

Borut Marincek  
Robert F. Dondelinger  
*Editors*

# Emergency Radiology



Imaging  
and Intervention

 Springer

Borut Marincek · Robert F. Dondelinger (Eds.)

---

**EMERGENCY RADIOLOGY – Imaging and Intervention**



Borut Marincek · Robert F. Dondelinger (Eds.)

---

# **EMERGENCY RADIOLOGY – Imaging and Intervention**

With 483 Figures, 25 in Color and 49 Tables

 Springer

Prof. Dr. Borut Marincek  
Institute of Diagnostic Radiology  
University Hospital Zurich  
Rämistrasse 100  
8091 Zurich  
Switzerland

Prof. Dr. Robert F. Dondelinger  
Department of Medical Imaging  
University Hospital Sart Tilman  
Domaine Universitaire du Sart Tilman B 35  
4000 Liège  
Belgium

Library of Congress Control Number: 2006933176

ISBN-10 3-540-26227-X Springer Berlin Heidelberg New York  
ISBN-13 978-3-540-26227-5 Springer Berlin Heidelberg New York

This work is subject to copyright. All rights are reserved, whether the whole or part of the material is concerned, specifically the rights of translation, reprinting, reuse of illustrations, recitation, broadcasting, reproduction on microfilms or in any other way and storage in data banks. Duplication of this publication or parts thereof is permitted only under the provisions of the German Copyright Law of September 9, 1965, in its current version, and permission for use must always be obtained from Springer-Verlag. Violations are liable for prosecution under the German Copyright Law.

Springer-Verlag is a part of Springer Science+Business Media  
springer.com

© Springer-Verlag Berlin Heidelberg 2007

The use of general descriptive names, registered names, trademarks, etc. in this publication does not imply, even in the absence of a specific statement, that such names are exempt from the relevant protective laws and regulations and therefore free for general use.

Product liability: the publishers cannot guarantee the accuracy of any information about dosage and application contained in this book. In every individual case the user must check such information by consulting the relevant literature.

Editor: Dr. Ute Heilmann, Heidelberg  
Desk Editor: Wilma McHugh, Heidelberg  
Cover design: eStudio Calamar, Girona Spain  
Reproduction and Typesetting: AM-productions GmbH, Wiesloch  
Production: LE-TeX Jelonek, Schmidt & Vöckler GbR, Leipzig

Printed on acid-free paper 21/3100/YL 5 4 3 2 1 0

## Preface

Why write a book on emergency radiology? In many countries, hospital emergency departments have become a major part of the healthcare safety net. In the last decade economically-driven structural changes in health care delivery have caused a dramatic increase in emergency department visits. In response to capacity and staffing pressures, hospitals are developing and implementing a variety of strategies designed to improve patient flow and reduce overcrowding in the emergency department. Several factors are considered critical for success, such as having the right multidisciplinary teams in place and optimizing the use of imaging tests. For a critical care physician it is paramount to obtain the images quickly and for them to be interpreted accurately.

To accomplish this, the emergency radiology division should be located adjacent to or within the emergency department. High quality emergency radiology services combine state-of-the art equipment and unsurpassable expertise available 24 hours a day. The demands for radiologists with specific knowledge in diagnostic and interventional emergency radiology is continuously increasing. The emergency radiology services should be equipped with sophisticated imaging (especially Multidetector Computed Tomography, MDCT) and information technologies (Picture Archiving and Communication System, PACS). The rapid development of MDCT technology has dramatically changed CT applications. In many imaging centers the volume of MDCT scans is growing at least 10% annually while the number of radiographic studies

decline. There is an increasing trend towards the use of MDCT to evaluate traumatic injuries and non-traumatic emergencies. The use of workstations for reporting and for further image reconstruction becomes standard practice. On the occasion of the European Congress of Radiology (ECR) 2003 and 2004 a Categorical Course on “Emergency Radiology” has been organized to assess current developments and concepts in this rapidly growing field. Numerous radiologists, all outstanding and internationally renowned experts in their field, have made superb contributions in an ECR syllabus. These authors have now made a second effort and updated their contributions for this book. The chapters in the book mirror the topics presented in the ECR course, encompassing imaging approaches as well as interventional aspects. A separate section is devoted to pediatric emergencies.

We would like to express our thanks and appreciation to all contributors for their excellent written material. This comprehensive work would not have been accomplished without their enthusiasm.

We hope this book will be a “Go-To” reference to general radiologists who have to deal with traumatic and non-traumatic emergencies. Similarly, it should serve as reference for emergency medicine physicians. Finally, radiology residents should find this book useful when covering the emergency department.

Zurich  
Liège

Borut Marincek  
Robert F. Dondelinger

## Foreword

As emergency medicine continues to evolve as a formal clinical discipline, the need for emergency radiology to be integrated in its four essential fields of action, including clinical practice, a defined body of knowledge, a rigorous training program, and an active research environment are of primary importance.

Radiological diagnosis and management presently play an instrumental role in providing the highest standards of care in the acutely ill or multitrauma patient who enters the emergency department, and it is imperative that radiologists and other clinicians be well aware and adequately informed of the actual trends and concepts, as well as the latest advances, in this rapidly growing field.

The book provides unique and authentic descriptions of the role of imaging and intervention in practically all facets of traumatic and non-traumatic, as well as acute and life-threatening, conditions of modern medicine.

The book is divided into seven sections. Following introductory in-depth coverage of the present use of 3D imaging in the dedicated emergency room and the role of imaging in the management of polytrauma patients, the book describes in great detail imaging and intervention of all common, and less common, traumatic and non-trau-

matic neurological, thoracic, abdominal, gastrointestinal, pelvic, musculoskeletal, vascular, and pediatric emergencies.

The editors, Borut Marincek and Robert Dondelinger, are internationally renowned authorities with unparalleled clinical experience in emergency radiology. In addition to writing their own contributions to several individual chapters, they have been very successful in involving a number of leading specialists in the field, from both Europe and the United States, who convey a breadth and depth of experience and insight, and enrich our understanding and capabilities of imaging and intervention in emergency medicine.

I congratulate the editors and all the distinguished contributors to this comprehensively written and superbly illustrated volume, most sincerely, for their outstanding work. I am confident that this excellent book will meet with success among specialists in all disciplines involved in emergency medicine, and will serve as the main reference source in the field.

Nick C. Gourtsoyiannis, MD, PhD, FRCR (Hon)  
Heraklion, 22 May 2006

# Contents

## SECTION ONE Emergency Radiology: Role of Imaging

1.1	Role of Imaging in the Management of Trauma Victims P.-A. Poletti, A. Platon, C.D. Becker	
1.1.1	Introduction . . . . .	3
1.1.2	Imaging Algorithms for Trauma Patients . . .	3
1.1.3	Sonography . . . . .	7
1.1.4	CT Scan . . . . .	8
1.1.5	Follow-up Imaging during Conservative Treatment . . . . .	18
References	. . . . .	20
1.2	Role of 3D Imaging in the Emergency Room L. Husmann, S. Leschka, H. Alkadhi, S. Wildermuth	
1.2.1	Introduction . . . . .	25
1.2.2	Imaging . . . . .	25
1.2.3	Conclusion . . . . .	35
References	. . . . .	35

## SECTION TWO Traumatic Injuries: Imaging and Intervention

2.1	Hemostatic Arterial Embolization in Trauma Victims at Admission R.F. Dondelinger, G. Trotteur, B. Ghaye	
2.1.1	Introduction . . . . .	41
2.1.2	Classification of Trauma Patients . . . . .	41
2.1.3	Trauma Patient Triage with Computed Tomography . . . . .	45
2.1.4	Indications of Therapeutic Arteriography . .	47
2.1.5	Arteriographic Demonstration of Posttraumatic Hemorrhage . . . . .	48
2.1.6	Arteriographic Hemostatic Embolization Technique . . . . .	48
2.1.7	Organ-Specific Hemostatic Embolization . .	51
2.1.8	Conclusion . . . . .	58
References	. . . . .	58

2.2	Imaging and Intervention in Post-traumatic Complications (Delayed Intervention) P.P. Goffette	
2.2.1	Introduction . . . . .	61
2.2.2	Liver and Bile Ducts . . . . .	62
2.2.3	Spleen . . . . .	75
2.2.4	Pancreas . . . . .	83
2.2.5	Kidneys, Adrenals, Urinary Bladder . . . . .	86
2.2.6	Gastrointestinal Tract . . . . .	88
2.2.7	Vascular Complications . . . . .	89
2.2.8	Diaphragm . . . . .	92
2.2.9	Conclusion . . . . .	92
References	. . . . .	92
2.3	Imaging of Head Injuries N. Bešenski	
2.3.1	Introduction . . . . .	99
2.3.2	Clinical Findings . . . . .	99
2.3.3	Imaging . . . . .	100
2.3.4	Biomechanical Considerations of Brain Injury . . . . .	102
2.3.5	Classification of Brain Injury . . . . .	108
2.3.6	Closed-Head Injury . . . . .	109
2.3.7	Imaging of Diffuse Axonal Injury (Shearing Injury) . . . . .	114
2.3.8	Early Secondary Lesions in Brain Injury . . .	118
2.3.9	Late Sequelae of Trauma . . . . .	120
2.3.10	Conclusion . . . . .	122
References	. . . . .	123
2.4	Imaging of Facial Injuries U. Salvolini, G. Polonara, S. Salvolini	
2.4.1	Introduction . . . . .	125
2.4.2	Imaging . . . . .	125
2.4.3	Nasal Fractures . . . . .	127
2.4.4	Complex Midfacial Fractures . . . . .	128
2.4.5	Isolated Fractures . . . . .	131
2.4.6	Foreign Bodies and Penetrating Injuries . . .	133
2.4.7	Complex Facial Fractures . . . . .	133
2.4.8	Mandibular Fractures . . . . .	136
2.4.9	Conclusion . . . . .	138
References	. . . . .	138

<b>2.5</b>	<b>Imaging of Spinal Injuries</b>				
	H. Imhof				
2.5.1	Introduction	141			
2.5.2	Injury Assessment and Imaging	142			
2.5.3	Imaging	142			
2.5.4	Classification	144			
	References	153			
<b>2.6</b>	<b>Imaging of Thoracic Injuries</b>				
	G. Gavelli, G. Napoli, P. Bertaccini, G. Battista, R. Fattori				
2.6.1	Introduction	155			
2.6.2	Clinical and Imaging Findings	156			
2.6.3	Conclusion	175			
	References	176			
<b>2.7</b>	<b>Vascular Injuries of the Thorax: Multi-Detector-Row CT and 3D Imaging</b>				
	H. Alkadhi, S. Leschka, S. Wildermuth				
2.7.1	Introduction	179			
2.7.2	Clinical Findings	179			
2.7.3	Imaging	180			
2.7.4	Conclusion	187			
	References	187			
<b>2.8</b>	<b>Imaging of Abdominal and Pelvic Injuries</b>				
	S. Leschka, H. Alkadhi, L. Husmann, S. Wildermuth				
2.8.1	Introduction	189			
2.8.2	Clinical Findings	190			
2.8.3	Imaging	191			
2.8.4	Conclusion	201			
	References	201			
<b>2.9</b>	<b>Imaging and Intervention of Large Arterial Trauma</b>				
	M. Schoder, M. Prokop, J. Lammer				
2.9.1	Introduction	205			
2.9.2	Supraaortic Arch Vessels	206			
2.9.3	Pelvic Arteries and Lower Limbs	208			
2.9.4	Thoracic Aorta	212			
2.9.5	Abdominal Aorta	218			
2.9.6	Abdominal Aortic Branches	220			
2.9.7	Conclusion	220			
	References	220			
<b>2.10</b>	<b>Pelvic Fractures</b>				
	N.H. Theumann, P. Schnyder, F. Portier				
2.10.1	Introduction	225			
2.10.2	Incidence	225			
2.10.3	Anatomy and Biomechanics	225			
2.10.4	Imaging	228			
2.10.5	Classifications	231			
2.10.6	Pelvic Trauma Management	246			
2.10.7	Complications	247			
2.10.8	Conclusion	248			
	References	248			
<b>2.11</b>	<b>Traumatic Injuries: Imaging of Peripheral Musculoskeletal Injuries</b>				
	M.A. Müller, S. Wildermuth, K. Bohndorf				
2.11.1	Introduction	251			
2.11.2	General Part: Imaging Modalities	251			
2.11.3	Soft Tissue Injuries in General	253			
2.11.4	Upper Extremity	254			
2.11.5	Lower Extremity	273			
	References	288			
<b>SECTION THREE</b>					
<b>Non-Traumatic Neurologic Emergencies: Imaging and Intervention</b>					
<b>3.1</b>	<b>Imaging of Cerebral Ischemia</b>				
	I. Grunwald, C. Roth, P. Papanagiotou, W. Reith				
3.1.1	Introduction	293			
3.1.2	Intracerebral Hemorrhage	293			
3.1.3	Acute Ischemic Stroke	294			
3.1.4	Clinical Terms of “Stroke”	296			
3.1.5	Lacunar Infarctions	308			
3.1.6	Stroke in Children	308			
3.1.7	Dissection	308			
3.1.8	Hypoxic–Ischemic Encephalopathy	309			
3.1.9	Venous Infarction	309			
	References	310			
<b>3.2</b>	<b>Neuroradiological Emergency Interventions</b>				
	C. Brekenfeld, J. Gralla, R. Wiest, M. El-Koussy, L. Remonda, C. Ozdoba, G. Schroth				
3.2.1	Introduction	313			
3.2.2	Acute Haemorrhage in Neuroradiology	313			
3.2.3	Acute Ischaemic Stroke	323			
3.2.4	Discussion	326			
	References	327			
<b>SECTION FOUR</b>					
<b>Non-Traumatic Thoracic Emergencies: Imaging and Intervention</b>					
<b>4.1</b>	<b>Acute Chest Pain: Diagnostic Strategies</b>				
	L. Bonomo, M.L. Storto, A.R. Larici, R. Marano				
4.1.1	Introduction	331			
4.1.2	Diagnostic Imaging in Non-cardiac Acute Chest Pain	331			
4.1.3	Aortic Diseases	333			
4.1.4	Multidetector-Row CT and Acute Chest Pain	342			
	References	344			
<b>4.2</b>	<b>CT Diagnosis of Acute Pulmonary Embolism</b>				
	B. Ghaye and R.F. Dondelinger				
4.2.1	Introduction	347			
4.2.2	History	348			
4.2.3	The CTPA Technique	348			
4.2.4	Image Interpretation	349			
4.2.5	Estimation of the Age of the Embolus	354			

4.2.6 Results . . . . . 354  
 4.2.7 Interpretation Pitfalls . . . . . 358  
 4.2.8 Severity Assessment  
 of Pulmonary Embolism . . . . . 361  
 4.2.9 Alternative Diagnoses . . . . . 362  
 4.2.10 Other Advantages . . . . . 363  
 4.2.11 Limitations of CTPA . . . . . 364  
 4.2.12 CT of PE in Emergency Conditions . . . . . 364  
 4.2.13 Conclusion . . . . . 365  
 References . . . . . 365

**4.3 CT Venography in an Integrated Diagnostic Strategy of Acute Pulmonary Embolism and Venous Thrombosis**  
 B. Ghaye and R.F. Dondelinger

4.3.1 Introduction . . . . . 371  
 4.3.2 History . . . . . 372  
 4.3.3 Diagnostic Imaging of DVT . . . . . 372  
 4.3.4 Direct CT Venography . . . . . 372  
 4.3.5 Indirect CT Venography . . . . . 373  
 4.3.6 Venous Anatomy . . . . . 375  
 4.3.7 Image Interpretation . . . . . 378  
 4.3.8 Interpretive Pitfalls . . . . . 379  
 4.3.9 Potential Benefits of Combined CTPA  
 and CTV . . . . . 383  
 4.3.10 Clinical Results . . . . . 388  
 4.3.11 Conclusion . . . . . 388  
 References . . . . . 388

**4.4 Imaging and Treatment of Thoracic Fluid and Gas Collections**  
 C. Noukoua Tchuisse, B. Ghaye, R.F. Dondelinger

4.4.1 Introduction . . . . . 391  
 4.4.2 Diagnostic Imaging . . . . . 391  
 4.4.3 Imaging Guidance Modalities . . . . . 394  
 4.4.4 Percutaneous Drainage  
 of Thoracic Fluid Collections . . . . . 395  
 4.4.5 Pulmonary Collections . . . . . 401  
 4.4.6 Mediastinal Collections . . . . . 403  
 4.4.7 Complications of Percutaneous  
 Catheter Drainage . . . . . 406  
 4.4.8 Conclusion . . . . . 406  
 References . . . . . 406

**SECTION FIVE  
 Non-Traumatic Abdominal Emergencies:  
 Imaging and Intervention**

**5.1 Acute Abdominal Pain: Diagnostic Strategies**  
 S. Leschka, H. Alkadhi, S. Wildermuth,  
 B. Marincek

5.1.1 Introduction . . . . . 411  
 5.1.2 Clinical Findings . . . . . 411  
 5.1.3 Imaging . . . . . 413  
 5.1.4 Conclusion . . . . . 429  
 References . . . . . 431

**5.2 Imaging of Acute Intestinal Obstruction**  
 P. Taourel, C. Uriot, G. Laffargue, A. Lesnik,  
 F. Guillon, J.M. Bruel

5.2.1 Introduction . . . . . 435  
 5.2.2 Diagnosis of Mechanical Obstruction . . . . . 435  
 5.2.3 Diagnosis of Site . . . . . 437  
 5.2.4 Diagnosis of Cause . . . . . 437  
 5.2.5 Diagnosis of Complications . . . . . 446  
 5.2.6 Impact and Diagnostic Strategy . . . . . 449  
 References . . . . . 450

**5.3 Imaging and Intervention in Gastrointestinal Hemorrhage and Ischemia**  
 J.I. Bilbao Jaureguizar, I. Vivas Pérez,  
 D. Cano Rafart, A. Martínez de la Cuesta

5.3.1 Introduction . . . . . 453  
 5.3.2 Gastrointestinal Hemorrhage . . . . . 454  
 5.3.3 Intestinal Ischemia . . . . . 461  
 References . . . . . 467

**5.4 Imaging and Intervention in Sepsis**  
 T. Geoghegan, M.J. Lee

5.4.1 Introduction . . . . . 471  
 5.4.2 Ultrasound . . . . . 471  
 5.4.3 Computed Tomography . . . . . 472  
 5.4.4 Radionuclide Scintigraphy . . . . . 472  
 5.4.5 Diagnostic Fluid Aspiration . . . . . 473  
 5.4.6 Percutaneous Abscess Drainage . . . . . 474  
 5.4.7 Results of Percutaneous Abscess Drainage . . . . . 476  
 5.4.8 Conclusion . . . . . 479  
 References . . . . . 479

**5.5 Imaging and Intervention in Acute Biliary Conditions**  
 Y. Menu and M.-P. Vuillerme

5.5.1 Introduction . . . . . 481  
 5.5.2 Acute Cholecystitis . . . . . 481  
 5.5.4 Emphysematous Cholecystitis . . . . . 485  
 5.5.5 Gangrenous Cholecystitis . . . . . 485  
 5.5.6 Perforation of the Gallbladder . . . . . 485  
 5.5.7 Mirizzi Syndrome . . . . . 485  
 5.5.8 Cholecystostomy . . . . . 487  
 5.5.9 Acute Cholangitis . . . . . 487  
 5.5.11 Conclusion . . . . . 491  
 References . . . . . 491

**5.6 Imaging and Intervention in Acute Pancreatic Conditions**  
 G. Mansueto, D. Cenzi, A.A. Gumbs, M. D’Onofrio

5.6.1 Introduction . . . . . 493  
 5.6.2 Pancreatic Infections . . . . . 493  
 5.6.3 Involvement of Adjacent Organs, Structures  
 and Spaces . . . . . 503  
 5.6.4 Vascular Involvement . . . . . 510  
 References . . . . . 519

**5.7 Non-traumatic Uroradiological Emergencies**  
 D. Rickards

5.7.1 Introduction . . . . . 523

5.7.2 Obstruction of the Upper Urinary Tract . . . 523

5.7.3 Treatment of Acute Urinary Obstruction . . . 530

5.7.4 Spontaneous Haemorrhage  
 from the Urinary Tract . . . . . 533

5.7.5 Spontaneous Bladder Rupture . . . . . 534

5.7.6 Testicular Torsion . . . . . 534

5.7.7 Priapism . . . . . 535

References . . . . . 535

**SECTION SIX  
 Non-Traumatic Vascular Emergencies:  
 Imaging and Intervention**

**6.1 Imaging and Intervention in Acute Non-Traumatic Arterial Conditions**  
 W. Cwikiel

6.1.1 Introduction . . . . . 539

6.1.2 Pulmonary and Bronchial Arteries . . . . . 539

6.1.3 Acute Arterial Gastrointestinal Bleeding . . . 544

6.1.4 Conclusion . . . . . 546

References . . . . . 546

**6.2 Imaging and Intervention in Acute Venous Occlusion**  
 P. Haage and T. Krings

6.2.1 Introduction . . . . . 549

6.2.2 Acute Venous Occlusion  
 of the Lower Extremity . . . . . 549

6.2.3 Acute Pelvic Vein and Inferior Vena  
 Cava Occlusion . . . . . 552

6.2.4 Acute Mesenteric Vein Occlusion . . . . . 554

6.2.5 Acute Venous Occlusion of the Upper  
 Extremity . . . . . 556

6.2.6 Acute Venous Occlusion of Arteriovenous  
 Hemodialysis Access . . . . . 557

6.2.7 Acute Cerebral Vein Thrombosis . . . . . 560

References . . . . . 568

**6.3 Management of Occluded Hemodialysis Shunts, Grafts, and Venous Access**  
 D. Vorwerk

6.3.1 Introduction . . . . . 571

6.3.2 Clinical Situation . . . . . 571

6.3.3 Complications . . . . . 577

6.3.4 Technique of Fibrinolysis . . . . . 578

6.3.5 Technique of Catheter Stripping . . . . . 578

References . . . . . 578

**SECTION SEVEN  
 Imaging Pediatric Emergencies**

**7.1 Pediatric Neurological Emergencies**  
 J.W.J. McCann and E.Phelan

7.1.1 Introduction . . . . . 583

7.1.2 Clinical Findings . . . . . 584

7.1.3 Hypoxic–Ischaemic Encephalopathy . . . . . 584

7.1.4 The Preterm Infant . . . . . 585

7.1.5 The Term Infant . . . . . 587

7.1.6 Congenital Infection . . . . . 588

7.1.7 Acquired Infection . . . . . 589

7.1.8 Non-accidental Injury . . . . . 590

7.1.9 Acute Disseminated Encephalomyelitis . . . . 592

7.1.10 Hypertensive Encephalopathy . . . . . 593

7.1.11 Cerebral Sinovenous Thrombosis  
 and Venous Infarction . . . . . 594

7.1.12 Arterial Infarction . . . . . 595

7.1.13 Metabolic Disorders . . . . . 595

7.1.14 Drugs: Asparaginase, Methotrexate  
 and Cyclosporin . . . . . 596

7.1.15 Epilepsy: Structural Abnormalities . . . . . 596

7.1.16 Endocrine-Related Encephalopathy . . . . . 597

7.1.17 Conclusion . . . . . 597

References . . . . . 597

**7.2 Thoracic Emergencies**  
 L. Breysem and M.-H. Smet

7.2.1 Introduction . . . . . 601

7.2.2 The Chest and Respiratory Tract in Children:  
 Physiological Aspects and Differences  
 with Adults . . . . . 601

7.2.3 Clinical Symptoms . . . . . 602

7.2.4 Imaging of Non-traumatic Pediatric  
 Thoracic Emergencies . . . . . 603

7.2.5 Imaging of Traumatic Pediatric Thoracic  
 Emergencies . . . . . 617

7.2.6 Conclusion . . . . . 618

References . . . . . 618

**7.3 Non-traumatic Abdominal Emergencies**  
 M.I. Tawil

7.3.1 Introduction . . . . . 621

7.3.2 Imaging . . . . . 622

7.3.3 The Diseases . . . . . 623

7.3.4 Conclusion . . . . . 642

References . . . . . 642

**Subject Index . . . . . 653**



## List of Contributors

### H. Alkadhi

Institute of Diagnostic Radiology  
University Hospital Zurich  
Rämistrasse 100  
8091 Zurich  
Switzerland  
E-mail: hatem.alkadhi@usz.ch

### G. Battista

Department of Radiology  
University of Bologna  
Via Massarenti, 9  
40100 Bologna  
Italy  
E-mail: battista@aosp.bo.it

### C.D. Becker

Department of Diagnostic and Interventional Radiology  
University Hospital  
24, Rue Micheli-du-Crest  
1211 Geneva  
Switzerland  
E-mail: christoph.becker@hcuge.ch

### P. Bertaccini

Department of Radiology  
University of Bologna  
Via Massarenti, 9  
40100 Bologna  
Italy  
E-mail: paolabertaccini@libero.it

### N. Bešenski

Department of Radiology  
Medical University of South Carolina  
169 Ashley Avenue  
Charleston, SC 29245  
USA  
E-mail: besenski@musc.edu

### J.I. Bilbao Jaureguizar

Servicio de Radiología  
University Clinic of Navarra  
Avda Pio XII, s/n, Apt. 192  
31080 Pamplona  
Spain  
E-mail: jibilbao@unav.es

### K. Bohndorf

Department of Radiology  
Zentralklinikum Augsburg  
Stenglinstraße 2  
86156 Augsburg  
Germany  
E-mail: radiol-klin.augsburg@gmx.de

### L. Bonomo

Department of Radiology  
Univ. Cattolica del Sacro Cuore  
Largo A. Gemelli  
00168 Rome  
Italy  
E-mail: lbonomo@rm.unicatt.it

### C. Brekenfeld

Institute of Diagnostic and  
Interventional Neuroradiology  
Inselspital  
University Hospital Berne  
Freiburgerstrasse 4  
3010 Berne  
Switzerland  
E-mail: caspar.brekenfeld@insel.ch

### L. Breysem

Department of Radiology  
University Hospitals Gasthuisberg  
Herestraat 49  
3000 Leuven  
Belgium  
E-mail: luc.breysem@uz.kuleuven.ac.be

**J.M. Bruel**

Department of Imaging  
Hospital St. Eloi  
80, rue Augustin Fliche  
34295 Montpellier  
France  
E-mail: jm-bruel@wanadoo.fr

**D. Cano Rafart**

Servicio de Radiología  
University Clinic of Navarra  
Avda Pio XII, s/n, Apt. 192  
31080 Pamplona  
Spain  
E-mail: dcanor@unav.es

**D. Cenzi**

Department of Radiology  
University Hospital "GB Rossi"  
Piazza L.A. Scuro 10  
37134 Verona  
Italy  
E-mail: danielacenzi@katamail.com

**W. Cwikiel**

Department of Diagnostic Radiology  
University of Michigan Hospital  
1500 E. Medical Center Drive  
Ann Arbor MI, 48109-0030  
USA  
E-mail: cwikiel@med.umich.edu

**R.F. Dondelinger**

Department of Medical Imaging  
University Hospital Sart Tilman  
Domaine Universitaire du Sart Tilman B35  
4000 Liège  
Belgium  
E-mail: rdondelinger@chu.ulg.ac.be

**M. El-Koussy**

Institute of Diagnostic and  
Interventional Neuroradiology  
Inselspital  
University Hospital Berne  
Freiburgerstrasse 4  
3010 Berne  
Switzerland  
E-mail: marwan.el-koussy@insel.ch

**R. Fattori**

Department of Radiology  
University of Bologna  
Via Massarenti, 9  
40100 Bologna  
Italy  
E-mail: ross@med.unibo.it

**G. Gavelli**

Department of Radiology  
University of Bologna  
Via Massarenti, 9  
40100 Bologna  
Italy  
E-mail: ggavelli@med.unibo.it

**T. Geoghegan**

Department of Radiology  
Beaumont Hospital and Royal College of Surgeons  
Beaumont Road  
Dublin 9  
Ireland  
E-mail: geoghegancrosbie@eircom.net

**B. Ghaye**

Department of Medical Imaging  
University Hospital Sart Tilman  
Domaine Universitaire du Sart Tilman B35  
4000 Liège  
Belgium  
E-mail: bghaye@chu.ulg.ac.be

**P.P. Goffette**

Department of Medical Imaging  
Angiography and Interventional Radiology Unit  
Saint-Luc University Hospital  
Louvain Medical School  
10, avenue Hippocrate  
1200 Brussels  
Belgium  
E-mail: goffette@rdgn.ucl.ac.be

**J. Gralla**

Institute of Diagnostic and  
Interventional Neuroradiology  
Inselspital  
University Hospital Berne  
Freiburgerstrasse 4  
3010 Berne  
Switzerland  
E-mail: jan.gralla@insel.ch

**I. Grunwald**

Department of Diagnostic and  
Interventional Neuroradiology  
University of Saarland  
66424 Homburg  
Germany

**F. Guillon**

Department of Surgery  
Hospital St. Eloi  
80, rue Augustin Fliche  
34295 Montpellier  
France  
E-mail: f-guillon@chu-montpellier.fr

**A.A. Gumbs**

Department of Surgery  
Yale University School of Medicine  
New Haven, CT, 06512  
USA  
E-mail: rgumbs@howard.edu

**P. Haage**

Department of Diagnostic and Interventional Radiology  
Helios Klinikum Wuppertal  
University Hospital Witten/Herdecke  
Heusnerstraße 40  
42283 Wuppertal  
Germany  
E-mail: phaage@wuppertal.helios-kliniken.de

**L. Husman**

Institute of Diagnostic Radiology  
University Hospital Zurich  
Rämistrasse 100  
8091 Zurich  
Switzerland  
E-mail: lars.husmann@usz.ch

**H. Imhof**

University Clinic for Diagnostic Radiology  
Medical University of Vienna  
Währinger Gürtel 18–20  
1090 Vienna  
Austria  
E-mail: osteo-mr@meduniwien.ac.at

**T. Krings**

Department of Neuroradiology  
RWTH Aachen University  
Pauwelsstrasse 30  
52057 Aachen  
Germany  
E-mail: wkrings@t-online.de

**G. Laffargue**

Department of Imaging  
Hospital Lapeyronie  
371, avenue du Doyen Gaston Giraud  
34295 Montpellier Cedex 5  
France  
E-mail: f-laffargue@chu-montpellier.fr

**J. Lammer**

Ludwig-Bolzmann Institut  
für Interdisziplinäre Gefäßforschung  
AKH-University Clinics  
Währinger Gürtel 18–20  
1090 Vienna  
Austria  
E-mail: johannes.lammer@meduniwien.ac.at

**A.R. Larici**

Department of Radiology  
Univ. Cattolica del Sacro Cuore  
Largo A. Gemelli  
00168 Rome  
Italy  
E-mail: ar.larici@rm.unicatt.it

**M. Lee**

Department of Radiology  
Beaumont Hospital and Royal College of Surgeons  
Beaumont Road  
Dublin 9  
Ireland  
E-mail: mlee@rcsi.ie

**S. Leschka**

Institute of Diagnostic Radiology  
University Hospital Zurich  
Rämistrasse 100  
8091 Zurich  
Switzerland  
E-mail: sebastian.leschka@usz.ch

**A. Lesnik**

Department of Imaging  
Hospital Lapeyronie  
371, avenue du Doyen Gaston Giraud  
34295 Montpellier Cedex 5  
France  
E-mail: a-lesnik@chu-montpellier.fr

**G. Mansueto**

Department of Radiology  
University Hospital “GB Rossi”  
Piazza L.A. Scuro 10  
37134 Verona  
Italy  
E-mail: giancarlo.mansueto@univr.it

**R. Marano**

Department of Radiology  
Univ. G. D’Annunzio Chieti  
Via dei Vestini  
66100 Chieti  
Italy  
E-mail: r.marano@rad.unich.it

**B. Marincek**

Institute of Diagnostic Radiology  
University Hospital Zurich  
Rämistrasse 100  
8091 Zurich  
Switzerland  
E-mail: borut.marincek@usz.ch

**A. Martínez de la Cuesta**

Servicio de Radiología  
University Clinic of Navarra  
Avda Pio XII, s/n, Apt. 192  
31080 Pamplona  
Spain  
E-mail: amartinc@unav.es

**J.W.J. McCann**

Our Lady's Hospital for Sick Children  
Crumlin  
Dublin 12  
Ireland  
E-mail: wolfram.machann@roentgen.uni-wuerzburg.de

**Y. Menu**

Service de Radiologie Broca  
Hôpital de Bicêtre  
78, rue du Général Leclerc  
94275 Le Kremlin-Bicêtre  
France  
E-mail: yves.menu@bct.ap-hop-paris.fr

**M.A. Müller**

Institute of Diagnostic Radiology  
University Hospital Zurich  
Rämistrasse 100  
8091 Zurich  
Switzerland  
E-mail: mathias.mueller@stag.ch

**G. Napoli**

Department of Radiology  
University of Bologna  
Via Massarenti, 9  
40100 Bologna  
Italy  
E-mail: gabrin@gmail.com

**C. Noukoua Tchuisse**

Department of Medical Imaging  
University Hospital Sart Tilman  
Domaine Universitaire du Sart Tilman B35  
4000 Liège  
Belgium  
E-mail: noukouac@yahoo.fr

**M. D'Onofrio**

Department of Radiology  
University Hospital "GB Rossi"  
Piazza L.A. Scuro 10  
37134 Verona  
Italy  
E-mail: mdonofrio@univr.it

**C. Ozdoba**

Institute of Diagnostic and  
Interventional Neuroradiology  
Inselspital  
University Hospital Berne  
Freiburgerstrasse 4  
3010 Berne  
Switzerland  
E-mail: christoph.ozdoba@insel.ch

**P. Papanagiotou**

Department of Diagnostic and  
Interventional Neuroradiology  
University of Saarland  
66424 Homburg  
Germany  
E-mail: panagiotis.papanagiotou@hotmail.com

**E. Phelan**

Our Lady's Hospital for Sick Children  
Crumlin  
Dublin 12  
Ireland  
E-mail: eithne.phelan@olhsc.ie

**A. Platon**

Department of Diagnostic and  
Interventional Radiology  
University Hospital  
24, Rue Micheli-du-Crest  
1211 Geneva  
Switzerland  
E-mail: alexandra.platon@hcuge.ch

**P.-A. Poletti**

Department of Diagnostic and  
Interventional Radiology  
University Hospital  
24, Rue Micheli-du-Crest  
1211 Geneva  
Switzerland  
E-mail: pierre-alexandre.poletti@hcuge.ch

**G. Polonara**

Department of Radiology  
 University Hospital  
 Via Conca, 71, Torrette  
 60020 Ancona  
 Italy  
 E-mail: g.polonara@ao-umbertoprime.marche.it

**F. Portier**

Hôpital Ambroise Paré  
 1, rue d'Eylau  
 13006 Marseille  
 France  
 E-mail: fraportier@wanadoo.fr

**M. Prokop**

University Clinics of Radiodiagnostics  
 AKH University Clinics  
 Währinger Gürtel 18–20  
 1090 Vienna  
 Austria  
 E-mail: mathias.prokop@gmail.com

**I. Quasar Grunwald**

Department of Diagnostic and  
 Interventional Neuroradiology  
 University of Saarland  
 66424 Homburg  
 Germany  
 E-mail: i.grunwald@web.de

**W. Reith**

Department of Diagnostic and  
 Interventional Neuroradiology  
 University of Saarland  
 66424 Homburg  
 Germany  
 E-mail: nrreith@uniklinikum-saarland.de

**L. Remonda**

Institute of Diagnostic and  
 Interventional Neuroradiology  
 Inselspital  
 University Hospital Berne  
 Freiburgstrasse 4  
 3010 Berne  
 Switzerland  
 E-mail: luca.remonda@insel.ch

**D. Rickards**

University College Hospitals London  
 235 Euston Road  
 London NW12BU  
 UK  
 E-mail: david.rickards@uclh.nhs.uk

**C. Roth**

Department of Diagnostic and  
 Interventional Neuroradiology  
 University of Saarland  
 66424 Homburg  
 Germany  
 E-mail: christian.roth@gmx.com

**S. Salvolini**

Department of Ophthalmology  
 University Hospital  
 Via Conca, 71, Torrette  
 60020 Ancona  
 Italy  
 E-mail: u.salvolini@univpm.it

**U. Salvolini**

Department of Radiology  
 University Hospital  
 Via Conca, 71, Torrette  
 60020 Ancona  
 Italy  
 E-mail: u.salvolini@univpm.it

**P. Schnyder**

Department of Diagnostic and  
 Interventional Radiology  
 University Hospital (CHUV)  
 Rue du Bugnon 46  
 1011 Lausanne  
 Switzerland  
 E-mail: pierre.schnyder@chuv.hospvd.ch

**M. Schoder**

Department of Angiography and  
 Interventional Radiology  
 AHK University Clinics  
 Währinger Gürtel 18–20  
 1090 Vienna  
 Austria  
 E-mail: maria.schoder@akhwien.at

**G. Schroth**

Institute of Diagnostic and  
 Interventional Neuroradiology  
 Inselspital  
 University Hospital Berne  
 Freiburgstrasse 4  
 3010 Berne  
 Switzerland  
 E-mail: gerhard.schroth@insel.ch

**M.-H. Smet**

Department of Radiology  
University Hospitals Gasthuisberg  
Herestraat 49  
3000 Leuven  
Belgium  
E-mail: marleen.smet@uz.kuleuven.ac.be

**M.L. Storto**

Department of Radiology  
Univ. G. D'Annunzio Chieti  
Via dei Vestini  
66100 Chieti  
Italy  
E-mail: ml.storto@radiol.unich.it

**P. Taourel**

Department of Imaging  
Hospital Lapeyronie  
371, avenue du Doyen Gaston Giraud  
34295 Montpellier Cedex 5  
France  
E-mail: p-taourel@chu-montpellier.fr

**M.I. Tawil**

Department of Radiology  
Royal Liverpool Children's Hospital NHS Trust –  
Alder Hey  
Eaton Road  
Liverpool L12 2AP  
UK  
E-mail: Mohamed.Tawil@rlc.nhs.uk

**N. Theumann**

Department of Diagnostic and Interventional Radiology  
University Hospital (CHUV)  
Rue du Bugnon 46,  
1011 Lausanne  
Switzerland  
E-mail: nicolas.theumann@chuv.ch

**G. Trotteur**

Department of Medical Imaging  
University Hospital Sart Tilman  
Domaine Universitaire du Sart Tilman B35  
4000 Liège  
Belgium  
E-mail: g.trotteur@chu.ulg.ac.be

**C. Uriot**

Department of Imaging  
Hospital Lapeyronie  
371, avenue du Doyen Gaston Giraud  
34295 Montpellier Cedex 5  
France  
E-mail: curior@chu-montpellier.fr

**I. Vivas Pérez**

Servicio de Radiología  
University Clinic of Navarra  
Avda Pio XII, s/n, Apt. 192  
31080 Pamplona  
Spain  
E-mail: isvivasp@unav.es

**D. Vorwerk**

Department of Diagnostic and Interventional Radiology  
Klinikum Ingolstadt  
85080 Ingolstadt  
Germany  
E-mail: dierk.vorwerk@klinikum-ingolstadt.de

**M.-P. Vuillerme**

Service de Radiologie Broca  
Hôpital de Bicêtre  
78, rue du Général Leclerc  
94275 Le Kremlin-Bicêtre  
France  
E-mail: marie-pierre.vuillierme@bjn.ap-hop-paris

**R. Wiest**

Institute of Diagnostic and  
Interventional Neuroradiology  
Inselspital  
University Hospital Berne  
Freiburgerstrasse 4  
3010 Berne  
Switzerland  
E-mail: roland.wiest@insel.ch

**S. Wildermuth**

Institute of Radiology  
Kantonsspital St. Gallen  
9007 St. Gallen  
Switzerland  
E-mail: simon.wildermuth@kssg.ch

## **Section ONE**

# **Emergency Radiology: Role of Imaging**





# Role of Imaging in the Management of Trauma Victims

P.-A. Poletti, A. Platon, C.D. Becker

## 1.1

### Contents

1.1.1	Introduction	3
1.1.2	Imaging Algorithms for Trauma Patients	3
1.1.2.1	Multi-trauma Patients	3
1.1.2.2	Mild or Low-Energy Trauma	4
1.1.3	Sonography	7
1.1.4	CT Scan	8
1.1.4.1	CT Protocols	8
1.1.4.2	CT Interpretation	10
1.1.5	Follow-up Imaging during Conservative Treatment	18
1.1.5.1	Brain and Cervical Spine Injuries	18
1.1.5.2	MR in Non-neurological Trauma Situations	19
	References	20

### 1.1.1 Introduction

Trauma is a major public health concern throughout the world, and probably the most serious of all health problems facing developed countries (Harlan et al. 1990). In the Western industrialized countries, injuries are the leading cause of death up to the age of 44 years (Colucciello 1993). The improvement in imaging techniques that occurred during the past 30 years have deeply modified the conception and the understanding of trauma patients management. Before the advent of computed tomography (CT) and sonography, surgery was liberally used for both diagnostic and therapeutic purposes with the drawback of non-therapeutic surgical procedures being associated with a significant increase of morbidity (e.g., about 20% for a negative laparotomy). The progressive use of contrast-enhanced CT allowed a better selection of patients for surgery and also reduced the amount of life-threatening injuries that could remain overlooked at initial assessment as well as improved monitoring of patients, in whom a non-surgical therapeutic approach has been attempted. In addition, surgeons have gained confidence in imaging for the monitoring of patients treated non-operatively (Regel et al.

1995; Mirvis and Shanmuganathan 2003; Daffner 2001). The growing role of imaging in the management of trauma victims, along with the development of more sophisticated technologies, increases the workload and the responsibility of the emergency radiology team; therefore, the emergency radiologist on call must be aware of the fundamentals of trauma radiology, to depict the life-threatening diagnoses, avoid the classical radiological pitfalls, and to allow the immediate application of the life-saving therapeutic procedures.

The goal of this chapter is to address the current concepts of imaging trauma patients, from admission in the emergency facility to follow-up investigation in the ICU

### 1.1.2 Imaging Algorithms for Trauma Patients

#### 1.1.2.1 Multi-trauma Patients

At the time of their admission in the emergency room, trauma patients are often confused, unconscious, or intubated. Clinical examination alone has been shown to be unreliable for excluding traumatic injuries (Rodriguez et al. 1982; Schurink et al. 1997; Poletti et al. 2004a; Brown 2005), and the examiner's suspicion must therefore rely on the trauma mechanism rather than on the patients' complaints or physical examination. According to the Advanced Trauma Life Support (ATLS; Bell et al. 1999) recommendations, the following imaging studies are systematically performed at the resuscitation area, in most of the trauma centers, for the initial evaluation of any trauma patients involved in a high-energy accident or with loss of consciousness:

1. An antero-posterior (AP) chest radiograph, to detect life-threatening injuries which may require immediate treatment (e.g., tension pneumothorax, massive hemothorax, flail chest) or further investigation (e.g., widening of mediastinum, suggestive of a major vessel injury; Fig. 1)
2. An AP pelvic radiograph, to detect a severe pelvic fracture, which could mandate immediate application of a pelvic belt

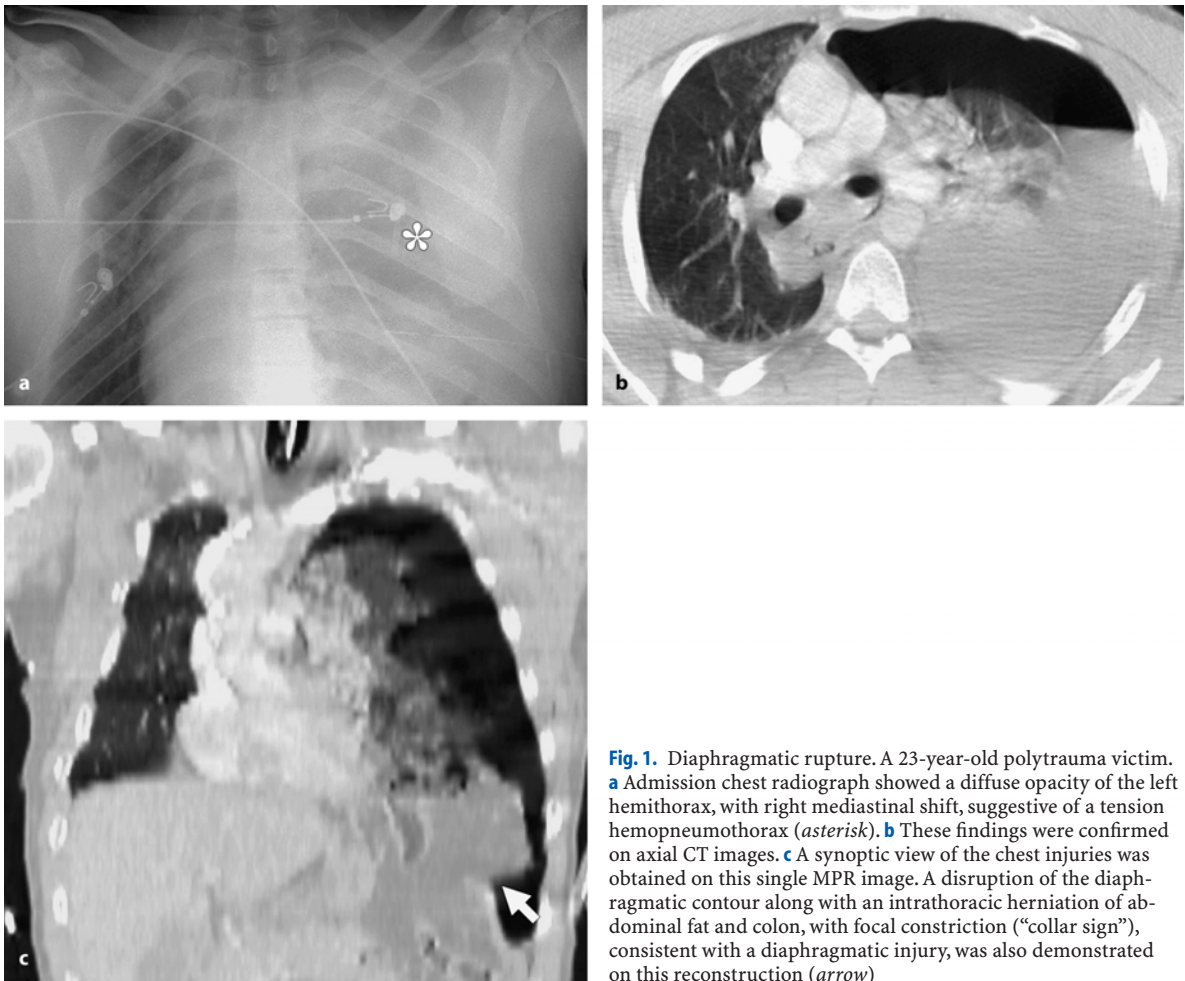


**Fig. 1.** Diaphragmatic rupture. A 23-year-old polytrauma victim. **a** Admission chest radiograph showed a diffuse opacity of the left hemithorax, with right mediastinal shift, suggestive of a tension hemothorax (*asterisk*). **b** These findings were confirmed on axial CT images. **c** A synoptic view of the chest injuries was obtained on this single MPR image. A disruption of the diaphragmatic contour along with an intrathoracic herniation of abdominal fat and colon, with focal constriction (“collar sign”), consistent with a diaphragmatic injury, was also demonstrated on this reconstruction (*arrow*)

3. A lateral cervical spine radiograph, to detect a major cervical spine injury. Due to the low sensitivity of this examination, its utility is subject to controversy, especially in unconscious patients: even if the lateral cervical spine radiograph is normal, the presence of a cervical fracture should be suspected until CT examination has been performed (Brohi et al. 2005; Wintermark et al. 2003). Inadequate lateral views should not be repeated, to avoid unnecessary loss of time (Fig. 2; Brohi et al. 2005)
4. An abdominal sonography, for quick detection of free intra-peritoneal fluid indicating abdominal bleeding. This examination can be easily, quickly, and safely performed in trauma patients with a small mobile ultrasound unit, although its sensitivity in detecting hepatic, splenic, and renal trauma in the acute phase is limited (Poletti et al. 2003; McGahan et al. 1997)

As soon as the vital functions have been stabilized, the patient is brought in the CT facility to undergo a total body CT examination. Conventional radiograph examination of

the limbs is usually performed immediately after CT, provided that it does not delay a life-saving procedure. Conventional spine radiograph can be replaced by 2D reconstructions obtained from multidetector-row CT (MDCT) examination, which is more accurate to depict fractures (Wintermark et al. 2003)

#### 1.1.2.2 Mild or Low-Energy Trauma

Some authors, essentially in the U.S., advocate performing a CT for the triage of every trauma patient, to rule out cranio-cerebral, cervical, or thoraco-abdominal injury (Livingston et al. 1991; Tocino et al. 1984; Rhea et al. 1989; Shackford et al. 1992). The requirement for more cost-effective use of health care resources and the concern to avoid overuse of CT, with its significant inherent radiation exposure, raises the question as to whether all patients with mild or low-energy trauma (e.g., traffic accidents at a speed below 50 km/h) require a complete radiological investigation of the cervical spine, brain, chest, or abdomen. Proto-

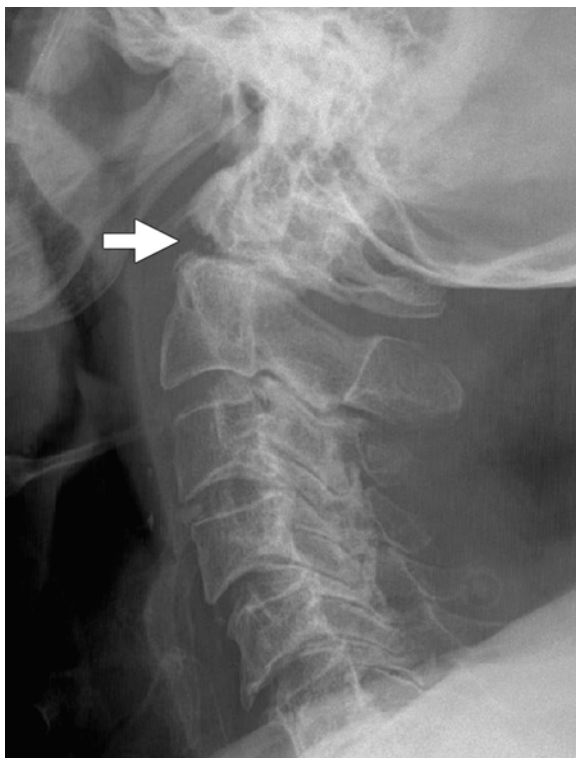


**Fig. 2.** Dens fracture. An 87-year-old patient was admitted after a fall. He complained of diffuse tenderness of the neck. Admission lateral cervical spine radiograph showed an interruption of the anterior aspect of C2 (arrow), with posterior displacement of the dens. The patient then underwent CT examination (not shown)

cols taking into consideration the patient's clinical presentation and the mechanism of injury for the decision to immediately perform CT or assess patient with conventional radiographs, sonography, and clinical observation, have been adopted by many emergency centers, including ours

### Brain

Skull radiographs are no longer systematically recommended in the assessment of head trauma. Indeed, some series reported that management or outcome is not significantly affected by skull film findings, because a skull fracture alone does not indicate a serious internal head injury (Masters 1980; Masters et al. 1987). Computed tomography is now widely recognized as the first choice imaging for the initial evaluation of patients with head injury. To limit controversy about the rational use of CT in patients with minor head injuries, a prospective trial was conducted in ten large Canadian hospitals, which led to the development of the Canadian CT Head Rule (Stiell et al. 2001). The Canadian CT Head Rule defines minor head injuries as witnessed loss of consciousness, definite amnesia, or witnessed disorientation in a patient with a GCS >13. Two levels of risks are identified among minor head injuries

Patients with any of these high-risk factors are at substantial risk for requiring neurosurgical intervention and CT should be performed:

1. GCS score <15 at 2 h after surgery
2. Suspected open or depressed skull fracture
3. Any sign of basal skull fracture (hemotympanum, "raccoon eyes," cerebrospinal fluid otorrhea/rhinorrhea, Battle's sign)
4. Vomiting, more than two episodes
5. Age >65 years

Factors for medium risk of brain injury, in which CT could detect clinically important lesions, but where no intervention is required, are:

1. Amnesia before impact >30 min
2. Dangerous mechanism (pedestrian struck by motor vehicle, occupant ejected from motor vehicle, fall from height >1 m or five stairs)

The high-risk factors were reported to be 100% sensitive for predicting need for neurological intervention and the medium-risk factors to be 98.4% sensitive for predicting important brain injury

The Canadian CT Head Rule is believed to be effective regardless of possible drug or alcohol intoxication, since no association was demonstrated, in the multicenter survey, between these criteria and the presence of an important brain injury; however, a correlation between intoxication and brain injury was reported in another study (Haydel et al. 2000), which suggested to include drug or alcohol intoxication in the criteria to perform CT in patients with minor head injury

### Cervical Spine

Two groups have proposed clinical prediction rules to determine which patients should undergo imaging of the cervical spine and which should not. The National Emergency X-Radiography Utilization Study (NEXUS) includes five criteria to rule out a cervical fracture without performing any imaging, with a sensitivity of 99.6% and a specificity of 12.9% (Hoffman et al. 1998, 2000; Mahadevan et al. 1998):

1. No posterior midline cervical spine tenderness
2. No evidence of intoxication
3. A normal level of alertness
4. No focal neurological deficit
5. No painful distracting injury

The more recent Canadian Cervical Spine Clinical Prediction Rule Study (CCSPRS; Stiell et al. 2001b) is based on the following items to rule out a cervical spine fracture:

1. Absence of three high-risk criteria (age >65 years, dangerous mechanism, paresthesias in extremities)
2. Five low-risk criteria (simple rear-end motor vehicle collision, sitting position in the emergency department,

ambulatory at any time since trauma, delayed onset of neck pain, absence of midline cervical-spine tenderness)

3. The ability of patients to rotate their neck of at least 45° bilaterally

A recent comparative survey reported CCSPRS criteria to be more sensitive and specific than NEXUS, and their use would have resulted in lower radiography rates (Stiell et al. 2003). When a cervical spine fracture cannot be ruled out by the above-mentioned criteria, imaging must be performed. The sensitivity of the three-view radiographs in identifying a cervical fracture has been reported to be in the range from 38 to 65% (Daffner 2001; Brown 2005; Schenarts et al. 2001), and their potential to miss significant or unstable injuries has been well established (Schenarts et al. 2001; Nunez et al. 1996; Griffen et al. 2003). Many recent studies have demonstrated that CT with coronal and sagittal reformations may replace conventional radiographs for the systematic evaluation of the cervical spine in blunt trauma, because of its higher sensitivity (close to 100%; Daffner 2001; Brown 2005; Barba et al. 2001) and cost-effectiveness (Daffner 2001; Blackmore et al. 1999; Blackmore 2003). Patients with focal neurological signs, evidence of cord or disc injury, and patients whose surgery require pre-operative cord assessment should be imaged by MR (Richards 2005). Although MR has been advocated to clear ligamentous injuries in trauma patients with persistent neck pain, a study reported that MR may not be performed after a normal cervical spine CT and in the absence of motor deficit (Schuster 2005). In most centers, emergency MR examinations in acute trauma victims are still difficult to obtain, for technical and practical logistical reasons

### Chest

If the need of performing chest CT after a high-energy trauma is well established, essentially for the assessment of an aortic injury or an occult pneumothorax in an unconscious patient (Rhea et al. 1989; Karaaslan 1995; Mirvis et al. 1998; Trupka 1997), there is no consensus with regard to the decision to perform CT after a mild or minor trauma. Despite the fact that CT is a highly sensitive imaging modality for the thorax, many authors reported that injuries detected by CT and not visible on chest radiograph are minor and not life-threatening (Rizzo 1995; Smejkal 1991; Poole et al. 1993; Pillgram-Larsen 1993); therefore, in the absence of another reason to perform CT in an alert patient the systematic use of CT after a mild chest trauma would not be cost-effective. In other series, CT detected more lesions than chest radiograph, which induced therapy changes in many patients, but had no impact on the improvement in clinical outcome (Guerrero-Lopez et al. 2000). Furthermore, a normal mediastinum by erect chest radiograph (no widening of the mediastinum and the

paraspinal lines, normal aortic contour, clear aorticopulmonary window, no mediastinal shift, no apical pleural cap sign, etc.) was reported to be sufficient per se to exclude a traumatic aortic injury (98% negative predictive value) without need of further assessment (Mirvis and Shanmuganathan 2003; Mirvis et al. 1998)

In our institution, we perform CT only in selected cases of minor chest trauma patients, when the clinical presentation and/or the chest radiograph are suggestive for a severe injury, when the patient cannot be properly clinically evaluated (intoxicated, unconscious), or when a spinal fracture is suspected (Brown et al. 2005; Wintermark et al. 2003; Sheridan et al. 2003). Computed tomography should also be considered in a trauma patient who has to sustain surgery with assisted ventilation, to rule out an occult pneumothorax which may evolve into a life-threatening tension pneumothorax (Sheridan et al. 2003; Strieter and Lynch 1988)

### Abdomen

Radiological management of patients admitted for a suspicion of a blunt abdominal trauma, and especially patient selection for an abdominal CT, is still the subject of controversy (McGahan et al. 1997; Yoshii et al. 1998; Bode 1999; Richards and Derlet 1998). Computed tomography is an excellent tool for abdominal trauma assessment (Brasel 1996), but its systematic use after minor trauma in a busy emergency center may lead to inappropriate delays in patient care, is costly, and requires radiation exposure to a young patient population. Some authors recommend the use of an initial sonographic examination to determine the need for abdominal CT: if abdominal sonography is normal, most of these authors observe a 12- to 24-h period of clinical abdominal observation before discharging a patient without performing a CT (Bode et al. 1999; Lingawi and Buckley 2000). If clinical observation cannot be undergone for organizational reasons (e.g., leak of medical care resources), the following combination of radiological and laboratory data are reported to be sufficient to exclude an intra-abdominal injury in an alert patient (GCS>13) with no tenderness or guarding at palpation:

1. Normal chest radiograph
2. No free intraperitoneal fluid at sonography
3. Normal hematocrit, normal white blood cell count, and normal serum glutamic oxaloacetic transaminase (sGOT)

About 12% of abdominal trauma patients fulfill these criteria (Poletti et al. 2004a). All other patients should undergo CT or clinical observation.



### 1.1.3 Sonography

Although CT is now universally considered the key imaging modality for the evaluation of severe, hemodynamically stable, trauma patients, the major role of sonography for the early demonstration of hemopericardium, hemothorax, or hemoperitoneum in the initial assessment of hemodynamically unstable patient is also widely recognized; however, there is still controversy about the rational use of either modality in hemodynamically stable patients who underwent mild or low-energy trauma. The emergency physician must be aware of the indications, drawbacks, and limitations of sonography and CT in the evaluation of trauma patients, to achieve a rational use of both modalities, according to the available resources, in a given medical environment. Sonography is widely accepted as an effective initial triage tool to evaluate trauma victims with suspected blunt abdominal injuries, because it can be performed rapidly in the admission area and because it is repeatable, noninvasive, nonirradiating, and inexpensive. The sensitivity of sonography for the detection of free intraperitoneal fluid is generally considered to be excellent, and there is general consensus that abdominal sonography is superior to diagnostic peritoneal lavage (DPL; Yoshii et al. 1998; Richards and Derlet 1998; Brasel et al. 1996; Lingawi and Buckley 2000; McKenney et al. 1994; Boulanger et al. 1995, 1996). In a victim of polytrauma who is hemodynamically unstable at admission, the presence of a major quantity of free intraperitoneal fluid on sonography warrants emergency laparotomy.

Patient-related drawbacks of sonography include a limited diagnostic access window and lack of cooperation. Even more important, however, is that sonography is operator dependent. In clinical practice, two main trends have recently emerged with regard to the utilization of sonography in the setting of blunt abdominal trauma in adults; one of these consists of regarding and using sonography as a rapid and reliable diagnostic test mainly for depiction of free fluid, performed by emergency medical staff with a relatively limited level of training in sonography, including non-radiologist physicians or surgeons. This method has been termed "focused assessment sonography for trauma" (FAST; Shackford 1993; Scalea et al. 1999; McGahan and Richards 1999). The FAST protocol includes real-time sonographic scanning of four regions, namely, the right upper quadrant with particular attention to the hepatorenal fossa (Morrison's pouch), the left upper quadrant (subphrenic space and splenorenal recess), the pelvis with special attention to the pouch of Douglas, and the pericardium. The rationale of limiting FAST to free fluid lies in the fact that it is difficult for most emergency physicians and surgeons to acquire and maintain the skills that are necessary to make a reliable assessment with sonography of the parenchymal abdominal organs with regard to the presence of injuries. Although the usefulness of FAST for clinical decision making has been discussed by many investigators, a direct com-

parison between studies is not simple since methodology varies so much among studies, particularly with regard to the reference standard. Consequently, the reported sensitivity of FAST for intraperitoneal free fluid varies between 63 and 96% (McGahan and Richards 1999; Forster et al. 1993).

Adequate training requirements for FAST are still subject to controversy, especially concerning the number of protocolized examinations necessary before an operator can be considered capable of performing and accurately interpreting this examination. Although some authors feel that at least 200 or more supervised examinations are necessary for credentialing in FAST (Scalea et al. 1999), others have proposed that "as few as ten examinations may be required for the clinician sonographer to become competent" (Shackford et al. 1999). Experience in a level-1 trauma center in North America does not substantiate the latter appreciation. In a prospective study, surgeons' ability for depicting free peritoneal fluid was evaluated in comparison with CT results. The standard for credentialing in FAST in this center was 6 h of theoretical and practical training, adequate performance on videotape test set, and 20 supervised patient examinations. Under these conditions of training, the sensitivity of FAST for depicting free fluid when compared with CT results was only 36%, with a specificity of 97% (P.A. Poletti et al., unpublished data). Similar observations were reported by other authors (Miller et al. 2003).

In a recent series on 1090 patients FAST was performed by senior radiologists, and the results were compared with a 12-h clinical follow-up. Under these conditions, FAST achieved a 94% sensitivity and 100% negative predictive value for major abdominal injuries; however, the prevalence of visceral injuries in this series was relatively low, and only 124 CT exams were performed, namely in the presence of positive or indeterminate FAST results and in 4 patients with clinical deterioration after a negative sonographic examination (Lingawi and Buckley 2000); thus, the results of this study may overestimate the sensitivity of sonography. Many studies have also stressed the limitation of FAST as an indirect method for depicting abdominal injuries without concurrent hemoperitoneum. Indeed, intra-abdominal visceral injuries without intraperitoneal free fluid have been described at CT in 23–34% of blunt trauma patients (Poletti et al. 2004b; Chiu 1997; Shanmuganathan et al. 1999); 12–17% of them ultimately needed surgery or embolization for management of organ injuries (Poletti et al. 2004b; Shanmuganathan et al. 1999); thus, the risk of missing abdominal visceral injuries seems inevitable if the diagnosis is based on the presence of intraperitoneal fluid alone.

In order to enhance the sensitivity of sonography for the detection of intraperitoneal injuries, some investigators, mainly from Europe and Asia, have advocated to perform, rather than FAST, a complete abdominal sonography study by a well-trained operator to depict both free fluid and parenchymal injuries (Yoshii et al. 1998; McGahan and Richards 1999; Röthlin et al. 1993). Injuries of solid organs, particularly the liver and spleen, consist of hyperechoic,

hypoechoic, or mixed (both hyper- and hypoechoic) lesions. The presence of free intraperitoneal gas suggests the presence of perforation of a hollow organ. Although the sensitivity of sonography to depict organ injuries was reported to be 88% or more, many series used an uneventful 12- or 48 h clinical follow-up as the reference standard for a true-negative sonography examination (Yoshii et al. 1998; Bode et al. 1999; McKenney et al. 1996). Since this cannot reliably imply absence of organ injury, the true sensitivity of sonography may have been overestimated. In a series of 260 blunt trauma victims examined with sonography by R othlin et al. (1993) CT was later performed in 25%. The reported sensitivity of sonography was 98% for intra-abdominal fluid and 41% for organ lesions (R othlin et al. 1993). Yoshii et al. (1998) obtained a higher than 90% sensitivity to directly image liver, spleen, and kidney injuries by sonography, and a 34% sensitivity to depict bowel injuries (by free air detection). In the Geneva University Hospital, we prospectively compared sonography findings of 205 patients admitted after a blunt abdominal trauma with CT results exclusively. In this series, sonography by the combined criteria of free fluid and organ-related changes, yielded an overall sensitivity of 72% to suggest an intra-abdominal injury. The sensitivity for direct organ analysis alone did not exceed 41% (Poletti et al. 2003). This sensitivity was improved to 76% by using a second-generation sonographic contrast media in optimal conditions (Poletti et al. 2004b). Despite this important improvement in sonography technology, the presence of some life-threatening visceral injuries among the 24% false-negative sonographies suggests that contrast-enhanced sonography cannot be recommended yet to replace CT in the triage of hemodynamically stable trauma patients; however, this method could be an interesting alternative to control CT for the depiction of delayed splenic pseudoaneurysms (Poletti et al. 2004b; Catalano et al. 2004)

In summary, abdominal sonography is useful in the context of blunt trauma and may even be considered indispensable for initial screening and for selecting hemodynamically unstable victims with severe hemoperitoneum for immediate abdominal surgery. Operator experience plays an important role with regard to the diagnostic yield; however, even in experienced hands, sonography appears not sufficiently reliable to rule out organ injuries

### 1.1.4. CT Scan

The increasing role of contrast-enhanced CT in the management of the acute trauma victim may be explained by its ability to examine all body regions during a single examination with consistent quality. Although CT uses ionizing radiation and requires injection of iodinated contrast material, these drawbacks of CT are far outweighed by its benefits. Computed tomography enables not only reliable

detection of small quantities of free fluid with sensitivity similar to that of sonography, but is superior to sonography with regard to injuries of the visceral organs. Compared with sonography, CT is also much less dependent on the operator, less limited by technical factors, and is therefore more reproducible. This is a major advantage with regard to image-based monitoring of conservative treatment

Recent developments in MDCT technology did not only allow an increase speed of image acquisition, reconstruction, and resolution, but also the ability to obtain multiplanar reconstructions and immediate on-line interpretation at the workstation

Although therapeutic decisions cannot be based on radiological findings alone, the information provided by CT at admission and during conservative treatment may greatly facilitate patient management (Guerrero-Lopez et al. 2000; Federle et al. 1998; Poletti et al. 2000; Linsenmaier et al. 2002; Davis et al. 1998; Livingston et al. 1998, 2000). Injury severity scores, such as the organ injury scaling system (OIS) of the American Association for the Surgery of Trauma, have been proposed to facilitate clinical research (Moore et al. 1989, 1990, 1995). Since a variety of criteria can be assessed on the basis of CT, radiologists involved in trauma care should be familiar with the principles of grading injuries to the different visceral organs

#### 1.1.4.1 CT Protocols

Some MDCT scanning protocols are recommended below. Although a standard MDCT protocol is important in the setting of trauma, the examination needs to be tailored to the patient's condition, taking into consideration the different body regions to be examined simultaneously, and meet the requirements for eventual multiplanar reconstruction (Linsenmaier et al. 2002). If the patient's condition permits, 250–500 ml of water-soluble oral contrast material (2–5%) are administered via the nasogastric tube in the emergency department and an additional 250 ml in the CT suite immediately before scanning. Additional administration of rectal contrast material is an option in patients with pelvic trauma or a suspected colon injury. Scanning parameters may vary according to different types of equipment, and most major centers did set up their own specific protocols. Up to recently, we used in our institution the following pre-programmed "classical" protocols on our 16-detector row CT system:

1. Head (sequential): collimation of 16×1.5 mm, thickness (reconstruction) 3 mm
2. Maxillo-facial region (spiral): collimation 16×0.75 mm, thickness 1.5 mm, increment 0.7 mm, pitch 0.663
3. Cervical spine (spiral): collimation 16×1.5 mm, thickness 2 mm, increment 1 mm, pitch 0.66. Then, the patient's arms are raised over head, to reduce artifact at chest and abdomen examination



**Fig. 3.** Traumatic dissection of the right vertebral artery. A 30-year-old patient was admitted after a motor vehicle accident with hyperextension of the head. **a** Admission contrast-enhanced axial CT of the neck did not show opacification of the right vertebral artery at the level of C6 (*arrow*) and above (not shown). **b** Coronal

3D MR angiography displayed a tapering of the vertebral artery, 2 cm from origin (*arrow*), with a complete occlusion of its distal segment, consistent with a dissection. The patient received anticoagulant medication

4. Thoraco-abdominal region (spiral): automatic triggering. Collimation of 16×1.5 mm, pitch 1.35, thickness 3 mm, increment 3 mm. The thoracic spiral, at the arterial phase, ends at the superior aspect of the liver. The abdominal acquisition (hepatic dome to the symphysis pubis) is triggered 60–70 s after the beginning of injection

Preliminary scanning before administration of intravenous contrast material is not recommended for thoracic and abdominal CT examination, as it increases the radiation dose significantly, without adding relevant information with regard to contrast-enhanced series alone. An automated uniphasic bolus injection of 130–180 ml of intravenous iodinated contrast material (60–75%) is given at 2–4 ml/s; nonionic contrast material is preferable to ionic contrast material as it reduces the risk of vomiting with subsequent aspiration. A standard scan delay of 70–90 s may be used, but a longer delay may be preferable in patients with significant arterial hypotension in order to avoid artifacts in the early parenchymal phase or to miss extravasation of contrast material

Some leading emergency radiologists now advocate the routine use of a total body scan in one sweep from the circle of Willis through pubis symphysis. A brain CT is initially performed without contrast media injection, then arms are raised to undergo the total body CT. Using 16 detectors of 0.75 mm (1.5 mm for large patients) at acquisition, a continuous bolus of intravenous contrast media is administered at relatively high flow rates: 90 ml at 6 ml/s followed by 60 ml at 4 ml/s, with an automatic triggering (90 HU threshold at the level of the aortic arch). Based on a 1-year follow-up evaluation, this protocol would not only reduce the total scan time, but may also allow depiction of an important percentage of blunt cervical vascular injuries, which are probably underestimated by using the conventional protocol (Fig. 3; S.E. Mirvis and K. Shanmuganathan, pers. commun., American Society of Emergency Radiology, Tucson 2005). This protocol has been recently successfully adopted in our institution, with the following modifications to avoid pressure overload in the antebraichial catheter and also prevent too early opacification of the intra-abdominal viscera:

- reduction of the contrast flow-rate from 6ml/sec to 4 ml/sec

- use of a highly concentrated non-ionic contrast agent (400 mg Iodine/ml), to maintain the iodine concentration high.
- contrast volume of 100 ml in patients up to 75 kg, 120 ml in larger patients.
- automatic triggering using a threshold of 100 UH instead of 90 within the aortic arch.

In our preliminary experience, up to 10 min scan time can be saved by using the new protocol when compared with the “classical” one.

Repeated, delayed scanning may be necessary for better demonstration of the distribution of extravasated contrast material from the blood vessels, parenchymal organs, gastrointestinal tract, or urinary system. All images should be viewed immediately by the radiologist at the workstation with appropriate window settings. Depending on the questions that need to be answered, additional acquisitions may then be performed and two- or three-dimensional reconstructions can be obtained, if necessary. In patients with pelvic fracture, a CT cystogram should be performed after completion of the i.v. series, to evaluate the bladder wall integrity (Vaccaro and Brody 2000; Morgan et al. 2000; Morey et al. 2001). Indeed, bladder rupture is encountered in 5–10% of patients with pelvic fracture and in 10% of patients with gross hematuria (Morgan et al. 2000; Morey et al. 2001). Bladder rupture cannot be excluded by simply clamping the Foley catheter, but the bladder must be drained at first and adequate retrograde bladder distension must be achieved by instilling at least 350 ml of a diluted hydrosoluble iodinated solution (i.e., 25 ml of Ultravist 150; Iopromidum 150 mg/ml, Schering, Baar, Switzerland) in 350 ml of a sa-line solution) through the Foley catheter. The pelvis is then rescanned from above the iliac crest to the symphysis pubis. The presence of contrast material in the extra- or intra-peritoneal space reveals a bladder rupture. A CT cystogram is contraindicated if patient should undergo immediate angiographic hemostatic procedure after CT, since spillage of intra- or retro-peritoneal contrast media may interfere with the depiction of an actively bleeding site

#### 1.1.4.2 CT Interpretation

The increasing use of MDCT in the acute trauma victim has not only improved the ability to detect visceral injuries and to identify active bleeding sources by means of contrast extravasation, but has also influenced the understanding of the spontaneous course of injuries that can be treated conservatively in the situation of hemodynamic stability

Besides the technical standard of the CT equipment, the design, logistics, and staffing of the radiology emergency unit plays an important role (Wintermark et al. 2002). Presently, the emerging standard for centers involved in trauma care is integration of modern MDCT scanners in the emergency admission area. The time required for image acquisition is thus becoming secondary as compared with

the time required for patient transfer, positioning, and installation of adequate monitoring during the examination; therefore, many authors advocate performing whole-body or “head-to-toe” spiral CT protocols, once the decision to undergo CT has been taken, based on the above-mentioned criteria (Low 1997; Leidner 1998; West 2004). Complete realization of a cerebral, cervical, thoracic, and abdominal MDCT survey averages 40 min, with the following distribution: 45% for transportation; 35% for CT data acquisition itself; and 20% for data management by the technologist, including two-dimensional coronal and sagittal reconstructions (Wintermark 2002). The acquisition speed and artifact suppression algorithms as implemented in MDCT scanners has greatly improved the overall diagnostic quality of images in the acute trauma victim (Gralla et al. 2005). The MDCT scanning is readily performed while continuing resuscitation, and since MDCT scanner has been implemented in the emergency admission area of the University Hospital of Geneva, even suspected acute intraabdominal hemorrhage is no longer considered by our surgical colleagues as a general contraindication for the use of CT in the work-up of polytrauma

Some diagnostic findings to be looked at during the initial CT interpretation and typical pitfalls are summarized below

#### Brain and Cervical Spine

The presence of intra and extra-cerebral blood has to be carefully assessed. It usually appears as a hyper-attenuating area, although hyperacute, ongoing, or sub-acute bleeding may appear isodense to adjacent parenchyma. Different window/level settings should be used, and indirect signs of bleeding (mass effect) must be carefully sought, to reduce the risk of overlooking a thin-convexity hematoma. In the presence of a subarachnoid hemorrhage, if an aneurysmal rupture is compatible with the circumstances of the trauma, an angio-CT should complete the examination (Fig. 4)

In severe polytrauma patients, the early detection of diffuse axonal injuries (DAI) is of paramount importance in the estimation of the patient’s long-term neurological prognosis. The DAI results from shear-stress neuronal injuries consecutive to rash acceleration and deceleration of brain parenchyma, essentially at the gray/white junction. The most severe shearing forces, with classical involvement of midline structures (parasagittal white matter, corpus callosum, and dorsolateral brain stem) results in a worse prognosis than lesions located in lobar white matter alone (Fig. 5; Zimmerman et al. 1978; Hammoud and Wasserman 2002). Unfortunately, CT is of limited value in detecting the small foci of hypoattenuation at the gray/white matter junction, suggestive of DAI (Hammoud and Wasserman 2002). In addition, acute hemorrhagic shear injuries are also difficult to identify, due to beam-hardening artifacts (at the level of the brain stem and the posterior fossa), and to the quick resolution of acute hemorrhagic shear injuries



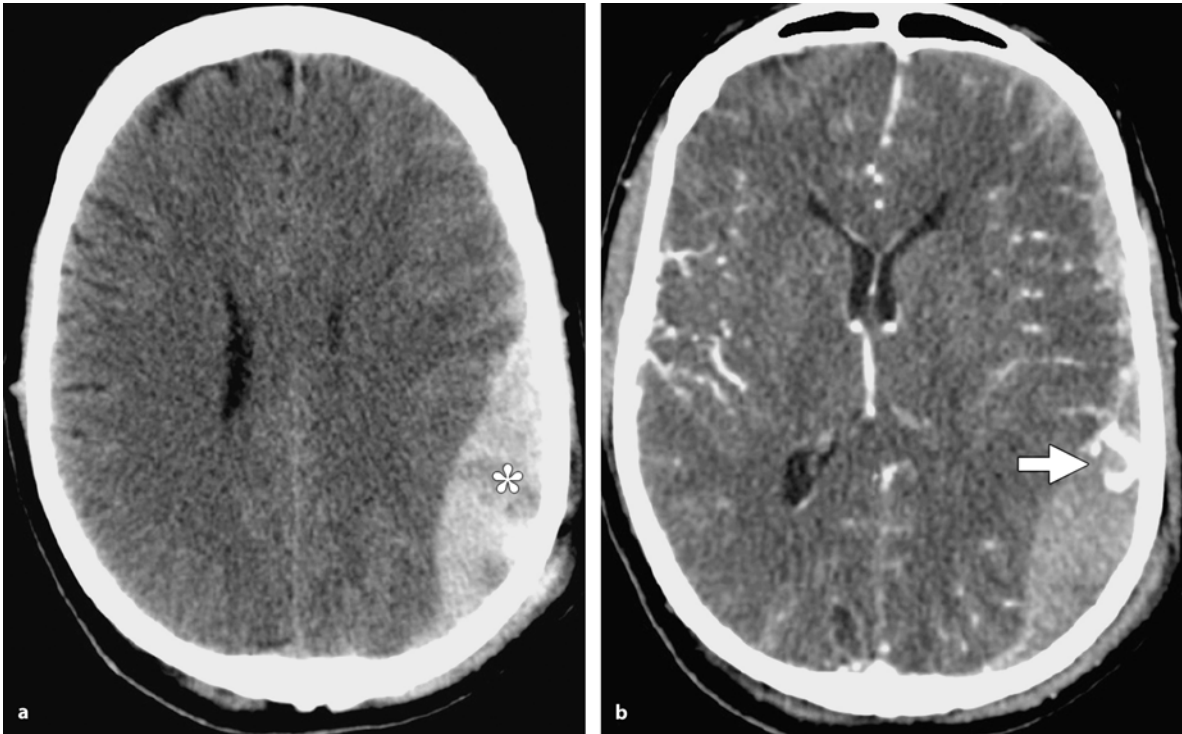


**Fig. 4.** Epidural hematoma. A 55-year-old patient was admitted after a loss of consciousness and fall. **a** Non-enhanced CT images display a biconvex high-density parietal hematoma (clotted blood), with area of hypoattenuation (unclotted blood) corresponding to recent bleeding (*asterisk*). An underlying skull fracture was visible on the bone window/level setting (not shown).

These features are characteristic of an epidural hematoma. **b** Contrast-enhanced angio-CT series were also obtained to rule out a ruptured aneurysm, suspected by the clinical history. A hyperdense blush of contrast was depicted within the epidural hematoma, corresponding to an active bleeding (*arrow*). The patient underwent immediate craniotomy



**Fig. 5.** Diffuse axonal injury. Admission axial brain CT in a patient who underwent a motor vehicle accident with sudden deceleration shows hyperdense lesion located in the splenium of corpus callosum (*arrow*), consistent with diffuse axonal injury

Facial bones must be examined on 1-mm axial sections, using a dedicated bone algorithm for reconstructions. The important limitation of routine CT images for the proper evaluation of bone fractures has been demonstrated (Holland and Brant-Zawadzki 1984)

When screening the cervical spine, special attention should be paid to the inter-vertebral and inter-articular joint evaluation. Indeed, up to 46% of dislocations and subluxations can be overlooked in a succinct analysis, if axial images are only considered (Woodring and Lee 1992). Similarly, axial images are not sufficient to rule out horizontal fractures, especially at the cranio-cervical junction (Van Goethem et al. 2005). The MPR reformatting views, rapidly obtained in various plans from helical CT data, are therefore mandatory for a correct assessment of the cervical spine in a trauma patient (Fig. 6)

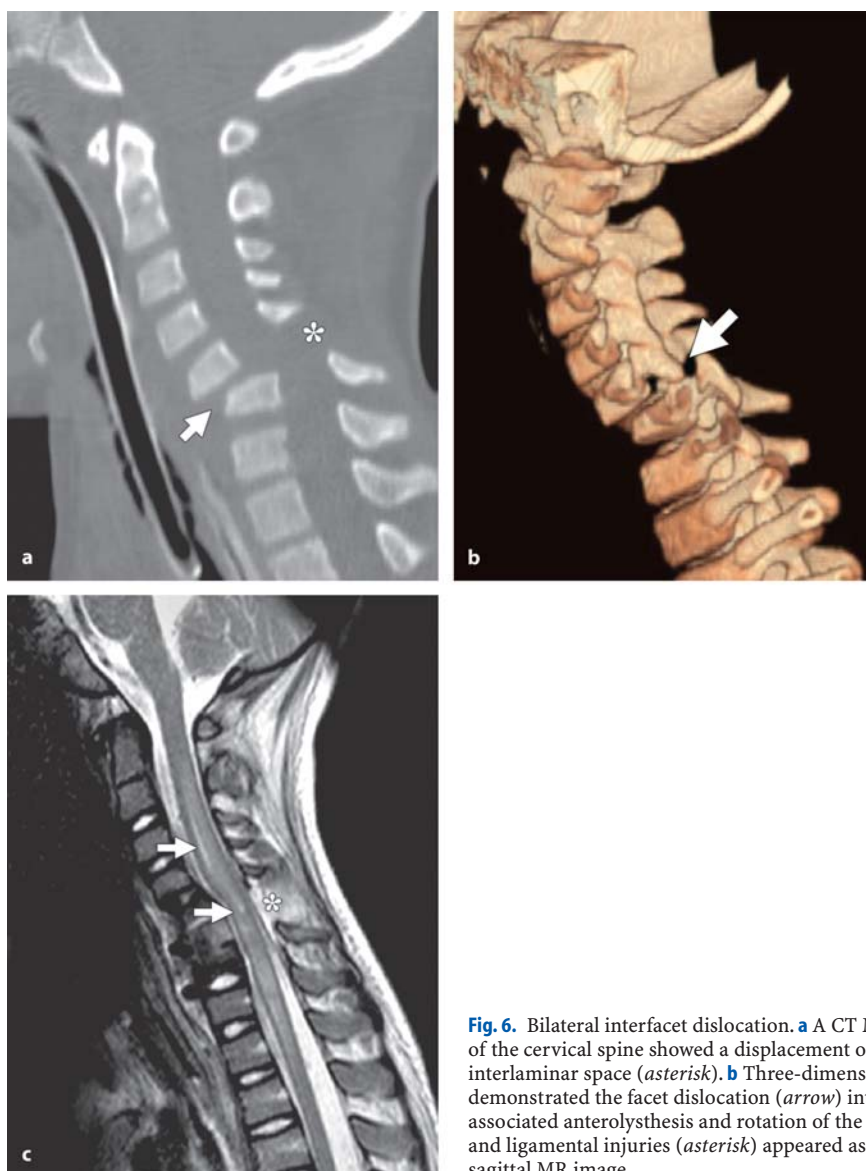


**Fig. 6.** Bilateral interfacet dislocation. **a** A CT MPR midsagittal reconstruction of the cervical spine showed a displacement of C5 on C6 (*arrow*) and widened interlaminar space (*asterisk*). **b** Three-dimensional CT reconstruction clearly demonstrated the facet dislocation (*arrow*) into the neural foramen and the associated anterolysthesis and rotation of the vertebra. **c** Cord contusions (*arrows*) and ligamentous injuries (*asterisk*) appeared as hyperintense area on T2-weighted sagittal MR image

### Chest

The diagnosis of aortic injuries can be challenging for the emergency radiologist on call (Fig. 7). It has been reported that, in the absence of proper diagnosis and treatment, about 32–50% of patients initially surviving aortic injury die within 24 h after trauma and 74% within 2 weeks (Mirvis et al. 1998; Frick et al. 1997; Williams et al. 1994; Symbas et al. 1998). Despite the fact that spiral CT was reported to be almost 100% sensitive and specific for the identification of blunt traumatic aortic injuries (Mirvis and Shanmuganathan 2003; Mirvis et al. 1998; Wintermark et al. 2002), the radiologist should be aware that injuries occurring in atypical locations, such as

the ascending aorta or the aortic arch (in close proximity to aortic branches), may be confusing on axial CT images (Mirvis and Shanmuganathan 2003; Mirvis et al. 1998). In addition, anatomic variants, such as the ductus diverticulum or a diverticular origin of the bronchial artery, may mimic aortic injury in the presence of adjacent mediastinal blood (Mirvis and Shanmuganathan 2003; Mirvis et al. 1998). Conversely, an aortic injury can be excluded in the absence of mediastinal blood, or if a mediastinal hemorrhage can be explained by a vertebral or sternal fracture (in the absence of vascular injury; Mirvis and Shanmuganathan 2003; Mirvis et al. 1998)

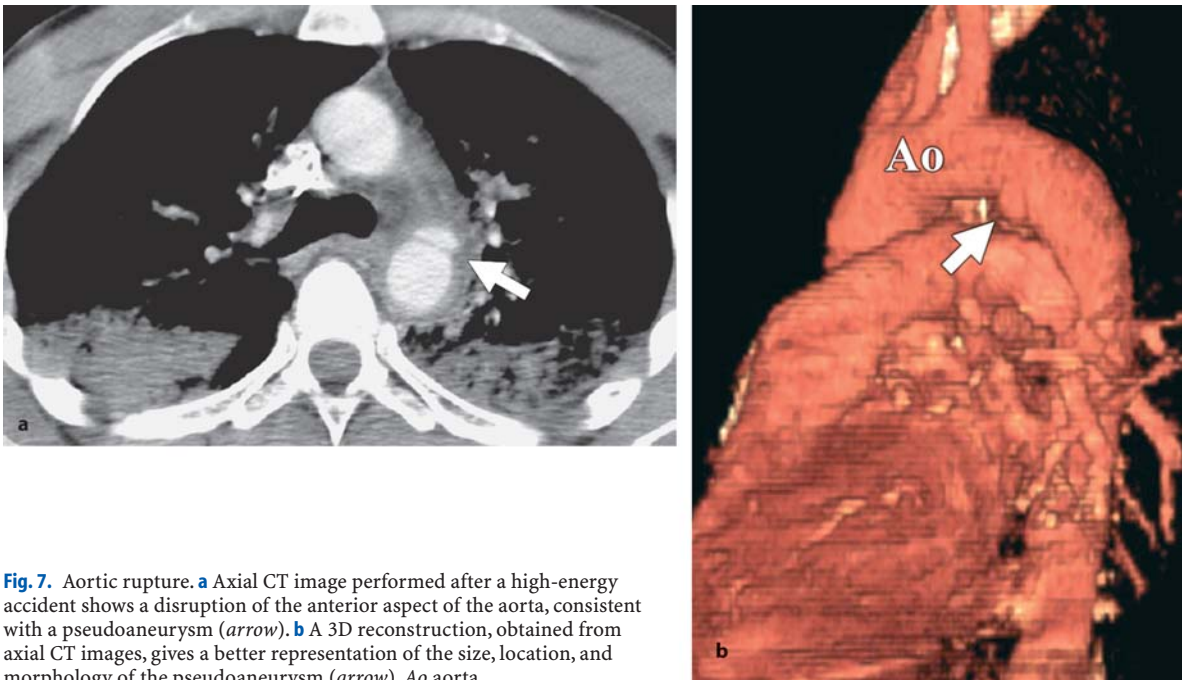


**Fig. 7.** Aortic rupture. **a** Axial CT image performed after a high-energy accident shows a disruption of the anterior aspect of the aorta, consistent with a pseudoaneurysm (arrow). **b** A 3D reconstruction, obtained from axial CT images, gives a better representation of the size, location, and morphology of the pseudoaneurysm (arrow). Ao aorta

### Spleen and Liver

The spleen is the most frequently injured abdominal organ in the context of blunt trauma. The spleen has been involved in one-third of all patients with proven blunt abdominal injury seen at the Geneva University Hospital over the past 2 years. Although there is an increasing trend toward conservative management of splenic injuries in adults, caution is required because secondary hemorrhage, e.g., delayed splenic rupture may lead to failure of nonsurgical treatment in 10–31% of cases (Shackford and Molin 1990; Cogbill et al. 1989; Feliciano et al. 1992). CT scanning with power injection of contrast media has been shown to be up to 98% accurate for detecting blunt splenic injuries (Brasel et al. 1998). Typical diagnostic findings observed on CT include, besides hemoperitoneum, capsular disruption, perisplenic, intrasplenic, and subcapsular hematoma, active contrast extravasation and intrasplenic pseudoaneurysm (Moore et al. 1995; Buntain et al. 1988; Resciniti et al. 1988; Mirvis et al. 1989a). Care must be taken to avoid image acquisition in a too early phase since the inhomogeneous parenchymal pattern is difficult to interpret. Perfusion defects do not always reflect a vascular injury but may also be due to contusion or correspond to reversible local reactive hypoperfusion in the hypotensive state

One of the most important challenges in imaging splenic trauma is to help determine which patients can be safely managed conservatively and which patients need surgery. Because the surgical injury scale for splenic trauma (Moore et al. 1995) includes several criteria that cannot

be evaluated with CT, various CT-based grading systems for splenic injury therapy have been proposed. Although initial reports regarding the ability of such grading systems to predict the need for surgery were optimistic (Moore et al. 1995; Resciniti et al. 1988; Mirvis et al. 1989a), subsequent studies have not substantiate their value in predicting the outcome of nonoperative management (Brasel et al. 1998; Becker et al. 1994; Kohn et al. 1994); therefore, the use of CT-based grading systems described to date does not seem to be warranted for clinical decision making

Recently, increased attention has been given to the presence of posttraumatic vascular abnormalities within the splenic parenchyma (Federle et al. 1998; Davis et al. 1998; Hagiwara et al. 1996; Gavant et al. 1997; Shanmuganathan et al. 2000a). The CT evidence of a focal intrasplenic or perisplenic collection with an attenuation similar to that of the aorta or a major adjacent artery and greater than that of the spleen has been termed “intrasplenic contrast blush” or “intrasplenic pseudoaneurysm” and has been reported to be a highly predictive sign for failure of nonoperative management (Fig. 8). Gavant et al. (1997) reported that the contrast blush sign was visible on CT in 82% of trauma victims with failed attempts at nonoperative management for splenic blunt injuries, whereas only 13% of the patients in whom nonoperative management was successful had any sign of vascular abnormality of the spleen. Federle et al. (1998) reported the presence of active contrast extravasation with CT in 43% of victims who required surgical intervention and its absence in 86% who required no intervention; therefore, some investigators, including ourselves,





**Fig. 8.** Vascular injury of the spleen. A 42-year-old man was admitted after a fall. **a** Admission abdominal sonography (not shown) was normal, without evidence of intra-peritoneal fluid. An extended splenic injury was depicted at CT, as multiple hypodense areas (*asterisks*) within the normally enhancing parenchyma. A focal blush of contrast media, consistent with a vascular injury, is depicted in the periphery of the spleen (*arrow*). **b** A pseudoaneurysm was demonstrated at angiography (*arrow*) and successfully embolized. **c** The pseudoaneurysm is no longer visible at control angiography

have begun to use the CT sign of contrast blush as an indication for angiographic embolization (Davis et al. 1998; Shanmuganathan et al. 2000a), whereas others believe that further data are needed to confirm the usefulness of this sign for guidance of treatment (Omert et al. 2001). Depiction of a contrast blush in a traumatized spleen is recognized in most emergency centers as an indication for angiographic embolization (Richards 2005; Schuster et al. 2005), although some controversy still persists (Karaaslan et al. 1995). Mirvis and Shanmuganathan (2003) recently proposed a new CT-based grading system for splenic trauma, adapted from the AAST surgical classification system, that takes into account the major vascular findings, in addition to the extent of anatomic disruption of the parenchyma. According to this classification, splenic arteriography and embolization are indicated, as an alternative to surgery, in the presence of active intraparenchymal and sub-capsular bleeding, splenic vascular injuries (pseudoaneurysms or arterio-venous fistulae), and shattered spleen (fragmentation into three or more sections)

The most common direct CT signs of blunt liver injury include capsular tear (disruption), intraparenchymal lac-

eration or fracture, and subcapsular or intraparenchymal hematoma. Signs of vascular injuries include, besides active contrast extravasation and periportal tracking of blood, partial devascularization due to vascular injury. Several attempts have been made to grade liver injury by means of CT in order to help guide clinical management. Although these classifications are useful for clinical research, they have not been found useful for guiding clinical management, since even high-grade injuries with involvement of three or more segments may often respond favorably to conservative treatment (Becker et al. 1998)

Intrahepatic vascular injuries have been reported more frequently in association with injuries of higher CT grades than those with lower CT grades (Sugimoto et al. 1994; Fang et al. 1998). Vascular injuries have been analyzed in the context of blunt liver trauma (Poletti et al. 2000). Extension of hepatic injury into the main trunk of one or more hepatic veins occurred in 91% of patients in whom non-surgical management failed, but in only 41% of patients in whom nonsurgical management was successful (Fig. 9). All CT studies that were false negative for active arterial bleeding were cases of extensive injury involving two segments or more had at least one major hepatic vein involved by the

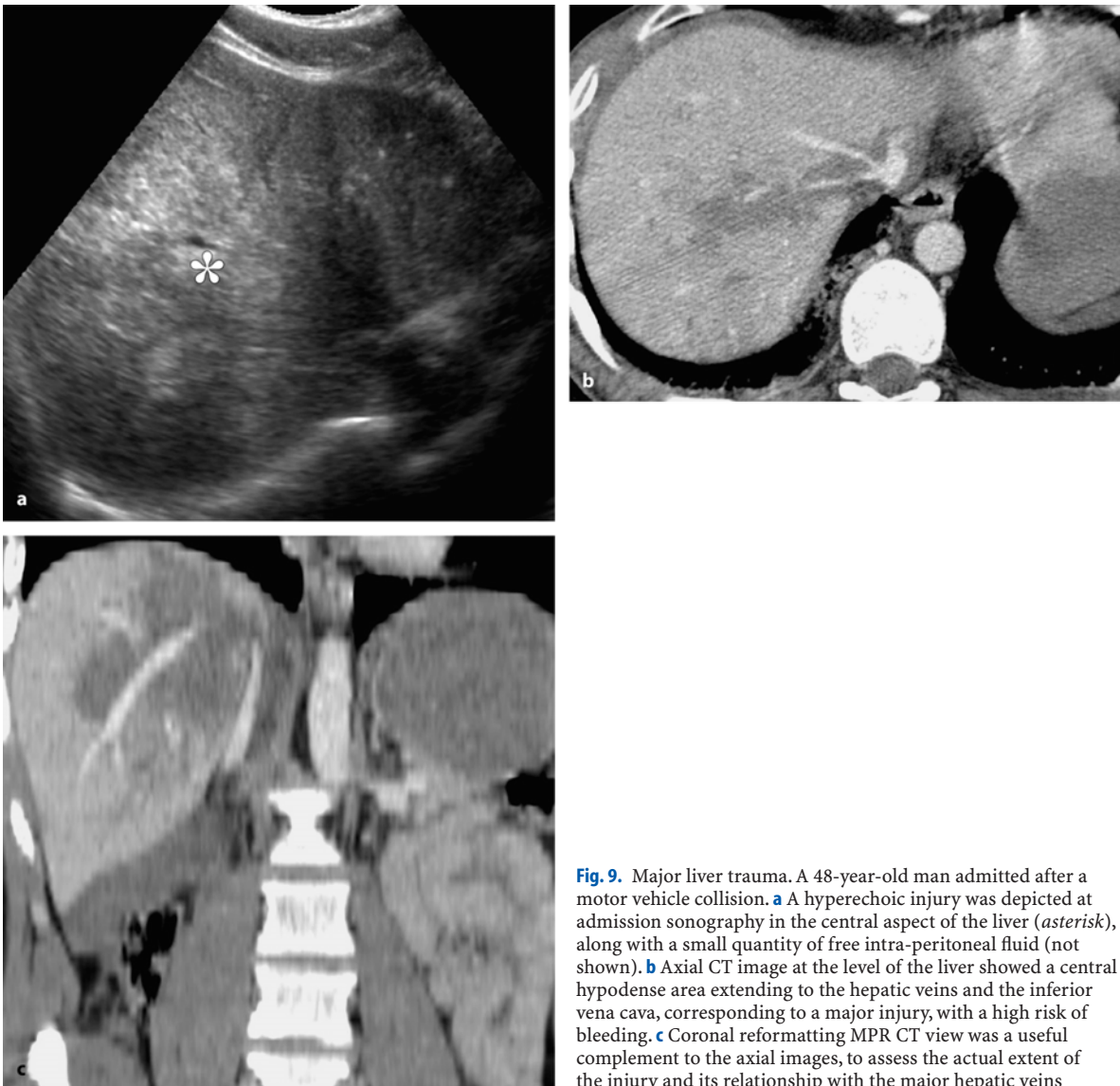


**Fig. 9.** Major liver trauma. A 48-year-old man admitted after a motor vehicle collision. **a** A hyperechoic injury was depicted at admission sonography in the central aspect of the liver (*asterisk*), along with a small quantity of free intra-peritoneal fluid (not shown). **b** Axial CT image at the level of the liver showed a central hypodense area extending to the hepatic veins and the inferior vena cava, corresponding to a major injury, with a high risk of bleeding. **c** Coronal reformating MPR CT view was a useful complement to the axial images, to assess the actual extent of the injury and its relationship with the major hepatic veins

injury. Conversely, the absence of both pooling of contrast and major hepatic venous involvement was considered to be the most reliable CT evidence to exclude active hepatic bleeding at angiography or surgery, with a sensitivity of 100% (25 of 25 cases). Further research is necessary to develop a prognostic CT-based liver trauma classification, which should probably take into consideration the presence of vascular injuries along with their localization

#### **Gastrointestinal, Pancreatic, and Diaphragmatic Injuries**

Traumatic bowel lesions include contusion, hematoma, partial or full laceration of the bowel circumference, and bowel transection. Injuries of the mesentery may affect the vascular structures and thus lead to either bleeding or

vascular occlusion with subsequent necrosis and eventual perforation of the corresponding bowel structures

The CT signs of injury to the gastrointestinal tract are often subtle. Of high clinical importance, a first group of signs indicates full-thickness bowel perforation and, consequently, immediate surgical exploration; these include visible discontinuity of the gastrointestinal wall and leakage of enteric contrast material or luminal contents into the peritoneal cavity or retroperitoneum, or extravasation of vascular contrast material. Although free extraluminal, extra- or intraperitoneal air adjacent to the anterior abdominal wall or bowel loops may be a valuable indirect sign of bowel perforation, this may also result from other causes, e.g., dissection of interstitial air in the presence of pneumothorax or after chest tube placement, or after peri-

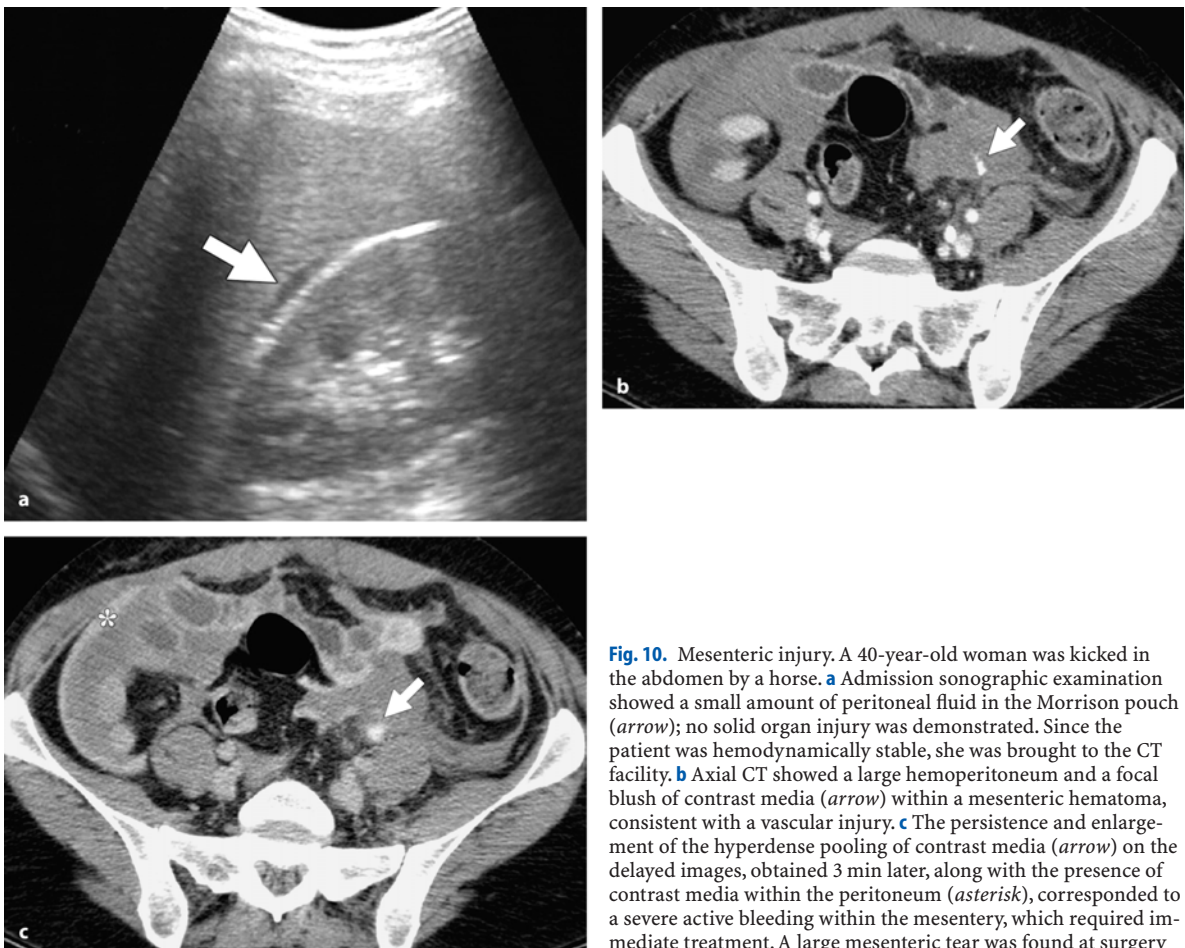


**Fig. 10.** Mesenteric injury. A 40-year-old woman was kicked in the abdomen by a horse. **a** Admission sonographic examination showed a small amount of peritoneal fluid in the Morrison pouch (arrow); no solid organ injury was demonstrated. Since the patient was hemodynamically stable, she was brought to the CT facility. **b** Axial CT showed a large hemoperitoneum and a focal blush of contrast media (arrow) within a mesenteric hematoma, consistent with a vascular injury. **c** The persistence and enlargement of the hyperdense pooling of contrast media (arrow) on the delayed images, obtained 3 min later, along with the presence of contrast media within the peritoneum (asterisk), corresponded to a severe active bleeding within the mesentery, which required immediate treatment. A large mesenteric tear was found at surgery

toneal lavage (Hamilton et al. 1995). The quantities of free air are often very small and require image viewing with wide window settings. A second group of ancillary CT signs include focal thickening of the bowel wall of the small bowel wall (>3 cm) intramesenteric fluid or hematoma, or a “streaky” appearance of the mesenteric fat due to inhomogeneous infiltration (Hagiwara et al. 1995; Dowe 1997)

The combination of all of the above-described diagnostic signs at CT yielded a sensitivity of 85–95% for the detection of injuries of the gastrointestinal tract (Becker et al. 1998b). The study design needs to be considered when interpreting the results. In a recent retrospective analysis of 230 patients, CT achieved a 94 and 99% sensitivity in detecting bowel and mesenteric injuries, respectively (Killeen et al. 2001), whereas in a prospective study the reported sensitivity and specificity were 64 and 97%, respectively (Butela et al. 2001). The ability of CT to predict the need for exploratory laparotomy was retrospectively analyzed by classifying bowel injuries as surgical in the presence of a moderate to large amount of free fluid without evidence of solid organ injury or in the presence of extraluminal air or oral contrast material, and as

nonsurgical in the absence of these signs. The need for surgery was predictable with a sensitivity of 92% and a specificity of 94% (Killeen et al. 2001). Mesenteric injuries were considered surgical in the presence of an active extravasation of contrast within the mesentery, or when a bowel wall thickening was associated with mesenteric hematoma (Fig. 10). Focal mesenteric hematoma or mesenteric infiltration was considered nonsurgical. Although CT enabled detection of mesenteric injuries with high accuracy (96%), the ability to distinguish surgical from nonsurgical mesenteric injuries was poor (sensitivity 37%, specificity 96%)

Depiction of a pancreatic traumatic injury may be challenging on the admission CT; it has been considered the most common cause of diagnostic errors of interpretation of CT studies of blunt trauma patient (Cook et al. 1986). The diagnosis of pancreatic transection may also be difficult to recognize on CT (Mirvis and Shanmuganathan 2003). Pancreatic injuries may appear as low-attenuation area with focal or diffuse enlargement of the gland (contusions) or as linear irregular hypodensities (Fig. 11). Thickening of the anterior pararenal fascia was reported the most commonly





**Fig. 11.** Duodenal, pancreatic and renal injuries. A 22-year-old woman was involved in a motor vehicle collision. An hemoperitoneum was depicted at admission sonography. Since the patient was hemodynamically stable, she underwent an abdominal CT, which showed a discontinuity (rupture) of the anterior aspect of the duodenal wall (*arrow*), a transection of the pancreatic body (*arrowhead*), and a devascularized left kidney (*asterisk*). These findings were confirmed at surgery

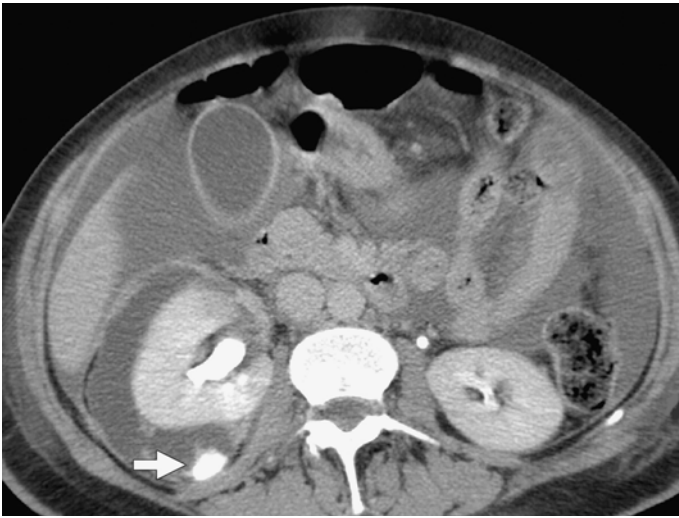


**Fig. 12.** Post-traumatic urinoma. A CT scan performed 1 week after an abdominal trauma with right kidney laceration. This delayed phase, obtained 3 min after injection of contrast media, shows opacified urine (*arrow*) filling the perirenal fluid collection, corresponding to a urinoma

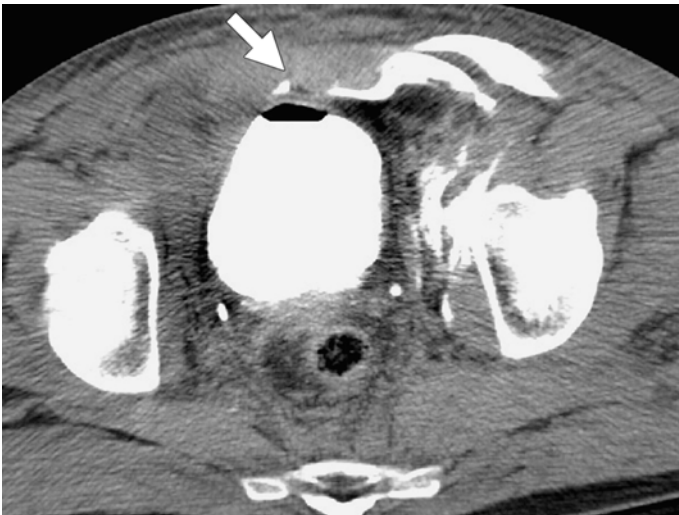


**Fig. 13.** Bladder rupture. Patient admitted after a motor vehicle collision. A pelvic fracture was depicted on standard radiograph and CT images (not shown). A retrograde CT cystography shows an anterior contrast leak into the prevesical space and into the anterior abdominal wall. (*arrow*), demonstrating an extra-peritoneal bladder rupture

observed finding associated with pancreatic injury (Jeffrey et al. 1983). The integrity of the main pancreatic duct must be assessed by ERCP, since stricture or disruption of the main pancreatic duct may be cause of delayed complications, months to years after initial injury (Carr et al. 1989)

Early diagnosis of diaphragmatic rupture is essential in order to avoid complications due to intrathoracic herniation or even strangulation of gastrointestinal organs (see Fig. 1). When using routine axial sections rupture of the diaphragmatic dome, which usually occurs on the left side, may be missed in one-third of cases unless 2D sagittal or coronal reformatting is used (Tocino et al. 1984; Rhea et al. 1989). The demonstration of a waist-like constriction across the air containing structures, “the collar sign” (Shanmuganathan et al. 2000b; Killeen et al. 1999), the most common CT finding of diaphragmatic rupture, is considered pathognomonic of the diagnosis (Mirvis and Shanmuganathan 2003)

### Kidney and Urinary Bladder

Approximately 75–85% of renal injuries may be considered minor (grade I or II according to the AAST classification system; Santucci et al. 2001) and heal spontaneously (Mirvis and Shanmuganathan 2003; Thomason et al. 1989). Common CT findings include lesions such as contusions (seen as ill defined perfusion defects), superficial lacerations, segmental renal ischemic infarcts (seen as segmental perfusion defects), and subcapsular or perirenal hematoma. Major renal injuries (grades III–V) must be rapidly identified, since they may require angiography or surgery. They consist in deep renal lacerations, in lacerations extending into the collecting system with contained urine leak, in renal vascular pedicle injuries and in devascularized kidney (Santucci et al. 2001). Multiplanar and 3D reconstructions are highly recommended for optimal display of the relationship of the parenchyma, the hilar vessels, and the proximal collecting system, or to display the extent of arterial injury. Delayed helical acquisition provides valuable additional information regarding the renal collecting system, the ureters, the urinary bladder (intra or retroperitoneal rupture), and may also help distinguish between contrast extravasation from the renal pelvis (posttraumatic urinoma) and active hemorrhage (Figs. 12, 13)

## 1.1.5 Follow-up Imaging during Conservative Treatment

Once the initial radiological evaluation of the trauma patients has been completed, follow-up imaging can still play an important role in monitoring of conservative treatment and detection of early or delayed complications. We discuss here the most common situations in which follow-up imaging is recommended after trauma

### 1.1.5.1 Brain and Cervical Spine Injuries

Patients with head injury may occasionally develop a delayed hematoma in an area without obvious injury depicted at initial CT (Bruce 2000). In 199 patients with severe head injury, Lipper et al. (1979) reported ten (8.4%) delayed intra-cerebral hematoma and nine (7.6%) delayed extracerebral hematoma. In a survey by Lobato et al. (1997) of 587 patients with severe head injuries who underwent a control CT, 23.6% developed new diffuse brain swelling, and 20.9% a new focal mass lesion, not previously seen on admission CT. In the same series, 51.2% of patients developed significant CT changes (improvement or impairment) and their final outcomes were more closely related to the control than to the initial CT. Most delayed hematomas occur within 2–4 days of injury and are associated with poor outcome (Lipper et al. 1979; Lobato et al. 1997). As mentioned above, acute hematoma in patients with coagulopathy, or ongoing bleeding, may appear isoattenuating with brain parenchyma (Wilms et al. 1992; Greenberg et al. 1995) and may therefore be overlooked at initial CT. Follow-up CT or MR will reveal such hematoma, since the attenuation of an acute clot will increase over time. For these reasons, some authors recommend to systematically repeat CT to identify worsening of traumatic head injuries (Servadei et al. 1995), whereas others advocate a more selective use of CT, as an adjunct to neurological evaluation (Brown et al. 2004; Chao et al. 2001)

Further MR imaging is recommended when benign CT findings are unable to explain an impaired neurological status (Parizel et al. 1998, 2005; Paterakis 2000). Recent series reported that diffusion imaging should be added to conventional MR sequences, to reveal additional shearing injuries (Rugg-Gunn et al. 2001; Lin et al. 2001; Ducreux et al. 2005)

Magnetic resonance may also be used as a complement to CT to precisely evaluate the extent of post-traumatic ischemia and infarction in patients with brain edema or herniation (Server et al. 2001)

After a cervical spine injury, MR should be performed in patients with neurological deficit, to assess the extent and type of cord (and/or discal) injury, to detect ligament sprains or tears, and to evaluate flow in the major cervical vessels (see Figs. 3, 4)

### Chest Injuries

Due to its large availability, conventional chest radiograph is the first-line imaging modality in the follow-up of chest trauma patients. Images are generally performed in supine or semi-erect position, because the general condition of the multi trauma patients usually precludes obtaining a true erect position. In the same patient, the quality of consecutive bedside radiographs is subject to great technical variability, due to the patient's different positions, when compared with consecutive images in erect position. Then,



differentiating between technical factors, variations and true alterations in the cardiopulmonary status is often a difficult challenge for the radiologist and the ICU physician (Ovenfors and Hedgcock 1978). Many series have reported the limitation of conventional radiographs in identifying intra-thoracic abnormalities in critically ill patients (Voggenreiter et al. 2000; Mirvis et al. 1987; Tocino et al. 1985; Wagner and Jamieson 1989). The advent of MDCT technology, essentially the reduction of motion artifacts in patients unable to breath-hold, has conferred to this imaging method a crucial complementary role to conventional radiology in the follow-up of the chest trauma patients (Ovenfors and Hedgcock 1978; Voggenreiter et al. 2000; Tocino et al. 1985). Comparative evaluations of chest radiograph with CT findings in critically ill trauma patients revealed that only 25–40% of hemo/pneumothoraces and pulmonary contusions are detected by chest radiograph (Trupka et al. 1997; Voggenreiter et al. 2000; McGonigal et al. 1990; Toombs et al. 1981). Consequently, some authors advocate the liberal use of chest sonography in the ICU, arguing a significant influence on treatment planning in up to 41% of patients, when CT is not available or cannot be performed (Yu et al. 1992). The limitation of chest radiograph was also reported in the detection of abnormality smaller than 8×5×4 cm (abscesses or empyema; Voggenreiter et al. 2000). Computed tomography was found to add significantly more diagnostic information in up to 70% critically ill patients than was available from the corresponding bedside radiographs (Mirvis et al. 1987); however, there is no consensual algorithm yet relevant to the indications for CT in the follow-up of chest trauma patients (McGonigal et al. 1990; Navarrete-Navarro et al. 1996). In a prospective assessment of the efficiency of chest CT in 39 trauma patients, Voggenreiter et al. (2000) adopted well-defined clinical criteria to perform secondary chest CT. Under these conditions of use, significant information that influenced therapeutic management was obtained in 66% of patients with deterioration of gas exchanges, in 61% of patients with sepsis, and in 40% of patients to guide the duration of intermittent prone positioning

### Abdominal Injuries

It is noteworthy that splenic artery pseudoaneurysms are not necessarily apparent on the CT scans obtained at admission, but only on subsequent imaging after 1–3 days, thus underlining the usefulness of CT-based follow-up CT in patients who undergo nonoperative management of a blunt splenic injury (Voggenreiter et al. 2000); therefore, some authors recommend to perform a routine follow-up CT on patients with splenic injury, within 48–72 h post-admission (Mirvis and Shanmuganathan 2003; Davis et al. 1998; Federle 1989)

As mentioned above, some preliminary data suggest that contrast-enhanced sonography could play a role for the delayed assessment of splenic vascular abnormalities,

when CT is unavailable or not easily feasible, due to the impaired general conditions of the patients (Poletti et al. 2004b); however, these observations (based on a small number of patients) need to be validated by further prospective studies

Diagnostic arteriography cannot be recommended as a routine procedure in patients with blunt hepatic trauma. It should be performed in the presence of visible contrast extravasation on CT even in a hemodynamically stable patient, because there is a risk that conservative management may fail unless transcatheter embolization or surgery is performed (Yoshii et al. 1998; Bode et al. 1999). Arteriography also seems warranted in hemodynamically stable patients with major blunt liver injuries along with major hepatic venous involvement (Poletti et al. 2000)

Although delayed hepatic rupture is uncommon, delayed complications of blunt liver injuries include formation of a biloma due to injury of a major bile duct or the gallbladder, formation of a posttraumatic pseudoaneurysm, or abscess in the context of major tissue devascularization or large hematoma are important issues (Poletti et al. 2000; Becker et al. 1998a,b; Mirvis et al. 1989b)

In patients undergoing conservative treatment of renal injuries, follow-up with CT may be recommended under certain conditions; these include large retroperitoneal hematomas, large urinoma, major devascularized or “shattered” segments, and transarterial embolization treatment of vascular lesions such as pseudoaneurysm or arterio-venous fistula (Regel et al. 1995). Follow-up is also indicated whenever there is a suspicion of a pre-existing cystic or solid renal mass. Other authors reported that performing a systematic control CT in every patient with grade-III or higher renal lesion 2–4 days after trauma would detect more than 90% of delayed urological complications and may be cost-effective (Blankenship et al. 2001)

Monitoring of conservatively treated trauma victims by means of repeat CT studies enables early detection of a variety of other delayed complications of trauma, e.g., bowel devascularization, pseudoaneurysm or arterio-venous fistula, pancreatic pseudocysts, abscess, etc.; however, except for vascular injuries, there is no universally accepted criteria for performing follow-up imaging in abdominal trauma patients. Indications for radiological investigations should therefore be tailored to the clinical and biological parameters

---

#### 1.1.5.2 MR in Non-neurological Trauma Situations

Very few reports have investigated the role of MR imaging (MRI) in the work-up of hemodynamically stable trauma patients, in non-neurological indications. Indeed, beside its limited availability in most emergency centers, MRI is difficult to use in uncooperative patients and in the presence of metallic components such as skin ECG electrodes and life-support equipment. Some authors reported the use of



**Fig. 14.** Post-traumatic bile leak. A 24-year-old patient was involved in a motor vehicle collision. **a** Admission CT shows a grade-4 liver injury (*asterisk*) and intra-peritoneal fluid (*arrows*), without active bleeding. The patient underwent non-operative management. Due to a progressive increase of intra-peritoneal fluid content, he underwent an MR cholangiography examination

3 days after admission. **b** An MR cholangiography with intravenous injection of mangfodipir trisodium (Teslascan), a bilio-specific contrast agent, showed a central bile duct injury (*arrow*), with active extravasation of contrast agent along the right inferior aspect of the liver (*arrowheads*). These findings were important to determine the most appropriate therapeutic procedure

MRI as a complement to non-enhanced CT in patients with a major contra-indication of injection of iodinated contrast agent (Hedrick et al. 2005) or to evaluate the integrity of the diaphragm (Shanmuganathan et al. 1996), the pancreatic ducts (Fulcher and Turner 1999), or the biliary tree (Fig. 14; Pilleul et al. 2004). Unfortunately, these reports remain anecdotal, and the use of MR is not yet integrated in the current diagnostic management of trauma patients, except for neurological indications (mentioned previously); however, this situation may change in the future, as access to MR becomes facilitated

## References

- Barba CA, Taggart J, Morgan AS, et al. A new cervical spine clearance protocol using computed tomography. *J Trauma* 2001;51:652–657
- Becker CD, Spring P, Glatli A, Schweizer W. Blunt splenic trauma in adults: Can CT findings be used to determine the need for surgery? *Am J Roentgenol* 1994;162:343–347
- Becker CD, Mentha G, Terrier F. Blunt abdominal trauma in adults: role of CT in the diagnosis and management of visceral injuries. Part 1: liver and spleen. *Eur Radiol* 1998a;8:553–562
- Becker CD, Mentha G, Schmidlin F, Terrier F. Blunt abdominal trauma in adults: role of CT in the diagnosis and management of visceral injuries. Part 2: Gastrointestinal tract and retroperitoneal organs. *Eur Radiol* 1998b;8:772–780
- Bell RM, Krantz BE, Weigelt JA. ATLS: a foundation for trauma training. *Ann Emerg Med* 1999;34:233–237
- Blackmore CC, Ramsey SD, Mann FA, Deyo RA. Cervical spine screening with CT in trauma patients: a cost-effectiveness analysis. *Radiology* 1999;212:117–125
- Blackmore CC. Evidence-based imaging evaluation of the cervical spine in trauma. *Neuroimaging Clin N Am* 2003;13:283–291
- Blankenship JC, Gavant ML, Cox CE, Chauhan RD, Gingrich JR. Importance of delayed imaging for blunt renal trauma. *World J Surg* 2001;25:1561–1564
- Bode PJ, Edwards MJ, Kruit MC, van Vugt AB. Sonography in a clinical algorithm for early evaluation of 1671 patients with blunt abdominal trauma. *Am J Roentgenol* 1999;172:905–911
- Boulanger BR, Brenneman FD, McLellan BA, Rizoli SB, Culhane J, Hamilton P. A prospective study of emergent abdominal sonography after blunt trauma. *J Trauma* 1995;39:325–330
- Boulanger BR, McLellan BA, Brenneman FD, et al. Emergent abdominal sonography as a screening test in a new diagnostic algorithm for blunt trauma. *J Trauma* 1996;40:867–874
- Brasel KJ, Borgstrom DC, Kolewe KA, Weigelt JA. Abdominal computed tomography scan as a screening tool in blunt trauma. *Surgery* 1996;120:780–784
- Brasel KJ, DeLisle CM, Olson CJ, Borgstrom DC. Splenic injury: trends in evaluation and management. *J Trauma* 1998;44:283–286
- Brohi K, Healy M, Fotheringham T, et al. Helical computed tomographic scanning for the evaluation of the cervical spine in the unconscious, intubated trauma patient. *J Trauma* 2005;58:897–901
- Brown CV, Weng J, Oh D, et al. Does routine serial computed tomography of the head influence management of traumatic brain injury? A prospective evaluation. *J Trauma* 2004;57:939–943
- Brown CV, Antevil JL, Sise MJ, Sack DI. Spiral computed tomography for the diagnosis of cervical, thoracic, and lumbar spine fractures: its time has come. *J Trauma* 2005;58:890–896

- Bruce DA. Imaging after head trauma: why, when and which. *Childs Nerv Syst* 2000;16:755–759
- Buntain WL, Gould HR, Maull KI. Predictability of splenic salvage by computed tomography. *J Trauma* 1988;28:24–34
- Butela ST, Federle MP, Chang PJ, et al. Performance of CT in detection of bowel injury. *Am J Roentgenol* 2001;176:129–135
- Carr ND, Cairns SJ, Lees WR, Russell RC. Late complications of pancreatic trauma. *Br J Surg* 1989;76:1244–1246
- Catalano O, Lobianco R, Sandomenico F, Mattace Raso M, Siani A. Real-time, contrast-enhanced sonographic imaging in emergency radiology. *Radiol Med (Torino)* 2004;108:454–469
- Chao A, Pearl J, Perdue P, et al. Utility of routine serial computed tomography for blunt intracranial injury. *J Trauma* 2001; 51:870–876
- Chiu WC, Cushing BM, Rodriguez A, et al. Abdominal injuries without hemoperitoneum: a potential limitation of focused abdominal sonography for trauma (FAST). *J Trauma* 1997;42: 617–623
- Cogbill TH, Moore EE, Jurkovich GJ, et al. Nonoperative management of blunt splenic trauma: a multicenter experience. *J Trauma* 1989;29:1312–1317
- Colucciello SA. Blunt abdominal trauma. *Emerg Med Clin North Am* 1993;11:107–123
- Cook DE, Walsh JW, Vick CW, Brewer WH. Upper abdominal trauma: pitfalls in CT diagnosis. *Radiology* 1986;159:65–69
- Daffner RH. Helical CT of the cervical spine for trauma patients: a time study. *Am J Roentgenol* 2001;177:677–679
- Davis KA, Fabian TC, Croce MA, et al. Improved success in nonoperative management of blunt splenic injuries: embolization of splenic artery pseudoaneurysms. *J Trauma* 1998;44:1008–1013
- Dowe MF, Shanmuganathan K, Mirvis SE, Steiner RC, Cooper C. CT findings of mesenteric injury after blunt trauma: implications for surgical intervention. *Am J Roentgenol* 1997;168:425–428
- Ducreux D, Huynh I, Fillard P, et al. Brain MR diffusion tensor imaging and fibre tracking to differentiate between two diffuse axonal injuries. *Neuroradiology* 2005;47:604–608
- Fang JE, Chen RJ, Wong YC, et al. Pooling of contrast material on computed tomography mandates aggressive management of blunt hepatic injury. *Am J Surg* 1998;176:315–319
- Federle MP. Splenic trauma: Is follow-up CT of value? *Radiology* 1995;194:23–24
- Federle MP, Courcoulas AP, Powell M, Ferris JV, Peitzman AB. Blunt splenic injury in adults: clinical and CT criteria for management, with emphasis on active extravasation. *Radiology* 1998;206:137–142
- Feliciano PD, Mullins RJ, Trunkey DD, Crass RA, Beck JR, Helfand M. A decision analysis of traumatic splenic injuries. *J Trauma* 1992;33:340–348
- Forster R, Pillasch J, Zielke A, Malewski U, Rothmund M. Ultrasonography in blunt abdominal trauma: influence of the investigators' experience. *J Trauma* 1993;34:264–269
- Frick EJ, Cipolle MD, Pasquale MD, et al. Outcome of blunt thoracic aortic injury in a level I trauma center: an 8-year review. *J Trauma* 1997;43:844–851
- Fulcher AS, Turner MA. Magnetic resonance pancreatography (MRP). *Crit Rev Diagn Imaging* 1999;40:285–322
- Gavant ML, Schurr M, Flick PA, Croce MA, Fabian TC, Gold RE. Predicting clinical outcome of nonsurgical management of blunt splenic injury: using CT to reveal abnormalities of splenic vasculature. *Am J Roentgenol* 1997;168:207–212
- Gralla J, Spycher F, Pignolet C, Ozdoba C, Vock P, Hoppe H. Evaluation of a 16-MDCT scanner in an emergency department: initial clinical experience and workflow analysis. *Am J Roentgenol* 2005;185:232–238
- Greenberg J, Cohen WA, Cooper PR. The "hyperacute" extraaxial intracranial hematoma: computed tomographic findings and clinical significance. *Neurosurgery* 1985;17:48–56
- Griffen MM, Frykberg ER, Kerwin AJ, et al. Radiographic clearance of blunt cervical spine injury: Plain radiograph or computed tomography scan? *J Trauma* 2003;55:222–227
- Guerrero-Lopez F, Vazquez-Mata G, Alcazar-Romero PP, Fernandez-Mondejar E, Aguayo-Hoyos E, Linde-Valverde CM. Evaluation of the utility of computed tomography in the initial assessment of the critical care patient with chest trauma. *Crit Care Med* 2000;28:1370–1375
- Hagiwara A, Yukioka T, Satou M, et al. Early diagnosis of small intestine rupture from blunt abdominal trauma using computed tomography: significance of the streaky density within the mesentery. *J Trauma* 1995;38:630–633
- Hagiwara A, Yukioka T, Ohta S, Nitatori T, Matsuda H, Shimazaki S. Nonsurgical management of patients with blunt splenic injury: efficacy of transcatheter arterial embolization. *Am J Roentgenol* 1996;167:159–166
- Hamilton P, Rizoli S, McLellan B, Murphy J. Significance of intra-abdominal extraluminal air detected by CT scan in blunt abdominal trauma. *J Trauma* 1995;39:331–333
- Hammoud DA, Wasserman BA. Diffuse axonal injuries: pathophysiology and imaging. *Neuroimaging Clin N Am* 2002;12: 205–216
- Harlan LC, Harlan WR, Parsons PE. The economic impact of injuries: a major source of medical costs. *Am J Public Health* 1990;80:453–459
- Haydel MJ, Preston CA, Mills TJ, Luber S, Blaudeau E, DeBlieux PM. Indications for computed tomography in patients with minor head injury. *N Engl J Med* 2000;343:100–105
- Hedrick TL, Sawyer RG, Young JS. MRI for the diagnosis of blunt abdominal trauma: a case report. *Emerg Radiol* 2005;11: 309–311
- Hoffman JR, Wolfson AB, Todd K, Mower WR. Selective cervical spine radiography in blunt trauma: methodology of the National Emergency X-Radiography Utilization Study (NEXUS). *Ann Emerg Med* 1998;32:461–469
- Hoffman JR, Mower WR, Wolfson AB, Todd KH, Zucker MI. Validity of a set of clinical criteria to rule out injury to the cervical spine in patients with blunt trauma. National Emergency X-Radiography Utilization Study Group. *N Engl J Med* 2000; 343:94–99
- Holland BA, Brant-Zawadzki M. High-resolution CT of temporal bone trauma. *Am J Roentgenol* 1984;143:391–395
- Jeffrey RB, Jr., Federle MP, Crass RA. Computed tomography of pancreatic trauma. *Radiology* 1983;147:491–494
- Karaaslan T, Meuli R, Androux R, Duvoisin B, Hessler C, Schnyder P. Traumatic chest lesions in patients with severe head trauma: a comparative study with computed tomography and conventional chest roentgenograms. *J Trauma* 1995;39:1081–1086
- Killeen KL, Mirvis SE, Shanmuganathan K. Helical CT of diaphragmatic rupture caused by blunt trauma. *Am J Roentgenol* 1999;173:1611–1616
- Killeen KL, Shanmuganathan K, Poletti PA, Cooper C, Mirvis SE. Helical computed tomography of bowel and mesenteric injuries. *J Trauma* 2001;51:26–36
- Kohn JS, Clark DE, Isler RJ, Pope CF. Is computed tomographic grading of splenic injury useful in the nonsurgical management of blunt trauma? *J Trauma* 1994;36:385–390
- Leidner B, Adiels M, Aspelin P, Gullstrand P, Wallen S. Standardized CT examination of the multitraumatized patient. *Eur Radiol* 1998;8:1630–1638
- Linsenmaier U, Krotz M, Hauser H, et al. Whole-body computed tomography in polytrauma: techniques and management. *Eur Radiol* 2002;12:1728–1740
- Lin DD, Filippi CG, Steever AB, Zimmerman RD. Detection of intracranial hemorrhage: comparison between gradient-echo images and b(0) images obtained from diffusion-weighted echo-planar sequences. *Am J Neuroradiol* 2001;22:1275–1281
- Lingawi SS, Buckley AR. Focused abdominal US in patients with trauma. *Radiology* 2000;217:426–429
- Lipper MH, Kishore PR, Girevendulis AK, Miller JD, Becker DP. Delayed intracranial hematoma in patients with severe head injury. *Radiology* 1979;133:645–649

- Livingston DH, Loder PA, Koziol J, Hunt CD. The use of CT scanning to triage patients requiring admission following minimal head injury. *J Trauma* 1991;31:483-489
- Livingston DH, Lavery RF, Passannante MR, et al. Admission or observation is not necessary after a negative abdominal computed tomographic scan in patients with suspected blunt abdominal trauma: results of a prospective, multi-institutional trial. *J Trauma* 1998;44:273-280
- Livingston DH, Lavery RF, Passannante MR, et al. Emergency department discharge of patients with a negative cranial computed tomography scan after minimal head injury. *Ann Surg* 2000;232:126-132
- Lobato RD, Gomez PA, Alday R, et al. Sequential computerized tomography changes and related final outcome in severe head injury patients. *Acta Neurochir (Wien)* 1997;139:385-391
- Low R, Duber C, Schweden F, Lehmann L, Blum J, Thelen M. Whole body spiral CT in primary diagnosis of patients with multiple trauma in emergency situations. *Rofo* 1997;166:382-388 [in German]
- Mahadevan S, Mower WR, Hoffman JR, Peeples N, Goldberg W, Sonner R. Interrater reliability of cervical spine injury criteria in patients with blunt trauma. *Ann Emerg Med* 1998;31:197-201
- Masters SJ. Evaluation of head trauma: efficacy of skull films. *Am J Roentgenol* 1980;135:539-547
- Masters SJ, McClean PM, Arcarese JS, et al. Skull X-ray examinations after head trauma. Recommendations by a multidisciplinary panel and validation study. *N Engl J Med* 1987;316:84-91
- McGahan JP, Rose J, Coates TL, Wisner DH, Newberry P. Use of ultrasonography in the patient with acute abdominal trauma. *J Ultrasound Med* 1997;16:653-654
- McGahan JP, Richards JR. Blunt abdominal trauma: the role of emergent sonography and a review of the literature. *Am J Roentgenol* 1999;172:897-903
- McGonigal MD, Schwab CW, Kauder DR, Miller WT, Grumbach K. Supplemental emergent chest computed tomography in the management of blunt torso trauma. *J Trauma* 1990;30:1431-1435
- McKenney M, Lentz K, Nunez D, et al. Can ultrasound replace diagnostic peritoneal lavage in the assessment of blunt trauma? *J Trauma* 1994;37:439-441
- McKenney MG, Martin L, Lentz K, et al. 1000 consecutive ultrasounds for blunt abdominal trauma. *J Trauma* 1996;40:607-611
- Miller MT, Pasquale MD, Bromberg WJ, Wasser TE, Cox J. Not so FAST. *J Trauma* 2003;54:52-60
- Mirvis SE, Shanmuganathan K. *Imaging in trauma and critical care*, 2nd edition. Saunders Ed. 2003
- Mirvis SE, Tobin KD, Kostrubiak I, Belzberg H. Thoracic CT in detecting occult disease in critically ill patients. *Am J Roentgenol* 1987;148:685-689
- Mirvis SE, Whitley NO, Gens DR. Blunt splenic trauma in adults: CT-based classification and correlation with prognosis and treatment. *Radiology* 1989a;171:33-39
- Mirvis SE, Whitley NO, Vainwright JR, Gens DR. Blunt hepatic trauma in adults: CT-based classification and correlation with prognosis and treatment. *Radiology* 1989b;171:27-32
- Mirvis SE, Shanmuganathan K, Buell J, Rodriguez A. Use of spiral computed tomography for the assessment of blunt trauma patients with potential aortic injury. *J Trauma* 1998;45:922-930
- Moore EE, Shackford SR, Pachter HL, et al. Organ injury scaling: spleen, liver, and kidney. *J Trauma* 1989;29:1664-1666
- Moore EE, Cogbill TH, Malangoni MA, et al. Organ injury scaling, II: pancreas, duodenum, small bowel, colon, and rectum. *J Trauma* 1990;30:1427-1429
- Moore EE, Cogbill TH, Jurkovich GJ, Shackford SR, Malangoni MA, Champion HR. Organ injury scaling: spleen and liver (1994 revision). *J Trauma* 1995;38:323-324
- Morey AF, Iverson AJ, Swan A, et al. Bladder rupture after blunt trauma: guidelines for diagnostic imaging. *J Trauma* 2001;51:683-686
- Morgan DE, Nallamala LK, Kenney PJ, Mayo MS, Rue LW III. CT cystography: radiographic and clinical predictors of bladder rupture. *Am J Roentgenol* 2000;174:89-95
- Navarrete-Navarro P, Vazquez G, Bosch JM, Fernandez E, Rivera R, Carazo E. Computed tomography vs clinical and multidisciplinary procedures for early evaluation of severe abdomen and chest trauma: a cost analysis approach. *Intensive Care Med* 1996;22:208-212
- Nunez DB, Jr., Zuluaga A, Fuentes-Bernardo DA, Rivas LA, Becerra JL. Cervical spine trauma: How much more do we learn by routinely using helical CT? *Radiographics* 1996;16:1307-1321
- Omert LA, Salyer D, Dunham CM, Porter J, Silva A, Protetch J. Implications of the "contrast blush" finding on computed tomographic scan of the spleen in trauma. *J Trauma* 2001;51:272-278
- Ovenfors CO, Hedgcock MW. Intensive care unit radiology. Problems of interpretation. *Radiol Clin North Am* 1978;16:407-439
- Parizel PM, Ozsarlak O, Van Goethem JW, et al. Imaging findings in diffuse axonal injury after closed head trauma. *Eur Radiol* 1998;8:960-965
- Parizel PM, Van Goethem JW, Ozsarlak O, Maes M, Phillips CD. New developments in the neuroradiological diagnosis of craniocerebral trauma. *Eur Radiol* 2005;15:569-581
- Paterakis K, Karantanis AH, Komnos A, Volikas Z. Outcome of patients with diffuse axonal injury: the significance and prognostic value of MRI in the acute phase. *J Trauma* 2000;49:1071-1075
- Pilleul F, Billaud Y, Gautier G, et al. Mangafodipir-enhanced magnetic resonance cholangiography for the diagnosis of bile duct leaks. *Gastrointest Endosc* 2004;59:818-822
- Pillgram-Larsen J, Lovstakken K, Hafsahl G, Solheim K. Initial axial computerized tomography examination in chest injuries. *Injury* 1993;24:182-184
- Poletti PA, Mirvis SE, Shanmuganathan K, Killeen KL, Coldwell D. CT criteria for management of blunt liver trauma: correlation with angiographic and surgical findings. *Radiology* 2000;216:418-427
- Poletti PA, Kinkel K, Vermeulen B, Irmay F, Unger PF, Terrier F. Blunt abdominal trauma: Should US be used to detect both free fluid and organ injuries? *Radiology* 2003;227:95-103
- Poletti PA, Mirvis SE, Shanmuganathan K, et al. Blunt abdominal trauma patients: Can organ injury be excluded without performing computed tomography? *J Trauma* 2004a;57:1072-1081
- Poletti PA, Platon A, Becker CD, et al. Blunt abdominal trauma: Does the use of a second-generation sonographic contrast agent help to detect solid organ injuries? *Am J Roentgenol* 2004b;183:1293-1301
- Poole GV, Morgan DB, Cranston PE, Muakkassa FF, Griswold JA. Computed tomography in the management of blunt thoracic trauma. *J Trauma* 1993;35:296-300
- Regel G, Lobenhoffer P, Grotz M, Pape HC, Lehmann U, Tscherner H. Treatment results of patients with multiple trauma: an analysis of 3406 cases treated between 1972 and 1991 at a German Level I Trauma Center. *J Trauma* 1995;38:70-78
- Resciniti A, Fink MP, Raptopoulos V, Davidoff A, Silva WE. Nonoperative treatment of adult splenic trauma: development of a computed tomographic scoring system that detects appropriate candidates for expectant management. *J Trauma* 1988;28:828-831
- Rhea JT, Novelline RA, Lawrason J, Sacknoff R, Oser A. The frequency and significance of thoracic injuries detected on abdominal CT scans of multiple trauma patients. *J Trauma* 1989;29:502-505
- Richards PJ. Cervical spine clearance: a review. *Injury* 2005;36:248-270
- Richards JR, Derlet RW. Computed tomography for blunt abdominal trauma in the ED: a prospective study. *Am J Emerg Med* 1998;16:338-342
- Rizzo AG, Steinberg SM, Flint LM. Prospective assessment of the value of computed tomography for trauma. *J Trauma* 1995;38:338-342



- Rodriguez A, DuPriest RW, Jr., Shatney CH. Recognition of intra-abdominal injury in blunt trauma victims. A prospective study comparing physical examination with peritoneal lavage. *Am Surg* 1982;48:457-459
- Röthlin MA, Naf R, Amgwerd M, Candinas D, Frick T, Trentz O. Ultrasound in blunt abdominal and thoracic trauma. *J Trauma* 1993;34:488-495
- Rugg-Gunn FJ, Symms MR, Barker GJ, Greenwood R, Duncan JS. Diffusion imaging shows abnormalities after blunt head trauma when conventional magnetic resonance imaging is normal. *J Neurol Neurosurg Psychiatry* 2001;70:530-533
- Santucci RA, McAninch JW, Safir M, Mario LA, Service S, Segal MR. Validation of the American Association for the Surgery of Trauma organ injury severity scale for the kidney. *J Trauma* 2001;50:195-200
- Scalea TM, Rodriguez A, Chiu WC, et al. Focused assessment with sonography for trauma (FAST): results from an international consensus conference. *J Trauma* 1999;46:466-472
- Schenarts PJ, Diaz J, Kaiser C, Carrillo Y, Eddy V, Morris JA, Jr. Prospective comparison of admission computed tomographic scan and plain films of the upper cervical spine in trauma patients with altered mental status. *J Trauma* 2001;51:663-669
- Schurink GW, Bode PJ, van Luijt PA, van Vugt AB. The value of physical examination in the diagnosis of patients with blunt abdominal trauma: a retrospective study. *Injury* 1997;28:261-265
- Schuster R, Waxman K, Sanchez B, et al. Magnetic resonance imaging is not needed to clear cervical spines in blunt trauma patients with normal computed tomographic results and no motor deficits. *Arch Surg* 2005;140:762-766
- Servadei F, Nanni A, Nasi MT, et al. Evolving brain lesions in the first 12 hours after head injury: analysis of 37 comatose patients. *Neurosurgery* 1995;37:899-906
- Server A, Dullerud R, Haakonsen M, Nakstad PH, Johnsen UL, Magnaes B. Post-traumatic cerebral infarction. Neuroimaging findings, etiology and outcome. *Acta Radiol* 2001;42:254-260
- Shackford SR. Focused ultrasound examinations by surgeons: the time is now. *J Trauma* 1993;35:181-182
- Shackford SR, Molin M. Management of splenic injuries. *Surg Clin North Am* 1990;70:595-620
- Shackford SR, Wald SL, Ross SE, et al. The clinical utility of computed tomographic scanning and neurologic examination in the management of patients with minor head injuries. *J Trauma* 1992;33:385-394
- Shackford SR, Rogers FB, Osler TM, Trabulsky ME, Clauss DW, Vane DW. Focused abdominal sonogram for trauma: the learning curve of nonradiologist clinicians in detecting hemoperitoneum. *J Trauma* 1999;46:553-564
- Shanmuganathan K, Mirvis SE, White CS, Pomerantz SM. MR imaging evaluation of hemidiaphragms in acute blunt trauma: experience with 16 patients. *Am J Roentgenol* 1996;167:397-402
- Shanmuganathan K, Mirvis SE, Sherbourne CD, Chiu WC, Rodriguez A. Hemoperitoneum as the sole indicator of abdominal visceral injuries: a potential limitation of screening abdominal US for trauma. *Radiology* 1999;212:423-430
- Shanmuganathan K, Mirvis SE, Boyd-Kranis R, Takada T, Scalea TM. Nonsurgical management of blunt splenic injury: use of CT criteria to select patients for splenic arteriography and potential endovascular therapy. *Radiology* 2000a;217:75-82
- Shanmuganathan K, Killeen K, Mirvis SE, White CS. Imaging of diaphragmatic injuries. *J Thorac Imaging* 2000b;15:104-111
- Sheridan R, Peralta R, Rhea J, Ptak T, Novelline R. Reformatted visceral protocol helical computed tomographic scanning allows conventional radiographs of the thoracic and lumbar spine to be eliminated in the evaluation of blunt trauma patients. *J Trauma* 2003;55:665-669
- Smejkal R, O'Malley KF, David E, Cernaianu AC, Ross SE. Routine initial computed tomography of the chest in blunt torso trauma. *Chest* 1991;100:667-669
- Stiell IG, Wells GA, Vandemheen K, et al. The Canadian CT Head Rule for patients with minor head injury. *Lancet* 2001a;357:1391-1396
- Stiell IG, Wells GA, Vandemheen KL, et al. The Canadian C-spine rule for radiography in alert and stable trauma patients. *J Am Med Assoc* 2001b;286:1841-1848
- Stiell IG, Clement CM, McKnight RD, et al. The Canadian C-spine rule versus the NEXUS low-risk criteria in patients with trauma. *N Engl J Med* 2003;349:2510-2518
- Strieter RM, Lynch JP III. Complications in the ventilated patient. *Clin Chest Med* 1988;9:127-139
- Sugimoto K, Horiike S, Hirata M, Ohwada T, Maekawa K. The role of angiography in the assessment of blunt liver injury. *Injury* 1994;25:283-287
- Symbas PJ, Horsley WS, Symbas PN. Rupture of the ascending aorta caused by blunt trauma. *Ann Thorac Surg* 1998;66:113-117
- Thomason RB, Julian JS, Mostellar HC, Pennell TC, Meredith JW. Microscopic hematuria after blunt trauma. Is pyelography necessary? *Am Surg* 1989;55:145-150
- Tocino IM, Miller MH, Frederick PR, Bahr AL, Thomas F. CT detection of occult pneumothorax in head trauma. *Am J Roentgenol* 1984;143:987-990
- Tocino IM, Miller MH, Fairfax WR. Distribution of pneumothorax in the supine and semirecumbent critically ill adult. *Am J Roentgenol* 1985;144:901-905
- Toombs BD, Sandler CM, Lester RG. Computed tomography of chest trauma. *Radiology* 1981;140:733-738
- Trupka A, Waydhas C, Hallfeldt KK, Nast-Kolb D, Pfeifer KJ, Schweiberer L. Value of thoracic computed tomography in the first assessment of severely injured patients with blunt chest trauma: results of a prospective study. *J Trauma* 1997;43:405-420
- Vaccaro JP, Brody JM. CT cystography in the evaluation of major bladder trauma. *Radiographics* 2000;20:1373-1381
- Van Goethem JW, Maes M, Ozsarlak O, van den Hauwe L, Parizel PM. Imaging in spinal trauma. *Eur Radiol* 2005;15:582-590
- Voggenreiter G, Aufmkolk M, Majetschak M, et al. Efficiency of chest computed tomography in critically ill patients with multiple traumas. *Crit Care Med* 2000;28:1033-1039
- Yoshii H, Sato M, Yamamoto S, et al. Usefulness and limitations of ultrasonography in the initial evaluation of blunt abdominal trauma. *J Trauma* 1998;45:45-50
- Yu CJ, Yang PC, Chang DB, Luh KT. Diagnostic and therapeutic use of chest sonography: value in critically ill patients. *Am J Roentgenol* 1992;159:695-701
- Wagner RB, Jamieson PM. Pulmonary contusion. Evaluation and classification by computed tomography. *Surg Clin North Am* 1989;69:31-40
- West OC. How to image from head to pubis for blunt abdominal trauma using GE LightSpeed QX/i. *Emerg Radiol* 2004;11:68-76
- Williams JS, Graff JA, Uku JM, Steinig JP. Aortic injury in vehicular trauma. *Ann Thorac Surg* 1994;57:726-730
- Wilms G, Marchal G, Geusens E, et al. Isodense subdural haematomas on CT: MRI findings. *Neuroradiology* 1992;34:497-499
- Wintermark M, Poletti PA, Becker CD, Schnyder P. Traumatic injuries: organization and ergonomics of imaging in the emergency environment. *Eur Radiol* 2002;12:959-968
- Wintermark M, Mouhsine E, Theumann N, et al. Thoracolumbar spine fractures in patients who have sustained severe trauma: depiction with multi-detector row CT. *Radiology* 2003;227:681-689
- Woodring JH, Lee C. The role and limitations of computed tomographic scanning in the evaluation of cervical trauma. *J Trauma* 1992;33:698-708
- Zimmerman RA, Bilaniuk LT, Genneralli T. Computed tomography of shearing injuries of the cerebral white matter. *Radiology* 1978;127:393-396



# Role of 3D Imaging in the Emergency Room

L. Husmann, S. Leschka, H. Alkadhi, S. Wildermuth

## 1.2

### Contents

1.2.1 Introduction	25
1.2.2 Imaging	25
1.2.2.1 Postprocessing Techniques	25
1.2.2.2 Clinical Applications	27
1.2.3 Conclusion	35
References	35

### 1.2.1 Introduction

Diagnostic imaging is a major support system to emergency services. Available imaging methods in the emergency department are conventional X-ray, ultrasound, magnetic resonance (MR), angiography, and computed tomography (CT). Computed tomography is considered the most valued tool in the diagnostic workup of trauma patients and of patients with various nontraumatic emergencies [1–4] and is performed in up to 67% of patients presenting to the emergency room [5]. In emergency situations, the patient's room time in the CT suite and the early diagnosis and initiation of treatment have a profound influence on the patient's outcome [6]. The correct choice of scan protocols and especially an optimized work flow are of vital importance. Presently, the new multislice CT generations with improved performance in speed and spatial resolution, and the use of three-dimensional (3D) imaging, offer new possibilities for optimal patient treatment in the emergency room

The 3D imaging of CT data sets was introduced shortly after clinical CT scanning became a reality in the late 1970s. Early applications most frequently involved areas with high CT attenuation, which were unlikely to be affected by patient motion or breathing, such as the bones of the craniofacial regions and the skull. The advent of multidetector-row computed tomography (MDCT) in the late 1990s represented a fundamental step from a cross-sectional towards a true three-dimensional imaging modality. It created immense new opportunities but also required changes in radiological viewing methods and data handling [7, 8]. On one hand, the reduction of the collimated

slice thickness ( $<3$  mm) realizes the isotropic voxel, which is the prerequisite for sophisticated two-dimensional (2D) and 3D postprocessing algorithms. The physician is now enabled to interactively segment out organs or organ systems and this will help with more accurate detection of disease as well as quantification of disease volumes. On the other hand, the number of images acquired per scan has also increased considerably, making conventional image interpretation slice by slice more difficult and more time-consuming; therefore, exact and predicative postprocessing applications are increasingly required [9] to speed up the viewing process for both the radiologist and the referring physician

Work-flow issues are obviously a critical factor in the success of a 3D applications, especially in the emergency room. The timely performance of a CT scan will be negated if there is a time lag until the 3D images are generated. Although many 3D studies do not require an immediate turnaround, other applications are very time-sensitive (e.g., suspected mesenteric ischemia or suspected aortic dissection). In the trauma setting, 3D reformations have been proven very useful for detecting and characterizing spinal, pelvic, maxillofacial, and extremity fractures, as well as for detecting acute vascular injuries with CT angiography [10]. Even when the 3D images are not the principal diagnostic tool, they can increase confidence in the correctness of a diagnosis and facilitate communication with surgeons and referring physicians [11]

This chapter focuses on the technical fundamentals of postprocessing techniques and on current 2D and 3D applications with a focus on emergency room usability

### 1.2.2 Imaging

#### 1.2.2.1 Postprocessing Techniques

Sectional images derived from CT are not really 2D but represent a slice of a particular volume with a certain thickness; thus, the pixels visualized on CT images are called voxels because of their 3D nature. The main issue in visualizing volume data is how to display 3D data as a 2D image with-

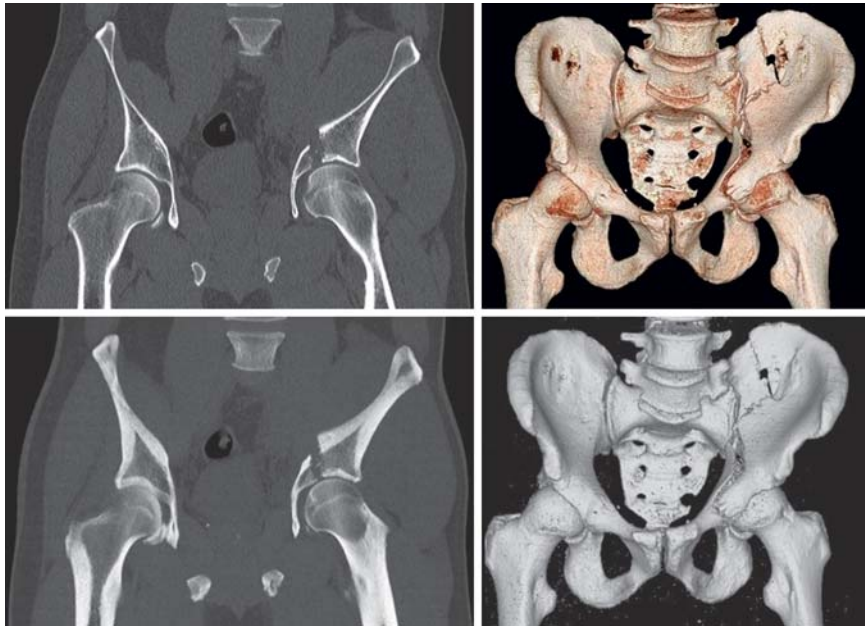


**Fig. 1.** A 52-year-old patient brought to the emergency room after a car accident. Four different postprocessing techniques of pelvic fractures of the same were performed. *Top left:* multiplanar reconstructions; *top right:* volume rendering; *bottom left:* maximum intensity projection; *bottom right:* surface rendering

out losing too much information. Several techniques for displaying data cubes of sectional volume data are well developed and used in the emergency department. Figure 1 shows an example of a fractured pelvis postprocessed with the four modalities described in this chapter

### Surface Rendering

Surface Rendering, also called Shaded Surface Display, was one of the earliest methods for 3D display, and is now available in most commercially available 3D medical imaging packages. Surface rendering is a process in which apparent surfaces are determined within the volume of data and an image representing the derived surfaces is displayed. In this method thresholding is commonly used to extract the desired object of interest from the background in an image or data volume. Each voxel within the data set is determined to be a part of or not a part of the object of interest, usually by comparing the voxel intensity to some threshold value, thereby defining the “surface” of the object. The remainder of the data set is then discarded [12]. Surface contours are generated by approximating and connecting the shape of interdata boundaries and typically modeled as a number of overlapping polygons. A virtual light source is computed for each polygon, and the object is displayed with the resulting surface shading

Surface-rendered images have the clearest volume depth cues of all 3D images and have the advantage of superior speed and flexibility in image rendering, allowing real-time rendering and thereby enhancing user interactivity. However, the resulting image is simplified by using <10% of the available data; therefore, possibly misleading interpreta-

tions of the displayed structures may occur, especially in structures that do not have naturally well-differentiated surfaces, and thus limiting the usefulness of surface-rendered images. Because of these limitations, the method has continuously been abandoned in recent years and volume rendering has become the present method of choice [13]

### Volume Rendering

Volume rendering (VR) is now increasingly being incorporated into commercially available imaging software packages. It renders the entire volume of data rather than just surfaces, and provides transparent volumetric display through relative shadings of brightness, opacity, and color, and is particularly helpful for the visualization of complex anatomy and pathology. Because of the large amounts of information incorporated into the resulting image, powerful computers are necessary to perform volume rendering at a reasonable speed

The VR takes the entire volume of data, adds the contribution of each voxel along a line from the viewer’s eye through the data set, and displays the resulting composite for each pixel of the display. The resulting displayed value is affected by both opacity and the value of underlying voxels; therefore, VR does not involve a sharp distinction between “object” and “background” but considers the influence of partial-volume effects as well. Furthermore, volume-based rendering allows a combined display of different aspects such as opaque and semi-transparent surfaces, cuts, and maximum intensity projections (MIP). Threshold values and other parameters can be interactively changed, thus, making it an ideal technique for interactive data exploration



The VR is presently the most important 3D postprocessing algorithm with constantly increasing clinical indications. The main disadvantage is the large calculation effort that makes the procedure cumbersome to run on normal workstations

### Multiplanar Reconstructions

The new generations of MDCT scanners acquire high-resolution data with nearly isotropic voxels, allowing multiplanar reconstructions (MPR) in any arbitrary plane interactively determined by the viewer. Generally, MPR are helpful whenever pathology cannot be accurately assessed on axial images alone, mostly when pathological interfaces are orientated parallel to the axial plane or when structures cannot be displayed in their entirety when they run through a number of slices

The MPR are most important in skeletal CT and in CT angiography and should additionally be employed whenever the radiologist expects additional information. In the emergency room coronal MPR with a thickness of approximately 500  $\mu\text{m}$  provide an image quality and diagnostic accuracy which is comparable to that of a conventional bedside chest radiography or to that of a portable pelvis film. These reconstructions could serve as an equivalent baseline image in trauma patients in whom the initial conventional radiograph is omitted because the emergency radiological evaluation has to be accelerated

### Maximum Intensity Projection

Maximum intensity projection (MIP) is widely available in commercial 3D software packages and is particularly useful in creating angiography-like images and urography-like displays from CT data [14]. The MIP algorithm evaluates each voxel along a line from the viewer's eye through the volume of data and selects the maximum voxel attenuation value as the value of the corresponding display pixel. This implies that the resulting MIP image is a 2D projection image. A 3D impression, which is not generated intentionally in the MIP procedure, can be deceptive. To accentuate the spatial relationships a series of MIP images can be generated by incrementing the viewing direction in small steps and viewing these images in a cine loop; the latter, however, is rarely necessary in clinical routine work

The MIP has a number of limitations and shortcomings that must be taken into account to properly interpret the images. The displayed pixel intensity only represents the material with the highest attenuation along the projected ray. High-intensity structures, such as vessel-wall calcification, will obscure information from intravascular contrast material. Selection of the highest pixel value also increases the background mean of the image, particularly in enhancing structures such as the kidney and liver, thereby decreasing the visibility of vessels in these structures. The

MIP images are typically not displayed with surface shading or other depth cues, which can make assessment of 3D relationships difficult. Also, volume averaging (the effect of finite volume resolution) coupled with the MIP algorithm commonly leads to MIP artifacts: a string of beads appearance in MIP images of normal vessels passing obliquely through a volume

### 1.2.2.2 Clinical Applications

The evaluation of CT studies in the emergency room should routinely be performed on dedicated workstations, allowing interactive viewing and viewing in "scroll-through" or cine modes. The following algorithmic approach for a general workflow is helpful in most patients:

1. Initial viewing of the axial images in a scroll-through mode
2. Interactive viewing in the coronal plane to complement axial image viewing
3. In case of equivocal findings, additional sagittal, oblique, or curved planar reconstructions may facilitate diagnosis
4. In suspected vascular or ureteral disease, MIP are usually reconstructed in dedicated planes and slab thickness is adapted to include the volume of interest
5. In suspected vascular, musculoskeletal or cardiac pathology, VR images may be helpful in understanding complex pathology and for reporting the results to clinical colleagues
6. Finally, all diagnoses should again be verified on axial images to avoid false-positive findings, because all post-processing techniques have the potential hazard of losing valuable information

### Vascular Emergency

In vascular imaging MIP and VR of image data from MDCT angiography can enable visualization that is equal or superior to that obtained with catheter angiography [3] and at the same time accelerates the work flow in the emergency department [15]. In CT angiography MPR are used to define the longitudinal extent of pathology and measure vascular diameters truly perpendicular to the course of the vessel. The MPR along with axial images are preferable in the diagnosis of carotid artery disease because overlying calcified plaque does not disturb the evaluation of the vessels [6]

In the diagnosis of active bleeding 3D imaging is also very helpful [16, 17]. The MIP images clearly depict extravasation of contrast material and are thereby useful in the confirmation of active bleeding (Fig. 2), but the lesion and neighboring organs often are not visible because of low attenuation [3]. The VR enables simultaneous the localization of the source of blood flow and the visualization of adjacent anatomic structures on the same image



**Fig. 2.** A 72-year-old man with acutely ruptured abdominal aortic aneurysm. Active bleeding is demonstrated both on axial and coronal images (arrows). The extent of the aneurysm is preferably evaluated on coronal multiplanar reconstructions

Among others, volume rendering of MDCT data enhances diagnosis and planning of subsequent procedures for pulmonary vessels, aortic dissection, and aneurysms, as well as cerebral aneurysms, vascular anomalies, renal artery stenosis, and peripheral artery disease. The VR is superior to shaded-surface display of vessels, because there is no need for threshold segmentation to exclude disturbing surrounding tissues, which could result in incomplete visualization of vessels and consecutive misinterpretation of pathologies

### Aortic Dissection

In the assessment of aortic dissection the following CT information is essential: (a) confirmation of diagnosis; (b) localization of the dissection; (c) extent of dissection; (d) classification of dissection; and (e) involvement of any branch [18]. One also needs to be aware of the pitfalls that may mimic aortic dissection; these include streak artifacts generated by high-attenuation contrast material in adjacent veins, and aortic wall motion as well as aortic arch branches, mediastinal veins, pericardial recess, thymus, atelectasis, pleural thickening, or effusions adjacent to the aorta [19]

With 3D imaging the correct diagnosis and the measurement of the extent of aortic dissection can be facilitated (Fig. 3). The MPR images provide a better display of the complexity of aortic dissection and often demonstrate the location of an intimal tear and the anatomical relationships between the flap and the adjacent great vessels. Curved planar reformations are particularly useful in assessing stenosis in the aortic branches and in displaying the relationships of mural atheroma, thrombus, intimal flaps, and dissection into branching vessels [20]

### Aortic Aneurysm

The MPR images provide additional advantages in assessment of aneurysms, compared with the use of axial images alone. Due to the tortuosity and curvature of the thoracic aorta, the size of an aneurysm is most accurately measured when the reconstruction images are generated perpendicular to the aortic flow lumen. The accurate sizing is especially important in the planning for endoluminal prostheses [21], and in their follow-up [22]

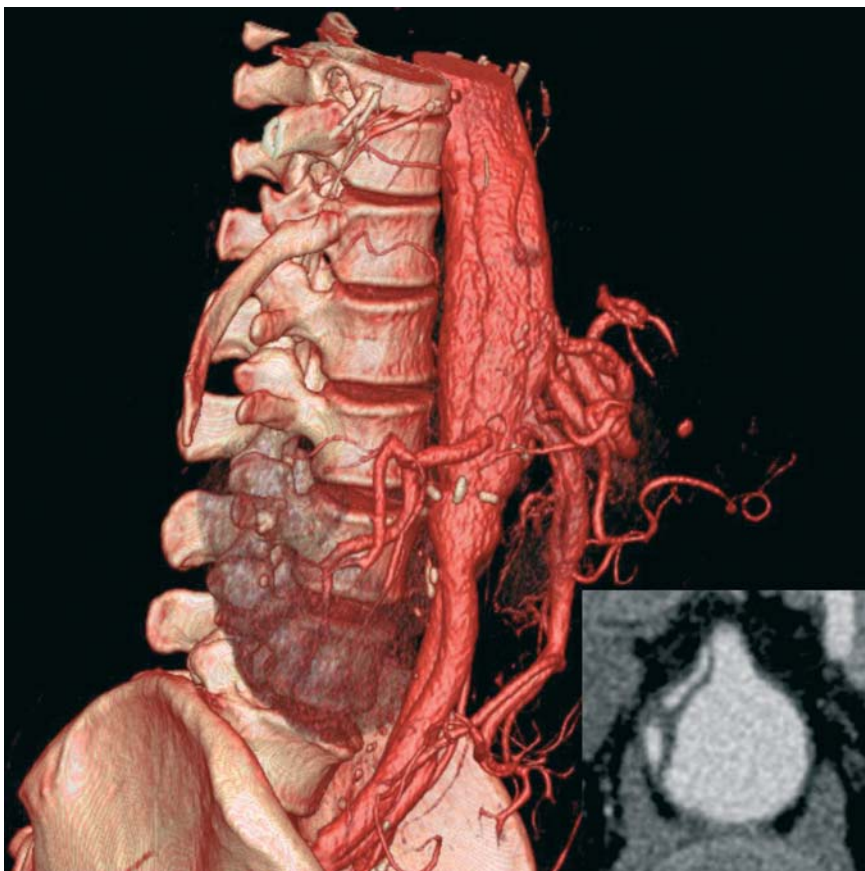


**Fig. 3.** A 65-year-old man with acute abdominal aortic dissection. Typical diagnostic findings are demonstrated on axial images. The extent of the aneurysm can be evaluated on volume-rendered (VR) reconstructions

### Aortic Rupture

Rupture of an aortic aneurysm (Fig. 2) is one of the most urgent vascular conditions and requires rapid intervention. Most patients who reach the hospital alive are sufficiently stable to undergo CT and consideration of endovascular aneurysm repair [23]. The diagnosis may be made on the basis of axial images, but most of the measurements required for determination of the optimal dimension and type of aortic stent-graft require 3D reconstructions [3]

The CT is an effective screening tool for aortic injury in that CT can help reduce the need for transcatheter aortography. Through MPR as well as 3D reconstructions, possible involvement of the aortic main branches and their relationship to primary lesions are easily detected. Sagittal reconstruction images from helical scans result in an aortogram that is generally adequate for surgical planning [24] and for depicting aortic lacerations longer than 15 mm [25]

### Pulmonary Embolism

The diagnosis of pulmonary embolism (PE) is usually most beneficially established on the basis of individual transverse sections, although extensive or isolated findings of

PE, as well as normal pulmonary vasculature, can be visualized in a comprehensive manner by means of 3D reconstructions (Fig. 4). A 3D display may also aid diagnosis in some instances. At a subsegmental level, for example, the diagnostic benefit of radial MPR in the diagnosis of thromboembolism could be shown [26]. Furthermore, 3D imaging helps to prevent diagnostic pitfalls, allowing, for example, correct interpretation of hilar lymphatic tissue adjacent to central pulmonary arteries [27]. There are indications that focal lung disease can be diagnosed accurately by using MIP reconstructions that beneficially “condense” large-volume multidetector-row CT data sets [28]. The development of dedicated algorithms for computer-aided detection may be helpful in the future for identification of pulmonary emboli in large-volume multidetector row CT data sets [29]

### Coronary Artery Disease

Acute coronary syndromes (ACS) can be caused by myocardial infarction or unstable angina, which is diagnosed based on ECG findings and biomarkers. Patients with myocardial infarction preferably undergo conventional coronary angiography and no further imaging work-up is required in the emergency room. Patients with unstable



**Fig. 4.** A 77-year-old woman with shortness of breath after 2 weeks of treatment of pulmonary infection. Coronal maximum intensity projection (MIP) reconstructions show a large thrombus in the right pulmonary artery

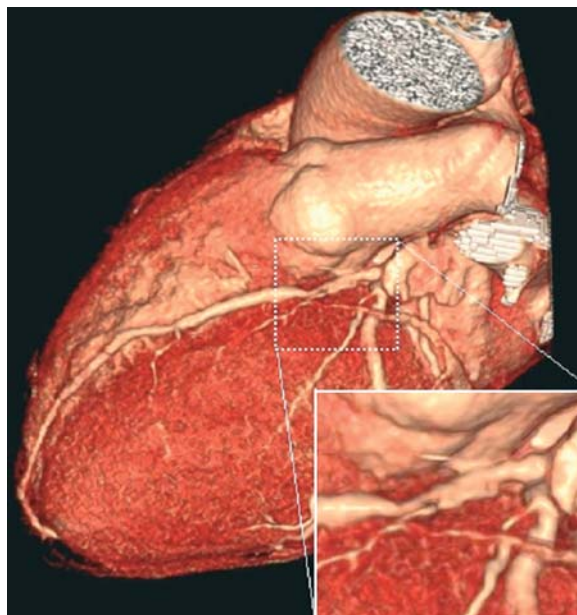


**Fig. 5.** A 60-year old man presents with first-time onset of chest pain after exercise. The VR reveals a significant stenosis of the proximal segment of the left anterior descending artery

angina are hospitalized with conservative treatment or conventional coronary angiography is performed in cases of objective evidence of myocardial ischemia and in approximately 2% of the cases, they are in appropriately discharged home [30]. Although conventional coronary angiography has a low morbidity of 1–2% and mortality of 0.1% [31], it is a relatively expensive technique, is inconvenient for patients, and in most cases conventional coronary angiography remains a diagnostic procedure with no intervention being performed [32]. A 64-slice CT has demonstrated the ability to detect coronary artery stenoses with high accuracy and a negative predictive value of 99% [33]. In the future 64-slice CT should be the method of choice to rule out coronary artery disease (CAD) in patients with a low likelihood of CAD in the emergency department to reduce morbidity and lower costs [34]

For the evaluation of coronary arteries axial planes and MPR are used. The most useful planes are, firstly, a plane parallel to the atrioventricular groove allowing a longitudinal visualization of the right coronary artery and the left circumflex coronary artery, and secondly, a plane parallel to the interventricular groove allowing a visualization of the left anterior descending coronary artery. Additional orthogonal views of the coronary vessels allow a better evaluation of stenosis

Curved MPR and VR (Fig. 5) is performed to provide an overview of the coronary anatomy and to demonstrate findings, but it should not be used for the assessment of stenotic lesions

## Abdominal Emergency

### Gallstones

Dislocation of gallstones in the biliary duct may lead to biliary colic. The most reliable CT finding is the depiction of the stone within the biliary duct. The MPR facilitates the detection of small calculi in the biliary system, often leading to distal common bile duct obstruction [35, 36]

### Appendicitis

Although the preoperative diagnosis of acute appendicitis can be established on the basis of clinical findings, the symptoms of appendicitis may be atypical and mimic other gastrointestinal or genitourinary conditions. When MDCT is performed in the emergency room, multiplanar viewing provides improved appendiceal visualization and enhances confidence as to the presence or absence of acute appendicitis [37]. Coronal reformations are especially useful for visualizing the appendix in an unusual location and also help guide surgical planning (Fig. 6)

### Diverticulitis

For the diagnosis of diverticulitis, CT is the imaging technique of choice for depicting complications, including walled-off perforation, intraperitoneal perforation, fistulae, and bowel obstruction [38]. Coronal reformations may provide improved differentiation between normal and abnormal bowel walls. The use of near-isotropic volumes





**Fig. 6.** A 30-year-old man presents with fever, elevated white blood cell count, and acute abdominal pain in the right lower quadrant. Coronal MPR depict an dilated appendix in a retro-ileal position, with circumferential mural enhancement, peri-appendiceal fat stranding, extra-luminal gas, and a small calcified appendicolith in the appendiceal apex (*arrow*)



**Fig. 7.** A 56-year-old man presents with chronic constipation and acute abdominal pain. Plain radiography did not provide sufficient information, so a multidetector-row CT (MDCT) examination was performed, showing distended small bowel loops measuring up to 4.2 cm in diameter. As the level of obstruction was difficult to identify on axial images alone, 3D imaging was used to accurately visualize the site of transition and the underlying pathology. Open abdominal surgery revealed a small bowel adenocarcinoma

results in reconstructions of imaging planes optimized to the bowel segment in question, or, when curved reconstructions are used, fistulae can be delineated in their entire course. Additional benefits of CT include the guidance of therapeutic intervention in complicated forms of diverticular disease [39] and the provision of an alternative diagnosis in patients without diverticulitis

### Inflammatory Bowel Disease

The diagnostic value of CT is based on the excellent visualization and documentation of extent and severity of bowel wall inflammation and the diagnosis of extra-intestinal complications. Because there is considerable overlap in the CT findings of ulcerative colitis and Crohn's disease, the use of MPR significantly improves observer confidence in image interpretation, even if additional abnormalities are not revealed [40]

### Bowel Obstruction

Computed tomography is increasingly used to identify the site, severity, and underlying cause of obstruction, and to determine the presence of complications [41]. Especially, the

determination of the transition point from dilated to nondilated bowel can be difficult on axial slices alone [42, 43]. Post-processing may enhance detection of the site of obstruction, diagnosis of adhesions, and analysis of the relationship between normal and abnormal bowel wall (Fig. 7) [44]

### Ischemic Bowel Disease

Computed tomography has been shown to be very useful for the diagnosis of bowel ischemia [45]. By evaluating the mesenteric vasculature, CT may sometimes be able to detect the underlying cause, such as atherosclerotic plaques, thrombus or occlusion. Evaluation of axial images and multiplanar display are usually sufficient for detecting alterations of the bowel wall and the main mesenteric vessels, whereas VR images have the advantage of demonstrating mesenteric vessels, from their origin to distal branches, on a single projection [46]

### Ureteral Stone Disease

Helical CT has been found to be more sensitive than excretory urography to plan treatment of patients with flank pain caused by obstructing ureteral stones [47]. The use of



**Fig. 8.** A 65-year-old man with abdominal pain and a status after nephrectomy on the right. Uretal stone disease was ruled out with MDCT. Thick MPR allow image quality similar to excretory urographs (*top left*). Volume rendering facilitates anatomic orientation

oblique–coronal reconstructions is more effective for precise stone localization and measurement than axial slices [48]. The use of curved reformations provides unequivocal images focused on the ureteral stone. The VR facilitates anatomic orientation (Fig. 8)

#### Acute Pancreatitis

Computed tomography is the imaging modality of choice in classifying pancreatitis and in detecting complications such as pseudoaneurysms, porto-mesenteric venous occlusion, pseudocysts, or abscess. Curved planar reformations are useful in displaying the whole tortuous pancreas, tracing the cholangiopancreatic duct and peri-pancreatic vessels, and highlighting the relationship of lesions with surrounding anatomic structures [49]

#### Musculoskeletal and Soft Tissue Emergency

When a CT of the abdomen or chest is initially scheduled in the emergency room, coronal and sagittal CT reconstructions of the pelvis, the thoracic or lumbar spine, and the chest accelerate the image work-up and decrease the radiation dose for the patient, when the plain films to

screen the lung, the spine, and the pelvis (Fig. 9) in a multiple trauma patient are omitted. Additionally, reconstructions of the thoracic and lumbar have been shown to be significantly superior in diagnostic accuracy as compared with plain films in detecting spine fractures [50]

#### Musculoskeletal Emergency

In trauma imaging MPR are performed on a routine basis along with axial images, because they convey additional information about the course of a fracture or the extent of deformities. They allow precise quantification of the displacement of the fragments, but they do not display a global comprehensible view of the lesions. The VR clearly demonstrates complex injuries and complicated spatial information about the relative positions of fracture fragments. Subtle fractures, particularly those oriented in the axial plane, are better seen on VR images. Particularly in areas with highly complex anatomy, such as the face, the pelvis, or the calcaneus, or in patients with complex fractures, 3D reformations have been proven very useful for detecting and characterizing spinal [51, 52], pelvic [53, 54], maxillofacial (Fig. 10) [55, 56], chest [57], and extremity (Fig. 11) [58, 59] fractures



**Fig. 9.** A 71-year-old man brought to the emergency room after a fall. Volume-rendered images show a depressed skull fracture

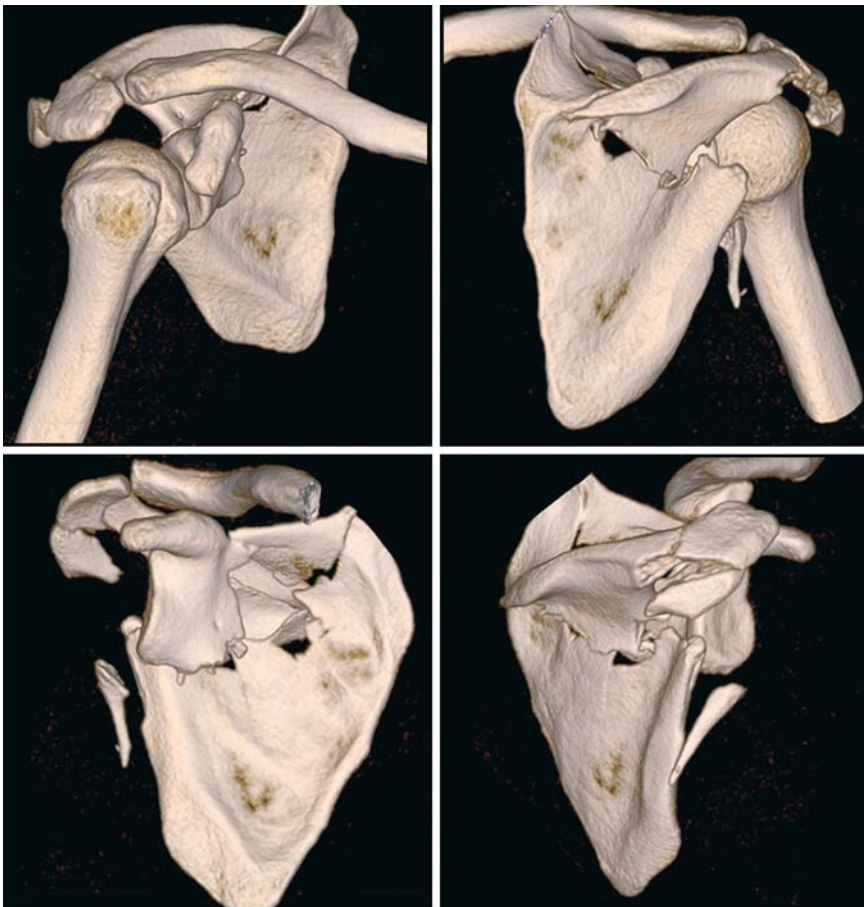


**Fig. 10.** A 23-year-old man brought to the emergency room after a motorbike accident. Volume-rendered images show a comminuted fracture of the scapula, involving the acromion





**Fig. 11.** **a** A 30-year-old man brought to the emergency room after a fall from great height. A CT angiography was performed. Volume-rendered images show a comminuted fracture of the tibia with dislocated fragments and their relationship to the arteries. **b** The subtraction of the bones from the volume-rendered images facilitates the evaluation of the arteries

The use of intravenously administered contrast material allows simultaneous evaluation of osseous and vascular structures within the affected area (Fig. 12)

#### **Soft Tissue Emergency**

Many emergency CT examinations are performed for the evaluation of suspected abscesses, masses, sialadenitis, and upper-airway trauma [1]. Coronal and sagittal MPR

adapted to the anatomic situation are particularly helpful for demonstrating the craniocaudal extent of acute pathology [60]. The 3D airway models, for example, appear as “casts” of the airway and provide information similar to that of laryngograms and tracheobronchograms [61], and these models can be rotated and imaged from various perspectives to show the extent of acute abnormality that impinges on or affects the upper airway





**Fig. 12. a** A 62-year-old man brought to the emergency room after a car accident. The conventional plain radiograph reveals fractures and displacement of the upper (*arrowhead*) and lower (*thick arrow*) pubic rami disruption of the sacro-iliac joints (*thin arrow*). **b** A thick MPR was reconstructed from MDCT data of the same patient as in **a**, displaying similar image quality as the plain radiograph

### 1.2.3 Conclusion

In the emergency room the increased acquisition speed of MDCT together with the high resolution accelerate the diagnostic work-up of traumatic and nontraumatic emergency conditions, thus potentially leading to earlier therapy and decreased mortality. Caused by the immensely increasing number of acquired images and augmented by frequently needed orthogonal reformations, 3D VR visualization of CT volume data sets have become essential also in the emergency department

This chapter explains the impact of postprocessing application on the acceleration of the work-flow and on the communication between physicians in the emergency department, and it also demonstrates, using multiple examples, that the accuracy on diagnostic findings and the support for diagnostic findings can strongly benefit from 3D imaging

### References

1. Novelline RA, Rhea JT, Bell T. Helical CT of abdominal trauma. *Radiol Clin North Am* 1999; 37:591–612, vi–vii
2. Harris JH Jr. Reflections: emergency radiology. *Radiology* 2001; 218:309–316
3. Frauenfelder T, Wildermuth S, Marincek B, Boehm T. Nontraumatic emergent abdominal vascular conditions: advantages of multi-detector row CT and three-dimensional imaging. *Radiographics* 2004; 24:481–496
4. Alkadhi H, Wildermuth S, Desbiolles L et al. Vascular emergencies of the thorax after blunt and iatrogenic trauma: multi-detector row CT and three-dimensional imaging. *Radiographics* 2004; 24:1239–1255
5. Gralla J, Spycher F, Pignolet C, Ozdoba C, Vock P, Hoppe H. Evaluation of a 16-MDCT scanner in an emergency department: initial clinical experience and workflow analysis. *Am J Roentgenol* 2005; 185:232–238
6. Philipp MO, Kubin K, Hormann M, Metz VM. Radiological emergency room management with emphasis on multidetector-row CT. *Eur J Radiol* 2003; 48:2–4

7. Prokop M. General principles of MDCT. *Eur J Radiol* 2003; 45 (Suppl 1):S4–S10
8. Rubin GD. 3-D imaging with MDCT. *Eur J Radiol* 2003; 45 (Suppl 1):S37–S41
9. Kirchgeorg MA, Prokop M. Increasing spiral CT benefits with postprocessing applications. *Eur J Radiol* 1998; 28:39–54
10. Soto JA, Lucey BC, Stuhlfaut JW, Varghese JC. Use of 3D imaging in CT of the acute trauma patient: impact of a PACS-based software package. *Emerg Radiol* 2005; 11:173–176
11. Salvolini L, Bichi Secchi E, Costarelli L, Nicola M de. Clinical applications of 2D and 3D CT imaging of the airways: a review. *Eur J Radiol* 2000; 34:9–25
12. Blank M, Kalender WA. Medical volume exploration: gaining insights virtually. *Eur J Radiol* 2000; 33:161–169
13. Kuszyk BS, Heath DG, Bliss DF, Fishman EK. Skeletal 3-D CT: advantages of volume rendering over surface rendering. *Skeletal Radiol* 1996; 25:207–214
14. Noroozian M, Cohan RH, Caoili EM, Cowan NC, Ellis JH. Multislice CT urography: state of the art. *Br J Radiol* 2004; 77 (Spec no 1):S74–S86
15. Prokop M. Multislice CT angiography. *Eur J Radiol* 2000; 36:86–96
16. Munera F, Soto JA, Nunez D. Penetrating injuries of the neck and the increasing role of CTA. *Emerg Radiol* 2004; 10:303–309
17. Schertler T, Pfammatter T, Eid K, Wildermuth S. Embolization of the splenic artery after splenic gunshot wound. *Swiss Surg* 2003; 9:87–91 [in German]
18. Takahashi K, Stanford W. Multidetector CT of the thoracic aorta. *Int J Cardiovasc Imaging* 2005; 21:141–153
19. Batra P, Bigoni B, Manning J et al. Pitfalls in the diagnosis of thoracic aortic dissection at CT angiography. *Radiographics* 2000; 20:309–320
20. Quint LE, Francis IR, Williams DM et al. Evaluation of thoracic aortic disease with the use of helical CT and multiplanar reconstructions: comparison with surgical findings. *Radiology* 1996; 201:37–41
21. Sakalihan N, Limet R, Defawe OD. Abdominal aortic aneurysm. *Lancet* 2005; 365:1577–1589
22. Kramer SC, Seifarth H, Pamler R, Fleiter T, Gorich J. Geometric changes in aortic endografts over a 2-year observation period. *J Endovasc Ther* 2001; 8:34–38
23. Lloyd GM, Bown MJ, Norwood MG et al. Feasibility of preoperative computer tomography in patients with ruptured abdominal aortic aneurysm: a time-to-death study in patients without operation. *J Vasc Surg* 2004; 39:788–791
24. Dyer DS, Moore EE, Mestek MF et al. Can chest CT be used to exclude aortic injury? *Radiology* 1999; 213:195–202
25. Patel NH, Stephens KE, Jr., Mirvis SE, Shanmuganathan K, Mann FA. Imaging of acute thoracic aortic injury due to blunt trauma: a review. *Radiology* 1998; 209:335–348
26. Pech M, Wieners G, Lopez-Hanninen E et al. The diagnostic value of radial multiplanar reformatting (MPR) in the CT-diagnosis of pulmonary embolism. *Rofo* 2004; 176:1576–1581 [in German]
27. Remy J, Remy-Jardin M, Artaud D, Fribourg M. Multiplanar and three-dimensional reconstruction techniques in CT: impact on chest diseases. *Eur Radiol* 1998; 8:335–351
28. Gruden JF, Ouanounou S, Tigges S, Norris SD, Klausner TS. Incremental benefit of maximum-intensity-projection images on observer detection of small pulmonary nodules revealed by multidetector CT. *Am J Roentgenol* 2002; 179:149–157
29. Schoepf UJ, Costello P. CT angiography for diagnosis of pulmonary embolism: state of the art. *Radiology* 2004; 230:329–337
30. Pope JH, Aufderheide TP, Ruthazer R et al. Missed diagnoses of acute cardiac ischemia in the emergency department. *N Engl J Med* 2000; 342:1163–1170
31. Papaconstantinou HD, Marshall AJ, Burrell CJ. Diagnostic cardiac catheterisation in a hospital without on-site cardiac surgery. *Heart* 1999; 81:465–469
32. Dorgelo J, Willems TP, Geluk CA, van Ooijen PM, Zijlstra F, Oudkerk M. Multidetector computed tomography-guided treatment strategy in patients with non-ST elevation acute coronary syndromes: a pilot study. *Eur Radiol* 2005; 15:708–713
33. Leschka S, Alkadhi H, Plass A et al. Accuracy of MSCT coronary angiography with 64-slice technology: first experience. *Eur Heart J* 2005; 26:1482–1487
34. Sato Y, Matsumoto N, Ichikawa M et al. Efficacy of multislice computed tomography for the detection of acute coronary syndrome in the emergency department. *Circ J* 2005; 69:1047–1051
35. Cahir JG, Freeman AH, Courtney HM. Multislice CT of the abdomen. *Br J Radiol* 2004; 77 (Spec no 1):S64–S73
36. Urban BA, Fishman EK. Tailored helical CT evaluation of acute abdomen. *Radiographics* 2000; 20:725–749
37. Paulson EK, Jaffe TA, Thomas J, Harris JP, Nelson RC. MDCT of patients with acute abdominal pain: a new perspective using coronal reformations from submillimeter isotropic voxels. *Am J Roentgenol* 2004; 183:899–906
38. Werner A, Diehl SJ, Farag-Soliman M, Duber C. Multi-slice spiral CT in routine diagnosis of suspected acute left-sided colonic diverticulitis: a prospective study of 120 patients. *Eur Radiol* 2003; 13:2596–2603
39. Kaiser AM, Jiang JK, Lake JP et al. The management of complicated diverticulitis and the role of computed tomography. *Am J Gastroenterol* 2005; 100:910–917
40. Raptopoulos V, Schwartz RK, McNicholas MM, Movson J, Pearlman J, Joffe N. Multiplanar helical CT enterography in patients with Crohn's disease. *Am J Roentgenol* 1997; 169:1545–1550
41. Maglinte DD, Reyes BL, Harmon BH et al. Reliability and role of plain film radiography and CT in the diagnosis of small-bowel obstruction. *Am J Roentgenol* 1996; 167:1451–1455
42. Alkadhi H, Boehm T, Hahnloser D, Marincek B, Wildermuth S. Images of interest. Gastrointestinal: adenocarcinoma of the ileum. *J Gastroenterol Hepatol* 2005; 20:648
43. Khurana B, Ledbetter S, McTavish J, Wiesner W, Ros PR. Bowel obstruction revealed by multidetector CT. *Am J Roentgenol* 2002; 178:1139–1144
44. Aufort S, Charra L, Lesnik A, Bruel JM, Taourel P. Multidetector CT of bowel obstruction: value of post-processing. *Eur Radiol* 2005; 15:2323–2329
45. Kirkpatrick ID, Kroeker MA, Greenberg HM. Biphasic CT with mesenteric CT angiography in the evaluation of acute mesenteric ischemia: initial experience. *Radiology* 2003; 229:91–98
46. Wildermuth S, Leschka S, Alkadhi H, Marincek B. Multislice CT in the pre- and postinterventional evaluation of mesenteric perfusion. *Eur Radiol* 2005; 15:1203–1210
47. Fielding JR, Silverman SG, Samuel S, Zou KH, Loughlin KR. Unenhanced helical CT of ureteral stones: a replacement for excretory urography in planning treatment. *Am J Roentgenol* 1998; 171:1051–1053
48. Nadler RB, Stern JA, Kimm S, Hoff F, Rademaker AW. Coronal imaging to assess urinary tract stone size. *J Urol* 2004; 172: 962–964
49. Gong JS, Xu JM. Role of curved planar reformations using multidetector spiral CT in diagnosis of pancreatic and peripancreatic diseases. *World J Gastroenterol* 2004; 10:1943–1947
50. Sheridan R, Peralta R, Rhea J, Ptak T, Novelline R. Reformatted visceral protocol helical computed tomographic scanning allows conventional radiographs of the thoracic and lumbar spine to be eliminated in the evaluation of blunt trauma patients. *J Trauma* 2003; 55:665–669
51. Wintermark M, Mouhsine E, Theumann N et al. Thoracolumbar spine fractures in patients who have sustained severe trauma: depiction with multi-detector row CT. *Radiology* 2003; 227:681–689

52. Hauser CJ, Visvikis G, Hinrichs C et al. Prospective validation of computed tomographic screening of the thoracolumbar spine in trauma. *J Trauma* 2003; 55:228–234
53. Falchi M, Rollandi GA. CT of pelvic fractures. *Eur J Radiol* 2004; 50:96–105
54. Borrelli J Jr, Goldfarb C, Catalano L, Evanoff BA. Assessment of articular fragment displacement in acetabular fractures: a comparison of computerized tomography and plain radiographs. *J Orthop Trauma* 2002; 16:449–456
55. Buitrago-Tellez CH, Schilli W, Bohnert M, Alt K, Kimmig M. A comprehensive classification of craniofacial fractures: post-mortem and clinical studies with two- and three-dimensional computed tomography. *Injury* 2002; 33:651–668
56. Linnau KE, Stanley RB Jr, Hallam DK, Gross JA, Mann FA. Imaging of high-energy midfacial trauma: what the surgeon needs to know. *Eur J Radiol* 2003; 48:17–32
57. Alkadhi H, Wildermuth S, Marincek B, Boehm T. Accuracy and time efficiency for the detection of thoracic cage fractures: volume rendering compared with transverse computed tomography images. *J Comput Assist Tomogr* 2004; 28:378–385
58. Buckwalter KA, Farber JM. Application of multidetector CT in skeletal trauma. *Semin Musculoskelet Radiol* 2004; 8:147–156
59. Pretorius ES, Fishman EK. Volume-rendered three-dimensional spiral CT: musculoskeletal applications. *Radiographics* 1999; 19:1143–1160
60. Quint LE, Whyte RI, Kazerooni EA et al. Stenosis of the central airways: evaluation by using helical CT with multiplanar reconstructions. *Radiology* 1995; 194:871–877
61. Zeiberg AS, Silverman PM, Sessions RB, Troost TR, Davros WJ, Zeman RK. Helical (spiral) CT of the upper airway with three-dimensional imaging: technique and clinical assessment. *Am J Roentgenol* 1996; 166:293–299



## **Section Two**

# **Traumatic Injuries: Imaging and Intervention**



# Hemostatic Arterial Embolization in Trauma Victims at Admission

R.F. Dondelinger, G. Trotteur, B. Ghaye

## 2.1

### Contents

2.1.1	Introduction	41
2.1.2	Classification of Trauma Patients	41
2.1.3	Trauma Patient Triage with Computed Tomography	45
2.1.3.1	Significance of Hemoperitoneum for Patient Triage	45
2.1.3.2	Significance of Organ Injury Demonstration and Injury Severity Grading	45
2.1.3.3	Demonstration of Ongoing Hemorrhage	46
2.1.4	Indications of Therapeutic Arteriography	47
2.1.5	Arteriographic Demonstration of Posttraumatic Hemorrhage	48
2.1.6	Arteriographic Hemostatic Embolization Technique	48
2.1.6.1	Principles	48
2.1.6.2	Percutaneous Arterial Access	49
2.1.6.3	Catheterization Technique for Diagnostic Arteriography	49
2.1.6.4	Carbon Dioxide Arteriography	49
2.1.6.5	Implementation of an Integrated CT-Angiography Unit	49
2.1.6.6	Arterial Hemostatic Embolization Techniques	50
2.1.7	Organ-Specific Hemostatic Embolization	51
2.1.7.1	Splenic injuries	51
2.1.7.2	Hepatic Injuries	51
2.1.7.3	Renal Injuries	53
2.1.7.4	Retroperitoneal Injuries	55
2.1.7.5	Pelvic Injuries	56
2.1.7.6	Other Injuries	58
2.1.8	Conclusion	58
	References	58

### 2.1.1 Introduction

Currently, suicide and trauma are the leading causes of death in the male population under 25 and 40 years of age, respectively, and are responsible for the loss of more years of life than cancer and cardiovascular diseases combined (Trunkey 1983). Traumatic injuries of the central nervous system, heart, and great vessels are responsible for the

deaths that occur at the site of accident, whereas visceral hemorrhage is the principal cause of mortality during the first 4 h following trauma. The vast majority of nonbleeding internal injuries are compatible with survival; therefore, urgent patient admission (“load and go”), rapid resuscitation, and hemodynamic stabilization are the prerequisites for setting management priorities, followed when possible by aggressive and reliable investigation of all posttraumatic injuries for the selection of appropriate treatment

Urgent intervention is the cornerstone of hemostasis. Arteriographic embolization has been shown for several decades to represent a useful adjunct in the treatment of persistent or recurrent postoperative bleeding, and to be a reasonable primary alternative to surgery in retroperitoneal or pelvic bleeding, or in selected patients with abdominal visceral hemorrhage

### 2.1.2 Classification of Trauma Patients

History taking of the mechanism of trauma is helpful in anticipating the presence of potential posttraumatic injuries and to sense their severity. Despite the availability of powerful imaging, the gross clinical findings always take precedence in the sequence of management and imaging. Trauma victims may be classified into three categories for management orientation:

- Patients in class I, who remain hemodynamically unstable despite resuscitation, are directed to the operating room. “Focused Assessment with Sonography for Trauma” (FAST) or a standardized “six-point trauma ultrasonography (US) examination” was introduced as a means of rapid evaluation of the abdomen (and pericardium) in the shock room, and has replaced diagnostic peritoneal lavage, to decide on immediate laparotomy or thoracotomy, without additional imaging (Chiu et al. 1997; Rozycki 1998; Scalea 1999; Nunez et al. 2001)
- Patients in class II are marginally stable, and will probably require surgery (Fig. 1); however, when ongoing retroperitoneal hemorrhage is suspected, these patients should undergo angiography (Ben Menachem et al.



**Fig. 1.** An 18-year-old man was admitted after a car crash. The patient was marginally stable at admission and degraded rapidly during immediate CT examination, which, however, could be completed before emergency laparotomy was performed. **a** Massive contrast extravasation (*asterisk*) within a large area of contusion of the right lobe of the liver. Large perihepatic and perisplenic hemoperitoneum. **b** Extraperitoneal contrast extravasation (*arrow*) is seen in the right anterior pararenal space associated with a perirenal hematoma

1981). Patients with unstable pelvic bone fractures primarily undergo external orthopedic fixation, followed by angiographic evaluation, when pelvic bleeding persists. Presently, many of the marginally stable patients benefit from computed tomography (CT), preceding orthopedic fixation and therapeutic pelvic or retroperitoneal angiography. Marginally stable patients with suspected thoracic or abdominal visceral bleeding can also undergo CT, if the local logistics allow to perform the examination without delay in the resuscitation environment (Fig. 2)

- Patients in class III are hemodynamically stable and are systematically evaluated with CT. Some patients with clinical suspicion of minimal single-organ injury may undergo US or CT without the need for a formal hospital admission

In summary, according to this classification, based on the hemodynamic status, patients either undergo immediate surgery, or hemostatic angiography, alone or in combination with surgery, or they are included in a trial of expectant conservative management





**Fig. 2.** A 50-year-old man was involved in a traffic accident. The patient was marginally stable at admission. Thoracic and abdominal CT were obtained. **a** Thoracic CT showed an irregular contour of the lumen of the descending thoracic aorta (*arrow*) suggestive of a remnant of ductus arteriosus. No peri-aortic hematoma was present. **b** Abdominal CT evidenced extensive contusion of the spleen and intrasplenic foci of persistent contrast extravasation (*arrows*). Notice also a large left pleural effusion. **c** At the inframesocolic level, massive contrast extravasation (*arrows*) is observed at the root of the mesentery. **d** Frontal abdominal display shows the mesenteric hematoma and persistent bleeding (*arrow*) and evidences a large pelvic fluid collection (*asterisk*), displacing the gastrointestinal tract. **e, f** Pelvic fractures of the iliopectic and ischiopubic rami and pelvic hematoma without contrast extravasation are shown. **g** Immediate arteriography was performed following CT

examination. Thoracic aortography confirmed irregularities of the luminal contour (*arrow*), suggesting local posttraumatic mural changes than a remnant of ductus arteriosus. Conservative treatment was applied. **h** Splenic arteriography showed intraplenic arterial displacement in the contused area and contrast extravasation at the lower pole (*arrow*). **i** Hemostatic embolization was obtained with coils. Conservative treatment. **j** Superior mesenteric arteriography showed a local proximal nonobstructive dissection without contrast extravasation (*arrow*). Conservative treatment. **k** Pelvic arteriography showed local contrast extravasation (*arrow*) of a muscular branch of the left superior gluteal artery. **l** No residual extravasation was seen after selective arterial embolization with microcoils. **m** The patient remained hemodynamically stable. A CT scan obtained 10 h later confirm extraperitoneal rupture of the urinary bladder

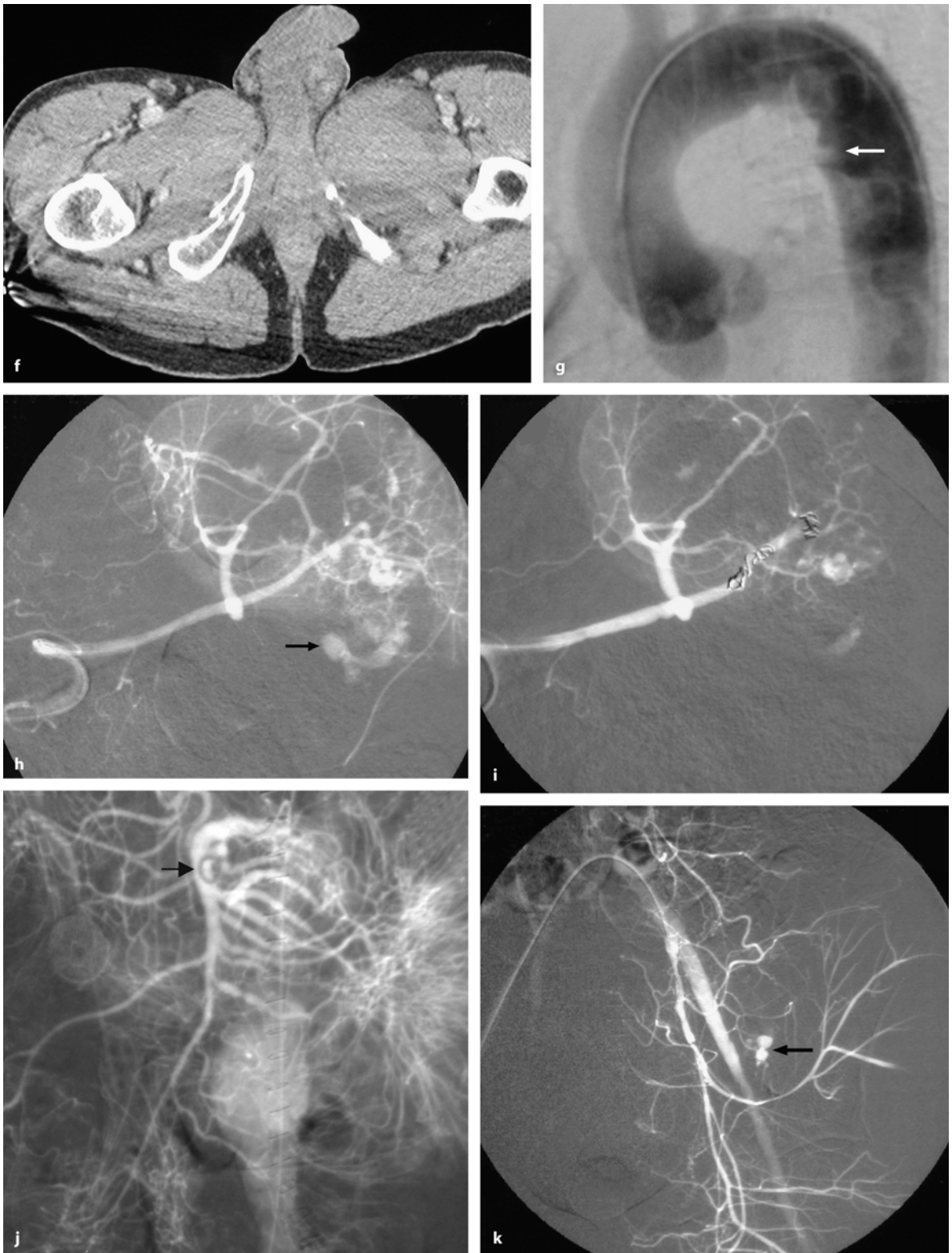


Fig. 2. (continued)

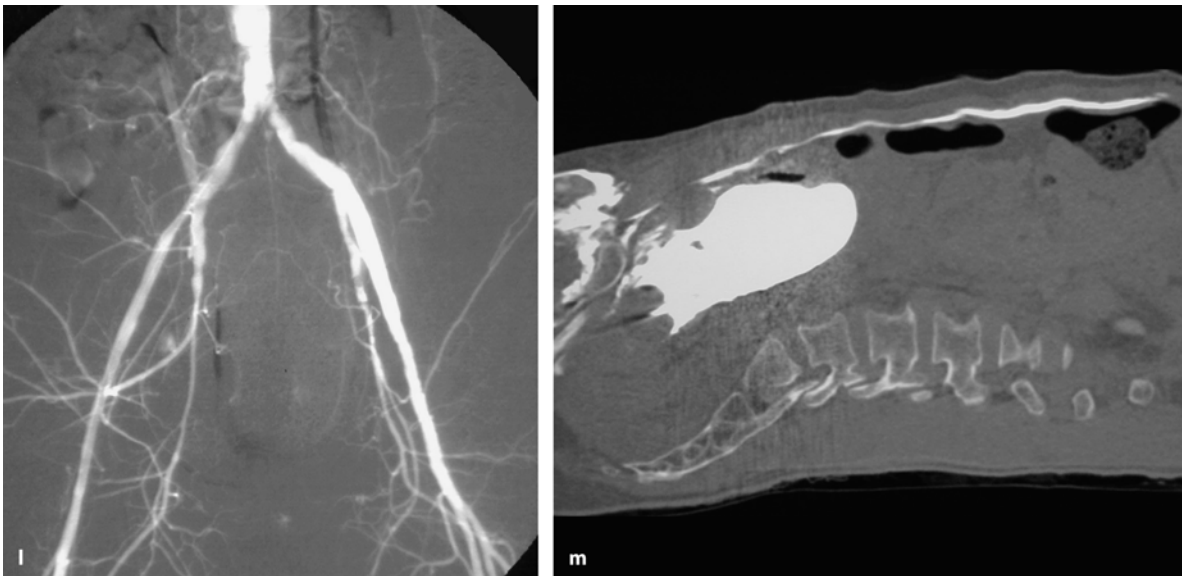


Fig. 2. (continued)

### 2.1.3 Trauma Patient Triage with Computed Tomography

Computed tomography largely contributes to management orientation of trauma victims. Spiral CT has been recognized as the modality of choice for investigation of blunt trauma, allowing for a rapid screening of injuries of the brain, face, thorax, abdomen, spine, and pelvis

#### 2.1.3.1 Significance of Hemoperitoneum for Patient Triage

Both CT and US are able to detect with confidence hemoperitoneum and have largely superseded diagnostic peritoneal lavage; however, the observation of hemoperitoneum is relatively irrelevant for management of stable patients. Peritoneal fluid confirms visceral bleeding but is not a reliable indicator of need for hemostasis. In our experience, 1% of all adult patients with blunt abdominal trauma have hemoperitoneum without detectable abdominal organ injury and 4.3% have no intraperitoneal injury (Dondelinger and Trotteur 2004). In children, 11% were reported to have “unexplained” isolated peritoneal fluid (Taylor and Sivit 1995). In these patients, hemoperitoneum may be caused either by minimal mesenteric bleeding, or by extension of retroperitoneal hematoma into the peritoneal cavity through a ruptured parietal peritoneal leaflet (Freeman and Fischer 1976; Hubbard et al. 1979). On the other hand, we and others have observed parenchymal hepatosplenic injuries of moderate severity grade and

without hemoperitoneum in 11–25% of the cases, when CT was urgently performed after trauma (Dondelinger and Trotteur 2004; Ochsner et al. 2000; Deleuse et al. 2001; Dondelinger et al. 2004)

#### 2.1.3.2 Significance of Organ Injury Demonstration and Injury Severity Grading

There is general agreement that cross-sectional imaging evidences hemoperitoneum more easily than specific abdominal organ injury. A significant false-negative rate of 20–30% might be expected in the diagnosis of parenchymal injuries when using FAST. In hemodynamically stable patients, FAST was shown to be unreliable in comparison with CT, with a sensitivity of only 30% (Mutabagani et al. 1999). Furthermore, in polytrauma patients, US is not applicable to brain, lung, and bone injury

Early CT reports on the first 200–500 patients that were investigated for abdominal or pelvic trauma showed that there were only a few false-positive or false-negative interpretations of abdominal examinations (Federle et al. 1982; Federle 1983). Most papers published thereafter credited CT with overall sensitivities higher than 90% and specificities close to 100% in the diagnosis of abdominal parenchymal injuries in adults and in the pediatric age group. More differentiated injury-specific sensitivities were published for the pancreas (0%), gastrointestinal tract (42%), and urinary bladder (50%; Udekwu et al. 1996). Some publications also reported lower sensitivities of 85, 84, and 67% for renal, hepatic, and splenic injuries, respectively (Lang 1990); however, the accepted statement is that only a few



percent of errors are observed in thoracoabdominal CT, and most missed injuries are generally not responsible for posttraumatic death and do not carry a life-threatening posttraumatic complication

The amount of hemoperitoneum correlates with the need for laparotomy, but the demonstration of high-grade parenchymal injury is not a good predictor for intervention. The amount of hemoperitoneum correlates with the severity of splenic injury, but not with hepatic injury in our experience (Dondelinger and Trotteur 2004). High-grade (III–IV) splenic and hepatic injury may require more often hemostatic intervention than lower-grade injury, but low-grade liver trauma (grades I and II) responds to expectant nonoperative treatment more consistently than splenic injury

### 2.1.3.3 Demonstration of Ongoing Hemorrhage

It is well established that overall 50–70% of all liver and splenic injuries have stopped bleeding at time of operation and can be treated conservatively, without surgery (Sclafani et al. 1984; Moore 1984; Anderson et al. 1986; Beal 1990; Sclafani et al. 1995); therefore, imaging should be able to disclose “active bleeding,” which is expected to serve best as a triage of patients for urgent hemostatic intervention or expectant conservative treatment

As CT is able to detect minimal density gradients, it was hypothesized that small amounts of extravasated contrast medium could be recognized and that CT could give equivalent or superior results to angiography in the diagnosis of active hemorrhage. In fact, ongoing bleeding (25–370 HU, mean 132) can be differentiated from clotted blood (40–70 HU) by measurement of CT attenuation values ( $p < 0.001$ ; Shanmuganathan et al. 1993)

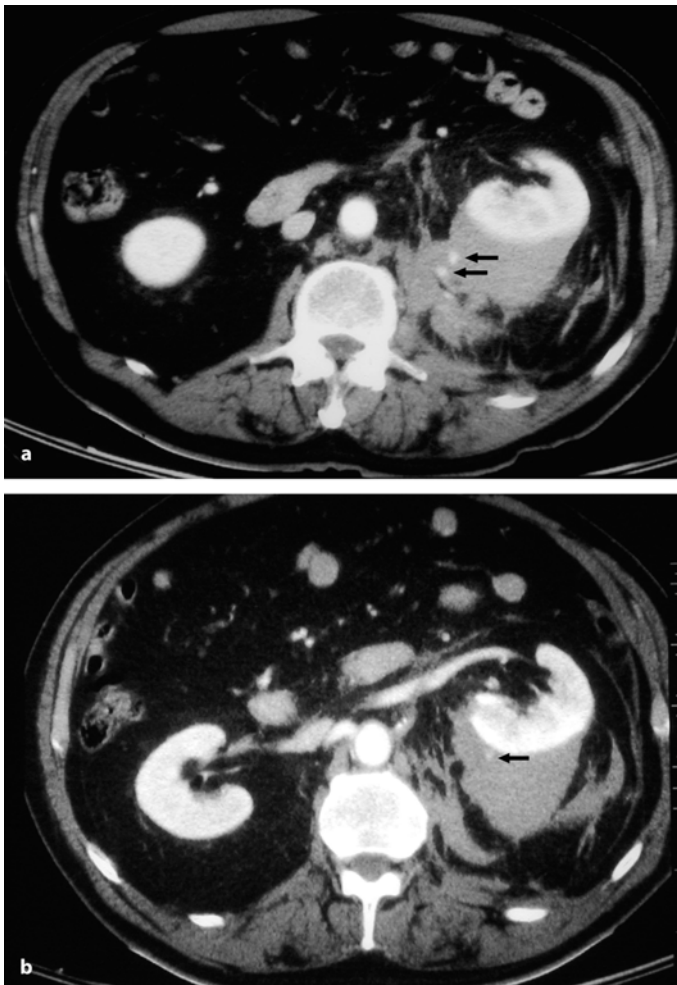


**Fig. 3.** This patient remained hemodynamically stable after a blunt trauma to the left flank. **a** Computed tomography at admission showed a moderate left peri- and pararenal hematoma without significant renal injury, and two small foci of contrast extravasation (*arrows*) within the hematoma. **b** The CT was repeated 24 h later, and still showed a small spot of extravasated contrast material (*arrow*), without increase in volume of the hematoma. No angiography was performed

Extravasation of contrast medium was shown in the spleen to have a high predictive value for surgery even in injuries of minor or moderate grade (Gavant et al. 1997; Federle et al. 1998); however, there is no prospective study comparing CT and angiography in the detection of post-traumatic bleeding. In our personal experience, more than 90% of these angiographies are indicated by a positive CT for contrast extravasation and 90% of angiographies are therapeutic by hemostatic embolization (Kurdziel et al. 1987; Dondelinger and Kurdziel 1991)

Computed tomography may show an intraparenchymal capillary blush, a pseudoaneurysm, an arteriovenous fistula, or contrast accumulation outside the organ capsule, or dilution of contrast medium in peritoneal fluid or sedimenting within a hematoma. Contrast diluting or sedimenting in peritoneal fluid, or increasing size of a hematoma on serial CT examinations, is a definite sign of ongoing bleeding. On the other hand, contrast seen in a hematoma, that does not increase in size, a parenchymal blush, a pseudoaneurysm, or an arteriovenous fistula do not necessarily indicate per se persisting bleeding (Fig. 3). Some posttraumatic vascular lesions, particularly those of small size, may thrombose spontaneously and completely regress without intervention. It is quite common to observe blushes of contrast in pelvic or retroperitoneal muscles, which have a benign prognosis compared with similar images seen in a plain parenchyma; therefore, the hemodynamic status of the patient, the number of blood transfusions, his or her ability to coagulate, metabolic parameters, and the overall assessment of severity of injury and type and number of associated lesions should be considered before indicating arteriography for hemostasis. Among CT findings, contrast extravasation is the most reliable sign for deciding on angiographic intervention or surgery

### 2.1.4 Indications of Therapeutic Arteriography

As trauma victims are triaged by clinical assessment and CT for conservative management or intervention, arteriography is no longer used as a primary tool in demonstrating thoracoabdominal injury. In the pre-CT era, arteriography was first shown to be accurate in demonstrating renal injury (Lang 1976), but correlation was poor with the pathological findings in splenic injury and arteriography was found an unreliable predictor of management decision. A false-negative angiogram was observed in 24% of patients with splenic injury (Fisher et al. 1981). Similar criticism could be extrapolated to other parenchymal or extraparenchymal injuries, studied angiographically. Over the past 20 years, with the advent of US and CT, the role of arteriography in trauma changed from a diagnostic to a therapeutic modality

Despite the fact that hemostatic embolization was recognized as an efficient means of treatment, arteriography is often not considered at the early posttraumatic phase while blood loss is still compensated and coagulation and other homeostatic parameters are still within normal limits. Arteriography is often requested when surgery has failed to obtain definite hemostasis, or when resuscitation was protracted. Time loss has been significantly decreased in the diagnostic process in specialized trauma centers, by scanning of trauma victims on a CT unit that is installed within the emergency environment. Diagnostic efficiency has also been increased by the availability of radiologists who are dedicated to trauma and on-call around the clock. Despite the interest of radiologists in trauma, therapeutic angiography is not applied to its full potential. Reasons for its underemployment are multifold: the absence of an integrated global diagnostic and therapeutic approach of the trauma patient by radiologists is a major limitation. General radiologists who read the CT examination of a trauma patient have a different approach than a trauma-dedicated interventional radiologist. Residents who read CT examinations in the emergency room and are not interested in sharing responsibility in therapy are inadequate partners for case discussion with trauma surgeons or intensive care physicians on management options. Due to the dramatic decrease of diagnostic visceral angiographies, it takes many years to train a radiologist in all aspects of interventional angiography. Besides the logistic and functional problems encountered in a radiology department in offering a full range “radiological trauma service,” other factors may lead to an untimely implementation of hemostatic angiography or surgical treatment (Ben Menachem et al. 1981; Ben Menachem 1988):

- Over-reliance on a technically inadequate CT examination, or declaring that injuries recognized on CT are not at risk of bleeding
- Miscalculation of the severity of injury: a shock status should not be attributed to brain injury alone, unless proved otherwise. Children compensate for considerable blood loss by maintaining normal blood pressure for a longer period of time than adults. Clinical examination and laboratory findings are not reliable predictive factors of need for hemostatic intervention in children or adults. Absence of contrast medium extravasation on a positive CT for injuries is not a sign of definite hemostasis. A patient may rebleed, when arterial pressure has increased again, and vasoconstriction has ceased, or after endogenous clot lysis. The most severe injury seen on CT is not necessarily one that will rebleed: a severe splenic contusion might have stopped bleeding, whereas an injured lumbar artery goes on bleeding profusely
- Inadequate assessment of the mechanism of injury: in blunt trauma, right, left, and midline package abdominal injury must be understood to extrapolate all potential organs that might be involved together in the same anatomical area. Injuries created by contra-coup are

located on the opposite side to the impact, and can be a concomitant source of bleeding (Rao et al. 1997)

- Inadequate assessment of postoperative hemorrhage: a missed or an inadequately treated vascular injury, rather than a wash-out coagulopathy, should be searched for when hemorrhage persists or recurs after operation. A marginally stable patient who is transferred to a specialized trauma center after a damage control laparotomy should undergo systematic arteriography, before reintervention, to disclose either a missed or an additional iatrogenic vascular injury, created during the first intervention. Computed tomography alone may not be sufficient, as selective arteriography is able to show more small vascular injuries than CT
- A classical adage recommends “never put an unstable patient on the X-ray table”: CT and angiography can be obtained in the emergency room environment, whereas resuscitation is ongoing. Unnecessary patient transfer can be avoided by the use of a combined CT-angio room (Capasso et al. 1996; Kos et al. 1999). Unstable patients with retroperitoneal hemorrhage that is best treated by selective embolization should be deliberately moved to the angiography suite, provided that medical and paramedical radiological expertise is available to the same degree as in the surgical facility

**Table 1.** Arteriographic signs of vascular or parenchymal injury

Arterial cut-off
Mural irregularities or flap
Laceration
Thrombosis
Dissection
Free flow contrast extravasation
Stagnant intraparenchymal accumulation of contrast
Parenchymal blush
Stagnant arterial or venous flow
Diffuse vasoconstriction
Pseudoaneurysm
Arteriovenous fistula
Vessel displacement
Intraparenchymal avascular zones
Disruption of visceral contour
Displaced organ

contained way, into a pseudoaneurysm or an arteriovenous fistula that may persist, thrombose and regress or enlarge and rupture later. In our experience, there is an excellent overall correlation between CT and arteriography in demonstrating active bleeding, and the combination of the two modalities enhances diagnostic capabilities (Kurdziel et al. 1987; Capasso et al. 1996)

## 2.1.5 Arteriographic Demonstration of Posttraumatic Hemorrhage

Angiography was introduced as a diagnostic modality of visceral injury in the mid 1950s, and was used extensively during the 1960s and 1970s and less thereafter in the evaluation of visceral or large vessel trauma (Norell 1957; Vogler and Bergmann 1963). Arteriographic signs of vascular or parenchymal injury are listed in Table 1, but some are not specific for a traumatic origin when taken as an isolated finding

Overall, angiography confirms posttraumatic arterial bleeding in about 80–90% of cases. Results are affected mainly by false negatives, caused by intermittent vasospasm, spontaneous vasoocclusion of a bleeding artery by thrombus formation coexistence of several bleeding sites, venous, or capillary bleeding that is not shown by arteriography, or technical inability to catheterize selectively the bleeding artery. False positives are due to erroneous film interpretation: an adrenal blush, gastric or intestinal wall, a vessel seen end-on or overlying vessels, and stagnant capillary flow or venous stasis should not be taken for contrast extravasation, or for a vascular lesion

The arteriographic pathognomonic sign of extraluminal contrast extravasation is not 100% prognostic for ongoing hemorrhage: a limited extravasation within a parenchyma or within a hematoma may evolve in a self-

## 2.1.6 Arteriographic Hemostatic Embolization Technique

### 2.1.6.1 Principles

After having localized one or several sources of hemorrhage angiographically, hemostasis is obtained by catheter embolization. Hemostatic endovascular embolization technique is different in principle from (chemo)embolization for tumor mass or organ function reduction or vasoocclusion of a vascular malformation. Spontaneous hemostasis is induced by vasoconstriction and formation of a clot at the site of vascular tear and subsequent scar formation by granulation tissue or vessel recanalization. Catheter-mediated treatment should be derived from the physiological process of hemostasis:

- A temporary arterial occlusion with resorbable material may be sufficient to initiate local thrombus formation. Late vessel recanalization is not a concern
- Vasoocclusion should take place exclusively at the site of vascular injury
- No or minimal tissue loss should be induced by embolization
- Recurrent bleeding should be avoided by formation of a stable clot



---

### 2.1.6.2 Percutaneous Arterial Access

Percutaneous access is gained in general by a right or left femoral approach. When major pelvic bone fractures or severe tissue damage is present at the inguinal region, the opposite femoral side or a left brachial or axillary arterial puncture is chosen. In a hypotensive patient with a faint pulse, ultrasound Doppler guidance or bone landmarks may be helpful under fluoroscopy control to guide vessel puncture. When the femoral vein was inadvertently punctured, venous access should be preserved and a hemostatic valve sheath should be placed. The sheath can serve as a landmark for the arterial puncture, and as an additional large-flow infusion line. A 5-F valve sheath is adequate for diagnosis and embolization, and is particularly useful in trauma angiography, allowing for rapid catheter exchange or immediate withdrawal of a catheter blocked with plugged embolization agents or a partially delivered coil

---

### 2.1.6.3 Catheterization Technique for Diagnostic Arteriography

Despite the fact that 90% of angiographies are based on contrast extravasation, which was shown by CT, a midstream thoracic or abdominal and pelvic aortogram should always be obtained before selective catheterization (Sclafani 1985). An aortogram shows the mapping of aortic collaterals, anatomical variants, and unsuspected traumatic or nontraumatic preexisting lesions. It also establishes priorities in selective catheterization, when several bleeding sites coexist. Selective arteriography is based on CT and midstream aortography findings. Preshaped sidewinder Simmons type or Cobra shaped 4- or 5-F catheters are usually adequate for most catheterizations. Catheter manipulation should be carried out rapidly, but gently, avoiding creation of endothelial injury, which prevents from further catheterization. Vasoconstriction in a shocked patient favors arterial dissection by the catheter tip and thrombosis. Hydrophilic catheters and guidewires are helpful. A negative midstream aortogram does not eliminate the possibility of extravasation, as concentration of contrast medium, flow, and pressure conditions are different at the site of vascular injury during an aortic or a selective arterial injection. Care must be applied to obtain a selective arteriogram of the hepatic, splenic, or renal artery, for instance, with a proximal position of the catheter tip. A too distal catheterization may miss significant branches, such as an upper pole splenic artery, or a proximal division of a renal or common hepatic artery

---

### 2.1.6.4 Carbon Dioxide Arteriography

Carbon dioxide digital subtraction angiography (CO<sub>2</sub> DSA) was introduced in the early 1980s and thereafter was applied to the diagnosis of vascular injury in a limited number of studies (Sato et al. 1991; Hashimoto et al. 1997; Hawkins et al. 1997). The assumption was that thanks to the lower viscosity of CO<sub>2</sub>, compared with iodinated contrast medium, even minute bleeding through a minimal tear in the vascular wall can be seen. In one series, intra-arterial CO<sub>2</sub> DSA demonstrated extravasation in 52% of the cases, whereas iodinated contrast extravasation in only 13% of the same patients (Hashimoto et al. 1997). It has not been proven whether or not extravasation shown by CO<sub>2</sub> DSA, and which was not evidenced on iodine DSA, requires hemostasis in all cases. Injection into the hepatic artery shows arteriportal shunting in normal liver, and CO<sub>2</sub> may still pass in the gastrointestinal lumen after embolization, despite demonstration by iodine angiography of complete vaso-occlusion; therefore, CO<sub>2</sub> DSA is at risk of overdiagnosing extravasation or arteriportal fistula and when used alone, without iodine angiography, may lead to overtreatment. The CO<sub>2</sub> DSA is too sensitive to determine significance of bleeding and to appreciate the end point of embolization (Hawkins et al. 1997). Advantages of CO<sub>2</sub> DSA are absence of allergic reaction, or nephrotoxicity or other significant side effects, low cost, unlimited permissible volume, and easy passage through the smallest catheter; however, due to the possible gas embolism in the brain or myocardium, intra-arterial injection is contraindicated in arteries located above the diaphragm

---

### 2.1.6.5 Implementation of an Integrated CT-Angiography Unit

The use of an integrated CT-angiography unit has undeniable advantages in urgent angiographic management of posttraumatic hemorrhage (Capasso et al. 1996; Kos et al. 1999). Both machines are preferably installed in the Emergency Department environment and are linked with a common patient support. The table may be shifted or turned from the CT to the angiography position, and vice versa, as in the prototype unit that we have designed. Other room configurations have been envisioned, such as an alignment of the CT gantry and the C-arm, making pivoting of the table unnecessary, or a mobile angiography C-arm and/or a mobile CT gantry (Fig. 4). The CT and angiography unit can also be installed separately in adjacent rooms for independent use and are brought together on rails, only when needed. No mobilization of the patient, or of the anesthesiology team or ancillary equipment, is required. Prolonged transit time of the trauma patient in the radiology suite and the risk of severe hypothermia is



**Fig. 4.** A CT scanner and an angiography unit with a mobile C-arm are installed together in the emergency environment. Both units are served by a common patient support, avoiding patient mobilization and time loss between CT examination and hemostatic arteriographic embolization

avoided. Absence of patient mobilization minimizes creation or increase of damage in hypotensive patients or those presenting with spinal or pelvic bone fractures

A radiologist who is an expert in trauma imaging, including CT and vascular diagnostic and interventional procedures, should be on duty to insure the full potential of such an integrated CT-angiography suite. Reading the CT examinations is now done exclusively on the console, using the cine mode, and the decision to treat arterial hemorrhage by embolization should be made immediately at the end of the CT examination by the multidisciplinary trauma team

#### 2.1.6.6 Arterial Hemostatic Embolization Techniques

Selective catheterization is directed without time loss to the bleeding artery, but an overview angiographic run, demonstrating the entire organ or region, is mandatory before selective catheterization to recognize all arteries feeding the bleeding site. The bleeding arterial branch should be catheterized as selectively as possible to avoid undesirable tissue infarction, or amputation of organ function. Injection of the embolizing agent is thus precisely targeted, the tip of the catheter being placed proximal to the site of extravasation. This is the regular technique for intra-

parenchymal end arteries such as in the splenic or renal parenchyma. Five-French catheters are usually too large for a selective catheterization of the site of hemorrhage; 3-F or 2-F catheters, which are introduced coaxially, are best suited for a targeted deposition of embolization material. Selective angiograms by manual injection of several milliliters of contrast, are sufficient to check the catheter position and flow conditions before embolization. Road-mapping technique, multiple projections, and direct magnification are useful

The principal agents used for vaso-occlusion in trauma include gelfoam soaked in an antibiotic solution, coils, and particles. Gelfoam pledgets of variable size are cut and injected with a syringe containing contrast medium. Small fragments of gelfoam pass through the lumen of a 3-F catheter. Gelfoam powder should be avoided, as it may result in too distal embolization, carrying the risk of tissue infarction or late abscess formation. Coils come in different shape, length, and diameter. Their main advantage is a precise targeted delivery. When properly selected, secondary coil migration after delivery almost never occurs. Coils with a tornado configuration allow for immediate luminal occlusion by a compact coiling. Particulate material of small size (100–500  $\mu\text{m}$ ) is used during flow directed embolization of a bleeding source, which is located in a small vessel. The risk of fan embolization in adjacent territories is higher with particles than with gelfoam pledgets

Vaso-occlusion can also be simply achieved by an occlusive catheterization of an end artery, such as in the kidney or spleen. Iatrogenic posttraumatic intrarenal pseudoaneurysm or arteriovenous fistula may thrombose, by simply stopping the flow for several minutes, whereas the tip of the catheter is maintained in an occluded position. In non-iatrogenic injury, however, this technique is not recommended, as several potentially hemorrhaging injuries might coexist on the same artery, or the ability of the patient to coagulate may be impaired, resulting in rebleeding

When an arterial rupture with discontinuous flow is evidenced in a lobar liver artery, for instance, a sandwich embolization technique is used, placing coils distal and proximal to the arterial interruption. When a pseudoaneurysm is present, a similar sandwich technique should be used, but never intrasaccular filling with coils. Indeed, the pseudowall of a recent posttraumatic pseudoaneurysm is extremely fragile and may rupture at the contact of the guidewire or catheter tip. Intrasaccular filling with coils increases the pressure in the sac, which may result in acute or delayed rupture and fatal hemorrhage if the parent vessel remains patent

Embolization with coils in the splenic artery, proximal to the hilar branching, was described as an equivalent to the surgical Keramidas procedure. The intervention consists of ligation of the splenic artery at the splenic hilum, without creating necrosis to the spleen, which remains vascularized through epiploic, short gastric, and transcapsular arteries (Keramidas 1979). This technique might be used in

high-grade splenic injury, without extravasation seen, as a preventive treatment of rebleeding. Proximal embolization of the renal and hepatic artery is contraindicated, as irreversible renal ischemia would follow as well as severe disturbances of the liver function, particularly in a patient with traumatic shock

A large artery that shows a cut-off on arteriography should be embolized systematically with coils, proximal to the complete vessel interruption, even in the absence of contrast medium extravasation, to avoid rebleeding after resolution of vasospasm and endogenous thrombolysis. High-pressure injection of contrast medium through a catheter placed close to a large thrombosed artery (iliac artery for instance) should be avoided, as a primary hemostatic thrombus may be fragmented by pressure and the ruptured vessel may open again to extravasation. The burst effect of injection of CO<sub>2</sub> may have similar effects

A tangential vascular wall rupture in a large-caliber patient artery (iliac, subclavian artery) can be treated by urgent placement of a covered metal stent. Posttraumatic rupture of the thoracic aorta at the level of the isthmus or descending portion have been treated in semiurgent conditions by placement of a stent graft (Rousseau et al. 1999)

## 2.1.7 Organ-Specific Hemostatic Embolization

### 2.1.7.1 Splenic injuries

In the spleen, transcatheter hemostatic arterial embolization is carried out in selected patients, as an alternative to surgical spleen preserving interventions (Chuang and Reuter 1975). Indications are based on focal intra- or extrasplenic contrast medium extravasation seen on CT. In the spleen, helical CT confidently predicts extravasation observed on splenic arteriography and the need for hemostatic arterial embolization (Shanmuganathan et al. 2000). Splenic arteriography precisely localizes a pseudoaneurysm or an arteriovenous fistula or thrombosis of a disrupted arterial branch. The systematic use of microcatheters that are introduced coaxially through a guiding catheter, placed in the proximal part of the splenic artery, allows a selective catheterization of a bleeding intrasplenic branch. Technical failures caused by tortuosity of the splenic artery are thus limited. As intrasplenic arteries are terminal vessels, selective embolization of the branch, proximal to the site of extravasation, gives a definitive vaso-occlusion, without risk of recanalization by collateral or retrograde flow. When several intrasplenic bleeding sites are documented, each branch feeding an extravasation should be selectively catheterized and embolized close to the vascular injury, to limit the extent of splenic tissue infarction. Minicoils or particulate agents are most often used in the smallest arterial branches. Placement of macro-

coils or large gelfoam fragments in the main splenic artery at the hilar bifurcation, as an equivalent to arterial ligation (Keramidas intervention), should be avoided except in a shattered spleen, as a prevention of rebleeding, when no extravasation is seen (Fig. 5; Keramidas 1979). Reducing the pressure in the intrasplenic arteries by a proximal embolization in the main splenic artery might not be sufficient to obtain a permanent hemostasis, and massive splenic gastric wall or pancreatic infarction is a potential complication when a too proximal embolization has been performed

Selective embolization, without the need for subsequent splenic surgery, being part of the initial management protocol and based on extravasation seen on CT or angiography, is successful in 87–95% of cases (Sclafani et al. 1991; Hagiwara et al. 1996). In another study, an intrasplenic blush of contrast was seen on CT in 8% of patients with blunt splenic injury, and confirmed to be a pseudoaneurysm on arteriography; 20 of 26 patients were successfully embolized, and 6 underwent splenectomy for technical failure of embolization (Davis et al. 1998). In a personal experience of 19 patients managed with arterial splenic embolization at admission, bleeding was stopped in 17 without requiring splenectomy. Computed tomography shows on postembolization examinations splenic infarcts in two-thirds of the patients after proximal embolization and in all cases after distal vaso-occlusion. Gas in the embolized splenic area or in small arterial branches may be seen, particularly after gelfoam embolization. Necrotic areas, liquefaction, and air/fluid level are suggestive of abscess formation (Killeen et al. 2001)

### 2.1.7.2 Hepatic Injuries

Hepatic artery embolization was shown to be a valuable adjunct in the management of posttraumatic hepatic hemorrhage (Boijssen et al. 1966; Bass and Crosier 1977; Allison et al. 1985). Embolization on an emergency basis and as a primary hemostatic treatment was reported in small series of patients (Fig. 6; Bass and Crosier 1977; Allison et al. 1985; Jander et al. 1977; Rubin and Katzen 1977; Hashimoto et al. 1990). Emergency arterial liver embolization can be performed in marginally stable patients with complex liver injury in specialized centers. Other reports illustrated the value of arterial embolization for ongoing or recurrent hemorrhage, despite laparotomy (Bass and Crosier 1977; Wagner et al. 1985; Toma et al. 1994). General indications for angiography and arterial hepatic embolization are evidence of continuous hemorrhage, or patients who remain borderline after resuscitation and in whom contrast medium extravasation or intraparenchymal blush or contrast staining is seen on CT (Sherman 1996; Gorich et al. 1999; Harper and Maull 2000). Such a management requires optimal organization and skills in the radiology department (Sugimoto et al. 1994). Patients with early ongoing hepatic

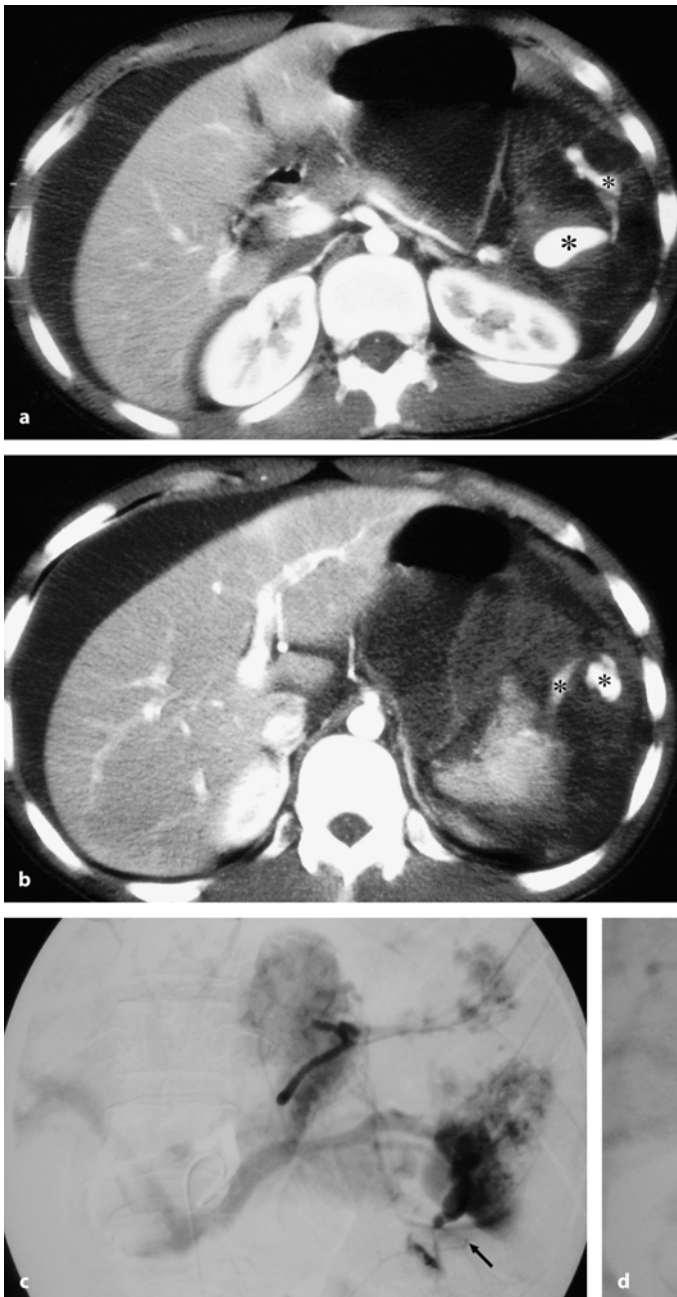


**Fig. 5.** This patient was admitted in shock after blunt abdominal trauma. **a,b** A CT scan at admission showed a shattered spleen with multiple sites of contrast extravasation (*asterisk*), an intra- and perisplenic hematoma and perihepatic hemoperitoneum. **c** Splenic arteriography was obtained on an integrated CT-angiography unit, without patient transfer. The parenchymal phase showed a fragmented spleen and contrast extravasation at the lower pole of the spleen (*arrow*). **d** Embolization of the splenic artery with large gelfoam fragments was obtained at the level of the hilar bifurcation (*arrow*) for immediate and definitive hemostasis

bleeding after primary surgical hemostasis, and patients who are referred after a crash laparotomy should also undergo arteriography, and when necessary, embolization, obviating reoperation (Toma et al. 1994). Patients who rebleed after an initially successful embolization should be treated again angiographically. Arterial embolization is said to contribute to the overall better outcome of liver injuries, which is also explained by a relative decrease of major liver injuries and improved surgical results for major injury (Richardson et al. 2000)

In a recent study, arterial embolization was shown to be 100% effective to treat extravasation of contrast medium in the liver, following blunt hepatic injury, in a cohort of hemodynamically stabilized patients with 52% grade-3 and grade-4 injury. Of patients submitted to angiography, 54% showed contrast extravasation. Following embolization, CT was repeated during 3 weeks, once a week. A pseudoaneurysm was detected during follow-up in 6% of patients and treated by embolization. Overall mortality was 0%; however, 2 patients developed severe hepatic hem-



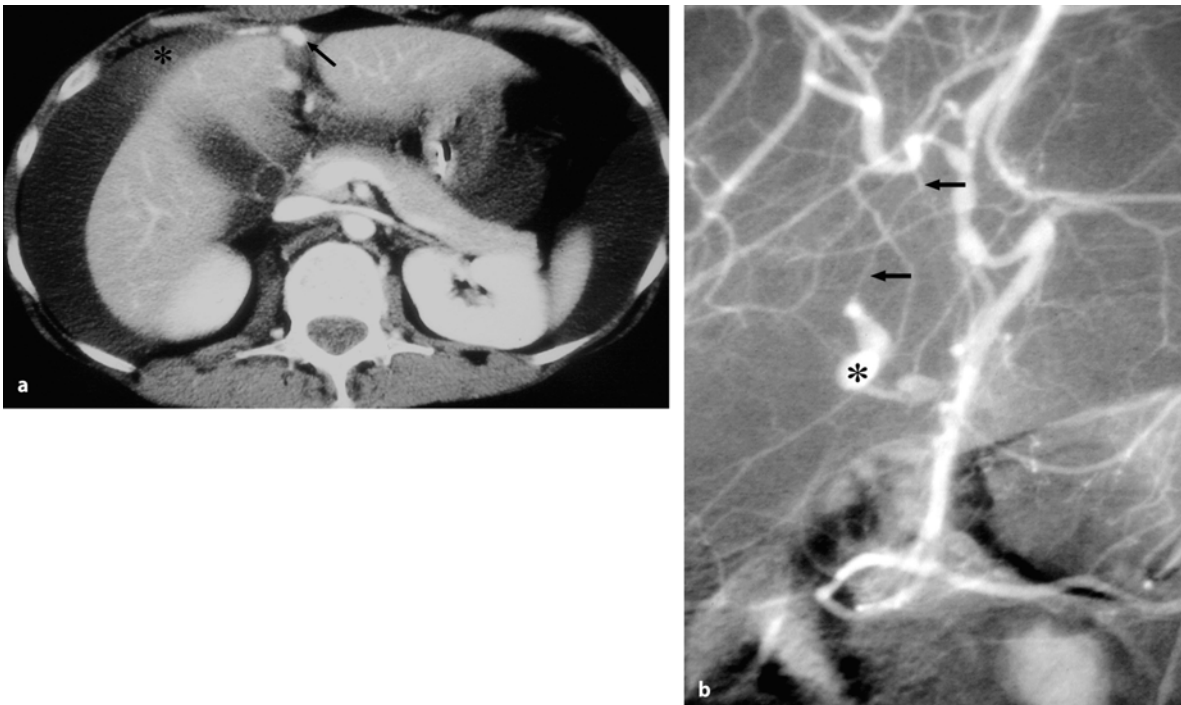


**Fig. 6.** A nurse was involved in a traffic accident on her way home from work. **a** A CT scan at admission showed massive perihepatic and perisplenic hemoperitoneum and extravasation of contrast medium, originating from the anterior liver convexity (*arrow*) and diluting in the hemoperitoneum (*asterisk*). No major liver contusion was seen. **b** The patient was marginally stable. Hepatic arteriography showed bleeding (*asterisk*) originating from a small branch

of the quadrate lobe artery (segment IV; *arrows*). The quadrate lobe artery was embolized with multiple coils, and two additional coils were placed proximally in the right hepatic artery to prevent rebleeding by collateral flow, as the patient had developed a washout coagulopathy after massive blood transfusions. The patient was stabilized without hemostatic abdominal surgery

orrhage at 2 and 3 weeks following admission, requiring a second emergency embolization of a bleeding pseudoaneurysm (Hagiwara et al. 1977). In another study, 16 of 30 patients with blunt liver injury underwent arterial hemostatic embolization. Patients were markedly unstable and had hemoperitoneum, deep liver laceration (grade III) and contrast extravasation on angiography in 14 of 16 patients. Patients were stabilized after embolization and no major complications were observed (Murakami et al. 1993). In another study of 24 patients with posttraumatic vascular lesions, transcatheter occlusion was successful in 88% of cases. Cause of failure was inability to catheterize the lesion with the catheter, persistent flow in an arteriovenous fistula after embolization, and late recurrence (Schwartz et al. 1993). Patients with grade-IV and grade-V hepatic injury, and who remain hemodynamically stable with continued resuscitation, could undergo hepatic arteriography and embolization. Treatment was effective in 10 of 11 patients (Giraulo et al. 1998)

Recent experience in high-grade liver injury (grades IV and V) managed with a surgical, angiographic, and endoscopic biliary approach showed an overall mortality of 14%, and hepatic-surgery-related mortality of 9% (8% for grade IV and 22% for grade V; Asensio et al. 2000)

Complications of arterial hepatic embolization mainly include rebleeding due to incomplete vaso-occlusion or coagulopathy, and later hepatic infarction or abscess, bile duct, or gallbladder necrosis or bilo-hematoma. Hepatic infarct is most likely to occur when the portal vein or a lobar branch is occluded concomitantly to arterial embolization (Takakuwa et al. 1993). Delayed rebleeding after embolization is reported only in a small percentage of patients. Emphasis is put on the possible relation between a biloma and formation of a pseudoaneurysm that is responsible of secondary hemorrhage, despite initially successful embolization (Hagiwara et al. 1993)

### 2.1.7.3 Renal Injuries

Renal contusions are accessible to conservative management in the majority of the cases; however, avulsion of the vascular pedicle must be treated surgically in the first hours following injury to preserve renal function. Renal arteriography is indicated, based on CT findings, when extravasation of contrast is seen in or around the kidney. Extravasation should not be confused with extravasated opaque urine, resulting from a previous contrast injection

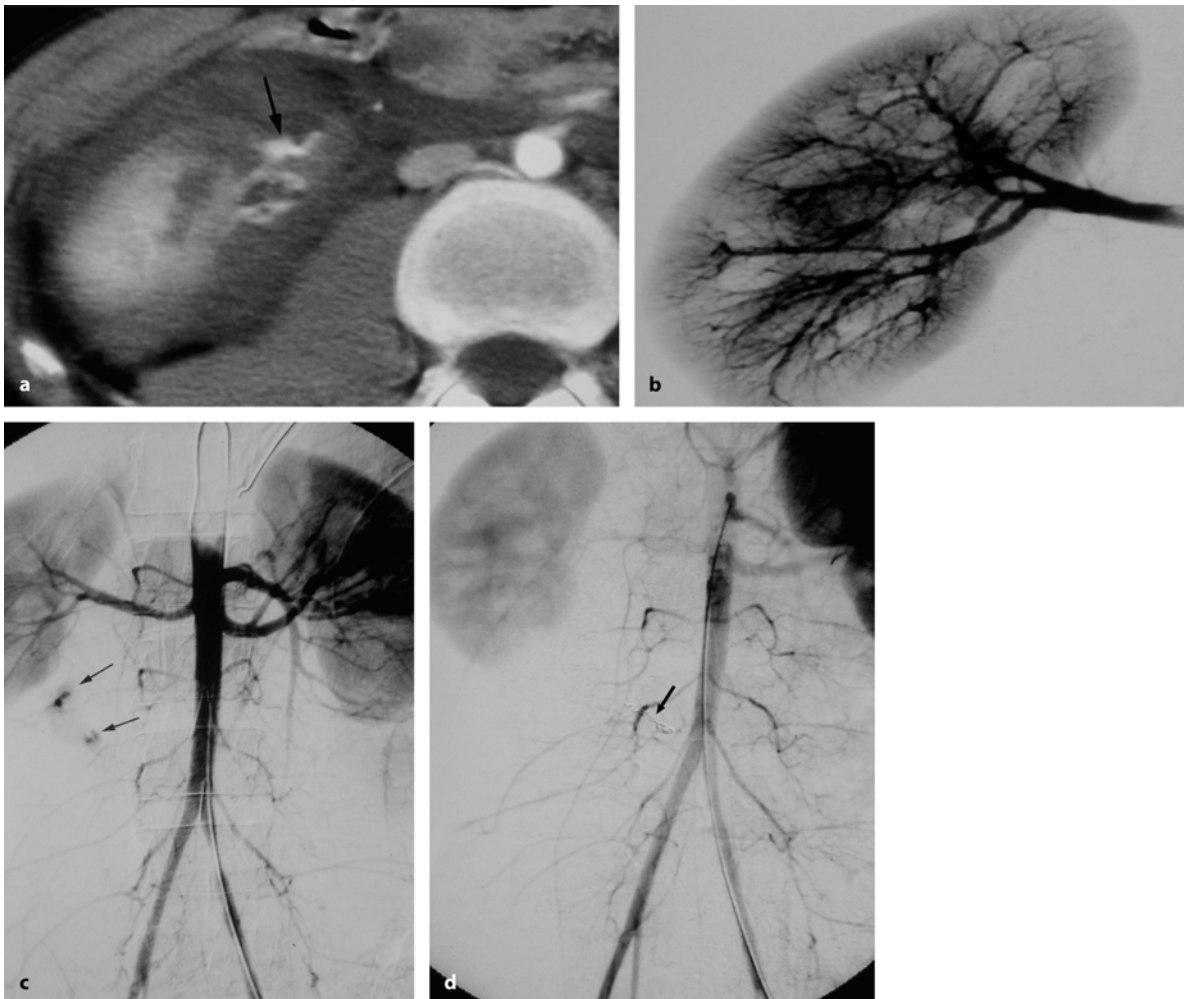


**Fig. 7.** Young patient with a blunt right flank impact. **a** A CT scan at admission shows, at the arterial phase, contrast extravasation around the lower pole of the right kidney, a limited renal parenchyma contusion, and perirenal and retroperitoneal hematoma. **b** Selective arteriography of the right kidney was normal. Note flattening of the contour of the lower pole, suggesting

the presence of a polar artery. **c** Abdominal aortography shows two foci of contrast extravasation (*arrows*) originating from a small lower pole renal artery, originating from the distal abdominal aorta. **d** After embolization of the lower pole renal artery with microcoils, no extravasation is seen on abdominal aortography. Note position of microcoils (*arrows*)

(brain CT, IVP, others). In some hemodynamically unstable patients, with evidence of a flank impact and suspicion of massive renal and/or retroperitoneal hemorrhage, urgent arteriography may be obtained without a previous CT examination. Renal arteriography must include a midstream aortogram to confirm the presence of a normal contralateral kidney and display the number and origin of renal arteries (Fig. 7). Embolization should be carried out rapidly, before a subcapsular hematoma severely compresses the underlying renal parenchyma, and makes selective intrarenal catheterization difficult or impossible. Number and location of the bleeding sites must be precisely identified by serial angiographic runs during and after embolization. The use of 3-F catheters for selective distal intraparenchymal catheterization is standard

(Fig. 8). When multiple intraparenchymal arteries bleed, requiring total nephrectomy, complete vaso-occlusion is an alternative, allowing to control other associated injuries first and perform nephrectomy later in a stabilized patient

Hemostatic embolization in the kidney is successful in 82–100% as a primary treatment (Fisher and Ben-Menachem 1985). When hematuria persists or recurs, renal arteriography should be repeated, and when positive, a persistent or new vascular injury should be reembolized. Less than 10% of severe complications are noticed following embolization, including sepsis, urinary fistula, or renal infarction (Fisher et al. 1989; Larsen and Pentecost 1992)



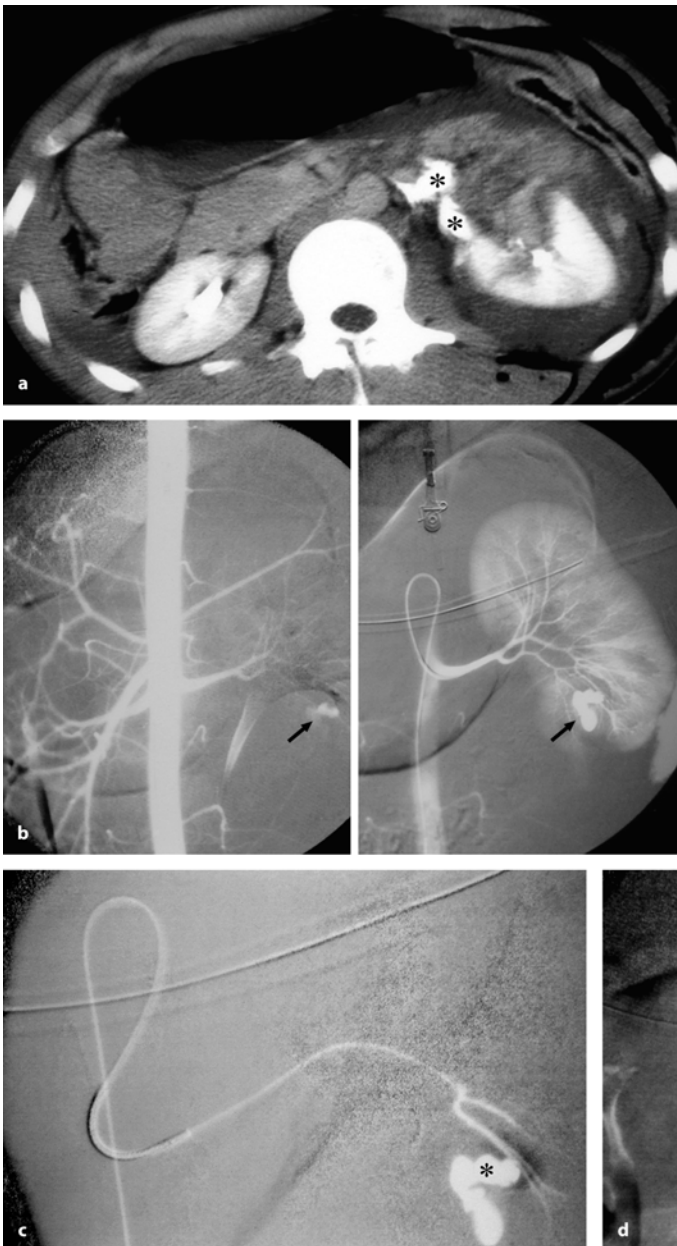


**Fig. 8.** This patient was admitted in preshock after a blunt impact in the left flank. **a** A CT scan showed contrast extravasation at the arterial phase, accumulating at the hilum of the left kidney. Extravasated high-density arterial contrast (*asterisk*) should not be mistaken for extravasated urine at the late phase, after IV contrast medium injection. **b,c** Midstream abdominal aortography and left renal arteriography were obtained immediately after CT on a combined CT-angiography unit. Contrast extravasation (*arrow*) is better seen on selective renal arteriography than on aortography. Note diffuse arterial vasoconstriction due to retroperitoneal hemorrhage. The bleeding site was evidenced angiographically (*asterisk*) and treated by selective embolization with microcoils by a coaxial catheterization technique. **d** Left renal arteriography after embolization shows vascular amputation of the lower-pole renal parenchyma. Note position of microcoils (*arrows*)

#### 2.1.7.4 Retroperitoneal Injuries

Posttraumatic retroperitoneal bleeding is primarily investigated and treated angiographically. Often, surgery carries the risk of cataclysmic hemorrhage by dissection of the retroperitoneal space and loss of passive tamponade of a hematoma. Classically, one or several lumbar arteries bleed, and giant pseudoaneurysms can be found. Other arterial branches, such as originating from intercostal, inferior phrenic, adrenal, pancreaticoduodenal, and other arteries, may participate in feeding a retroperitoneal hem-

orrhage (Fig. 9; Chang et al. 1978; Haydu et al. 1978; Fankuchen et al. 1981). These arteries should be catheterized selectively, when a retroperitoneal hematoma increases in size and no extravasation is demonstrated on abdominal aortography and selective lumbar arteriography. In some cases, when selective arteriography and intravenously injected CT are negative for contrast extravasation, a selective arterially enhanced CT may be the only modality, which is able to show the bleeding (Kos et al. 1999). When a lumbar or intercostal artery must be embolized at the thoracolumbar level, the origin of a spinal artery must be recognized, and inadvertent embolization is avoided by



**Fig. 9.** An 80-year-old woman was admitted after blunt abdominal trauma. The patient became unstable several days after admission and complained of left flank pain. A CT scan showed a large left retroperitoneal hematoma without contrast extravasation. **a,b** An arterially enhanced CT examination was obtained on an integrated CT-angiography unit. The catheter was placed selectively in the left inferior epigastric artery (*arrow in a*). Extravasation was seen (*arrow in b*) within the left retroperitoneal hematoma. **c** No extravasation was seen on selective digital subtraction angiography of the left inferior epigastric artery. **d** Despite the negative arteriography, but positive CT, the left inferior epigastric artery was embolized with microcoils (*arrow*). The patient stabilized after hemostatic embolization

distal catheterization and the use of large-size particles. The metameric levels adjacent to the bleeding lumbar artery should also be occluded to prevent rebleeding by revascularization through vertical interlumbar connections

#### 2.1.7.5 Pelvic Injuries

Posttraumatic pelvic bleeding is of arterial, venous, or bone origin. Arterial injuries are the most severe and are predominantly observed in anterior/posterior pelvic compression injuries types 2 and 3, lateral compression injuries type 3, vertical compression injuries, and combined injury mechanisms. The instability of pelvic bone fractures is a

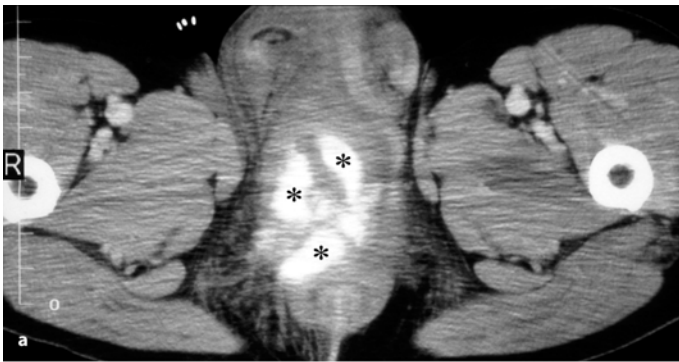
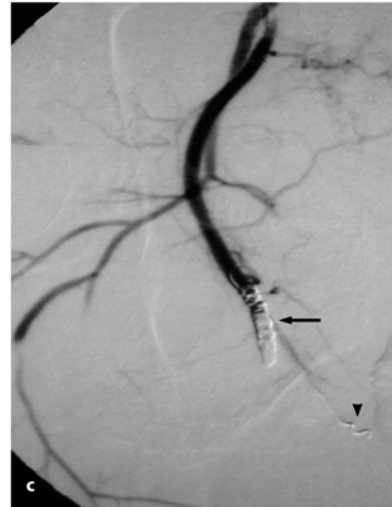
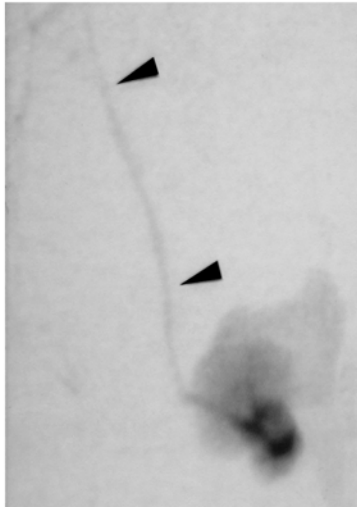
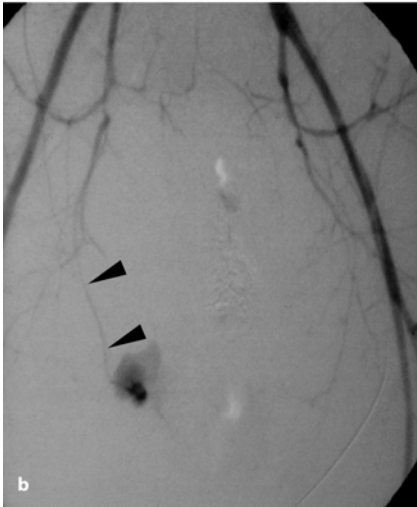


**Fig. 10.** **a** A CT scan obtained at admission in a young patient with complex pelvic fractures shows massive perineal contrast extravasation (*asterisks*). **b** Pelvic aortography and selective arteriography of the right internal pudendal artery (*arrowheads*) shows distal contrast extravasation. **c** Distal embolization with small microcoils (*arrowhead*) was inefficient, due to impaired coagulation after multiple blood transfusions. Hemostasis was achieved after placement of a dozen of coils in the main arterial trunk (*arrow*)



good predictor of the need for hemostatic embolization and prompts rapid orthopedic fixation as a first treatment (Mears 1980; Burgess et al. 1990)

As for retroperitoneal bleeding, surgical dissection is not indicated to obtain hemostasis, and urological interventions should be postponed after angiographic intervention (Ben Menachem 1988; Ben Menachem 1985; Ben Menachem and Bahramipour 1997). A contralateral femoral approach to the suspected side of bleeding is chosen for arteriography. An abdominal and a pelvic aortogram are obtained to demonstrate all potential bleeding sites. The bleeding artery is catheterized by a coaxial crossover technique using a 3-F catheter inside a 5-F Cobra catheter (Fig. 10). Arteries that are involved in posttraumatic pelvic hemorrhage are, in decreasing order of frequency: superior gluteal; internal pudendal; lateral sacral; iliolumbar; obturator; urinary bladder; and inferior gluteal arteries. The treatment of posttraumatic pelvic hemorrhage has raised a considerable interest in the literature. Pelvic trauma is responsible of 6–8% of death of all trauma patients. Rupture of a main pelvic artery carries a mortality of 50–75%, and the main cause of death from pelvic trauma is arterial hemorrhage. Furthermore, pelvic injury is frequently associated with other abdominal, aortic, and neurological injuries (Katz et al. 1992)

A deep selective catheterization of the bleeding artery is obtained for embolization. Gelfoam powder or liquid embolization agents (alcohol) are avoided because of the risk of nerve damage in the pelvis. Vaso-active drugs should not be injected intra-arterially, as induced vasospasm prevents selective catheterization and distal embolization. In the most unstable patients, a unilateral proximal embolization of the internal iliac artery is performed for urgent occlusion of all internal branches. Gelfoam pledgets soaked in an antibiotic solution and coils can be used in combination

Patients with pelvic hemorrhage may bleed profusely and show a wash-out coagulopathy at time of embolization after multiple blood transfusions; therefore, embolization, and compact coiling are mandatory for a definite mechanical vessel occlusion. In case of laceration of an iliac artery, placement of one or two occlusion balloons before surgery may be a lifesaving procedure (Ben Menachem 1988; Ben Menachem et al. 1985)

Embolization in posttraumatic pelvic hemorrhage is overall successful in 85–94% of patients (Jander and Russinovich 1980). Potential complications are pelvic visceral necrosis, fistulization, ischemic pneumopathy, and impotence, due to too massive embolization or vaso-occlusion of overlapping arterial territories

### 2.1.7.6 Other Injuries

Urgent hemostatic embolization may also be indicated for treatment of vascular injuries in other areas, such as the face and neck, thorax, scapular region, and limbs. Limb artery lesions are most often secondary to penetrating injury. Embolization must be precisely targeted to the bleeding arterial branch, avoiding occlusion of the main limb arteries

### 2.1.8 Conclusion

Trauma prevention and care does not attract the attention that it deserves. Research expenditures on trauma in Europe and the United States are very low in comparison with those of cancer or cardiovascular diseases; however, over the years modern medical imaging has become a cornerstone of management of trauma victims. Multislice CT is well established as an optimal screening modality for poly-trauma patients, provided the equipment is installed in emergency admissions and permanently operational. Although instantaneous imaging is able to detect the extend and severity of injuries, clinical symptoms and findings always take precedence in decision making on patient management. After reviewing the examination on the console, the radiologist should be able to formulate precisely the findings and should take part in the discussion on the clinical significance of the injuries observed and on management options, as long as arteriographic hemostatic embolization at admission is a considered an option

### References

- Allison DJ, Jordon H, Hennessy O (1985) Therapeutic embolization of the hepatic artery: a review of 75 procedures. *Lancet* 1:595
- Anderson R, Alwmark A, Gullstrand P, Offerbarti K, Bengmark S (1986) Non-operative treatment of blunt trauma to liver and spleen. *Acta Chir Scand* 152:739–741
- Asensio JA, Demetriades D, Chahwan S et al. (2000) Approach to the management of complex hepatic injuries. *J Trauma* 48: 66–69
- Bass EM, Crosier JH (1977) Percutaneous control of posttraumatic hepatic hemorrhage by gelfoam embolization. *J Trauma* 17:61–63
- Baum S, Roy R, Finkelstein AK, Blakemore WS (1965) Clinical applications of selective coeliac and superior mesenteric arteriography. *Radiology* 84:279–294
- Beal SL (1990) Fatal hepatic hemorrhage: an unsolved problem in the management of complex liver injuries. *J Trauma* 30:163–169
- Ben Menachem Y (1988) Pelvic fractures: diagnostic and therapeutic angiography: in Bassett FH (ed): Instructional course lectures. Park Ridge, IL: American Academy of Orthopaedic Surgeons 37:139–141
- Ben Menachem Y, Bahramipour P (1997) Interventional radiologic damage control. *Semin Intervent Radiol* 14:151–162
- Ben Menachem Y, Fisher RG, Ward RE (1981) Are “occult” intra-abdominal and extraperitoneal injuries really occult. *Radiol Clin North Am* 19:125–140
- Ben Menachem Y, Handel SF, Ray RD, Childs TL (1985) Embolization procedures in trauma: a matter of urgency. *Semin Intervent Radiol* 2:107–117
- Boijesen E, Judkins MP, Simay A (1966) Angiographic diagnosis of hepatic rupture. *Radiology* 86:66–72
- Burgess AR, Eastridge BJ, Young JWR et al. (1990) Pelvic ring disruptions: effective classification system and treatment protocols. *J Trauma* 30:848–856
- Capasso P, Trotteur G, Flandroy P, Dondelinger RF (1996) A combined CT and angiography suite with a pivoting table. *Radiology* 199:561–563
- Chang J, Katzen BT, Sullivan KP (1978) Transcatheter gelfoam embolization of posttraumatic bleeding pseudoaneurysms. *AJR* 131:645–650
- Chiu WC, Cushing BM, Rodriguez A et al. (1997) Abdominal injuries without hemoperitoneum: a potential limitation of focused abdominal sonography for trauma (FAST). *J Trauma* 42:817–822
- Chuang VP, Reuter SR (1975) Selective arterial embolization for the control of traumatic splenic bleeding. *Invest Radiol* 10:18–24
- Davis KA, Fabian TC, Croce MA et al. (1998) Improved success in nonoperative management of blunt splenic injuries: embolization of splenic artery pseudoaneurysms. *J Trauma* 44:1008–1013
- Deleuse P, Boverie JH, Ghaye B, Dondelinger RF (2001) Systematic CT evaluation of thoracic and abdominal blunt trauma: immediate vs delayed film reading. *Eur Radiol (S)* 11:144
- Dondelinger RF, Kurdziel JC (1991) A plea for conservative non-operative management of hepatic contusion. *Ann Chir* 45: 863–876
- Dondelinger RF, Trotteur G (2004) Hemostatic arterial embolization in blunt trauma victims at admission. In: Dondelinger RF (ed) *Imaging and intervention in abdominal trauma*. Springer, Berlin Heidelberg New York, pp 533–556
- Dondelinger RF, Deleuse P, Ponghis G, Willems V (2004) Systematic CT examination of thoraco-abdominal trauma victims at admission. In: Dondelinger RF (ed) *Imaging and intervention in abdominal trauma*. Springer, Berlin Heidelberg New York, pp 504–512
- Fankuchen EI, Martin EC, Karlson KB, Mattern RF, Casarella WJ (1981) Small coils for large hemorrhages. *AJR* 136:816–818
- Federle MP (1983) Computed tomography of blunt abdominal trauma. *Radiol Clin North Am* 21:461–475
- Federle MP, Crass RA, Jeffrey RB, Trunkey DD (1982) Computed tomography in blunt abdominal trauma. *Arch Surg* 117:645–650
- Federle MP, Courcoulas AP, Powell M, Ferris JV, Peitzman AB (1998) Blunt splenic injury in adults: clinical and CT criteria for management, with emphasis on active extravasation. *Radiology* 206:137–142
- Fisher RG, Ben-Menachem Y (1985) Embolization procedures in trauma: the extraperitoneal abdomen. *Semin Intervent Radiol* 2:148–157
- Fisher RG, Foucar K, Estrada B, Ben-Menachem Y (1981) Splenic rupture in blunt trauma: correlation of angiographic and pathological records. *Radiol Clin North Am* 19:141–146
- Fisher RG, Ben-Menachem Y, Wigham C (1989) Stab wounds of the renal artery branches: angiographic diagnosis and treatment by embolization. *AJR* 152:1231–1235
- Freeark RJ, Love L, Baker RJ (1968) The role of aortography in the management of blunt abdominal trauma. *J Trauma* 8:557–571
- Freeman T, Fischer RP (1976) The inadequacy of peritoneal lavage in diagnosing acute diaphragmatic rupture. *J Trauma* 16:538–540



- Gavant ML, Schurr M, Frick PA et al. (1997) Predicting clinical outcome of nonsurgical management of blunt splenic injury: using CT to reveal abnormalities of splenic vasculature. *AJR* 168:207–211
- Giraulo DL, Luk S, Palter M et al. (1998) Selective hepatic arterial embolization of grade IV and V blunt hepatic injuries: an extension of resuscitation in the nonoperative management of traumatic hepatic injuries. *J Trauma* 45:353–359
- Gorich J, Rilinger N, Brado M et al. (1999) Non-operative management of arterial liver hemorrhages. *Eur Radiol* 9:85–88
- Hagiwara A, Yukioka T, Shimazaki S, Megawa T, Matuda H (1993) Delayed hemorrhage following catheter arterial embolization for blunt hepatic injury. *Cardiovasc Intervent Radiol* 16:380–383
- Hagiwara A, Yukioka T, Ohta S, Nitatori T, Matsuda N, Shimazaki S (1996) Nonsurgical management of patients with blunt splenic injury: efficacy of transcatheter arterial embolization. *AJR* 167:159–166
- Hagiwara A, Yukioka T, Ohta S et al. (1997) Nonsurgical management of patients with blunt hepatic injury: efficacy of transcatheter arterial embolization. *AJR* 169:1151–1156
- Harper HC III, Maull KI (2000) Transcatheter arterial embolization in blunt hepatic trauma. *South Med J* 93:663–665
- Hashimoto S, Ido K, Hiramatsu K et al. (1990) Expanding role of emergency embolization in the management of severe blunt hepatic trauma. *Cardiovasc Intervent Radiol* 13:193–197
- Hashimoto S, Hiramatsu K, Sato M (1997) CO<sub>2</sub> as an intra-arterial digital subtraction angiography (IADSA) agent in the management of trauma. *Semin Intervent Radiol* 14:163–173
- Hawkins IF, Caridi JG, Wiechmann BN, Kerns SR (1997) Carbon dioxide (CO<sub>2</sub>), digital subtraction angiography in trauma patients. *Semin Intervent Radiol* 14:175–180
- Haydu P, Chang J, Knox G, Neelson TF Jr (1978) Transcatheter arterial embolization of a traumatic lumbar artery false aneurysm. *Surgery* 84:288–291
- Hubbard SG, Bivins BA, Sachatello CR, Griffen WO Jr (1979) Diagnostic errors with peritoneal lavage in patients with pelvic fractures. *Arch Surg* 114:844–846
- Jander HP, Russinovich AE (1980) Transcatheter gelfoam embolization in abdominal, retroperitoneal and pelvic hemorrhage. *Radiology* 136:337–344
- Jander HP, Laws HL, Kogutt MS, Mihlas AA (1977) Emergency embolization in blunt hepatic trauma. *AJR* 129:249–252
- Katz MD, Teitelbaum GP, Pentecost MJ (1992) Diagnostic arteriography and therapeutic transcatheter embolization for post-traumatic pelvic hemorrhage. *Semin Intervent Radiol* 9:4–12
- Keramidas DC (1979) The ligation of the splenic artery in the treatment of traumatic rupture of the spleen. *Surgery* 85: 530–533
- Killeen KL, Shanmuganathan K, Boydcranis R, Scalea TM, Mirvis SE (2001) CT findings after embolization for blunt splenic trauma. *J Vasc Interv Radiol* 12:209–214
- Kos X, Fanchamps JM, Trotteur G, Dondelinger RF (1999) Radiologic damage control: evaluation of a combined CT and angiography suite with a pivoting table. *Cardiovasc Intervent Radiol* 22:124–129
- Kurdziel JC, Dondelinger RF, Hemmer M (1987) Radiological management of blunt polytrauma with computed tomography and angiography: an integrated approach. *Ann Radiol* 30:121–124
- Lang EK (1976) The role of arteriography in trauma. *Radiol Clin N Am* 14:353–370
- Lang EK (1990) Intra-abdominal and retroperitoneal organ injuries diagnosed on computed tomograms obtained for assessment of renal trauma. *J Trauma* 30:1161–1168
- Larsen DW, Pentecost MJ (1992) Embolotherapy in renal trauma. *Semin Intervent Radiol* 9:13–18
- Love L, Greenfield GB, Braun TW, Moncada R, Freeark RJ, Baker RJ (1968) Arteriography in splenic trauma. *Radiology* 91:96–102
- Matalon TSA, Athanasoulis CA, Margolies NM et al. (1979) Hemorrhage with pelvic fractures: efficacy of transcatheter embolization. *AJR* 133:859–864
- Mears D (1980) External fixation of pelvic fractures. *Orthop Clin North Am* 11:465–479
- Moore EE (1984) Critical decision making in the management of hepatic trauma. *Am J Surg* 6: 712–716
- Murakami R, Tajima H, Kumazaki T (1993) Transcatheter hepatic arterial embolization for the treatment of blunt hepatic injury. *Nippon Igaku Hoshasen Gakkai Zasshi* 53:395–402
- Mutabagani KH, Coley BD, Zumberge N et al. (1999) Preliminary experience with focused abdominal sonography for trauma (FAST) in children: Is it useful? *J Pediatr Surg* 34:48–52
- Norell HG (1957) Traumatic rupture of the spleen diagnosed by abdominal aortography. *Acta Radiol* 48:449–452
- Nunez LW, Simmons S, Kozar R, Kinback R, Hallowell MJ, Mulhern C Jr (2001) Feasibility and profitability of a radiology department providing trauma US as a part of a trauma alert team. *Acad Radiol* 8:88–95
- Ochsner MG, Knudson MM, Pachter HL et al. (2000) Significance of minimal or no intraperitoneal fluid visible on CT scan associated with blunt liver and splenic injuries: a multicenter analysis. *J Trauma* 49:505–510
- Panetta T, Sclafani SJA, Goldstein AS et al. (1985) Percutaneous transcatheter embolization for massive bleeding from pelvic fractures. *J Trauma* 25:1021–1029
- Rao PM, Rhea JT, Novelline RA (1997) CT diagnosis of acute abdominal trauma. *Semin Intervent Radiol* 14:111–124
- Richardson DJ, Franklin GA, Lukan JK et al. (2000) Evolution in the management of hepatic trauma: a 25-year perspective. *Ann Surg* 232:324–330
- Rousseau H, Soula P, Perreault P et al. (1999) Delayed treatment of traumatic rupture of the thoracic aorta with endoluminal covered stent. *Circulation* 99:498–504
- Rozycki GS, Ballard RB, Feliciano DV, Schmidt JA, Pennington SD (1998) Surgeon-performed ultrasound for the assessment of truncal injuries: lessons learned from 1540 patients. *Ann Surg* 228:557–567
- Rubin BE, Katzen BT (1977) Selective hepatic artery embolization to control massive hepatic hemorrhage after trauma. *AJR* 129:253–256
- Sato M, Fujisawa H, Hagiwara A et al. (1991) Traumatic hemorrhage of the spleen diagnosed by CO<sub>2</sub> DSA. *JJAAM* 2:728–732
- Scalea TM, Rodriguez A, Chiu WC et al. (1999) Focused assessment with sonography for trauma (FAST): results from an international consensus conference. *J Trauma* 46:466–472
- Schwartz RA, Teitelbaum GP, Katz MD, Pentecost MJ (1993) Effectiveness of transcatheter embolization in the control of hepatic vascular injuries. *J Vasc Interv Radiol* 4:359–365
- Sclafani SJA (1985) Angiographic control of intraperitoneal hemorrhage caused by injuries to the liver and spleen. *Semin Intervent Radiol* 2:139–147
- Sclafani SJ, Shaftan GW, McAuley J et al. (1984) Interventional radiology in the management of hepatic trauma. *J Trauma* 24: 256–262
- Sclafani SJA, Weisberg A, Scalea TM, Philips TF, Duncan AO (1991) Blunt splenic injuries: nonsurgical treatment with CT, arteriography and transcatheter arterial embolization of the splenic artery. *Radiology* 181:189–196
- Sclafani SJA, Shaftan GW, Scalea TM et al. (1995) Nonoperative salvage of computed tomography diagnosed splenic injuries: utilization of angiography for triage and embolization for hemostasis. *J Trauma* 39:818–825
- Shanmuganathan K, Mirvis SE, Sover ER (1993) Value of contrast-enhanced CT in detecting active hemorrhage in patients with blunt abdominal or pelvic trauma. *AJR* 161:65–69
- Shanmuganathan K, Mirvis SE, Boyd-Kranis R, Takada T, Scalea T (2000) Nonsurgical management of blunt splenic injury: use of CT criteria to select patients for splenic arteriography and potential endovascular therapy. *Radiology* 217:75–82
- Sherman HF (1996) Letter to the editor. *J Trauma* 40:171
- Sugimoto K, Horiike S, Hirata M, Ohwada T, Maekawa K (1994) The role of angiography in the assessment of blunt liver injury. *Injury* 25:283–287

- Takakuwa T, Yokota J, Sugimoto T (1993) Liver infarction produced by dual vessels occlusion due to trauma and TAE: long follow up using CT, US and MRI. *Med J Osaka Univ* 41/42:23-27
- Taylor GA, Sivit CJ (1995) Posttraumatic peritoneal fluid: Is it a reliable indicator of intraabdominal injury in children? *J Pediatr Surg* 30:1644-1648
- Toma G de, Mingoli A, Modini C, Cavallaro A, Stipa S (1994) The value of angiography and selective hepatic artery embolization for continuous bleeding after surgery in liver trauma: case reports. *J Trauma* 37:508-511
- Trunkey DD (1983) Trauma. *Sci Am* 249:28-35
- Udekwo PO, Gurkin B, Oller DW (1996) The use of computed tomography in blunt abdominal injuries. *Am Surg* 62:56-59
- Vogler E, Bergmann M (1963) Angiography in blunt kidney trauma. *RöFo* 98:675-685
- Wagner WH, Lundell CJ, Donovan AJ (1985) Percutaneous angiographic embolization for hepatic arterial hemorrhage. *Arch Surg* 120:1241-1249



## Imaging and Intervention in Post-traumatic Complications (Delayed Intervention)

P.P. Goffette

# 2.2

### Contents

2.2.1	Introduction	61
2.2.2	Liver and Bile Ducts	62
2.2.2.1	Type and Incidence of Complications	62
2.2.2.2	Vascular Complications	62
2.2.2.3	Endovascular and Percutaneous Management	67
2.2.2.4	Results and Complications	69
2.2.2.5	Fluid Collections, Sepsis and Varia	75
2.2.3	Spleen	75
2.2.3.1	Clinical Presentation and Imaging	77
2.2.3.2	Fluid Collection	82
2.2.4	Pancreas	83
2.2.4.1	Vascular Complications	83
2.2.4.2	Ductal Complications and Fluid Collections	83
2.2.5	Kidneys, Adrenals, Urinary Bladder	86
2.2.5.1	Vascular Complications	86
2.2.5.2	Urinary Tract Complications	88
2.2.6	Gastrointestinal Tract	88
2.2.6.1	Stomach-Duodenum	88
2.2.6.2	Small Bowel and Large Bowel	88
2.2.7	Vascular Complications	89
2.2.7.1	Superior Mesenteric Artery	89
2.2.7.2	Aorta, Lumbar and Iliac Arteries	91
2.2.7.3	Inferior Vena Cava	91
2.2.8	Diaphragm	92
2.2.9	Conclusion	92
	References	92

### 2.2.1 Introduction

During the past 2 decades, non-operative management (NOM) of abdominal trauma has become the standard of care in children [90, 121, 149, 152, 173, 231]. Based on the excellent success rate in child population (90–95%), this approach has been extended to adult trauma patients (rate 65–90%) [24, 135, 154, 162]. Recent work has suggested that patients regaining haemodynamic stability after arrival to

the trauma centre and carefully selected patients with abdominal gunshot wounds can also be safely managed non-operatively [32, 39, 54, 90, 178, 261, 263]. Experience has been uniform in confirming that instability supersedes injury grade or the extent of haemoperitoneum for determining the need for early surgery [178, 263]. Several factors have promoted the use of conservative therapy, including (a) the widespread use of high-speed spiral CT scan which enables precise evaluation and grading of solid organ injury, may demonstrate parenchymal self-limited or massive peritoneal bleeding [62, 64, 166], and reduces the risk of unrecognized hollow viscus injuries [48, 262, 276], (b) the high success rate and clinical benefits of angiographic embolisation as primary therapeutic option for intra- or retroperitoneal bleeding [5, 55, 64, 95, 96, 213, 267], (c) a better understanding of the natural history and pathophysiology of organ injuries and associated complications [62, 149, 173] and (d) a rate up to 67% of non-therapeutic exploratory ceiotomies for the conventional management of hepatic and splenic injuries. This trend is reinforced by the cost-effectiveness evaluation of care, as physicians and administrators look for ways to cut costs without sacrificing quality of care. The enthusiasm of NOM is undergoing a critical analysis, inasmuch as the benefits of such treatment may be obviated by subsequent delayed complications not previously encountered after surgery [5, 27, 32, 74, 86, 177, 263]. As NOM approach has been extended to severe trauma previously considered as candidate for surgery, the incidence of delayed and uncommonly encountered complications has consequently increased. These complications have been identified as factors that may lead to failure of NOM of liver, splenic and renal injuries in both children and adults. Causes of delayed complications are multiple and include (a) abnormal or insufficient injury healing process, (b) retention of necrotic tissue, (c) secondary infection of initially sterile collections and (d) underestimation of injury severity. Historically, most of these complications have been treated surgically [171]. These complications, which do not necessarily negatively influence the final outcome, are often predictable, virtually obligatory consequences of the successful NOM of high-grade or complex abdominal injuries. Presently, recent advanced technologies allow detection and recogni-

tion of them non-invasively, and management of the large majority of them by minimally invasive techniques including interventional radiology, endoscopy and laparoscopy. Between 50 and 60% of those patients with grade-IV or grade-V liver or splenic lacerations require some type of interventional treatment; therefore, indiscriminate discharge of patients with solid organ injury managed conservatively may be potentially harmful

## 2.2.2 Liver and Bile Ducts

### 2.2.2.1 Types and Incidence of Complications

Liver trauma secondary complications are reported in up to 64% of the patients [43, 131, 171]. As the conservative management of any grade of blunt hepatic injury is becoming the primary approach, complications, previously not encountered after surgery, are now more commonly described and can occur weeks to months after injury, often after the patient's discharge [4, 8, 22, 33, 39, 86, 90, 121, 137, 141, 152, 160, 162, 171, 187, 219, 262]. These delayed complications, involving the liver and biliary tract, arise either as a result of direct liver trauma, such as bile duct disruptions, bile peritonitis, biloma, intra-abdominal abscess formation, delayed haemorrhage, non-bleeding vascular malformations, haemobilia and bilhaemia, or occur in the course of post-traumatic critical care such as acute acalculous cholecystitis [27, 33, 48, 96, 135, 152, 178, 183, 215]. Liver-related complications appear to be less frequent in patients managed without operation than in those managed surgically [27]; however, the prolonged hospital stay associated with NOM of liver injury has been reported as a limiting criterion for NOM [141]. Overall complication rates in patients undergoing non-operative treatment are reported to be between 9.5 and 24% in adults [4, 26, 27, 30, 33, 47, 48, 52, 86, 96, 135, 160, 162] and between 7 and 10% in children [90, 137, 152, 215]. Deep liver injuries are more likely to disrupt major blood vessels and bile ducts [171]. Open celiotomy remains useful in patients requiring debridement of necrotic liver, decompression of compartment syndrome or a detailed examination of all abdominal organs [86]. Following NOM of liver trauma, mortality or severe morbidity is usually caused by associated intra- or extra-abdominal injuries unrelated to the liver injury [62, 262]

Delayed complications following NOM of liver trauma, reported by the most relevant series between 1990 and 2005, are summarised in Table 1. Those complications after NOM of blunt abdominal trauma in children reported by the most relevant series are presented in Table 2

### 2.2.2.2 Vascular Complications

#### Clinical Presentation and Imaging

##### Delayed Haemorrhage

Delayed or recurrent haemorrhage is the most common reported complication of the NOM of hepatic injuries with an overall incidence between 2.4 and 5% [24, 32, 47, 137, 178], but the exact prevalence of such secondary bleeding is unknown. Indeed, when strict guidelines for NOM are followed, the incidence of delayed haemorrhage ranged from 0% to <3.5% [180] with only 0.7–1.7% of patients requiring surgery. An incidence of 1–3% has been reported in children series [21, 62, 90, 170, 221, 231]. Delayed haemorrhage-related deaths after either surgical or conservative management were reported in both children [14, 72, 90, 137] and adults [79, 80, 84, 96, 180, 246]. Delayed haemorrhage may be related to either an expanding initial minimal injury or to a biloma-induced pseudo-aneurysm, and may result in an expanding haematoma or free intraperitoneal rupture. The incidence of secondary rupture of hepatic haematoma is reported between 0 and 14%. The time elapsed between trauma and rupture ranges from 8 h to 30 days [47, 72, 94]. This complication should be suspected in the setting of an initial injury involving >50% of the liver, in patients with ongoing transfusion requirements, a drop in the haemoglobin level value or continued blood loss demonstrated by serial follow-up CT scan [72, 221]. Persistent complaints of right upper quadrant abdominal and right shoulder pain after injury could be a sentinel sign [221]. Duodenal obstruction due to left liver lobe hypertrophy induced by a haematoma-related right portal vein occlusion has been reported in a child with a grade-IV liver injury [72]. When a delayed haemorrhage is suspected in patients initially managed conservatively, either an immediate laparotomy or an abdominal CT will be performed depending on the haemodynamic stability. Indeed, this complication may also be safely approached non-surgically assuming that the criteria used in the initial management of blunt hepatic trauma are applied

##### Vascular Abnormalities

The incidence of post-traumatic pseudo-aneurysms (PPA), eventually associated with an arteriovenous fistula (AVF), varies between 1 and 3% after penetrating trauma and remains below 1% after blunt trauma in adults [198, 180]. These lesions have been reported even less frequently in children [9, 12, 88, 111, 152, 225, 235]. Intrahepatic development of PPA after surgical haemostasis for delayed haemorrhage after blunt liver trauma may also occur [111]. Potential complications of a hepatic PPA include decompression into the biliary system causing haemobilia, rupture and associated haemorrhage, direct enteric fistulisation into the duodenum and development of jaundice [1, 46, 69, 84, 88, 111, 127, 195]. The use of absorbable gelatin

**Table 1.** Delayed complications after non-operative management of blunt liver trauma (1990–2005). *NOM* non-operative management, *NA* not available, *E* embolisation at admission,  $\psi$ A pseudoaneurysm, *AVF* arteriovenous fistula

Reference	No. of patients	Liver injury grading	No. of patients	Re-bleeding	Biliary	Abscess	Missed injury	Successful radiological intervention or observation	Surgery	Success NOM (%)
[131]	52	I-II 65%, III-V 35%	1 (2%)	1	0	0	0	0	1	98
[27]	26	I-II 62%, III-V 38%	5 (19%)	0	Leaks 2, biloma 3	0	0	Biloma 3	2	92
[29]	142	NA	6 (4%)	1	Leaks 1, biloma 1	2	1	Biloma 1, abscess 2	3	94
[160]	72	I-II 54%, III-V 46%	2 (3%)	2 ( $\psi$ A)	0	0	0	0	2	97
[219]	30	I-II 34%, III-V 66%	1 (3%)	1	0	0	0	Embol. 1	0	100
[22]	46	I-II 30%, III-V 70%	7 (15%)	2	Leaks 2, biloma 1	2	0	Biliary 2, abscess 2	4	91
[180]	404	I-II 50%, III-V 50%	21 (5%)	14	Biloma 2	3	2	Drainage 4, embol. 4	6	93
[24]	50	I-II 76%, III-V 28%	3 (6%)	2 ( $\psi$ A)	Leak 1	0	0	Drainage 1, embol. 2	0	96
[96]	54 (15E)	I-II 48%, III-V 52%	4 (7%)	3 ( $\psi$ A)	Biloma 4 (3 with $\psi$ A)	0	0	Drainage 1, embol. 3	0	100
[33]	135	I-II 30%, III-V 70%	32 (24%)	12	Leaks 5 obstruct, 2 bilhaemia 1	0	1	Embol. 10, ERCP 7, drainage 10	5	96
[48]	52	I-II 30%, III-V 70%	3 (6%)	1 (AVF)	Biloma + 1 leak	0	1	Embol. 1, drainage 1	1	98
[86]	153	NA	19 (12%) <sup>a</sup>	5	Leak 7, biloma 1	1	0	Drainage 2, biliary 1, conservative 1	15	91
[162]	26(E)	III-V 100%	13 (50%)	2	Leak 6, Biloma 1	4	0	Drainage 4, embol. 2, ERCP 1	6	78
[262]	47(7E)	I-II 38%, III-V 62%	2 (4%)	2 (1 $\psi$ A)	0	0	0	Embol. 2	0	100
[135]	230	III-V 100%	25 (11%) <sup>b</sup>	13	16	5	0	Embol. 12, ERCP 7, drainage 6, laparotomy 4	8	97

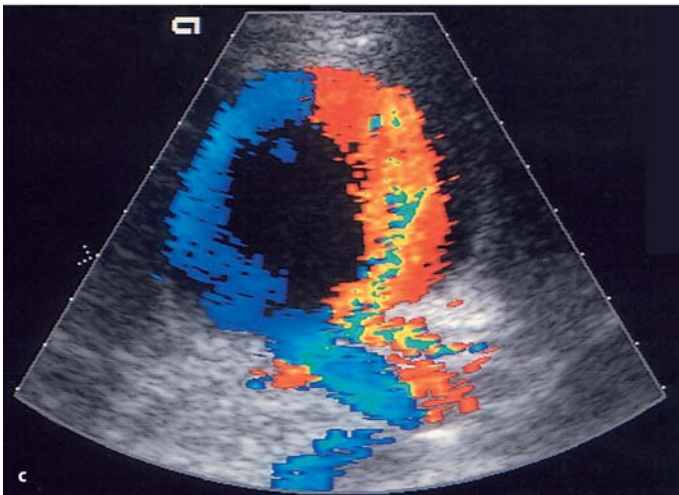
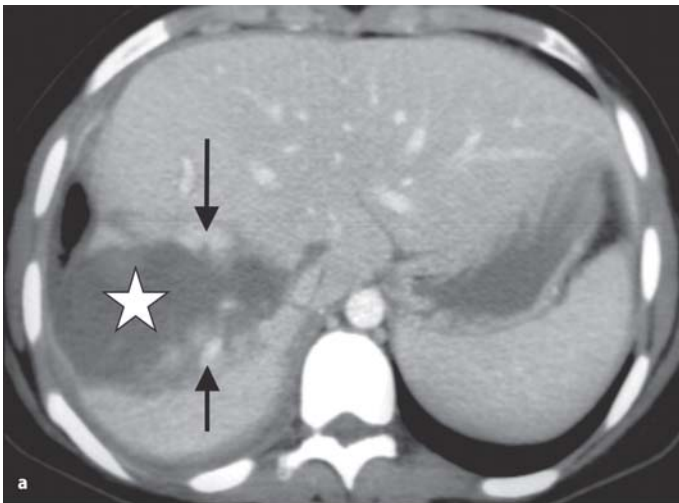
<sup>a</sup> Abdominal compartment syndrome in 5 patients<sup>b</sup> Thirty-seven complications including three abdominal compartment syndromes

Table 2. Delayed complications after non-operative management (NOM) of blunt abdominal trauma in children

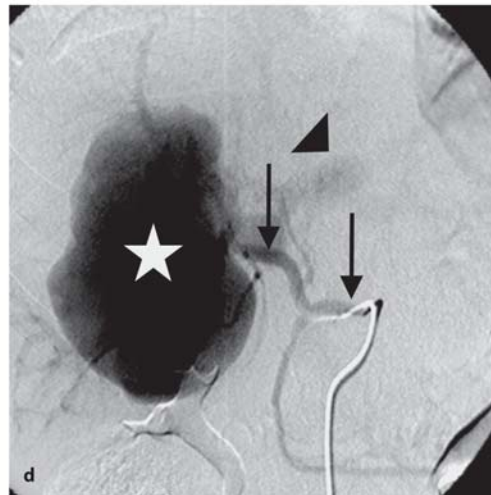
Reference	No. of patients	Organ	No. of patients	Type	DELAYED COMPLICATIONS				
					Surgery	Mortality	Missed hollow viscus injury	Success NOM (%)	
[170]	49	Liver	4 (8%)	Haemobilia 1, bile leaks 3	1	0	0	98	
[21]	156	Liver, spleen	2 (1.5%)	Hepatic bleeding, segmental liver necrosis	2	0	2; Surgery	97	
[276]	68	Liver-spleen, pancreas	4 (6%)	Liver haematoma, haemoperitoneum splenic abscess pancreatic pseudo-cyst	0	0	3; Surgery	96	
[231]	175	Liver-spleen, pancreas	9 (5%)	Hepatic bleeding 1, splenic rupture 1, splenic cyst 3, pancreatic cysts 4	3	0	1; Surgery	97	
[221]	75	Liver	2 (3%)	Delayed bleeding	2	0	0	91 <sup>a</sup>	
[115]	26	Pancreas	8 (31%)	Pseudo-cyst 7, fistula 1	-	0	0	73 <sup>b</sup>	
[177]	170	Liver, spleen, kidney	4 (2.5%)	Hypertension 2, wound infection 1, septicaemia 1	1	0	0	99	
[121]	75	Liver, grades I-II 41, III-V 34	3 (4%)	Bleeding 2, bile leaks 1	2	1	0	97	

<sup>a</sup> Mortality-related to head injuries

<sup>b</sup> Mortality due to other thoraco-abdominal injuries



**Fig. 1.** A 22-year-old woman presented with grade-IV right liver laceration with massive haemoperitoneum after a ski fall. She underwent an emergent laparotomy with hepatorrhaphy. **a** Early post-operative CT scan shows a large right posterior contusion area (*star*) surrounded by vascular structures (*arrows*). **b** Two-week follow-up CT scan demonstrates simultaneous enhancement of the aorta, intra-hepatic portal vein branches and a large pseudo-aneurysm (*star*) developed within the contusion. **c** Colour Doppler sonography confirms the hypothesis of an arterial pseudo-aneurysm and demonstrates arterialised flow within the right portal branches, suggesting a combined arterioportal fistula. **d** Hepatic angiography clearly shows a huge pseudo-aneurysm (*star*), supplied by the right hepatic artery (*arrows*), with early filling of the right portal vein (*arrowhead*). **e** Gianturco Coils (4) embolisation of the right hepatic artery (*arrow*) is initially performed with technical success. **f** The embolisation led to only partial resolution of the pseudo-aneurysm. Indeed, a persistent flow pouch (*arrow*) in the aneurysmal sac is disclosed on the first control CT scan following the arterial embolisation. *Curved arrow* points the intra-arterial coils. **g** The remaining circulating cavity (*star*) is supplied by multiple small branches arising from the gastroduodenal, as well as left hepatic and intra-hepatic arteries (*arrows*). The right hepatic artery remains occluded. **h** Embolisation of all remaining arterial feeders could not be considered because of the risk of massive liver necrosis due to fistula-related persistent hepatofugal portal flow. Direct percutaneous transhepatic approach of the aneurysmal sac (*stars*) with a 5-F Teflon needle (*arrows*) under sonographic guidance is performed to complete the embolisation procedure. **i** The aneurysmal sac is filled with 12 15- to 20-mm steel macro-coils (*arrows*) and several large gelatin sponge torpedos. The intra-hepatic portal branches (*curved arrows*) remain patent with exception for the right postero-lateral branch. **j** Control CT scan four weeks after the percutaneous procedure confirms complete obliteration of the pseudo-aneurysm retracted around the steel coils (*arrow*). A small residual biloma (*star*) and a marked left liver lobe hypertrophy due to right posterior portal branch occlusion are observed





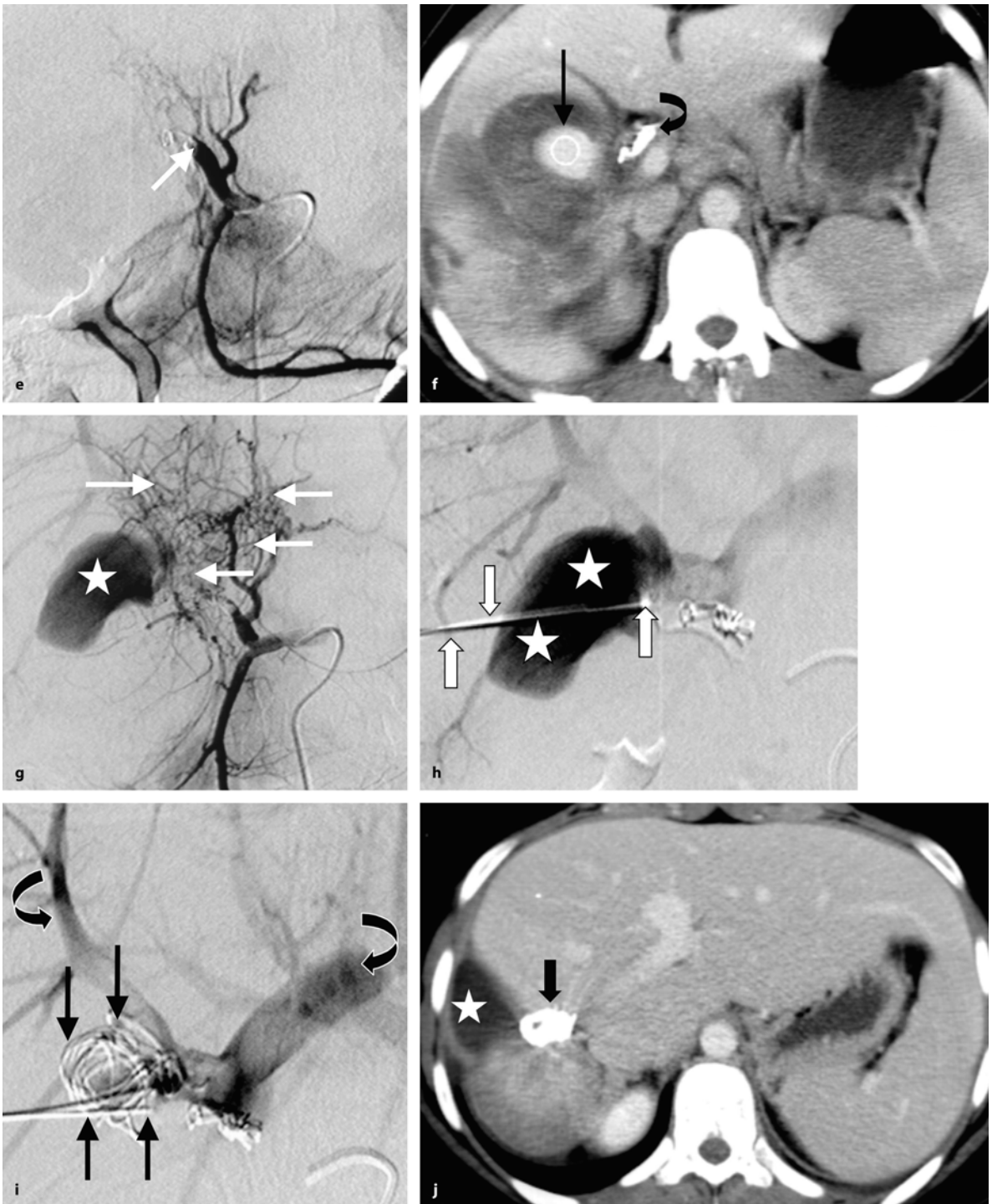


Fig. 1. (continued)

sponge for primary haemostasis in patients with high-grade hepatic injury and who secondarily develop biloma is associated with a higher risk of pseudo-aneurysm formation than after steel-oil embolisation [98]. In contrast to splenic pseudo-aneurysms, hepatic aneurysms have a high rupture rate up to 44% [69, 88, 156, 176, 225] that dictates a more aggressive management. Although they are sometimes disclosed or demonstrated by CT scan, the detection or confirmation of PPA usually requires angiography which is the most sensitive technique for the diagnosis. The main reasons for high false-negative rate of CT scan (35%) and US (40–50%) include small-size PPA and suboptimal contrast enhancement. Multidetector helical CT scan angiography seems of particular interest to detect non-invasively small-size vascular malformations [166, 77]. Spontaneous thrombosis of hepatic PPA has been rarely reported in children [235]. A conservative approach mandates repeated clinical and sonographic controls combined with restriction in physical activities until diminution of aneurysmal thrombosis [166, 235]

Intra-hepatic arteriovenous fistula (AVF) is rarely observed and classically located between a hepatic arterial branch and a portal vein (Fig. 1). Hepatic artery-to-hepatic vein fistula are much less common. Traumatic arterio-portal fistulas may form from direct lacerations of adjacent arteries and veins or more commonly via a connection with a pseudo-aneurysm [124, 143, 209, 248]. Patients with arterio-portal fistulae may develop crampy abdominal pain several days to years after injury, gastrointestinal bleeding, ascitis and mesenteric ischaemia resulting from portal hypertension and high cardiac output failure resulting from chronic large-size shunt [61, 129, 205, 212]. Porto-hepatic fistula is rarely observed, may be combined with a portal pseudo-aneurysm and requires technical refinements for treatment [239]

### Haemobilia

Traumatic haemobilia, first described by Sandblom in 1948 [199] as “an hemorrhage into the biliary tract”, has been noted after surgical repair of liver injuries and may be more frequently associated with central liver injuries. The incidence of haemobilia after conservative management of hepatic injury is between 0.5 and 2%, most cases being secondary to blunt liver trauma [46, 198]. Haemobilia, which usually develops within 2–4 weeks of liver injury [9, 41, 46, 103, 198] but may occur later than 1 month after, should be suspected when melena or haematemesis follow hepatic trauma [152, 195, 204]. This complication is often related to the development of a deeply located pseudo-aneurysm secondary to a high-grade liver injury (Fig. 2). Direct endoscopic visualisation of blood issuing from the Vater papilla or angiographic demonstration of bleeding into the bile ducts or gallbladder will confirm the clinical suspicion. Because of intermittent and slow-flow bleeding due to intrabiliary clotting, bleeding through the papilla or into the biliary tree is rarely observed [103, 195]

### 2.2.2.3 Endovascular and Percutaneous Management

Angiographic embolisation is the first-line treatment of delayed vascular complications. Surgery, including selective artery ligation and/or hepatectomy, remains indicated only in cases of embolisation failure or for large intrahepatic cavities with suspected superinfection [46, 84, 214]. If surgery is considered, preoperative embolisation should be performed to avoid catastrophic intra-operative massive bleeding [46]. The angiographic investigation should include superior mesenteric and inferior phrenic arteries study in order to detect injuries of aberrant or replaced arterial supplies [198]

#### Techniques

Ideally, embolisation should be done as close as possible to the injury site (a) to decrease the risk of massive liver ischaemia, (b) to avoid retrograde collateral flow from branches distal to the embolisation area and (c) to preserve the remaining patent arterial branches which are of utmost importance for the resorption of the local contusion and haematoma [103, 111, 204, 207]. The use of a coaxial microcatheter systems (Tracker-18 and Tracker-325-Target Therapeutics, Fremont, Calif.; or 3-F Focus microcatheter, Terumo, Japan) allows vessel occlusion close to the vascular lesion. Such microcatheters can deliver a variety of embolic agents including complex helical or straight platinum microcoils, gelfoam particles, alcohol and isobutyl-2-cyanoacrylate. Besides facilitating very distal vascular occlusions in spasm-prone injured blood vessels, a coaxial microcatheter system also allows for easier and more rapid catheterisation of the targeted vessel. If distal embolisation is not feasible because of vessel or aneurysm size or location, a single proximal coil may provide a sufficient blood flow reduction inducing secondary thrombosis over time [88, 225]. Embolisation with glue could be useful to occlude pseudo-aneurysms not accessible for coils placement, especially those located in a very thin or severely affected vessel or when multiple efferent arteries originate from pseudo-aneurysm [274]. For pseudo-aneurysms arising from large proximal branches of the hepatic artery, both distal and proximal embolisations should be performed to reduce the risk of PPA reconstitution by retrograde collaterals [103]. Because of an increased risk of liver ischaemia, this technique should be employed with caution, especially in patients with compromised portal flow

The AVFs are technically more challenging since high flow states may result in non-target embolisation of occlusive materials to the peripheral portal branches. The first-line endovascular approach consists of a careful deposition of a large fibriled coil which may provide a matrix for the nesting of smaller coils placed to induce complete mechanical blockage of the feeding arteries as close as possible to the fistulus nidus [61, 129, 191, 249]. When superselective

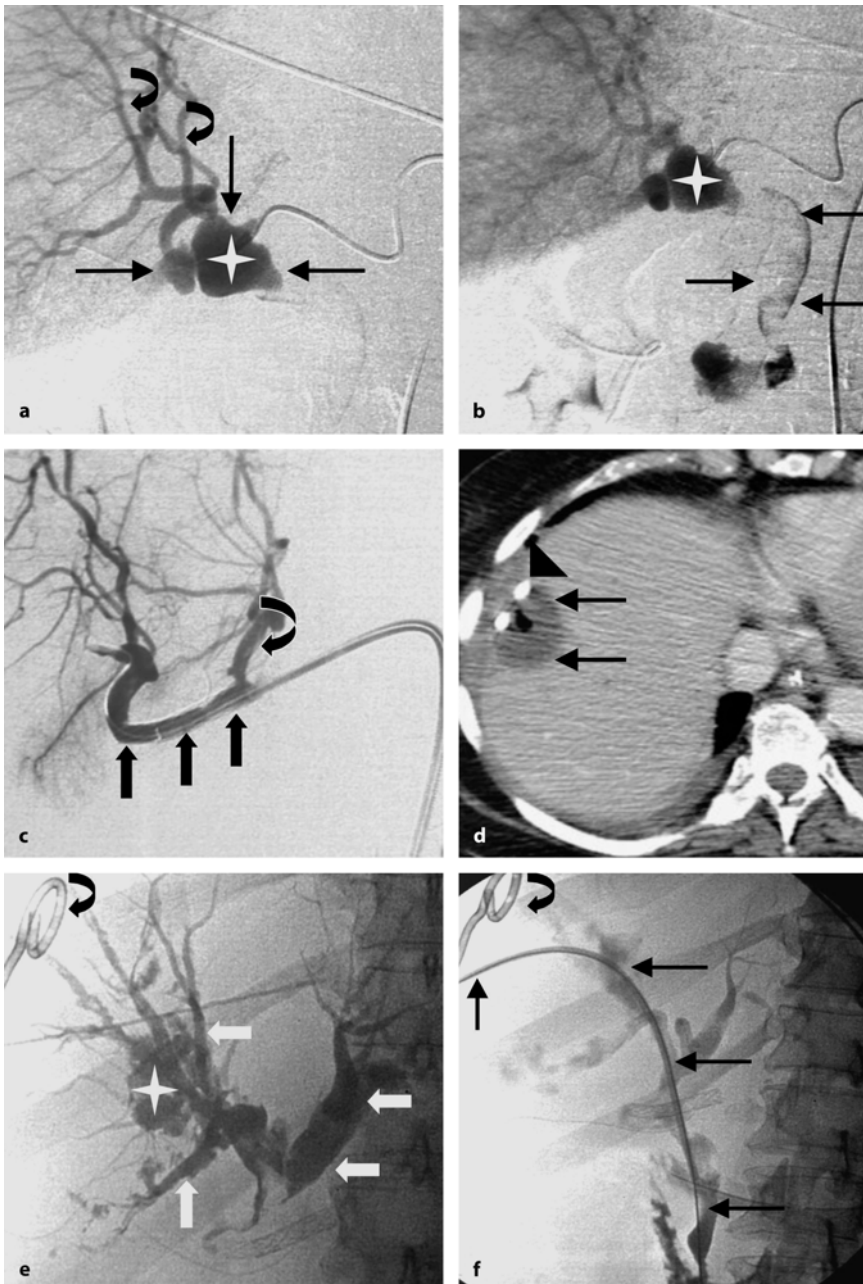


**Fig. 2.** A 55-year-old woman was treated conservatively for a grade-IV blunt liver trauma. Intra- and perihepatic bilomas were drained percutaneously. On day 7 she presented with sudden upper quadrant pain, massive GI bleeding and shock. Endoscopic retrograde cholangiography demonstrates massive haemobilia. An emergent arteriography was performed. **a** Selective hepatic injection shows a biloculated (arrows) pseudo-aneurysm (star) arising from the right hepatic artery. Intrahepatic arterial branches look patent (curved arrows). **b** The late phase of the same injection clearly demonstrates bleeding from the pseudo-aneurysm (star) into the common bile duct (arrows) with blood accumulation in the papilla. **c** Instead of total occlusion of the right hepatic artery with coils, the pseudo-aneurysm is excluded selectively by placement of two covered stents (Jostent, JOMED; arrows) just behind

the origin of the left hepatic artery (curved arrow). Distal emboli in one peripheral branch were not treated. **d** Secondary peripheral (arrows) abscesses, probably related to peripheral arterial occlusion, were drained percutaneously (arrowhead). **e** Because of progressive jaundice with intrahepatic bile duct dilatation, a percutaneous cholangiography was performed and shows marked dilatation of bile ducts (arrows) due to near complete occlusion of the common hepatic duct. Peripheral (curved arrow) and hilar bilomas (star) were drained. **f** An external-internal transpapillary biliary drain (arrows) is primarily inserted percutaneously and secondary exchanged for an internal plastic endoprosthesis. Delayed extra-hepatic bile duct stricture (curved arrow) was treated surgically on elective basis

occlusion of the arterial feeders is not feasible, the siphoning effect of the lesion may allow proximal injection of large-sized particulate material because of preferential travel to the appropriate site [207]. A direct percutaneous approach to a PPA is a valuable alternative to classical embolisation when the endovascular arterial route has failed or when back-flow from peripheral branches still supply the PPA (Fig. 1) [9, 45, 148, 156, 260]. Direct puncture of the aneurysmal cavity with a small-gauge Teflon needle should ideally be performed under colour Doppler guidance [9]. For small-size or deeply located lesions, a combined C-arm fluoroscopy during arterial contrast injection could be essential for exact needle placement and for limiting the number of needle passes, thereby reducing potential haemorrhagic or biliary complications [148]. Numerous embolic agents have been injected including stainless steel coils [148, 260], thrombin [156] or thrombin-soaked gelfoam pledgets [45] and/or the association of different materials with gelfoam. Non-arterial route, such as transhepatic drainage catheter tract or biliary T-tube tract, can be used as an alternative way for embolisation of hepatic artery pseudo-aneurysm developing adjacent to a biliary drainage catheter [194, 204]. In case of injuries to the proximal or hilar segment of the hepatic artery or disruption of a porto-hepatic vein, endovascular treatment with bare stent or stent-graft implantation could be considered as a possible alternative to surgical repair. New-generation, more flexible and reduced-size covered-stents allow to navigate easily through very sinuous arterial access

## Results and Complications

The technical success rate of embolisation of post-traumatic hepatic vascular complications is around 88 and 94% [207, 249]. Technical failures are due to the inability to select the appropriate vessel for embolisation and to persistent high-flow AVF. Persistent slow flow within the lesion or delayed recurrences may usually be controlled by re-embolisation [103, 143, 148]. Complications of embolisation include hepatic necrosis, abscess formation, non-targeted embolisation, gallbladder infarction and catheter-induced vessel damage. In the right hepatic artery, selective embolisation, beyond the cystic artery level, reduces the risk of gallbladder infarction [162]. Percutaneous transhepatic approach-related complications include coil migration, especially in case of biliary–arterial fistula, superinfection to treat by percutaneous drainage and tract bleeding [6]. This last side effect may be avoided by placing a few coils or gelfoam pieces inside the tract after completion of the procedure. Only few cases of complications after embolisation for haemobilia or PPA, such as hepatic necrosis, rebleeding, coil misplacement or migration into the common bile duct, have been reported [20, 78]. Misplacement or retrograde coil migration may be related to the catheter used for delivering or an inappropriate coil sizing

### 2.2.2.4 Biliary Complications

#### Bilhaemia

The bilhaemia syndrome, an extremely rare complication with a high mortality rate if untreated, is usually caused by a pathological communication between intrahepatic bile ducts and the hepatic venous system following the formation of an extensive liver haematoma within necrotic tissue. Passage of bile from the disrupted bile ducts into the intra hepatic venous blood stream is due to an increased biliary–venous pressure gradient of 15–20 cm H<sub>2</sub>O and will occur during the resorption of the bilio-haematoma [19, 240]. This clinical entity is characterised by the rapid development of jaundice after blunt hepatic trauma corresponding to a marked increase of the total serum bilirubin level, without sign of hepatic failure [19]. Localisation of the bilio-venous fistula requires a direct opacification of the bile duct either by an endoscopic retrograde cholangiography, a cholangiography via a T-tube or a fine-needle percutaneous cholangiography. The ideal treatment of post-traumatic bilhaemia is a combined endoscopic sphincterotomy and biliary endostenting [19, 76]. Alternative therapeutic options include surgery either by fistula resection or drainage of the collection and T-tube suction drainage, and percutaneous approach by direct occlusion of the fistula with a catheter [240] or insertion of a drainage catheter in the causative biloma in order to decrease the pressure and allow closure of the shunt [19]

#### Bile Leaks

The NOM of abdominal trauma may result in a delayed recognition of significant bile leaks either from a liver injury or from extra-hepatic source in both adults and children [22, 53, 215, 242]. The true incidence of intra-hepatic bile duct injuries after blunt abdominal trauma is unknown. Indeed, many peripheral bile ducts injuries go unrecognised as most are below the threshold of current imaging techniques and heal without complications [238]. Depending on the criteria and method used to diagnose bile leakage, the incidence of significant bile leaks resulting in biloma or biliary fistula in patients treated conservatively after liver injury ranges from 0.5 to 20% [22, 29, 32, 47, 107, 180, 215, 238]. A higher incidence up to 22.5% has been observed following major liver trauma or after extended resection following hepatic injuries [8, 49, 135]. Traditionally, surgical interventions, such as biliary–enteric anastomosis, primary duct repair, and ligation of lobar bile duct, have been the preferred treatment modalities for significant biliary injuries [238]. Endoscopic retrograde cholangiography (ERCP), rarely indicated in the first few days after hepatic trauma, could be performed as an alternative to surgery in cases of persistent bile leaks, bilhaemia or haemobilia (Fig. 3) [27, 41, 114, 135, 208, 216, 238, 243]. A new classification of biliary injuries, emphasizing the anatomic location of the injured duct and the location of the leaking bile, and recommendations regarding the combined percutaneous and endoscopic management of these complications, have been recently published [238]



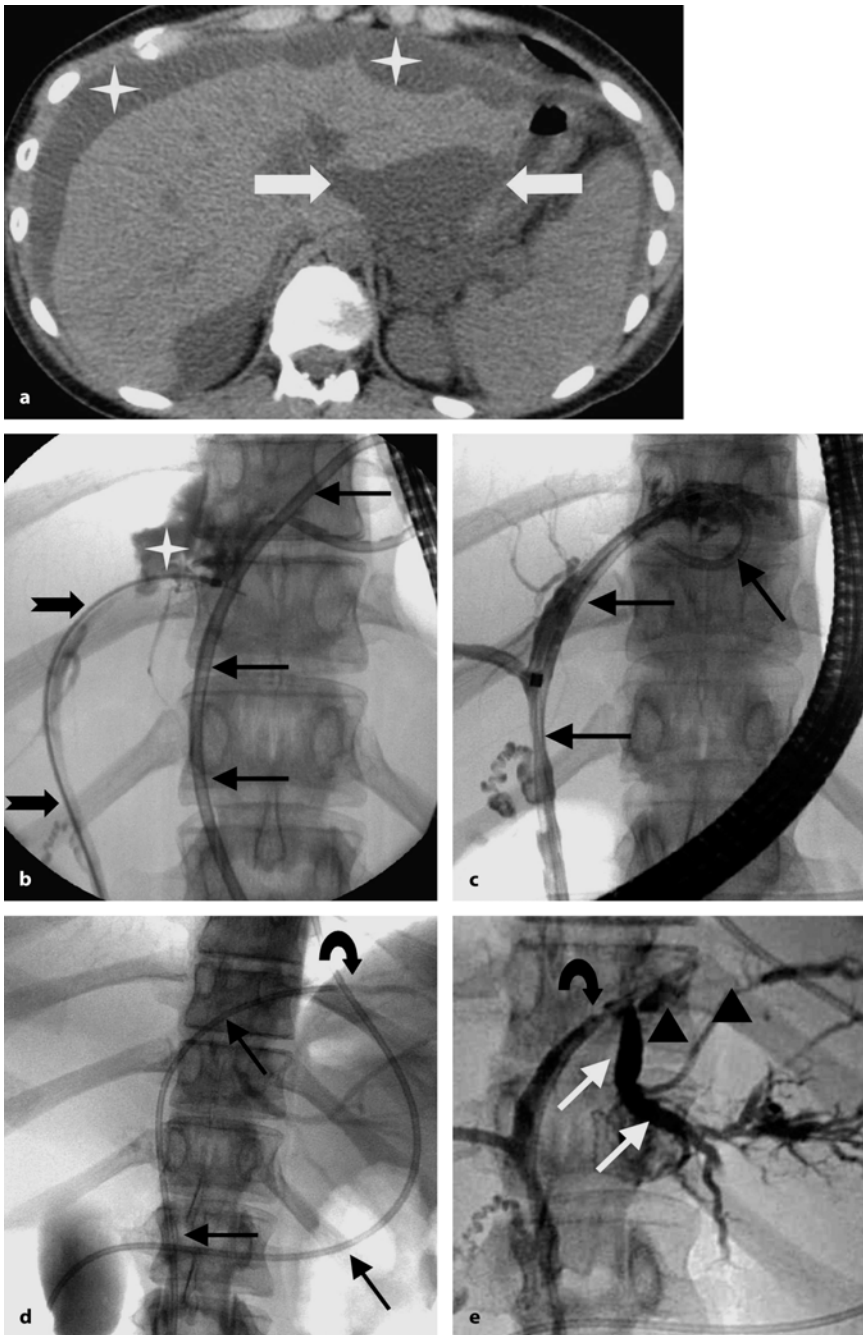


**Fig. 3.** A 19-year-old polytrauma female developed massive bilious ascites 3 days after a grade-III blunt liver injury managed conservatively. She complained of severe upper abdominal tenderness and develops biliary peritonitis. **a** Under sonographic guidance two 12-F drains are placed percutaneously in the right perihepatic (stars) and left retrohepatic (arrows) spaces, leading to a near complete resolution of symptoms. Magnetic resonance cholangiography demonstrates biliary leaks from the left hepatic duct. **b** Endoscopic retrograde cholangiography (ERCP) confirms a left bile duct (thick arrows) rupture supplying an intrahepatic biloma (star) contiguous to the percutaneous drain (thin arrows) placed initially in the left retrohepatic biloma. **c** A naso-biliary drain (arrows) is placed in the proximal left bile duct after unsuccessful attempt to catheterize the peripheral branches of the segment II. **d** Five days later, a re-attempt to place a naso-biliary drain (arrows)

more distally (curved arrow) succeeds. **e** Eight days later, control ERCP discloses dilatation of segment-III bile ducts (arrows) due to a tight stenosis (curved arrow), and retrograde displacement of the naso-biliary drain away from the injured bile duct (arrowheads). **f** After failure of an endoscopic approach, a percutaneous transhepatic access (arrows) succeeded to cross a tight posttraumatic stenosis (curved arrow). **g, h** After balloon dilatation of the stenosis (white arrows) via the percutaneous access, a plastic endoprosthesis (thin arrows) is insert by a “rendez-vous” technique. The stent cross entirely the injured left bile duct (thick arrow). **i** Control ERCP performed 3 months later discloses a sequela focal bile duct stricture (arrowhead) inducing severe bile ducts dilatation (arrows). **j** The stricture is successfully managed by long-term large stent implantation (arrows). At 6 months follow-up, the patient remains asymptomatic



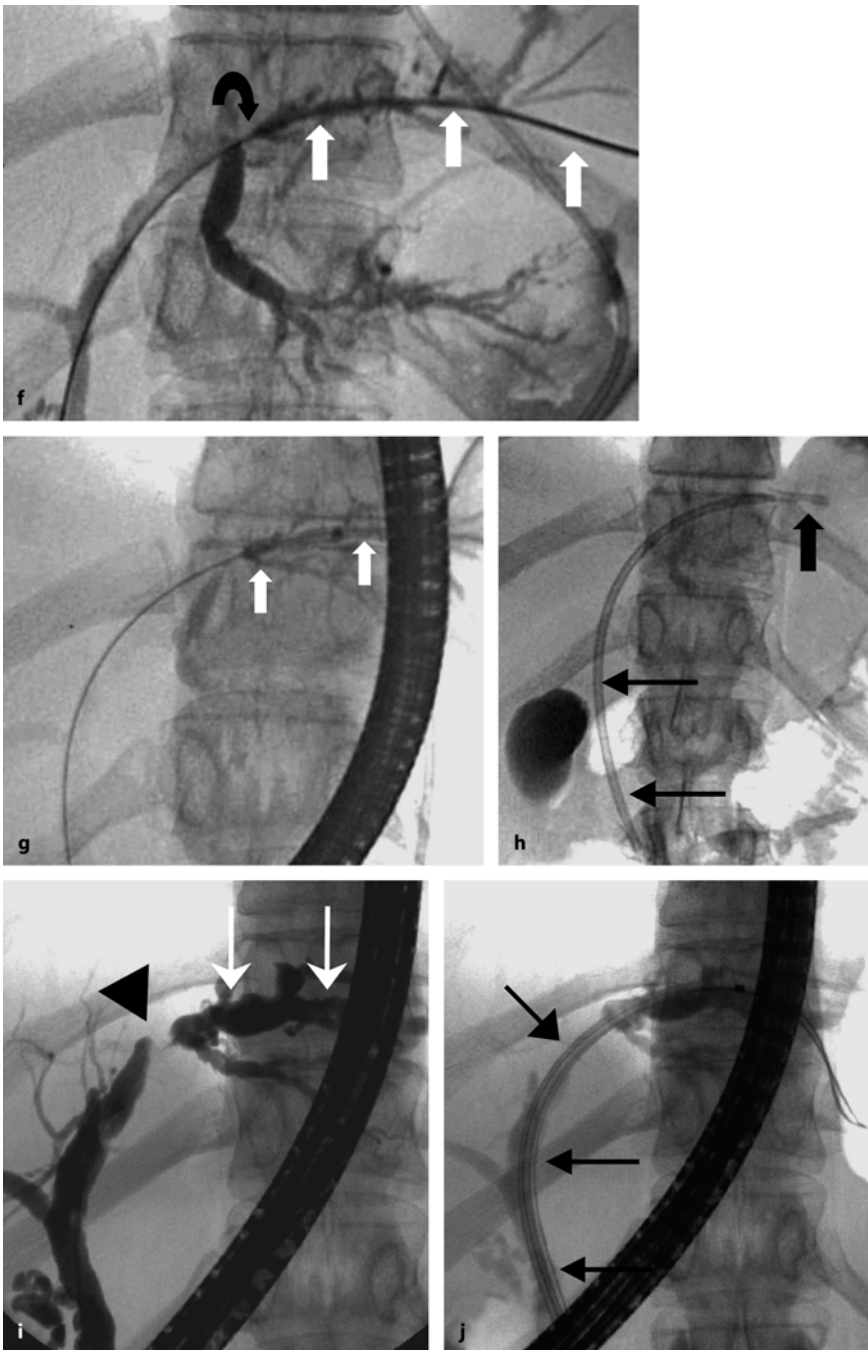


**Fig. 3.** (continued)

### Biloma

Bilomas, reported with an incidence ranging from 2 to 12%, may be asymptomatic or present with right-side upper quadrant fullness or pain. Persistence or continued growth of a cystic intra- or perihepatic collection after hepatic trauma should suggest the diagnosis of biloma which may be confirmed by a percutaneous aspiration of bile or demonstration of a communication with the biliary tree by <sup>99m</sup>Tc-PIPIDA cholescintigraphy [270, 278]. A clinical range of presentation for bilomas from 11 days to 2.5 years has been described [180]. Small bilomas <3 cm in diameter usually do not require treatment and resolve with conservative management unless they become infected. Bilomas >3 cm should systematically be treated, preferentially by percutaneous drainage or surgically to avoid pseudoaneurysm development [96]. Indeed, the presence of bile delays liver wound healing by the inflammatory reaction induced nearby the vessels. This process could lead to rupture of blood vessel wall with the development of a pseudoaneurysm (Fig. 1) [33]. The drainage should remain in place until the communication between the biliary system and the biloma cannot longer be demonstrated by direct opacification or nuclear imaging [33, 51]. If the bile output is not significant early (<50 ml/day), the drain is normally removed within 2 weeks. Those patients with high-output leaks (>50 ml/day) should remain with drainage catheter in place until the output is negligible to prevent recurrence [162]

### Biliary Fistula

The chief investigational tools to search and diagnose biliary fistula are nuclear hepato-biliary scan (HIDA) and ERCP [107, 114, 208, 216, 278]. Hepato-biliary nuclear scanning with technetium <sup>99m</sup>-dimethyl iminodiacetic acid (HIDA) is a sensitive test for studying the hepatic parenchyma and demonstrating the presence or absence of biliary leaks because it is concentrated and excreted into the biliary ductal system. Once a biliary fistula is diagnosed, a percutaneous cholangiogram, or often preferentially a ERCP, is required to determine whether the source of bile is from either a peripheral biliary radical or a main branch of one of the major hepatic duct [8, 49, 243]. Conventional therapy has usually involved surgical intervention with debridement, ductal repair and controlled drainage to seal the fistula [27, 170]; however surgery is often difficult as demonstrated by the high mortality rate, ranging from 5 to 8%, for redo surgery to control biliary fistulas after hepato-biliary surgery. Direct surgical exploration and ligation of the extra- or intra-hepatic duct, hepatic resection or a Roux-en-Y hepatico-jejunostomy remains an option when conservative methods have failed. Endoscopic treatments, including sphincterotomy, nasobiliary drainage or biliary stent insertion, are effective tools for the management of post-traumatic bile leakage (Fig. 3) [49, 51, 107, 114, 162, 188, 208, 216, 243, 259]. A temporary

stent, placed to bridge a common bile duct laceration or bypass either right or left main hepatic ducts defect, will induce subsequent healing of the fistula, confirmed by follow-up ERCP and/or radionuclide scan before stent removal [8, 51, 58, 107, 136, 216, 243]. An additional endoscopic sphincterotomy may be useful to reduce fistula output by decreasing the intra-biliary pressure (Fig. 4) [208, 259]. Ablation of the pressure gradient within the common bile duct will enhance flow away from the fistula and down the common duct into the duodenum. Although endoscopic sphincterotomy alone may result in closure of a peripheral biliary fistula [208], these injuries are best treated by such combined percutaneous biloma drainage and endoscopic sphincterotomy [136, 188, 216, 243]. If the distal bile duct is strictured, balloon dilatation or insertion of a large diameter stent will be required. The value of endoscopic treatment may be limited when ERCP does not detect the biliary fistula because of sequestration [243]. In this setting, a primary percutaneous transhepatic biliary drainage is recommended despite difficult catheterisation of non-dilated intrahepatic bile ducts. Thoracobiliary fistulas, including pleurobiliary and bronchobiliary communications are rare, but severe delayed complications of synchronous diaphragmatic and hepatic injuries treated non-operatively [167, 266]. Endoscopic retrograde cholangiopancreatography is the imaging modality of choice because it has the potential of therapeutic intervention by sphincterotomy and/or stent placement (Fig. 4) [167, 217, 266]. In some cases both secure closure of diaphragmatic perforations and adequate drainage of all bilious collections are required for successful management [217]

### Bile Peritonitis

Liver trauma patients, without evidence of associated injury based on initial and follow-up physical examination and CT scan, and who subsequently developed fever, persistent abdominal pain and leucocytosis, should be highly suspected to develop bile peritonitis [27, 34, 89]. Biliary nuclear scan are the keys to the diagnosis of bile peritonitis [34, 188, 278]. The development of large bile leak with secondary bile ascites and bile peritonitis has generally mandated laparotomy [89], which is aimed at the evacuation and irrigation of the peritoneal cavity, localisation of the bile leak, possible repair of the duct and finally drainage. The combination of sequential laparoscopic surgery and endoscopic or percutaneous stenting provides a minimally invasive alternative to conventional laparotomy [34, 89, 135]. Laparoscopy is extremely useful to evacuate bile and/or blood, place drain for adequate irrigation and drainage of the peritoneal cavity and assess the extent of the liver injury, the gallbladder and the extra-hepatic tree [32, 34, 135, 178]; thereafter, ERCP should be performed for three reasons: firstly, for precise delineation of the source of the bile leak, secondly, to exclude pathology in the distal biliary tree such as blood clots, incidental stricture or



**Fig. 4.** This 38-year-old man had sustained a right flank gunshot injury. The bullet crossed from the right lateral chest wall to the left paravertebral space through the inferior pulmonary lobe and upper part of the right liver lobe. Due to complete transection of the spinal cord, the patient was paraplegic at admission. A massive right hemothorax was initially drained percutaneously. **a, b** Admission contrast-enhanced CT scan of the upper abdomen shows the bullet located just behind the T11 vertebral body (*white arrows*) and a large contusion of the dome of the liver (*black arrows*). No active bleeding is observed inside this grade-III liver injury (*star*). A non-significant haemoperitoneum is visible around the spleen. The patient was managed conservatively. **c** Because of progressive resorption (*stars*) on serial CT and good clinical course, the bilio-haematoma is initially not drained. **d** At day 9 after the injury, the presence of bile in the pleural drain is highly suspicious of a bilio-pleural fistula. An endoscopic retrograde cholangiography confirms the peripheral biliary leaks (*arrows*) supplying the intrahepatic biloma (*star*). **e** A bilio-pleural fistula (*black arrows*) between the biloma (*star*) and the right pleural space (*arrowhead*) is clearly demonstrated after selective cholangiography (*white arrow*). **f** A naso-biliary drain (*arrows*) with its distal tip located within the peripheral leakage is used in combination with a sphincterotomy to manage this biliary complication. A complementary percutaneous drainage of the intrahepatic biloma would be necessary for complete healing of the leak. **g** A CT scan obtained at day 36 shows almost complete resolution of the hepatic injury (*star*). A residual small scar (*curved arrow*) is still visible

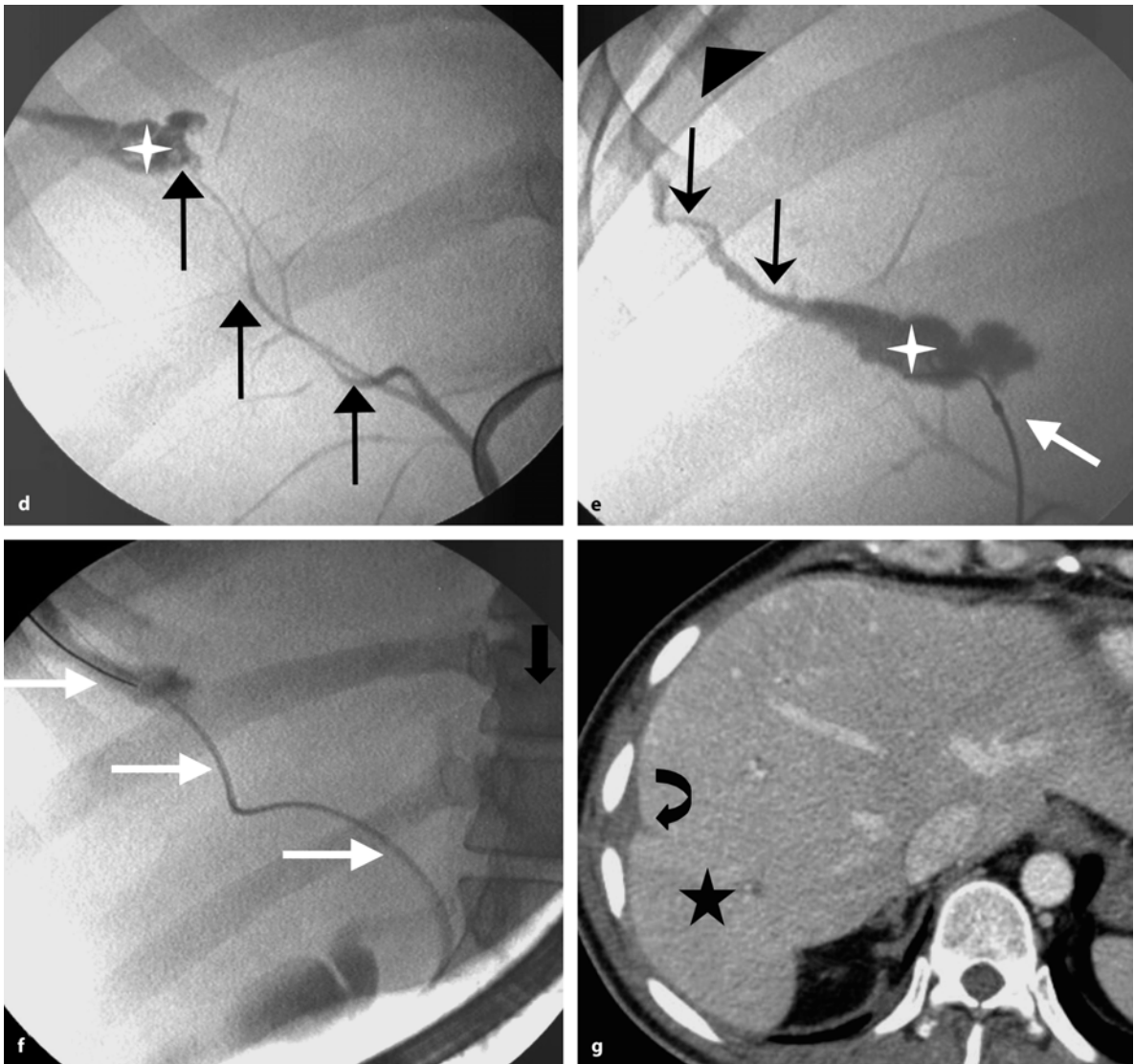


Fig. 4. (continued)

choledocholithiasis, which could interfere with closure of the bile leak, thirdly, to stent the bile leak, if possible; Fig. 3) [32, 34, 89, 188]

### Biliary Strictures

Secondary biliary strictures due to blunt abdominal injuries are often delayed diagnosis until the appearance of clinical manifestations such as jaundice or abnormal laboratory results (Fig. 3) [277]. This delayed complication is rarely reported but may result in permanent damage to the bile duct causing secondary cirrhosis in case of very late diagnosis [218]. Several mechanisms of traumatic bile duct injury have been suggested including traumatic compression of the gallbladder causing acute common bile duct ductal distension, compression of the common bile duct against the spine, lat-

eral shear stress to the supra-pancreatic duct and disruption of the segmental blood supply to the bile duct causing ischemia [277]. As common CT scan and ERCP findings are non-specific and could mimic malignant strictures, a correct diagnosis based on these imaging findings without clinical history of trauma [218, 277] may be difficult to do. Surgery has been traditionally used to treat benign biliary strictures, but with a high post-operative recurrence rate up to 18%. Presently, permanent or temporary endoscopic or percutaneous stent placement, depending on the injury site, should be considered the primary therapeutic option, allowing for both biliary decompression and duct stricture management (Fig. 3) [40, 277]. When the bile duct dilatation and stenting could not be performed via ERCP or percutaneous routes, surgical reconstruction or bilio-enteric anastomosis, depending on the injured site, should be performed [218, 277]



### 2.2.2.4 Fluid Collections, Sepsis and Varia

Sepsis related to liver injury, most commonly pneumonia, abdominal abscess or wound infection, accounts for up to 15% of deaths and is the second cause of death after haemorrhage in liver trauma [59]. A high incidence, between 15 and 27% [8, 59], is reported after major hepatic trauma, in patients requiring liver haemostasis, multiple surgeries and who had more than one organ injured or GI perforation [85, 108, 154]. The rate of intra-abdominal abscesses is not increased with NOM [154]. Cysts, which may result from incomplete resolution of bilio-haematoma, are being recognised with greater frequency as CT scan become increasingly available [136]. As bile cysts may sometimes resolve spontaneously, they should not be drained unless the patient is symptomatic or febrile or the cyst is seen to expand on serial scans. The CT or sonographic-guided percutaneous aspiration of any suspicious collection should be performed, followed by an immediate gram stain of the aspirate. If negative, no attempt at drainage should be done in order to avoid iatrogenic contamination of sterile collection. Liver abscesses are predominantly found in patients treated operatively for their primary liver injury [13, 63, 85]. As a complication of NOM of liver trauma, liver abscess is an uncommon entity, with an incidence ranging from 0.7 to 4.3% [108, 109]. It is usually seen in severe injury and prolonged hospitalisation may be required in this patient group [109, 154, 180]. Predisposing factors related to the formation of a liver abscess after trauma include associated enteric injuries, extensive parenchymal damage, inadequate debridement of devitalised liver tissue, untreated bile leaks and persistent post-operative haemorrhage [109]. As CT-guided percutaneous drainage of liver abscess is widely accepted as the mainstay of treatment, being successful in 78–100% of patients [4, 176, 180, 276], all patients with a well-organised intrahepatic abscess should primarily undergo a trial of medical treatment and percutaneous drainage. As a large majority of these abscesses are noted

within 12 days after complex liver injury of at least grade III, scheduled repeat CT scan within 72 h after injury for early detection and management and the prophylactic use of antibiotics may be justified in patients with complex liver injury [109]. Laparoscopy may be useful to drain large retained haemoperitoneum or infected perihepatic collections not accessible by percutaneous approach [34]. The incidence and management of trauma-related liver abscess are summarised in Table 3. Abdominal compartment syndrome usually requires laparotomy in order to alleviate compression-related symptoms [135]. Gallbladder infarction is not always a remote complication and should be considered in patients who have undergone hepatic embolisation after trauma [162]. The development of huge pleural effusion after blunt liver injury has been rarely reported [72]

### 2.2.3 Spleen

Patients with splenic injury, treated either surgically or non-operatively, have the potential for developing life-threatening delayed complications such as delayed re-bleeding, vascular malformations, parenchymal or subcapsular pseudo-cysts and splenic or subphrenic abscesses [15, 26, 42, 50, 55, 74, 93, 181, 213, 267, 275]. Although associated with higher grades of injury, a blush sign on admission CT do not mandate systematically embolisation in children [62, 149]. Conversely the presence of a blush sign may portend failure of NOM in adults [5]. After NOM of splenic injury, the incidence of complications is reported to be up to 17.6% in adults [42, 50, 206, 267] and from 0 to up 7.5% in children [74, 231]. These complications, especially in cases of arteriovenous fistula, could lead to failure of NOM of blunt splenic injuries in both children and adults [50, 93, 231, 267]. Delayed complications associated with NOM of spleen trauma and detailed by the most relevant series between 1990 and 2005 are summarised in Table 4

**Table 3.** Liver abscess after hepatic injury. (Adapted from [109])

Reference	No. of patients	Mechanism of liver injury	Management of liver injury	No. of abscesses	Management of abscess	Abscess-related mortality
[13]	295	Blunt + penetrating	Operative	23 (7.8%)	Surgery	4 (17%)
[63]	482	Blunt + penetrating	Operative	34 (7.1%)	Surgery 25, Percutaneous drainage 9	3 (8.8%)
[22]	46	Blunt	Non-operative	2 (4.3%)	Percutaneous drainage	0
[180]	404	Blunt	Non-operative	3 (0.7%)	Percutaneous drainage 2, surgery 1	0
[154]	518	Blunt	Non-operative	0	–	0
[108]	674	Blunt	Operative ( <i>n</i> =279); non-operative ( <i>n</i> =395)	15 (5.4%); 6 (1.5%)	Surgery, Surgical drainage 3, Percutaneous drainage 2, conservative 1	0



**Table 4.** Delayed complications after non-operative management (NOM) of splenic trauma, E embolisation at admission, NA not available;  $\psi$ A pseudo-aneurysm

Reference	No. of patients	CT grade of injury	No. of patients	Type	DELAYED COMPLICATIONS		
					Treatment	Mortality	Success NOM
[44]	112	I-II 71%, III-IV 29%	13 (12%)	Bleeding 12, pancreatic cyst 1	Splenectomy 13	0	99 (88%)
[213]	90 (-E), 150, 60 (+E)	I-II 71%, III-IV 29%, I-II 37%, III-IV 63%	9 (0.6%)	Bleeding 4, abscess 3, haematoma 2	Splenectomy 4, drainage 2, conservative 3	4	143 (95%)
[95]	13 (-E), 28, 15 (+E)	I-II 77%, III-IV 23%, I-II 27%, III-IV 73%	0	0	0	0	26 (93%)
[42]	87	NA	7 (8%)	Bleeding 5, abscess 1, cyst 1	Splenectomy 5, embolisation 2, (pseudo-aneurysm)	0	82 (94%)
[50]	332 (+E20)	I-II 62%, III-IV 38%	16 (5%)	Bleeding 16	Splenectomy 16	0	310 (93%)
[181]	102	I-II 66%, III-IV 34%	2 (2%)	Bleeding 2	Splenectomy 2	0	100 (98%)
[74]	40 (children)	I-II 60%, III-IV 40%	3 (7%)	$\psi$ A 2, abscess 1	Spontaneous resolution 2, drainage 1	0	40 (100%)
[93]	140 (+E)	I-II 13%, III-V 87%	27 (19%)	Bleeding 16, abscess 4, infarct 2, missed injury 4, iatrogenic arterial injury 1	Splenectomy 18, embolisation 7, conservative 1, groin exploration 1	0	122 (87%)
[55]	8 (+E), 132 (-E)	NA	3 (2%)	Bleeding 2, hematoma 1	Splenectomy 2, drainage 1	0	137 (98%)
[15]	37 (+E), 67, 30 (-E)	III-V, I-III	2 (5%), 2 (6%)	Bleeding 1, hematoma 1, bleeding 2	Splenectomy 1, drainage 1, splenectomy 2	0	63 (94%)

### 2.2.3.1 Clinical Presentation and Imaging

During the course of a NOM of splenic trauma (Table 5), the sudden onset of delayed bleeding may be the result of either lysis of a subcapsular clot that had sealed parenchymal tears immediately after injury [15, 172], or rupture of a post-traumatic false aneurysm or arteriovenous fistula. In 70% of patients, the haemorrhage occurs within 2 weeks of the injury, but secondary haemorrhage in rare instances can occur months after injury [26, 172, 197]. As 75–90% of adults with pseudo-aneurysm or arteriovenous fistula [50], and all such lesions in the paediatric population [88, 104, 150, 155, 168], occur only in patients having grade-III or greater injury, a follow-up CT is reasonable and mandatory only in patients with such graded injury

#### Delayed Rupture

The so-called delayed splenic rupture represents injury in evolution including both missed primary rupture and true secondary rupture due to either clot lysis aside the injured arterial wall or expanding subcapsular haematoma by osmotic phenomenon [65, 130]. A distinction should be made between true delayed rupture (normal initial CT scan) and delayed recognition of rupture (no initial or misread initial CT scan; Fig. 5) [65]. The true clinical entity of delayed rupture is defined as bleeding occurring more than 48 h after blunt trauma in a previously haemodynamically stable patient following an initially normal CT scan [130]. The early utilisation of CT scan, before subcapsular haematoma has growth enough to be visible, may be also the reason for the delay in the detection of some discrete splenic injuries [3, 16]. The incidence of true delayed rupture, estimated to be as high as 5–40% of all splenic injuries [159] before the CT scan era, seems to be as low as 1–2% [3, 172] if considering delayed recognition of splenic injuries. If strict criteria are used, only a few case reports can be considered as true delayed splenic rupture [65, 142]. No predicting factor for a delayed splenic rupture has been recognised [26]. Isolated post-traumatic enlargement of the spleen could be a possible sign of delayed rupture [18]. The only consistent sign of impending rupture might be an increase in size of a subcapsular haematoma. Such delayed ruptures can present atypically and after minor trauma often forgotten by the patient [3]. One theory suggests that increased capsular pressure secondary to clot lysis and increased oncotic pressure later causes free rupture of the capsule and massive bleeding [65, 130]. A second theory is that surrounding organs or omentum tamponades a perisplenic haematoma which later ruptures freely into the peritoneal cavity [3, 130, 159, 172]. Delayed splenic rupture has been reported to occur as long as 2–5 years post-injury [26]. The significance of delayed splenic rupture lies in its higher mortality rate (5–15%) as compared with these of the primary splenic injury (1–3%)

[44, 130]. Although splenectomy has been the standard treatment for delayed splenic rupture [3], more conservative management with or without embolisation is gaining wider acceptance in selected populations [65], should the criteria for conservative management be fulfilled (Fig. 5) [65, 130, 142]

#### Pseudo-aneurysm

The mechanism for the development of traumatic splenic artery pseudo-aneurysm is related to intimal trauma and disruption of elastic fibres associated with deceleration injury, leading to intimal fragmentation and weakening of the arterial wall [50, 104, 241]. Rapid enlarging intra-splenic post-traumatic pseudo-aneurysm may develop from pulpar laceration and haematoma continuously supplied with blood from injured intra-splenic arteries. Vascular blushes on contrast-enhanced CT scan were proven to be contained intra-splenic haematoma with active haemorrhage that slowly enlarge and finally rupture in most cases [104, 206]

From intra-operative inspection of the spleen, it was found that the CT contrast blush is a contained intra-splenic haematoma with active haemorrhage that slowly enlarges and ruptures finally in most cases [104, 126]. The natural history of splenic false aneurysm is unclear, but they have been implicated as the source of secondary delayed splenic haemorrhage in both children and adults [42, 50, 88, 206]. Delayed presentation or diagnosis is due to, respectively, progressive clot lysis at the site of arterial wall injury or to a technical failure in term of timing of contrast bolus injection on initial CT scan [50]. Although bolus-enhanced CT scan with prompt imaging after iodine injection is highly sensitive to detect intra-splenic vascular malformation [73, 87, 126, 150, 168], it may fail to demonstrate small areas of abnormal enhancement, only identifiable using high-resolution ultrasound. Magnetic resonance imaging could also be effective for the diagnosis of intra-splenic pseudo-aneurysm by demonstrating a flow void within the pseudo-aneurysm [87, 126]. The incidence of false aneurysm appears to be lower in children than in adults and its evolution seems less predictable [74, 88, 104, 275]. Unlike splenic artery aneurysm in adult patients, the severity of the splenic injury does not have predictive value for development of such lesions in children [275]. As false aneurysm may remain asymptomatic for a long time period, the possibility of this complication should be investigated even in asymptomatic child with mild splenic injury [150, 275]. Such lesions in children and young people are more likely to resolve spontaneously and less likely to bleed than in older patients [74, 88, 173, 275]. The thicker capsule and more elastic parenchyma of the paediatric spleen, resulting to a self-tamponade, may contribute to spontaneous pseudo-aneurysm thrombosis [74, 206]. It seems then justified to follow-up stable paediatric patients with splenic pseudo-aneurysm with repeated colour

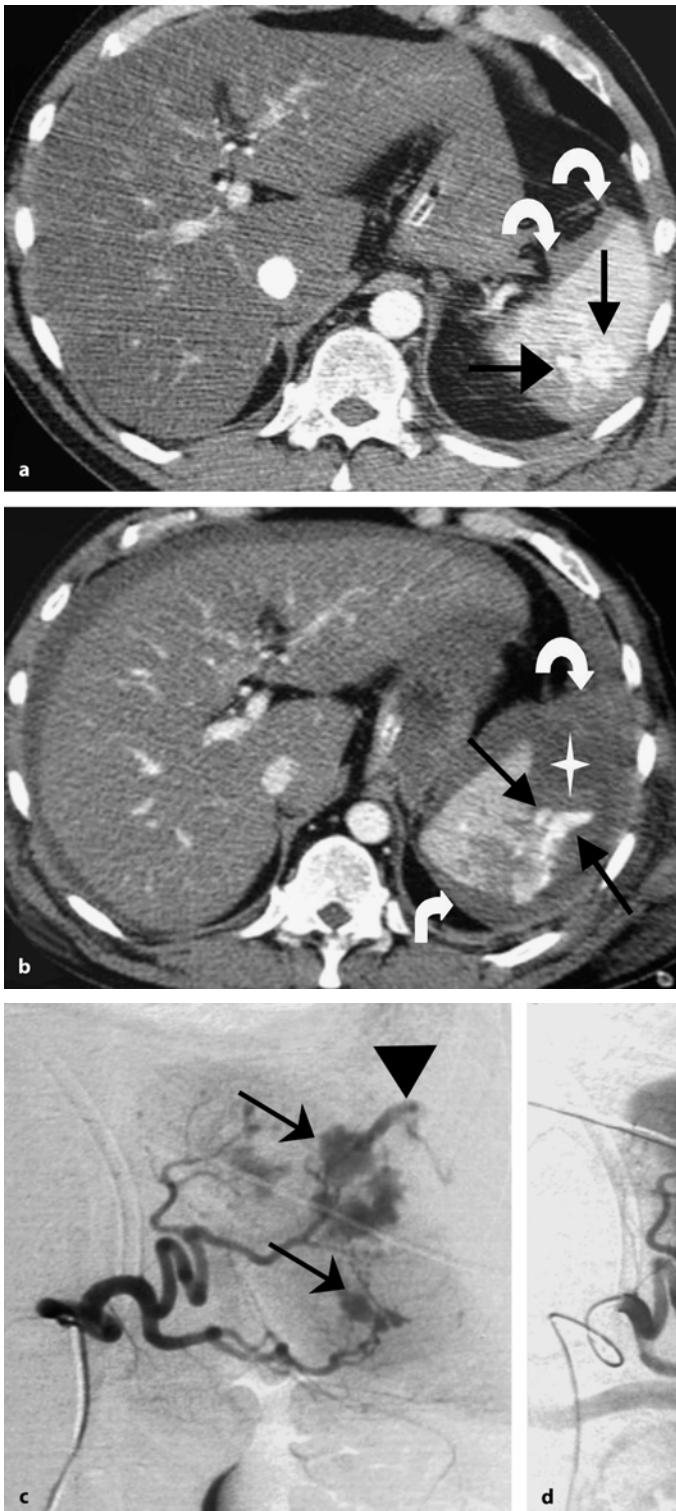


**Fig. 5.** This 49-year-old polytraumatised man was managed conservatively for a grade-IV blunt splenic trauma. **a** Despite small parenchymatous areas of abnormal enhancement (*arrows*) and perisplenic haematoma (*curved arrows*), an angiographic investigation was not performed initially because of preserved haemodynamic stability. **b** On day 5, the patient developed a sudden left abdominal pain with haemodynamic shock. Immediate control CT scan reveals a delayed splenic rupture (*star*) with active extra-splenic bleeding (*arrows*) and an increased perisplenic haematoma (*curved arrows*). **c, d** A selective splenic angiogram (**c** early and **d** late phases) demonstrates two areas of intraparenchymatous extravasation (*arrows*) and active perisplenic bleeding (*arrowheads*) with peritoneal leak (*star*). Because of marked tortuosity of the distal splenic artery, superselective catheterisation of the different bleeding vessels with microcatheters was considered too time-consuming in this emergency setting; therefore, small-size gelfoam pledgets were injected through the 4-F catheter as distally as possible in the splenic artery. **e** Control angiogram shows complete arrest of bleeding and occlusion of two feeding arteries (*arrows*). The upper and lower poles of the spleen (*stars*) are preserved. **f** Early (day 4) control CT scan shows enlarging subcapsular and perisplenic haematoma (*stars*) surrounding the remaining splenic parenchyma (*arrow*). This haematoma requires two times needle aspiration to avoid tertiary rupture

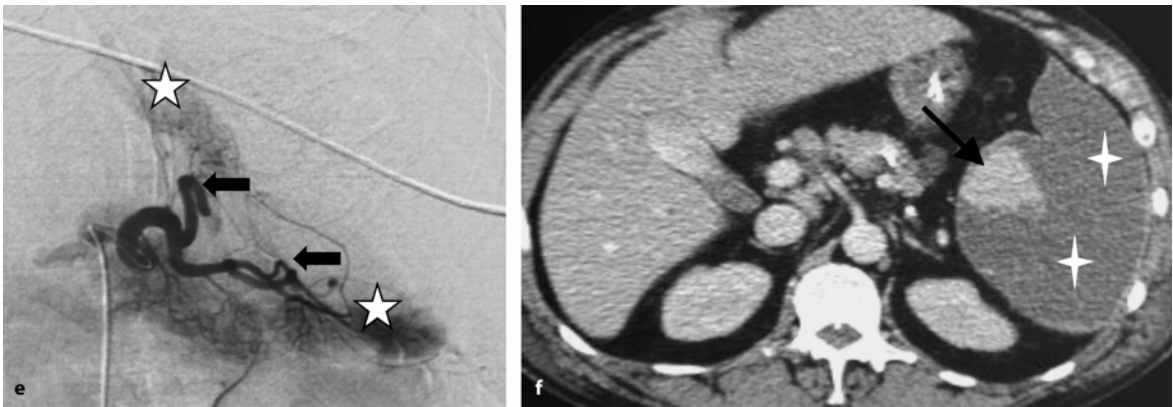
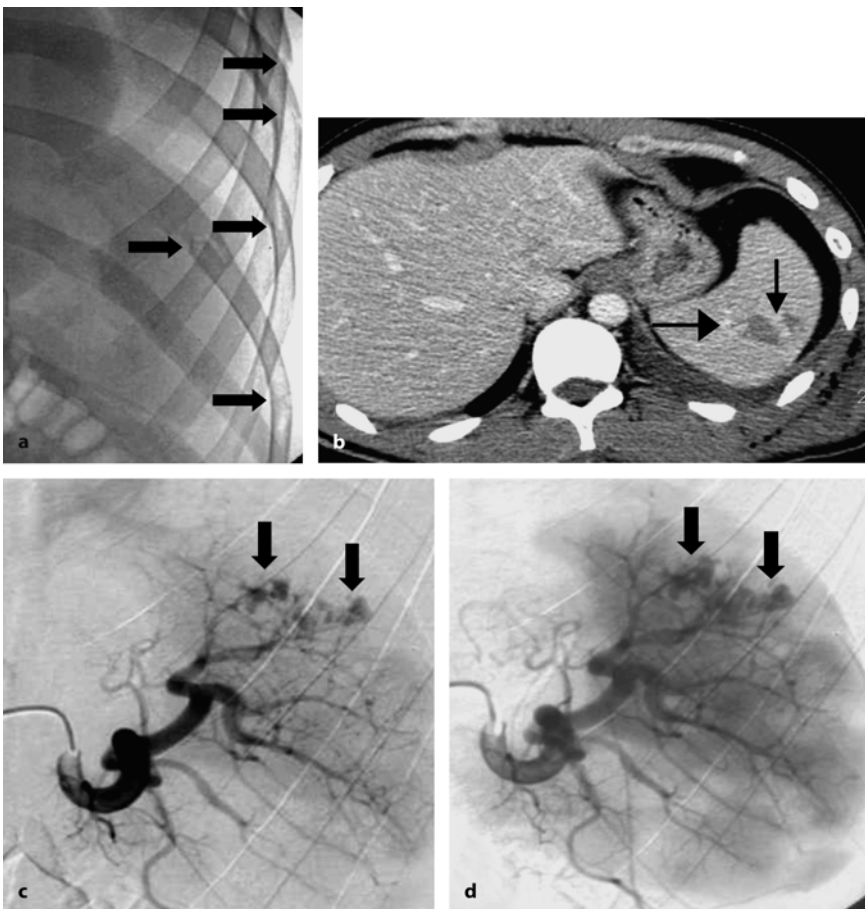


Fig. 5. (continued)



**Fig. 6.** A 27-year-old man presented with moderate left flank tenderness but severe respiratory shortness after a motor vehicle accident. A massive left-side haemopneumothorax is immediately drained percutaneously. A CT scan revealed a grade-II splenic injury. **a** Control chest X-Ray shows fractures of the of the seventh, eighth, ninth, and tenth ribs (arrows) with resorption of the pleural effusion. **b** Routine control enhanced CT scan at day 6 discloses two irregular enhanced areas (arrows) around the contusion in the upper pole of the spleen. **c, d** Splenic arteriogram (**c** early phase, **d** late phase) confirms the hypothesis of two posttraumatic pseudo-aneurysms (arrows) developed within the injured area. No arteriovenous fistula

is observed. **e** Superselective catheterisation of arteries feeding both aneurysms (catheter Progreat 2.7, Terumo Corporation, Tokyo, Japan) is performed. Contrast injection confirms good positioning of the tip of the microcatheter (arrow). **f** Both aneurysms are selectively embolised by distal occlusion of respective feeder with two microcoils (Hilal 2/2, William Cook Europe, Denmark) each (arrows). **g** Control angiogram shows complete exclusion of both aneurysms (arrows) while the proximal arterial feeders remain open. A limited amount of peripheral devascularisation (star) is observed. **h** At 2 weeks control CT, a peripheral triangular-shape area of hypoperfusion is observed in front of the coils (arrowheads)



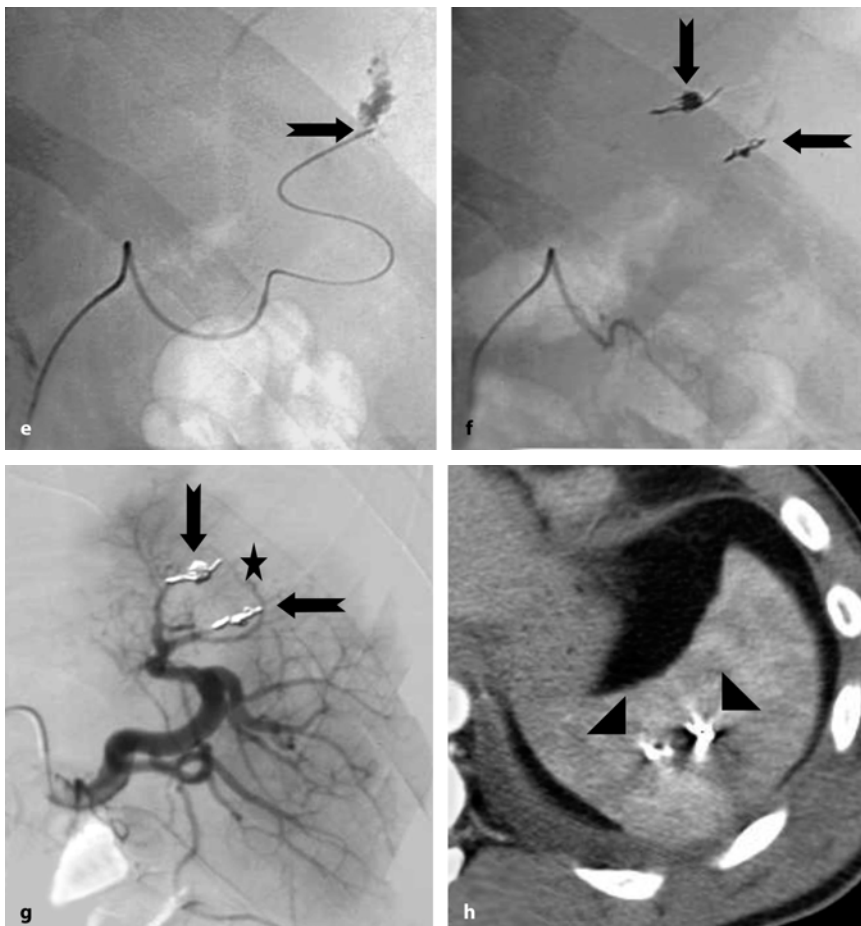


Fig. 6. (continued)

Doppler examinations expecting spontaneous resolution of this lesion. In adults, most pseudo-aneurysms, which occur more likely in higher-grade splenic injuries [50, 74], progress over time and ultimately rupture, leading to delayed splenic haemorrhage in days, months or even years after the inciting event [50, 181, 206]. As all paediatric cases and a large majority of adult pseudo-aneurysms are noted on delayed imaging studies (Fig. 6), the need for follow-up studies to document splenic injury healing is obvious especially in grade-IV and grade-V injuries [275]

#### Arteriovenous Fistula

Post-traumatic splenic arteriovenous fistulae are rare, very uncommon in the paediatric age group [155, 168] and usually associated with a newly developed pseudo-aneurysm (Fig. 6). Low-flow splenic arteriovenous fistulae may be asymptomatic for an extended time interval and are disclosed either during routine sonographic follow-up [168] or by auscultation of a continuous systolic murmur. Symptoms resulting from a chronic high-flow splenic arteriove-

nous fistula are numerous, including a continuous thrill, diarrhoea due to congestion of mesenteric veins, ascitis, chronic abdominal pain from bowel ischaemia related to a mesenteric steal syndrome [155] and hypovolaemic shock due to rupture of an associated pseudo-aneurysm [196, 201]. In long-standing fistulae, splenomegaly and portal venous hypertension or high output cardiac failure may occur

#### Endovascular Management

Therapeutic options include observation, angiographic embolisation, splenectomy or surgery with splenic preservation. Selective embolisation of the artery tributary to the vascular malformation should be considered as the first choice treatment (Figs. 6, 7). In adults, an aggressive use of embolisation seems mandatory to decrease the failure rate of NOM due to late rebleeding related to false aneurysm rupture [42, 50, 74, 175]. As spontaneous thrombosis is the rule in children, an expectant attitude is more indicated in young patients, should repeated sonographic control be feasible [88, 164]





**Fig. 7.** A 55-year-old man complains of persistent left flank pain with two episodes of discrete haematuria after a minor motorcycle accident. The haemodynamic condition is preserved. **a, b** Enhanced abdominal CT scan performed 8 days after trauma is unremarkable for the urinary tract but discloses isolated multiple abnormal vascular blushes (*arrows*) inside the upper pole of the spleen. No haemoperitoneum or subcapsular haematoma are visible. **c** Proximal splenic arteriogram confirms the hypothesis of a multilobulated pseudo-aneurysm (*arrows*) supplied by one peripheral splenic arterial branch. **d** Contrast injection after superselective catheterisation of the feeder with a microcatheter (Progreat 2.4, Terumo corporation, Japan; *thin arrows*) discloses an early venous filling (*thick arrows*) following opacification of the pseudo-aneurysm (*curved arrows*). These findings are compatible with an arteriovenous fistula. **e** Diluted glue (Glubran 2, GEM, Italy) 20% / Lipiodol (80%; Guerbet, Aulnay-sous-Bois, France) is injected through the microcatheter directly into the pseudo-aneurysm (*curved arrows*). Glue leak on the venous lining is visible (*arrows*). **f** Control angiogram shows a complete exclusion of the arteriovenous malformation (*curved arrows*), a limited area of parenchymal devascularisation (*arrows*) and preserved patency of the intrasplenic arterial branches. **g** On non-enhanced CT control performed 2 weeks after embolisation, the glue cast outlines the aneurysmal cavity (*star*)

## Techniques and Results

In acute setting, isolated coil occlusion of the proximal splenic artery is the preferred technique when multiple extravasation areas are documented within the splenic parenchyma. The theory behind these techniques is that occluding the proximal splenic artery will decrease blood pressure to the organ, therefore promoting thrombosis of the visualised areas of extravasation, with a low risk of tissue infarction [15, 70, 93, 95, 213]. This technique may also be applied as an alternative to splenectomy in case of delayed bleeding without angiographic demonstration of a true vascular malformation [70, 93] but is not valuable to exclude focal vascular malformations. As most of them will arise from intra-parenchymal branches, the most efficient and safe means to definitively occlude splenic pseudo-aneurysm or arteriovenous fistula, without risk of sepsis, is to perform a superselective embolisation in order to spare collateral vessels (Figs. 6, 7) [50, 87, 126, 155, 175, 196]. This technique often requires use of a micro-catheter or flow-directed catheter (Fig. 6) [87, 155, 196]. Available micro-catheters may be successfully advanced into small branches with low risk of spasm or intimal damage, allowing micro-coil deposition on both sides of the pseudo-aneurysm neck (Fig. 7) or glue (Fig. 6) or particles injection. As an immediate and permanent occlusion is intended, micro- or Gianturco coils are the first-choice embolic agents [87, 126, 155, 175, 196]. Moreover, coils need less pressure for deposition than the considerable pressure required to force gelfoam out of a micro-catheter. This force may be transmitted to the fragile pseudo-aneurysm wall that consequently may rupture [151]. Gelfoam has some other disadvantages as it temporally occludes the vessel, raising the risk of future recanalisation, and may migrate and occlude small arteries within the spleen, causing complications such as pain and infection due to peripheral necrosis [151]. Detachable balloons could also be used to manage large saccular pseudo-aneurysms [10]. Transcatheter autologous thrombin injection into the aneurysmal neck to induce thrombosis of the pseudo-aneurysm represents an alternative embolic agent, avoiding placement of foreign material into injured splenic parenchyma [60]. The incidence of segmental splenic infarction and intra-splenic air is increased with distal embolisation [128]. Infarcts after distal embolisation tend to be larger and occur just distal to the embolisation material, whereas infarcts after proximal embolisation tend to be smaller, multiple and located in the periphery. Limited infarction rate (>25% of the gland) have no clinical implications because these infarcts are often associated with minimal symptoms [15, 92, 93, 128]. Gas may be present within a sterile infarct after embolisation with gelfoam. An air/fluid level within a subcapsular collection is a strong predictor of abscess that requires percutaneous drainage [15, 128]. Clinical success rates of embolisation range between 85 and 96% in adult patients [10, 42, 50, 126, 151, 175, 184]. Albeit partial or total splenectomy has been traditionally performed to manage

ruptured pseudo-aneurysms in children [104, 168, 201], embolisation has been recently described in a few cases [73, 155]

### 2.2.3.2 Fluid Collection

#### Pseudo-cyst

Splenic pseudo-cysts, either subcapsular or intra-parenchymal, are occasionally observed after blunt abdominal trauma, mainly those managed non-operatively [179] or after initial embolisation [93]. Because of delayed development of subcapsular haematomas, post-traumatic cysts may form in patients with initially discrete splenic injuries [181]. They form by the organisation of an intra-splenic haematoma. The blood is partially or completely absorbed leaving a brownish-green fluid surrounded by a fibrous capsule. An asymptomatic cyst, which develops following abdominal trauma and ruptures, possibly years later, is a potential mechanism for delayed splenic rupture. Clinical presentation include local or referred pain to the left shoulder as a result of phrenic irritation, abdominal distention and splenomegaly-related symptoms such as early satiety, emesis, dysphagia, left lower lobe atelectasia. Asymptomatic cysts of <5 cm may be managed expectantly, since most involute within 3 months to 3 years [179]. Conversely, cysts >5 cm in diameter seem to be prone to the complications of rupture (25% of risk) and infection and therefore should be treated prophylactically [25, 179]. Percutaneous aspiration, followed by catheter insertion for infusion of tetracycline, could be the initial approach. Splenorrhaphy or resection of the cyst-bearing portion of the spleen with marsupialisation [38, 42, 179, 257] is indicated after failure of the percutaneous approach which occurs in 10% of cases

#### Abscess

Splenic abscess may present within several months or years after the causal injury [174, 182, 251]. Due to the parenchymal disruption, trauma creates a situation that increases the susceptibility of the spleen to develop suppuration. Splenic abscess and septicaemia has also been observed after proximal splenic artery coil occlusion performed as primary haemostatic measure [10, 93] or after distal embolisation [128, 174, 213, 251]. During the first weeks after splenic embolisation, splenic abscess and infarcts are the two major concerns. A 3% splenic abscess rate and a 3% aseptic infarct rate are reported after initial embolisation [93]. Abscess formation seems higher in patients having undergone combined proximal coil and selective distal embolisation [93]. Because of the high mortality rate of post-traumatic splenic abscess treated medically, splenectomy has been the mainstay of treatment of this complication [42, 174, 176, 276]. Presently, drainage of splenic abscesses is usually performed with a success rate up to 90% in

unilocular and 75% for multilocular lesions [74, 176, 276]. Splenic abscesses complicating primary embolisation may be treated by percutaneous or intraoperative drainage [93, 128]

### Pleural Effusion

Massive pleural effusion after splenic injury may develop as a sympathetic reaction to the visceral trauma or may be caused by simultaneous injuries to the diaphragm, pleura or lung [133]

## 2.2.4 Pancreas

The rate of complications after pancreatic trauma is between 8 and 62% [49, 116, 145]. Injury to the main pancreatic duct is the principal determinant for the development of early significant complications such as pseudo-cysts, internal and external pancreatic fistulas, haemorrhage and abscesses [2, 49, 117, 185]. Delayed ductal strictures, occurring from 3 months to 21 years after apparent recovery from the original pancreatic injury, are reported [23, 30, 145]

### 2.2.4.1 Vascular Complications

Post-traumatic pancreatic pseudo-aneurysm is rare, more commonly observed after initial surgical trauma management (5–10%) and usually the result of secondary pancreatitis with enzymatic digestion of the arterial wall. Half of these lesions may rupture either into the GI tract via the pancreatic (hemorrhage pancreaticus) or common bile duct, or into a pseudo-cyst, rarely into the peritoneal cavity. Early angiography is useful both to confirm the clinical suspicion of post-traumatic pseudo-aneurysm and to perform selective embolisation of a peripancreatic pseudo-aneurysm, arteriovenous fistula or bleeding vascular injury. Embolisation, which has a success rate between 80 and 90%, is a viable and attractive alternative to surgery in patients who are often poor surgical candidates [10, 202]. Covered stent may be useful to manage trauma-related arterial rupture or post-operative bleeding vascular injury (Fig. 8)

### 2.2.4.2 Ductal Complications and Fluid Collections

#### Clinical Presentation and Imaging

The CT scan and ultrasonography play a major role not only in the detection and follow-up of ductal complications, but also in the guidance of percutaneous aspiration or drainage of post-traumatic pancreatic collections [226]. Endoscopic retrograde cholangiography (ERCP) remains

the first-line imaging technique when a complete duct transection is suspected, allowing accurate anatomical delineation of the duct injury and facilitating operative strategy [49, 117, 125, 145]. Magnetic resonance cholangiography (MRCP) is helpful to detect or exclude non-invasively pancreatic duct damage and/or pancreas-specific complications following trauma, such as pseudo-cyst not opacified at ERCP [75]

### Fistulae

Fistula, which is the most common complication after pancreatic injury (4.5–35%), is usually secondary to a pancreatic ductal discontinuity after blunt trauma [2, 117]. Frequent low-output fistulae are almost always self-limiting processes resolving spontaneously within 2 weeks to 3 months of injury [185, 259]. High-output fistula or fistula complicated by an increasing or infected collection require an aggressive management including percutaneous or endoscopic drainage, skin protection, nutritional support and intravenous administration of somatostatin in order to hasten external fistula closure [28, 259]. Endoscopic insertion of a plastic stent may be an alternative to conventional surgical techniques such as side-to-side duct-Roux-en-Y loop anastomosis or distal pancreatectomy to seal a major pancreatic duct laceration [2, 49, 185]

### Pseudo-cysts

Post-traumatic pancreatic pseudo-cysts, reported with an incidence rate from 15 to 36%, occur preferentially in the paediatric population [2, 230, 231], may be the result of a missed pancreatic injury and may arise weeks to months after the initial injury. The strategy in the management of traumatic pancreatic pseudo-cysts will depend on the site and nature of the duct injury, the maturity of the cyst wall, the urgency to treat and will differ from children to adults [2, 185]. Depending on the location of the ductal injury, pseudo-cysts and their complications, such as secondary infection, spontaneous perforation and massive haemorrhage, may require aspiration, external drainage or partial pancreatectomy, but conservative management has also been successful in selected cases, mostly in the paediatric population [117]. Spontaneous resolution of cysts after medical treatment is observed in 25–46% in children, and in less than 20% in adults [30, 115, 125, 147]. To manage large or complicated post-traumatic pancreatic pseudo-cysts in children, percutaneous drainage is primarily performed instead of simple needle aspiration which is inappropriate for long-term management of pseudo-cysts refractory to medical treatment [147, 231, 269, 276]. As nearly all post-traumatic pancreatic pseudo-cysts in children are uninfected, reduce-size 8.3- to 10-F drainage catheters are large enough to provide therapeutic long-term drainage [2]. Larger sump drainage catheters are needed in adults or to drain efficaciously septated or infected pseudo-cysts.



**Fig. 8.** After emergent surgical repair (left pancreatectomy with splenic preservation) of a major blunt pancreatic injury with complete distal duct disruption, this 42-year-old man had a good initial recovery. **a** Limited pancreatic fluid collection (*white arrows*) and surgical clips near the patent splenic artery (*black arrow*) are visible on day 8 control CT scan. **b** The patient presents on post-operative day 12 with massive haemoperitoneum and shock requiring emergent abdominal arteriography. A selective splenic injection shows irregular borders (*arrows*) of the splenic artery near the surgical clips. A segmental arterial dissection is suspected. **c** Forceful injection through a large guiding catheter (*arrow*) clearly demonstrates free bleeding (*stars*) arising from the abnormal arterial segment. **d, e** The vascular injury was successfully treated by insertion of a covered stent (Fluency, Bard-Angiomed GmbH, Germany; *arrows*) in the splenic artery that looks patent on control angiogram after stent placement. A circumferential stricture (*arrowhead*) is due to spasm. Dramatic haemodynamic stabilisation is obtained after this endovascular intervention



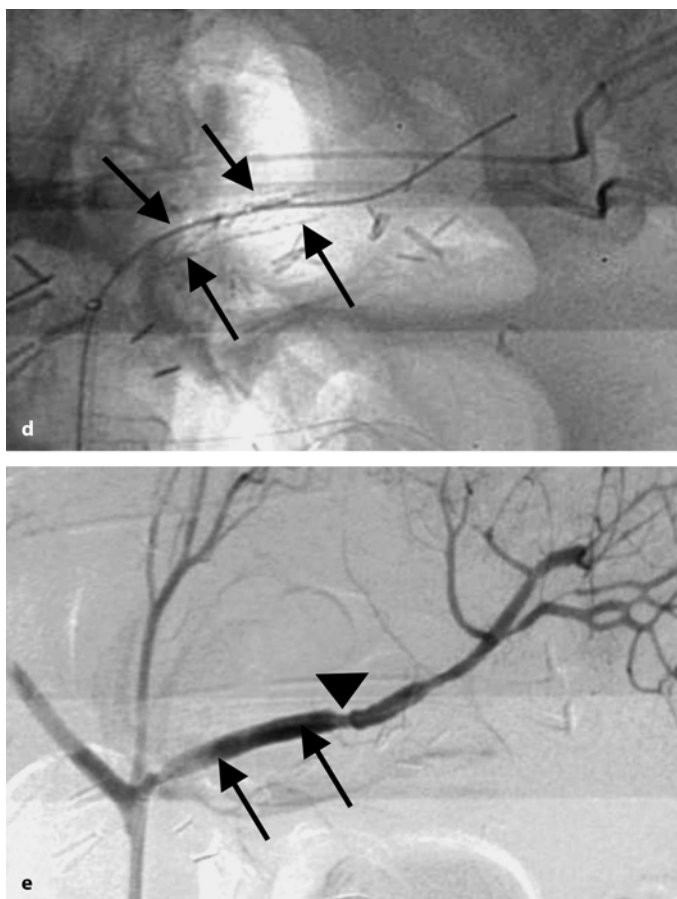


Fig. 8. (continued)

Before catheter removal, a trial of oral feeding, with the drainage catheter clamped, is recommended. This trial should be done once the patient is asymptomatic and drainage nearly ceased. This usually occurs around 3–4 weeks after drainage [147, 269]. Fluid reaccumulation, recurrent pain or a major rise in amylase value are indicators of persistent communication between the cyst and the pancreatic duct, requiring prolonged drainage [125, 269]. Most commonly, complete distal duct injuries are managed by spleen-sparing pancreatectomy and major cephalic duct trauma by endoscopic cystostomy and duct stenting [125]; however, successful percutaneous drainage in such condition has been reported [269]. Occasionally, the gland can heal spontaneously and the duct appears to recanalize [269]. Pseudo-cysts due to major proximal duct injury require frequently surgical resection or internal drainage, depending on the maturity of the cyst wall [117]

#### Abscess and Pancreatitis

Pancreatitis and abscess formation after pancreatic injuries are serious complications with a high risk of death unless it is early diagnosed and drained under CT guidance

or surgically [145, 185]. The treatment to be initiated is the standard care applicable to any acute severe pancreatitis [117, 272]. Most pancreatic abscesses, reported with an incidence from 10–25%, represent inadequately drained fluid collections secondarily contaminated by Gram-negative intestinal flora

#### Long-Term Complications

Long-term complications of ductal trauma are fibrosis and stricture formation most commonly encountered when ductal section has been incomplete. They may cause recurrent episodes of acute pancreatitis [23, 30, 145]. Duct stenosis may induce fibrotic atrophy of the parenchyma with secondary changes of chronic pancreatitis in the obstructed segment of the gland. Pancreatoenteric drainage or resection of the obstructed segment of pancreas provides prompt and effective relief [23, 30, 145]. Diabetes mellitus after pancreatic injury is rare unless necrosis reaches 80–90% of the gland [272]. Exocrine function impairment is unusual provided that pancreatic fluid has access to the duodenum [269]



## 2.2.5 Kidneys, Adrenals, Urinary Bladder

Long-term sequelae from renal injuries depend on the type and extend of the injury, and how long the injury goes unrepaired. Major complications sometimes may occur in patients who have sustained isolated major renal injuries, but most often result from associated injury and/or the development of sepsis or associated organ failure [35, 132]. Complications resulting directly from the renal injury or its repair occur in <10% of patients [35, 158]. Early complications occurring within 4 weeks of trauma include delayed renal bleeding, persistent urinary extravasation with urinoma formation and perinephric abscess [94, 97, 132, 144, 158]

Late complications include pseudo-aneurysm and/or arteriovenous fistula formation, hydronephrosis, cyst or stones formation, chronic pyelonephritis, urinary fistulisation and hypertension, which is uncommon and may occur either early or several years after a repaired or untreated injury [158]. Serial follow-up studies with CT scan and/or ultrasonography are recommended after grade-III or grade-IV injury to detect and document these potential complications mainly observed after non-surgical treatment [35, 158]

### 2.2.5.1 Vascular Complications

#### Pseudo-aneurysm, Arteriovenous Fistula and Venous Lesions

Secondary haemorrhage is the most common and serious delayed complication of renal injury and is usually due to a traumatic pseudo-aneurysm (PSA) or an arteriovenous fistula (AVF) bleeding into the pyelocaliceal system or perinephric area [94, 97, 100, 113, 140, 144, 236, 245, 256]. This complication occurs in 18–19% of patients treated conservatively after penetrating injury [7–102], in 13–18% of patients with deep cortical lacerations (grades III and IV) due to blunt trauma [66, 97, 100, 113, 132, 138, 140, 144, 161, 200, 237, 245] and in 3–15% of patients following primary surgical exploration after trauma [102, 132]. The PSA development after blunt abdominal trauma is less common than after penetrating trauma and is believed to result from rapid deceleration-induced, full- or partial-thickness injury to arteries supplying the renal parenchyma [99, 100, 113, 161, 245]. After the initial arterial injury, surrounding tissues such as the vascular adventitia, renal parenchyma, or Gerota's fascia may contain the haemorrhage. The combination of hypotension and coagulation results in the temporary cessation of bleeding. The degradation of the clot and surrounding necrotic tissue results in recanalisation between the intravascular and extravascular spaces and, subsequently, the formation of a pseudo-aneurysm [66, 138, 161]. Regarding the risk of PSA or AVF development after major renal trauma, it has been suggested that a

CT scan should be performed 3–6 months after any high-grade injury [17, 91]. Bleeding into the renal collecting system usually causes haematuria and, in rare cases, may produce renal insufficiency from clot retention. Pseudo-aneurysm, which may cause a mass effect on the collecting system, haematuria or extracapsular haemorrhage, may be evident as large, enhancing collection within the kidney on CT scan [57, 66, 100, 138, 228, 245]. An AVF may present either in isolation [236, 258] or in combination with a pseudo-aneurysm (Fig. 9). The danger in not treating these injuries is the risk of delayed rupture, renal loss, cardiac failure (Fig. 9) and death. Arterio-caliceal fistulae, which occur when an arterial injury communicates with the renal collecting system, usually result in profuse haematuria [113]. These fistulae may be very difficult to identify on both CT scan imaging and renal arteriography because of residual contrast in the collecting system from previous studies [119]. An angiographic investigation is mandatory in the presence of recurrent gross haematuria, bruit over the kidney or when de novo systemic hypertension develop after previous renal injury [91, 97, 158, 161, 200, 256]. Most PSA and arteriovenous fistulas occurring after major renal trauma do not heal spontaneously. As secondary nephrectomy for delayed renal haemorrhage is required in half of patients when surgery is considered, angiography is the gold standard to diagnose and treat renal PSA or AVF in any patient who presents recurrent or delayed post-traumatic haematuria. Angiography not only confirms the presence of PSA and or AVF, but also provides anatomic localisation and assessment of the renal parenchyma (Fig. 9) [97]. Although endovascular embolisation may result in partial renal infarction, the primary use of this technique is justified because less loss of renal parenchyma is to be expected from catheter embolisation than from an attempt at conservative operative repair such as renal branches ligation or fistula excision [237]. The PSA or AVF embolisation is usually performed through a micro-catheter placed through a 5- or 6-F guiding catheter in order to induce minimal renal parenchyma loss, especially in case of single functioning kidney [110, 140, 237, 253]. The use of coaxial micro-catheters greatly facilitates the procedure whenever superselective embolisation of an interlobar branch is attempted [57, 234]. Various embolic materials, including Gianturco coils or platinum micro-coils, gelfoam pledgets, detachable balloons, glue and hydrogel particles, may be used, depending on the location, size and accessibility of the feeding artery [57, 97, 99, 110, 138, 140, 237, 245, 253, 256]. As PSA has a very thin wall that may easily rupture, the use of embolic material that can be gently applied through catheter without increasing the intravascular pressure is preferable. As retrograde filling of the renal vasculature with subsequent reinjection of a previously embolised PSA by collaterals is very unlikely, proximal coils occlusion of the feeding artery alone usually offers permanent occlusion. For AVF or arterio-caliceal fistula occlusion, coils or micro-coils properly sized to the feeding

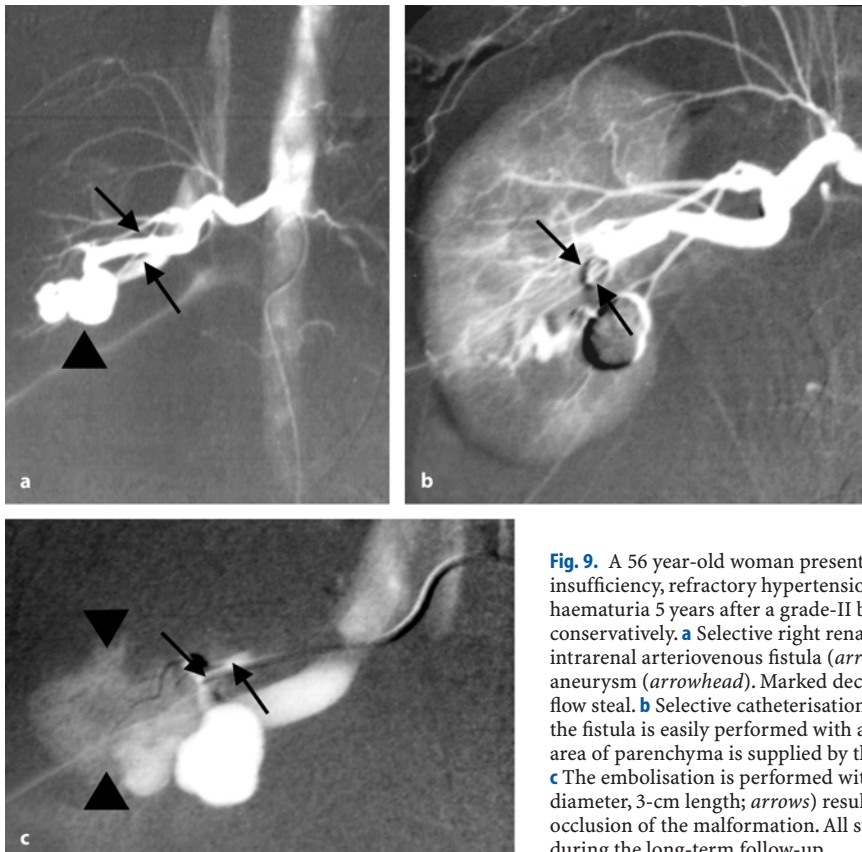


**Fig. 9.** A 56 year-old woman presented with a progressive right cardiac insufficiency, refractory hypertension and recurrent episodes of discrete haematuria 5 years after a grade-II blunt right renal injury treated conservatively. **a** Selective right renal arteriogram shows a massive intrarenal arteriovenous fistula (*arrows*) with an in between pseudo-aneurysm (*arrowhead*). Marked decrease in renal perfusion is due to flow steal. **b** Selective catheterisation of the dilated branch supplying the fistula is easily performed with a 4-F catheter (*arrows*). A limited area of parenchyma is supplied by the same artery (*arrowheads*). **c** The embolisation is performed with three Gianturco coils (4-mm diameter, 3-cm length; *arrows*) resulting in immediate and complete occlusion of the malformation. All symptoms completely disappeared during the long-term follow-up

vessel are embolic agents of choice, since they offer a better deployment control, compared with gelfoam pledgets, and are less likely to pass through the fistula into the venous system than smaller particles or gelfoam pieces (Fig. 9) [258]. Bleeding control after embolisation is achieved in 80–100% of patients [97, 99, 119, 138, 140, 234, 256]. In case of bleeding recurrence, embolisation can be repeated obviating surgical nephrectomy [256]. Complications due to renal artery embolisation are observed in 8–10% of cases and usually do not require any additional intervention. [71, 234, 256]. Truncal or hilar renal arteriovenous fistula could be managed by placement of a covered stent as an alternative to surgical repair [236]. For patients suffering from major renal stab wounds, primary renal angiography with segmental targeted or pre-emptive embolisation is an alternative management strategy to initial surgical exploration [91, 97, 102, 234, 256]. Isolated renal vein thrombosis after trauma has been reported twice [122]. Trauma-induced renal vein thrombosis, which always occurs in combination with an arterial or parenchymal injury, may be treated conservatively with long-term anticoagulation instead of historical thrombectomy or nephrectomy [122]

### Hypertension

Renal trauma-related hypertension, probably due to renal infarction, may be observed both after blunt and penetrating injury. This complication may result from any type of treatment, including observation and surgery. Hypertension and renal failure are observed in 10% of the patients undergoing surgery for major renal trauma [132]. Recent data suggest that the true incidence of post-traumatic hypertension is close to 5% (up to 33%). Possible mechanisms for the development of post-traumatic hypertension include renal artery occlusion or stenosis, renal artery compression, severe renal contusion, arteriovenous fistula or pseudo-aneurysm, and chronic contained subcapsular haematoma with subsequent renal scarring reducing flow to the kidney and inducing renin-mediated hypertension (Page kidney) [123, 250]. Hypertension may be transient and observed anywhere from 2 weeks to 8 months after injury and may resolve spontaneously within 1 year after injury. In selected cases, percutaneous embolisation of the damage vessels may be considered to exclude the renal artery injury responsible for the hypertension

### Renal Failure

The true incidence of post-traumatic renal failure after major renal trauma is around 6.5%, going up to 10% after surgery for major reno-vascular trauma [132]. In case of bilateral renal artery injuries, every attempt must be made to revascularise at least one kidney. Endovascular stent placement may be considered in those cases of intimal tear of the renal artery [186]

#### 2.2.5.2 Urinary Tract Complications

##### Urinary Leaks

Persistent extravasation or urinoma, secondary to laceration of the renal collecting system or ureter with subsequent urinary leak into the perirenal or retroperitoneal spaces, are the most frequent complications of expectant management with an incidence between 13–16%. These patients are at an increased risk of developing a perinephric abscess and therefore placed on prophylactic antibiotics. The incidence of these urological complications correlates significantly with increasing grade of trauma (grade II 15%, grade IV 43%) [17, 81]. The vast majority of urinary extravasation will seal spontaneously while persistent urinomas (30%) may be successfully treated by percutaneous placement of 10-F drainage catheter under CT or sonographic guidance. Persistence of a urinoma longer than several days, despite optimal percutaneous drainage, is indicative of a continuous leak from the collecting system and requires percutaneous nephrostomy to ensure urine diversion, thereby avoiding secondary renal exploration [17, 132, 210]. The combination of percutaneous drainage catheters with either antegrade ureteral stents or nephroureteral catheters diverts the urine away from the area of leakage and promotes primary healing of the collecting system [250]. Antegrade ureteral stenting is recommended for the management of persistent massive ureteral leaks after prolonged urine diversion or to treat ureteral dehiscence after primary surgical repair [81, 132, 210]. Selective embolisation of the renal parenchyma producing the urine filling a refractory urinoma has been proven to be effective in ceasing urine flow and may be therefore a less invasive alternative to surgery [106]. A leakage from the urinary tract causing urinoma, and can lead to urinothorax, which is a rare complication of blunt renal trauma [169]. Ureteral injuries are best treated by percutaneous nephrostomy with antegrade ureteral stenting. The retrograde approach may be difficult or impossible because of a large area of ureteral transection, an intervening urinoma or tortuosity of the ureter. Ureteral stents are usually left in place for 8–12 weeks to allow the ureter to heal [81, 250]

##### Urinary Stenosis

Late complications of non-penetrating ureteral injuries are rarely reported. High-pressure angioplasty balloon catheter can be used to dilate trauma-induced ureteral

stenosis or secondary stricture after primary surgical repair [50%]. A success rate of 50% is reported [82] Ureteropelvic junction injuries, traditionally described in children, consist of laceration or avulsion of the ureter. Delayed post-traumatic ureteropelvic junction obstruction may occur several year after blunt trauma [82, 83]

## 2.2.6 Gastrointestinal Tract

### 2.2.6.1 Stomach-Duodenum

The two major complications after duodenal trauma are post-operative fistula, reported with an incidence between 2 and 16% [117], and duodenal obstruction. Duodenal fistula has an overall mortality rate of 2% [31]. Most of the low-output duodenal fistulas closed spontaneously with NOM. In patients with a high-output fistula, without duodenal diversion or in those where the fistula remains open after a period longer than 2 weeks, a surgical diversion should be considered to avoid the development of severe malnutrition, intra-abdominal sepsis or extensive skin necrosis. Duodenal obstruction occurs in 5–8% of patient after duodenal trauma, either after primary surgical duodenal repair or during the follow-up of large duodenal haematoma. Most commonly seen in children, who are at higher risk than adults because of their weaker abdominal musculature, duodenal haematoma, which usually involves the second portion of the duodenum, may extend proximally and distally to the first and third portions in 25% of patients [224]. Because of the likelihood of spontaneous resolution and high post-operative morbidity rate, a non-operative treatment should be tried for at least 3–4 weeks in case of partial obstruction [31]. A different laparotomy technique may be necessary in some cases of incomplete obstruction because of delay in diagnosis, unsatisfactory improvement with non-surgical treatment, rupture of the haematoma or late duodenal obstruction. Extending duodenal haematoma involving the papilla with subsequent common bile duct and Wirsung obstruction has been reported. In this setting, a surgical decompression should be performed to avoid severe cholangitis or pancreatitis [247]. Intramural duodenal haematoma requires early surgical evacuation or local repair only in the presence of uncontrolled haemorrhage, transmural perforation or haemodynamic instability. In case of continuous bleeding, embolisation therapy is a possible alternative to surgical haemostatic procedure

### 2.2.6.2 Small Bowel and Large Bowel

##### Stenosis

Delayed small or large bowel stricture, observed in both adults and children [105, 118] after conservative management of blunt abdominal trauma, may result from various

pathological mechanisms. The classical features of this entity include a time interval between trauma and onset of symptoms ranging from 3 days to 11 months [105, 118, 146, 254] and clinical and radiological signs of obstruction with a long ileal of colonic stenosis; however, highly different clinical manifestations are observed between patients with ileal stenosis (ileus) and those with colonic stenosis (rectal bleeding and diarrhoea) [105, 118, 146]. The pathological findings of post-traumatic ischaemic small bowel stenosis may be similar to those observed in patients with acute intestinal ischaemia or spontaneous ischaemic jejuno-ileitis. These findings suggest that injury-related focal segmental intestinal ischaemia plays an important role in the pathogenesis of post-traumatic intestinal stenosis [105, 134, 254]. These stenoses may be complicated by penetration or perforation probably due to ischaemic ulceration [134]. Whereas CT scan is a reliable method in detecting the level and cause of obstruction by demonstration of mural thickening of a loop associated with a localised mesenteric haematoma [254], enteroclysis can test the distensibility and fixation of the small bowel and therefore provides evaluation of the severity of partial mechanical small bowel obstruction better than CT scan. Injury-related delayed colonic obstruction may result from a combination of several factors including interference of the blood supply by damage to small vessels, oedema and haematoma secondary to the injury itself and progressive fibrosis with gradually increasing obstruction [146]. The relatively high rate of involvement of the left colon may be explained by the under-developed marginal arterial system in that region making it more susceptible to damage-induced blood supply interruption [146, 265]. Surgery with segmental resection will restore a normal condition to all these patients

### Perforation

Delayed ileal or colonic perforation after blunt trauma usually occurs in patients sustaining other injuries, mainly spinal trauma [273], but also as an isolated event [163, 252]. Delayed perforation of the sigmoid colon may be caused by desinsertion of sigmoid mesentery [163]. Seat-belt flexion–distraction fracture of the spine, so-called Chance fracture, and intramural haemorrhage of the intestine observed after low-impact velocity (5m/s), may be associated with delayed development of ileal perforation or enterocolic fistula [273]. Patients with persistent vague abdominal pain after a blunt spinal trauma appear to be at high risk for delayed abdominal perforation and should be monitored carefully [273]. In a post-traumatic setting, the combination of localised bowel wall thickening with intramesenteric haematoma, as well as extravasation of bowel contrast material, is highly suggestive of trauma-induced vascular compromise

## 2.2.7 Vascular Complications

### 2.2.7.1 Superior Mesenteric Artery

Injuries to the mesenteric vessels are highly lethal and challenging complications of penetrating and blunt abdominal trauma [37]. A few cases of delayed rupture of post-traumatic intramural jejunal or duodenal pseudoaneurysms are reported. They are usually revealed by a massive gastrointestinal haemorrhage due to erosion or perforation into an adjacent hollow viscus [127] or by delayed intraperitoneal rupture [68]. Late haemorrhage after trauma may be explained by a weakened arterial media resulting in a subsequent delayed dissection and rupture [68]. Post-traumatic SMA arteriovenous fistulae, commonly observed after penetrating trauma but also after blunt injury or following primary surgical repair, may be occult for a prolonged period (Fig. 10) [203, 255]. Early recognition and treatment of this lesion is mandatory to avoid subsequent major complications such as bowel ischaemia, venous congestion, intra-peritoneal rupture or secondary portal hypertension [56, 101, 255]. In case of large, proximal or of long-standing duration fistula, signs of right heart failure may also be present [203]. Any clinical suspicion, such as an abdominal bruit or palpable thrill, should require a selective arteriography delineating the mesenteric and portal circulation, localizing the fistula and allowing an elective planned surgical or endovascular approach. The fistulous communication may also result from the formation of a post-traumatic or post-operative pseudoaneurysm which subsequently ruptures into the SMV [56–101]. Despite spontaneous closure had been described [233], a mortality of 25–35% is reported for untreated traumatic mesenteric arteriovenous fistulae. Surgical therapeutic options, including ligation of both arterial and venous sides or fistula resection with arterial and venous reconstruction by saphenous vein or synthetic interposition grafting [37, 203], carry an operative mortality rate from 18 to 28% [56]. Several studies have shown that percutaneous embolisation is a safe, reliable and effective alternative with a low complication rate compared with surgery [68, 255]. Steel coils and detachable balloons are the materials of choice for embolisation (Fig. 10) [56, 101]; however, additional gelfoam pledgets placement after primarily stainless steel coils packing may be necessary to achieve an immediate and complete obliteration of high-flow fistula. If the pseudoaneurysm could not be selectively treated, segmental SMA exclusion by coils placement on both sides of the aneurysmal neck may be an effective therapy. Following initial surgery or after emergent SMA ligation performed to control massive bleeding, embolisation of recurrent SMA fistula using giant steel coils may be successful [52]. Risks associated with embolisation include pseudoaneurysm rupture from catheter manipulation, inadvertent coil deployment in a SMA sidebranch resulting in focal





**Fig. 10.** This 61-year-old man had a history of motor vehicle accident with rupture of the mesenteric roof requiring emergent surgical repair. Six years later, he presented with massive ascitis. Discrete fibrotic changes were observed on liver biopsy specimen. Contrast-enhanced CT scan in axial (**a**) and coronal multiplanar reconstruction (**b**) show diffuse ascitis and a marked enlarged superior mesenteric vein (SMV; *arrows*). The early enhancement of the dilatated SMV is highly suggestive for a chronic mesenteric arterio-venous fistula. **c** An SMA arteriography confirms the hypothesis of a distal mesenteric arterio-venous fistula (*arrow*) supplied by a distal branch of the ileo-caecal artery. **d, e** Superselective ileo-

caecal artery catheterisation demonstrates a 1-cm diameter pseudo-aneurysm (*arrow*) interposed between two arterial feeders (*arrowhead*) and the dilated veins (*curved arrow*). **f** The pseudo-aneurysm is selectively occluded by on site deposition of nine Gianturco coils through a 4-F catheter positioned in the pouch (*arrow*). Immediate (**g**) and 6-month follow-up (**H**) controls SMA arteriography show a complete obliteration of the fistula (*arrow*), preservation of the arterial feeders and a marked increased perfusion of the peripheral mesenteric arteries (*curved arrows*) due to the suppression of the blood steal phenomenon induced by the fistula





**Fig. 10.** (continued)

intestinal ischaemia and coil embolisation through the fistula [220], which could lead to portal vein branches occlusion [56, 192]. If the transarterial route is unsuitable or has failed to occlude a mesenteric arteriovenous fistula, a percutaneous transhepatic transvenous approach, aiming at occluding the draining vein as close as possible to the fistulous tract, should be considered [36]

### 2.2.7.2 Aorta, Lumbar and Iliac Arteries

Occult pseudo-aneurysms or stenosis of the abdominal aorta and iliac arteries branches usually occur following gunshot or stab wound injuries [11] but may also be observed after blunt trauma [112, 189, 222]. This diagnosis, delayed in one-third of patients, should be suspected in traumatised patients presenting persistent back pain, bruit, claudication or decreased peripheral pulses [112, 189, 222]. These lesions can be managed by surgical bypass [222] or endovascular stent-grafts with a reduced peri-operative morbidity. Traumatic aortocaval or pelvic arteriovenous fistulae, commonly secondary to penetrating injuries, should be suspected in cases of lower limb oedema, varicosities, pain, neurological deficit, audible bruit or right cardiomegaly [193, 268]. These lesions may currently be treated percutaneously either by endovascular arterial stent-graft implantation allowing to keep patent the parent artery or by vessel occlusion achievable with various embolic agents including glue, coils and detachable balloon [193, 268]. Bilateral internal iliac artery embolisation with gelfoam, which is commonly performed to arrest massive bleeding after pelvic trauma, does not product lasting adverse effects on urogenital function [190]. Delayed skin and muscle necrosis of the gluteal region following internal iliac artery embolisation may lead to uncontrollable gluteal

infection [244]. Traumatic rupture of a lumbar artery, which is associated mainly with lumbar vertebrae fractures, may lead to a massive retroperitoneal haemorrhage and shock, or to pseudo-aneurysm formation and retroperitoneal haematoma [223]. Lumbar artery pseudo-aneurysm, which is a well-known complication of retroperitoneal penetrating trauma [211–227] but a rare complication of blunt abdominal trauma [223], may determine a back pulsatile mass, bruit or thrill, or may cause painful nerve root compression [223]. Embolisation should be performed as close as possible to the aneurysmal neck to avoid both distal reinjection by collaterals from adjacent metameric levels and non-target occlusion of spinal cord collateral supply [211, 223, 227]. If the endovascular approach is not feasible, pseudo-aneurysm occlusion may be performed by a direct posterior percutaneous approach under combined CT scan and angiographic guidance

### 2.2.7.3 Inferior Vena Cava

Secondary thrombosis of the supra- or retro-hepatic inferior vena cava (IVC) may occur following partial- or full-thickness caval wall injury at the diaphragmatic hiatus, as this portion is fixed and more vulnerable to shearing forces. Traumatic hepatic venous outflow obstruction may also result from IVC compression by parenchymal and/or subcapsular liver haematoma producing sufficient mass effect to compress the confluence main hepatic veins–retrohepatic IVC [165]. Decompression of the IVC and hepatic veins by percutaneous or surgical drainage of the collection is curative in most cases [157]

## 2.2.8 Diaphragm

Traumatic diaphragmatic hernia (TDH) is believed to occur in 1–5% of patients with blunt trauma to the abdomen [228]. Bilateral diaphragm rupture is a rare occurrence and, therefore, is often overlooked, which contributes to the high morbidity and mortality seen in these patients [229]. Delayed TDH, which may occur months to years after the causative injury [153, 228, 232, 264, 271], should be considered in the setting of non-specific respiratory and bowel symptoms, in patients with abnormal shadows in the thoracic region and who have recently sustained injury or who have a past history of major abdominal trauma [228, 229, 264, 271]. Delayed rupture may occur when the diaphragmatic muscle is devitalised at the time of initial injury but remains a barrier against herniation until several days later, when the inflammatory process weakens it [3, 229]. Patients with a large TDH often remain asymptomatic for a long time [153, 228]. Delayed diaphragmatic bowel herniation secondary to a retroperitoneal stab wound will occur predominantly on the left side, since the bulk of the liver prevents herniation through defects on the right [67, 264, 271]. The morbidity and mortality of management of chronic TDH are formidable, being significantly higher in blunt TDH (60%) than in penetrating TDH (40%). This finding is because blunt trauma generates higher pressures causing larger diaphragmatic tears and greater degrees of evisceration [228]. Tension fecopneumothorax usually requires combined closure of the diaphragmatic defect and a Hartmann's procedure [264, 271]. Gastro-pleural fistula may develop months to years after an unrecognised or untreated traumatic diaphragmatic perforation [120]. This complication, known to cause severe complications such as tension pneumothorax, can also manifest with insidious onset and chronic complaints. In this setting, discontinuation of oral feeding may relieve symptoms and promote spontaneous closure of the fistulous tract [120]. Inferior phrenic artery injury, responsible for a delayed haemothorax after a NOM of a blunt splenic injury, may be successfully managed by particles embolisation, (personal communication). Delayed inferior vena cava stenosis induced by a traumatic diaphragmatic hernia has been occasionally reported [139]. In this condition, the IVC is angulated and markedly narrowed below the right atrium. Herniation of right lobe of the liver may be associated. The surgical reduction of the herniated viscus and repair of the ruptured diaphragm are definite treatments [139].

## 2.2.9 Conclusion

As more patients with complex solid abdominal organ injuries are treated non-operatively and the criteria for NOM continue to expand, more patients will need some type of interventional procedure to treat complications that historically were managed by laparotomy

The application of the non-surgical approach and interventional radiology to manage delayed complications after abdominal trauma imposes prerequisite conditions: the clinician has to be aware of the natural history of abdominal trauma and the expected associated complications; an oriented clinical and radiological follow-up has to be performed; and the radiologist must have a training and skill in the different and complementary techniques required for the diagnosis and treatment of these complications. In addition, the approaches and treatment modalities may differ in adults compared with children. Some complications observed in children may resolve more frequently spontaneously (i.e. splenic pseudo-aneurysm), whereas treatment is indicated in adult (rupture and bleeding from the same aneurysm). The knowledge of this different natural history is mandatory in order to apply the most appropriate care to patients. Some post-traumatic lesions still require surgery (i.e. hollow viscus stenosis, diaphragmatic rupture, late-onset distal pancreatic duct stenosis). Finally, the optimal attitude is to combine the different complementary techniques in a multidisciplinary fashion. The shortcomings associated with NOM with or without embolisation, of solid abdominal organs injuries, are offset by the commonly used multidisciplinary approach in which interventional radiologists, gastroenterologists and urologists are teamed with trauma surgeon to resolve non-operatively most of the negative sequelae of these non-operative treatments

## References

1. Aboujaoude M, Noel B, Beaudoin M et al. (1996) Pseudoaneurysm of the proper hepatic artery with duodenal fistula appearing as a late complication of blunt abdominal trauma. *J Trauma* 40:123–125
2. Akhrass R, Yaffe MB, Brandt CP et al. (1997) Pancreatic trauma: a ten-year multi-institutional experience. *Am Surg* 63:598–604
3. Allen TL, Greenlee RR, Price RR (2002) Delayed splenic rupture presenting as unstable angina pectoris: case report and review of the literature. *J Emerg Med* 23:165–169
4. Al-Mulhim AS, Mohammad HA (2003) Non-operative management of blunt hepatic injury in multiple injured adult patients. *Surgeon* 1:81–85
5. Alonso M, Brathwaite C, Garcia V et al. (2002) EAST patient management guidelines for the non-operative management of blunt injury to the liver and spleen. *Trauma Practice Guidelines*, Eastern Association for the Surgery of Trauma. <http://www.east.org/tpg/chap6body.html>

6. Araoz PA, Andrews JC (2000) Direct percutaneous embolization of visceral artery aneurysms: techniques and pitfalls. *J Vasc Interv Radiol* 11:1195–1200
7. Armenakas NA, Duckett CP, McAninch JW (1999) Indications for nonoperative management of renal stab wounds. *J Urol* 161:768–771
8. Asensio JA, Demetriades D, Chahwan S et al. (2000) Approach to the management of complex hepatic injuries. *J Trauma* 48:66–69
9. Baha B, Meyer PG, Brunelle F et al. (2001) A case of hepatic pseudoaneurysm treated with percutaneous embolization in a child with multiple trauma. *Ann Fr Anesth Reanim* 20(9):786–790
10. Baker RS, Tisnado J, Cho S et al. (1987) Splanchnic artery aneurysm and pseudoaneurysm: transcatheter embolization. *Radiology* 163:135–139
11. Bardiche R, Bove T, Demanet et al. (1999) Traumatic pseudoaneurysm of the abdominal aorta. *Acta Chir Belg* 99:174–176
12. Basile KE, Sivit CJ, Sachs PB et al. (1999) Hepatic arterial pseudoaneurysms: a rare complication of blunt abdominal trauma in children. *Pediatr Radiol* 29:306–308
13. Bender JS, Geller ER, Wilson RF et al. (1989) Intra-abdominal sepsis following liver trauma. *J Trauma* 29:1140–1144
14. Berman SS, Mooney EK, Weireter LJ et al. (1992) Late fatal hemorrhage in pediatric liver trauma. *J Pediatr Surg* 27:1546–1548
15. Bessoud B, Denys A, Calmes JM et al. (2006) Nonoperative management of traumatic splenic injuries: Is there a role for proximal splenic artery embolization. *AJR* 186:779–785
16. Black JJ, Sinow RM, Wilson SE et al. (1992) Subcapsular hematoma as a predictor of delayed splenic rupture. *Am Surg* 58:732–735
17. Blankenship JC, Gavatt ML, Cox CE et al. (2001) Importance of delayed imaging for blunt renal trauma. *World J Surg* 25:1561–1564
18. Blocker C, Brandon JC, Izenberg SD et al. (1998) Posttraumatic enlargement of the spleen: a possible sign of delayed rupture. *Emerg Radiol* 5:263–265
19. Blum U, Buitrago-Tellez CH, El Seif M et al. (1993) Post-traumatic bilhemia: conservative management by percutaneous drainage. *Cardiovasc Intervent Radiol* 16:55–57
20. Bokhari F, Nagy K, Roberts R et al. (1999) Complications of angiographic embolization for traumatic hemobilia. *J Trauma* 47:977–978
21. Bond SJ, Eichelberger MR, Gotschall CS et al. (1996) Nonoperative management of blunt hepatic and splenic injury in children. *Ann Surg* 223:286–289
22. Boone DC, Federle M, Billiar TR et al. (1995) Evolution of management of major hepatic trauma: identification of patterns of injury. *J Trauma* 39:344–350
23. Bradley EL (1991) Chronic obstructive pancreatitis as a delayed complication of pancreatic trauma. *HPB Surg* 5:49–59
24. Brasel KJ, DeLisle CM, Olson CJ et al. (1997) Trends in the management of hepatic injury. *Am J Surg* 174:674–677
25. Bravo JL, Mangalmurti CS, Kowalak M (1998) Management of a ruptured post-traumatic splenic pseudocyst: case report. *J Trauma* 45:165–167
26. Brown RL, Irish MS, McCabe AJ et al. (1999) Observation of splenic trauma: When is a little too much? *J Pediatr Surg* 34:1124–1126
27. Bynoe RP, Bell RM, Miles WS et al. (1992) Complications of nonoperative management of blunt hepatic injuries. *J Trauma* 32:308–315
28. Cabay JE, Boverie JH, Dondelinger RF (1998) Percutaneous catheter drainage of external fistulas of the pancreatic duct. *Eur Radiol* 8:445–448
29. Carles J, Dubuisson V, Douws C et al. (1994) Conservative treatment of hepatic injuries. Management and course. *Chirurgie* 95:444–450
30. Carr ND, Cairns SJ, Lees WR et al. (1989) Late complications of pancreatic trauma. *Br J Surg* 76:1244–1246
31. Carrillo EH, Richardson JD, Miller FB (1996) Evolution in the management of duodenal injuries. *J Trauma* 40:1037–1045
32. Carrillo EH, Platz A, Miller FB et al. (1998) Non-operative management of blunt hepatic trauma. *Br J Surg* 85:461–446
33. Carrillo EH, Spain DA, Wohltman CD et al. (1999) Interventional techniques are useful adjuncts in non-operative management of hepatic injuries. *J Trauma* 46:619–627
34. Carrillo EH, Reed DN Jr, Gordon L et al. (2001) Delayed laparoscopy facilitates the management of biliary peritonitis in patients with complex liver injuries. *Surg Endosc* 15:319–322
35. Carroll PR, JW McAninch, Klosterman P et al. (1990) Renovascular trauma: risk assessment, surgical management, and outcome. *J Trauma* 30:547–552
36. Cekirge S, Özmen M, Akata D et al. (1998) Endovascular treatment of a superior mesenteric arteriovenous fistula by a transhepatic portal venous approach. *AJR* 171:1283–1284
37. Chiriano J, Abou-Zamzam AM Jr, Teruya TH et al. (2005) Delayed development of a traumatic superior mesenteric arteriovenous fistula following multiple gunshot wounds to the abdomen. *Ann Vasc Surg* 19:470–473
38. Christimaz D, Le Coutre C (1987) Traumatic splenic cysts. *Eur J Pediatr Surg* 42:193–195
39. Ciraulo DL, Luk S, Palter M et al. (1998) Selective hepatic arterial embolization of grade IV and V blunt hepatic injuries: an extension of resuscitation in the nonoperative management of traumatic hepatic injuries. *J Trauma* 45:353–359
40. Citron SJ, Martin LG (1991) Benign biliary stricture: treatment with percutaneous cholangioplasty. *Radiology* 178:339–341
41. Clancy TE, Warren RL (1997) Endoscopic treatment of biliary colic resulting from hemobilia after nonoperative management of blunt hepatic injury: case report and review of the literature. *J Trauma* 43:527–529
42. Cocanour CS, Moore FA, Ware DN et al. (1998) Delayed complications of nonoperative management of blunt adult splenic trauma. *Arch Surg* 133:619–624
43. Cogbill TH, Moore EE, Jurkovich GJ et al. (1988) Severe hepatic trauma: a multicenter experience with 1335 liver injuries. *J Trauma* 28:1433–1438
44. Cogbill TH, Moore EE, Jurkovich GJ et al. (1989) Nonoperative management of blunt splenic trauma: a multicenter experience. *J Trauma* 29:1312–1317
45. Cope C, Zeit R (1986) Coagulation of aneurysms by direct percutaneous thrombin injection. *AJR* 147:383–387
46. Croce MO, Fabian TC, Spiers et al. (1994) Traumatic hepatic artery pseudoaneurysm with hemobilia. *Am J Surg* 168:235–238
47. Croce MO, Fabian TC, Menke PG et al. (1995) Nonoperative management of blunt hepatic trauma is the treatment of choice for hemodynamically stable patients. Results of a prospective trial. *Ann Surg* 221:744–753
48. Cuff RF, Cogbill TH, Lambert PJ (2000) Nonoperative management of blunt liver trauma: the value of follow-up abdominal computed tomography scans. *Am Surg* 66:332–336
49. D'Amours SK, Simons RK, Scudamore CH et al. (2001) Major intrahepatic bile duct injuries detected after laparotomy: selective nonoperative management. *J Trauma* 50:480–484
50. Davis KA, Fabian TC, Croce MA et al. (1998) Improved success in nonoperative management of blunt splenic injuries: embolization of splenic artery pseudoaneurysms. *J Trauma* 44:1008–1013
51. De Backer A, Fierens H, De Schepper A et al. (1998) Diagnosis and nonsurgical management of bile leak complicated by biloma after blunt liver injury: report of two cases. *Eur Radiol* 8:1619–1622
52. Deitrick J, McNeill P, Posner MP et al. (1990) Traumatic superior mesenteric artery–portal vein fistula. *Ann Vasc Surg* 4:72–76
52. Delgado Millan MA, Deballon PO (2001) Computed tomography, angiography and endoscopic retrograde cholangiopancreatography in the nonoperative management of hepatic and splenic trauma. *World J Surg* 25:1397–1402

54. Demetriades D, Gomez H, Chahwan S et al. (1999) Gunshot injuries to the liver: the role of selective nonoperative management. *J Am Coll Surg* 188:343–348
55. Dent D, Alsabrook G, Erickson BA et al. (2004) Blunt splenic injuries: high nonoperative management rate can be achieved with selective embolization. *J Trauma* 56:1063–1067
56. Desai SB, Modhe JM, Aulakh BG et al. (1987) Percutaneous transcatheter steel-coil embolization of a large proximal post-traumatic superior mesenteric arteriovenous fistula. *J Trauma* 27:1091–1094
57. Dinkel HP, Danuser H, Triller J (2002) Blunt renal trauma: minimally invasive management with microcatheter embolization. Experience in nine patients. *Radiology* 223:723–730
58. Eid A, Almogy G, Pikarsky AJ et al. (1996) Conservative treatment of a traumatic tear of the left hepatic duct: case report. *J Trauma* 41:912–913
59. Eng RH, Tecson-Tumang F, Corrado ML (1981) Blunt trauma and liver abscess. *Am J Gastroenterol* 76:252–255
60. Engelke C, Quarmby J, Ubhayakar G et al. (2002) Autologous thrombin: a new embolization treatment for traumatic intrasplenic pseudoaneurysm. *J Endovasc Ther* 9: 36–37
61. English WP, Johnson MB, Borman KR et al. (2001) Mesenteric ischemia: an unusual presentation of traumatic intrahepatic arteriportal fistula. *Am Surg* 67:865–867
62. Eubanks III JW, Meier DE, Hicks BA et al. (2003) Significance of “Blush” on computed tomography scan in children with liver injury. *J Pediatr Surg* 38:363–366
63. Fabian TC, Croce MA, Stanford GG et al. (1991) Factors affecting morbidity following hepatic trauma. A prospective analysis of 482 injuries. *Ann Surg* 213:540–548
64. Fang J, Chen R, Wong Y et al. (2000) Classification and treatment of pooling of contrast material on computed tomographic scan of blunt hepatic trauma. *J Trauma* 49:1083–1088
65. Farhat GA, Abdu RA, Vanek VN (1992) Delayed splenic rupture: Real or imaginary? *Am Surg* 58:340–348
66. Farrell TM, Sutton JE, Buchard KW (1996) Renal artery pseudoaneurysm: a cause of delayed hematuria in blunt trauma. *J Trauma* 41:1067–1068
67. Feliciano DV, Cruse PA, Mattox KL (1988) delayed diagnosis of injuries to the diaphragm after penetrating wounds. *J Trauma* 28:1135–1144
68. Ferrella TJ (1992) Delayed rupture of the middle colic artery secondary to blunt abdominal trauma. *Ann Emerg Med* 21:428–430
69. Finley DS, Hinojosa MW, Paya M et al. (2005) Hepatic artery pseudoaneurysm: a report of seven cases and a review of the literature. *Surg Today* 35:543–547
70. Firstenberg MS, Plaisier B, Newman JS et al. (1998) Successful treatment of delayed splenic rupture with splenic artery embolization. *Surgery* 123:584–586
71. Fischer RG, Ben-Menachem Y, Whigham C (1989) Stab wounds of the renal artery branches: angiographic diagnosis and treatment by embolization. *AJR* 152:1231–1235
72. Fisher JC, Moulton SL (2004) Nonoperative management and delayed hemorrhage after pediatric liver injury: new issues to consider. *J Pediatr Surg* 39:619–622
73. Fitoz S, Atasoy C, Dusunceli E et al. (2001) Post-traumatic intrasplenic pseudoaneurysms with delayed rupture: color Doppler sonographic and CT findings. *J Clin Ultrasound* 29:102–104
74. Frumiento C, Sartorelli K, Vane D (2000) Complications of splenic injuries: expansion of the nonoperative theorem. *J Pediatr Surg* 35:788–791
75. Fulcher AS, Turner MA, Yelon JA et al. (2000) Magnetic resonance cholangiopancreatography (MRCP) in the assessment of pancreatic duct trauma and its sequelae: preliminary findings. *J Trauma* 48:1001–1007
76. Gable DR, Allen JW, Harrell DJ et al. (1997) Endoscopic treatment of posttraumatic “Bilhemia”: case report. *J Trauma* 43:534–536
77. Galeon M, Goffette P, Van Beers et al. (1997) Post-traumatic intra-hepatic pseudoaneurysm: diagnosis with helical CT angiography and management with embolization *J Belge Radiol* 80:287–288
78. Garby KB, King TS, Tsai FY (1997) Recurrence of pseudoaneurysm after successful embolization. *J Endovasc Surg* 4:385–388
79. Gates JD (1994) Delayed hemorrhage with free rupture complicating the nonsurgical management of blunt hepatic trauma: a case report and review of the literature. *J Trauma* 36:572–575
80. Geis WP, Schulz KA, Giacchino JL et al. (1981) The fate of unruptured intrahepatic hematomas. *Surgery* 90:689–697
81. Ghali AM, Elfadil MA, El Malik A et al. (1999) Ureteric injuries: diagnosis, management and outcome. *J Trauma* 46:150–158
82. Giannarini G, Grossetti B, Crisci A et al. (2004) Post-traumatic ureteropelvic junction obstruction. *Arch Ital Urol Androl* 76:100–102
83. Glazer K, Wetscher G, Pointner R et al. (1994) Traumatic bilhemia. *Surgery* 116:24–28
84. Goettler CE, Stallion A, Grisoni ER et al. (2002) Delayed hemorrhage after blunt hepatic trauma: case report. *J Trauma* 52:556–559
85. Goins WA, Rodriguez A, Joshi M et al. (1990) Intra-abdominal abscess after abdominal trauma. *Ann Surg* 212:60–65
86. Goldman R, Zilkoski M, Mullins R et al. (2003) Delayed celiotomy for the treatment of bile leak, compartment syndrome, and other hazards of nonoperative management of blunt liver injury. *Am J Surg* 185:492–497
87. Goletti O, Ghiselli G, Lippolis PV et al. (1996) Intrasplenic post-traumatic pseudoaneurysm: echo color Doppler diagnosis. *J Trauma* 41:542–454
88. Gow KW, Murphy JJ III, Blair GK et al. (1996) Splanchnic artery pseudo-aneurysms secondary to blunt abdominal trauma in children. *J Pediatr Surg* 31:812–815
89. Griffen M, Ochoa J, Boulanger BR (2000) A minimally invasive approach to bile peritonitis after blunt liver injury. *Am Surg* 66:309–312
90. Gross M, Lynch FP, Cauty T et al. (1999) Management of pediatric liver injuries: a 13-year experience at a pediatric trauma center. *J Pediatr Surg* 34:811–817
91. Guerriero WG (1988) Etiology, classification and management of renal trauma. *Surg Clin N Am* 68:1071–1084
92. Haan J, Bochicchio G, Kramer M et al. (2003) Air following splenic embolization: infection or incidental findings. *Am Surg* 69:1036–1039
93. Haan JM, Biffi W, Knudson MM et al. (2004) Splenic embolization revisited: a multicenter review. *J Trauma* 56:542–547
94. Hagiwara A, Yukioka T, Shimazaki S et al. (1993) Delayed hemorrhage following transcatheter arterial embolization for blunt hepatic injury. *Cardiovasc Intervent Radiol* 16:380–383
95. Hagiwara A, Yukioka T, Ohta S et al. (1996) Nonsurgical management of patients with blunt splenic injury: efficacy of transcatheter arterial embolization. *AJR* 167:159–166
96. Hagiwara A, Yukioka T, Ohta S et al. (1997) Nonsurgical management of patients with blunt hepatic injury: efficacy of transcatheter arterial embolization. *AJR* 169:1151–1156
97. Hagiwara A, Sakaki S, Goto H et al. (2001) The role of interventional radiology in the management of blunt renal injury: a practical protocol. *J Trauma* 51:526–531
98. Hagiwara A, Tarui T, Murata A et al. (2005) Relationship between pseudoaneurysm formation and biloma after successful transarterial embolization for severe hepatic injury: permanent embolization using stainless steel coils prevents pseudoaneurysm formation. *J Trauma* 59:49–53
99. Halachmi S, Chait P, Hodapp J et al. (2003) Renal pseudoaneurysm after blunt renal trauma in a pediatric patient: management by angiographic embolization. *Urology* 61:224



100. Han KK, Goldstein DW, Pantuck AJ et al. (1998) Angiographic management of pseudoaneurysm and arteriocalyceal fistula following blunt trauma: case report and review of the literature. *Can J Urol* 5:654–657
101. Hennessy OF, Gibson RN, Allison DJ (1986) Use of giant steel coils in the therapeutic embolization of a superior mesenteric artery–portal vein fistula. *Cardiovasc Intervent Radiol* 9:42–45
102. Heyns CF, van Vollenhoven P (1992) Increasing role of angiography and segmental artery embolization in the management of renal stab wounds. *J Urol* 147:1231–1234
103. Hidalgo F, Narvaez JA, Rene M et al. (1995) Treatment of hemobilia with selective hepatic artery embolization. *J Vasc Interv Radiol* 6:793–798
104. Hiraide A, Yamamoto H, Yahata K et al. (1994) Delayed rupture of the spleen caused by an intrasplenic pseudoaneurysm following blunt trauma: a case report. *J Trauma* 36:743–744
105. Hirota C, Iida M, Aoyagi K et al. (1995) Posttraumatic intestinal stenosis: clinical and radiographic features in four patients. *Radiology* 194:813–815
106. Horikami K, Matsuoka Y, Nagaoki K et al. (1997) Treatment of post-traumatic urinoma by means of selective arterial embolization. *J Vasc Interv Radiol* 8:221–224
107. Howdieshell TR, Purvis J, Bates WB et al. (1995) Biloma and biliary fistula following hepatorrhaphy for liver trauma: incidence, natural history, and management. *Am Surg* 61:165–168
108. Hsieh CH (2002) Comparison of hepatic abscess after operative and nonoperative management of isolated blunt liver trauma. *Int Surg* 87:178–184
109. Hsieh CH, Chen RJ, Fang JF et al. (2003) Liver abscess after non-operative management of blunt liver injury. *Langenbecks Arch Surg* 387:343–347
110. Huppert PE, Duda SH, Erley CM et al. (1993) Embolization of renal vascular lesions: clinical experience with microcoils and tracker catheters. *Cardiovasc Intervent Radiol* 363–367
111. Inoguchi H, Mii S, Sakata H et al. (2001) Intrahepatic pseudoaneurysm after surgical hemostasis for a delayed hemorrhage due to blunt liver injury: report of a case. *Surg Today* 31:367–370
112. Israel LJ, Morano JU (1996) Abdominal aortic injury in blunt abdominal trauma. *Emerg Radiol* 3:296–297
113. Jebara VA, El Rassi I, Achouh PE et al. (1999) Renal artery pseudoaneurysm after blunt abdominal trauma. *J Vasc Surg* 27:362–365
114. Jenkins MA, Ponsky JL (1995) Endoscopic retrograde cholangiopancreatography and endobiliary stenting in the treatment of biliary injury resulting from liver trauma. *Surg Laparosc Endosc* 5:118–120
115. Jobst MA, Canty TG, Lynch FP (1999) Management of pancreatic injury in pediatric blunt abdominal trauma. *J Pediatr Surg* 34:818–823
116. Jones RC (1985) Management of pancreatic trauma. *Am J Surg* 150:698–704
117. Jurkovich GJ, Carrico CJ (1994) Pancreatic trauma. *Surg Clin North Am* 70:575–593
118. Kaban G, Somani RA, Carter J (2004) Delayed presentation of small bowel injury after blunt abdominal trauma: case report. *J Trauma* 56:1144–1145
119. Kantor A, Scafani S, Scalea T et al. (1989) The role of interventional radiology in the management of genitourinary trauma. *Urol Clin North Am* 16:255–265
120. Karacan Ö, Savas S, Akçay S et al. (2003) Gastropleural fistula as a delayed complication of blunt abdominal trauma: spontaneous closure of the lesion. *Internet J Gastroenterol*
121. Karkiner A, Temir G, Utku M et al. (2005) The efficacy of non-operative management in childhood blunt hepatic trauma. *Ulus travma derg* 11:128–133
122. Kau E, Patel R, Shah O (2004) Isolated renal vein thrombosis after blunt trauma. *Urology* 64:807–808
123. Kawashima A, Sandler CM, Franck MC et al. (2001) Imaging of renal trauma: a comprehensive review. *Radiographics* 21:557–574
124. Kayser S, Marincek B, Schlumpf R et al. (1996) Rapidly progressive portal hypertension 23 years after post-traumatic arterioportal fistula of the liver. *Am J Gastroenterol* 91:1442–1446
125. Keller MS, Stafford PW, Vane DW (1997) Conservative management of pancreatic trauma in children. *J Trauma* 42:1097–1100
126. Kennedy JA, Majury C, Kelly I et al. (1999) Post traumatic pseudoaneurysm of an intrasplenic segmental artery; a mechanism of delayed splenic rupture. *Injury* 30:535–536
127. Kestenberg WL, Mittal VK (1992) Post-traumatic pseudoaneurysm of the left hepatic artery initially appearing as gastrointestinal hemorrhage secondary to hepatic artery: duodenal fistula. A case study. *Am Surg* 58:451–455
128. Killeen KL, Shanmuganathan K, Boyd-Kranis R et al. (2001) CT findings after embolization for blunt splenic trauma. *J Vasc Interv Radiol* 12:209–214
129. Kirchgatterer A, Baldinger C, Lenglinger F et al. (1998) Portal hypertension due to traumatic hepatic arterioportal fistula: report of successful embolization. *Eur J Gastroenterol Hepatol* 10:1057–1059
130. Kluger Y, Paul DS, Raves JJ et al. (1994) Delayed rupture of the spleen: myths, facts, and their importance: case reports and literature review. *J Trauma* 36:568–571
131. Knudson MM, Lim RC, Oakes DD et al. (1990) Nonoperative management of blunt liver injuries in adults: the need for continued surveillance. *J Trauma* 30:1494–1500
132. Knudson MM, Harrison PB, Hoyt DB et al. (2000) Outcome after major renovascular injuries: a Western Trauma Association Multicenter Report. *J Trauma* 49:1116–1122
133. Koehler PR, Jones R (1980) Association of left-sided pleural effusions and splenic hematomas. *AJR* 135:851–853
134. Konobu T, Murao Y, Miyamoto S et al. (1999) Posttraumatic intestinal stenosis presenting as a perforation: report of a case. *Surg Today–Jpn J Surg* 29:564–567
135. Kozar RA, Moore JB, Niles SE et al. (2005) Complications of nonoperative management of high-grade blunt hepatic injuries. *J Trauma* 59:1066–1071
136. Krige JEJ, Bornman PC, Terblanche J (1997) Liver trauma in 446 patients. *South Afr J Surg* 35:10–15
137. Landau A, van As AB, Numanoglu A et al. (2006) Liver injuries in children: the role of selective non-operative management. *Injury* 37:66–71
138. Lee DG, Lee SJ (2005) Delayed hemorrhage from a pseudoaneurysm after blunt renal trauma. *Int J Urol* 12:909–911
139. Lee HK, Kim IO, Kim WS et al. (1995) Stenosis of the inferior vena cava caused by a traumatic diaphragmatic hernia: case report. *Pediatr Radiol* 25:S175–S177
140. Lee RS, Porter JR (2003) Traumatic renal pseudoaneurysm: diagnosis and management techniques. *J Trauma* 55 972–978
141. Leone RJ Jr, Hammond JS (2001) Non-operative management of pediatric blunt hepatic trauma. *Am Surg* 67:138–142
142. Leppaniemi A, Haapiainen R, Standertskjold-Nordenstam CG et al. (1988) Delayed presentation of blunt splenic injury. *Am J Surg* 155:745–749
143. Lerut J, Vauthey N, Triller J et al. (1992) Intrahepatic arterioportal fistula following conservative treatment of a traumatic liver rupture: case report. *J Trauma* 33:760–764
144. Levy JB, Baskin LS, Ewalt DH et al. (1993) Nonoperative management of blunt pediatric major renal trauma. *Urology* 42:418–424
145. Lin BC, Chen RJ, Fang JF et al. (2004) Management of blunt major pancreatic injury. *J Trauma* 56:774–778
146. Lublin M, Chauvin S, Kashani M et al. (2004) Delayed colonic stricture and obstruction after blunt abdominal trauma: a case report and review of the literature. *J Trauma* 57:193–195



147. Lucaya J, Vazquez E, Caballero F et al. (1998) Non-operative management of traumatic pancreatic pseudocysts associated with pancreatic duct laceration in children. *Pediatr Radiol* 28:5–8
148. Lukancic SP, Nemcek AA, Vogelzang RL (1991) Post-traumatic intra-hepatic arterial pseudo-aneurysm: treatment with direct percutaneous puncture. *J Vasc Interv Radiol* 2:335–337
149. Lutz N, Mahboudi S, Nance ML et al. (2004) The significance of contrast blush on computed tomography in children with splenic injuries. *J Pediatr Surg* 39:491–494
150. Lynch JM, Meza MP, Newman B et al. (1997) Computed tomography grade of splenic injury is predictive of the time required for radiographic healing. *J Pediatr Surg* 32:1093–1096
151. MacDermott VG, Shlansky-Goldberg R, Cope C (1994) Endovascular management of splenic artery aneurysms and pseudoaneurysms. *Cardiovasc Intervent Radiol* 17:179–184
152. MacGillivray DC, Valentine RJ (1989) Nonoperative management of blunt pediatric liver injury: late complications: case report. *J Trauma* 29:251–254
153. Maekawa T, Yabuki K, Satou K et al. (1997) A patient with a traumatic right diaphragmatic hernia occurring 4 years after sustaining injury: statistical observations of a delayed diaphragmatic hernia caused by uncomplicated injury in Japan. *Nippon Geka Hokan* 66:116–125
154. Malhotra AK, Fabian TC, Croce MA et al. (2000) Blunt hepatic injury: a paradigm shift from operative to nonoperative management in the 1990s. *Ann Surg* 231:804–813
155. Maloo MK, Burrows PE, Shamberger RC (1999) Traumatic splenic arteriovenous fistula: splenic conservation by embolization. *J Trauma* 47:173–175
156. Marcheix B, Dambrin C, Cron C et al. (2004) Transhepatic percutaneous embolization of a post-traumatic pseudoaneurysm of hepatic artery. *Ann Chir* 129:603–606
157. Markert DJ, Shanmuganathan K, Mirvis SE et al. (1997) Budd-Chiari syndrome resulting from intrahepatic IVC compression secondary to blunt hepatic trauma. *Clin Radiol* 52:384–387
158. McAninch JW (1993) Editorial: renal trauma. *J Urol* 150:1778
159. McIndoe AH (1931) Delayed hemorrhage following traumatic rupture of the spleen. *Br J Surg* 20:249–268
160. Meredith JW, Young JS, Bowling J et al. (1994) Nonoperative management of blunt hepatic trauma: The exception or the rule? *J Trauma* 36:529–534
161. Miller DC, Forauer A, Faerber GJ (2002) Successful angioembolization of renal artery pseudoaneurysms after blunt abdominal trauma. *Urology* 59:444
162. Mohr AM, Lavery RF, Barone A et al. (2003) Angiographic embolization for liver injuries: low mortality, high morbidity. *J Trauma* 55:1077–1082
163. Mourad M, Desrousseaux B, Atat I et al. (1992) Delayed perforation of the sigmoid colon following closed abdominal trauma. A propos of a case report. *Acta Chir Belg* 92:172–175
164. Nagar H, Kessler A, Weiss J (1997) Traumatic intraparenchymal splenic pseudoaneurysms in a child: nonoperative management. *J Trauma* 43:552–555
165. Nagy KK, Duarte B (1990) Post-traumatic inferior vena caval thrombosis: case report. *J Trauma* 30:218–221
166. Navarro O, Babyn P, Pearl R (2000) The value of routine follow-up imaging in pediatric blunt liver trauma. *Pediatr Radiol* 30:546–550
167. Navsaria PH, Adams S, Nicol AJ (2002) Traumatic thoracobiliary fistulae: a case report with a review of the current management options. *Injury* 33:639–643
168. Oguzkurt L, Balkanci F, Ariyurek M et al. (1996) Traumatic aneurysm and arteriovenous fistula of the splenic artery. *Pediatr Radiol* 26:195–197
169. Oguzulgen IK, Oguzulgen AI, Sinik Z et al. (2002) An unusual cause of urinothorax. *Respiration* 69:273–274
170. Oldham KT, Guice KS, Ryckman F et al. (1986) Blunt liver injury in childhood: evolution of therapy and current perspective. *Surgery* 100:542–549
171. Olsen WR (1982) Late complications after central liver injuries. *Surgery* 92:733–743
172. Olsen WR, Polley TZ (1977) A second look at delayed splenic rupture. *Arch Surg* 112:422–425
173. Omert LA, Saylor D, Dunham CM et al. (2001) Implications of the “Contrast blush” finding on computed tomographic scan of the spleen in trauma. *J Trauma* 51:272–278
174. Ooi LLPG, Leong SS (1997) Splenic abscess from 1987 to 1995. *AM J Surg* 174:87–92
175. Owens CA, Alkadri A, Yaghamai B et al. (2001) Massive intraperitoneal hemorrhage from traumatic intrasplenic pseudoaneurysms: treatment using superselective embolotherapy. *Int Surg* 86:201–205
176. Owings JT, Engle SJ (1995) Combined hepatic abscess and arterial pseudoaneurysms from blunt trauma: a case report and management strategy. *J Trauma* 38:634–638
177. Ozturk H, Dokucu AI, Onen A et al. (2004) Non-operative management of isolated solid organ injuries due to blunt abdominal trauma in children: a fifteen-year experience. *Eur J Pediatr Surg* 14:29–34
178. Pachter HL, Hofstetter SR (1995) The current status of non-operative management of adult blunt hepatic injuries. *Am J Surg* 169:442–454
179. Pachter HL, Hofstetter SR, Elkowitz A et al. (1993) Traumatic cysts of the spleen: the role of cystectomy and splenic preservation: experience with seven conservative patients. *J Trauma* 35:430–436
180. Pachter HL, Knudson MM, Esrig B et al. (1996) Status of non-operative management of blunt hepatic injuries in 1995: a multicenter experience with 404 patients. *J Trauma* 40:31–38
181. Pachter HL, Guth AA, Hofstetter SR et al. (1998) Changing patterns in the management of splenic trauma: the impact of nonoperative management. *Ann Surg* 227:708–717
182. Paris S, Weiss SM, Ayers VVH et al. (1994) Splenic abscess. *Am Surg* 60:358–361
183. Parks RW, Chrysos E, Diamond T (1999) Management of liver trauma. *Br J Surg* 86:1121–1135
184. Patel NY, Cogbill TH, Gundersen LF (1996) Angioembolization of multiple intrasplenic pseudoaneurysms as a result of blunt trauma. *J Vasc Surg* 24:299–301
185. Patton JH, Lyden SP, Croce MA et al. (1997) Pancreatic trauma: a simplified management guideline. *J Trauma* 43:234–239
186. Paul JL, Otal P, Perreault P et al. (1999) Treatment of posttraumatic dissection of the renal artery with endoprosthesis in a 15-year-old girl. *J Trauma* 47:169–172
187. Pearl LB, Trunkey DD (1999) Compartment syndrome of the liver. *J Trauma* 47:796–798
188. Poli ML, Lefebvre F, Ludot H et al. (1995) Nonoperative management of biliary tract fistulas after blunt abdominal trauma in a child. *J Pediatr Surg* 30:1719–1721
189. Raghavendran K, Singh G, Arnoldo B et al. (2004) Delayed development of infrarenal abdominal aortic pseudoaneurysm after blunt trauma: a case report and review of the literature. *J Trauma* 57:1111–1114
190. Ramirez JJ, Velmahos GC, Best CR et al. (2004) Male sexual function after bilateral internal iliac artery embolization for pelvis fracture. *J Trauma* 56:734–739
191. Redmond PL, Kumpe DA (1988) Embolization of an intrahepatic arterioportal fistula: case report and review of the literature. *Cardiovasc Intervent Radiol* 11:274–279
192. Repasky RG, Tisnado J, Freedman AM (1993) Transcatheter embolization of a superior mesenteric artery pseudoaneurysm and arteriovenous fistula. *J Vasc Interv Radiol* 4:241–244
193. Roberts A, Hays DA, McFarland DR (1996) Coil embolization of an internal iliac artery arteriovenous fistula with a Wall-stent. *J Vasc Interv Radiol* 7:611–613
194. Rosen RJ, Rothberg (1982) Transhepatic embolisation of hepatic artery pseudoaneurysm following biliary drainage. *Radiology* 145:532–533

195. Rousseau A, Regimbeau JM, Vibert E et al. (2004) Pseudoaneurysm after blunt liver trauma: a potential delayed complication. *Ann Chir* 129:41–45
196. Salis A, Pais SO, Vennos A et al. (1999) Superselective embolization of a traumatic intrasplenic arteriovenous fistula. *J Trauma* 46:186–188
197. Samaiya A, Gupta S, Chumber S et al. (2001) Blunt abdominal trauma with delayed rupture of splenic hematoma in a hemophilic patient. *Hemophilia* 7:331–334
198. Samek P, Bober J, Vrzuga A et al. (2001) Traumatic hemobilia caused by false aneurysm of replaced right hepatic artery: case report and review. *J Trauma* 51:153–158
199. Sandblom P (1948) Hemorrhage into the biliary tract following trauma: “Traumatic hemobilia”. *Surgery* 24:571–586
200. Santucci RA, McAninch JM (2001) Grade IV renal injuries: evaluation, treatment, and outcome. *World J Surg* 25:1565–1572
201. Sarioglu A, Tanyel FC, Ariyurek M et al. (1996) Aneurysmatic arteriovenous fistula complicating splenic injury. *Eur J Pediatr Surg* 6:183–185
202. Sato N, Yamaguchi K, Shimizu S et al. (1998) Coil embolization of bleeding visceral pseudoaneurysms following pancreatectomy. *Arch Surg* 133:1099–1102
203. Saunders MS, Riberi A, Massullo EA (1992) Delayed traumatic superior mesenteric arteriovenous fistula after a stab wound: case report. *J Trauma* 32:101–106
204. Savader SJ, Trerotola SO, Merine DS et al. (1992) Hemobilia after percutaneous transhepatic biliary drainage: treatment with transcatheter embolotherapy. *J Vasc Interv Radiol* 3:345–352
205. Schmidt B, Bhatt GM, Abo MN (1980) Management of post-traumatic vascular malformations of the liver by catheter embolization. *Am J Surg* 140:332–335
206. Schurr MJ, Fabian TC, Gavant M et al. (1995) Management of blunt splenic trauma: computed tomographic contrast blush predicts failure of non-operative management. *J Trauma* 39:507–513
207. Schwartz RA, Teitelbaum GP, Katz MD et al. (1993) Effectiveness of transcatheter embolization in the control of hepatic vascular injuries. *J Vasc Interv Radiol* 4:359–365
208. Scioscia PJ, Dillon PW, Cilley RE et al. (1994) Endoscopic sphincterotomy in the management of posttraumatic biliary fistula. *J Pediatr Surg* 29:3–6
209. Sclafani SJA, Nayaranaswamy T, Mitchell WG (1981) Radiologic management of traumatic hepatic artery: portal vein arteriovenous fistulae. *J Trauma* 21:576–580
210. Sclafani SJA, Goldstein AS, Lipkowitz GS (1984) Radiologic management of disrupted ureteral anastomosis and infected urinoma after gunshot wound. *J Trauma* 24:1060–1062
211. Sclafani JA, Florence LO, Phillips TF et al. (1987) Lumbar arterial injury: radiologic diagnosis and management. *Radiology* 165:709–714
212. Sclafani SJA, Herskowitz M, Rachlin S et al. (1995) Intestinal plethora: an early sign of acute posttraumatic hepatic artery–portal vein arteriovenous fistula. *Emerg Radiol* 2:380–383
213. Sclafani SJA, Shaftan GW, Scalea TM et al. (1995) Nonoperative salvage of computed tomography–diagnosed splenic injuries: utilization of angiography for triage and embolization for hemostasis. *J Trauma* 39:818–827
214. Settmacher U, Nussler NC, Pfitzmann R et al. (2001) Surgical treatment of a post-traumatic hepatic artery aneurysm. *Eur J Vasc Endovasc Surg* 21:77–78
215. Sharif K, Pimpalwar AP, John P et al. (2002) Benefits of early diagnosis and preemitive treatment of biliary tract complications after major blunt liver trauma in children. *J Pediatr Surg* 37:1287–1292
216. Sharpe RP, Nance ML, Stafford PW (2002) Nonoperative management of blunt extrahepatic biliary duct transection in the pediatric patient: case report and review of the literature. *J Pediatr Surg* 37:1612–1616
217. Sheik-Gafoor MH, Singh B, Moodley J (1998) Traumatic thoracobiliary fistula: report of a case successfully managed conservatively, with an overview of current diagnostic and therapeutic options. *J Trauma* 45:819–821
218. Sherman HF, Higler JS, Jones LM et al. (1992) Delayed diagnosis of extrahepatic biliary injury. *Eur J Surg* 158:575–578
219. Sherman HF, Savage BA, Jones LM et al. (1994) Nonoperative management of blunt hepatic injuries: Safe at any grade? *J Trauma* 37:616–621
220. Shih FC, Wang SJ, Dang KJ et al. (1994) Successful management of traumatic mesenteric arteriovenous fistula after failure of steel coil embolization: case report. *J Trauma* 37:682–686
221. Shilyansky J, Navarro O, Superina RA et al. (1999) Delayed hemorrhage after nonoperative management of blunt hepatic trauma in children: a rare but significant event. *J Pediatr Surg* 34:60–64
222. Shindo S, Ogata K, Katahira S et al. (1997) Delayed manifestation of aortic stenosis after blunt abdominal trauma: report of a case. *Surg Today* 27:76–79
223. Siablis D, Panagopoulos C, Karamessini M et al. (2003) Delayed diagnosis of a false aneurysm after lumbar arterial injury: treatment with endovascular embolization: a case report. *Spine* 28:E71–E73
224. Sidhu MK, Weinberger E, Healey P (1998) Intramural duodenal hematoma after blunt abdominal trauma. *AJR* 170:38
225. Sidhu MK, Shaw DWW, Daly CP et al. (1999) Post-traumatic hepatic pseudoaneurysms in children. *Pediatr Radiol* 29:46–52
226. Siegel MJ, Sivit CJ (1997) Pancreatic emergencies. *Radiol Clin North Am* 35:815–830
227. Silberzweig JE (1999) Ruptured lumbar artery pseudoaneurysm: a diagnostic dilemma in retroperitoneal hemorrhage after abdominal trauma. *J Trauma* 46:531–532
228. Singh S, Kalan MM, Moreyra CE et al. (2000) Diaphragmatic rupture presenting 50 years after the traumatic event. *J Trauma* 49:156–159
229. Sirbu H, Busch T, Spillner J et al. (2005) Late bilateral diaphragmatic rupture: challenging diagnostic and surgical repair. *Hernia* 9:90–92
230. Sivit CJ, Eicheberger MR, Taylor GA et al. (1992) Blunt pancreatic trauma in children: CT diagnosis. *AJR* 158:1097–1100
231. Sjövall A, Hirsh K (1997) Blunt abdominal trauma in children: risks of nonoperative treatment. *J Pediatr Surg* 1169–1174
232. Slim K (1999) Ruptures and injuries to the diaphragm. *J Chir* 136:67–75
233. Smith GR, Northrop CH (1987) Stab wound causing mesenteric–portal arteriovenous fistula: an unusual case with a spontaneous closure. *J Trauma* 16:408–411
234. Sofocleous CT, Hinrichs C, Hubbi B et al. (2005) Angiographic findings and embolotherapy in renal arterial trauma. *Cardiovasc Intervent Radiol* 28:39–47
235. Soudack M, Epelman M, Gaitini D (2003) Spontaneous thrombosis of hepatic posttraumatic pseudoaneurysms: sonographic and computed tomographic features. *J Ultrasound Med* 22:99–103
236. Sprouse LR II, Hamilton IN Jr (2002) The endovascular treatment of a renal arteriovenous fistula: placement of a covered stent. *J Vasc Surg* 36:1066–1068
237. Steffens MG, Bode PJ, Lycklama à Nijeholt AA et al. (1996) Selective embolization of pseudo-aneurysms of the renal artery after blunt abdominal injury in a patient with a single kidney. *Injury* 27:219–220
238. Stein M, Battistella FD (2003) Percutaneous management of traumatic biliary injuries. *Semin Interv Radiol* 20:141–149
239. Stroz P, Asch M, Salem S et al. (1996) Transhepatic embolization of a portohepatic venous fistula. *J Vasc Interv Radiol* 7:705–707
240. Struyven J, Cremer M, Pirson P et al. (1982) Posttraumatic bilhemia: diagnosis and catheter therapy. *AJR* 138:746–747

241. Sugg SL, Gerndt SJ, Hamilton BJ et al. (1995) Pseudoaneurysms of the intraparenchymal splenic artery after blunt abdominal trauma: a complication of nonoperative therapy and its management. *J Trauma* 39:593–595
242. Sugimoto K, Asari Y, Sakagushi T et al. (1993) Endoscopic retrograde cholangiography in the nonsurgical management of blunt liver injury. *J Trauma* 35:192–199
243. Sugiyama M, Atomi Y, Matsuoka T et al. (2000) Endoscopic biliary stenting for treatment of persistent biliary fistula after blunt hepatic injury. *Gastrointest Endosc* 51:42–44
244. Suzuki T, Shindo M, Kataoka Y et al. (2005) Clinical characteristics of pelvic fracture patients with gluteal necrosis resulting from transcatheter arterial embolization. *Arch Orthop Trauma Surg* 125:448–452
245. Swana HS, Cohn SM, Burns GA et al. (1996) Renal artery pseudoaneurysm after blunt abdominal trauma: case report and literature review. *J Trauma* 40:459–461
246. Taff ML, Wolodzko AA, Boglioli LR (1990) Sudden death due to delayed rupture of hepatic subcapsular hematoma following blunt abdominal trauma. *Am J Forensic Med Pathol* 11:270–274
247. Takishima T, Hirata M, Kataoka Y et al. (2000) Delayed development of obstructive jaundice and pancreatitis resulting from traumatic intramural hematoma of the duodenum: report of a case requiring deferred laparotomy. *J Trauma* 49:160–162
248. Tanaka H, Iwai A, Sugimoto H et al. (1991) Intrahepatic arterioportal fistula after blunt hepatic trauma: cases reports. *J Trauma* 31:143–146
249. Teitelbaum GP, Reed RA, Larsen D et al. (1993) Microcatheter embolization of non-neurologic traumatic vascular lesions. *J Vasc Interv Radiol* 4:149–154
250. Titton RL, Gervais DA, Boland GW et al. (2002) Renal trauma: radiologic evaluation and percutaneous treatment of nonvascular injuries. *AJR* 178:1507–1511
251. Toevs CC, Beilman GJ (2000) Splenic abscess 10 years after splenic trauma: a case report. *Am Surg* 66:204–205
252. Totte E, Van Hee R, Discart H et al. (2000) Isolated colonic injury following blunt abdominal trauma. *Acta Chir Belg* 100:71–73
253. Triller J, Krebs T, Ackermann D (1993) Superselective embolization of traumatic renal pseudoaneurysm with a Tracker-18 catheter and microcoils. *Eur Radiol* 3:261–263
254. Tsushima Y, Yamada S, Aoki J et al. (2001) Ischaemic ileal stenosis following blunt abdominal trauma and demonstrated by CT. *Br J Radiol* 74:277–279
255. Uflacker R, Saadi J (1982) Transcatheter embolization of superior mesenteric arteriovenous fistula. *AJR* 139:1212–1214
256. Uflacker R, Paolini RM, Lima S (1984) Management of traumatic hematuria by selective renal artery embolization. *J Urol* 132:662–667
257. van der Zee DC, Kramer WL, Ure BM et al. (1999) Laparoscopic management of a large posttraumatic splenic cyst in a child. *Surg Endosc* 13:1241–1242
258. van der Zee JA, van den Hoek J, Weerts JGE (1995) Traumatic renal arteriovenous fistula in a 3-year-old girl, successfully treated by percutaneous transluminal embolization. *J Pediatr Surg* 30:1513–1514
259. Vassiliu P, Toutouzas KG, Velmahos GC et al. (2004) A prospective study of post-traumatic biliary and pancreatic fistuli. The role of expectant management. *Injury* 35:223–227
260. Vauthey JN, Tomczak RJ, Helmberger T et al. (1997) The arterioportal fistula syndrome: clinicopathologic features, diagnosis, and therapy. *Gastroenterology* 113:1390–1401
261. Velmahos GC, Chahwan S, Falabella A et al. (2000) Angiographic embolization for intraperitoneal and retroperitoneal injuries. *World J Surg* 24:539–545
262. Velmahos GC, Toutouzas K, Radin R et al. (2003) High success with nonoperative management of blunt hepatic trauma: the liver is a sturdy organ. *Arch Surg* 138:475–481
263. Velmahos GC, Toutouzas KG, Radin R et al. (2003) Nonoperative treatment of blunt injury to solid abdominal organs: a prospective study. *Arch Surg* 138:844–851
264. Vermillion JM, Wilson EB, Smith RW (2001) Traumatic diaphragmatic hernia presenting as a tension fecopneumothorax. *Hernia* 5:158–160
265. Vromen A, Beglaibter N, Feigen E et al. (1993) Delayed large bowel obstruction after blunt abdominal injury. *Eur J Surg* 159:447–448
266. Waelbers A, Duval EL, Vervloessem D (2005) Posttraumatic cholethorax in a child: case report and review of the literature. *Pediatr Crit Care Med* 6:355–358
267. Wahl WL, Ahrns KS, Chen S et al. (2004) Blunt splenic injury: operation versus angiographic embolization. *Surgery* 136:891–899
268. Waldrop JL Jr, Dart BW, Barker DE (2005) Endovascular stent graft treatment of a traumatic aortocaval fistula. *Ann Vasc Surg* 19:562–565
269. Wales PW, Shuckett B, Kim PC et al. (2001) Long-term outcome after nonoperative management of complete traumatic pancreatic transection in children. *J Pediatr Surg* 36:823–827
270. Weissmann HS, Chun KJ, Frank M et al. (1979) Demonstration of traumatic bile leakage at cholescintigraphy and ultrasonography. *AJR* 133:843–847
271. Wick M, Martin D, Muller EJ et al. (2000) Intrathoracic displacement of the transverse colon as a late complication after abdominal knife stab wound. A case report. *Unfallchirurg* 103:908–909
272. Wilson RH, Moorehead RJ (1991) Current management of trauma to the pancreas. *Br J Surg* 78:1196–1202
273. Winton TL, Girotti MJ, Sterns EE (1985) Delayed intestinal perforation after nonpenetrating abdominal trauma. *Can J Surg* 28:437–439
274. Yamakado K, Nakatsuka A, Tanaka N et al. (2000) Transcatheter arterial embolisation of ruptured pseudoaneurysms with coils and n-butyl cyanoacrylate. *J Vasc Interv Radiol* 11:66–72
275. Yardeni D, Polley TZ Jr, Coran AG (2004) Splenic artery embolization for post-traumatic splenic artery pseudoaneurysm in children. *J Trauma* 57:404–407
276. Yoo SY, Lim KS, Kang SJ (1996) Pitfalls of nonoperative management of blunt abdominal trauma in children in Korea. *J Pediatr Surg* 31:263–266
277. Yoon KH, Ha HK, Kim MH et al. (1998) Biliary stricture caused by blunt abdominal trauma: clinical and radiologic features in five patients. *Radiology* 207:737–741
278. Zeman RK, Lee CH, Stahl R et al. (1984) Strategy for the use of biliary scintigraphy in non-iatrogenic biliary trauma. *Radiology* 151:771–777

# Imaging of Head Injuries

Nada Bešenski

## 2.3

### Contents

2.3.1	Introduction	99
2.3.2	Clinical Findings	99
2.3.3	Imaging	100
2.3.4	Biomechanical Considerations of Brain Injury	102
2.3.5	Classification of Brain Injury	108
2.3.5.1	Open-Head Injury/Missile Head Injury	108
2.3.6	Closed-Head Injury	109
2.3.6.1	Extra-axial hemorrhage	109
2.3.6.2	Intra-axial Lesions	112
2.3.6.3	Cortical Contusion	112
2.3.7	Imaging of Diffuse Axonal Injury (Shearing Injury)	114
2.3.7.1	Brain-stem Injury	117
2.3.8	Early Secondary Lesions in Brain Injury	118
2.3.8.1	Diffuse Cerebral Edema	118
2.3.8.2	Secondary Intraparenchymal Hemorrhage	119
2.3.8.3	Brain Herniation	119
2.3.9	Late Sequelae of Trauma	120
2.3.9.1	Shaken-Baby Syndrome	121
2.3.10	Conclusion	122
	References	123

### 2.3.1 Introduction

Traumatic brain injury (TBI) and its consequences are a big public health problem. The cost of severe TBI to the individual, family, and society are extremely high. Traumatic brain injury has a high incidence, ranging from about 100 per 100,000 to 800 per 100,000 people across European countries with an average incidence rate of 0.32% (Berg 2004). Motor vehicle crashes, falls, assaults, guns, sports, and recreational activities are the major causes of TBI. The fact that the incidence of persons injured in traffic accidents is higher than in falls reflects an “epidemic” of trauma as a consequence of increased traffic accidents in general (Frankowski et al. 1985;

Pavic et al. 1994). Adolescents, young adults, and those over 75 years are most at risk. The term “traumatic head injury” is often used synonymously with TBI, although it may not be associated with the same neurological deficit

### 2.3.2 Clinical Findings

The clinical considerations for patients suffering a brain injury are included into and judged by the Glasgow Coma Scale (GCS) and imaging at the moment of trauma. Relating to the Glasgow Coma Scale, TBI can be clinically categorized as severe (GCS  $\leq 8$ ), moderate (GCS 9-12), or mild (GCS 13-15). Kuhne et al. (2003) showed that independently of the initially good GCS, a high percentage of patients suffered from severe intracranial lesions. In the hyperacute setting the patient’s level of consciousness is a poor predictor of long-term outcome, because loss of consciousness is highly variable in the early hours after injury and can be substantially altered by the central nervous system side effects of acute medical treatment. Despite these limitations, the GCS remains the most widely used scoring system in acute cerebral disorders because it is simple and reproducible, and because its use requires a little training

The indications for imaging are severely impaired consciousness, focal neurological signs, and penetrating head injury. Clinically, this is a high-risk group. A moderate-risk group are the injured persons with minor disturbances of consciousness, progressive headaches, fracture of the skull base, and those with multiple injuries. The low-risk group are patients with mild or moderate posttraumatic headaches, without a loss of consciousness. The focal neurological signs are sometimes masked by a serious general state of the patient (coma, shock)

Traumatic brain injury is related to a significant risk of mortality, particularly directly after the injury, and surviving patients often suffer severe consequences in terms of cognitive, physical, emotional, and social functioning. The TBI can result often in the disturbance of behavioral or emotional functioning. All these impairments may be either temporary or permanent and cause partial or total functional disability or psychosocial maladjustment. In-



creasing evidence shows that even mild TBI can cause brain damage suggesting that structural and physiological factors may contribute to some cognitive syndromes and postconcussion syndrome. Particular and common clinical problems may cause endocrinological disturbances due to pituitary hormone abnormalities in trauma patients. They may occur in up to 50% of survivors of TBI who were investigated several months or longer following the event. Data showed that posttraumatic neuroendocrine abnormalities occur early and with high frequency, which may have significant implications for recovery and rehabilitation of TBI patients (Agha et al. 2004). Generally, each patient with head injury should be evaluated individually based upon clinical findings

### 2.3.3 Imaging

Imaging of head trauma in the emergency setting is performed to detect potentially treatable lesions before a secondary neurological damage occurs. Although skull fractures can be detected by a different plain X-ray examination, they are obsolete. Computerized tomography (CT) and magnetic resonance imaging are the most common techniques in patients who suffered brain injury. Cihangiroglu et al. (2002) analyzed over 20,000 imaging studies done in brain injury and compared the results with the experience in the literature. A detailed comparison has been done relative to CT, MRI, SPECT, and PET in traumatic brain injury is demonstrated in Table 1

Scout CT scan and thin slices with bone window are reliable in detecting of depressed skull fractures and are much more sensitive than plain X-ray

In daily routine CT is still the method of choice in acute TBI evaluation. Despite the well-recognized contribution of MR to the investigation of most of acute neurological pathologies, MRI is still not a routine procedure for the initial investigation of patients with acute head injury; however, MR can give the insight into the full extent of traumatic lesions, insight which cannot be obtained by use of CT

Generally, the density of traumatic brain lesions demonstrated by CT can be hyperdense, hypodense, or mixed (combined). Pathoanatomically hyperdense lesions on CT correspond to bleeding, whereas hypodense ones correspond to edema or destruction of axons and necrosis; therefore, hypodense lesions are also important. Around hyperdense lesions hypodense areas can be frequently found depending on the time of scanning in relation to the traumatic event concerned. On the control CT we can follow the evolution of hyperdense lesions into hypodense ones (resorption of hemorrhage), but also the evolution of hypodense into hyperdense areas (Fig. 1; Grčević 1984, 1988; Jadro-Santel et al. 1989; Besenski and Jadro-Santel 1992); therefore, CT is a suitable method to follow the dynamics of lesion development, giving insight into the corresponding pathological development of brain injury (living pathology; Grčević, 1982)

Wintermark et al. (2004a) demonstrated that CT perfusion provides additional information with respect to focal brain traumatic injuries when compared with conventional cerebral CT. They showed that perfusion CT has a higher sensitivity for the diagnosis of cerebral contusions when compared with admission on unenhanced cerebral CT with a sensitivity 87.5% vs a sensitivity of 39.6%, respectively. The CT perfusion provides quantitatively accurate assessment of brain perfusion. It is a minimal-risk procedure giving insight into the region cerebral blood vol-

**Table 1.** Comparison of CT, MRI, SPECT, and PET in traumatic brain injury. (From Cihangiroglu 2002)

Pathology	Skull radiography	CT	MRI	SPECT/PET
Skull fracture	+	+++	?	
Extra-axial hemorrhage		+++	+++ /++++	
Epidural hematoma		+++	++++	
Subdural hematoma		++	+++	
Subdural hygroma		+++	++ /+++	
Subarachnoid hemorrhage		+++	++++	
Intraventricular hemorrhage				
Intra-axial pathology				
Diffuse axonal injury		+ /++	++++	
Cortical contusion		+++	+++ /++++	
Brain-stem injury		+ /++	++++	
Secondary effects of trauma				
Cerebral herniation		++	++++	
Diffuse cerebral edema		+++	+++	
Vascular complication		++	+++ /++++	
Child abuse	+	+++	+ /++	
Intracranial metabolic changes			++	+++

+ poor, ++ fair, +++ good, +++++, excellent, ? in chronic setting, MR spectroscopy



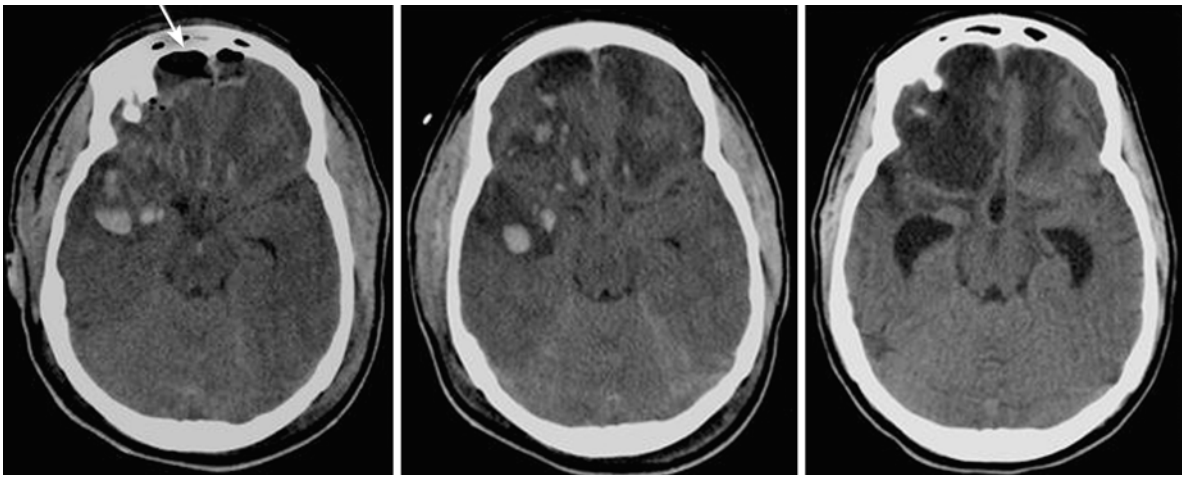


**Fig. 1.** Computed tomography performed on first day, 5 days and 5 weeks after trauma, demonstrated resorption of hemorrhagic lesion in the basal aspect of frontal lobes with encephalomalacia and

hydrocephalus as a final result. Note pneumocephalus in the frontal area on the first scan (*arrow*)

ume(rCBV), mean transit time(MTT), and regional cerebral blood flow (rCBF) values. The CT perfusion is a less operator-dependent technique with respect to its results than other non-invasive techniques, such as transcranial Doppler. Performing CT perfusion in severe head-trauma patients involves only minimal additional contrast (40 vs 120 ml for the chest/abdomen/pelvis CT) and minimal radiation dose. It presents complementary tools to invasive cerebral perfusion pressure measurement (CPP), which is used in the clinical routine as a general indicator of brain perfusion (Wintermark et al. 2004b). Wintermark et al. (2004b) demonstrated a significant correlation of invasive measurements of CPP values with noninvasive CT perfusion measurements of the rCBV, MTT, and rCBF values, as well as with the extent of perfusion CT abnormalities. The CPP measurements are basic in intracranial hypertension monitoring. Intracranial hypertension accounts for about half of all death in trauma patients after admission

Perfusion CT affords insight into regional brain perfusion alterations due to head trauma, with the major advantage of being able to depict regional heterogeneity. Perfusion CT also offers prognostic information with respect to functional outcome, even as early as admission. Patients with altered brain perfusion might be considered for more aggressive and early treatment to prevent intracranial hypertension, whereas patients with preserved brain perfusion might benefit from less invasive treatment. It might allow clinicians to distinguish between patients with preserved autoregulation (or pseudoregulation) and those with impaired autoregulation

Undoubtedly, MRI can substantially enlarge the scope visualization of the lesions, especially at the preacute stages. The MR is especially sensitive in detecting small lesions because of its excellent spatial resolution

The availability of MR imaging data obtained in comatose patients after head injury is scarce, because MR imaging is somewhat cumbersome to perform in patients requiring ventilation. The MR is very sensitive in detecting hyperacute hemorrhages, but since trauma patients are usually unstable and should be monitored, MR is slightly inferior to CT scanning in hyperacute trauma setting. In addition, special equipment is required to obtain MR images in a patient who is respirator dependent; therefore, there is a paucity of MR imaging data obtained in comatose head-injured patients during the acute phase while the patient is dependent on the ventilator. All of this makes MR of little daily practical value in the hyperacute phase of head injury

However, if MR is performed at any other time after a traumatic event, gradient-recalled-echo (GRE) sequences and diffusion-weighted images (DWI) with apparent diffusion coefficient (ADC map) should be included into routine MR protocol in trauma patients. Generally, MR signal intensity varies depending on sequences and time scanning after trauma. The GRE sequences are very sensitive in detection of blood-degradation products (hemorrhagic lesions) as well as former hematoma without hemosiderin (Wardlaw and Statham 2000); however, GRE T2\* are less sensitive in depicting nonhemorrhagic lesions than are fluid-attenuated inversion recovery (FLAIR), T2-weighted spin-echo, and DWI sequences. The DWI is the most sensitive sequence in detection of acute ischemia and edema. The DWI sequence depicts changes in the diffusion rates of water molecules. Many studies have shown respective value of each aforementioned sequence in depicting changes in total brain water content (e.g., vasogenic edema, nonhemorrhagic lesions); thus, the complementary sensitivity of the sequences for the different types of pathophysiological processes increases correlation of lesions with final outcome

There are many published data dealing with MRS, PET, and SPECT findings in TBI with general agreement that those techniques are very sensitive in detecting posttraumatic changes and functional lesions. Magnetic resonance spectroscopy (MRS), PET, and SPECT may explain long-standing effects on trauma in the chronic clinical setting

In TBI there is a specific metabolite spectra demonstrated on MRS with a strong correlation between outcome and MRS (Ross et al. 1998). A spectral feature of the decrease NAA/creatine and increased choline/creatine and myo-inositol/creatine ratios in parietal white matter may be a marker for diffuse axonal injury in patients with TBI as recommended by Yoo et al. (2005), since there is a significant correlation with those spectra and the functional status of the patients. Significant loss of normal functioning neurons are present in TBI, but there is no evidence of anaerobic metabolism using lactate as a surrogate marker, which leads to questioning the role of ischemia as a major mechanism of damage since no lactate was found in TBI (Macmillan et al. 2002)

In trauma patients, significant changes in N-acetyl aspartate (NAA) and choline were found in both gray and white matter as compared with controls, and these alterations correlated with injury severity. Correlations have been reported between these biochemical changes (reduction in NAA, increase in choline) measured at 1–6 months after TBI and the clinical outcome of the patients. But, according to Payen et al. (2005), there are methodological issues which still impede to recommend MRS as a tool for predicting neurological outcome in the clinical setting

A number of studies using PET for the evaluation of patients with head trauma have been reported in the literature. The major limitation of PET imaging is that it cannot distinguish between functional abnormalities specifically related to structural damage from those which are not associated with clear structural damage; therefore, it is essential that PET images be compared with the corresponding anatomical images generated by MR or CT

The SPECT studies have yielded results similar to those with PET scans in patients with head trauma. The SPECT generally has been more available and less costly than PET and thus is more practical than PET for the routine evaluation of brain injury. The SPECT is capable of detecting abnormalities in cerebral blood flow that indicate areas of dysfunction in brain injury. But it has not yet been shown whether or not PET and SPECT can detect more lesions than MR imaging. Studies have shown that SPECT and PET may correlate better with outcome and cognitive dysfunction compared with MR and CT

Finally, current opinion about neuroimaging modalities is that CT remains the first imaging modality, allowing a quick diagnosis of most injuries, especially those which require an emergency treatment. But its predictive value in coma outcome is low. Although MR is more sensitive, it does not, in acute stage, lead to therapeutic modifications. It also increases the cost, and is thus not necessary. In the

subacute or chronic stage after a severe head injury or whenever a patient becomes stable, MR is the method of choice because of its much higher sensitivity and very high predictive power, considering values of new MR technique as DWI and diffusion tensor imaging (DTI). Both MRA and CT angiography may show cranial vessel injury which need specific therapeutic procedures

Computed tomography is the diagnostic mainstay for evaluation of patients with acute injury. Magnetic resonance imaging is preferred in sub-acute and chronic injuries to evaluate the full extent of injury

### 2.3.4 Biomechanical Considerations of Brain Injury

To interpret the imaging findings in a brain injury properly, the biomechanical and pathological conditions during the traumatic event need to be known. The forces need for a head injury are translational (translational forces produce linear movement of the brain), rotational, or angular

Due to the forces of acceleration, linear translation, as well as rotational and angular acceleration, the brain undergoes deformation and distortion depending on the site of impact of traumatizing force direction, severity of the traumatizing force, and tissue resistance of the brain

At the moment of trauma lacerations of parenchyma, supportive and vascular brain structures occur in the epicenter of the primary irreversible damage. These epicenters are consequences of the effects produced by the maximal forces combined with a minimal capacity of the resistance of the brain tissue. It is important to keep in mind that not all types of the brain cells are equally vulnerable. The most vulnerable cells are axons and the most resistant structures are blood vessels

These epicentric, focal lesions are surrounded by larger areas of less severely, but still irreversibly damaged, tissue which is hardly visible by naked-eye inspection but is demonstrated by microscopic examination giving impression of diffuse damage, known as a diffuse axonal injury (DAI) or shearing injury, a special category of brain injury (Fig. 2); therefore, the term DAI is a misnomer, since lesions are focal. It is not a diffuse injury to the whole brain, but rather predominates in discrete regions of brain following high-speed, long-duration acceleration/deceleration injuries. The mechanism for DAI is shear-strain deformation, a change in shape of the brain without a change in volume (Arfanakis et al. 2002). There is a microscopic mechanism of the DAI. Histopathological studies show that the extent of axonal injury always exceeds one that is visualized macroscopically. All imaging modalities underestimate the true extent of DAI, but some of them, such as DWI, DTI, and MRS, reflect microscopic setting of DAI

Microscopically shearing injury initially produces characteristic axonal bulbs or retraction balls, with subsequent

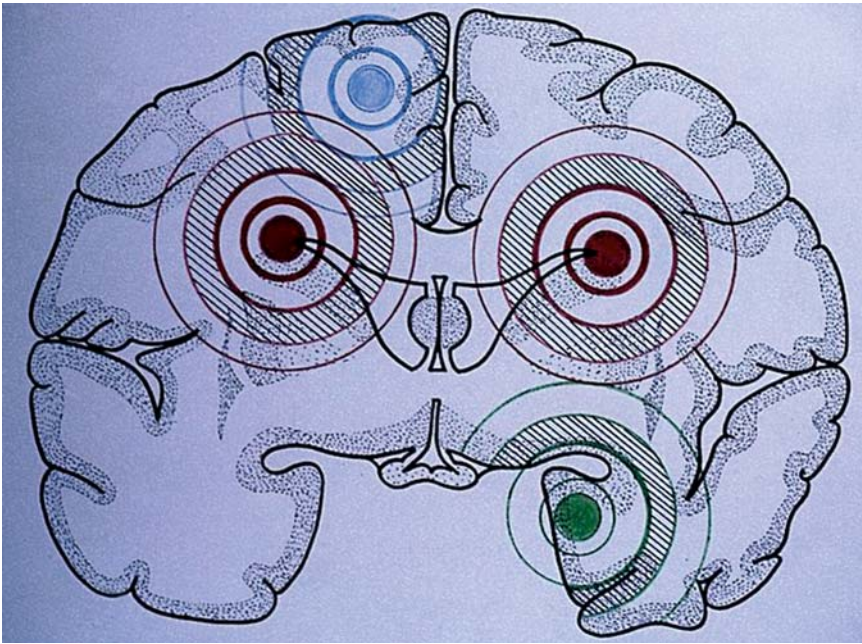


**Fig. 2.** Diffuse axonal injury (DAI) from the pathological point of view

progression to microglial clusters and then long-tract degeneration (Amon et al. 1999). The histological features of DAI depend on the length of time after injury; but within a day or so after injury, there is evidence of damage to axons in the form of axonal bulbs. With time, the microscopic features correspond to Wallerian-type axonal degeneration as the axon disintegrates. This is probably due to metabolic disruption from damage to the internal organelles and a loss of membrane integrity (Meythaler et al. 2001)

Disruption of the cytoskeletal network and axonal membranes characterizes DAI in the first few hours after TBI. In humans with mild traumatic brain injury the first evidence of DAI is believed to be focal neurofilament misalignment. The effect continues for several hours after injury causing local swelling and expansion of the axonal cylinder. Over time, lobulation of the focal swelling takes place, followed by disconnection of the axon at 30–60 h after injury. After disconnection, the proximal and distal segments of the axon become sealed by a continuous axolemma and encompassed by an independent myelin sheath. That axolemmal permeability is not altered after mild traumatic injury, but in the moderate and severe traumatic brain injury a change in the axolemmal permeability is the first evidence of injury. After several hours the neurofilaments become misaligned leading to local swelling and disconnection (Arfanakis et al. 2002). The disconnection of the various target sites is assumed to translate into the resultant morbidity. There is slow progression from axonal swelling to axonal bulb and weeks later to the development of small clusters of microglia throughout the parasagittal white matter, the corpus callosum the internal capsule, and the deep gray matter that usually continues for months to

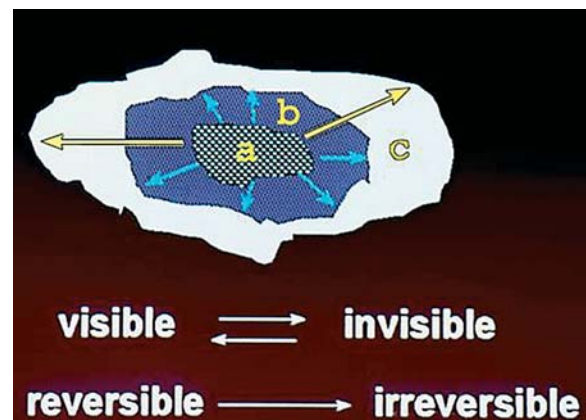


**Fig. 3.** Epicentric lesion with traumatic penumbra in DAI. Epicentric lesion (a). Irreversibly damaged tissue (b). Penumbra (c)

2 years. In the first 2 years after trauma, there is active myelin degeneration which represents the final stage of the process. Neuropathological studies distinguish between three grades of DAI. In grade-1 lesions, there is widespread axonal damage in the cerebral white matter, corpus callosum and brain stem, without hemorrhage. Lesions of grades 2 and 3 show extensive white matter damage with tissue-tear hemorrhages in the corpus callosum and brain stem, respectively (Graham et al. 2002)

The second type of lesion which occurs at the moment of a traumatic event are primarily reversible lesions also related to the epicenters and are distributed at the peripheral epicentric zones. They are termed traumatic penumbra such as an ischemic penumbra (Fig. 3). This change



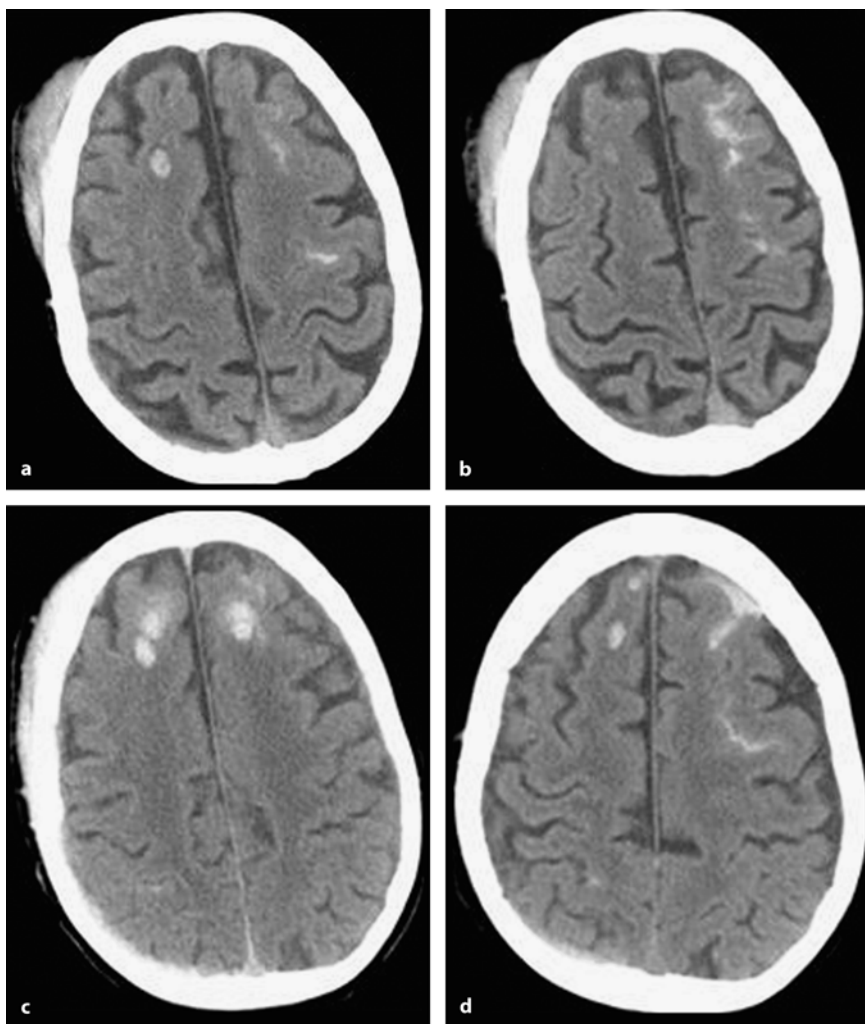


**Fig. 4.** Patient suffered DAI. First CT (**a, b**) showed focal hemorrhagic lesion within subcortical white matter on the right with subarachnoid hemorrhage on the left. Due to traumatic penumbra on follow-up study 24 h later (**c, d**), a new hemorrhagic lesion appeared on the left (**c**) which was not seen on the first CT. Note also a more prominent hemorrhage on the *right* on control CT

represents a *locus minoris resistentiae* to various favorable or unfavorable secondary factors during the early or later posttraumatic period leading visible lesions to perhaps become invisible, and vice versa. Reversible lesions can turn into the irreversible ones. That is the reason why delayed scans may demonstrate lesions not apparent on initial scans. (Fig. 4; Gentry 1991). Primary CT findings performed immediately after injury are usually negative in 10–30% of cases. On the repeated scanning, 75% of this number were positive (Tatalovic-Osterman et al. 1991)

These two types of lesions (epicentric zones associated with area of penumbra) represent a complex which clearly defines the beginning of a traumatic cerebral disease

The course of a traumatizing force and its effect on brain damage in a closed-head injury were systematically studied (Grčević 1984, 1988; Leestma and Grčević 1988; Lindenberg and Freytag 1957, 1960; Sellier and Unterharnscheidt 1963). Some works have emphasized the value of CT data in the study of the biomechanical condition of the brain injury (Jadro-Santel et al. 1989; Tatalovic-Osterman et al. 1991)

Brain damage in a closed-head injury of acceleration/deceleration type depends on the site of impact and on the course of traumatizing forces. It is known that according to the site of impact and traumatizing force direction the lesions can be expected in some peculiar sites in the damaged brain. The attempt has been made to reconstruct traumatic force direction using CT in the entire traumatized brain as we well as in the corpus callosum (CC; Besenski et al. 1992, 1996). Linear translation was taken as criterion for conclusions about the course of the traumatizing force, since this type of acceleration is relatively easy to reconstruct and is common in traumatic event. Forty-five standard CT examinations of patients with closed acceleration/deceleration head injury with the aim to reconstruct the site of impact and the course of traumatizing force were analyzed (Besenski et al. 1996). The site of impact and the course of traumatizing force were reconstructed and graphically presented based on CT findings of soft tissue changes, skull fractures, cortical contusions, and parenchymal lesions. A comparison between the computerized

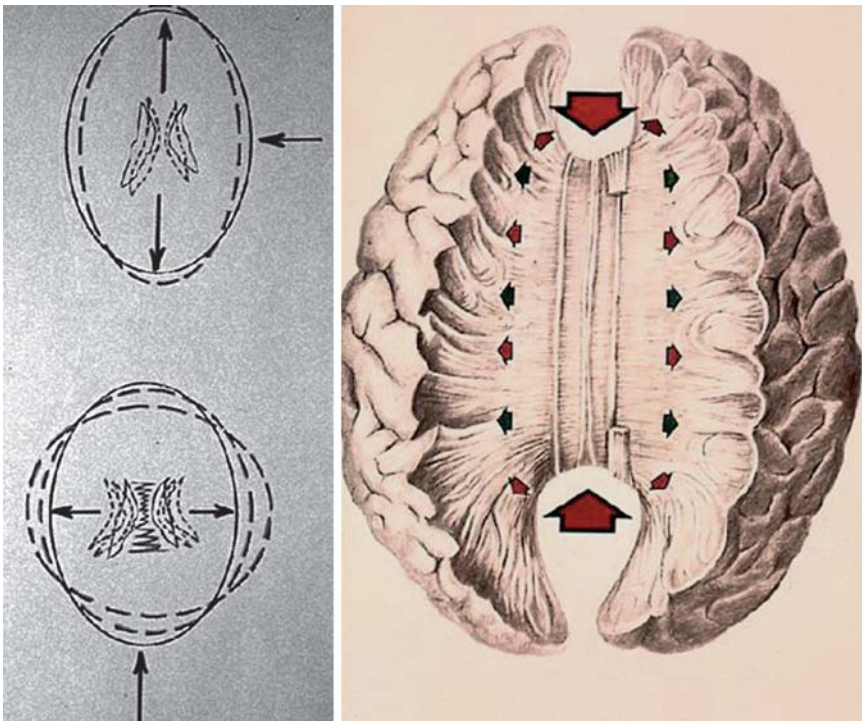


**Fig. 5.** The “inner cavitation effect” with outstretching of the corpus callosum. The longer diameter of the head is shortened and the shorter latero-lateral direction is widened due to cerebrospinal fluid (arrows)

graphic presentation of the site of impact, direction of the traumatic force, and the location of lesions revealed a high correlation between them. In 80% of cases the site of impact could be visualized only by CT. These results showed that CT is very useful for a reconstruction of the site of impact and of the course of the traumatizing force in acceleration head injury. Data obtained by this procedure may have far-reaching prognostic and forensic implications

It has been demonstrated on experimental trauma model that the crucial factors to the extent of injury are the type of acceleration and deceleration (angular rather than translation), the duration of acceleration and deceleration (long rather than short), and the direction of head movement (coronal rather than sagittal; Meythaler et al. 2001)

Generally, a linear translation of acceleration in a closed-head injury can run along the longer or along the shorter diameter of the skull in L-L direction. In such cases an extraaxial lesion (SDH, EDH, SAH) can occur. The L-L courses of a traumatizing force usually lead to quite pronounced coup and countercoup contusions. Contusions are considerably less frequently present in a fronto-occipital (F-O) or an occipito-frontal (O-F) direction of the traumatizing force. The brain stem can also be damaged, but it is damaged more often if the traumatic force acts along the longer diameter of the head. The course of a traumatizing force can run in fronto-occipital (F-O) or occipito-frontal (O-F) medial or oblique paramedial, left or right direction, named as a centroaxial course of the linear translation of an acceleration/deceleration type of trauma. Frontal blows are the most frequent type of a head injury in traffic acci-

dents, whereas the occipito-frontal direction of the traumatizing forces appear most frequently in falls

The centroaxial blows produce a different pattern of lesion located mostly in the deep structures. A biomechanical explanation of the deep, centroaxial lesions was offered by Grčević et al. (1984, 1988), Lindenberg and Freytag (1957, 1960), and Sellier and Unterharnscheidt (1963). They put forth the hypothesis of L-L expansion of the ventricles inner cavitation effect. If traumatic force acts along the longer diameter of the head, F-O or OF, medial or paramedial, the longer diameter of the head will be shortened and the shorter L-L diameter will be widened due to cerebrospinal fluid (CSF) which cannot be compressed. That causes the out-stretching of the corpus callosum (CC) and other midline structures (septum pellucidum, fornix, tella chorioidea of the third ventricle) with a displacement of the lateral ventricular wall resulting in a lesion within these structures (Figs. 5, 6). These structures are often affected. Each deviation from this medial line results in asymmetry of the pattern of lesion. The pattern completely disappears in latero-lateral linear acceleration injuries (Jadro-Santel et al. 1989). Lesions consist of hemorrhages and necrotic lacerations of various degrees. In cases with centroaxial blows DAI occurs as well as brain-stem lesions

By neuropathological analysis of the CC in 54 cases of deep trauma, Zarkovic et al. (1991) showed a significant congruence of the topographic pattern of lesions and the vectors of linear translation of acceleration. In their material the rostral portions of CC were most frequently involved



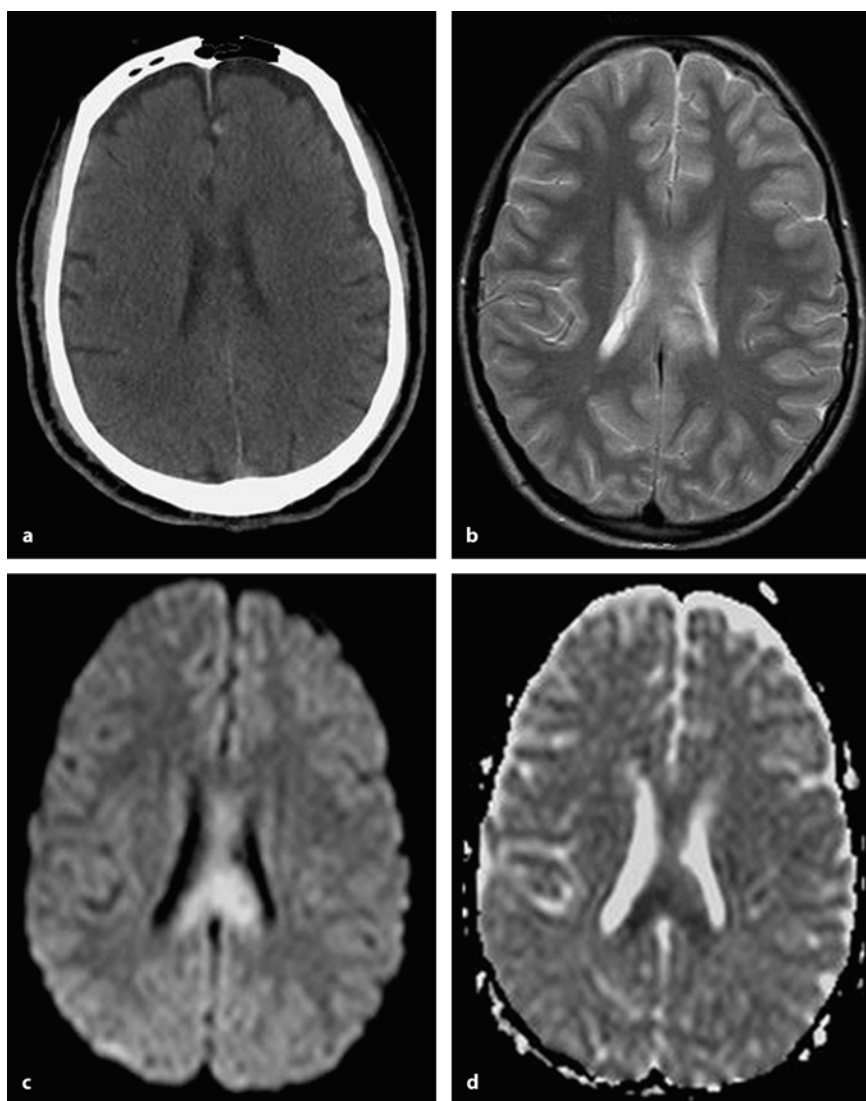


**Fig. 6.** Typical corpus callosum traumatic changes. The CT demonstrated multiple hemorrhagic foci within the callosal body and small one in frontal cortical parasagittal area on the left. **a** Hypodense chronic frontal SDH. Magnetic resonance in another case exhibits large hyperintense lesion within the callosal body on T2 (**b**). Diffusion-weighted imaging (**c**) and ADC map (**d**) demonstrate signal abnormality in the same region

Since the CC is an especially interesting formation in the complex of closed-head injury, there is a study of patterns of lesions of CC in inner cerebral trauma visualized by CT (Besenski et al. 1992). The topographic variations of the lesions of CC were analyzed and correlated to these with the known biomechanical conditions of the traumatic event. In all cases of semioblique frontal–occipital course of linear translation of acceleration the signs of lesions in the frontal part of the CC on the side of the blow and more-or-less marked changes in the splenium of CC on the contralateral side were found. Similar congruence was found with semioblique occipito-frontal translations. The results showed significant congruence between the course of linear translation of acceleration and the sites of the lesions for brain and for CC. This congruence permits CT to be used to reconstruct the course of linear translation and the site of the main blow (Besenski et al. 1992, 1996).

The findings of even small lesion in the CC on CT indicates the need for further investigation of other structures which are usually involved in DAI performing MR as soon as possible

A parasagittal complex (PSC) consists of peculiar and significant lesions localized in the subcortical WM of the parasagittal areas of the brain from the frontal to the occipital region. The PSC is an associated and almost constant phenomenon of the pattern of deep intra-axial lesions. These lesions are a result of the stretching and tearing of long perforating veins which are attached to the sagittal sinus and suffer through a “gliding” of the brain in the rotating anteroposterior movements of the head in frontal blows (Fig. 7). The PSC occurs much less frequently in cases with occipital blows

The periventricular area belongs to the most frequently affected parts in deep intra-axial lesions. The biomechanical

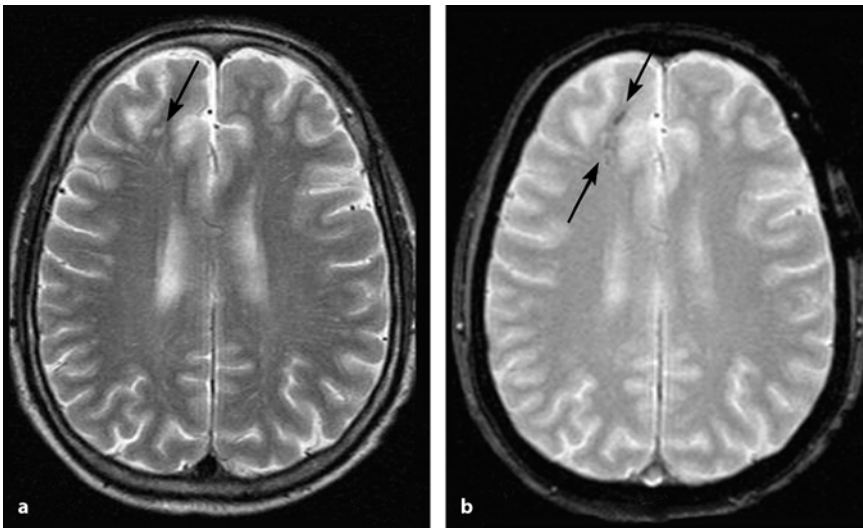


**Fig. 7.** Subtle signal abnormality within white matter/gray matter junction parasagittal on the right on T2-weighted images (*arrow, a*), and more prominent on GRE T2\* sequences (*arrows, b*)



**Fig. 8.** Multiple periventricular lesion in DAI with evidence of intraventricular hemorrhage. Note very subtle hyperdense foci bilaterally in parasagittal area (*arrows*)



**Fig. 9.** A huge hippocampal hematoma on the right seen on CT. Note a prominent soft tissue swelling on the right with preseptal edema and retrobulbar hematoma on the right eye (*arrow*)

cal explanation of a periventricular complex (PVC) may be sought in the same mechanism which produces a lesion of CC (inner cavitation effect). These lesions are small, appearing in an acute phase, usually hemorrhagic and multiple, with a predilection in the WM of the lateral ventricular corners. They are often found in patients with long survival. Demyelination and glial sclerosis were first described in these lesions by Strich (1956). Such a small lesion may play an important role in the development of a persistent vegetative state (Fig. 8)

Lesions in the basal ganglia and the thalamus can be considered as a part of the centro-axial pattern, but they may also be the result of other mechanisms. A downward shifting of the brain due to large EDH, SDH, or a large

countercoup complex, as well as lateral blows, may cause thalamic lesions, too

In the cases of centroaxial blows, especially upper frontal and vertex blows, the brain can be shifted towards tentorial hiatus causing lesions of the hippocampus and the parahippocampal region (Fig. 9). These structures are damaged by L-L force direction as well as in centroaxial blows due to a direct physical conflict of the hippocampus with the rigid edge of the tentorium. The cortical areas suffer cuts, laceration, and disruptions followed by hemorrhage, necrosis, or edema. During the herniation, circulation is impaired and infarctions occur (Grčević 1984, 1988). Lesions of the hippocampal complex are difficult to visualize on CT scans (Jadro-Santel et al. 1989)

Pathoanatomically, a brain-stem lesion is a frequent, if not regular, component of the deep centroaxial pattern of lesions accompanied by diffuse hemispheric damage consisting of hemorrhage, laceration, contusion, and infarction (Grčević 1988; Jadro-Santel et al. 1989; Besenski and Jadro-Santel 1992)

Lesions in the different sites due to the known biomechanism of the closed acceleration/deceleration brain injury need to be interpreted dynamically and not separately with special attention given to minimal brain lesions. Minimal brain lesions may complete the mosaic for a reconstruction of biomechanical condition in each case, which may be important from both clinical and forensic standpoints (Besenski and Jadro-Santel 1992; Besenski 2002)

Using CT and new MR techniques the mechanism of closed-brain injury can be demonstrated in a living traumatized patient without or before pathological section is performed

### 2.3.5 Classification of Brain Injury

Generally, a TBI can be divided into two groups: open-head injury and closed-head injury. By definition, in a closed-head injury dura is intact, in contrast to open-head injury, when dura is torn. Using imaging techniques the manifestations of a head trauma can be divided into primary and secondary lesions. The pathological features of both the primary and secondary lesions attributed to TBI should be understood by anyone caring for head injured patients

Primary lesions are those that occur at the time of trauma as a direct result of the traumatic force. Primary lesions are: scalp laceration/hematoma; skull fractures; the extra-axial (extra-cerebral) hemorrhage (epidural hematoma, subdural hematoma, subarachnoid hemorrhage, intraventricular hemorrhage); and intra-axial lesions (cortical contusion, diffuse axonal injury, and brain-stem injury). Since scalp laceration/hematoma are easily detectable by naked-eye inspection, no special attention will be paid to them in this article. Skull fracture can be detected by CT or X-ray. Skull fractures are most common in persons injured by falls (Leestma and Grčević 1988). Skull fractures do not correspond with the severity of brain injury and are of small importance; however, exceptions are fractures of sinuses, orbit, and midface. High-resolution CT is necessary for evaluating facial or orbital fracture and basilar skull fractures with 3D model

Twenty-five percent of cases with fatal injuries do not demonstrate a skull fracture, although the incidence of intracranial hematomas in patients who have skull fractures is much higher than in those who do not (MacPherson et al. 1990)

Basilar skull fracture can be easily overlooked on routine 5-mm-thick sections and the small gas pocket can be a clue about possible skull base fracture. Pneumocephalus implies that the fracture may be connected to the paranasal

sinuses or mastoid cell. Orbital emphysema indicates that the lamina papiracea or orbital floor is fractured. If the question of basilar skull fracture is important to evaluate the initial patient management, especially if the question of vascular or nerve injuries is raised, the choice of 2 mm slice thickness can be made prospectively with optimal window setting and coronal reconstruction

Basal skull fractures that extend across the carotid canal body of sphenoid bones have a high incidence of vascular injury. Fracture near anterior clinoid process or clinocarotid canal may cause internal carotid artery (ICA) or optic nerve injury. Traumatic ICA dissection appears in cervical, petrous, or intracavernous segment. Vertebral artery dissection involves distal segment of artery and is accompanied with skull or cervical vertebral fracture. If we are worried about possible damage of neurovascular structure, additional CT angiography or MR angiography is a method of choice to exclude or confirm vascular injury

Secondary lesions occur as a consequence of primary lesions usually as a result of mass effect or vascular compromise. They represent diffuse cerebral edema and swelling, cerebral herniation, traumatic ischemia, and infarction and hypoxic injury. Differentiation between primary and secondary lesions is clinically important as secondary lesions are often preventable, whereas primary lesions are consequence of direct mechanical changes and are not preventable

Using imaging techniques it is possible to make fine distinction between the two, as well as to define an open- vs closed-brain injury

#### 2.3.5.1 Open-Head Injury/Missile Head Injury

Open-head injury (e.g., gunshot wounds to the head) are usually fatal injuries, despite all medical and surgical interventions. The energy impacted into the head by penetrating missiles is primarily dependent on their velocity and mass, whereas the missile track within the brain is also related to the design and configuration of the projectile, the firing distance, and weapon orientation (Siccardi et al. 1991; Kirckpatrick 1998) When a high-velocity bullet enters the body and ploughs through the tissue, the material in its path will thoroughly disintegrate

There are several different type of open brain injury: penetrating type if missile stays within the brain parenchyma causing missile canal. The second type is tangential damage of scalp, dura, and bones. In such cases there might be contusion of the brain but no missile canal. The third type is a perforating type if missile has passed through the brain causing bones and dura to be damaged twice. In perforating type missile path is completely formed with entrance and exit wound, in-driven shell, and bone fragments. All this can be visualized by CT

The CT is indispensable in missile head wounds, because it is faster than any other method and provides more detailed



**Fig. 10.** Multiple in-driven bones with retained shell fragments temporo-occipital on the left with diffuse edema and pneumocephalus (arrow) in case with penetrating type of open head injury

information on the extent of brain injury and the presence of retained bone and/or shell fragments (Fig. 10). This information is of utmost importance for decisions on treatment

Imaging analysis in missile head injury should include the following steps: assess missile path; determine the extent and type of wound, bone fragments, and in-driven shell fragments; and follow-up evolution of missile head injury. Intraventricular hemorrhage and ventricular lacerations are the main components of such injuries. Ventricular injury is a poor prognostic factor for penetrating cranial gunshot wounds. Many such patients have major vascular lesions; therefore, CT angiography or conventional angiography, depending on type of trauma and degree of injury, should also be considered

Besenski et al. (1995) studied 154 patients who had suffered open, missile head injury. In 54% of cases CT was performed 1–24 h after injury, and in 27% follow-up CT was obtained showing evolution of hemorrhage, edema, cerebritis, abscess, secondary vascular lesions, necrosis, encephalomalacia, and hydrocephalus. According to their results, the most dynamic changes occurred 7–14 days after injury in patients with open-head injury

## 2.3.6 Closed-Head Injury

### 2.3.6.1 Extra-axial hemorrhage

There are three types of extracerebral hemorrhage: epidural hematoma (EDH); subdural hematoma (SDH); and subarachnoidal hemorrhage (SAH). Intraventricular hemorrhage (IVH) can also be included in this group, considering ventricles as extraaxial, meaning extraparenchymal structures

The EDH is usually arterial in origin and often results from a skull fracture (95%) that disrupts the middle meningeal artery. Air within EDH suggests sinus or mastoid fracture. In 10% of cases EDH are located in posterior fossa with usually venous origin, commonly found in children

Because EDH exists in the potential space between the dura and the inner table of the skull, such hematomas can cross dural attachment but not cranial sutures (Fig. 11; Gean 1994). On CT acute EDH appears as well-defined biconvex hyperdense extra-axial collection. Occasionally within an acute EDH heterogeneous foci appear containing irregular areas of lower attenuation. This finding indicates active extravasation of fresh unclothed blood (swirl sign) and warrants immediate surgical attention (Fig. 12). Acute EDH are isointense or slightly hypointense on T1-weighted images with variable signal intensity on T2-weighted images being commonly hypointense. Subacute/early chronic are hyperintense on T1-weighted images with black line between EDH and brain representing displaced dura. Early subacute EDH are hypointense on T2-weighted images, whereas late subacute/early chronic are hyperintense on T2-weighted images, showing also displaced dura as a black line between brain and EDH

The SDH is usually venous in origin, resulting from the stretching or tearing of cortical veins. Movement of the brain within subdural space causes stretching and tearing of the bridging veins which extend from the cortex to the dural sinuses

Most such hematomas are supratentorial, located along the convexity, frequently seen along the falx and tentorium from the anterior to the posterior falx, typically crescent shaped (Fig. 13). Unlike epidural hematoma, subdural hematoma can cross sutural margins, but not dural attachments

In the acute stage a traumatic SDH shows the same imaging findings on CT (being hyperdense) and on MR as any other acute non-traumatic hemorrhage. Diffuse swelling of the underlying hemisphere is common with SDH with or without midline shift or possible brain herniation. Because of the increase in tissue fluid, edema causes decreased attenuation on CT images with a loss of gray matter/white matter differentiation. The brain stem and cerebellum are usually spared and may appear relatively hyperdense to cerebral hemispheres (white cerebellum sign). Focal areas of edema are frequently associated with cerebral contusions and may contribute significantly to mass effect

On MR in hyperacute phase SDH is isointense or slightly hypointense on T1-weighted images, iso- to hyperintense on T2-weighted images, and is hyperintense to CSF on FLAIR. In acute stage on MR they are iso- to moderately hypointense on T1 and hypointense on T2 (Fig. 14)

During the transition in appearance from acute to chronic SDH, an isodense phase occurs, usually between several days and 3 weeks after the acute event. Such iso-



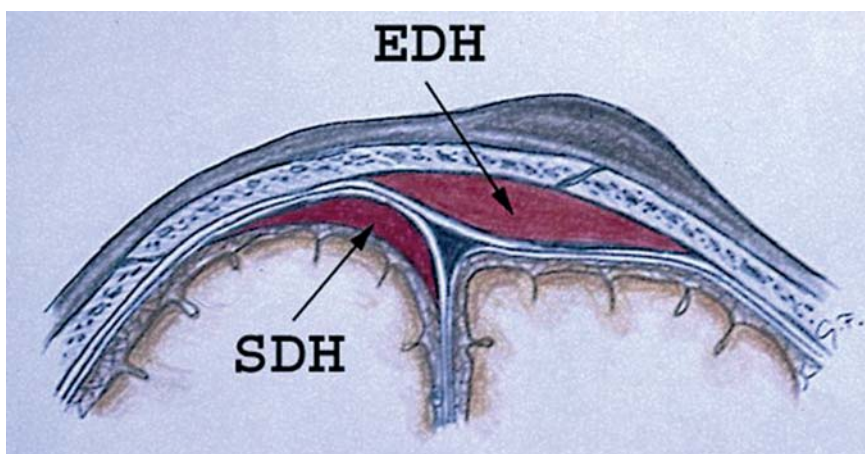


**Fig. 11.** Epidural hematoma (EDH) and subdural hematoma (SDH) relative to the meningeal anatomy. (Adapted from Gean 1994)



**Fig. 12.** Non-contrast axial CT scan demonstrates huge acute left frontal epidural hematoma with mass effect and prominent low-density area (swirl sign) corresponding to active bleeding with unretracted liquid clot (arrow)



**Fig. 13.** An acute right-sided SDH spreading along the right convexity into the interhemispheric fissure with edema of underlying brain parenchyma causing left-sided midline shift. Note also hyperdensity within subarachnoid spaces in the left hemisphere representing acute subarachnoid hemorrhage

dense, subacute SDH can be overlooked on CT scans. Analyzing CT possible pitfalls might appear because SDH might be small, isodense or mixed density on CT; therefore, usage of appropriate window is extremely helpful

One must pay attention to the following: gray-white matter interface is medially displaced, the border between the extra-axial collection and the underlying brain is barely discernible and failure of surface sulci to reach the inner calvarial table is present

In some cases fibrovascular proliferation subdivides the clot and forms neomembranes which may be present in subacute SDH. They enhance because of lack of BBB (Fig. 15) Contrast enhancement can help identify non-acute, isodense, SDH by demonstrating an enhancing cap-

sule or displaced cortical vessels. Hemorrhage resolve through the intervention of macrophagy and production of collagen dura-arachnoids cells forming membrane first on the dural surface. Fragile blood vessels within membrane cause re-hemorrhage. Occasionally re-bleeding occurs during the evolution of a SDH causing a heterogeneous appearance from the mixture of fresh blood and partially liquefied hematoma. A sediment level or "hematocritic effect" or fluid-fluid level may be seen either from rebleeding or in patients with clotting disorders

Fluid-fluid level occur secondary to layering of blood cells. The upper layer will be bright on T1 and T2 and the lower layer will be isointense to brain on T1 and hypointense on T2. The lower portion of the collection is of



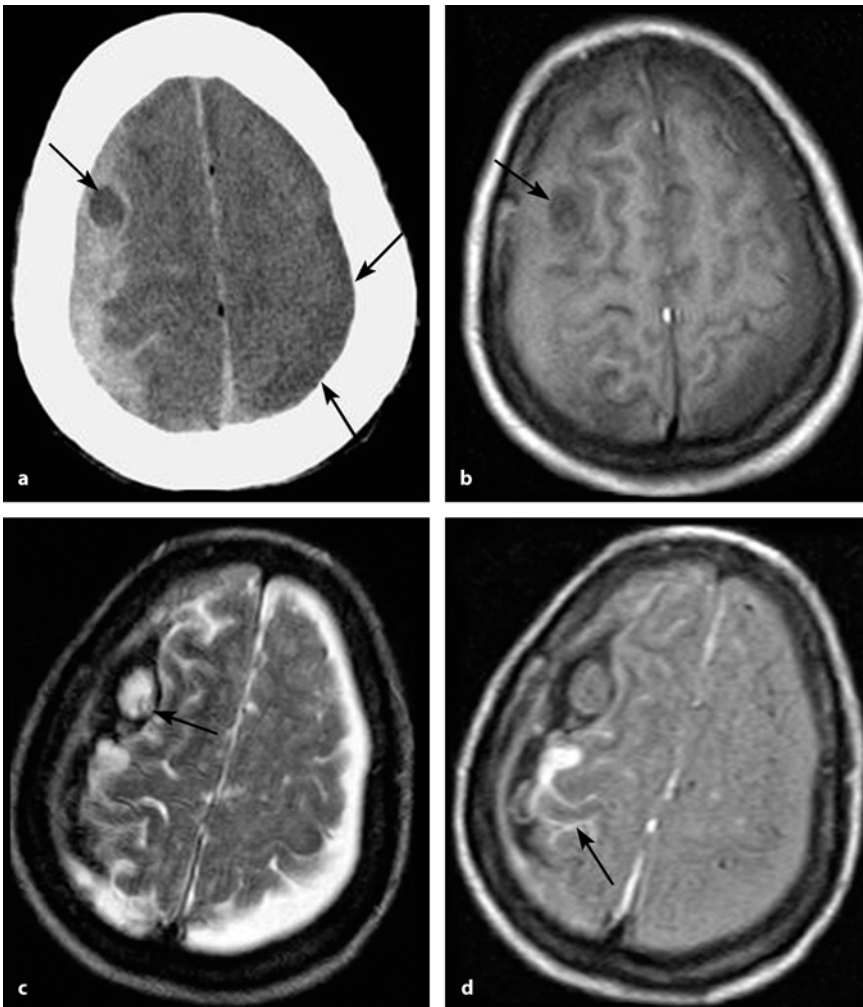


**Fig. 14** Non-contrast CT (a) and T1 (b), T2 (c), and FLAIR (d) in an 83-year-old woman who fell from wheelchair. The CT showed acute SDH on the right with unclotted clot (arrow), evidence of cortical subarachnoidal hemorrhage, and subacute to chronic subdural hematoma on the left (arrows). There is blood within inter-hemispheric fissure. The MRI demonstrated bilateral SDH, chronic on the left and acute on the right. Left is slightly hypointense on T1 and hyperintense on T2 and FLAIR. Heterogenous T2 signal within the right SDH corresponds to an acute hemorrhage with active extravasation on the right (arrow). Acute subarachnoidal hemorrhage is best seen on FLAIR on the right as signal hyperintensity in cortical subarachnoidal spaces (arrow, d)



**Fig. 15.** Postcontrast axial CT demonstrates enhancement of neomembranes in subacute left-sided subdural hematoma (short arrows). Note that sulci and gyri (long arrows) are displaced from the calvarian table to midline with evidence of midline shift to the right

lower density than is the superior portion (Fig. 16). This represents gravitational setting of blood breakdown products in the inferior aspect of the collection. In general SDH evolve in pattern similar to intracerebral hemorrhage

Chronic SDH can not be distinguished from hygroma by CT. Using MR distinction between hygroma and SDH is easy. MR appearance of chronic SDH and hygromas are variable depending on the evolution of hemorrhage like in any other hemorrhage. Chronic SDH has low attenuation values, very similar to CSF on CT. Due to methemoglobin, old SDH are usually hyperintense on T1-weighted images and FLAIR. The GRE T2\*-weighted images are the most sensitive sequences for SDH when it is isointense on other standard sequences

A subdural hygroma is the accumulation of watery (serous) fluid resembling CSF in the subdural space following CSF signal intensities on MR. The SDH hygroma are a consequence of a traumatic tear of the arachnoid which result in the leak of CSF into subarachnoidal space. Hygromas may develop immediately or after a delay following head injury. Most hygromas form above the tentorium,

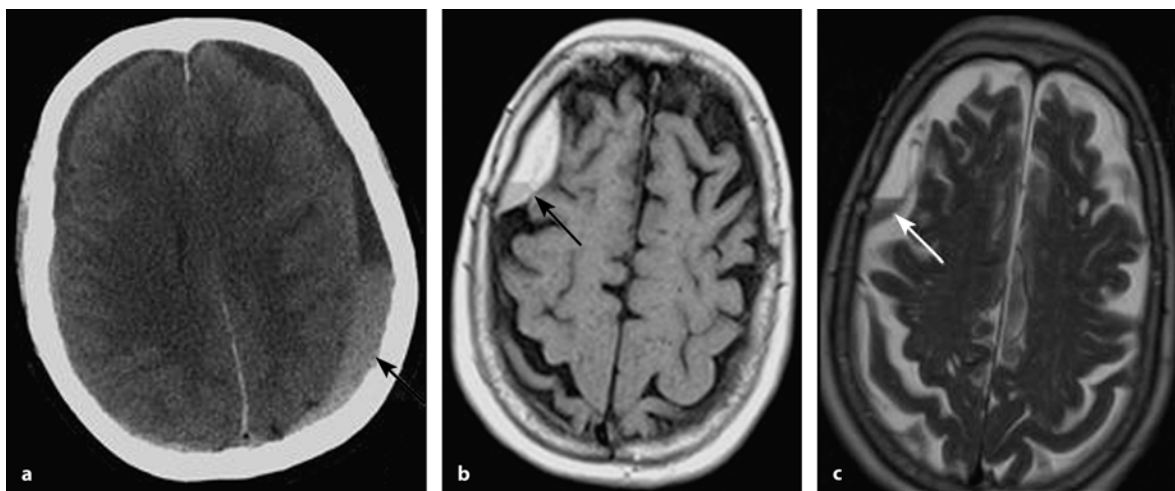


**Fig. 16.** Computed tomography demonstrated bilateral chronic SDH, more prominent on the left with evidence of rebleeding in occipitoparietal region (a). T1 (b) and T2 (c) in different cases showed fluid–fluid level (arrow) secondary to layering of blood cells



**Fig. 17.** Acute diffuse traumatic subarachnoid hemorrhage. Note hyperdensity within interpeduncular cistern (arrow)

unilaterally or bilaterally over the cerebral hemispheres. Traumatic subdural hygromas make up to 13% of surgically treated subdural lesions

On imaging, traumatic SAH and IVH exhibited the same findings as in non-traumatic cases

Traumatic SAH results from disruption of small subarachnoidal vessels or direct extension into the subarachnoidal space by a contusion or hematoma (Fig. 17). Blood is within subarachnoidal spaces within pial and arachnoidal membranes. On CT images there is a high density within sulci and cisterns in setting of trauma

Hyperdensity within interpeduncular cisterns is the most liable indicator of SAH and may be the only manifestation of subtle SAH. The SAH produces dramatic hyperin-

tensity in the normally hypointense CSF on FLAIR. Magnetic resonance has been proven to have sensitivity equal to, or even greater than, CT in subarachnoidal hemorrhage detection. Very young and very old SAH enlarge subarachnoid space. The SAH blood tends to remain in the oxy-hemoglobin state due to the high oxygen tension of CSF causing slow transformation of oxy- to paramagnetic breakdown products such as deoxy or methemoglobin

In the chronic phase decreased signal on T2-weighted images because of hemosiderin deposit in subarachnoid spaces can be recognized easily

During MR examination GRE sequences are highly recommended with the aim of detecting hemosiderin even a few years after the trauma has happened

The IVH results from a rotationally induced tearing of subependymal veins on the surface of ventricles or by direct extension of parenchymal hematoma into the ventricular system. Horizontally sediment blood CSF level in occipital horns is a typical feature for IVH. The SAH and IVH cause hydrocephalus commonly

### 2.3.6.2 Intra-axial Lesions

With cortical contusions, a diffuse axonal injury (DAI, or “shearing” injury) has been identified as the most important cause of significant morbidity in patients with TBI

### 2.3.6.3 Cortical Contusion

Cortical contusions are bruises and laceration of the brain which are covered by dura which occur due to disruption of small capillaries and extravasation of whole blood. In cortical contusions blood is mixed with native tissue opposite to

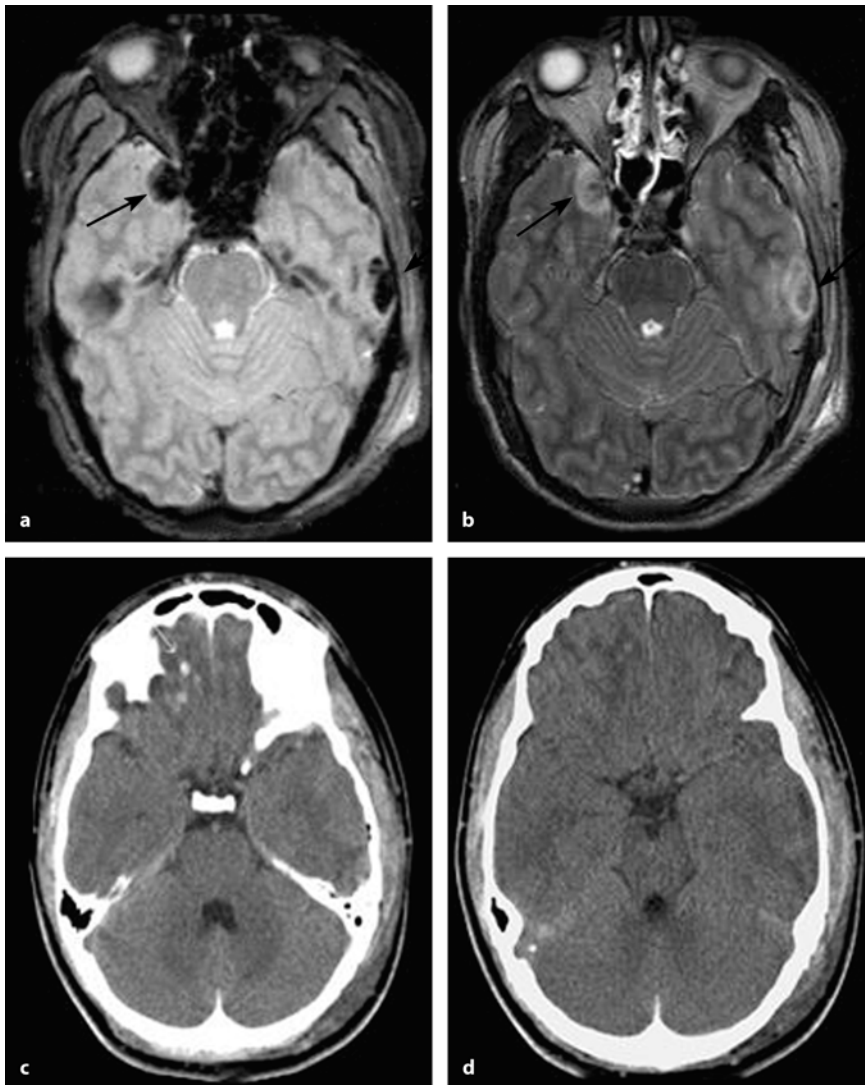


**Fig. 18.** Typical location of cortical contusion seen on GRE T2\* (arrow, **a**) and T2 (arrow, **b**). Acute hemorrhagic contusions surrounded with edema (high signal on T2) in the temporal lobes bilaterally not seen on CT in the temporal region (**c, d**). Very small hemorrhagic foci are seen in basal aspect of the right frontal lobe (**c**)

intraparenchymal hematoma with lack of blood mixture with brain tissue. In the first stage of cortical contusion hemorrhage is associated with necrosis. In the second phase resorption and organization of hemorrhage occur followed by final or defect stage containing CSF. Contusions are wedge-shaped lesions with their base on the cortical surface and their tip pointed toward the center of the brain. Their shape, character, and anatomical distribution are not compatible with vascular distribution, which is characteristic of brain infarction. Their main characteristic is that they are diffuse, often multiple rare solitary, wedge shaped and superficial, present in the cortical or subcortical region

There are some predilections for a certain portion of the brain where contusions occur, e.g., bases of the frontal lobes and the tips, bases, and lateral surfaces of the temporal lobes due to brain gliding upon the uneven (rough) surface of the skull base. Focal contusion may also occur at the

site of depressed skull fracture. Four to 6 months after trauma, this lesion becomes cystic (encephalomalacia) as focal or diffuse atrophy, being hypodense on CT with CSF signal characteristic on MRI

Countercoup contusional lesions are usually a little bit larger than coup lesions. During the first week after a traumatic event lesions are multiple, exhibiting the characteristic CT pattern of mixed areas of hypo- and hyperdensity (salt and pepper) due to hemorrhage with necrosis. Cortical contusions can lead to regional ischemia caused by extensive release of excitotoxic amino acids leading to increased cytotoxic brain edema and raised intracranial pressure. There is experimental evidence that parenchymal damage in the setting of TBI may be related to the loss of calcium and potassium homeostasis, the release of excitotoxic amino acids, free radicals, and tissue acidosis (Braun et al. 2000; Hoelper et al. 2000)

Cortical contusions are underestimated by CT and are best depicted by MRI. On MRI they show inhomogeneous signal due to admixture of edema and hemorrhage on T1-weighted images in acute phase, being hyperintense on FLAIR (Fig. 18). On T2-weighted images they are bright because of edema with hypointense hemorrhagic foci on GRE. Those foci are usually not seen on other sequences

### 2.3.7 Imaging of Diffuse Axonal Injury (Shearing Injury)

Imaging of diffuse axonal injury (DAI) is one of the most common types of primary neuronal injury in a patient with severe head trauma. It is stressed that DAI rarely occurs in isolation. It has been estimated that severe DAI not accompanied by an intracranial mass lesion occurs in al-

most 50% of patients with severe head injury and causes 35% of all deaths. Diffuse axonal injury is the most common cause of persistent vegetative state and severe disability in TBI (Meythaler et al. 2001; Graham et al. 2002; Parizel et al. 1998). At the moment of impact loss of consciousness is typical. Tissue damage can be extensive with involvement of multiple brain areas and multiple functional systems, and can result in profound neurological deficit

The DAI is characterized by a widespread disruption of axons that occurs at the time of an acceleration or deceleration injury. Histologically, DAI is a widespread disruption of axons in brain stem, parasagittal white matter of the cerebral cortex, and corpus callosum which occurs during abrupt acceleration or deceleration and is consistent in terms of the features of TBI

At present, DAI lesions tend to be small, only a few millimeters in diameter, and multiple (15–20) lesions can be found in severely injured patients. This type of lesion oc-

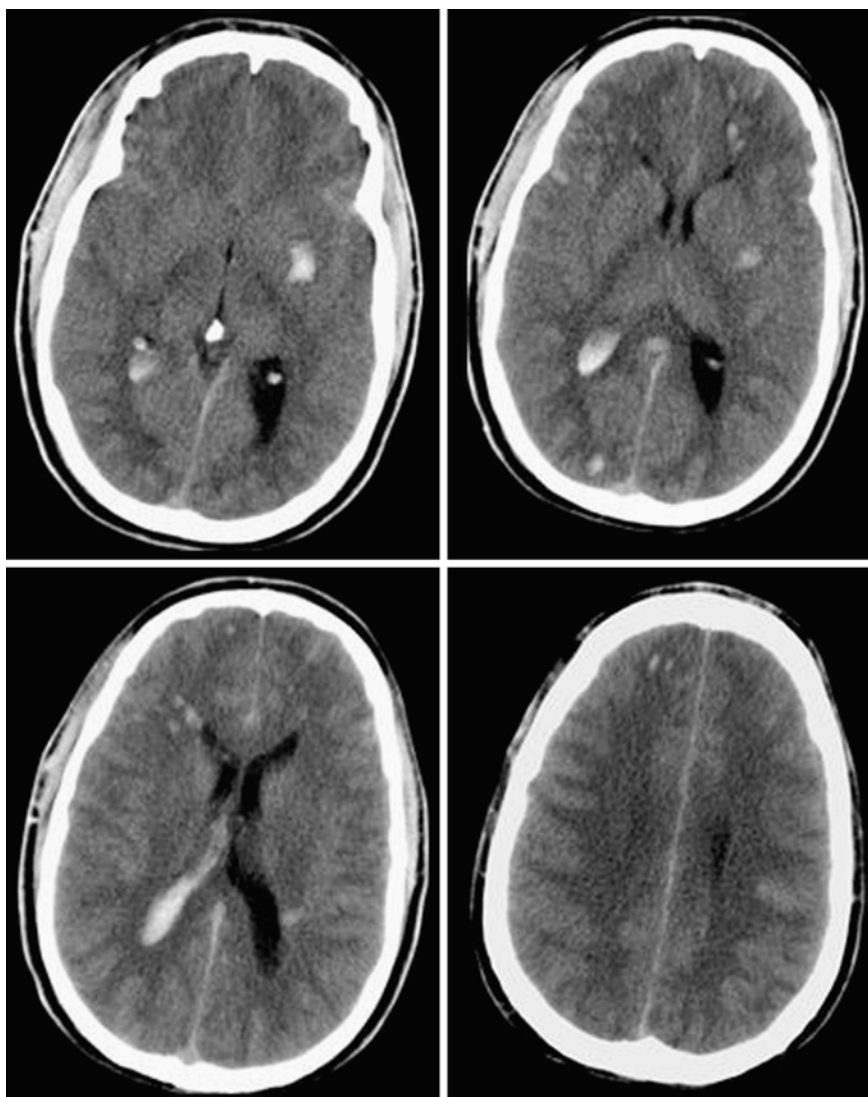


**Fig. 19.** The DAI with typical appearance of multiple hemorrhagic lesion in typical location



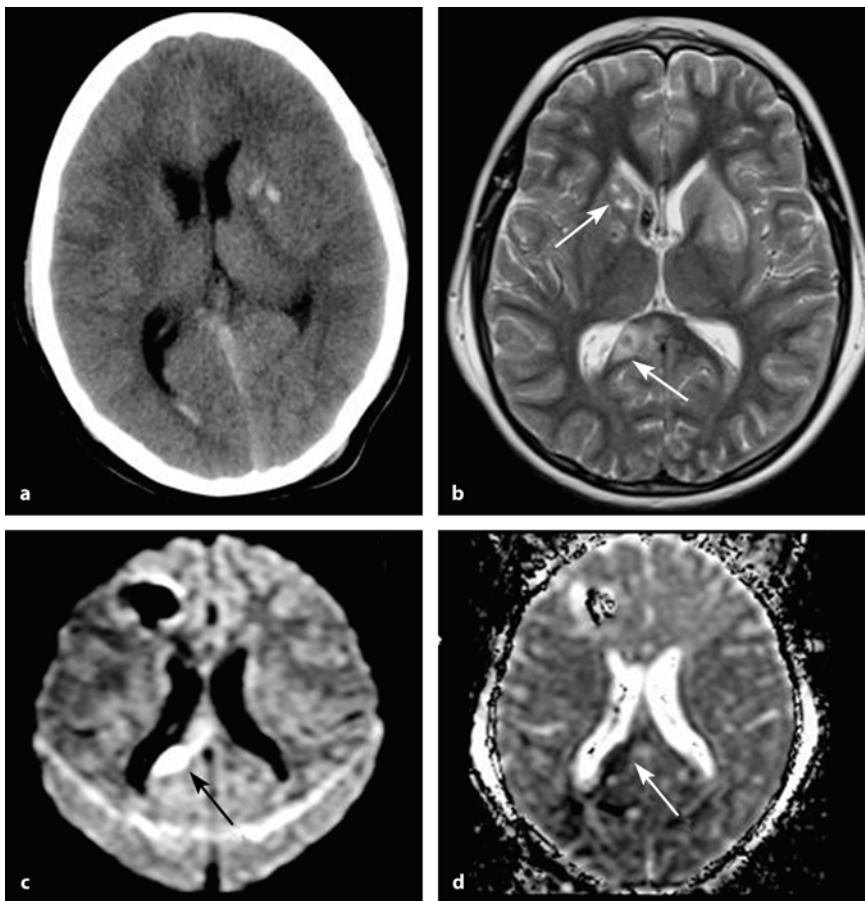


**Fig. 20.** Computed tomography (a) demonstrates left basal ganglia lesion with intraventricular hemorrhage in patient who suffered DAI. Two days later, T2 (b) shows high signal in the left basal ganglia with additional lesions seen in splenium and cauda nuclei on the right (arrows). The DWI (c) and ADC (d; scan obtained above the basal ganglia) demonstrate signal abnormality in splenium on the right involving the callosal body (arrow). Signal abnormality on DWI and ADC frontal on the right correspond to changes related to catheter placement seen on other slices and sequences

occurs in a specific location of the traumatic brain (Parizel et al. 1998; Kostas Paterakis et al. 2000; Gentry 1994; Gentry et al. 1998). This peculiar pattern of lesions, caused mostly by a centroaxial traumatic force, is located within the corpus callosum complex (septum pellucidum, fornix, tela choroidea), gray matter/white matter junction (different density and elasticity between the two) in parasagittal subcortical areas, and deep periventricular white matter (not superficial), especially in the frontal area at the corner of ventricles, basal ganglia, internal capsule, hippocampal and parahippocampal region, brain stem, and cerebellum (Figs. 19, 20); therefore, these areas should be examined very thoroughly, seeking for a minimal lesion

Regarding the location of DAI, three different stages have been established (Gentry 1994). Magnetic resonance is much more sensitive than CT in its detection, especially in non-hemorrhagic lesions (Parizel et al. 1998; Kostas Paterakis et al. 2000; Gentry 1994; Gentry et al. 1998). Sometimes hypodensities on CT can be caused by artifacts (common on basal CT scans due to bones of skull base) and do not correspond to non-hemorrhagic lesions seen in DAI. As corpus callosum is commonly involved in DAI asymmetry of portions of the CC, relative narrowing and irregularity of the inner ventricular contours helps to

determine if the lucencies seen in the CC correspond to edema and necrosis of the CC, or if they are artifacts on CT (Besenski et al. 1992)

The MR appearance of DAI depends on several factors, including the time since injury, the presence of hemorrhage or blood break-down products, and the type of sequences used (Gentry 1991, 1994; Gillgini et al. 2005). The DAI is frequently associated with tissue-tear hemorrhage. The GRE sequences during MRI permit the identification of most blood products such as oxyhemoglobin, methemoglobin, and hemosiderin, which are all paramagnetic substances in the white matter. It is known that gradient T2\* are more sensitive than T2-weighted spin-echo images for detection of hemorrhage. As an alternative to GRE to assess brain DAI in severe TBI patients, especially if uncooperative and medically unstable, turbo proton echoplanar spectroscopic imaging sequences (t-PEPSI) can be used due to its very short scan time and high sensitivity to the hemorrhage foci (Gillgini et al. 2005)

The DIA is considered to be caused by excitotoxic mechanism, particularly those involving glutamate and N-methyl-D-aspartate (NMDA) receptor. Due to traumatic defect in the axonal membrane, the leakage of glutamate occurs into the extracellular space causing axonal swelling



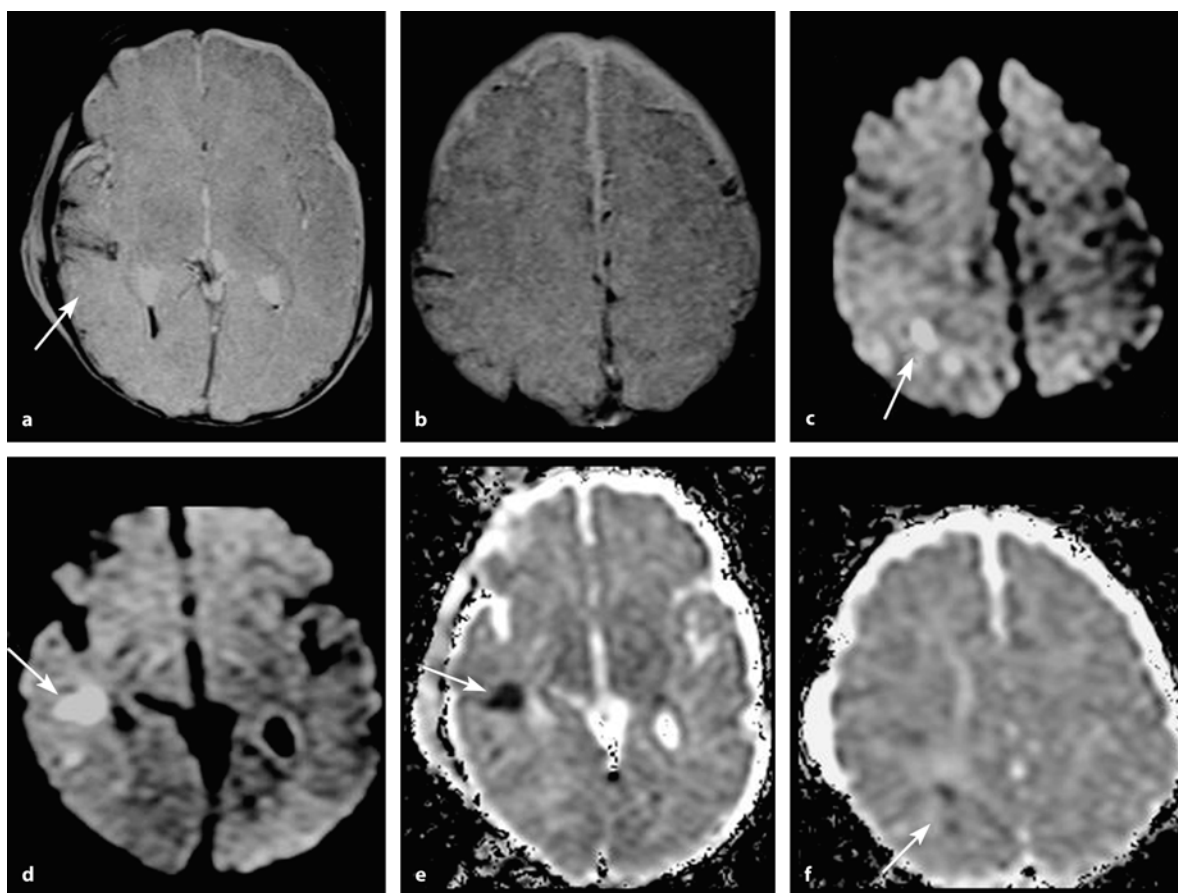


**Fig. 21.** Child at the age of 5 months. Computed tomography was completely normal (not shown). Magnetic resonance was performed 4 days later. All standard MR sequences demonstrated no signal abnormality. The GRE T2\* showed possible small hy-

pointense signal in the right peritrigonal area (*arrow, a*). Subcortical area was normal also on GRE T2\* (*b*). The DWI (*c, d*) and ADC (*e, f*) demonstrated multiple abnormalities in the right peritrigonal area and right subcortical region (*arrows*)

and cytotoxic edema of glial cells, which may contribute to diffusion abnormalities resulting in necrosis, axonal degeneration, and gliosis. Excessive extracellular glutamate leads to axonal swelling and cytotoxic edema of glial cells, which may contribute to diffusion abnormalities resulting in necrosis, axonal degeneration, and gliosis (Moritani et al. 2005)

The new MR imaging technique, DWI, including diffusion tensor imaging (DTI), can provide information about brain ultrastructure by quantifying isotropic and anisotropic water diffusion. Furthermore, DWI/ADC maps can differentiate between lesion with increased vs decreased diffusion

The DWI shows restricted diffusion (usually seen in ischemia) as increased, high signal intensity on DWI sequences and hypointense signal intensity on ADC map. Increased diffusion exhibits high signal on both, DWI and ADC map

The DWI is valuable in closed-head injury because it identifies additional shearing injuries not visible on T2,

FLAIR, or GRE T2\* sequences (Fig. 21). The DWI depicted the largest number of lesions (365 of 488, or 75%), followed by FLAIR (61%), T2-weighted fast spin echo (50%), and T2\*-weighted GRE (43%; Schaefer et al. 2004). The majority of the lesions identified on DWI showed decreased diffusion on the corresponding ADC maps. Lesions with increased ADC results in an increased amount of extracellular water (vasogenic edema)

It is still uncertain whether persistently decreased ADC represents ongoing ischemic changes, cytotoxic edema, or demyelination, or whether it is more indicative of the underlying intrinsic process of TBI. This is in contrast to the decline in ADC values seen with acute ischemia, which tends to persist for the first week and then normalize and ultimately rise

Experimental studies by Hanstock et al. (1994) showed that these lesions occur when the trauma does not reduce blood flow enough to induce ischemia. The second possible mechanism for diffusion restriction in DAI might be acute hemorrhage often present in DAI. Small areas of hemor-

rhage may significantly impede water mobility, because of high viscosity, and concentrated intact blood cells and the formation of a fibrin clot cause decrease in ADC; or thirdly, cytotoxic edema may be present similar to a non-hemorrhagic stroke. Decreased ADC can be demonstrated in patients with DAI in the acute setting and may persist into the subacute period, beyond that described for cytotoxic edema in ischemia suggesting alternative mechanisms at work in DAI (Amon et al. 1999)

Histological abnormalities seen in DAI decrease the diffusion along axons and increase the diffusion in directions perpendicular to them. Those changes in diffusion can be evaluated by DTI. In DAI misalignment of the axonal membranes may increase restriction in diffusion parallel to the main axis of the neurons. Misalignment of the axonal membranes in DAI could be responsible for reduction of anisotropy. The second phase of DAI includes an impairment of axoplasmic transport and local accumulation of organelles causing local swelling and expansion of the axonal cylinder. This change in shape may also increase restriction in the diffusion along the main axis of the fibers and decrease local diffusion anisotropy. Following lobulation disconnection may occur that might lead to the death of the distal and proximal segments of the neuron (Arfanakis et al. 2002). The DAI might be detected in patients with mild traumatic brain injury through a reduction of the diffusion anisotropy using DTI. This could have significant implications not only for the diagnosis but also for the treatment of these patients. Arfanakis et al. (2002) found reduced anisotropy in white matter 24 h after trauma in five patients with mild TBI using DTI; therefore, they concluded that DTI may be a powerful technique for in vivo detection of DAI

The DTI may be a valuable biomarker for the severity of tissue injury and predictor of outcome. Volume of lesions on diffusion-weighted MR images provides the strongest correlation with a score of subacute on modified Rankin scale at discharge. Total lesion number also correlates well with modified Rankin score. The DTI reveals changes in the white matter that are correlated with both acute GCS and Rankin scores at discharge (Huisman et al. 2004; Huisman et al. 2003)

The DAI is not in the category of surgery, but if not recognized and treated adequately, prognosis is poor with long-term disability; therefore, small lesions seen in DAI need to be recognized because an early and correct diagnosis with early treatment improve outcome in patients with TBI

### 2.3.7.1 Brain-stem Injury

In 30 patients with moderate and severe TBI brain-stem injuries were detected in 26.6% of the patients (Aguas et al. 2005). Many of those patients with brain-stem injury die very soon after the accident

Lesions of the brain stem can be primary or secondary. Histologically primary lesions can be divided into three

categories: hemorrhage; necrosis; and lesions of axons including swelling, or fragmentation, with a formation of retraction bulbs

Primary brain-stem injury occurs due to downward shift at moment of impact, mostly rotational forces representing contusion and/or shearing injury being manifested on imaging as contusions or DAI. A primary brain-stem lesion after a closed-head trauma due to contusional coup injury against the tentorial edge was initially demonstrated by Lindenberg (1964). Brain-stem contusions are usually caused by tentorial coup injury caused as many other contusions, mostly in latero-lateral direction, act with traumatic force when soft brain tissue collides with firm tentorial edge. Those changes are located at the brain-stem surface at the level of tentorial incisura. A midbrain contusion due to tentorial coup injury must be particularly differentiated from DAI, the most common form of primary brain-stem injury, which occur in cases with centroaxial traumatic force direction. The DAI usually affects the rostral dorsolateral aspect of the midbrain and upper pons. Commonly, lesions are seen in the periaqueductal region in comparison with a secondary lesion which usually appears in the ventral part of the brain stem (Fig. 22). The DAI of brain-stem lesions do not occur in isolation, but rather in association with DAI which usually involves the corpus callosum, cerebral hemispheres, and cerebellum, in addition to brain stem

Secondary brain-stem injury is a consequence of downward displacement due to increased ICP and edema; it includes infarction, hemorrhages, or compression of the brain stems as a result of the adjacent or systemic pathology. A secondary brain-stem lesion that occurs as a result of downward herniation or hypoxia-ischemia usually involves the ventral or ventrolateral aspect of the brain stem in contrast to a primary DAI brain-stem lesions which are most common in the dorsolateral aspect of the brain stem. The brain-stem infarction is another often secondary brain-stem lesion which accompanies transtentorial herniations as a result of damage to the medial pontine branches of the basilar artery. In some cases, such as secondary lesion Duret hemorrhages, a characteristic secondary midline hematoma in the tegmentum of the rostral pons occurs due to transtentorial herniation. It is believed to result from the stretching or tearing of penetrating arteries as the brain stem is caudally displaced

During CT or MR examination special attention should be paid to an analysis of the brain stem, especially in differentiation between primary and secondary lesions

On imaging a primary brain-stem lesion after a closed-head trauma can be differentiated as contusion or DAI. Brain-stem injury can be recognized based on both, direct and indirect signs on imaging. Direct signs include hematoma and edema. Indirect signs are compression of the basal cisterns (complete or incomplete), hemorrhage, and compression of the fourth ventricle and transtentorial herniation

According to Hashimoto et al. (1993), only 8.8% of brain stem injuries can be detected by CT. Firsching detected



**Fig. 22.** A huge acute periaqueductal hematoma on the right associated with subarachnoid hemorrhage, frontal SDH, and pneumocephalus (arrow)

brain-stem lesions in 64% of patients who suffered severe brain injury by MR (Firsching et al. 1998). Sometimes brain-stem lesions are difficult to detect on cranial CT scanning because of bone artifacts within the lower portions of the posterior fossa. Magnetic resonance is absolutely the method of choice in brain-stem injury analyses and is also valuable in predicting the outcome (Hashimoto et al. 1993; Firsching et al. 1998; Shibita et al. 2000)

### 2.3.8 Early Secondary Lesions in Brain Injury

The secondary effects of a craniocerebral trauma are sometimes of greater importance than direct manifestations such as focal hematoma, contusion, or DAI

Early secondary alterations represent diffuse cerebral edema, hypoxia, infarction, necrosis, secondary hemorrhage, and cerebral herniation. Most secondary injuries are caused by an increased intracranial pressure or cerebral herniations. They occur in the early posttraumatic period

Using CT and MR all early secondary lesions can be easily distinguished from the late sequelae which are the final result of brain injury. The late sequelae include hydrocephalus, pneumocephalus, CSF leak, and encephalomalacia. From the group of early secondary lesions we describe only chosen topics that might be a threat to the patient's life

#### 2.3.8.1 Diffuse Cerebral Edema

Diffuse brain swelling is a common manifestation of head trauma. It may occur either because of an increase of cerebral blood volume or an increase of tissue fluid content.

Hyperemia refers to an increase of blood volume, whereas edema refers to an increase in tissue fluid; both lead to generalized mass effect with effacement of sulci, suprasellar and quadrigeminal plate cistern, and compression of the ventricular system. Homogeneous attenuation of brain parenchyma is present on CT scans with a loss of gray matter/white matter interface (Fig. 23). Cerebellum may appear relatively hyperdense in comparison with hypodense edematous cerebral hemispheres (white cerebellum sign). Diffuse cerebral edema is developed in 10–20% of severe TBI within 24–48 h after impact. Basically, two types of edema can be present in TBI, vasogenic and cytotoxic. Vasogenic edema follows an increase in permeability of blood–brain barrier (BBB) and an accumulation of plasma protein-rich fluid within extracellular space. It is usually most obvious in white matter. Cytotoxic edema, also called cellular edema, is caused by parenchymal cell dysfunction. There is a swelling of parenchymal cells without BBB disruption, and is most apparent in gray matter. Cytotoxic edema is associated with a decrease of extracellular fluid volume. Using DWI these two types of edema can be distinguished very easily (Fig. 24)

In the study by Barzo et al. (1997), the reduction in ADC extending out of several weeks as seen in their experimental trauma animal model are postulated to result from neurotoxic edema. Increased interstitial water associated with vasogenic edema results in increased diffusion, as opposed to cytotoxic edema which is associated with increased intracellular water and restricted (decreased diffusion) as typically seen in acute infarction

Increased diffusion in vasogenic edema appears to be bright, hyperintense signal abnormality on both DWI and ADC map. Changes with decreased, restricted diffusion (cytotoxic edema, bright on DWI, hypointense on ADC map) is believed to be irreversible, whereas changes with increased diffusion (vasogenic edema) are thought to be reversible. The ability to discriminate between these two types of edema and therefore be able to predict whether or not a lesion will progress is of great therapeutic and prognostic importance; therefore, in the future, DWI may be useful in determining treatment strategies for acute head injury

In cases of severe, diffuse cerebral edema “pseudo-subarachnoid hemorrhage” is seen when the brain becomes very low in attenuation and dura and circulating blood in the cranial vasculature appears unusually hyperdense on CT. Cerebral swelling from hyperemia is most commonly seen in children and adolescents due to loss of normal cerebral autoregulation. The main problem of closed-head injury is brain swelling as a result of all perifocal tissue damages. In children a brain swelling starts developing as early as 20–30 min after a head injury and advances very fast; therefore, the observation of consciousness in children is necessary, even in cases with a mild head injury (Zimmeman et al. 1978; Ross and Ross 1989)

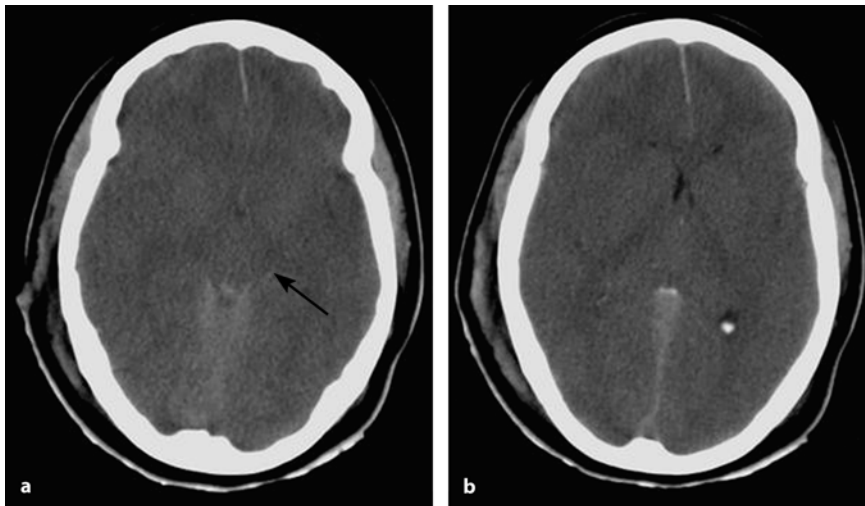


**Fig. 23.** Prominent diffuse edema seen on CT. Perimesencephalic cisterns are compressed (*arrow, a*). Gray matter/white matter differentiation is decreased, sulci and gyri are effaced. Ventricles are split (*b*)

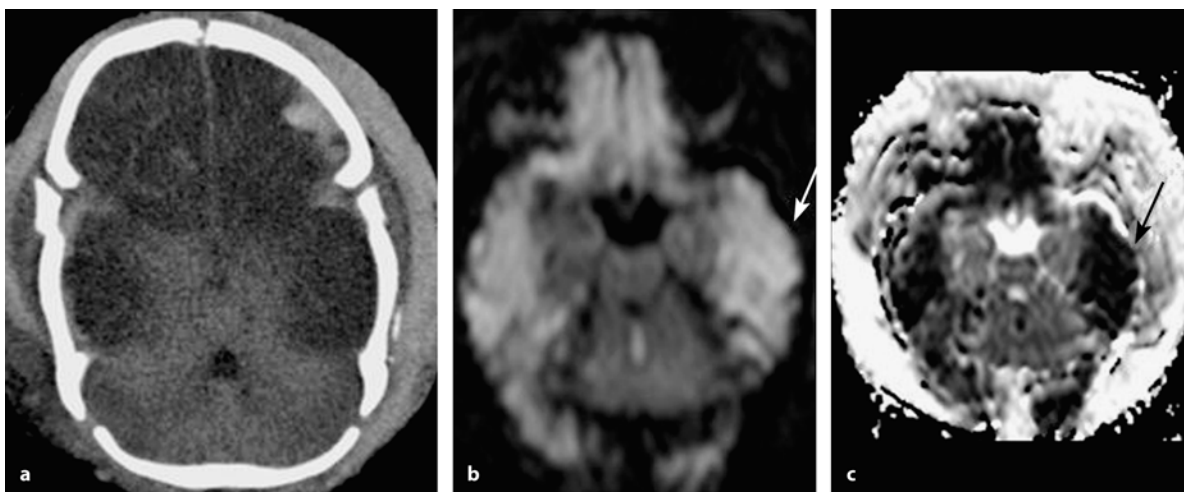


**Fig. 24.** Computed tomography in a baby at 5 months of age demonstrated “white cerebellum sign” due to diffuse edema of cerebral hemispheres. Three days later, corresponding area of the

brain showed hyperintense signal on DWI (*arrow, b*) being hypointense on ADC (*arrow, c*) performed 3 days later representing restricted diffusion (most likely cytotoxic edema)

### 2.3.8.2 Secondary Intraparenchymal Hemorrhage

Secondary ICH can also appear later secondary to delayed hemorrhage, which is another cause of clinical deterioration during the first several days after head trauma. As the hematoma matures and clot retraction occurs, it becomes surrounded by a hypodense rim of edema. Intracerebral hematomas have less expressed perifocal edema than cortical contusions, because they represent the bleeding into the normal parenchyma. The secondary parenchymal hemorrhage can occur anywhere within the brain but tend to be in deeper parts of the brain

### 2.3.8.3 Brain Herniation

Cerebral herniations are caused by a mechanical displacement of the brain, cerebrospinal fluid, and blood vessels from one cranial compartment to another. Using CT or MR different types of brain herniation can be recognized, as follows: subfalcine; transtentorial (descending and rarely ascending due to upward herniation of the cerebellum); transphenoidal (transalar descending and ascending); tonsillar (cerebellar tonsils are forced through the foramen magnum); and external herniation of the brain through bone defect. All types of herniation are signs of a serious cerebral injury accompanied by displacement of blood vessels and nerves. The most common type of herniation in trauma pa-



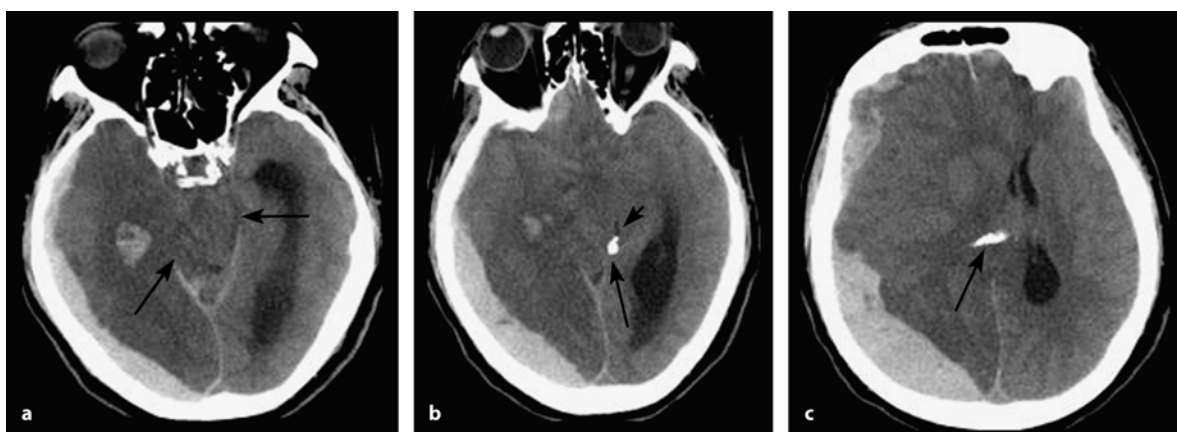


**Fig. 25.** Typical transtentorial herniation associated with subfalcine herniation and midline shift to the left seen on noncontrast CT. Huge acute SDH on the right associated with hippocampal hematoma causing dilatation of the contralateral temporal horn and perimesencephalic cistern compression (arrows, **a**). Down-

ward displacement of the calcified pineal gland (long arrow) and posterior part of the third ventricles (short arrow, **b**). Normal calcified but displaced right chorioid plexus due to midline shift (arrow, **c**). Subfalcine herniation

tients are subfalcine, transtentorial, and uncal. External herniation in postoperative period is also not uncommon

In cases involving subfalcine herniation, the cingulate gyres is displaced across the midline under the falx and anterior cerebral artery is displaced resulting in secondary ischemia and infarction. Subfalcine herniations occur in cases with EDH, SDH, or any other hemispheric mass lesion. On imaging mass lesion bowing of falx with compression of ipsilateral ventricle is seen. The contralateral ventricle is enlarged due to obstruction of the foramen of Monro. Anterior cerebral artery infarction can occur. Subfalcine herniation can be associated often with descending transtentorial herniation

A downward displacement of the temporal lobes and brain stem through tentorial incisura is termed descendent transtentorial herniation. Descending transtentorial herniation is a very serious consequence of brain injury. On imaging it can be recognized by a dilatation of the contralateral ventricular system, especially contralateral temporal horn, compression of the basal cisterns, downward shift of pineal calcification, and midline shift of the brain parenchyma (Fig. 25). Posterior cerebral artery compression with occipital lobe infarction and Duret hemorrhage can also be seen. The mortality rate in such cases is very high

Ascending transtentorial herniation may appear due to superior displacement of the vermis in cases with huge posterior fossa mass. Features of ascending transtentorial herniation are obliterated fourth ventricle and effacement of superior cerebellar and quadrigeminal cisterns. Compression of aqueduct causes hydrocephalus, where compromise of superior cerebellar artery results in cerebellar infarction

In transalar herniation the brain is displaced across the sphenoid wing. Uncal herniation is medial temporal lobe herniation through tentorial notch due to temporal mass (focal hematoma)

Features of uncal herniations on imaging are shift of mesencephalon, widening of ipsilateral cerebellopontine angle cistern, obliteration of the suprasellar cistern, aqueductal compression, PCA compression with infarction, hydrocephalus, and descending transtentorial herniation

Tonsillar herniation can be demonstrated by inferior displacement of the cerebellar tonsils through foramen magnum due to posterior fossa or supratentorial mass. Cisterna magna obliteration with associated PCA infarction and hydrocephalus are common features

In external herniation brain tissue extrudes externally through a skull defect (surgical or traumatic defect) due to increased ICP. This extracranial displacement of the brain tissue with swelling of the adjacent brain at the margin of the defect can be seen easily on imaging. Sometimes pressure necrosis with possible venous compression and venous infarction are also present

### 2.3.9 Late Sequelae of Trauma

Late sequelae of trauma can also be detected by imaging. They are mostly hydrocephalus, pneumocephalus, ischemia/infarction, cerebrospinal fluid leak, leptomenigeal cyst, encephalomalacia, and atrophy

Focal encephalomalacia consists of tissue loss with surrounding gliosis and is a frequent manifestation of remote head injury. The appearance of encephalomalacia is not specific for posttraumatic injury, but its locations are characteristic: the anteroinferior part of frontal and temporal lobes (predilections for cortical contusions). All of late sequelae have known features on imaging associated with many other brain pathological conditions

### 2.3.9.1 Shaken-Baby Syndrome

Shaking-baby syndrome (SBS) is characterized with association of intracranial injury (SDH, EDH, SAH, parenchymal lesions), retinal hemorrhages, and metaphyseal long-bone fractures. Ophthalmological examination is a poor screening method for occult head injury and one should proceed to CT or MR in abused children. Many children with acute inflicted head injury have evidence of old injury when they are diagnosed. Using MR distinction between old and new injury can be very easy and reliable. Imaging plays a major role in establishing the diagnosis of SBS. The SBS is the most common cause of death in the age group <1 year of life. By clinical examination one cannot differentiate with certainty between accidental and inflicted injury, especially in the absence of external signs of violence

During shaking rotational forces occur causing to turn brain on its central axis or at the attachment to the brain stem. Cervical hyperextension causes stretch injury to the neuroaxis. Relatively large head and puny neck muscle render the infant particularly vulnerable to whiplash injury (Blumenthal). With violent shaking the initial brain injury is caused by hypoxia. The initial cause of the hypoxia is res-

piratory difficulty. Apnea and breathing problems have been commonly observed in infants who have been shaken. Necropsies on such infants reveal brain-stem damage. This damage is unique to infancy when there is a big head with poor neck muscle. Movement of the brain causes also stretching and tearing of the bridging veins resulting in SDH, the appearance of which is very typical and most common for SBS. Those bridging veins are very vulnerable in young babies. The SDH of varying age, or located in the interhemispheric fissure, are highly suggestive of shaking injury. Since skull base in infants is smooth and the white matter is unmyelinated and very soft, contusions and skull fractures are seldom present (Blumenthal 2002)

Non-contrast CT needs to be the initial investigation of choice to detect acute SDH or any other hemorrhage. Ideally, CT would be complemented by MR 2–3 days later, because MR is better at delineating the intraparenchymal damage, especially the non-hemorrhagic form, and can easily distinguish different ages of hematomas in cases of repetitious injury which is not uncommon. Especially DWI is the most sensitive technique in not only cerebral ischemia detection but in age determination of ischemia associated with shaking injury. The time-dependent signal intensity changes on DWI during MRI may be of great im-

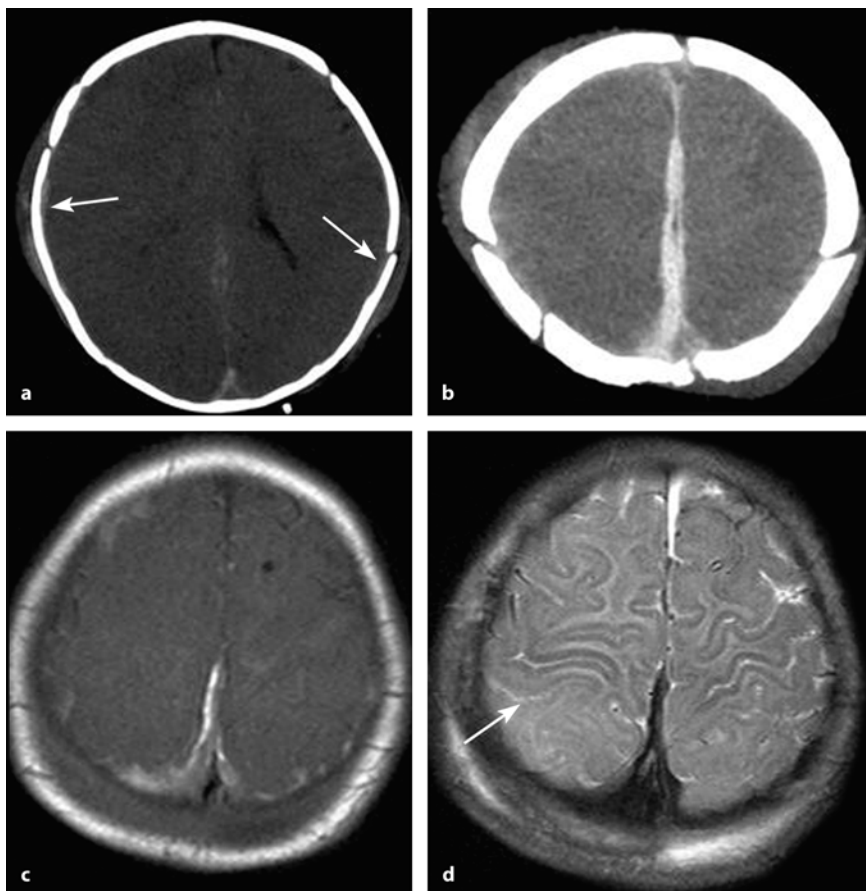


**Fig. 26.** An 8-month-old abused child with evidence of global hypoxia on MR. A CT exam shows bilateral parietal fractures, bilateral SDH (arrows) associated with diffuse edema (a). The SDH is spreading into interhemispheric fissure. b T1 showed iso- to hyperintense signal corresponding to acute SDH (c). T2 showed additional hyperdensity in the cortex dominantly in the region of the right Rolandic sulcus (arrow, d)

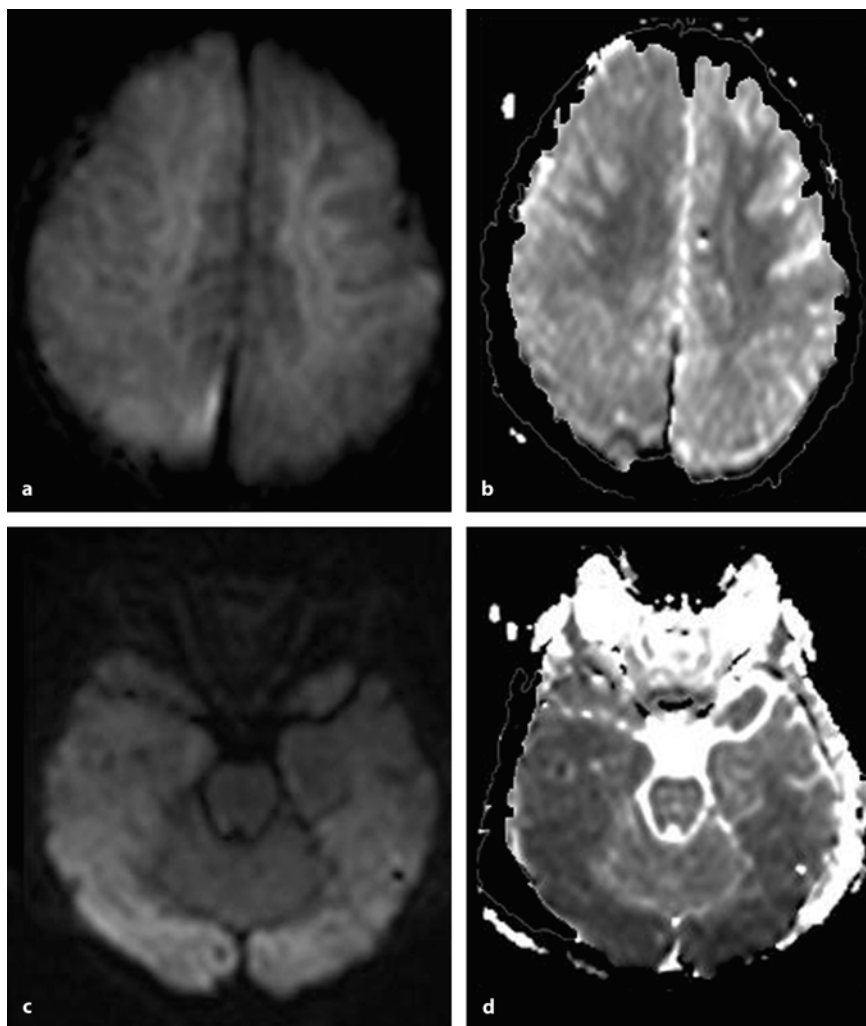


**Fig. 27.** The same case as shown in Fig. 26. The DWI showed diffuse cortical hyperintense signal dominantly in the convexity (a) and occipitoparietal area (c). The ADC was hypointense in the corresponding area (b, d), representing global hypoxia

portance in forensic medicine. The DWI can detect acute ischemic changes in the cortex which is involved in SHS as decreased diffusion indicating cytotoxic edema. Parenchymal damage in SBS is predominantly due to diffuse hypoxic/ischemic encephalopathy and not to diffuse axonal injury (Figs. 26, 27; Parizel et al. 2003). This findings are in concordance with histopathological studies confirming that global severe hypoxic damage is far the most common histological findings in inflicted head injury in children, and DAI is less common. On the contrary, DAI is very common in adult brain injury. The possible explanation for that is the somewhat different biomechanisms of injury in adults, in comparison with infants, keeping in mind the disproportion of the head and neck in infants

### 2.3.10 Conclusion

Computed tomography scanning is the current first imaging technique to be used after head injury. Using CT scalp, bone, extra-axial hematomas, and parenchymal injury can be demonstrated. Computed tomography is rapid and easily performed, also in monitored patients. It is the most relevant imaging procedure for surgical lesions

Magnetic resonance imaging is more sensitive for all posttraumatic lesions, except skull fractures, but scanning time is longer, and the problem with the monitoring of patients outside the MRI field is present. If CT does not demonstrate pathology adequately, MRI is warranted. Follow-up is done best with MRI, as it is more sensitive to parenchymal changes. Using imaging, primary from secondary lesions can be distinguished, which is extremely important for patient management

To interpret the imaging findings in brain injury properly, the biomechanics of brain injury need to be known. The knowledge of the mechanism of the closed acceleration/deceleration type of brain injury is very important and can help in detecting even minimal traumatic brain lesions, especially on CT. Lesions in different sites on CT and MR scans due to the known biomechanism of the closed acceleration/deceleration brain injury should be interpreted dynamically and not separately, with special attention given to minimal brain lesions. Minimal brain lesions may complete the mosaic for a reconstruction of biomechanical condition in each case, which may be important from both clinical and forensic standpoints

Finally, CT still remains the first-line examination to detect immediately life-threatening lesions. Magnetic resonance imaging is the examination of choice for full assessment of brain lesions

## References

- Agha A, Rogers B, Mylotte D, et al (2004) Neuroendocrine dysfunction in the acute phase of traumatic brain injury. *Clin Endocrinol (Oxf)* 60(5):584–91
- Aguas J, Begue R, Diez J (2005) Brainstem injury diagnosed by MRI. An epidemiologic and prognostic reappraisal. *Neurocirugia (Astur)* 1:14–20
- Amon Y, Liu, Maldjian JA, Bagley L, et al (1999) Traumatic brain injury. Diffusion-weighted MR Imaging findings. *Am J Neuroradiol* 20:1636–41
- Arfanakis K, Haughton VM, Carew JD, et al (2002) Diffusion tensor MR imaging in diffuse axonal injury. *Am J Neuroradiol* 5:794–802
- Barzo P, Marmarou A, Fatorous P, et al (1997) Contribution of vasogenic edema and cellular edema to traumatic brain swelling measured by diffusion-weighted imaging. *J Neurosurg* 87: 900–7
- Berg J (2004) Economic evidence in traumas: a review. *Eur J Health Econom* 5 (Suppl 1) 84–91
- Besenski N (2002) Traumatic injuries: imaging of head injuries. *Eur Radiol* 6:1237–52
- Besenski N, Jadro-Santel D (1992) CT detection of minimal brain lesions in closed cerebral trauma. *Neurol Croat* 41:33–42
- Besenski N, Jadro-Santel D, Grcevic N (1992) Patterns of lesions of corpus colosum in inner cerebral trauma visualized by computed tomography. *Neuroradiology* 34:126–30
- Besenski N, Jadro-Santel D, Jelavic-Kojoc F, et al (1995) CT analysis of missile head injury. *Neuroradiology* 37:207–11
- Besenski N, Broz R, Jadro-Santel D, et al (1996) The course of traumatizing force in acceleration head injury: CT evidence. *Neuroradiology* 38:36–41
- Blumenthal I (2002) Shaken baby syndrome. *Postgrad Med J* 78: 732–5
- Braun M, Cordoliani YS, Dosch JC (2000) Head and brain injuries. Place of imaging. *Ann Fr Anesth Reanim* 4:296–8
- Cihangiroglu M, Ramsey RG, Dohrmann GJ (2002) Brain injury: analysis of imaging modalities. *Neurol Res* 1:7–18
- Firsching R, Wioschneck D, Diedrich M, et al (1998) Early magnetic resonance imaging of brainstem lesions after severe head injury. *J Neurosurg* 89:707–12
- Frankowski, RF, Annerggers JF, Whitman S (1985) Epidemiological and descriptive studies. The descriptive epidemiology of head trauma in the United States. In: Becker DP, Polishock J (eds) Central nervous system trauma status report. National Institute of Neurological and Communicative Disorders and Stroke. National Institutes of Health, Bethesda, Maryland
- Gean AD (1994) Imaging of head trauma. Raven Press, New York, pp 76–8
- Gentry LR (1991) Primary neuronal injuries. *Neuroimaging Clin N Am* 1:411–32
- Gentry LR (1994) Imaging of closed head injury. *Radiology* 297:1–17
- Gentry LR, Godersky JC, Thompson BH (1998) MR imaging of head trauma: review of the distribution and radiopathologic features of traumatic lesions. *Am J Neuroradiol* 9:101–10
- Gillgni E, Sabatini U, Hagberg GE, et al (2005) Fast detection of diffuse axonal damage in severe traumatic brain injury: comparison of gradient-recalled echo and turbo proton echo-planar spectroscopic imaging MRI sequences. *Am J Neuroradiol* 5:1140–8
- Graham DI, Gennarelli TA, McIntosh TK (2002) Blunt head injury. In: Graham DI, Lantos PL (eds) Greenfield's neuropathology, 7th edn. New York, NY: Arnold, 824–79
- Grčević N (1984) Investigations of neuropathology and pathogenetical mechanisms of closed brain injury of the acceleration-deceleration type. Final report of project no. 02-05-1. The National Institute of Health, Bethesda, Maryland
- Grčević N (1988) The concept of inner cerebral trauma. *Scan J Rehabil Med* 17 (Suppl):1–7
- Hanstock CC, Faden AL, Bendall RM, et al (1994) Diffusion weighted images differentiates ischemic tissue from traumatized tissue. *Stroke* 25:843–8
- Hashimoto T, Nakamura N, Richard KE, et al (1993) Primary brainstem lesions caused by closed head injury. *Neurosurg Rev* 16:291–8
- Hoelper BM, Reinert MM, Zauner A, et al (2000) rCBF in hemorrhagic, nonhemorrhagic and mixed contusions after severe head injury and its effect on perilesional cerebral blood flow. *Acta Neurochir (Suppl)* 76:21–5
- Huisman TA, Sorensen AG, Hergan R, et al (2003) Diffusion weighted imaging for the evaluation of diffuse axonal injury in closed head injury. *J Comput Assist Tomogr* 27:5–11
- Huisman TA, Schwamm LH, Schaefer PW, et al (2004) Diffusion tensor imaging as potential biomarker of white matter injury in diffuse axonal injury. *Am J Neuroradiol* 25:370–6
- Jadro-Santel D, Grcevic N, Besenski N, et al (1989) The inner cerebral trauma: the correlative pathology with CT scans. In: Aichner F, Gerstenbrandt F, Grcevic N (ed) *Neuroimaging II*. Stuttgart–New York: Fischer, pp 263–73
- Kirkpatrick JB (1998) Gunshots and other penetrating wounds of the central nervous system. In: Leestma JE, Kirkpatrick JB (eds) *Forensic neuropathology*. Raven Press, New York, pp 276–99
- Kuhne CA, Homann M, Ose C, et al (2003) Emergency room patients. *Unfallchirurg* 106: 380–6
- Leestma JE, Grčević N (1988) Impact injuries to the brain and head. In: Leestma JE, Kirkpatrick JB (eds) *Forensic Neuropathology*, New York: Raven Press, pp 409–16
- Lindenberg R, Freytag E (1957) Morphology of cortical contusions. *AMA Arc Pathol* 63:23–42
- Lindenberg R, Freytag E, (1960) The mechanism of cerebral contusions. *AMA Arc Pathol* 69:440–69
- Lindenberg R (1964) Significance of the tentorium in head injury from the blunt forces. *Clin Neurosurg* 12:1
- Macmillan CS, Wild JM, Wardlaw JM, et al (2002) Traumatic brain injury and subarachnoid hemorrhage: in vivo occult pathology demonstrated by magnetic resonance spectroscopy may not be “ischaemic”. A primary study and review of the literature. *Acta Neurochir (Wien)* 144:853–62



- MacPherson BCM, MacPherson P, Jennett B (1990) CT incidence of intracranial contusion and hematoma in relation to the presence site and type of skull fracture. *Clin Radiol* 42:321–6
- Meythaler JM, Peduzzi JD, Eleftheriou E, et al (2001) Current concepts: diffuse axonal injury-associated traumatic brain injury. *Arch Phys Rehabil* 82:1461–71
- Moritani T, Smoker WK, Y Sato Y, et al (2005) Diffusion weighted imaging of acute excitotoxic brain injury. *Am J Neuroradiol* 126:216–28
- Parizel PM, Ozsarlak O, Van Goethem JW, et al (1998) Imaging findings in diffuse axonal injury after closed head trauma. *Eur Radiol* 8:965–9
- Parizel PM, Ceulemans B, Laridon A (2003) Cortical hypoxic-ischemic brain damage in shaken baby (shaken impact) syndrome. Value of diffusion-weighted MRI. *Pediatr Radiol* 33:868–71
- Paterakis K, Karantanas AH, Komnos A, et al (2000) Outcome of patients with diffuse axonal injury: the significance and prognostic value of MRI in the acute phase. *J Trauma* 49:1071–5
- Pavic D, Kralj K, Besenski N, et al (1994) Some epidemiological features of fatal head injury. *Neurol Croat* 43:3–7
- Payen JF, Francony G, Fauvage B, et al (2005) Interest of magnetic resonance spectroscopy in predicting severity and outcome in traumatic brain injury. *Ann Fr Anesth Reanim* 5:522–7
- Ross PS, Ross AM (1989) Should patients with normal cranial CT scans following minor head trauma be hospitalized for observation? *Pediatr Emergency Care* 5:216–17
- Ross BD, Ernst T, Kreis R, et al (1998) 1H MRS in acute traumatic brain injury. *Magn Reson Imaging* 8:829–40
- Schaefer W, Huisman TA, Sorensen AG, et al (2004) Diffusion weighted MR imaging in closed head injury: high correlation with initial Glasgow coma scale score on modified Rankin scale at discharge. *Radiology* 1:58–66
- Sellier K, Unterharnscheidt F (1963) Mechanik und pathomorphologie der Hirnschaden nach stumpfer Gewaltein Wirkung auf den Schaedel. *Hefte Unfallheilkunde* 76:1–140
- Shibita Y, Matsumura A, Meguro K, et al (2000) Differentiation of mechanism and prognosis of traumatic brain stem lesions detected by magnetic resonance imaging in the acute stage. *Clin Neurol Neurosurg* 102:124–8
- Siccardi D, Cavaliere R, Pau A, et al (1991) Penetrating craniocerebral missile head injuries in civilians: a retrospective analysis of 314 cases. *Surg Neurol* 35:455–60
- Strich SJ (1956) Diffuse degeneration of the cerebral white matter in severe dementia following head injury. *J Neurosurg Psychiatry* 19:163–85
- Tatalovic-Osterman LJ, Jadro-Santel D, Besenski N (1991) Diagnostic possibilities of the closed head injuries of acceleration type using computed tomography. *Neurol Croat* 40:231–45
- Wardlaw JM, Statham PFX (2000) How often is haemosiderin not visible on routine MR following traumatic intracerebral haemorrhage? *Neuroradiology* 42:81–4
- Wintermark M, van Melle G, Schnyder P, Revelly JP, Chiolero R, Porchet F, Regli L, Meuli R, Maeder P, Chiolero R (2004a) Admission perfusion CT: prognostic value in patients with severe head trauma. *Radiology* 2:211–20
- Wintermark M, Chiolero R, van Melle G, Revelly JP, Porchet F, Regli L, Meuli R, Schnyder P, Maeder P (2004b) Relationship between brain perfusion computed tomography variables and cerebral perfusion pressure in severe head trauma patients. *Crit Care Med* 32:1579–87
- Yoo SJ, Lee JH, Kim ST, et al (2005) Evaluation of traumatic brain injured patients in correlation with functional status by localized 1H-MR spectroscopy. *Clin Rehabil* 19: 209–15
- Zarkovic K, Jadro-Santel D, Grcevic N (1991) Distribution of traumatic lesions of corpus callosum in “inner cerebral trauma”. *Neurol Croat* 40:129–56
- Zimmernan RA, Bilanuik LT, Buce D, et al (1978) Computed tomography of pediatric head trauma: acute general brain swelling. *Radiology* 126:403–8

# Imaging of Facial Injuries

U. Salvolini, G. Polonara, S. Salvolini

## 2.4

### Contents

2.4.1 Introduction	125
2.4.2 Imaging	125
2.4.3 Nasal Fractures	127
2.4.3.1 Tripod Fracture	127
2.4.4 Complex Midfacial Fractures	128
2.4.5 Isolated Fractures	131
2.4.6 Foreign Bodies and Penetrating Injuries	133
2.4.7 Complex Facial Fractures	133
2.4.8 Mandibular Fractures	136
2.4.9 Conclusion	138
References	138

### 2.4.1 Introduction

Injuries to the facial bones and adjacent soft tissues are common. The sheer pace of modern life with high-speed travel as well as an increasingly violent and intolerant society have made facial trauma a form of social disease from which no one is immune (Batnitzki and McMillan 1990). The combination of traffic accidents and blows sustained during fights and assaults accounts for more than 80% of all injuries to the facial skeleton (Rogers 1982).

### 2.4.2 Imaging

Severe trauma to the face is a strong indication for radiological investigation; however, before any technical act is performed, the patient's vital functions must be stabilized and the clinical state carefully evaluated to rule out other, more serious injuries. Radiological evaluation of facial injuries may be difficult due to the complex anatomy of the region and to the difficulties in obtaining high-quality

imaging studies in severely traumatized patients (Hermans et al. 1997; Druelinger et al. 2000). Its goal is to establish the number and exact location of the fractures, determine the dislocation of the bony fragments, and assess concomitant soft tissue complications (Ghysen et al. 2000).

Dolan and Jacoby (1978) have described three imaginary lines of bone continuity that are helpful to evaluate the bony contours and identify fractures with plain X-ray examination. Any disruption in the continuity of these lines, and any difference in contour between the two sides of the face, suggest a fracture and warrant closer evaluation (Fig. 1).

There is general agreement (Batnitzki and McMillan 1990) that the exact anatomic identification and quantification of facial fractures, the recognition of the true extent of bone displacements, and the precise assessment of major bone and soft tissue complications can be effectively and accurately imaged with high-resolution computed tomography (CT). In the recent past, conventional radiography was considered by some authors to be the technique of choice for the initial evaluation of the maxillo-facial skeleton. Some researchers believe that plain films should be used to focus CT examination when this is indicated (Druelinger et al. 2000). The view has also been expressed that substantial hospital savings could be made through the selective use of CT in the diagnosis of facial fractures after blunt trauma, because CT scans are expensive, time-consuming, and labor intensive, and sometimes add little clinical information to that obtained by physical examination and plain films (Thai et al. 1997). As the cost of facial CT declines, and the gap with that of plain films decreases, helical CT is expected to become the screening modality of choice depending on the cost structure at each given hospital (Rhea et al. 1999), even though the risk of harmful ionizing radiation to the lens should never be underestimated (Lund and Halaburt 1982).

There are certain facial soft tissue injury zones that correlate with facial fractures: these are more common in patients affected by lip laceration, intraoral laceration, periorbital contusion, subconjunctival hemorrhage, and nasal laceration; consequently, the acronym LIPS-N has been proposed (Holmgren et al. 2005) to be used in conjunction with a physical examination when assessing if a trauma pa-



**Fig. 1.** Dolan and Jacoby's three lines of reference as seen on the Waters view. (Modified from Batnitzki and McMillan 1990)

tient who is getting head CT in acute trauma situations should also get facial CT, to avoid missing facial fractures on initial imaging evaluation. To save the patient unnecessary radiation exposure, health care costs, and time spent in the emergency radiology department, according to a retrospective review (Lewandowski et al. 2004) the absence at standard head CT scan of an air-fluid level within the paranasal sinuses or of a fracture of the maxillary, orbital, or zygomatic osseous structure could preclude the need for a dedicated facial CT scan.

In trauma patients, CT shows a larger number of fracture fragments and fracture lines than conventional radiography, and better depicts the position and orientation of displaced fracture fragments (Daffner 1997, 1998; Novelline et al. 1999). Computed tomography can also demonstrate soft tissue injuries.

In acutely injured patients, unenhanced axial CT provides the most effective, safe, reasonably rapid diagnostic imaging tool (Novelline et al. 1999); direct coronal CT can also be performed.

The speed of helical technology permits CT examination of seriously ill patients in emergency care as well as of patients who, because of its duration, would not have tolerated CT in the past. Helical technology (Fig. 2) also allows multiple, sequential CT scans to be quickly obtained in the same patient, a great advance for multiple-trauma patients (Novelline 1999). We suggest routine non-enhanced helical scanning of the face with 3-mm collimation, a soft tissue reconstruction algorithm, and a pitch of 1 (or 1.5, to reduce radiation dose), and slice reconstruction at 1.5 mm intervals using a high-resolution algorithm for the bone; thinner 1 mm collimation may occasionally be indicated to detect subtle trauma, such as fractures of the optic canal.

In the transverse plane, sections should be obtained from above the frontal sinuses to below the alveolar process of the maxilla, and in the coronal plane from in front of the nasal bones to behind the sphenoid sinuses. If a mandibular fracture is also clinically suspected, the scan should be extended to include the entire mandible in the transverse plane and the temporo-mandibular joints in the

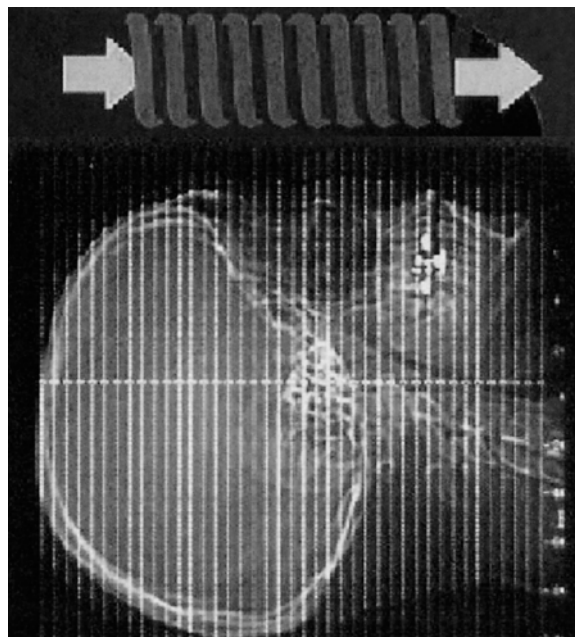


**Fig. 2.** Spiral CT: scanning protocol for the facial area

coronal plane. In any case, the transaxial remains the dominant modality (Kassel et al. 1983).

If the patient cannot be positioned for primary coronal scanning, which requires hyperextension of the neck, the coronal planes can be reconstructed using computer reformations, even though this involves a loss of spatial resolution (Brant-Zawadzki et al. 1982) depending on the thickness of the direct axial scans. A 3D bony surface model can also be reconstructed on the workstation. Multiplanar reconstructions improve the representation of skeletal injuries, especially along a horizontal plane parallel to the axial scans (Laine et al. 1993).

The integration of axial imaging with multiplanar and 3D surface reconstructions improves the understanding of the injury and thus diagnosis in the vast majority of cases (Preda et al. 1998).

A 3D reconstruction is quantitatively accurate also for surgical planning and treatment evaluation of cranio-facial structures (Cavalcanti et al. 1999), also in forensic post-mortem examinations (Myers et al. 1999).

Magnetic resonance imaging (MRI) of maxillo-facial structures affords several advantages, including absence of ionizing radiations, multiplanar capability, and excellent soft tissue contrast: its main limitation is the difficulty of imaging the cortical bone. For these reasons, whereas its use is limited in the detection of fracture sites, it optimally images soft tissue involvement (Tonami et al. 1991). Before performing MRI, the presence of metallic fragments needs to be ruled out. Magnetic resonance imaging is complementary to CT in the evaluation of maxillo-facial complex fractures; CT is superior to MRI in detecting fracture sites, but MRI provides valuable information about soft tissue

lesions. Situations in which MRI is preferable to CT include unexplained neurological deficits, visual or extraocular muscle impairment, both pre- and postoperative, and fractures with a high probability of intracranial complications.

Multiple coronal MR images covering the entire orbit should first be obtained, then additional images should be performed in another plane, the axial or the oblique sagittal plane according to the direction of the inferior rectus muscle.

### 2.4.3 Nasal Fractures

The nose is the most prominent projection of the face and therefore sustains the largest number of fractures, accounting for half of all facial bone fractures (Muraoka and Nakai 1998). As fractures of the nasal bones are usually readily apparent on clinical examination, a radiographic examination is generally unnecessary and can be performed to confirm the clinical diagnosis, for medico-legal purposes, or to attempt to determine the displacement of the fracture fragments (Schultz and de Villers 1975).

Radiology plays a minor role in the management of nasal bone fractures, unless there is extension to other facial bones. De Lacey and co-workers (1977) concluded from a study of 100 patients with nasal bone trauma that it is an unnecessary procedure and should be carried out only upon specific request by an ENT surgeon.

#### 2.4.3.1 Tripod Fracture

The tripod fracture, or zygomatico-maxillary complex fracture, is the second most common isolated fracture of the midface (Noyek et al. 1983). The principal lines of fracture involve the three distinct processes of the zygomatic bone: orbital; zygomatic; and maxillary (Figs. 3–6).

As the zygoma becomes separated from its three attachment points, there is a widening of the zygomatico-frontal suture, and a fracture of the inferior orbital rim involving the postero-lateral wall of the maxillary sinus and of the zygomatic arch. The CT demonstrates the details of the simple or complex fracture.

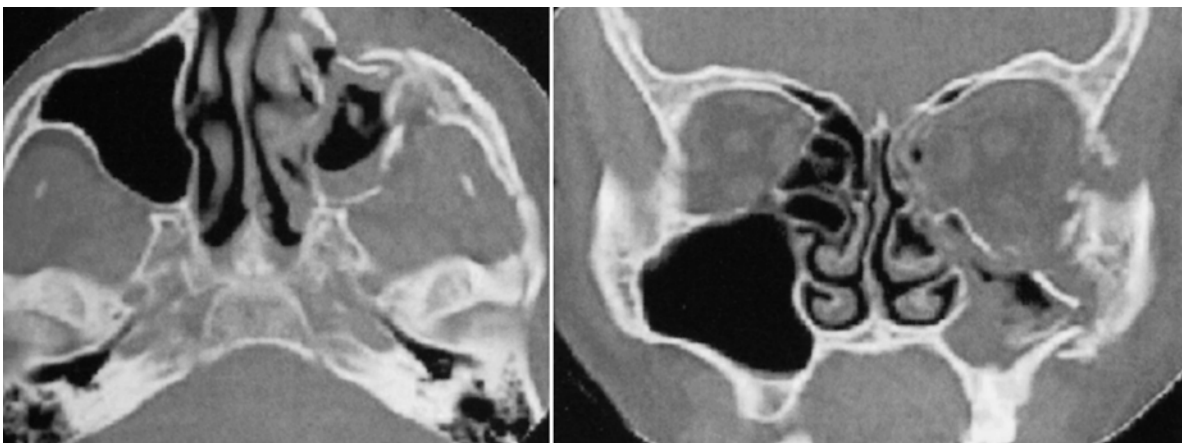


Fig. 3. Tripod fracture; axial (*left*) and coronal CT (*right*)

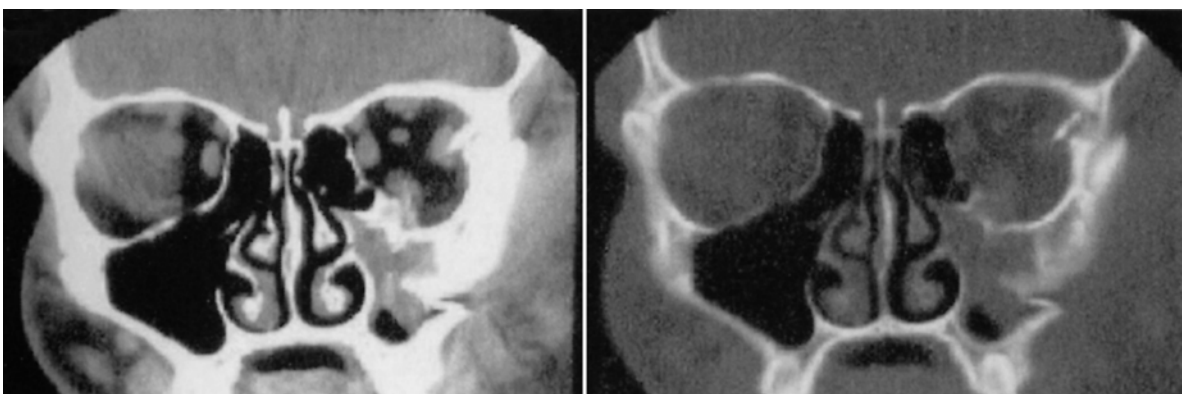
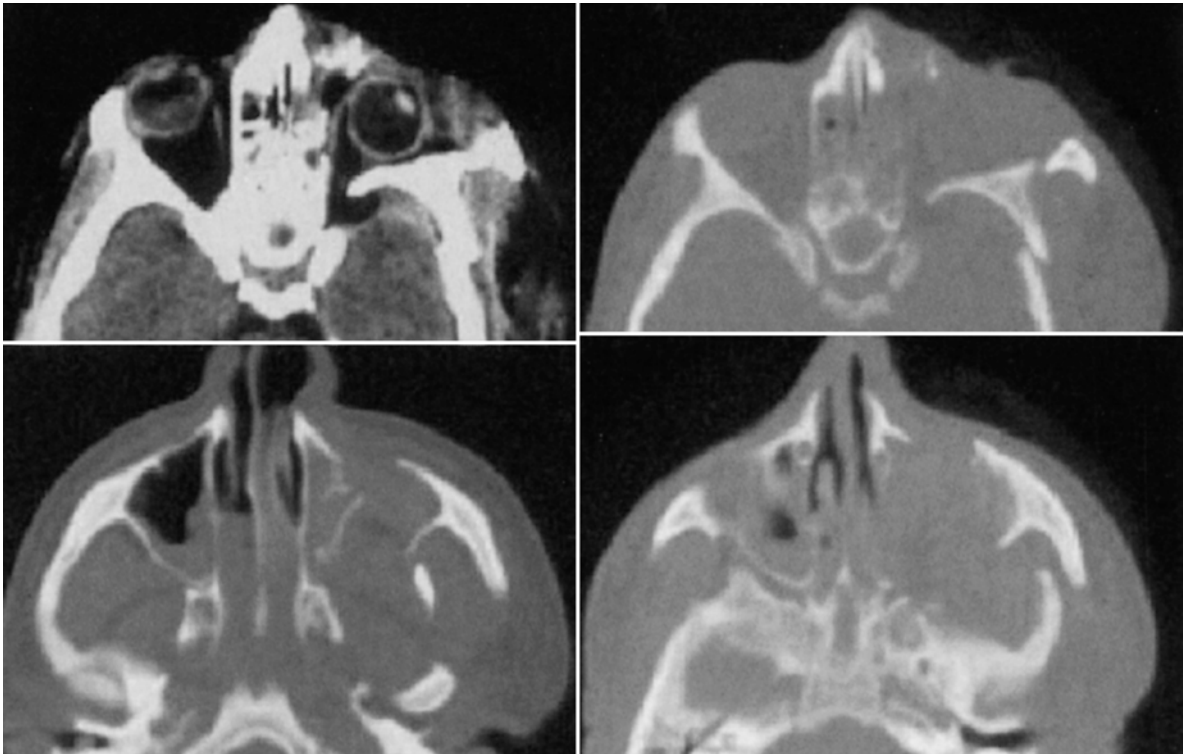
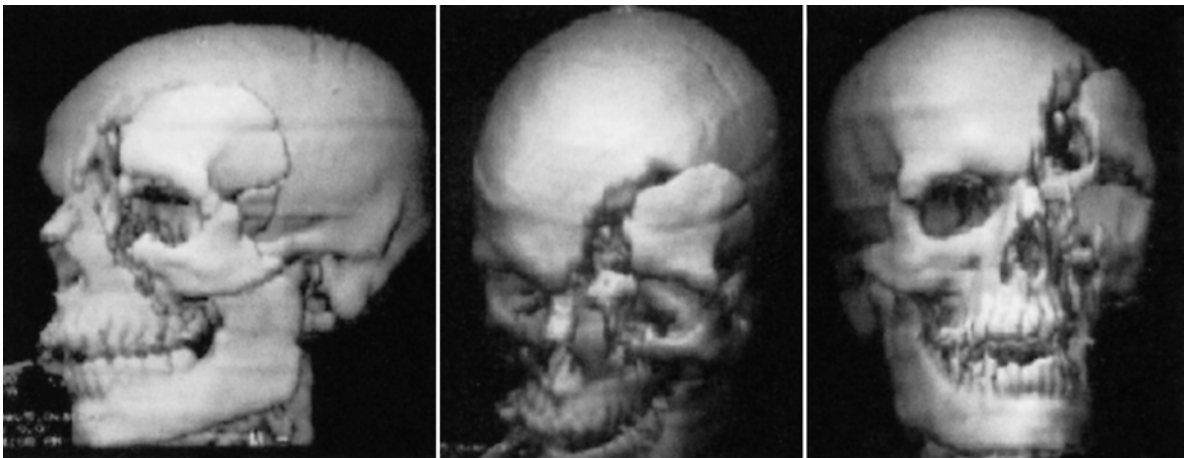


Fig. 4. Depressed tripod fracture involving the orbital muscles; coronal CT





**Fig. 5.** Tripod fracture with rotation of the fragment compressing the optic nerve; axial CT



**Fig. 6.** Complex tripod fracture associated with fronto-orbital fracture as demonstrated by CT using 3D bony surface reconstruction

#### 2.4.4 Complex Midfacial Fractures

In 1901 Le Fort (1901a–c) published his magnum opus comprising three famous papers on upper jaw fractures: cadaver heads were subjected to variable degrees of trauma, then dissected, and the fracture patterns carefully determined.

Le Fort outlined three lines of fracture, reflecting the relative areas of weakness within the facial skeletal structure, which form the basis of what has come to be known as Le Fort's classification of facial fractures (Batnitzki and McMillan 1990).

As originally described by Le Fort in 1901, the classification regarded symmetric fractures of the facial bones extending back to, and involving, the pterygoid plates. Since



**Fig. 7.** Le Fort type-I fracture: floating palate; coronal CT

injuries are often asymmetric, they are usually designated as Le Fort-type fractures.

In Le Fort-type I fracture (Fig. 7) the fracture runs transversely through the maxilla and the nasal vault, just above the alveolar portion of the maxilla, at the level of the hard palate, through the floor of the maxillary sinuses to the lower portion of the pterygoid plates. As a result, there is a “floating palate” displaced posteriorly. This fracture was described by Guerin in 1866.

Le Fort type-II fracture is also called pyramidal fracture because the central portion of the face becomes separated as a pyramidal fragment. Across the nose bridge, it runs on either side lateral to the nasal cavity through the medial orbital rim, obliquely across the anterior maxillary antra and the zygomatic arches, extending posteriorly and reaching the pterygoid plates.

Le Fort type-III fracture (Figs. 8–10) entails the complete separation of the facial skeleton from the cranium (cranio-facial dysjunction). It begins in the naso-frontal area and extends through the medial, lateral, and posterior

walls of the orbits involving the ethmoid and the sphenoid sinus and ending in the pterygoid plates.

By definition, Le Fort fractures are bilateral and symmetric injuries. Le Fort’s experiments were carried out with modest impact forces compared with those generated in a high-speed car crash; presently, combinations of injuries are more common than the three original types. In addition, the classification of facial fractures by these criteria alone is inadequate, as they do not include minor osseous injuries that may be of greater significance than the major ones (Gentry et al. 1983a,b). Dolan and co-workers (1984) have suggested the term “smash injuries” to describe these severely comminuted fractures of the facial skeleton: naso-ethmoidal complex fractures, involving the entire naso-frontal and ethmoidal region.

Computed tomography has allowed adoption of a method of classification of facial fractures based on the involvement of the facial pillars (buttresses or struts): three horizontal, two coronal, and five sagittally oriented struts have been described (Bensimon and Herman 1994; Dupuis

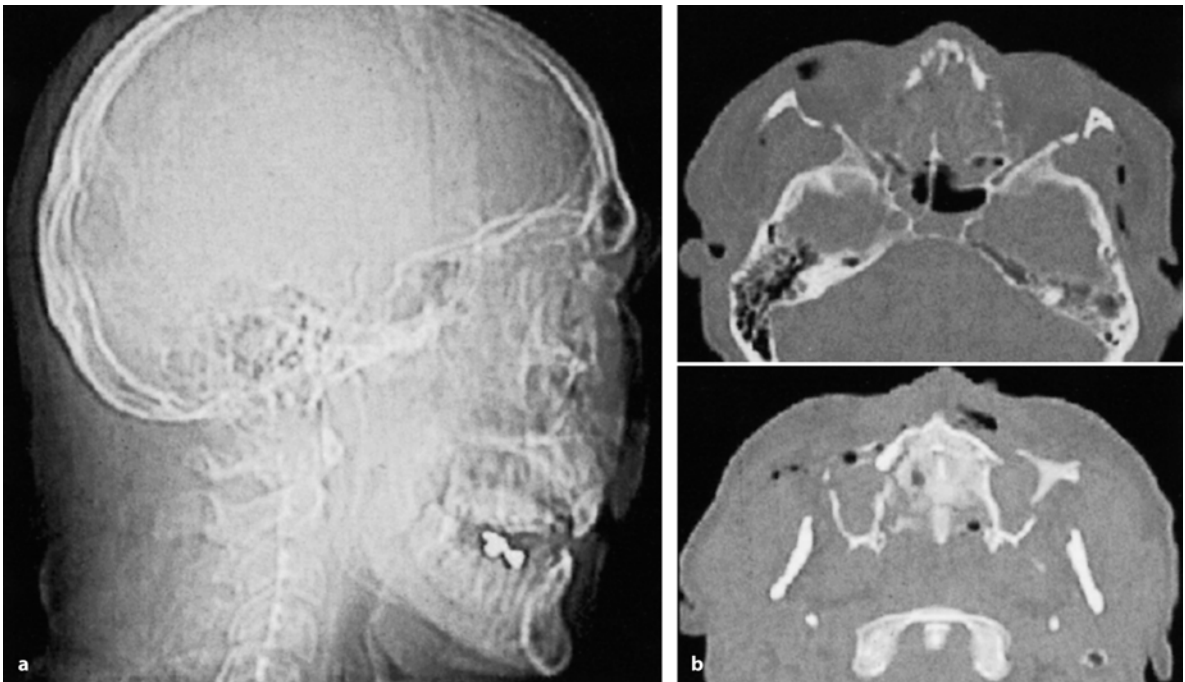


**Fig. 8.** Le Fort type-III fracture: cranio-facial dysjunction; scanography (*left*) and axial CT (*right*)

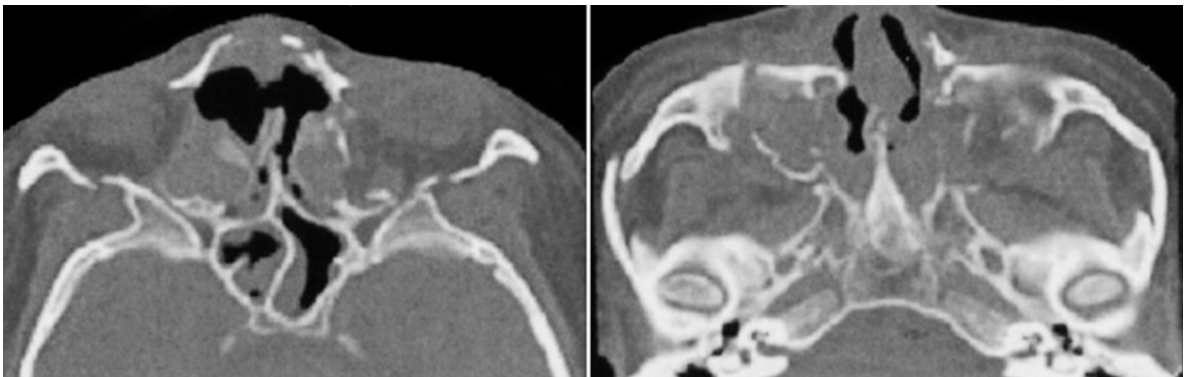


**Fig. 9.** Le Fort type-III fracture, axial CT

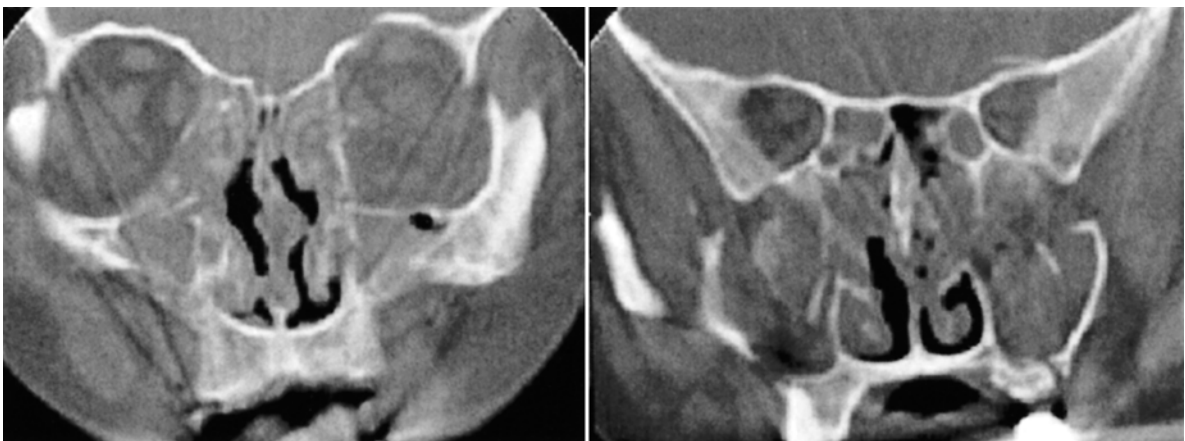


**Fig. 10.** Le Fort type-III fracture, coronal CT



et al. 1994). Limited fractures can be differentiated from transfacial ones by the lack of involvement of the pterygoid plates in the former. These fractures can also be subdivided into solitary and complex (Laine et al. 1993). This classification scheme may be defined as fractures of vertical buttresses and horizontal beams (Donat et al. 1998). When describing fractures of the face, the diagnosis is best confined to the actual anatomic structures involved.

### 2.4.5 Isolated Fractures

Isolated fractures of the maxillary antrum are uncommon. They are characterized radiographically by an anterolateral wall fracture or by a depressed fracture of the anterior wall of the maxillary antrum (Fig. 11).

Fractures of the frontal sinuses may be linear and non-displaced, or comminuted and depressed. They may be confined to the anterior wall of the sinus or also involve the posterior wall (Fig. 12). Extensive comminuted fractures in the naso-ethmoid region commonly extend into the base of the frontal sinus and the cribriform plate.

Fractures of the ethmoid cells generally occur as part of more extensive Le Fort-III injuries, but may also be isolated. They may be observed on the roof of the ethmoid labyrinth, in the region of the cribriform plate (Fig. 13). When they involve the medial orbital wall, the fracture is suspected for the presence of orbital emphysema (Fig. 14) (Brasileiro et al. 2005), whereas the fracture of the cribriform plate can be inferred from the detection of pneumocephalus.

The term “blowout” fracture indicates a specific “hydraulic mechanism” that results in a fracture first described by Pfeiffer (1943): it is a fracture of the orbital floor; the orbital rim remains intact and the adjacent intraorbital contents prolapse into the maxillary antrum through the defect in the floor (O’Hare 1991).

The impairment of muscle function underpins the special severity of a blow-out fracture. According to Smith and Regan (1957), the mechanism of injury is as follows: part of the impact of the blow is absorbed by the orbital rim, which

remains intact, but the force of the blow causes a backward displacement of the eye and an increase in intraorbital pressure, with a resultant fracture of the orbital floor or medial wall, and a consequent herniation of orbital soft tissues into the maxillary antrum or ethmoid cells (Fig. 15). Pure eth-

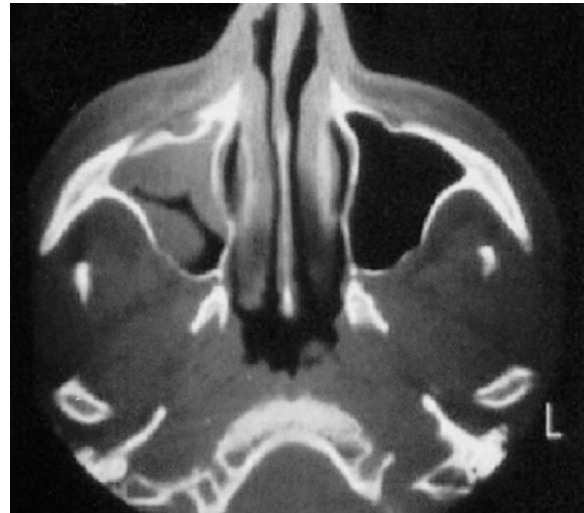


**Fig. 11.** Depressed fracture of the anterior wall of the maxillary antrum; axial CT

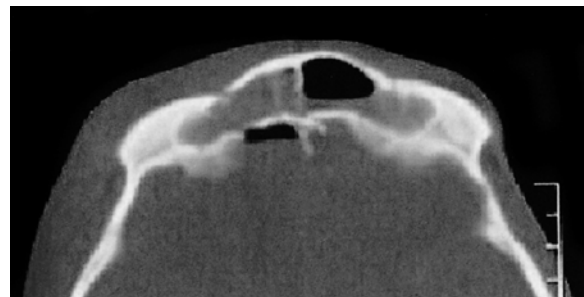


**Fig. 12.** Fracture of both the anterior and the posterior wall of the frontal sinus; pneumocephalus and intrasinusal hemorrhage; axial CT

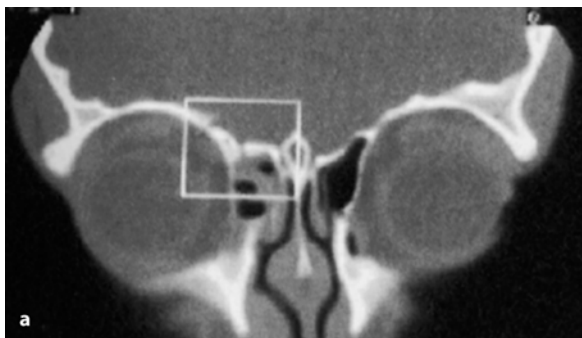


**Fig. 13.** Complex fracture of the ethmoid cells; coronal (left) and axial CT (right)



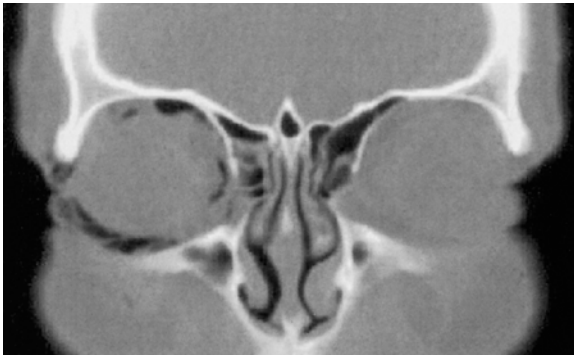


**Fig. 14.** Right orbital emphysema indicates fracture of the adjacent sinuses; coronal CT

moldal blow-out fractures are rare. In an orbital blow-out fracture, entrapment of the connective tissue septa, which join the periorbita to the rectus muscle sheaths and the tendinous ring connecting them, may cause a downward drag on the medial or lateral rectus muscle via the tendinous ring which joins them to the inferior rectus muscle. Magnetic resonance imaging may be performed soon after the trauma: although small bone fragments are not well visualized, the identification of hyperintense prolapsed orbital fat enables localization of the fracture site; MRI also provides useful information on the relationship between fracture and extraocular muscles (Figs. 15, 16) (Tonami et al. 1991; Tonami et al. 1987). Magnetic resonance imaging also allows satisfactory evaluation of scar tissue formation.

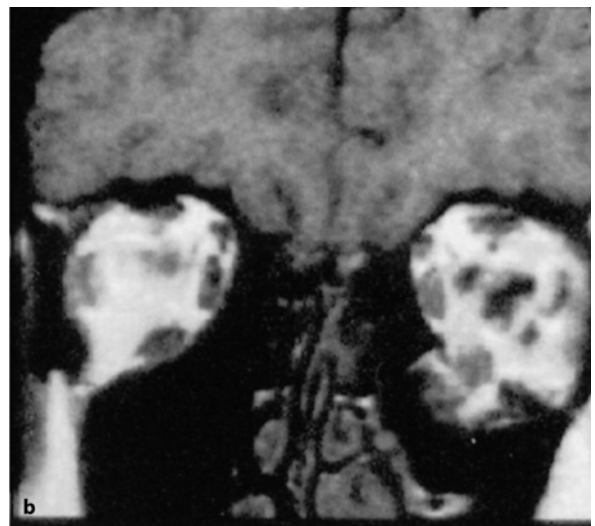
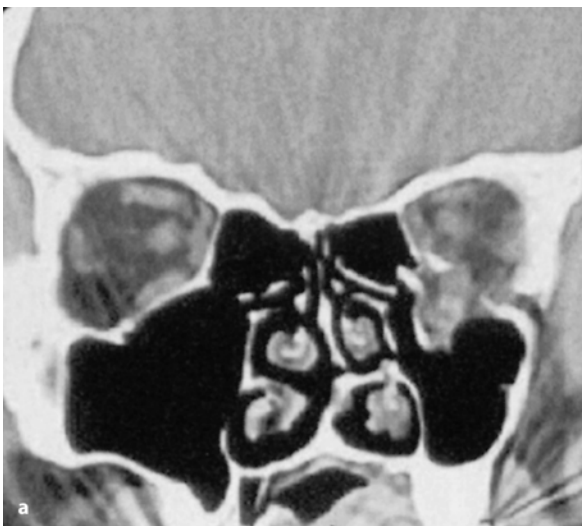


**Fig. 15.** Blow-out fracture; of the orbit coronal CT (*left*) and MRI (*right*)



**Fig. 16.** Blow-out fracture of the orbit; oblique sagittal MRI

### 2.4.6 Foreign Bodies and Penetrating Injuries

Computed tomography is particularly valuable in demonstrating penetrating injuries and foreign bodies in the face (Fig. 17) and orbit (Fig. 18). Materials such as stone, glass without significant lead content, and wood may not be evident on conventional radiographs. Although the radiological appearance may show considerable variety, CT is the basic diagnostic technique and MRI the method of second choice.

### 2.4.7 Complex Facial Fractures

Complex facial structures, especially those associated with cranio-cerebral or spinal injuries, are better and more safely assessed with CT. Complications to soft tissue structures (orbit, brain) are diagnosed at the time of study and provide information often not obtainable with other modalities (Kassel et al. 1983).

Complex orbital rim and fractures of the internal orbital skeleton are best analyzed with high-resolution axial CT, especially associated with multiplanar and body-surface reconstruction (Fig. 19). Optic canal fractures are



**Fig. 17.** Metallic foreign body penetrates the right fronto-ethmoidal region; scanography (*left*) and axial CT (*right*)

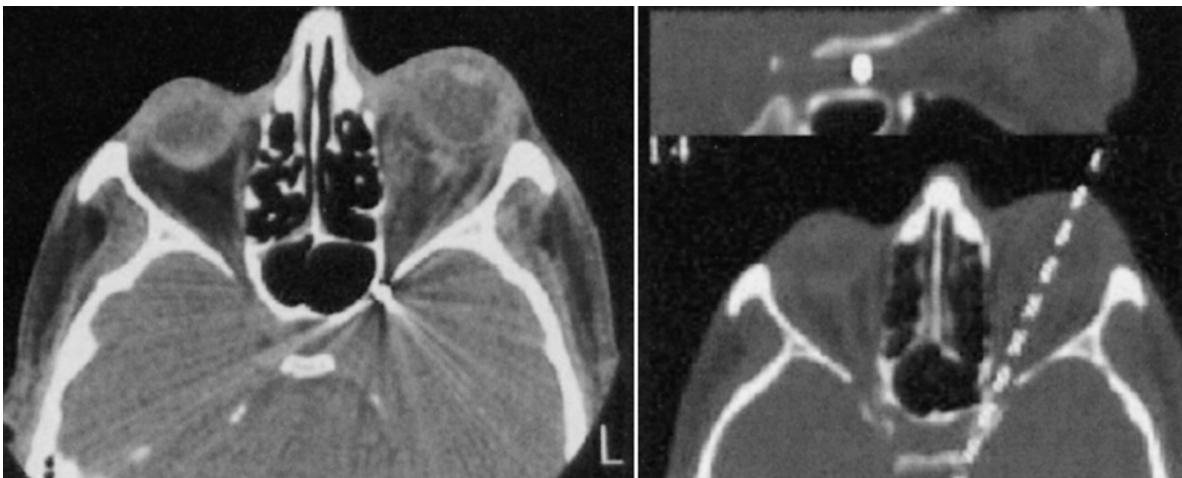


**Fig. 18.** Small metallic foreign body inside the left optic canal; axial CT (*left*) and reformatted oblique sagittal CT (*right*)

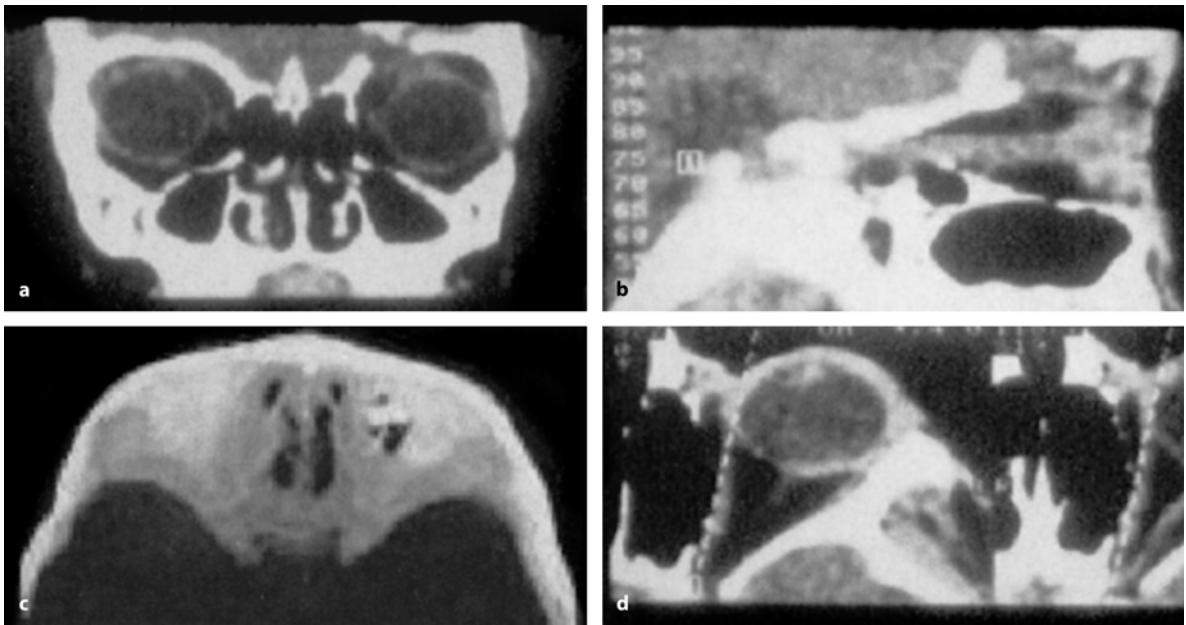


**Fig. 19.** Fracture of the orbital roof involving the superior oblique muscle; reformatted CT: coronal (*top left*) oblique sagittal (*top right*) and 3D bony surface reconstruction (*bottom left*)



**Fig. 20.** Complex gunshot fracture of the left orbit; axial CT



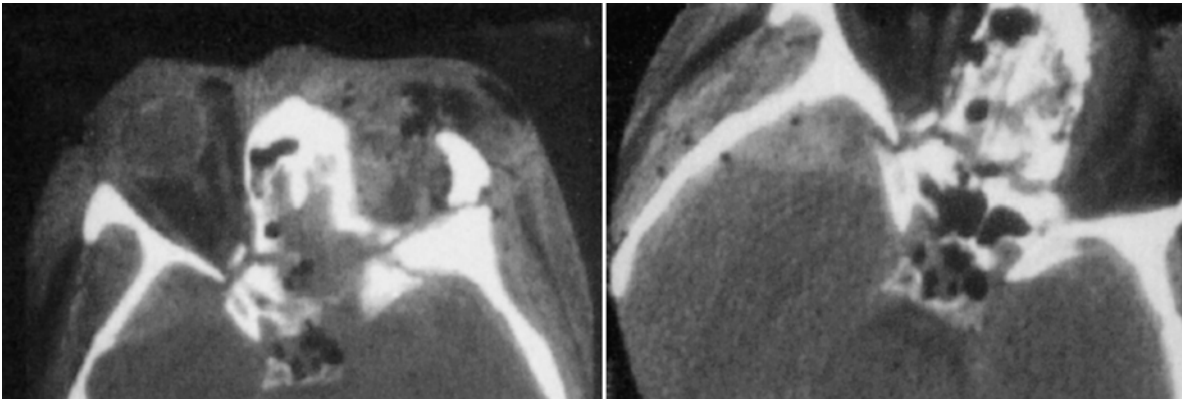


**Fig. 21.** Fracture of the orbital apex involving the optic canal and the ethmoidal region; axial CT

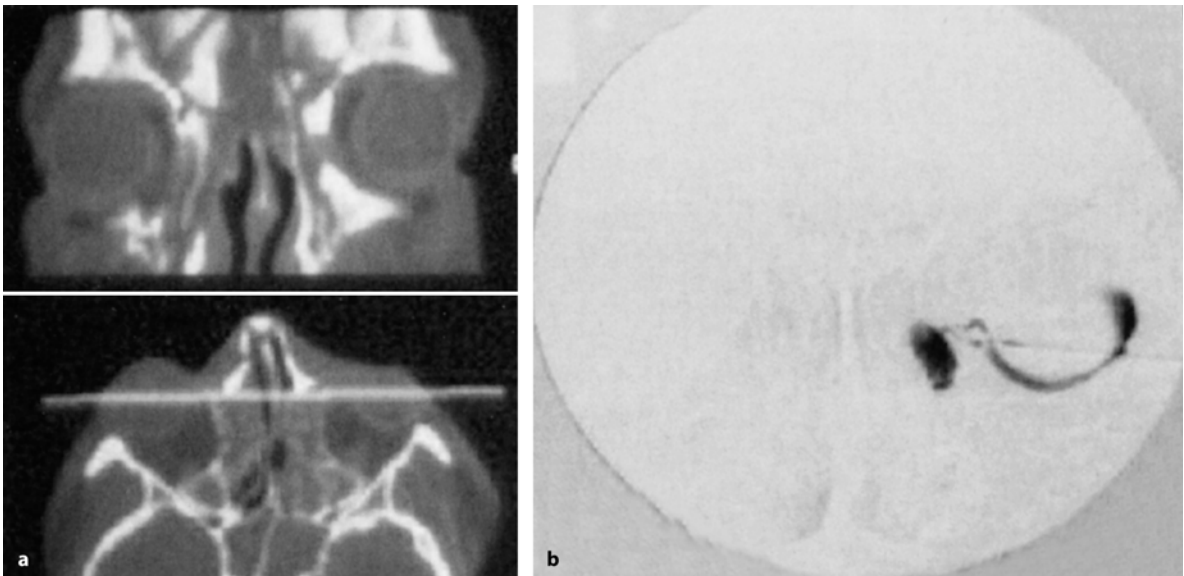


**Fig. 22.** Complex fracture of the fronto-orbital region involving the left naso-lacrimal duct. Reformatted coronal CT (*left*) and digital dacryocystography (*right*) demonstrates duct occlusion

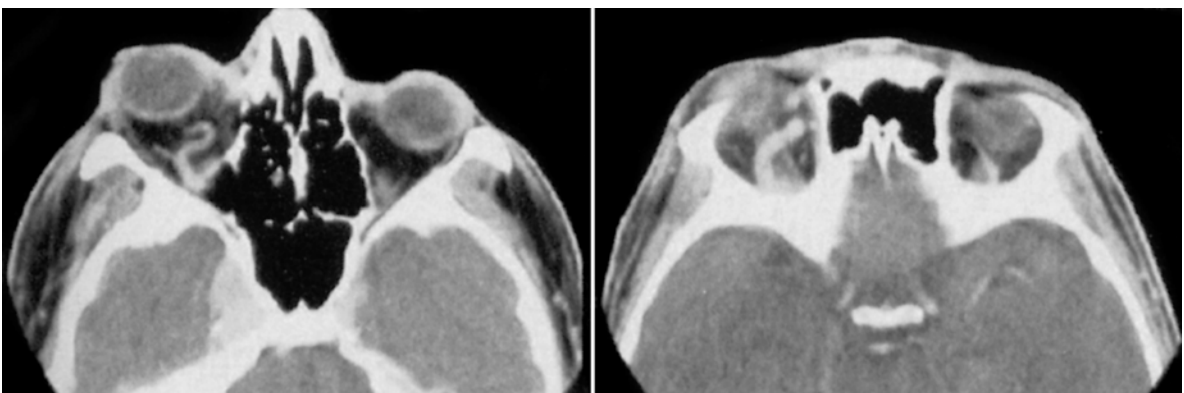


**Fig. 23.** Carotido-cavernous fistula axial CT after intravenous contrast medium demonstrates the thickened right superior ophthalmic vein and enlarged cavernous plexus



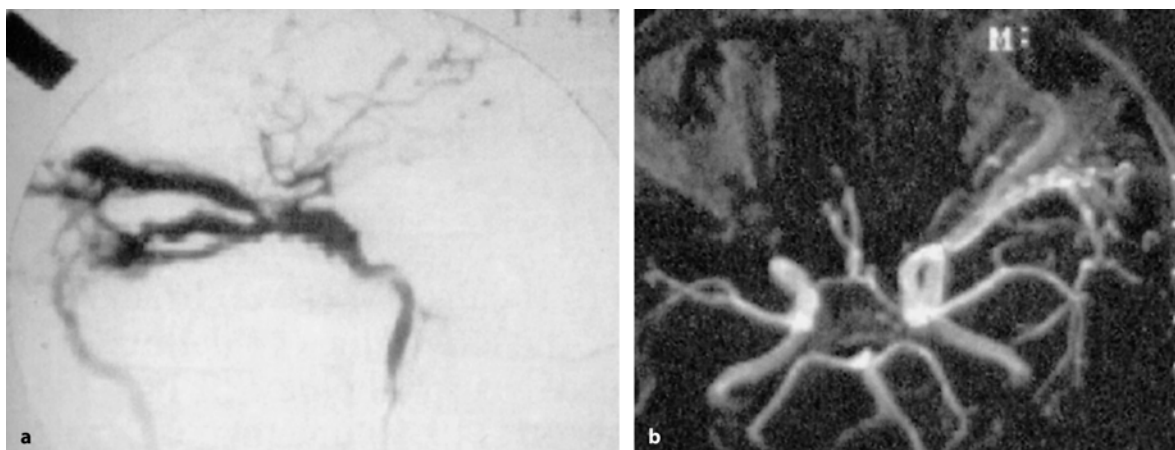


**Fig. 24.** Carotido-cavernous fistula MRI depicts thickened left orbital muscles and superior ophthalmic vein

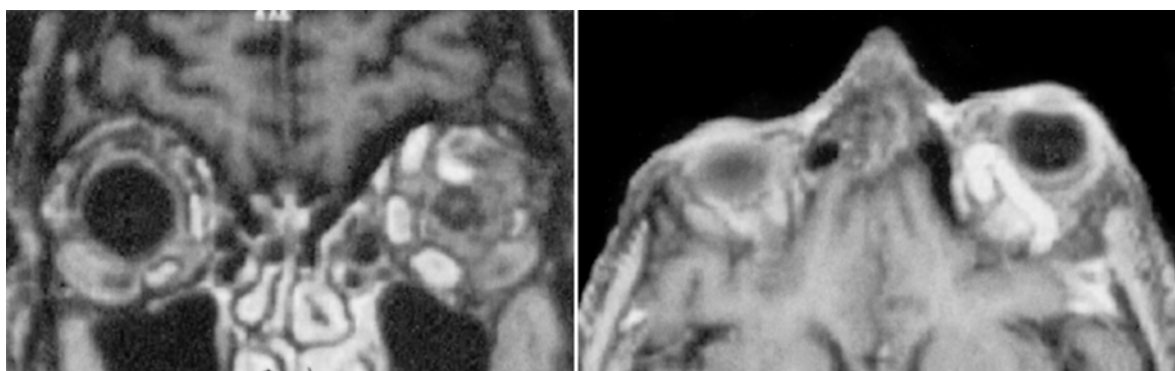


**Fig. 25.** Same case as in Fig. 24. Digital subtraction angiography (*left*) confirms the carotido-cavernous fistula seen with angio-MRI (*right*)

visualized with thin 1-mm-section high-resolution CT scanning [43]. Spiral CT is rapid and is thus used in acutely injured patients (Figs. 20–22). Magnetic resonance imaging is helpful in evaluating carotid-cavernous sinus fistulas (Figs. 23–25) (Mauriello et al. 1999).

#### 2.4.8 Mandibular Fractures

Fractures of the mandible are often subtle and easily overlooked unless disciplined search patterns are employed. Radiological evaluation can determine the extent of alveolar ridge fractures and the relation of the dental apices to the fracture line. In most instances, maxillary alveolar process fracture is transverse and limited to the alveolar process, most commonly in the incisor area.

Panoramic views and plain films are usually adequate to evaluate solitary mandibular injuries; CT scans are useful in selected cases. Often the mandible will fracture at two sites: at the location of the impact (symphysis) and where



**Fig. 26.** Ortho-panoramic radiography demonstrates the mandibular fracture

the force is dissipated (condylar neck) (Figs. 26, 27) (Hermans et al. 1997).

As the traction of the external pterygoid muscle displaces the condylar fragment medially and anteriorly (Figs. 27, 28), the fracture is inferred from the so-called empty glenoid fossa (Fig. 29). The glenoid cavity can be involved also in complex skull-base fractures (Fig. 30).

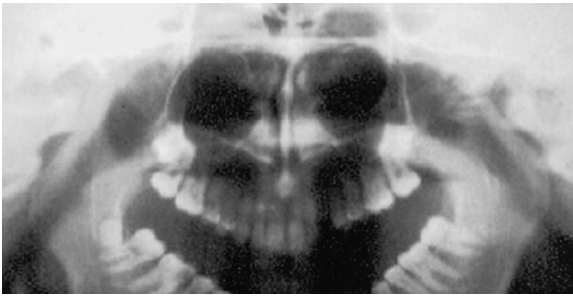


**Fig. 27.** Fracture of the left mandibular condyle the anterior luxation is well depicted on the ortho-panoramic film



**Fig. 28.** Fracture of the left mandibular condyle the medial luxation is demonstrated on direct coronal CT

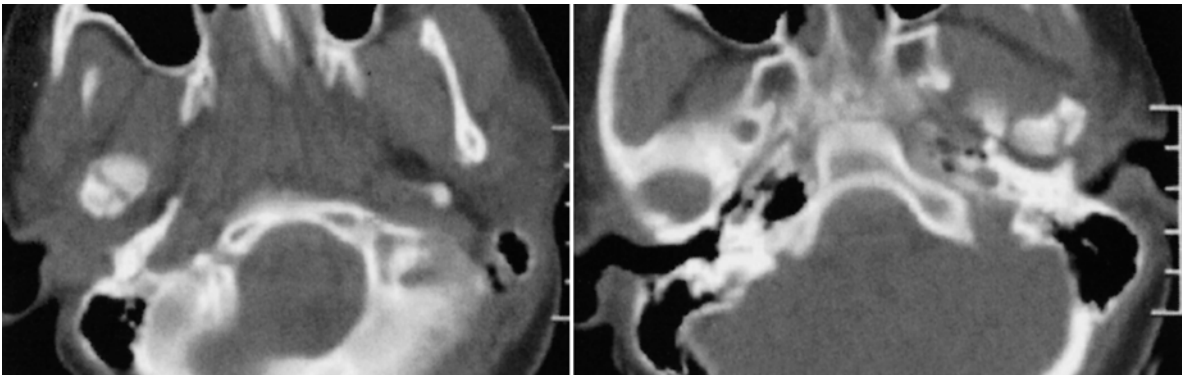


**Fig. 29.** Bilateral fracture of the condyle to the right of the glenoid fossa is “empty”; axial CT

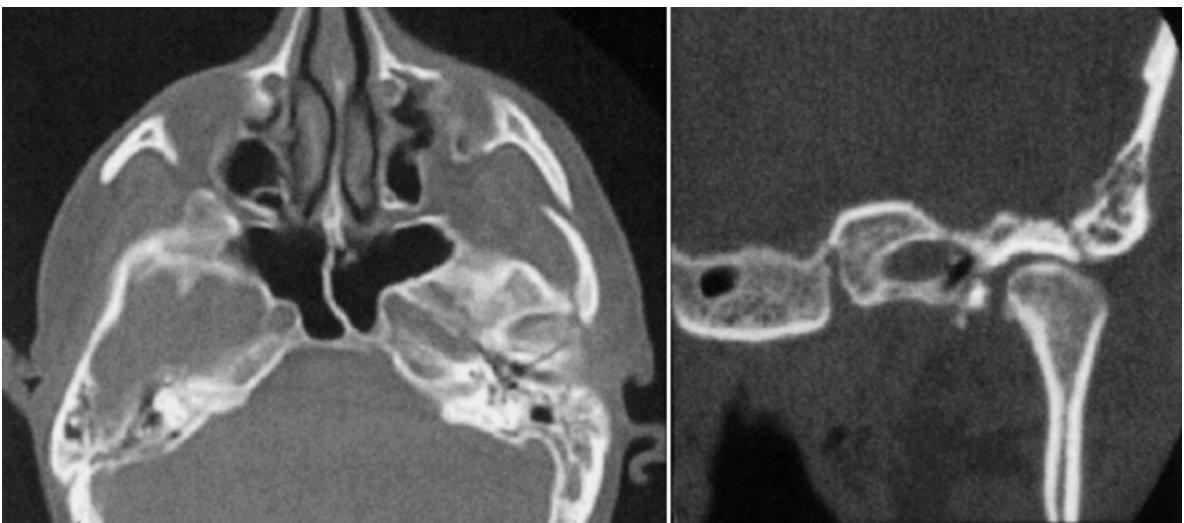


**Fig. 30.** Complex fracture involving left zygomatic arch, glenoid cavity, and petrous bone; axial (*left*) and coronal CT (*right*)

## 2.4.9 Conclusion

Injuries to the face ordinarily receive a low priority: in fact, early evaluation of facial injuries cannot be postponed. The acutely injured patient being scanned for intracranial trauma should be examined for facial injuries at the same time.

It is also necessary to know that maxillofacial trauma may mask intracranial injuries, prompting intensive care treatment: according to Holrieder et al. (2004), nearly 10% of patients with craniomaxillofacial fractures sustain intracranial hemorrhages. Moreover, among 400 patients with facial injuries of varying degree, Schultz (1967) found an incidence of 4% of cervical spine fractures, many of which were asymptomatic. For this reason, routine inclusion of the upper cervical spine in head CT is appropriate when evaluating patients with significant head trauma (Kirshenbaum et al. 1990). In a prospective investigation of 582 consecutive patients with facial fractures for evidence of a concomitant cervical spine injury, six were found to have it (Beirne et al. 1995). Many fractures are missed or incompletely shown at radiography, especially in uncooperative trauma victims. Helical CT can depict significant fractures not shown by plain radiography and should be added routinely to the initial screening for cervical spine fractures in multiple trauma victims (Nunez et al. 1996).

## References

- Batnitzki S, McMillan JH (1990) Facial trauma. In: McCort JJ, Mindelzun RE (eds) *Trauma radiology*. Churchill Livingstone, New York, pp 301–338
- Beirne JC, Butler PE, Brady FA (1995) Cervical spine injuries in patients with facial fractures: a 1-year prospective study. *J Oral Maxillofac Surg* 24:26–29
- Bensimon JL, Herman P (1994) Pathologie non tumorale du massif facial (TDM et IRM). In: *Encyclopédie Médico-Chirurgicale, Radiodiagnostic, Neuroradiologie–Appareil locomoteur*. Editions Techniques, Paris, 31–675-A-10
- Brant-Zawadzki MN, Minagi H, Federle MP, Rowe LD (1982) High resolution CT with image reformation in maxillofacial pathology. *AJR* 138:477–483
- Brasileiro BF, Vieira Cortez AL, Asprino L, Passeri LA, Moraes M de, Mazzonetto R, Fernandes Moreira RW (2005) Traumatic subcutaneous emphysema of the face associated with paranasal sinus fractures: a prospective study. *J Oral Maxillofac Surg* 63:1080–1087
- Cavalcanti MG, Haller JW, Vannier MW (1999) Three-dimensional computed tomography landmark measurement in craniofacial surgical planning: experimental validation in vitro. *J Oral Maxillofac Surg* 57:690–694
- Daffner RH (1997) Imaging of facial trauma. *Curr Probl Diagn Radiol* 26:153–184
- Daffner RH (1998) Imaging of facial trauma. *Semin Musculoskelet Radiol* 2:65–82
- De Lacey GJ, Wignall BK, Hussain S, Reidy JR (1977) The radiology of nasal injuries: problems of interpretation and clinical relevance. *Br J Radiol* 50:412–414
- Dolan KD, Jacoby CG (1978) Facial fractures. *Semin Roentgenol* 13: 37–51
- Dolan K, Jacoby C, Smoker W (1984) The radiology of facial fractures. *Radiographics* 4: 575–663
- Donat TL, Endress C, Mathog RH (1998) Facial fracture classification according to skeletal support mechanisms. *Arch Otolaryngol Head Neck Surg* 124:1306–1314
- Druelinger I, Guenther M, Marchand EG (2000) Radiographic evaluation of the facial complex. *Emerg Med Clin North Am* 18:393–410
- Dupuis MG, Dosch JC, Badoz A (1994) Imagerie des traumatismes du massif facial. In: *Encyclopédie Médico-Chirurgicale, Radiodiagnostic, Neuroradiologie–Appareil Locomoteur*. Editions Techniques, Paris, 31–652-B-10
- Gentry LR, Manor WF, Turski PA, Strother CM (1983a) High-resolution CT analysis of facial struts in trauma. 1. Normal anatomy. *AJR* 140:523–532
- Gentry LR, Manor WF, Turski PA, Strother CM (1983b) High-resolution CT analysis of facial struts in trauma. 2. Osseous and soft-tissue complications. *AJR* 140: 533–541
- Ghysen D, Ozsarlak O, van den Hauwe L, Van Goethem J, De Schepper AM, Parizel PM (2000) Maxillo-facial trauma. *JBR-BTR* 83:181–192
- Hermans R, Van der Goten A, De Foer B, Baert AL (1997) Imaging of maxillo-facial trauma. *JBR-BTR* 80:25–29
- Hohlrieder M, Hinterhoelzl J, Ulmer H, Hackl W, Schmutzhard E, Gassner R (2004) Maxillofacial fractures masking traumatic intracranial hemorrhages. *Int J Oral Maxillofac Surg* 33:389–395
- Holmgren EP, Dierks EJ, Assael LA, Bell RB, Potter BE (2005) Facial soft tissue injuries as an aid to ordering a combination head and facial computed tomography in trauma patients. *J Oral Maxillofac Surg* 63:651–654
- Kassel EE, Noyek AM, Cooper PW (1983) CT in facial trauma. *J Otolaryngol* 12:2–15
- Kirshenbaum KJ, Nadimpalli SR, Fantus R, Cavallino RP (1990) Unsuspected upper cervical spine fractures associated with significant head trauma: role of CT. *J Emerg Med* 8:183–198
- Krimmel M, Cornelius CP, Stojadinovic S, Hoffmann J, Reinert S (2001) Wooden foreign bodies in facial injury: a radiological pitfall. *Int J Oral Maxillofac Surg* 30: 445–447
- Le Fort R (1901a) Etude expérimentale sur les fractures de la mâchoire supérieure. *Rev Chir de Paris* 23:208–227
- Le Fort R (1901b) Etude expérimentale sur les fractures de la mâchoire supérieure. *Rev Chir de Paris* 23:360–379
- Le Fort R (1901c) Etude expérimentale sur les fractures de la mâchoire supérieure. *Rev Chir de Paris* 23:479–507
- Laine FJ, Conway WF, Laskin DM (1993) Radiology of maxillo-facial trauma. *Curr Probl Diagn Radiol* 22:145–188
- Lewandowski RJ, Rhodes CA, McCarroll K, Hefner L (2004) Role of routine nonenhanced head computed tomography scan in excluding orbital, maxillary, or zygomatic fractures secondary to blunt head trauma. *Emerg Radiol* 10:173–175
- Linnau KF, Hallam DK, Lomoschitz FM, Mann FA (2003) Orbital apex injury: trauma at the junction between the face and the cranium. *Eur J Radiol* 48:5–16
- Lund E, Halaburt M (1982) Irradiation dose to the lens of the eye during CT of the head. *Neuroradiology* 22:181–184
- Mauriello JA Jr, Lee HJ, Nguyen L (1999) CT of soft tissue injury and orbital fractures. *Radiol Clin North Am* 37:241–252
- Muraoka M, Nakai Y (1998) Twenty years of statistic and observation of facial bone fracture. *Acta Otolaryngol (Suppl)* 538:261–265
- Myers JC, Okoye MI, Kiple D, Kimmerle EH, Reinhard KJ (1999) Three-dimensional (3D) imaging in post-mortem examinations: elucidation and identification of cranial and facial fractures in victims of homicide utilizing 3D computerized imaging reconstruction techniques. *Int J Legal Med* 113:33–37
- Novelline RA, Rhea JT, Rao PM, Stuk JL (1999) Helical CT in emergency radiology. *Radiology* 213:321–339

- Noyek AM, Kassel EE, Wortzman G, Jazrawy H, Greyson ND, Zizmor J (1983) Contemporary radiologic evaluation in maxillofacial trauma. *Otolaryngol Clin North Am* 16:473–508
- Nunez DB, Zuluaga A, Fuentes-Bernardo DA, Rivas LA, Becerra JL (1996) Cervical spine trauma: How much more do we learn by routinely using helical CT? *Radiographics* 16: 1307–1318
- O'Hare TH (1991) Blow-out fractures: a review. *J Emerg Med* 9:253–263
- Pfeiffer RL (1943) Traumatic enophthalmos. In: *Adv Ophthalmic Plast Reconstr Surg* (1987) 6:301–312
- Preda L, La Fianza A, Maggio EM di, Dore R, Schifino MR, Mevio E, Campani R (1998) Traumi complessi del massiccio facciale: apporto diagnostico dell'imaging TC multiplanare e tridimensionale ottenuto con tecnica spirale. 96:178–184
- Rhea JT, Rao PM, Novelline RA (1999) Helical CT and three-dimensional CT of facial and orbital injury. *Radiol Clin North Am* 37:489–513
- Rogers LF (1982) *Radiology of skeletal trauma*. Churchill Livingstone, New York, pp 229–271
- Schultz RC (1967) Facial injuries from automobile accidents: a study of 400 consecutive cases. *Plast Reconstr Surg* 40:415–425
- Schultz RC, de Villers YT (1975) Nasal fractures. *J Trauma* 15: 319–327
- Smith B, Regan F (1957) Blow-out fracture of the orbit: mechanism and correction of internal orbital fracture. *Am J Ophthalmol* 44:733–739
- Thai KN, Hummel RP III, Kitzmiller WJ, Luchette FA (1997) The role of computed tomographic scanning in the management of facial trauma. *J Trauma* 43:214–217
- Tonami H, Nakagawa T, Ohguchi M, Takarada A, Yamamoto I, Karino K, Sasaki K (1987) Surface coil MR imaging of orbital blow-out fractures: a comparison with reformatted CT. *AJNR* 8:445–449
- Tonami H, Yamamoto I, Matsuda M, Tamamura H, Yokota H, Nakagawa T, Takarada A, Okimura T (1991) Orbital fractures: surface coil MR imaging. *Radiology* 179:789–794





# Imaging of Spinal Injuries

H. Imhof

## 2.5

### Contents

2.5.1 Introduction	141
2.5.2 Injury Assessment and Imaging	142
2.5.3 Imaging	142
2.5.4. Classification	144
2.5.4.1 Cervical Spine	144
2.5.4.2 Thoracolumbar Spine	146
2.5.4.3 Cervical Spine Fractures	148
2.5.4.4 Special Cervical Spine Fractures	150
2.5.4.5 Thoraco-Lumbar Spine Fractures	151
References	154

### 2.5.1 Introduction

In the European Union, there are over 130,000 victims of severe spinal injuries each year; about 15,000 involve the cervical spine. It has been shown that 23–57% of spinal fractures are missed by standard radiography compared to

multi-detector (multi-slice) CT, and there are already many advocates who stress that in severe spinal trauma MDCT should be the first imaging modality (Hauser et al. 2003; Boehm et al. 2004).

There are two key objectives of the clinical–radiological assessment. The first is to ascertain the presence of spinal and eventually concomitant injuries. Up to 47% of patients with severe spine trauma have associated injuries: 26% with head injuries; 24% with chest injuries; and 23% long-bone injuries. Approximately 10–14% of all spinal fractures and dislocations are associated with spinal cord injury. Injuries of the cervical spine are by far the ones most commonly associated with neurological deficit, occurring in about 40% of cases (Rogers 1982). In 85% of cases, cord injury occurs at the time of the accident, whereas 5–10% develop in the immediate post-injury period (Galanski and Wippermann 1999). The majority of spinal and cord injuries occur in the lower cervical spine and at the cervico-thoracic junction and thoraco-lumbar region (Fig. 1).

The second objective is to ascertain the presence of a neurological deficit. Neurological assessment can be performed according to the guidelines developed by the American Spinal Injury Association.

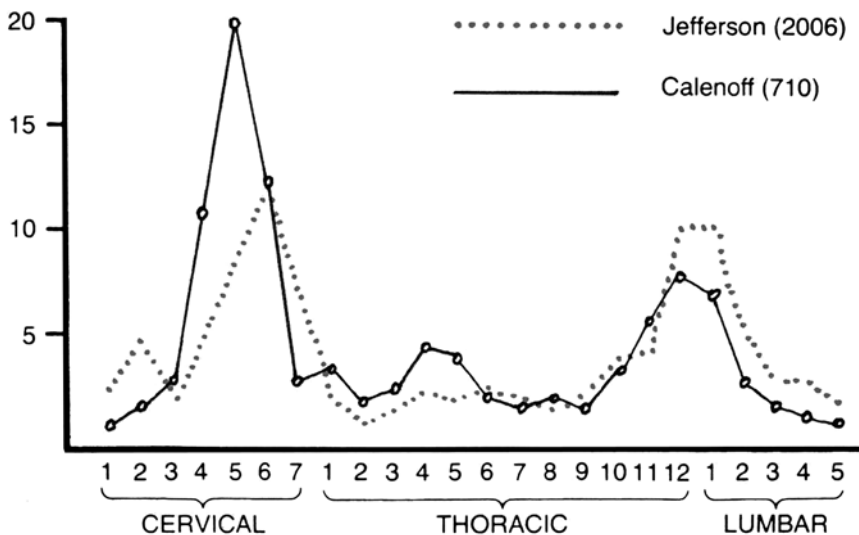


**Fig. 1.** Frequency of spinal fractures in correlation to segments

## 2.5.2 Injury Assessment and Imaging

Until about 2000 it was thought that in about 30–50% of patients, radiography alone could be diagnostic and that no further imaging is needed, provided that the clinical symptoms are in agreement with the imaging findings. The rest of the cases should be studied with cross-sectional imaging. Occult fractures, soft tissue injuries (cord, vessel, ligament, muscle, etc.), or bone marrow injuries should be best studied with MRI, and unclear calcifications or bony problems with CT. Any questionable findings on physical examination or plain radiographs should be thoroughly investigated because of the possible devastating sequelae of a missed injury.

The statements above are no more generally accepted, because MDCT has a much higher accuracy in fracture detection than conventional radiographs but costs much more per examination; therefore, to be most cost-effective with a high diagnostic yield, one should try to divide the incoming emergency patients in two groups, one with a low risk and a second group with a high risk. According to the Canadian National Emergency X-Radiography Utilization Study (NEXUS), patients who fulfill those first criteria have a low risk with a negative predictive value of 99.8% (Table 1; Dickinson et al. 2004).

Moreover, a prediction rule was developed consisting of three questions (“Canadian C-spine rule”; Stiell et al. 2003). According to these rules, the probability of (cervical) spine injury was extreme, and imaging was not at all indicated if the following three determinations were made: (a) the absence of a high-risk factor (age >65 years, dangerous mechanism, paraesthesia in extremities); (b) the presence of a low-risk factor (simple rear-end motor vehicle collision, sitting position in the emergency department, ambulatory at any time since injury, delayed onset of neck pain, or absence of midline cervical tenderness); or (c) the patient was able to rotate the neck actively 45° to the left and right.

On the other hand, high-risk patients are such – according to the so-called Harbourview Criteria – who have suffered a high-energy trauma (>50 kmh, fall from more than 3 m height, motor-vehicle crash with death at scene), or have high-risk clinical parameters such as significant head injury, neurological signs referable to the cervical spine, as well as pelvic or multiple-extremity fractures (Hanson et al. 2000).

Patients of the high-risk group must get a (MD)CT examination as first choice. Low-risk patients can be exam-

**Table 1.** NEXUS criteria for low-risk cervical spine fracture

- No midline cervical tenderness
- No focal neurological deficit
- Normal alertness
- No intoxication
- No painful, distracting inquiry

ined with conventional radiographs or just be observed clinically. If there is any unclear result with conventional radiographs, MDCT, or even MRI, must be used.

An indication for an additional MR examination exists also in all patients with an unclear neurological deficit and/or signs of instability and neurological problems.

## 2.5.3 Imaging

Conventional imaging (Harris and Mirvis 1996; Eustace 1999; Licina et al. 2005) starts with anteroposterior (AP), lateral, oblique, and in the cervical spine, with open-mouth views (three- or five-view plain-film series). A technically adequate lateral view of the cervical spine should include all seven cervical vertebrae and the T1–T4 vertebrae. This will allow the assessment of the four longitudinal lines:

1. A line connecting the anterior margins of the vertebral bodies
2. A line connecting the posterior margin of the vertebral bodies
3. The spinolaminar line joining the junctions of the laminae with the anterior margin of the spinous processes
4. A line joining the tips of spinous processes (Fig. 2)

On the AP view, a line connecting the tips of spinous processes should be perfectly straight (Fig. 3), and two lines connecting the outer borders of the vertebral bodies should be parallel. The distance between the middle line and the outer parallel lines must be equal. Anteroposterior and lateral views allow assessment of vertebral alignment, height of vertebral bodies, end plates, and disk spaces. (Attention should be paid to the integrity of the lateral vertebral body margins, pedicles, and posterior vertebral line!) Prevertebral soft tissue widening or mediastinal or paralumbar soft tissue widening are excellent positive clues for possible fractures, but normal soft tissues do not exclude a fracture.

The MDCT is the present standard examination in all high-risk patients. In many emergency centers, due to the advent of multi-detector CT, the CT examination has advanced from the “CHARLIE” time slot (first 30 min) to the initial 5-min (“BRAVO” slot) position and becomes much more time critical. In these cases the CT exam is started with the head and neck (slice thickness: 3 mm with collimation of 16×0.75 mm), continued by thorax and abdomen (slice thickness: 5 mm with collimation of 16×1.5 mm). During the second part of the exam contrast medium is applied intravenously (Boehm et al. 2004; Mutschlov and Kanz 2002). The CT helps in visualizing bony abnormalities, the spinal canal, facet joints, spinous processes, and spinal alignment. Bony fragments within the spinal canal can also be easily demonstrated (Table 2). Isotropic 3D or 2D sagittal and coronal reformations are an essential standard part of the CT examination.

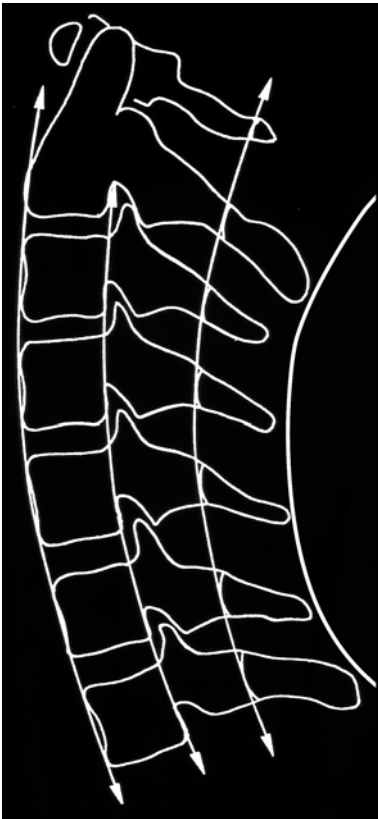


**Fig. 2.** The lateral cervical spine. *Parallel lines* are drawn along the anterior vertebral bodies, posterior vertebral bodies, and connecting the spinolaminar lines

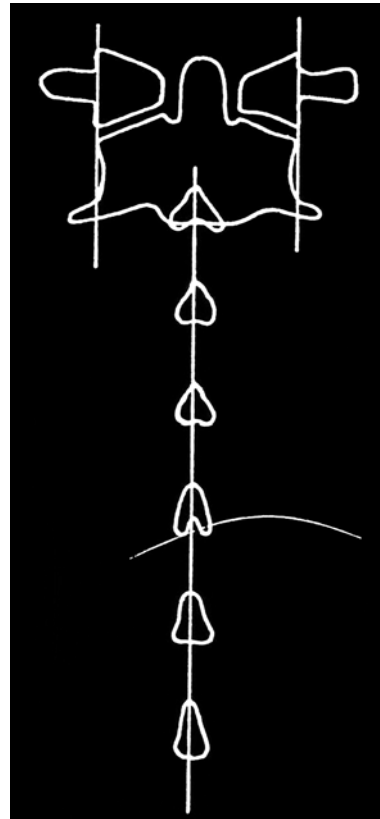


**Fig. 3.** Drawing of the anteroposterior cervical spine: a line through the spinous processes should be fairly straight

**Table 2.** Systematic inspection of the images in cervical spine trauma

Anatomical region	Pathology	CT (radiographs)	MRI
Alignment	Subluxation/dislocation	++	+
Spinal cord	Edema		++
	Swelling		++
	Hemorrhage	+	++
	Compression		++
	Dissection		++
Epidural space	Disk herniation	+	++
	Bone fragment	++	
	Hematoma	+	++
Spinal column	Vertebral body fracture	++	
	Posterior element fracture	++	
	Dislocation	++	
	Bony edema		++
	Spondylosis	++	
Ligaments	Anterior longitudinal ligament rupture		++
	Posterior longitudinal ligament rupture		++
	Interlaminar ligament (flava) rupture		++
	Supra- or interspinous ligament rupture		++
Vascular (+contrast)	Occlusion/dissection	+	+



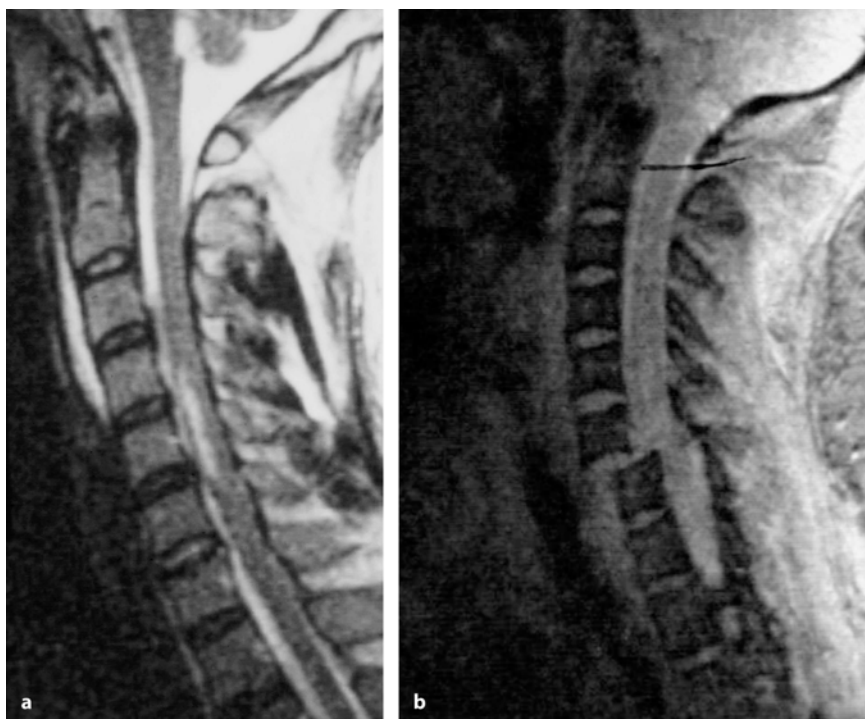


**Fig. 4.** **a** Sagittal, T2-weighted MRI of the cervical spine: hyperintense bleeding within the cord and paravertebral tissues. **b** Sagittal, proton-density-weighted MRI of the cervical spine: transection of the cervical spine and cord at C6/7

**Table 3.** Imaging protocol in severe spinal trauma (high-risk patients)

Question	Imaging procedure	
Trauma with spinal involvement?	MDCT	
Unclear bony fracture?	High-resolution MDCT	
Bony fragments?	High-resolution MDCT	
Facet joints?	High-resolution MDCT	
Spinal canal?	High-resolution MDCT	
Cord injury?	T1 SE MRI	sagittal
Epidural space?	T2 fast SE MRI	sagittal
Vascular supply?	T2 STIR MRI	sagittal
Disk herniation?	T2* GRE MRI	sagittal
Ligament/muscle rupture?	T1 SE MRI	axial
Bone marrow edema?	T2 fast SE MRI	axial

Patients with a neurological deficit are best studied with MRI, which is capable of demonstrating cord injuries (edema, hematoma, infarction, transection, disk herniations, rupture of ligaments, and/or muscles, nerve root disruption, and bone marrow edema; Fig. 4; Tables 2, 3).

When CT and MRI are available, we do not recommend open-mouth views or oblique views of the spine. The accuracy of CT and MRI are much higher than that of plain radiographs. Dynamic views (flexion and extension) are contraindicated in the acutely traumatized spine. In the unconscious high-risk patient, CT and MRI are often required. Myelography and CT-myelography are used only in cases where MRI is not available, and in rare questions of dural sac tears or nerve root problems.

## 2.5.4. Classification

Classification of spinal injury has great relevance. It facilitates communication among clinicians, assists in making treatment decisions, and aids in predicting outcome. It also provides a standardized language to assist research.

### 2.5.4.1 Cervical Spine

Unlike the thoracolumbar spine, the cervical spine does not lend itself to a single classification system. The atypical C0–C2 region necessitates separate consideration of differ-

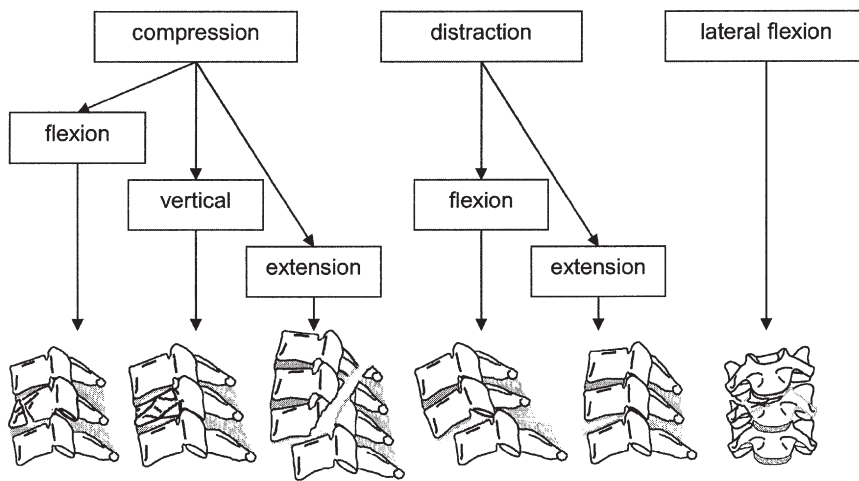


**Fig. 5.** A mechanistic classification of subaxial cervical injuries

ent injury patterns, including atlanto-occipital dissociations, occipital condyle fractures, fractures of the atlas, atlanto-axial rotatory instabilities, odontoid fractures, and traumatic spondylolisthesis of the axis. Fortunately, well-established and accepted classification systems exist for each of these injuries. In the subaxial cervical spine, it seems that the Allen and Ferguson classification system (Allen et al. 1982) is most widely used. It is mechanistic and divides injuries into six groups, each named according to the dominant force leading to failure and the presumed position of the head at the time of injury (Fig. 5). Each phylogeny has a number of stages, representing increasing

severity of injury. Adoption of the classification system can facilitate communication and minimize confusion, avoiding ill-defined terms such as teardrop injury (which can refer to highly unstable flexion-compression injury or a more benign extension-avulsion injury). It can improve injury assessment by ensuring that fracture patterns are carefully scrutinized in order to classify them.

For example, the less common extension/compression-type injury can often be confused with a flexion-distraction (facet dislocation) injury, as both result in a forward displacement of the cephalad vertebra, but these injuries behave quite differently and require different treatment approaches. Attempts have been made to apply the concepts of the AO thoracolumbar classification to the cervical spine to gain the benefits of a hierarchical classification that reflects increasing injury severity and helps dictate treatment; however, because of inherent differences between the two anatomical regions, there are limitations of this approach and the classification has not been widely accepted.

**Table 4a.** Radiographic findings of cervical spine instability

<ul style="list-style-type: none"> <li>- Widened interspinous space or facet joints &gt;50%</li> <li>- Anterior listhesis &gt;3.5 mm</li> <li>- Narrowed or widened disc space</li> <li>- Focal angulation of more than 11°</li> <li>- Vertebral compression more than 50%</li> </ul>
---

**Table 4b.** Functional classification of cervical spine fractures and dislocations

Mechanism of injury	Type	Stable	Unstable
Hyperflexion	Anterior subluxation (sprain)	+	
	Bilateral interfacetal dislocation		+
	Simple wedge fracture	+	
	Clay-shoveler's fracture	+	
	Teardrop fracture		+
	Odontoid fracture	+	+
Hyperextension	Dislocation (sprain or strain)	+	
	Avulsion fracture of the posterior arch of C1	+	
	Fracture of the posterior arch of C1	+	
	Teardrop fracture of C2	+	
	Laminar fracture		+
	Hangman's fracture		+
Vertical compression	Fracture or dislocation		+
	Jefferson's fracture		+
	Burst fracture	+	

Nevertheless, still in many centers, biomechanical concepts with additional diagnostic signs for instability are used (Table 4a,b).

#### 2.5.4.2 Thoracolumbar Spine

There are two classification systems in common use, the Denis system and the AO classification (modified Magerl's classification). The Denis system (Denis 1983), based on the concept of the three-column spine, became a near-universal standard after its introduction, and remains so in many parts of the world (Table 5). It divides major spinal injuries into four categories: compression; burst; seat-belt type; and fracture dislocation. The advantage of the Denis system is that it uses familiar descriptive terms, making it easier to remember. But it has a number of disadvantages. The middle column upon which it is based is a conceptual rather than an anatomical structure, consisting of the posterior longitudinal ligament and the posterior part of the vertebral body and annulus. While some studies support its significance in determining spinal stability (Panjabi et al. 1995), others have found that the integrity of the posterior elements is more important (James et al. 1994). Another disadvantage is that it is not hierarchical, with no pattern of increasing injury severity within or across groups. This decreases its value in assisting with treatment decisions or outcome prediction. It does not specifically recognize the burst fracture with posterior bony or ligamentous injury, the presence of which has important treatment implications. Because of this lack of clarity in many centers additional signs for instability are used (Table 6).

The thoracolumbar injury classification adopted by AO was developed in 1994 (Magerl et al. 1994). As with other AO classifications, it is hierarchical, and based on an al-

phanumerical grid (e.g., A.1.2.3). It is mechanistic rather than descriptive, and unlike the Denis system, is based on two columns, the anterior compression-resistant vertebral body and the posterior elements that resist tension. The distinctions between and within the three groups (types A–C) reflect injury severity and guide treatment (Table 7). “A”-type fractures are compression injuries to the anterior column. They may be crush fractures (A1), split fractures (A2), or burst fractures (A3), but the posterior tension band is intact. “B”-type injuries are distraction injuries. The fact that the posterior tension band is disrupted is important. In B1 injuries, the posterior disruption is primarily ligamentous, and B2 injuries involve posterior bony dis-

**Table 5.** Components of the three columns of the thoraco-lumbar spine (Denis)

Column	Components
Anterior	Anterior longitudinal ligament Anterior annulus fibrosus Anterior two-thirds of vertebral body
Middle	Posterior one-third of vertebral body Posterior annulus fibrosus Posterior longitudinal ligament
Posterior	Posterior elements Facet capsules Interlaminar ligaments (flava) Supra- or interspinous ligaments

**Table 6.** Radiographic findings of thoraco-lumbar spine instability

- Fracture dislocation >25%
- Posttraumatic kyphosis >30°
- Additional sternal/rib fractures
- >2-mm difference in ventral body height

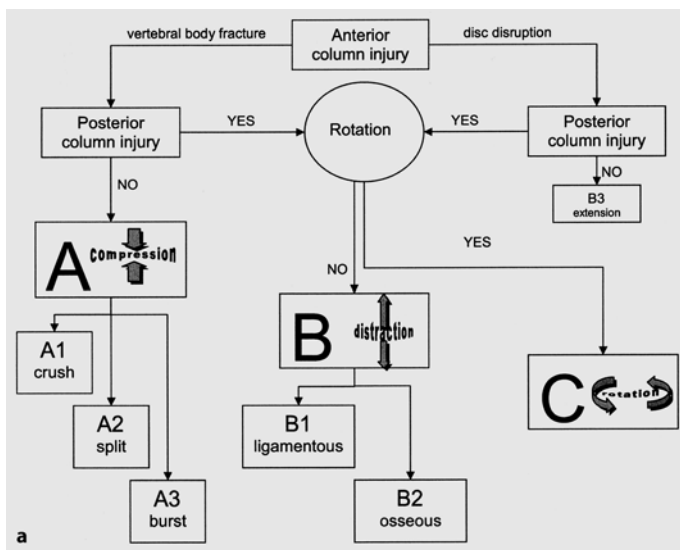
**Table 7.** Radiological signs of type-A/type-B/type-C injuries of the thoraco-lumbar spine according to AOT (Magerl)

Type-A injury	
<b>Compression fracture</b>	Reduction of vertebral body height
A1 impaction fracture	Body splitting
A2 splitting fracture	Enlarge interpedicle distance
A3 chest fracture	Intraspinous fragments
<b>Type-B injury</b>	
<b>Distraction fracture</b> (injury of body and dorsal parts with distraction)	Enlarged spinous process distance
B1 dorsal, ligament tear	Luxation/subluxation of the facet joints
B2 dorsal, osseous tear	Overhanging dorsal edge
B3 ventral, tear-through disk	Transverse fracture
	Fragments of dorsal body rim
<b>Type-C injury</b>	Lateralization of body
<b>Torsion injury</b> (injury of body and dorsal parts with rotation)	Pedicle asymmetry
C1 type-A injury with rotation	Dislocation of spinous process
C2 type-B injury with rotation	Fracture of transverse process
C3 rotation and shearing	One-sided luxation/subluxation
	Fracture of dorsal ribs
	Unilateral Fracture
	Exarticulation

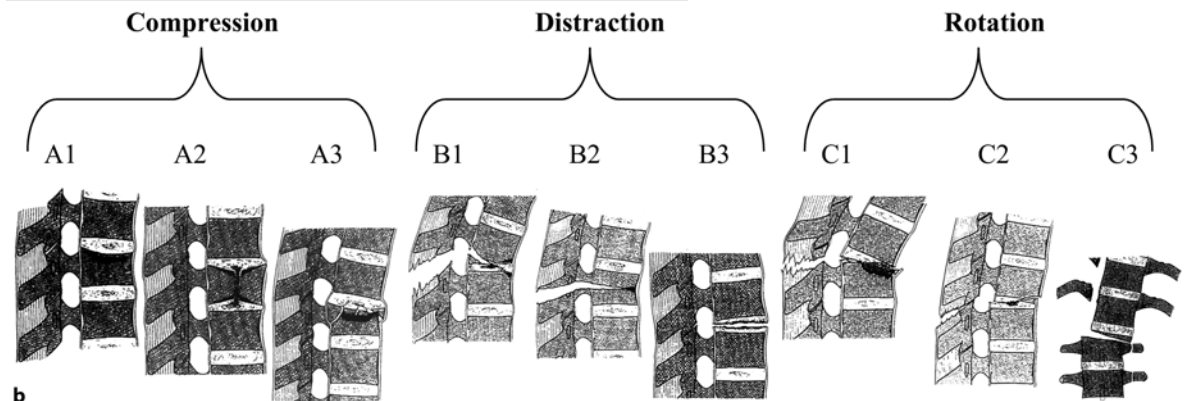
ruption. Both B1 and B2 injuries also involve the anterior column, and do so in one of two ways: the first is with disruption of the disc, and the other is with an A3 burst-type injury to the vertebral body. It is vital to distinguish this B-type “complex” burst fracture with posterior disruption from the more stable “simple” A3 burst fracture, as added disruption of the posterior tension band has important treatment implications. This distinction is often overlooked, especially if the injury is ligamentous. Its presence is suggested by local tenderness and swelling with a palpable gap on examination, eventually increased interspinous distance on plain X-ray and sagittal reformatted CT scan, and increased posterior soft tissue signal intensity on sagittal T2-weighted MRI. A B3 injury is a rare extension

injury through the disc. This is the exception to the rule, where the posterior column may be intact. “C”-type injuries are high-energy injuries to both anterior and posterior columns with associated rotation. They are subclassified according to whether they are primarily A-type injuries with rotation (C1), B-type injuries with rotation (C2), or rotational shear injuries (C3).

While precise classification of fractures using the AO system is useful for research, use of the classification at a more basic level, by understanding the fundamental concepts and using a simple algorithm to determine the broad groups, makes the system a very useful clinical tool (Fig. 6; Licina et al. 2005).



**Fig. 6. a** Algorithm for classifying thoracolumbar injuries according to the AO comprehensive classification. **b** Actual spinal injuries. The AO classification with the three types of subtypes: A compression; B distraction; and C rotation





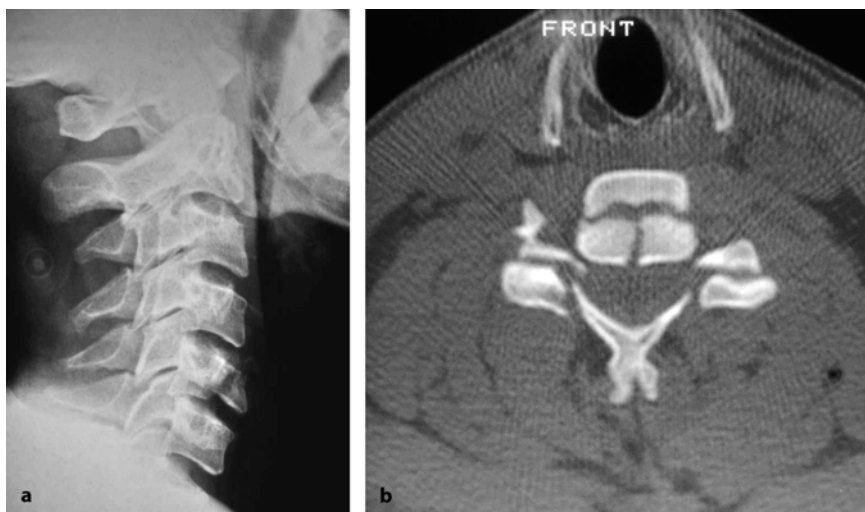


**Fig. 7.** Flexion teardrop (burst) fracture of  $C_5$ . **a** Lateral radiograph of the cervical spine shows the teardrop fragment anteriorly. **b** Axial CT shows vertebral-body fractures and dislocation of the facet joints

### 2.5.4.3 Cervical Spine Fractures

In the cervical spine, concepts to guide treatment exist but are not as clearly defined as in the thoraco-lumbar spine by the classification system. In general, injuries involving both the anterior and posterior columns require surgical stabilization, especially if they involve the soft tissues (i.e., the disc anteriorly and the ligaments posteriorly). Examples are high-grade flexion-compression (flexion teardrop) fractures and flexion-distraction injuries (bifacetal dislocations).

Flexion-compression fractures are usually treated with anterior vertebrectomy and plate fixation. Bifacet dislocations may be treated with anterior discectomy and fusion, or posterior fixation alone. In some cases where there is gross circumferential soft tissue disruption, anterior and posterior fixation may be indicated.

According to the basic mechanics, four different fracture types can be differentiated (Table 4b). Signs of instability should be included in each report (Table 4a).

#### Hyperflexion Injuries

Flexion injury of the cervical spine results in anterior rotation or translation of a vertebra segment in the sagittal plane. This injury is caused by direct trauma to the head and neck while they are in a flexed position, or by other forces that cause hyperflexion of the cervical spine.

Prominent features of flexion injuries are disruption of the posterior ligamentous complex: the interlaminar ligaments; the facet-joint capsules; and the posterior part of the annulus fibrosus. In the acute phase, the injury is stable, although the incidence of delayed instability is high, varying from 20 to 50%. Hyperflexion injuries are commonly associated with acute disc herniation. The flexion teardrop fracture is caused by severe flexion and axial loading. The



**Fig. 8.** Sagittal, T2-weighted MRI of the cervical spine: anterior subluxation of  $C_2$  on  $C_3$  with disc herniation and cord compression. Severe edema and bleeding in the dorsal spinal parts and soft tissues

posterior and anterior ligaments as well as the disc are disrupted. An anterior inferior corner fracture of the vertebral body is typically present. Cord injury is commonly associated with flexion teardrop fracture (Figs. 7, 8). The clay-shoveler's fracture, the simple wedge fracture tends to be stable, whereas the bilateral interfacetal dislocation and teardrop fracture are unstable.



**Fig. 9.** Bilateral facet-joint dislocation with anterior subluxation of C<sub>5</sub> on C<sub>6</sub>

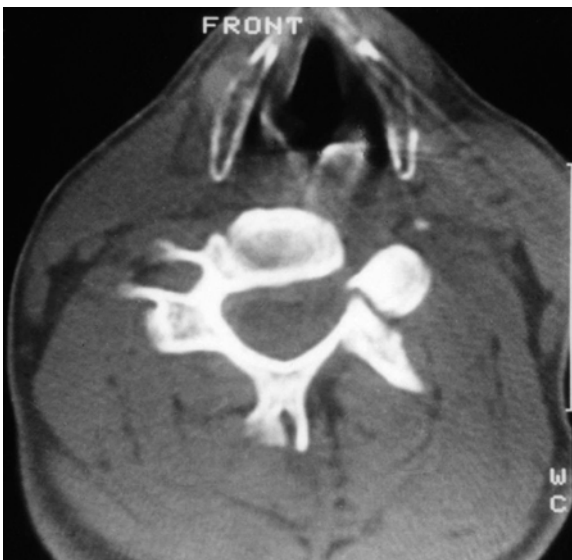


**Fig. 10.** Axial CT section shows left-sided facet joint fracture/dislocation

When a significant rotational component accompanies hyperflexion, unilateral or bilateral facet dislocation may occur. The vertebral body of the dislocated vertebra is anteriorly displaced. Widening of the interspinous process distance is present and the articulating facets are no longer in opposition (Figs. 9, 10).

### Hyperextension Injuries

Extension injury of the cervical spine results in posterior rotation or translation of the injured vertebral segment in the sagittal plane. It often results from an anterior impact to the face, or forehead, or from sudden deceleration (Fig. 11). The facial trauma often gives a clue to the hyperextension mechanism. Rupture of the anterior longitudinal ligament is frequently accompanied by disruption of the intervertebral disc. An avulsion fracture of the anterior arch of the atlas and small-extension teardrop fractures can be seen in C<sub>2</sub> and C<sub>3</sub> with hyperextension injuries.

In the more severe hyperextension injuries, two columns are disrupted, with resultant instability. Such fractures include the hangman's fracture, which involves the pars interarticularis in C<sub>2</sub> and adjacent structures (Fig. 12). Effendi et al. (1981) classified the hangman's fractures into three types, depending on the location of the fracture. Most commonly, this fracture occurs in frontal car accidents where the driver and/or co-frontal passenger are not using their seat belts. When the C<sub>2</sub>-C<sub>3</sub> disc ruptures with extension into the anterior and posterior longitudinal ligaments, anterior subluxation of C<sub>2</sub> on C<sub>3</sub> occurs, indicating instability. Hyperextension injuries assume great importance in patients with ankylosing spondylitis, and in patients with congenital or acquired cervical stenosis.

### Vertical Compression

Axial loading of the cervical spine results from forces transmitted through the skull and occipital condyles to the cervical spine. Typical representatives are atlas fractures and the Jefferson fracture, and burst fractures of the lower cervical spine (Fig. 13). The Jefferson fracture, which is a special atlas fracture, consists of simultaneous disruption of the anterior and posterior arches of C<sub>1</sub> with or without disruption of the transverse atlantal ligament. Identification of transverse ligament disruption, with resultant atlanto-axial instability, is crucial in the thorough evaluation of this injury. An overhang (i.e., lateral displacement) of the lateral masses of C<sub>1</sub> on the lateral masses of C<sub>2</sub> greater than 7 mm implies instability due to tearing of transverse ligament. Two-dimensional coronal CT reformation can illustrate the overhang of the C<sub>1</sub> lateral masses.

Atlas fractures which include only the anterior or posterior parts are stable, however.

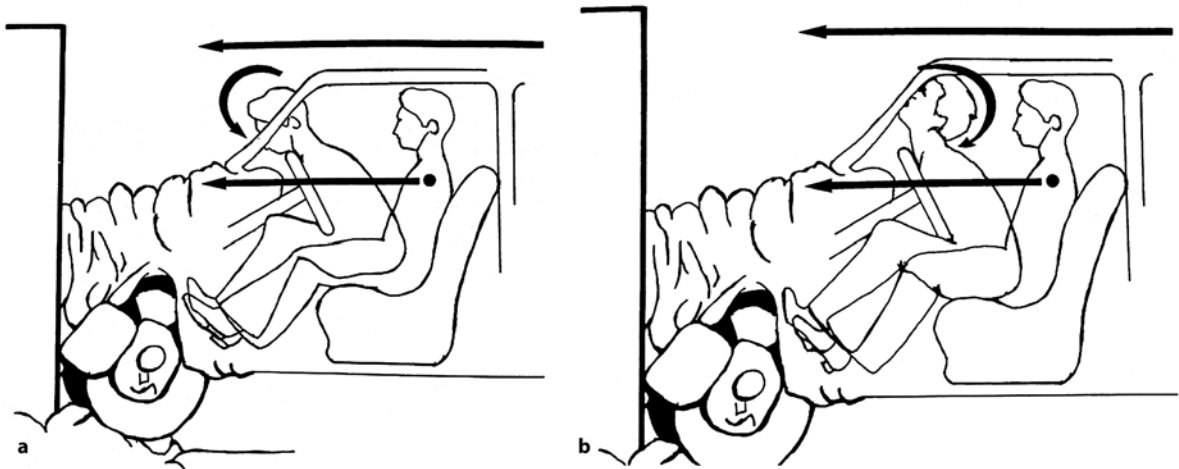


**Fig. 11.** Drawing of a frontal car collision. There are anterior-flexion forces on the head (a) and hyperextension forces (b)

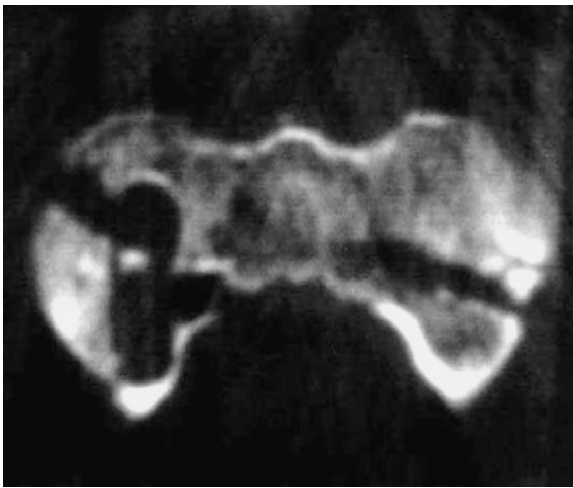


**Fig. 12.** Hangman's fracture (C2 hyperextension fracture)

#### 2.5.4.4 Special Cervical Spine Fractures

Odontoid fractures are the most frequent injury in the atlanto-axial region. The mechanism of injury in odontoid fractures is not well understood. Hyperflexion is believed to play a major role. Anderson and D'Alonzo (1974) classified odontoid fractures into three types based on the location of the fracture (Figs. 14, 15): type I is a stable avulsion fracture of the tip of the dens. Some authors believe that this type is not existent; type II is the most common odontoid fracture, and it represents a transverse unstable fracture at the base of the dens. Displacement of the fractured dens is frequent and the incidence of non-union is high; in type III, the fracture line extends into the superior body of C<sub>2</sub> and is unstable.

Atlanto-occipital dissociations (complete or incomplete) are rare and in many cases deadly. Imaging should be

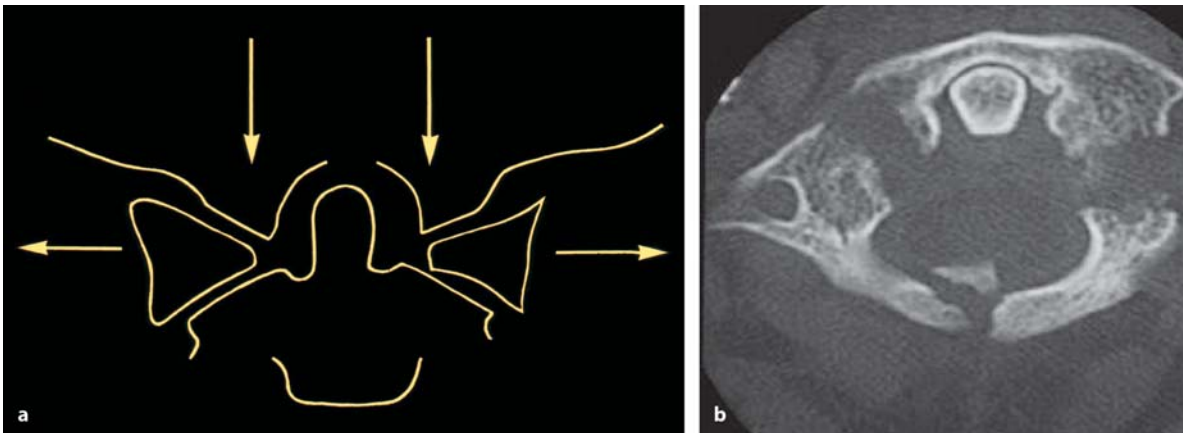


**Fig. 13.** Jefferson fracture. a Drawing with lateral overlay of the atlas. b Axial CT with fracture of the anterior and posterior arches (Jefferson fracture)

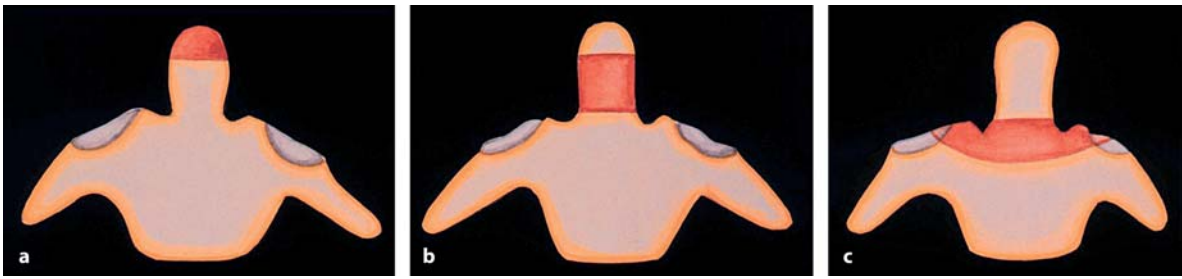


**Fig. 14.** Three types of odontoid process fractures. **a** Avulsion fracture of the tip of the odontoid process. **b** Fracture through the base of the odontoid process. **c** Fracture through the body of C<sub>2</sub>

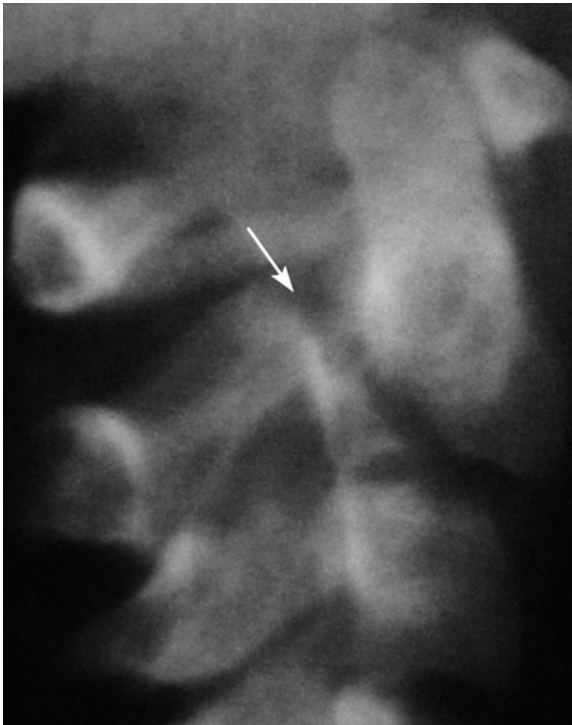


**Fig. 15.** Lateral tomogram: odontoid fracture (*arrow*), type III

done by CT when diagnosis is evident. Condylar fractures, which are burst fractures, are not so uncommon as previously thought. They are unstable if there is extension into the condylus and/or there is an avulsion of the alar ligament. An arterial involvement should be suspected in all cases.

#### 2.5.4.5 Thoraco-Lumbar Spine Fractures

In the thoracolumbar spine, the AO classification system provides some guidelines for surgery. Some fractures are clearly stable (such as A1 crush fractures) and some are highly unstable (such as C3 rotational shear injuries); how-

ever, there is a gray zone between these extremes that encompasses injuries such as severe A3 burst fractures, which are stable except for a compressive force, and undisplaced B2 bony Chance-type fractures, which are unlikely to further displace. This concept is schematically demonstrated in Fig. 16. In almost all cases, C fractures require surgical stabilization; the majority require anterior and posterior fixation to resist translation and shear. Most B fractures should also be considered for surgery. The posterior tension band is disrupted, reducing resistance to flexion and predisposing to kyphosis. Surgery usually involves reconstructing the tension band with posterior instrumentation. Occasionally, minimally displaced primarily osseous injuries can be treated with an orthosis.

Based on anatomy and biomechanisms, the thoracic and lumbar spine can be divided into three segments: T<sub>1</sub>-T<sub>10</sub>; T<sub>11</sub>-L<sub>4</sub>; and L<sub>5</sub>.

The upper thoracic spine or T<sub>1</sub>-T<sub>10</sub> is the largest and most rigid segment of the spine. About 10-20% of all spinal fractures occur in the upper thoracic spine. The T<sub>1</sub>-T<sub>10</sub> segment is distinguished by the presence of the rib cage, which restricts motion and adds stiffness and stability to the spine. To produce a fracture in the upper thoracic spine, considerable energy is required and, therefore, such injuries are often associated with non-contiguous vertebral fractures (Qaiyum et al. 2001). Sixty-three percent of patients with upper thoracic spine trauma present with neurological deficit due to spinal cord injury (Rogers et al. 1980). The cord damage is believed to be due to the relatively small canal size and reduced blood supply to the mid-thoracic cord (Bohlman 1985).

There are two conditions which can mimic vertebral fractures: physiological wedging and Scheuermann's disease. Physiological wedging is most pronounced in the lower thoracic spine and is especially common in males. A wedging ratio of 0.80 in males and 0.87 in females, at T<sub>8</sub> to T<sub>12</sub> levels, is considered within normal limits (Lauridsen et al. 1984).

The other mimicker of vertebral fractures is Scheuermann's disease, where an abnormality of vertebral growth cartilage results in vertebral wedging which persists into adulthood. In the setting of trauma, this deformity can be easily confused with a compression fracture.



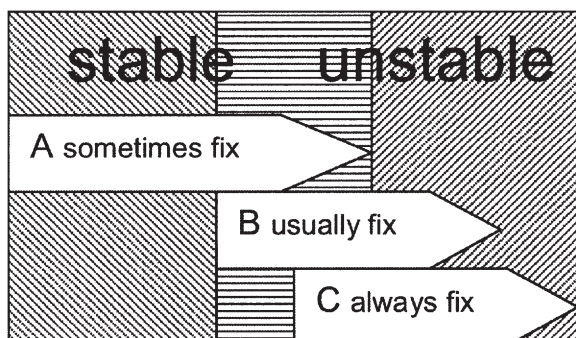


**Fig. 16.** Stability of thoracolumbar fractures according to AO classification and indications for surgical stabilization

Spines that are fused by diseases such as ankylosing spondylitis, diffuse skeletal hyperostosis (DISH), or severe degenerative disc disease with bridging osteophytes are considered separately. Fractures in this group are very unstable since all three columns are disrupted. The mechanism is due to hyperextension and they can occur from relatively minor trauma (Weinstein et al. 1982).

According to the biomechanics, four fracture types can be differentiated in the thoraco-lumbar spine, as described below.

### Compression Fracture

Compression fracture is a common fracture accounting for about half of all thoracolumbar junction injuries. Compression fractures represents failure of the anterior column while the middle column remains intact. The posterior column can remain intact or it may fail in tension. The mechanism of injury is due axial loading acting on a flexed spine. The fracture typically involves the superior end plate of the vertebral body producing anterior wedging and disruption of the anterior cortex (Fig. 17).

### Burst Fractures

Burst fractures are relatively common. Nearly half of these fractures are associated with neurological deficit. They are characterized by either failure of the anterior and middle columns or of all three columns (Fig. 18). The majority of these fractures are associated with retropulsion of a bony fragment resulting in spinal stenosis. Burst fractures represent a dynamic event where the final position of the retropulsed fragment is not representative of the canal stenosis that occurred during the injury (Wilcox et al. 2003).



**Fig. 17.** Cervical spine (lateral): anterior vertebral body compression of C7; straightening of the spine

### Flexion–Distraction Injuries (Chance Fracture)

Chance fracture is a rare injury resulting from hyperflexion where the axis of rotation is centered anterior to the spine (Vaccaro et al. 2003). The posterior and middle columns fail in tension while the anterior column fails either in tension or compression depending on whether the axis of rotation is at, or anterior to, the anterior column. The classical Chance fracture involves the bony elements of a single vertebra. It horizontally splits the spinous process, laminae, pedicles, and vertebral body. On the lateral radiograph, there is increased height of the vertebral body posteriorly, whereas the anterior portion of the vertebral body shows mild compression (Fig. 19). Chance fractures have a high association with intra-abdominal injuries (45%). About 15% of patients with these injuries suffer from a neurological deficit.

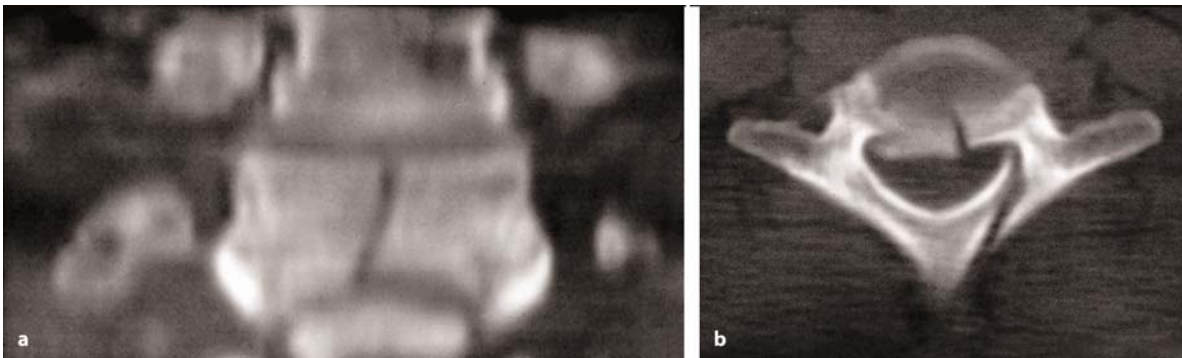


**Fig. 18.** **a** Coronal CT: burst fracture with compression of the vertebral body. **b** Axial CT: burst fracture with compression of the spinal canal



**Fig. 19.** Sagittal, T2-weighted fast-spin-echo MRI: Chance fracture (complete) with compression of the spinal cord (patient had neurological deficit)



**Fig. 20.** Sagittal reformation CT: dislocation with rotation of the facet joints C5/C6 (arrow)

### Fracture–Dislocation

Fracture dislocations represent one of the most serious spinal injuries. Of these fractures, 75% are associated with a neurological deficit. The mechanism of injury includes flexion with rotation, flexion with distraction, and shear forces. This injury is characterized by displacement of one vertebral body over an adjacent vertebral body resulting in horizontal translation or rotation at the level of the injury. Fracture dislocations are very unstable injuries since all three columns are disrupted. Radiography may demonstrate malalignment of the vertebral bodies and spinous processes. Facet dislocation is often seen in severe cases. Sagittal and coronal CT-reformatted images and 3D images are now routinely obtained for thorough evaluation of the extent of this injury (Fig. 20).

## References

- Allen BL Jr, Ferguson RL, Lehmann TR, O'Brien RP (1982) A mechanic classification of closed, indirect fractures and dislocations of the lower cervical spine. *Spine* 7:1–27
- Anderson LD, D'Alonzo RT (1974) Fractures of the odontoid process of the axis. *J Bone Joint Surg Am* 56:1663–1691
- Boehm T, Alkadhi H, Schertler T, Baumert B, Roos J, Marincek B, Wildermuth S, Mutschler W (2004) Einsatz der Mehrschicht-Spiral-CT beim traumatologischen Notfall und ihre Auswirkungen auf den Untersuchungs- und Behandlungsalgorithmus. *Fortschr Röntgenstr* 176:1734–1742
- Bohlman HH (1985) Treatment of fractures and dislocations of the thoracic and lumbar spine. *J Bone Joint Surg Am* 67:165–169
- Brown CV, Antevil JL, Sise MJ, Sack DI et al. (2003) Spiral computed tomography for the diagnosis of cervical, thoracic, and lumbar spine fractures: its time has come. *J Trauma* 58:890–896
- Denis F (1983) The three column spine and its significance in the classification of acute thoracolumbar spinal injuries. *Spine* 8:817–831
- Dickinson G, Stiell IG, Schull M, Brison R, Clement CM, Vandemheen KL, Cass D, McKnight D, Greenberg G, Worthington JR, Reardon M, Morrison L, Eisenhauer MA, Dreyer J, Wells GA. (2004) Retrospective application of the NEXUS low-risk criteria for cervical spine radiography in Canadian emergency departments. *Ann Emerg Med* 43:515–517
- Effendi B, Roy D, Cornish B, Dussault RG, Laurin CA (1981) Fractures of the ring of the axis: a classification based on the analysis of 131 cases. *J Bone Joint Surg Br* 63:319–327
- Eustace STJ (1999) Magnetic resonance imaging of orthopaedic trauma. Lippincott Williams and Wilkins, Philadelphia
- Galanski M, Wippermann B (1999) Kompendium der traumatologischen Röntgendiagnostik. Springer, Berlin Heidelberg New York
- Hanson JA, Blackmore CC, Mann FA et al. (2000) Cervical spine screening: a decision rule can identify high risk patients to undergo screening helical CT of the cervical spine. *AJR* 174:713–718
- Harris JH, Mirvis JH (1996) The radiology of acute cervical spine trauma. Williams and Wilkins, Baltimore
- James KS, Wenger KH, Schlegel JD, Dunn HK (1994) Biomechanical evaluation of the stability of thoracolumbar burst fractures. *Spine* 1:1731–1740
- Lauridsen KN, Carvalho A de, Andersen AH (1984) Degree of vertebral wedging of the dorso-lumbar spine. *Acta Radiol Diagn (Stockh)* 25:29–32
- Licina P, Nowitzke A, Panjabi MM, James R, Magerl W, Allen BL (2005) Approach and considerations regarding the patient with spinal injury. *Int J Care Injured* 36:S-B2-S-B12
- Magerl F, Allen BL Jr, Ferguson RL, Lehmann TR, O'Brien RP et al. (1994) A comprehensive classification of closed, indirect fractures and dislocations of the lower cervical spine. *Spine* 7:1–27
- Mutschler W, Kanz KG (2002) Interdisziplinäre Schockraumversorgung: Die Aufgaben der Radiologie aus unfallchirurgischer Sicht. *Radiologe* 42:506–517
- Panjabi MM, Oxland TR, Kifune M, Arand M, Wen L, Chen A (1995) Validity of the three-column theory of thoracolumbar fractures. A biomechanic investigation. *Spine* 15:1122–1127
- Qaiyum M, Tyrrell PN, McCall IW, Cassar-Pullicino VN et al. (2001) MRI detection of unsuspected vertebral injury in acute spinal trauma: incidence and significance. *Skeletal Radiol* 30:299–304
- Rogers LF (1982) Radiology of skeletal trauma. Churchill Livingstone, Edinburgh
- Rogers LF, Thayer C, Weinberg PE, Kim KS (1980) Acute injuries of the upper thoracic spine associated with paraplegia. *AJR* 134:67–73
- Stiell IG, Clement CM, McKnight RD, Brison R, Schull MJ, Rowe BH, Worthington JR, Eisenhauer MA, Cass D, Greenberg G, MacPhail I, Dreyer J, Lee JS, Bandiera G, Reardon M, Holroyd B, Lesiuk H, Wells GA (2003) The Canadian C-spine rule versus the NEXUS low-risk criteria in patients with trauma. *N Engl J Med* 25:2510–2518
- Vaccaro AR, Kim DH, Brodke DS, Harris M, Chapman JR, Schildhauer T, Routt ML, Sasso RC (2003) Diagnosis and management of thoracolumbar spine fractures. *J Bone Joint Surg Am* 85:2456–2470
- Weinstein PR, Karpman RR, Gall EP, Pitt M et al. (1982) Spinal cord injury, spinal fracture, and spinal stenosis in ankylosing spondylitis. *J Neurosurg* 57:609–616
- Wilcox RK, Boerger TO, Allen DJ, Barton DC, Limb D, Dickson RA, Hall RM et al. (2003) A dynamic study of thoracolumbar burst fractures. *J Bone Joint Surg Am* 85:2184–2189

## Imaging of Thoracic Injuries

G. Gavelli, G. Napoli, P. Bertaccini,  
G. Battista, R. Fattori

# 2.6

### Contents

2.6.1	Introduction	155
2.6.2	Clinical and Imaging Findings	156
2.6.2.1	Chest Wall Injuries	156
2.6.2.2	Parenchymal Lung Injuries	159
2.6.2.3	Extra-alveolar Air	162
2.6.2.4	Pleural Effusion and Hemothorax	163
2.6.2.5	Tracheobronchial Injury	164
2.6.2.6	Thoracic Esophageal Disruption	165
2.6.2.7	Diaphragmatic Injury	166
2.6.2.8	Blunt Cardiac and Pericardial Injury	169
2.6.2.9	Traumatic Aortic Injury	169
2.6.3	Conclusion	175
	References	176

### 2.6.1 Introduction

Traumatic injuries are the fourth cause of death in the United States and in Western Europe, and the first cause of death in population less than 45 years old. Thoracic trauma, which more frequently is a blunt trauma (70%), represents 10–15% of all traumas and is responsible for 25% of fatalities due to traumatic injuries.

The mortality rate of chest trauma ranges from approximately 15.5 to 77% if shock and head injuries (Glasgow score 3–4) are associated.

The accurate diagnosis of injuries related to thoracic chest trauma depends on a complete knowledge of the different clinical and radiological manifestations. Even though it is well known that it is less sensitive and accurate than computed tomography (CT), chest radiography, usually performed on supine position at the moment of hospital admission, represents the first diagnostic approach to patients sustaining blunt chest trauma. Moreover, many patients have very unstable clinical conditions which make it difficult to bring them to the radiology department, and therefore a chest X-ray, performed at the bedside of the patient with limitations due to poor positioning, poor inspiration, or artifacts related to overlying monitoring equipment, can be the only diagnostic tool in the evaluation of such patients.

Since the chest X ray is essential in providing information regarding life-threatening conditions, such as tension pneumothorax, hemothorax, flail chest, and mediastinal abnormalities, the radiologist must have deep knowledge of the possibilities and limits of this modality, which may not point out, or may underestimate, all these conditions.

Poor-quality radiographs are, therefore, not acceptable especially when it becomes difficult or impossible to exclude life-threatening conditions and an alternative imaging study should be performed.

In selected cases, it could be very useful to perform an additional lateral radiograph with horizontal incidence of the ray because the evaluation of pleural effusion, pneumothorax, and the identification of sternal fractures may be easier.

As mentioned previously, a CT study must be performed in all chest trauma patients in whom there is even the smallest diagnostic doubt on plain film.

Computed tomography has come to assume an increasingly important role in the evaluation of patients with known or suspected chest injuries. Chest CT is much more sensitive and accurate than chest plain film in the detection of almost all thoracic lesions, particularly those involving vessels, heart, pericardium, airways, mediastinum, and chest wall, including the spine and diaphragm.

Moreover, CT depicts more accurately the presence and the real extent of lung involvement as well as the entity of pneumothorax and/or pleural effusion, and has been shown to determine an impact on therapeutic treatment in a significant number of patients.

The recent introduction of multi-detector row CT (MDCT) has represented a real revolution in non-invasive evaluation of trauma patients offering many advantages in the imaging work-up strategy of these patients. The remarkable increase of acquisition speed, together with the possibility of a thinner collimation, provides a higher quality of the study, minimizing the motion artifacts and allowing the scanning of the same or larger volume of interest in less time with an increased temporal and spatial resolution. Such relevant increase in spatial resolution has also a great impact on post-processing multiplanar 2D and 3D reformations and volume-rendered images, often improving the final diagnosis.



Moreover the faster acquisition reduces the amount of contrast material needed to study both vascular structure and parenchymal organs.

For all these features, computed tomography of the chest is being increasingly used in the routine work-up of the trauma patients, which often includes scans of the brain and the abdomen.

Magnetic resonance imaging, despite some advantages (i.e., lack in ionizing radiation, no need for iodinated contrast medium), still has a limited role in evaluation of chest trauma, and angiography is being used less and less.

The use of ultrasound at the bedside of the patient is still not well defined in the study of the traumatized patients.

In the present chapter we present the principal radiological features which can be reported in patients who sustain blunt chest trauma.

## 2.6.2 Clinical and Imaging Findings

### 2.6.2.1 Chest Wall Injuries

Rib fractures are the most common finding after blunt chest trauma, with an incidence reported up to 40%. Chest radiograph has a low sensitivity (18–50%) in detecting rib fractures, and it is even more insensitive in showing costochondral fractures (Primak and Collins 2002; Tocino and Miller 1987).

Fractures of the ribs rarely have particular clinical significance but they are an indicator of the severity of trauma, especially in old patients with non-compliant chest wall. In fact, in elderly patients, complications occurs more frequently as the number of fractures increase, with a relative increase in mortality (Sirmali et al. 2003).

It is also very important to remember that, on the contrary, children's and young patients' ribs are more flexible, so the absence of rib or other skeletal injuries can be misleading since even severe trauma can occur without chest wall lesions (Sirmali et al. 2003).

In the majority of cases, ribs from IV to IX are involved after chest trauma. Fractures of the first two or three ribs and of the clavicle indicate a violent trauma since they are thicker and well protected by the thoracic muscles and can cause lesions of the brachial plexus or the supra-aortic vessels (3–15%; Fermanis et al. 1985). Study of the subclavian vessels must be carried out in emergency when bone fragments are widely dislocated, when there is evidence of mediastinal hemorrhage, extrapleural hematoma, and if neuropathy of the brachial plexus can be clinically demonstrated.

Moreover, these fractures are frequently associated with other chest lesions, and in particular, more than 90% of tracheobronchial lesions are associated with fractures of at least one of the first three ribs.

Finally, fracture of the lower ribs (IX–XII) can be associated with traumatic lesions of liver, spleen, and kidneys.

Rib fractures are often accompanied by focal extrapleural hematomas, which can be seen as a bulging of the soft tissue density convexly bordering the lungs.

An apical extrapleural hematoma which increases in dimensions is highly suggestive of active arterial bleeding and requires further investigation and eventually angiographic intervention.

Flail chest, the most severe lesion of the thoracic wall found in blunt chest trauma, is caused by a fracture of three or more ribs in at least two different sites (Fig. 1). A paradoxical movement of this flail segment of the thoracic wall occurs during respiratory cycle, which favors the onset of atelectasis and hinders physiological drainage of the bronchial secretions. This situation can lead to respiratory failure, especially if parenchymal injuries are associated, requiring intensive respiratory therapy.

The resulting morbidity and mortality rates depend on the age of the patient and the extension and gravity of the thoracic lesions associated (contusions and/or parenchymal lacerations, atelectasis, mediastinal lesions, hemothorax, pneumothorax, and associated extrathoracic lesions).

In 8–10% of blunt chest traumas, sternal fractures are found. It is a marker of a high-energy trauma and is related to a direct impact from the steering wheel or to the use of seat belts. The most common site of the sternal fractures is approximately 2 cm down from the manubrio-sternal joint (Figs. 2, 3). Sternal fracture usually cannot be diagnosed on frontal chest radiographs, whereas the lateral projections can detect it with high sensitivity.

Sternal fractures, especially those with dislocation of the “bony stump” (so-called displaced sternal fracture), can cause vascular lesions, mediastinal hemorrhage, and cardiac contusions, and therefore, carry a mortality ranging from 25 to 45%.

Spiral CT, with sagittal and coronal reformations, should be the examination of choice in the suspicion of sternal fracture, because it identifies with high accuracy both the fracture, especially that with minimal dislocation often unrecognized on conventional radiographs, and the associated lesions.

Inspection and palpation (Shanmuganathan and Mirvis 1999) generally suggest the presence of sternoclavicular fracture.

An anterior fracture, the most common, generally has no clinical significance, whereas a posterior fracture of the parasternal tract of the clavicle can cause lesions of the brachiocephalic vessels, nerves, esophagus, and trachea.

A scapular fracture is indicative of a high-energy trauma, since it is protected by the surrounding muscles. Scapular fracture is missed on chest radiograph in up to 43% of cases, and 72% of these fractures are visible evaluating retrospectively the initial radiographs.

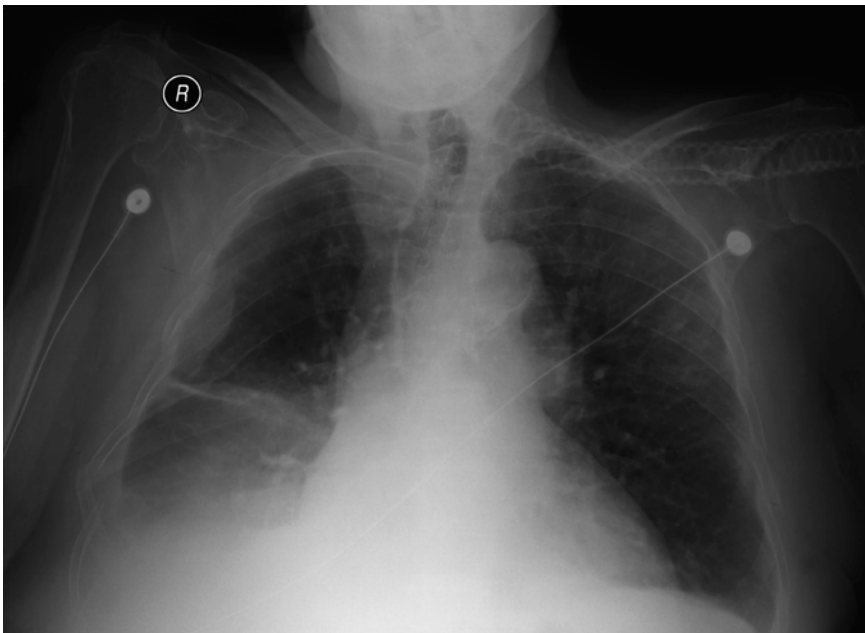


**Fig. 1.** Blunt trauma with chest wall injury. Supine chest X-ray shows multiple rib fractures in different points on the right (flail chest) with ipsilateral hemothorax and hematoma of the soft tissues surrounding the more cranial fractures

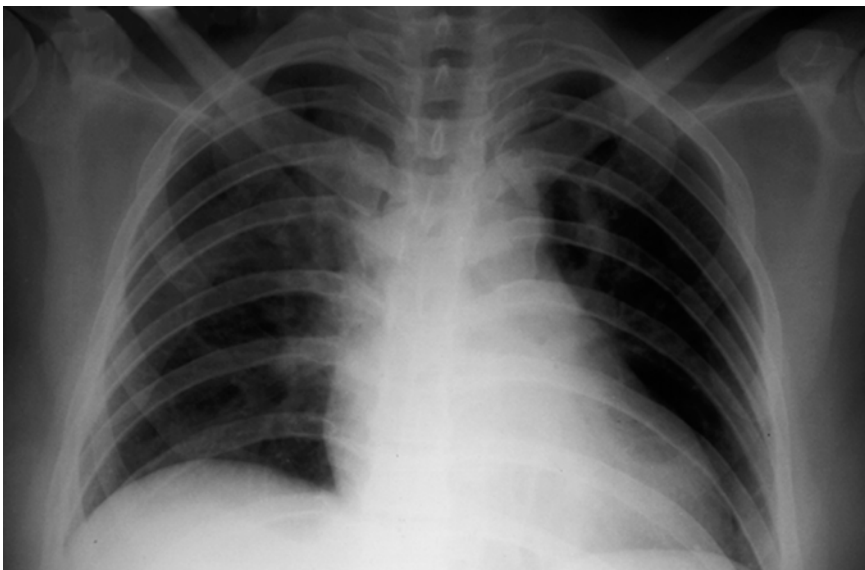


**Fig. 2.** Sternal fracture in a patient with blunt trauma of the anterior upper chest wall. Supine chest X-ray shows a slight widening of the superior mediastinum raising suspicion of mediastinal hematoma

Since large forces are needed to fracture the scapula, associated lesions (rib fractures, pneumothorax, hemothorax, or pulmonary contusions) are found in up to 40% of patients. Obviously, CT is more sensitive than chest radiographs in detecting both the fracture and the associated lesions.

A rare but serious traumatic lesion is the scapulo-thoracic dissociation. The diagnosis of this lesion is based on the finding of lateral dislocation of the scapula on a non-rotated frontal chest radiograph.

The displacement must be more than 2 cm from the line of the spinous processes with respect to the contralateral scapula and confirmed by more radiographs (Wicky et al. 2000).

In general, CT scans performed in order to evaluate the mediastinum demonstrate scapulo-thoracic dissociation with the lateral fracture of the scapula and better points out edema or surrounding hematomas. The patient can present, moreover, with brachial plexopathy and rupture of the sub-

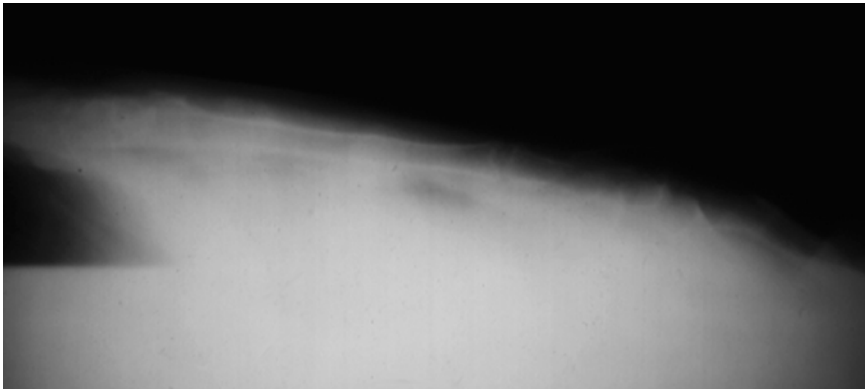


**Fig. 3.** Sternal fracture in a patient with blunt trauma of the anterior upper chest wall. A cross table lateral view of the same patient demonstrates a fracture of the sternal manubrium

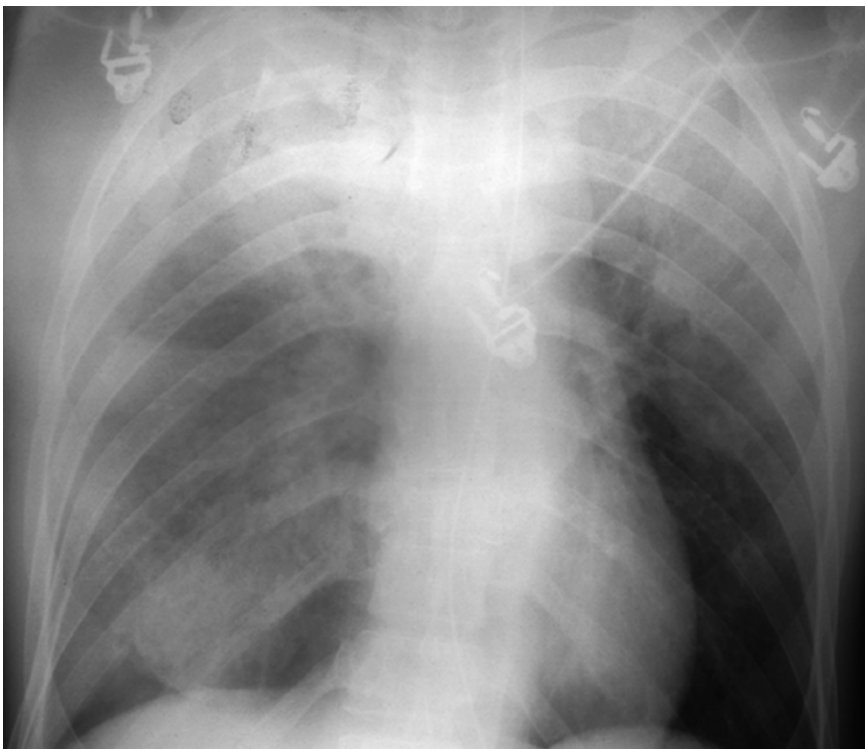


**Fig. 4.** Patient with paraplegia resulting from a motor vehicle accident. Supine chest X-ray shows reduced height of T9 associated with pleural effusion and multiple parenchymal contusions on both lungs

clavian or axillary artery, resulting in a potentially life-threatening hemorrhage needing angiographic intervention.

Fracture of the humerus, clavicle, and sternum are often associated. Pulmonary hernias, caused by associated lesion of the ribs, as well as intercostal and pectoral muscles and their fasciae, are rare. When small and non-strangulating, these hernias do not require surgical treatment and usually resolve spontaneously.

Fractures of the thoracic spine account for 25–30% of all spine fractures, and significant neurological deficits can be associated in up to 62% of patients, the highest incidence as

compared with fracture elsewhere in the spine. Most of these fractures are the consequence of hyperflexion or axial loading injuries since rotation is limited by the thoracic cage, especially in the upper portions (Rivas et al. 2003).

The chest radiograph usually is inadequate in detecting spinal fractures, especially those located in the upper portion, because the film can be difficult to interpret due to patient motion, overlying support lines, tubes, or anatomical structures, associated lesions, as well as the fact that the initial findings can be subtle (Rivas et al. 2003); however, radiological signs of thoracic spine fractures include corti-

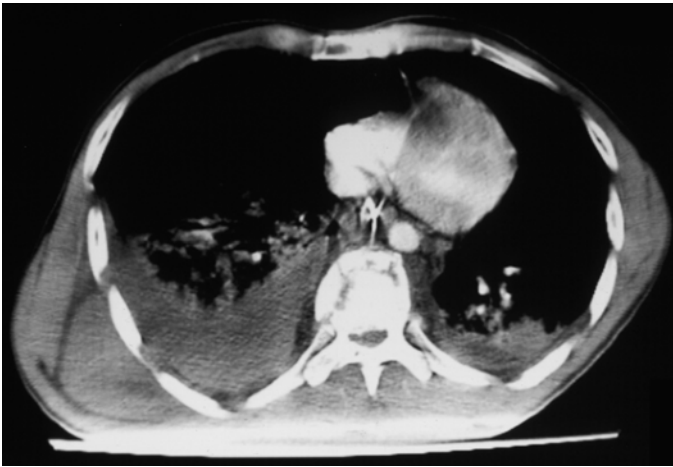


**Fig. 5.** Patient with paraplegia resulting from a motor vehicle accident. The CT scan confirms multifragment fracture of the body of T9, bilateral pleural effusion, and contusions, but also depicts a right pneumothorax not visible on plain chest film



**Fig. 6.** Same as Fig. 5

cal disruption, abnormal alignment, deformity, and/or height loss of vertebral bodies, mediastinal opacities, and/or widening of paraspinal lines.

Computed tomography is the most suitable method for evaluating spinal fractures and should be obtained with sagittal and coronal reformations in order to define the type of fracture and its stability (Figs. 4–6; Lomoschitz et al. 2003; Mirvis 2004; Rivas et al. 2003; Thoongsuwan et al. 2005).

Even if it is not usually performed, especially in the acute phase due to imaging time and difficult monitoring of the patients, MRI can be useful in the evaluation of spinal cord, soft tissue and ligaments, paravertebral soft tissue, and nerve roots (Thoongsuwan et al. 2005).

### 2.6.2.2 Parenchymal Lung Injuries

#### Pulmonary Contusions

Pulmonary contusions, first described in 1761 by Morgagni, are the most common of severe pulmonary lesions caused by chest blunt trauma and are seen in 17–70% of patients with severe trauma (Cohen 1997; Greene 1987). It is one of the principal factors determining morbidity and post-traumatic mortality. Contusions are generally found in the pulmonary regions near solid structures such as vertebrae, ribs, liver, and heart, as a result of the energy transmitted by the direct impact to the chest wall (Lomoschitz et al. 2003; Mirvis 2004; Rivas et al. 2003; Thoongsuwan et al. 2005). The fracture or damaging of small vessels and the capillary alveolar membrane causes blood extravasation and edema into interstitium and alveolar spaces. Although the contusions are not always accompanied by pulmonary lacerations, CT evaluation often shows numerous lacerations not evidenced on radiographs where usually only contusions are seen. The





**Fig. 7.** Polytraumatized patient with respiratory failure. A CT scan shows important left-sided contusions and a wide pulmonary laceration in the ipsilateral lower lobe. It also demonstrates left hemothorax, pneumomediastinum, right chest wall emphysema, and, in particular, an anterior subpleural pneumatocele in the right lung which required surgery before performing mechanical ventilation



**Fig. 8.** Patient with blunt chest trauma and respiratory failure. On supine chest X-ray there are subtle densities on the upper left side with a small basal ipsilateral pneumothorax

extension of parenchymal damage depends on the severity of the trauma, and thus, in general, on the rapidity of the onset of clinical and radiological signs.

Severe contusions manifest themselves early and quickly, within 3–4 h (and always within 24 h). Pulmonary lesions cause intrapulmonary shunts, reduced compliance, and ventilation–perfusion mismatch. The clinical signs of severe contusions include hemoptysis, tachypnea, bronchorrea, hypoxemia, and reduced cardiac output. The mortality varies from 14 to 40% according to the extension and severity of the contusion and the presence of associated thoracic and non-thoracic lesions.

In light or moderate forms of pulmonary contusions, the initial clinical and radiological signs of respiratory

alterations are minimal or absent. It must be emphasized that, apart from severity, the initial clinical and radiological signs of pulmonary contusions almost always underestimate the real definitive extension of the lesions.

The radiological aspect of the contused lung varies from inhomogeneous slender and ill-defined infiltrates to pneumonic-like consolidations which are non-lobar, non-segmental, or subsegmental, and predominantly localized in peripheral sites, adjacent to the site of injury, usually solid structures (vertebrae, ribs).

Contusions can be monolateral, bilateral, focal, multifocal, or diffused throughout an entire lung or both lungs, and are processes that do not respect fissure boundaries. The air bronchogram may be absent as a result of a

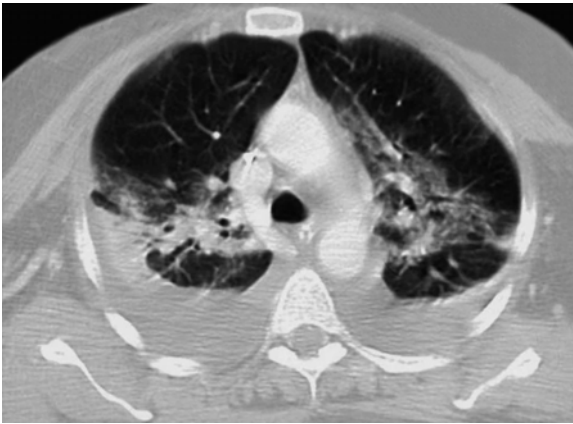


**Fig. 9.** Patient with blunt chest trauma and respiratory failure. An MDCT scan reveals multiple contusions, even on the right side, with bilateral pleural effusion



**Fig. 10.** Patient with blunt chest trauma and respiratory failure. A repeated MDCT examination after 3 weeks shows an almost complete healing of the lesions

bronchial obstruction caused by secretions or blood (Lomoschitz et al. 2003; Mirvis2004; Rivas et al. 2003; Thoongsuwan et al. 2005).

The radiological signs of pulmonary contusion can be masked by associated pathologies such as atelectasis, ab-ingestis infiltrates, and hemothorax.

Uncomplicated pulmonary contusions begin to resolve on the chest radiograph after 48–72 h and tend to heal completely or with little scarring after 1–2 weeks (Figs. 7–9). Contusions which do not show progressive improvement after 7–8 days must be considered carefully because of possible association with superimposed pathologies (infections, atelectasis, ARDS, lacerations).

### Pulmonary Lacerations

Pulmonary laceration is a serious consequence of severe blunt chest trauma and it can be caused by lung perforation due to rib fractures, by inertial deceleration, or by penetrating trauma (Lomoschitz et al. 2003; Mirvis2004; Rivas et al. 2003; Thoongsuwan et al. 2005). Pulmonary lacerations are usually associated with hemoptysis and hemothorax. Pulmonary lacerations are often not identified on chest X-rays, because they are frequently surrounded by contused areas; therefore, before the advent of CT, they were considered an unusual finding. Computed tomography is more sensitive and accurate in delineating the presence and the extension of pulmonary lacerations as well as the associated complications (Fig. 10). Morphologically, laceration is a “tear” of the lung that becomes ovoid or elliptical in shape due to the elastic recoil of the lung parenchyma.

When the space created by the lacerations fills with air coming from bronchial lesions, a pneumatocele develops (radiologically, an ovoid radiolucency); however, when the space fills with blood originating from vessels laceration, a hematoma develops (radiologically, a uniform mass-like

opacity) which can be included in the differential diagnosis with coin lesions (Lomoschitz et al. 2003; Thoongsuwan et al. 2005).

Pneumatocele and hematoma can coexist and air–fluid levels are frequently found. Complex lesions may have a bizarre appearance of post-traumatic cavities.

According to the literature, lacerations can be classified into four types based on the mechanism of injury (Thoongsuwan et al. 2005):

1. Type 1: pulmonary laceration resulting from sudden compression of the chest wall against the closed glottis, wherein the air-containing parenchyma ruptures (usually large and located deep in the parenchyma)
2. Type 2: pulmonary laceration occurring from shearing forces as the lung is compressed on the vertebral bodies (typically elliptical and located in the paraspinal regions)
3. Type 3: pulmonary lacerations developing as a consequence of fractured rib puncture (small, peripheral, often multiple and adjacent to a fractured rib).
4. Type 4: pulmonary lacerations resulting from a pre-existing pleuropulmonary adhesion which causes the lung tear when the chest wall is compressed or fractured (usually surgical or post-mortem findings). Pulmonary lacerations are usually benign lesions which resolve in 3–5 weeks, sometimes with residual scarring, especially if clot was present in the lesion (Lomoschitz et al. 2003).

Nevertheless, when the patient is mechanically ventilated and, in particular, is affected by ARDS, the post-traumatic pneumatocele can rapidly become larger, thus compressing the surrounding functional parenchyma and determining further impairment of respiratory function, and then lasts for months.

Mechanical ventilation can also favor the onset of infections and abscesses.

Direct connection of the laceration with a bronchus and the pleura determines a bronchopleural fistula with pneumothorax or hemopneumothorax (Lomoschitz et al. 2003; Mirvis 2004; Rivas et al. 2003). A pneumothorax, especially during mechanical ventilation, can become a "tension" pneumothorax. A persistent air leak in the pleural cavity may not respond to drainage and requires surgical intervention.

### 2.6.2.3 Extra-alveolar Air Pneumothorax

Pneumothorax is a frequent complication after blunt or penetrating chest trauma, occurring in about 30–40% of patients. Pneumothorax usually occurs from alveolar rupture, secondary to lung lacerations or alveolar compression after crush injuries, with air leakage into the interstitium and pleural space, but it can also be the consequence of direct puncture of the visceral pleura by a fractured rib or tracheo-bronchial injuries. Moreover, it can be an iatrogenic complication following venous cannulation, thoracentesis or related to barotraumas in mechanically ventilated patients.

The diagnosis of this entity is of great importance because even small pneumothoraces may enlarge and become symptomatic, especially in positive-pressure ventilated patients. The diagnosis of air in the pleural cavity is made by visualizing the visceral pleura as a thin straight line with absence of parenchymal markings outside of it. The anatomic localization of pneumothorax depends on the position of the patient, the quantity of air, the presence of pleural adhesions, and atelectasis.

In the erect or semi-erect patient, air rises to the apical or lateral part of the hemithorax. In the supine patient, air tends to collect along the anterior and medial margin of the thoracic wall, i.e., in the anterior costophrenic sulcus which is the most elevated space in this position. This is the reason why 30–50% of the small pneumothoraces in traumatized patients cannot be seen on a frontal supine chest X-ray. In these cases a lateral supine radiograph with horizontal incidence of the ray allows to reach the diagnosis in almost all patients.

The importance to reach the diagnosis is emphasized by the fact that approximately one-third of the patients will develop a tension pneumothorax if not diagnosed and therefore not treated (Tocino and Miller 1987; Wall et al. 1983).

In traumatized patients who have undergone a CT scan of the abdomen, it is better to also include a study of the pulmonary base. It is sufficient to perform only few scans in order to arrive at an early diagnosis of a small pneumothorax which had not been suspected.

It must be remembered that in the radiograph of a supine patient, air collection in the most non-dependent part of the thoracic cage (Gordon 1980; Rhea et al. 1979) determines hyperlucency at the pulmonary base at the level of the upper abdomen, lowering the diaphragm, deepening

of the lateral costophrenic sulcus (so-called deep sulcus sign), and a double diaphragm sign (air which outlines the central dome and the anterior insertion of the hemidiaphragm).

The free air shows up the cardiac margins, the ascending aorta, the aortic knob, and the superior vena cava. The paracardiac fat pad and the lateral border of the inferior vena cava are demarcated by free air collection.

On the supine radiograph, free air in the medial posterior recess is seen as a hyperlucent line delineating the paraspinal line, the descending aorta, and the posterior costophrenic sulcus.

Free air collection in the pulmonary ligaments is an infrequent condition causing a linear hyperlucent band with a convex lateral profile and the superior limit turned forward the upper hilum. This condition must not be confused with the posteromedial pneumothorax, which has a triangular morphology.

Several studies have documented the higher sensitivity of CT when compared with the supine plain film in the evaluation of all these different situations, and this supports the increasing reliance on CT in the screening of the thoracic trauma patients (Lomoschitz et al. 2003; Mirvis 2004; Mirvis et al. 1996; Rivas et al. 2003; Thoongsuwan et al. 2005; Wicky et al. 2000). Recently, US has been proposed as an alternative imaging tool in the detection of small, subtle pneumothoraces, overlooked on chest radiographs, showing promising sensitivity, specificity, and accuracy. The diagnosis is based on the loss of lung sliding and absence of comet-tail artifacts at the hyperechoic pleural interface (Rowan et al. 2002). Further studies are necessary to validate these initial results.

Tension pneumothorax is one of the more frequent life-threatening complications following chest trauma (Koenig and West 2004; Lomoschitz et al. 2003; Mirvis 2004; Rivas et al. 2003; Thoongsuwan et al. 2005).

It develops when there is a consistent air leak and the air penetrates into the pleural cavity during inspiration and does not exit during expiration. It can occur also when the patient, who was not diagnosed as having a pneumothorax, is put on mechanical ventilation.

Tension pneumothorax is a medical emergency. It is diagnosed on clinical signs and symptoms and the treatment usually precedes the radiographic evaluation; however radiological signs are related to high intrathoracic pressure which determines contralateral dislocation of the mediastinum, flattening, or inversion of the ipsilateral diaphragm, widening of the intercostals spaces, and notable collapse of the ipsilateral lung.

The presence of extensive atelectases or pleural adhesions may present with atypical air locations, even with the patient in an erect position.

Treatment of pneumothorax usually involves chest tube placement. When a pneumothorax is not resolved, a malpositioned chest tube must always be suspected. Pleural

adhesions can prevent the chest drainage tube from reaching a loculated pneumothorax.

### **Pneumomediastinum**

Pneumomediastinum is characterized by the presence of air in the mediastinum. It occurs both in blunt (10%) and penetrating traumas. The air can enter into the mediastinum as a consequence of tracheobronchial rupture (<2%), esophageal rupture, and above all, alveolar rupture (95%; Lomoschitz et al. 2003; Primak and Collins 2002; Rivas et al. 2003). As a result of alveolar rupture, air invades the interstitium and subsequently reaches the mediastinum (Macklin effect; Rivas et al. 2003).

Mediastinal emphysema can also be a consequence of facial, laryngeal, and cervical tracheal fractures or perforation of retroperitoneal intestinal ansae (Rivas et al. 2003).

Generally, pneumomediastinum is a benign condition and asymptomatic, but it can sometimes cause chest pain and dyspnea. When the pneumomediastinum is extensive, air can spread extraperitoneally along the anterior wall of the abdomen or in the peritoneal cavity, simulating a primary pneumoperitoneum, or can rupture through the pleura and cause a pneumothorax.

Tension pneumomediastinum, a rare condition, can hinder the venous return to the heart with cardiovascular compromise similar to a cardiac tamponade (Ma and Mateer 1997).

The radiological signs are represented by hyperlucent bands which highlight the parietal pleura and the other mediastinal structures.

Mediastinal air may also cause the “continuous diaphragm sign” delineating the cardiac base and the upper central surface of the diaphragm. It is often better seen in a lateral view rather than on frontal chest view. Computed tomography is the most sensitive method for identifying pneumomediastinum (Rivas et al. 2003; Thoongsuwan et al. 2005; Wicky et al. 2000).

It is not always easy to distinguish pneumomediastinum from pneumothorax and pneumopericardium. In the pneumothorax and pneumopericardium, the air moves easily with change of position, whereas in pneumomediastinum it is trapped in the soft tissue and does not move significantly with the position of patient.

### **Pneumopericardium**

Pneumopericardium is rarely found as a consequence of blunt trauma. It can result more frequently from penetrating trauma, surgery, and gastrointestinal or tracheobronchial fistulas. In patients affected with pneumomediastinum, air rarely reaches the pericardial sac through the periadventitial space or the pulmonary veins. Radiologically, the air outlines the cardiac shadow and it is delineated superiorly from the reflection of the pericardium to the

root of the large vessels. Small quantities of air along the left ventricle can simulate pneumothorax or mediastinal emphysema. Very rarely it can cause cardiac tamponade by restriction of cardiac filling. The development of tension pneumopericardium, which results in a small cardiac shadow on the radiograph, must be treated rapidly with pericardial drainage (Lomoschitz et al. 2003).

### **2.6.2.4 Pleural Effusion and Hemothorax**

A pleural effusion after acute chest trauma is present in approximately 50% of major chest traumas and usually represents a hemothorax (Rivas et al. 2003; Shanmuganathan and Mirvis 1999; Stark 1993).

Bleeding into the pleural space frequently occurs several hours after trauma and is frequently bilateral. Hemothorax can have multiple causes, such as intercostal vessel lacerations, pulmonary lacerations, diaphragmatic or mediastinal tears, or traumatic insertion of vascular lines (Cohen 1997).

A small hemothorax typically occurs in association with traumatic pneumothorax. When hemothorax is due to lung contusion, it is generally self-limited, but when it is due to lung lacerations or mediastinal lesions, it is often massive and protracted.

Blood originating from a venous source is self-limited without mass effect, whereas bleeding of arterial origin is under greater pressure and may continue to accumulate with compression of the heart and mediastinum to the contralateral side (Lomoschitz et al. 2003; Shanmuganathan and Mirvis 1999).

In the upright position, the radiograph shows an opaque meniscus that dulls the costophrenic and pericardiophrenic angles and increases the density of the entire hemothorax (Gavelli et al. 2002). In the supine patient, blood collects posteriorly and the only radiological sign may be an increased density of the hemothorax with persistent visualization of the parenchymal markers (Tocino et al. 1985; Wall et al. 1983).

In both upright and supine position, hemorrhage collects laterally along the wall and at the apex of the lung producing a band of density on the radiograph, the so-called apical cap (Lomoschitz et al. 2003). In the supine patient, a band of paraspinous density may also appear.

Subpulmonic effusions can mimic an elevated diaphragm producing a “pseudodiaphragm” contour. This pseudodiaphragm has typically a flattened contour adjacent to the heart with a curvilinear aspect of its external portion and a more laterally located peak than that of a normal diaphragm (Gavelli et al. 2002).

Pleural effusions below 200–300 ml cannot usually be detected in the supine radiograph. Standard radiology suggests performing radiographs using a horizontal beam on patients in the supine position or, if possible, on the side involved, in order to evaluate the effusion, and, partially,



the underlying parenchyma (Hessen maneuver; Rivas et al. 2003; Stark 1993).

Bedside sonography has been increasingly used as a routine method to exclude effusion or to evaluate its extent and composition and, possibly, to guide thoracentesis (Ma and Mateer 1997).

In ultrasonography, the pleural serous effusion is classically anechoic. Sometimes it can be difficult to make a differential diagnosis between exudative effusion and hemothorax using only ultrasonography.

Computed tomography is superior to radiography in identifying a pleural collection and can aid in distinguishing serous effusions (low-attenuation values) from hemothorax (high attenuation values, varying from 35 to 70 HU; Rivas et al. 2003; Trupka et al. 1997).

On occasion, active hemorrhage can also be detected by spiral CT with injection of contrast media (Mullinix and Foley 2004).

Another cause of pleural effusions after acute trauma is chylothorax due to interruption of the thoracic duct. On CT scans, chylothorax can be recognized on the basis of its very low-attenuation values.

### 2.6.2.5 Tracheobronchial Injury

Tracheobronchial ruptures due to thoracic trauma are relatively rare, reported in 2.8–5.4% of autopsies of trauma victims and in 0.4–1.5% of patients in clinical series of major blunt thoracic trauma (Shanmuganathan et al. 1996, 2000). Patients with tracheobronchial injury suffer from a high prehospital mortality rate (Lomoschitz et al. 2003).

More than 80% of bronchial injuries occur in the main bronchi within 2.5 cm of the carina, with the right side more commonly than the left side (Rivas et al. 2003; Shanmuganathan et al. 1996, 2000).

Tracheobronchial injuries are usually associated with other thoracic emergencies, such as pneumothorax, pneumomediastinum, and vascular lesions, which often obscure the diagnosis.

Because of the low frequency of the injury and the non-specific signs and symptoms, there often is a delay in diagnosis (Lomoschitz et al. 2003). The classic findings of ruptured airways are pneumothorax, pneumomediastinum, and subcutaneous emphysema (Tocino and Miller 1987). The presence of persistent large pneumothorax, despite an adequate thoracostomy tube, increasing subcutaneous emphysema and mediastinal air, and persistent atelectasis, should raise suspicion for tracheobronchial injury (Lomoschitz et al. 2003).

Pneumomediastinum occurs alone when the lesion is located medial to the pulmonary ligament, whereas pneumothorax occurs alone when the lesion involves the main bronchus distal to the insertion of the pulmonary ligament.

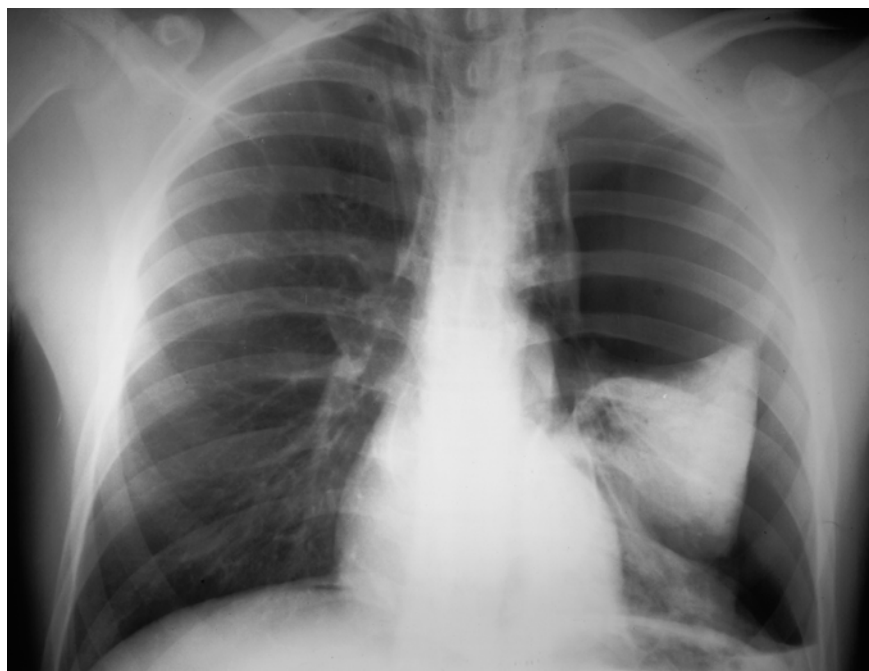


**Fig. 11.** Supine chest radiograph shows the typical, but rare, fallen-lung sign, pathognomonic of tracheobronchial rupture. The lung is detached from its mainstem bronchus and is connected to the mediastinum only with the vascular hilum, which is abnormally caudal in position

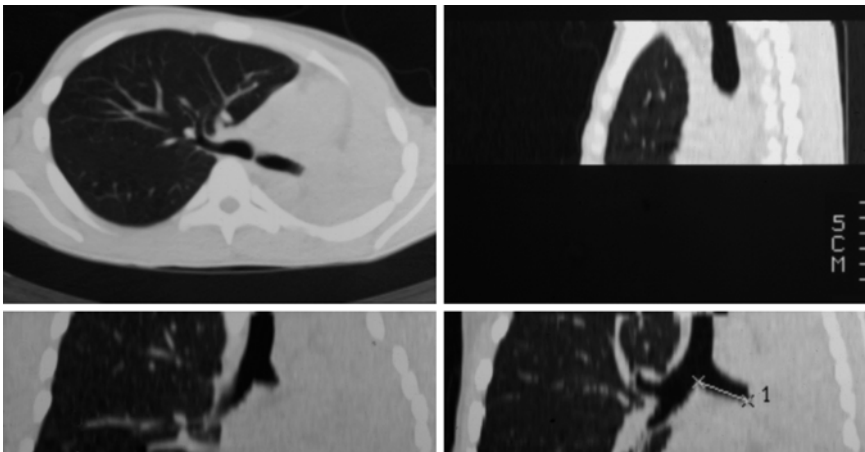


**Fig. 12.** Bronchial rupture. Spiral CT scan with multiplanar reformations demonstrates the presence of a clot inside the left bronchus caused by a bronchial tear confirmed by bronchoscopy

Other indirect radiographic signs of tracheal rupture include deviation of the endotracheal tube tip to the right, overdistension of the endotracheal balloon cuff, and migration of the balloon to the endotracheal tube tip (Lomoschitz et al. 2003; Thoongsuwan et al. 2005).

The “bayonet sign” (a thin tapering air-filled structure of the proximal end of the ruptured bronchus), which can be visualized on chest radiographs, is a rare but important finding (Gavelli et al. 2002).

Another rare but pathognomonic finding is the “fallen lung sign” caused by the detachment of the lung from its mainstem bronchus with consequent fall into the most dependent portion of the thoracic cavity (Tack et al. 2000). The hilum of the collapsed lung appears remarkably caudal in position (Fig. 11).

Complications of undiagnosed tracheobronchial injuries include airway stenosis and lung atelectasis, tracheoesophageal fistula, empyema, and mediastinitis (Rivas et al. 2003).

Helical CT with sagittal and coronal reconstructions, is more sensitive and specific than radiography (Chen and Wilson 1991; Gavelli et al. 2002; Shanmuganathan and Mirvis 1999; Tocino and Miller 1987; Tocino et al. 1985; Wan et al. 1997; Wintermark et al. 2001). Computed tomography can reveal minimum quantities of air in the mediastinum and can be able to directly identify the traumatic lesion (Figs. 12, 13).

Although CT can explicitly diagnose tracheal tears in patients with endotracheal tubes, the bronchoscopy is the diagnostic method to confirm the suspicion of inconclusive cases (Rossbach et al. 1998).

The use of MDCT improved multiplanar reformations of the tracheobronchial tree and may assist in the diagnosis of injuries. Multiplanar reformations and volumetric images are being used with great success and the virtual bronchoscopy is very useful to confirm small tracheobronchial lacerations (Visvikis et al. 2002).

Early diagnosis is essential in order to obtain successful surgical treatment and optimal long-term results.



**Fig. 13.** Tracheal rupture. A CT scan shows pneumomediastinum, subcutaneous emphysema and left pneumothorax persisting after tube placement. Rupture of the posterior tracheal wall is clearly depicted

### 2.6.2.6 Thoracic Esophageal Disruption

Esophageal perforation must be excluded in any case of mediastinal penetrating trauma; however, esophageal injuries can occur from a direct blow by being crushed between the spine and the trachea or through rupture by a bony fragment from a vertebral body fracture (Rivas et al. 2003).

Esophageal rupture is extremely rare as a complication of blunt trauma (it occurs in 10% of cases of esophageal perforation and in about 1/1000 cases of blunt chest trauma).

Most patients with esophageal disruption have other significant associated thoracic injuries. Radiographic signs are not specific and include persistent cervical and mediastinal emphysema, pleural fluid, and abnormal mediasti-

nal contour caused by leakage of fluids, hematoma, or mediastinitis (Gavelli et al. 2002; Rivas et al. 2003).

Contrast esophagography is the ideal method (90% sensitivity) for evaluating suspected esophageal perforation. Contrast studies should be performed first with water-soluble contrast and, if no leaks are detected, with barium sulfate contrast.

Esophagoscopy is also a highly sensitive diagnostic tool, and the association of the two methods allows for the highest diagnostic accuracy. These studies, however, may be difficult to perform in the critically ill patient.

Computed tomography scanning is used to distinguish thoracic injuries from blunt or penetrating trauma (i.e., demonstration of a ballistic tract or knife wounds).

At CT, the presence of air bubbles in the mediastinum, which are localized adjacent to the esophagus, suggests complete esophageal perforation.

The HCT or MDCT scan provides a rapid and non-invasive means to evaluate missile trajectories (Rivas et al. 2003).

The perforation may occasionally become apparent some time after the trauma as a result of ischemia.

### 2.6.2.7 Diaphragmatic Injury

Diaphragmatic injuries occur in 0.8–8% of patients who sustain blunt trauma. Up to 90% of diaphragmatic ruptures from blunt trauma occur in young men after motor vehicle accident (Iochum et al. 2002).

When not recognized, diaphragmatic rupture has a mortality rate of about 30% (Gelman et al. 1991; Murray et al. 1996; Wicky et al. 2000; Worthy et al. 1995), since it is frequently associated with other severe life-threatening abdominal or thoracic conditions.

Injuries to the left hemidiaphragm occur more frequently than to the right side following blunt trauma, possibly due to a protective effect of the liver on the right hemidiaphragm (Iochum et al. 2002); however, the relative paucity of right-side injuries may also have been associated with underdiagnosis (Killeen et al. 1999).

Most tears affect the peripheral portion of the diaphragm, whereas both bilateral tears and extension of the tears into the central tendon are uncommon. Mechanisms of injuries include a lateral impact, which distorts the chest wall and shears the diaphragm, and a direct frontal impact, which leads to increased intraabdominal pressure (Shanmuganathan et al. 2000).

Diaphragmatic injuries are always associated with other traumatic pathologies (pleural effusions, lung injury, aortic injury, hepatic injury, splenic injury, fractures, acute gastric distention, paralysis of the phrenic nerve) and this often prevents an early diagnosis (Shah et al. 1995).

Diaphragmatic injuries remains a diagnostic challenge for both radiologist and surgeons.

The detection with chest radiography is limited (diagnosis of 27–60% of left-sided rupture but only 17% of right side; Gelman et al. 1991; Killeen et al. 1999; Rizoli et al. 1994; Shanmuganathan et al. 1996; Shanmuganathan et al. 2000) and a delayed diagnosis increases the chance of visceral herniation and strangulation.

It is particularly important to perform chest radiographs in series, especially in patients supported by mechanical ventilation in which positive intrathoracic pressure may delay herniation of the abdominal organs through a diaphragmatic lesion (Gavelli et al. 2002).

The following radiological signs can be detected on chest radiographs: an abnormal course of the nasogastric tube; an elevated or intrathoracic location of abdominal organs; obliteration, elevation, or distortion of the diaphragm; pleural effusion; contralateral shift of the mediastinum; air–fluid levels in the lower thorax; and fractures of the lower ribs (Figs. 14, 15).

Gastrointestinal contrast studies usually demonstrate waist-like constriction of the herniated organs (stomach, colon) at the site of the tear in the diaphragm (Fig. 16; Gavelli et al. 2002).

The use of HCT and MDCT with high-quality sagittal or coronary reconstructions has remarkably increased the sensitivity and specificity (71 and 100%, respectively) compared with unsatisfactory results of conventional CT (Figs. 17, 18; Killeen et al. 1999; Shanmuganathan et al. 2000).

Radiological findings of CT, which demonstrate the rupture of the diaphragm, are represented by intrathoracic herniation of the abdominal organs and the omentum.

The CT findings suggestive of diaphragmatic rupture include (Bergin et al. 2001; Iochum et al. 2002; Murray et al. 1996): (a) direct discontinuity of the hemidiaphragm; this sign is the most sensitive CT finding in diaphragmatic rupture (sensitivity of 73% and specificity of 90%) but a normal variant, frequently on the left in elderly women, is represented by a continuity defect of the diaphragm in the posterolateral position; (b) intrathoracic herniation of abdominal viscera, particularly the stomach and colon, with a reported sensitivity of 55% and a specificity of 100%; (c) the “collar sign”, representing the edges of the diaphragmatic rupture wrapped around the herniated abdominal viscera (sensitivity of 63% with MDTC); and (d) the “dependent viscera sign” is an additional sign observed by Bergin et al. (2001) in 90% of cases. This finding is an early indication of diaphragmatic tear on axial image and represents the loss of posterior support by the diaphragm of the liver (right), stomach, and bowel (left), allowing them to abut the posterior ribs.

Magnetic resonance with direct coronal and sagittal images is the ideal method for optimal visualization of the entire hemidiaphragm, particularly on the left side. Both cardiac and respiratory gating should be used to diminish motion artifacts; however, these techniques are not well adapted to polytraumatized patients, but the development

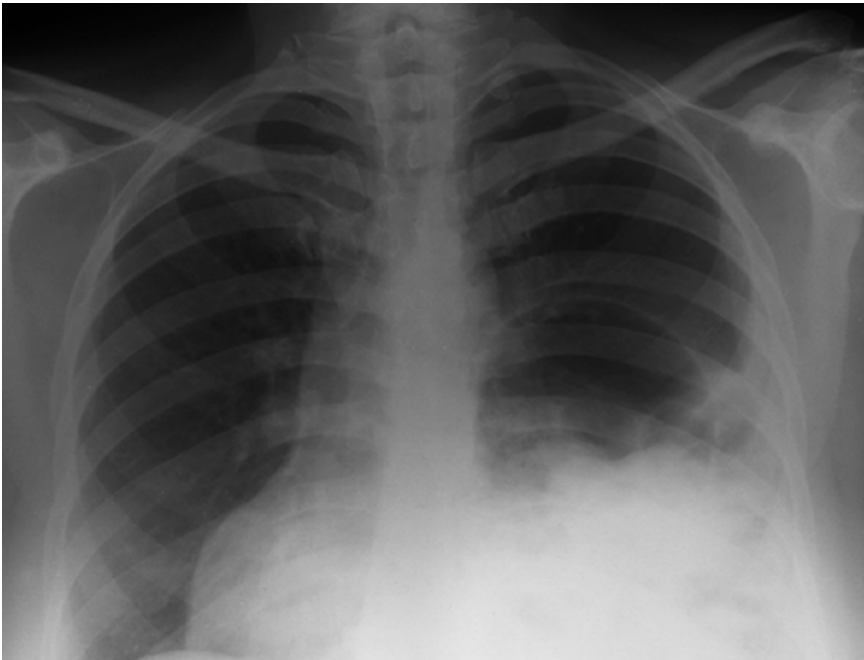


**Fig. 14.** Thoracoabdominal trauma with diaphragmatic rupture. Supine chest film shows left hemothorax with associated pulmonary contusions. Note the moderate right shift of the mediastinal shadow and the presence of a thin, curved radiopaque band caused by the interface between lung and herniated stomach



**Fig. 15.** Chest radiograph with the introduction of water-soluble contrast media through the nasogastric tube. The apex of the nasogastric tube is turned up and placed within the thorax because of stomach herniation through a diaphragmatic rupture after a thoracoabdominal trauma

of faster imaging sequences, improved MR imaging-compatible physiological monitoring, and improved life-support equipment allow MR imaging of most hemodynamically stable trauma patients (Sirmali et al. 2003).

The MR study of diaphragm is performed with sagittal and coronal spin-echo T1-weighted imaging. The normal diaphragm appears as a continuous hypointense thin band of soft tissue outlined by the hyperintense peritoneal and mediastinal fat on the left and by the liver on the right.

Additional pulse sequences (single-shot fast spin echo and fast gradient echo) are particularly well suited for analysis of the diaphragm, are rapidly performed, and decrease respiratory and motion artifacts (Shanmuganathan et al. 1996).

The MR imaging signs of diaphragmatic rupture include abrupt disruption of the contour of the diaphragm and intrathoracic herniation of abdominal fat or viscera. Generally, the use of MR imaging is reserved for patients with uncertain CT diagnosis.

Ultrasonography is widely used in patients with abdominal trauma, but although it may sometimes help in detecting diaphragmatic injury, it is no longer considered particularly useful (Wicky et al. 2000).





**Fig. 16.** Thoracoabdominal trauma with diaphragmatic rupture. A radiograph after barium swallow displays a significant right mediastinal shift with the herniation of the entire stomach into the left hemithorax



**Fig. 17.** Thoracoabdominal trauma. On admission chest radiograph there is a massive opacification of the right hemithorax with gas images suggestive of intrathoracic herniated bowel loops



**Fig. 18.** Thoracoabdominal trauma. Axial CT scan shows a herniated bowel loop with wall thickening due to ischemic damage

### 2.6.2.8 Blunt Cardiac and Pericardial Injury

The spectrum of cardiac and pericardial injuries includes cardiac contusion, coronary injuries, pericardial tears, rupture of the free wall, septum and heart valves, as well as conduction defects.

On the whole, cardiac injuries have been reported in 10–16% of patients admitted after blunt trauma (Olsovsky et al. 1997).

The incidence of cardiac rupture ranges from 0.2 to 2% of major blunt chest trauma victims and usually involves the right atrium (Olsovsky et al. 1997; Perchinsky et al. 1995). Mortality rates of 54% for atrial rupture and 29% for ventricular rupture are reported. Chest radiography is of limited value in detecting cardiac injuries following trauma. There can be several nonspecific radiographical signs such as congestive cardiac failure, cardiomegaly, pneumopericardium, or ventricular aneurysms.

Computed tomography can demonstrate hemopericardium, pneumopericardium, and active arterial bleeding with development of a hematoma which can compress right cardiac chambers.

Transthoracic or transesophageal echocardiography is essential and must be performed without delay. It may detect regional wall abnormalities, lower ejection fractions, patency of the valves, ventricular aneurysms, pericardial effusions, and intracardiac shunts.

A pericardial effusion of an acutely injured patient usually represents blood, and an acute cardiac tamponade may be caused by a 250- to 300-ml pericardial effusion, thus making emergency drainage necessary. A safe approach is represented by percutaneous drainage under sonographic guidance since pericardial effusion in supine patients generally accumulates in the non-dependent portion of the pericardial sac.

A cardiac tamponade may be also caused by a tension pneumopericardium that represents a complication of air within the pericardial sac, generally from penetrating trauma. In these cases, the cardiac silhouette appears progressively smaller on serial radiographs (Lomoschitz et al. 2003).

Angiography and echocardiography remain the diagnostic methods of choice for excluding lesions of the coronary arteries and left ventricular dysfunction.

Magnetic resonance can be performed to confirm and better evaluate the extension of cardiac lesions, particularly in the event of myocardial contusions.

### 2.6.2.9 Traumatic Aortic Injury

Traumatic aortic injury is a lesion of the aortic wall extending from the intima to the adventitia, occurring as a result of a trauma. As previously stated, trauma is the fourth cause of death in the United States and the leading cause of death in individuals under the age of 45 years. Among lethal traumatic lesions, aortic rupture is secondary only to

head trauma: 25% of deaths resulting from motor vehicle accidents are associated with aortic rupture, accounting for 8000 victims per year in the U.S. (Ben-Menachem 1993). Air bags and seatbelts do not protect against this type of lesion. Such injuries can be expected to gain prominence in road traffic injury statistics, since the frequency of lethal injuries in head-on collisions is lowered by the mandatory use of restraints, which protect the victim from thoracic and head lesions but not from the mechanism producing aortic rupture. A recent study by Richens and co-workers (2002) demonstrate that, presently, the most common scenario leading to aortic lesion is the side impact. Interestingly, in this scenario, the lesion can occur at low-severity impact. The aortic segment subjected to the greatest strain by rapid deceleration forces is just beyond the isthmus, where the relatively mobile thoracic aorta is joined by the ligamentum arteriosus. Aortic rupture occurs at this site in 90% of the clinical series. The ascending aorta may be involved in the proximity of the innominate artery or in its proximal segment immediately superior to the aortic valve (Fattori et al. 1997). Other less common locations are distal segments of the descending aorta or the abdominal infrarenal segment. The lesion is transverse and involves all or part of the aortic circumference with different extension into the aortic layers. Intimal hemorrhages without any laceration have been described in pathological series but were not recognized in the clinical setting before the advent of high-resolution tomographic imaging modalities. When a laceration is present it may extend through the media into the adventitia layer with false aneurysm formation. Peri-aortic hemorrhage occurs irrespective of the type of lesion. Complete rupture leads to immediate death in 85% of cases. If a complete rupture of the aorta does not occur at the time of trauma, the adventitia and the surrounding structures stabilize the continuity of the aortic wall by development of an adventitial hematoma. If anti-hypertensive therapy acting to reduce wall stress is prompt in these patients, the risk of aortic rupture is limited. For many years traumatic aortic injury has been considered a surgical emergency needing immediate surgical repair, with absolute priority over any other associated lesions; however, the use of heparin necessary to perform extra-corporeal circulation and a major thoracotomy in polytraumatized patients resulted in a high operative mortality. In the past few years several studies reported a reduction of mortality managing patients with medical therapy in the acute phase and postponing the surgical repair of the aortic lesion after clinical stabilization (Hunt et al. 1996; Pate et al. 1996). Delayed surgery of the post-traumatic aneurysm provides a low operative mortality ranging from 0 to 10% and a low risk of spontaneous aortic rupture in the interval between trauma and surgery. Now the development of endovascular techniques provides additional alternatives for the treatment of traumatic aortic injury.

## Chest Radiography

As a high percentage of blunt chest trauma patients with aortic rupture do not present with indicative clinical signs, the routine chest radiograph becomes an essential tool for identifying subjects with suspected aortic injury (Fig. 19; Marnocha and Maglante 1985; Mirvis et al. 1987; Wintermark et al. 2002).

A variety of radiological signs have been considered as indicators of aortic injury, but there is a great difference in the diagnostic importance of such signs in the various studies. The following are the most frequent and important abnormalities seen on the plain chest radiograph reported in the literature:

1. **Mediastinal widening.** In older studies, emphasis has been placed on mediastinal widening as the principal finding on chest radiograph. A mediastinal width >8 cm at the level of the aortic knob on a 100-cm AP supine chest X-ray was a highly sensitive sign of aortic injury; however, there are obviously many problems in interpreting chest radiographs of acutely polytraumatized patients. A widened mediastinum can be due to causes other than aortic rupture, including bleeding from small mediastinal vessels (arteries or veins), excessive mediastinal fat, thymic tissue, adjacent lung contusion, and ectatic vessels. In addition, with the patient supine, the superior mediastinal shadow is physiologically wider as a result of an increase in systemic blood volume and poor inspiration. The ratio of the mediastinal width to chest width (M/C ratio) of 0.28, applied by Marnocha and Maglante (1985), was found to be 100% sensitive but only 15% specific. Increasing the criterion to a ratio of 0.38 or above produced a specificity of 60%, but sensitivity fell to 40%. This experience, confirmed by subsequent studies, has shown that mediastinal widening, evaluated either subjectively or quantitatively, is a sensitive but relatively non-specific sign of aortic injury.
2. **Abnormal aortic contour.** In patients with blunt chest trauma, an irregular, enlarged, or indistinct aortic outline can be caused by either peri-aortic/mediastinal hemorrhage or by an enlarging aneurysm which is primarily located at the level of the isthmus. Loss of aortic knob and obscuration of the descending aorta outline have shown in many studies a good sensitivity (53–100%) but a low specificity (21–63%) for the diagnosis of aortic injury. False positives can also occur in patients with lung contusions.
3. **Aortopulmonary window opacification.** The opacification of the clear space between the aorta and the left pulmonary artery as a potential indicator of aortic injury has a high negative predictive value (83–86%).
4. **Shift of the trachea and nasogastric tube.** Deviations of the trachea reflect the presence of central mediastinal blood, fluid, masses, or aneurysms of the isthmus or descending aorta. Blunt chest trauma can produce hematomas of the anterior or posterior mediastinum originating from injuries of the sternum, ribs, vertebrae, and their associated vessels.
5. **Widening of paraspinous lines.** Mediastinal hemorrhage with widening of either the left or right paraspinous stripe may occur as a result of major arterial injuries, but can also be caused by venous bleeding and vertebral and/or rib fractures; therefore, in the evaluation of these features, the radiologist should be aware of the possibility of false positives due to injuries not related to aortic rupture. Mirvis et al. (1987) reported a poor sensitivity (12 and 2% for left and right paraspinous lines, respectively) and a high specificity (97 and 99%) of both these abnormalities without concomitant fractures of the thoracic cage. They suggested that sensitivity was likely to be affected by failure to visualize distinct paraspinous lines on underexposed chest films.
6. **Widening of the paratracheal stripe.** The diagnostic value of the widening of the right paratracheal stripe to 5 mm or more has been emphasized in previous studies as predictor of a mediastinal hemorrhage. In most of the literature, this finding is not reported to be significant.
7. **Depressed left mainstem bronchus.** In blunt chest trauma, the left mainstem bronchus (below 40° from the horizontal line) may be depressed and also displaced to the right by a mediastinal hematoma or by an aneurysm at the isthmus. Mirvis et al. (1987) confirmed the high specificity of this finding, but also reported a very poor sensitivity (4% on the supine view and 1% on the erect view) related in part to problems in accurately visualizing bronchi on underexposed radiographs.
8. **Apical cap.** Hemorrhage from an aortic tear dissecting along the left subclavian artery can extend into the extrapleural space over the apex of the lung, especially the left lung, producing a soft tissue density. In general, this sign has a sensitivity of 9–63% and a specificity of 75–96%.

There is wide agreement in the literature that no single radiographic sign or combination of signs has sufficient sensitivity and specificity to confirm or exclude the presence of aortic injury. As Mirvis et al. (1987) have pointed out, most of the signs described previously are more valuable by their absence as indicators of normality, than by their presence as indicators of aortic rupture. In the identification of a normal chest film, the true erect view has shown a higher negative predictive value (98%) than the supine view (96%). The same authors found that the observation of a normal aortic arch and descending aorta, a clear aortopulmonary window, and absence of a tracheal shift or widened left paraspinous line has a 91–92% negative predictive value for aortic injury; therefore, chest radiograph on admission remains the essential screening test for identifying traumatized patients in whom an aortic tear is strongly suspected and who thus require further imaging investigations.

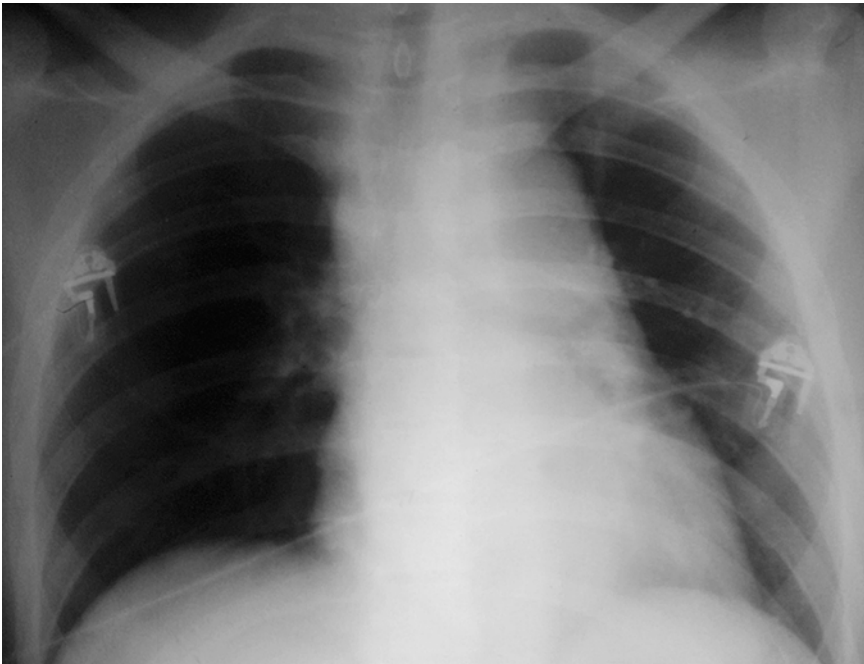


**Fig. 19.** Chest X-ray. Mediastinal widening with enlargement of the paratracheal stripe. The apical cup is visible at the left apex due to hemorrhage of the epi-aortic vessels

### Computed Tomography

Over the past few years, several studies have evaluated the role of standard CT in the diagnosis of aortic injury yielding controversial results. Before the introduction of HCT in clinical practice, CT diagnosis of aortic rupture relied primarily on the detection of mediastinal hematomas as an indirect sign, rather than on the detection of direct signs of aortic injury.

In most trauma centers, the next diagnostic step included the performance of aortography to confirm or exclude the aortic origin of the mediastinal bleeding. If hematoma was not present, aortography was not carried out. As pointed out by Raptopoulos (1994) in a commentary, the characteristics of mediastinal hematoma on CT scans have not been described in detail in the majority of reports. In interpreting the mediastinum for the detection of hemorrhage, false-positive findings may occur as a result of thymus tissue, peri-aortic atelectasis of the left lower lobe, volume averaging of the pulmonary artery with mediastinal fat and left medial pleural effusion. The hematoma secondary to aortic rupture is mostly peri-aortic and may extend along the descending aorta. In blunt chest trauma patients, a mediastinal hemorrhage may be present for other reasons, such as bleeding from small mediastinal vessels (arteries or veins), often in association with fractures of the thoracic cage. Furthermore, if the adventitia is intact, aortic rupture may occur without hemorrhage. For these reasons, the interpretation of a positive CT scan based only on the presence of mediastinal hematoma causes a large number of negative aortograms with a resulting low specificity. In order to in-

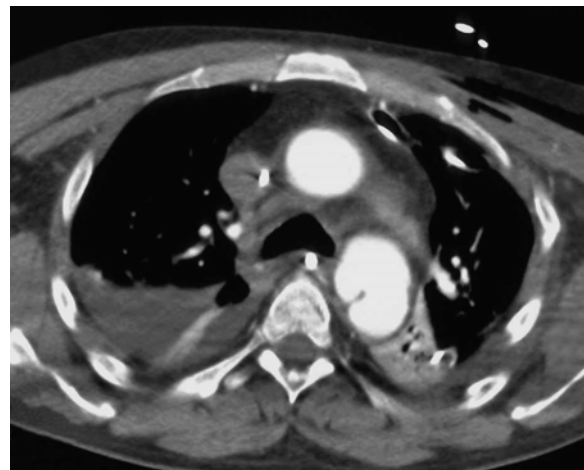


**Fig. 20.** An MDCT of a traumatic aortic lesion (grade 3). A pseudoaneurysm is visible with an anterior extrinsication

crease the specificity of CT, direct signs of aortic rupture must be considered. These signs include aortic pseudoaneurysm, an abrupt change in the aortic contour, intimal tear, intramural hematoma, extravasation of contrast material from the aorta, diminished caliber of the descending aorta (pseudocoarctation), and double aortic lumen. Problems in the evaluation of these direct findings may arise from artifacts due to respiratory and voluntary movement of the traumatized patients, cardiovascular motion, and from streak artifacts caused by nasogastric tubes, external





**Fig. 21.** An MDCT of a traumatic aortic lesion (grade 3). A volume-rendering reconstruction better displays the morphology of the pseudoaneurysm and its relationship with the supra-aortic vessels (arrow, **a**). An MDCT performed 1 year after endovascular stent positioning shows complete resolution of the post-traumatic pseudoaneurysm (arrow/arrowhead, **b-d**)

leads, or other devices; presence of effusion in the upper pericardial recess can mimic a double lumen. With conventional CT, motion and respiratory artifacts were common, and the detection of subtle aortic injuries with axial plane extension may also be obscured by volume averaging with the normal aortic lumen. Another limit of conventional CT is the inability to display images of pseudoaneurysm in the longitudinal plane, which is their major axis, failing to provide anatomic details useful for surgery such as relationships between the aortic lesion and the brachiocephalic vessels.

The advent of HCT and, recently, of MDCT, overcomes most of these limitations (Alkadi et al. 2004; Koenig and West 2004; Mirvis et al. 2004; Mirvis et al. 1996; Wicky et al. 1998; Wintermark et al. 2002), and it is particularly useful in critically injured patients with suspected associated neurological, visceral, or retroperitoneal lesions, some of which may be more critical than an aortic injury. Gavanti et al. (1996) used HCT exclusively to screen 1518 patients with non-trivial blunt chest trauma, 127 of whom presented abnormal findings at CT and underwent aortography. Helical CT was found to be more sensitive than aortography (100 vs 94.4%) but less specific (81.7 vs 96.3%, respec-

tively) in detecting aortic lesions. False positives are reported in cases of prominent mediastinal vessels adjacent to the aorta (i.e., a right bronchial artery) or in cases of volume averaging of the left brachiocephalic or left superior intercostal veins. The authors conclude that negative findings on helical CT of the aorta, even in the presence of mediastinal hematoma, is sufficient to exclude aortic rupture. Presently, many therapeutic approaches are possible in traumatic aortic rupture, depending on the anatomic features as well as the severity of the aortic lesion (Figs. 20, 21); therefore, the following CT grading system has been proposed in the estimation of the severity of aortic injury (Morris and Gavant 1999):

1. Grade 0: normal aorta and mediastinum.
2. Grade 1: abnormal mediastinum and normal aorta. Five to 10% of blunt trauma present with isolated mediastinal hematoma in the absence of an aortic lesion.
3. Grade 2: minimal aortic injury. Aortic intimal injuries extending for 1 cm or less may be difficult to detect and should be differentiated from atherosclerotic plaques.
4. Grade 3: confined aortic injury. This is the most common type of aortic lesion, easily identified due to the formation of pseudoaneurysm.
5. Grade 4: total aortic disruption. The aortic contour is irregular, poorly defined, and contrast medium extravasation into the extra-adventitia space is visible.

Comparing the diagnostic value of transesophageal echocardiography (TEE) and HCT in a consecutive series of 110 patients, Vignon et al. (2001) found one false negative with TEE in a traumatic lesion of the innominate artery, identified by HCT. On the other hand, HCT missed four cases of intimal/medial injuries at the aortic isthmus; however, the sensitivity and specificity of HCT in the detection of traumatic aortic lesions was approximately 100% in other reports (Wicky et al. 1998).

The development of multidetector-row CT in the late 1990s represented the most significant advancement in helical CT, especially in the evaluation of vascular system. Thinner collimations, faster gantry rotation times, large detector arrays, powered X-ray tubes, and increased table speed dramatically improved image quality. Recent further improvement of MDCT scanners, just a few years ago, with the introduction of 16–64 detector rows, give a submillimetric, isotropic 3D data acquisition of extended anatomical ranges in less time, enabling high-quality vascular imaging with 2D–3D artifact-free reconstructions from virtually any angle and in any desirable plane (Alkadi et al. 2004). Since it provides high-quality images in a short time, MDCT represents a method of great diagnostic value, potentially the method of first choice in the acute phase for the evaluation of blunt chest trauma patients with suspected aortic injury, particularly in polytraumatized patients with other thoracic and extrathoracic associated lesions.

## Echocardiography

Transesophageal echocardiography (TEE), developed by Frazin in 1976, has evolved as the optimal modality in acute non-traumatic aortic pathology. The capability of providing high-resolution images of the aortic wall rapidly, even at the patient's bedside, allowed it to become the method of choice in the diagnosis of suspected acute aortic injuries (Vignon et al. 1995). The use of TEE in aortic injury was first reported in the 1990s, initially in small series of patients with blunt chest trauma and successively in wider prospective trials (Buckmaster et al. 1994; Smith et al. 1995). The diagnosis is based on the identification of aortic tear as a mobile echogenic flap, perpendicular to the aortic isthmus. The aortic contour is generally deformed because of the formation of a pseudoaneurysm. There are several advantages in the use of TEE in the evaluation of aortic injury. Echocardiography can be performed quickly at the bedside, without interrupting resuscitative and therapeutic measures. It is a non-invasive technique and does not require the administration of contrast media. Moreover, it may provide information on possible associated cardiac contusions or valvular lesion. Nevertheless, in a polytraumatized patient, some disadvantages of TEE may become particularly problematic. It cannot be performed in patients with facial fractures or cervical spine fractures, representing 5–25% of the trauma victims. The descending aorta is scanned in close proximity to the esophagus and possible near-field artifacts may occur due to excessive gain and reverberation. Because of the interposition of the trachea, there can be some limitations in visualizing the upper portion of the ascending aorta as well as the arteries of the aortic arch, the next most common locations for aortic injury after the aortic isthmus. These problems are evident in the literature in several cases of false-positive and false-negative results. Serious consequences of a missed diagnosis or of an unnecessary thoracotomy in an already ill patient demand a high degree of accuracy from any diagnostic test applied in aortic injury evaluation. The TEE may be considered an effective test in the evaluation of aortic injury, providing helpful information regarding the aortic lesion; nevertheless, considering the operator dependence of the method and some pitfalls in detecting specific portions of the aortic segments, its use as sole diagnostic test for ruptured thoracic aorta requires a careful approach.

## Aortography

For more than 20 years aortography has been the only imaging modality for studying aortic pathology and it has been considered to be the gold standard in confirming or excluding the presence of traumatic aortic rupture. Biplane cineangiography assures high temporal resolution images and accurate evaluation of the isthmus of the aorta by a single injection of 50 ml of contrast medium. The entire thoracic aorta as well as the intrathoracic portions of the brachio-

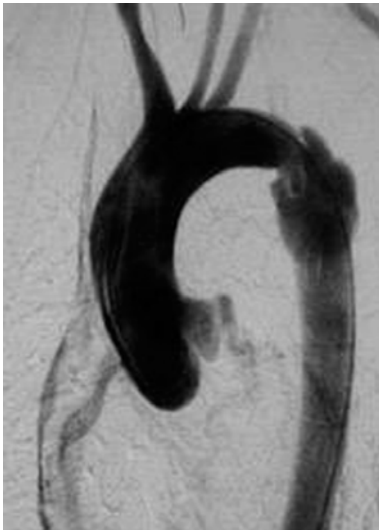


**Fig. 22.** Digital subtraction aortography (left anterior oblique view). An aortic lesion with pseudoaneurysm formation is visible

cephalic vessels should be visualized to exclude location of aortic rupture other than at the isthmus, occurring in 5% of clinical series. The diagnosis is based on the detection of the intimal/medial tear visible as a linear irregular filling defect within the lumen of the aorta. When the tear extends deep into the media, the pseudoaneurysm appears on the aortogram as a focal bulge in the column of contrast material (Fig. 22). The combined findings that are highly specific for aortic rupture are a focal bulge with delayed washout of contrast material and a linear filling defect at the level of the ligamentum arteriosum. Focal bulge alone cannot be considered diagnostic of traumatic aortic rupture. A focal convexity, involving the opposite wall asymmetrically, may be present at the thoracic aortic isthmus in 25% of cases due to ductus diverticulum, and tend to be more prominent in older patients. It accounts for 1–2.8% of false-positive results of aortography in the diagnosis of aortic injury [30]. Other abnormalities that can simulate aortic injury include atherosclerotic plaques, aortitis, and streaming or mixing artifacts. A false-negative diagnosis of rupture with angiography may occur up to 12% of cases due to poor opacification by contrast agents, inadequate projections, or thrombosis of the pouch. By design, small intimal tears or intimal intraparietal lesions cannot be visualized by angiography, as demonstrated in reports comparing angiography with high-resolution tomographic modalities such as TEE, MRI, and CT. Due to its invasive approach and contrast media administration, aortography generally has a complication rate of 1–2%, which tends to be higher in acute patients. Kram et al. (1987) reported 10.5% of complications in 76 victims of blunt chest trauma undergoing aortography, one of which required blood transfusion for severe groin hemorrhage. Although it is difficult to

demonstrate a precise cause and effect relationship, several cases of death during aortography have been reported. Contrast media extravasation into the mediastinum or massive leakage from the aneurysm after injection of contrast media have even been documented by Del Rossi et al. (1990).

In the era of high-resolution non-invasive imaging modalities, aortography should not be recommended in polytraumatized patients with suspected TAR.

### Magnetic Resonance

The role of MRI in diagnostic evaluation of aortic diseases has been widely documented, resulting, in comparative studies, in one of the most accurate diagnostic techniques in the detection of acute and chronic aortic pathology. A long examination time as well a difficult access to the patient has been considered the main limitation of MRI in acute aortic pathology. Although the development of fast MRI techniques has enabled the examination to be shortened to a few minutes, MRI has been under-utilized in critically ill patients. The value of MRI in detecting traumatic aortic rupture has been reported in a series of 24 consecutive patients in comparison with angiography and CT [8]. The diagnostic accuracy was 100% for MRI, 84% for angiography (two false negatives, in two cases of limited partial lesion), and 69% for CT (two false negatives and three false positives). Moreover, in almost all cases, MRI was able to differentiate the type of lesion, according to Parmley's classification. Because of the presence of methemoglobin, intimal hemorrhage has high signal intensity and can be clearly detected. On sagittal spin-echo sequence, the longitudinal visualization of the thoracic aorta allows identification of a partial lesion (a tear limited to the anterior or to the posterior wall) from a circumferential lesion developing on the entire aortic circumference. This discrimination is of prognostic significance, because circumferential lesion may have a greater risk of rupture [10]. The presence of periaortic hematoma, or pleural and mediastinal hemorrhagic effusion, may also be considered a sign of instability. The characteristics of MRI to detect the hematic content of a collection by its high signal intensity is very useful in polytraumatized patients. In the same sequence used to evaluate the aortic lesion, without any additional time, the wide field of view of MRI gives a comprehensive evaluation of chest trauma, such as lung contusion and edema, pleural effusion, and rib fractures (Figs. 23, 24). Furthermore, if delayed surgery is considered, MRI may be used to monitor thoracic and aortic lesions because of its non-invasiveness and repeatability. The development of fast techniques that reduce examination time to a few minutes, and allow better accessibility to the patients, may contribute to a feasible use of this powerful diagnostic tool in traumatic aortic rupture.



**Fig. 23.** Sagittal spin-echo MR image demonstrates a partial lesion of the isthmus aorta. An intimal tear involving only the anterior wall is visible. Note the high signal intensity of the peri-aortic effusion



**Fig. 24.** Axial spin-echo MR image of the same patient shows the associated pulmonary contusions (high signal intensity), peri-aortic hematoma, right pleural effusion, and rib fractures

### Optimal Diagnostic Approach

Although the new surgical strategies demonstrated low rates of spontaneous mortality of traumatic aortic lesion observed in the clinical setting, traumatic aortic rupture has to be considered a potentially evolving lesion; therefore, a prompt and accurate diagnosis is necessary in order to initiate pharmacological control of arterial blood pressure and stratify the risk of delayed or emergency surgical repair (Nzewi et al. 2005).

Chest X-ray is routinely performed in all blunt thoracic trauma victims and plays an essential role in raising the suspicion of aortic injury. On the basis of positive chest X-ray, several imaging modalities are currently available to confirm or exclude the presence of the lesion. The choice of approach has to take account of the patient's clinical condition. In the case of severe hemodynamic instability, TEE has the advantage that it can be performed at the patient's bedside without interrupting resuscitative and therapeutic measures. In the more stable patients, the ideal modalities are those able to give high definition images of the aortic wall and to obtain information on the other organs and structures affected by the traumatic impact. Both MRI and CT demonstrated these characteristics, providing a high accuracy in the diagnosis of aortic injury coupled to the capability to evaluate thoracic, head, or abdominal lesions. Because of a better access to the patient and widespread availability, HCT may be considered the method of first choice in a severe polytrauma. If delayed surgery is considered, either MRI or HCT may be used to monitor thoracic and aortic lesions because of its non-invasiveness and repeatability.

### 2.6.3 Conclusion

Diagnostic imaging plays a fundamental role in the evaluation of patients who sustain chest trauma, which is associated with high morbidity and mortality and is the leading cause of death in patients under 45 years old and the fourth cause of death in Western countries.

Chest X-ray still represents the first imaging tool in the work-up strategy of chest trauma victims, allowing the detection of most life-threatening conditions; however, chest radiograph has shown low sensitivity and specificity, especially in critically ill patients, and the radiologist must have deep knowledge of the possibilities and limits of this imaging modality, which may not point out or underestimate even life-threatening lesions.

For these reasons and due to its high accuracy, CT has assumed an increasing role in the evaluation of chest trauma patients. The introduction of MDCT has significantly improved the diagnostic capability of this technique, so much so that it has been recently proposed as a screening tool, especially in major traumas.



## References

- Alkadi H, Wildermuth S, Desbiolles L, et al (2004) Vascular Emergencies of the Thorax after Blunt and Iatrogenic Trauma: Multi-detector Row CT and Three Dimensional Imaging. *Radiographics* 24:1239-1255.
- Ben-Menachem Y (1993) Rupture of the thoracic aorta by broad-side impacts in road traffic and other collisions: further angiographic observations and preliminary autopsy findings. *J Trauma* 35:363-367.
- Bergin D, Ennis R, Keogh C, et al (2001) The "Dependent Viscera" Sign in CT Diagnosis of Blunt Traumatic Diaphragmatic Rupture. *AJR* 177:1137-1140.
- Buckmaster MJ, Kearney PA, Johnson SB, et al (1994) Further experience with transeophageal echocardiography in the evaluation of thoracic aortic injury. *J Trauma* 37:989-995.
- Chen JC, Wilson SE (1991) Diaphragmatic injuries: recognition and management in sixty-two patients. *Am Surg* 57:810-815.
- Cohen MC (1997) Pulmonary contusion: Review of the clinical entity. *J Trauma* 42:973-979.
- Del Rossi AJ, Cernaianu AC, Madden LD et al (1990) Traumatic disruptions of the thoracic aorta: treatment and outcome. *Surgery* 108:864-870.
- Fattori R, Celletti F, Bertaccini P et al (1996) Delayed surgery of traumatic aortic rupture: role of Magnetic Resonance Imaging. *Circulation* 94:2865-2870.
- Fattori R, Bertaccini P, Celletti F et al (1997) Intramural posttraumatic hematoma of the ascending aorta in a patient with a double aortic arch. *Eur Radiol* 7:51-53.
- Fattori R, Celletti F, Descovich B et al (1998) Evolution of post traumatic aneurysm in the subacute phase: magnetic resonance imaging follow-up as a support of the surgical timing. *Eur J Cardiothorac Surg* 13:582-587.
- Fermanis GG, Deane SA, Fitzgerald PM (1985) The significance of first and second ribs fractures. *Aust N Z J Surg* 55:383-386.
- Gavant ML, Flick P, Menke P, et al (1996) CT aortography of thoracic aortic rupture. *AJR* 166:955-961.
- Gavelli G, Canini R, Bertaccini et al (2002) Traumatic injuries: imaging of thoracic injuries. *Eur Radiol* 12:1273-1294.
- Gelman R, Mirvis SE, Gens D (1991) Diaphragmatic rupture due to blunt trauma: sensitivity of plain chest radiographs. *AJR* 156:51-57.
- Gordon R (1980) Deep sulcus sign. *Radiology* 136:25-27.
- Greene R (1987) Lung alterations in thoracic trauma. *J Thorac Imaging* 2:1-11.
- Hunt JP, Baker CC, Lentz CW et al (1996) Thoracic aorta injuries: management and outcome of 144 patients. *J Trauma* 40:547-556.
- Iochum S, Ludwig T, Walter F, et al (2002) Imaging of diaphragmatic injury: a diagnostic challenge?. *RadioGraphics* 22:S103-S118.
- Killeen KL, Mirvis SE, Shanmuganathan K (1999) Helical CT of diaphragmatic rupture caused by blunt trauma. *AJR* 173:1611-1616.
- Koenig TR, West OC (2004) Diagnosing Acute Traumatic Aortic Injury with Computed Tomography Angiography: Signs and Potential Pitfalls. *Curr Probl Diagn Radiol* May/June 97-105.
- Kram HB, Wohlmuth DA, Appel PL, et al (1987) Clinical and radiographic indications for aortography in blunt chest trauma. *J Vasc Surg* 6:168-176.
- Lomoschitz FM, Eisenhuber E, Linnau KF, et al (2003) Imaging of chest trauma: radiological patterns of injuries and diagnostic algorithms. *Eur J Radiol* 48:61-70.
- Ma OJ, Mateer JR (1997) Trauma ultrasound examination versus chest radiography in the detection of hemothorax. *Ann Emerg Med* 29:312-315.
- Marnocha KE, Maglinte DDT (1985) Plain film criteria for excluding aortic rupture in blunt chest trauma. *AJR* 144:19-21.
- Mirvis SE (2004) Diagnostic Imaging of Acute Thoracic Injury. *Seminars in Ultrasound, CT, and MRI* 25(2):156-179.
- Mirvis SE, Bidwell JK, Buddemeyer EU, et al (1987) Value of chest radiography in excluding traumatic aortic rupture. *Radiology* 163:487-493.
- Mirvis SE, Shanmuganathan K, Miller BH, et al (1996) Traumatic aortic injury: diagnosis with contrast-enhanced thoracic CT-five-year experience at a major trauma center. *Radiology* 200:413-422.
- Morris L, Gavant ML (1999) Helical CT grading of traumatic aortic injuries. *Radiol Clin North Am* 37 (3):553-574.
- Morse SS, Glickman MG, Greenwood L et al (1988) Traumatic aortic rupture: false-positive aortographic diagnosis due to atypical ductus diverticulum. *AJR* 150:793-796.
- Mullinix AJ, Foley WD (2004) Multidetector Computed Tomography and blunt thoracoabdominal trauma. *J Comput Assist Tomogr* 28:S20-S27.
- Murray JG, Caoili E, Gruden JF, et al (1996) Acute rupture of the diaphragm due to blunt trauma: diagnostic sensitivity and specificity of CT. *AJR* 166:1035-1039.
- Nzewi O, Slight RD, Zamvar V (2005) Management of Blunt Thoracic Aortic Injury. *Eur J Vasc Endovasc Surg.* (Article in press).
- Olsovsky MR, Wechsler AS, Topaz O (1997) Cardiac trauma: diagnosis, management, and current therapy. *Angiology* 48:423-432.
- Pate JW, Fabian TC, Walker W (1995) Traumatic rupture of the aortic isthmus: an emergency? *World J Surg* 19:119-126.
- Perchinsky MJ, Long WB, Hill JG (1995) Blunt cardiac rupture: the Emanuel trauma Center experience. *Arch Surg* 40:852-856.
- Primak SL, Collins J (2002) Blunt nonaortic chest trauma: radiographic and CT findings. *Emergency Radiology* 9:5-12.
- Raptopoulos V (1994) Chest CT for aortic injury: maybe not for everyone. *AJR* 162:1053-1055
- Rhea JT, van Sonnenburg E, McLoud TC (1979): Basilar pneumothorax in the supine adult. *Radiology* 133:593-595.
- Richens D, Kotidis K, Neale M (2002) Rupture of the aorta following road traffic accidents in United Kingdom 1992-1999. The results of the co-operative crash injury study. *European Journal of Cardio-Thoracic Surgery* 23:143-148.
- Rivas LA, Fishman JE, Munera F, et al (2003) Multislice CT in thoracic trauma. *Radiol Clin North Am* 41:599-616.
- Rizoli SB, Brennenan FD, Boulanger BR, et al (1994) Blunt diaphragmatic and thoracic aortic rupture: An emergency injury complex. *Ann Thorac Surg* 58:1404-1408.
- Rowan KR, Kirkpatrick AW, Liu D, et al (2002) Traumatic Pneumothorax Detection with Thoracic US: Correlation with Chest Radiography and CT-initial experience. *Radiology* 225:210-214.
- Roszbach MM, Johnson SB, Gomez MA, et al (1998) Management of major tracheobronchial injuries: a 28-year experience. *Ann Thorac Surg* 65:182-186.
- Shah R, Sabanathan S, Mearns AJ, et al (1995) Traumatic rupture of diaphragm. *Ann Thorac Surg* 60:1444-1449.
- Shanmuganathan K, Mirvis SE (1999) Imaging diagnosis of nonaortic thoracic injury. *Radiol Clin North Am* 37 (3):533-551.
- Shanmuganathan K, Mirvis SE, White CS, et al (1996) MR imaging evaluation of hemidiaphragms in acute blunt trauma: experience with 16 patients. *AJR* 167:397-402.
- Shanmuganathan K, Killeen KL, Mirvis SE, et al (2000) Imaging of diaphragmatic injuries. *J Thorac Imaging* 15:104-111.
- Sirmali M, Turut H, Topcu S, et al (2003) A comprehensive analysis of traumatic rib fractures: morbidity, mortality and management. *European Journal of Cardiothoracic Surgery* 24:133-138.
- Smith MD, Cassidy JM, Souther S et al (1995) Transeophageal echocardiography in the diagnosis of traumatic rupture of the aorta. *N Engl J Med* 332:356-362.
- Stark P (1993) Pleura. In Stark P (ed) *Radiology of Thoracic Trauma*. Andover Medical Publisher, Boston, pp 54-72.
- Tack D, Defrance P, Delcour C, et al (2000) The CT fallen-lung sign. *Eur Radiol* 10(5):719-721.

- Thoongsuwan N, Kanne JP, Stern EJ (2005) Spectrum of Blunt Chest Injuries. *J Thorac Imaging* 20(2):89-97.
- Tocino I, Miller MH (1987) Computed tomography in blunt chest trauma. *J Thorac Imaging* 2:45-59.
- Tocino IM, Miller MH, Fairfax WR (1985) Distribution of pneumothorax in supine and semi-recumbent critically ill patients. *AJR* 144:901-905.
- Trupka A, Waydas C, Hallfeldt KK, et al (1997) Value of thoracic CT in the first assessment of severely injured patients with blunt chest trauma: results of a prospective study. *J Trauma* 43:405-412.
- Vignon P, Gueret P, Vedrinne J et al (1995) Role of transesophageal echocardiography in the diagnosis and management of traumatic aortic disruption. *Circulation* 92:2959-2968.
- Vignon P, Boncoeur MP, Francois B, et al (2001) Comparison of multiplane transesophageal echocardiography and contrast-enhanced helical CT in the diagnosis of blunt traumatic cardiovascular injuries. *Anesthesiology* 94(4):615-622.
- Visvikis GA, Hinrichs CR, Shah K (2002) Virtual endoscopy for evaluation of tracheal trauma. *Emergency Radiology* 9:162-164.
- Wall SD, Federle MP, Jeffrey RB et al (1983): CT diagnosis of unsuspected pneumothorax after blunt trauma. *AJR* 141:919-921.
- Wan YL, Tasi KT, Yeown KM, et al (1997) CT findings of bronchial transection. *Am J Emerg Med* 15:176-177.
- Wicky S, Capasso P, Meuli R, et al (1998) Spiral CT aortography: an efficient technique for the diagnosis of traumatic aortic injury. *Eur Radiol* 8:828-833.
- Wicky S, Wintermark M, Schnyder P, et al (2000) Imaging of blunt chest trauma. *Eur Radiol* 10:1525-1538.
- Wintermark M, Schnyder P, Wicky S (2001) Blunt traumatic rupture of a mainstem bronchus: spiral CT demonstration of the "fallen lung" sign. *Eur Radiol* 11:409-411.
- Wintermark M, Wicky S, Schnyder P (2002) Imaging of acute traumatic injuries of the thoracic aorta. *Eur Radiol* 12:431-442.
- Worthy SA, Kang EY, Hartman TE, et al (1995) Diaphragmatic rupture: CT findings in 11 patients. *Radiology* 194:885-888.



# Vascular Injuries of the Thorax: Multi-Detector-Row CT and 3D Imaging

H. Alkadhi, S. Leschka, S. Wildermuth

## 2.7

### Contents

2.7.1	Introduction	179
2.7.2	Clinical Findings	179
2.7.3	Imaging	180
2.7.3.1	Thoracic CT Angiography Imaging Protocol	180
2.7.3.2	Traumatic Aortic Transection	180
2.7.3.3	Traumatic Aortic Intramural Hematoma	183
2.7.3.4	Traumatic Myocardial Rupture	185
2.7.3.5	Traumatic Extra-aortic Vascular Injury	187
2.7.4	Conclusion	187
	References	187

### 2.7.1 Introduction

Radiology remains an ever-evolving discipline. Introduction of new modalities frequently impacts on the optimal diagnostic pathway for evaluation of a given clinical syndrome. Traditionally, catheter angiography has been considered the gold standard for evaluating patients with traumatic vascular injuries. It was until the beginning of the 1980s that the chest, and especially the thoracic aorta, remained difficult areas to evaluate with computed tomography (CT). Cardiovascular and respiratory motion and insufficient resolution of small aortic injuries limited the utility of conventional single-slice CT. Because the risk of fatal exsanguinations was high, patients often directly underwent thoracic catheter aortography to exclude traumatic aortic injuries [1]. The improvements in reducing motion and volume averaging artifacts of helical CT with continuous data acquisition in the early 1990s allowed for the first time a reliable demonstration of the aortic wall and lumen so that helical chest CT became sufficient for diagnosing traumatic vascular injuries [2]. Presently, multi-detector-row CT plays the dominant and critical role in the evaluation of patients with traumatic thoracic vascular emergencies. With recent hardware and software developments, vascular injuries of the entire torso, including the

thoracic aorta, can be detected quickly, even while the patient is being resuscitated and assessed [3–5].

Basically, two different mechanisms cause vascular injury as a result from thoracic trauma: compressive and deceleration forces. Compressive forces result from blows or external compression against the spine and can cause lacerations resulting in vessel rupture. Deceleration forces cause stretching and linear shearing forces between fixed and more freely moveable objects resulting in lacerations or injuries of blood vessels. Penetrating injuries may be produced by a variety of devices, such as knives and high-velocity projectiles, and each is associated with a different injury pattern. In the setting of blunt thoracic trauma where a penetrating wound does not indicate the potentially injured organs, CT has the capability of rapidly assessing multiple anatomic regions within the same examination.

This chapter highlights the pivotal role of multi-detector-row CT with use of two- and three-dimensional CT data post-processing techniques for the visualization and diagnosis of potentially lethal traumatic vascular injuries.

### 2.7.2 Clinical Findings

Approximately 80% of patients with blunt traumatic aortic or cardiac injury die from exsanguination at the scene of the accident [6]. In the remaining 20%, the mortality rate of acute traumatic aortic injury in the absence of surgical treatment is high [7]. On the other hand, 70% of patients with blunt traumatic lesion who reach the hospital alive will survive, provided that appropriate treatment is initiated. Development of coordinated emergency medical services with trained trauma centers together with recent advances in diagnostic imaging modalities may allow for prompt and accurate diagnosis and thus can improve the trauma patients' outcome [7, 8].

Clinically, the majority of traumatic aortic injuries are silent until the onset of sudden hemodynamic decompensation; therefore, the initial clinical examination is usually neither sensitive nor specific and the symptoms unspecific [9]. Common symptoms in cases of transmural aortic lesions with mediastinal hematoma are retrosternal and



interscapular chest pain, dyspnea, hoarseness, and coughing, whereas acute coarctation syndromes can represent with upper limb hypertension and lower limb hypotension as well as with precordial or interscapular systolic ejection murmur. Because the chest walls are elastic, most kinetic energy is absorbed by the intrathoracic viscera rather than by the thoracic cage itself; therefore, 40% of patients with acute traumatic aortic injury show no external sign of chest wall trauma [9]. Sternal, clavicular, scapular, or upper and paravertebral rib fractures are not specific for aortic injuries but indicate the severity of thoracic trauma and thus should raise the suspicion for blunt aortic injuries [10, 11].

## 2.7.3 Imaging

### 2.7.3.1 Thoracic CT Angiography Imaging Protocol

The CT imaging protocol has to be optimized for maximizing the diagnostic yield and for the most complete and accurate volume coverage. For assessment of vascular emergencies, collimation, pitch, and intravenous contrast material injection protocols must be tailored to the region of interest (ROI) for the given anatomic area. At our institute, imaging of thoracic vascular emergencies is performed with a 16-row MDCT scanner (Sensation 16, Siemens, Forchheim, Germany) which is integrated into the emergency room [8]. The technical parameters, contrast bolus regimen, and the image reconstruction parameters of our emergency CT protocol are presented in Table 1. Scanning is performed from the diaphragm to the thoracic outlet. Three main post-processing techniques for the axial CT data sets are commonly used: multi-planar reconstructions (MPR); maximum intensity projections (MIP); and volume rendering (VR). The MPR allow the scanned volume to be viewed in any arbitrary plane interactively determined by the viewer. These reconstructions are especially useful when following vessels. The MIP are obtained by projecting onto an image plane the voxels with the highest

attenuation encountered through the whole volume. This technique is useful for evaluation of structures that are not lying in a single plane; however, disadvantages arise from the fact that vessels close to bones may be obscured. The VR images are useful for visualization of complex vessel anatomy and pathology and to best advantage delineates tortuous vessels and smaller branches [12]. It is also the favored method for reporting and demonstrating purposes to the referring surgeon. These post-processing techniques are used as the initial and only imaging modality for assessment of vascular pathology and for surgical or interventional treatment planning, thus obviating conventional catheter angiography and hereby leading to reduced costs [13].

### 2.7.3.2 Traumatic Aortic Transection

In traumatic aortic transection, rupture results as the tear extends from the intima and media into the adventitial layer of the aortic wall [14, 15]. Subsequent mediastinal hemorrhage develops and extends cranially along the extrapleural space and leads to left apical extrapleural capping. Subsequently, the mediastinal hematoma may extend into the pleural space resulting in a hemothorax. Approximately 90% of blunt traumatic aortic injuries occur at the level of the aortic isthmus immediately distal to the origin of the left subclavian artery [9, 14, 15]. Seven to 8% of traumatic aortic transections are located in the aortic root and are often associated with aortic valve tears, cardiac contusions or ruptures, coronary artery tears, and/or hemopericardium with pericardiac tamponade [16, 17]. In approximately 2% of cases, traumatic ruptures of the descending aorta occur at the level of the diaphragm [16, 17].

Conventional chest radiography is commonly the first imaging examination of victims of deceleration injury that arrive to the emergency room. Suspicious findings suggesting mediastinal hemorrhage include superior mediastinal widening, an abnormal aortic contour, aorta-pulmonary window opacification, deviation of a nasogastric tube to the right, displacement of an endotracheal tube off the

**Table 1.** Technical scan parameters, contrast regimen, and image reconstruction parameters for thoracic angiography with 16-channel CT. CM contrast medium

Scanning parameters		Contrast regimen and reconstruction parameters	
Collimation	16×1.5	CM amount (ml)	120
Gantry rotation time (s)	0.375	CM administration technique	Bolus tracking in ascending aorta
Tube potential (kV)	120	Start of acquisition (HU)	120
Tube current (mAs) <sup>a</sup>	150	Section width (mm)	2
Feed per rotation (mm)	20	Increment (mm)	1
Radiation dose (mSv) <sup>b</sup>	4.0 (M)	Field of view (mm)	~380
	5.3 (F)		

<sup>a</sup> Effective tube current is on-line modulated using the CareDose technique

<sup>b</sup> Radiation dose calculations according to anthropomorphic mathematical phantoms [46]. Values for male (M) and female (F) patients are given

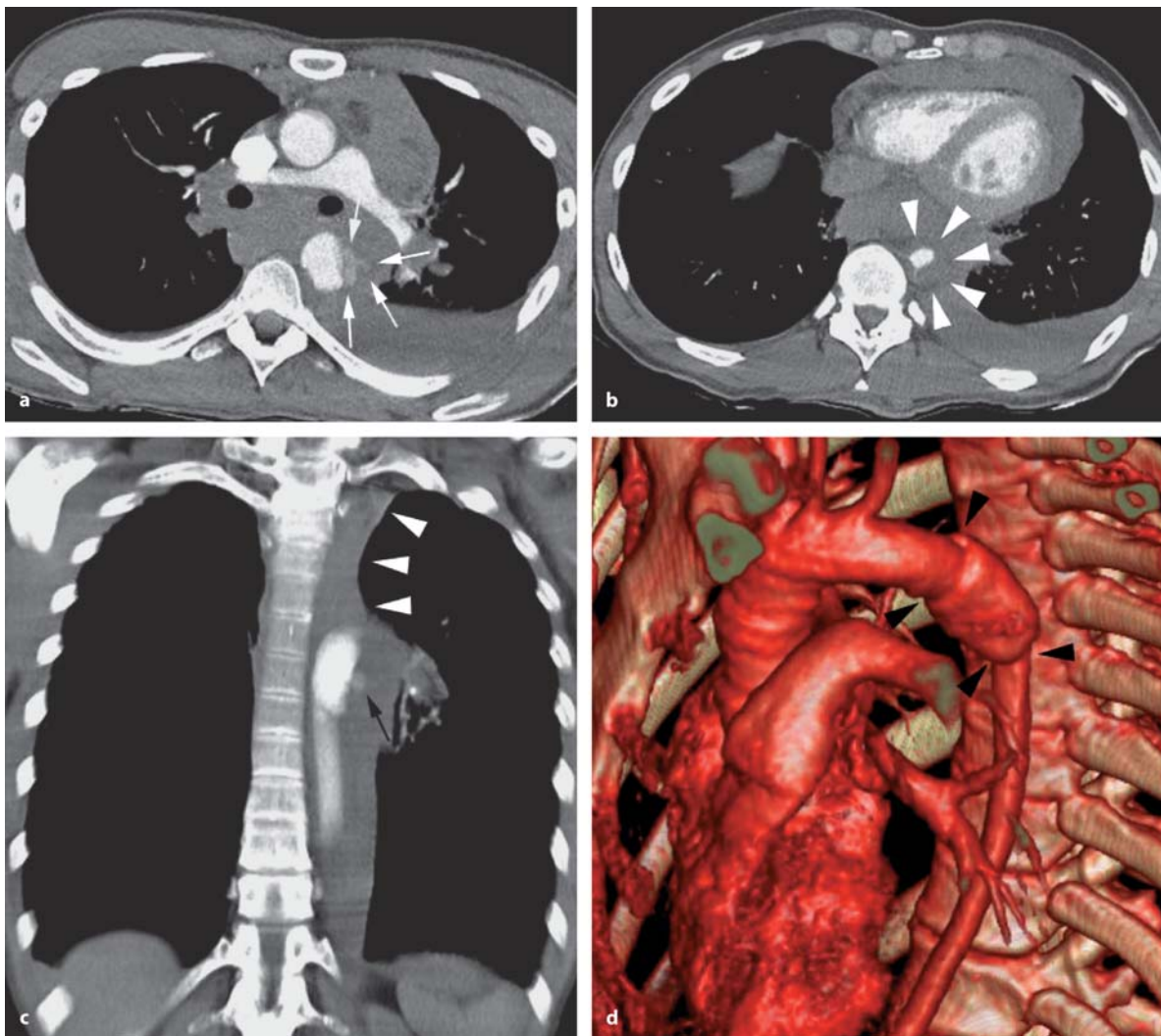


**Fig. 1.** A 42-year-old man involved in a traffic accident with blunt thoracic trauma. **a** Axial CT image at the level of the pulmonary arteries demonstrates acute subadventitial contrast medium extravasation (*arrows*) indicating acute traumatic aortic transection with consecutive hemomediastinum and left-sided hemothorax. **b** Axial CT image at a lower level shows additional acute intramural hematoma (*arrowheads*) in the descending aorta. Note the

two intercostal arteries crossing the intramural hematoma. **c** Coronal thin maximum intensity projection (MIP) reconstruction demonstrates the contrast material extravasation (*arrow*) and the left apical extrapleural capping (*arrowheads*). **d** Oblique sagittal clip plane of volume-rendering reconstruction allows 3D anatomic delineation of the aortic transection site (*arrowheads*), thereby facilitating surgical and interventional treatment planning.

midline, an abnormal left paratracheal stripe, and depression of the left main bronchus [18]. Finally, a left-sided apical extrapleural cap or a left-sided hemothorax are radiological features typically associated with aortic lesions. All patients with an “unclearable” mediastinum by radiography should undergo further imaging; however, a radiographically normal mediastinum does not exclude aortic injury. Over 50% of patients with a normal initial chest radiograph suffer from multiple thoracic injuries on CT scans, among which 7–8% are potentially fatal aortic lesions [19–21]. On the other hand, radiographic evaluation for evidence of mediastinal blood is often falsely positive

and can be caused by, for example, vascular engorgement, mediastinal lipomatosis, or lymphadenopathy; therefore, findings suggesting mediastinal hemorrhage on supine chest radiographs have a sensitivity of 90%, a specificity of 25%, and a negative predictive value of 95% for major vascular injury [21, 22].

Catheter angiography has traditionally been the gold standard for evaluating acute aortic disease. Aortography findings of aortic transection include visualization of an intimal tear, aortic contour or caliber abnormality, pseudoaneurysm formation, and contrast extravasation. Thoracic aortography can detect blunt traumatic aortic injuries with

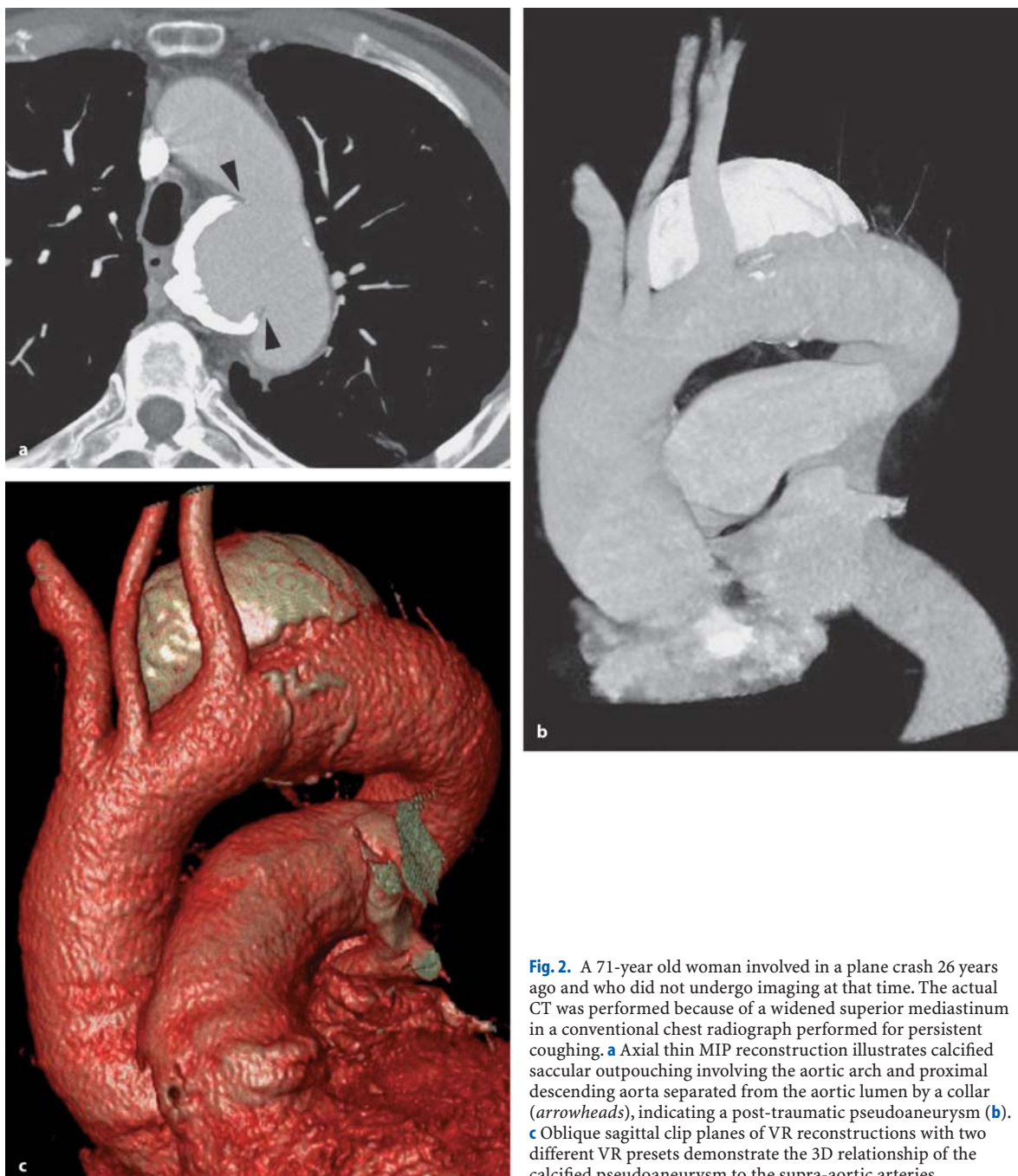


**Fig. 2.** A 71-year old woman involved in a plane crash 26 years ago and who did not undergo imaging at that time. The actual CT was performed because of a widened superior mediastinum in a conventional chest radiograph performed for persistent coughing. **a** Axial thin MIP reconstruction illustrates calcified saccular outpouching involving the aortic arch and proximal descending aorta separated from the aortic lumen by a collar (*arrowheads*), indicating a post-traumatic pseudoaneurysm (**b**). **c** Oblique sagittal clip planes of VR reconstructions with two different VR presets demonstrate the 3D relationship of the calcified pseudoaneurysm to the supra-aortic arteries

a sensitivity of 96% and a specificity of 98% [23]. False-negative examinations are most often related to incomplete series or inadequate injections, false-positive examinations are often caused by a prominent ductus diverticulum or from ulcerated atheromas [9]. The major disadvantage of thoracic catheter aortography (besides its invasiveness) is the time needed to initiate and complete the examination, which can considerably delay other diagnostic and therapeutic procedures.

Multi-detector-row CT is considered the modality of choice for the evaluation of traumatic aortic transections [24]. At our hospital, thoracic CT angiography is virtually performed in all patients where the severity of the accident and the chest radiography findings are compatible with blunt traumatic aortic injury. The classic CT appearance of a ruptured aorta features a sleeve of subadventitial contrast medium with a tear involving the whole vessel wall (Fig. 1). The CT also accurately demonstrates hemomediastinum



and hemothorax as being indirect signs of traumatic aortic injury. The location of the hemomediastinum is of diagnostic significance: for example, hemorrhage surrounding the aorta and other vascular structures is more suggestive of vascular injury than blood, which is confined to the retrosternal space adjacent to a sternal fracture. Computed tomography was found to have a sensitivity and negative predictive value equivalent to that of aortography [25] with a sensitivity, specificity, and accuracy of 96, 99, and 99%, respectively [22, 26–28]. Moreover, CT has been shown to have a 100% sensitivity for the detection of traumatic aortic transection on the basis of the combined findings of mediastinal hemorrhage and aortic injury. A negative CT examination with a normal mediastinum and a regular aorta surrounded by normal fat has a 100% negative predictive value for acute traumatic aortic transection [3]. When the aortic rupture remains unrecognized or untreated, a pseudoaneurysm will develop which features a sacular outpouching separated from the aortic lumen by a collar and which may partially calcify in the chronic phase (Fig. 2).

### 2.7.3.3 Traumatic Aortic Intramural Hematoma

Acute intramural hematoma (AIH) is referred to as a variant of dissection, i.e., non-communicating aortic dissection [29, 30]. In contrast to the classical aortic dissection, which is characterized by an intimo-medial tear [31, 32], necropsy data on intramural hematomas have shown the lack of an entry tear [30]. The false lumen is then created by a hemorrhage into the aortic media, most likely after rupture of the vasa vasorum that penetrate the outer half of the media from the adventitia and arborize at this level [31–33]. In patients with traumatic AIH the thickening of the aortic wall is generally circular [30]. The AIH weakens the aorta and may progress either to rupture of the aortic wall externally or to inward disruption of the intimal layer, the latter leading to a communicating aortic dissection [32]. The reported mean thickness of type-A and type-B intramural hematoma is  $12.7 \pm 6.9$  and  $10.5 \pm 3.5$  mm, respectively [34]. As the normal thickness of the aortic wall is

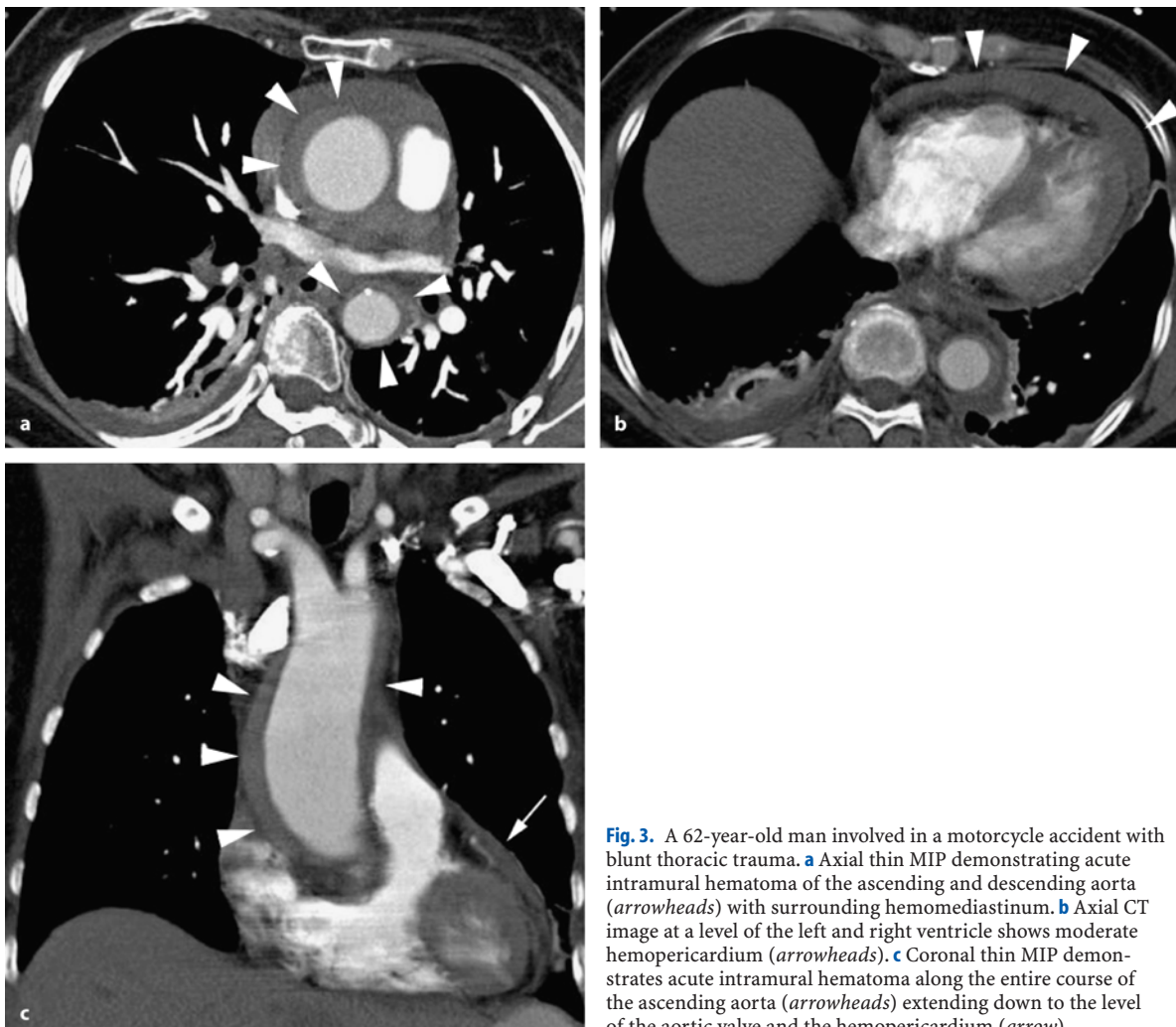


**Fig. 3.** A 62-year-old man involved in a motorcycle accident with blunt thoracic trauma. **a** Axial thin MIP demonstrating acute intramural hematoma of the ascending and descending aorta (*arrowheads*) with surrounding hemomediastinum. **b** Axial CT image at a level of the left and right ventricle shows moderate hemopericardium (*arrowheads*). **c** Coronal thin MIP demonstrates acute intramural hematoma along the entire course of the ascending aorta (*arrowheads*) extending down to the level of the aortic valve and the hemopericardium (*arrow*)



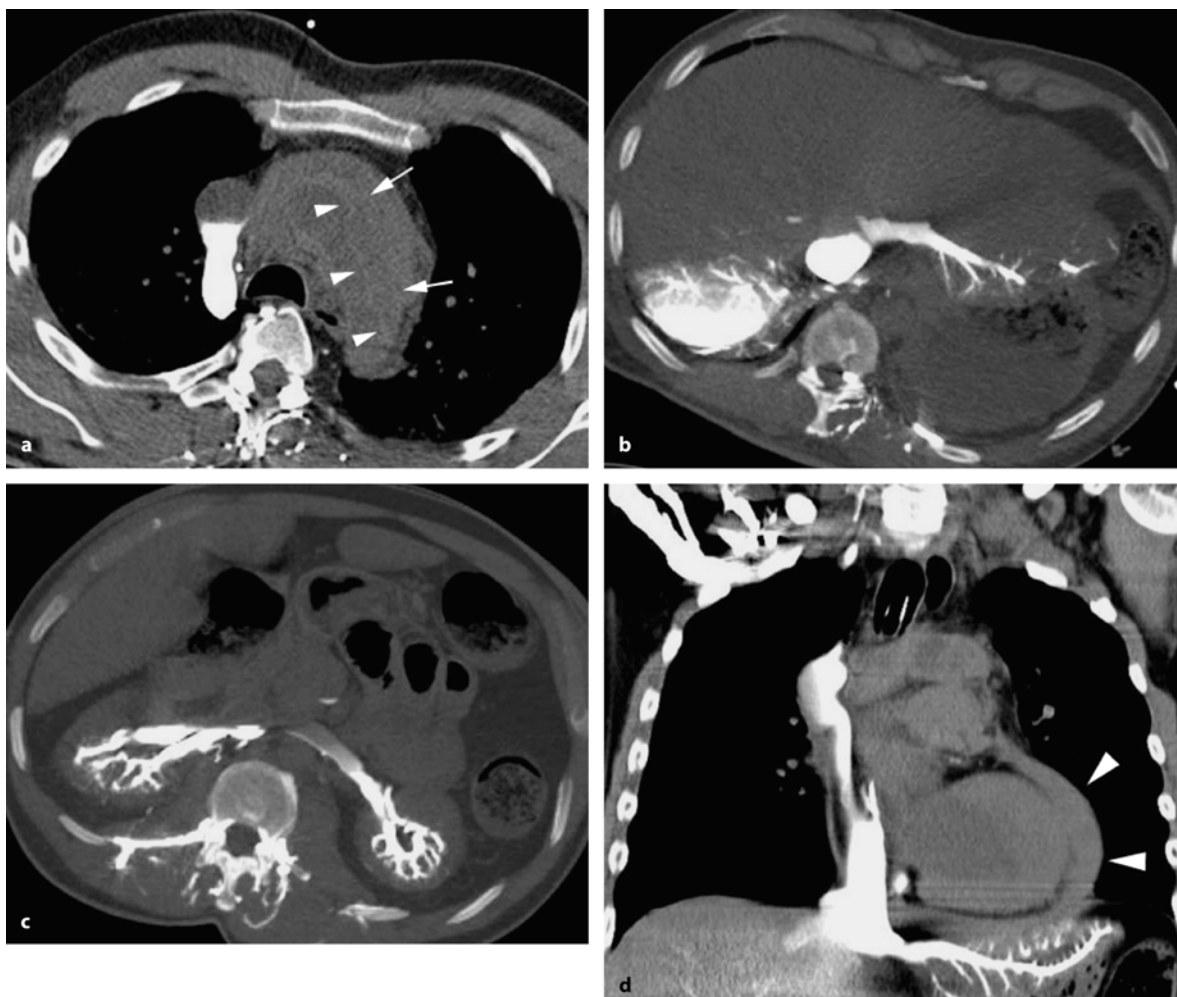


**Fig. 4.** A 38-year old man after a skydiving accident with blunt thoracic trauma. During CT examination, acute and severe hemodynamic deterioration occurred and the patient subsequently died on the scanner table. **a** Axial CT at the level of the aortic arch demonstrates acute intramural hematoma characterized by a hyperdense longitudinal area in the vessel wall. Hyperdensity enables to distinguish the intramural hematoma from the aortic lumen medially (*arrowheads*) and the hemomediastinum laterally (*arrows*). **b** Axial CT image at the level of the upper abdomen

demonstrates pooling of contrast medium due to acute congestive heart failure via the inferior vena cava into the right and left hepatic veins. **c** Axial CT image demonstrates additional pooling of the contrast medium in both kidneys via renal veins. Note pooling of contrast material also in perivertebral and in the epidural, intraspinal venous plexus. **d** Coronal thin MIP reconstruction demonstrates large hemopericardium and pooling (*arrowheads*) of contrast material via the superior vena cava, the right atrium, and the inferior vena cava, eventually reaching the left hepatic vein

usually  $<3$  mm, a wall thickness  $\geq 5$  mm is considered sufficient for diagnosing AIH in patients with typical clinical symptoms of aortic syndromes.

Transesophageal echocardiography (TEE) has a reported sensitivity of 97% and a specificity of 100% for the diagnosis of acute intramural hematoma [35]. Conventional catheter angiography has been shown to have a lower sensitivity of 83% (specificity 100%) because it may fail to demonstrate changes in the media in the absence of an intimal lesion [35]. Multi-detector-row CT approaches a sensitivity of 100% and a negative predictive value of 100% [36, 37].

At CT, demonstration of a continuous, usually crescentic, high-attenuation area along the aortic wall without

visualization of an intimal flap is characteristic before contrast medium injection, which fails to be enhanced after injection of contrast medium (Fig. 3) [24, 34]; thus, acute intramural hematoma must be distinguished from mural thrombus by identification of the intima: a mural thrombus lies on top of the intima, which is frequently calcified, whereas an intramural hematoma is subintimal [32].

Imaging findings play a significant role for risk stratification in patients with AIH [34]. Complete resorption of the hematoma is possible with pure medical treatment, and the clinical results of “aggressive” medical treatment are better in type-A intramural hematoma than in classical aortic dissection, which suggests the important role for

imaging studies in the selection of therapeutic strategies [34]. Hematoma thickness and aortic diameter are important predictors of adverse clinical events, including death and development of a classic aortic dissection [34, 38]. Similarly, presenting clinical features are important predictors of early mortality. The high prevalence of fluid extravasates, pericardial and pleural effusion, and mediastinal hemorrhage is a frequent finding in AIH. Among them, cardiac tamponade can be considered the largest challenge to the emergency physicians, as mortality is much higher in patients with cardiac tamponade (Fig. 4).

### 2.7.3.4 Traumatic Myocardial Rupture

Myocardial ruptures are rarely diagnosed in blunt chest trauma patients since most of these patients die at the scene of the accident [6]; however, for the survivors,

prompt diagnosis and surgery are mandatory and save up to 80% of patients [39]. Depiction of myocardial ruptures relies mainly on a high clinical index of suspicion and on echocardiography, particularly on TEE [40].

Conventional chest radiography demonstrates in 70% of patients a widened mediastinum, due to either hemo-pericardium or mediastinal hematoma. A left hemothorax occurs when the pericardium and pleura have been simultaneously torn [41]. The TEE demonstrates a hemo-pericardium with or without cardiac tamponade and may disclose focal thrombi or abnormal Doppler blood flows, both indirect signs of a myocardial lesion. The myocardial rupture itself is only rarely observed [40].

Computed tomography does not allow the diagnosis of a myocardial rupture in the majority of patients, but demonstrates indirect signs such as hemo-pericardium. Very rarely, a small spot of contrast material or even contrast material leak can be observed (Fig. 5) [41].

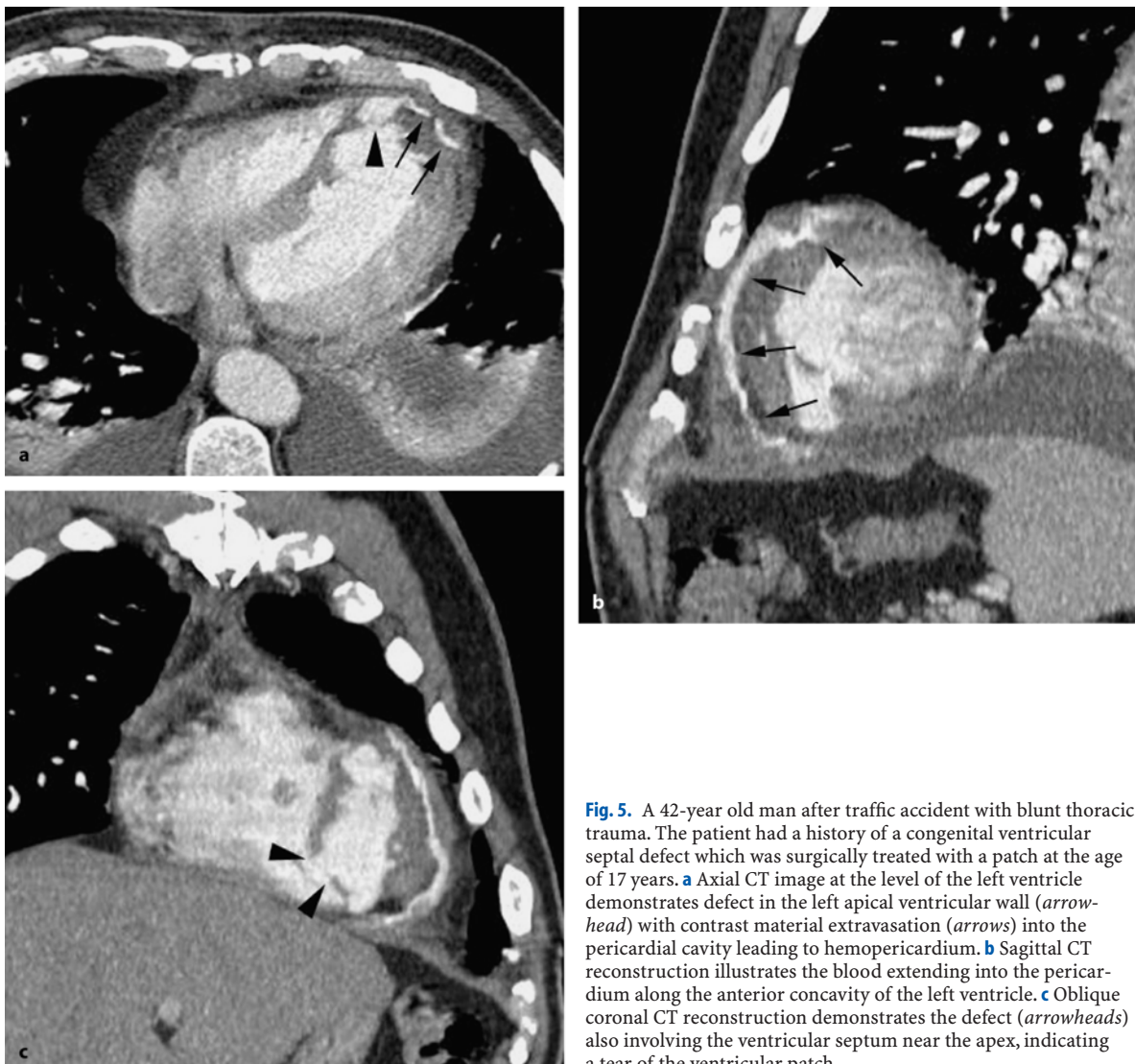


**Fig. 5.** A 42-year old man after traffic accident with blunt thoracic trauma. The patient had a history of a congenital ventricular septal defect which was surgically treated with a patch at the age of 17 years. **a** Axial CT image at the level of the left ventricle demonstrates defect in the left apical ventricular wall (*arrowhead*) with contrast material extravasation (*arrows*) into the pericardial cavity leading to hemo-pericardium. **b** Sagittal CT reconstruction illustrates the blood extending into the pericardium along the anterior concavity of the left ventricle. **c** Oblique coronal CT reconstruction demonstrates the defect (*arrowheads*) also involving the ventricular septum near the apex, indicating a tear of the ventricular patch

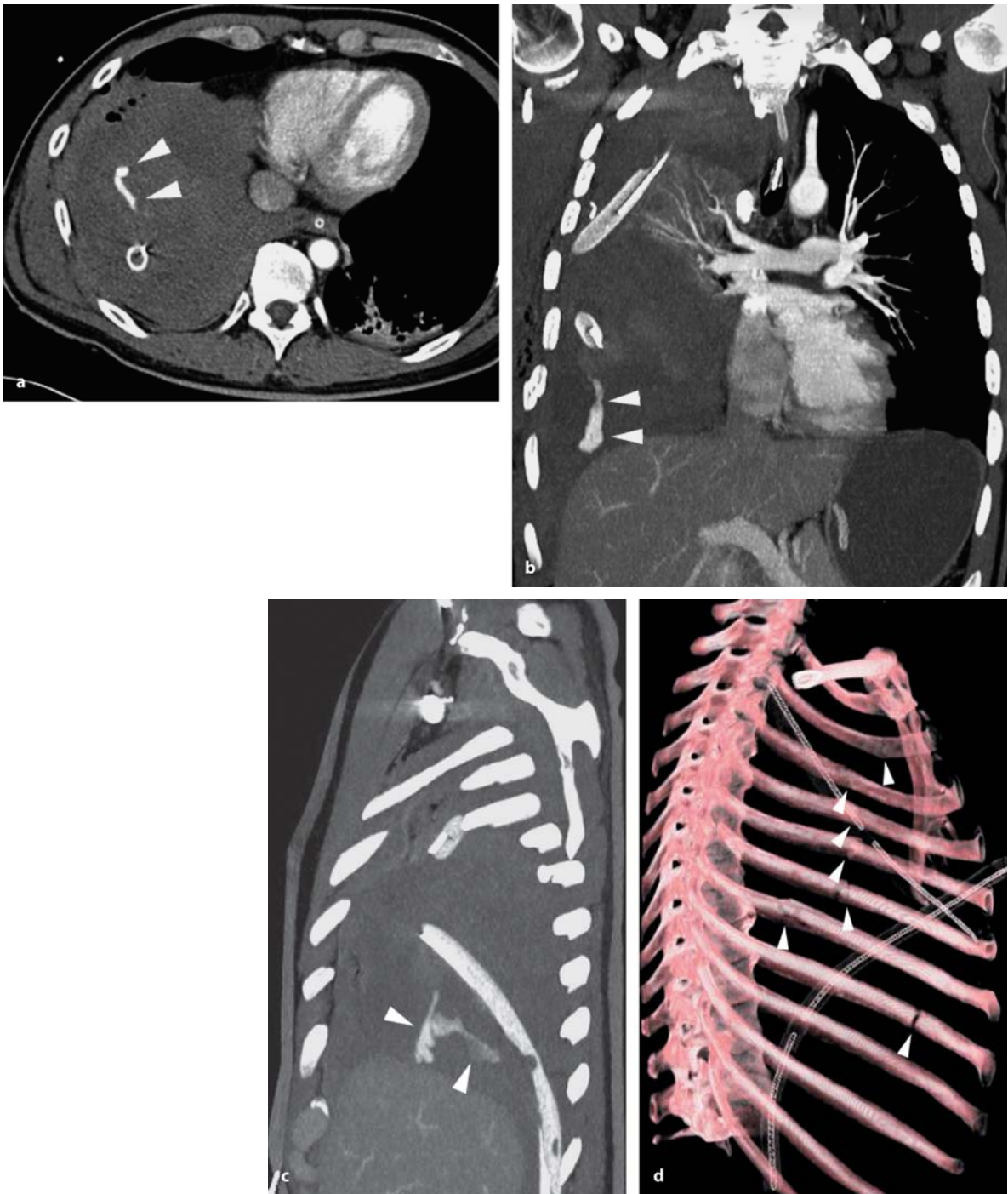


**Fig. 6.** A 58-year old man suffering from blunt thoracic trauma after falling from a balcony. **a** Axial CT image at the level of the lower thorax demonstrates right-sided hemothorax with subtotal atelectasis of the right lung, an inserted chest tube, and a jet of contrast material (*arrowheads*), indicating active arterial bleeding into the right pleural cavity. **b** Coronal thin MIP reconstruction shows active arterial bleeding (*arrowheads*) most probably origi-

nating from a right diaphragmatic artery. **c** Sagittal thin MIP reconstruction illustrates the active bleeding jet directed both cranially and caudally (*arrowheads*). **d** Sagittal clip plane of VR reconstruction illustrates a single image in the right thoracic cage with a total of seven serial rib fractures (*arrowheads*), thus indicating the possible underlying cause of the traumatic laceration of a diaphragmatic vessel. Note the two inserted chest tubes



### 2.7.3.5 Traumatic Extra-aortic Vascular Injury

Traumatic vascular injury of thoracic vessels other than the aorta is encountered in <1% of trauma patients who reach the hospital alive [9]. When present, they are multiple in 69% and are associated with blunt aortic lesions in 20% of cases. Depending on the injured vessel, hemorrhage can be located either in the mediastinum or in the pleural space. Fractures of the ribs and the sternum are the most common of all major chest injuries, occurring in almost 40% of patients who sustained a severe, non-penetrating trauma [42, 43]. Complications of rib and sternal fractures are considered to be more important than the fracture itself. For example, fractures of upper ribs suggest a severe trauma with potential great vessel and brachial plexus injury, whereas fractures of the lower ribs can be accompanied by lacerations of upper abdominal organs. Complications of rib fractures include pulmonary contusion, atelectasis, flail chest, pneumothorax, laceration of the pericardium and diaphragm, and hemothorax. Hemothorax usually derives from bleeding of intercostal and internal mammary arteries and is caused by vessel wall injury from fractured ribs [44]. Very rarely, hemothorax can be caused by traumatic laceration of diaphragmatic vessels from broken ribs (Fig. 6).

Multi-detector-row CT is the method of choice, not only for the diagnosis of thoracic cage fractures [45] but also for the diagnosis of associated soft tissue and vascular injury. It thus allows the evaluation of the underlying cause of vessel injury, the visualization of the injured vessel itself, and allows the delineation of the sequelae of bleeding.

### 2.7.4 Conclusion

Multi-detector-row CT is being increasingly embraced as the most important non-invasive tool for imaging thoracic vessels. It has proven efficacy in the diagnosis of vascular pathology and has even surpassed the diagnostic capabilities of conventional angiography. The advancements have led CT to a transform from a pure cross-sectional 2D into a true 3D imaging modality by allowing to display the data in any straight or curved plane and to approach the data from any desired vantage point. It can therefore be considered a reliable technique for the definitive evaluation of patients with traumatic, thoracic vascular injuries.

### References

1. Tomiak MM, Rosenblum JD, Messersmith RN, Zarins CK (1993) Use of CT for diagnosis of traumatic rupture of the thoracic aorta. *Ann Vasc Surg* 7:130–139
2. Gavant ML, Menke PG, Fabian T, Flick PA, Graney MJ, Gold RE (1995) Blunt traumatic aortic rupture: detection with helical CT of the chest. *Radiology* 197:125–133
3. Mirvis SE, Shanmuganathan K, Miller BH, White CS, Turney SA (1996) Traumatic aortic injury: diagnosis with contrast-enhanced thoracic CT: five-year experience at a major trauma center. *Radiology* 200:413–422
4. Mirvis SE, Kostrubiak I, Whitley NO, Goldstein LD, Rodriguez A (1987) Role of CT in excluding major arterial injury after blunt thoracic trauma. *Am J Roentgenol* 149:601–605
5. Wicky S, Capasso P, Meuli R, Fischer A, Segesser L von, Schnyder P (1998) Spiral CT aortography: an efficient technique for the diagnosis of traumatic aortic injury. *Eur Radiol* 8:828–833
6. Bintz M, Gall WE, Harbin D (1992) Blunt myocardial disruption: report of an unusual case and literature review. *J Trauma* 33:933–934
7. Frick EJ et al. (1997) Outcome of blunt thoracic aortic injury in a level I trauma center: an 8-year review. *J Trauma* 43:844–851
8. Boehm T et al. (2004) Application of multislice spiral CT (MSCT) in multiple injured patients and its effect on diagnostic and therapeutic algorithms. *Rofo* 176:1734–1742 [in German]
9. Wintermark M, Wicky S, Schnyder P (2002) Imaging of acute traumatic injuries of the thoracic aorta. *Eur Radiol* 12:431–442
10. Lee J, Harris JH Jr, Duke JH Jr, Williams JS (1997) Noncorrelation between thoracic skeletal injuries and acute traumatic aortic tear. *J Trauma* 43:400–404
11. Gupta A, Jamshidi M, Rubin JR (1997) Traumatic first rib fracture: Is angiography necessary? A review of 730 cases. *Cardiovasc Surg* 5:48–53
12. Wildermuth S, Leschka S, Alkadhi H, Marincek B (2005) Multislice CT in the pre- and postinterventional evaluation of mesenteric perfusion. *Eur Radiol* 15:1203–1210
13. Lawler LP, Fishman EK (2001) Multi-detector row CT of thoracic disease with emphasis on 3D volume rendering and CT angiography. *Radiographics* 21:1257–1273
14. Richens D, Field M, Neale M, Oakley C (2002) The mechanism of injury in blunt traumatic rupture of the aorta. *Eur J Cardiothorac Surg* 21:288–293
15. Macura KJ, Corl FM, Fishman EK, Bluemke DA (2003) Pathogenesis in acute aortic syndromes: aortic aneurysm leak and rupture and traumatic aortic transection. *Am J Roentgenol* 181:303–307
16. Creasy JD, Chiles C, Routh WD, Dyer RB (1997) Overview of traumatic injury of the thoracic aorta. *Radiographics* 17:27–45
17. Ben-Menachem Y (1993) Rupture of the thoracic aorta by broadside impacts in road traffic and other collisions: further angiographic observations and preliminary autopsy findings. *J Trauma* 35:363–367
18. Macura KJ, Szarf G, Fishman EK, Bluemke DA (2003) Role of computed tomography and magnetic resonance imaging in assessment of acute aortic syndromes. *Semin Ultrasound CT MR* 24:232–254
19. Woodring JH (1990) The normal mediastinum in blunt traumatic rupture of the thoracic aorta and brachiocephalic arteries. *J Emerg Med* 8:467–476
20. Exadaktylos AK, Sclabas G, Schmid SW, Schaller B, Zimmermann H (2001) Do we really need routine computed tomographic scanning in the primary evaluation of blunt chest trauma in patients with “normal” chest radiograph? *J Trauma* 51:1173–1176
21. Mirvis SE et al. (1987) Value of chest radiography in excluding traumatic aortic rupture. *Radiology* 163:487–493



22. Patel NH, Stephens KE Jr, Mirvis SE, Shanmuganathan K, Mann FA (1998) Imaging of acute thoracic aortic injury due to blunt trauma: a review. *Radiology* 209:335–348
23. Ahrar K, Smith DC, Bansal RC, Razzouk A, Catalano RD (1997) Angiography in blunt thoracic aortic injury. *J Trauma* 42:665–669
24. Alkadhi H et al. (2004) Vascular emergencies of the thorax after blunt and iatrogenic trauma: multi-detector row CT and three-dimensional imaging. *Radiographics* 24:1239–1255
25. Parker MS et al. (2001) Making the transition: the role of helical CT in the evaluation of potentially acute thoracic aortic injuries. *Am J Roentgenol* 176:1267–1272
26. Mirvis SE, Shanmuganathan K, Buell J, Rodriguez A (1998) Use of spiral computed tomography for the assessment of blunt trauma patients with potential aortic injury. *J Trauma* 45:922–930
27. Wicky S, Wintermark M, Schnyder P, Capasso P, Denys A (2000) Imaging of blunt chest trauma. *Eur Radiol* 10:1524–1538
28. Gavant ML (1999) Helical CT grading of traumatic aortic injuries. Impact on clinical guidelines for medical and surgical management. *Radiol Clin North Am* 37:553–574, vi
29. Raab BW, Vosschenrich R, Fischer U, Funke M, Grabbe E (2001) Intramural hematomas of the aorta. *Radiologe* 41:653–659 [in German]
30. Vilacosta I et al. (1997) Natural history and serial morphology of aortic intramural hematoma: a novel variant of aortic dissection. *Am Heart J* 134:495–507
31. Vilacosta I, Roman JA (2001) Acute aortic syndrome. *Heart* 85:365–368
32. Macura KJ, Corl FM, Fishman EK, Bluemke DA (2003) Pathogenesis in acute aortic syndromes: aortic dissection, intramural hematoma, and penetrating atherosclerotic aortic ulcer. *Am J Roentgenol* 181:309–316
33. Choi SH et al. (2001) Useful CT findings for predicting the progression of aortic intramural hematoma to overt aortic dissection. *J Comput Assist Tomogr* 25:295–299
34. Song JK (2004) Diagnosis of aortic intramural haematoma. *Heart* 90:368–371
35. Goarin JB, Cluzel P, Gosgnach M, Lamine K, Coriat P, Riou B (2000) Evaluation of transesophageal echocardiography for diagnosis of traumatic aortic injury. *Anesthesiology* 93:1373–1377
36. Dyer DS et al. (1999) Can chest CT be used to exclude aortic injury? *Radiology* 213:195–202
37. Dyer DS et al. (2000) Thoracic aortic injury: How predictive is mechanism and is chest computed tomography a reliable screening tool? A prospective study of 1561 patients. *J Trauma* 48:673–682
38. Song JM et al. (2003) Usefulness of the initial noninvasive imaging study to predict the adverse outcomes in the medical treatment of acute type A aortic intramural hematoma. *Circulation* 108 (Suppl 1):II324–328
39. Shalaby RI, Rajendran U, Regunathan R (1999) Blunt traumatic rupture of the heart: case report and selected review. *Ann Thorac Cardiovasc Surg* 5:123–129
40. Symbas NP, Bongiorno PF, Symbas PN (1999) Blunt cardiac rupture: the utility of emergency department ultrasound. *Ann Thorac Surg* 67:1274–1276
41. Wintermark M, Delabays A, Bettex D, Schnyder P (2001) Blunt trauma of the heart: CT pattern of atrial appendage ruptures. *Eur Radiol* 11:113–116
42. Sirmali M et al. (2003) A comprehensive analysis of traumatic rib fractures: morbidity, mortality and management. *Eur J Cardiothorac Surg* 24:133–138
43. Athanassiadi K, Gerazounis M, Moustardas M, Metaxas E (2002) Sternal fractures: retrospective analysis of 100 cases. *World J Surg* 26:1243–1246
44. Simon BJ, Chu Q, Emhoff TA, Fiallo VM, Lee KF (1998) Delayed hemothorax after blunt thoracic trauma: an uncommon entity with significant morbidity. *J Trauma* 45:673–676
45. Alkadhi H, Wildermuth S, Marincek B, Boehm T (2004) Accuracy and time efficiency for the detection of thoracic cage fractures: volume rendering compared with transverse computed tomography images. *J Comput Assist Tomogr* 28:378–385
46. Kalender WA, Schmidt B, Zankl M, Schmidt M (1999) A PC program for estimating organ dose and effective dose values in computed tomography. *Eur Radiol* 9:555–562

# Imaging of Abdominal and Pelvic Injuries

S. Leschka, H. Alkadhi, L. Husmann, S. Wildermuth

## 2.8

### Contents

2.8.1	Introduction	189
2.8.2	Clinical Findings	190
2.8.2.1	Mechanisms of Injury	190
2.8.2.2	Physical Examination	190
2.8.3	Imaging	191
2.8.3.1	Plain Radiography	191
2.8.3.2	Ultrasound	191
2.8.3.3	Computed Tomography	192
2.8.3.4	Imaging Findings in Abdominal and Pelvic Organ Injuries	193
2.8.4	Conclusion	201
	References	201

### 2.8.1 Introduction

In the United States and Western Europe, trauma represents the third leading cause of death, behind cardiovascular diseases and cancers [1]. Disproportionately striking the young and male population, trauma is responsible for the loss of more productive years of life than cancer and cardiovascular disease combined [2]. Trauma most often results from traffic accidents, free or accidental falls from a height, recreational accidents, and violence [3–5]. In multiple traumatized patients, abdominal injuries occur in 19% [6] to 43% [7], and are responsible for a similar rate of death in the early hours after trauma as severe head injuries [7]. While traumatic injuries of the central nervous system, the heart, and the great vessels often lead to death at the site of the accident, patients with abdominal and pelvic injuries more often survive the arrival at the emergency hospital. Rapid diagnosis and treatment of patients with suspected blunt abdominal trauma is a difficult and challenging task for the trauma surgeon, because physical examination in trauma patients is often unreliable and non-specific [1]. Unlike penetrating wounds, the multi-systemic injuries often seen with blunt trauma make an accurate and complete triage more complex [8]. On the one hand, morbidity and lethality of abdominal trauma is

highly dependent on timely therapeutic intervention [9]. On the other hand, missed abdominal injuries are one of the leading avoidable causes of death in multiple traumatized patients [10], thus raising the need for rapid and valid diagnostic evaluation. Diagnostic peritoneal lavage (DPL) has been recommended as screening tool because of its high sensitivity [11]; however, DPL is invasive, limited to injuries in the peritoneal cavity, and has the risk of severe complications such as visceral perforation [12]. The introduction of ultrasound (US) and computed tomography (CT) has improved the diagnostic approach to patients with suspected abdominal and pelvic injuries. Both modalities have widely replaced DPL, due to their high sensitivity for free intra-abdominal fluid. Ultrasound has been widely accepted as the first step in radiological assessment. Ultrasound is of particular value in deciding whether immediate surgical exploration is indicated for intraperitoneal hemorrhage in the hemodynamically unstable patient. If patients are hemodynamically stable, more sophisticated assessment of the injuries can be achieved by CT [4, 5]. With CT evaluation, a comprehensive and complete survey of the injuries is obtained, which allows categorizing trauma patients according to the pattern and severity of their lesions and could help to decide on the required therapeutic procedures. Even if the individual injury is not detectable, CT imaging usually obtains enough information to guide further special diagnostic studies such as endoscopic retrograde cholangio-pancreaticography or invasive angiography. Compared with US, CT imaging has the great advantage of rapid evaluation of the head, spine, chest, abdomen, pelvis, and extremities during a single examination. Moreover, its ability to detect and monitor injuries of the parenchymal abdominal organs (e.g., liver, spleen, kidney) and to compare the imaging findings with the outcome has changed the therapeutic attitude towards non-operative management in the past few years [9]. The development of multi-detector-row CT (MDCT) provides distinct advantages including scanning the entire abdomen and pelvis in a single breath-hold by shortening in acquisition time, thin-collimated submillimeter isotropic imaging, and more precise separation in contrast bolus exploitation. The implementation of MDCT in the emergency ward will further increase its role in evaluating abdominal

and pelvic injuries. As a third evolving imaging modality, magnetic resonance imaging (MRI) offers some distinct advantages over CT, including lack of radiation exposure and less nephrotoxic contrast agent application. Due to several technical restrictions inherent in MRI, including the need for special equipment for anesthesia, difficult patient access, lengthy examination times, and the lack of rapid availability of MRI in the emergency setting, MRI has currently only a minor role in the evaluation of patients with suspected abdominal trauma [13].

Although the practical approach with regard to imaging procedures has been simplified and standardized in the past few years, choice and employment of any particular radiological investigation depends on the equipment available at a particular facility and the urgency of demand particularly in life-threatening situations; thus, the performing radiologist should be familiar with the diagnostic potential of the several imaging modalities in the context of abdominal trauma and the imaging features of the individual abdominal and pelvic injuries.

---

## 2.8.2 Clinical Findings

In general, the abdomen consists of three distinct anatomical compartments. Firstly, the peritoneal cavity includes the vast majority of abdominal organs. The upper intrathoracic segment is covered by the bony thorax and includes diaphragm, liver, spleen, stomach, and transverse colon; thus, slightly protected by the thoracic cage, injuries of these organs are more often transmitted indirectly. Secondly, the retroperitoneum includes the retroperitoneal vessels, pancreas, kidneys, ureters, and portions of duodenum and colon. Injuries to these structures are notoriously difficult to diagnose, because the retroperitoneum is remote from physical and US examination and is not sampled by DPL. Thirdly, the pelvic segment includes rectum, bladder, iliac vessels, and the internal genitalia in women. Although these organs are protected from direct forces to the skeletal pelvis, injuries are difficult to diagnose early because of unreliable physical examination or US studies.

---

### 2.8.2.1 Mechanisms of Injury

By the mechanism of injury, abdominal and pelvic trauma are classified as blunt or penetrating. Penetrating wounds due to knife or firearm incidents are a cause in societies with a high-rate of violence or with a culture of the use of these weapons such as in the United States and South Africa. In penetrating trauma, the entry sites do not accurately predict the nature of deeper injury due to the displacement of moveable abdominal organs. In addition, gunshot wounds may have a circuitous trajectory and thus may injure multiple non-contiguous structures.

In western Europe, blunt abdominal trauma is eight to ten times more frequently than penetrating trauma [6, 7]. Identifying the injury pattern may increase the detection of subtle findings [14]. Injuries in blunt abdominal trauma may be caused by compressive or deceleration forces. Injuries by compressive forces occur when solid parenchymal or hollow organs are blown against a fixed structure such as the spine. Right-sided compression may injure the lung, right hepatic lobe, right kidney, and iliac wing. Left-sided blows may injure the lung, spleen, left kidney, pancreatic body and tail, and the iliac wing. Seat-belt or midline compression injuries may affect the left hepatic lobe, pancreatic head and body, duodenum, renal vascular pedicle, and less commonly, the intestine and aortoiliac vessels. Injuries by decelerating forces occur when differential movement occurs between adjacent structures resulting in stretching and linear shearing forces between fixed and more moveable structures such as the vessels.

The individual abdominal and pelvic organs differentially react on the traumatizing force. The solid abdominal viscera may lacerate, infarct, or suffer vascular, ductal, or pyelocalyceal disruption. The bladder and intestines may rupture. In abdominal pelvic trauma, the direction of applied force often results in an identifiable constellation of injuries. The distribution of injury patterns not only depends on the direction but also on the amount of energy transfer to the abdomen. For instance, pancreatic or small bowel injuries are more often accompanied with liver injuries than with splenic injuries due to the greater force needed to damage the liver [15].

---

### 2.8.2.2 Physical Examination

Information on the accident obtained from a witness help to estimate the severity of injuries. The physical examination focuses primarily on the abdomen. By inspection, the distribution of hematoma or open wounds help to determine the region of the highest energy transfer. Contusion marks of a seat belt are more frequently accompanied with injuries of duodenum, small bowel, and pancreas [16]. If bleeding in the subcutaneous tissue is present, injuries of the bowel are up to ten times more frequent than without [9]. Other helpful clinical findings indicating an abdominal or pelvic injury are hematuria, hemothorax, pneumothorax, and fractures of the lower ribs or the pelvis [17]. In addition, guarding and tenderness of the abdomen are highly suggestive of abdominal injury [17]. Pain is not only limited to the abdominal impact zone, but may also be located in the shoulder in the case of subdiaphragmatic hematoma or in the back in retroperitoneal injuries [9].

Although history and physical examination are the first evaluation step, traumatized patients are often not cooperative and the clinical methods of diagnosis are unreliable [9]. As reported by Schurink and colleagues [1], almost half of the multiple injury patients have an unequivocal physi-

cal examination; therefore, the clinical diagnostic part should be as complete and accurate as possible to identify patients with life-threatening conditions and guide the further diagnostic approach, but should not result in an excessive delay in diagnosis and therapeutic procedures.

---

### 2.8.3 Imaging

The approach to investigation of abdominal/pelvic trauma should be done in a simple and systematic manner to reduce the time needed for evaluation. Algorithms dedicated to all eventualities are generally not expedient in the clinical practice, because the optimal diagnostic approach is largely determined by the experience of the physician and radiologist, by the presenting symptoms and signs of the patient, and the radiological armamentarium available in the emergency situation.

Two initial situations of the patient's presentation have to be initially clarified: firstly, patients presenting with respiratory insufficiency have to be intubated prior to any further clinical or radiological investigation. Secondly, patients who are hemodynamically unstable require immediate operation. Hemodynamically instability includes non-responders and transient responders to initial small-volume fluid substitution. If the patient is pulseless at arrival in the emergency ward but has witnessed recent or actual signs of life (e.g., pulseless electrical activity), transfer to the operating room and immediate laparotomy should be performed without further investigation. If palpable pulses are present, the only decision to be made in these patients is where is the bleeding source. Bedside US is recommended for accurate and fast identification of the bleeding site [18–22]. Blood amounts causing hemodynamically instability could be accurately identified by US [23, 24]. The US investigation should include the peritoneal and retroperitoneal cavity, the pelvic segment, and the pleural spaces.

If initial life-endangering respiratory or circulatory conditions have been excluded, further radiological investigations should be performed to accurately identify solid and visceral organ injuries by CT. If the patient is unconscious at presentation the CT evaluation of the head is indicated, and extension of the scan volume to the abdominopelvic region is recommended if the patient's presentation raises the suspicion of abdominal or pelvic injuries.

---

#### 2.8.3.1 Plain Radiography

An supine chest radiography is generally performed in all severely injured trauma patients to evaluate for life-threatening thoracic conditions and to assess the correct position of an intratracheal intubation after implantation in patients with respiratory insufficiency. Free subdiaphrag-

matic air may predict perforation of hollow abdominal organs or open abdominal wounds, whereas fractured lower ribs predict injuries in the upper abdominal organs. Herniation of abdominal viscera may be present in the case of traumatic diaphragmatic rupture.

On the other hand, plain abdominal radiography is not useful in emergency situation [3]. Because of significant diagnostic limitations, the impact of plain abdominal radiography has declined even in the traditional indication of pneumoperitoneum.

The initial imaging evaluation of a multiple-trauma patient with suspected pelvic fractures traditionally consists of a single plain pelvic radiography in the antero-posterior view. However, conventional radiographs in the emergency setting suffer from an impaired image quality due to poor positioning and overlaying structures, and the accuracy for diagnosing pelvic injuries is low [25, 26]; therefore, several authors suggested omission of the plain pelvic radiography in patients who will undergo abdomino-pelvic MDCT anyway as part of the initial emergency imaging evaluation [27–29]. This would result in a shorter total examination time, in reduced costs, a reduction of patient discomfort, and a decrease in total gonadal irradiation, which is important in the young trauma population [30].

In a recent study performed at our hospital we demonstrated, that post-processing of axial MDCT data sets allows generation of coronal ultra-thick multi-planar reconstructions of the pelvis, which is similar to plain pelvic radiography in terms of visibility of critical anatomical landmarks, and accuracy for the assessment of pelvic fractures [31]; therefore, when it is decided to expedite the emergency imaging evaluation by omitting the plain pelvic radiography and directly performing a MDCT examination, such coronal ultra-thick MPR could serve as an alternative equivalent without lacking the baseline examination for further treatment monitoring and follow-up [31].

---

#### 2.8.3.2 Ultrasound

Ultrasound is widely accepted as an effective initial triage tool to evaluate trauma victims with suspected blunt abdominal trauma. Emergency US for trauma is performed bedside and simultaneously with clinical assessment in the first minutes after arrival. In addition, it is repeatable, non-invasive, non-irradiating, and inexpensive. Because of the high sensitivity of US for the detection of free intraperitoneal fluid, US has replaced DPL in the detection of hemoperitoneum and in determining the need for immediate surgery [20]. In emergency radiology, there are mainly two trends for using US in the evaluating of blunt abdominal trauma. The first trend, usually performed in North America, is the use of US mainly as a rapid and reliable diagnostic test for free intra-abdominal fluid, performed by emergency medical staff with a limited level in training in US. This method has been termed “focused assessment



sonography for trauma" (FAST) [32, 33]. The US protocol includes scanning of four regions: the right upper quadrant with particular attention to the Morrison's pouch; the left upper quadrant with the subphrenic space and splenorenal recess; the pelvis with particular attention to the Douglas' pouch; and the pericardium. The limitation of FAST is due mainly to the varying experience of investigators and adequate training requirements for FAST are still controversial [34, 35]. Consequently, the reported sensitivity of FAST for intraperitoneal fluid varies between 63 and 91% [36, 37]. In a recent study performed by senior radiologists, FAST achieved a sensitivity of 94% and a negative predictive value of 100% for major abdominal injuries [38]. A recently published meta-analysis reported that the bias-adjusted sensitivity of screening US for trauma is low with a combined sensitivity of 66% [39].

The second trend widely accepted in European institutions is that standard abdominal US should be performed by a well-trained operator and should involve both a full abdominal exploration with particular attention to the peritoneal pouches for any indication of hemoperitoneum, and a systematic solid organ analysis to detect any solid-organ injuries [40, 41]. In a series of 1239 patients evaluated with US for detection of intra-abdominal injuries and the identification of individual organ injuries, Yoshii and colleagues reported a sensitivity of 94% and a specificity of 95%. Individual organ injuries were identified with sensitivities of 92.4, 90.0, 92.2, 71.4, and 34.7% for the liver, spleen, kidneys, pancreas, and intestine, respectively [41]. R othlin and colleagues reported a sensitivity for the demonstration of intra-abdominal fluid of 98% and for organ lesions of 41% [40]. In addition, recently published meta-analyses of emergency US for blunt abdominal trauma concluded that, despite its high specificity, US has an unexpectedly low sensitivity for the detection of both free fluid and organ lesions [42, 43].

In summary, abdominal US is useful in the context of blunt trauma and may even be considered indispensable for initial screening and for selecting hemodynamically unstable victims with severe hemoperitoneum for immediate surgery [44]; however, even in experienced hands, US is not useful to rule out organ injuries reliably. Therefore, in clinically suspected abdominal trauma and hemodynamically stability, CT must be performed regardless of the initial US findings.

### 2.8.3.3 Computed Tomography

If the patient is hemodynamically stable, CT is widely accepted as the imaging modality of choice for the detection of abdominal and pelvic injuries, to help for decision making on the appropriate treatment, and to monitor the course of healing of injuries. In the past, the time required for CT, including transport to and from the radiology department and interpretation of the CT images, exceeded

60 min [12]. With the evolution from single-slice CT to current MDCT scanners, the time needed for image acquisition has been markedly reduced. In our institution, implementation of the CT equipment located next to the emergency ward has greatly enhanced our ability to provide a rapid CT examination of the trauma victim. Other important advantages of MDCT include thin-collimated submillimeter isotropic imaging enabling high-quality reconstructions in any desired plane, and improved contrast bolus exploitation allowing precise separation of multiple phases of enhancement, which is especially useful in the evaluation of vascular diseases.

At the University Hospital Zurich, our standard MDCT abdominal imaging protocol for patients with abdominal trauma includes an automated intravenous bolus injection of 120 ml non-ionic contrast agent (e.g., 270 mg of iodine per milliliter) at an injection rate of 3 ml/s. In general, the following scanning parameters are used: tube voltage 120 kV; tube current 225 mA; slice collimation 16×0.75 mm. Images are routinely performed in the parenchymal phase of enhancement with imaging starting 85 s after the beginning of contrast agent injection. Axial slices are routinely reconstructed at a thickness of 2 mm with 1 mm increment for evaluation and at a thickness of 5 mm (5 mm increment) for reporting. For suspected vascular injuries, additional arterial phase imaging should be performed starting with a delay of 30 s after contrast agent application. In these cases, narrow collimation (1 mm slice thickness, 0.5 mm increment) is suggested. If indicated, delayed scanning more than 5 min after contrast bolus injection is recommended for better demonstration of extravasated contrast in injuries of the urinary tract.

All images are interactively reviewed on dedicated radiological workstations mainly using axial source images and individually adapted multiplanar reconstructions. Administration of oral contrast agent (e.g., 800–1000 ml water-soluble contrast agent containing 2% iodine) is considered to be useful especially for suspected bowel injury. The oral contrast may be applied through a nasogastric tube and scanning is performed immediately afterwards. Occasionally, rectal contrast agent (e.g., 100 ml water-soluble contrast containing 2% iodine) instilled via rectal enema may be beneficial if colonic injuries are suspected on the basis of penetrating injury, or on the basis of hemochezia in a patient with pelvic fractures.

The data obtained from CT scanning performed to evaluate seriously injured multiple-trauma patients for abdominal visceral injury can be reformatted to screen for thoracic and lumbar spine fractures, providing accurate screening while eliminating the time, expense, and radiation exposure associated with conventional film radiography [45, 46].

### 2.8.3.4 Imaging Findings in Abdominal and Pelvic Organ Injuries

#### Diaphragm

Traumatic diaphragmatic rupture occurs in 3–8% of patients with major trauma [47] and are more frequently observed in blunt than in penetrating trauma [48, 49]. In addition, associated abdominal and extra-abdominal injuries are more frequent in blunt traumatic diaphragmatic rupture [48]. Most cases occur in young men after motor vehicle accidents [50, 51]. The rupture site usually affects the left-sided part of the diaphragm which is anatomically less protected than the liver-shielded right-sided part [13, 52]. In addition, the rupture size is usually smaller on the right side compared with the left diaphragm (Fig. 1) [13]. Traumatic diaphragmatic rupture rarely accounts for immediate mortality and may be asymptomatic until complications occur. If the diagnosis is missed, the patients may develop intrathoracic visceral herniation and gastrointestinal strangulation with a morbidity and mortality rate of up to 60% [53]. Chest radiography is insensitive in detecting diaphragmatic rupture, with sensitivity of 46% for left-sided and 17% for right-sided ruptures [54]. The signs of diaphragmatic rupture in chest radiographs are masked in most patients by accompanied findings of pleural effusion, atelectasis, pulmonary contusion, or non-specific diaphragmatic elevation [55, 56]. Computed tomography is the imaging modality of choice in the evaluation of acute traumatic diaphragmatic rupture with a reported sensitivity of 63–71% and a specificity of 87–100% [57, 58]. The most reliable CT findings predicting blunt diaphragmatic rupture are diaphragmatic discontinuity, diaphragmatic thickening, segmental non-recognition of the diaphragm, intrathoracic herniation of abdominal viscera, elevation of the diaphragm, and both hemothorax and hemoperitoneum reaching together a cumulative sensitivity of 100% [59]. Other CT findings include contrast medium extravasation at the level of the diaphragm, presumed laceration of the diaphragm by a fractured rib, thoracic fluid abutting intra-abdominal viscera, and waist-like constriction of the bowel, the so-called collar sign [59]. Another helpful finding is the dependent viscera sign, which is present on the right side if the upper one-third of the liver abuts the posterior ribs, and on the left side if the stomach or the bowel abuts the posterior ribs [60]. The application of coronal image reconstructions is recommended to facilitate demonstration of the extent of diaphragmatic rupture as well as the content of the hernia.

#### Liver and Gallbladder

Hepatic injuries are common after blunt abdominal or right-sided thoracic trauma. The typical injury pattern in right hepatic lobe trauma is shearing adjacent to the hepatic veins, whereas left hepatic lobe injury is usually secondary to midline compression [14]. To date, the vast ma-



**Fig. 1.** Right-sided traumatic diaphragmatic rupture. Coronal reconstruction of contrast-enhanced CT scan in a 31-year-old man after a motorcycle accident shows herniation of the liver into the right hemithorax

majority of hepatic injuries are managed conservatively [61, 62]. Surgical treatment is restricted to severe injuries with active bleeding and/or complete destruction of an entire hepatic lobe [63–67].

Computed tomography is well suited to delineate the presence, extent, and location of blunt injuries of the hepatic parenchyma. Minor hepatic injury findings include contusion and laceration (Fig. 2). Extension of the laceration through the liver capsule results in hemoperitoneum. Laceration of the posterior surface of the liver is often accompanied with extraperitoneal bleeding and injuries of retroperitoneal organs [68]. More severe injuries include subcapsular or intraparenchymal hematoma, and partial devascularization due to parenchymal contusion, or direct rupture of major arterial or portal branches. According to the segmental nomenclature of Couinaud, segments V–VIII are involved in approximately 75% of cases [4, 69]. Periportal areas of low density tracking the course of the portal vein and its branches is a frequent finding in hepatic injury (Fig. 3) [70]. Trauma-associated periportal tracking is thought to be due to lymphedema following systemic volume overload, tension pneumothorax, pericardial tamponade, or hematoma obstructing the hepatic venous outflow. Discontinuity of the biliary tree due to traumatic rupture often only becomes detectable with some delay as loculated intrahepatic biloma or extrahepatic bile collections.



**Fig. 2.** Severe contusion and laceration of the liver. Contrast-enhanced CT scan in a 22-year-old man involved in a car accident shows low-density areas in the right liver lobe with inhomogeneous contrast enhancement of the adjacent parenchyma and small parahepatic and perisplenic fluid collections



**Fig. 3.** Periportal tracking in a 44-year-old man after a motorcycle accident. Contrast-enhanced CT depicts periportal areas of low density tracking the course of the portal vein and its branches indicative of hepatic injury

In patients treated conservatively, repeated CT studies are recommended to monitor the course of spontaneous healing and to detect vascular or biliary complications. Although complications of conservative treatment infrequently occur, delayed hepatic rupture in initially stable patients has been observed several days after trauma [71, 72].

Gallbladder injury is rare and in most cases associated with traumatic liver and duodenal lesions [73]. Injuries to

the gallbladder include wall contusion and rupture. Complete gallbladder avulsion is a rare complication, which may result in the gallbladder lying freely within the peritoneal cavity [72]. The CT finding of an ill-defined contour of the gallbladder wall, a collapsed gallbladder in a fasting patient, mass effect on the duodenum, or high-density intraluminal hemorrhage, especially in the presence of pericholecystic fluid, strongly suggests primary gallbladder injury [74].

## Spleen

The spleen is the most frequently affected organ in blunt abdominal trauma, accounting for approximately 40% of abdominal organ injuries [73]. Left lower rib fractures are frequently associated [5]. The spectrum of splenic trauma includes contusion, parenchymal laceration, subcapsular hematoma, perisplenic hematoma, fragmentation of the parenchyma, and disruption of hilar vessels.

Computed tomography is a sensitive method for detecting blunt splenic trauma and enables distinguishing different patterns of injury. Contusion appears as a hypodense area within normally perfused splenic parenchyma. Laceration appears as linear perfusion defect. Subcapsular hematoma typically shows a lenticular shape with compression of the adjacent splenic parenchyma. Because the splenic capsule cannot be confidently visualized, it is sometimes difficult to distinguish between a subcapsular and a perisplenic hematoma. Perfusion defects due to segmental devascularization from vascular pedicle injury can be difficult to distinguish from contusions or local reactive hypoperfusion in the hypotensive patient [5]. The term “shattered spleen” relies to multiple crossing lacerations (Fig. 4).

While splenectomy has long been the standard treatment for splenic injuries, non-surgical treatment is now an accepted practice to reduce the risk of infectious complications inherent with asplenia [75–78]. Although non-operative management has documented success rates of 95% in children [75] and approximately 70% in adults [79], delayed splenic rupture is a well-recognized complication. Based on the CT findings and the clinical context, this complication is classified as true delayed splenic rupture, delayed diagnosis of splenic injury, rupture due to failure of non-surgical treatment, and failure of splenic salvage at surgery [80]. Unfortunately, there are no reliable CT findings which predict the risk of delayed splenic rupture, and even a negative CT study cannot exclude the possibility of a delayed splenic rupture [81]. A variety of CT-based signs and injury scales have been correlated with the outcome of treatment in order to decide on which patients can be safely managed conservatively and which require surgery [82–86]. Resciniti and colleagues [82] introduced a CT-based scoring system that assigns points according to the injury of splenic parenchyma, splenic capsule, and the presence of free abdominal and pelvic fluid. A score of <2.5 indicates that patients could be safely managed conservatively, whereas patients with a score of  $\geq 2.5$  often needed surgery [82]; however, subsequent studies using this scoring system reported that conservative treatment was successful in 47–92% of cases with a score of  $\geq 2.5$ , whereas 0–17% of patients with a score <2.5 required urgent surgery after an interval of days or even weeks of admission [83, 84, 86, 87].



**Fig. 4.** Splenic rupture in a 34-year-old man involved in an industrial accident with high-compression forces to the left flank. Coronal reconstruction and axial image (*inset*) of contrast-enhanced CT revealed the disruption of the spleen with left-sided hemoretroperitoneum and free perihepatic fluid collection

## Pancreas

Pancreatic injuries are uncommon occurring in <2% of blunt abdominal trauma patients [88, 89]. In up to 90% of cases, pancreatic injuries are associated with injuries to the liver, stomach, duodenum, and spleen [90, 91]. The pancreas is mostly vulnerable to midline compression forces resulting in impact against the adjacent spine, particularly affecting the pancreatic body [91]. Pancreatic injuries may be difficult to diagnose clinically. If these injuries are overlooked, they may result in delayed complications such as recurrent pancreatitis, fistula, abscess, and hemorrhage increasing the mortality to 20% [88]. The risk of abscess or fistula formation with disruption of the pancreatic duct approaches 25 and 50%, respectively [92, 93]. In contrast, patients without duct disruption develop abscess and fistula in <10% of cases [93]. Death occurring in the first 48 h following the traumatic event are usually due to acute hemorrhage from injury to the portal vein, splenic vein, or inferior vena cava [90, 91, 94], whereas death due to delayed complications is usually due to sepsis [93]; therefore, imaging should focus on the integrity of the duct or findings that suggest damage to the pancreatic duct in order to identify the patients requiring surgical intervention [72].

Computed tomography is routinely used as the first-line imaging modality in patients with suspected pancreatic



trauma. Patterns of pancreatic injury may include contusion, superficial or partial laceration, and complete transection or disruption. Direct CT signs of pancreatic injury, including pancreatic enlargement, focal linear non-enhancement, comminution, and inhomogeneous enhancement, are often subtle initially but become more pronounced in severe cases or when posttraumatic pancreatitis develops within a few days [72]. Often non-specific but more evident are the secondary CT findings including peripancreatic fat stranding, peripancreatic fluid collections, fluid separating the splenic vein from the pancreatic parenchyma, hemorrhage, and thickening of the left anterior pararenal fascia [72]. Wong and colleagues [89] proposed to predict the presence or absence of ductal disruption based on the depth of laceration. Their CT grading scheme classifies pancreatic injuries as follows: grade A, pancreatitis or superficial laceration (<50% pancreatic thickness); grade B1, deep laceration (>50% pancreatic thickness) of the pancreatic tail; grade B2, transaction of the pancreatic tail; grade C1, deep laceration of the pancreatic head; and grade C2, transaction of the pancreatic head. Grade-A injuries are usually seen with an intact pancreatic duct, whereas grades B and C correlate with duct disruption. With the advent of MDCT, thin-collimation and dedicated post-processing algorithms facilitate the depiction of the pancreatic and intrapancreatic bile ducts [95].

### Bowel and Mesentery

Bowel or mesentery injury occur in 3–7% of patients with blunt abdominal trauma [5, 73]. The jejunum and ileum are the most commonly affected bowel segments, followed by the colon and duodenum [96, 97]. The stomach is rarely affected [96]. Duodenal injuries usually affect the second and third portion due to their close proximity to the spine [73], and are frequently associated with lesions of the pancreatic head [5]. The differentiation between duodenal perforation and duodenal hematoma is of major clinical interest since duodenal perforation requires immediate surgery, whereas duodenal hematoma may be treated conservatively [98]. The jejunum and ileum are commonly injured near the point of fixation (e.g., the ligament of Treitz or the ileocecal valve) [73]. Colonic injuries most frequently involve the transverse colon, the sigmoid colon, and the cecum [73]. Triple contrast agent application using intravenous, oral, and rectal contrast may be helpful in identifying colonic injuries.

Computed tomography has been shown to be an accurate imaging modality for the assessment of bowel and mesentery injury [96–101]. Discontinuity of the gastrointestinal wall and spillage of contrast material or luminal contents into the peritoneal or retroperitoneal cavity are direct signs of free wall perforation requiring surgical exploration. Extraluminal air is a valuable indirect sign of bowel perforation [98–101]; however, in trauma patients extraluminal air may also be due to other etiologies including dissection of interstitial air from the chest due to pneu-

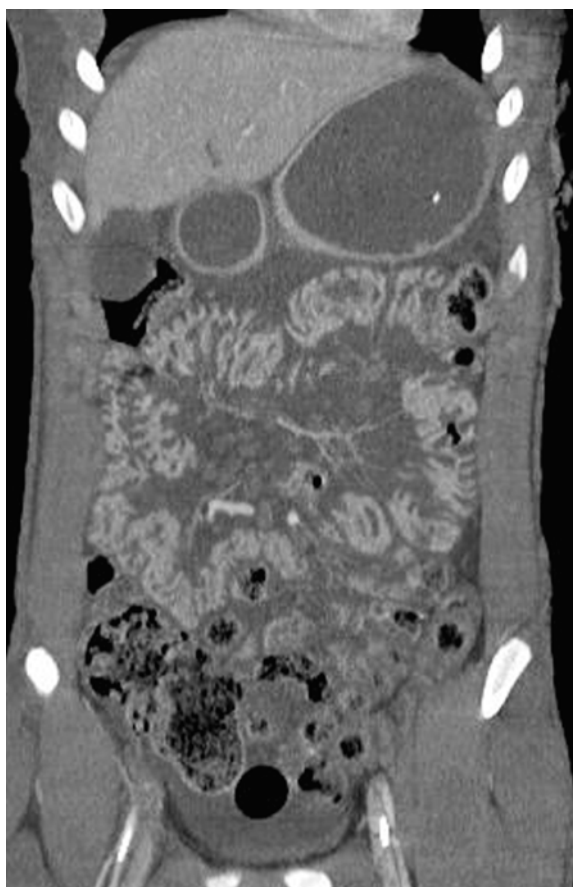


**Fig. 5.** Shock bowel. Contrast-enhanced CT in a 16-year-old boy with third-degree burn. Coronal reconstruction shows the collapsed small bowel with wall enhancement and edematous thickening of the mesentery following hypotension and a high volume of fluid substitution

mothorax, and deep abdominal wounds communicating with the outside. For accurate detection of small quantities of extraluminal air, CT images should be viewed with lung window setting. Other indirect CT signs which suggest bowel injury include focal bowel wall thickening, streaky appearance of the mesenteric fat, and unexplained free fluid localized between the mesenteric loops [99, 101, 102]; however, generalized bowel wall thickening is a non-specific finding in trauma patients, because it may be also observed after aggressive fluid substitution, after prolonged hypotension (“shock bowel”), and in the presence of a compromised central venous return (Fig. 5) [103]. Identification on CT of focal high-density clotted blood (“sentinel clot”) is an accurate sign of injury to an adjacent organ [104]. The overall sensitivity of the direct and indirect CT signs of bowel injury is reported to be between 85 and 95% [96, 97, 99, 101].

Mesentery injury may be caused by crushing forces against the spine or tangential shearing forces resulting in

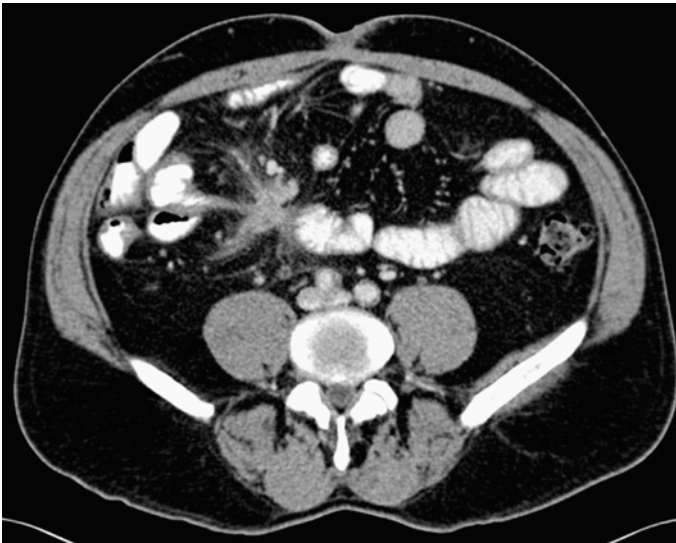


**Fig. 6.** Mesenteric injury. Contrast-enhanced CT in a 34-year-old woman after an accidental fall from a height reveals hematoma of the mesentery remote from the spine indicating mesenteric injury most probably due to shearing forces

avulsion of the mesentery from its point of fixation [73]. The CT evaluation may show extravasation of contrast agent in the case of active bleeding. Other CT findings include intramesenteric fluid collections (Fig. 6), hemoperitoneum, and thickening of bowel loops in bowel ischemia. To define the need for surgery, Dowe and colleagues [100] observed that the CT finding of mesenteric bleeding or bowel wall thickening associated with mesenteric hematoma or infiltration in the blunt trauma patient indicates a high likelihood of a mesenteric or bowel injury requiring surgery.

#### Adrenal Glands

Adrenal injuries have been reported in 2% of patients undergoing CT for blunt abdominal trauma [105]. Adrenal injury is usually unilateral, right sided, and associated with ipsilateral intra-abdominal and intrathoracic injuries [105, 106]. The vast majority of adrenal injuries are of less clinical significance with the traumatic changes spontaneously resolving within 2 months [105]. Occasionally, specific treatment is required, if a large right-sided adrenal hematoma compresses the inferior vena cava, or if bilateral adrenal hemorrhage results in adrenal insufficiency [107–109].

Adrenal injuries may sometimes be seen on US investigations as enlarged, hyperechoic masses with a bright central echo that becomes cystic on follow-up examinations [110]. In most cases changes in the adrenal glands presenting with only subtle findings require CT for detection and follow-up. On CT, adrenal gland injuries appear as round or ovoid-shaped hematomas arising in the center of the gland commonly associated with stranding of the perirenal or periadrenal fat [5]. Posterior pararenal hemorrhage may mimic a thickened diaphragmatic crus [105]. Active bleeding due to injuries to the suprarenal arteries may also be visualized on CT [13].

#### Kidney and Ureter

Renal trauma is the most common retroperitoneal injury. A variety of pre-existing pathological conditions (e.g., hydronephrosis, renal cyst, horseshoe kidney, angiomyolipoma, renal carcinoma) render a kidney more susceptible to injury due to minor trauma [5, 111]. Major renal hemorrhage after minor trauma should therefore raise the suspicion of an underlying renal pathology. Renal injury include contusion, laceration, subcapsular hematoma, shattered kidney, and renal artery occlusion. Approximately 80% of the injuries are contusions and minor lacerations that heal spontaneously without complications [5]. In the setting of microscopic hematuria after blunt abdominal trauma, radiological imaging for evaluation of a renal injury is unnecessary [112, 113]; however, in hemodynamically stable patients with macrohematuria, CT is the imaging modality of choice because information relating to morphology and function may be obtained in a single examination. Renal contusion appears as focal zones of decreased enhancement or as a striated nephrogram because of temporarily impaired tubular excretion. Intrarenal hematomas appear as poorly marginated areas without enhancement. Subcapsular hematoma typically shows lenticular shape due to displacement of the renal cortex. In minor hemorrhage, extrarenal hematomas remain confined to the perirenal space and extend into the adjacent retroperitoneal compartments in severe hemorrhage. Renal laceration appear as a linear or wedge-shaped hypodense area. According to depth, lacerations are classified as being cortical, corticomedullary, or completely involving the renal collecting system. Renal fracture involves the medial and lateral surface of the kidney through the hilum. The term “shattered kidney” defines lacerations crossing the kidney resulting in multiple fragments [13]. Although CT images obtained in the corticomedullary phase are well

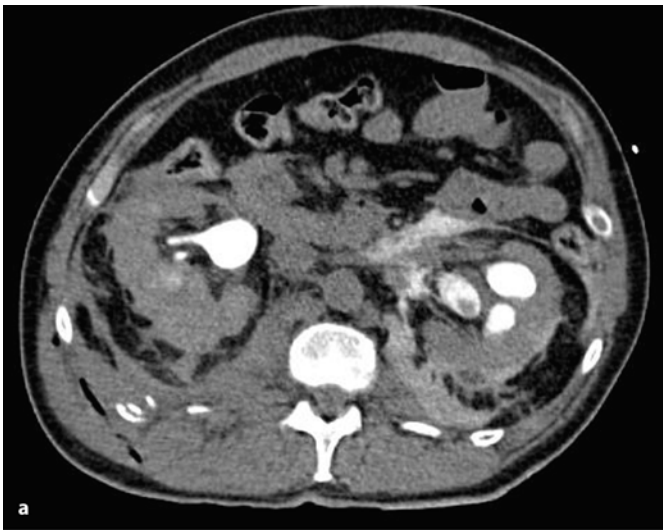


**Fig. 7.** Bilateral renal rupture. A 20-year-old man involved in a car accident as pedestrian with bilateral renal rupture on contrast-enhanced CT scan was referred from an outside hospital for further evaluation. Unenhanced CT examination in axial (a) and coronal

reconstruction (b) performed at our hospital 3 h after the accident shows rupture of both kidneys with bilateral hemoretroperitoneum. In addition, the left-sided urinary collecting system was disrupted with contrast extravasation in the pararenal space

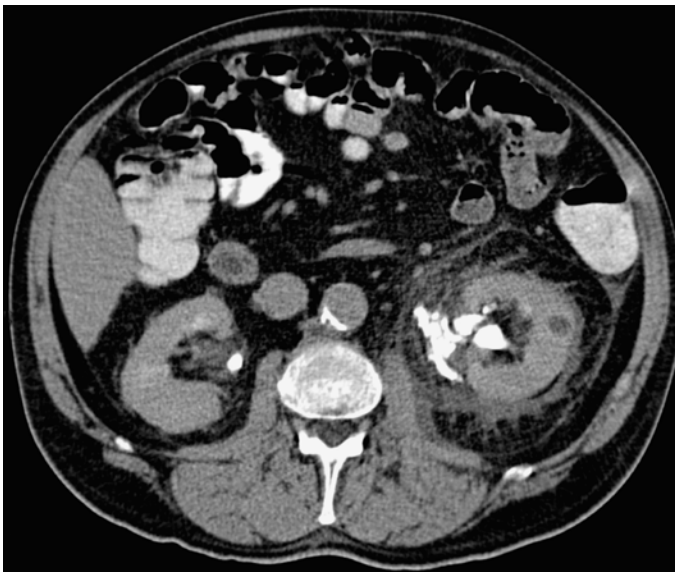


**Fig. 8.** Disruption of the renal pelvis. Contrast-enhanced CT in a 30-year-old woman after a free fall from a height depicts hematoma around the left kidney and contrast material extravasation indicative of ruptured renal pelvis

sued to diagnose parenchymal lesions, a triphasic contrast application protocol is recommended including an early arterial phase of enhancement to diagnose injuries to the renal arteries, and an additional delayed scanning to demonstrate extravasation of contrast material from the urinary tract (Figs. 7, 8) [13].

Besides parenchymal injuries, renal vascular injuries are common and may be distinguished as different types. Occlusion of the main renal artery may be due to a sub-intimal tear with subsequent thrombosis or to arterial avulsion [5], resulting in absence of the parenchymal nephrogram on contrast-enhanced CT scan. Cortical en-



hancement caused by patent capsular arteries originating proximally to the occlusion should always raise the suspicion of an injury to the main renal artery [73, 114, 115]. Occlusion of interlobar arcuate branches results in segmental infarction typically appearing as a wedge-shaped unenhanced area [116]. Traumatic lesions to the renal vein result in an enlarged kidney, ipsilaterally prolonged corticomedullary junction time, and a cortical rim enhancement usually thicker than that observed in arterial devascularization [116].

Ureteral injuries are more frequently seen in penetrating than in blunt trauma. If extravasation of contrast-opacified urine is not observed, the combination of large urinoma, non-opacified distal ureter, and an intact ipsilateral kidney should always raise the suspicion of a rupture of the ureter or the ureteropelvic junction [5].

Comparing CT findings with the outcome of treatment have made the organ injury scale most useful in classifying renal injuries [117]; therefore, injuries of grades I–III, including traumatic lesions of small segmental or polar arteries or interlobar or arcuate branches, tend to heal spontaneously and can be managed conservatively. In grade-IV lesions, conservative treatment is often expedient; however, in the presence of associated intraperitoneal or pancreatic injuries infectious complications are more common; thus, primary surgical exploration has been recommended [118]. Other complications of conservative treatment in major lacerations include continuing hemorrhage, development of a false aneurysm, hematoma, and formation of a perirenal abscess. Grade-V trauma usually require surgical revision. Computed tomography is not only important for the detection of renal injuries, but also in deciding for their appropriate management and in monitoring the course of healing in conservative treatment.

### Hemoperitoneum

Free-fluid collections are a common CT finding of patients with blunt abdominal trauma. Measurement of the attenuation values may help distinguishing between extravasated blood, bile, and ascetic fluid [4]. Typical attenuation values of acutely extravasated blood are 30–45 Hounsfield units (HU). After some hours, concentration of hemoglobin due to layering phenomena, clot formation, and clot retraction increases the attenuation value to 50–60 HU or even more. Attenuation values begin to decrease after 48 h due to clot lysis [104, 119]. Small amounts of intraperitoneal blood initially accumulate adjacent to the site of bleeding and identification on CT of focal high-density clotted blood (“sentinel clot sign”) is an valuable indirect sign of injury to an adjacent organ, even if the lesion could not be identified [104]. A retrospective CT study of 116 patients by Orwig and colleagues [104], the sentinel clot sign was present in 84% of visceral injuries with only three false-positive cases. Whereas CT visualized the visceral injury itself in 86% of cases, the sentinel clot was the only clue as to the source



**Fig. 9.** Hemoperitoneum. Coronal reconstruction of contrast-enhanced CT scan in a 44-year-old man reveals massive hemoperitoneum in the Morison's pouch, perihepatic and perisplenic spaces, and the paracolic gutters. High-attenuation areas around the mesenteric vessels are indicative of vascular injury

of hemorrhage in 14%. Small amounts of free intra-abdominal fluid without hyper-attenuating values are usually of no clinical significance if situated in the major peritoneal compartment; however, even small amounts of free fluid between the mesenteric loops are suggestive of mesentery or bowel injury raising the need for further investigation [102]. As the amount of extravasated blood increases, the location extend within in the communicating peritoneal spaces and identification of the initial bleeding site is more difficult (Fig. 9). By counting the number of involved compartments (e.g., Morison's pouch, perihepatic and perisplenic spaces, paracolic gutters, Douglas' pouch), the amount of hemoperitoneum can be estimated by CT in a semiquantitative fashion as minor hemoperitoneum (one compartment, approximately 100–200 ml), moderate hemoperitoneum (two compartments, approximately 250–500 ml), and severe hemoperitoneum (more than two compartments, >500 ml) [4].



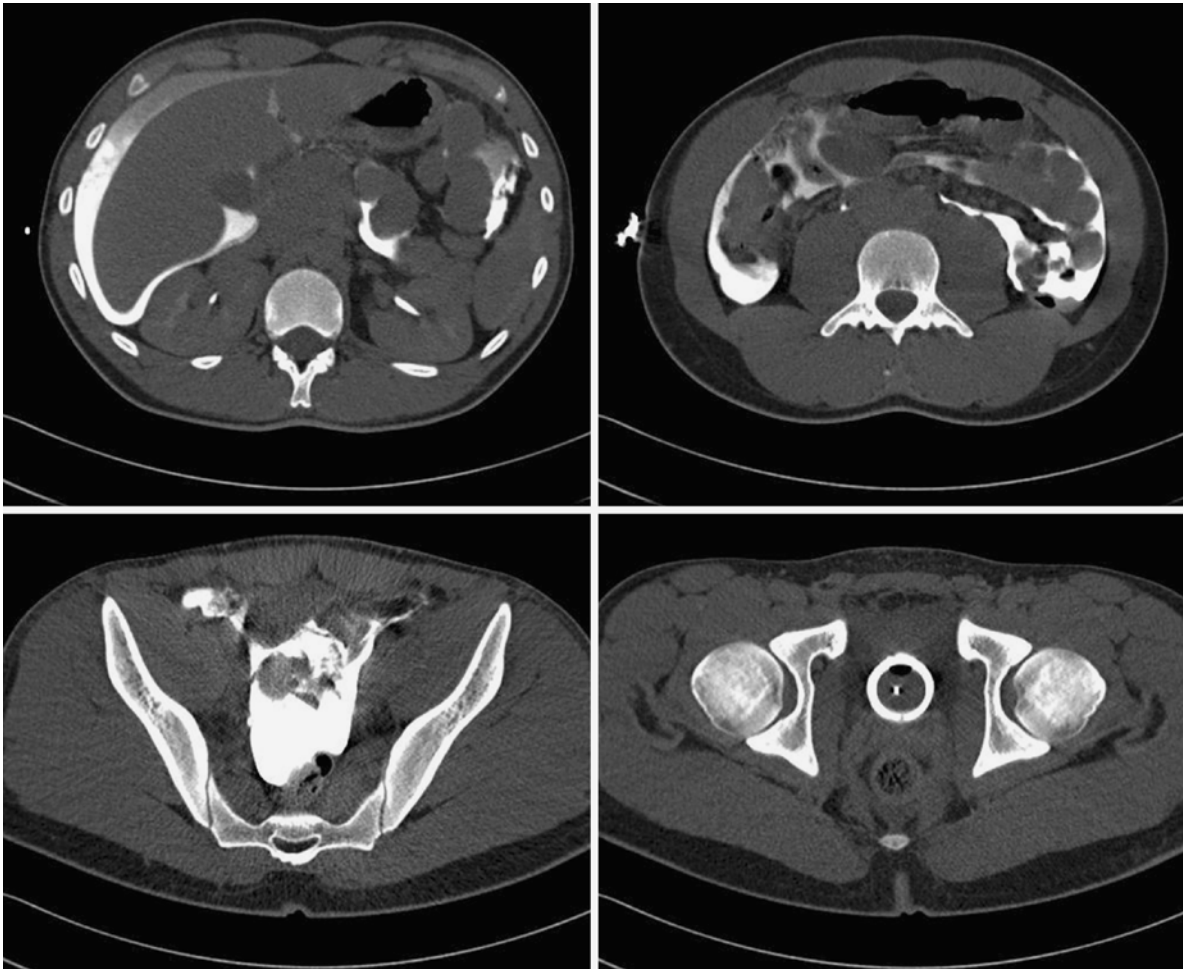


**Fig. 10.** Bladder rupture. Serial axial images of CT scan with administration of contrast material via a bladder catheter in a 29-year-old man after a motorcycle accident show intraperitoneal

rupture of the bladder with contrast extravasation in the peritoneal spaces

In the retroperitoneum, minor hemorrhage may only be visible as fascial thickening. Moderate hemorrhage is usually confined to the retroperitoneal space adjacent to its origin (e.g., perirenal space, anterior or posterior pararenal space). Large hemorrhages affect multiple communicating retroperitoneal spaces and can extend along the fasciae into the pelvis [4].

With contrast-enhanced CT imaging, active bleeding sites can be detected by extravasation of intravenously applied contrast media [120]. Identification of active bleeding sites is of utmost importance, as it may indicate a life-threatening condition requiring emergency treatment [121–124]. Furthermore, recognition of active hemorrhage on CT may help in guiding surgical treatment and transarterial embolization [4].

### Pelvic Visceral Injuries

Most pelvic visceral injuries involve bladder and urethra, whereas gastrointestinal tract and gynecological injuries are rare following blunt trauma. In patients with unstable pelvic fractures, injuries of the lower urinary tract occur in 25% of these cases, compared with only 6% for patients with stable pelvic fractures [125].

Urinary bladder injury is seen in 8% of patients with pelvic fracture [126], and typically occurs following severe trauma with other visceral injuries [127]. Macroscopic hematuria, the presence of pubic rami fractures, and hemorrhagic shock upon admission are highly indicative of bladder injury [128]. Simple contusion of the bladder results in wall hematoma and is associated with frank hematuria. Extra-peritoneal rupture may be due to direct perforation by a bony fragment, rupture of pubo-vesical ligaments near the bladder neck after symphysis injury, or contusion of a distended bladder [128]. The rupture often

involves the anterior bladder wall near the neck. Findings include lack of urination, absence of a bladder distension, and uro-hematoma especially in the space of Retzius. Intra-peritoneal bladder rupture is more frequently caused by direct perforation of a bony fragment than by rupture of a distended bladder [128]. The rupture site is often plugged by the omentum or bowel loops, making it difficult to detect. Computed tomography with delayed scanning has a sensitivity equivalent to that of retrograde cystography [129]. The identification of contrast extravasation into the peritoneal cavity is of utmost importance, since extra-peritoneal rupture is managed without surgery and intra-peritoneal rupture requires immediate explorative surgery (Fig. 10).

Urethral injury occurs in approximately 5% of all pelvic traumas and affects males almost exclusively [128]. Two-thirds of cases are associated with pubic rami fractures or sacro-iliac joint injuries [130]. A retrograde urethrogram is usually performed to evaluate the urethra in patients with suspected urethral injuries. Recent studies observed promising results of in evaluating urethral injuries [131, 132]. The CT findings of elevation of the prostatic apex, extravasation of urinary tract contrast material, distortion or obscuration of the uro-genital diaphragm fat plane, hematoma of the ischiocavernosus muscle, distortion or obscuration of the prostatic contour, distortion or obscuration of the bulbocavernosus muscle, and hematoma of the obturator internus muscle were more common in patients with pelvic fractures and associated urethral injuries than in patients with uncomplicated pelvic fractures [133].

## 2.8.4 Conclusion

Trauma to abdominal and pelvic structures often occurs in the setting of multisystemic injury. Rapid and accurate diagnosis is a mainstay in reducing mortality and morbidity of these patients. Choice and employment of any particular radiological investigation would depend on the radiological armamentarium available and the urgency of demand in the life-threatening situation. While US has an important role in the early triage to detect massive hemoperitoneum, CT is the cornerstone in the evaluation of stable patients because of its impact on patient management and reduction of associated mortality. The advantages of CT include the high accuracy in screening the extent of intra- and retroperitoneal injuries, detection of active arterial extravasation and associated spine and pelvic injuries, and detection of small amounts of free abdominal air and fluid, which may be the only finding of significant injury. The tendency toward conservative management of parenchymal abdominal injuries enhances the use of CT as a modality for monitoring the natural development of injuries.

## References

- Schurink GW, Bode PJ, van Luijt PA, van Vugt AB (1997) The value of physical examination in the diagnosis of patients with blunt abdominal trauma: a retrospective study. *Injury* 28:261–265
- Trunkey DD (1983) Trauma. Accidental and intentional injuries account for more years of life lost in the U.S. than cancer and heart disease. Among the prescribed remedies are improved preventive efforts, speedier surgery and further research. *Sci Am* 249:28–35
- Wintermark M, Poletti PA, Becker CD, Schnyder P (2002) Traumatic injuries: organization and ergonomics of imaging in the emergency environment. *Eur Radiol* 12:959–968
- Becker CD, Mentha G, Terrier F (1998) Blunt abdominal trauma in adults: role of CT in the diagnosis and management of visceral injuries. Part 1: liver and spleen. *Eur Radiol* 8:553–562
- Becker CD, Mentha G, Schmidlin F, Terrier F (1998) Blunt abdominal trauma in adults: role of CT in the diagnosis and management of visceral injuries. Part 2: Gastrointestinal tract and retroperitoneal organs. *Eur Radiol* 8:772–780
- Bardenheuer M, Obertacke U, Waydhas C, Nast-Kolb D (2000) Epidemiology of the severely injured patient. A prospective assessment of preclinical and clinical management. *AG Polytrauma of DGU. Unfallchirurg* 103:355–363 [in German]
- Nast-Kolb D, Waydhas C, Kastl S, Duswald KH, Schweiberer L (1993) The role of an abdominal injury in follow-up of polytrauma patients. *Chirurg* 64:552–559 [in German]
- Shanmuganathan K (2004) Multi-detector row CT imaging of blunt abdominal trauma. *Semin Ultrasound CT MR* 25: 180–204
- Feussner H, Papaziosgas W, Siewert JR (1999) Modern diagnostic workup of blunt abdominal trauma. *Chirurg* 70:1246–1254 [in German]
- Enderson BL, Maull KI (1991) Missed injuries. The trauma surgeon's nemesis. *Surg Clin North Am* 71:399–418
- Root HD, Hauser CW, McKinley CR, Lafave JW, Mendiola RP Jr (1965) Diagnostic Peritoneal Lavage. *Surgery* 57:633–637
- Davis JW, Hoyt DB, Mackersie RC, McArdle MS (1990) Complications in evaluating abdominal trauma: diagnostic peritoneal lavage versus computerized axial tomography. *J Trauma* 30: 1506–1509
- Weishaupt D, Grozaj AM, Willmann JK, Roos JE, Hilfiker PR, Marincek B (2002) Traumatic injuries: imaging of abdominal and pelvic injuries. *Eur Radiol* 12:1295–1311
- Mullinix AJ, Foley WD (2004) Multidetector computed tomography and blunt thoracoabdominal trauma. *J Comput Assist Tomogr* 28 (Suppl 1):S20–S27
- Miller PR, Croce MA, Bee TK, Malhotra AK, Fabian TC (2002) Associated injuries in blunt solid organ trauma: implications for missed injury in nonoperative management. *J Trauma* 53:238–242
- Chandler CF, Lane JS, Waxman KS (1997) Seatbelt sign following blunt trauma is associated with increased incidence of abdominal injury. *Am Surg* 63:885–888
- Cushing BM, Clark DE, Cobean R, Schenarts PJ, Rutstein LA (1997) Blunt and penetrating trauma: Has anything changed? *Surg Clin North Am* 77:1321–1332
- Partrick DA, Bensard DD, Moore EE, Terry SJ, Karrer FM (1998) Ultrasound is an effective triage tool to evaluate blunt abdominal trauma in the pediatric population. *J Trauma* 45: 57–63
- Dolich MO, McKenney MG, Varela JE, Compton RP, McKenney KL, Cohn SM (2001) 2576 ultrasounds for blunt abdominal trauma. *J Trauma* 50:108–112
- McKenney M et al (1994) Can ultrasound replace diagnostic peritoneal lavage in the assessment of blunt trauma? *J Trauma* 37:439–441

21. Thaler W (1995) Can ultrasound replace diagnostic peritoneal lavage in the assessment of blunt trauma? *J Trauma* 39:393–395
22. Fernandez L et al. (1998) Ultrasound in blunt abdominal trauma. *J Trauma* 45:841–848
23. Rozycki GS, Ballard RB, Feliciano DV, Schmidt JA, Pennington SD (1998) Surgeon-performed ultrasound for the assessment of truncal injuries: lessons learned from 1540 patients. *Ann Surg* 228:557–567
24. Sisley AC, Rozycki GS, Ballard RB, Namias N, Salomone JP, Feliciano DV (1998) Rapid detection of traumatic effusion using surgeon-performed ultrasonography. *J Trauma* 44:291–297
25. Schädel-Höpfner M, Celik I, Stiletto R, Giannadakis K, Froelich JJ, Gotzen L (2002) Computed tomography for the assessment of posterior pelvic injuries in patients with isolated fractures of the pubic rami in conventional radiography. *Chirurg* 73:1013–1018
26. Kaulbach C, Heller M, Triebel HJ, Spielmann RP, Richartz-Heller M (1989) Radiologic diagnosis of acetabular fractures. *Radiologe* 29:501–507
27. Vo NJ, Gash J, Browning J, Hutson RK (2004) Pelvic imaging in the stable trauma patient: is the AP pelvic radiograph necessary when abdominopelvic CT shows no acute injury? *Emerg Radiol* 10:246–249
28. Duane TM, Cole FJ, Weireter LJ, Britt LD (2001) Blunt trauma and the role of routine pelvic radiographs. *Am Surg* 67:849–852
29. Duane TM, Tan BB, Golay D, Cole FJJ, Weireter LJJ, Britt LD (2002) Blunt trauma and the role of routine pelvic radiographs: a prospective analysis. *J Trauma* 53:463–468
30. Jurik AG, Jensen LC, Hansen J (1996) Total effective radiation dose from spiral CT and conventional radiography of the pelvis with regard to fracture classification. *Acta Radiol* 37:651–654
31. Leschka S, Alkadhi H, Boehm T, Marincek B, Wildermuth S (2005) Coronal ultra-thick multiplanar CT reconstructions (MPR) of the pelvis in the multiple trauma patient: an alternative for the initial conventional radiograph. *Rofo* 177:1405–1411
32. Ballard RB et al. (1999) An algorithm to reduce the incidence of false-negative FAST examinations in patients at high risk for occult injury. Focused assessment for the sonographic examination of the trauma patient. *J Am Coll Surg* 189:145–150
33. Boulanger BR, Kearney PA, Brennehan FD, Tsuei B, Ochoa J (2000) Utilization of FAST (focused assessment with sonography for trauma) in 1999: results of a survey of North American trauma centers. *Am Surg* 66:1049–1055
34. Scalea TM et al. (1999) Focused assessment with sonography for trauma (FAST): results from an international consensus conference. *J Trauma* 46:466–472
35. Gracias VH et al. (2001) Defining the learning curve for the focused abdominal sonogram for trauma (FAST) examination: implications for credentialing. *Am Surg* 67:364–368
36. McGahan JP, Richards JR (1999) Blunt abdominal trauma: the role of emergent sonography and a review of the literature. *Am J Roentgenol* 172:897–903
37. Forster R, Pillasch J, Zielke A, Malewski U, Rothmund M (1993) Ultrasonography in blunt abdominal trauma: influence of the investigators' experience. *J Trauma* 34:264–269
38. Lingawi SS, Buckley AR (2000) Focused abdominal US in patients with trauma. *Radiology* 217:426–429
39. Stengel D, Bauwens K, Rademacher G, Mutze S, Ekkernkamp A (2005) Association between compliance with methodological standards of diagnostic research and reported test accuracy: meta-analysis of focused assessment of US for trauma. *Radiology* 236:102–111
40. Röthlin MA, Naf R, Amgwerd M, Candinas D, Frick T, Trentz O (1993) Ultrasound in blunt abdominal and thoracic trauma. *J Trauma* 34:488–495
41. Yoshii H et al. (1998) Usefulness and limitations of ultrasonography in the initial evaluation of blunt abdominal trauma. *J Trauma* 45:45–50
42. Stengel D, Bauwens K, Porzolt F, Rademacher G, Mutze S, Ekkernkamp A (2003) Emergency ultrasound for blunt abdominal trauma: meta-analysis update 2003. *Zentralbl Chir* 128:1027–1037 [in German]
43. Stengel D et al (2001) Systematic review and meta-analysis of emergency ultrasonography for blunt abdominal trauma. *Br J Surg* 88:901–912
44. Poletti PA, Wintermark M, Schnyder P, Becker CD (2002) Traumatic injuries: role of imaging in the management of the polytrauma victim (conservative expectation). *Eur Radiol* 12:969–978
45. Sheridan R, Peralta R, Rhea J, Ptak T, Novelline R (2003) Reformatted visceral protocol helical computed tomographic scanning allows conventional radiographs of the thoracic and lumbar spine to be eliminated in the evaluation of blunt trauma patients. *J Trauma* 55:665–669
46. Albrecht T, Schlippenbach J von, Stahel PF, Ertel W, Wolf KJ (2004) The role of whole body spiral CT in the primary work-up of polytrauma patients: comparison with conventional radiography and abdominal sonography. *Rofo* 176:1142–1150 [in German]
47. Meyers BF, McCabe CJ (1993) Traumatic diaphragmatic hernia. Occult marker of serious injury. *Ann Surg* 218:783–790
48. Simpson J, Lobo DN, Shah AB, Rowlands BJ (2000) Traumatic diaphragmatic rupture: associated injuries and outcome. *Ann R Coll Surg Engl* 82:97–100
49. Carter YM, Karmy-Jones RC, Stern EJ (2001) Delayed recognition of diaphragmatic rupture in a patient receiving mechanical ventilation. *Am J Roentgenol* 176:428
50. Morgan AS, Flancaum L, Esposito T, Cox EF (1986) Blunt injury to the diaphragm: an analysis of 44 patients. *J Trauma* 26:565–568
51. Wienczek RG Jr, Wilson RF, Steiger Z (1986) Acute injuries of the diaphragm. An analysis of 165 cases. *J Thorac Cardiovasc Surg* 92:989–993
52. Peloponissios N, Halkic N (1999) Diaphragmatic rupture after closed injury. *Schweiz Med Wochenschr* 129:1230 [in German]
53. Drews JA, Mercer EC, Benfield JR (1973) Acute diaphragmatic injuries. *Ann Thorac Surg* 16:67–78
54. Gelman R, Mirvis SE, Gens D (1991) Diaphragmatic rupture due to blunt trauma: sensitivity of plain chest radiographs. *Am J Roentgenol* 156:51–57
55. Dee PM (1992) The radiology of chest trauma. *Radiol Clin North Am* 30:291–306
56. Shapiro MJ, Heiberg E, Durham RM, Luchtefeld W, Mazuski JE (1996) The unreliability of CT scans and initial chest radiographs in evaluating blunt trauma induced diaphragmatic rupture. *Clin Radiol* 51:27–30
57. Murray JG, Caoili E, Gruden JF, Evans SJ, Halvorsen RA Jr, Mackersie RC (1996) Acute rupture of the diaphragm due to blunt trauma: diagnostic sensitivity and specificity of CT. *Am J Roentgenol* 166:1035–1039
58. Killeen KL, Mirvis SE, Shanmuganathan K (1999) Helical CT of diaphragmatic rupture caused by blunt trauma. *Am J Roentgenol* 173:1611–1616
59. Nchimi A et al (2005) Helical CT of blunt diaphragmatic rupture. *Am J Roentgenol* 184:24–30
60. Bergin D, Ennis R, Keogh C, Fenlon HM, Murray JG (2001) The "dependent viscera" sign in CT diagnosis of blunt traumatic diaphragmatic rupture. *Am J Roentgenol* 177:1137–1140
61. Mirvis SE, Whitley NO, Vainwright JR, Gens DR (1989) Blunt hepatic trauma in adults: CT-based classification and correlation with prognosis and treatment. *Radiology* 171:27–32
62. Boone DC, Federle M, Billiar TR, Udekwu AO, Peitzman AB (1995) Evolution of management of major hepatic trauma: identification of patterns of injury. *J Trauma* 39:344–350



63. Meredith JW, Young JS, Bowling J, Roboussin D (1994) Nonoperative management of blunt hepatic trauma: The exception or the rule? *J Trauma* 36:529–534
64. Malhotra AK et al. (2000) Blunt hepatic injury: a paradigm shift from operative to nonoperative management in the 1990s. *Ann Surg* 231:804–813
65. Croce MA et al (1995) Nonoperative management of blunt hepatic trauma is the treatment of choice for hemodynamically stable patients. Results of a prospective trial. *Ann Surg* 221:744–753
66. Patton JH Jr, Croce MA, Fabian TC (1995) Blunt hepatic trauma: trends in nonoperative management. *J Tenn Med Assoc* 88:101–102
67. Pachter HL et al (1996) Status of nonoperative management of blunt hepatic injuries in 1995: a multicenter experience with 404 patients. *J Trauma* 40:31–38
68. Patten RM, Spear RP, Vincent LM, Hesla RB, Jurkovich GJ (1993) Traumatic laceration of the liver limited to the bare area: CT findings in 25 patients. *Am J Roentgenol* 160:1019–1022
69. Becker CD, Gal I, Baer HU, Vock P (1996) Blunt hepatic trauma in adults: correlation of CT injury grading with outcome. *Radiology* 201:215–220
70. Shanmuganathan K, Mirvis SE, Amoroso M (1993) Periportal low density on CT in patients with blunt trauma: association with elevated venous pressure. *Am J Roentgenol* 160:279–283
71. Gates JD (1994) Delayed hemorrhage with free rupture complicating the nonsurgical management of blunt hepatic trauma: a case report and review of the literature. *J Trauma* 36:572–575
72. Gupta A, Stuhlfaut JW, Fleming KW, Lucey BC, Soto JA (2004) Blunt trauma of the pancreas and biliary tract: a multimodality imaging approach to diagnosis. *Radiographics* 24:1381–1395
73. Novelline RA, Rhea JT, Bell T (1999) Helical CT of abdominal trauma. *Radiol Clin North Am* 37:591–612
74. Erb RE, Mirvis SE, Shanmuganathan K (1994) Gallbladder injury secondary to blunt trauma: CT findings. *J Comput Assist Tomogr* 18:778–784
75. Cogbill TH et al. (1989) Nonoperative management of blunt splenic trauma: a multicenter experience. *J Trauma* 29:1312–1317
76. Williams MD, Young DH, Schiller WR (1990) Trend toward nonoperative management of splenic injuries. *Am J Surg* 160:588–592
77. Delgado Millan MA, Deballon PO (2001) Computed tomography, angiography, and endoscopic retrograde cholangiopancreatography in the nonoperative management of hepatic and splenic trauma. *World J Surg* 25:1397–1402
78. Pimpl W, Dapunt O, Kaindl H, Thalhamer J (1989) Incidence of septic and thromboembolic-related deaths after splenectomy in adults. *Br J Surg* 76:517–521
79. Shackford SR, Molin M (1990) Management of splenic injuries. *Surg Clin North Am* 70:595–620
80. Kluger Y et al. (1994) Delayed rupture of the spleen: myths, facts, and their importance: case reports and literature review. *J Trauma* 36:568–571
81. Pappas D, Mirvis SE, Crepps JT (1987) Splenic trauma: false-negative CT diagnosis in cases of delayed rupture. *Am J Roentgenol* 149:727–728
82. Resciniti A, Fink MP, Raptopoulos V, Davidoff A, Silva WE (1988) Nonoperative treatment of adult splenic trauma: development of a computed tomographic scoring system that detects appropriate candidates for expectant management. *J Trauma* 28:828–831
83. Becker CD, Spring P, Glatli A, Schweizer W (1994) Blunt splenic trauma in adults: Can CT findings be used to determine the need for surgery? *Am J Roentgenol* 162:343–347
84. Kohn JS, Clark DE, Isler RJ, Pope CF (1994) Is computed tomographic grading of splenic injury useful in the nonsurgical management of blunt trauma? *J Trauma* 36:385–390
85. Buntain WL, Gould HR, Maull KI (1988) Predictability of splenic salvage by computed tomography. *J Trauma* 28:24–34
86. Elmore JR, Clark DE, Isler RJ, Horner WR (1989) Selective nonoperative management of blunt splenic trauma in adults. *Arch Surg* 124:581–586
87. Umlas SL, Cronan JJ (1991) Splenic trauma: Can CT grading systems enable prediction of successful nonsurgical treatment? *Radiology* 178:481–487
88. Ilahi O, Bochicchio GV, Scalea TM (2002) Efficacy of computed tomography in the diagnosis of pancreatic injury in adult blunt trauma patients: a single-institutional study. *Am Surg* 68:704–708
89. Wong YC, Wang LJ, Lin BC, Chen CJ, Lim KE, Chen RJ (1997) CT grading of blunt pancreatic injuries: prediction of ductal disruption and surgical correlation. *J Comput Assist Tomogr* 21:246–250
90. Bradley EL III et al. (1998) Diagnosis and initial management of blunt pancreatic trauma: guidelines from a multiinstitutional review. *Ann Surg* 227:861–869
91. Madiba TE, Mokoena TR (1995) Favourable prognosis after surgical drainage of gunshot, stab or blunt trauma of the pancreas. *Br J Surg* 82:1236–1239
92. Akhrass R, Yaffe MB, Brandt CP, Reigle M, Fallon WF Jr, Malangoni MA (1997) Pancreatic trauma: a ten-year multi-institutional experience. *Am Surg* 63:598–604
93. Wilson RH, Moorehead RJ (1991) Current management of trauma to the pancreas. *Br J Surg* 78:1196–1202
94. Dawson AR, Webster CH, Howe HC, Theron EJ, Meiring L (1985) Rupture of the head of the pancreas by blunt trauma. A case report. *S Afr Med J* 67:560–562
95. Itoh S, Ikeda M, Ota T, Satake H, Takai K, Ishigaki T (2003) Assessment of the pancreatic and intrapancreatic bile ducts using 0.5-mm collimation and multiplanar reformatted images in multislice CT. *Eur Radiol* 13:277–285
96. Sherck J, Shatney C, Sensaki K, Selivanov V (1994) The accuracy of computed tomography in the diagnosis of blunt small-bowel perforation. *Am J Surg* 168:670–675
97. Hagiwara A et al. (1995) Early diagnosis of small intestine rupture from blunt abdominal trauma using computed tomography: significance of the streaky density within the mesentery. *J Trauma* 38:630–633
98. Kunin JR, Korobkin M, Ellis JH, Francis IR, Kane NM, Siegel SE (1993) Duodenal injuries caused by blunt abdominal trauma: value of CT in differentiating perforation from hematoma. *Am J Roentgenol* 160:1221–1223
99. Rizzo MJ, Federle MP, Griffiths BG (1989) Bowel and mesenteric injury following blunt abdominal trauma: evaluation with CT. *Radiology* 173:143–148
100. Dowe MF, Shanmuganathan K, Mirvis SE, Steiner RC, Cooper C (1997) CT findings of mesenteric injury after blunt trauma: implications for surgical intervention. *Am J Roentgenol* 168:425–428
101. Mirvis SE, Gens DR, Shanmuganathan K (1992) Rupture of the bowel after blunt abdominal trauma: diagnosis with CT. *Am J Roentgenol* 159:1217–1221
102. Levine CD, Patel UJ, Wachsberg RH, Simmons MZ, Baker SR, Cho KC (1995) CT in patients with blunt abdominal trauma: clinical significance of intraperitoneal fluid detected on a scan with otherwise normal findings. *Am J Roentgenol* 164:1381–1385
103. Mirvis SE, Shanmuganathan K, Erb R (1994) Diffuse small-bowel ischemia in hypotensive adults after blunt trauma (shock bowel): CT findings and clinical significance. *Am J Roentgenol* 163:1375–1379
104. Orwig D, Federle MP (1989) Localized clotted blood as evidence of visceral trauma on CT: the sentinel clot sign. *Am J Roentgenol* 153:747–749
105. Burks DW, Mirvis SE, Shanmuganathan K (1992) Acute adrenal injury after blunt abdominal trauma: CT findings. *Am J Roentgenol* 158:503–507



106. Sivit CJ, Ingram JD, Taylor GA, Bulas DI, Kushner DC, Eichelberger MR (1992) Posttraumatic adrenal hemorrhage in children: CT findings in 34 patients. *Am J Roentgenol* 158:1299–1302
107. Hinrichs CR, Singer A, Maldjian P, Abu-Judeh H, Dadarwala A (2001) Inferior vena cava thrombosis: a mechanism of post-traumatic adrenal hemorrhage. *Am J Roentgenol* 177:357–358
108. Valls C, Andia E, Gil I, Conde I (1992) Bilateral posttraumatic adrenal hemorrhage detected with CT. *Am J Roentgenol* 159:433–434
109. Gomez RG, McAninch JW, Carroll PR (1993) Adrenal gland trauma: diagnosis and management. *J Trauma* 35:870–874
110. Murphy BJ, Casillas J, Yrizarry JM (1988) Traumatic adrenal hemorrhage: radiologic findings. *Radiology* 169:701–703
111. Rhyner P, Federle MP, Jeffrey RB (1984) CT of trauma to the abnormal kidney. *Am J Roentgenol* 142:747–750
112. Cass AS, Vieira J (1987) Comparison of IVP and CT findings in patients with suspected severe renal injury. *Urology* 29:484–487
113. Carlin BI, Resnick MI (1995) Indications and techniques for urologic evaluation of the trauma patient with suspected urologic injury. *Semin Urol* 13:9–24
114. Catalano O, Lobianco R, Esposito M, Sandomenico F, Siani A (1999) Contrast media extravasation in upper abdominal injuries: detection with spiral computerized tomography. *Radiol Med (Torino)* 97:138–143 [in Italian]
115. Steinberg DL, Jeffrey RB, Federle MP, McAninch JW (1984) The computerized tomography appearance of renal pedicle injury. *J Urol* 132:1163–1164
116. Glazer GM, Francis IR, Brady TM, Teng SS (1983) Computed tomography of renal infarction: clinical and experimental observations. *Am J Roentgenol* 140:721–727
117. Moore EE et al. (1989) Organ injury scaling: spleen, liver, and kidney. *J Trauma* 29:1664–1666
118. Husmann DA, Gilling PJ, Perry MO, Morris JS, Boone TB (1993) Major renal lacerations with a devitalized fragment following blunt abdominal trauma: a comparison between nonoperative (expectant) versus surgical management. *J Urol* 150:1774–1777
119. Federle MP, Jeffrey RB Jr (1983) Hemoperitoneum studied by computed tomography. *Radiology* 148:187–192
120. Willmann JK et al. (2002) Multidetector CT: detection of active hemorrhage in patients with blunt abdominal trauma. *Am J Roentgenol* 179:437–444
121. Fang JF et al (2000) Classification and treatment of pooling of contrast material on computed tomographic scan of blunt hepatic trauma. *J Trauma* 49:1083–1088
122. Fang JF et al (1998) Pooling of contrast material on computed tomography mandates aggressive management of blunt hepatic injury. *Am J Surg* 176:315–319
123. Shanmuganathan K, Mirvis SE, Reaney SM (1995) Pictorial review: CT appearances of contrast medium extravasations associated with injury sustained from blunt abdominal trauma. *Clin Radiol* 50:182–187
124. Shanmuganathan K, Mirvis SE, Sover ER (1993) Value of contrast-enhanced CT in detecting active hemorrhage in patients with blunt abdominal or pelvic trauma. *Am J Roentgenol* 161:65–69
125. Chan L, Nade S, Brooks A, Deane S (1994) Experience with lower urinary tract disruptions associated with pelvic fractures: implications for emergency room management. *Aust N Z J Surg* 64:395–399
126. Hochberg E, Stone NN (1993) Bladder rupture associated with pelvic fracture due to blunt trauma. *Urology* 41:531–533
127. Flancaum L, Morgan AS, Fleisher M, Cox EF (1988) Blunt bladder trauma: manifestation of severe injury. *Urology* 31:220–222
128. Chaumoitre K, Portier F, Petit P, Merrot T, Guillon PO, Panuel M (2000) CT imaging of pelvic injuries in polytrauma patients. *J Radiol* 81:111–120 [in French]
129. Horstman WG, McClennan BL, Heiken JP (1991) Comparison of computed tomography and conventional cystography for detection of traumatic bladder rupture. *Urol Radiol* 12:188–193
130. Lowe MA, Mason JT, Luna GK, Maier RV, Copass MK, Berger RE (1988) Risk factors for urethral injuries in men with traumatic pelvic fractures. *J Urol* 140:506–507
131. Chou CP et al (2005) CT voiding urethrography and virtual urethroscopy: preliminary study with 16-MDCT. *Am J Roentgenol* 184:1882–1888
132. Kamat N (2004) Dynamic three-dimensional spiral computed tomographic cysto-urethrography: a novel technique for evaluating post-traumatic posterior urethral defects. *BJU Int* 94:191
133. Ali M, Safriel Y, Sclafani SJ, Schulze R (2003) CT signs of urethral injury. *Radiographics* 23:951–963

# Imaging and Intervention of Large Arterial Trauma

M. Schoder, M. Prokop, J. Lammer

## 2.9

### Contents

2.9.1	Introduction	205
2.9.2	Supraaortic Arch Vessels	206
2.9.2.1	Innominate and Subclavian Artery	206
2.9.2.2	Carotid and Vertebral Arteries	206
2.9.3	Pelvic Arteries and Lower Limbs	208
2.9.3.1	Pelvic Arteries	208
2.9.3.2	Lower Limbs	211
2.9.4	Thoracic Aorta	212
2.9.4.1	Thoracic Aortic Transection	212
2.9.4.2	Thoracic Aortic Dissection	214
2.9.5	Abdominal Aorta	218
2.9.5.1	Blunt Abdominal Aortic Injuries	218
2.9.5.2	Stent-Graft Designs	218
2.9.5.3	Imaging and Stent-Graft Implantation	218
2.9.6	Abdominal Aortic Branches	220
2.9.7	Conclusion	220
	References	220

### 2.9.1 Introduction

Traumatic injury to the aorta and its major branches often cause an acute life-threatening situation. The length of time between injury and treatment is one of the major determinants for patient outcome. In many trauma centers, contrast-enhanced CT is increasingly used for initial diagnosis in the evaluation of the multi-trauma patient. Introduction of multi-detector row CT with the ability of two- and three-dimensional post-processing techniques has offered a number of advantages in the diagnostic work-up of emergency patients [1–5].

Great vessel injuries can occur by a direct mechanism due to a penetrating or a blunt trauma. Penetrating injuries are usually caused by cutting, stabbing and firearm as-

saults, or are iatrogenic in nature. Non-bleeding vessels with injuries of the vessels' adventitia and media may cause delayed emergency situations due to rupture of a pseudoaneurysm or fistula formation. Furthermore, a dissection may lead to vessel thrombosis and end-organ malperfusion; therefore, in all cases of suspected trauma to a vascular structure, a meticulous search must be performed to rule out a trauma to a large vascular structure.

In complete traumatic perforation of the aorta and bleeding into the pleural or peritoneal cavity, the patient is usually in severe shock or already dead upon arrival to the emergency room; however, in small perforations with bleeding into the mediastinum or retroperitoneal space, the patient may be hemodynamically stable for a longer period of time.

Complete avulsion of an arterial branch at its origin from the main artery always causes hemorrhage, but if the vessel has a small diameter, bleeding may stop due to retraction and coil up of the intimal layer. In such a case the injury may be temporary asymptomatic and may be overseen.

Injuries from blunt trauma are less predictable than those from penetrating trauma because of the complex forces with wide variations in distribution and direction. Injury pattern varies from a sub-intimal hemorrhage, with or without an intimal tear, to complete aortic disruption. Intimal dissections and tears in branch vessels range from asymptomatic to occluding.

Indirect vessel injuries include vessel spasms caused by mechanical irritation due to compression or displacement, and may be serious enough to damage an organ or limb. Extensive stretching of a vessel may also cause a dissection, coil up of the intima or rupture.

An emergent and life-threatening situation deriving from large vessels can be due to any of the following

1. Bleeding
  - a. Traumatic transection
  - b. Perforating injuries
  - c. Rupture of pseudoaneurysm, dissection

2. Thrombosis
  - a. Traumatic vessel injury
  - b. Hypercoagulability syndrome
3. Embolization
  - a. Foreign-body embolization
  - b. Organ artery or peripheral artery embolization
  - c. Pulmonary artery embolization
4. Malperfusion syndromes
  - a. Traumatic compression or spasm
  - b. Avulsion of vessels
  - c. Thrombosis
  - d. Static or dynamic true lumen compression in dissection

---

## 2.9.2 Supraaortic Arch Vessels

The neck is divided into three zones:

1. Zone I: from the thoracic outlet up to the cricoid cartilage
2. Zone II: mid-segment of the neck between the cricoid cartilage and the angle of the mandible
3. Zone III: from the mandibular angle up to the base of the skull [6]

---

### 2.9.2.1 Innominate and Subclavian Artery

The great vessels can be injured by blunt or penetrating mechanisms. Injuries in zone I are commonly caused by chest trauma. The most frequent cause is a penetrating trauma [7] in subclavian and axillary injuries which constitute 5–10% of arterial trauma in civilians [8]. Rupture of the innominate artery is a rare injury from blunt trauma with the majority of patients is victims of motor vehicle collisions [9, 10]. Laceration of the brachiocephalic artery at the origin from the aortic arch may cause a mediastinal hematoma, which is seen primarily on chest CT. If contrast bolus CT angiography (CTA) with 3D reconstructions, such as multiplanar reformation (MPR), curved planar reconstruction (CPR), and maximum intensity projection (MIP), do not clearly demonstrate the site of vascular laceration, catheter angiography is necessary. In a study by Ahrar et al. 17 of 89 patients who suffered from blunt thoracic trauma presented with great vessel injuries [11]. In 70% of patients the vessel injury was not clinically suspected. At the thoracic outlet blunt trauma is frequently caused by a seat belt injury [12]. The presence of a peripheral pulse does not exclude a proximal arterial injury; therefore, all patients presenting with thoracic and periclavicular trauma should be examined for a vascular trauma. Conventional angiography has been replaced by CTA in many trauma centers [13–15].

Inadvertent puncture and catheter insertion into the subclavian artery may occur during cannulation of the subclavian vein. Removal of the arterial catheter can cause massive hemorrhage with compression of the brachial plexus. Furthermore, if both the artery and the adjacent vein are injured, formation of an arteriovenous fistula (AVF) can be formed. Another sequelae is the occurrence of a pseudoaneurysm with a high risk for rupture (Fig. 1).

Because surgical exploration in this area is difficult, endovascular stent-graft placement has become an alternative treatment option in selected patients. Reported short-term patency rates of 100% by du Toit et al. [16] and Patel and colleagues [17] are encouraging. Hilfiker and associates [18] described their experience in 9 patients with AVFs and pseudoaneurysms resulting in a primary and secondary patency of 89 and 100%, respectively, after a mean follow-up of 29 months. When feasible, an alternative to stent graft subclavian repair for a misplaced central catheter is the implementation of a percutaneous closure device, such as Angioseal or Perclose, for occlusion of the arterial catheter hole [19].

---

### 2.9.2.2 Carotid and Vertebral Arteries

The overall incidence of penetrating carotid artery injuries in head and neck trauma is approximately 0.45% [20]. Blunt injury to the carotid and vertebral artery is higher than once thought. Early reports described an incidence of blunt carotid injury in 0.08% [21]; however, recent series reported an incidence of 0.86% in a meticulously screened population [22]. Vertebral artery injury is common with cervical spine fracture and is reported to be associated with a 33–46% incidence of injury in this setting [23–25].

Penetrating trauma, often due to stabbing injuries or a gunshot, can cause arterial injuries anywhere along the path of one or more of the craniocervical vessels.

Patients with penetrating neck injuries in zone II and no signs of vascular injury can be managed on the basis of physical examination alone. In case of a blunt carotid artery trauma, color-coded duplex sonography is the first imaging modality, and allows exclusion of cervical internal carotid artery dissection [26]; however, a diagnosis of dissection must be confirmed with MRI and MRA [26, 27]. The vertebral artery is more difficult to examine because of its passage through the foramen transversarium. Furthermore, injuries in zone III are almost inaccessible to ultrasound exploration and must be explored by MR-, CT, or conventional angiography, which still is the “gold standard” for diagnosis of blunt cerebrovascular injuries [28, 29].



**Fig. 1.** **a** The CT scan shows huge pseudoaneurysm after inadvertent puncture of the right innominate artery. **b** Angiogram delin-

eates the pseudoaneurysm. **c** After placement of a balloon-expandable stent-graft, the pseudoaneurysm is successfully excluded

For the arteriographic appearance of carotid and vertebral injuries Biffi et al. [30] proposed following grading scale:

- Grade I: arteriographic appearance of irregularity of the vessel wall or dissection/intramural hematoma with <25% luminal stenosis
- Grade II: intraluminal thrombus or raised intimal flap is visualized, or dissection/intramural hematoma with 25% or more luminal narrowing
- Grade III: pseudoaneurysms
- Grade IV: vessel occlusion
- Grade V: transections

When a screening protocol is used, grade-I and grade-II injuries are the most commonly seen [31]. Anticoagulant and antiplatelet therapy is currently the accepted treatment in patients without contraindication, and improved outcomes were reported in patients who were treated medically compared with patients who did not receive therapy [31–33]; however, as evaluated by Biffi et al. [31], 8% of grade I, and 43% of grade-II lesions progressed to pseudoaneurysm necessitating interventional treatment. Surgical treatment is often difficult because many blunt carotid injuries occur in zone III (Fig. 2); therefore, stent placement may be appropriate for vessels demonstrating an evolving or progressing dissection or pseudoaneurysm (Fig. 3) [34, 35].



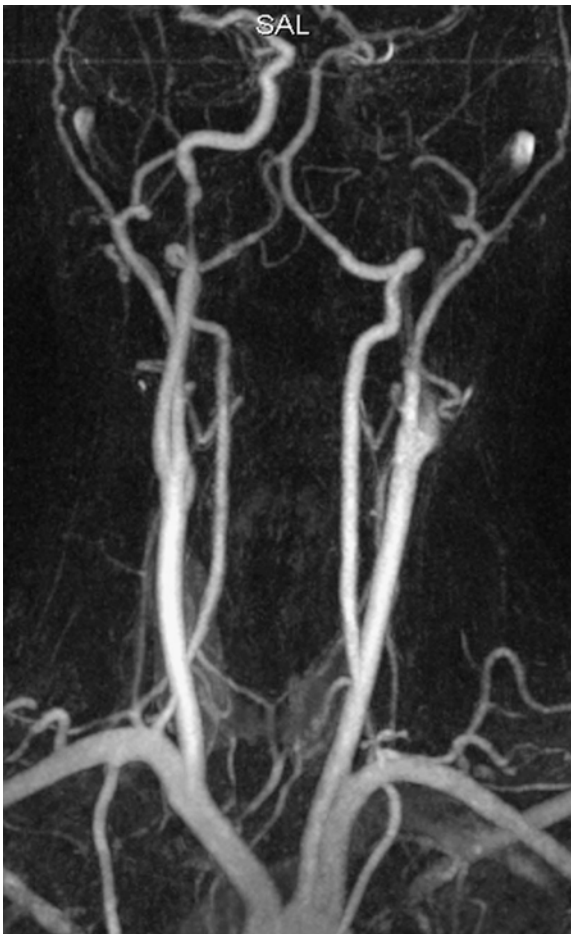


**Fig. 2.** The MR angiogram shows grade-II lesion (>25% luminal narrowing) of the right internal carotid artery, and grade-IV lesion (occlusion) of the left internal carotid artery

## 2.9.3 Pelvic Arteries and Lower Limbs

### 2.9.3.1 Pelvic Arteries

In complex pelvic fractures, recent articles reported hemodynamic instability of patients due to bleeding in 3–10% of cases [36, 37]. Blood loss and resulting coagulopathy are recognized causes for death in patients with “unstable” pelvic fractures. Arterial bleeding in these patients is usually caused by disruption of smaller branches of the internal iliac artery that traverse deep in the pelvis. Angiography and selective embolization of bleeding arteries has been reported with a high initial success rate of 95–100% [36–39], and has therefore become the treatment of choice in unstable patients. Injuries of the common and external iliac arteries associated with pelvic fractures are uncommon. If it occurs, the injury pattern is dominated by intimal disruption which may result in vessel dissection, thrombosis, and occlusion with malperfusion of the lower limb. Besides conventional surgical repair by use of prosthetic grafts [40], there are a few case reports presenting patients who were treated successfully by endovascular stent placement [41, 42].

Iatrogenic injuries by catheter angiography and percutaneous transluminal angioplasty (PTA) can cause acute occlusive dissection of an iliac artery. If the collateral flow is insufficient, the limb is threatened necessitating acute revascularization, which can be achieved with stent placement in the majority of cases. Plaque perforation and rupture are rare complications of PTA, observed in only <0.005% of cases. Acute bleeding into the spongy perivascular tissue of the retroperitoneum can rapidly lead to large hematomas extending up to the diaphragm. Immedi-



**Fig. 3.** Posttraumatic lesion in zone III of the neck. **a** Diagnostic angiogram shows dissection and pseudoaneurysm (grade-III lesion) of the internal carotid artery. **b** After stent-graft implantation

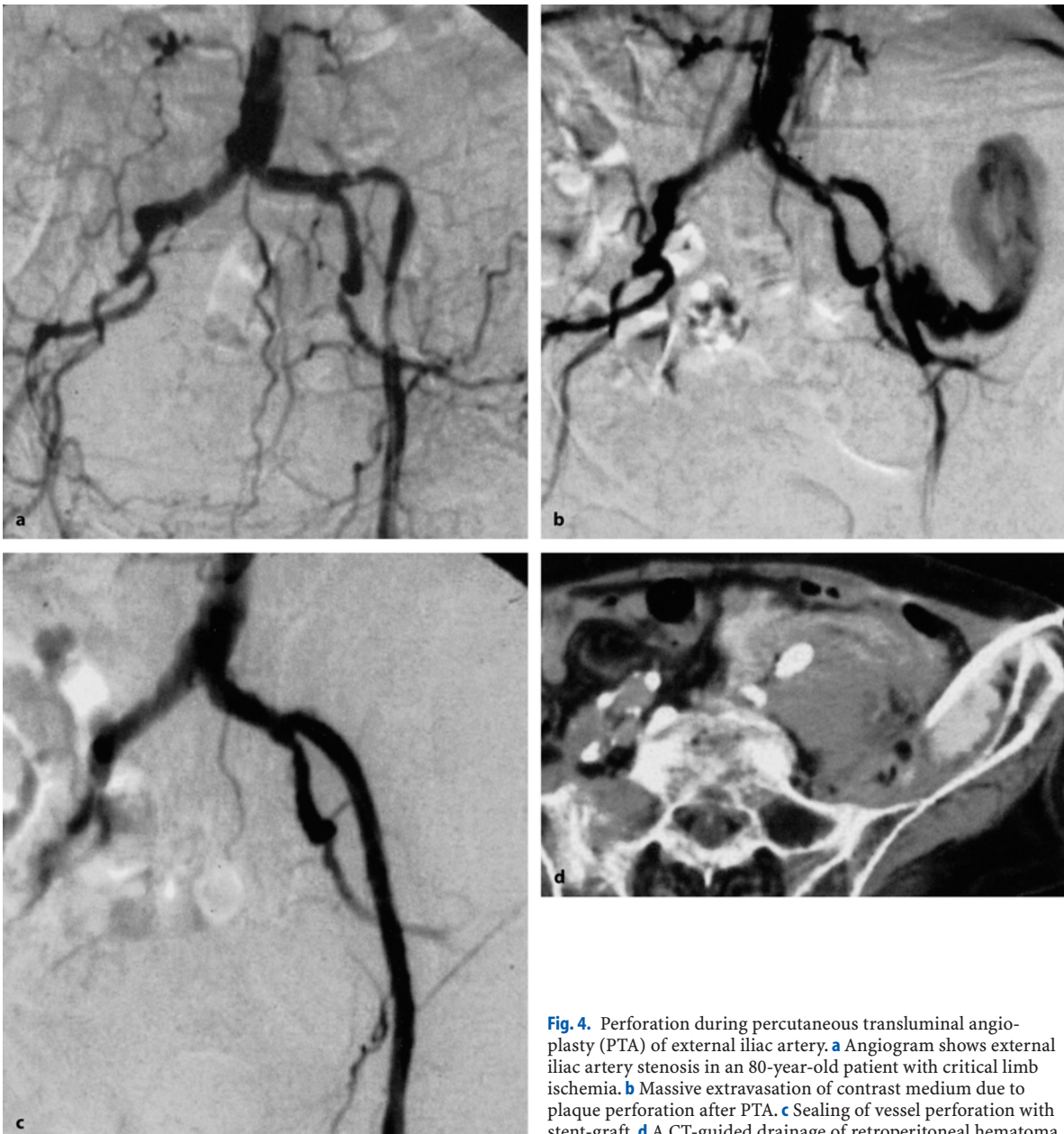


**Fig. 4.** Perforation during percutaneous transluminal angioplasty (PTA) of external iliac artery. **a** Angiogram shows external iliac artery stenosis in an 80-year-old patient with critical limb ischemia. **b** Massive extravasation of contrast medium due to plaque perforation after PTA. **c** Sealing of vessel perforation with stent-graft. **d** A CT-guided drainage of retroperitoneal hematoma

ate inflation of an angioplasty balloon leads to temporary bleeding control. Subsequent sealing of the leak can be achieved with stent-graft implantation (Fig. 4). An arteriovenous fistula can occur after surgical and endovascular

interventions and may cause venous aneurysms or bleeding. It can be treated by embolization with coils, endovascular occlusion with a stent-graft (Fig. 5), or surgical ligation.

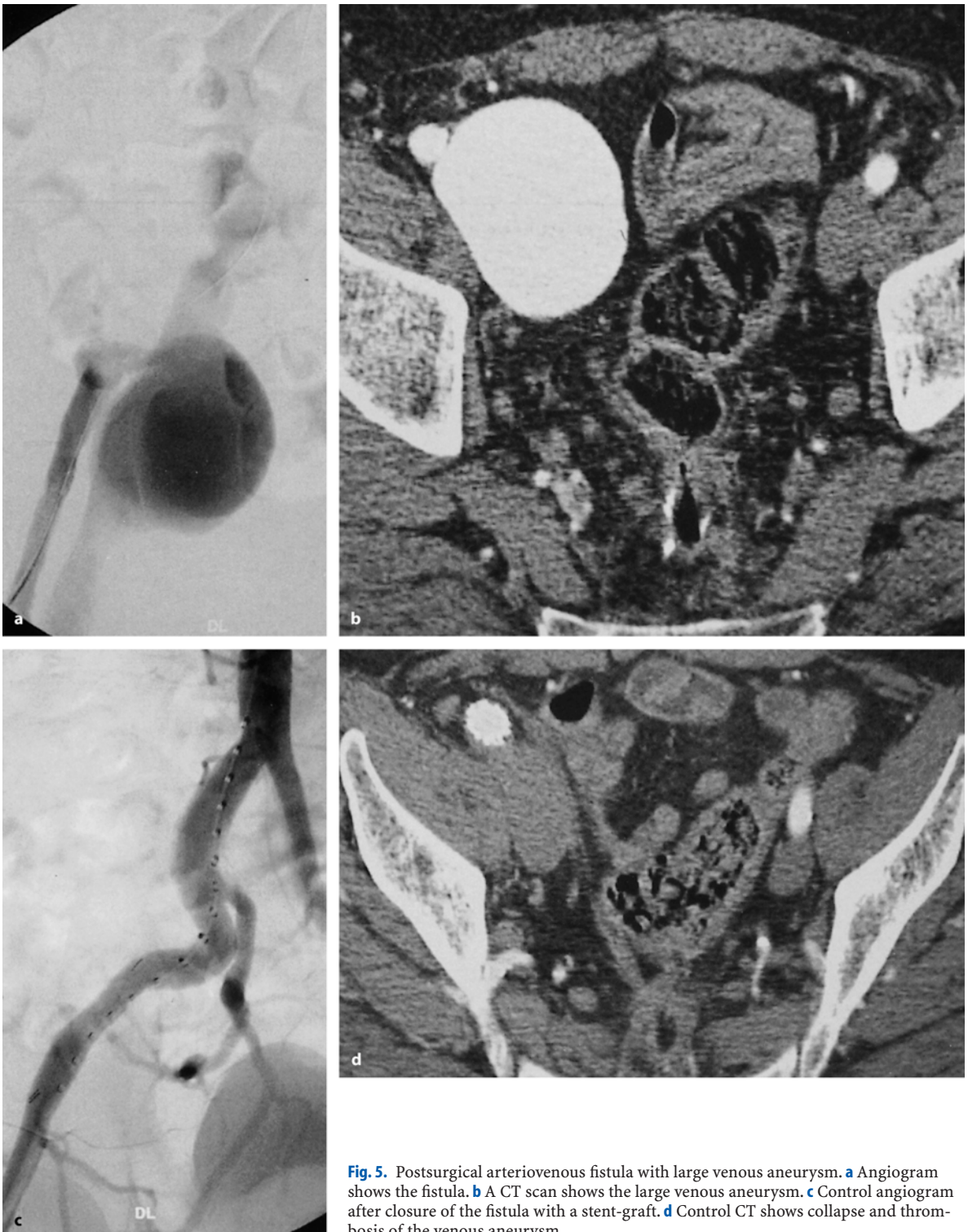


**Fig. 5.** Postsurgical arteriovenous fistula with large venous aneurysm. **a** Angiogram shows the fistula. **b** A CT scan shows the large venous aneurysm. **c** Control angiogram after closure of the fistula with a stent-graft. **d** Control CT shows collapse and thrombosis of the venous aneurysm



### 2.9.3.2 Lower Limbs

Generally, arterial injury of the lower extremity combined with fractures or knee dislocation is not very frequent [43, 44]. The greatest series of 550 civilian patients who suffered from non-iatrogenic lower limb arterial injuries was published by Hafez and colleagues [45]. In their patients, 19% had a blunt injury, whereas the remaining patients had penetrating injuries from firearm or stab wounds. They found that the clinical presence of sensory or motor dysfunction and compartment syndrome, as well as additional compound fractures, were associated with a significant increase in limb loss. In unstable patients, clinical presence of hemorrhage and extremity ischemia with absent distal pulses requires immediate surgical intervention. To rule out occult arterial lesions in the trauma setting, ankle-brachial index (ABI) measurements have been evaluated. Lynch and Johansen found, when compared with angiograms, that an ABI of  $<0.9$  had a sensitivity of 87% and a specificity of 97% for arterial disruption [46]. In some centers, duplex ultrasonography was found to have a high sensitivity and specificity in diagnosis of flow limiting lesions in penetrating or blunt injuries [47, 48]. Helical CT angiography in the diagnosis for arterial injuries has been reported to have a 90–100% sensitivity in the diagnosis of significant arterial lesions [49].

If there is suspicion of vascular injuries in stable patients, intra-arterial digital subtraction angiography (DSA) remains the gold standard for the evaluation of intimal tears, dissections, occlusions, AVFs, and pseudoaneurysms. Angiographic findings of arterial termination are caused

by complete avulsion with bleeding or vessel occlusion due to intimal tears and dissections (Fig. 6). Limb-threatening ischemia can also occur with arterial spasm. In this setting, intra-arterial infusion of vasodilators has been reported to

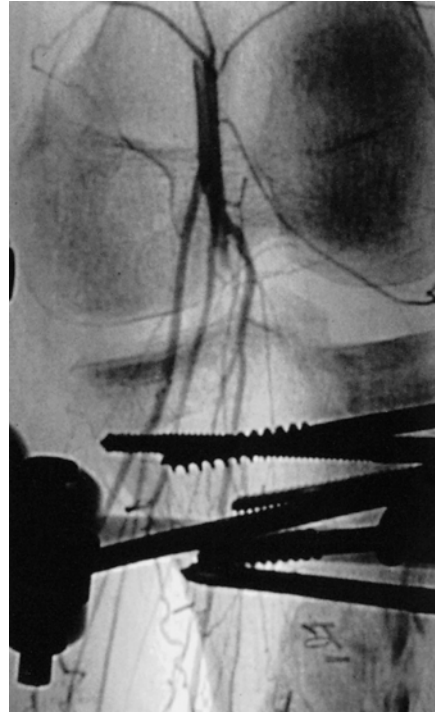


**Fig. 6.** Angiogram shows posttraumatic occlusion of the popliteal artery

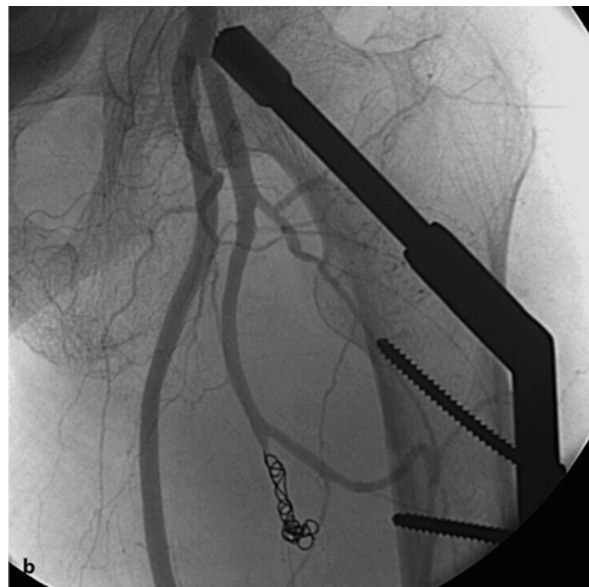


**Fig. 7.** Iatrogenic pseudoaneurysm and bleeding after orthopedic surgery. **a** Angiogram shows pseudoaneurysm of profound femoral artery branches. **b** Successful occlusion after coil embolization



improve blood flow [50]. Endovascular control of bleeding from pseudoaneurysms and AVFs in non-critical vascular territories can be achieved by selective or super-selective embolization of arterial branches using coils, gelatin sponge, or glue (Fig. 7) [51]. Prevention of back bleeding from collateral vessels is vital when employing this technique. The operator must intentionally achieve initial distal vessel occlusion beyond the arterial injury prior to proximal embolization. In selected patients, stent-grafts were successfully used in the treatment of traumatic and iatrogenic arterial rupture, pseudoaneurysms, and AVFs [52–55].

Iatrogenic pseudoaneurysms, usually located in the common femoral artery or close to the superficial femoral artery origin, may result in 1–9% after retrograde catheterization and 1–18% after an antegrade puncture. In small pseudoaneurysms, the treatment of choice is ultrasound-guided compression. After compression for 20–40 min, a thrombosis of the fresh pseudoaneurysm occurs in 70–80% [56, 57]. Injection of a thrombin solution is also very effective (thrombosis rate >90%), primarily in pseudoaneurysms with a narrow neck [58, 59]. In broad-based aneurysms, surgery must be performed.

## 2.9.4 Thoracic Aorta

### 2.9.4.1 Thoracic Aortic Transection

Approximately 70% of blunt thoracic aortic injuries result from motor vehicle collisions [60], and is reported to be lethal in 75–90% of patients at the time of injury [61–63]. Moreover, 10–13% of survivors who reach the hospital die within a few hours if appropriate therapy is delayed [64–66]. Multiple-organ injuries are frequent in these patients with an average of two associated injuries in survivors [62]. In 1–2% of the patients with traumatic aortic injuries the diagnosis is initially missed. If these patients survive, development of chronic traumatic false aneurysms with a high risk for rupture may occur [61, 67, 68].

Uncertainty remains regarding the pathogenic etiology of blunt thoracic injuries [69]. Several hypotheses have been proposed regarding mechanical forces acting through the aorta during the blunt trauma. The favored theories combine the occurrence of rapid deceleration with shearing stress and chest compression. In addition to stretching of the aorta, the mobility of the ascending aorta and the aortic arch relative to the fixed distal descending aorta has been emphasized as a contributory factor [70, 71]. Crass et al. [72] assume that rupture is due to an entrapment of the aorta between the manubrium, first rib, medial clavicles or sternum, and the vertebral column. Some authors attribute a sudden increase of the internal blood pressure as a possible mechanism [73, 74]. More recent theories propose that blunt trauma results from a combination including shear

stress, torsion, and stretching combined with hydrostatic forces [75].

The possibility for a blunt thoracic aortic injury should be considered in any person who was exposed to a large amount of force such as major motor vehicle accident, fall from a significant height, or a collision. Plain chest X-ray is often the first-line screening tool. Although there are diagnostic limitations, aortic rupture may be suspected in widening of the mediastinum, obscuring of the aortic knob, opacification of the aorto-pulmonary window, widened paratracheal and para-spinous stripes, or an apical capping; however, a negative chest X-ray does not exclude aortic injuries, as found in 12% of cases in the series by Gammie et al. [64]. Helical CT scanning has become the recommended screening tool in many centers [76–78]. Multi-slice scanner allow rapid diagnosis and their accuracy has been improved by the availability of two- and three-dimensional reconstructions. Diagnostic difficulties might be caused by imaging issues such as streak and aortic motion artifacts [79]. To overcome this diagnostic uncertainty by cardiac motion, retrospective or prospective electrocardiographically synchronized multi-slice CT has been shown to be relevant in imaging of the ascending aorta. Intra-arterial digital subtraction angiography has been the “gold standard” in diagnosis of thoracic aortic injuries. Presently, diagnostic angiography is used as a supplementary diagnostic tool in selected cases.

The most common site of the aortic tear is at the antero-medial aspect of the aortic isthmus, distal to the left subclavian artery and proximal to the third intercostals artery. In the autopsy series by William et al. [63], aortic rupture at the isthmus is reported in 65% of cases with complete transection at this area in 66%. Other locations of injuries were the ascending aorta (14%), the distal descending aorta (12%), and the abdominal aorta (9%). In patients who reach the hospital alive, the injury site is the aortic isthmus in over 85% [80].

The majority of aortic injuries are transverse intimal tears with or without involvement of the medial layer. Occasionally, spiral, longitudinal, and ragged ruptures occur. The classic appearance of the ruptured isthmus on contrast-enhanced CT or angiography is the characteristic sleeve of subadventitial contrast medium (Fig. 8). In disruption of the intimal and medial layer pseudoaneurysms are frequently seen on CTA (Fig. 9). Parmely and associates [61] classified aortic lesions into six groups: (a) intimal hemorrhage; (b) intimal hemorrhage with laceration; (c) medial laceration; (d) complete laceration of the aorta; (e) false aneurysm formation; and (f) periaortic hemorrhage.

The feature of an aortic dissection after blunt trauma is seen infrequently, and has been reported only sporadically [81, 82]; however, a factor that has to be considered in relation to traumatic dissection is the concomitance of an underlying natural disease.

Because patients with traumatic injuries of the thoracic aorta have high in-hospital mortality rates due to rupture

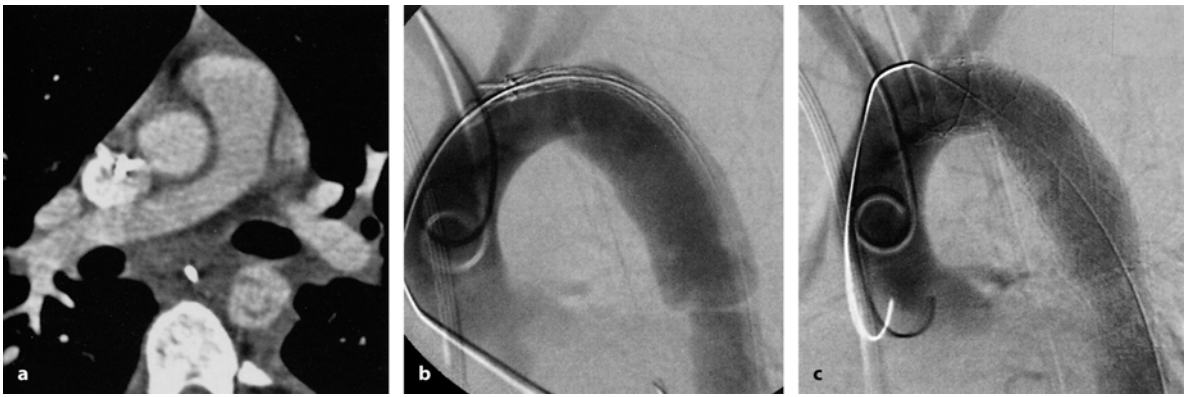


**Fig. 8.** Incomplete rupture of the aortic isthmus after frontal collision. **a** Ruptured isthmus on contrast CT features a sleeve of dissect-

ed intima and media. **b** Angiogram shows dilated aorta after partially ruptured aorta at the isthmus. **c** After stent-graft implantation



**Fig. 9.** Incomplete rupture of the aortic isthmus after broadside collision. **a** A CT scan demonstrates partial rupture of the aortic wall at the lesser curvature with a pseudoaneurysm. **b** Angiogram

shows acute pseudoaneurysm at lesser curvature. **c** After stent-graft implantation. **d** A CT follow-up 1 week after stent-graft implantation

[65], urgent treatment of blunt thoracic injuries is warranted; however, in patients who present with associated life-threatening injuries, and who have stable conditions regarding the aortic injury, a delayed repair of the thoracic aorta may be considered. Fabian et al. [78] have shown that concomitant medical management with anti-hypertensive therapy decreased the risk for rupture. Close imaging follow-up of these patients is mandatory, and aortic repair is indispensable if sign of deterioration occur.

The traditional therapy for blunt thoracic injury is conventional surgical repair. Despite advances in surgical techniques and critical care medicine, the operative mortality remains 12–32% [65, 66, 83, 84]. Besides perioperative complications, such as bleeding, respiratory failure, renal failure, myocardial infarction, and stroke, paraplegia remains the most catastrophic adverse event after surgery. Despite different surgical techniques in surgical repair, the risk of postoperative paraplegia remains high, reportedly ranging from 4 to 19% [65, 66, 85].

Since the first endovascular application of a self-fixing synthetic prosthesis for the treatment of a traumatic thoracic aortic aneurysm by Volodos et al. [86] in 1988 this less invasive procedure became an alternative modality to open surgical repair in a selected population of patients. Although the numbers of patients reported in literature is still small, paraplegia was not described [87–92]. In these articles, the postoperative deaths reported were related to comorbid injuries and were not associated with the stent-graft. The single graft-related death reported by Lachat et al. [87] occurred secondary to hemorrhage from a proximal endoleak. This reflects one of the potential complications after stent-graft repair which is caused by incomplete sealing at the attachment sites [88, 89]. Despite the technical success rate of 100% in almost all series, the main anatomical challenge is the relatively small aortic diameter in young victims. Analysis by Borsa et al. [93] yielded a mean aortic diameter of 19.3 mm adjacent to the injured aortic segment in 50 patients. Currently available stent-grafts have a diameter of at least 24 mm, which might lead to an inappropriate oversize of the device resulting in incomplete expansion or collapse [94]. Regardless of anatomical limitations, stent-graft repair is shown to have remarkably better outcomes compared with surgery. There are a few studies comparing treatment outcome between open and endovascular repair of blunt aortic injuries [84, 95]. Rousseau et al. [84] reported their experience in 70 patients over a 22-year period. In 28 patients who were treated urgently, the mortality and paraplegia rates were 21 and 7%, respectively, whereas none of the patients treated with stent-graft repair died or had paraplegia. Although all available studies show promising results after endovascular repair of blunt aortic injuries, there is a significant gap in reported data pertaining to long-term outcomes of stent-graft repair and necessity of subsequent revisions in the younger patient population.

### 2.9.4.2 Thoracic Aortic Dissection

In patients at risk for arterial dissection, a minor trauma can initiate the disease process. Hypertension is the most common factor predisposing the aorta to dissection. Further causalities, such as inherited connective tissue disorders (i.e., Marfan's syndrome, Ehler-Danlos syndrome and annuloaortic ectasia and familial aortic dissection), degenerative, atherosclerotic, inflammatory or toxic processes, as well as traumatic events, may precede an aortic dissection. Another stated risk factor is pregnancy [96, 97], and approximately 50% of women under 40 years old who suffer from aortic dissection are pregnant.

Arteriosclerosis followed by cystic medial necrosis is the main risk factor for dissection of the aging aorta. Thickening and fibrosis of the intimal layer and adventitial fibrosis with obstruction of the vasa vasorum may lead to compromised nutrition of the medial layer, which causes medial smooth muscle cell necrosis. Chronic hypertensive injury to the stiffened aortic wall may ultimately lead to aneurysms and dissection. In a post-mortem study, aortic rupture was found in 0.9% as the cause for sudden death. In 62% an aortic dissection was present, in 37% an aneurysm was present, and 1.5% demonstrated a false aneurysm [98]. Iatrogenic injuries that may result in aortic dissection are cardiopulmonary resuscitation, aortic surgery, and endovascular interventions.

Two classifications of aortic dissection refer to the extent of the dissection and the usual site of the tear:

1. Stanford classification. (a) Type A: dissection of the ascending aorta with or without involvement of the descending aorta. (b) Type B: dissection of the descending aorta (Fig. 10).
2. DeBakey classification. (a) Type 1: dissection of the entire aorta; (b) Type 2: dissection of the ascending aorta; and (c) Type 3: dissection of the descending aorta.

A new classification, as proposed by the Task Force on aortic dissection, encompasses a subdivision of radiological and pathological variants of aortic dissection [99]:

1. Class 1: classical aortic dissection with an intimal flap between the true and false lumen
2. Class 2: medial disruption with formation of intramural hematoma/hemorrhage
3. Class 3: discrete/subtle dissection without hematoma, eccentric bulge at tear site
4. Class 4: plaque rupture leading to aortic ulceration, penetrating aortic atherosclerotic ulcer with surrounding hematoma, usually adventitial
5. Class 5: iatrogenic and traumatic dissection



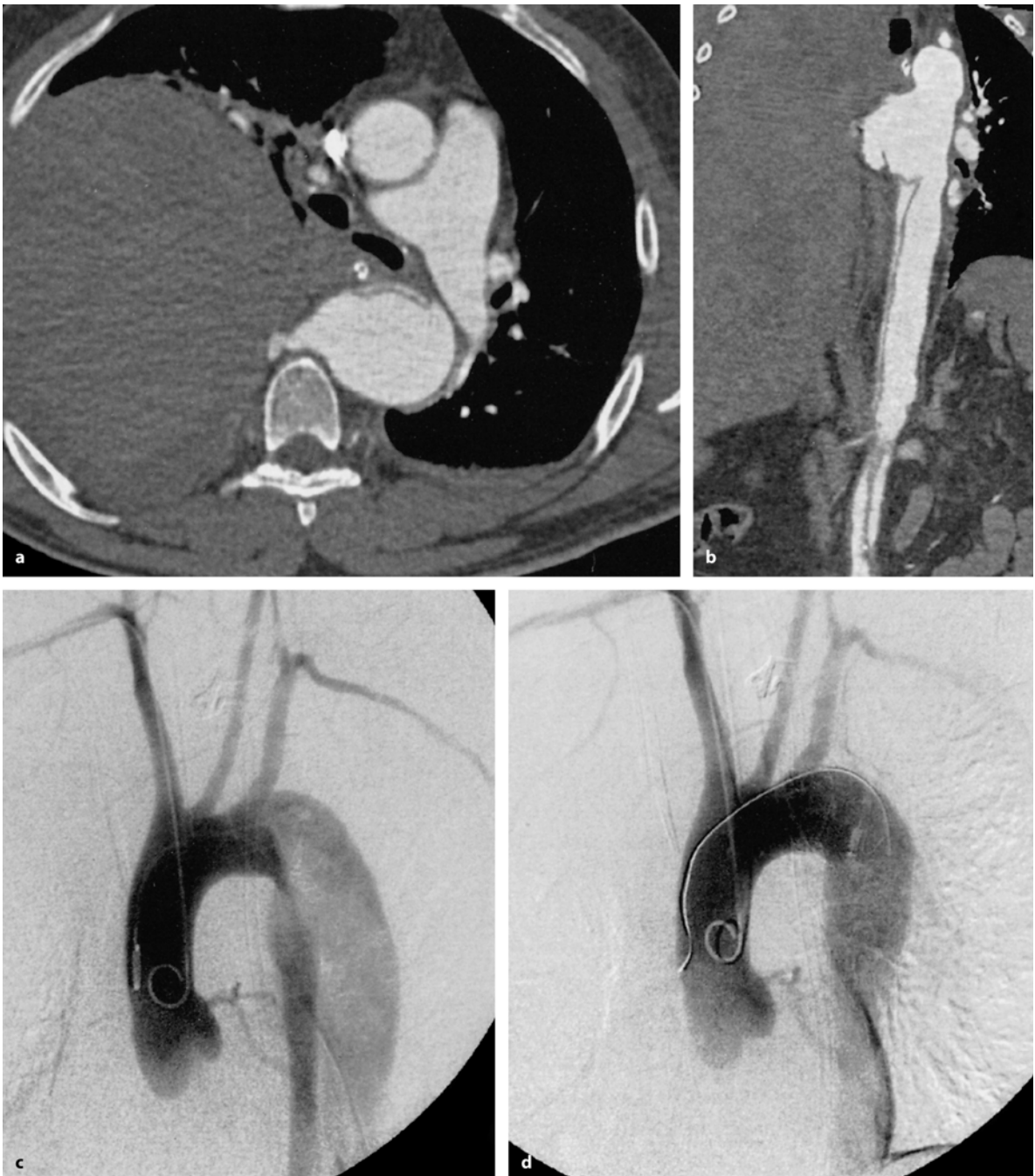


**Fig. 10.** Posttraumatic dissection Stanford type B with perforation into the right pleural space. **a** The CT scan shows small true and large false lumen, the perforation site, and right-sided hemotho-

rax. **b** Multiplanar reconstruction with false lumen perforation. **c** Angiogram shows proximal entry tear close to the left subclavian artery. **d** Closure of the entry tear after stent-graft implantation



### Clinical Course

Aortic dissection has a high mortality rate in the acute stage. The mortality rate within the first 48 h was reportedly 50–68% or 1–1.4% per hour [98, 100–103]. The most common cause of death is aortic rupture (80%). The spontaneous course of intramural hematoma is malignant as well. The development of class-1 dissection is found in up to 40%, rupture in up to 26%, and death in 20–80% [104–111]. Medical and surgical therapy reduced the 1-year mortality rate in Stanford type-A dissections to 48–68% and to 15–30% in Stanford type-B dissections [103].

There are a characteristic set of symptoms that a patient may experience with aortic dissection. The most common clinical feature is sudden onset of severe chest or back pain that is stabbing or tearing. If coronary arteries are involved, myocardial ischemia may blur the clinical symptoms. Acute aortic valve incompetence accompanies type-A aortic dissections in up to 50% of patients. Hemiplegia can result from carotid artery involvement, and paraplegia from a compromised Adamkiewicz artery. A highly compressed true lumen or extension of the intimal flap into branch vessels may result in malperfusion of the visceral and renal arteries, and can cause acute limb ischemia.

Pain management with morphine derivatives, anti-hypertensive therapy, and imaging of the aorta are the first steps once the patient arrives in the emergency room.

Imaging must provide the following information:

1. Confirmation of the diagnosis
2. Localization of the primary tear
3. Distal extension of the dissection
4. Classification of the aortic dissection
5. Side branch involvement with organ malperfusion

### Criteria for Treatment Priority

Any dissection involving the ascending aorta is an indication for acute surgery. Information is needed as to whether aortic regurgitation and coronary artery involvement is also present. In dissections involving the descending aorta, information is needed about branch vessel involvement and organ malperfusion. Static narrowing occurs when the line of dissection intersects the branch vessel origin and the false lumen hematoma is propagating into the vessel wall with narrowing of the true lumen. In dynamic obstruction, the dissection flap spares the side branch vessel but collapses across the branch vessel origin occluding the lumen (Fig. 11) [112, 113].

Transthoracic echocardiography (TTE) has a sensitivity of 77–80% and transesophageal echocardiography (TEE) 89–99% for detecting a type-A dissection. Pericardial effusion and aortic regurgitation can be assessed accurately. The distal part of the ascending aorta and the anterior portion of the aortic arch are the “blind spots” of both imaging modalities [114–119]. Furthermore, TEE has a limited field of view with inability to visualize the distal extension below the celiac trunk.

Contrast-enhanced spiral CT has a sensitivity of 90–95% [117, 118]. Cross-sectional images, MIP, MPR, and CPR should be performed to enable a complete diagnosis. Side branch involvement, even of the coronary arteries, can be demonstrated with high accuracy. Limitations are the inability to diagnose aortic regurgitation and to localize the primary tear. Motion artifacts of the ascending aorta may mimic a dissection in a single slice.

The CT criteria for the true lumen are as follows:

1. Occasionally surrounded by intimal calcifications

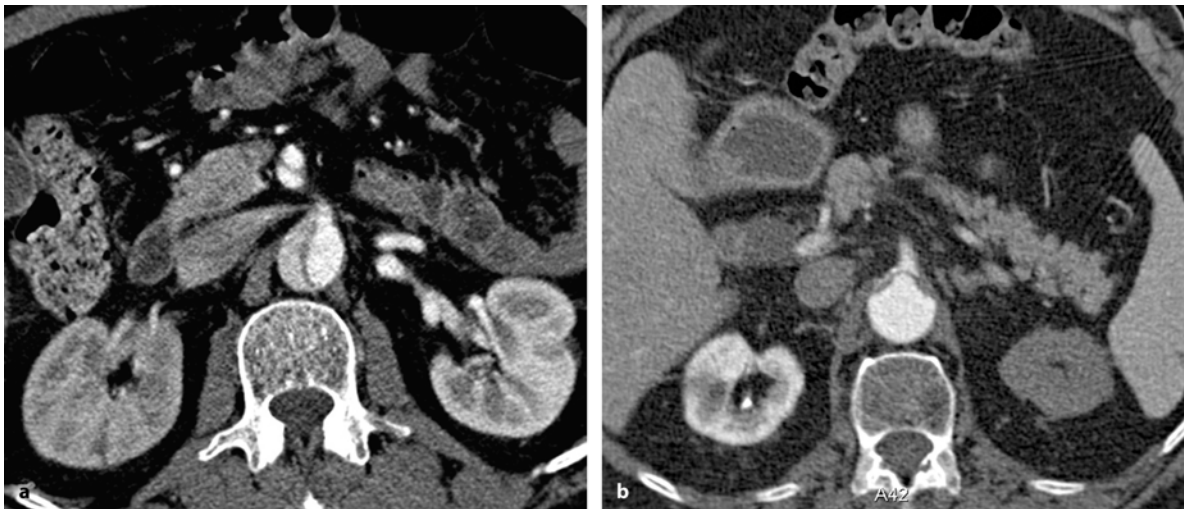


**Fig. 11.** **a** Static narrowing of the superior mesenteric artery (SMA) with intersection of the vessel origin by the intimal flap. **b** Dynamic narrowing of the SMA and occlusion of left renal

artery with malperfusion of the kidney by collapse of the intimal flap across vessels origin

2. Early contrast filling
3. Origin of most side branches
4. Anterior localization in the abdominal aorta
5. Compression by the false lumen

Magnetic resonance imaging has a >90% sensitivity for diagnosis of aortic dissection for all segments of the aorta, including side branches [115, 117, 119–122]. Single breath-hold acquisition using 3D fast low-angle shot (FLASH) gradient-echo sequences with gadolinium enhancement (0.3 mmol/kg b.w., 1.5 cc/s) are used. Cross-sectional images and MIP should be performed to enable a complete diagnosis. Side branch involvement, even of the coronary arteries, can be demonstrated with high accuracy if fat saturation is applied.

Aortography has a sensitivity of only 77–88%, because class-2 and class-3 dissections may be overlooked [123]. Aortography is used only for detailed imaging before endovascular treatment. Rapid acquisition mode (>12 frames/s) with a 45–50 cc contrast medium bolus (300 mg J/ml) with a flow rate of 20–25 cc/s are required and are useful in localizing the entry tear in type-B dissections.

### Therapy

In acute type-A dissections, the standard approach is surgery under deep hypothermic circulatory arrest with extracorporeal circulation and replacement of the ascending aorta by a tube graft or by a composite graft if the aortic valve is involved [103, 124].

In acute type-B dissection treatment the decision is based on dissection complexity. Complicated type-B dissections require surgical [125] or endovascular therapy. Uncomplicated type-B dissections are treated medically by antihypertensive therapy and close monitoring.

### Complicated Type-B Dissection

Complicated type-B dissection consists of the following:

1. Visceral, renal, and limb ischemia
2. Peri-aortic or mediastinal hematoma
3. Hemorrhagic pleural effusion
4. Dissection in an aneurysmal aorta
5. Rapidly expanding aortic (false lumen) diameter
6. Refractory pain
7. Malignant hypertension

In interventional therapy, the primary aim is occlusion of the entry tear with subsequent decompression, collapse, and thrombosis of the false lumen and true lumen expansion [126–135]. This can be achieved by transfemoral insertion of a tubular stent-graft (Fig. 12). Single-shot antibiotic prophylaxis is administered prior to the procedure, and 5000 IU of heparin are given intravenously in non-ruptured dissections. Under general or spinal anesthesia, the common femoral or iliac artery is surgically exposed for the access site. An angiogram is obtained using a pigtail catheter to demonstrate the proximal entry tear and to determine the optimal stent-graft landing zones; thereafter, for insertion of the device, the pigtail catheter is replaced

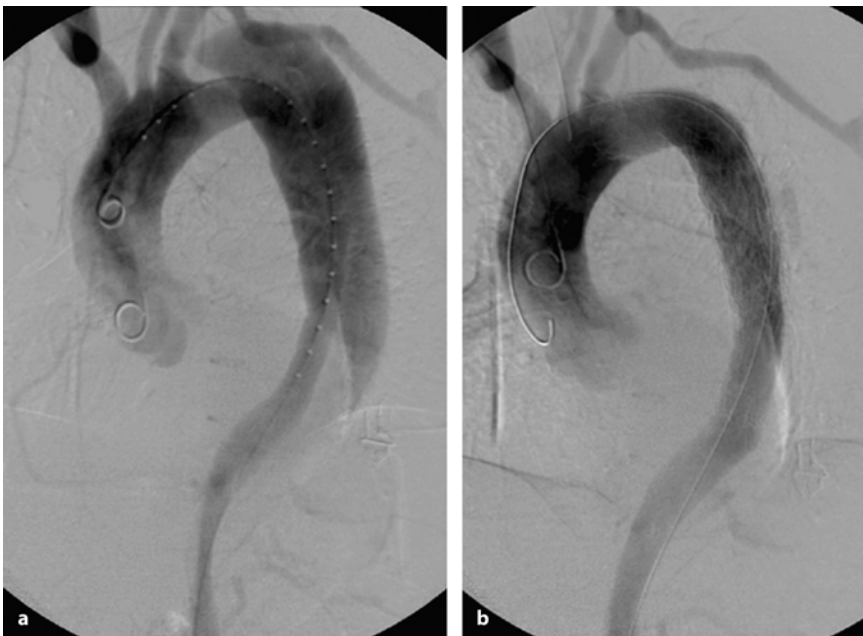


**Fig. 12.** Acute aortic type-B dissection. **a** Angiogram demonstrates the proximal entry tear and compression of the true lumen. **b** Closure of the entry tear and true lumen expansion after stent-graft implantation

by an extra-stiff guide wire. The diameter of the stent-graft is chosen between the diameter of the true lumen and the total aortic diameter. In an left anterior 60° oblique view, the stent-graft is deployed in such a position that it overlaps the entry tear by approximately 2 cm. Overstenting of the left subclavian artery may be required. The stent-graft should cover the proximal part of the descending aorta to facilitate false lumen collapse and thrombosis; however, the distal part of the descending aorta should remain uncovered to ensure perfusion of the anterior spinal artery (Adamkiewicz).

Primary closure of the entry tear after stent-grafting was reported in 89–100% [126–136], and false lumen thrombosis of the descending aorta is reported in 70–100% of cases [127, 128, 130, 136]. Dake and associates concluded that restoration of blood flow was sufficient after stent-graft repair in all compromised branch vessels exclusively by a dynamic process. In vessels affected additionally by a static component, deployment of an uncovered stent within the true lumen of the obstructed artery was necessary in 60%. [128].

Fenestration of the dissection membrane between the true and false lumens is indicated if branch vessel perfusion is compromised by a hypertensive false lumen [137]. For fenestration, an intravascular ultrasound (IVUS) catheter is placed in the false lumen, which generally tends to have the larger diameter. For puncture of the dissection flap a curved, hollow metal needle (i.e., transjugular liver access set) is used. Under IVUS control, the false lumen is punctured usually in the infrarenal aorta, and over a stiff guide wire, the membrane is fenestrated with a balloon of at least 15 mm in diameter. If equalization of pressure and satisfactory perfusion of branch vessels is not achieved, fenestrations at several levels may be required.

---

## 2.9.5 Abdominal Aorta

### 2.9.5.1 Blunt Abdominal Aortic Injuries

Injury of the abdominal aorta by blunt trauma is unusual. In an autopsy series by Parmley et al. [61], 400 patients presented with aortic injuries of which 4% were located in the abdominal aorta; however, in patients who are admitted in the emergency room, 0.05–15% of all aortic injuries were abdominal traumas [138, 139]. Blunt forces can result in minor intimal tears only, an intramural hematoma, an aortic dissection with peripheral ischemia or paraplegia, and in pseudoaneurysms and complete disruption. The most frequent site of injury is found to be located distal to the inferior mesenteric artery and is frequently caused by seat belts [140, 141]. In blunt abdominal injury, associated visceral lesions were found in 42% of patients [142]. In these patients there exists a risk for operative contamination. Because of the less invasive approach, endovascu-

lar techniques are an alternative to surgery in stable patients who have an appropriate anatomical condition. In instances of retroperitoneal bleeding, pseudoaneurysms, or aortocaval fistulas, implantation of stent-grafts led to satisfactory results in a few reported cases [141, 142]. In dissections, implantation of bare stents has been shown to be successful with thrombosis of the false lumen [143–146].

---

### 2.9.5.2 Stent-Graft Designs

Stent-grafts have a self-expandable stent structure covered by an ultra-thin polyester or expanded polytetrafluoroethylene (ePTFE) fabric. Commercially available devices are either an aorto-monoiliac device, or a bifurcated device with the majority having a modular design. Some designs have an uncovered stent structure at the proximal end for suprarenal fixation, which may be advantageous in patients with short infrarenal necks.

---

### 2.9.5.3 Imaging and Stent-Graft Implantation

Contrast-enhanced CTA with reconstructions (MPR, CPR, MIP) is the most important examination before stent-graft implantation. Alternatively, MRA is a valuable examination method for patients with renal insufficiency. In selected cases angiography with a marker catheter is performed for accurate length measurements. Identification of the following anatomical characteristics are critical for successful stent-graft implantation:

1. Infrarenal anchoring zone: length; configuration; diameter; irregularity by thrombus or calcification; and angulation
2. Angulation or stenosis of the aorto-iliac junction
3. Iliac arteries: ectasia; tortuosity; stenosis; occlusion; and aneurismal dilatation
4. Aortic branch vessels: stenosis or occlusion of visceral arteries and aberrant renal arteries
5. Internal iliac artery: aneurysm

Depending on the stent-graft design, unilateral or bilateral surgical exposure of the femoral or iliac artery is required for the access site. In the use of a bifurcated stent-graft, the main body is advanced under fluoroscopic control over an extra-stiff guide wire. An angiogram is performed to demonstrate the renal arteries. Deployment of the trunk should be as close as possible to the renal arteries. Suprarenal fixation of the uncovered part of stent-grafts usually does not cause renal artery thrombosis or embolization. Modeling of the stent-graft with the use of a Latex balloon within the infrarenal neck and the iliac artery landing zone may be necessary for proper sealing between the aorta and the stent-graft. A crucial part of the procedure is the correct placement of the contralateral iliac stent-graft segment. Cannulation of the contralateral stub leg can be per-

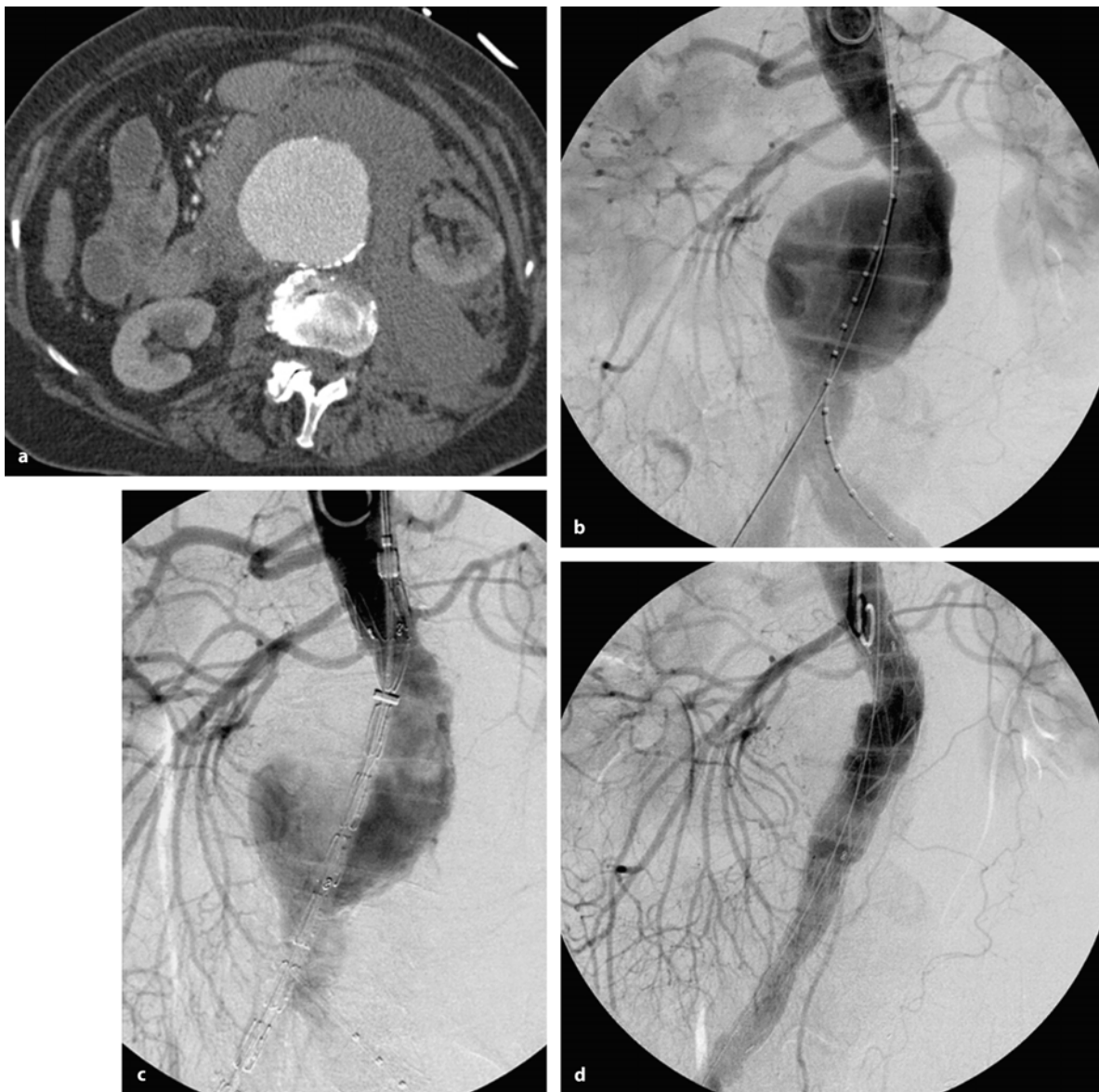


**Fig. 13.** Ruptured infrarenal aortic aneurysm. **a** Diagnostic CT shows a huge retroperitoneal hematoma with dislodgement of the left kidney. **b** Angiogram before endovascular repair. **c** Partially de-

ployed aorto-uni-iliac prosthesis. **d** Successful exclusion of the aneurysm after stent-graft implantation

formed by direct retrograde access with an angled catheter. Another option is a crossover technique with a Simmons 1 Sidewinder catheter, and a soft curved glide wire, which is snared in the iliac artery and pulled out; thereafter, a pig-tail-catheter is advanced over the guide wire into the aortic segment. After insertion of an extra stiff guide wire, the stent-graft limb is positioned within the stub leg. After modeling of the iliac limb, a control angiogram is performed to demonstrate endoleak-free exclusion of the aortic lesion and to confirm patency of renal arteries.

In an emergency situation, placement of a bifurcated stent-graft is feasible only if the patient is hemodynamical-

ly stable. In unstable patients, the ruptured aneurysm can be excluded much quicker with an aorto-mono-iliac stent-graft (Fig. 13). Once the aneurysm is excluded and the patient is stabilized, a cross-over bypass must be implanted for contralateral limb perfusion.

Experiences of endovascular stent-graft repair in abdominal aortic bleeding in the trauma setting are limited. There are a few authors reporting their experience with treatment of ruptured aortoiliac aneurysms [147–149]. Ohki and Veith [147] managed 80% of ruptured aneurysms by implantation of aorto-unifemoral PTFE grafts. Additionally, balloon occlusion of the suprarenal



aorta was performed via transbrachial access in hemodynamically unstable patients. Operative mortality in ruptured abdominal aortic aneurysms is still high with an estimated value of 41% for the year 2000 [150]. For endovascular repair, 30-day mortality rates are reported to be from 10 to 14% [147–149].

## 2.9.6 Abdominal Aortic Branches

Traumatic laceration of the hepatic, splenic, mesenteric, and renal arteries is rare. Patients usually suffer from blunt trauma due to traffic accidents. The typical trauma is a deceleration injury with an intimal rupture in the artery 1–2 cm from the aorta. Partial traumatic transection or dissection of branch vessels may sometimes heal spontaneously; however, thrombus formation on the intimal flap may lead to arterial thrombosis. Complete occlusion of the artery may also be caused by an avulsion of the arterial pedicle. Upper abdominal pain, shock in the event of bleeding, and elevated LDH in the event of thrombosis are symptoms of hepatic and splenic artery laceration. Flank pain and hematuria are the leading symptoms of renal pedicle laceration. Contrast CT will demonstrate an unenhanced organ, which may be homogeneous or segmental, irregularities of the artery, and a periarterial hematoma. Catheter angiography is necessary to show the details of the pathology and may lead to interventional treatment such as stenting in case of dissection, recanalization with or without fibrinolysis, and stent-graft placement in case of a deep vessel injury.

Abdominal organ artery aneurysms are most commonly seen at the splenic artery. Hepatic, mesenteric, and renal artery aneurysms are rare [151, 152]. The causes include arteriosclerosis, mycotic aneurysms due to perivascular inflammation (i.e., pancreatitis), systemic vasculitis, such as polyarteritis nodosa or systemic lupus erythematosus (SLE), fibromuscular dysplasia (FMD), soft tissue disorders (i.e., Marfan's syndrome), and traumatic pseudoaneurysms. Arteriosclerotic and large aneurysms are usually calcified. Inflammatory aneurysms have the highest tendency to rupture. The risk of rupture and chronic embolization are the indications for treatment. Bypass surgery, coil embolization, and stent-graft implantation are the therapeutic options [153].

## 2.9.7 Conclusion

The broad variety of non-invasive vascular imaging modalities enables an accurate diagnosis of patients with an acute vascular problem. Contrast-enhanced spiral CT is the most reliable modality for imaging of large vessel emergencies. Angiography may be necessary for detailed

information and before intervention. Embolization and stent-grafts are used to close large vascular lacerations, ruptured aortic aneurysms, and the entry tear of dissections. Interventional radiology methods play a major role in managing vascular emergencies.

## References

- Gavatt ML, Menke PG, Fabian T, Flick PA, Graney MJ, Gold RE. Blunt traumatic aortic rupture: detection with helical CT of the chest. *Radiology* 1995;197:125–133
- Alkadh H, Wildermuth S, Desbiolles L, Schertler T, Crook D, Marinck B, Boehm T. Vascular emergencies of the thorax after blunt and iatrogenic trauma: multidetector row CT and three-dimensional imaging. *Radiographics* 2004;24:1239–1255
- Sheridan MK, Blackmore CC, Linnau KF, Hoffer EK, Lomoschitz F, Jurkovich GJ. Can CT predict the source of arterial hemorrhage in patients with pelvic fractures? *Emerg Radiol* 2002;9:188–194
- Yoon W, Kim JK, Jeong YY, Seo JJ, Park JG, Kang HK. Pelvic arterial hemorrhage in patients with pelvic fractures: detection with contrast-enhanced CT. *Radiographics* 2004;24:1591–1606
- Miller-Thomas MM, West OC, Cohen AM. Diagnosing traumatic arterial injury in the extremities with CT angiography: pearls and pitfalls. *Radiographics* 2005;25 (Suppl 1):S133–S142
- Saletta JD, Lowe RJ, Lim LT, Delk S et al. Penetrating trauma of the neck. *J Trauma* 1976;16:579–587
- Hoff SJ, Reilly MK, Merrill WH, Stewart J, Frist WH, Morris JA Jr. Analysis of blunt and penetrating injury of the innominate and subclavian arteries. *Am Surg* 1994;60:151–154
- Hyre CE, Cikrit DF, Lalka SG, Sawchuk AP, Dalsing MC. Aggressive management of vascular injuries of the thoracic outlet. *J Vasc Surg* 1998;27:880–885
- Symbas JD, Halkos ME, Symbas PN. Rupture of the innominate artery from blunt trauma: current options for management. *J Cardiac Surg* 2005;20:455–459
- Hirose H, Moore E. Delayed presentation of rupture of a post-traumatic innominate artery aneurysm. A case report and review of the literature. *J Trauma* 1997;42:1187–1195
- Ahrar K, Smith DC, Bansal RC, Razzouk A, Catalano RD. Angiography in blunt thoracic aortic injury. *J Trauma* 1997;42:665–669
- Sommer A, Meairs S, Gueckel F, Cornelius A, Schwartz A. Traumatic brachiocephalic pseudoaneurysm presenting with delayed stroke: a case report. *Neuroradiology* 2000;42:742–745
- Aksoy M, Tunca F, Yanar H, Guloglu R, Ertekin C, Kurtoglu M. Traumatic injuries to the subclavian and axillary arteries: a 13-year review. *Surg Today* 2005;35:561–565
- Staller B, Mùnera F, Sanchez A, Nuñez DB Jr. Helical and multi-slice CTA following penetrating trauma to the subclavian and axillary arteries. *Emerg Radiol* 2005;11:336–341
- Chen MYM, Miller PR, McLaughlin CA, Kortesis BG, Kavanagh PV, Dyer RB. The trend of using computed tomography in the detection of acute thoracic aortic and branch vessel injury after blunt thoracic trauma: Single-center experience over 13 years. *J Trauma* 2004;56:783–785
- du Toit DF, Strauss DC, Blaszczyk M, de Villiers R, Warren BL. Endovascular treatment of penetrating thoracic outlet arterial injuries. *Eur J Vasc Endovasc Surg* 2000;19:489–495
- Patel AV, Veith FJ, Kerr A, Sanchez LA. Endovascular graft repair of penetrating subclavian artery injuries. *J Endovasc Surg* 1996;3:382–388
- Hilfiker PR, Razavi MK, Kee ST, Sze DY, Semba CP, Dake MD. Stent-graft therapy for subclavian artery aneurysms and fistulas: Single-center mid-term results. *J Vasc Interv Radiol* 2000;11:578–584

19. Nicholson T, Ettles D, Robinson G. Managing inadvertent arterial catheterization during central venous access procedures. *Cardiovasc Intervent Radiol* 2004;27:21–25
20. Asensio JA, Valenziano CP, Falcone RE, Grosh JD. Management of penetrating neck injuries: the controversy surrounding zone II injuries. *Surg Clin North Am* 1991;71:267–296
21. Davis JW, Holbrook TL, Hoyt DB, Mackersie RC, Field TO Jr, Shackford SR. Blunt carotid artery dissection: incidence, associated injuries, screening and treatment. *J Trauma* 1990;30:1514–1517
22. Biffi WL, Moore EE, Ryu RK et al. The unrecognized epidemic of blunt carotid arterial injuries: early diagnosis improves neurologic outcome. *Ann Surg* 1998;228:462–470
23. Miller PR, Fabian TC, Croce MA, Cagianos C, Williams JS et al. Prospective screening for blunt cerebrovascular injuries. Analysis of diagnostic modalities and outcomes. *Ann Surg* 2002;236:386–395
24. Biffi WL, Moore EE, Elliot JP et al. The devastating potential of blunt vertebral injuries. *Ann Surg* 2000;23:672–681
25. Willis BK, Greiner F, Orrison WW et al. The incidence of vertebral artery injury after midcervical spine fracture or subluxation. *Neurosurgery* 1994;34:435–441
26. Benninger DH, Georgiadis D, Gandjour J, Baumgartner RW. Accuracy of color duplex ultrasound diagnosis of spontaneous carotid dissection causing ischemia. *Stroke* 2006;37:377–381
27. Lanczik O, Szabo K, Hennerici M, Gass A. Multiparametric MRI and ultrasound findings in patients with internal carotid artery dissection. *Neurology* 2005;65:469–471
28. Tay KY, U-King-Im JM, Trivedi RA et al. Imaging the vertebral artery. *Eur Radiol* 2005;15:1329–1343
29. Biffi WL, Ray CE, Moore EE, Mestek M, Johnson JL, Burch JM. Noninvasive diagnosis of blunt cerebrovascular injuries: a preliminary report. *J Trauma* 2002;53:850–856
30. Biffi WL, Moore EE, Offner PJ, Brega KE, Franciose RJ, Burch JM. Blunt carotid arterial injuries: implications of a new grading scale. *J Trauma* 1999;47:845–853
31. Biffi WL, Ray CE, Moore EE et al. Treatment related outcomes from blunt cerebrovascular injuries. *Ann Surg* 2002;235:699–707
32. Fabian TC, Patton JH Jr, Croce MA et al. Blunt carotid injury: importance of early diagnosis and anticoagulant therapy. *Ann Surg* 1996;223:513–525
33. Cothren CC, Moore EE, Biffi WH et al. Anticoagulation is the gold standard therapy for blunt carotid injuries to reduce stroke rate. *Arch Surg* 2004;139:540–545
34. Duke BJ, Ryu RK, Coldwell DM, Brega KE. Treatment of blunt injury to the carotid artery by using endovascular stents: an early experience. *J Neurosurg* 1997;87:825–829
35. Cohen JE, Leker RR, Gotkine M, Gomori M, Ben-Hur T. Emergent stenting to treat patients with carotid artery dissection. *Stroke* 2003;34:e254–e257
36. Fangio P, Asehnoune K, Edouard A, Smail N, Benhamou D. Early embolization and vasopressor administration for management of life-threatening hemorrhage from pelvic fracture. *J Trauma* 2005;58:978–984
37. Wong YC, Wang LJ, Ng CJ, Tseng IC, See LC. Mortality after successful transcatheter arterial embolization in patients with unstable pelvic fractures: rate of blood transfusion as a predictive factor. *J Trauma* 2000;49:71–75
38. Velmahos GC, Toutouzas KG, Vassiliu P et al. A prospective study on the safety and efficacy of angiographic embolization for pelvic and visceral injuries. *J Trauma* 2005;52:303–308
39. Gourlay D, Hoffer E, Routt M, Bulger E. Pelvic angiography for recurrent traumatic pelvic arterial hemorrhage. *J Trauma* 2005;1168–1174
40. Carrillo EH, Wohltmann CD, Spain DA, Schmiege RE Jr, Miller FB, Richardson JD. Common and external iliac artery injuries associated with pelvic fractures. *J Orthop Trauma* 1999;13:351–355
41. Sternbergh WC III, Conners III MS, Ojeda MA, Money SA. Acute bilateral iliac artery occlusion secondary to blunt trauma: successful endovascular treatment. *J Vasc Surg* 2003;38:589–592
42. Shah SH, Ledgerwood AM, Lucas CE. Successful endovascular stenting for common iliac artery injury associated with pelvic fracture. *J Trauma* 2003;55:383–385
43. Starr AJ, Hunt JL, Reinert CM. Treatment of femoral fracture with associated vascular injury. *J Trauma* 1996;40:17–21
44. Stannard JP, Sheils TM, Lopez-Ben RR, McGwin G Jr, Robinson JT, Volgas DA. Vascular injuries in knee dislocations: the role of physical examination in determining the need for arteriography. *J Bone Joint Surg Am* 2004;86:910–915
45. Hafez HM, Woolgar J, Robbs JV. Lower extremity arterial injury: results of 550 cases and review of risk factors associated with limb loss. *J Vasc Surg* 2001;33:1212–1219
46. Lynch K, Johansen K. Can Doppler pressure measurement replace “exclusion” arteriography in the diagnosis of occult extremity arterial trauma? *Ann Surg* 1991;214:737–741
47. Ordog GJ, Balasubramaniam S, Wasserberger J et al. Extremity gunshot wounds. Part one. Identification and treatment of patients at high risk of vascular injury. *J Trauma* 1994;36:358–368
48. Bynoe RP, Miles WS, Bell RM. Noninvasive diagnosis of vascular trauma by duplex ultrasonography. *J Vasc Surg* 1991;14:346–352
49. Busquets AR, Acosta JA, Colon E, Alejandro KV, Rodriguez P. Helical computed tomographic angiography for the diagnosis of traumatic arterial injuries of the extremities. *J Trauma* 2004;56:625–628
50. Dickerman R, Gewertz B, Foley D, Fry W. Selective intraarterial tolazoline infusion in peripheral arterial trauma. *Surgery* 1977;81:605–609
51. Aksoy M, Taviloglu K, Yanar H, et al. Percutaneous transcatheter embolization in arterial injuries of the lower limbs. *Acta Radiol* 2005;5:471–475
52. Werner GS, Ferrari M, Figulla HR. Superficial artery rupture after balloon angioplasty: treatment with implantation of a balloon-expandable endovascular graft. *J Vasc Interv Radiol* 1999;10:1115–1117
53. Risberg B, Lonn L. Management of vascular injuries using endovascular techniques. *Eur J Surg* 2000;166:196–201
54. Thalhammer C, Kirchherr AS, Uhlich F, Waigand J, Gross CM. Postcatheterization pseudoaneurysms and arteriovenous fistulas: repair with percutaneous implantation of endovascular covered stents. *Radiology* 2000;214:127–131
55. Önal B, Ilgit ET, Koşar Ş, Akkan K, Gümüş T, Akpek S. Endovascular treatment of peripheral vascular lesions with stent-grafts. *Diagn Intervent Radiol* 2005;11:170–174
56. Katzenschlager R, Ugurluoglu A, Achmadi A et al. Incidence of pseudoaneurysm after diagnostic and therapeutic angiography. *Radiology* 1995;195:463–466
57. Ugurluoglu A, Katzenschlager R, Achmadi A et al. Ultrasound guided compression therapy of iatrogenic pseudoaneurysms: advantage of routine duplex ultrasound control of the puncture site following transfemoral catheterization. *Vasa* 1997;26:110–116
58. Paulson EK, Sheafor DH, Kliwer MA, Nelson RC, Eisenberg LB, Sebastian MW, Sketch MH Jr. Treatment of iatrogenic femoral arterial pseudoaneurysms: comparison of US-guided thrombin injection with compression repair. *Radiology* 2000;215:403–408
59. Owen RJ, Haslam PJ, Elliott ST, Rose JD, Loose HW. Percutaneous ablation of peripheral pseudoaneurysms using thrombin: a simple and effective solution. *Cardiovasc Intervent Radiol* 2000;23:441–446
60. Groskin SA. Selected topics in chest trauma. *Semin Ultrasound CT MR* 1996;17:119–141
61. Parmley LF, Mattingly TW, Manion WC, Jahnke EH. Nonpenetrating traumatic injury of the aorta. *Circulation* 1958;17:1086–1101
62. Smith RS, Chang FC. Traumatic rupture of the aorta: still a lethal injury. *Am J Surg* 1986;15:660–663
63. Williams JS, Graff JA, Uku JM, Steinig JP. Aortic injury in vehicular trauma. *Ann Thorac Surg* 1994;57:726–730

64. Gammie JS, Shah AS, Hattler BG et al. Traumatic aortic rupture: diagnosis and management. *Ann Thorac Surg* 1998;66:1295–1300
65. OPELL UO von, Dunne TT, DeGroot MK, Zilla P. Traumatic aortic rupture: twenty-year metaanalysis of mortality and risk of paraplegia. *Ann Thorac Surg* 1994;58:585–593
66. Fabian TC, Richardson DJ, Croce MA et al. Prospective study of blunt aortic injury: multicenter trial of the American Association for the surgery of trauma. *J Trauma Injury Infect Crit Care* 1997; 42:374–383
67. Finkelmeier BA, Mentzer RM, Kaiser DL, Tegtmeyer CJ, Nolan SP. Chronic traumatic thoracic aneurysm: influence of operative treatment of natural history. *J Thorac Cardiovasc Surg* 1982;84:257–266
68. Demers P, Miller C, Mitchell RS, Kee ST, Chagonjian L, Dake MD. Chronic traumatic aneurysms of the descending thoracic aorta: mid-term results of endovascular repair using first- and second-generation stent-grafts. *Eur J Cardiothorac Surg* 2004;25:394–400
69. Richens D, Field M, Neale M, Oakley C. The mechanism of injury in blunt traumatic rupture of the aorta. *Eur J Cardiothorac Surg* 2002;21:288–293
70. Sevitt S. The mechanism of traumatic rupture of the thoracic aorta. *Br J Surg* 1977;64:166–173
71. Shkrum MJ, McClafferty KJ, Green RN, Nowak ES, Young JG. Mechanism of aortic injury in fatalities occurring in motor vehicle collisions. *J Forensic Sci* 1999;44:44–56
72. Crass JR, Cohen AM, Motta AO, Tomaszewski JF, Wiesen EJ. A proposed new mechanism of traumatic aortic rupture: the osseous pinch. *Radiology* 1990;176:645–649
73. Kroell CK, Gadd CW, Schneider DC. Biomechanics in crash injury research. *ISA Trans* 1974;13:183–198
74. Lundewall J. The mechanics of traumatic rupture of the aorta. *Acta Pathol Microbiol Scand* 1964;62:34–36
75. Moar JJ. Traumatic rupture of the thoracic aorta. An autopsy and histopathological study. *S Afr Med* 1985;67:383–385
76. Downing SW, Sperling JS, Mirvis SE et al. Experience with spiral computed tomography as the sole diagnostic method for traumatic aortic rupture. *Ann Thorac Surg* 2001;72:495–502
77. Mirvis SE, Shanmuganathan K, Buell J, Rodriguez A. Use of spiral computed tomography for the assessment of blunt trauma patients with potential aortic injury. *J Trauma* 1998;45:922–930
78. Fabian IC, Devis KA, Gavant ML et al. Prospective study of blunt aortic injury. Helical CT is diagnostic and antihypertensive therapy reduces rupture. *Ann Surg* 1998;227:666–677
79. Qanadli SD, El Hajjam M, Mesurolle B et al. (1999) Motion artefacts of the aorta simulating aortic dissection on spiral CT. *J Comput Assist Tomogr* 23:1–6
80. Tatou E, Steinmetz E, Jazayeri S, Benhamiche B, Brenot R, David M. Surgical outcome of traumatic rupture of the thoracic aorta. *Ann Thorac Surg* 2000;69:70–73
81. Bashar AH, Kazui T, Washiyama N et al. Stanford type-A aortic dissection after blunt chest trauma: case report with a reflection on the mechanism of injury. *J Trauma* 2002;52:380–381
82. Gammie J, Katz WE, Swanson ER, Peitzmann AB. Acute aortic dissection after blunt chest trauma. *J Trauma* 1996;40:126–127
83. Sweeney MS, Young TH, Frazier OH, Adams PR, Kapusta MO, Macris MP. Traumatic aortic transection: eight year experience with the clamp-sew technique. *Ann Thorac Surg* 1997;64:384–387
84. Rousseau H, Dambrin C, Marcheix B et al. Acute traumatic aortic rupture: a comparison of surgical and stent-graft repair. *J Thorac Cardiovasc Surg* 2005;129:1050–1055
85. Kodali S, Jamieson WR, Leia-Stephens M, Miyagishima RT, Janusz MT, Tyers GF. Traumatic rupture of the thoracic aorta. A 20-year review: 1969–1989. *Circulation* 1991;84:III40–III46
86. Volodos NL, Karpovich IP, Shekhanin VE, Troian VI, Iakovenko LF. A case of distant transfemoral endoprosthesis of the thoracic artery using a self-fixing synthetic prosthesis in traumatic aneurysm. *Grudn Khir* 1988;6:84–86
87. Lachat M, Pfammater T, Witzke H et al. Acute traumatic aortic rupture: early stent-graft repair. *Eur J Cardiothorac Surg* 2002;21:959–963
88. Fattori R, Napoli G, Lovato L et al. Indications for, timing of, and results of catheter-based treatment of traumatic injury of the aorta. *Am J Radiol* 2002;179:603–609
89. Orend KH, Scharrer-Pamler R, Kapfer X, Kotsis T, Görlich J, Sunder-Plassmann L. Endovascular treatment in diseases of the descending thoracic aorta: 6-year result of a single center. *J Vasc Surg* 2003;37:91–99
90. Neuhauser B, Czermak B, Jaschke W, Waldenberger P, Fraedrich G, Perkmann R. Stent-graft repair of acute traumatic thoracic aortic rupture. *Am Surg* 2004;70:1039–1044
91. Dunham MB, Zygun D, Petrasko P, Kortbeck JB, Karmy-Jones R, Moore RD. Endovascular stent-grafts for acute blunt aortic injury. *J Trauma* 2004;1173–1178
92. Peterson BG, Matsumura JS, Morasch MD, West MA, Eskandari MK. Percutaneous endovascular repair of blunt thoracic aortic transection. *J Trauma* 2005;59:1062–1065
93. Borsari JJ, Hoffer Ek, Karmy-Jones R, et al. Angiographic description of blunt traumatic injuries to the thoracic aorta with specific relevance to endograft repair. *J Endovasc Ther* 2002;9 (Suppl II):II84–II91
94. Idu MM, Reekers JA, Balm R, Ponsen KJ, de Mol BA, Legemate DA. Collapse of a stent-graft following treatment of a traumatic thoracic aortic rupture. *J Endovasc Ther* 2005;12:503–507
95. Ott MC, Stewart TC, Lawlor DK, Gray DK, Forbes TL. Management of blunt thoracic injuries: endovascular stents versus open repair. *J Trauma* 56:565–570
96. Roberts WC. Aortic dissection: anatomy, consequences and causes. *Am Heart J* 1981;101:195–214
97. Weissmann-Brenner A, Schoen R, Divon NY. Aortic dissection in pregnancy. *Obstet Gynecol* 2004;103:1110–1113
98. Young R, Ostertag H. Häufigkeit, Ätiologie und Rupturrisiko des Aortenaneurysmas. Eine Autopsiestudie. *Dtsch Med Wochenschr* 1987;112:1253–1256
99. Erbel R, Alfonso F, Boileau C et al. Diagnosis and management of aortic dissection: recommendations of the Task Force on aortic dissection, European Society of Cardiology. *Eur Heart J* 2001;22:1642–1681
100. Erbel R, Oelert H, Meyer J et al. Influence of medical and surgical therapy on aortic dissection evaluated by transesophageal echocardiography. *Circulation* 1993;87:1604–1615
101. Masuda Y, Takanashi K, Takasu J, Morooka N, Inagaki Y. Expansion rate of thoracic aortic aneurysms and influencing factors. *Chest* 1992;102:461–466
102. Kunz R. Aneurysmata bei 35.380 Autopsien. *Schweiz Med Wochenschr* 1980;110:142–148
103. DeBakey ME, McCollum CH, Crawford ES et al. Dissection and dissecting aneurysms of the aorta: twenty-year follow-up of five twenty-seven patients treated surgically. *Surgery* 1982;92:1118–1134
104. Nienaber CA, Kodolitsch Y von, Peterson B, Loose R, Helmchen A, Spielmann R. Intramural haemorrhage of the aorta: diagnostic and therapeutic implications. *Circulation* 1995;92:1465–1472
105. O’Gara PT, Sanctis RW de. Acute aortic dissection and its variants. *Circulation* 1999;92:1376–1378
106. Shimizu H, Yohino H, Udagawa H et al. Prognosis of aortic intramural haemorrhage compared with classic aortic dissection. *Am J Cardiol* 2000;85:792–795
107. Kang DH, Song JK, Lee IS et al. Clinical and echocardiographic outcomes of aortic intramural haemorrhage compared with acute aortic dissection. *Am J Cardiol* 1998;81:202–206
108. Stanson AV, Kazmier FJ, Chollier LG. Penetrating atherosclerotic ulcer of the thoracic aorta: natural history and clinicopathology correlation. *Ann Vasc Surg* 1986;1:15–23
109. Cooke JP, Kazmier FJ, Orszulak TA. The penetrating aortic ulcer: pathologic manifestations, diagnosis and treatment. *Mayo Clin Proc* 1988;63:718–725



110. Die K, Uchida H, Otsuji H et al. Acute aortic dissection with intramural haematoma: possibility of transition to classic dissection or aneurysm. *J Thorac Imaging* 1996;11:46–52
111. Coady MA, Rizzo JA, Elefteriades JA. Pathologic variants of thoracic aortic dissections. Penetrating atherosclerotic ulcers and intramural hematomas. *Cardiol Clin* 1999;17:637–657
112. Lee DY, Williams DM, Abrams GD. The dissected aorta. II. Differentiation of the true from the false lumen with intravascular US. *Radiology* 1997;203:32–36
113. Williams DM, Lee DY, Hamilton BH et al. The dissected aorta. III. Anatomy and radiology diagnosis of branch vessel compromise. *Radiology* 1997;203:37–44
114. Erbel R, Engberding R, Daniel W, Roelandt J, Visser CM, Renollet H. Echocardiography in diagnosis of aortic dissection. *Lancet* 1989;1:457–461
115. Nienaber CA, Spielmann RP, Kodolitsch Y von et al. Diagnosis of thoracic aortic dissection. Magnetic resonance imaging versus transesophageal echocardiography. *Circulation* 1992;85:434–447
116. Mohr-Kahaly S, Erbel R, Renollet H et al. Ambulatory follow-up of aortic dissection by transesophageal two-dimensional and color coded Doppler echocardiography. *Circulation* 1989;80:24–33
117. Sommer T, Fehske W, Holzknicht N et al. Aortic dissection: a comparative study of diagnosis with spiral CT, multiplanar transesophageal echocardiography and MR imaging. *Radiology* 1996;199:347–352
118. Iliceto S, Ettore G, Francisco G, Antonelli G, Biasco G, Rizzon P. Diagnosis of aneurysm of the thoracic aorta: comparison between two noninvasive techniques: two-dimensional echocardiography and computed tomography. *Eur Heart J* 1984;5:545–555
119. Nienaber CA, Kodolitsch Y von, Nicolas V et al. The diagnosis of thoracic aortic dissection by noninvasive imaging procedures. *N Engl J Med* 1993;328:1–9
120. Prince MR, Narasimham DL, Jacoby WT et al. Three-dimensional gadolinium-enhanced MR angiography of the thoracic aorta. *Am J Roentgenol* 1996;166:1387–1397
121. Deutsch HJ, Sechtem U, Meyer J, Theissen P, Schicha H, Erdmann E. Chronic aortic dissection: comparison of MR imaging and transesophageal echocardiography. *Radiology* 1994;192:645–650
122. Pele NJ, Herfkens RJ, Shimakawa A, Enzmann DR. Phase contrast cine magnetic resonance imaging. *Magn Reson Q* 1991;7:229–254
123. Bansal RC, Chandrasekaran K, Ayala K, Smith DC. Frequency and explantation of false negative diagnosis of aortic dissection by aortography and transesophageal echocardiography. *J Am Cardiol* 1995;25:1393–1401
124. Glower DD, Speier RH, White WB. Management and long-term outcome of aortic dissection. *Ann Surg* 1991;214:31–41
125. Elefteriades JA, Lovoulos CJ, Coady MA, Tellides G, Kopf GS, Rizzo JA. Management of descending aortic dissection. *Ann Thorac Surg* 2002;67:2002–2005
126. Williams DM, Lee DY, Hamilton BH et al. (1997) The dissected aorta: percutaneous treatment of ischaemic complications; principles and results. *J Vasc Interv Radiol* 8:605–665
127. Nienaber CA, Fattori R, Lund G et al. (1999) Nonsurgical reconstruction of thoracic aortic dissection by stent-graft placement. *N Engl J Med* 340:1539–1545
128. Dake MD, Kato N, Mitchell RS, Semba CP, Razavi MK, Shimono T, Hirano T, Takeda K, Yada I, Miller DC (1999) Endovascular stent-graft placement for the treatment of acute aortic dissection. *N Engl J Med* 20:1585–1586
129. Czermak BV, Waldenberger P, Fraedrich G, Dessl AH, Roberts KE, Bale RJ, Perkmann R, Jaschke WR (2000) Treatment of Stanford type B aortic dissection with stent-grafts: preliminary results. *Radiology* 217:544–550
130. Beregi JP, Prat A, Gaxotte V, Delomez M, McFadden EP (2000) Endovascular treatment for dissection of the descending aorta. *Lancet* 356:482–483
131. Lonn L, Delle M, Falkenberg M et al. Endovascular treatment of type-B thoracic aortic dissections. *J Cardiac Surg* 2003;18:539–544
132. Nienaber CA, Ince H, Weber F et al. Emergency stent-graft placement in thoracic aortic dissection and evolving rupture. *J Cardiac Surg* 2003;18:464–470
133. Leurs LJ, Bell R, Degrieck Y, Thomas S, Hobo R, Lundbom J. Endovascular treatment of thoracic aortic diseases: combined experience from the EUROSTAR and United Kingdom thoracic endograft registries. *J Vasc Surg* 2004;40:670–680
134. Bortone AS, De Cillis E, D'Agostino D, Schinosa L et al. Endovascular treatment of thoracic aortic disease. *Circulation* 2004;110:II262–II267
135. Duebener LF, Lorenzen P, Richardt G et al. Emergency endovascular stent-grafting for life-threatening acute type-B aortic dissection. *Ann Thorac Surg* 2004;78:1261–1267
136. Eggebrecht H, Herold U, Kuhnt O et al. Endovascular stent-graft treatment of aortic dissection: determinants of post-interventional outcome. *Eur Heart J* 2005;26:489–497
137. Hartnell GG, Gates J. Aortic fenestration: a why, when, and how-to guide. *Radiographics* 2005;25:175–189
138. Brathwaite CEM, Rodriguez A. Injuries of the abdominal aorta from blunt trauma. *Am Surg* 1992;58:350–352
139. Michaels AJ, Gerndt SJ, Taheri PA et al. Blunt force injury of the abdominal aorta. *J Trauma* 1996;41:105–109
140. Randhawa MP Jr, Menzoian JO. Seat belt aorta. *Ann Vasc Surg* 1990;4:370–377
141. Vernhet H, Marty-Ané CH, Lesnik A et al. Dissection of the abdominal aorta in blunt trauma: management by percutaneous stent placement. *Cardiovasc Intervent Radiol* 1997;20:473–476
142. Berthet JP, Marty-Ané CH, Veerapen R, Picard EP, Mary H, Alric P. Dissection of the abdominal aorta in blunt trauma: endovascular or conventional surgical management? *J Vasc Surg* 2003;38:997–1004
143. Teruya TH, Bianchi C, Abou-Zamzam AM, Ballard JL, Linda L. Endovascular treatment of a blunt traumatic abdominal injury with a commercially available stent graft. *Ann Vasc Surg* 2005;19:474–478
144. Picard E, Marty-Ané CH, Vernhet H et al. Endovascular management of traumatic infrarenal abdominal aortic dissection. *Ann Vasc Surg* 1998;12:515–521
145. Tucker S Jr, Rowe VI, Rao R, Hood DB, Harrel D, Weaver FA. Treatment options for traumatic pseudoaneurysms of the paravisceral abdominal aorta. *Ann Vasc Surg* 2005;19:613–618
146. Waldrop JL, Dart IV BW, Barker DE. Endovascular stent graft treatment of a traumatic aortocaval fistula. *Ann Vasc Surg* 2005;19:562–565
147. Ohki T, Veith FJ. Endovascular grafts and other image-guided catheter-based adjuncts to improve the treatment of ruptured aortoiliac aneurysms. *Ann Surg* 2000;232:466–479
148. Orend KH, Kotsis T, Scharrer-Pamler R et al. Endovascular repair of aortic rupture due to trauma and aneurysms. *Eur J Vasc Endovasc Surg* 2002;23:61–67
149. Hechelhammer L, Lachat ML, Wildermuth S, Bettex D, Mayer D, Pfammatter T. Mid-term outcome of endovascular repair of ruptured abdominal aortic aneurysms. *J Vasc Surg* 2005:752–757
150. Brown MJ, Sutton AJ, Bell PR, Sayers RD. A meta-analysis of 50 years of ruptured abdominal aortic aneurysm repair. *Br J Surg* 2002;89:714–730
151. Carr SC, Pearce WH, Vogelzang RL, McCarthy WJ, Nemcek AA Jr, Yao JS. Current management of visceral artery aneurysms. *Surgery* 1996;120:627–633
152. Yoon HK, Lindh M, Uher P, Lindblad B, Ivancev K. Stent-graft repair of a splenic artery aneurysm. *Cardiovasc Intervent Radiol* 2001;24:200–203
153. Schoder M, Cejna M, Langle F, Hittmaier K, Lammer J. Glue embolization of a ruptured celiac trunk pseudoaneurysm via the gastroduodenal artery. *Eur Radiol* 2000;10:1335–1337





# Pelvic Fractures

N. Theumann, P. Schnyder

## 2.10

### Contents

2.10.1 Introduction	225
2.10.2 Incidence	225
2.10.3 Anatomy and Biomechanics	225
2.10.3.1 Pelvic Ring	225
2.10.3.2 Acetabulum	227
2.10.4 Imaging	228
2.10.4.1 Plain films	228
2.10.4.2 Computed Tomography	230
2.10.4.3 Magnetic Resonance Imaging	231
2.10.5 Classifications	231
2.10.5.1 Pelvic Ring Fractures	231
2.10.5.2 Classification of Acetabulum	243
2.10.6 Pelvic Trauma Management	246
2.10.6.1 Clinical Evaluation	246
2.10.6.2 Imaging Strategies	246
2.10.6.3 Treatment	247
2.10.7 Complications	247
2.10.7.1 Death Rate	247
2.10.7.2 Associated Lesions	248
2.10.8 Conclusion	248
References	248

### 2.10.1 Introduction

Pelvic trauma includes a great variety of very polymorphous lesions, differing from each other by their anatomical aspect, their context, and the following therapeutic implications:

1. Isolated bone tear needing no particular treatment
2. Acetabular fractures with major functional prognosis
3. High-energy trauma with pelvic ring disruption, vital lesions, and hemorrhage implying emergency hemostasis.

In order to be efficient, the radiologist first has to know the diagnostic value of each radiological technique, in order to suggest the investigation strategy appropriate to any given clinical situation. He/she must then be able to accurately describe fractures and include them into a classification in agreement with the clinician.

### 2.10.2 Incidence

Pelvic ring fractures amount to 1.5% of all joint fractures [39, 41]. Simple fractures without great displacement affect mainly elderly women with low-energy trauma. Severe displaced lesions affect younger, essentially male, patients in a context of high-energy trauma, resulting in multiple trauma (polytrauma) in 75% of cases [17, 20, 48]. Melton et al. [39] reported 175 pelvic fractures over 10 years, including 84 fragmented and isolated lesions, 71 simple pelvic ring ruptures, and 20 severe fractures. Among the latter fractures, 48% were provoked by high-energy trauma and 2% by simple falls. The average age of the first group was approximately 33 years, whereas in the second, it was approximately 69 years. Low-energy trauma provoked fragmented or simple lesions in 95% of cases. The gender ratio was to 2 women for 1 man. Pohlemann et al. [49] report 200 serious fractures (10.5%) out of a series of 1409 cases within 20 years. The most frequent causes of pelvic trauma relate to car accidents (50–60%) and car–pedestrian crash (14–18%) [9, 13, 15, 38, 65]. In a recent review of traffic accidents, 4.1% of cases presented pelvic ring lesions; among these, 47% of cases were car passengers, 31% pedestrians, 12% motorcyclists, and 10% cyclists [50]. In the same group, only those seat-belt-fastened patients for whom the speed gradient exceeded 30 km/h suffered pelvic ring lesions, whereas the unbelted ones suffered lesions with lower speed gradients.

### 2.10.3 Anatomy and Biomechanics

#### 2.10.3.1 Pelvic Ring

The pelvis is a ring composed of three bones: the sacrum dorsally, and two innominate bones front-medially. The sacrum joins to the innominate bone by the sacroiliac (SI) joints. The two innominate bones join frontally by the symphysis pubis. The innominate bone includes three separate ossifications: the ilium; the ischium; and the pubis.

The posterior stability of the ring is assumed by the posterior tension band, which includes the posterior and interosseous sacroiliac ligaments. This ligamentous com-

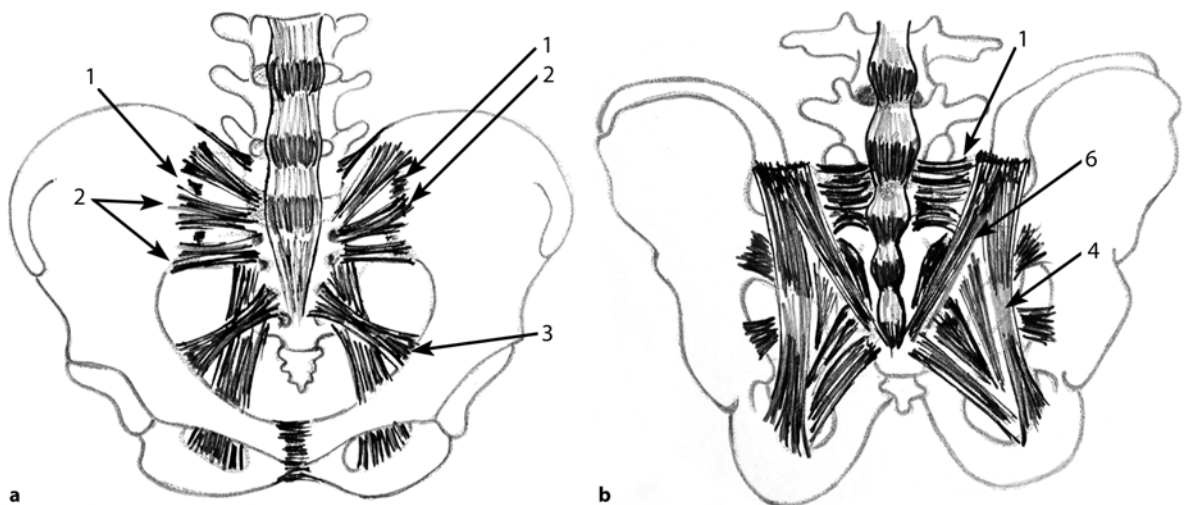


**Fig. 1.** Normal pelvic ligaments. **a** Anterior view. **b** Posterior view. 1 Interosseous sacroiliac ligament; 2 anterior sacroiliac ligaments; 3 sacro-spinous ligaments; 4 sacro-tuberous ligaments; 5 symphysis pubis; 6 posterior sacroiliac ligaments

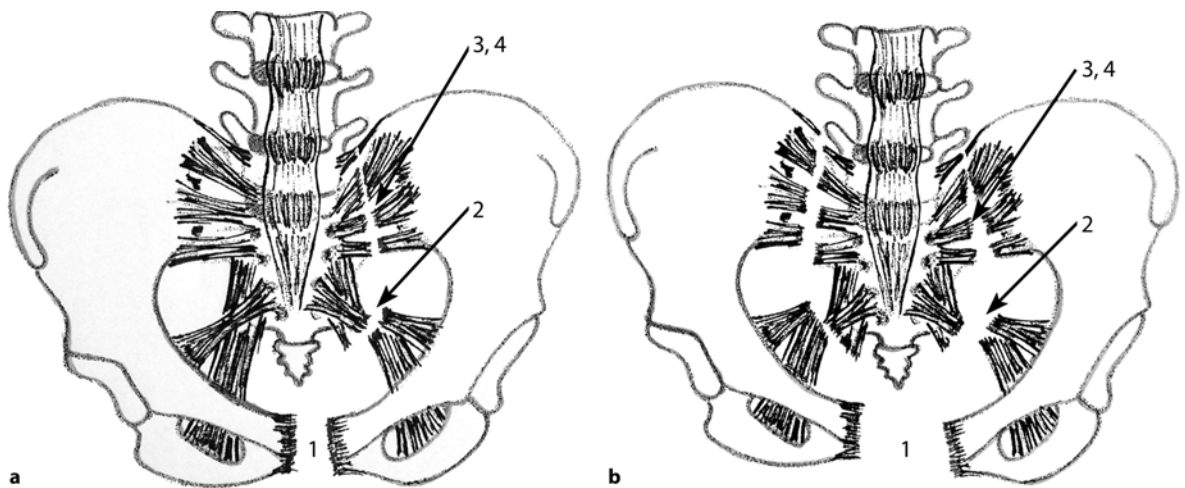


**Fig. 2.** Antero-posterior compression. **a** “Low energy”. **b** “High energy”. 1 Symphysis diastasis; 2 sacrospinous and sacrotuberous ligament disruption; 3 anterior sacroiliac ligaments disruption; 4 posterior sacroiliac ligaments disruption

plex and the sacro-tuberous ligaments resist vertical translation between the ilia and the sacrum. The anterior sacroiliac, symphyseal, and sacrospinous ligaments are transversely oriented and resist rotation of the pelvis (Fig. 1) [30, 61]. For the pelvis, the instability is defined by two displacements: rotational and vertical. The forces, caused by rotational displacements, tend either to open and externally rotate the pelvis, or to close and internally rotate it. Vertical instability indicates disruption of the posterior tension band and implies cranio-caudal, rotational, and antero-posterior displacement [30].

Three basic mechanisms lead to pelvic ring disruptions [14, 28, 45]. They are based on the direction of the force imparted to the pelvis at the time of injury.

### Antero-posterior Compression

The antero-posterior (AP) compression injury pattern (Fig. 2) is due to a force directly applied to the pubis or to the posterior pelvis and results in iliac external rotation deformity. The symphyseal separation suggests damage to the ligamentous structures and possible instability. The presence of a vertical obturator ring fracture, a diastasis of both the symphysis pubis and the sacroiliac joint, are important points of this pattern and serve as stability hallmarks [14, 30, 61, 71].

### Lateral Compression

The lateral compression injury pattern (Fig. 3) or iliac internal rotation injury is the result of a lateral blow to the side of the pelvis. This fracture affects either one or both sides of the pelvic ring. Anteriorly, the fracture fragments frequently override the adjacent fragments. Posteriorly, the fracture fragments are impacted (mainly in elderly patients), or there is a diastasis of the sacroiliac joint (mainly in the younger patients, sometimes associated with ligamentous disruption [14, 30, 55, 71].

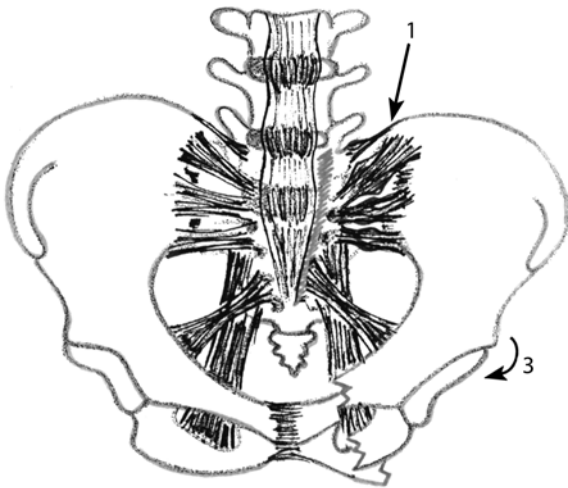


**Fig. 3.** Lateral compression. 1 Impacted fractures of the sacrum; 2 horizontal overlapping ring fracture; 3 internal rotation of the left hemipelvis

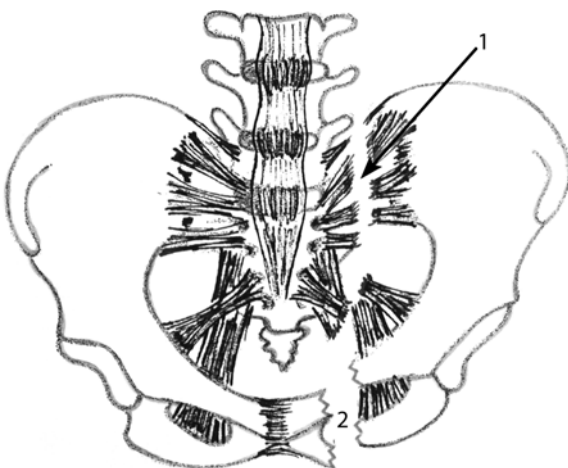


**Fig. 4.** Vertical shear pattern. 1 Anterior and posterior ligamentous disruption; 2 obturator ring fractures

### Vertical Shear

The vertical shear pattern (Fig. 4) is often an unstable state, when it appears after a vertical axial fall, with presence of anterior and posterior fractures of the pubic rami, fractures of the sacrum, sacroiliac diastasis, or iliac wing fracture. A typical finding is always present as a superior and usually asymmetric displacement of the involved hemipelvis secondary to the vertical axial fall [28].

#### 2.10.3.2 The Acetabulum

The acetabulum is composed by two columns: the large anterior one and the small posterior one. An inverted “Y” is formed by these two columns, which support the hip (Fig. 5) [23, 26, 36, 37]. The anterior column begins at the inferior pubic ramus and extends above the acetabulum into the iliac wing. The posterior column is shaped by the ischium and extends to the greater sciatic notch and the sacroiliac joint. The inferior junction of the two columns forms the ischio-pubic junction. The quadrilateral plate shapes the medial wall of the acetabulum. It is a thin layer of bone between the hip joint and the pelvis. In addition to the two columns, the bone stability of the hip is increased by the presence of anterior and posterior walls, the latter being larger than the former.

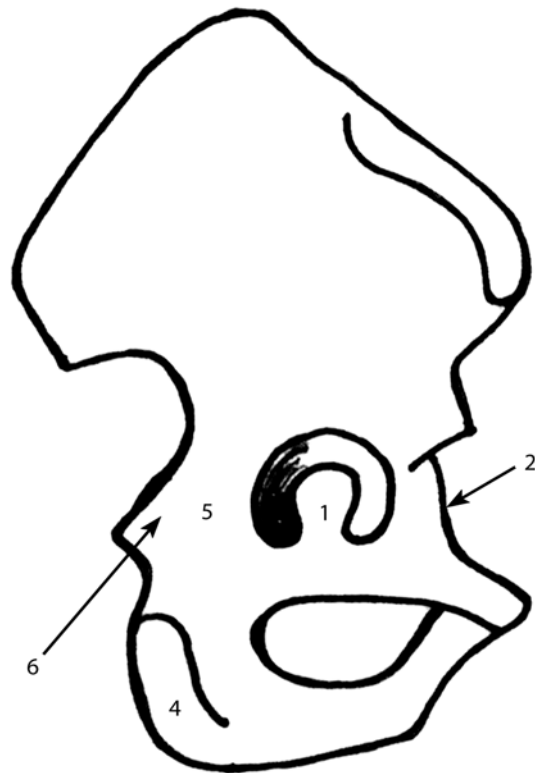


**Fig. 5.** Normal acetabular anatomy. 1 “Inverted Y”; 2 ilio-pectineal line; 3 anterior wall; 4 ischial tuberosity; 5 posterior wall; 6 sciatic notch



## 2.10.4 Imaging

### 2.10.4.1 Plain Films

The AP view of the pelvis is the basic incidence for pelvic trauma. It allows identification of ischio-iliac line, ilio-pectineal line (ilio-pubic line), as well anterior and posterior acetabular walls (Fig. 6). The ilio-pectineal line is formed by the anterior structure of acetabulum. The ilio-ischial line is formed by posterior structures of the acetabulum [18].

More specifically to each type of fracture, numerous incidences have been evaluated among which Pennal's incidences are mostly used in pelvic ring investigations and Judet's incidences in acetabulum investigations.

#### Pelvic Ring Investigation

Pelvic inlet (tube angled 45° caudad; Fig. 7) and outlet (tube angled 45° cephalad; Fig. 8) views may be added to AP view when pelvic fracture is suspected [14, 30, 55, 56]. They are known as Pennal's incidences. Inlet view proves best to display AP displacement of hemi-pelvis as well as horizontal rotation, whereas outlet view allows identification of vertical displacement, superior displacement of hemi-pelvis thus being evaluated in comparison with the levels of posterior elements. Anteriorly, symphysis pubis and pubis rami are inspected, whereas posteriorly iliac crests, sacrum, sacral foramina, sacroiliac joints, and L5 transverse processes are evaluated to rule out possible injuries. Particular attention is paid to the sacrogluteal line, which corresponds to

the continuation of the ilio-pectineal line around the greater sciatic notch and onto the body of the sacrum. This hallmark is useful in identifying posterior fractures. The arcuate lines of the sacrum, representing the dense cortical bone between the sacral foramina, should also be examined. A distortion or break in it indicates a lesion [35].

#### Acetabular Investigation

If an acetabular fracture is suspected, three more incidences are mandatory in addition to the AP view: an AP view centered on the injured hip and two "Judet's" oblique views obtained with patient rotated 45° right posterior oblique (iliac oblique view; Fig. 9) and left posterior oblique (obturator oblique view; Fig. 10), in the supine position [33]. In the majority of cases, these four incidences are sufficient to classify these fractures and to propose therapeutic strategy.

The two oblique views and the classic AP view of the hip allow identification of the six fundamental landmarks: the acetabular roof; the acetabular anterior lip; the acetabular posterior lip; the ilio-ischial line, the ilio-pectineal (ilio-pubic) line; and the tear drop. The ilio-ischial line is shaped by posterior parts. The ilio-pectineal line is shaped by anterior parts of the acetabulum. If disruption of the landmarks are noted on plain films, the fracture can often be classified properly. The iliac oblique view shows the iliac wing, useful to display a fracture that extends above the acetabulum into the iliac wing. The obturator oblique view shows fractures of the obturator ring, of the posterior wall of the acetabulum, and of the greater sciatic notch [46].

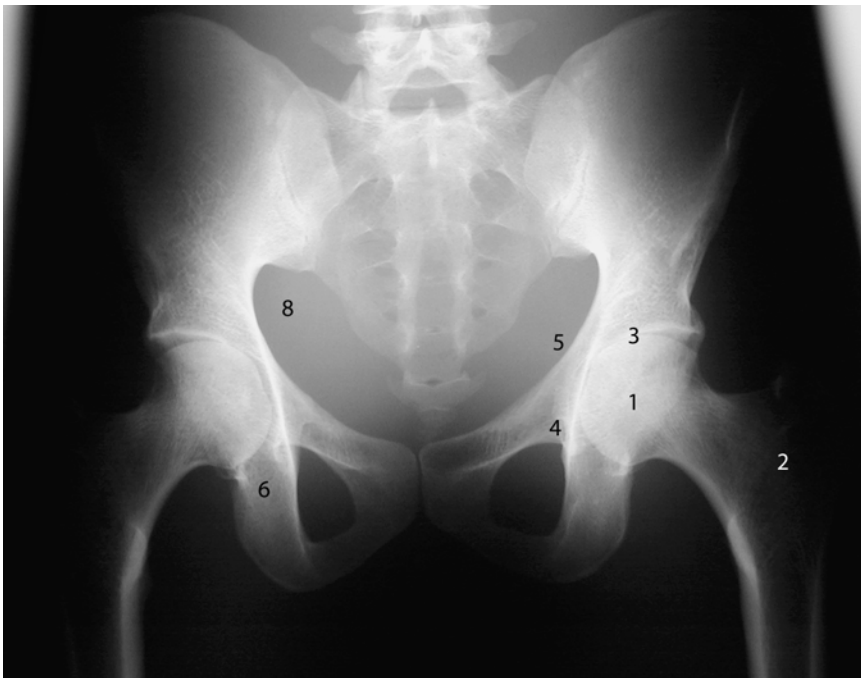


**Fig. 6.** Normal anatomy, antero-posterior view. 1 Anterior lip; 2 posterior lip; 3 roof; 4 ilio-ischial line; 5 Ilio-pectineal line; 6 tear drop; 7 sacro-gluteal line; 8 arcuate line

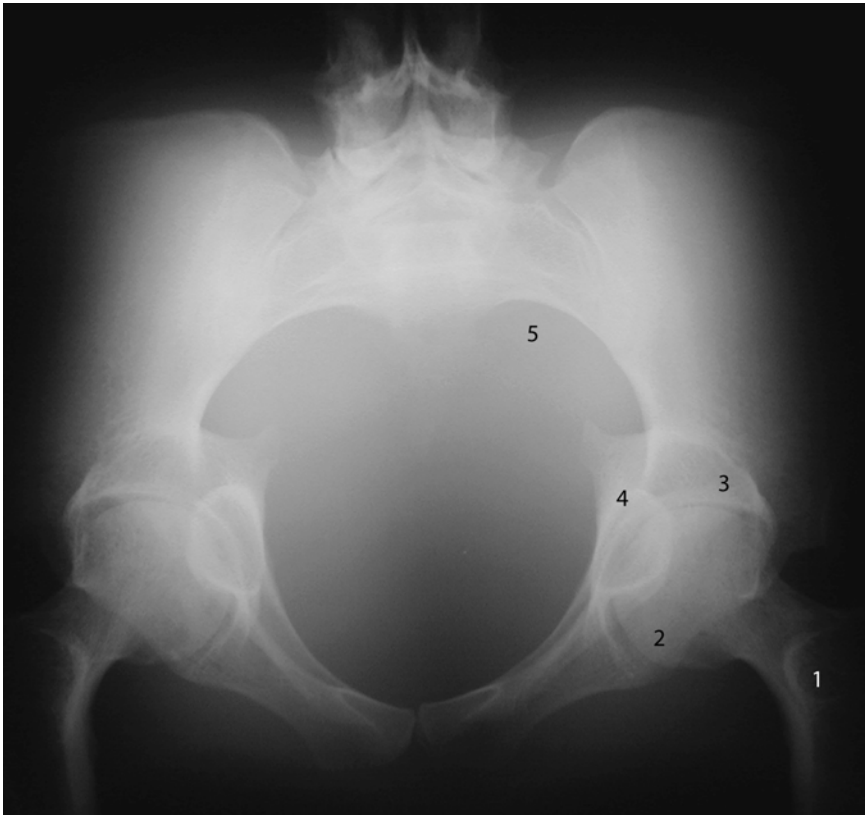


**Fig. 7.** Inlet view. 1 anterior lip; 2 posterior lip; 3 roof; 4 ilio-pectineal line; 5 anterior border of the sacral body

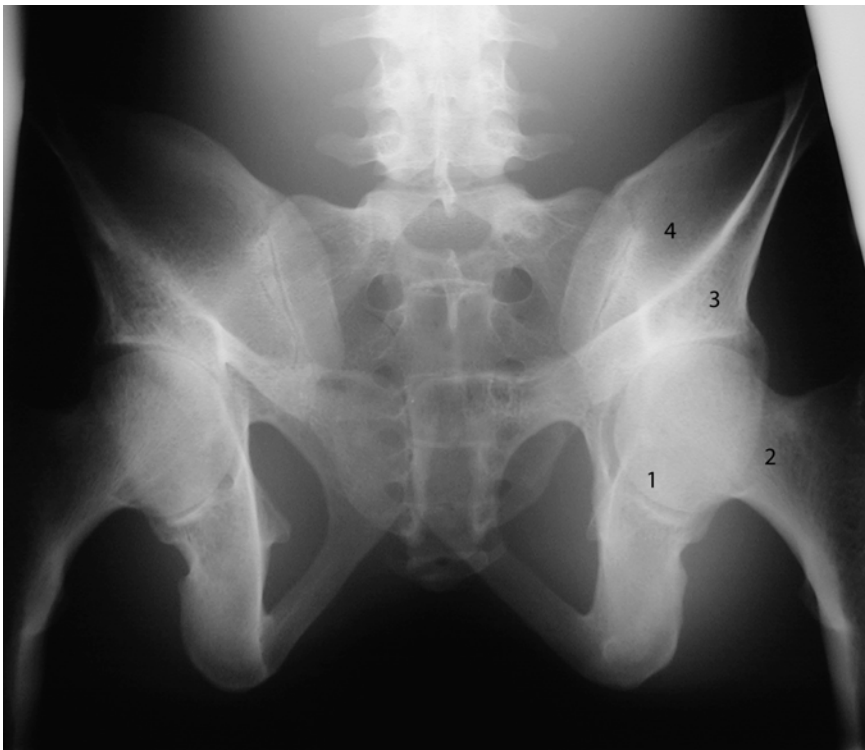


**Fig. 8.** Normal anatomy, outlet view. 1 Anterior lip; 2 posterior lip; 3 roof; 4 ilio-pectineal line

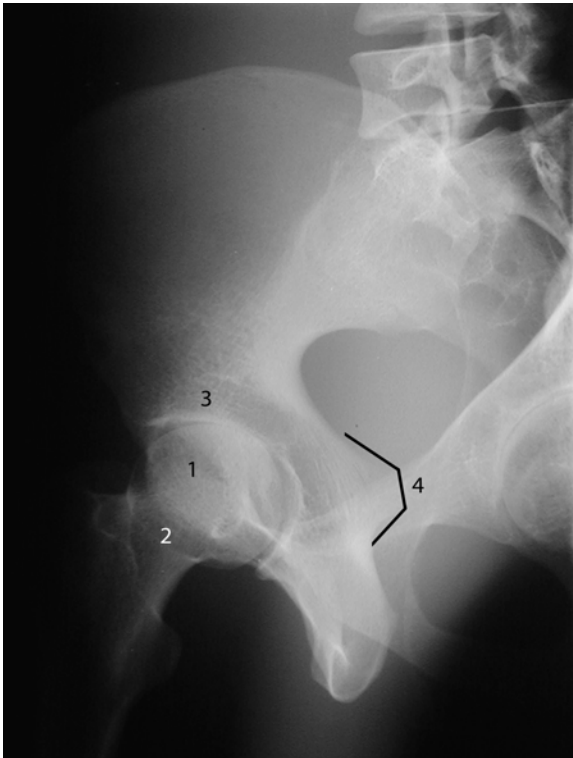


**Fig. 9.** Normal anatomy, iliac oblique view. 1 Anterior lip; 2 posterior lip; 3 roof; 4 greater sciatic notch; 5 quadrilateral surface

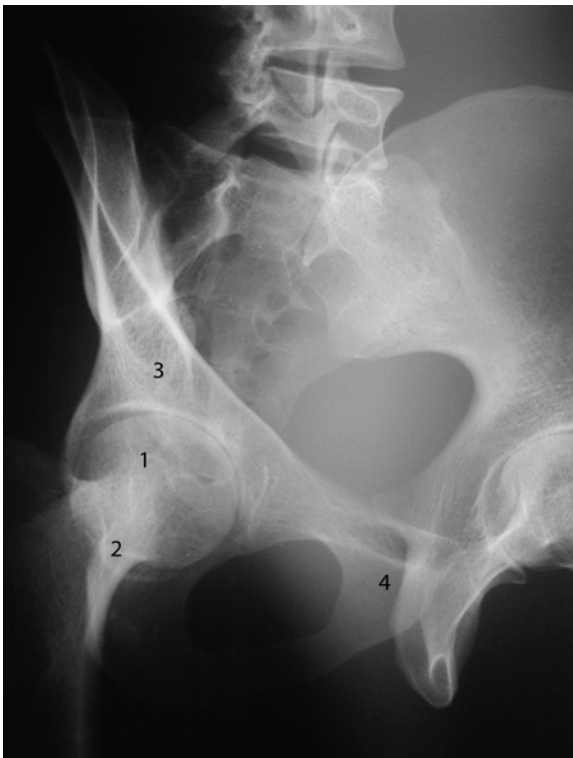


**Fig. 10.** Normal anatomy, obturator oblique view. 1 Anterior lip; 2 posterior lip; 3 roof; 4 pelvic brim

## 2.10.4.2 Computed Tomography

### Diagnostic Value

Computed tomography has become an outstanding tool in pelvic imaging [21]. Its technological improvements (helical and multi-detector technologies) have recently increased its potential. In some cases, its performance has proved to be superior to plain films. About 30% of pelvic fractures detected by CT are missed by plain film [2, 55, 59]. In sacral trauma, plain films missed 29% of sacroiliac diastasis, 57% of acetabular rim fractures, and 34% of vertical shearing fractures [40]. Plain films also missed up to 40% of intra-articular fragments and 50% of femoral head fractures visualized with CT [26, 64]. It must be mentioned that detection of additional fractures will change patient management [22, 64]. Computed tomography has some limitations. Some authors relate false negatives [72], but use of new-generation CT machines might show better results [67]. Moreover, CT allows complete investigation of visceral pelvic lesions and of associated thoracic, abdominal, and even brain lesions [10, 31, 66].

### Indications

Because of its performance, CT indications tend to increase. For Hunter et al. [28] they may be detailed as follows:

1. Acetabular fractures
2. Dislocations of the hip
3. All potential or recognized sacral fractures
4. All potential or recognized sacroiliac injuries
5. Any question of stability in pelvic fractures

### Technical Considerations

Several protocols can be taken into consideration according to the context:

1. In cases of pelvic trauma, complete pelvis investigation can be performed with 5-mm slices every 5 mm allowing for a wide area of investigation, from above the iliac crests down to the ischia, with a sufficient investigation quality. Depending on the context, an intravenous contrast agent injection is useful in investigating visceral lesions all in one examination. Associated examination of the abdomen seems mandatory, as abdomen and pelvis remain the same traumatic entity [10, 19]. The CT acquisition should occur at least 60 s after injection of contrast agent to make sure of a good visceral impregnation and mainly to allow for the detection of an active hemorrhage (contrast agent leak). Such a protocol allows appreciation of both osseous and visceral lesions.
2. If an acetabular lesion is suspected from the clinical examination and plain films, or during detection CT, thinner slices, ranging between 1 and 3 mm, joint or overlapping, are mandatory. They allow better analysis of the lesions and good-quality multiplanar reconstructions (MPRs). If not performed before, a systematic in-

vestigation of all the pelvis with 5-mm slice thickness is recommended to complete acetabular examination.

3. Multiplanar reconstructions are useful in the interpretation of complex fractures, mainly for the acetabulum. They often need thinner acquisition (3-mm slices or less) and overlapping reconstruction to improve imaging quality; however, even with 5-mm-thick slice acquisitions, MPRs may be of interest. In this latter case quality may be improved by overlapping of axial slices. Reconstruction in anatomical planes may be added to the classic sagittal and frontal reconstruction planes (sacrum plane, iliac wing plane, etc.).
4. A 3D reconstruction is favored by surgeons but should only be used as a tool to the understanding of complex fractures, in particular for the acetabular fractures or important displacements of the fragments. Their reading should always be achieved with axial and/or MPRs, which remain the best analysis tools.
5. In case of doubt about sacral lesions, acquisitions in the oblique coronal plane, inclining the gantry according to the great sacral axis, often improve imaging quality. In most of cases, however, MPRs are sufficient.

### Multislice CT And Pelvic Trauma

Multidetector technology allows extended possibilities in trauma investigation: large area of exploration; faster acquisition; thinner thickness of slices and easy reformation in the appropriate plane; and dimensional imaging and thick-slice (wedge) MPRs (mimicking conventional radiographs). At our institution, pelvic investigation of multiple-trauma patients is systematically included in a complete thoracic, abdominal, and pelvic examination realized with multislice CT. Use of high peak voltage is recommended for imaging bone. We use 140 kVp for spine and pelvis. This increases the likelihood of penetrating the bone and at the same time reduces the total dose to the patient (lower milliamperes per second, mAs) [8].

Imaging post-operative patients with metallic implants may present a challenge. Metal causes artifacts such as beam hardening. The metal artifacts depend on the composition of the hardware (titanium produces the least artifacts, cobalt chrome alloys produce the most). Artifact also depends on the geometry of the implant (its thickness and orientation), and is most severe in the direction of the thickest portion of the artifact. Metal artifacts also depend on kVp and mAs, reconstruction algorithm, and the MPR slice thickness and orientation. Use of high kVp reduces artifacts by increasing the likelihood of X-ray penetration. Increasing mAs increases photon flux, striking the CT detectors, and also reduces artifacts, but this must be balanced against increased radiation dose. Use of bone or edge enhancement should be avoided as it increases hardware artifact. It is recommended that standard bony or soft tissue reconstruction algorithms be used when imaging patients with dense metal implants. Use of thicker slice widths for MPR reduces metal artifacts by averaging pixels [8].

The MSCT images are reconstructed using filtered back projection or reconstruction algorithms. The higher the kernel number, the sharper the image, and the lower the number, the smoother the image. We recommend detailed or sharp reconstruction algorithms for MPR.

Image reconstruction (MPRs and 3D) at increments near or equal to 50% of the slice width is recommended. For 3D imaging, we recommend the use of the smoothest available volume zoom (filter or algorithm), e.g., B10. This is because suboptimal or poor-quality images are obtained if there is excess noise on the original (axial) slices from which the 3D images are obtained, and this is most likely if a bone algorithm is used. Production of two sets of images from the raw data is therefore required if MPR and 3D images are needed.

The large volume of data produced is also a challenge and time-consuming for the reporting radiologist. Soft-copy (workstation) reviewing and reporting may reduce the time spent handling the large numbers of images. Selected images can then be produced on hard copy to best communicate the pathology to the clinicians.

### Protocol

The protocol is as follows: patient lying supine, arms comfortably on the chest or above the head and lower legs supported. No breathing command is required. Raw data acquisition is as follows: 140 mAs; 140 kV; and rotation time 0.5 s. Image data sets of 1-mm-width slices on 0.8 mm increments on both sharp kernel (B70) and very smooth kernel (B10) are acquired. This allows faster and accurate detection of visceral and osseous lesions in one go. Secondary multiplanar and 3D reconstructions with 2-mm-thick slices are of great quality, even for acetabular fractures. If needed, better quality may be obtained with 1.25- or 1-mm-thick slices in addition to initial exploration.

### 2.10.4.3 Magnetic Resonance Imaging

Some studies have shown the superiority of MRI under particular circumstances such as the detection of intra-articular splinters, appreciation of the femoral head, and detection of hidden fractures mainly in the elderly [52]; however, its use remains minor with pelvic trauma in their acute phase.

## 2.10.5 Classifications

### 2.10.5.1 Pelvic Ring Fractures

One of the first descriptions of pelvic fracture (iliac wing fracture) was reported by Duverney in 1751 [35]. Until the 1950s, classifications of pelvic ring fractures were based only on anatomical descriptions of the lesions. Pennal and Sutherland [45] suggested the first mechanistic classifica-



tion of these fractures. They distinguished several fracture categories according to the mechanism of lesion: AP or lateral compression or vertical shearing; thus were set the bases of most of the classifications established so far. In 1981 Bucholz [7] gave a clear definition of the anterior and posterior pelvic ring and insisted on the frequent occurrence of unknown lesions of the posterior ring. They suggested an anatomical classification based on the importance of these lesions of the posterior ring.

In the late 1980s, Tile and Young developed two classifications which have been the most used in the past years. Tile [60, 61] modified Pennal's classification. He introduced the idea that management of these fractures was directly related to the importance and direction of instability; thus, he insists on the importance of the appreciation of the stability. But the classification did not include description of complex fractures. Fractures are classified using their principal elementary lesion. At the same time, Young and Burgess developed a classification [71] that includes mechanism of the lesion and radiographic (AP plain film) grading of severity. This classification emphasizes the level of energy imparted [9, 72]. They also noted that the mechanism may not always be identified and therefore introduced the category called "combined mechanical injury." Later, Dalal et al. [15] demonstrated that the Young–Burgess classification could be of value in predicting associated injuries and in prioritizing the work-up during resuscitation of acutely ill patient; however, all these classifications still remain difficult to apply. On one hand, the link between trauma mechanism and

anatomical lesions can be difficult to define. On the other hand, the appreciation of lesion stability remains ill-defined in emergency cases, as it often relies on incompletely validated radiological criteria. Tile, in association with the thoughts of a working group of the AO (Association for Osteosynthesis), suggested an alphanumeric classification in order to harmonize the therapeutic management and the prognostic evaluation (Table 1) [42, 61]. This Tile/AO classification seems to be the most frequently used classification at present. It is our reference classification. It allows description of the mechanisms involved, the elementary lesions, and the therapeutic consequences implied.

The Tile/AO classification suggests three subdivided main categories (Fig. 11).

### Type-A Fracture

Type-A fracture is an incomplete fracture with neither disruption of the pelvic ring nor lesion of the posterior band (Fig. 11a). Type-A1 fracture corresponds to an avulsion fracture of the pelvic ring. It usually concerns teenagers at the end of their growth and may involve the anterior–superior, anterior–inferior, or ischial spine. The avulsion of the anterior–superior spine is caused by the sudden contraction of the sartorius, whereas that of the anterior–inferior spine is caused by the contraction of the rectus femoris. The avulsion of the pubic tubercle is caused by the contraction of the pectineus (Fig. 12).

**Table 1.** Tile/AO classification of pelvic fractures

Mechanism	Classification	Features	Stability
	Type A	A1: apophyseal avulsions A2: stable iliac wing fracture or stable minimally displaced ring fracture A3: sacro-coccygeal fractures	Stable
Anterior compression	Type B1	External rotation or "open-book" injuries B1.1: unilateral anterior sacroiliac disruption B1.2: sacral fracture	Partially stable (complete rupture of anterior arch, incomplete rupture of posterior arch)
Lateral compression	Type B2	Internal rotation injuries B2.1: anterior compression fracture of the sacrum B2.2: partial sacroiliac joint fracture B2.3: incomplete posterior iliac wing fracture	Partially stable (complete rupture of anterior arch, incomplete rupture of posterior arch)
Anterior compression	Type B3	Bilateral external rotation (bilateral "open book") B3.1: bilateral B1 B3.2: B1 and B2 B3.3: bilateral B2	Partially stable (complete rupture of anterior arch, incomplete rupture of posterior arch)
Vertical shear	Type C	C1: complete unilateral rupture C1.1: iliac fracture C1.2: sacroiliac dislocation C1.3: sacral fracture C2: bilateral injury (B+C types) C3: bilateral complete rupture	Unstable (complete rupture of both anterior and posterior arches)

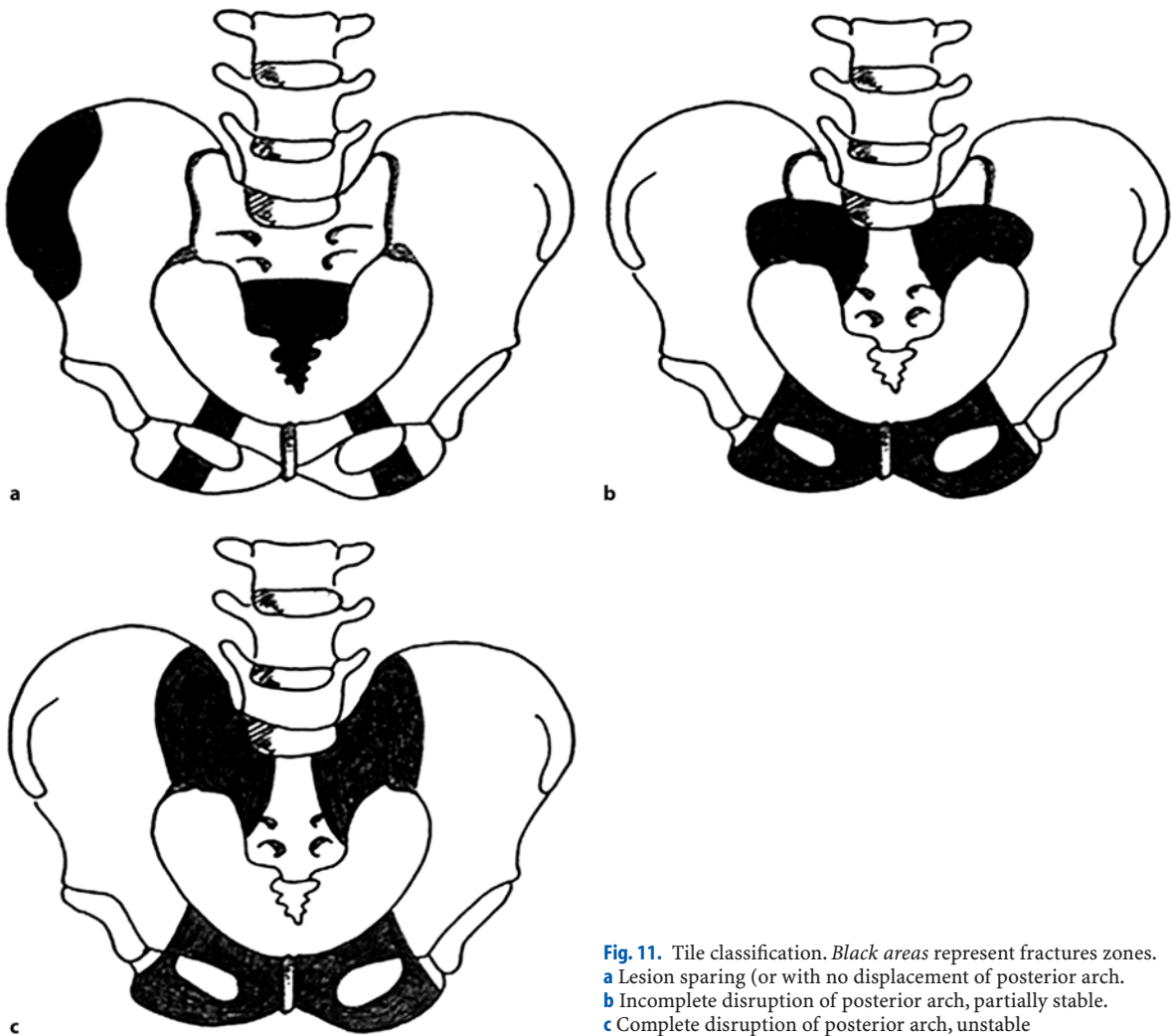


**Fig. 11.** Tile classification. *Black areas* represent fractures zones.  
**a** Lesion sparing (or with no displacement of posterior arch).  
**b** Incomplete disruption of posterior arch, partially stable.  
**c** Complete disruption of posterior arch, unstable

Type-A2.1 fracture corresponds to a stable iliac wing fracture caused by direct blow on the ilium and does not involve pelvic ring, which remains stable (Fig. 13).

Type-A2.2 fracture relates to a stable, minimally, or undisplaced fracture of the pelvic ring and usually affects elderly women with osteoporosis after a fall. The mechanism corresponds to a lateral compression, cracking the pubic rami. (Fig. 14).

Type-A2.3 fracture relates to anterior ring fractures or four pillar fractures and involves the four pubic rami frontally, without posterior injury. These fractures are caused by a direct blow or by a high-energy trauma of shearing or lateral compression (Fig. 15).

### Type A3 Are Sacral or Coccygeal Fractures

Type A3.1 implies fractures of the coccyx or sacro-coccygeal dislocation common after a sitting fall and may be the source of prolonged pain, but no neurological disability can be observed. The transverse fractures of the sacrum distal to the gluteal line do not involve the pelvic ring.

Type A3.2 relates to undisplaced fractures and rarely causes neurological deficit.

Type A3.3 corresponds to displaced and translated fractures with injury to the sacral nerve roots.

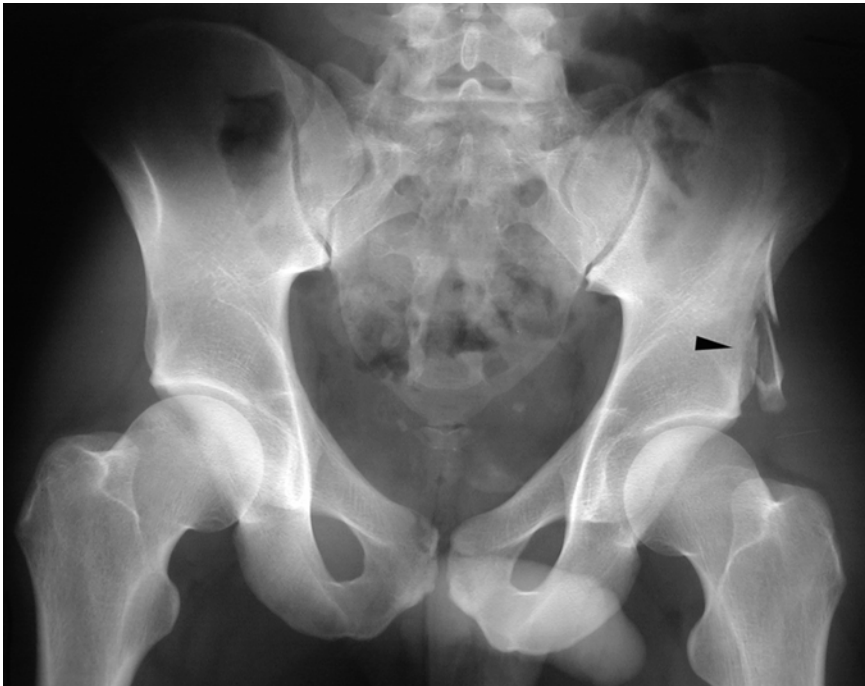


**Fig. 12.** Type-A1 fracture. Antero-posterior view. Fracture- avulsion of the right antero-inferior iliac spine

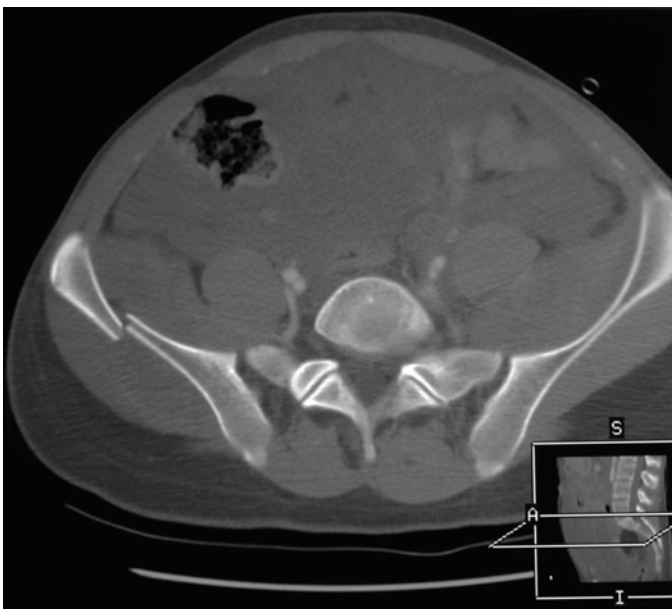


**Fig. 13.** Type-A2.1 fracture. Isolated right iliac wing fracture

### Type-B Fracture

It relates to disruption (or fracture) of the symphysis pubis, associated with anterior sacroiliac joint disruption (unilateral or bilateral; Fig. 11b). The posterior sacroiliac ligaments, responsible for the vertical stability, remain untouched. The typical lesion is caused by an AP compression applied to the anterior–superior iliac spines of the fixed pelvis. A posterior blow against the posterior–superior iliac

spine may produce a similar fracture. Displacement of the symphysis pubis is an important feature of this type. If the splitting of the symphysis pubis is <2.5 cm, it cannot be associated with a disruption of either the pelvic floor or the sacro-spinous ligament. But if it is wider than 2.5 cm, then it is often associated with a disruption of either the pelvic floor or the sacro-spinous ligament. In the latter case, a much higher occurrence of visceral injury can be observed.

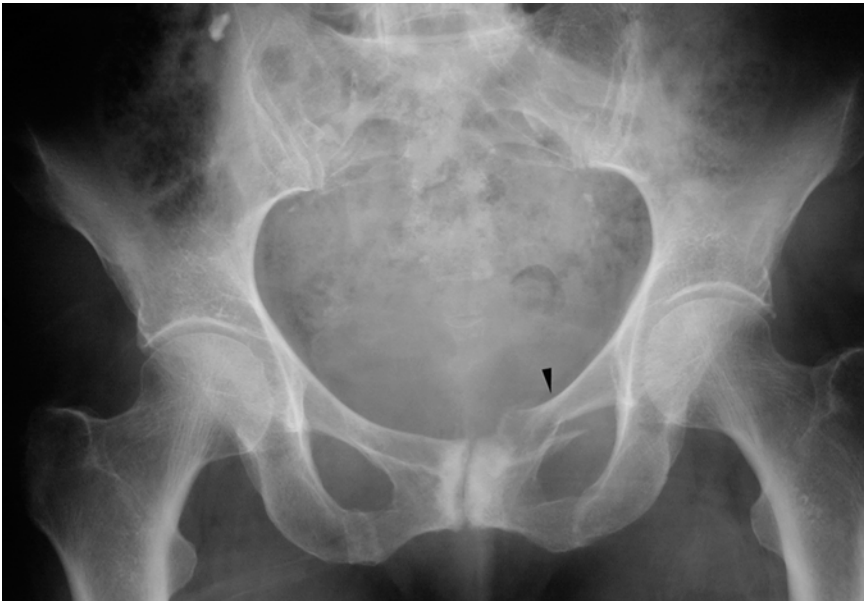


**Fig. 14.** Type-A2.2 fracture. Antero-posterior view. Left unilateral pubic rami fractures (*arrowhead*)

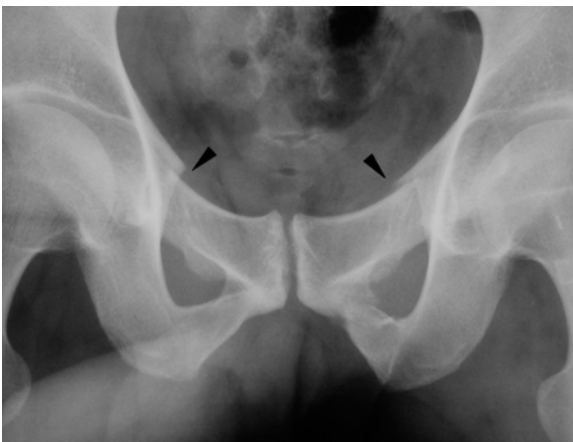


**Fig. 15.** Type-A2.3 fracture. Antero-posterior. Bilateral pubic rami fractures (*arrowheads*)

Type B1 relates to a unilateral “open-book” injury usually caused by a violent external rotation of one femur. The typical situation is that of the motorcyclist who puts out a leg for balance and gets caught by a stationary object such as a road panel or a tree. The external rotation force usually disrupts the symphysis pubis first, and as the external rotation goes on, a disruption of the pelvic floor, of the fascia, and of the sacrospinous and anterior sacroiliac ligaments follows.

The variants include type B1.1 (sacroiliac joint anterior disruption) and B1.2 (sacral fractures; Fig. 16).

Type B2 relates to lateral compression injuries characterized by unilateral partial disruption of the posterior arch maintaining the vertical or posterior stability (internal rotation). A lateral compressive force directed at the

pelvic ring may cause two types of injury, the first in which the anterior and posterior lesions occur on the same side of the pelvis, and the second in which the displacement is shown on the opposite side. In the latter case, the relative stability is maintained by the osseous impaction (no muscle or ligament tears). Variants include B2.1 (anterior crush fracture of the sacrum), B2.2 (partial sacroiliac joint fracture/subluxation), and B2.3 (incomplete iliac fracture; Figs. 17, 18).

Type B3 stands for the classical, bilateral “open-book” injury. Despite the relative stability of the pelvic ring, maintained by the posterior sacroiliac ligaments, the pelvic floor disruption causes visceral injuries. Variants include B3.1 (bilateral B1), B3.2 (B1 on one side and B2 on the other side), and B3.3 (bilateral B2; Fig. 19).



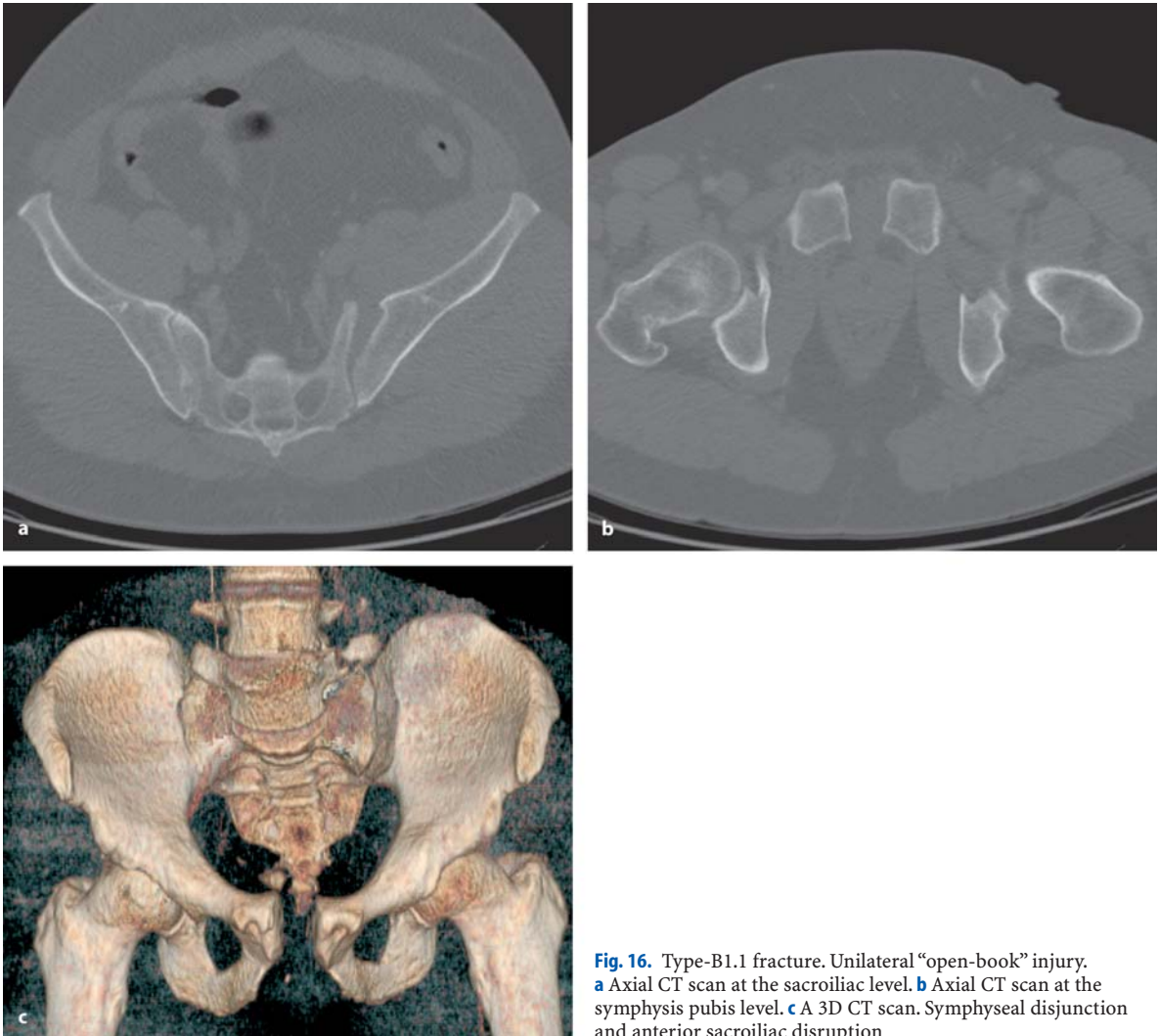


**Fig. 16.** Type-B1.1 fracture. Unilateral “open-book” injury. **a** Axial CT scan at the sacroiliac level. **b** Axial CT scan at the symphysis pubis level. **c** A 3D CT scan. Symphyseal disjunction and anterior sacroiliac disruption



**Fig. 17.** Type-B2.1 fracture. Lateral compression, stable fracture. **a** Antero-posterior view. Left pubic rami fracture. **b** A CT scan. Anterior compression fracture of right superior sacroiliac joint

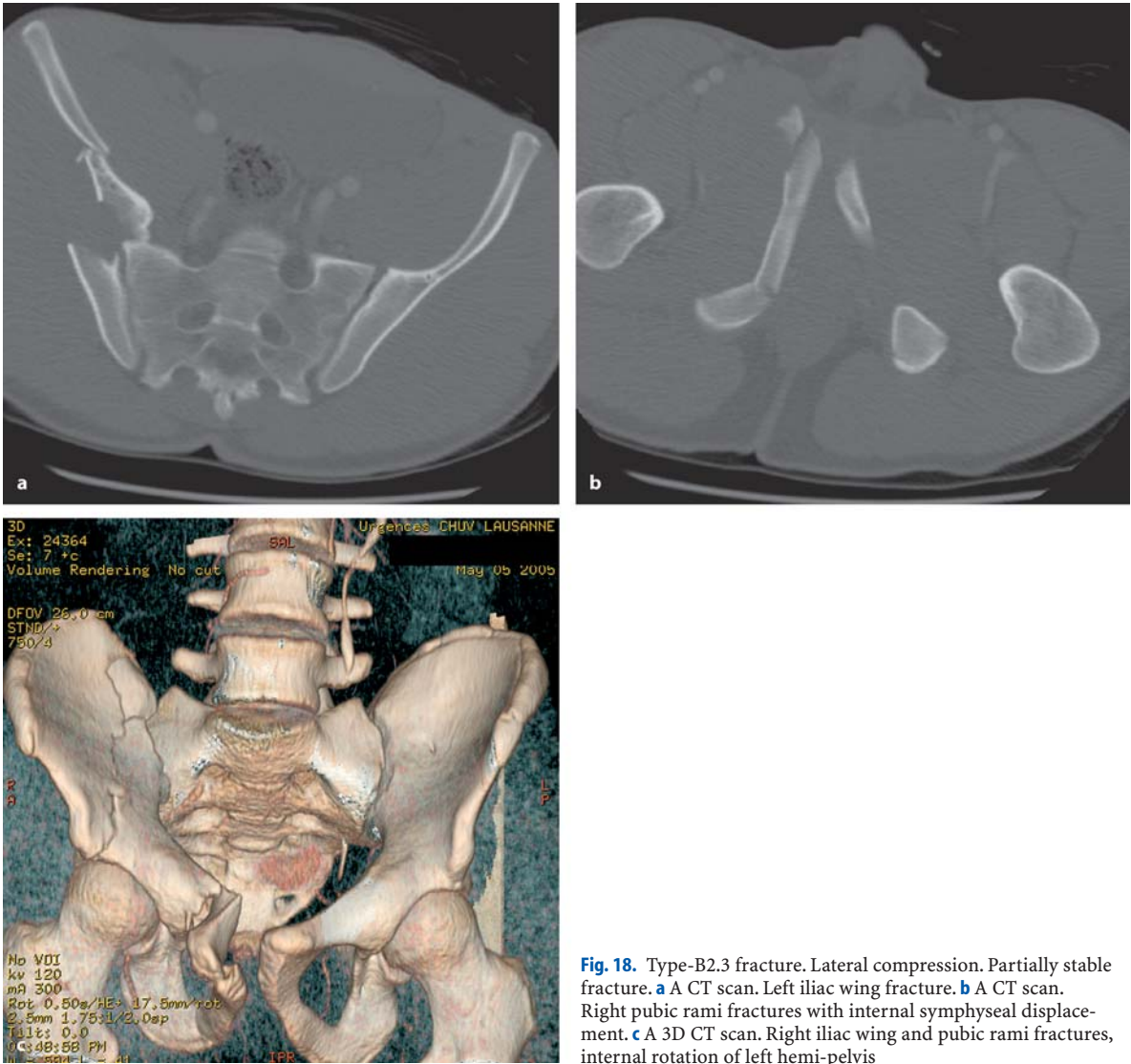


**Fig. 18.** Type-B2.3 fracture. Lateral compression. Partially stable fracture. **a** A CT scan. Left iliac wing fracture. **b** A CT scan. Right pubic rami fractures with internal symphyseal displacement. **c** A 3D CT scan. Right iliac wing and pubic rami fractures, internal rotation of left hemi-pelvis



**Fig. 19.** Type-B3 fracture. **a** Antero-posterior view. “Open-book” lesion with symphyseal diastasis and bilateral sacroiliac disruption. **b** Antero-posterior view. Same patient after external fixation and reduction of diastasis

### Type-C Fracture

Type-C fracture relates to unstable injuries with complete disruption of the posterior–sacroiliac complex, involving vertical shearing forces. These unilateral or bilateral fractures are almost always caused by severe trauma such as falls from heights, crushing injuries, or motor vehicle accidents. They cause massive disruption of both the pelvic ring and the surrounding soft tissues.

Type C1 corresponds to unilateral injuries of the hemipelvis.

Type C1.1 relates to shear fractures of the ilium, which begin at the inferior part of the sacroiliac joint and run to the iliac crest at the rear.

Type C1.2 stands for sacroiliac dislocations. These fractures can only be associated with extreme violence, as the sacroiliac ligaments are the strongest in the human body (Fig. 20).

Type C1.3 deals with fractures of the sacrum caused by high-energy shearing forces.

Type C2 stands for bilateral injuries of the pelvis ring in which one side remains partially stable and thus corresponds to a type-B injury, e.g., in sacral fractures, whereas the opposite relates to an unstable type-C injury, such as an iliac fracture (Fig. 21).

Type C3 deals with bilateral injuries in which both hemi-pelves are unstable (Fig. 22).

### Incidence

Type-A lesions represent to 52%, type B to 27%, and type C to 21% of all cases [50]. Type-B and type-C lesion percentage grows with the speed implied in the trauma.



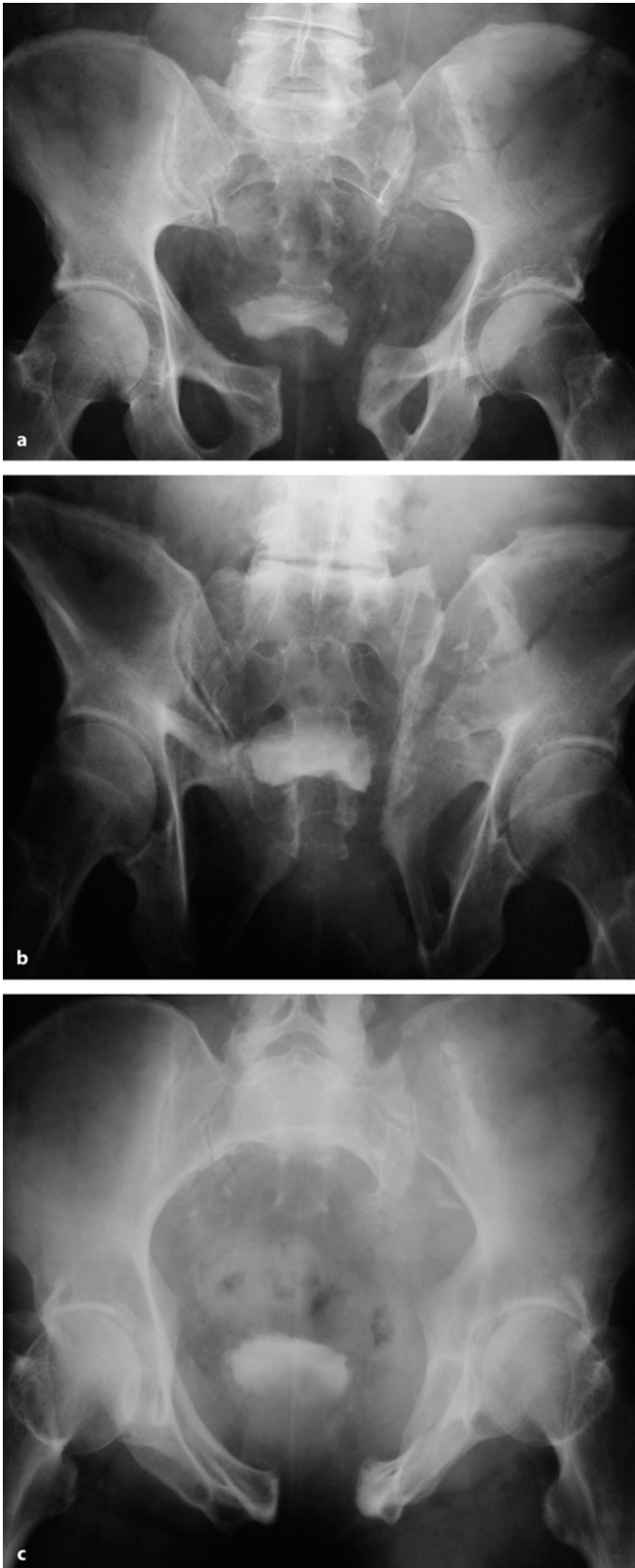


**Fig. 20.** Type-C1.2 fracture. Major trauma, unstable fracture of pelvic ring. **a** Antero-posterior view. Symphyseal diastasis, left sacroiliac disruption and iliac wing fracture. **b** Outlet view. Note the ascension of the left hemi-pelvis related to complete posterior ligaments disruption. **c** The inlet view confirms the posterior displacement of the left iliac wing. **d** Same patient after temporary external fixation. **e** Same patient after internal fixation

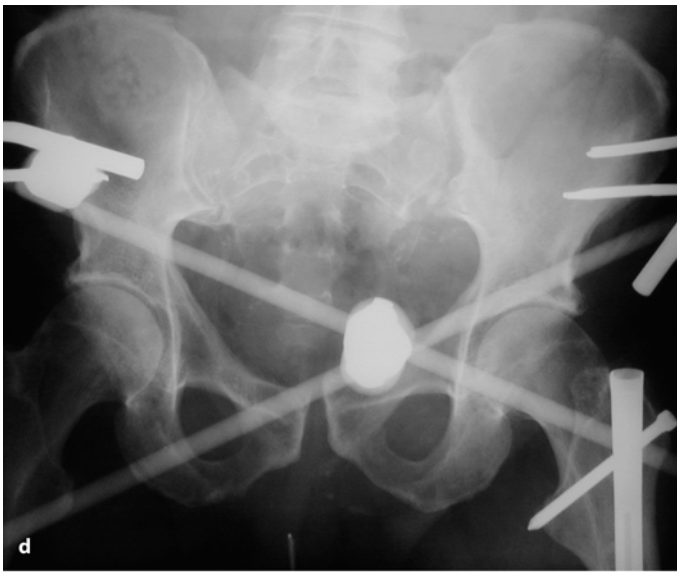


Fig. 20. (continued)





**Fig. 21.** Type-C2. fracture. Bilateral sacral fracture complete on the right (unstable) and incomplete on the left side (stable). A) AP view. Bilateral pubic rami fractures and right sacral fracture . (Note the rupture of right arcuate lines). B) Axial CT scan.



**Fig. 22.** Type-C3. fracture. Bilateral instability. Antero-posterior view. Bilateral iliac wing fractures, symphyseal disjunction

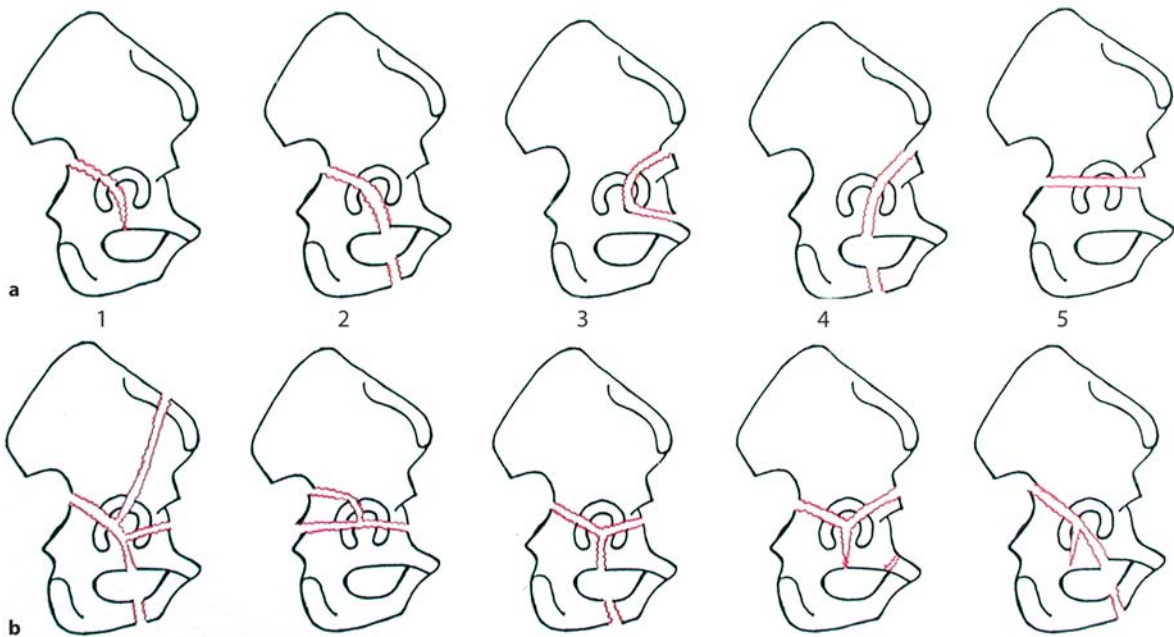


**Fig. 23.** Acetabular fractures. Letournel's and Judet's classification. **a** Elementary fractures. 1 Posterior wall fracture; 2 posterior column fracture; 3 anterior wall fracture; 4 anterior column fracture; 5 transverse fracture. **b** Associated fractures. 1 Two-column frac-

ture; 2 transverse posterior wall fracture; 3 T-type fracture; 4 Anterior wall posterior hemi-transverse fracture; 5 posterior column posterior wall fracture

### 2.10.5.2 Classification of Acetabular Fractures

The study of acetabular trauma has to be closely connected to Letournel and Judet's works. After establishing the bases of standard radiography from outstanding anatomical studies, which allowed them to introduce the concept of the two columns of the hip bone, they developed a classification of acetabular fractures still in use at present [29, 33].

This classification is divided into ten patterns, consisting of five elementary and five associated patterns. (Fig. 23) Elementary fractures run in a single plane, whereas associated fractures are combinations of elementary patterns.

Elementary fractures are as follows:

1. Anterior wall fractures
2. Anterior column fractures
3. Posterior wall fractures
4. Posterior column fractures
5. Transverse fractures

Associated fractures are as follows:

1. T-shaped fractures
2. Complete two-column fractures
3. Transverse and posterior wall fractures
4. Posterior column and posterior wall fractures
5. Anterior column posterior hemi-transverse fractures (uncommon)

Acetabular fractures are uncommon, and thus, this classification remains difficult to remember; however, among

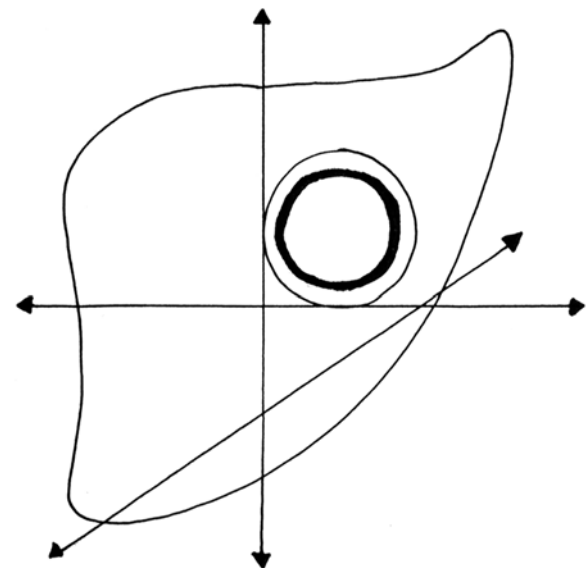


**Fig. 24.** The axial plane of main fracture orientation depending on fracture type. (Level: roof of the acetabulum). A Wall fracture. B Column fracture. C Transverse fracture

these ten fracture types, five of them are very common: complete two-column fracture, transverse, T-shaped, transverse with posterior wall, and posterior wall fractures constitute about 90% of acetabular fractures; thus, knowl-



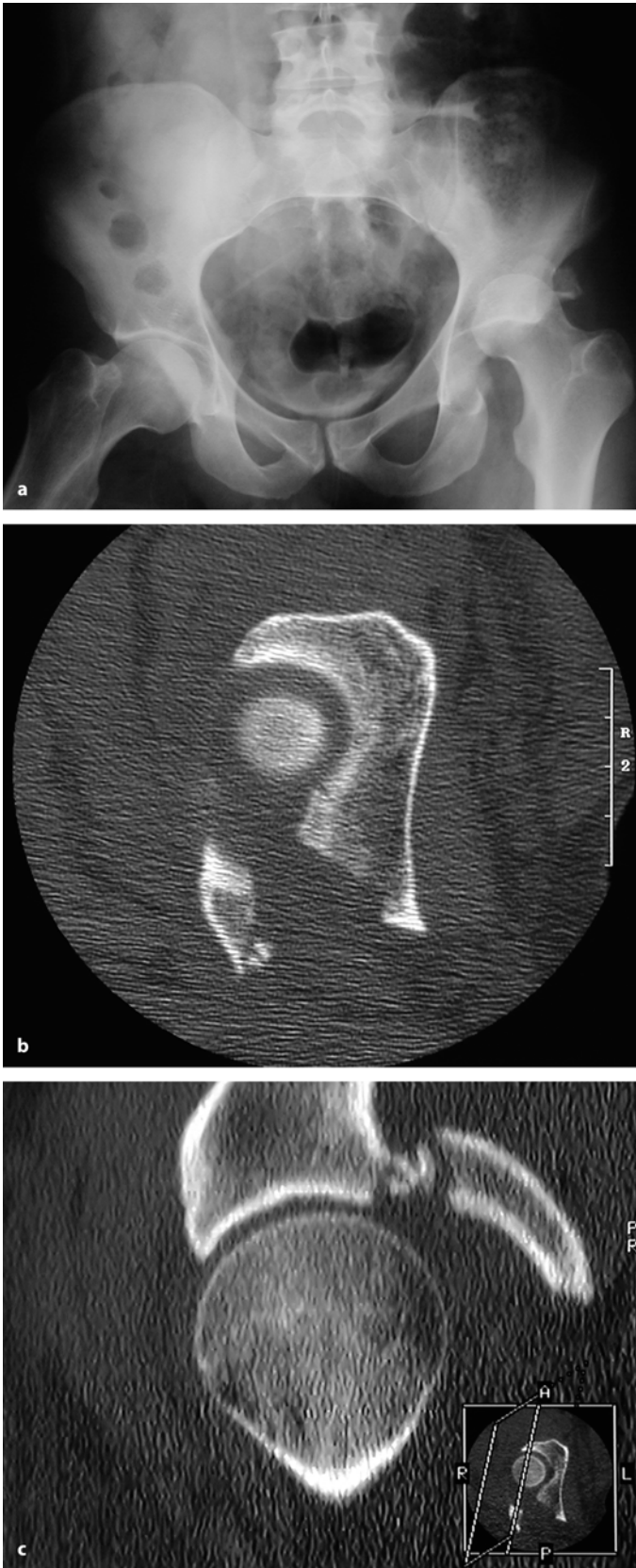


**Fig. 25.** Posterior wall fracture. **a** Antero-posterior view. **b** Axial CT scan. **c** A CT sagittal reconstruction confirms posterior wall fracture and suggests potential posterior instability



**Fig. 26.** Two-column fracture of the acetabulum. **a** Axial CT scan at the level of the roof of the acetabulum. **b,c** A 3D CT scan: two-column fracture of the acetabulum and pubic rami fractures

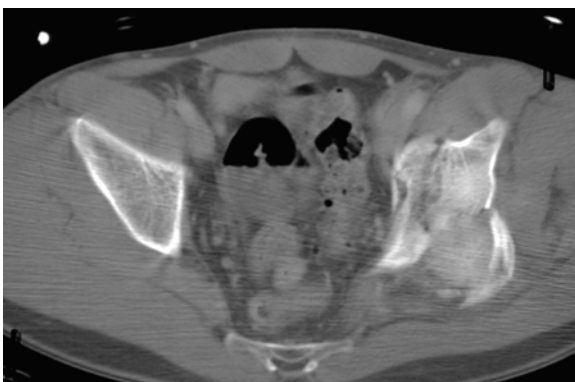
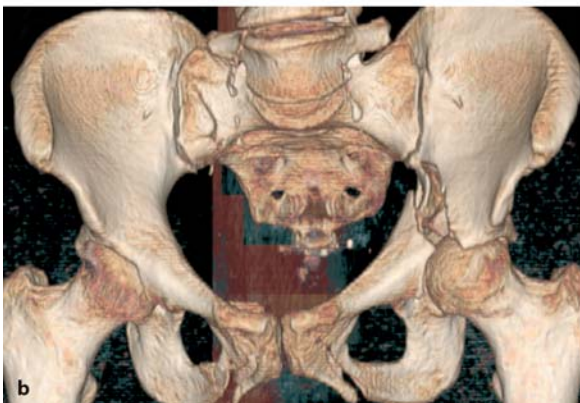


**Fig. 27.** Transverse posterior wall fracture. Axial CT scan. Note the sagittal fracture line and the tearing of the posterior wall associated with posterior luxation of the femoral head

edge of these five types allows correct assessment of 90% of all acetabular fractures [5]. Grouping the different categories could be another way to simplify this classification. Brandser et al. [5] suggest three major categories: trans-

verse-type fractures; column-type fractures; and wall-type fractures. Computed tomography is helpful in recognizing these three categories, by identifying main orientation fracture on a slice through the roof of the acetabulum (Fig. 24) [28, 32].

We prefer Tile's grouping [61] in anterior, posterior, and transverse fractures. In our experience, these groups are easier both to memorize and to identify from radiological data (Figs. 25–27).

#### Anterior Fractures

Anterior fractures include the anterior wall and the anterior column fractures. They are often associated with a pelvic fracture, and, as such, are considered as pelvic ring rather than acetabulum fractures. These injuries are caused by a lateral blow to the greater trochanter when the leg is externally rotated. An anterior hip dislocation is rarely associated, when compared with posterior fracture types, and is almost always associated with posterior hip dislocation. With anterior injury, the complications are less frequent and the overall prognosis remains better than in

other types [61]. The anterior wall fracture usually begins at the anterior–inferior iliac spine and passes below through the cotyloid fossa, up to the junction of the articular dome and the superior ramus. The anterior column fracture is characterized by a fracture line that extends from the middle of the pubic ramus to any point above the anterior segment of the iliac crest [46].

### Posterior Fracture

Posterior fractures include the posterior wall and the posterior column fractures. Posterior fractures are usually caused by a blow to the flexed knee (also called “dashboard” injury), and therefore associated knee injuries are common. Posterior dislocation of the hip is frequent and almost always present when the posterior wall is fractured. This complication affects the prognosis, since the prevalence of vascular necrosis and sciatic nerve lesions is markedly increased [61]. The posterior wall fracture is identified by a disruption of the posterior border, best seen on the obturator oblique view. The posterior column fracture is completely detached, because it usually originates in the greater sciatic notch and crosses the weight-bearing dome and the obturator foramen. The plain film shows medial displacement of the femoral head [46].

### Transverse and T-Type Fractures

Transverse and T-type fractures are commonly caused by high-energy shearing forces. They appear simple but often have the worst prognosis. In a pure transverse fracture, the fracture line extends transversely from the anterior to the posterior column. So the weight-bearing dome portion remains attached to the ilium. This type of fracture presents three subdivisions: (a) the transtectal transverse fracture which goes through the weight-bearing dome; (b) the juxtatectal transverse fracture, which occurs just above the cotyloid fossa; (c) the infratectal transverse fracture, which affects the whole weight-bearing dome. The T-type fracture essentially consists in a transverse fracture with a vertical component, splitting the cotyloid fossa. The posterior column thus becomes a loose fragment [46].

## 2.10.6 Pelvic Trauma Management

### 2.10.6.1 Clinical Evaluation

Cross questioning and anamnesis should define the type and mechanism of trauma. A high-energy mechanism relates to crush lesions, traffic accidents, and defenestration, whereas a low-energy mechanism has the characteristics of confounding or muscular contractions. Defining the initial shock spot leads to a particular mechanism and a certain type of lesion: AP compression relates to “open-book”

lesions; lateral impact on the great trochanter or iliac wing is associated with rotation lesions; and shearing strain in axial trauma on one or both members (defenestration, dashboard syndrome) connects with unstable lesions of the posterior ring. Investigation should look for impact lesions or graze on the pelvis, whereas clinical check-up should look for pain at palpation or pelvic manipulation. The value of this clinical investigation varies according to the patient’s state, as follows:

- In a patient without spinal column lesion, a normal clinical status of the pelvis rules out pelvic ring fracture, and thus radiological investigation need not be performed [57, 73].
- On the other hand, if pain occurs at palpation or manipulation, or if the clinical findings cannot be trusted for sure (unconscious or intoxicated patient, spinal column lesion), radiological investigation is mandatory; however, one must be careful in pelvic clinical evaluation, which may lead to aggravation of fracture displacement or hemorrhage.

### 2.10.6.2 Imaging Strategies

Initial clinical evaluation leads to different situations, as given below.

#### Minor Trauma Limited to the Hip

Radiological appraisal must include four basic incidences: AP pelvic view; front-hip view; and oblique views. Normal views of good quality can rule out fractures. In case of doubt or recognized lesion, further exploration with CT is highly advisable. It allows confirmation of fractures, definition of characteristics, and it allows the radiologist to look for associated lesions and plan surgical management.

#### Major Trauma

It should be carefully analyzed, whether it is a predominant pelvic trauma or a complex trauma, in a conscious or unconscious patient (see Table). In any case, the patient must be considered as polytraumatized with possible hidden visceral or osseous lesions. Radiological assessment must be included in a multidisciplinary approach and correspond to pre-established protocols in order to optimize management, as follows:

- First, AP pelvic view as well as AP thoracic and profile cervical spine views should be performed in any patient. Inlet and outlet views may complete assessment, systematically or on request.
- The patient’s hemodynamic state will then determine further treatment. If the patient’s hemodynamic situation is unstable, treatment of hemorrhage is the priority. Bedside US abdominal screening must be performed. In case of abnormal US or thoracic views, hem-

**Table 2.** Young–Burgess classification of pelvic fractures. *SP* symphysis pubis, *ST* sacrotuberous ligament, *SS* sacrospinous ligament, *ASI* anterior sacroiliac ligaments, *PSI* posterior sacroiliac ligaments; *R* rotationally, *V* vertically, *P* posteriorly

Fracture type	Classification	Features	Stability
Anterior compression	Antero-posterior compression: types I–III	External rotation or “open-book” injuries Type I: SP disrupted ST, SS, ASI, and PSI spared Type II: SP, ST, SS, and ASI disrupted PSI spared Type III: SP, ST, SS, ASI, and PSI disrupted	Type I: stable Type II: R unstable, V, and P stable Type III: R, V, and P unstable
Lateral compression	Lateral compression: types I–III	Internal rotation injuries Type I: ipsilateral sacral compression Type II: type I with associated iliac wing fracture Type III: types I or II with contralateral “open-book” injury (“windswept pelvis”)	Type I: stable Type II: R unstable, V stable Type III: R unstable, V stable
Vertical shear	Vertical shear	Disruption of SP, ST, SS, ASI, and PSI Vertical displacement of one hemipelvis Posterior disruption may include sacral or iliac fractures with sparing of ASI and PSI	R, V, and P unstable
Complex	Complex	Variable	Variable

orrhage management is suggested first. In case of isolated pelvis fracture with normal US and thoracic views, indication for angiography with possible hemostatic embolization must be decided (after external pelvic fixation). In case of stable hemodynamics, complete body lesion (visceral and osseous) assessment should be performed. Thoracic, abdominal, and pelvic investigation is advisable in the same examination, with whole-body CT (as described above). This leads to the more specific and least time-consuming assessment and allows better therapeutic management.

### 2.10.6.3 Treatment

The great variety of clinical situations explains the diversity of possible treatments. Some principles can be established, keeping in mind that therapeutic indications rely upon precise lesion assessment [4, 62, 63].

In case of pelvic ring lesions, stabilization of patient’s hemodynamics must first be achieved. This may consist of external fracture stabilization, surgical hemostatic treatment, or hemostatic embolization. The radiologist has to know the importance of angiography in the management of hemorrhagic blows in pelvic trauma (techniques and indications are developed in another chapter). The external fixation of fracture is essential for hemodynamic stabilization, contributing to hemostasis [69, 70]. A 2-cm symphyseal diastasis can increase pelvic volume in the adult from a normal of 1.5 l to as much as 5 l [28].

After completing hemostasis, the choice of orthopedic management will rely upon the associated visceral (neurological, thoracic, or abdomino-pelvic) or osseous (femoral or acetabular) lesions. Type-A lesions rarely lead to surgical fixing. Type-B or type-C lesions usually need osteosynthesis. Because of the complexity of type-C lesions, a clear

evaluation of the real profit implied by surgical fixing must be made. This should consider neurological complications, skin necrosis, or sepsis. If surgery is required, it must be completed within the first 3 weeks after trauma to prevent lesions from fixing or turning irreducible. If performed, internal fixation allows easier reduction and stabilization of fracture and facilitates patient mobilization.

For the acetabulum, emergencies consist of the associated displacement of the femoral head, which must be reduced immediately. A suspected injury of the gluteal artery with a sciatic notch fracture is also an emergency and has to lead to angiography with possible embolization in mind. In other cases, reduction of an acetabular fracture is not an emergency and best recovers when treated within the third to seventh day after trauma. In all cases, the main preoccupation must lie in the restoration of the articular congruence in order to prevent early coxarthrosis; however, the indications are often difficult to treat, due to fracture complexity, age, osseous potential, and associated lesions.

In cases of association of pelvic ring and acetabular fractures, priority is given to management of pelvic ring fracture.

## 2.10.7 Complications

### 2.10.7.1 Death Rate

The death rate in pelvic trauma ranges between 5 and 15%, but may reach 50% of cases [9, 13, 15, 16, 24, 41, 49, 55].

The cause of death directly relates to pelvic trauma in 12% of cases [41]. This rate is closely connected to the associated lesions, to the importance of trauma, and to the patient’s age [25, 56]. The Injury Severity Score (ISS) and patient’s hemodynamic state seem to be the best prognos-



tic features. The value of the fracture type as a prognostic tool has also been evoked. In Pohlemann's series, death rate amounts to 11.7% in the type A, 14.9% in the type B, and 23% in the type C [48]. The best prognostic improvement factors are multidisciplinary management and early fracture fixing [6, 47, 54]. For a same ISS and comparable age group, the death rate can be reduced three times in cases of early fracture management [3].

In pelvic fractures with intense bleeding, mainly in cases of pelvic ring disruption, transfusion is mandatory in nearly 50% of cases [13]. These hemorrhages cause half of the fatalities [51] and may sometimes occur in isolated acetabular lesions.

### 2.10.7.2 Associated Lesions

Associated vascular and visceral lesions are frequent and are discussed in another chapter. Briefly, brain lesions occur in 26–55%, and abdominal lesions in 16–26%, of cases [1, 55, 58]. Pulmonary lesions are frequent, with aortic isthmus rupture occurrences increased six times when associated with pelvis fractures [12, 43, 44]. Lower urinary track lesions are found in 4–17% of cases in the urethra and 5–25% of cases in the bladder [11, 27, 34, 55, 68]. Anorectal or gynecological lesions are rare and most often secondary to open trauma. Peripheral nerve lesions represent 10% of cases, mainly complicating sacrum fractures (40% of cases) [53]. Posterior femoral head dislocation goes along with sciatic lesions in 20% of cases [32].

## 2.10.8 Conclusion

Pelvic fractures form a polymorphous group, described as follows:

- In the isolated acetabular fractures, function is mainly at stake. Radiological assessment relies upon good-quality plain films completed by CT imaging in fine slices with MPR. Letournel's classification remains the reference. Management mainly consists of re-establishing a joint congruence to prevent early coxarthrosis.
- Pelvic fractures often occur in violent trauma and are associated with visceral lesions, putting vital prognosis at stake. Radiological assessment must be included in multidisciplinary management and CT imaging stands for the most complete and least time-consuming device, allowing for investigation of both visceral and osseous lesions. In cases of hemodynamic shock, external fracture stabilization and embolization of pelvic bleeding are preponderant. Tile/AO's classification is the most used classification at present. It allows good description of mechanisms and lesions and more adaptable management.

## References

1. Ben-Menachem Y, Coldwell DM, Young JW, Burgess AR (1991) Hemorrhage associated with pelvic fractures: causes, diagnosis, and emergent management. *Am J Roentgenol* 157:1005–1014
2. Berg EE, Chebuhar C, Bell RM (1996) Pelvic trauma imaging: a blinded comparison of computed tomography and roentgenograms. *J Trauma* 41:994–998
3. Bone LB, McNamara K, Shine B, Border J (1994) Mortality in multiple trauma patients with fractures. *J Trauma* 37:262–265
4. Bonneville P (1996) Rupture de l'anneau pelvien. *Encycl Med Chir*:14-072-A-10
5. Brandser E, El-Khoury G, Marsh J (1995) Acetabular fractures: a systematic approach to reclassification. *Emerg Radiol* 2:18–28
6. Browner BD, Cole JD, Graham JM, Bondurant FJ, Nunchuck-Burns SK, Colter HB (1987) Delayed posterior internal fixation of unstable pelvic fractures. *J Trauma* 27:998–1006
7. Bucholz RW (1981) The pathological anatomy of Malgaigne fracture: dislocations of the pelvis. *J Bone Joint Surg Am* 63:400–404
8. Buckwalter KA, Rydberg J, Kopecky KK, Crow K, Yang EL (2001) Musculoskeletal imaging with multislice CT. *Am J Roentgenol*; 176:979–986
9. Burgess AR, Eastridge BJ, Young JW, Ellison TS, Ellison PS Jr, Poka A, Bathon GH, Brumback RJ (1990) Pelvic ring disruptions: effective classification system and treatment protocols. *J Trauma* 30:848–856
10. Chaumoitre K, Portier F, Petit P, Merrot T, Guillon PO, Panuel M (2000) CT imaging of pelvic injuries in polytrauma patients. *J Radiol* 81:111–120 [in French]
11. Colapinto V (1980) Trauma to the pelvis: urethral injury. *Clin Orthop Relat Res*:46–55
12. Conolly WB, Hedberg EA (1969) Observations on fractures of the pelvis. *J Trauma* 9:104–111
13. Cryer HM, Miller FB, Evers BM, Rouben LR, Seligson DL (1988) Pelvic fracture classification: correlation with hemorrhage. *J Trauma* 28:973–980
14. Daffner RH (1990) Pelvic trauma. In: McCort JJ, Mindelzun RE (eds) Churchill Livingstone, New York, pp 339–380
15. Dalal SA, Burgess AR, Siegel JH, Young JW, Brumback RJ, Poka A, Dunham CM, Gens D, Bathon H (1989) Pelvic fracture in multiple trauma: classification by mechanism is key to pattern of organ injury, resuscitative requirements, and outcome. *J Trauma* 29:981–1002
16. Davidson BS, Simmons GT, Williamson PR, Buerk CA (1993) Pelvic fractures associated with open perineal wounds: a survivable injury. *J Trauma* 35:36–39
17. Eastridge BJ, Burgess AR (1997) Pedestrian pelvic fractures: 5-year experience of a major urban trauma center. *J Trauma* 42:695–700
18. Ersoy G, Karcioğlu O, Enginbas Y, User N (1995) Should all patients with blunt trauma undergo "routine" pelvic X-ray? *Eur J Emerg Med* 2:65–68
19. Federle M (1995) Should patients who undergo CT scanning of the abdomen for blunt trauma always have a CT scan of the pelvis as well, regardless of the severity and location of the trauma? *Am J Roentgenol* 164:762
20. Gansslen A, Pohlemann T, Paul C, Lobenhoffer P, Tschernke H (1996) Epidemiology of pelvic ring injuries. *Injury* 27 (Suppl 1):S-A13-20
21. Geusens E, Brys P, Maleux G, Janzing H (2000) Imaging in pelvic trauma. *JBR-BTR* 83:173–180
22. Gill K, Bucholz RW (1984) The role of computerized tomographic scanning in the evaluation of major pelvic fractures. *J Bone Joint Surg Am* 66:34–39
23. Goulet JA, Bray TJ (1989) Complex acetabular fractures. *Clin Orthop Relat Res*:9–20

24. Gruen GS, Leit ME, Gruen RJ, Peitzman AB (1994) The acute management of hemodynamically unstable multiple trauma patients with pelvic ring fractures. *J Trauma* 36:706–711
25. Gustavo Parreira J, Coimbra R, Rasslan S, Oliveira A, Fregoneze M, Mercadante M (2000) The role of associated injuries on outcome of blunt trauma patients sustaining pelvic fractures. *Injury* 31:677–682
26. Harley JD, Mack LA, Winquist RA (1982) CT of acetabular fractures: comparison with conventional radiography. *Am J Roentgenol* 138:413–417
27. Heare MM, Heare TC, Gillespy T III (1989) Diagnostic imaging of pelvic and chest wall trauma. *Radiol Clin North Am* 27: 873–889
28. Hunter JC, Brandser EA, Tran KA (1997) Pelvic and acetabular trauma. *Radiol Clin North Am* 35:559–590
29. Judet R, Judet J, Letournel E (1964) Fractures of the acetabulum: classification and surgical approaches for open reduction. Preliminary report. *J Bone Joint Surg Am* 46:1615–1646
30. Kellam P, Browner B (1992) Fractures of the pelvic ring. In: Browner BD, Jupiter JB, Levine AM, Trafton PG (eds) *Skeletal trauma*. Saunders, Philadelphia, pp 849–897
31. Killen KL, DeMeo JH (1999) CT detection of serious internal and skeletal injuries in patients with pelvic fractures. *Acad Radiol* 6:224–228
32. Laude F, Puget J, Martimbeau C (1999) Fracture du cotyle. *Encycl Med Chir*:14-073-A-10
33. Letournel E (1993) Fracture of the acetabulum, 2nd edn. Springer, Berlin Heidelberg New York
34. MacCort J, Mindelzun R (1994) Bladder injury and pelvic fractures. *Emerg Radiol* 1:47–51
35. MacLeod M, Powell JN (1997) Evaluation of pelvic fractures. Clinical and radiologic findings. *Orthop Clin North Am* 28: 299–319
36. Martinez CR, Pasquale TG di, Helfet DL, Graham AW, Sanders RW, Ray LD (1992) Evaluation of acetabular fractures with two- and three-dimensional CT. *Radiographics* 12:227–242
37. Mayo KA (1987) Fractures of the acetabulum. *Orthop Clin North Am* 18:43–57
38. McIntyre RC Jr, Bensard DD, Moore EE, Chambers J, Moore FA (1993) Pelvic fracture geometry predicts risk of life-threatening hemorrhage in children. *J Trauma* 35:423–429
39. Melton LJ III, Sampson JM, Morrey BF, Ilstrup DM (1981) Epidemiologic features of pelvic fractures. *Clin Orthop Relat Res*:43–47
40. Montana MA, Richardson ML, Kilcoyne RF, Harley JD, Shuman WP, Mack LA (1986) CT of sacral injury. *Radiology* 161: 499–503
41. Mucha P Jr, Farnell MB (1984) Analysis of pelvic fracture management. *J Trauma* 24:379–386
42. Muller M, Allgower M, Schneider R (1990) *Manual of internal fixation*, 3rd edn. Springer, Berlin Heidelberg New York
43. Ochsner MG Jr, Champion HR, Chambers RJ, Harviel JD (1989) Pelvic fracture as an indicator of increased risk of thoracic aortic rupture. *J Trauma* 29:1376–1379
44. Ochsner MG Jr, Hoffman AP, Pasquale D di, Cole FJ Jr, Rozycki GS, Webster DW, Champion HR (1992) Associated aortic rupture–pelvic fracture: an alert for orthopedic and general surgeons. *J Trauma* 33:429–434
45. Pennal G, Sutherland G (1961) Fractures of the pelvis. American Academy of Orthopaedic Surgeons Film Library
46. Perry DC, DeLong W (1997) Acetabular fractures. *Orthop Clin North Am* 28:405–417
47. Phillips TE, Contreras DM (1990) Timing of operative treatment of fractures in patients who have multiple injuries. *J Bone Joint Surg Am* 72:784–788
48. Pohlemann T, Bosch U, Gansslen A, Tscherne H (1994) The Hannover experience in management of pelvic fractures. *Clin Orthop Relat Res*:69–80
49. Pohlemann T, Gansslen A, Stief CH (1998) Complex injuries of the pelvis and acetabulum. *Orthopade* 27:32–44 [in German]
50. Pohlemann T, Richter M, Otte D, Gansslen A, Bartram H, Tscherne H (2000) Mechanism of pelvic girdle injuries in street traffic. Medical-technical accident analysis. *Unfallchirurg* 103:267–274 [in German]
51. Poole GV, Ward EF, Muakkassa FF, Hsu HS, Griswold JA, Rhodes RS (1991) Pelvic fracture from major blunt trauma. Outcome is determined by associated injuries. *Ann Surg* 213:532–539
52. Potter HG, Montgomery KD, Heise CW, Helfet DL (1994) MR imaging of acetabular fractures: value in detecting femoral head injury, intraarticular fragments, and sciatic nerve injury. *Am J Roentgenol* 163:881–886
53. Rai SK, Far RF, Ghovanlou B (1990) Neurologic deficits associated with sacral wing fractures. *Orthopedics* 13:1363–1366
54. Riemer BL, Butterfield SL, Diamond DL, Young JC, Ravess JJ, Cottsington E, Kislak K (1993) Acute mortality associated with injuries to the pelvic ring: the role of early patient mobilization and external fixation. *J Trauma* 35:671–677
55. Rogers L (1992) *Radiology of skeletal trauma*, 2nd edn. Churchill Livingstone, New York, pp 991–1105
56. Routh M (1993) Pelvic fractures. In: Hansen ST, Swiontkowski MF (eds) *Orthopaedic trauma protocols*. Raven Press, New York, pp 225–236
57. Salvino CK, Esposito TJ, Smith D, Dries D, Marshall W, Flisak M, Gamelli RL (1992) Routine pelvic X-ray studies in awake blunt trauma patients: a sensible policy? *J Trauma* 33:413–416
58. Siegmeth A, Mullner T, Kukla C, Vecsei V (2000) Associated injuries in severe pelvic trauma. *Unfallchirurg* 103:572–581 [in German]
59. Their ME, Bensch FV, Koskinen SK, Handolin L, Kiuru MJ (2005) Diagnostic value of pelvic radiography in the initial trauma series in blunt trauma. *Eur Radiol* 15:1533–1537
60. Tile M (1988) Pelvic ring fractures: Should they be fixed? *J Bone Joint Surg Br* 70:1–12
61. Tile M (1995) Fractures of the pelvis and acetabulum. Lippincott Williams and Wilkins, Baltimore
62. Tile M (1996) Acute pelvic fractures: I. Causation and classification. *J Am Acad Orthop Surg* 4:143–151
63. Tile M (1996) Acute pelvic fractures: II. Principles of management. *J Am Acad Orthop Surg* 4:152–161
64. Vas WG, Wolverson MK, Sundaram M, Heiberg E, Pilla T, Shields JB, Crepps L (1982) The role of computed tomography in pelvic fractures. *J Comput Assist Tomogr* 6:796–801
65. Vazquez WD, Garcia VF (1993) Pediatric pelvic fractures combined with an additional skeletal injury is an indicator of significant injury. *Surg Gynecol Obstet* 177:468–472
66. Watura R, Cobby M, Taylor J (2004) Multislice CT in imaging of trauma of the spine, pelvis and complex foot injuries. *Br J Radiol* 77 (Spec no 1):S46–S63
67. Wedegartner U, Gatzka C, Rueger JM, Adam G (2003) Multislice CT (MSCT) in the detection and classification of pelvic and acetabular fractures. *Rofo* 175:105–111 [in German]
68. Werkman HA, Jansen C, Klein JP, Ten Duis HJ (1991) Urinary tract injuries in multiply-injured patients: a rational guideline for the initial assessment. *Injury* 22:471–474
69. Wolinsky PR (1997) Assessment and management of pelvic fracture in the hemodynamically unstable patient. *Orthop Clin North Am* 28:321–329
70. Yang AP, Iannacone WM (1997) External fixation for pelvic ring disruptions. *Orthop Clin North Am* 28:331–344
71. Young J, Burgess A (1987) Radiological management of pelvic ring fracture. Urban and Schwarzenberg, Baltimore
72. Young JW, Burgess AR, Brumback RJ, Poka A (1986) Pelvic fractures: value of plain radiography in early assessment and management. *Radiology* 160:445–451
73. Yugueros P, Sarmiento JM, Garcia AF, Ferrada R (1995) Unnecessary use of pelvic X-ray in blunt trauma. *J Trauma* 39:722–725



# Traumatic Injuries: Imaging of Peripheral Musculoskeletal Injuries

M.A. Müller, S. Wildermuth, K. Bohndorf

## 2.11

### Contents

2.11.1	Introduction	251
2.11.2	General Part: Imaging Modalities	251
2.11.2.1	Conventional Radiography (Projection Radiography)	251
2.11.2.2	Computed Tomography	252
2.11.2.3	Magnetic Resonance Imaging	252
2.11.2.4	Ultrasound	253
2.11.3	Soft Tissue Injuries in General	253
2.11.3.1	Muscle Injuries	253
2.11.3.2	Tendinous and Ligamentous Injuries on US	254
2.11.4	Upper Extremity	254
2.11.4.1	The Clavicle and its Articulations	254
2.11.4.2	Shoulder and Proximal Humerus	256
2.11.4.3	Elbow	260
2.11.4.4	Distal Forearm and Wrist	265
2.11.4.5	Metacarpals and Fingers	271
2.11.5	Lower Extremity	273
2.11.5.1	Hip	273
2.11.5.2	Knee	276
2.11.5.3	Ankle	282
2.11.5.4	Foot	285
	References	288

### 2.11.1 Introduction

Since the publication of the first peripheral musculoskeletal radiograph in Roentgen's first description of X-rays in 1895, demonstrating a hand, projection radiography has remained the most important and, in many cases the only needed, imaging modality for fracture and other musculoskeletal injury diagnosis. The clinical importance of this radiographic application is illustrated by the rapid diffusion of X-ray knowledge in the first years after its discovery, as shown by the following example: One of the first known clinical applications of radiology in soft tissue imaging and searching for foreign bodies for preoperative assessment was performed 1897, not in a big city but in the village of Poschiavo in a secluded valley in Switzerland [67].

In past years, computed tomography (CT) has gained an important place in the emergency evaluation of fractures and in planning surgery of complex injuries. Magnetic resonance imaging (MRI) and ultrasound (US) are important imaging modalities in the evaluation of soft tissues in addition to the clinical examination.

### 2.11.2 General Part: Imaging Modalities

#### 2.11.2.1 Conventional radiography (Projection radiography)

Two projections perpendicular to each other preceded by clinical examination are generally the first and often the only necessary diagnostic approach in evaluation of extremity trauma. Clinical prediction rules and cost-effectiveness analyses are valuable evidence-based tools for selecting optimal imaging approaches [1]. Conventional radiographs can almost always be obtained under difficult circumstances, like in the acute setting of severe trauma and in unstable patients. Surgical planning is guided primarily by clinical and conventional radiographic findings. General fracture signs are radiolucent fracture lines, cortical discontinuities or angulations, and periosteal and trabecular irregularities. Radiodense lines can represent impacted fractures. In general, conventional radiography diagnoses fractures quickly and provides relevant information as to whether the adjacent joint is involved and about the position and number of fracture fragments. Due to the divergence of the X-ray beam, the region of interest should be centered on the image to minimize contortion of relevant structures, leading, for example, to widening of fracture lines in the film periphery. In the evaluation of the shaft of a long bone, it is necessary to include both adjacent joints in the examination. In skeletal regions with complex anatomy or superimposed soft tissues, additional special views designed to eliminate superimposed structures can be used, but sometimes further imaging modalities are used to complete the assessment. Following treatment, conventional radiographs are mandatory to confirm treatment results and clinical diagnosis of possible complica-



tions such as infection, reflex osteodystrophy, or inadequate internal fixation.

In evaluation of soft tissue injury, conventional radiographs have limited value. In some joints, soft tissue changes can be used as indirect fracture signs. If clinical examination is not conclusive, further evaluation of soft tissue injuries is usually performed with US or MRI.

Digital techniques allow new features for acquisition, post-processing, interpretation, reporting and storage of images. Advantages are obvious in the acute trauma setting. Becoming filmless is also an important progress in a continuous evaluation of the healing process, because there is no further searching for lost films.

The role of conventional tomography and arthrography has declined. Arthrography is presently mostly performed before a CT or MRI examination.

---

### 2.11.2.2 Computed tomography

Display of complex fractures and assessment of fracture extension into joint surfaces are the main indications for CT imaging in the acute trauma setting. Most peripheral body parts can be positioned to prevent exposure of radiation-sensitive tissues. Multidetector CT (MDCT) has improved the ability to image patients with skeletal trauma. Advantages of MDCT include extremely short scan times, the ability to produce very high-quality multiplanar reformations (MPR), and 3D reconstructions based on the ability to acquire virtually isotropic images. Computed tomography of bony structures requires high spatial resolution. The thinnest possible slice width and a bone-reconstruction algorithm will maximize image quality. Imaging of large joints, such as the shoulder, requires slightly thicker slices to ensure reasonable image quality, particularly if surface rendering is to be performed [2]. The use of high kilovoltage levels increases the likelihood of penetrating the bone. The limiting factor becomes the level of noise in the reconstructed image set. Submillimeter slices can be used to demonstrate minimally depressed fractures. The higher the kernel number, the sharper the image; therefore, detailed or sharp reconstruction algorithms are recommended for single slices. In contrast, for 3D imaging, there is the smoothest available kernel recommended for lowering the noise in the original slices; therefore, production of two image sets from the raw data is required. Overlap of 20% for image reconstruction will give good image quality for most routine scans [3]. Besides transversal slices, MPR should be the first modality of assessment because 3D reconstructions can obscure fine detail. A 3D shaded-surface display (SSD) and volume-rendering technique (VRT) can show articular surfaces. As volume rendering makes use of the entire acquired volume data set and does not use intermediate geometrical representations, such as polygons in SSD, it overcomes the problem of accurate representation

of surfaces [4]. The possibility to visualize structures beneath the surface while still seeing the surface, and especially the display of minimal displaced fractures and dislocated fragments together with the fact that volume rendering is much less affected by hardware artifacts, favors the use of VRT.

The MDCT also is helpful in healing assessment following operative stabilization. In particular, the slice overlap and pitch of  $<1$  create a substantial flux, which allows for imaging through orthopedic hardware [5]. High-milliampere technique reduces metallic artifact (titanium produces the least artifacts, cobalt chrome the most).

With CT arthrography, also ligamentous injuries can be detected. The technique is particularly useful in patients who require multiplanar imaging for preoperative planning and patients who cannot undergo MR arthrography. The CT arthrography can be a valuable imaging choice for the evaluation of the postoperative menisci [6]. Advantages of CT arthrography include higher spatial resolution and often minimal metallic artifacts.

---

### 2.11.2.3 Magnetic Resonance Imaging

Magnetic resonance imaging has improved diagnostic imaging of traumatic ligamentous, muscle, and tendon lesions, and is the preferred method of investigation for stress and insufficiency fractures. T2-weighted images are highly sensitive to bone marrow edema. Presence of bone marrow edema and absence of a fracture line is suggestive of trabecular microfracture. Computed tomography is an alternative in imaging stress fractures, but is generally less sensitive particularly in absence of a fracture line. Magnetic resonance arthrography can be performed as direct technique with intraarticular contrast medium injection – in acute traumatized joints, joint effusion can have the same effects – or as indirect technique with intravenous administration of contrast medium. Indications for direct and indirect arthrography are sometimes controversial [7]. When imaging ligaments and tendons, it is important to be aware of the magic-angle phenomenon. This artifact can lead to a signal increase in fibrous strictures which are crossing the vector of the magnetic field at an angle of about  $55^\circ$ . Sequences with a short echo time are most vulnerable to this phenomenon.

Recent studies have tried to assess the value of a short dedicated extremity MRI examination in different anatomic regions in the acute emergency setting for prediction of need for treatment. In the ankle, although there is high sensitivity in the detection of occult fractures, the sensitivity in detection of avulsion fractures is low. The radiographic result as a single predictor of the need for therapy appeared to be of higher predictive value than the MRI result. An MRI in the initial evaluation of ankle trauma may be valuable in a setting where ruptured ankle ligaments are immediately re-

paired surgically [8], but actually this is not the case. In acute knee trauma, neither abnormal nor normal MRI results had significant added predictive value. A prediction of the need for treatment after acute knee trauma can be made on the basis of age, trauma mechanism, and the radiographic results [9], and MRI not seems to be useful. In the wrist, the addition of MRI leads to a significant increase in the power of patients who would need additional treatment, but MRI is not helpful in identification of patients who do not need further treatment [10]. The contribution of MRI was the identification of radiographically occult fractures of the scaphoid and the distal radius, and not the diagnosis of soft tissue injury; therefore, emergency MRI should usually remain reserved for the brain and spine.

#### 2.11.2.4 Ultrasound

Ultrasound can play an important role in musculoskeletal trauma. In the emergency setting, focused US is the first imaging modality in evaluation of muscle, tendon, and ligament injury if the results of the clinical examination have to be confirmed or are not conclusive. Advantages are easy availability, lack of radiation, low costs, functional imaging, and easy comparison with the noninjured contralateral side. Disadvantages are operator dependence, long learning curve, and the low consistency of the studies. The disadvantage of a limited field of view may be overcome with extended field of view functions.

High-resolution sonography can also reveal subtle changes of the bone surface not detected on plain radiographs, such as subperiosteal fluid collections, and can differentiate soft tissue lesions from bone lesions. Fractures can be visualized as “step-off” cortical disruption, angular, or buckle deformity of the cortex at the fracture site or subperiosteal blood/fluid collection and overlying soft tissue edema. Searching for fractures is impractical in clinical routine; however, skeletal areas overlying the trunk (sternum, ribs, clavicle) can be easily examined [11]. Intraarticular bone fragments can be best visualized in highly mobile joints (e.g., shoulder); however, interpretation of the deep articular portion remains problematic. Ultrasound can also be used to assess fracture healing in the early phase, where radiographic findings are subtle: the initial hypoechoic appearance of the fracture is replaced by the image of a hyperechoic callus, which increases in volume and casts a greater posterior shadow with maturation. Doppler sonography may demonstrate progressive formation of new vessels. This technique has also a potential value to demonstrate new bone formation and to measure the distraction gap in patients who undergo Ilizarov callus distraction procedures [12]. Ultrasound may also have potential in the detection of occult fractures and in the assessment of the joint cartilage in accessible locations.

Sonography is especially helpful in detecting radio-transparent foreign bodies. Foreign bodies that recently penetrated the skin can be difficult to see due to the artifact from air. One should mark the position of the foreign body on the skin and note the depth. The first imaging modality for searching foreign bodies remain conventional radiographs, because they demonstrate more exactly the size of the bodies [13].

## 2.11.3 Soft Tissue Injuries in General

### 2.11.3.1 Muscle Injuries

Muscle tears and sprains are very common, particularly in the lower limb. Muscles prone to injury are two-joint muscles such as biceps brachii, hamstring muscles, rectus femoris, and gastrocnemius. The muscle–tendon junction is most prone to injury. With US, three injury grades can be distinguished [14]: stretch injury shows in general a localized increase in echogenicity, but diffuse hypoechoic areas may also be observed (grade I). In partial tears, US reveals focal fiber disruption or hematoma that appear hypoechoic and are usually located at the muscle–tendon junction (grade II; Fig. 1). Complete muscle rupture shows the separated margins and mass-like appearance of the bunched retracted muscle (grade III). Magnetic resonance imaging is equally efficacious in detection, demonstrating hyperintense areas in T2-weighted images, but muscle edema can sometimes complicate the decision between grade-I and grade-II injuries.

Muscle contusion results in fibre disruption, often accompanied by intramuscular hematoma. Hematomas in US appear commonly well defined and oval; however, they may have irregular margins when associated with fibre disruption.

Sequelae of muscle injury include muscle hernias, best demonstrated with dynamic US evaluation, fibrous scarring (linear or stellate hyperechoic areas), calcific myonecrosis, and myositis ossificans, typically localized in the adductor muscles. Ultrasound is more efficient in demonstrating myositis ossificans compared with MRI, because of its higher sensitivity in demonstrating the calcifications in orientation in the long axis of the muscle. The MRI appearance of myositis ossificans can be confusing, and the differentiation from a soft tissue tumor can be difficult. In contrast to myositis ossificans, calcific myonecrosis shows amorphous calcification. Computed tomography as best image modality shows a plate-like calcification extending throughout at least one muscle compartment. Magnetic resonance imaging shows a partially cystic mass without soft tissue enhancement.

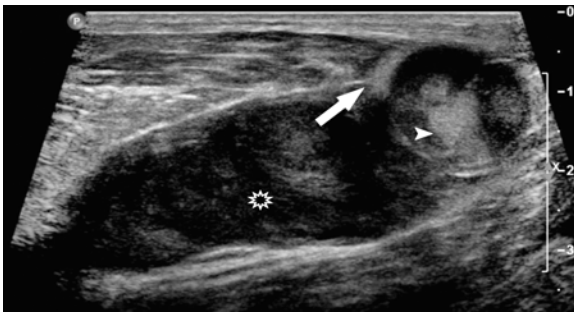


**Fig. 1.** Ultrasound image of the leg in the sagittal plane demonstrates a large hypoechoic blood collection (*asterisk*) with hyperechoic areas (*arrowhead*), consistent with coaguli, originating from the musculotendinous junction (*arrow*) of the medial gastrocnemius muscle

### 2.11.3.2 Tendinous and Ligamentous Injuries on US

The normal tendon is brightly echogenic with internal fibrillar pattern. One must be aware of the anisotropic property of tendons, which can produce focal hypoechoic pattern and has to be differentiated from a tendon defect. When a tendon sheath is present, partial tendon rupture is associated with a collection of fluid in the sheath and fluid-filled clefts within the tendon. In tendons without a sheath, a partial tear appears as hypoechoic cleft within the tendon. Diagnosis of a complete rupture in the acute stage is facilitated by the presence of fluid within the tendon sheath or by the presence of a hematoma separating the retracted ends of the tendon. Dynamic imaging is mandatory to reveal absence of the normal sliding motion during contraction and relaxation. Measuring the distance between the distant tendon ends in flexion and extension is important.

In acute ligamentous sprain, the following conditions can be seen: enlargement of the ligament; an anechoic zone crossing the ligament or replacing one end of the ligament; and an anechoic band following the superficial border of the ligament representing edema. Potential other signs are avulsion of the bony insertion, an anechoic zone forming a subcutaneous pouch, and edema of the subcutaneous tissue with lymphatic distension [15]. Clinical evaluation is often sufficient to correctly classify benign or severe sprains. Sonographic investigations are thus reserved for difficult and inconclusive cases. Every superficial ligament can be studied and compared with its counterpart on the other side, potentially avoiding misinterpretation.

## 2.11.4 Upper Extremity

### 2.11.4.1 The Clavicle and its Articulations

#### Clavicular Fractures

Clavicular fractures are common and were first described by Hippocrates in 400 BC. They are classified according to their localization. Most frequent are fractures within the middle third (group 1; Fig. 2). They are usually transverse and complete with a typical step-off at the fracture side. Pectoralis major, pectoralis minor, and latissimus dorsi pull the distal segment downward and medial, causing overriding of the medial fragment. Scapular rotation may rotate the distal segment. Trapezius and sternocleidomastoid also tend to distract the fracture segments. Important characteristics are the degree of angulation and the amount of override of the fracture components. Fractures of the lateral third (group 2) are commonly associated with injury to the coracoclavicular ligaments and should not be confused with acromioclavicular dislocation type 2 or type 3. They are subclassified according to the state of the coracoclavicular ligaments: intact (type I); detached from the medial fragment and maybe partially torn (type II; Fig. 3); and involvement of the articular surface without ligamentous injury (type III). Group-3 fractures are fractures of the medial third. Although the clavicle is the first bone to ossify, the medial clavicular epiphysis does not appear until the mid-teens and does not fuse until the mid-20s [16]; therefore, in children and young persons, fractures through the physal plate can be confused with sternoclavicular dislocations, but physal fractures are more likely.

Due to the specific anatomic position of the clavicle, one is not able to get two perpendicular views. The basic protocol is an anteroposterior (AP) view and a 45–50° cephalic angulated view (tangential view), which produces more detailed information about the medial aspect of the clavicle and about the AP relationship of fracture fragments. In addition, axillary views of the shoulder can be used to document the extent of fracture–dislocations in the AP direction. Standard radiographs may be inadequate to assess completely distal fractures. In this case, stress posteroanterior views of both shoulders with weights, and anterior and AP 45° oblique views are described as a possible evaluation protocol [17]. The risk of stress radiographs in assessment of distal clavicular fractures is the displacement of otherwise minimally displaced type-II distal clavicular fractures. Computed tomography may be helpful for detection of subtle fractures of the sternal side of the clavicle [18] and also for demonstration of presence and extent of articular surface injuries.

Associated injuries, such as rib fractures, scapular fractures, acromioclavicular dislocations, and head and neck injuries, are more common in severe fractures. Complications of clavicle fractures are rare. In the acute phase, injuries to the neurovascular bundle include subclavian artery injury



**Fig. 2.** Clavicular fracture of the middle third (group 1) with the typical step-off at the fracture side



**Fig. 3.** Clavicular fracture in the lateral third. The widening of the acromioclavicular joint space (*arrowhead*) is suspicious for possible ligamentous damage (group 2, type II)

and brachial plexus lesions with involvement of the medial cord in middle-third fractures. Pleural injuries with pneumothorax are rare. Abundant callus formation or significant fracture deformity can cause compression of the subclavian vessels, most commonly compression of the subclavian vein with subsequent thrombosis. Compression of the carotid artery can occur after medial fractures and lead to syncope by a steal mechanism. Brachial plexus irritation is also possible. In vascular complications, CT angiography is useful for therapy planning. Distal clavicular fractures predisposes to malunion.

### Acromioclavicular Dislocation

The evaluation of an acromioclavicular joint separation often necessitates stress radiographs and comparison images of the uninjured side. The normal joint space width is between 5 and 8 mm (2 mm in the elderly), an asymmetry of 2–4 mm may be normal. The normal coracoclavicular interval is 11–13 mm. Asymmetry of the distance between the coracoid process and the clavicle of >5 mm also suggests ligamentous injury. The undersurface of the acromion should be in the same horizontal plane as the undersurface of the distal clavicle. There are nontraumatic entities such as hyperparathyroidism and rheumatoid arthritis that may also widen the acromioclavicular joint. Radiography should be performed with an AP view and a 10–15° cephalic view, clearing the outer edge of the clavicle from the acromion process.

Acromioclavicular lesions are usually radiologically graded according to Tossy: normal without and with weights; representing ligamentous sprain (type 1: radiologically normal, clinically abnormal); normal without, but abnormal with weights, representing disruption of the acromioclavicular ligament and sprained, but intact coracoclavicular ligament (type 2: slight elevation of the distal clavicle with respect to the acromion and/or widening of the joint space), and upward displacement of the distal clavicle without weights representing disruption of the acromioclavicular and coracoclavicular ligament. Rockwood has added three additional types, all of which are subsets of type 3. Type 4 involves the clavicle grossly displaced dorsally. Concomitant dorsal dislocation of the lateral clavicle should be assessed by axillary views of the shoulder. Type 5 injuries represent vertical separation of the clavicle from the scapula. Type 6 injuries involve the clavicle dislocating inferior into either a subacromial or a subcoracoid position. In severe causes, there is detachment of the deltoid and the trapezoid muscle. There may be additional fractures of the clavicle, the coracoid process or the acromion. Old ligamentous injuries may cause heterotopic ossification. Osteolysis of the distal clavicle is another complication that may contribute to an additional widening of the acromioclavicular joint space.

### Sternoclavicular Dislocation

The direction of dislocation refers to the position of the clavicular head, commonly anterior or posterior. Anterior dislocation is more frequent and not associated with mediastinal injury. Posterior dislocation can be associated with compression or rupture of the trachea, rupture of the esophagus, occlusion or compression of the subclavian or carotid artery, laceration of the superior vena cava, injury to the recurrent laryngeal nerve or pneumothorax [19]. Three subtypes of dislocation can be differentiated in both directions: sprain, but no ligamentous disruption (type I); partial disruption of the sternoclavicular and costoclavicular ligaments resulting in subluxation (type II); and complete disruption of the ligaments, leading to dislocation (type III). Anterior and posterior dislocation are difficult to diagnose both clinically and radiographically, and delay in diagnosis and treatment is common. Sternoclavicular dislocation should be suspected whenever the medial clavicles are not at the same height level on a trauma chest radiograph and especially posterior dislocation, when there is evidence of hematoma in the upper mediastinum [20]. An AP view may demonstrate asymmetry of the medial ends of the clavicle, but determination of anterior or posterior displacement is often impossible. An AP view of the sternum with 40° cephalic angulation (Rockwood view) is the mostly used additional projection, because perpendicular views are not possible. In anterior dislocation, the affected clavicle is projected superior to the contralateral clavicle



and in posterior dislocation it is projected inferior. Other views, such as oblique views or a cross-table lateral view with the arm in extension (Heinig view), can also be used. Due to the difficult interpretation of conventional radiographs, CT is the preferred imaging modality for evaluation of the sternoclavicular joint. The CT angiography is obtained for evaluation of mediastinal hematoma or in posterior dislocation.

#### 2.11.4.2. Shoulder and Proximal Humerus

For conventional radiological evaluation of the shoulder joint, a true AP (glenoidal–tangential) view combined with a transscapular Y view (true lateral projection perpendicular to the true AP view) is required. Other possible second projections are an axillary view (with abduction of the arm about 60–90°) and/or modified axillary view with the patient's arm abducted 45° [21]. The latter projections are often impracticable in the acutely injured patient, because abduction of the arm can be painful. Additional AP projections in internal and external rotation can demonstrate the greater and lesser tuberosity, respectively. A transscapular Y view with an 5° caudal angulation of the central beam represents the supraspinatus outlet view with can help in evaluation of acromion and subacromial space.

#### Glenohumeral Dislocations

Glenohumeral joint dislocations are very common and account for approximately 50% of all articular dislocations. Glenohumeral subluxations are transient, momentary, and not visible on radiographs. Anterior dislocations are most frequent and may be further subclassified as subcoracoid (most common; Fig. 4), subglenoid, subclavicular, and intrathoracic. Posterior dislocations can be subclassified as subacromial (most common; Fig. 5), subglenoid, and subspinous. They are rare and typically subsequent to seizures, electrocution, or a posterior force with the arm in internal rotation. Other types of shoulder dislocation are superior and inferior. Superior dislocations are obligatory associated with fractures of the acromion, clavicle, coracoid process, or tuberosities, and severe damage to the soft tissue of the fornx humeri. *Luxatio erecta* is often associated with neurovascular compromise. Intrathoracic dislocation is often associated with neurovascular and pulmonary complications.

In the transscapular Y view, the humeral head should be projected exactly in the center of the Y, formed by the scapular body, the coracoid process, and the acromion process. Any dislocation of the humeral head should be detected on this projection. In the true AP view, any overlap of humeral head and glenoid is suspect. Combination of these views can demonstrate each type of dislocation. Posterior dislocations are sometimes difficult to diagnose, but the

transscapular Y view should clearly demonstrate the dislocation. In the AP projection, a directed search for the rim sign (joint space width >6 mm), the trough line, (an impaction fracture of the anteromedial humeral head, seen as vertical dense line) and lack of congruency of articular surfaces of humerus and glenoid may avoid misinterpretation. Another characteristic finding in posterior dislocation is internal rotation of the humerus; therefore, posterior dislocation should be suspected in any patient with limited external rotation. Postreduction radiographs have to be analyzed for adequate reduction and accompanying osseous lesions.

Dislocations are often accompanied by associated injuries. In anterior dislocation, there is often an impaction injury of the posterolateral aspect of the humeral head, called Hill-Sachs lesion (Fig. 6). In posterior dislocations, there are impaction fractures of the anteromedial humeral head (reverse Hill-Sachs lesion). There may also be an associated fracture of the greater tuberosity (avulsion of the supraspinatus tendon) in anterior dislocation or a fracture of the lesser tuberosity (avulsion of the subscapularis tendon) in posterior dislocation. Internal rotation views or a Grashey projection with an additional 45° caudal angulation of the central ray can demonstrate a Hill-Sachs lesion. Evaluation of Hill-Sachs lesions and other fractures is also possible with sonography. But CT – after closed reduction – remains the most important further imaging modality whenever even small osseous lesions are suspected.

The Bankart lesion represents a tear of the antero-inferior labrum, often associated with injury to the anterior labrocapsular complex. The posterior glenoid rim can be involved in posterior dislocation. Both MRI or CT arthrography can evaluate cartilaginous labrum injuries. The MRI may show loss of the normal triangular appearance of the labrum or fluid signal within the labrum. Ultrasound may play a role in demonstrating integrity of the labrum and in identifying labral cysts as complication of labral avulsion, which can lead to suprascapular nerve entrapment. There may also be cartilaginous or osseocartilaginous fractures at the antero-inferior aspect of the glenoid, described as bony Bankart lesion (Fig. 7), eventually visible on the AP view. Presence and severity of an osseous Bankart lesion is best evaluated with CT. Humeral avulsions of the glenohumeral joint are only visible on conventional radiographs if there is a small bony fragment, typically linear and medial to the neck of the humerus, associated with a linear radiolucency in the humeral neck (bony HAGL lesion), which may mimic a bony Bankart lesion. The HAGL lesion may cause important anterior instability. They can be visualized with CT or MR arthrography [22]. The MRI arthrography is superior to native MRI. If MRI is performed in the first week after the injury, joint effusion can serve as intra-articular contrast medium, and MRI can be performed without arthrography [23]. Recurrent dislocation is the most common complication following acute

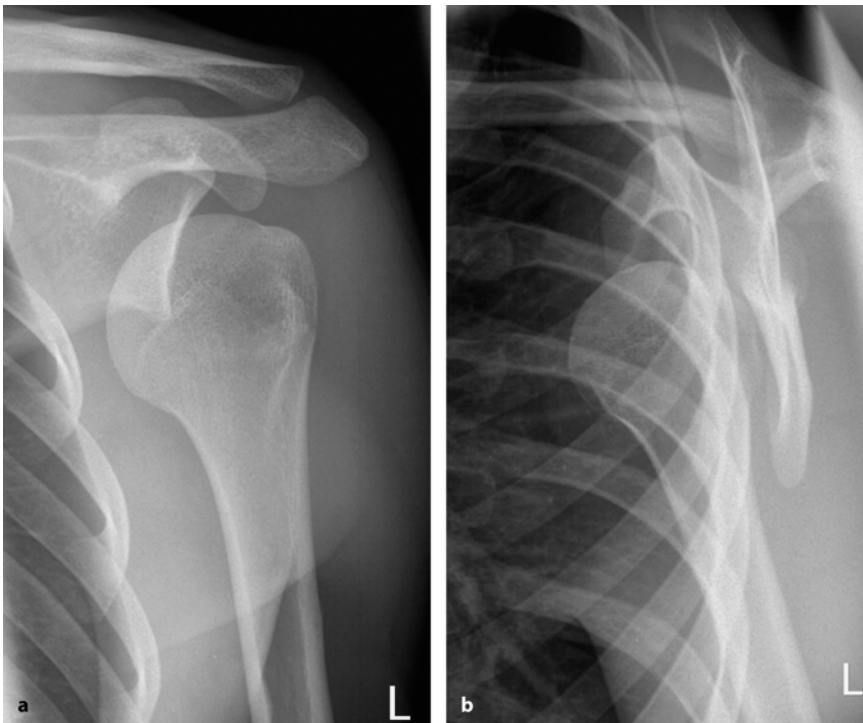


**Fig. 4.** **a** The glenoidal-tangential view of the shoulder demonstrates an excessive overlap between the humeral head and the glenoid, suspicious for dislocation. **b** The transscapular Y-view confirms the anterior-subcoracoid position of the dislocated humeral head



**Fig. 5.** **a** The glenoidal-tangential view of the shoulder demonstrates only a small overlap between the humeral head and the glenoid. The humeral head is in internal rotation (the greater tuberosity is not visible in profile). A discrete trough-line (arrowhead) is seen. **b** The transscapular Y-view clearly demonstrates the dislocation in a posterior-subacromial position

traumatic anterior dislocation. Other complications include rotator cuff tears, neural injuries affecting the axillary nerve, and rare vascular injuries to the axillary artery. A reverse Hill-Sachs lesion can lead to recurrent posterior dislocation. The MRI arthrography may also be performed

for further evaluation of rotator cuff injuries. Sonography may be used in the acute assessment of rotator cuff lesions, where thinning of the cuff and echogenic bands may represent partial rupture. In big lesions, there may also be hypochoic lesions.



**Fig. 6.** The postreductional anteroposterior view of the shoulder after anterior humeral dislocation demonstrates a Hill-Sachs lesion: an impaction injury (*arrowhead*) of the posterolateral humeral head



**Fig. 8.** Two-part fracture of the proximal humerus at the surgical neck with malrotation of the head segment. Note the osteoporotic bone structure



**Fig. 7.** The postreductional coronal CT MPR after anterior humeral dislocation demonstrates a fracture of the inferior glenoid rim (*arrowhead*), consistent with bony Bankart lesion

### Fractures of the Proximal Humerus and Humeral Shaft

Fractures of the proximal humerus account about the most common fractures in the elderly, particularly in osteoporotic women. Nondisplaced or impacted fractures at the chiralurgical neck are typical (Fig. 8). Fractures in younger people generally indicate severe trauma and are often asso-

ciated with fracture–dislocations of the glenohumeral joint or head-splitting fractures. Neer’s classification is widely used and bases on the division of the proximal humerus in four parts along the physseal lines: articular head; greater tuberosity; lesser tuberosity; and humeral shaft. Grading of fractures is based on the total number of fracture parts. A modification of Neer’s classification incorporates the differentiation between fracture and fracture–dislocation according to whether the articular segment is dislocated or not. They can be classified according to the direction of the dislocation as well as to the number of fracture fragments. A fracture is defined as displaced if there is displacement of >1 cm and/or angulation >45° of any of the four parts. Malrotation of the humeral head segment in the joint does not count as dislocation. The subscapularis muscle causes medial and anterior displacement of the lesser tuberosity, whereas the supraspinatus, teres minor, and infraspinatus muscles cause superior and posterior displacement of the greater tuberosity. The pectoralis major muscle causes medial displacement of the humeral shaft. Isolated avulsion of the lesser tuberosity at the insertion of the subscapularis muscle, associated with posterior glenohumeral dislocation and biceps tendon dislocation, is rare.

If movement of the arm is eventually possible, it may be useful to obtain in addition to the standard views an AP view in external rotation, demonstrating the greater tuberosity in profile and an AP view in internal rotation, demonstrating the lesser tuberosity. Intraarticular fractures of the humeral head often distend the joint capsule with blood, displacing the humeral head inferiorly, termed pseudosubluxation, because there is no anterior or posterior displacement. In isolated lesser tuberosity avulsion, the

avulsed lesser tuberosity may retract and lie inferior and medial to the glenoid and then be misinterpreted as calcific tendonitis of the biceps tendon. Computed tomography is of importance in complex comminuted fractures and fracture-dislocations in preoperative planning to define the displacement and rotation of fragments and in demonstration of impression fractures (following dislocation), head splitting fractures and loose bodies. Definition of the amount of the involved joint surface is important and best performed with CT. 3D reconstructions can be useful.

Complications of proximal humerus fractures are injuries of the brachial plexus and/or the axillary artery, sometimes directly caused by osseous fragments and more common in anteriorly displaced fractures. Three-part and four-part fractures are often accompanied by longitudinal rotator cuff tears. Three- and four-part fractures may also disrupt the blood supply and lead to osteonecrosis of the humeral head. Extensive damage and traumatization of soft tissue has proved to be also a major contributing factor to osteonecrosis. The CT angiography or duplex sonography may be helpful in predicting and grading of vascular injury. Magnetic resonance imaging of the neck and the axilla can be used for staging brachial plexus injury and rotator cuff tears. Another complication which may be prevented by early mobilization is frozen shoulder, caused by fibrosis and adhesive capsulitis. Myositis ossificans is rare, mostly occurring after chronic displaced fracture dislocations.

Shaft fractures of long bones are usually classified after AO in simple fractures, wedge fractures and complex (comminuted) fractures. A fracture between the rotator cuff and pectoralis major will have abduction and rotation of the proximal fragment, a fracture between the pectoralis major and the deltoid will have anterior and medial displacement of the proximal fragment and a fracture below the deltoid insertion will have abduction of the proximal fragment. For fracture evaluation, AP and lateral views are best with the entire bone included. Radial nerve injury is the most frequent complication of humeral shaft fractures, mostly occurring in distal-third spiral fractures. The nerve may become trapped between displaced fragments or during closed manipulation. Most radial nerve injuries are incomplete. Vascular injuries, usually involving the axillary artery and less common the brachial artery, are infrequent. Ultrasound or CT angiography can reveal vascular damage. Delayed union or nonunion may occur in transverse fractures.

### Fractures and Dislocations of the Scapula

Scapular fractures are usually high-energy-traumatic direct fractures and in 80% of cases associated with other injuries. Fractures of the scapular body (Fig. 9) and spine are the most common type and are most commonly associated with further injuries. Involvement of the superior border of the scapula is infrequent. Fractures of the scapular body are described in terms of location, displacement, and comminution.



**Fig. 9.** Scapular fracture: The CT VRT in a posterior view demonstrates an isolated fracture at the inferior aspect of the lateral margin (arrowhead), not extending to the superior border

Scapular neck fractures are the second most common type, representing either transverse extensions from scapular body fractures or avulsions from the glenoid rim. Sometimes they are impacted and with the fracture line running from the suprascapular notch towards the lateral margin. Displaced fractures of the scapular neck are considered stable if there is no additional injury of the ipsilateral clavicle or acromioclavicular ligaments. Unstable fractures need surgical treatment.

Glenoid fractures are intraarticular fractures and can be divided into five types after Ideberg: avulsion fracture from the glenoid rim, frequently subsequent to glenohumeral dislocation (type I); transverse and oblique fractures exiting caudally (type II); transverse fracture exiting superiorly (type III); fractures exiting through the medial border of the scapula (type IV); and the combination of a type-II and type-IV fracture (type V). Greater than 2- to 3-mm displacement or  $>45^\circ$  angulation are indications for surgical repair.

Fractures of the coracoid process represent commonly avulsion fractures from either the coracoclavicular ligaments or the short head of the biceps tendon, with fracture lines extending across the base of the coracoid. Avulsion fractures can be caused by muscle contraction (high-voltage injuries, seizures). Coracoid fractures can also occur by direct trauma or by the impact of a dislocating humeral head, especially in superior dislocation. Involvement of the body of the scapula or the glenoid fossa indicates an unstable fracture. Fractures of the acromion typically occur at



the junction of the scapular spine and acromion process lateral to the acromioclavicular joint and are mostly nondisplaced. There are some anatomic variants at the scapula that should not be confused with a fracture such as os acromiale (nonunited acromion apophysis; in 60% bilateral), secondary ossification centers of the inferior angle, as well as those proximal and distal at the coracoid process and nutrient foramina near the glenoidal neck.

Scapular fractures are usually obvious on a chest radiograph or on a shoulder AP view. Glenoidal-tangential views allow evaluation of the anterior portion of the acromion, the glenoid, and the entire coracoid process. The coracoid process is best visualized with 25–40° cephalic angulation of the beam. The CT should be performed if involvement of the glenoid is possible. Goals of the CT examination are to determine if glenoid fractures are intra-articular and to assess congruency of the articular surface. The 3D reconstructions are helpful to demonstrate the relationship of fracture lines to the glenohumeral joint, to display complex fractures, and for surgical planning.

When a scapular fracture is present, associated injuries are common to the head, chest wall, and shoulder girdle. Rib fractures are most common, sometimes visible on the standard shoulder or chest radiographs. Lung contusion, pneumothorax, and clavicle fractures are also very common. Scapular fractures can also occur in association with acromioclavicular and glenohumeral dislocation, especially fractures of the scapular spine, the acromion, and the glenoid. Neurovascular complications are also possible. Lesion of the suprascapular nerve is possible in fractures of the scapular body and neck or in coracoid fractures, if there is involvement of the suprascapular notch.

Scapulothoracic dissociation is a serious injury, indicating partial amputation. It represents a continuum of injury, whereby patients may have a varying degree of neurovascular compromise. Classification schemes are based on clinical findings. It is characterized by lateral displacement of the involved scapula >1 cm comparing distances from the scapular medial border with the spinous processes and/or acromioclavicular separation, sternoclavicular separation, or distracted clavicular fractures on a trauma AP chest radiograph. Bilateral injuries can render side-to-side comparison meaningless and patients with less severe injuries may have few, if any, radiographic findings. Scapulothoracic dislocation indicates disruption of the forequarter musculature, often accompanied with stretching and avulsing of the subclavian and brachial vessels and the brachial plexus [24]; therefore, the dissociation not only causes extensive muscular bleeding, but may also create a large potential space, into which hemorrhage can occur. Soft tissue swelling without soft tissue defect indicates large hematoma. The CT angiography can assess skeletal, soft tissue, and vascular damage.

Scapulothoracic dissociation should be distinguished from the rare scapulothoracic dislocation, which is traumatic separation of the inferior scapulothoracic articulation without neurovascular injury.

## Soft Tissue Lesions

A specific type of labral tear, which involves both anterior and posterior labral quadrants and which can extend into the biceps tendon, is known as superior labrum anterior posterior tear (SLAP lesion). It is best evaluated with MRI arthrography [25]. Evaluation with US is also possible [26]. Several anatomic variants in labral morphology exist that can be confused with acute traumatic injury, such as sublabral foramen or a Budford complex, consisting of a thickened middle glenohumeral ligament and a deficient anterosuperior labrum.

The MRI is highly accurate in diagnosing rotator-cuff tears by fluid signal in tendons, and it can measure the degree of tendon retraction and distinguish partial-thickness from full-thickness tears. In the acutely traumatized shoulder joint, assessment of integrity of the rotator cuff and assessment of position and integrity of biceps tendon may be an indication for sonography. Sonography may also show dislocation or subluxation of the biceps tendon or rupture of the pectoralis major tendon [27].

---

### 2.11.4.3 Elbow

Standard plain-film views are an AP view in the supine position with full extension and a lateral view with the elbow flexed 90° and the lower arm and the hand in neutral position. If full extension of the elbow below 90° not is possible in an acutely injured patient, it is possible to take an AP projection of the upper arm and the forearm as alternative. Horsfield and Siegerist [3] describe an alternative AP view of the radial head by the patient sitting with the back to the examination table and moving the elbow backwards over the cassette until it is flexed at approximately 45° with the hand in supination and the arm moved 45–20° laterally. A vertical central ray is aligned to a point 5 cm proximal to the olecranon process [28]. The resultant image demonstrates most of the radial head in an AP projection. Additional views include internal and external oblique views, the coronoid view, and the radio-capitellum view, the latter positioned as for a neutral lateral view and with additional cephalic angling of the central beam 45°. Stress views are occasionally used to provide indirect evidence of ligamentous trauma; however, pain may limit the degree of distractive force that can be applied. In complex cases, CT or MR will lead to precise diagnosis.

Important bony lines are the anterior humeral line along the anterior cortex of the distal humerus, prolongation of which normally passes through the middle third of the capitellum and more anteriorly in the presence of supracondylar fracture and the radiocapitellar line bisecting the proximal radius proximally to the tuberosity, which should pass through the middle three-fifths of the capitellum and which confirms articulation between the radial head and the capitellum. The radiocapitellar line fails to pass through



**Fig. 10.** Pathological fat-pad signs. Elevation of the anterior fat pad (*arrow*) and appearance of the posterior fat pad (*arrowhead*) demonstrate joint effusion. In the acute trauma setting, this image is suspicious for an occult radial head fracture. There is no visible osseous lesion



**Fig. 11.** A vertical fracture line in the capitellum (*arrowhead*) extends into both condyles, resulting in a comminuted complete intraarticular bicondylar fracture. There is proximal displacement of the medial condyle and slight angulation

the capitellum, if the radial head is dislocated by a fracture or as a component of a Monteggia lesion. Both lines should cross in the middle third of the capitellum. Evaluation of conventional radiographs includes assessment of the soft tissues in the lateral projection. Fat pads are thin layers of fat between the synovial and fibrous joint capsule. Any intraarticular fluid collection causes fat pad displacement. Elevation of the anterior fat pad or appearance of the posterior fat pad is a sensitive index of joint effusion (Fig. 10). In the acute trauma setting, a fracture is the most common cause for joint effusion. Although these signs are strong indicators, they are not specific for trauma and rupture of the capsule will negate the fat pad sign. The absence of joint effusion in adults does not exclude fracture. Ventral displacement, blurring, or obliteration of the supinator fat stripe is typical in fractures of the radial head and neck and should lead to further investigations, if there is no obvious fracture. Swelling or hemorrhage of the olecranon bursa are commonly associated with olecranon fractures and should lead to search for subtle bony irregularities.

### Distal Humerus Fractures

Classification of distal humerus fractures is usually performed in the AP view with exception of the capitellum fracture. They can be classified after AO as extraarticular (supracondylar, epicondylar), partial intraarticular (trans-

condylar), or complete intraarticular (T- or Y-shaped bicondylar fractures). Of all distal humeral fractures in adults, 95% are intraarticular.

Supracondylar fractures can be divided into extension-type fractures, which are extraarticular and frequently associated with volar compartment syndrome, or brachial artery and nerve injuries, and into the much less common flexion-type fractures, which occur mostly in older people and are often combined with a sharp proximal fragment responsible for soft tissue and tendinous injuries resulting in an open fracture. Supracondylar humeral fractures usually involve the ulnar nerve but also may involve the radial and median nerves. Epicondylar fractures are usually intraarticular in adults. The medial epicondyle is more commonly involved and can also be associated with ulnar nerve injury. If a fracture of either the medial or lateral epicondyle includes the lateral aspect of the trochlea, it is considered unstable. Transcondylar fractures are more common in osteoporotic patients. Adult fractures of the distal portion of the humerus are typically intraarticular and composed of a vertical fracture line through the trochlea, branching into one or both condyles in a T- or Y-configuration; there may be significant comminution (Fig. 11). The condylar fragments tend to be displaced and rotated by their muscular attachments. Combined fractures of the humeral shaft (usually complex dislocated bicondylar fractures) and forearm are not uncommon and result in the

grossly unstable “floating elbow.” Significant soft tissue injuries may be associated with these fractures.

Fractures of the capitellum may be subtle, particularly on the AP radiograph, showing often only a lack of definition of the articular cortex of the capitellum. The articular fragment is often shaped like a half circle, displaced proximally to the radial head and frequently rotated 90°, so that the articular surface faces ventrally. Osteochondral injury may be present and associated disruption of the medial collateral ligament. Fractures of the capitellum occur in association with fractures of the radial head, but proximal dislocation of the radial head fracture fragments is rare, hence a confusion of the fragments can be avoided.

Distal humerus fractures are typically obvious on conventional radiographs, but the images must be examined for less obvious fractures of the olecranon, the capitellum, or the radial head, and for any dislocation. Complex fractures should be evaluated with CT. Displaced or neglected fractures of the distal humerus can rarely injure the brachial artery, which can lead to disabling ischemic injury to the muscles of the forearm and hand, known as Volkmann contracture.

As sequelae, soft tissue calcifications and scarring around the elbow are common even with minimal trauma. Hypertrophic callus can obliterate the radial, the coronoid, or the olecranon fossa, resulting in restricted of motion.

Osteochondritis dissecans following repeated micro-trauma typically occurs at the capitellum and the medial epicondyle. Loose bodies may be located in the synovial recess such as the radial neck recess, coronoid fossa, olecranon fossa, and less commonly in the lateral and medial recesses. They may be loose, trapped in synovial folds, or adherent to the synovial lining. Loose bodies can usually be diagnosed on conventional radiographs, when calcified. Computed tomography can demonstrate very small osseous fragments [29]. The MR arthrography, which has been shown to be more sensitive than conventional MRI, is the imaging modality of choice in searching for cartilaginous bodies [30]. Ultrasound can confirm intraarticular cartilaginous fragments and show also noncalcified loose bodies as focal hyperechoic foci.

Avulsion fractures occur typically in younger persons. Injuries to the physis can be diagnosed on conventional radiographs as physeal widening, soft tissue swelling, joint effusion, or a combination thereof. If there is clinical concern of a Salter-I fracture with normal conventional radiographs, MRI can be used to identify possible intraarticular fracture, subchondral edema, or adjacent soft tissue swelling. In avulsion injuries of the medial epicondyle, it is important to look for possible intraarticular loose bodies with MR or ultrasound, because they may cause limitation of motion. The MRI can also be useful in searching for stress fractures of the epicondyles, which are more common in the medial epicondyle [31].



**Fig. 12.** Radial head fracture with involvement of about 25 % of the radial head and displacement of >2 mm (Mason type 2). Note the pathological anterior fat pad sign (arrowhead)

### Proximal Radius Fractures

Radial head fractures are the most common elbow injuries in adults. About half of radial head and neck fractures are nondisplaced. Single-line fractures are typically oriented vertically to the radial aspect of the joint surface and show a cortical disruption at the peripheral margin (Fig. 12). Frequently, the fragment is slightly depressed. Mason’s classification of displaced fractures is commonly used: displacement <2 mm and angulation <20–30° (type I); segmental fractures of one-quarter of the radial head with displacement or compression >2 mm or angulation >20–30° (type II); and involvement of the entire radial head, often with comminution (type III). Comminuted fractures may be associated with shortening of the radius, resulting in proximal migration of the distal radioulnar joint (Essex-Lopresti fracture). None of the existing classifications take account of injuries of the interosseous membrane that are commonly associated with injuries of the distal radioulnar joint. They are commonly diagnosed by physical examination.

Slightly depressed fractures may be radiographically indicated by appearance of a double line of cortical bone. The AP view sometimes shows a line of increased density or only a slight angulation between the radial head and neck, probably without visible fracture line in nondisplaced fractures. Minimal cortical and trabecular irregularities can be suspicious. Evaluation of soft tissue signs can be helpful. The presence of a joint effusion (pathological fat-pad signs) in combination with the appropriate clinical findings is probably diagnostic of a nondisplaced radial fracture. In difficult cases, additional oblique images, such as the radio-capitellum view, may be obtained, or repeated radiographs.

Fractures of the radial head may be associated with fractures of the capitellum. The key to diagnosis is the typical proximal and ventral position of the capitellar frag-

ment, which is unusual for radial fragments. Fractures of the carpus may be associated with proximal radial fractures. A wrist radiograph is mandatory in all cases of severely comminuted proximal radius fractures. Calcification of the capsule and ligaments, ectopic ossifications, and shortening of the intraosseous membrane may be long-term sequelae.

### Proximal Ulna Fractures

Olecranon fractures are common in the elderly. In most cases, the fracture line runs transversely, involving the trochlear notch. If the periosteum is completely torn, separation of the proximal fragment may occur due to traction by the triceps muscle. The Mayo classification distinguishes three fracture types: nondisplaced (type I); displaced and stable (type II; Fig. 13); and displaced and unstable (type III). Each type is subdivided into simple (A) or comminuted (B) fractures. A fracture of the olecranon must meet three criteria to be considered stable: displacement <2 mm; may not increase in 90° elbow flexion; and the ability to extend the elbow articulation against gravity must be maintained. The group of displaced fractures is subdivided into avulsion fractures, oblique (most from proximal and medial to distal and lateral) and transverse fractures, comminuted fractures, and fracture–dislocations. Avulsion of the tip of the olecranon most often occurs due to indirect trauma. Comminuted fractures and fracture–dislocations involve the mid-portion and the proximal portion of the olecranon. If located distally, both types typically involve the collateral ligaments, resulting in instability. Fracture of the anterior trochlear notch extending toward the coronoid process often follows anterior dislocation of the elbow. It is commonly associated with anterior displacement of a distal ulnar fragment and a disrupted radiocapitellar joint (anterior fracture–dislocation of the elbow). Olecranon fractures can also occur in more serious trauma, the injuries of which tend to be open fractures with contamination of the elbow joint.

Transverse fractures may be overlooked on the AP view, but are obvious on the lateral view. Undisplaced oblique fractures may be difficult to visualize on radiographs. It can be necessary to obtain angulated lateral projections to demonstrate the fracture. Soft tissue indicators of a fracture are soft tissue swelling in the olecranon bursa and fat-pad sign, which may provide a diagnostic clue in subtle nondisplaced fractures. Gas within the elbow joint indicates joint contamination. Triceps tendon tears are uncommon, but may be associated with avulsion fractures. The tendon tear and an associated avulsion fracture may be identified by US with the goal to determinate the extent of the tear, to distinguish a partial tear from a nonretracted rupture and to assess the degree of retraction [32]. Fractures of the anterior trochlear notch should lead to careful inspection of the radiocapitellar alignment to exclude a subtle anterior fracture–dislocation. The ulnar nerve pass-



**Fig. 13.** Olecranon fracture with a typical fracture line in transverse orientation and displacement >2 mm (arrowhead)

ing the ulnar ridge is endangered in olecranon fractures as well as during fracture healing by hypertrophic callus.

Coronoid fractures are rarely isolated and most commonly associated with posterior elbow dislocation. Fracture lines are typically obscured by the radius but can be depicted on the lateral view. Coronoid fractures are classified after Regan and Morrey into three types, each subdivided in type A without and type B with elbow dislocation: avulsion fracture of the coronoid tip (type I); involvement of up to 50% coronoid process (type II); and >50% (type III) of the coronoid process. Isolated and nondisplaced fractures can be overlooked at AP and lateral views and are best demonstrated on oblique views. In cases of posterior elbow dislocation, the tip of the coronoid process is depicted as a free fragment with a typical triangular shape. Definite evaluation of the coronoid should be done on the postreduction radiograph.

### Elbow Dislocation

Elbow dislocations are common posterior (Fig. 14) or posterolateral dislocations of the radius and the ulna relative to the humerus and often occur in combination with fractures of the distal humerus or olecranon. Less commonly, the elbow may dislocate laterally, medially, anteriorly, or posteromedially. Divergent dislocations with the radius and ulna displaced in different directions are rare but grossly unstable due to the disruption of all of the ligaments at the elbow plus the proximal interosseous membrane [33]. Other frac-





**Fig. 14.** Posterior elbow dislocation with displaced coronoid process fragment (*arrowhead*)

tures may be seen in the lateral condyle, capitellum, or olecranon. Other types of fracture–dislocations include a fracture of the distal portion of the olecranon with radial head dislocation (anterior fracture–dislocation) as well as an extraarticular fracture of the proximal portion of the ulna with radial head dislocation (Monteggia’s fracture–dislocation). Most dislocations are obvious, but radiographs must be analyzed carefully for any associated fractures, especially coronoid process fractures. Associated soft tissue lesions include injury to ligaments and tendons, and injury to the brachial artery occurs especially in open fractures. Computed tomography is helpful for staging fracture–dislocations. Heterotopic ossification may follow elbow dislocation.

### Soft Tissue Injuries

The most common soft tissue injury is stretching of the capsule and collateral ligaments, resulting at least in hemarthrosis indicated by a fat-pad sign. Ruptures of the ulnar collateral ligament are commonly located at its humeral insertion or in the middle third. There are also reported ruptures of its insertion on the coronoid process with associated avulsion flake. Ruptures of the radial collateral ligament occur mostly in complete elbow dislocation and may lead to posterolateral instability. Possible associated lesions are osteochondral lesions at the radial head. Traumatic tendon injuries or avulsions are rare and usually due to preexisting degenerative change. Rupture of the distal biceps tendon usually occurs at or near its insertion at

the radial tuberosity. Less severe injuries may include partial tears, tendinitis, or intramuscular hematoma. Soft tissue injuries may also occur secondary to fractures caused by sharp fragments. Hematomas in the olecranon bursa may be identified on conventional radiographs, and these can be indicative of an obscure fracture of the olecranon. The MRI or preferably MRI arthrography can be used for evaluation of medial and lateral collateral ligament, demonstrating alterations in morphology, integrity, and signal intensity. Sonography can also be used for assessment of ulnar and lateral collateral ligament tears. Hypochoic clefts represent partial tear, and complete disruption of the normal ligamentous fibers represents full-thickness tear. Further indications for US are detection of joint effusion, evaluation of the distal biceps tendon including searching for tendon rupture, associated hematoma, tendon retraction, and distinguishing complete and partial tears.

### Radial and Ulnar Shaft Fractures

Due to the paired nature of the forearm bones and the presence of a tough interosseous membrane, fractures with displacement of one of the bones necessitates a fracture or dislocation of the other bone. Most commonly, both the radius and the ulnar shaft are fractured near the midshafts. Fractures are usually displaced and may be angulated. Rotation of the distal fragment is typical. Isolated fractures of the ulna are usually the result of a direct blow and tend to be in the distal third and are usually non or minimally displaced. Not uncommon, one of the bones is fractured while the other is displaced. The Monteggia’s fracture is a fracture of the ulna with dislocation of the proximal radius (Fig. 15). The fracture line can either run slightly oblique in the ulnar shaft, be located in the proximal ulna, or involve the olecranon, commonly running from proximal and radial to distal and ulnar. The dislocation of the radial head may be associated with a sloping fracture of the radial neck. Monteggia’s injury should be distinguished from the anterior fracture–dislocation of the elbow; the latter does not disrupt the capsular structures, but the Monteggia’s lesion results in disruption of the proximal radioulnar joint and the elbow collateral ligaments. Galeazzi’s fracture is a usually angulated and displaced distal radius fracture in combination with subluxation at the distal radioulnar joint. The resulting shortening of the radius necessitates the dislocation of the distal radioulnar joint. To avoid overlooking of fracture–dislocations, the elbow and wrist joint should be included in the radiographic evaluation of forearm shaft fractures. A neutral lateral view of the distal forearm should be searched for distal, dorsal, or ulnar displacement of the distal ulna relative to the distal radial metaphysis. Dislocated fractures of the radial head and neck may cause radial nerve palsy as well as a dislocation of the radial head in the case of a Monteggia’s injury. Cross-union of the ulnar and radial shafts is a possible complication after an Monteggia’s injury.



**Fig. 15.** Monteggia's lesion in the AP projection without significant displacement of the radial head. The proximal ulnar fracture demonstrates slight angulation of the proximal fragment. There is an associated displaced radial head fracture (*arrowhead*)

#### 2.11.4.4 Distal Forearm and Wrist

Standard radiographs should include a dorsovolar (DV) view in the neutral position and a true neutral lateral view. A standard DV view should profile the extensor carpi ulnaris groove. The articular surfaces of the carpal bones are normally aligned into three arcs. Arc I comprises the proximal articular surfaces of the scaphoid, the lunate and the triquetrum. Arcs II and III represent the parallel articular surfaces at the midcarpal joint. A broken arc or a step-off to any side of one or more arcs always indicates fracture, dislocation, or subluxation. As exception, in some people there may be small step-off at the lunotriquetral joint, which is normal. The widths of the distal radioulnar, radiocarpal, intercarpal, and carpometacarpal joint should be symmetrically 2 mm or less. Opposing articular surfaces at each joint should be parallel to each other. If a joint space is not in profile on the radiograph and there is suspicion of abnormality, fluoroscopic controlled views should be added. When a joint space is 4 mm or more, it is considered definitely abnormal. At the carpometacarpal articulations, the distal articular surfaces of the trapezoid, the capitate, and the hamate parallel the proximal articular surfaces of the second through fifth metacarpals in a form that roughly resembles an "M" [34]. The scaphoid fat stripe courses from the ulnar styloid to the trapezium. Swelling, displace-

ment, or obliteration is usually associated with scaphoid or other carpal fractures.

A true lateral view is defined by the scaphopisocapitate relationship: the ventral cortex of the pisiform bone should lie between the ventral cortices of the distal pole of scaphoid and the head of the capitate. The ulnar head and the distal radius should completely overlap on this projection. A line drawn along the central axis of the distal radius should pass through or very close to the central axis of the lunate, the capitate, and the third metacarpal. The proximal pole of the scaphoid should superimpose upon the lunate and triquetrum. A line drawn along the central axis of the distal ulna should intersect some portion of the triquetrum. Subtle subluxation can be diagnosed if this line passes dorsal to the triquetrum. The deep fat pad of the pronator quadratus is constantly seen on the lateral view. It is convexly bowed in a ventral direction or completely absent in pathological conditions, such as fractures, and can indicate occult fractures. Also the dorsal skin/subcutaneous fat zones can be evaluated. In the presence of significant dorsal wrist swelling, a fracture should be sought. Carpal tunnel view is an additional view which demonstrates an axial view of the hook of hamate, the pisiform, and the volar margin of the trapezium.

Computed tomography is helpful in complex cases (fracture comminution, displacement, or complex intra-articular extension). The MRI is helpful in patients with questionable occult fractures and osteochondral lesions, and for precise evaluation of the carpal ligaments and the triangular fibrocartilage complex (TFCC).

#### Distal Forearm Fractures and Dislocations

Distal radius fractures are the most common fractures of the skeleton. Several classification schemes for distal forearm fractures have been introduced (after Frykman, Melone, AO, Fernandez, and Jupiter), but none is widely accepted. The most common type of distal radius fractures is Colles fracture (Fig. 16), defined by dorsal displacement of the distal fragment. The term is characteristically described as an extraarticular fracture with impaction of the dorsal cortex, although this eponym may also be used for intraarticular fractures. Radiocarpal and distal radioulnar joint extension of the fracture lines, radial shortening, loss of radial inclination and palmar tilt, and associated ulnar styloid fractures can be observed. In many cases there is dorsal comminution, and in the majority of cases there is intraarticular involvement of either the radiocarpal or the radioulnar joint or both. In the Smith fracture (or reverse Colles fracture) the distal fragment is displaced or angulated in the palmar direction. Volar comminution is common. Articular involvement or fractures of the ulnar styloid are possible. Barton fractures and reverse Barton fractures are intraarticular fractures of the palmar (reverse Barton type; common in younger people) or the dorsal rim of the distal radius associated with palmar or dorsal



**Fig. 16.** **a** The DV view of the distal radius demonstrates intraarticular (*arrowhead*) distal radius fracture. **b** The lateral projection reveals dorsal displacement of the distal fragment; therefore, the diagnosis of Colles fracture can be made



**Fig. 17.** Chauffeur fracture: an undisplaced intraarticular fracture of the radial styloid process with origin in the junction of the scaphoid and lunate fossa and lateral course in an oblique direction

dislocation of the carpus. Chauffeur (or Hutchinson) fracture (Fig. 17) is an usually not significantly displaced oblique intraarticular fracture of the radial styloid process with the fracture line usually originating from the junction of the scaphoid and lunate fossae of the distal radial

articular surface and coursing laterally in a transverse or oblique direction. The osseous fragment can vary markedly in size. Comminution is possible. A die-punch fracture represents a depressed fracture of the articular surface of the lunate fossa. This fracture may be easily overlooked, but assessment of the palmar arcs will assist in identification. Degree and location of comminution are important characteristics.

Standard measurements include radial inclination (21–25°) and radial length (10–13 mm) on the DV radiograph and volar tilt (2–20°, average 11°) on the lateral radiograph [35]. Ulnar variation and bone quality (presence of osteoporosis) should also be mentioned. Obliteration or palmar translation of the pronator quadratus fat pad is suspicious for fracture. One should describe the course of the fracture line, fragment dislocation, radiocarpal and distal radioulnar articulations, and associated carpal injuries. More than 1–2 mm of step or gap deformity determine need of surgical treatment. Postreduction radiographs should be evaluated for articular congruity, and the same measurements as mentioned previously should be performed. The term malunion can be applied to any fracture with a dorsal tilt of 5° or greater, a radial inclination of 10° or less, or a loss of 5 mm or more of radial height. Ultrasound is also valuable in determining the postreduction evaluation [36]. Computed tomography provides more information on the presence of casts or splints, positioning difficulties, metallic hardware, and diffuse osteoporosis, and better reveals involvement of the distal radioulnar joint, the degree of comminution, and the extent of articular surface depression [37]. For staging of distal radius

fractures, it is also important to determine if the fracture is intra- or extraarticular, which is best visualized with CT; 3D reconstructions with view on the radial articular surface are recommended. The MRI can show occult fractures or bone contusions, parosseous and intraarticular hematomas, and ligamentous and chondral injuries.

Distal radius fractures are often associated with scaphoid fractures or intercarpal ligamentous injuries. Typical are scapholunate ligament injuries in Chauffeur fractures. Scapholunate ligament involvement is possible, if a fracture line runs directly intraarticular between the lunate and scaphoidal surface of the radius. Ulnar styloid fractures must be noted, because they may indicate injury to the TFCC and fracture severity and prognosis worsen. Other complications include lesions of the flexor and extensor tendons and compression of the median nerve. Radiocarpal dislocations are possible in the dorsal, palmar, and ulnar direction. Dorsal and palmar dislocations are associated with avulsion of the dorsal or palmar joint surface and radial or ulnar styloid process fractures.

Dislocations of the distal radioulnar joint are usually associated with distal radius and ulna fractures (termed Moore's fracture), although they can also occur as an isolated injury. According to the position of the ulnar head in relation to the distal radius, they are classified as dorsal (most cases), volar, or rotational. In rotational subluxation, the head of the ulna is fixed within the sigmoid notch in an abnormal position. Associated lesions of dorsal and palmar radioulnar ligaments may lead to instability with a range from isolated lesion to one of the radioulnar ligaments up to dislocation of the TFCC from either the radial or the ulnar surface. The key to radiographic diagnosis is the position of the ulnar styloid process which projects on the PA view on the midportion of the ulnar head and does not lie dorsal of the ulnar head on the lateral radiograph. A true neutral lateral radiograph is important for the diagnosis, as inadequate positioning may lead to misdiagnosis. On the DV radiograph, the distal radioulnar joint space is widened in many causes. Dislocation is present, if >50% of the joint surfaces do not articulate with each other; otherwise, it is termed subluxation. Computed tomography is the technique of choice for evaluation of distal radioulnar incongruency. On the axial plane, the ulnar head should be positioned at minimum to two-thirds into a space, formed by two lines through the dorsal and palmar radial surfaces. The CT scans in pronation and supination can show dynamic subluxation. The MRI may be helpful in identifying the injured radioulnar ligaments and in defining the amount of TFCC damage. Reflex sympathetic dystrophy may occur in association with fractures of the distal forearm and the carpal bones. Conventional radiographs and MRI can be helpful in diagnosis and follow-up as well as in staging.

## Wrist Fractures and Dislocations

The vulnerable zone of carpal injury includes structures demarcated by two concentric arcs. The lesser arc passes through the articulations of the lunate with the scaphoid, capitate, hamate, and triquetrum. The greater arc passes through the midportion of the scaphoid and the proximal aspect of the capitate, hamate, and triquetrum. The vulnerable zone also extends distally to include the distal pole of the scaphoid and the trapezium.

### Scaphoid Fracture

The scaphoid is the most frequent site of carpal fracture and intercarpal ligament injury. Scaphoid fractures occur commonly in the 15- to 40-year-old group and are usually located at the waist with the fracture line running transverse or slightly oblique to the long axis of the scaphoid (Fig. 18). Vertical fractures are rare. Avulsion fractures of the distal pole and the lateral tubercle are clinically less important. In unstable fractures, the distal fragment flexes in the palmar direction and moves with the carpal row, whereas the proximal fragment extends and moves with the lunate. This leads to the "humpback" deformity of the scaphoid associated with healed but formerly unstable angulated scaphoid fractures.

Radiographic assessment of scaphoid fractures and instability should include measurements of the capitulate angle between the long axis of the capitate and the midplane axis of the lunate (normal <30°) and the scapholunate angle between the long axis of the scaphoid and the midplane axis of the lunate (normal 30–60°) on the lateral radiograph. A scapholunate angle >80° or <30° indicates instability. Because the existing classification schemes (after Herbert [64], Cooney [65], and Russe [66]) consider only partial aspects, one should fully characterize the fracture by the orientation of the fracture, displacement, and angulation [35]. On standard DV radiographs, many scaphoid fractures are occult, because the fracture line runs commonly perpendicular to the long axis of the scaphoid, but this axis has a palmar inclination about 45°; therefore, in suspected lesions, additional coned-down and ulnar deviation views – with the ulnar deviation, the scaphoid extends from its volar tilt in the normal DV view and appears elongated on the DV radiograph – can be helpful in identification of scapholunate widening or a fracture line not visible on the standard view. Nevertheless, scaphoid fractures can be radiographically occult. Most authors recommend early realization of CT or MRI for definite evaluation, whereas immobilization of the wrist without definite diagnosis should not be performed further. The use of MRI at the time of presentation may be cost-effective if the costs of staying away from work are also considered [38].

A frequent normal variant on the radial margin of the waist of the scaphoid is a small angular tubercle whose margins may be mistaken for fracture. The opposing articular surface of the scaphoid should be examined carefully for ev-





**Fig. 18.** Scaphoid fracture in the middle third (*arrowhead*) with the typical orientation of the fracture line transverse to the long axis of the scaphoid

idence of discontinuity. If this cortex is intact, a fracture is very unlikely. Possible associated injuries are fractures of the radial styloid, capitate and lunate, scapholunate dissociation, perilunate dissociations, and other forms of carpal instability. Avascular necrosis of the proximal pole may complicate scaphoid fractures. Fractures at greatest risk include those displaced >1–2 mm, angulated >15°, and the likelihood directly increases by fracture location from distally to proximally. About 80% of scaphoid fractures occur in the vulnerable ischemic region. Gadolinium-enhanced MRI is important for early detection of this complication before conventional radiographic signs such as osteopenia, scaphoid collapse, and less commonly sclerosis are visible, and should be performed on clinical suspicion. If increased radiolucency develops along a fracture line, or if a round or oval focal area of radiolucency develops at the waist of the scaphoid, motion along a scaphoid fracture should be suspected. Scaphoid nonunion has been associated with the development of late arthritis of the wrist, commonly referred to as scaphoid nonunion advanced collapse (SNAC). When healing is uncertain or must be verified, CT can be helpful.

### Other Carpal Fractures

Triquetrum fractures generally occur on the dorsal surface at the attachment of the lunotriquetral, the dorsal radiotriquetral, or the intercarpal ligament as avulsion fractures (Fig. 19) or, less commonly, they involve the body. Transverse fractures usually reach the pisotriquetral joint. Avulsions of the palmar pole are difficult to detect and often associated with perilunate ligamentous lesions. Dorsal



**Fig. 19.** Irregular ossicles at the dorsal triquetrum surface (*arrowhead*), consistent with avulsion fracture of the dorsal pole

fractures are often nondisplaced and comminuted. They are best demonstrated on lateral radiographs, whereas transverse fractures can usually be seen on the DV radiograph. There should be no accessory ossicles just dorsal to the triquetrum. Steps in joint surfaces can be shown with CT or MRI. Triquetrum fractures, especially of the proximal radial corner, can occur in association with perilunate dislocations. After spontaneous reduction of such a dislocation, this fracture can remain the only indication of further dislocation.

Lunate fractures may occur as chip fractures of the dorsal or volar surface or occasionally as complete transverse fracture. Avulsions of the scapholunate or lunotriquetral ligament at the volar pole are possible and should be indicative of former perilunate dislocation. An accompaniment of volar perilunate subluxation or dislocation would support the diagnosis of translunate volar perilunate fracture subluxation or dislocation. Lunate fractures may be overlooked in the acute setting because the lunate is overlapped on standard radiographs. On the lateral view, a break in the volar or in the dorsal cortex, a radiolucency at the proximal pole or a impression at the distal pole may suggest a fracture. Fluoroscopic spot images, CT, or MRI can help in evaluation. Kienböck disease or avascular necrosis of the lunate is believed by some to be a chronic manifestation of lunate fractures; therefore, all patients with lunate fractures warrant periodic follow-up.

Hamate fractures occur either as a dorsally displaced articular fracture of the distal articular surface in association with an ulnar-sided metacarpal fracture and fourth and fifth carpometacarpal dislocation, or more commonly as a fracture of the base of the hook of the hamate, representing an avulsion fracture at the attachment of the transverse carpal ligament and the flexor carpi ulnaris tendon. Avulsions of the lateral tubercle are rare. Radiographic clues to

the diagnosis of fracture of the hook of the hamate may be the absence of the complete cortical ring of the hamulus on the DV view, absence of the hook, or sclerosis at the region of the hook, indicating reactive bone formation. In addition to standard views, a carpal tunnel radiograph, a 20° supine oblique view, an overpronation view, or a radial deviated lateral thumb-adducted view, further CT or MRI can show fractures of the hook of hamate. Os hamulus proprius, an unfused ossification center, may mimic an old fracture but is usually much larger. Nonunion is the most common complication following hook fractures. Basal fractures can cause chronic irritation of the ulnar nerve (“Syndrome de la loge de Guyon”) or rupture of the profound flexor tendons.

Trapezial fractures are often associated with a fracture of the first metacarpal base and/or subluxation or dislocation of the first carpometacarpal joint. The resulting fracture is longitudinal and intraarticular. Avulsions of the lateral or the dorsal tubercle are possible. Avulsion of the palmar tubercle at the attachment of the transverse carpal ligament can cause carpal tunnel syndrome. Diagnosis is possible with a carpal tunnel radiograph or with CT. Trapezoid fractures are rare and typically associated with dislocations. Isolated dislocations are also possible. Fractures and dislocations can generally be identified on conventional radiographs.

Pisiform fractures are comminuted or simple and may be associated with other upper-extremity fractures, resulting in delayed recognition. These fractures may be difficult to detect on standard radiographs. Carpal tunnel and pisotriquetral radiographs (a lateral projection with 20–25° supination) can demonstrate the pisiform in two projections, but CT or MRI are often needed. Sometimes, the pisiform may have more than one ossification center, which can mimic a fracture.

Capitate fractures are rare. They usually occur in association with scaphoid fractures or perilunate dislocations. Transverse fractures of the waist or the head are most common. Often the proximal fracture fragment is displaced and rotated or inverted and entrapped between the capitate and lunate with or without perilunate dislocation. One unusual type of greater arc injury is the scaphocapitate syndrome, characterized by a transverse fracture across the midportion of the capitate with 180° rotation of the proximal fragment, such that the proximal articular surface faces distally. This injury usually includes a fracture of the scaphoid. Demonstration of fractures may require angled-beam radiographs, CT, or MRI. Fractures of the capitate waist may rarely progress to avascular necrosis of the proximal pole. Greater arc injuries consist usually of multiple carpal bone fractures.

### Carpal Dislocations

Carpal dislocations are usually obvious on the lateral view, in which no carpal bone should cross either the volar or dorsal radial line. The key to identification of the most common lunate and perilunate dislocations is the position of the lunate and the capitate, which are under normal

conditions centered over the distal radial articular surface. Lesser arc injuries cause ligamentous disruption that leads to various types of perilunate instability and carpal malalignment. The initial stage disrupts the radioscaphoid ligament and the scapholunate ligament, leading to scapholunate dissociation or rotatory subluxation of the scaphoid. With dorsal migration of the proximal pole of the scaphoid, there is widening of the scapholunate joint space and foreshortening of the scaphoid on the DV radiograph. The second stage of progressive perilunate instability is created by disruption of the volar radiocapitate ligament, which allows dorsal dislocation of the capitate from the lunate, termed perilunate dislocation. In this case, on the lateral radiograph, the capitate crosses the dorsal radial line and the lunate lies behind the volar radial line. The majority of cases of perilunate dislocation are accompanied by a scaphoid waist fracture, termed transscaphoid perilunate dislocation or de Quervain fracture. These injuries may also lead to median neuropathy, chronic instability, malunion, or avascular necrosis. The third stage of progressive perilunate instability involves disruption of the volar and dorsal radiotriquetral ligaments and the lunotriquetral ligament. The resulting form of perilunate dislocation, sometimes referred to as midcarpal dislocation, may be characterized by additional avulsion fractures of the triquetrum. If such a fracture or a fracture of the radial styloid process fracture is present on standard radiographs, one should exclude perilunate dislocation.

The fourth stage of progressive perilunate instability is lunate dislocation, following disruption of the dorsal radiolunate ligament. The lunate is typically volar tilted, which results in the classic pie-shaped lunate on the DV view, which should not be confused with a fracture. On the lateral radiograph, the lunate crosses the volar radial line and the capitate does not cross the dorsal radial line. Most lunate dislocations do not have associated fractures. Irritation of the median nerve is also possible.

Not uncommonly, a mixed pattern of carpal dislocation is present. Fractures associated with carpal dislocations are often easier to identify on postreduction views. Computed tomography can be helpful in clarifying more complex cases. Other associated lesions include dislocation of the radial head or the elbow. In more severe injuries, more complex carpal dislocation up to the formation of a split hand is possible. Axial carpal dislocation is a rare injury indicated by widening between the carpal bones and their associated metacarpals in the distal carpal row. The fourth and fifth metacarpal–hamate joints are most often involved, and severe soft tissue injuries are common. Dislocations of the distal carpal bones may lead to irritation of the ulnar nerve.

### Tendinous and Ligamentous Injuries

Common soft tissue injuries are lesions of the triangular fibrocartilage complex (TFCC) or lesions of the scapholunate ligament; however, these lesions are less important in the

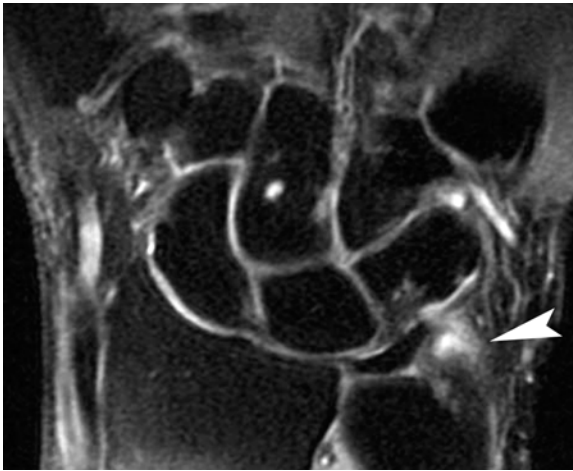


**Fig. 20.** The T2-weighted MRI image in the coronal plane demonstrates excessive fluid localization at the ulnar TFCC attachment without osseous lesion (arrowhead), consistent with TFCC avulsion (type-1b lesion)

acute setting. Traumatic TFCC tears are more common in younger patients and are frequently associated with distal radius fractures, particularly if there is radial shortening and dorsal angulation. They frequently occur close to the radial insertion. Ulnar attachment injury may be associated with an ulnar styloid fracture. Avulsions of the TFCC (Fig. 20) are less common and are identified at the ulnar aspect of the articular disc. In general, ulnar-sided TFCC injuries are more difficult to diagnose. In the Palmer classification, traumatic TFCC lesions are referred to as type-1 lesions, and subtypes include central perforation (1A), ulnar avulsion with or without distal ulnar fracture (1B), distal avulsion of the TFCC attachments to the lunate or the triquetrum (1C), and radial avulsion with or without sigmoid notch fractures (1D). The TFCC and ligamentous lesions are best evaluated with MRI arthrography. Pathological findings include altered morphology, linear fluid extending to the surface of the peripheral TFCC, and excessive fluid localizing, particularly if the fluid extends below the expected location of the prestyloid recess.

Abnormalities in the alignment of carpal bones are described as carpal instability. This can occur in association with scaphoid fractures, lunate/perilunate dislocations, or with interruption of the extrinsic and/or intrinsic carpal ligaments. There are static and dynamic instabilities. Carpal instabilities may also occur as normal variants; therefore, the examination should include both wrists. Scapholunate ligament injury accounts for the most common form of carpal instability. It may be suspected with a widening of the scapholunate interval of  $>2$  mm on a DV radiograph. Another common plain-film finding of scapholunate dissociation is the cortical ring sign on a true AP view without any ulnar or radial deviation, occurring due to abnormal orientation

of the scaphoid with rotation and appearing foreshortened on the DV radiograph. This rotatory subluxation of the scaphoid may progress to dorsal or volar intercalated segmental instability (DISI or VISI) with time. Diagnosis is usually confirmed by MRI. Dorsal intercalated segmental instability is present under the following conditions: scapholunate angle  $>60^\circ$  and capitolunate angle  $>30^\circ$ . Scapholunate advanced collapse represents the end stage. Tears of the lunotriquetral ligament may coexist with volar intercalated segmental instability (scapholunate angle  $<30^\circ$ ). Ulnar translocation is a less common form of carpal instability. Type I is diagnosed when the space between the radial styloid and the scaphoid is wider than the width of other intercarpal joints, or when more than one-half of the proximal articular surface of the lunate lies ulnar to the radius. In type II, there is marked scapholunate diastasis, but the scaphoid remains in the scaphoid fossa and the remainder of the carpus translocates ulnarly. In dorsal or palmar carpal subluxation, the total carpus is displaced dorsal or palmar to the midplane of the distal radius on the lateral view. It usually follows a fracture of the distal radius.

Tendon injuries can be visualized with US. It is necessary to consider that except for the flexor carpi ulnaris tendon, all tendons are surrounded by a synovial sheath, but not all along their course. The extensor pollicis brevis tendon is absent in up to 6% of normal individuals and the abductor pollicis longus tendon may have a multilamellar appearance, not to be confused with longitudinal tears. Multiple abductor pollicis longus tendons are found in 50% of patients [39]. Tenosynovitis of the third extensor compartment (extensor pollicis longus tendon) is often related to an irregular bony contour secondary to a previous fracture, typically involving Lister's tubercle. The flexor carpi radialis tendon occupies a narrow fibro-osseous tunnel at the level of the crest of the trapezium. Tendinitis and tendon rupture may be secondary to scaphoid fractures.

If CT is performed in assessment of wrist trauma, special 3D volume-rendering algorithms can show the flexor tendons, and with some limitations also the extensor tendons, and confirm the clinical diagnosis of tendon rupture. This technique may also be useful in assessment of the wrist tendons, when MRI or US cannot be used, like in the presence of metal hardware, surgical wounds, or open lacerations. Computed tomography may also be useful before tendon-transfer surgery is planned [40]. For evaluation of flexor or extensor tendon injuries as well as injuries to the median nerve, which are possible complications in distal radius fractures, MRI can be helpful.

### Carpometacarpal Dislocations

Dislocations of the second through fifth carpometacarpal joint are infrequent and associated with fractures of the adjacent carpals and metacarpals. Simultaneous dislocation of multiple joints occurs more commonly than dislo-

cation of a single joint. Combinations of the fourth and fifth or the second through fifth joints are most frequent. When a single joint is involved, the fifth is most common followed by the second joint. Dislocation usually occurs in dorsal direction. Fifth and/or fourth metacarpal/carpal dislocations are often associated with fractures of the hamate, typically an avulsion fracture of the dorsal lip. On a properly positioned DV view of the hand or wrist, the bases of the second through fifth metacarpals form parallel lines with the adjacent carpal bones. Loss of these parallel lines suggests malalignment, especially if any overlap is present. The diagnosis is established on the lateral view, where one or more metacarpal bases are not in proper alignment with the carpus.

#### 2.11.4.5 Metacarpals and Fingers

Dorsoventral (DV) and pronation/oblique projections, if the position of metacarpal bones is in question in combination with a lateral view, should be obtained as standard views. In finger injuries, radiographs of the injured finger give greater detail. The acquisition of radiographs of the whole hand is not necessary [41]. The dorsal skin/subcutaneous fat zones of the hand should be evaluated in the lateral plane. Dorsal hand swelling is strongly associated with fractures of the metacarpals II–V. Combination of dorsal wrist and hand swelling after trauma occurs in cases of carpometacarpal dislocation, proximal intraarticular fracture of one or more metacarpals II–V, or combinations of metacarpal and carpal fractures. Swelling of the thenar skin/subcutaneous fat plane are associated with fractures of the first metacarpal joint and sometimes with fractures of the proximal first phalanx. Hypothenar swelling may occur in cases with fractures of metacarpals II–V. Injuries at the metacarpophalangeal joints lead to focal swelling. Parallelism of articular joints and the lack of overlapping of articular surfaces is also worthy of mention.

#### Metacarpals

Fractures of the first metacarpal bone are most commonly located at the base or proximal portion. It is important to recognize whether the fracture is intraarticular (as is more common) or not. Bennet's fracture (also called fracture–dislocation; Fig. 21) is an oblique intraarticular fracture of the base of the first metacarpal. Commonly a small volar fragment of the base remains in position while the rest of the first metacarpal is dorsally and radially dislocated by the pull of the abductor pollicis muscle. Rolando's fracture is less common and represents a comminuted Bennet's fracture with a Y-, V-, or T-configuration. Winterstein's fracture is a proximal transverse extraarticular fracture of the first metacarpal with palmar angulation. Injury to the ulnar collateral ligament of the first metacarpophalangeal joint, usually at its distal point of insertion at the base of



**Fig. 21.** Bennett's fracture: a non comminuted intraarticular (*arrowhead*) fracture of the base of the first metacarpal with only slight angulation of the fracture fragment

the proximal phalanx, is called Gamekeeper's thumb or skier's thumb. There is often an associated osseous avulsion fracture at the insertion present. Complete tear is diagnosed by MCP joint laxity with  $>30^\circ$  angulation on stress radiographs. The torn ulnar collateral ligament can become displaced superficial to the adductor pollicis aponeurosis, which is called a Stener lesion and may require surgical treatment. Detection of this lesion is important and can be performed with sonography or MRI.

Fractures of the other metacarpals are common, frequently affecting the fifth metacarpal. Boxer's fracture is a transverse fracture of the neck of a metacarpal bone with volar angulation of the distal fracture fragment, common in the fifth metacarpal. These fractures are typically unstable secondary to fracture angulation and frequent comminution. Less than 40–50% of angulation can be tolerated in the fourth and fifth metacarpal joints. Fractures of the metacarpal base are also most commonly located in the fourth and fifth metacarpal joints. Shaft fractures may be transverse or oblique. Transverse fractures are frequently angulated due to the extension of the proximal fragment by the extensor carpi radialis and ulnaris muscle. Oblique fractures may result in shortening and rotational deformity; the latter is not evident on radiographs. Metacarpal fractures of the ring and the middle finger are more inherently stable than those of the index and fifth finger because of the dual support from the radial and ulnar deep transverse intermetacarpal ligaments.

#### Fingers

Proximal phalanx fractures are commonly located at the proximal portion and the midportion of the thumb or the index. Intraarticular involvement is rare. Occasionally, an avulsion fracture may occur at the lateral margin of the base



of the proximal or middle phalanx at the site of the collateral ligament attachment. Fractures may be oblique with a tendency for shortening and rotation of the digit or transverse with typical volar angulation. Phalangeal fractures should not show  $>10^\circ$  of angulation in any plane and no rotational malalignment should be present. Middle phalanx fractures are rare and the result of direct injuries. Typical locations are the distal shaft of the index and middle finger. The resultant angulation of a middle phalanx fracture depends upon their relation to the insertion of the flexor tendons. If the fracture line is distal, there results volar angulation of the proximal fragment; if proximal there is volar angulation of the distal fragment. Fractures of the distal phalanges, especially of the middle finger and the thumb, are the most common sites of fractures of the hand. The ungual tufts are most frequently fractured, varying from a simple marginal chip fracture to severely comminuted fractures. Transverse longitudinal fractures are less common and may be associated with displacement or angulation.

Dislocations of interphalangeal joints occur most commonly in the dorsal, but also in the lateral and the volar, direction, the latter being very uncommon. In simple dorsal dislocations, the volar plate is not interposed. Complex dorsal dislocations are defined by the interposition of the volar plate, the collateral ligament or the joint capsule and may not be reduced. The only radiographic sign of a complex dislocation is a persistent incongruity of the joint following reduction, if there is not a small avulsion fracture from the insertion of the volar plate at the base of the phalanx. Associated collateral ligament rupture is evidenced clinically by  $>10^\circ$  angulation at the extended PIP joint. The MRI can demonstrate the collateral ligament tear as discontinuity, detachment or thickening of the ligament together with increased T2-weighted signal intensity. Other signs may be obliteration of the fat planes around the ligament and extravasation of joint fluid. One should look carefully for associated fractures. Lateral dislocations show often only minimal displacement and are often subluxations.

### Soft Tissue Lesions and Avulsion Fractures

Mallet finger (Fig. 22) is either an intraarticular avulsion fracture of the dorsal base of the distal phalanx or a disruption of the distal terminal extensor tendon without fracture. Untreated mallet fingers may progress to a “swan neck” deformity with hyperextension of the proximal interphalangeal (PIP) joint. Avulsion of a middle part of the extensor tendon at the dorsal base of the middle phalanx is also possible. Subluxation or dislocation of the extensor digitorum communis tendon at the MCP joint occurs as a result of tearing of the sagittal bands of the extensor hood. Ulnar subluxation is more common and usually affects the middle finger. The MRI can be used for tendon injury staging and allows direct assessment of the position of the tendon.



**Fig. 22.** Mallet finger: an intraarticular avulsion of the dorsal base of the distal phalanx (*arrowhead*) representing osseous avulsion of the distal terminal extensor tendon

In flexor tendons there are five anatomic zones; the most important is zone I between the distal insertion of the flexor digitorum profundus (FDP) tendon and the distal insertion of the flexor digitorum superficialis (FDS) tendon and zone II (or no-man’s land) between the distal insertion of the FDS tendon and the distal palmar fold, where lacerations are most frequent and carry the most severe prognosis. Trauma in the proximal zones is associated with lesions of both flexor tendons and implies loss of active flexion. In addition, injuries to the major neurovascular structures have been reported. Jersey finger is an avulsion of the FDP tendon from the volar base of the distal phalanx. It is the most common closed injury to the flexor tendons. It can be staged as retraction of the tendon into the palm (type I), to the PIP (type II), or avulsion of a large bone fragment, associated with avulsion of the FDP tendon from this fracture fragment (type III). Isolated injury of the FDS tendon is rare; most cases are associated with FDP tendon injury. The MRI has been successfully used to diagnose tendon disruption and to visualize the locations of the ends of the lacerated tendon.

Volar plate avulsion can occur from the base of the middle phalanx or, less frequently, from the proximal insertion point of the checkrein ligaments on the proximal phalanx.

There can be simple avulsion, eventually progressing to swan-neck deformity (type-I lesion), more extensive involvement of the periarticular soft tissues with a major split between the components of the collateral ligament complex, and possible dorsal subluxation of the middle phalanx or even luxation (type II), or fracture–dislocations of the volar base of the middle phalanx (type III). A stable injury usually involves <40% of the articular surface leaving the collateral ligaments attached to the middle phalanx [42]. Volar plate avulsions can be detected on oblique or lateral radiographs. The avulsed fragment is often very small and undisplaced and can therefore be easily overlooked. The MRI is more sensitive.

In evaluation of the flexor pulley system, MRI and ultrasound have been successfully used, particularly in ruptures of the A2 and A4 ligaments, located at the middle portion of the proximal and the distal phalanx, respectively. These pulleys are most important for flexor tendon function, keeping them in close relation to the bone. Ruptures can be visualized directly. An indirect sign is detection of a gap >1 mm between the flexor tendon and the bone with the finger in forced flexion.

## 2.11.5 Lower Extremity

### 2.11.5.1 Hip

Standard radiographs include an AP projection of the pelvis and an axial or Lauenstein view of the hip. Two major trabecular groups within the femoral neck and head can be distinguished: the vertically oriented compressive and the tensile trabeculae. One should evaluate the preservation of symmetry of the femoral heads and hip-joint spaces. Dislocations or interposition of soft tissue and fragments may cause only subtle changes of congruency

and continuity of the bony contours of the femoral head and the articulating acetabulum. Of several described fat-pad signs, only an asymmetric prominent fat pad of the internal obturator muscle seems to be useful.

The advantage of CT is the evaluation of complex fractures, especially for evaluation of fracture extent of the femoral head and intraarticular fragments. In the femoral neck, application of CT is also possible for the diagnosis of unusual fractures and is useful in cases with rotational distortions. The MRI is useful in the diagnosis of insufficiency fractures, occult fractures, osteonecrosis, and for soft tissue evaluation.

### Dislocations and Fracture Dislocations

Dislocations of the hip are infrequent, because the strongest forces are required, and frequently associated with fractures of both the acetabulum and femoral head. The type of dislocation is defined by the position of the femoral head in relation to the acetabulum. Posterior dislocation is most common (Fig. 23), frequently associated with a fracture of the posterior acetabular rim. Posterosuperior (iliac) dislocation is more common than posteroinferior (ischial) dislocation. Posterosuperior dislocation may be missed on the AP radiograph, because the femoral head may project onto the acetabular fossa. Signs of dislocation may be the absence of visualization of the lesser trochanter due to posterior rotation and lack of exact congruency of the femoral head and acetabular fossa. In posteroinferior dislocation, the femoral head projects onto the ischial tuberosity. A fracture of the anteroinferior part or a ventral cortical impression of the femoral head and a fracture of the posterior acetabulum are often associated. These complications are sometimes difficult to visualize on conventional radiographs. The risk of avascular necrosis of the femoral head increases with the length of time the head remains disarticulated. Extent and location of the fracture,



**Fig. 23.** Posterosuperior hip dislocation. In this severe injured patient, acquisition of an image in a second plane is not possible, but the posterior direction of the dislocation can be suspected because the dislocated left femoral head seems to be smaller than the right femoral head; its position is closer to the film and therefore he suffers less geometrical magnification

involvement of weight-bearing surfaces of the femoral head and acetabulum, and the presence of intraarticular fragments are important parameters. Gas in the hip joint indicates a recent hip dislocation.

Anterior dislocation can be divided in superoanterior (pubic) dislocation, where the head of the femur is situated over the pubic crest and externally rotated and in inferoanterior (obturator or peroneal) dislocation, where the head of the femur is located in the region of the foramen. Associated injuries are fractures of the superolateral portion of the femoral head and less often fractures of the acetabular rim and the femoral neck, commonly impression fractures. Prognosis worsens if an impression of the femoral head is >4 mm.

Central dislocation occurs with medial displacement of the femoral head into the pelvis and marked comminution of the acetabulum. Rare dislocation variants are perineal, supracotyloid, infracotyloid, scrotal and luxatio erecta.

Postreduction radiographs have to be analyzed for intraarticular fragments and interposed soft tissue, indicating incomplete reduction. Comparative measurements between the acetabular roof and the femoral head laterally and medially between the femoral head and the medial line of the teardrop can be important. A total distance of more than 11 mm or a difference of >2 mm suggests large effusion or interposition of soft tissue. Computed tomography is the method of choice for evaluation for intraarticular bodies but is less sensitive for the diagnosis of nonosseous interponates. One should evaluate the femoral head and its congruence with the acetabulum. In the presence of asymmetry, soft tissue interposition should be suspected. The MRI can show muscle injuries, bone contusions, and lesions of the iliofemoral ligament. After hip dislocations, sciatic nerve palsy can be observed with a preference for the peroneal portion. There is a high frequency of associated injuries of the lower extremity.

### Fractures of the Femoral Head

Isolated fractures are rare because of the well-protected location by the acetabulum. Femoral head fractures are usually located at the anteroinferior aspect as shearing and compression fractures in posterior dislocations and at the superolateral femoral head in anterior dislocations. Compression fractures are more common, which may be difficult to diagnose on conventional AP radiographs. Computed tomography readily displays the defect. Because of the common association with hip dislocations, CT is recommended for full evaluation in the presence of femoral head fractures, which can demonstrate also minimal subluxations >2 mm.

Pipkin's classification is widely accepted and describes a fracture below the fovea with the fragment remaining in the acetabular cavity (type I), a fracture above the insertion of the round ligament (type II, most common), type-I and

type-II fractures with a fracture of the femoral neck (type III), and type-I or type-II fractures with a posterosuperior acetabular fracture (type IV). There exists also an AO classification. Posttraumatic avascular necrosis of the femoral head after hip dislocation is related to delayed reduction and the type of associated femoral head fracture. Pipkin type-III fractures have the worst prognosis. Heterotopic ossification is a common complication of operative procedures at the hip region.

Osteochondral lesions have a four-grade staging system on MRI: intact articular cartilage with signal changes in the subchondral bone (grade I); partial detachment of the cartilage and subchondral fragment (grade II); completely detached nondisplaced fragment (grade III); and detached and displaced fragment (grade IV). Diagnostic confidence is increased with grades III–IV osteochondral lesions [43].

### Fractures of the Femoral Neck

Femoral neck fractures may result from significant injury but can also occur spontaneously and in minor trauma in elderly women due to osteoporosis. They may be located either below the femoral head (subcapital; most common), through the neck (transcervical), or at the base (basicervical). They may be complete or incomplete as well as displaced, nondisplaced, or impacted. Subcapital fractures occur in the region where the nutrient vessels pierce the bone and can be injured by shearing of fragments.

Pauwels' fracture classification is mostly used, in which the angulation of the fracture line to the horizontal plane is related to the prognosis: 0–30° (type I) with the best prognosis, 30–70° (type II; Fig. 24), and >70° (type III). As limit between type-II and type-III fractures, some authors prefer a 50° angulation, corresponding to the original publication [44]. There exist also classifications of Garden considering the amount of dislocation and the disruption of the compressive trabeculation and an AO classification. The femoral head is usually in a valgus position; posterior rotation is best seen on axial views. In displaced fractures, the greater trochanter is externally rotated and displaced superiorly. Varus displacement of subcapital fractures is rare and may be difficult to diagnose. The proximal femur is a common site for pathological fractures. Subcapital fractures can have a pathological appearance in osteoporotic patients. Stress and insufficiency fractures are commonly located at the subcapital regions of the femoral neck superolaterally and at the base of the femoral neck inferiorly. These basicervical fractures are most commonly stress fractures, insufficiency fractures, and pathological fractures. Metastasis, renal osteodystrophy, and steroid therapy have to be excluded in the presence of a stress fracture. Stress fractures of the femoral neck may be subclassified into compression type and transverse/distraction type.

In incomplete subcapital fractures, radiographic findings may be limited to subtle cortical irregularities and a sclerotic line, a sclerotic line that breaks off the trabecular



**Fig. 24.** Subcapital femoral neck fracture (*arrowhead*) with the fracture line running about 45° angulated to the horizontal plane, consistent with Pauwels type-II fracture



**Fig. 25.** The coronal CT MPR demonstrates a nondisplaced trochanteric fracture with the fracture line paralleling the intra-trochanteric line (type I after the modified Evans classification)

pattern. Sclerotic areas in the subcapital region, representing impaction lines, may be mistaken for marginal osteophytes. This impaction lines are seen medially and the cortical break occurs superiorly. Osteoarthritis of the hip can also produce faint sclerotic lines which can be misinterpreted as fracture (pseudofracture). Complete fractures show a break of the medial cortex. Radiographic features of stress and insufficiency fractures are ill-defined lines of sclerosis and focal cortical lucency surrounded by sclerotic bone formation. The MRI is most sensitive to identify these lesions.

Avascular necrosis is the most important complication of femoral neck fractures, the highest incidence following subcapital fractures Pauwels type II and type III. The risk of ischemic complications decreases with a more lateral location of the fracture. Magnetic resonance imaging can reveal avascular necrosis only about 6 months after the initial trauma. Intracapsular fractures with associated intraarticular hematoma can also compromise the vascularization. Nonunion results from insufficient reduction and inadequate immobilization and is related to poor blood supply. Deep vein thrombosis and pulmonary embolism can occur in association with proximal femur fractures.

### Fractures of the Trochanteric Region

As compared with fractures of the femoral neck, trochanteric fractures are associated with higher force and comminution is common [45]. Elderly patients are more often affected. Trochanteric fractures are more extensive than femoral neck fractures and cause large hematomas. In contrast, due to better intraosseous blood supply and the extracapsular location, avascular necrosis and nonunion

are infrequent complications. Trochanteric fractures are divided in intertrochanteric, subtrochanteric, and avulsion fractures. The modified Evans classification divides intertrochanteric fractures into nondisplaced two-part fractures where the fracture line parallels the intertrochanteric line (type I; may be difficult to distinguish from basicervical fractures; Fig. 25), displaced two-part fractures (type II), three-part fractures with a displaced greater trochanter fragment (type III), three-part fractures with displacement of the calcar or lesser trochanter fragment (type IV) and four-part fractures with loss of both medial and posterolateral support (type V). Types I and II are considered stable, types III to V unstable. Less often, fracture lines extends into the subtrochanteric region, and occasionally, reverse fracture lines can be seen. Unstable fractures are also characterized by the postreductional presence of a defect zone, persistent dislocation of the greater trochanter or fracture or comminution of the greater trochanter itself. Isolated avulsion of the lesser trochanter is not indicative for instability. The degree of comminution may be difficult to assess on AP radiographs.

The definition of subtrochanteric fractures remains controversial, but they are usually considered to be within 5 cm below the lesser trochanter. In younger patients, they are usually related to high-energy trauma and tend to be comminuted and associated with significant soft tissue injuries and large hematomas. In elderly patients, fractures can occur from low-energy trauma and tend to be linear or spiral and only minimally comminuted. Subtrochanteric fractures can be divided in transverse and oblique fractures with or without a wedge fragment. Especially in transverse fractures, pathologic processes have to be ex-



cluded. If there is varus angulation, resulting in shortening of the affected extremity, fractures are unstable. Other important variables are continuity of the lesser trochanter and involvement of either the greater trochanter or the piriformis fossa.

Avulsion fractures are generally visible on conventional radiographs. Greater trochanter avulsions, more commonly in elderly patients, require further investigation. Associated intertrochanteric fractures are common and most occult. They are best demonstrated with MRI. Avulsion injuries of the lesser trochanter are rare in adults and should lead to search metastatic disease or systemic diseases such as chronic renal failure. Long-standing and mature avulsion may manifest as either hypertrophic ossification or as localized erosion caused by hyperemic osteolysis. The site of the lesion suggests the diagnosis and MRI can be used to exclude a mass lesion.

### Soft Tissue Lesions

Acute acetabular labral tearing is a precursor for degenerative joint disease. The differentiation from intraarticular loose bodies, synovitis, degenerative joint disease, and cartilage defects can be performed with MR arthrography. The criterion for diagnosis include contrast material tracking along the acetabular/labral interface on at least one image with or without anterior displacement of the labrum. The most common trauma-related tears are radial flap tears and longitudinal labral tears.

Groin disruption (Gilmore's groin) include one or more of the following: torn external oblique aponeurosis; torn conjoined tendon; conjoined tendon torn from the pubic tubercle; and dehiscence between the conjoined tendon and the inguinal ligament. There should be no evidence of hernia.

### 2.11.5.2 Knee

The AP and lateral views are taken as baseline study. In the AP view, the tibial plateaus are not visualized tangentially. Tangential demonstration needs a caudal angulation of 15°. The patella overlies the patellofemoral groove and the medial femoral condyle and the head of the fibula is overlapped by the lateral margin of the tibia on the AP projection. On the lateral view there can be seen a prefemoral fat pad below the quadriceps tendon and an infrapatellar fat pad between the patellar tendon and the femoral condyles. A blood-fat niveau on the lateral radiograph is indicative of joint damage. On an AP radiograph (Fig. 26), femoral and tibial condyles should not overlap, and on the lateral radiograph, both femoral condyles should exactly overlap. For definite fracture exclusion, some authors propose to add both oblique views. Internal oblique view with the leg internally rotated about 45° demonstrates the upper fibula, the tibiofibular joint, and the medial portion of the patella.



**Fig. 26.** A fat–fluid level (*arrowhead*) in the suprapatellar recess is indicative of hemarthrosis

The external oblique view demonstrates the lateral margin of the patella, the medial tibial plateau and the medial femoral condyle. Special projections include the notch view for the evaluation of patients with osteochondrosis dissecans or avulsion fractures and the patellar/tangential view for visualization of the joint surface, the medial and lateral joint facets and the patellofemoral groove. This view is required for exact evaluation of the position of the patella, patellar fractures, and the patellofemoral joint space. Stress views are difficult to perform in the injured knee. Computed tomography is useful for searching undisplaced fractures and evaluation of comminuted fractures of the femur and the tibia as well as for detection of small osseous fragments, following patellar dislocation.

### Distal Femur Fractures

Distal femur fractures are often high-velocity injuries. They are associated with ligamentous disruption of the knee, patellar fractures, fracture–dislocations of the hip and fractures of the tibial shaft and are classified according to the site and the extension of the fracture line as supracondylar, condylar, or intercondylar.

Supracondylar fractures are frequently transverse or slightly oblique with varying degrees of displacement and comminution. Extension of the fractures into the knee joint is common. Computed tomography helps to assess fracture extent and anatomy, if plain radiographic findings are not conclusive. Fractures of the femoral condyles are intraarticular fractures confined to one or both condyles. Fractures in which sagittal and coronal fracture lines are



**Fig. 27.** Combination of a comminuted distal femoral fracture and a comminuted proximal tibial fracture, resulting in a floating knee

isolated to the region of a condyle are more difficult to detect on radiographs and may require CT evaluation. Y- or T-shaped femur fractures with the sagittal component extending into the intercondylar notch may be described as intercondylar fractures. Computed tomography may be required for full evaluation of fracture lines and localization of fragments. Associated injuries are injuries to the popliteal artery, tibial shaft fractures, sometimes resulting in a floating knee (Fig. 27) or hip dislocations.

Minimally displaced fractures of the articular surfaces of the distal femur and proximal tibia may be extremely subtle, but accurate diagnosis is important because undetected fractures may lead to collapse of the joint surface and accelerated osteoarthritis. An effusion is often the most obvious sign of injury but accompanies frequently other joint disorders. A fat/fluid level on the lateral projection is very specific, but it is not often seen. The MRI may be necessary to confirm a subtle injury.

Avulsive cortical irregularity of the distal femur is most commonly an incidental finding which should not be mistaken for a bone tumor. The lesion may suddenly become painful.

### Proximal Tibial Fractures and Avulsion Fractures

The tibial plateau is the most common site of fractures of the proximal tibia. In a normal knee, the greater portion of the weight is transmitted through the medial femoral condyle to the medial tibial plateau, evidenced by a greater number of trabeculae within the medial femoral condyle and beneath the medial plateau. The lateral tibial plateau is weaker; therefore, isolated lateral plateau fractures are most common. Combined lateral and medial plateau fractures are more frequent than isolated medial plateau fractures. The most useful classification appears to be that of Schatzker. Types 1–3 involve the lateral plateau and imply a lower-energy trauma. Type 1 is a pure split or wedge fracture. Displacement may be lateral and distal. There is a high rate of ligamentous disruption and the lateral meniscus may be torn and displaced into the fracture site; those that involve the articular surface and rim are unstable. A type-2 fracture is a split-compression fracture, occurring mostly in the age group over 30 years and associated with cruciate and collateral ligament injury. A type-3 fracture is an isolated compression fracture that is commonly central to the condyle (Fig. 28) and occurs in older osteoporotic individuals after a less significant trauma. A mosaic-like pattern of multiple fractures of the articular surface is classic. These injuries carry a low risk of ligamentous injury. An intact articular rim usually provides stability unless the entire articular surface is involved. Lateral and posterior lesions are associated with greater instability. A type-4 fracture, typically after a high-energy trauma, involves the medial plateau and may be comminuted or depressed. The tibial spines are often involved. Associated injuries are common and include cruciate, lateral collateral, peroneal nerve, and popliteal vessel injury. A type-5 fracture is a bicondylar fracture with varying degrees of depression, displacement, and comminution. Neurovascular injury is not uncommon. A type-6 injury has associated diaphyseal and metaphyseal separation. Very high-energy trauma is implied and fractures may be very comminuted. Nonunion is common.

The fracture type can usually be suspected from the plain radiographs. Sometimes, fractures may not be obvious on the routine radiographs, particularly if there is no depression, because the usual AP radiograph is not tangential to the tibial joint surface. Depression fragments involving the anterior portion of the plateaus can be overlooked and depression fragments involving the posterior portion of the plateau can be overestimated. Computed tomography can detect fractures, confirm the suspected fracture type, and is useful in fracture staging and treatment planning. The examination demonstrates the course of the fracture line, the number, dislocation, and rotation of fragments, allowing precise demonstration of nondisplaced fragments, and the degree of depression and distraction. One should describe involvement of one or both condyles, extra- or intraarticular fractures, and the degree of comminution, impression, or depression of the articular surface. Impressions  $>2$  mm (to 10 mm), displacement  $>5$  mm, clinically diagnosed nonligament instability ( $>10^\circ$  varus or valgus instability in exten-



**Fig. 28.** The coronal CT MPR demonstrates a tibial plateau fracture with isolated impression of the lateral tibial plateau (type 3 after Schatzker)

sion), major ligament disruption, and displaced bicondylar fractures need operative treatment. The 3D reconstructions are helpful in therapy planning and may limit the number of additional views needed. The CT angiography may be needed to assess the presence of vascular injury, likely in 4-through 6-type injury [46]. The MRI may also be used, as it appears to define adequately the bony parameters and allows evaluation of associated soft tissue and ligamentous injuries. In the presence of bone contusion, MRI may show different bone marrow contusion patterns with bone marrow edema (BME) around the knee, which should lead to search for associated soft tissue abnormalities. Pivot shift injury shows BME in the lateral femoral condyle and posterior tibial plateau and is associated with anterior cruciate ligament (ACL) disruption. Dashboard injury shows BME in the anterior proximal tibia and is associated with posterior cruciate ligament (PCL) injury. In hyperextension injury, there are kissing contusion patterns of the anterior tibia and femur, associated with tears of the ACL and/or PCL. In clip injury, there is BME in the lateral femoral condyle associated with medial collateral ligament injury.

Subcondylar and intercondylar fractures in the condylar portion of the proximal tibia are defined by transverse or obliquely orientated fractures.

Avulsion fractures are usually well visible on conventional radiographs, but because of the associated soft tissue lesions, MRI should be performed.

Segond fracture, representing lateral capsular avulsions from the tibia posterior to Gerdy's tubercle, are often associated with anterior cruciate ligament tears, meniscal tears, and avulsions of the fibular head at the insertion of the bi-

ceps muscle or the fibular collateral ligament. The osseous fragment lies immediately distal to the lateral tibial plateau and appears as an elliptic piece of bone parallel to the tibia. Detection is best possible on an AP radiograph. If chronic, the avulsed fragment may become reattached to the tibia, where it forms an osteophyte-like bony excrescence. A true osteophyte, however, arises at the level of the joint line, whereas a chronic Segond fracture occurs below the joint line. Cortical avulsion fracture of the medial tibial plateau in association with posterior cruciate ligament tears are called medial Segond-type fracture.

In injury to Gerdy's tubercle, the attachment of the iliotibial tract, the detached fragment is usually much larger than the Segond fracture fragment and lies more anterior and distal. It is best demonstrated on a 45° external rotation view. This lesion is associated with lateral capsular, lateral collateral, and ACL injury.

Avulsion of the tibial eminence is more common in children, but can also occur in adults, associated with medial collateral ligament tears and focal bone contusions. The radiographic appearance varies with the degree of displacement. There is a staging system for fractures of the anterior tibial eminence. Nondisplaced or minimally displaced fractures (type A) consist of a horizontal fracture line at the base of the anterior portion of the tibial spine, best demonstrated on the lateral view. In type-B lesions, the fragment may be lifted upward as a hinge with a gap anteriorly and the fulcrum posteriorly. In type-C lesions, the fragment may be completely detached, in type-D lesions even inverted. Avulsion fractures of the posterior cruciate ligament of the tibia are rare and difficult to visualize on conventional radiographs. It can be associated with femoral fractures [47] or associated injuries of the cruciate ligament, collateral ligament, and menisci.

Condylar avulsions of the medial collateral ligament are associated with ligamentous sprains and tears, ACL tears, medial meniscal tears, and capsular disruptions. Tibial avulsion fractures of the semimembranous tendon, involve the posteromedial corner of the tibial plateau, and are rarely associated with ACL tears.

Stress and insufficiency fractures are commonly seen beneath the medial tibial plateau and at the junction of the mid- and proximal thirds of the tibia. Initial radiographs are frequently normal. The earliest conventional radiographic sign is loss of definition of the posterior cortex, followed by periostitis, central linear lucency, and finally, after a few weeks, there appears a plate-like 2- to 3-mm-wide band of endostal callus or sclerosis; periostal callus is rarely observed. The lesion is best shown with MRI and can be differentiated from early osteonecrosis and other knee disorders.

### Knee Dislocations

Dislocations of the knee require major force; therefore, possible associated injuries are visceral injuries and skull fractures. There are five types: anterior; posterior; lateral;



**Fig. 29.** Anterior dislocation of the tibia and the fibula. The image is indicative of major ligamentous and neurovascular damage

medial; and rotatory (posterolateral). Anterior dislocation (Fig. 29) is most common and is associated with tearing of the posterior capsule and posterior cruciate ligament. Posterior dislocations are the next most common type. Other types are rare but often associated with collateral ligament injuries. Involvement of both cruciate ligaments and one or both collateral ligaments is common. Especially in rotatory dislocation, irreducible intraarticular invagination of the medial capsule and the medial collateral ligament can be detected. The popliteal vessels and the tibial and peroneal nerve also may be injured during knee dislocations.

Knee dislocations are usually obvious on radiographs. Additional oblique views, CT, or CT arthrography should be performed to search for associated osteochondral fractures, fibular head fractures, avulsion injuries of the tibial spine, and to delineate the status of the popliteal artery in patients with vascular symptoms and signs. For the staging of associated soft tissue injuries, MRI is the method of choice.

### Proximal Fibular and Tibiofibular Joint Injuries

Fibular fractures are frequently combined with ligamentous injuries of the knee or fractures of the lateral tibial plateau or the ankle (Maisonneuve fracture). Associated injuries are rupture of the lateral capsular and ligamentous structures and injury to the peroneal nerve.

Dislocations of the tibiofibular joint are uncommon. They are classified whether the displacement of the fibular head is anterolateral (most common) or posteromedial or superior; the latter is invariably associated with fracture-

dislocations of the ankle or fractures of the distal tibia. In such cases, the whole tibia should be included in radiographic examination. In the other cases, radiographic findings associated with dislocation of the proximal tibiofibular joint may be subtle. The relationship of the fibular head to the osseous groove on the posterolateral aspect of the tibia should be carefully analyzed. If on an AP radiograph the fibular head is either completely obscured or completely uncovered by the tibia, dislocation of the proximal tibiofibular joint should be suspected. In some cases, oblique radiographs may reveal complete separation of the tibia and fibula.

A cortical avulsion of the fibular collateral ligament at its insertion can be identified on AP and lateral views and is often associated with arcuate ligament, popliteal tendon, and anterior cruciate ligament disruption. The avulsion fragments should not be confused with the rare sesamoid fibular bone or cyamella.

### Patellar Fractures, Dislocations, and Osteochondral Injuries

Patellar fractures are common, and unilateral injuries predominate. Transverse fractures are typical. They may divide the patella into equal-sized components or involve the superior or more commonly the inferior pole. Longitudinal and comminuted or stellate fractures are less common. Displacement of fracture fragments indicates disruption of the patellar retinaculum. Radiographic diagnosis is easy in most cases. Comminuted or transverse fractures are visible on frontal projections, whereas longitudinal fractures are best demonstrated on axial radiographs. Fractures of the patella should be differentiated from bipartite or multipartite patella (representing accessory ossification centers) and from the dorsal defect of the patella, both characteristically occurring superolaterally. The dorsal defect is best seen on the AP view, appearing as rounded, well-defined lucency, and should be easily distinguished from a fracture. Complications include displacement of fragments particularly in comminuted fractures and osteonecrosis.

Patellar dislocation is common among young people and may be defined as primary disruption of the patellofemoral relationship where the patella is displaced out of the sulcus. Predisposing factors are patellar or femoral dysplasia, ligamentous insufficiency, or patella alta. The dislocation is most common lateral; rare patterns of displacement include superior or rotational dislocations. Diagnosis on conventional radiographs is easy if the patella is actually dislocated. After spontaneous reduction, the diagnosis can be difficult and radiographs may reveal osteochondral fragments from the medial patella facet or the lateral femoral condyle or an abnormal angulation of the patella in the horizontal plane (patellar tilt). The MRI demonstrates BME in the inferomedial patella and in the anterolateral aspect of the lateral femoral condyle after lateral dislocation. Ruptures of the medial retinacula, eventually associated with osseous avulsions at the insertion at the



adductor tubercle, bone contusions, and osteochondral fractures, occur frequently with dislocation. Recurrent dislocation or subluxation may occur after an initial acute traumatic dislocation but develops more commonly from developmental abnormalities.

Osteochondral fragments containing a sizeable piece of bone can be visible on conventional radiographs, including tunnel and axial views. In adults, these fractures often occur at the junction of the calcified and uncalcified cartilage. Pure chondral fragments are not visible on plain film radiographs; therefore, staging is best accomplished with MRI. Lesions have been classified with the Outerbridge classification: Grade I is softening of the superficial aspect of the cartilage, grade II is fissuring of the cartilage limited to an area of 1 cm in diameter or less, grade III is fissuring of the cartilage extending to an area >1 cm in diameter, and grade IV is focal cartilaginous defect with exposure to subchondral bone. Free fragments can be located in the suprapatellar bursa, behind the patella, within the intercondylar notch or beside the femoral condyles within the joint space or in a Baker cyst.

Patellar sleeve fractures are acute avulsion fractures of the lower pole of the patella. The MRI may be required for better visualization of the extension of the fracture into the chondral tissue. True avulsion fractures of the superior pole of the patella are uncommon. They are evident on conventional radiographs and may not require further imaging.

### Extensor Mechanism Injuries

Extensor mechanism pathology can be related to the quadriceps mechanism, patellar tendon, or patellofemoral joint. These injuries are often accompanied by small avulsion fractures at either the proximal or distal pole of the patella, avulsion of the anterior tibial tubercle at the insertion of the infrapatellar tendon, or transverse fracture of the proximal or distal pole of the patella.

Quadriceps tendon rupture occurs most likely in patients with a previous history of cortisone injections, diabetes mellitus, renal failure, gout, or hyperparathyroidism, and is rare in healthy persons. Patellar tendon ruptures are more likely in patients with chronic patellar tendinitis and occurs usually at the junction with the inferior pole of the patella or less commonly with an avulsion fracture of the tibial tubercle.

Incomplete tendon tears are not associated with changes in patellar position. In complete tears there is soft tissue swelling, distortion of the soft tissue planes above or below the patella, and an inferior (patella *infera* or *baja*) or superior (patella *alta*) patellar position. The position of the patella can be described in the lateral projection after Insall-Salvati. The knee should be in a flexion about 20–70°. A quotient between the craniocaudal patellar length and the patellar tendon length (between the lower patellar pole and the tibial tuberosity) is formed. If the quotient is <0.75, there is patella *baja*; if the quotient is >1.15, there is patella

*alta*. The main clinical question is to distinguish a partial from a complete tear. For screening, usually US is recommended and MRI should be reserved for cases in which US cannot make the discrimination or if internal derangement of the knee is suspected.

Fractures of the anterior tibial tubercle are common. They are divided into three types: the tubercle hinged upward without displacement of the proximal base (type I); an avulsion of a smaller portion of the tubercle with proximal retraction (type II); and more severe injuries extending across the articular surface (type III). Avulsions of the tibial tuberosity are most frequently seen in young adolescents with ongoing Osgood-Schlatter disease [48] or with Sinding-Larsson-Johansson disease. Magnetic resonance imaging may play a significant role in distinguishing acute fractures from long-standing soft tissue inflammatory changes and fragmented nonfused tibial tuberosities.

### Soft Tissue Injuries Cruciate Ligaments

Plain-film signs of ACL injury are avulsion of the bony insertion site, anterior displacement of the tibia, a depth of the condylopatellar sulcus of 1.5 mm or more, and, very uncommonly, impaction fractures involving the posterior corner of the lateral tibial plateau or avulsion fractures of the posterior lateral tibial plateau [49].

The MRI is highly sensitive and specific in identification of ACL tears. Direct signs of ACL disruption include discontinuity of fibers (Fig. 30), abnormal slope of ACL, non-visualization of the ACL fibers on both sagittal and coronal planes, or avulsions of the anterior tibial spine. Indirect signs of ACL disruption include BME in lateral femoral condyle and posterior tibial plateau, deep sulcus sign (condylopatellar sulcus >2 mm), Segond fracture, kissing contusions of anterior tibia and femur, and anterior translation of the tibia relative to the femur. Nonspecific signs are buckling of the PCL, shearing injury to the Hoffa fat pad, and acute hemarthrosis. The diagnosis of partial tears is more difficult. There can be focal increased intraligamentous signal in T2-weighted images, posterior bowing, and attenuation of the bulk of the ACL. The MRI sensitivity and specificity is limited in partial tears [50]. Commonly associated injuries are tears of the posterior horn of either the medial or lateral meniscus, medial collateral ligament injuries, and posterolateral capsular injuries.

Posterior cruciate ligament injuries are less common and frequently involve its mid-substance and less commonly the proximal and distal limbs, which are more frequently involved in the setting of knee dislocation or combined injuries. Isolated PCL injuries are less common than injury combined with other ligamentous, capsular, and/or meniscal injury. Detection of such combined injuries is critical for treatment. Avulsion of the tibial attachment site of the PCL is the only plain radiographic sign of PCL injury. Primary MRI signs of PCL injury include high signal completely travers-



**Fig. 30.** An ACL tear: T1-weighted MRI image in the sagittal plane demonstrates discontinuity of the ACL fibers (*arrowhead*) and buckling of the distal ACL part

ing the fibers of the PCL on T2-weighted images in complete tear, high signal incompletely traversing the fibers of the PCL on T2-weighted images in partial tear, or an avulsion injury of the femoral insertion of the ligament. Secondary MRI signs are bone marrow edema involving the anterior proximal tibia or avulsion of the posterior tibia at the PCL insertion site. With a partial tear, there are intact fibers identified along the course of the ligament. Edema seen with PCL injuries is less conspicuous than in ACL tears [51]. Associated soft tissue injuries include disruption of the ACL, injury of the medial or less commonly the lateral collateral ligament, and injury of the medial meniscus, which is more common than in the lateral meniscus [52].

### Collateral Ligaments

In medial collateral ligament lesions, usually the proximal femoral attachment is injured. Plain-film signs of collateral ligament injury are uncommon. Occasionally, the joint space on the affected side may be widened. Avulsion of ligamentous attachment sites may be evident. The most common sign in chronic lesions is heterotopic ossification adjacent to the femoral origin of the medial collateral ligament, called Pellegrini-Steida disease. Lesions of the superficial parts of the collateral ligaments can also be staged on US examination. Injuries can be graded as minimal tear or strain injury with hypoechoic fluid parallel to the ligament (grade I), partial tear with hypoechoic fluid and ligament thickening (grade II), and complete tear with hematoma and disruption (grade III) [53]. In MRI, which can evaluate the entire ligament (best in the coronal plane), the grading is as follows: edema superficial to the fibers (grade I); edema extending partially through the ligament (grade II); and complete discontinuity (grade III; Fig. 31). The ACL and meniscal tears can occur in conjunction.



**Fig. 31.** An MCL tear: T1-weighted MRI image in the coronal plane demonstrates discontinuity of the MCL fibers (*arrowhead*) with ligamentous thickening, representing a grade-3 tear

Lesions of the posterolateral corner include lesions to the lateral collateral ligament, the arcuate ligament, the lateral capsule, and the popliteal muscle; the latter should be completely evaluated (muscle belly, muscle-tendon junction, tendon insertion). Isolated injury to the posterolateral corner of the knee is uncommon; injury usually occurs in conjunction with a cruciate ligament tear. On MRI, soft tissue swelling and edema of the subcutaneous fat along the lateral joint line are indicators of acute injury. Possible findings include tearing of the fibular collateral ligament, partial or complete popliteal musculotendinous tears, and less commonly popliteal disruption at its femur insertion site. There may also be injury to the arcuate ligament. The MRI grading is the same as for medial collateral ligament tears. Associated injury to the lateral head of gastrocnemius and/or the biceps femoris may be seen and an avulsion fracture of the proximal fibular head or “arcuate sign” may be present. There may also be a medial tibial plateau compression fracture.

### Menisci

Meniscal tears have been classified as horizontal, vertical, or radial. Traumatic meniscal tears are typically vertically and longitudinally oriented. Imaging of choice is MRI. Grading of meniscal signal include intrasubstance globular-appearing signal that does not extend to an articular surface (grade I), intrasubstance linear signal that does not extend to an articular surface (grade 2), and intrasubstance signal

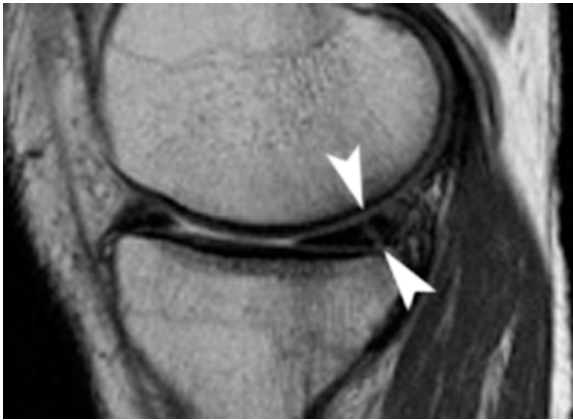


**Fig. 32.** Meniscus tear: T1-weighted MRI in the sagittal plane demonstrates intrasubstance high signal with extension to both surfaces (grade-3 signal) in the posterior horn of the medial meniscus (*arrowheads*)

that extends to either the superior or the inferior surface (grade 3; Fig. 32). Grades 1 and 2 represent intrasubstance degeneration in adults or prominent vascularity in a child. Grade-3 signal represents a tear. Criteria to detect meniscal tear are unequivocal grade-3 signal, abnormal meniscal morphology, displaced or missing meniscal tissue in the absence of surgical history, and meniscocapsular separation. The MRI signs associated with meniscal tears are: an absent bow-tie sign (the second sagittal image fails to have bow-tie appearance of the meniscus); the double PCL sign in a displaced bucket-handle tear of the medial meniscus; and the large anterior horn sign in a displaced bucket-handle tear of the lateral meniscus. The notch sign is when a small notch appears out of the articular surface of the meniscus. Another type of meniscal tear that is easily overlooked is an inferior displaced medial meniscus flap tear. It is best seen on the first sagittal image through the body of the meniscus, when the usual rectangular slab of the meniscus is absent; otherwise, a piece of meniscus can be seen inferior to the body segment.

Radial tears involve the inner edge of the meniscus; most occur in the posterior horns. The MRI can show a marching cleft or a truncated triangle. Peripheral tears occur at the attachment to the capsule, an area that has more vascularity. Important in the description of traumatic meniscal tears is the extent into the central avascular parts and the description of dislocated fragments. Meniscocapsular separation is a sign of instability.

Meniscal contusion usually occurs in association with an anterior cruciate ligament tear. Increased signal at the meniscal periphery can resemble a tear; however, it is amorphous rather than sharp and discrete. Adjacent bone contusion is often seen.

Normal variants that can lead to misdiagnosis of a meniscal lesion are meniscal flocule (wavy or folded ap-

pearance of the inner edge of medial meniscus, associated with ligamentous laxity), speckled appearance of the anterior horn of the lateral meniscus, caused by the insertion of fibers of the ACL, and a discoid lateral meniscus, particularly the Wrisberg's variant in which the posterior horn is not attached to the capsule and therefore mobile [54]. Normal anatomical structures in close proximity to meniscus can mimic a tear, such as the anterior transverse ligament (anterior horn, lateral meniscus), the meniscofemoral ligaments (posterior horn, lateral meniscus), the popliteal tendon and bursa (posterior horn, lateral meniscus), and the medial and lateral oblique menisco-meniscal ligament (bucket-handle tear). Also pathological conditions, such as gas within the joint, chondrocalcinosis, and articular cartilage defects, may mimic a tear.

Computed tomography arthrography and virtual arthroscopy has an excellent delineation of the articular bone and the contrast media in the joint cavity. Differentiation of a true meniscal tear is also possible, but intrameniscal pathology is not shown. Computed tomography has a limitation in terms of the delineation of structures outside the joint cavity such as the collateral ligaments and the PCL. Virtual arthroscopy may be helpful in detecting meniscal lesions. Although CT is not the gold standard, it may be helpful in some situations [55]. With air serving as contrast, MPR can show the cartilage of the knee joint [56].

### Tibial and fibular shaft Fractures

Shaft fractures are usually evident on plain-film radiographs. Visualization of the entire leg ensures that the fibular fractures, which are often not adjacent to tibial fractures can be seen. The amount of rotational deformity is best assessed if both the proximal and the distal joints are included in the image. Tibial fractures may also lead to compartment syndrome. In patients with tibial fractures associated with severe trauma, radiographic evaluation of the pelvis and proximal femur should be performed to avoid missing these injuries. Healing of tibial fractures may be problematic, and the most common site for delayed union or nonunion is the distal third of the tibia. Soft tissue defects, infection, large bone defects, markedly distracted fracture fragments, and segmentation may contribute to delayed union or nonunion.

### 2.11.5.3 Ankle

Standard views of ankle include an AP view and a lateral view that should include the base of the fifth metatarsal or a lateral view in combination with a mortise view. The diagnostically preferable view is a modified anteroposterior projection with the ankle rotated inwardly by about 15–20° (mortise view), demonstrating the medial and lateral joint space without overlap. Because of the axis of dorsal and

plantar flexion is not parallel to the film in the AP view, both malleoli will overlap the medial and lateral joint surface of the talus and flake fractures cannot be sufficiently well judged. This is not the case in the mortise view. Marginal benefits have been shown by combining all three views.

One should play close attention to the cortical outline, as flake fractures within the joint are easily overlooked. The width of the joint space should be 3–4 mm medially and <5 mm laterally. When the distance between the tibia and fibula exceeds 6 mm, one should suspect ligamentous injury. It is important to include the base of the fifth metatarsal in the lateral view, since avulsion fractures are not uncommon and manifest clinically like ankle fractures. Care should be taken not to interpret accessory bones as fractures. Certain fractures are not visible on standard projections. If there is convincing clinical evidence of substantial trauma, additional projections should be obtained. The 45° internal oblique view improves the visualization of the medial malleolus and the posterior facet of the talocalcaneal joint. The 45° external oblique view shows the contour of the anterior tubercle of the tibia and the lateral malleolus is seen from a different angle. Stress examinations have widely been replaced by MRI.

### Ankle Fractures

Ankle fractures are described as unimalleolar, when the medial or the lateral malleolus is involved, as bimalleolar, when both malleoli are fractured, as trimalleolar, when fracture involves the medial and lateral malleolus as well as the posterior lip (Volkman triangle) of the distal tibia, and as complex when comminuted fractures of the distal tibia and fibula occur. Weber's classification is widest used and focuses on the most important structures, such as the syndesmosis and the interosseous membrane, and relates their stability to the height of the fibular fracture. Type A is a transverse fracture of the distal fibula at the level or below the joint space. There may be an accompanying fracture of the medial malleolus and a tear of the anterior fibulotalar ligament. Type B is a spiral or oblique fracture of the fibula at the height of the joint space with partial or questionable destruction of the tibiofibular syndesmosis and may be accompanied by an avulsion fracture of the medial malleolus or a rupture of the deltoid ligament. Type C (Fig. 33) is a fibular fracture above the level of the ankle joint associated with a rupture of the posterior fibulotalar ligament and the syndesmosis, resulting in lateral instability. A Maisonneuve fracture results from ankle trauma with proximal propagation of force through the tibiofibular syndesmosis, which is ruptured up to that level. Ankle radiographs that demonstrate an isolated fracture of the posterior lip of the tibia or the medial malleolus should have a radiograph of the entire fibula. There are five stages of a Maisonneuve injury: tear of the anterior tibiofibular ligament; posterior malleo-



**Fig. 33.** Fracture of the distal fibula with the fracture level superior to the joint level (Weber type C)

lar (Volkman) fracture; joint capsule tear; proximal fibula fracture; and medial malleolar fracture or deltoid ligament tear. In general, dislocation of joint-forming osseous surfaces >2 mm needs surgical repair.

Volkman's fracture is a dorsal intraarticular tibial fracture. If the articular fragment measures >1 cm, reduction is indicated. All fractures with comminution of the distal tibial articular surface, often impressed, are referred to as pilon tibial fractures. There exist several classifications that describe the various degree of displacement of bone fragments and the joint surface involvement. Because even minimal incongruences of the tibial surface may lead to rapidly arthrotic change, almost all pilon tibial fractures (Fig. 34) require operative treatment. Even after optimal reposition, there remains a high risk of partial or even total necrosis of the talus. Complex comminuted fractures are further complicated by extensive soft tissue damage and perfusion deficits. Tillaux fractures are fractures in the anterior part of the distal tibia with a coronal course of the fracture line. In a triplane fracture, there are three fracture lines: the sagittal line, typically located at the epiphysis can be seen on the AP radiograph; the transverse line



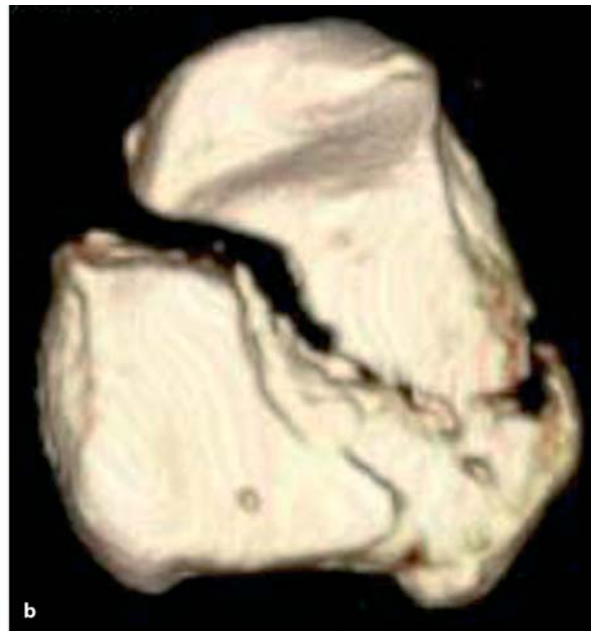


**Fig. 34.** **a** Pilon tibiale fracture: a comminuted intraarticular fracture of the distal tibia. **b** The CT VRT demonstrates position of the fracture fragments and gaps in the joint surface

on the AP and the lateral projection and the coronal line (typically located at the metaphysis) on the lateral line-projection.

In complex fractures, especially in pilon-tibiale, triplane, and Tillaux fractures, CT is helpful for surgical planning.

### Ligamentous and Tendinous injury

In a typical ankle sprain, the lateral ligaments fail in a predictive manner, with the anterior talofibular failing first, followed by the calcaneofibular ligament and finally by the posterior talofibular ligament. Ligamentous sprains are readily diagnosed with sonography and MRI; however, there are rare indications, e.g., clinical confusion between acute lateral ankle ligament complex injury and a distal tibiofibular syndesmosis injury. Targeted US can be very helpful when specific extraarticular complications are suspected [57]. Sprains may be divided into benign (the intraarticular effusion does not go through the ligament), middle-intensity (the ligament is lifted at the insertion, forming a pouch of liquid close to the bone or partial interruption of the ligament fibers is evident), and severe (a complete tear, allowing the effusion to reach the subcutaneous tissue). A severe tear is often central, as opposed to the insertion-site tears seen in middle-intensity lesions. Because of the close relationship between the calcaneofibular ligament and the fibular tendons and sheath, there is almost always an eruption of fluid

in the fibular tendon sheath associated with a complete and recent calcaneofibular tear. The tendons will be surrounded by fluid, forming a typical tenosynovitis. They will also move deeper towards the calcaneus bony margin because of loss of the ligamentous layer. The latter sign is most readily visualized during dorsal hyperflexion. Ultrasound can provide demonstration of the anterior talofibular ligament and allows dynamic assessment.

Sprains of the deltoid ligament can be associated with Achilles and posterior tibial tendon tears. Interposition of the ruptured deltoid ligament into the medial gutter, precluding reduction of extraarticular ankle fracture has been reported. As sequelae, there are possible impingement symptoms and concurrent chondral damage is common. The entire ligament is best evaluated with MRI, only the posterior component of the deep fibers is accessible to US.

In syndesmotic injuries there is most commonly a lesion of the anterior tibiofibular ligament while the posterior tibiofibular ligament remains intact. Avulsions at the tibial or fibular attachments may be associated with small cortical avulsion flake fractures. The radiographic signs of a syndesmotic injury may be subtle. The most reliable criterion for diagnosis on conventional radiographs is a tibiofibular clear space (representing the posterior aspect of the syndesmosis) on the AP view of  $>6$  mm. Another sign is the enlargement of the joint space between the medial malleolus and the talus. A CT can show subtle, radi-

ographically occult abnormalities in syndesmotomic alignment. Evaluation with MRI or US (acute tears manifest usually as anechoic cleft) is also possible.

If there is a targeted clinical question referable to one of the tendons about the ankle and the foot, ultrasound examination is useful because of its ability to perform provocative maneuvers and evaluate for possible tendon subluxation, usually involving the peroneal tendons after injury of the superior retinaculum. The MRI is an alternative if the differential diagnosis is broader and includes structures such as the spring ligament or osseous abnormality.

Injuries to the Achilles tendon are readily diagnosed with US. Evaluation of the tendon include distinguishing a ruptured tendon from a ruptured muscle–tendon junction, determining the position and size of the tendon deficit as well as the ability to oppose ruptured tendon ends with the foot plantar flexed and to distinguish tendinopathy from interstitial tear. The gap is most commonly direct above the calcaneus.

Evaluation of further tendons is possible with US or with MRI. It is important to note that most commonly the flexor hallucis longus tendon sheath, but also the tibialis posterior and flexor digitorum longus tendon sheath and the fibularis tendons can normally contain a small amount of fluid. The posterior tibialis tendon is normally about twice the diameter of the adjacent flexor digitorum longus tendon. Tendon tears in the ankle region may develop rather after chronic injury than in the acute setting. Dislocation of the posterior tibialis tendon along the outer aspect of the medial malleolus can occur in acute injury [58]. Tears of the posterior tibialis tendon can result in a painful flat foot deformity. If CT is performed for assessment of bony injuries, there can be a first assessment of possible tendon injury with 3D volume-rendering techniques as well as in the wrist [59].

#### 2.11.5.4 Foot

Standard radiographs of the foot include dorsoplantar (DP), 30° internal oblique views, and additional lateral views. The CT examinations of the hindfoot are very helpful, since they are able to show the complex anatomy and pathomorphological changes after injuries of the tarsus and can be considered as technique of choice for tarsal and subtalar joint trauma. The CT examination of talus, calcaneus, and the subtalar joint requires a minimum of 1-mm slices. Complex foot injuries, such as calcaneal fractures and tarsal injuries, and fracture–dislocations, such as the Lisfranc injury, are well demonstrated by CT. In a study for evaluation of imaging modalities in hyperflexion injuries, the conclusion was that conventional radiographs including weight-bearing views were not sufficient for routine diagnostic work-up of patients with acute hyperflexion injuries in the foot, and that CT should serve as the primary imaging technique for such patients [60].

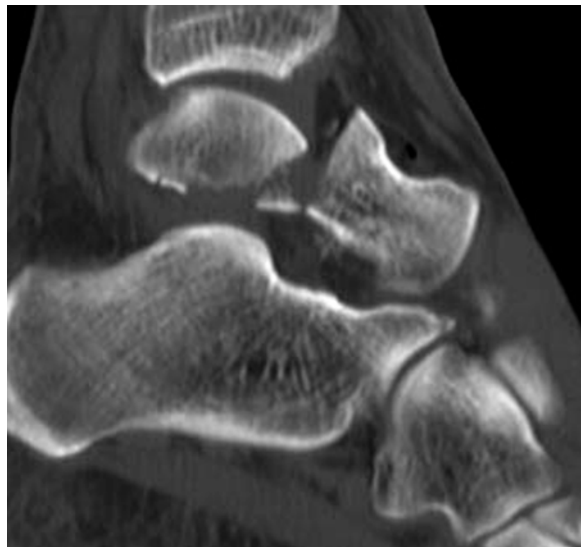


**Fig. 35.** The CT MPR in the sagittal plane demonstrates a talar neck fracture with dislocation of the subtalar joint. The navicular bone in this sagittal plane at the level of the talar joint surface is not visible; therefore, a dislocation in the talonavicular joint is present (type-IV lesion after Hawkins)

#### Talar Fractures

Fractures of the talus are not very frequent. Often, the neck of the talus is involved. The most commonly used classification of talar neck fractures is that established by Hawkins, defining the following categories: a fracture of the talar neck without dislocation or subluxation (type I); a lesion with subluxation or dislocation of the subtalar joint without dislocation of the ankle joint (type II); a lesion with complete dislocation of the body of the talus from the ankle joint as well as from the subtalar joint (type III); and a lesion associated with dislocation of the talonavicular joint (type IV; Fig. 35). The risk of avascular necrosis of the talar neck increases with higher fracture types. In type-IV fractures, the talar head is also at risk for avascular necrosis. Fractures of the body and the lateral and posterior processes are less common.

On conventional radiographs, fracture fragments of lateral-process fractures are easily overlooked because they are often overlapped by other bony structures. Small avulsions dorsal to the talar head are quite common but clinically not important. Neck and body fractures are associated with subtalar subluxation or posterior dislocation of the body; therefore, the position of the posterior facet of the subtalar joint has to be examined carefully. A CT examination is necessary if the amount of dislocation is unclear on conventional radiographs or for demonstration of avulsion fractures. An MRI scan can demonstrate avascular necrosis.

Acute traumatic chondral or osteochondral lesions typically occur at the medial or lateral talar dome margins and at the anterior or posterior margins of the plafond, and are

seen as small transverse fissures or chondral fractures. They can be evident on conventional radiographs as a curvilinear subchondral lucency. Nondislocated lesions are sometimes difficult to detect. Isolated chondral lesions in the ankle generally have a traumatic etiology and are associated with a negative prognosis after a fracture or ankle sprain. Could be slightly more sensitive than MR arthrography in detecting articular cartilage lesions [61].

Extended talar fractures are usually associated with lesions of the talonavicular joint or fractures of the navicular.

### Calcaneal Fractures

Calcaneus fractures are usually classified after Essex-Lopresti, which distinguishes between intraarticular and extraarticular fractures with regard to the subtalar joint. Extraarticular fractures are mostly avulsion fractures and classified into the “beak” type, horizontal and vertical types, and medial avulsions. They are usually easy to identify on conventional radiographs. Fractures of the anterior process are avulsions of the plantar calcaneonavicular ligament and are often overlooked in supination injuries.

Intraarticular fractures are in general complex fractures. The primary fracture line runs from posterolateral to anteromedial, and the secondary fracture lines run from the primary line to lateral. In intraarticular fractures, there are two subtypes. In the more common joint depression type (Fig. 36), the fracture line runs across the body just behind the subtalar joint. There is a lateralization of the central fragment which carries the posterior facet of the subtalar joint. Dislocation often causes impingement of peroneal tendons. The tongue type shows a tongue-like fragment in the lateral view and a straight fracture line running to the posterior margin of the calcaneus.

Plain-film examination of the calcaneus requires an axial as well as a lateral projection and different oblique views of the ankle. Böhler’s angle, formed by the intersection of two lines, one drawn from the posterior facet to the anterior superior calcaneus, the other drawn along the tuberosity and posterior facet, ranges between 20 and 40°. A reduction of Böhler’s angle may suggest a subtle intraarticular calcaneal fracture, but a normal angle does not exclude a fracture. The most important information for therapy concerns the comminution of the posterior facet of the subtalar joint and hindfoot alterations such as increased width and decreased height of the calcaneus. Additionally, information on the number and location of fragments and on soft tissue lesions is important. Computed tomography is the method of choice in the examination of intraarticular calcaneal fractures for evaluation of the joint surfaces, especially the anteromedial and posterior talocalcaneal facet and the calcaneocuboidal facet. It is important to describe dislocations >2 mm and to measure the subfibular space.

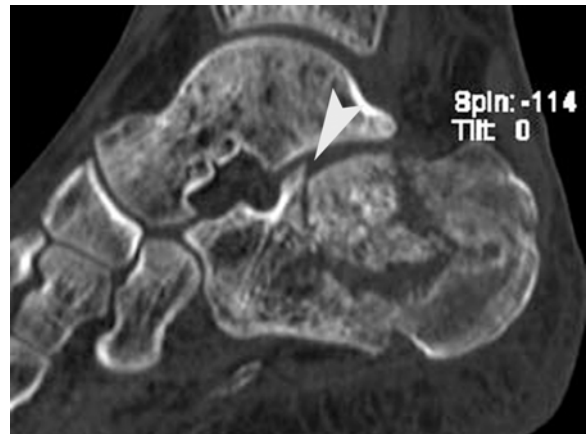


**Fig. 36.** The CT MPR in the sagittal plane demonstrates a comminuted calcaneus fracture with a secondary fracture line coursing in the superior surface just behind the tarsal sinus (intraarticular fracture, joint depression type after Essex-Lopresti)

Calcaneal insufficiency avulsion fracture is an extraarticular fracture in the posterior third of the calcaneus that is seen almost exclusively in diabetic patients. Radiographs show a curvilinear calcification adjacent to the posterior aspect of the ankle joint.

Complications of calcaneal fractures are compartment syndrome and tendon rupture. Calcaneal fractures are frequently bilateral and often combined with fractures of the thoracolumbar spine. Posttraumatic soft tissue calcifications can cause problems, especially if they are located close to articular facets.

### Midfoot Fractures

Midfoot fractures are not very common. Isolated fractures of the navicular bone represent most commonly dorsal avulsions close to the talonavicular joint, but they are relatively uncommon. In the midfoot, there are many of accessory bones. They are usually well defined and have round configuration. The os supranaviculare has to be distinguished from a dorsal avulsion, and the os tibiale externum from a tuberosity fracture. Vertical fractures of the body of the navicular may be associated with medial dislocation of the medial fragment, whereas horizontal lesions are associated with dorsal dislocation of the anterior fragment.

Isolated lesions of the cuboid are rare. There are some accessory ossification centers, such as os vesalianum and os peroneum, in close contact to the cuboid. Fractures of an os peroneum can occur in combination with rupture of the peroneus longus tendon.

Traumatic lesions of the cuneiform bones are generally associated with tarsometatarsal dislocations; therefore, such a lesion has to be excluded in the presence of a fracture of a cuneiform bone. Stress fractures are typically located at the navicular and at the cuboid.

### Midfoot Dislocations

Chopart's dislocation represents a rare complete and sole dislocation of the talonavicular and calcaneocuboid joints. Usually this lesion occurs in combination with avulsion fractures and fractures close to the articular facets or fractures of the facets. In most cases, the forefoot is displaced medially and less often laterally. Instead of involving the talonavicular joint, a midtarsal dislocation may involve the cuneonavicular joint. Chopart's dislocation has to be differentiated from the subtalar dislocation involving the talonavicular and the subtalar joints. Talar dislocation is unusual and the result of high-energy trauma. The risk of ischemic necrosis is very high. The talus usually is dislocated posteriorly [62].

In Lisfranc injuries, the metatarsals are usually subluxed or dislocated dorsally with respect to the tarsal bones. The classification differentiates between the more common homolateral and divergent types, based on the direction of the metatarsal dislocation. If the first metatarsal bone still has its normal relationship to the medial cuneiform and the four lateral metatarsals are dislocated laterally, this is called homolateral (Fig. 37). If the first metatarsal bone is displaced medially and the four lateral metatarsals are dislocated laterally, this is a divergent dislocation. Both types are usually associated with fractures of the base of the metatarsal and tarsal bones, especially in conjunction with the divergent type. In radiograph evaluation for Lisfranc injuries, a detailed evaluation of bone alignment is important. The DP view should be evaluated for a continuous, smooth contour of the second MT and middle cuneiform. The first intermetatarsal space should be continuous with the space between the first two cuneiforms. On the oblique view, the fourth MT and the cuboid should maintain a smooth contour, as should the lateral borders of the third MT and the lateral cuneiform. A lateral film should be evaluated for alignment of the second MT and the middle cuneiform. Displacement of >2 mm indicates the need for surgical treatment. The degree of instability is not present on these static studies, and as many as 10% of tarsometatarsal injuries cannot be visualized. Both CT and MRI can overcome this problem; CT in particular can be helpful for determining associated injuries that must be addressed to ensure a stable foot [63]. Assessment of fracture fragments and bony displacement is best accomplished with CT. Significant arterial injury may occur because the dorsalis pedis artery passes between the first and second metatarsal bones.

### Metatarsal Fractures

Traumatic lesions of the metatarsal bones are frequent. Transverse fractures of the proximal part of the fifth metatarsal are most common. The avulsion fracture of the tip of the proximal tuberosity should be differentiated from a true Jones fracture – an extraarticular transverse fracture through the junction of the diaphysis and metaphysis (usually 2 cm distal from the proximal tuberosity) – and a dia-



**Fig. 37.** The coronal CT MPR demonstrates subluxation of the second and third metatarsal joints associated with fractures of the bases of the second and third metatarsal and the cuneiform bones, consistent with Lisfranc luxation

physeal stress fracture of the diaphysis. The avulsion fracture is more frequent and is the result of abrupt pull of the peroneus brevis tendon or the lateral part of the aponeurosis. Malunion is a common complication in Jones fractures.

The metatarsals are a typical site of stress fractures in the foot, most frequently at the shaft of the second or third metatarsal. The first radiographic sign is a sclerotic line.

### Lesions of the Phalanges

One of the most common fractures of the foot is the traumatic lesion of the distal phalanx of the first toe. Fractures of the phalanges are usually minimally displaced and sometimes not easy to differentiate from skin folds. The major role of the radiographic examination is to detect articular involvement. Dislocations of the interphalangeal or the metatarsophalangeal joint can be combined with fractures and are either volar or dorsal. Lateral and medial dislocations are less common.

Excluding a traumatic lesion or a stress fracture of a sesamoid bone can be very difficult since the sesamoids can be bipartite and mimic fracture. A radiograph of



the opposite side can help to solve this problem because bipartite sesamoid bones are often bilateral. The medial sesamoid bone of the greater toe is more often fractured than the lateral. Usually these fractures are transverse or oblique. The MRI is also helpful in evaluating for sesamoid fractures and for the presence of subsequent osteonecrosis.

## References

- Blackmore CC (2005) Clinical prediction rules in trauma imaging: who, how and why. *Radiology* 235:371–374
- Buckwalter KA, Farber JM (2004) Application of multidetector CT in skeletal trauma. *Semin Musculoskelet Radiol* 8:147–156
- Watura M, Cobby M, Taylor J (2004) Multislice CT in imaging of trauma of the spine, pelvis and complex foot injuries. *Br J Radiol* 77:S46–S63
- Philipp MO, Kubin K, Mang T et al. (2003) Three-dimensional volume rendering of multidetector-row CT data: applicable for emergency radiology. *Emerg J Radiol* 48:33–38
- Farber JM (2004) Imaging of the wrist with multichannel CT. *Semin Musculoskelet Radiol* 8:167–173
- Farber JM (2004) CT arthrography and postoperative musculoskeletal imaging with multichannel computed tomography. *Semin Musculoskelet Radiol* 8:157–166
- Wirth S, Euler E, Pfeifer KJ (2005) Traumatische Veränderungen. In: Freyschmidt J (ed) *Handbuch diagnostische Radiologie, Bd. VII: Muskuloskelettales System I*. Springer, Berlin Heidelberg New York
- Nikken JJ, Oel EH, Ginai AZ (2005) Acute ankle trauma: value of a short dedicated extremity MRI examination in prediction of need for treatment. *Radiology* 234:134–142
- Oel EH, Nikken JJ, Ginai AZ (2005) Acute knee trauma: value of a short dedicated extremity MRI examination for prediction of subsequent treatment. *Radiology* 234:125–133
- Nikken JJ, Oel HG, Ginai AZ (2005) Acute wrist trauma: value of a short dedicated extremity MRI examination in prediction of need for treatment. *Radiology* 234:116–124
- Bücklein W, Vollert K, Wohlgenuth WA et al. (2000) Ultrasonography of acute musculoskeletal disease. *Eur Radiol* 10:290–296
- Cho KH, Lee YH, Lee SM et al. (2004) Sonography of bone and bone-related diseases of the extremities. *J Clin Ultrasound* 32:511–521
- Bianchi S, Martinoli C, Monet X et al. (2003) Hand- und Handwurzel-Ultraschall. *Radiologe* 43:831–840
- Hughes PM (2004) Low-energy injuries of the lower limb. In: *RSNA Categorical Course in Diagnostic Radiology 2004*, pp 197–215
- Peetrons P, Creteur V, Bacq C (2004) Sonography of ankle ligaments. *J Clin Ultrasound* 32:491–499
- Linnau KF, Blackmore CC (2002) Bony injuries of the shoulder. *Curr Probl Diagn Radiol* 31:29–47
- Neer CS II (1968) Fractures of the distal third of the clavicle. *Clin Orthop* 5:69–70
- Metz VM, Philipp MO (2004) Imaging low-energy upper extremity injuries. In: *RSNA Categorical Course in Diagnostic Radiology*, pp 187–196
- Ridpath CA, Wilson AJ (2000) Shoulder and humerus trauma. *Semin Musculoskelet Radiol* 4:151–170
- Ill TG (2004) High-energy blunt-force injuries to the upper extremity. In: *RSNA Categorical Course in Diagnostic Radiology*, pp 175–186
- Sofka CM, Pavlov H (2001) Sports injury update: imaging features. *Curr Probl Diagn Radiol* 30:174–187
- Bui-Mansfeld LT, Taylor DC, Uhorchak JM et al. (2002) Humeral avulsions of the glenohumeral ligament: imaging features and review of the literature. *AJR* 179:649–655
- Kreitner KF, Schultergürtel. In: Freyschmidt J (2005) *Handbuch diagnostische Radiologie, Bd. VII Muskuloskelettales System I*. Springer, Berlin Heidelberg New York
- Althausen PL, Lee MA, Finkemeier CG (2003) Scapulothoracic dissociation: diagnosis and treatment. *Clin Orthop Rel Res* 416:237–244
- Tirman PF, Smith ED, Stoller DW et al. (2004) Shoulder imaging in athletes. *Semin Musculoskelet Radiol* 8:29–40
- Zanetti M, Pfirrmann CW (2004) Bizepsprobleme: Ultraschall, Magnetresonanztomographie und MR-Arthrographie. *Radiologe* 44:591–596
- Martinoli C, Bianchi S, Prato N et al. (2003) US of the shoulder: non-rotator cuff disorders. *Radiographics* 23:381–401
- Horsfield D, Siegerist CF (2005) Radiography of the radial head: an alternative view. *Radiography* 11:201–206
- Steinborn M, Ellenbogengelenk. In: Freyschmidt J (2005) *Handbuch diagnostische Radiologie, Bd. VII: Muskuloskelettales System I*. Springer, Berlin Heidelberg New York
- Waldt S, Bruegel M, Ganter K et al. (2005) Comparison of multislice CT arthrography and MR arthrography for the detection of articular cartilage lesions of the elbow. *Eur Radiol* 15:784–791
- Potter HG, Ho ST, Altchek DW (2004) Magnetic resonance imaging of the elbow. *Semin Musculoskelet Radiol* 8:5–16
- Finlay K, Ferri M, Friedman L (2004) Ultrasound of the elbow. *Skeletal Radiol* 33:63–79
- Sonin A (2000) Fractures of the elbow and forearm. *Semin Musculoskelet Radiol* 4:171–191
- Resnik CS (2005) Wrist and hand injuries. *Semin Musculoskelet Radiol* 4:193–204
- Goldfarb CA, Yin Y, Gilula LA (2001) Wrist fractures: what the clinician wants to know. *Radiology* 219:11–28
- Chern TC, Jou JM, Yen SH (2002) Sonography for monitoring closed reduction of displaced extraarticular distal radial fractures. *J Bone Joint Surg Br* 84:194–203
- Catalano LW, Alton Barron O, Glickel SZ (2004) Assessment of articular displacement of distal radius fractures. *Clin Orth Rel Res* 423:79–84
- Gilula LA, Yin YM (eds) (1996) *Imaging of the wrist and hand*. Saunders, Philadelphia, p 425
- Daenen B, Houben G, Bauduin E et al. (2004) Sonography in wrist tendon pathology. *J Clin Ultrasound* 32:462–469
- Sunagawa T, Ishida O, Ishiburo M et al. (2005) Three-dimensional computed tomography imaging: its applicability in the evaluation of extensor tendons in the hand and wrist. *J Comput Assist Tomogr* 29:94–98
- Rogers LF, Kaye JJ (2001) Trauma of the appendicular skeleton. In: Schulthess GK von, Zollikofer CL (eds) *Syllabus: musculoskeletal diseases*, Springer, Berlin Heidelberg New York
- Clavero JA, Alomar X, Monill JM et al. (2002) MR imaging of ligament and tendon injuries of the fingers. *Radiographics* 22:237–256
- Overdeck KH, Palmer WE (2004) Imaging of hip and groin injuries in athletes. *Semin Musculoskelet Radiol* 8:41–55
- Stäbler A (2005) Hüftgelenk und proximaler Femur. In: Freyschmidt J (ed) *Handbuch Diagnostische Radiologie Bd. VII: Muskuloskelettales System I*. Springer, Berlin Heidelberg New York
- Yu JS (2004) Hip and femur trauma. *Semin Musculoskelet Radiol* 4:205–220
- Lawler LP, Corl FM, Fishman EK (2002) Multi- and single detector CT with 3D volume rendering in tibial plateau fracture imaging and management. *Crit Rev Comput Tomogr* 43:215–282
- Mellado JM, Ramos A, Camins E (2002) Avulsion fractures and chronic avulsion injuries of the knee: role of MRI. *Eur Radiol* 12:2463–2473

48. Stevens MA, El-Khoury GY, Kathol MH (1999) Imaging features of avulsion injuries. *Radiographics* 19:655–672
49. Tigges S, Fajman A (2000) Injuries about the knee and tibial/fibular shafts. *Semin Muskuloskelet Radiol* 4:221–239
50. White LM, Miniaci A (2004) Cruciate and posterolateral corner injuries in the athlete: clinical and MRI features. *Semin Muskuloskelet Radiol* 8:111–131
51. Potter HG (2000) The dislocated knee: imaging of the multiple-ligament injured knee. *Clin Sports Med* 19:425–441
52. Sanders TG, Miller MD (2005) A systematic approach to MRI interpretation of sports medicine injuries of the knee. *Am J Sports Med* 33:131–148
53. Friedman L, Finlay K, Jurriaans E (2001) Ultrasound of the knee. *Skeletal Radiol* 30:361–377
54. Helms CA (2002) The meniscus: recent advances in MRI of the knee. *AJR* 179:1115–1122
55. Lee W, Ho Sung K, Kim SJ et al. (2004) CT arthrography and virtual arthroscopy in the diagnosis of the anterior cruciate ligament and meniscal abnormalities of the knee joint. *Korean J Radiol* 5:47–54
56. Xiong C, Hao J (2004) Spiral CT arthrography of multiplanar reconstruction and virtual arthroscopy technique in diagnosis of knee with internal derangements. *Chin J Traumatol* 2:108–112
57. Linklater J (2004) Ligamentous, chondral and osteochondral ankle injuries in athletes. *Semin Muskuloskelet Radiol* 8:81–98
58. Tuite MJ (2002) MRI of the tendons of the foot and ankle. *Semin Muskuloskelet Radiol* 6:119–131
59. Choplin RH, Buckwalter KA, Rydberg J et al. (2004) CT with 3D rendering of the tendons of the foot and ankle: technique, normal anatomy and disease. *Radiographics* 24:343–356
60. Preidler KW, Peicha G, Lajtaj G et al. (1999) Conventional radiography, CT and MRI in patients with hyperflexion injuries of the foot: diagnostic accuracy in the detection of bony and ligamentous changes. *AJR* 173:1673–1677
61. Schmid MR, Pfirrmann CW, Hodler J et al. (2003) Cartilage lesions in the ankle joint: comparison of MR arthrography and CT arthrography. *Skeletal Radiol* 32:259–265
62. Mulligan ME (2000) Ankle and foot trauma. *Semin Muskuloskelet Radiol* 4:241–253
63. Sands AK, Grose A (2004) Lisfranc injuries. *Injury* 35:S-B71–S-B76
64. Herbert TJ (1990) The fractured scaphoid. *Quality Medical*, St. Louis, p 52
65. Cooney WP, Dobyns JH, Linscheid RL (1980) Fractures of the scaphoid: a rational approach to management. *Clin Orthop* 149:90–97
66. Russe O (1985) Fracture of the carpal navicular: diagnosis, non-operative treatment and operative treatment. *J Bone Joint Surg Am* 67:428–432 67. *Il Grigione Italiano* no. 13 (27.03.1897)



**Section Three**  
**Non-Traumatic**  
**Neurologic Emergencies:**  
**Imaging and Intervention**





# Imaging of Cerebral Ischemia

I. Grunwald, C. Roth, P. Papanagiotou, W. Reith

## 3.1

### Contents

3.1.1	Introduction	293
3.1.2	Intracerebral Hemorrhage	293
3.1.2.1	Computed Tomography	293
3.1.2.2	Digital Subtraction Angiography	294
3.1.2.3	Magnetic Resonance Imaging	294
3.1.3	Acute Ischemic Stroke	294
3.1.3.1	Computed Tomography	294
3.1.4	Clinical Terms of “Stroke”	296
3.1.4.1	Angiography	297
3.1.4.2	Computed Tomography	297
3.1.4.3	Magnetic Resonance Imaging	300
3.1.5	Lacunar Infarctions	308
3.1.6	Stroke in Children	308
3.1.7	Dissection	308
3.1.8	Hypoxic–Ischemic Encephalopathy	309
3.1.9	Venous Infarction	309
	References	310

### 3.1.1 Introduction

The need for increasingly early imaging has led to new emphasis on hyperacute changes on plain computed tomography (CT) and has also seen the widespread use of more complex imaging modalities in acute stroke.

Immediate brain imaging with CT for all stroke patients on admission is more cost-effective than deferred imaging, even when the possible interventions are limited to aspirin use and stroke unit care. A cost-effectiveness analysis has not yet been done to take into account thrombolytic treatment or modalities other than routine CT.

Around 85% of cases of stroke fulfilling the 1976 World Health Organization definition are ischemic in origin, with 10% caused by focal hemorrhage and 5% by subarachnoid hemorrhage (SAH). Since SAH rarely presents with sudden focal symptoms, this review ignores SAH.

Many ischemic strokes exhibit rapid early improvement, leading clinicians to apply the term “TIA”. Strictly speaking, this label is attached only when symptoms resolve entirely within 24 h. Most true TIAs last only minutes, and the longer the symptoms last, the greater the likelihood of a causative lesion being identified on imaging.

### 3.1.2 Intracerebral Hemorrhage

#### 3.1.2.1 Computed Tomography

Non-contrast CT (NCCT) remains the gold-standard means of detecting intracranial hemorrhage in acute stroke. Blood is hyperdense because of its high electron density (Fig. 1). As blood is broken down, density on CT declines by approximately 1.5 Hounsfield units (HU) per day. Old hemorrhage appears hypodense on CT within a time scale determined by the volume of the initial hematoma. Small bleeds may be indistinguishable from infarcts within days of the event. Anatomical location is relevant in determining the etiology of primary intracerebral hemorrhage (PICH), e.g., small vessel disease most commonly causes basal ganglia hemorrhage, whereas lobar hematoma is most commonly caused by amyloid angiopathy in the elderly. Lobar hemorrhage in younger patients may be due to underlying pathology, e.g., bleeds secondary to arteriovenous malformations (AVMs) typically extend from the cortical surface to the lateral ventricles, superior sagittal sinus thrombosis often gives bilateral parasagittal hemorrhages, and thrombosis of the vein of Labbe causes temporal lobe hemorrhage. Cavernomas may cause pontine or supratentorial lobar bleeds.

It is now recognised that a high proportion of hematomas expand within the first hours after onset, and that expansion is associated with poorer outcome [1]. With the preliminary demonstration that recombinant factor VII not only reduces hematoma expansion but also improves clinical outcomes in PICH treated within 3 h of onset [2], early recognition of PICH is likely to become an important diagnostic goal of acute imaging in its own right, and not simply a necessary step in exclusion before considering treatment for an ischemic event.

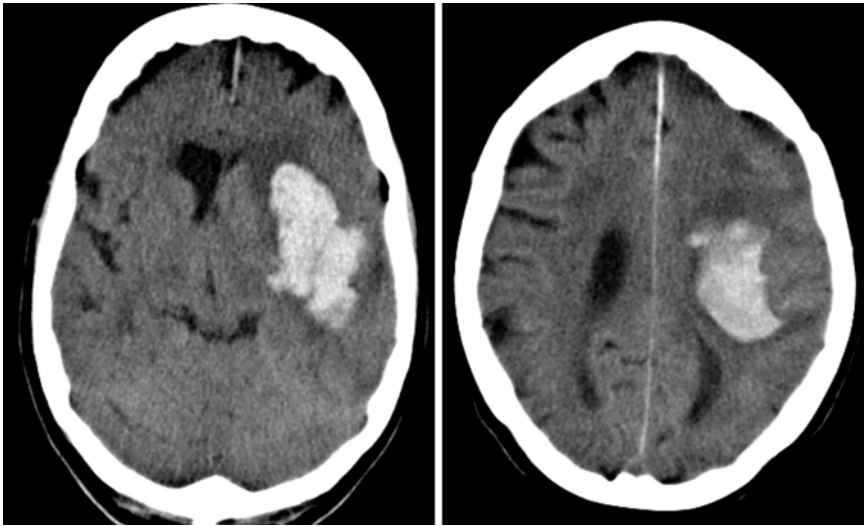


**Fig. 1.** Patient with known hypertension presented with a right-sided spontaneous hemiparesis. In the CT blood is seen in loco typico in the basal ganglia

### 3.1.2.2 Digital Subtraction Angiography

Surgical evacuation may still be considered for some hematomas, particularly superficial lobar hematomas, and there may be a need to undertake cerebral angiography in order to seek an underlying AVM before surgical decompression or evacuation can be planned. If surgery is not anticipated, it is usually advisable to defer vascular imaging studies for some months after an acute intracerebral hemorrhage since mass effect from any residual hematoma may obscure small low-pressure AVMs. External carotid studies may need to be included in addition to selective catheterisation of the internal carotid system in order to identify small dural arteriovenous shunts.

### 3.1.2.3 Magnetic Resonance Imaging

Susceptibility-weighted MRI sequences have been compared to CT in acute stroke and results to date suggest that MRI is a good alternative for the detection of hemorrhage [3]; however, further comparative evaluation is needed before MRI can be regarded as a substitute.

In investigation of stroke with delayed presentation, gradient-echo MRI is the investigation of choice for exclusion of old hemorrhage. On gradient-echo MRI, old bleeds are of low signal. Gradient-echo MRI increasingly identifies microhemorrhages in the brain in individuals with no clinical history to suggest intracerebral hemorrhage. These microbleeds may be a risk factor for spontaneous bleeds after thrombolytic treatment, and offer an explanation for the occurrence of hematomas that are remote from the site of ischemia for which treatment was given. It remains to be established definitively whether the presence of microbleeds on gradient-echo MRI represents a contraindication to systemic thrombolysis for ischemic stroke, although some investigators believe that it does.

## 3.1.3 Acute Ischemic Stroke

### 3.1.3.1 Computed Tomography

The NCCT remains the mainstay of emergency imaging of stroke in order to exclude intracranial hemorrhage. The NCCT may also identify other intracranial pathologies that mimic stroke such as tumor or encephalitis.

Ischemic tissue on NCCT appears hypodense because of a combination of reduced blood volume and cytotoxic edema. The rate of decline of tissue density is dependent upon severity and duration of ischemia (Fig. 2). Within the 3 h window for systemic thrombolytic treatment, hypodensity is usually subtle, if visible at all. More clearly visible hypodensity should always prompt reappraisal of the history around time of onset, since it suggests a greater duration of ischemia. Early ischemic change on NCCT (Table 1) is a term that encompasses changes that almost certainly represent a number of different pathological processes in acute ischemia whose significance varies. Previous radiological belief that CT within a few hours of stroke onset has low sensitivity is unfounded, at least in middle cerebral artery (MCA) occlusions, where Early ischemic changes are present in around 70% of cases within 3 h of onset. While the sensitivity of these changes is compromised by their subtlety, inter-observer reliability can be improved by systematic CT scan evaluation using systems such as the Alberta Stroke Programme early CT score (ASPECTS) [4]. Inter-observer agreement is improved significantly by clinical information being available. A recent large multi-observer comparative study found inter-observer agreement to be greater among neuroradiologists than stroke neurologists or general radiologists. The majority of early ischemic changes are features of reduced tissue density: it is not defined (and probably indefinable) at what point early ischemic changes merge into “visible hypodensity”. The arbitrary distinction between the two entities may be of clin-

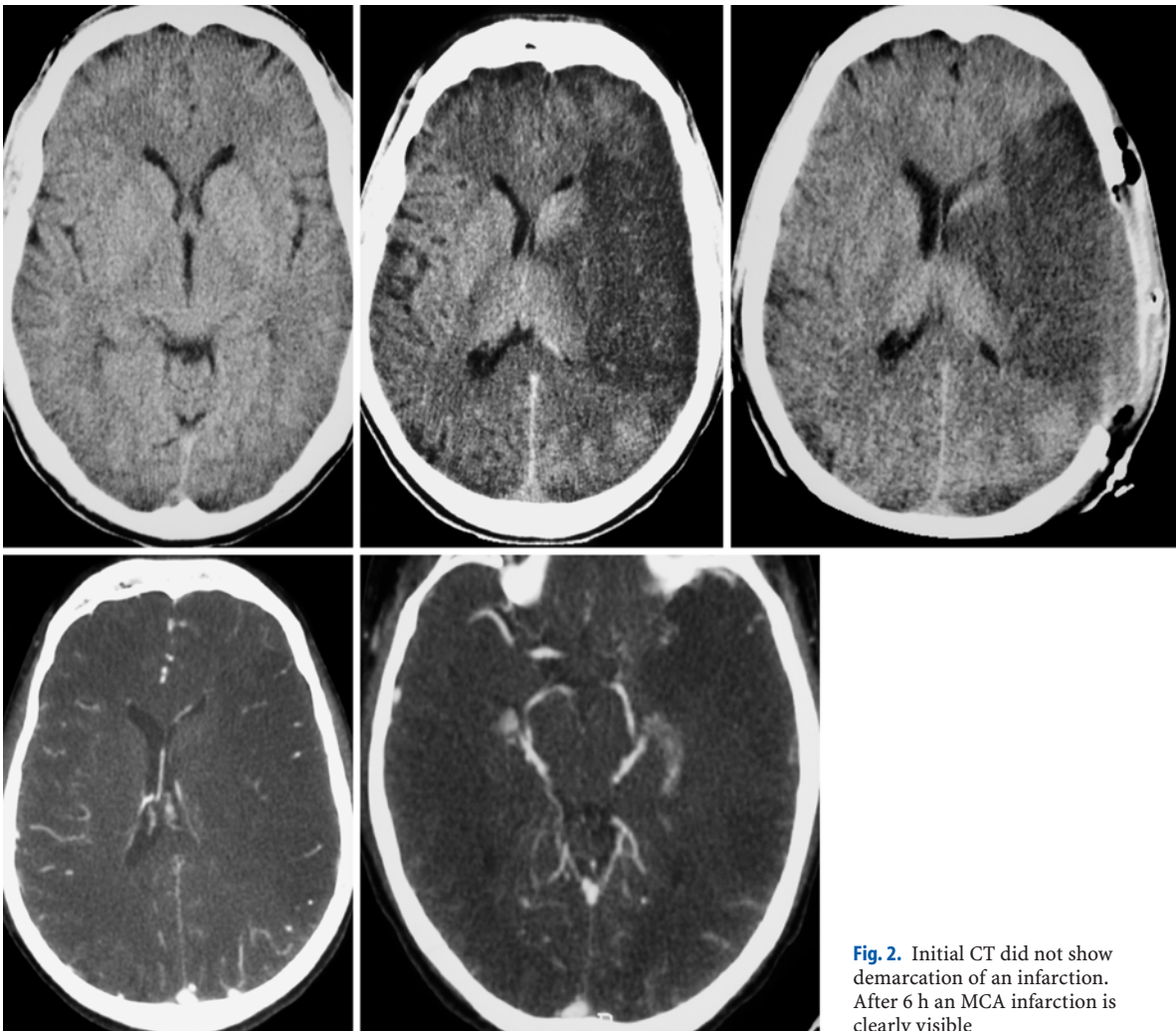


**Fig. 2.** Initial CT did not show demarcation of an infarction. After 6 h an MCA infarction is clearly visible

**Table 1.** Early ischemic changes on contrast-enhanced CT. MCA middle cerebral artery

- Hyperdense arteries (most commonly proximal MCA or MCA sylvian “dot”)
- Lentiform nucleus hypodensity
- Loss of “insular ribbon” (definition of gray from white matter)
- Loss of cortical gray–white matter differentiation
- Hemispheric sulcal effacement
- Local compression of lateral ventricle

ical significance, since visible hypodensity involving a large anatomical volume increases the risk of poor outcome and complications of thrombolytic treatment. Isodense brain swelling, another early ischemic change, in the acute phase probably represents increased blood volume, a physiological vasodilator response to ischemia indicating metaboli-

cally active tissue. Isodense swollen regions may therefore represent reversible ischemia. Early ischemic changes per se were not a pre-defined exclusion criterion in any thrombolysis trial, and therefore in themselves are not an exclusion from thrombolytic treatment. Extensive visible hypodensity is a risk factor for both poor outcome and higher risk of hemorrhage, which is unsurprising since the more obvious the hypodensity, the greater the severity (e.g., because of lack of collateral supply) or the duration of ischemia. Most defined early ischemic changes on CT, and systems such as ASPECTS, are concerned exclusively with stroke caused by occlusion of the carotid artery, the main trunk of the MCA, or the major branches of the MCA. The sensitivity of CT to ischemia within small penetrating artery territories, the posterior circulation, or scattered multifocal small infarcts that are often encountered in embolic stroke, is not established, and technical limitations mean that CT sensitivity in these scenarios is likely to be poor.





**Fig. 3.** This patient was brought to hospital with a right-sided hemiparesis, beginning 6 h prior to CT examination. In the CT a hyperdense middle cerebral artery (MCA) is clearly visible. This is one of the early signs of ischemia indicating a thrombus in the artery; however, it is not specific for MCA occlusion

Increased density of the MCA or other intracranial vessels on NCCT is indicative of thrombus partially or completely occluding the vessel (Fig. 3). The plane of section of CT means that main trunk MCA occlusions are seen as a linear hyperdensity in the sylvian fissure, whereas internal carotid artery (ICA) or branch MCA occlusions may be seen as hyperdense “dots” in cross section. “False-positive” hyperdense MCAs may be seen, particularly in conditions associated with increased hematocrit (e.g., polycythemia) or where hypodensity of brain parenchyma leads to increased contrast with normal vessels (e.g., herpes encephalitis).

### 3.1.4 Clinical Terms of “Stroke”

The term “ischemic penumbra,” originally applied to brain tissue perfused at values between the functional and morphological thresholds, has recently been extended to characterize ischemically affected but still viable tissue with uncertain chances for infarction or recovery [5]. Results have accumulated supporting the concept of the ischemic penumbra as a dynamic process of impaired perfusion and metabolism eventually propagating with time from the center of ischemia to the neighbouring tissue [6]. Very early it became evident that the tolerance of perfusional disturbance is related to its duration [7]. This relationship and secondary mechanisms extending the flow disturbance make the penumbra a dynamic process, progressing from the core to the periphery of vascular territories with im-

paired perfusion. In a new concept, “penumbra tissue” is an equivalent to “viable tissue,” the fate of which is undetermined because it might turn into necrosis but still has the potential of preserving morphological integrity and functional recovery. Because this concept renders the basis of therapeutic window in ischemic stroke, it has gained utmost clinical importance.

To salvage the viable tissue, aggressive treatment, such as fibrinolytic therapy, was developed and proved effective due to an improved outcome [8–10]. A drawback of fibrinolytic therapy is the considerable risk of intracranial hemorrhage, which could be lowered by appropriate patient selection.

Clinicians have long used the arbitrarily defined terms “stroke” and transient ischemic attack (TIA) to refer to the sudden loss of neurological function from a vascular mechanism. Symptoms resolving in <24 h have been referred to as TIA. The underlying tissue physiology of ischemia, whether reversible injury or infarction, does not always correspond to the clinical terms of TIA or stroke. Patients with TIA are commonly found to have areas of tissue infarction when imaged carefully. Many stroke clinicians come to favor a 1-h time limit for TIAs, improving the correlation of clinical and physiological terms. Neuroimaging has become tightly integrated in the study and management of cerebrovascular disease.

During the first hours of acute stroke, CT is still the imaging modality of choice to identify the underlying pathology [11].

In the decade since the first MR diffusion imaging of stroke patients, the technique has evolved and become familiar to those involved in acute intervention. Diffusion-weighted MRI has become a sensitive marker of infarction, and reversible diffusion abnormalities have been far less common clinically than in animal stroke models. Territories with perfusion and diffusion mismatch may define tissue at risk for infarction, but with potential recovery.

An alternative strategy with CT technology uses rapid CT for dynamic perfusion imaging, with similar goals in mind. It is hoped that acute stroke imaging can better guide interventions such as intravenous or intraarterial thrombolysis. While most attention has been focused on acute intervention, it is emphasized that the vast majority of patients are not seen in the appropriate time window for acute interventions. Less than 10% of all stroke patients are evaluated <3–6 h after the onset of clinical symptoms.

“Stroke” encompasses a heterogeneous group of cerebrovascular disorders with a variety of clinical presentations, pathology, etiology, prognosis, and treatment. There are four major types of stroke: cerebral infarction; primary intracerebral hemorrhage (ICH); subarachnoid hemorrhage (SAH); and venous occlusion.

Both CT and MRI can visualize the consequences of cerebral ischemia directly. Computed tomography and MR angiography, digital subtraction angiography (DSA), and transcranial Doppler ultrasonography show the vessels and

their pathology. Diffusion and perfusion MRI and perfusion imaging with CT give information about the localization of edema and the blood circulation within the brain. Magnetic resonance spectroscopy, positron emission tomography, and single photo emission CT are momentarily being used mainly for scientific questions.

#### 3.1.4.1 Angiography

Cerebral angiography is usually only performed in the hyperacute stage if thrombolytic therapy is being considered. With this it is hoped to reverse or decrease the size of infarction. Indications for diagnostic angiography include TIAs in a carotid distribution, amaurosis fugax, prior stroke in a carotid distribution, a high-grade stenotic lesion in a carotid artery, or the angiographic correlation of MRA or CTA stenotic findings. In 50% of all angiograms performed in the hyperacute stage, occlusion of a vessel is observed. This can be found with or without a distal meniscal filling defect. Other features are a slow antegrade flow with prolonged circulation time and delayed arterial emptying in the affected area. In addition, nonperfused areas as well as mass effect can be present. Often a vascular blush may be seen due to luxury perfusion; however, the need for angiography has been made less necessary due to the improvements of MRA, duplex ultrasound, and CTA.

#### 3.1.4.2 Computed Tomography

Computed tomography is considered the most important initial diagnostic study in patients with acute stroke. Underlying structural lesions, such as tumor, vascular malformation, or subdural hematoma, can mimic stroke clinically. Nonvascular lesions cause 1–2% of stroke syndromes [12]. Computed tomography provides a quick way of excluding conditions that may mimic ischemic stroke and may require a different treatment approach. It effectively discriminates between intracerebral hemorrhage as a possible cause for stroke-like symptoms and ischemic stroke.

The CT findings in acute cerebral infarction evolve with time. The most frequent finding is that of parenchymal low density which represents irreversibly damaged tissue. Computed tomography shows the neuropathological stages of infarction as hypodense areas. Low density is caused mainly by increased tissue water. In brain edema there is an increase in water that is accompanied by a parallel increase in sodium and a decrease in potassium. Experimental studies suggest a change of 2.6 Hounsfield units (HU) per 1% change in water content [13]. Early changes of ischemia occur in a small range of 5–10 HU. The ability of the eye to differentiate gray shades is limited to 15–20 steps, so that in a normal window range of 90 HU there is a change of approximately two shades in that early period. It is not astounding that these slight density changes can well

be overlooked on early CT. In prior studies the “sensitivity” of CT to parenchymal low density in the first 6 h after the onset of symptoms ranged from 56 to 95% [14]. This “sensitivity” depends on the duration and severity of ischemia, the size, type, and location of the infarction, and the examiner’s experience.

Although nearly 60% of CT scans obtained within the first few hours after infarction appear normal, there are numerous signs that can already be identified in strokes within the first 4 h or less.

#### Initial Stage: Early CT Findings

The appearance of ischemic infarction on CT follows a temporal pattern. Usually, three main stages can be distinguished. In the initial stage CT is commonly normal. The initial stage usually encompasses the first 24 h. Mild sulcal effacement is found. Early CT findings include a hyperattenuation of the artery [e.g., dense middle cerebral artery (MCA) sign; Fig. 3] gray/white interface loss along the lateral insular (loss of the insular ribbon sign), obscuration of the lentiform nucleus (Fig. 4a), and effacement of the gray/white junction along the cortex. A hyperdense MCA is caused by acute intraluminal thrombus. It is seen on non-contrast CT studies as high density of the MCA. It can also be caused by a calcified embolus within the artery.

#### Contrast CT

Routine use of contrast-enhanced CT is of limited additional diagnostic value in acute stroke and is not recommended, although concerns that blood–brain barrier breakdown would lead to contrast extravasation with risk of stroke worsening are not supported by evidence. Increased conspicuity of ischemic lesions within 6 h of onset on source images from CT angiography (CTA) examinations has been reported, but in effect the high-dose contrast administration for CTA yields an image representing cerebral blood volume (CBV). Decreased CBV corresponds with infarct core. The CT using routine doses of contrast is not validated in this respect, and in general the use of contrast agents should be to acquire additional information from CTA or CT perfusion (CTP), or to address specific diagnostic concerns about alternative pathologies.

#### CT Angiography

Computed tomographic angiography can provide important information concerning the current vessels status, and might help in the initiation of therapy in patients with acute hemispheric ischemia. Identification of patients with MCA occlusion (Fig. 4b), occlusion of the internal carotid artery bifurcation, and poor leptomeningeal collaterals is feasible with the use of CTA. Computed tomographic angiography in conjunction with CT can distinguish subgroups of acute ischemic stroke victims and thereby better

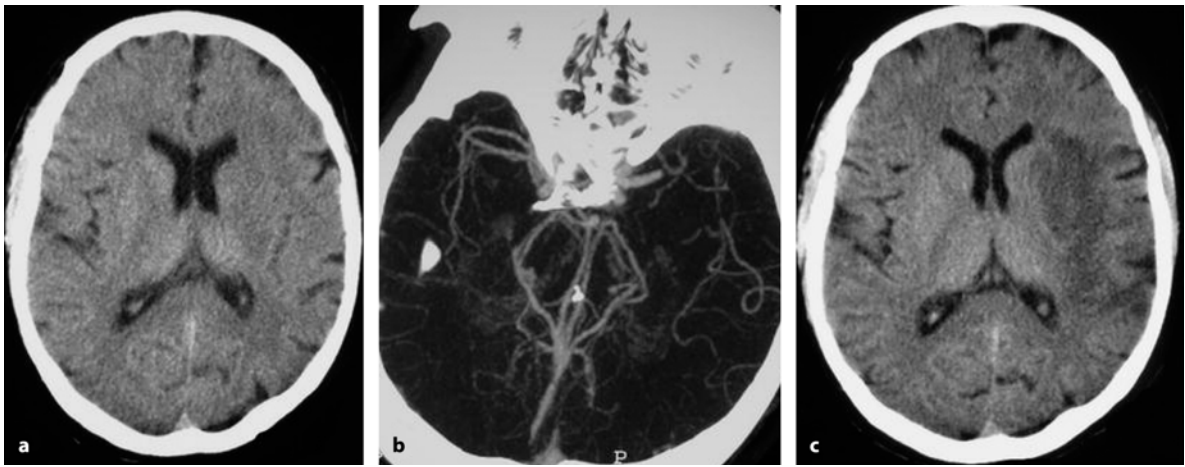


**Fig. 4a–c.** This 56-year-old patient presented with left-sided hemiparesis. **a** A CT scan revealed an obscuration of the lentiform nucleus as an early sign of cerebral ischemia. **b** The CT angiography confirmed an occlusion of the MCA. **c** In the control CT 24 h later, an ischemic infarction comprising mainly the lentiform nucleus is clearly visible

predict those subgroups most likely to benefit or not to benefit from thrombolytic therapy [14].

The CTA of intracranial vessels can identify the site of vessel occlusion, which may be of value in clinical management decisions. For example, the response to intravenous thrombolytic treatment of tandem occlusions of the ipsilateral ICA and MCA, carotid “T” occlusions, or of basilar artery thrombosis, is poor compared with isolated MCA occlusion, and in many centers is considered a potential indication for rescue therapy with intraarterial thrombolytics or mechanical embolus removal.

### CT Perfusion

Multidetector CT scanners allow the acquisition of several slices of brain repeatedly during the intravenous passage of high doses of iodinated contrast medium. The changes in the density–time curve for each pixel allow calculation of a number of parameters reflecting tissue perfusion by mathematical calculations based on the central volume principle. Typical derived parameters include mean transit time (MTT), time to bolus peak (TTP), and CBV, from which cerebral blood flow (CBF) can be calculated (as  $MTT/CBV$ ). The TTP and MTT in the first 3–6 h after stroke onset are predictive of final infarct volume in the absence of reperfusion, and represent tissue at risk (Fig. 5). Diminished CBV probably represents failure of autoregulatory responses and therefore tissue infarction. The difference between CBV and TTP or MTT lesions can be taken as an estimate of the “ischemic penumbra,” the volume of tissue at risk of infarction but still viable. The PCT has been validated against other techniques such as diffusion and perfusion MRI and quantitative PET. Claims that CTP is itself capable of quantitative blood flow measurement are not universally accepted.

### Developmental Stage

After day 1 the developmental stage spans over 5 weeks after the onset of symptoms. After 24 h, most large vessel infarctions are visible as hypodense areas involving both gray and white matter (Fig. 4c). The topography of the hyperdensity usually corresponds to a vascular territory. Most commonly the MCA territory is involved. At this stage mass effect is often present, due to edema. It corresponds to the size of infarction and is totally absent in small infarctions. The observed hypodensity on CT is due to ischemic changes at the cellular level producing cytotoxic edema. The increasing edema decreases the CT attenuation values. After approximately 2 weeks, mass effect begins to diminish. This causes an increase in the attenuation values and the CT appearance of the infarction may revert to normal density temporarily or possibly permanently [15]. This phenomenon is called fogging effect and is most likely due to the disappearance of the edema. It has also been suggested that during this period there is capillary dilatation and extravasation of macrophages which remove necrotic material.

Because of blood–brain barrier disruption, enhancement following contrast administration can often be seen in subacute infarctions. Other explanations for enhancement of the infarction include hypervascularization and luxury perfusion. Generally, it is agreed that extravasation of contrast material is the major mechanism [15]. This could be due to neovascularization around the infarction with an ill-developed blood–brain barrier so that leakage of contrast material occurs. Usually, the contrast enhancement appears later than the hypodensity. The maximum frequency and intensity is being reached during the second and third week. It then declines progressively and is rarely found after 10 weeks. Also, it is seldom seen within the first week, so that CT scans with contrast infusion before the fifth day after infarction have been considered pointless;

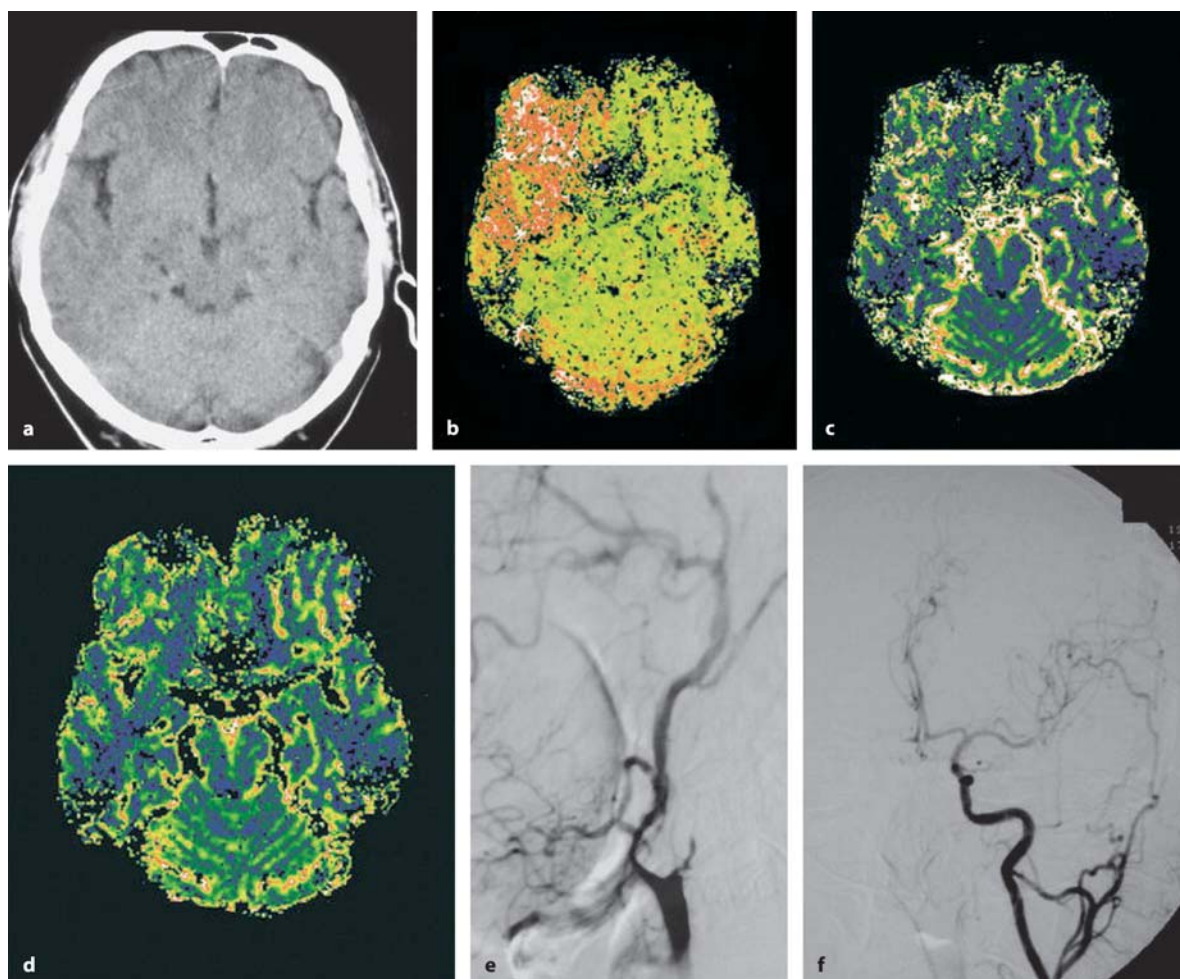


**Fig. 5.** **a** A CT scan of this 63-year-old patient with a left-sided hemiparesis revealed no abnormalities. **b** Perfusion-weighted CT showed a perfusion deficit in the mean transit time parameter

maps as well as on **c** the regional cerebral blood volume map and on **d** the regional cerebral blood flow map. DSA on the right hand side shows occlusion of the ICA (**e**)

however, it is useful when the scan appears normal due to the fogging effect.

An enhancing cerebral infarction may resemble a tumor or abscess. If in doubt, contrast enhancement and mass effect tend to disappear with infarction, whereas with tumor or abscess a gradual extension of the lesion is common. With infarction the enhancement follows a vascular topography. The hyperdensity affects the gray matter. With tumors the white matter is involved. This hyperdensity then has a digital pattern that traces the boundary of the peripheral white matter (vasogenic edema). The hypodensity seen with infarction is typically wedge shaped (cytotoxic edema).

Conventional or MR angiography would disclose an occluded MCA. Hypodensity of the lentiform nuclei on early studies is strongly associated with later hemorrhagic transformation of the initially ischemic infarction. In normotensive patients most hemorrhagic strokes occur with reperfusion of a previously ischemic infarction.

### Late Stages of Infarction

The late stages of infarction are those from the fourth to sixth week. By then mass effect has disappeared and the lesion is visualized on the CT scan as a definite hypodensity or cystic cavity. Contrast enhancement is usually absent. The lesion is transformed into a residual cavity with the same density as cerebral spinal fluid (CSF). There is a volume loss and gliosis. Well-delineated low-attenuation barriers are seen in the affected vascular distribution. The adjacent sulci become prominent and one usually finds a consecutive enlargement of the ipsilateral ventricle. This is due to the loss of cerebral tissue volume. Dystrophic calcification has been reported in infarcted brain but is very rare. The well-delineated hypodense area now seen represents focal encephalomalacia. The enlargement is due to the ex vacuo hydrocephalus as a consequence of the loss of cerebral tissue.



Arachnoid cysts that have the same density as CSF can sometimes be confused with an old cerebral infarction; however, these usually have some mass effect and are not associated with brain substance loss such as a widening of the ipsilateral lateral ventricle. In addition, due to CSF pulsations, a remodeling of the adjacent skull may have occurred.

### 3.1.4.3 Magnetic Resonance Imaging

Cerebral ischemia leads to early changes in the content of water in tissue; these are detected by MRI. Within the first 72 h it is more sensitive in the detection of acute cerebral ischemia than CT [16]. Infarction prolongs the MRI relaxation constants T1 and T2.

#### Spin-Echo Imaging

The MRI findings of cerebral ischemia change with time. In the acute phase the lesion is often isointense to normal brain on T1-weighted spin-echo images. Early changes, such as mass effect, sulcal effacement, and loss of gray/white matter interface, can be present.

T2-weighted images (T2WI) show hyperintensity in the area of the lesion due to the initial cytotoxic edema and later the additional vasogenic edema. Usually, these changes are not detected before 6–12 h. In the subacute stage low signal on T1 and high signal on T2 is observed. If hemorrhagic changes have occurred T2-weighted images show an increased signal in the peripheral regions. Chronic infarction has low signal on T1WI and high signal on T2WI as well as proton-density-weighted images.

#### Fluid-Attenuated Inversion Recovery Sequence

Fluid-attenuated inversion recovery (FLAIR) is a heavily T1- or T2-weighted sequence. Besides diffusion weighted images it is the most sensitive spin-echo technique for the imaging of cerebral infarction. Hyperintense signals from CSF and CSF-flow artifacts can make it difficult to spot lesions. The fluid-attenuated inversion recovery pulse sequence uses a long inversion time near the zero point of water, thus diminishing signals from CSF. In addition, a long echo time is used which makes the image T2-weighted but CSF appear dark.

#### Contrast-Enhanced MRI

Paramagnetic contrast agents lead to a shortening of T1. Vascular enhancement can sometimes be detected due to vasodilatation in ischemic areas [17]. Enhancement of adjacent meninges is observed within the first week in large cerebral infarction. This might be due to reactive hyperemia, collateral arterial flow, or venous engorgement. The affected parenchyma usually enhances at 6–14 days. Usually a gyriform enhancement is observed (Fig. 6).

#### Diffusion-Weighted MRI

After experimental studies [18–21], DWI has become a powerful tool in the evaluation of patients with stroke syndrome and is now used in daily clinical practice (Figs. 7, 8).

#### Principles of DWI

In a fluid environment, water molecules continuously move in a random fashion (Brownian diffusion) due to their inherent kinetic energy. Diffusion is higher in fluid environ-

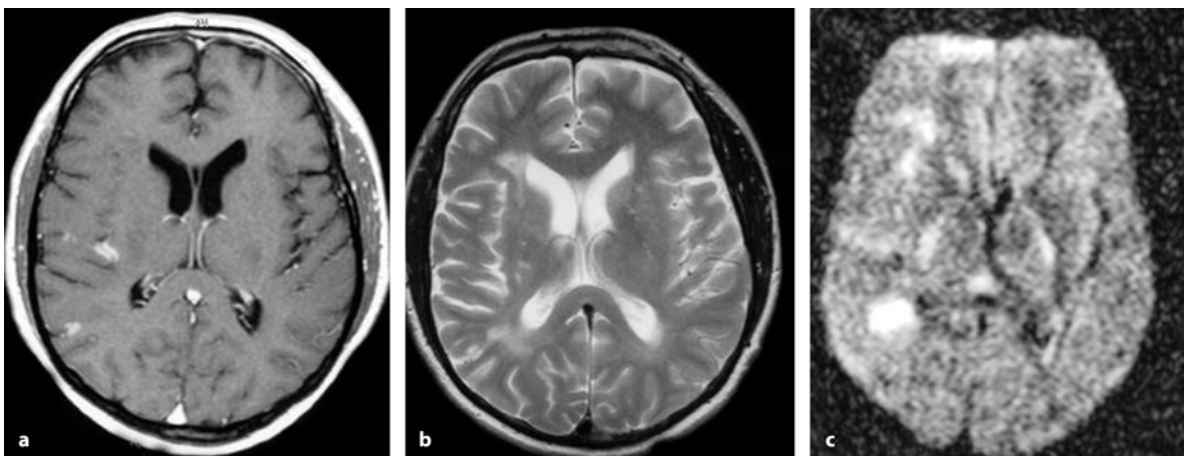


**Fig. 6a–c.** This 46-year-old patient had a light hemiparesis on the left side 5 days prior to MR examination. **a** The T1-weighted images (T1WI) after Gd-DTPA application showed a gyriform enhancement, confirming an ischemic area in the state of blood-

brain-barrier breakdown (e.g., the affected parenchyma usually enhances at 6–14 days), whereas **b** the T2-weighted images (T2WI) and **c** the diffusion-weighted images (DWI) show the infarction as a hyperintense area

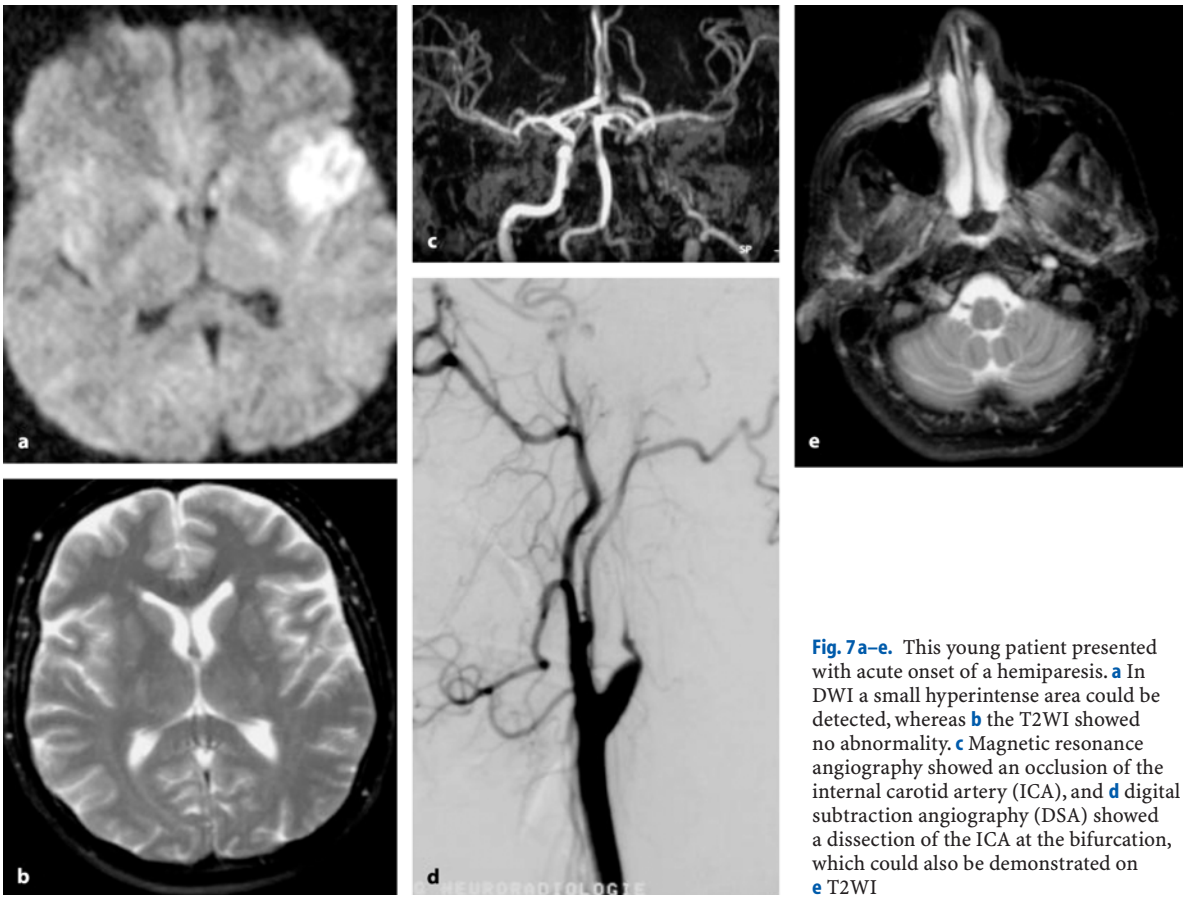


**Fig. 7a–e.** This young patient presented with acute onset of a hemiparesis. **a** In DWI a small hyperintense area could be detected, whereas **b** the T2WI showed no abnormality. **c** Magnetic resonance angiography showed an occlusion of the internal carotid artery (ICA), and **d** digital subtraction angiography (DSA) showed a dissection of the ICA at the bifurcation, which could also be demonstrated on **e** T2WI

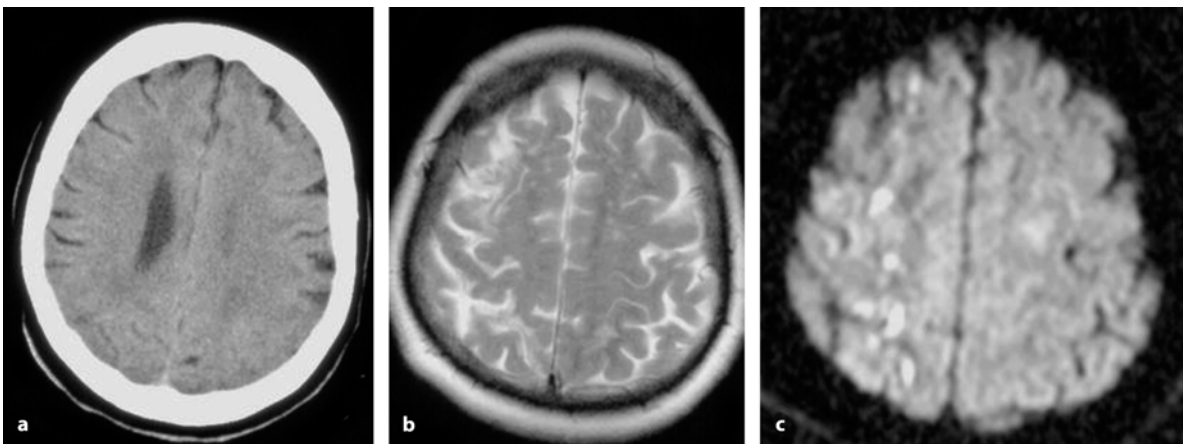


**Fig. 8a–c.** This patient with an occlusion of the anterior cerebral artery presented with a left-sided heiparesis 5 h prior to MR examination. **a** Computed tomography and **b** T2WI showed no abnor-

malities, whereas **c** in the DWI multiple hyperintense areas could be detected in the centrum semiovale; these areas correspond to watershed zone infarctions

ments than in solid environments due to increased restriction in diffusion in solid tissues. The DWI corresponds to the imaging representation of the relative intensity of diffusion of water molecules in each voxel. Diffusion-weighted imaging is based on the natural sensitivity of MR to motion, which is also the basis of MR phase-contrast angiography. In the presence of a magnetic field gradient protons carried by moving water molecules undergo a phase shift of their transverse magnetization.

The rate of diffusion, termed the diffusion coefficient ( $D$ ), is measured in units of area divided by time (e.g., square millimeters per second). The observed diffusion of molecules within biological environments is, however, determined by a variety of factors; these include the micro-environmental architecture which restricts or enhances diffusion in various anatomical directions (isotropic vs anisotropic diffusion), especially as the cellular structures are close together relative to the degree of water mobility in the central nervous system (CNS). To include this variety of known and unknown factors that influence observed diffusion, the rate of diffusion is termed the “apparent diffusion coefficient” (ADC) in living systems. The ADC values are measured in square millimeters per second.

In the most typical approach, MRI sequences are made sensitive to molecular diffusion by adding two extra gradient pulses that are equal in magnitude but opposite in direction. This balanced pair of gradient pulses was first added to a standard spin-echo (SE) sequence in 1965 by Stejskal and Tanner [22]. The degree of signal loss is determined by the degree of random motion (characterized by the diffusion coefficient) and by the strength and duration of the diffusion-encoding gradients.

The degree of signal drop can be enhanced by increasing the strength and duration of the diffusion-encoding gradients. This relationship is summarized in the following equation:

$$SD \bar{e}^{-bD} \quad (1)$$

where  $SD$  represents the signal drop,  $D$  the diffusion coefficient, and the variable  $b$  depends on the duration and strength of the diffusion-encoding gradients and can be calculated from the Stejskal-Tanner equation:

$$b = \gamma^2 G^2 \delta^2 (\Delta - \delta/3) \quad (2)$$

where  $\gamma$  is the gyromagnetic ratio, and  $G$ ,  $dgr$ , and  $Dgr$ , correspond to the amplitude, duration, and interval of the gradients, respectively.

As the DWI sequences rest upon a T2-weighted sequence the signal intensity of a voxel of tissue is equal to the signal intensity on a T2WI (or  $bap0$  s/mm<sup>2</sup>) decreased by an amount of signal drop related to the diffusion coefficient and the applied  $b$ -value. The resulting signal intensity can be calculated as follows:

$$SI = SI_0 \times e^{-bD} \quad (3)$$

where  $SI_0$  is the signal intensity on the T2-weighted image (or  $bap0$  s/mm<sup>2</sup>).

Diffusion-weighted imaging is characterized by the amplitude  $G$  of the gradients, the time  $Dgr$ , and  $dgr$ , corresponding to the duration of application of the gradients, the type of gradients, and the type of application of gradients, respectively, along the different spatial planes, and the simultaneous or separate applications of the gradients. The ADC can be calculated for each pixel of the MR image. The ADC value is an absolute quantitative measurement of water translational motion, which can be compared in serial examinations.

### DWI and Ischemic Lesions

During the hyperacute phase, ischemic lesions are characterized by the presence of hyperintensity on DWI without corresponding T2-weighted hyperintensity on  $b=0$  images. Diagnosis of cortical and subcortical lesions is easy, but diagnosis of lesions in the basal ganglia and brain stem can be more difficult. During the days following ischemia, the lesions remain hyperintense on  $b=1000$  images, but they become hyperintense on T2WI as well and visible on the  $b=0$  images, probably due to the development of edema. During the following weeks, the lesions remain hyperintense on the  $b=0$  images and then become progressively less hyperintense on the  $b=1000$  images, probably due to development of encephalomalacia and necrosis. Areas of marocystic encephalomalacia and necrosis are isointense to CSF, hyperintense on  $b=0$  images, and hypointense on  $b=1000$  images.

During the hyperacute phase of ischemia, the hyperintensity on  $b=1000$  images is due to a local decrease in ADC. The exact underlying mechanism leading to early ADC decrease remains uncertain; probable mechanisms are altered permeability, modification of perfusion and shift of water from the extracellular to the intracellular component with cytotoxic edema, modification of cell shape, and structural modifications of tissue with increased tortuosity of extracellular water-shift pathways. The most commonly cited theory is the one regarding the reduction of extracellular space secondary to cytotoxic edema due to Na-K pump dysfunction secondary to ischemia [23].

In DWI data is collected after a sensitization gradient is played out along a specified plane. The intensity of diffusion is measured along that specified plane. In some tissues, such as CSF and gray matter, the diffusion coefficient is the same in all spatial directions: isotropic diffusion. In white matter, where fibers are organized into fascicles or tracts, diffusion is much more intense along the spatial orientation of these tracts, whereas diffusion is reduced perpendicular to the long axis of these tracts: anisotropic diffusion. Therefore, the diffusion coefficient is dependent

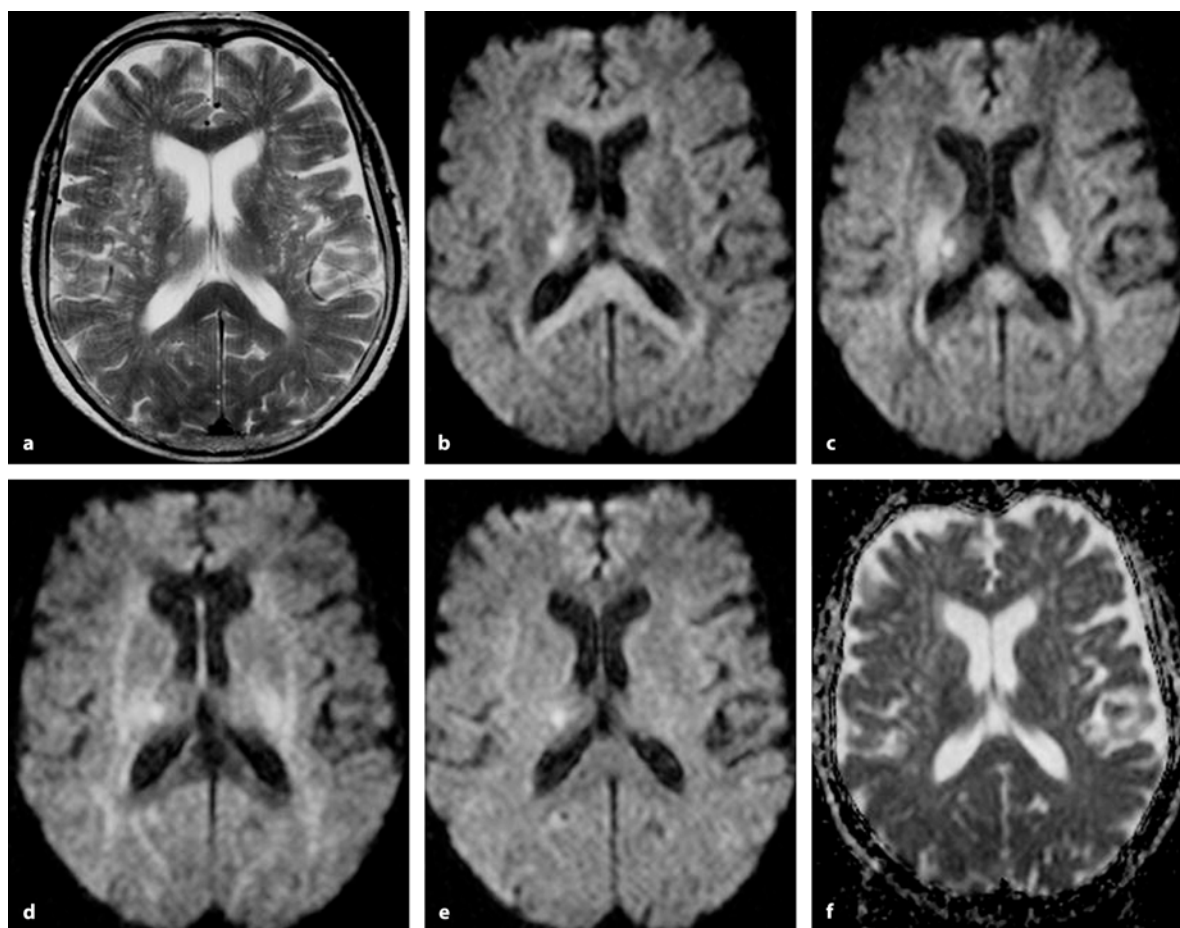


**Fig. 9a–f.** This patient presented with a hemisensory deficit with only mild paresis. **a** The T2WI showed no abnormalities besides relatively large perivascular spaces. In DWI data is collected after a sensitization gradient is played out along a specified plane. The intensity of diffusion is measured along that specified plane. In some tissues, such as cerebral spinal fluid and gray matter, the diffusion coefficient is the same in all spatial directions: isotropic diffusion. In white matter, where fibers are organized into fascicles or tracts, diffusion is much more intense along the spatial orientation of these tracts, whereas diffusion is reduced perpendicular to the long axis of these tracts: anisotropic diffusion. Diffusion gradient can be applied **b** along the x-axis, **c** along the y-axis, and **d** along the z-axis. **e** The so-called trace image consists of gradients in at least

three directions; therefore, the diffusion coefficient is dependent on the spatial orientation of the white matter tracts and on the direction of the sensitization gradients. In order to reduce the impact of these artifacts, DWI requires acquisition of images using sensitization gradients in at least three different spatial orientations. The acquisition of DW images with different  $b$ -values allows the calculation of the apparent diffusion coefficient (ADC). The ADC values of the single voxels can be displayed as an ADC map revealing the dispersion of the different ADC values within a slice of brain tissue (**f**). On an ADC map the signal intensity is equal to the magnitude of the ADC. An advantage of this representation is the independence of the signal intensity to T2 phenomena or to the magnetic field strength and gradient strength

upon the spatial orientation of the white matter tracts and direction of the sensitization gradients. In order to reduce the impact of these artifacts, DWI requires acquisition of images using sensitization gradients in at least three different spatial orientations. The exact causes of the anisotropic features of the white matter are not yet completely understood, but most investigators believe that the myelin sheaths play a contributory role. In addition to the axonal direction and myelination, physiological processes, such as axolemmic flow, extracellular bulk flow, capillary blood flow, and intracellular streaming, may also contribute to white matter anisotropy [24, 25].

The anisotropic nature of diffusion within the CNS can be visualized by evaluating DWI images obtained with diffusion gradients applied in different orthogonal directions (Fig. 9). Each image represents information about the direction and magnitude of the diffusion. Because the hyperintensities due to anisotropy can mimic pathology, most clinical imaging is performed by using methods to reduce these anisotropy artifacts, e.g., by acquiring multiple images, each with different gradient-encoding directions, and then averaging the images together (trace image). The resulting trace image is described as isotropic DWI image.



The degree of anisotropy can also be calculated and visualized as a separate map. By measuring the entire diffusion tensor the orientation of the principal axis of the diffusion tensor ellipsoid in space can be determined. The diffusion tensor describes the preferred direction of the water mobility, e.g., along the axons within a white matter bundle. Six different measurements (at a minimum) are required to describe water mobility in a three-dimensional space. These data allow to compute maps of fractional anisotropy (FA), which represent the ratio of the anisotropic component of the diffusion tensor to the whole diffusion tensor. On an FA map, the signal intensity is equal to the degree of anisotropy. Areas with marked anisotropy, such as regions with tightly packed white matter tracts (e.g., internal capsular, white matter of the spinal cord), appear hyperintense, and areas with low anisotropy (e.g., CSF, gray matter) appear hypointense. Changes in the degree of anisotropy can result from different disease processes, such as trauma or ischemia, and could serve as a sensitive and early indicator for injury or fiber tract integrity.

### Diagnostic Value of DWI

To date, the most important clinical application of diffusion-weighted imaging is focussed on the early identification of cerebral ischemia. The DWI has the ability to visualize changes in diffusion within minutes after the onset of ischemia [26–28]. This allows an evaluation of the extent of ischemia in a time frame where possible interventions (e.g., revascularization, thrombolytic agents, tPA) or the use of neuroprotective agents could limit or prevent further brain injury or possibly even reverse brain injury. This is of essential importance as conventional spin-echo MR sequences and conventional CT do not reliably detect infarction within the first hours after stroke onset (Fig. 10). Several studies have reported a limited sensitivity for ischemia within 6 h after stroke onset between 38 and 45% for CT, and 18 and 46% for conventional MR imaging [29, 30]. With an increasing time delay between onset of stroke and imaging the sensitivity consequently increases.

In approximately 3% of cases the diagnosis of an acute ischemic lesion by DWI is inaccurate due to variable etiologies, e.g., epilepsy, functional disorders, global transient amnesia, migraine, and intoxication [31]. In nearly 50% of patients with TIA, DWI may be normal, more commonly

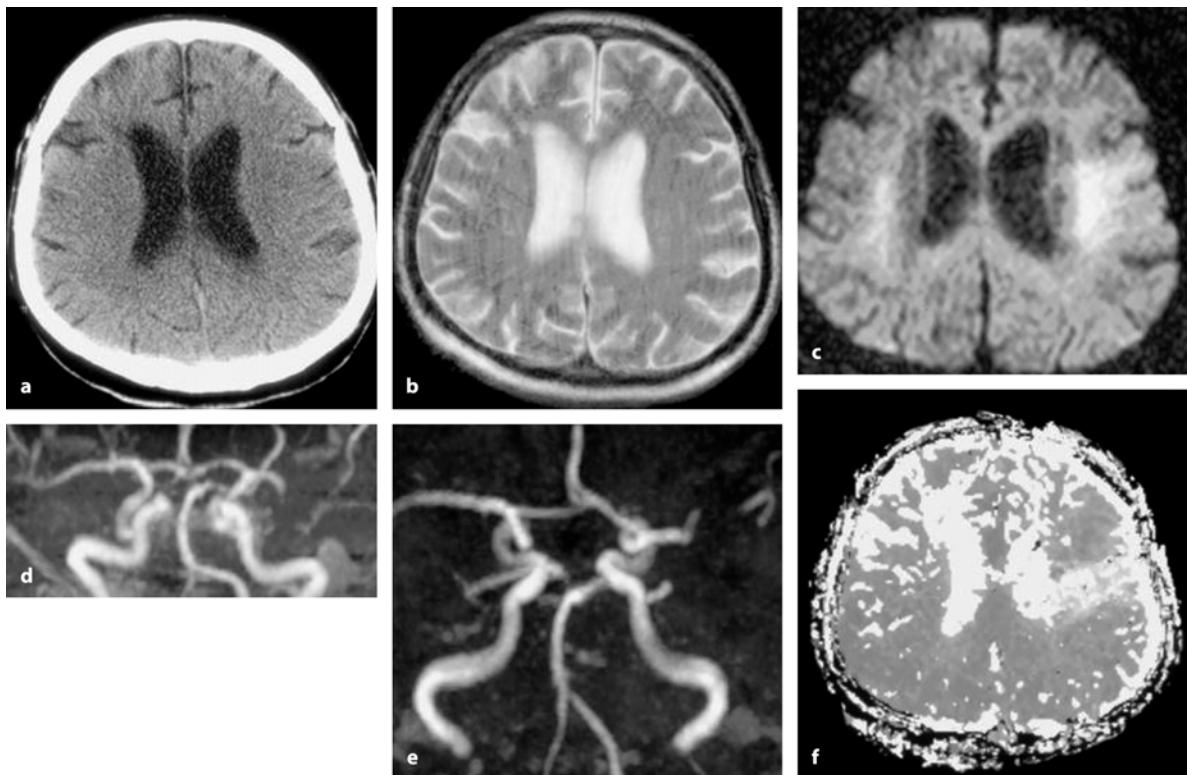


**Fig. 10a–f.** In the first few hours after the onset of stroke, perfusion-weighted imaging (PWI) abnormalities are often larger than the DWI lesion. This pattern (PWI deficit > DWI deficit) is frequently associated with subsequent lesion growth into the PWI/DWI mismatch region, indicating that the mismatch may

represent tissue at risk. **a** The CT and **b** the T2WI of a patient with onset of clinical symptoms 2 h earlier. **c** The DWI with a hyperintense lesion on the left and **d, e** MRA with an occlusion of the MCA. **f** The corresponding perfusion image with a perfusion deficit slightly larger than the DWI lesion

when duration of clinical symptoms is short, especially <1 h [32, 33]. On the other hand, approximately 50% of patients with TIA show lesions at DWI, and in a series of Cosnard et al. [34] 70% of the patients with complete regression of symptoms showed lesions which were mostly smaller than 1 cm<sup>3</sup>. The accuracy of DWI was improved when the sensitization gradients were applied sequentially because of reduced anisotropic artifacts. These artifacts could be responsible for false-positive results.

#### Apparent Diffusion Coefficient and ADC Maps

The acquisition of DW images with different *b*-values allows the calculation of the apparent diffusion coefficient (ADC). The ADC values of the single voxels can be displayed as an

ADC map revealing the dispersion of the different ADC values within a slice of brain tissue (see Fig. 11f). On an ADC map the signal intensity is equal to the magnitude of the ADC. An advantage of this representation is the independence of the signal intensity from T2-phenomena or from the magnetic field strength and gradient strength. Typically, ADC values are calculated by obtaining images with a *b*-value near to zero and 1000 s/mm<sup>2</sup>. Areas with a high diffusion have a high ADC value and appear consequently hyperintense on the ADC maps (CSF). Areas with restricted diffusion, like areas with acute ischemia, appear hypointense.

In normal brain parenchyma the mean ADC value was measured with  $0.740 \times 10^{-6}$  mm<sup>2</sup>/s with a standard variation of 0.031, without significant difference between similar structures between the left and right hemispheres. Between

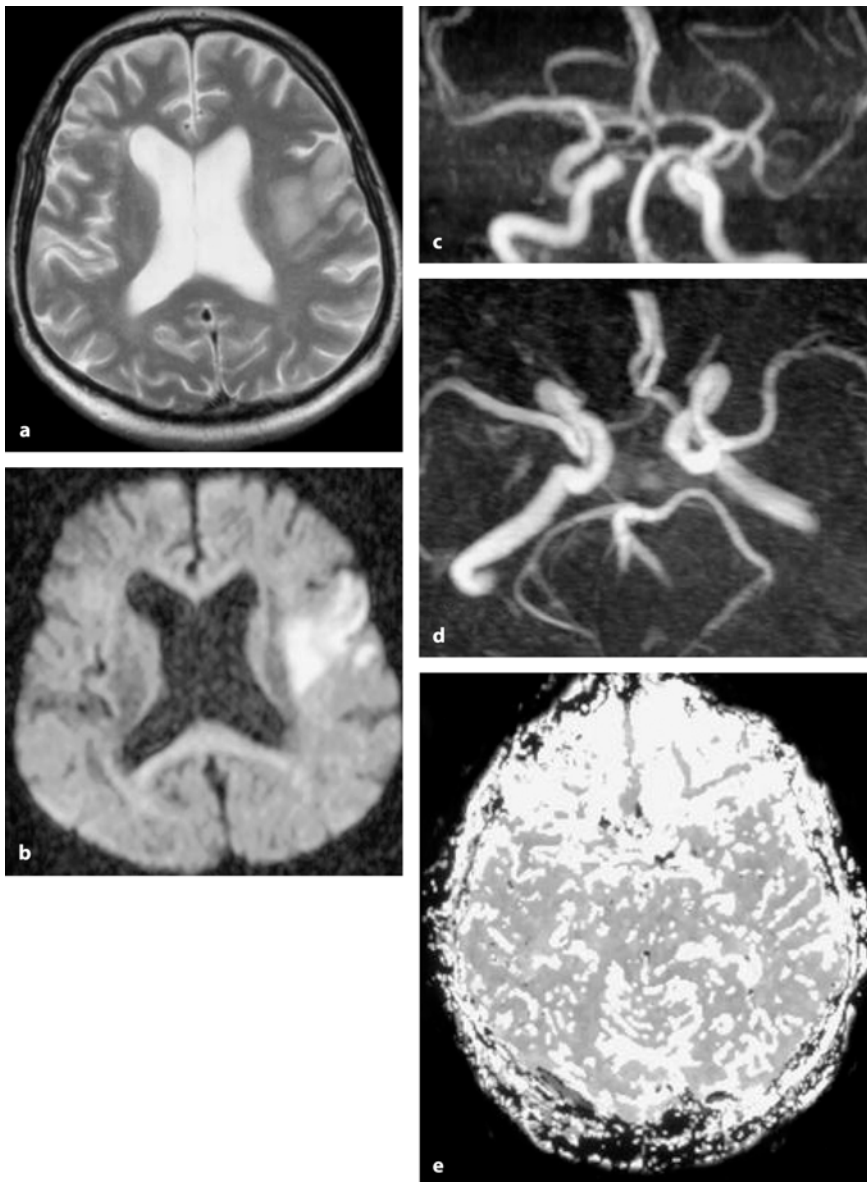


**Fig. 11a–e.** Same patient as in Fig. 7. The control MRI 3 days after the clinical onset of symptoms showed a small hyperintense area on **a** T2WI; **b** DWI showed the infarction slightly larger than on the first MR examination; **c, d** MRA showed the MCA now reopened. **e** The mean transit time maps now no longer revealed a perfusion deficit

different structures, such as the centrum semiovale, cerebellum, and the thalami, there were significant differences in ADC values ( $0.700 \times 10^{-6} \text{ mm}^2/\text{s}$  for the centrum semiovale and the cerebellum and  $0.790 \times 10^{-6} \text{ mm}^2/\text{s}$  for the thalami) [34]. Two studies reported significant increase in ADC values with increasing age, especially after 60 years of age (patients without macroscopic lesions) [35, 36].

In the literature the mean ADC values in ischemic lesions are quite variable, ranging from  $0.495 \times 10^{-6}$  to  $0.077 \times 10^{-6} \text{ mm}^2/\text{s}$  [28, 37].

### DWI in Routine Clinical Practice

Diffusion-weighted imaging is a valuable tool for diagnosing ischemic lesions at the hyperacute phase and for assessing the extent of lesions that are typically irreversible. Diffusion-weighted images are acquired in a few seconds using an echo-planar imaging SE sequence and are thus less sensitive to patient motion artifacts. The presence of ferromagnetic hardware may cause significant image degradation. Confirmation of acute ischemia is obtained by comparing  $b=0$  and  $b=1000$  images. The volume of lesions can be calculated by segmentation of images. The DWI and post-processing provide the clinicians with useful information for management of patients with stroke syndrome.

Diffusion-weighted imaging of the brain was first described in 1986 [38]. The ability to detect early ischemic changes was reported in 1990 [39]. Tissue changes in ischemic stroke are detectable by diffusion-weighted MRI (DWI) within minutes after the onset of symptoms; however, in daily routine CT is still the preferred imaging modality for patients with acute stroke. Diffusion-weighted imaging has been shown to be much more reliable than CT in the detection of early ischemic lesions and we believe that it should be used in acute ischemic stroke before aggressive therapeutic intervention.

### Perfusion-Weighted MRI

Magnetic resonance imaging should be performed on a 1.5-T whole-body MR scanner. A standard head coil can be used for radiofrequency transmission and detection. For perfusion-weighted MRI a T2\*-weighted fast low-angle shot (FLASH) sequence should be applied during bolus-injection of 0.1 mmol/kg Gd-DTPA in an antecubital vein. The injection rate is best performed using an MR injector with a flow rate of at least 2 ml/s with a subsequent flush of 0.9% saline solution. For calculating absolute rCBF values a two-slice technique can be used. Here one slice is placed at the level of the skull base, the other at the level of the basal ganglia. Sequence parameters on a Magnetom Vision (Siemens, Erlangen, Germany) are, for example, TR 55.2 ms, TE 20 ms, flip angle  $10^\circ$ , slice thickness 8 mm, matrix  $64 \times 128$ , effective time resolution 2.5 s, and 20 acquisitions. The total acquisition time of the dynamic study is then 50 s. Recently, it is possible to cover the whole brain and to calculate absolute rCBF values using EPI sequences.

### Theory

Assuming an exponential relationship between the relative signal reduction and the concentration of contrast medium, the resulting signal-time curves can be converted into concentration-time curves as follows [40–42]:

$$C(t) = \frac{-P}{TE} \cdot \ln \left( \frac{S(t)}{S(t_0)} \right) \quad (4)$$

where  $C(t)$  is the local concentration of contrast medium,  $P$  is the unknown proportionality factor,  $TE$  is the echo time,  $t_0$  is the arrival of the bolus, and  $S(t)/S(t_0)$  is the relative signal reduction.

According to Axel [43], rCBF can be calculated using the formula

$$rCBF = \frac{rCBV}{MTT} \quad (5)$$

where  $rCBV$  represents the fractional blood volume and  $MTT$  is the mean transit time. To solve Eq. (5) rCBV and  $MTT$  have to be known. They can be derived from the concentration–time curve.

The gamma-variate function has been shown to approximate closely an indicator–dilution curve without recirculation [42]. The gamma-variate function of the form

$$C(t) = \kappa \cdot (t - t_0)^\alpha \cdot e^{-(t - t_0)/k} \quad (6)$$

where  $\kappa$  and  $\alpha$  are parameters obtained from the curve fit. For each voxel the arrival of the bolus ( $t_0$ ) was calculated by the curve fitting routine. The curve fit beyond 70% of the maximum was extrapolated to baseline to eliminate the influence of indicator recirculation.

For correct measurements of rCBV the differences in plasma concentration and the differences between arterial and tissue hematocrit have to be considered. Absolute values of rCBV can be calculated, if the measured concentration time curves in tissue are normalized to the arterial concentration–time curve. According to Gobbel et al. [44] rCBV can be calculated as follows:

$$rCBV = \frac{1 - Hct_{art}}{1 - j \cdot Hct_{art}} \cdot \frac{AUC_{tis}}{AUC_{art}} \quad (7)$$

where  $Hct_{art}$  is arterial hematocrit, and  $j$  is a proportionality constant relating peripheral hematocrit to tissue hematocrit.  $AUC_{tis}$  is the area under the concentration–time curve for each voxel of tissue and  $AUC_{art}$  is the area under the concentration–time curve of the arterial input function.

Weisskoff et al. [45] have shown that even in a model with tubes of equal volume and flow, the first moment of the concentration–time curve would underestimate the mean transit time by 50%. The real mean transit time of the measured voxel  $\langle t_{tis} \rangle$  is related to the first and second moments of the distribution of transit times:

$$\langle t_{tis} \rangle = \frac{1}{2} \cdot \frac{\langle t^2 \rangle}{\langle t \rangle} \quad (8)$$

where  $\langle t \rangle$  and  $\langle t^2 \rangle$  are the first and second moments.

Using the relationship

$$\langle t^2 \rangle = \langle t \rangle^2 + \sigma^2 \quad (9)$$

where  $\sigma$  is standard deviation of the transit times and assuming that

$$\sigma = k \cdot \langle t \rangle \quad (10)$$

where  $k$  is an unknown constant, Eq. (8) can be rearranged to

$$\langle t \rangle = \frac{2}{1+k^2} \cdot \langle t_{tis} \rangle \quad (11)$$

A noninstantaneous bolus is always of finite duration and the measured tissue–concentration–time curve is a convolution of the real input concentration–time curve and the

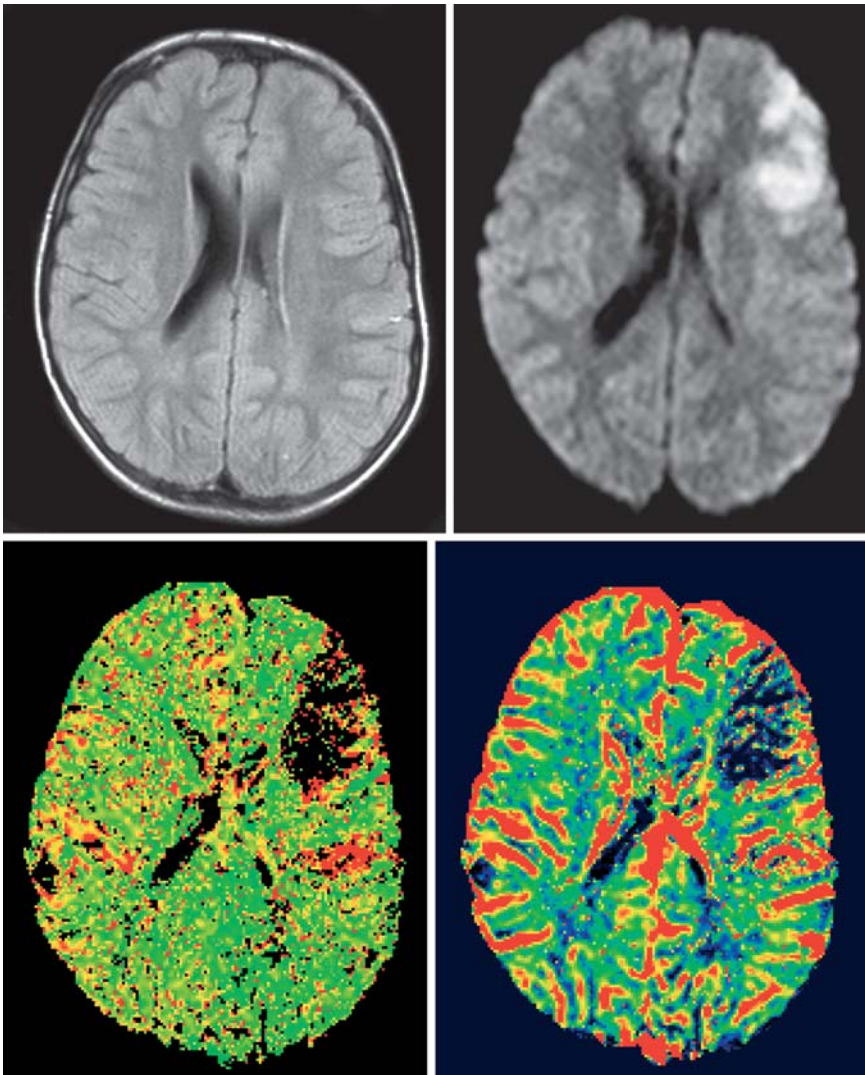
hypothetical curve resulting from an instantaneous bolus. As shown by Zierler [41] the mean transit time of the two convolved functions are additive, resulting in

$$MTT = \langle t \rangle = \frac{2}{1+k^2} \cdot (\langle t_{tis} \rangle - \langle t_{art} \rangle) \quad (12)$$

Combining Eqs. (7) and (12) rCBF can be calculated by

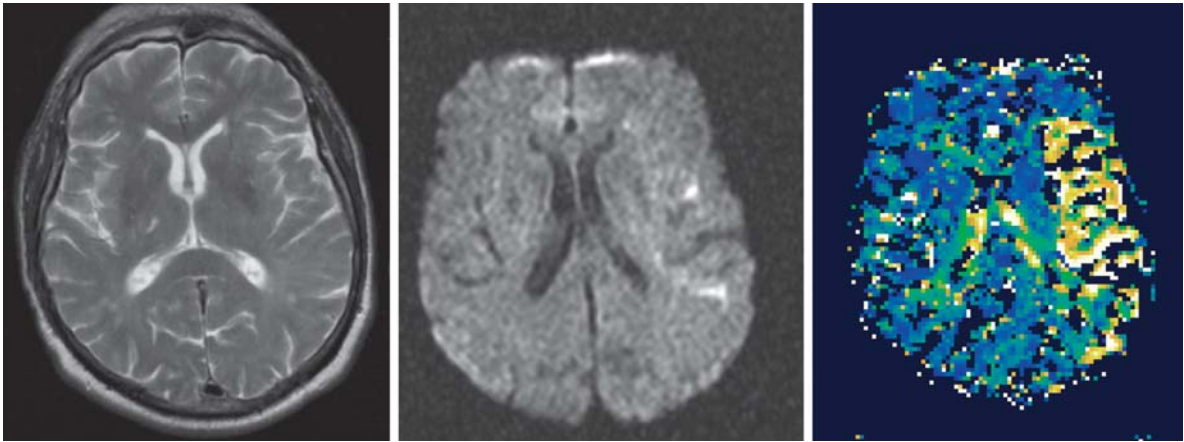
$$rCBF = \frac{1-Hct_{art}}{1-j \cdot Hct_{art}} \cdot \frac{AUC_{tis}}{AUC_{art}} \cdot \frac{1+k^2}{2} \cdot \frac{1}{(\langle t_{tis} \rangle - \langle t_{art} \rangle)} \quad (13)$$

Figure 12 demonstrates a patient with a left-sided hemiparesis 5 h prior to hospitalization. The FLAIR was normal (Fig. 12 a), whereas the perfusion images showed a deficit in the vascular territory of the right MCA. Figure 12b represents the DWI and Fig. 12c regional mean transit time map (Fig. 12d, the rCBF map).



**Fig. 12** No mismatch. On FLAIR the infarction is not yet visible, on DWI an infarction in the left MCA is visible. MTT and rCBF correspond to the delineation of the infarction on DWI





**Fig. 13** The infarction is hardly visible on DWI, whereas a perfusion deficit is seen in the left MCA territory

### Diffusion and Perfusion Imaging in Acute Stroke

It is interesting that despite the sensitivity of current imaging, it is presently not possible to identify an appropriate lesion in all patients with acute stroke deficits. Optimal stroke care requires close collaboration between the clinician and radiologist. Diffusion-weighted imaging makes an important contribution to stroke management, even in the subacute time frame, and should become widely available.

Figure 13 demonstrates the value of both diffusion- and perfusion-weighted MRI in the diagnostics of acute cerebral ischemia.

### 3.1.5 Lacunar Infarctions

Lacunar infarctions are associated with systemic arterial hypertension in approximately 90% of cases. They also occur as a result of arteriosclerosis with occlusion of the perforating branches. Frequent sites are putamen, caudate, thalamus, pons, internal capsulae, and corona radiata. There are some symptoms that are characteristic of lacunar infarction, e.g., a pure unilateral sensory loss due to lacunar infarction in the thalamus. A pure motor hemiparesis might be found in a lacunar infarction in the internal capsulae. Ataxic hemiparesis would lead us to look for an infarction in the pons. Generally, deficits, such as monoplegia, homonymous hemianopia, coma, or seizure, would not be expected in lacunar infarction [47].

Lacunar infarctions account for up to 25% of all strokes. They are typically located in the basal ganglia and thalamus. They are of small size and often multiple. Most commonly they are caused by embolic, atheromatous, or thrombotic lesions in the end arterioles that supply the deep cerebral gray matter. Due to their small size, they are often not recognized on CT scans. Some early subacute lacunar

infarctions may enhance following contrast administration [48]. On MR scans they are seen as round lesions, hyperintense on T2-weighted sequences (Fig. 14). On T1W1 they appear hypointense. The differential diagnosis includes enlarged perivascular Virchow-Robin spaces.

### 3.1.6 Stroke in Children

Pediatric stroke is very uncommon. Compared with adults, cerebral infarctions in children have different etiologies. The most common cause is an embolus from a congenital heart disease with right-to-left shunt. Traumatic or spontaneous dissection of the cerebral artery is also often seen. Although uncommon, idiopathic progressive arteriopathy (Moya-Moya disease) must also be considered. The symptoms usually start in childhood with repeated ischemic episodes. Progressive stenosis of the distal ICAs and proximal parts of the anterior and MCAs occur. Computed tomography scans show multiple infarctions. Usually, the anterior circulation is affected. Angiographic findings show enlarged lenticulo striatae and thalamo-perforating arteries, dural, leptomeningeal, and pial collateral vessels. This is called “puff-of-smoke” sign.

### 3.1.7 Dissection

Dissection of the large extracranial arteries may result in cerebral infarction. In dissection the intima is separated from the media. It is rarely seen in the elderly and is involved in up to 20% of pediatric cerebral infarctions [49]. The cause can be either the occlusion of the affected artery or embolism from the dissection. Dissection can also occur spontaneously and is often associated with trauma. After

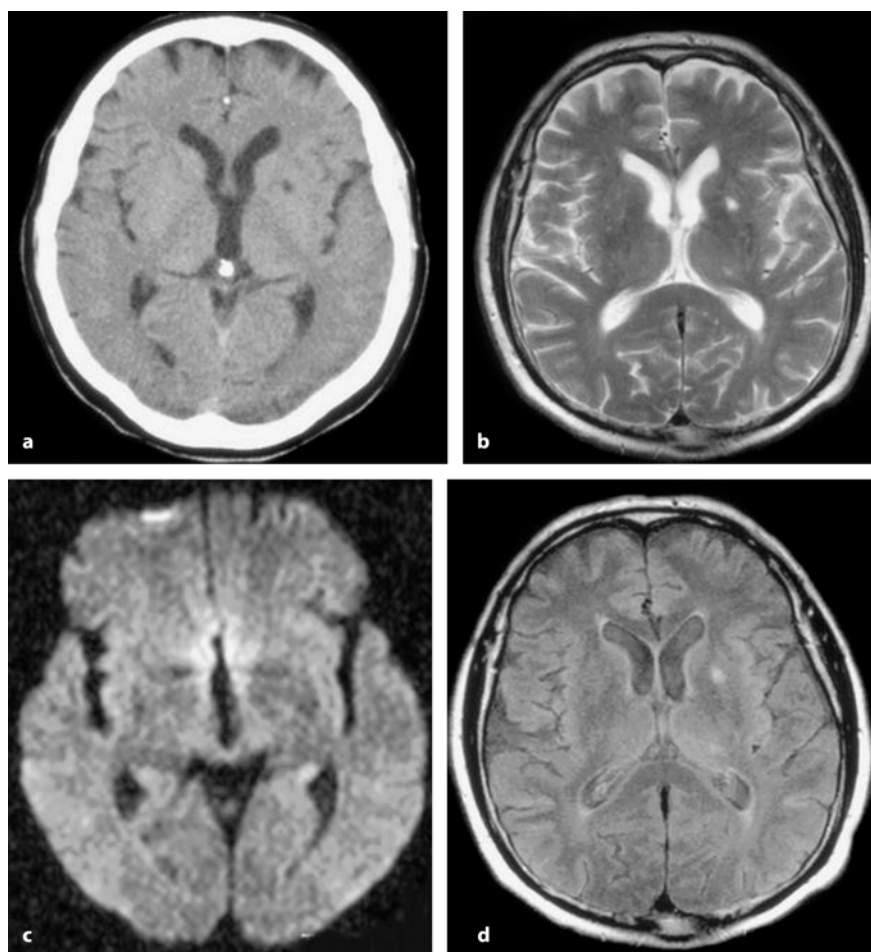


**Fig. 14 a–d.** Lacunar infarctions are associated with systemic arterial hypertension in approximately 90% of cases. They also occur as a result of arteriosclerosis with occlusion of the perforating branches. Frequent sites are putamen, caudate, thalamus, pons, internal capsulae, and corona radiata. There are some symptoms that are characteristic for lacunar infarction. **a** Computed tomography shows a small hypodense lesion, which is hyperintense on **b** the T2WI. **c** Diffusion-weighted imaging reveals no hyperintensity indicating that this lacunar infarction is older. **d** Fluid-attenuated inversion recovery image with a clearly visible lacunar infarction

chiropractic manipulations of the neck dissection can occur. Hypertension, Marfan's syndrome, and fibromuscular dysplasia are risk factors for spontaneous dissection.

On MR images the extraluminal hematoma may be seen as an area of increased T1 and T2 signal in subacute cases. Conventional MR and CT angiography can all be means to diagnose carotid or vertebral dissection. Spontaneous cervical internal carotid artery dissections generally have a good prognosis. Treatment is controversial, but usually, if a neurological deficit is present, heparinization is started.

### 3.1.8 Hypoxic–Ischemic Encephalopathy

In patients who have suffered a global anoxic/ischemic event, CT findings are often characteristic. A low-density band at the interface between major vascular territories is common. After perinatal asphyxia, initial CT scans can be more or less normal. After 24–48 h, a generalized cerebral edema occurs so that the brain now has a diffusely low density. Also a reversal sign may be present (reversal of the

gray/white matter densities). Hemorrhagic cortical necrosis with secondary calcification is often observed during the subsequent days. The surviving children usually have profound atrophic changes. Magnetic resonance imaging scans show high signal on T1WI in the basal ganglia, especially the ventro-lateral thalamus and posterior lateral lentiform nuclei.

### 3.1.9 Venous Infarction

Although the brain is equipped with numerous venous drainage with extensive collateration, the occlusion of a large sinus or a widespread vein obstruction will affect the cortex and underlying white matter. This will become congested and swollen and will eventually lead to venous infarction. Usually, they are bilateral and parasagittal, often multiple and hemorrhagic. Primary thrombosis is associated with hematological disorders (Fig. 15), the use of oral contraceptives, or inflammatory bowel disease. Thrombosis can also occur due to trauma, pregnancy, dehydration,

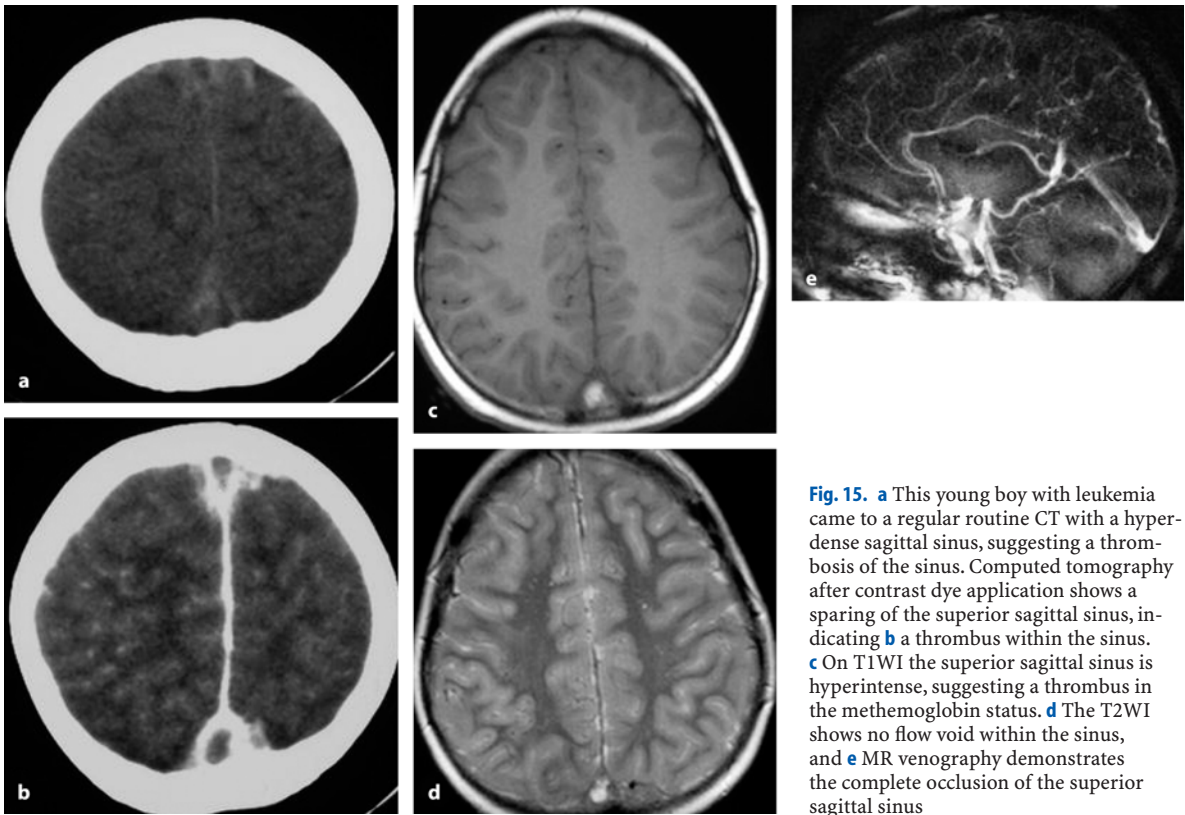


**Fig. 15.** **a** This young boy with leukemia came to a regular routine CT with a hyperdense sagittal sinus, suggesting a thrombosis of the sinus. Computed tomography after contrast dye application shows a sparing of the superior sagittal sinus, indicating **b** a thrombus within the sinus. **c** On T1WI the superior sagittal sinus is hyperintense, suggesting a thrombus in the methemoglobin status. **d** The T2WI shows no flow void within the sinus, and **e** MR venography demonstrates the complete occlusion of the superior sagittal sinus

malnutrition, heart disease, postoperative state, or cancer. Secondary thrombosis is mostly found due to a pyogenic infection. The patient complains of headache and might show a rapid neurological deterioration, even seizures and coma. The supersagittal sinus is commonly involved. Computed tomography scans can sometimes show a hyperdense thrombus within the thrombosed dural sinus or cortical veins (Fig. 15a). Cortical or subcortical hemorrhage in this region is often found. The CT scans with contrast enhancement may show the “empty delta sign” (Fig. 15b). This describes the enhancement around the thrombus, giving the appearance of a delta sign with a hollow center. Straight sinus occlusion may cause bilateral thalamic infarctions. On T1WI and T2WI the thrombosed sinus could be detected due to the loss of the normal signal void, especially on T2 (Fig. 15d) and FLAIR sequences as well as hyperintensities within the sinus representing the thrombus (Fig. 15c). Magnetic resonance angiography with 2D time of flight or phase contrast also shows venous or dural sinus occlusion as well as collateral venous flow (Fig. 15e). Both CT angiography and DSA reveal nonfilling of the thrombosed dural sinus. The thrombosed sinus is devoid of contrast and surrounded by dilated collateral venous channels. Injection in the aortic arc with the head imaged in a slightly oblique position is a good way to show all the craniocerebral vessels and their draining veins.

## References

1. Brott T, Broderick J, Kothari R et al. Early hemorrhage growth in patients with intracerebral hemorrhage. *Stroke* 1997;28:1–5
2. Mayer SA, Brun NC, Begtrup K et al. Recombinant activated factor VII for acute intracerebral hemorrhage. *N Engl J Med* 2005;352:777–785
3. Kidwell CS, Chalela JA, Saver JL et al. Comparison of MRI and CT for detection of acute intracerebral hemorrhage. *J Am Med Assoc* 2004;292:1823–1830
4. Barber PA, Demchuk AM, Zhang J et al. Validity and reliability of a quantitative computed tomography score in predicting outcome of hyperacute stroke before thrombolytic therapy. ASPECTS study group. *Alberta Stroke Programme early CT score. Lancet* 2000;355:1670–1674
5. Astrup J, Siesjö BK, Symon L (1981) Thresholds in cerebral ischemia: the ischemic penumbra. *Stroke* 12:723–725
6. Reith W, Hasegawa Y, Latour LL, Dardzinski B, Sotak CH, Fisher M (1995) Multislice diffusion mapping for 3D evolution cerebral ischemia in a rat stroke model. *Neurology* 45:172–177
7. Heiss W-D (1992) Experimental evidence for ischemic thresholds and functional recovery. *Stroke* 23:1668–1672
8. The National Institute of Neurological Disorders and Stroke rt-PA Stroke Study Group (1995) *N Engl J Med* 333:1581–1587
9. Hacke W, Kaste M, Fieschi C et al. (1995) Intravenous thrombolysis with recombinant tissue plasminogen activator for acute hemispheric stroke. The European Cooperative Acute Stroke Study (ECASS). *J Am Med Assoc* 274:1017–1020

10. Hacke W, Kaste M, Fiesci C et al. (1998) Randomised double-blind placebo-controlled trial of thrombolytic therapy with intravenous alteplase in acute ischemic stroke (ECASS II). Second European-Australasian Acute Stroke Study Investigators. *Lancet* 352:1245–1251
11. Kummer R von, Allen KL, Holle R et al. (1997) Acute stroke: usefulness of early CT findings before thrombolytic therapy. *Radiology* 205:327–333
12. Hunkey GJ, Warlow CP (1991) The role of imaging in the management of cerebral and ocular ischemia. *Neuroradiology* 33:381–390
13. Unger E, Littlefield J, Gado M (1988) Water content and water structure in CT and MR signal changes: possible influence in detection of early stroke. *Am J Neuroradiol* 9:687–691
14. Bourquain H, Elsner E, Gerber J, Müller A, Staube T, Kummer R von (1998) Prospektiver Wert der frühen CT bei zerebraler Ischämie. *Klin Neuroradiol* 8:135–136
15. Lev MH, Segal AZ, Farkas J, Hossain ST, Putman C, Hunter GJ, Budzik R, Harris GJ, Buonanno FS, Ezzeddine MA, Chang Y, Koroshetz WJ, Gonzalez RG, Schwamm LH (2001) Utility of perfusion-weighted CT imaging in acute middle cerebral artery stroke treated with intra-arterial thrombolysis: prediction of final infarct volume and clinical outcome. *Stroke* 32:2021–2028
16. Yuh W, Crain M, Loes D (1991) MR imaging of cerebral ischemia: findings in the first 24 hours. *Am J Neuroradiol* 12:621–629
17. Essig M, Kummer R von, Egelhof T, Winter R, Sartor K (1996) Vascular MR contrast enhancement in cerebrovascular disease. *Am J Neuroradiol* 17:887–894
18. Moseley ME, Cohen Y, Mintorovitch J et al. (1990) Early detection of regional cerebral ischemia in cats: comparison of diffusion and T2-weighted MRI and spectroscopy. *Magn Reson Med* 14:330–346
19. Kucharczyk J, Mintorovitch J, Asgari HS, Moseley ME (1991) Diffusion/perfusion imaging of acute cerebral ischemia. *Magn Reson Med* 19:311–315
20. Warach S, Gaa J, Siewert B et al. (1995) Acute human stroke studied by whole brain echo planar diffusion-weighted magnetic resonance imaging. *Ann Neurol* 37:231–241
21. Lovblad KO, Baird AE, Schlaug G et al. (1997) Ischemic lesion volumes in acute stroke by diffusion weighted MRI correlate with clinical outcome. *Ann Neurol* 42:164–170
22. Stejskal EO, Tanner JE (1965) Spin diffusion measurements: spin-echo in the presence of a time dependent field gradient. *J Chem Phys* 42:288–292
23. Li TQ, Chen ZG, Hindmarsh T (1998) Diffusion-weighted MR imaging of acute cerebral ischemia. *Acta Radiol* 39:460–473
24. Nomura Y, Sakuma H, Takeda K, Tagami T, Okuda Y, Nakagawa T (1994) Diffusional anisotropy of the human brain assessed with diffusion-weighted MR: relation with normal brain development and aging. *Am J Neuroradiol* 15:231–238
25. Wimberger DM, Roberts TP, Barkovich AJ, Prayer LM, Moseley ME, Kucharczyk J (1995) Identification of “premyelination” by diffusion-weighted MRI. *J Comput Assist Tomogr* 19:28–33
26. Provenzale JM, Sorensen AG (1999) Diffusion-weighted MR imaging in acute stroke: theoretic considerations and clinical applications. *Am J Roentgenol* 173:1459–1467
27. Chien D, Kwong KK, Gress DR, Buonanno FS, Buxton RB, Rosen BR (1992) MR diffusion imaging of cerebral infarction in humans. *Am J Neuroradiol* 13:1097–1102
28. Warach S, Gaa J, Siewert B, Wielopolski P, Edelman RR (1995) Acute human stroke studied by whole brain echo planar diffusion-weighted magnetic resonance imaging. *Ann Neurol* 37:231–241
29. Gonzalez RG, Schaefer PW, Buonanno FS et al. (1999) Diffusion-weighted MR imaging: diagnostic accuracy in patients imaged within 6 hours of stroke symptom onset. *Radiology* 210:155–162
30. Mohr J, Biller J, Hial S et al. (1995) Magnetic resonance versus computed tomographic imaging in acute stroke. *Stroke* 26:807–812
31. Ay H, Buonanno N, Bryan N, van Zijl PCM (1999) Normal diffusion-weighted MRI during stroke-like deficits. *Neurology* 52:1784–1792
32. Kidwell CS, Alger JR, Di Salle F et al. (1999) Diffusion MRI in patients with transient ischemic attacks. *Stroke* 30:1174–1180
33. Kimura K, Minematsu K, Yasaka M, Wada K, Yamaguchi T (1999) The duration of symptoms in transient ischemic attack. *Neurology* 52:976–980
34. Cosnard G, Duprez T, Grandin C, Dechambre S, Maigne F, Smith A (2000) Diffusion- and perfusion-weighted MR imaging during the hyperacute phase of stroke. *J Radiol* 81:858–869
35. Gideon P, Thomsen C, Henriksen O (1994) Increased self-diffusion of brain water in normal aging. *J Am Med Assoc* 4:185–188
36. Entgelter ST, Provencale JM, Petrella JR, DeLong DM, MacFall JR (2000) The effect of aging on the apparent diffusion coefficient of normal-appearing white matter. *Am J Roentgenol* 175:425–430
37. Nagesh V, Welch KMA, Windham JP et al. (1998) Time course of ADCw changes in ischemic stroke; beyond the human eye. *Stroke* 29:1778–1782
38. Le Bihan D, Breton E, Lallemand D, Grenier P, Cabanis EA, Laval-Jeantet M (1986) MR imaging of intravoxel incoherent motions: application to diffusion and perfusion in neurological disorders. *Radiology* 161:401–407
39. Moseley ME, Cohen Y, Mintorovitch L, Chileuitt L, Shimizu H, Kucharczyk J, Wendland MF, Weinstein PR (1990) Early detection of regional cerebral ischemia in cats: comparison of diffusion- and T2-weighted MRI and spectroscopy. *Magn Reson Med* 14:330–346
40. Axel L (1980) Cerebral blood flow determination by rapid sequence computed tomography. *Radiology* 137:679–686
41. Zierler KL (1962) Theoretical basis of indicator-dilution methods for measuring flow and volume. *Circ Res* 10:393–407
42. Reith W, Heiland S, Erb G, Benner T, Forsting M, Sartor K (1997) Dynamic contrast-enhanced T2\*-weighted MRI in patients with cerebrovascular disease. *Neuroradiology* 39:250–257
43. Axel L (1983) Tissue mean transit time from dynamic computed tomography by a simple deconvolution technique. *Invest Radiol* 18:94–99
44. Gobbel GT, Cann CE, Fike JR (1993) Comparison of xenon-enhanced CT with ultrafast CT for measurement of regional cerebral blood flow. *Am J Neuroradiol* 14:543–550
45. Weisskoff RM, Chesler D, Boxermann JL, Rosen BR (1993) Pitfalls in MR measurements of tissue blood flow with intravascular tracers: Which mean transit time? *Magn Reson Med* 29:553–559
46. Rempp K, Brix G, Wenz F, Becker CR, Gückel F, Lorenz WJ (1994) Quantification of regional cerebral blood flow and volume with dynamic susceptibility contrast-enhanced MR imaging. *Radiology* 193:637–641
47. Fisher CM (1982) Lacunar strokes and infarcts: a review. *Neurology* 32:871–876
48. Regli L, Regli F, Maeder P, Bogousslavski J (1993) Magnetic resonance imaging with gadolinium contrast in small deep (lacunar) cerebral infarcts. *Arch Neurol* 50:175–180
49. Russo CP, Smoker WRK (1996) Nonatheromatous carotid artery disease. *Neuroimaging Clin North Am* 6:811–830





## Neuroradiological Emergency Interventions

C. Brekenfeld, J. Gralla, R. Wiest, M. El-Koussy,  
L. Remonda, C. Ozdoba, G. Schroth

## 3.2

### Contents

3.2.1	Introduction	313
3.2.2	Acute Haemorrhage in Neuroradiology	313
3.2.2.1	Head and Neck Lesions	313
3.2.2.2	Intracranial Aneurysms	316
3.2.2.3	Venous Sinus Occlusion	319
3.2.2.4	Dural Arteriovenous Fistulas	319
3.2.2.5	Spinal Haemorrhage	322
3.2.3	Acute Ischaemic Stroke	323
3.2.3.1	Thrombolysis of Cerebral Arteries	323
3.2.3.2	Mechanical Revascularization of Cerebral Arteries	323
3.2.3.3	Central Retinal Artery Occlusion	324
3.2.3.4	Stenting of Cervical Arteries in Acute Stroke	324
3.2.4	Discussion	326
	References	327

### 3.2.1 Introduction

In the field of neuroradiology, improvements in imaging technology (diffusion-weighted MRI, DWI), 3D digital subtraction angiography (3D DSA) and endovascular devices (microcatheters, coils, stents) have opened the door to endovascular treatment even of life-threatening diseases in emergency situations. The advantage of endovascular therapy is that it is a minimally invasive approach that can be combined with diagnostic procedures. It is also fast and can be performed even in critically ill patients [34, 69, 71]. It does, however, require close cooperation between neurologists, neurosurgeons, craniofacial, head and neck surgeons, neuroanaesthesiologists and neuroradiologists.

Vessel access during neuroradiological emergency interventions is gained by insertion of a catheter sheath in the femoral artery or vein. The sheath and guiding catheters have to be thoroughly flushed with heparinized saline to prevent potentially disastrous thromboembolic complications in the spinal and cerebral arteries. In most emergency situations, head and neck procedures are best performed under general anaesthesia [37, 38] to ensure op-

timal working conditions for the interventional neuroradiologist by allowing acquisition of high-quality (1024×1024 matrix) digital subtraction angiography (DSA) images, stable biplane road maps or 3D projections, and to minimize the risk of vascular spasms due to catheter manipulation. In our institution, neuroleptic analgesia or light sedation based on benzodiazepines, such as diazepam or midazolam and opioids, are the alternative methods of choice for cooperative patients.

Herein several of the therapeutic options in interventional neuroradiology are discussed, including vessel embolization with particles, glue and coils, as well as vessel recanalization by thrombolysis, aspiration, balloon angioplasty and stent placement. Particular attention is given to the importance of the interdisciplinary management of neurovascular disorders.

### 3.2.2 Acute Haemorrhage in Neuroradiology

#### 3.2.2.1 Head and Neck Lesions

Acute haemorrhage in head and neck lesions can be caused by various factors and can lead to disastrous situations [52]. If conservative and/or surgical treatment is unsuccessful, catheter angiography can play a major role in localization of the source of bleeding and subsequent occlusion of the damaged vessel using the same endovascular approach.

The most frequent manifestation of acute haemorrhage in the head and neck region is epistaxis, which can be caused by tumour (Fig. 1), hypertension, trauma (Fig. 2), vascular malformation, Rendu–Osler–Weber disease, a bleeding disorder, iatrogenic or by infection (Fig. 3). Idiopathic epistaxis is usually a benign and self-limiting complaint with an ascending scale of treatments, such as injection of haemostatic agents, endoscopically guided electrocoagulation and anterior nasal packing. The conventional tools for immediate control of bleeding are internal maxillary artery ligation and posterior packing; the former has the drawback that it closes the endovascular approach, which should be preserved (especially in Rendu–Osler–



**Fig. 1.** An 18-year-old man with epistaxis from juvenile nasopharyngeal angiofibroma, class 3, treated with posterior packing. **a** Tumor and packing are well seen on sagittal T1-weighted MRI. **b** Selective angiography of the distal maxillary artery before embolization with particles shows the blush of the vascular tumor

Weber disease) for later embolization to stop acute re-bleeding. Posterior packing has the disadvantage of being painful and liable to complication by aspiration, sinus infection, or respiratory problems; it also has a high failure rate. Not burdened by either of these drawbacks, endovascular embolization has become an attractive alternative in the treatment of epistaxis.

Normally, the femoral approach and a 5.5-F JB2 diagnostic catheter (Valavanis, Cook, Bloomington, Ind.) is used to catheterize the ipsilateral common carotid artery. Biplane

DSA images are analysed to assess the source of bleeding, anatomical variations and potentially dangerous anastomoses from the external to the internal carotid or vertebral territory. Leaving the 5.5-F catheter as a guiding catheter, a coaxially inserted microcatheter (Tracker 18, 14 or 10; Boston Scientific, Fremont, Calif.) is advanced to the pterygopalatine portion of the maxillary artery, generally under biplane road map guidance. Embolization is performed using microparticles of polyvinyl alcohol (PVA) ranging in size between 45 and 250  $\mu\text{m}$  (Contour, Boston Scientific, Fremont, Calif.). Superselective angiography and, if necessary, embolization of the ipsilateral facial artery, is the next step in the neuroangiographic protocol. An ipsilateral common carotid artery injection is carried out to control the effect of treatment. It is essential that the contralateral side be investigated as well. If the common carotid injection demonstrates extensive blood supply from the contralateral side, which is the rule rather than the exception, superselective catheterization and embolization of that side is performed as described above.

In rare cases of Rendu–Osler–Weber disease, nasopharyngeal tumours or trauma, additional arteries (e.g. ascending pharyngeal, descending, and ascending palatine arteries) have to be included in this superselective embolization. In case of vascular tumours, additional angiography and elective preoperative embolization after emergency treatment may be necessary to obtain sufficient preoperative devascularization of the tumour.

One complication of direct abscess or tumour progression (frequently a squamous cell carcinoma) and/or therapy is carotid blow-out syndrome, in which patients are at high risk for arterial haemorrhage. The mechanisms include direct tumour invasion of the wall of the carotid artery or its branches, radiation injury, weakening of the vessel wall from multiple surgical dissections, carotid exposure owing to musculocutaneous flap necrosis, wound infections, pharyngocutaneous fistulas and/or the lack of surrounding supporting tissue. The angiographic pattern includes pseudoaneurysms of the carotid artery or of small branches. If, however, the vessel wall injury results in a local, compressive haematoma, rather than local or transoral haemorrhage, the damaged vessel may present as occluded. In such cases, as well as in traumatic bleeding with extensive soft tissue swelling, the embolic material must be fully prepared before selective angiography since this diagnostic procedure can dramatically increase the bleeding (Fig. 2).

Small-branch haemorrhages [59] are usually treated by superselective catheterization and glue (Histoacryl, Braun, Melsungen, Germany) injection at the site of the rupture. Proximal occlusion of the branch using coils may improve the acute situation; however, repeated use of the transarterial approach will become difficult or impossible if re-bleeding due to potential collaterals occurs.

In carotid blow-out syndrome the ruptured vessel wall can be bridged by a covered stent or one or more conventional stents or a combination of stents and coils (Fig. 3), where the coils are placed through the mesh of the stent

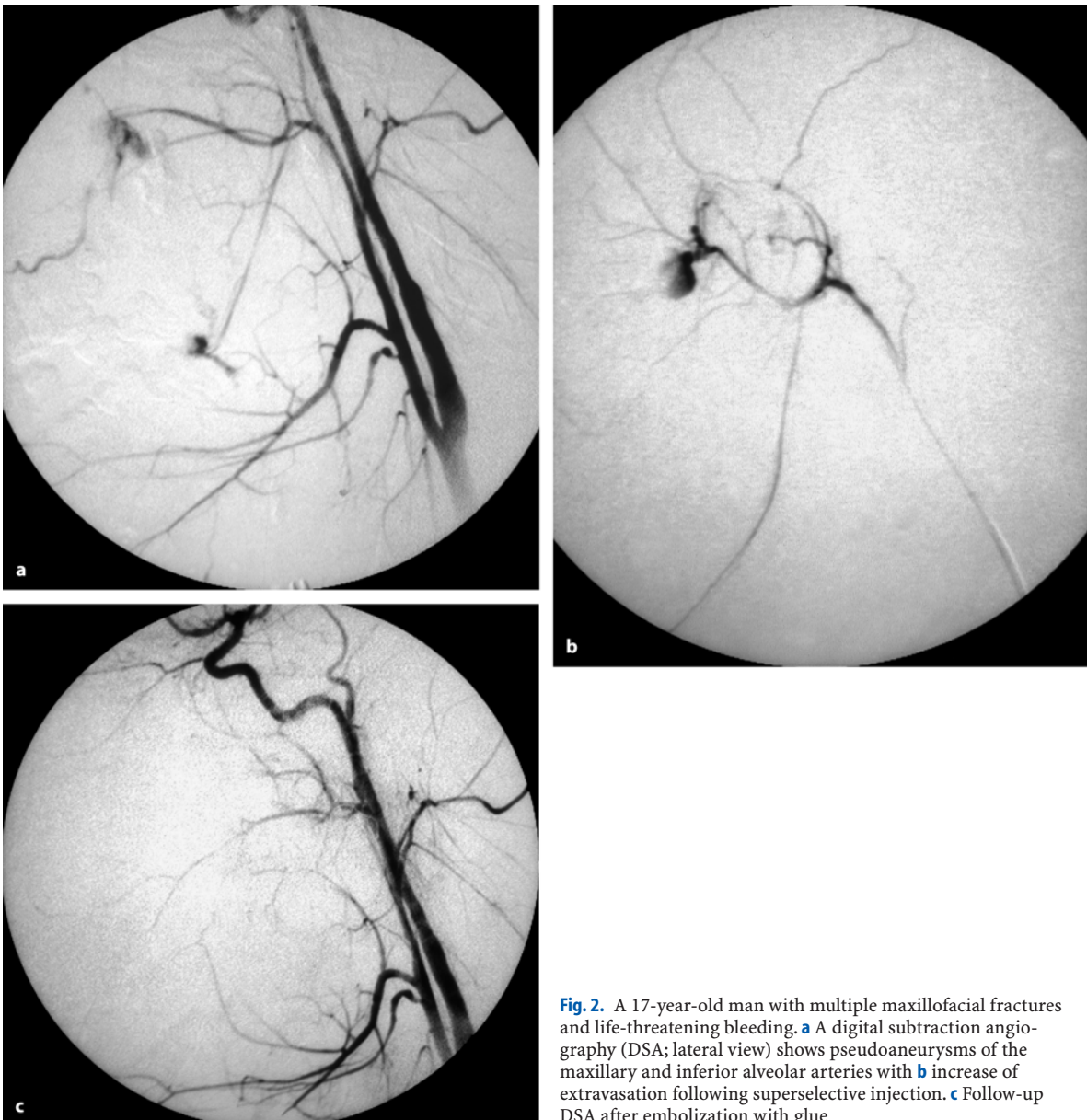


**Fig. 2.** A 17-year-old man with multiple maxillofacial fractures and life-threatening bleeding. **a** A digital subtraction angiography (DSA; lateral view) shows pseudoaneurysms of the maxillary and inferior alveolar arteries with **b** increase of extravasation following superselective injection. **c** Follow-up DSA after embolization with glue

directly into the pseudoaneurysm [10, 25, 52]. Fortunately, these recent advances in endovascular therapy have rendered surgical or balloon occlusion of ruptured common or internal carotid arteries almost obsolete. The complication rate of such procedures is high, principally because functional neuroangiographic tests [74] cannot be performed in these acutely ill patients.

Intraosseous arteriovenous malformations (AVM) of the maxilla or mandible are rare but can give rise to sudden massive oral haemorrhage [51]. The treatment of choice is transarterial and/or transvenous occlusion of the AVM. Percutaneous puncture of the AVM inside the bone can also be performed and glue and/or coils injected directly

into the venous pouch. Direct puncture of the venous pouch was achieved by our team using a computer-assisted navigation system [14]. Our neuroangiographic suite is designed as an operating theatre for just such occasions requiring combined interdisciplinary surgical and endovascular approaches [60]. Manual compression of the ipsilateral common carotid artery and jugular vein during the glue injection reduces the blood flow through the AVM and helps to avoid subsequent displacement of the acrylic glue.

Our group of 74 patients suffering from acute and sub-acute haemorrhage in the head and neck treated by the endovascular approach between 1992 and 1998 had a complication rate of 1.9% with a mortality rate of zero [52].



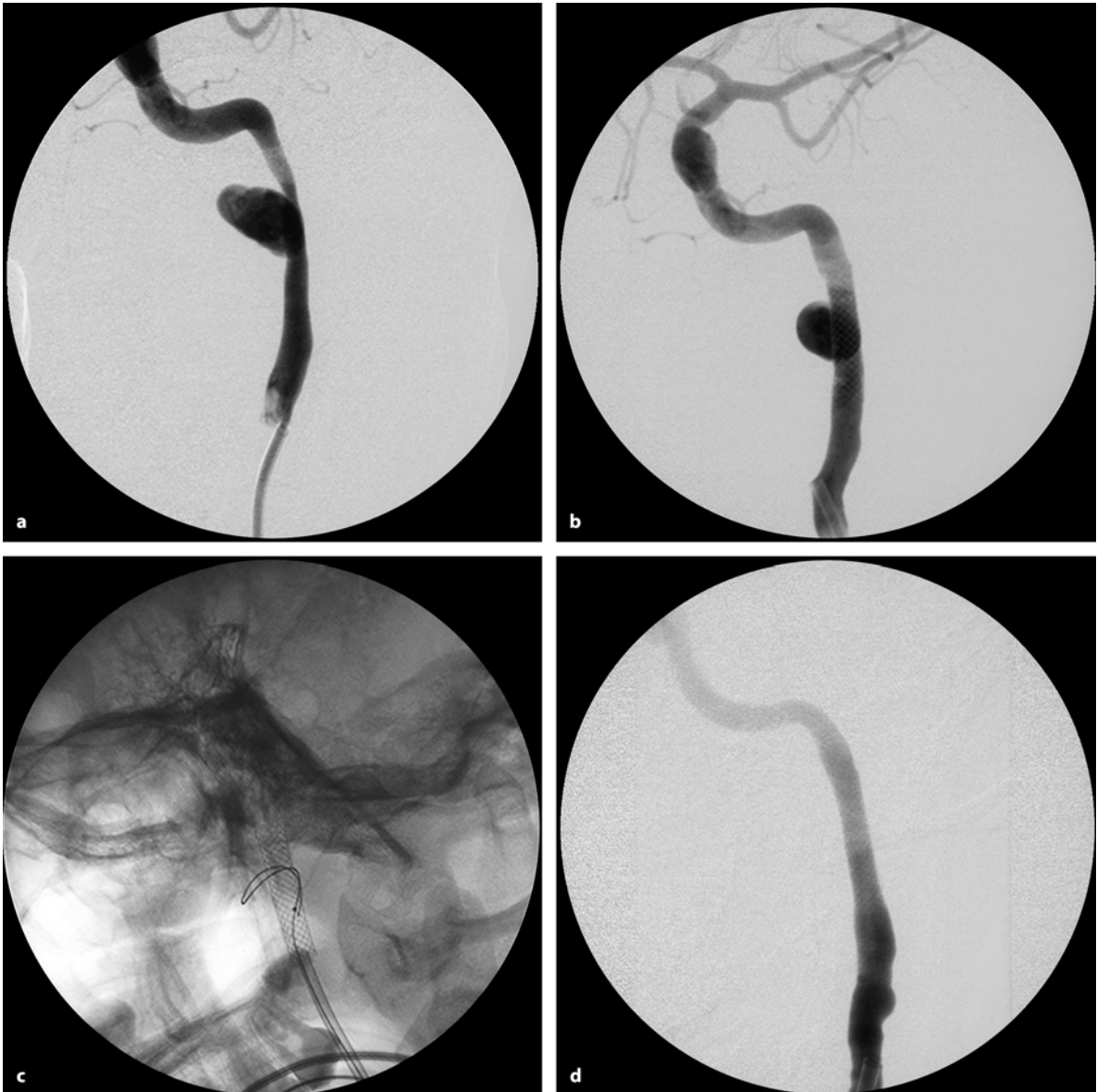


**Fig. 3.** **a** Lateral DSA shows a pseudoaneurysm of the internal carotid artery (ICA) as source of recurrent severe oral bleeding. The cervical segment of the ICA is stenotic due to parapharyngeal abscess formation. **b** A DSA (oblique view) after stent placement. The pseudoaneurysm is still perfused. **c** Unsubtracted angiogram

(oblique view). Unsuccessful coil treatment, because microcatheter could not be navigated through the mesh of the stent and **d** definite exclusion of the aneurysm after placement of a second covered stent (stent in stent technique)

### 3.2.2.2 Intracranial Aneurysms

The incidence of intracranial aneurysms has been reported at between 1.5 and 7% [7]. Aneurysm rupture causes 80% of all subarachnoid haemorrhages (SAH) [50], which commonly manifest in sudden explosive headache with or without neurological symptoms. Either CT or MRI are obligatory in all cases of aneurysmal SAH and must be followed by lumbar puncture if negative. The morbidity and

mortality of aneurysmal SAH are high and are caused by rebleeding, hydrocephalus and vasospasm. Occlusion of the aneurysm either by endovascular coiling or by surgical clipping effectively prevents rebleeding. A complete cerebral angiographic study is therefore the next step once the diagnosis of SAH has been established. Using 3D and/or high-resolution rapid sequences, the location of the aneurysm, its size and its relation to the parent vessel have to be visualized. Exact measurement of the neck, body and dome of the aneurysm is performed before the interven-

tion [67]. Depending on these measurements and on the clinical situation, the interdisciplinary neurosurgical/neuroradiological decision between early or late intervention and endovascular treatment is made in the neuroangiographic suite [63]. The International Subarachnoid Aneurysm Trial study (ISAT) that included 2143 patients revealed endovascular coil therapy to be generally superior to surgical clipping in acute SAB and aneurysms [41, 42].

Whereas diagnostic angiography is usually performed using local anaesthesia, endovascular treatment of the aneurysm or vasospasm usually requires general anaesthesia. The proximal parent vessel artery is catheterized with a 6-F guiding catheter. Using biplane road mapping, the microcatheter is advanced coaxially into the sac of the aneurysm (Fig. 4). Repeated angiograms through the guiding catheter with the introduced microcatheter allow monitoring of the progress of the treatment. The microguidewire is then removed and the detachable coil introduced through the microcatheter into the aneurysm sac. Both the microcatheter and the guiding catheter must be flushed with saline during the whole procedure.

A number of different coil systems are available, each with its own characteristics and pitfalls. The reader is therefore advised to become proficient with a single system to avoid complications. We normally use the Guglielmi detachable coil (GDC) system (Boston Scientific, Fremont, Calif.) which uses electrolysis for coil detachment [26, 27]. It is available in diameters of 0.010 and 0.015 in., the smaller size being used with a Tracker-10 microcatheter in acute aneurysms. Three-dimensional GDC coils were recently introduced and are especially useful in constructing the initial frame inside the aneurysm. Soft coils and ultrasoft coils are also available to be placed in the dead spaces between the initially implanted coils [43]. Other recent advances in the treatment of acute wide-neck aneurysms include a neck bridging device (Trispan; Fig. 4), a balloon-assisted technique [39, 44] and the combined application of an intravascular stent to bridge the wide neck of the aneurysm with subsequent intrasaccular placement of the coil through the mesh of the stent to protect the lumen of the parent artery [9, 20, 22, 72].

Potential complications of acute endovascular treatment of aneurysms are perforation of the aneurysm and thromboembolic complications [56, 68], e.g. thrombus formation at the coils or in a stent. Perforation most often occurs when the microguidewire or the coils are introduced into the aneurysm or when the microcatheter runs forward in an uncontrolled manner. In this situation it is crucial to leave the microcatheter in place and to continue with the coil treatment to prevent rebleeding [19]. It does not matter if a part of the coil extrudes from the aneurysm into the subarachnoid space. Coiling-related rerupture is more life-threatening in aneurysms of the basilar artery [68].

If sudden vessel occlusion occurs during intervention it might be due to vessel spasm or clot formation. To confirm vessel spasm, one should raise the patient's blood pressure



**Fig. 4.** Acute basilar-tip aneurysm. Both P1 segments of the posterior cerebral arteries are involved in the broad neck of the aneurysm, which was bridged by a trispan coil introduced from the left vertebral artery (**a** DSA, anteroposterior view). **b** Lateral DSA shows densely packed aneurysm after coil introduction from the right vertebral artery. The posterior cerebral arteries are well perfused

and wait a few minutes for the spasm to subside. If the occlusion does not resolve or local clot formation is observed, thrombolysis is the treatment of choice. A new alternative to intra-arterial urokinase is intravenous or intra-arterial application of abciximab, which acts as a platelet glycoprotein (GP) IIb/IIIa receptor inhibitor [6, 62]. Whereas urokinase is a plasmin activator, abciximab inhibits thrombocyte aggregation, which is thought to be the major cause of thromboembolic events in endovascular

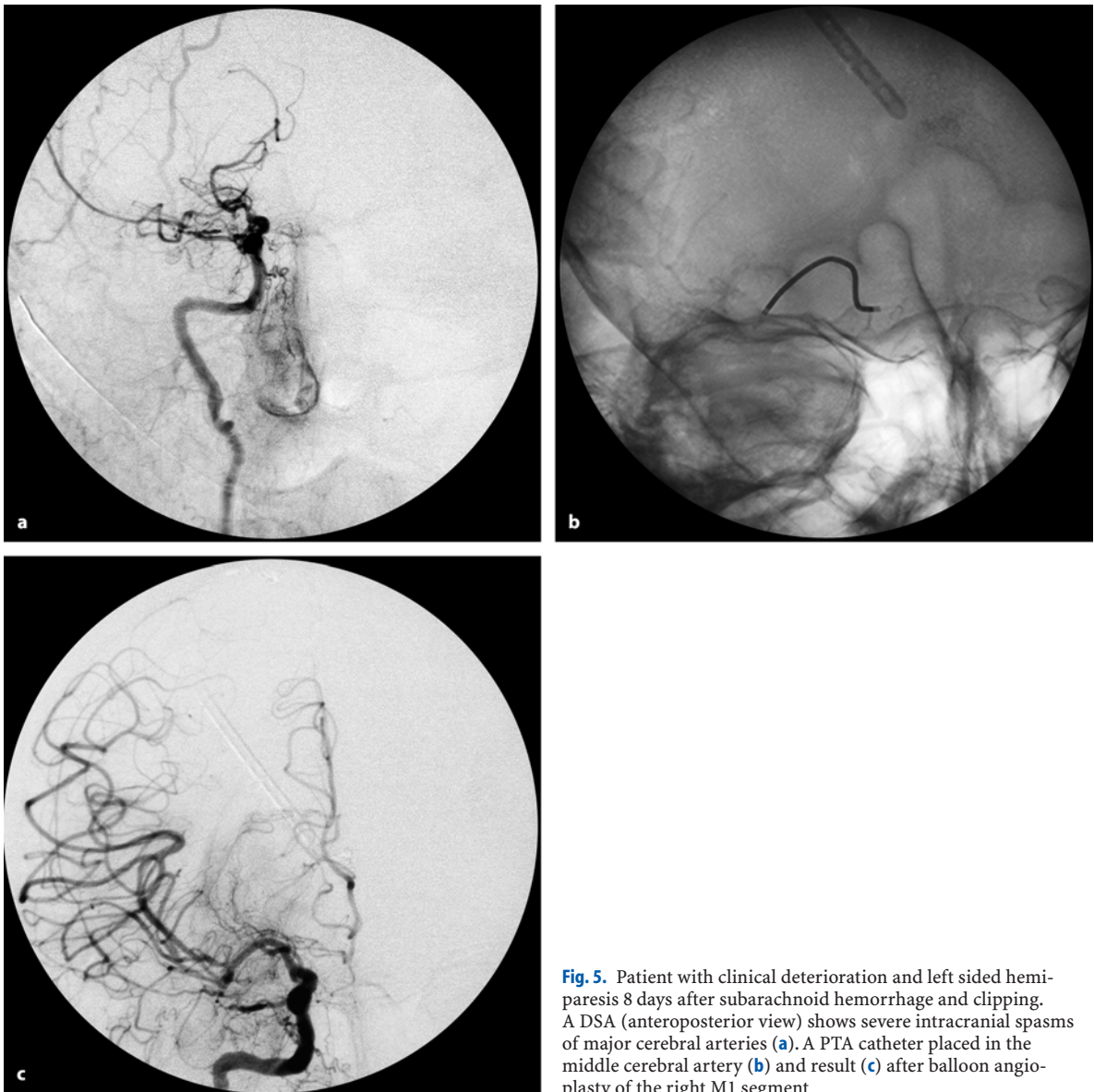


**Fig. 5.** Patient with clinical deterioration and left sided hemiparesis 8 days after subarachnoid hemorrhage and clipping. A DSA (anteroposterior view) shows severe intracranial spasms of major cerebral arteries (a). A PTA catheter placed in the middle cerebral artery (b) and result (c) after balloon angioplasty of the right M1 segment

interventions. Catheter-induced vasospasm can be resolved by local application of glycerol trinitrate or nimodipine.

With the advent of efficacious acute treatment of SAH by surgical or endovascular means, the prevention, monitoring and treatment of late complications such as vasospasm assumes increased importance [36]. Vasospasm typically develops between the fourth and fourteenth day following SAH. Changes associated with vasospasm include thickening and oedema of the vessel intima and media and surrounding inflammation. The degree and location of vasospasm are related to the amount of blood that the vessel adventitia is exposed to and the duration of exposure. Early clinical symptoms are due to altered con-

sciousness (patients become drowsy and confused), followed by focal neurological deficits, depending on the intensity of the spasm.

Angioplasty represents a significant breakthrough in the treatment of cerebral vasospasm. It should be performed as soon as possible after the onset of symptoms [21], or even in the absence of neurological deficits if transcranial Doppler ultrasound (mean velocities >200 cm/s in the middle cerebral artery) or functional MRI [36] indicate severe vasospasm. Angiography is the definitive method to directly localize and measure the degree of vasospasm. Vasospasm often occurs in multiple vessels, resulting in an additional reduction of collateral flow. Narrowing frequently extends over a long segment of the affected vessel,



significantly reducing cerebral perfusion even if narrowing of the luminal diameter is only 50%.

The GDC treatment of the aneurysm can be combined with endovascular therapy of vasospasm [45]. The basic transfemoral technique consists of a large (at least 7 F) guiding catheter being placed in the common or internal carotid or dominant vertebral artery, which allows repeated road maps and control DSA to be performed during the course of angioplasty. We prefer to use a polyethylene microballoon catheter (FasStealth, Boston Scientific, Fremont, Calif.) that can be navigated by a steerable microguidewire (Fig. 5), which is especially useful for entering the narrow segment of the vessel [33]. The most serious complication of angioplasty is vessel rupture, especially of intracranially arteries. To avoid this, the balloon diameter must be equal to or smaller than that of the treated vessel. In most cases, balloons with a diameter of 2.5 mm and a length of 15 mm are sufficient. These balloons utilize higher inflation pressures, which is useful in older, chronic vasospasms. Using a high-resolution road-map technique, the balloon can be kept out of small branches that would rupture upon balloon inflation.

### 3.2.2.3 Venous Sinus Occlusion

Cerebral venous thrombosis is less frequent than arterial thrombosis. The clinical severity depends upon the extent of the thrombus and on the availability of efficient venous collaterals. Although the reduction in brain perfusion and the degree of the resulting cytotoxic and vasogenic oedema can be visualized by MRI, estimating the capacity of the venous collaterals and thus the time course of this disease, even by angiography, is difficult [35]. Acute occlusion of the cerebral venous outflow may not be well tolerated and can lead to elevated intracranial pressure, venous congestion or brain oedema (pseudotumour cerebri), resulting in headache, focal neurological deficits, epileptic seizures and intracranial haemorrhage. The natural course is highly variable and mortality rates vary from 10 to 50% [12]. The usual therapy is partial thromboplastin time-regulated anticoagulation [70]: the partial thromboplastin time should be at least doubled and increased to target levels between 80 and 100 s, even if intracranial haemorrhage is already present.

In patients presenting with stupor or coma or with continued deterioration despite heparin treatment, direct endovascular thrombolysis should be considered. This technique involves placement of a guiding catheter in the jugular bulb via the transfemoral venous approach and insertion of the microcatheter directly into the thrombus in the dural sinus (Fig. 6). Urokinase is administered initially as a bolus of approximately 250,000 units and then as a continuous infusion of approximately 70,000 units/h. Recent reports describe accelerated recanalization of occluded dural sinuses by mechanical clot lysis, angioplasty and stent placement [8, 15, 16].

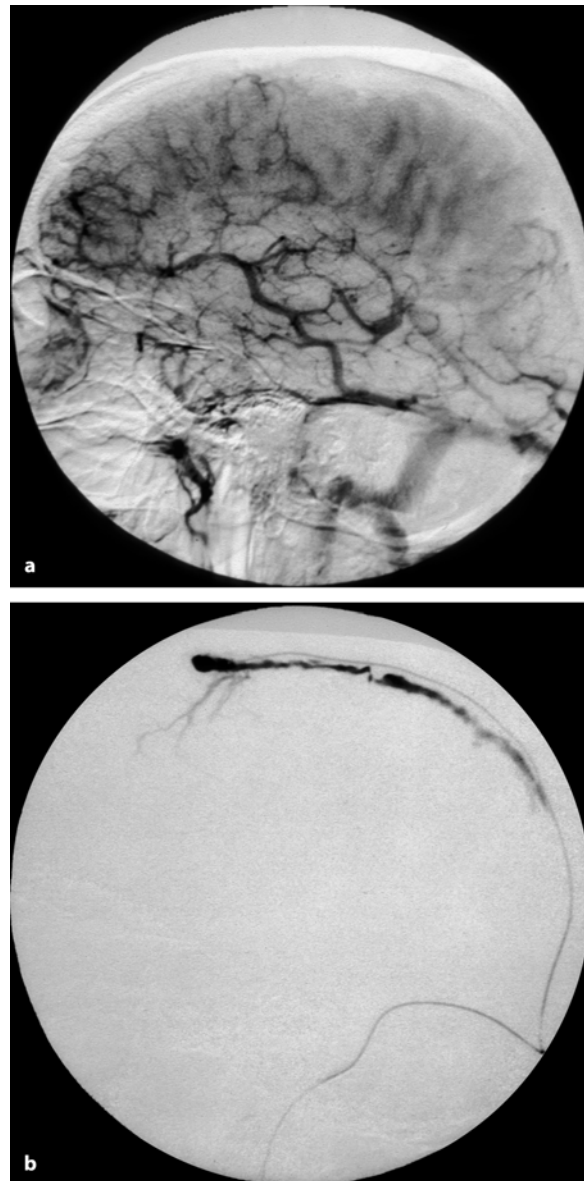


**Fig. 6.** A 26-year-old woman with rapidly progressive neurological deficits. **a** Lateral view of internal carotid DSA, late venous phase: occlusion of superior sagittal sinus. **b** Local application of urokinase while passing the thrombus with the microcatheter (lateral view of DSA)

### 3.2.2.4 Dural Arteriovenous Fistulas

Dural arteriovenous fistulas (DAVF) are foci of arteriovenous shunting that occur within the dura mater, most often in the wall of a dural sinus. As in dural sinus thrombosis, acute clinical symptoms can occur in DAVF with progressive narrowing and occlusion of the recipient dural sinus resulting in alteration of the drainage back into cortical veins (Fig. 7). Cortical venous drainage is associated with a



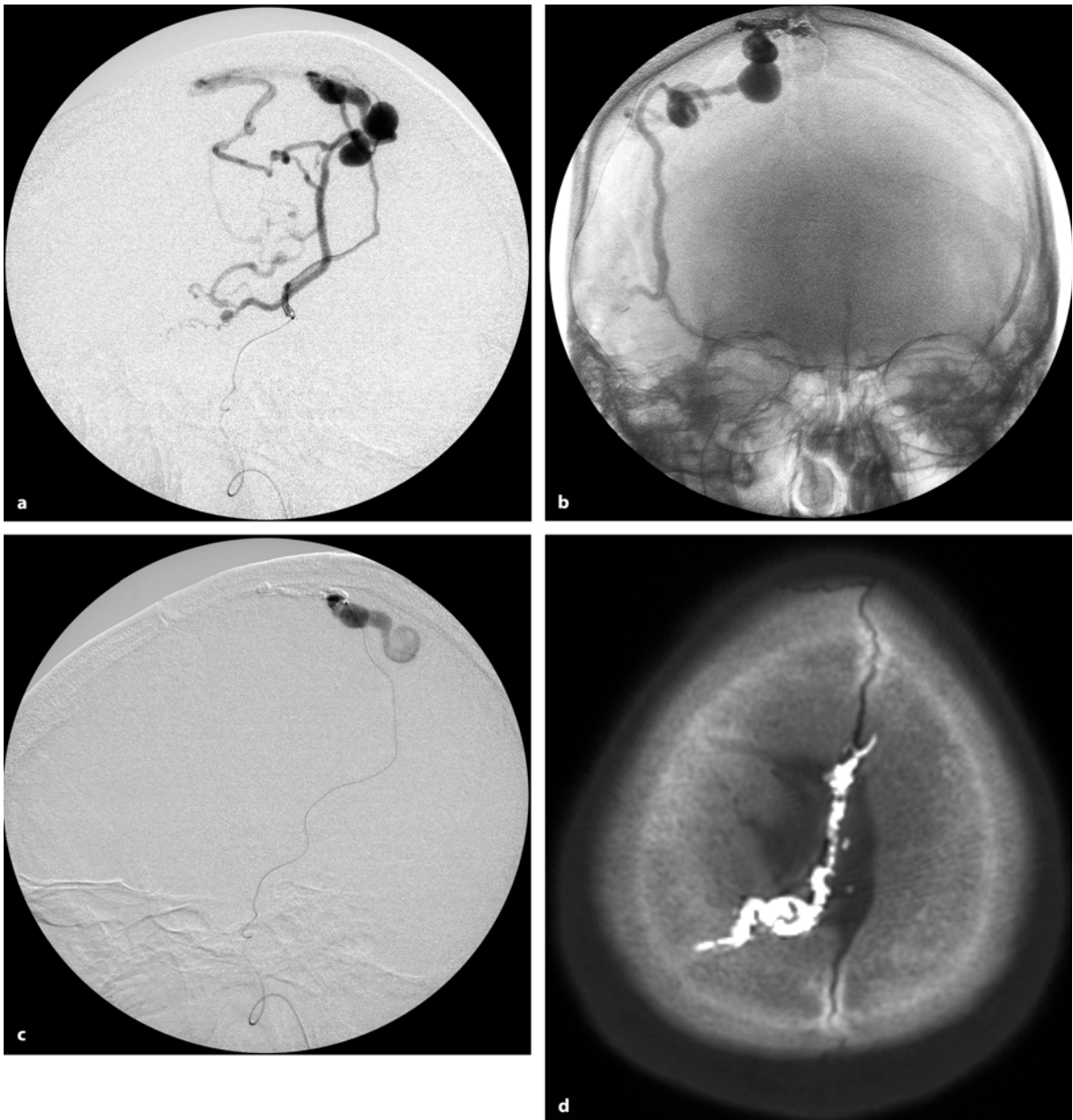


**Fig. 7.** Lateral DSA depicting dural arteriovenous fistulas at the superior sagittal sinus with retrograde filling of dilated cortical veins (a). b Anteroposterior view of unsubtracted angiogram, c lateral DSA after superselective catheterization of the middle meningeal

artery. The tip of the microcatheter is positioned directly in front of the fistula and glue embolization was subsequently performed. Follow-up CT depicts glue cast in the veins near to the sinus (d)

high incidence of acute haemorrhage, either subdural, subarachnoidal or intraparenchymal [17]. The frequent association of DAVF with dural sinus thrombosis can render treatment of DAVF even more difficult [46].

The DAVF can be treated by surgery, radiation or endovascular embolization alone or in combination. In the acute situation surgical access to the fistula can be difficult due to haemorrhage and multiple small feeding arteries. In these cases diagnostic angiography is combined with en-

dovascular embolization that best performed with glue to close the nidus of the fistula. The result of embolization with particles is often only transient and coiling occludes the feeding artery preventing further endovascular access. For glue embolization the microcatheter has to be placed in front of the nidus after introduction via the guiding catheter; the latter is used to stabilize the microcatheter as well as to perform road maps for navigation and follow-up angiograms.

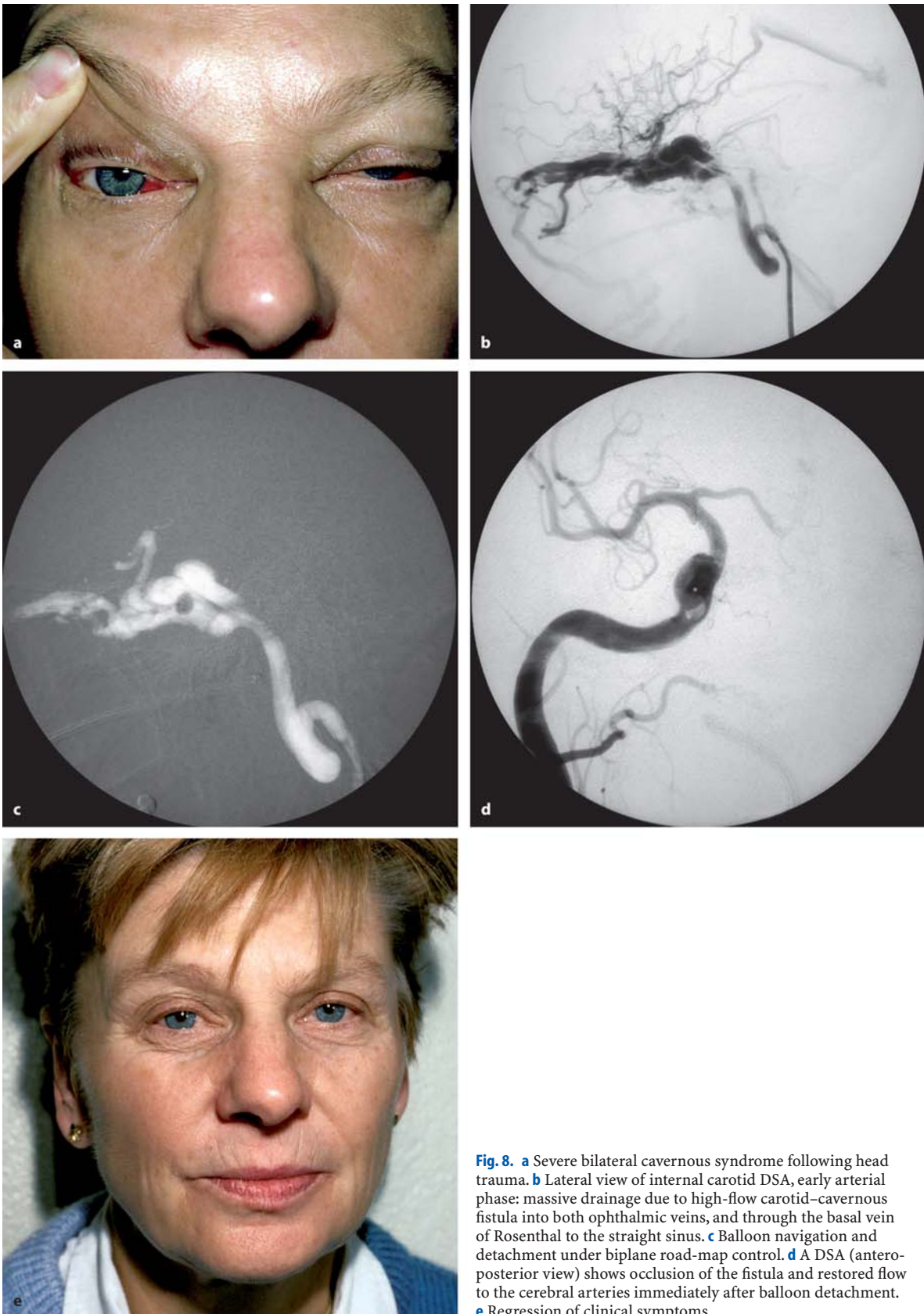


**Fig. 8.** **a** Severe bilateral cavernous syndrome following head trauma. **b** Lateral view of internal carotid DSA, early arterial phase: massive drainage due to high-flow carotid-cavernous fistula into both ophthalmic veins, and through the basal vein of Rosenthal to the straight sinus. **c** Balloon navigation and detachment under biplane road-map control. **d** A DSA (anteroposterior view) shows occlusion of the fistula and restored flow to the cerebral arteries immediately after balloon detachment. **e** Regression of clinical symptoms

Type-A carotid cavernous fistulas are usually traumatic and are typically caused by a large tear in the wall of the internal carotid artery. The high flow fistula results in engorgement and dilatation of the draining veins leading to elevated intracerebral and/or intraocular pressure, with possible cerebral ischaemia due to blood steal effects [18]. The treatment of choice for traumatic fistulas in this location consists of inflating one or more detachable balloons in the cavernous sinus in order to close the fistula and preserve the cerebral blood flow (Fig. 8). Alternatively, the cavernous sinus can be filled with coils. Additional use of a trispan catheter permits stable positioning of the balloon or coil [54]. The fistula can be obliterated by the intra-arterial or transvenous route via the inferior petrosal sinus or the superior ophthalmic vein.

### 3.2.2.5 Spinal Haemorrhage

Whereas haemorrhage is a frequent complication of cerebral AVM associated with aneurysms of feeding arteries, especially if located infratentorially [73], it is less frequent but often fatal if bleeding occurs from aneurysms associated with spinal, mostly intramedullary, AVMs [11]. Aneurysms are present in approximately 40% of cervical and 23% of thoracolumbar AVMs. The initial clinical symptoms of these vascular malformations are frequently caused by the bleeding aneurysm [55]. Early treatment with occlusion of the aneurysm is an important first step toward in improving the prognosis [40]. These aneurysms must therefore be identified by spinal angiography and treated by an endovascular approach (Fig. 9). Generally,

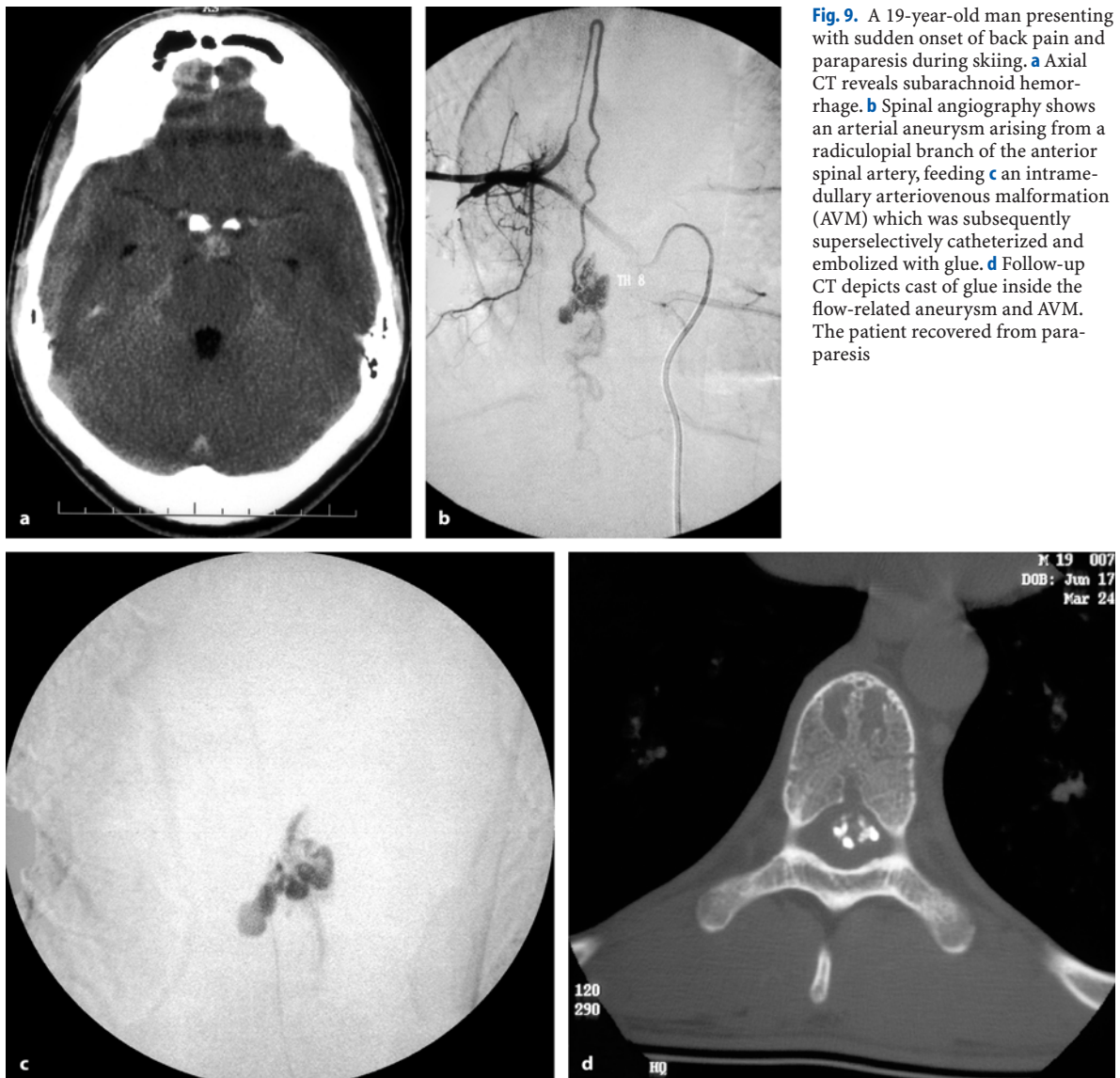


**Fig. 9.** A 19-year-old man presenting with sudden onset of back pain and paraparesis during skiing. **a** Axial CT reveals subarachnoid hemorrhage. **b** Spinal angiography shows an arterial aneurysm arising from a radiculopial branch of the anterior spinal artery, feeding **c** an intramedullary arteriovenous malformation (AVM) which was subsequently superselectively catheterized and embolized with glue. **d** Follow-up CT depicts cast of glue inside the flow-related aneurysm and AVM. The patient recovered from paraparesis



and especially so in emergency situations, global injection (aortography) is inappropriate as a primary modality of exploration. To detect a spinal source of bleeding, each intercostal and ilio-lumbar artery has to be catheterized selectively. In our institution this is done using a 5.2-F spinal catheter (Bernier spinal catheter, Cordis Corp., Miami Lakes, Fla.), which is available in three sizes to allow selective catheterization and stabilization [53]. In emergency cases, the lumen size and stability of this catheter are sufficient for it to be used subsequently as a guiding catheter for placement of the microcatheter into the spinal arterial axis.

### 3.2.3 Acute Ischaemic Stroke

Ischaemic stroke is an important cause of mortality and morbidity in industrialized countries. Until recently it was considered to be an untreatable condition. In situ thrombosis, often secondary to a local atherosclerotic stenosis or embolic occlusion of a cerebral artery, is by far the most common cause of ischaemic stroke. Both underlying mechanisms result in focal blockage of the cerebral circulation and initiate an ischaemic cascade that ultimately destroys the neurons. Early reopening of the blocked vessel can restore the oxygen supply and metabolism, thus preventing the death of the hypoperfused neurons [29] and potentially salvaging much of the hypoperfused cerebral tissue, especially in the ischaemic border zone, the so-called penumbra, and at best even at its core [30, 64]. In addition to chemical thrombolysis, which often takes more than 1 h to complete and carries a risk of haemorrhage, new mechanical approaches are under investigation and are discussed below.

#### 3.2.3.1 Thrombolysis of Cerebral Arteries

Several studies have shown that intravenous thrombolysis ((IVT) [58] and local intra-arterial thrombolysis (LIT) [24, 66] can be safely and efficaciously applied in everyday practice. IVT using rt-PA has been shown to be an effective treatment for ischaemic stroke within the first 3 h after onset of symptoms and was approved by the U.S. Food and Drug Administration [65]. LIT effectively recanalizes cerebral arteries and improves the neurological outcome [28]. In a prospective study pro-urokinase improved outcome of patients with acute M1 or M2 segment occlusions of the middle cerebral artery (MCA) when administered within 6 h of onset directly into the occluded vessel [23]. Because of the high mortality of acute vertebrobasilar occlusions LIT is performed in these patients even beyond the 6-h time window.

Until now application of LIT has been restricted to large medical centres where an interventional neuroradiologist

is part of the stroke team. Another drawback is the delay between diagnostic CT and/or MRI and LIT. This time delay can be minimized by interdisciplinary cooperation at the stroke center in the performance of the diagnostic work-up and LIT treatment [47].

In acute stroke diagnostic four-vessel angiography is performed, where the last vessel to be investigated is the clinically presumed occluded one. This diagnostic angiography is followed immediately by introduction of the microcatheter, the guiding catheter being already correctly placed. The initial three or four biplane series show the extent of direct or pial collateral flow to the hypoperfused brain region. After confirmation of cerebral vessel occlusion a microcatheter is navigated into this vessel using a biplane road map, and 200,000 to 1,000,000 IU urokinase (Urokinase HS, Medac, Wedel, Germany) is infused directly into or near the proximal end of the thrombus over a period of 60–90 min (Fig. 10). Application is stopped if recanalization occurs early and is confirmed by follow-up angiograms.

In addition to our analysis of the published results of 43 patients treated in Bern from 1992 to 1996 [24], we examined the clinical and radiological findings and functional outcome of 100 consecutive patients treated with LIT up to November 2000 for acute stroke due to MCA occlusion [2]. Our excellent or good outcomes (modified Rankin Scale <2) in 59% of patients with M1 or M2 occlusions and in 96% with M3 or M4 occlusions, as well as our recanalization rate of 76%, confirm the findings of other groups that LIT used within a time window of 6 h by an organized stroke team in a routine clinical setting can deliver safe and efficacious treatment of ischaemic stroke. Patients with occlusions of the carotid artery carry the worst prognosis [3]. In our series the rate of symptomatic intracerebral haemorrhage after LIT was 4.8%, in the PROACT II patients it was 10.2% and in the NINDS cohort 6.4%.

#### 3.2.3.2 Mechanical Revascularization of Cerebral Arteries

Even though thrombolysis is effective in the treatment of acute ischaemic stroke, its risk of haemorrhagic complication and the time needed to dissolve the thrombus have led to increasing interest in mechanical clot retrieval [13]. Several clot retrieval devices are now available, but no method has yet been established. The MERCI device is typical of distal devices: a microcatheter is inserted past the thrombus, where the device is deployed distal to the occlusion, catches the thrombus and pulls it back into the guiding catheter. To avoid thromboembolism, the procedure is done with proximal balloon protection to achieve flow arrest [61]. In addition to thromboembolism, methods employing distal devices also entail a risk of vessel dissection and perforation.



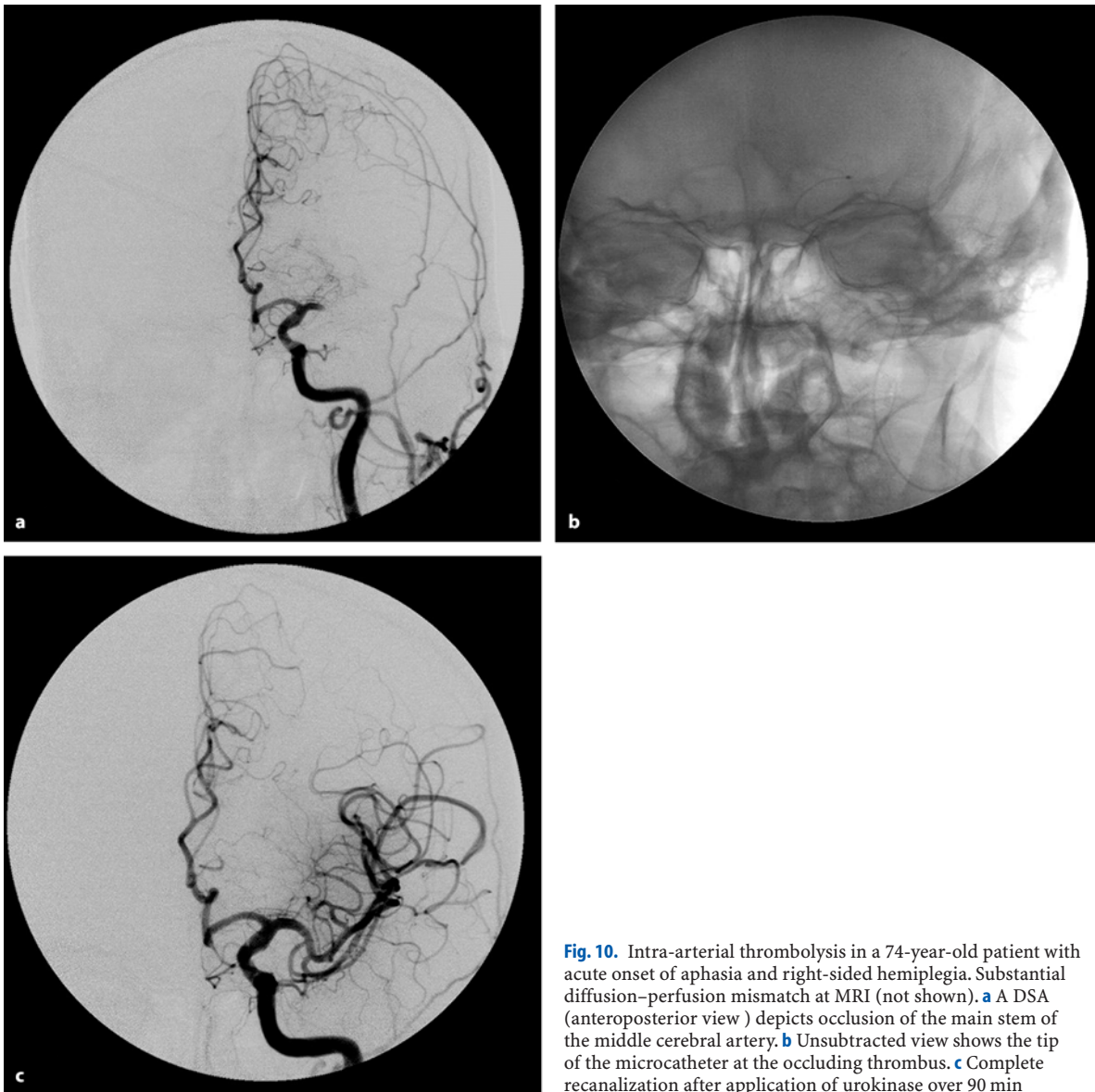


**Fig. 10.** Intra-arterial thrombolysis in a 74-year-old patient with acute onset of aphasia and right-sided hemiplegia. Substantial diffusion–perfusion mismatch at MRI (not shown). **a** A DSA (anteroposterior view) depicts occlusion of the main stem of the middle cerebral artery. **b** Unsubtracted view shows the tip of the microcatheter at the occluding thrombus. **c** Complete recanalization after application of urokinase over 90 min

### 3.2.3.3 Central Retinal Artery Occlusion

Because the retina is part of the brain, many principles of fibrinolysis in brain vessels can also be applied to central retinal artery occlusions. In acute central retinal artery occlusion conventional therapies, such as anterior chamber paracentesis, ocular massage or pentoxifylline or carboanhydrase inhibitors, hardly change the unfavourable course [5]. The first attempts to use selective thrombolysis to treat this disease were made in 1992 [57]. In a retrospective study comparing 37 patients treated with LIT to 19 control patients receiving conservative treatment only, LIT significantly enhanced the chances of visual improvement [4].

Urokinase served as the fibrinolytic agent and was applied at dosages from 100,000 to 1,000,000 IU via microcatheter in the proximal segment or at the origin of the ophthalmic artery. In two patients, a transient ischaemic attack was observed during the procedure and one patient suffered a minor stroke. No symptomatic haemorrhages occurred.

### 3.2.3.4 Stenting of Cervical Arteries in Acute Stroke

Often the acute ischaemic stroke is associated with high-grade stenosis or pseudoocclusion of the ipsilateral internal carotid artery that can encumber access to the cerebral arteries and might cause early reocclusion. Should this

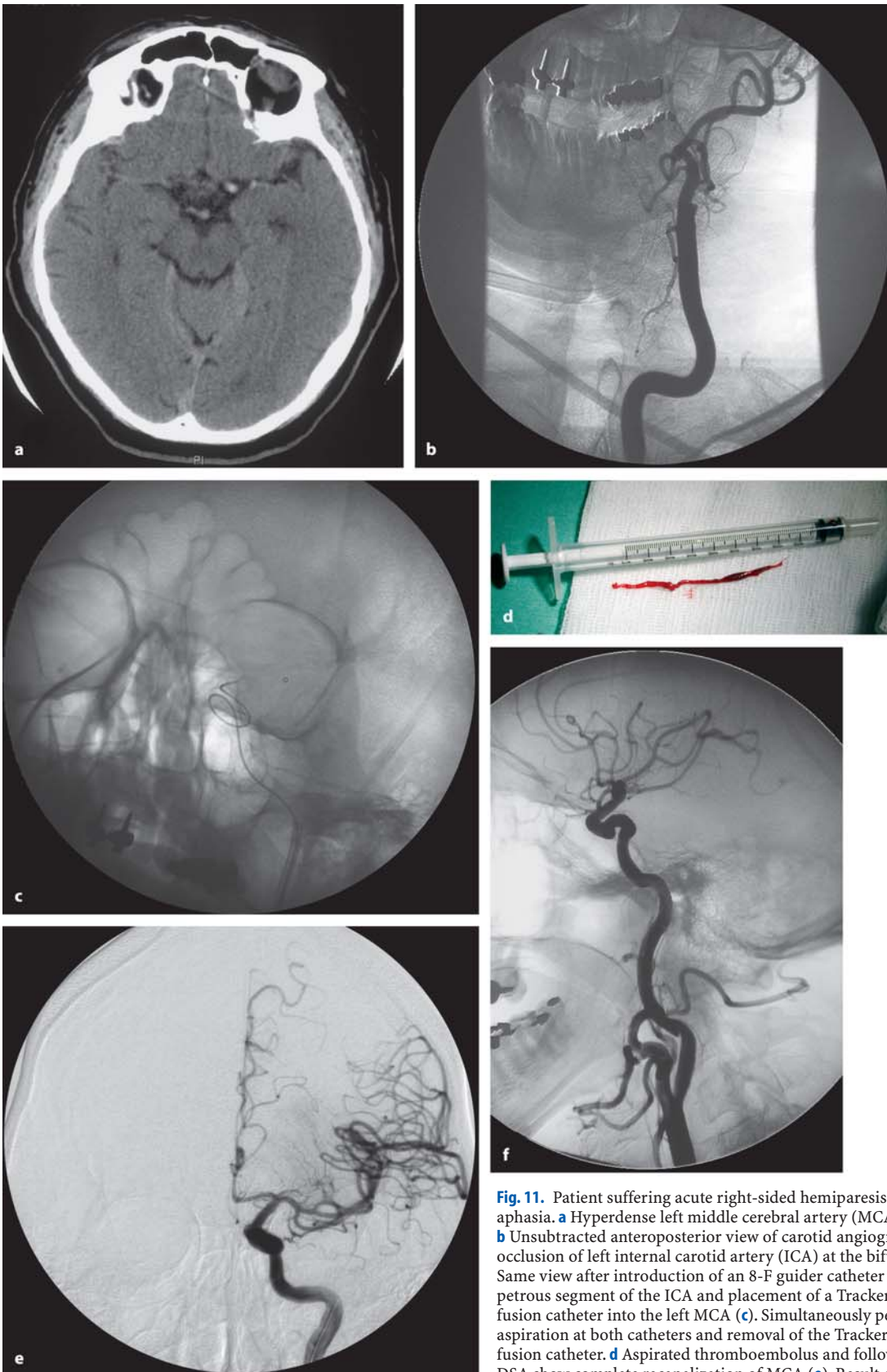


**Fig. 11.** Patient suffering acute right-sided hemiparesis and aphasia. **a** Hyperdense left middle cerebral artery (MCA) at CT. **b** Unsubtracted anteroposterior view of carotid angiogram shows occlusion of left internal carotid artery (ICA) at the bifurcation. Same view after introduction of an 8-F guider catheter into the petrous segment of the ICA and placement of a Tracker-38 infusion catheter into the left MCA (**c**). Simultaneously performed aspiration at both catheters and removal of the Tracker-38 infusion catheter. **d** Aspirated thromboembolus and follow-up DSA show complete recanalization of MCA (**e**). Result after finally performed stent placement for ICA-stenosis (**f**)

occur, the proximal stenosis or occlusion must first be treated by stent placement and/or angioplasty. For this purpose the tip of a 7- or 8-F guiding catheter is placed into or beyond the stenosis. Often it is possible to aspirate large amounts of thrombotic material through a catheter with such a large lumen. Subsequently a stent is deployed and the stenosis dilated (Fig. 11). This technique was performed in 25 of our 312 patients and can be followed by intracranial thrombolysis as described above [49].

Thrombolysis is feasible in cervical artery dissection, with or without stent placement, if stroke symptoms are progressive [1]. Stenting is also feasible in vertebral artery stenosis or occlusion combined with basilar thrombosis [48].

### 3.2.4 Discussion

With recent advances in devices and techniques for interventional neuroradiology, such as microcatheters and 3D DSA, neuroendovascular surgery is playing an ever increasing role in both the diagnosis and treatment of acute head and neck lesions and cerebrovascular disease. This chapter is intended to provide information regarding the current state of the art of this field. This, however, cannot replace proper training, which has been established for diagnostic as well as for interventional neuroradiology/neuroendovascular surgery [31, 32].

Diagnostic and interventional angiography are usually performed in neuroangiography suites which should be equipped with a high-resolution biplane angiography system and the capacity to perform biplane road map and/or 3D reconstruction by rotational subtraction angiography. Some neurocentres offer the additional possibility of performing combined endovascular and surgical procedures in the neuroangiography suite. In our department, the angiography suite is used for the interdisciplinary treatment of bleeding vascular malformations of the face, of giant aneurysms, and for retrograde catheterization of supra-aortic vessels.

We routinely use femoral puncture involving the insertion of a 6- to 9-F catheter sheath depending on the procedure, therapeutic goals and embolic material to be used. In emergency cases, both the angiographic work-up and subsequent intervention are performed in a single session. Even in this situation, however, the angiographic work-up follows a specific protocol that encompasses all functional aspects of the affected vascular territory relevant to the planned therapeutic procedure. Selective and superselective neuroangiography should provide specific information relevant to the endovascular treatment, e.g. flow characteristics, dangerous arterio-arterial anastomoses, collateral circulation, the type and geometry of feeding arteries, and the quality of venous drainage. During the procedure, it is essential that rapid and effective communication is maintained between the neuro-

radiologist and the neurologist/neurosurgeon/ENT surgeon, as well as the neuroanaesthesiologist. While providing endovascular treatment of acute ischaemic stroke, e.g. at least one neurologist from our institution's stroke unit follows the patient through all diagnostic procedures and is present, together with one technician, one nurse the anaesthesia personnel and at least one neuroradiologist, in the neuroangiography suite during intervention, even at night and on weekends. His or her functions also include keeping the patient's relatives well informed during the procedure and/or obtaining informed consent if special techniques must be performed or if the patient is part of an ongoing scientific study. The neurologist also measures the neurological severity of the disease using international scores, e.g. the National Institutes of Health Stroke scale (NIHSS), Glasgow Coma scale, or the Hunt and Hess scale in acute subarachnoid bleeding.

The introduction of electrolytically detachable platinum coils and of neck-bridging trispan coils and stents has prompted many centres to adopt the endovascular approach as the treatment of choice for acute aneurysms; however, even in patients undergoing endovascular treatment, interdisciplinary management of the ruptured aneurysm and complications following subarachnoid hemorrhage is mandatory to improve the outcome of these critically ill patients.

In acute life-threatening bleeding of head and neck lesions, endovascular embolization is a complementary alternative to surgical therapy; each can be performed as part of a combined approach if angiography and/or another imaging modality are available in the operation room, or if the angiography suite is designed to serve an operation room as well. In our experience, it can be dangerous for the radiologist to make compromises in this situation: the result can be disastrous, e.g. if a complication occurs and only poor fluoroscopy without DSA and/or road-map options is available in the operation room.

In acute ischaemic stroke, the endovascular approach has several advantages over IVT. In the endovascular approach the thrombolytic agent can be applied directly to the thrombus itself, thus delivering treatment directly to the occluded vessel while causing less disturbance of systemic coagulation parameters than intravenous thrombolysis. In addition, endovascular therapy can be applied any time within an protracted time frame ("therapeutic window"), it visualizes individual vessel pathology and provides information on collateral circulation. The endovascular approach permits documentation of recanalization, thus facilitating timely adjustment of the thrombolytic agent dosage. If occlusion persists, other techniques for revascularization of the occluded vessel might be tried, such as aspiration of the thrombus or mechanical clot disruption. In cases of high-grade stenosis or pseudo-occlusion of the supra-aortic vessels, PTA and stent implantation can be performed to restore the cerebral blood flow through the same endovascular approach.

## References

- Arnold M, Nedeltchev K, Sturzenegger M et al (2002) Thrombolysis in patients with acute stroke caused by cervical artery dissection: analysis of 9 patients and review of the literature. *Arch Neurol* 59:549–553
- Arnold M, Schroth G, Nedeltchev K et al (2002) Intra-arterial thrombolysis in 100 patients with acute stroke due to middle cerebral artery occlusion. *Stroke* 33:1828–1833
- Arnold M, Nedeltchev K, Mattle HP et al (2003) Intra-arterial thrombolysis in 24 consecutive patients with internal carotid artery T occlusions. *J Neurol Neurosurg Psychiatry* 74:739–742
- Arnold M, Koerner U, Remonda L et al (2005) Comparison of intra-arterial thrombolysis with conventional treatment in patients with acute central retinal artery occlusion. *J Neurol Neurosurg Psychiatry* 76:196–199
- Augsburger JJ, Magargal LE (1980) Visual prognosis following treatment of acute central retinal artery obstruction. *Br J Ophthalmol* 64:913–917
- Aviv RI, O'Neill R, Patel MC et al (2005) Abciximab in patients with ruptured intracranial aneurysms. *Am J Neuroradiol* 26:1744–1750
- Bannerman RM, Ingall GB, Graf CJ (1970) The familial occurrence of intracranial aneurysms. *Neurology* 20:283–292
- Barnwell SL, Higashida RT, Halbach VV et al (1991) Direct endovascular thrombolytic therapy for dural sinus thrombosis. *Neurosurgery* 28:135–142
- Benitez RP, Silva MT, Klem J et al (2004) Endovascular occlusion of wide-necked aneurysms with a new intracranial microstent (Neuroform) and detachable coils. *Neurosurgery* 54:1359–1367
- Benndorf G, Campi A, Schneider GH et al (2001) Overlapping stents for treatment of a dissecting carotid artery aneurysm. *J Endovasc Ther* 8:566–570
- Biondi A, Merland JJ, Hodes JE et al (1992) Aneurysms of spinal arteries associated with intramedullary arteriovenous malformations. II. Results of AVM endovascular treatment and hemodynamic considerations. *Am J Neuroradiol* 13:923–931
- Boussier MG, Chiras J, Bories J et al (1985) Cerebral venous thrombosis: a review of 38 cases. *Stroke* 16:199–213
- Breckenfeld C, Remonda L, Nedeltchev K et al (2005) Endovascular neuroradiological treatment of acute ischemic stroke: techniques and results in 350 patients. *Neur Res* 27 (Suppl 1):29–35
- Caversaccio M, Bachler R, Ladrach K et al (1999) The “Bernese” frameless optical computer aided surgery system. *Comput Aided Surg* 4:328–334
- Chaloupka JC, Mangla S, Huddle DC (1999) Use of mechanical thrombolysis via microballoon percutaneous transluminal angioplasty for the treatment of acute dural sinus thrombosis: case presentation and technical report. *Neurosurgery* 45:650–656
- Chow K, Gobin YP, Saver J et al (2000) Endovascular treatment of dural sinus thrombosis with rheolytic thrombectomy and intra-arterial thrombolysis. *Stroke* 31:1420–1425
- Cognard C, Gobin YP, Pierot L et al (1995) Cerebral dural arteriovenous fistulas: clinical and angiographic correlation with a revised classification of venous drainage. *Radiology* 194:671–680
- Debrun GM (1993) Endovascular management of carotid cavernous fistulas. In: Valavanis A (ed) *Interventional neuroradiology*. Springer, Berlin Heidelberg New York
- Doerfler A, Wanke I, Egelhof T et al (2001) Aneurysmal rupture during embolization with Guglielmi detachable coils: causes, management, and outcome. *Am J Neuroradiol* 22:1825–1832
- dos Santos Souza MP, Agid R, Willinsky RA et al (2005) Microstent-assisted coiling for wide-necked intracranial aneurysms. *Can J Neurol Sci* 32:71–81
- Eskridge JM, Newell DW, Pendleton GA (1990) Transluminal angioplasty for treatment of vasospasm. *Neurosurg Clin N Am* 1:387–399
- Fiorella D, Albuquerque FC, Han P et al (2004) Preliminary experience using the Neuroform stent for the treatment of cerebral aneurysms. *Neurosurgery* 54:6–16
- Furlan A, Higashida R, Wechsler L et al (1999) Intra-arterial proUK for acute ischemic stroke. The PROACT II study: a randomized controlled trial. *Polype in Acute Cerebral Thromboembolism*. *J Am Med Assoc* 282:2003–2011
- Gonner F, Remonda L, Mattle H et al (1998) Local intra-arterial thrombolysis in acute ischemic stroke. *Stroke* 29:1894–1900
- Gralla J, Brekenfeld C, Schmidli J et al (2004) Internal carotid artery aneurysm with life-threatening hemorrhages in a pediatric patient: endovascular treatment options. *J Endovasc Ther* 11:734–738
- Guglielmi G, Vinuela F, Sepetka I et al (1991) Electrothrombolysis of saccular aneurysms via endovascular approach. Part 1: Electrochemical basis, technique, and experimental results. *J Neurosurg* 75:1–7
- Guglielmi G, Vinuela F, Dion J et al (1991) Electrothrombolysis of saccular aneurysms via endovascular approach. Part 2: Preliminary clinical experience. *J Neurosurg* 75:8–14
- Hacke W, Zeumer H, Ferbert A et al (1988) Intra-arterial thrombolytic therapy improves outcome in patients with acute vertebralbasilar occlusive disease. *Stroke* 19:1216–1222
- Heiss WD (1992) Experimental evidence of ischemic thresholds and functional recovery. *Stroke* 23:1668–1672
- Heiss WD, Grond M, Thiel A et al (1997) Ischemic brain tissue salvaged from infarction with alteplase. *Lancet* 349:1599–1600
- Higashida RT (2000) Evolution of a new multidisciplinary subspecialty: interventional neuroradiology/neuroendovascular surgery. *Am J Neuroradiol* 21:1151–1152
- Higashida RT, Hopkins LN, Berenstein A et al (2000) Program requirements for residency/fellowship education in neuroendovascular surgery/interventional neuroradiology: a special report on graduate medical education. *Am J Neuroradiol* 21:1153–1159
- Kothbauer K, Schroth G, Seiler RW et al (1995) Severe symptomatic vasospasm after rupture of an arteriovenous malformation. *Am J Neuroradiol* 16:1073–1075
- Lausjaunias P, Berenstein A (1987) *Surgical neuro-angiography*, vols 1–4. Springer, Berlin Heidelberg New York
- Lovblad KO, Bassetti C, Schneider J et al (2001) Diffusion-weighted MR in cerebral venous thrombosis. *Cerebrovasc Dis* 11:169–176
- Lovblad KO, el-Koussy M, Guzman R et al (2001) Diffusion-weighted and perfusion-weighted MR of cerebral vasospasm. *Acta Neurochir (Suppl)* 77:121–126
- Luginbuehl M, Schroth G, Dick T (1997) Interventional neuro-radiology and minimally invasive neurosurgery. *Curr Opin Anaesthesiol* 10:287–296
- Luginbuehl M, Remonda L (1999) Interventional neuroradiology. Recent developments and anaesthesiologic aspects. *Minerva Anesthesiol* 65:445–454
- Malek AM, Halbach VV, Phatouros CC et al (2000) Balloon-assist technique for endovascular coil embolization of geometrically difficult intracranial aneurysms. *Neurosurgery* 46:1397–1406
- Mattle HP, Schroth G, Seiler RW (2000) Dilemmas in the management of patients with arteriovenous malformations. *J Neurol* 247:917–928
- Molyneux A, Kerr R, Stratton I et al (2002) International Subarachnoid Aneurysm Trial (ISAT) of neurosurgical clipping versus endovascular coiling in 2143 patients with ruptured intracranial aneurysms: a randomised trial. *Lancet* 360:1267–1274



42. Molyneux AJ, Kerr RS, Yu LM et al (2005) International subarachnoid aneurysm trial (ISAT) of neurosurgical clipping versus endovascular coiling in 2143 patients with ruptured intracranial aneurysms: a randomised comparison of effects on survival, dependency, seizures, rebleeding, subgroups, and aneurysm occlusion. *Lancet* 366:809–817
43. Mordasini P, Schroth G, Guzman R et al (2005) Endovascular treatment of posterior circulation cerebral aneurysms by using Guglielmi detachable coils: a 10-year single-center experience with special regard to technical development. *Am J Neuroradiol* 26:1732–1738
44. Moret J, Cognard C, Weill A et al (1997) Reconstruction technique in the treatment of wide-neck intracranial aneurysms. Long-term angiographic and clinical results. Apropos of 56 cases. *J Neuroradiol* 24:30–44
45. Murayama Y, Song JK, Uda K et al (2003) Combined endovascular treatment for both intracranial aneurysm and symptomatic vasospasm. *Am J Neuroradiol* 24:133–139
46. Murphy KJ, Gailloud P, Venbrux A et al (2000) Endovascular treatment of a grade-IV transverse sinus dural arteriovenous fistula by sinus recanalization, angioplasty, and stent placement: technical case report. *Neurosurgery* 46:497–500
47. Nedeltchev K, Arnold M, Brekenfeld C et al (2003) Pre- and in-hospital delays from stroke onset to intra-arterial thrombolysis. *Stroke* 34:1230–1234
48. Nedeltchev K, Remonda L, Do DD et al (2004) Acute stenting and thromboaspiration in basilar artery occlusions due to embolism from the dominating vertebral artery. *Neuroradiology* 46:686–691
49. Nedeltchev K, Brekenfeld C, Remonda L et al (2005) Internal carotid artery stent implantation in 25 patients with acute stroke: preliminary results. *Radiology Epub ahead of print.*
50. Pakarinen S (1967) Incidence, aetiology, and prognosis of primary subarachnoid hemorrhage. A study based on 589 cases diagnosed in a defined urban population during a defined period. *Acta Neurol Scand* 43 (Suppl 29):1–28
51. Remonda L, Schroth G, Ozdoba C et al (1995) Facial intracranial arteriovenous malformations: CT and MR features. *J Comput Assist Tomogr* 19:277–281
52. Remonda L, Schroth G, Caversaccio M et al (2000) Endovascular treatment of acute and subacute hemorrhage in the head and neck. *Arch Otolaryngol Head Neck Surg* 126:1255–1262
53. Remonda L, Heini P, Schroth G (2002) Acute tumor hemorrhage during spinal angiography. *Rofo* 174:114–116
54. Remonda L, Frigerio SB, Buhler R et al (2004) Transvenous coil treatment of a type a carotid cavernous fistula in association with transarterial trispan coil protection. *Am J Neuroradiol* 25:611–613
55. Rodesch G, Lasjaunias P, Berenstein A (1993) Embolisation of arteriovenous malformations of the spinal canal. In: Valavanis A (ed) *Interventional neuroradiology*. Springer, Berlin Heidelberg New York
56. Ross IB, Dhillon GS (2005) Complications of endovascular treatment of cerebral aneurysms. *Surg Neurol* 64:12–18
57. Schmidt D, Schumacher M, Wakhloo AK (1992) Microcatheter urokinase infusion in central retinal artery occlusion. *Am J Ophthalmol* 113:429–434
58. Schmulling S, Grond M, Rudolf J et al (2000) One-year follow-up in acute stroke patients treated with rtPA in clinical routine. *Stroke* 31:1552–1554
59. Schroth G, Wichmann W, Valavanis A (1991) Aneurysm of the lingual artery. Endovascular treatment. *Neuroradiology* 33:451–452
60. Schroth G, Do DD, Remonda L et al (1997) Special technics for angioplasty of the brachiocephalic vessels. *Rofo* 167:165–173 [in German]
61. Smith WS, Sung G, Starkman S et al (2005) Safety and efficacy of mechanical embolectomy in acute ischemic stroke: results of the MERCI trial. *Stroke* 36:1432–1438
62. Song JK, Niimi Y, Fernandez PM et al (2004) Thrombus formation during intracranial aneurysm coil placement: treatment with intra-arterial abciximab. *Am J Neuroradiol* 25:1147–1153
63. Steiger HJ, Medele R, Bruckmann H et al (1999) Interdisciplinary management results in 100 patients with ruptured and unruptured posterior circulation aneurysms. *Acta Neurochir* 141:359–366
64. Taleb M, Lovblad KO, El-Koussy M et al (2001) Reperfusion demonstrated by apparent diffusion coefficient mapping after local intra-arterial thrombolysis for ischemic stroke. *Neuroradiology* 43:591–594
65. The National Institute of Neurological Disorders and Stroke rt-PA Stroke Study Group (1995) Tissue plasminogen activator for acute ischemic stroke. *N Engl J Med* 333:1581–1587
66. Theron JG, Coskun O, Huet HF et al (1996) Local intra-arterial thrombolysis in the carotid territory. *Interv Neuroradiol* 1:111–126
67. Toennies KD, Oishi S, Koster D et al (1997) The accuracy of distance measurements in bi-plane angiography. *Proc SPIE Med Imaging* 3031:19–30
68. Tummala RP, Chu RM, Madison MT et al (2001) Outcomes after aneurysm rupture during endovascular coil embolization. *Neurosurgery* 49:1059–1066
69. Valavanis A (ed) (1993) *Interventional neuroradiology*. Springer, Berlin Heidelberg New York
70. Villringer A, Einhaupl KM (1997) Dural sinus and cerebral venous thrombosis. *New Horiz* 5:332–341
71. Vinuela F, van Halbach V, Dion JE (eds) (1992) *Interventional neuroradiology. Endovascular therapy of the central nervous system*. Raven Press, New York
72. Wanke I, Doerfler A, Schoch B et al (2003) Treatment of wide-necked intracranial aneurysms with a self-expanding stent system: initial clinical experience. *Am J Neuroradiol* 24:1192–1199
73. Westphal M, Grzyska U (2000) Clinical significance of pedicle aneurysms on feeding vessels, especially those located in infratentorial arteriovenous malformations. *J Neurosurg* 92:995–1001
74. Wielepp JP, Schroth G, Häusler R et al (1998) Preoperative determination of stroke risk with EDC SPECT before therapeutic carotid artery occlusion. In: Bergmann H, Köhn H, Sinzinger H (eds) *Radioactive isotopes in clinical medicine and research XXIII*. Birkhäuser, Basel, pp 353–356



## **Section Four**

# **Non-Traumatic Thoracic Emergencies: Imaging and Intervention**

# Acute Chest Pain: Diagnostic Strategies

L. Bonomo, M.L. Storto, A.R. Larici, R. Marano

## 4.1

### Contents

4.1.1 Introduction . . . . .	331
4.1.2 Diagnostic Imaging in Non-cardiac Acute Chest Pain . . . . .	331
4.1.3 Aortic Diseases . . . . .	333
4.1.3.1 Aortic Dissection . . . . .	333
4.1.3.2 Aortic Intramural Hematoma . . . . .	338
4.1.3.3 Penetrating Atherosclerotic Ulcer . . . . .	341
4.1.4 Multidetector-Row CT and Acute Chest Pain . . . . .	342
References . . . . .	344

### 4.1.1 Introduction

Acute chest pain may arise from any structure in the thoracic cavity so that a wide spectrum of disorders may manifest with this symptom, including both cardiac and non-cardiac diseases. From 10 to 31 % of patients presenting to the emergency department with chest pain have acute coronary ischemia (i.e., acute myocardial infarction or unstable angina) [48]. In a study of 660 consecutive referrals to a “one-stop” clinic, only 27% of patients had a cardiac cause for their symptoms [4].

In most cases, patients with acute coronary ischemia show the classical anginal symptoms of chest tightness and left arm pain. If these symptoms are present and if an electrocardiogram shows evidence of ischemia, a cardiac etiology for pain is favored [44]. On the other hand, non-cardiac chest pain may demonstrate a variety of characteristics with radiation and migration. Causes of non-cardiac chest pain include aortic diseases, pulmonary embolism, pulmonary hypertension, pericarditis, pneumothorax, pneumomediastinum, esophageal diseases, and chest wall disorders. In a series of 70 patients with non-cardiac chest pain undergoing spiral CT scan of the chest, Oliver et al. [36] found aortic diseases as the origin of pain in 25 cases, pulmonary embolism in 4 patients, pericarditis in 4, and perforated duodenal ulcer in 1 patient; other causes of thoracic pain were present in 8 patients. Chest pain has also

been described in patients with sickle cell disease and acute chest syndrome [8]. This syndrome, which is responsible for 25% of all deaths in sickle cell disease, is characterized by fever, pleuritic pain, dyspnea, leukocytosis, and new lung opacities on chest radiographs. Possible causes are fat embolism from bone infarcts or “in situ” thrombosis secondary to increased blood viscosity. Recently, a transient thrombus in the descending aorta has been reported in a young patient with sickle cell disease and severe chest pain [9].

The evaluation of patients presenting with chest pain is challenging for the clinicians. Although clinical history, physical examination, and the presence of risk factors are important in establishing the etiology of symptoms, imaging modalities are frequently utilized to confirm or to refute a provisional diagnosis. In fact, radiologists are commonly involved in the diagnostic work-up of patients with chest pain, particularly when a cardiac disease has been ruled out.

Non-cardiac causes of acute chest pain are reviewed in this chapter with special reference to the most recent published literature and emphasis on acute aortic diseases. The emerging role of multidetector-row CT (MDCT) in patients with acute chest pain is also discussed. Pulmonary embolism is discussed in Chap. 4.2.

### 4.1.2 Diagnostic Imaging in Non-cardiac Acute Chest Pain

Chest radiography usually represents the first imaging modality performed in patients presenting with acute chest pain. It may be diagnostic in patients with pneumothorax, pneumomediastinum, rib fractures, and acute infections. Other conditions producing acute chest pain of non-cardiogenic etiology, such as aortic aneurysms or dissections, and pulmonary embolism, may be suspected from the chest film, but the overall sensitivity is much lower. Widening of the superior mediastinum and displacement of aortic wall calcifications, in the appropriate clinical setting, may suggest the diagnosis of aortic dissection; however, these findings may be difficult to evaluate since most patients with suspected dissection are examined with



portable radiography. Comparison with previous films, if available, may be extremely helpful and reveal changes in the aortic contour that are nearly pathognomonic for aortic dissection. The presence of a Hampton hump, Westermark sign, or pulmonary artery enlargement may indicate pulmonary embolism, although the sensitivity of these findings is quite low.

Computed tomography (CT) using helical technology is fast and easy to perform and, most importantly, can be obtained at any time of day or night. Newer CT scanners, especially those using multidetector arrays, can cover large anatomic areas with good spatial resolution and short scan duration [15]. The CT can help validating the diagnosis of pulmonary embolism, aortic aneurysms and dissection, pericardial effusions and thickening, and mediastinal hematomas. In patients with pneumothorax or pneumomediastinum, high-resolution CT scans can be useful in defining the cause of disease.

Appropriate technique is important to maximize the sensitivity and specificity of CT. Non-contrast CT scans are mandatory in patients with clinical suspect of aortic disease in order to better visualize calcifications, which may be seen in association with atheromas, within longstanding luminal thrombi, or along the intimal flap of a dissection (Fig. 1) [20, 36]. Moreover, acute hematomas, either in the aortic wall or leaking into the mediastinum, are best seen before contrast due to their high density as compared with flowing blood or mural thrombus (Fig. 2). Thin collimations in the order of 3–5 mm are recommended in CT scanning of thoracic aorta in order to improve spatial resolution and visualization of subtle abnormalities and small vascular branches [20, 43]. Use of contrast material should also be optimized in vascular studies with accurate selection of scan delay. Multiplanar and 3D reformatted images can be useful for better evaluation of the anatomic relationships and extent of vascular diseases.

Magnetic resonance imaging (MRI) allows noninvasive assessment of the mediastinum and thoracic aorta in multiple projections. Although the relatively long scan duration and the limited access to the patient may represent a drawback of MRI, this imaging modality can be useful in the assessment of patients presenting with acute chest pain and suspected aortic dissection by either showing the intimal flap or demonstrating associated findings of aortic regurgitation and branch vessel involvement. The MRI also has some utility in showing spinal abnormalities and nerve root compression as a source of chest pain [44].

A variety of sequences are available. The ECG-gated spin-echo studies provide excellent anatomic detail of the heart and thoracic aorta and remain the basis for many MRI algorithms [15]. Cine MRI and other gradient-echo techniques allow visualization of flowing blood and may help differentiate slow flowing blood from clot [13]. Gadolinium-enhanced 3D MR angiography techniques now permit rapid acquisition of MR angiograms of both aorta and branch vessels [22].



**Fig. 1.** Aortic dissection in a 72-year-old patient. Non-contrast CT scan (a) shows displacement of some calcifications toward the aortic lumen. The contrast-enhanced CT scan at the same level (b) clearly demonstrates an intimal flap in the aortic arch with calcifications along it

Echocardiography is also frequently performed in patients with acute chest pain. When compared with other imaging modalities, transthoracic echocardiography (TTE) and transesophageal echocardiography (TEE) have the unique advantage of portability and can be readily available in the emergency department or easily performed at the bedside. Echocardiography can help define the cardiac origin of chest pain in patients with elusive clinical findings and non-diagnostic electrocardiogram by demonstrating ventricular wall motion abnormalities [44]. More importantly, the absence of regional wall motion abnormalities makes the diagnosis of myocardial infarction unlikely with a negative predictive value of about 95% [2]. Echocardiography may additionally be helpful in diagnosing other causes of chest pain such as pericarditis, pericardial effusion, pulmonary embolism, and aortic dissection.

Films of the cervical and thoracic spine may be indicated to establish vertebral abnormalities, whereas barium

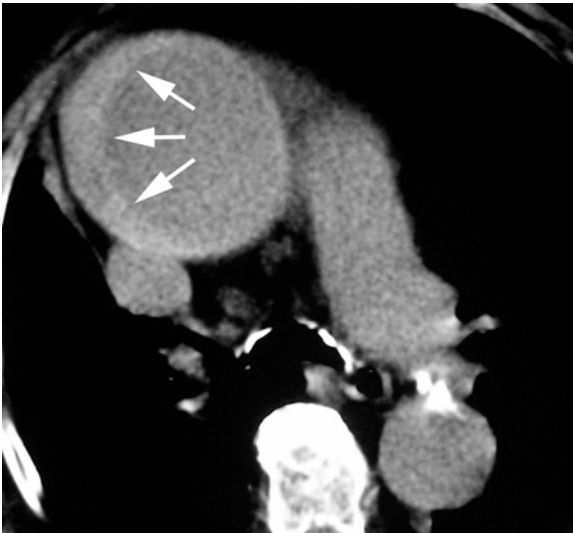


**Fig. 2.** Intramural hematoma. Non-contrast CT scan demonstrates a crescent-shaped high-attenuating rim along the anterior, right lateral, and posterior wall of the ascending aorta (arrows). Also note a dilatation of the ascending aorta

swallow or endoscopy may be of help in diagnosing esophageal spasm or reflux as possible etiology of the chest pain [44].

In 1995 an ACR (American College of Radiology) Task Force on Appropriateness Criteria and its expert panels have developed criteria for determining appropriate imaging examinations for diagnosis and treatment of specific medical conditions. Most of these criteria were subsequently reviewed in 1999. Although the availability of equipment or personnel may influence the selection of appropriate imaging procedures in an individual situation, ACR criteria represent a useful guide for both radiologists and referring physicians. According to these criteria, in patients with acute chest pain and suspected aortic dissection chest radiography, CT angiography, MRI or MR angiography, and TEE are the most appropriate procedures [13]. A chest radiograph should always be obtained in order to rule out other diseases, whereas the selection of a subsequent imaging modality will depend on clinical circumstances and availability. In centers where an experienced operator is available, TEE may be the preferred first-line imaging that can provide sufficient information to determine whether emergency surgery is necessary; however, CT angiography is likely to be more readily available on a 24-h basis and can provide information on branch vessel involvement.

Although faster sequences may lead to extent its use, at present MRI is more useful in stable patients, and those with chronic dissection. Aortography is less appropriate and should be limited to those situations in which information about branch vessel involvement is required by the surgeon and not provided by CT.

### 4.1.3 Aortic Diseases

After the introduction and diffusion of modern diagnostic techniques that provide high-resolution images of the thoracic aorta, intramural hematoma and penetrating ulcer have been increasingly recognized as causes of acute aortic disease in addition to classic aortic dissection. Although the pathogenesis of these three entities differ, they have been collectively called “acute aortic syndrome” because of common clinical manifestations and considerable overlap in natural history [46, 49].

#### 4.1.3.1 Aortic Dissection

Aortic dissection can be defined as a collection of blood within the media which communicates with the true lumen through one or more intimal tears. In most cases, the triggering event is a tear in the intima through which blood surges into the middle to outer third of the media and dissects longitudinally the vessel layers with formation of a double channel aorta [8, 34, 46]. The dissecting column of blood propagates most often in an anterograde direction, under the influence of systolic forces, although retrograde extension can occur. Degenerative changes in the media, cystic medial necrosis, and hypertension are important predisposing factors of aortic dissection.

Intimal tears are most commonly located a few centimeters above the aortic valve, along the right antero-lateral wall of the ascending aorta, where hydrodynamic forces are greatest, or in the proximal segment of the descending aorta just beyond the insertion of the ligamentum arteriosum [34, 36, 46]. Many patients with classic aortic dissection also have a re-entry tear somewhere along the aorta or several communications between the true and false lumen. Alternatively, the dissecting hematoma can rupture through the adventitia with consequent hemopericardium and cardiac tamponade or hemothorax. Distortion or disruption of the aortic valve may lead to aortic regurgitation.

Various systems based on anatomic characteristics have been proposed to classify aortic dissection. In the widely used Stanford classification, type-A dissections involve the ascending aorta, regardless of the site of intimal tear and the distal extent of dissection, whereas type-B dissections involve any portion of the descending aorta distal to the left subclavian artery. Approximately 60% of acute dissections are type A. The dissection may also be labeled as acute, when it is diagnosed within 14 days of the onset of symptoms, or chronic, if it is diagnosed later. The risk of complications including acute aortic insufficiency, occlusion of the coronary vessels, and rupture of the dissection into the pericardium or pleural cavity approximates 90% in type-A dissection and necessitates immediate surgical repair. This risk is much lower in type-B dissection, which can be controlled medically.

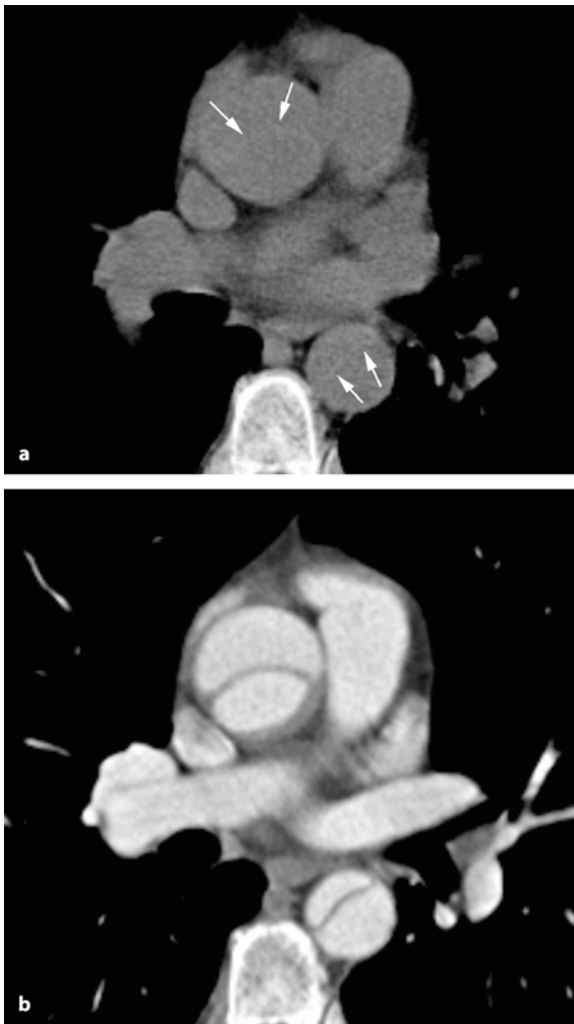


**Fig. 3.** Type-A aortic dissection. A subtle hyperattenuating, thin line can be seen on non-contrast CT scan (a) within the lumen of both ascending and descending aorta (arrows). This thin line corresponds to an intimal flap, as shown on the contrast-enhanced CT scan (b). The patient had severe anemia which could explain the relative high attenuation of the flap



**Fig. 4.** Type-A aortic dissection. Contrast-enhanced CT scans (a, b) show a thin, curvilinear structure within the opacified ascending and descending aorta, representing an intimal flap. The flap is curved toward the false lumen in the ascending aorta, and toward the true lumen in the descending aorta. Also note the greater cross-sectional area of the false lumen relative to the true lumen; this latter is compressed by the false lumen at the level of descending aorta. F false lumen

The classic symptom of acute aortic dissection is pain that is described as crushing, burning, tearing, or ripping. Maximal intensity is often experienced at the onset, as opposed to the crescendo pain of myocardial infarction. Pain may radiate to the back, abdomen, and flanks in a migratory pattern consistent with the course of dissection. In a series of 72 patients with aortic dissection, pain represented the initial symptom in 66 cases and was referred to anterior chest in 46 patients, back in 7, and to other sites in the remaining 13 patients [26].

The main criterion used for diagnosis of dissection is the identification of an intimal flap within the aorta separating two lumens. Secondary and less specific criteria include compression of the true lumen by the false lumen,

widening of the aorta, and thickening of the aortic wall [20, 31, 41, 43]. Displacement of intimal calcifications toward the aortic lumen may also be seen.

Occasionally, unenhanced CT scans of patients with aortic dissection may show internal displacement of intimal calcifications (Fig. 1), a finding that can be confused with an aneurysm with calcified mural thrombus [3]. In some cases, the intimal flap can be recognized on unenhanced CT scans as a subtle hyperattenuating line, as a consequence of severe anemia (Fig. 3).

On contrast-enhanced CT scans, the intimal flap is seen as a thin, curvilinear lucency within the opacified aorta (Figs. 1, 3-5). The flap can be either flat or curved toward

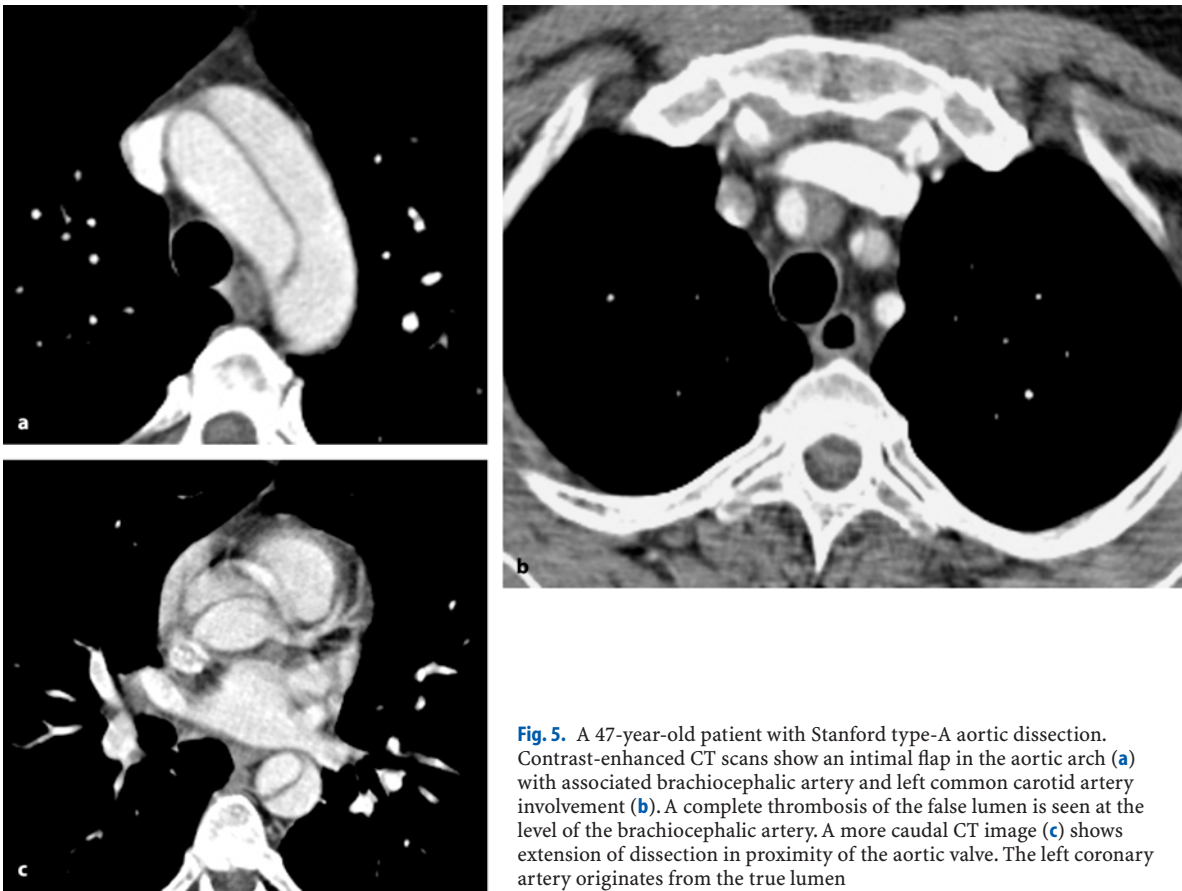


**Fig. 5.** A 47-year-old patient with Stanford type-A aortic dissection. Contrast-enhanced CT scans show an intimal flap in the aortic arch (a) with associated brachiocephalic artery and left common carotid artery involvement (b). A complete thrombosis of the false lumen is seen at the level of the brachiocephalic artery. A more caudal CT image (c) shows extension of dissection in proximity of the aortic valve. The left coronary artery originates from the true lumen

the false or, less commonly, the true lumen [21]. Sometimes, it shows a serpiginous course, particularly in the aortic arch, or may be highly mobile thus mimicking the aspect of a complex dissection with more than two lumens. Axial images are usually sufficient to identify a dissection in nearly all cases; however, multiplanar reformations can provide more accurate evaluation of extent of the dissection and effect on aortic branches [33].

Motion artifacts of the ascending aorta may impair image quality and simulate an intimal flap or a false lumen. These artifacts are related to movements of the aortic wall in the interval from end-diastole to end-systole and appear as a curvilinear interface in the ascending aorta [25, 41]. In most cases artifacts occur left anterior and right posterior on both unenhanced and contrast-enhanced images and change from one section to another. Care must be taken not to misdiagnose an extra aortic structure as a false lumen. The left innominate vein, the left intercostals vein, the left superior pulmonary vein, and the superior pericardial recess can all mimic a false channel, as can pleural thickening and lung atelectasis adjacent to the descending aorta [41].

Accurate differentiation between the true and false lumen, as well as correct assessment of luminal origins of branch vessels, has become particularly important for

planning endovascular treatment of dissection (Fig. 6) [3, 21]. In most cases, the identity of the true lumen may be determined by its continuity with a non-dissected segment of aorta; moreover, the false lumen usually shows a cross-sectional area larger than the true lumen (Fig. 4). Another useful indicator of the false lumen is the “beak sign,” defined as the presence of an acute angle between the dissection flap and the outer wall of aorta (Fig. 7). The space formed by the acute angle can be filled with contrast medium or low-attenuation material [21]. Cobwebs are also present only in the false lumen [3, 21]. They appear as thin, linear filling defects in the false lumen that are attached to the wall at one end and represent residual ribbons of media incompletely shared off by the dissection (Fig. 7); however, the cobweb sign is of limited usefulness because of its rarity. The finding was present in 9% scans in a series of 51 patients recently reported [21]. A newly described finding for distinguishing true from false lumen in aortic dissection at CT is the intimomedial rupture that is the direct visualization of the intimomedial entrance tear from true to false lumen [18]. This sign has been observed in 5 of 59 (8%) patients with aortic dissection as a distinct defect along the intimal flap with the free edges of the flap pointing toward the false lumen [18].



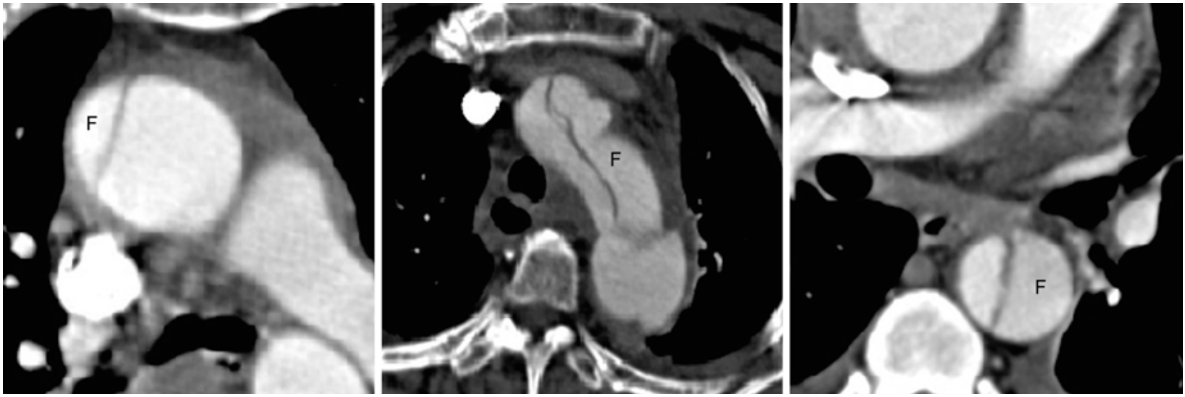


**Fig. 6.** Differentiating true lumen and false lumen. The false lumen is frequently located along the right antero-lateral aspect of the ascending aorta, the left lateral aspect of the aortic arch and the left postero-lateral aspect of the descending aorta. *F* false lumen

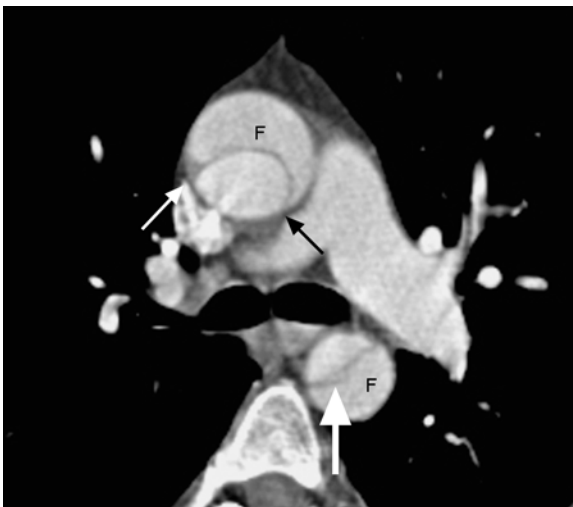


**Fig. 7.** Differentiating true lumen and false lumen. Contrast-enhanced CT scan shows a curved ascending aortic flap and a flat descending aortic flap. Beak sign is present in the false lumen and can be easily appreciated at the level of ascending aorta (*thin white and black arrows*). The right false lumen beak in the ascending aorta (*thin white arrow*) is partially opacified and partially filled with thrombus. A cobweb is also faintly visualized in the false lumen at the level of descending aorta (*thick white arrow*). This represents a residual fragment of the aortic media separated during dissection. *F* false lumen

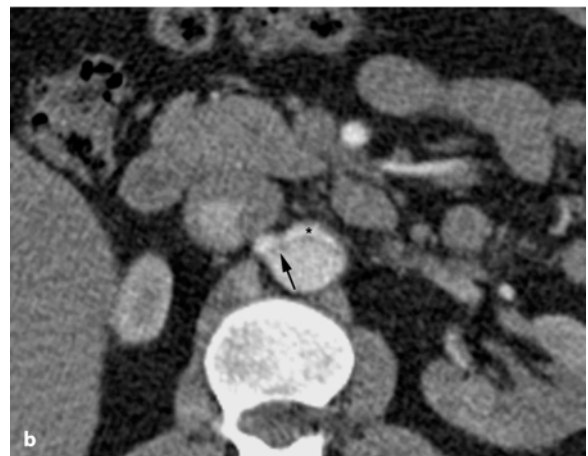
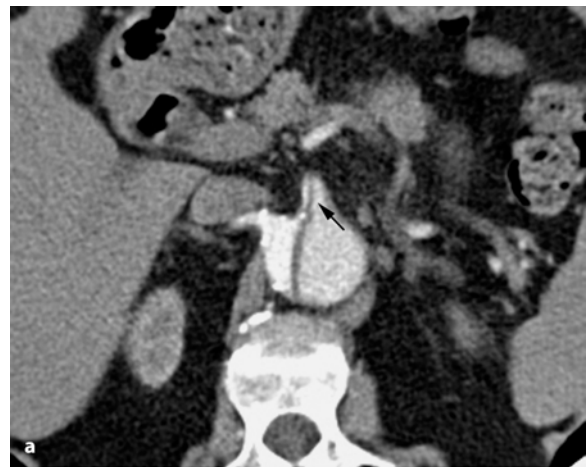


**Fig. 8.** Static and dynamic obstruction of abdominal arterial branches. Contrast-enhanced CT scan (**a**) shows the intimal flap entering the superior mesenteric artery (*arrow*) and causing static obstruction of the vessel. A CT scan obtained in a different patient with type-B aortic dissection (**b**) shows a collapsed true lumen (*asterisk*) and an intimal flap covering the origin of the right renal artery (*arrow*). This results in a dynamic obstruction of the renal artery

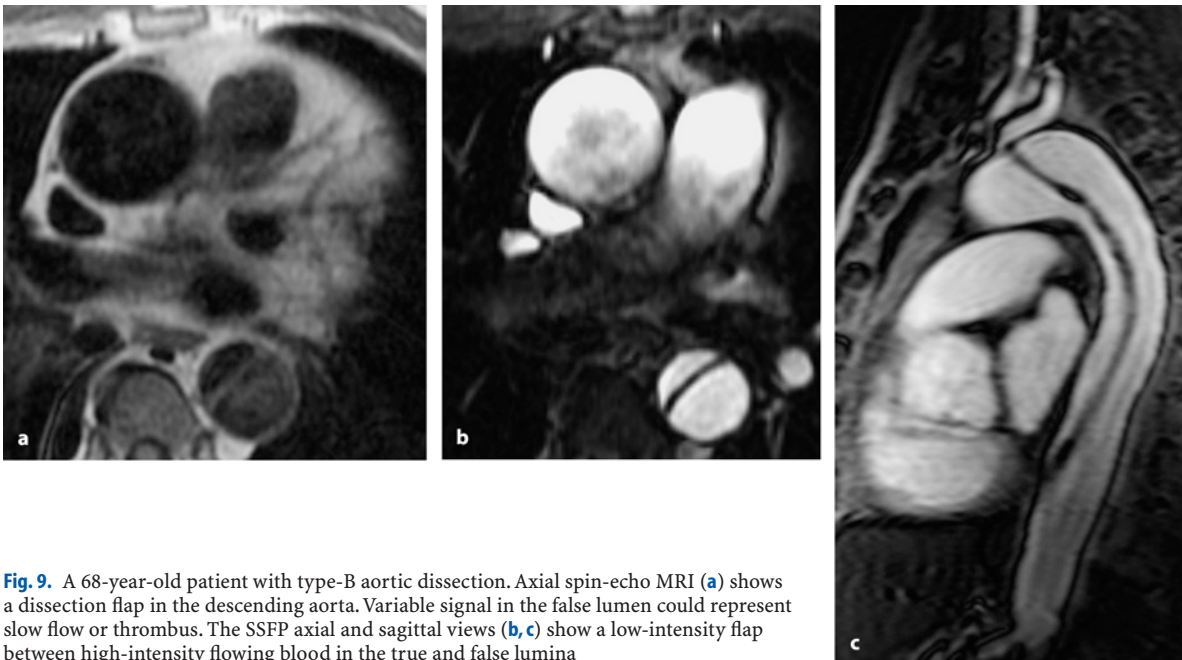


**Fig. 9.** A 68-year-old patient with type-B aortic dissection. Axial spin-echo MRI (**a**) shows a dissection flap in the descending aorta. Variable signal in the false lumen could represent slow flow or thrombus. The SSFP axial and sagittal views (**b, c**) show a low-intensity flap between high-intensity flowing blood in the true and false lumina

Definition of branch vessel origin is also important when a percutaneous treatment of aortic dissection is planned since branch vessels being supplied by the false lumen may be occluded unless surgically bypassed [3, 18]. Equally important is assessment of flap extension and branch vessel obstruction (Fig. 8) that can occur either when the dissection flap enters the vessel origin (static obstruction) or when the intimal flap prolapses and covers the vessel origin like a curtain thus causing obstruction during systole (dynamic obstruction) [3, 45]. Distinction between the two mechanisms of branch vessel compromise is important because they require different treatment: static obstruction can be treated locally with intravascular stent placement, whereas dynamic obstruction requires fenestration of the intimal flap to reduce pressure in the false lumen.

A variety of MRI techniques can be used for imaging thoracic aorta; however, spin-echo imaging and gadolinium-enhanced MR angiography, with gradient-recalled-echo imaging used in selected cases, are typically performed for accurate evaluation of both aortic lumen and wall [22]. On ECG-gated spin-echo sequences, the intimal flap can be seen as a well-defined curvilinear structure of intermediate signal intensity separating the true and false lumen when blood flow is above a critical rate. Slow-flowing blood in the false lumen produces different signal patterns which can be difficult to distinguish from thrombus (Fig. 9). On gradient-echo images, the flap appears as a low-intensity linear structure between high-intensity flowing blood in the true and false channels. Because gradient-recalled-echo imaging is flow sensitive, slow flow, which

would show a flow-related signal increase, can be easily differentiated from thrombus, which would have inherent low signal [22].

As with CT there are a number of diagnostic pitfalls using MRI. Adjacent structures, such as the left brachiocephalic vein, the left superior pulmonary vein, and the superior pericardial recess may mimic a false lumen. Apparent thickening of the aortic wall due to motion artifacts or atherosclerotic plaques may be confused with a thrombosed false lumen.

Several criteria have been used for the diagnosis of aortic dissection by TEE. The pathognomonic echocardiographic appearance of dissection is an undulating linear density within the aortic lumen separating a true and false lumen which have different Doppler color flow patterns; however, these criteria are restrictive and dissection should be suspected whenever the normal appearance of the aortic wall consisting of a single dominant echo is replaced by two separate echoes, one presumably representing the intima plus the inner media and the second representing the outer media and adventitia [49]. Reverberation artifacts are common in dilated ascending aortas and can lead to false-positive diagnoses of dissection. On the other hand, false negatives may occur when small dissections limited to the upper ascending aorta or proximal aortic arch are not visualized because of interference from the air-filled trachea.

Important roles for imaging are to confirm or exclude aortic dissection and to differentiate between type A and type B, information that decides not only whether surgery is indicated but also the surgical approach. Additional in-

formation that is useful for assessing prognosis and selecting the appropriate therapy includes the presence and extent of branch vessel involvement, the site of entry and re-entry tear, the presence and severity of aortic insufficiency, the presence or absence of thrombosis in the false lumen, and the presence of extravasated blood in the mediastinal, pleural, or pericardial spaces.

Each of the four main imaging modalities, i.e., aortography, CT, MRI, and TEE, have advantages and disadvantages in the evaluation of suspected aortic dissection and their relative accuracy has been debated in the medical literature.

Aortography has long been considered the study of choice for evaluation of patients with suspected aortic dissection; however, this procedure is invasive, time-consuming, and, most importantly, has limited sensitivity which is reported to be as low as 88% [7]. Moreover, when the flow in the false lumen is slow or thrombosed, aortography can rely on indirect signs only, such as deformation and extrinsic compression of the true lumen.

Non-invasive imaging modalities have played an increasingly important role in the diagnosis of aortic dissection. Continuous advances in CT technology with introduction of spiral CT and multidetector-row CT have allowed the development of a new minimally invasive vascular imaging technique. In 1996, Sommers et al. reported on a series of 49 symptomatic patients with clinical suspicion of aortic dissection; spiral CT showed a sensitivity and specificity of 100% in the detection of thoracic dissection and allowed accurate assessment of supra-aortic vessel involvement with an accuracy of 96% [43]. In a more recent study including 45 patients with type-A aortic dissection and 12 patients with type-A intramural hematoma, Yoshida et al. reported an accuracy of 100% for correct diagnosis with spiral CT in comparison with surgical findings [50]. For detection of the entry tear and assessment of arch branch vessels, the accuracy of spiral CT were 84 and 98%, respectively. Similar results have been reported for MRI in the evaluation of aortic dissection with a sensitivity of 93-100% and specificity of 94-97% [31, 43]. Main limitations of CT are the inability to identify aortic regurgitation and the need for contrast administration, which may be a limiting factor in patients with severe cardiac failure [43]. Weaknesses of MRI include limited access to the patients and difficult monitoring of vital signs. Moreover, patients with cardiac pacemaker cannot undergo MRI.

Reported sensitivity and specificity for monoplane and biplane TEE range from 97.7 to 100% and from 68 to 97%, respectively [7, 31]. In fact, the major problem of TEE is the inability to see through the air in the trachea and the left main bronchus which results in limited exploration of the aortic arch and the distal part of the ascending aorta. Multiplanar TEE may overcome these difficulties and has shown sensitivity and specificity values of 100 and 94%, respectively, in the detection of aortic dissection [43]. The TEE also has the advantage of being readily available and

fast. It can be performed at the bedside, making it ideal for use in unstable patients; however, TEE is operator dependent and has a quite limited field of view with impossibility to visualize the distal extension of dissection below the celiac trunk.

#### 4.1.3.2 Aortic Intramural Hematoma

Intramural hematoma (IMH), first described by Krukemberg in 1920, represents a variant of dissection characterized by the absence of an intimal tear [27, 46]. In these cases, the false lumen is created by a hemorrhage into the aortic media, most likely after rhexis of the vasa vasorum that penetrates the outer half of the aortic media from the adventitia.

The IMH accounts for 3-13% of all acute aortic dissections in autopsy series [27]; however, the reported incidence of IMH in clinical studies using TEE, CT, or MRI is higher and ranges between 13 and 27% [27, 32, 49]. This discrepancy may be due to inability of imaging modalities to detect small intimal tears or low flow states in non-communicating dissections. Another possible interpretation of these data is that some patients who initially present with IMH develop an intimal tear and progress to classic aortic dissection prior to death, thus accounting for the lower incidence of dissection without entry tear at autopsy.

Although controversies still exist about the appropriate treatment of IMH, most authors suggest that patients with IMH should be managed with the same empirical guidelines that have been successfully adopted for patients with classical dissection [20, 32, 34]. Specifically, involvement of the ascending aorta (type-A IMH) should prompt urgent repair, whereas initially stable patients with IMH of the descending aorta (type-B IMH) can be treated medically with frequent clinical and radiological reassessment to rule out progression.

Chest or back pain on a substrate of chronic hypertension characterize the clinical presentation of IMH. Aortic regurgitation is common in patients with ascending aorta hematoma, whereas other physical findings of classic dissection (pulse differential, ischemic, and neurological symptoms) are less frequently seen [32].

The diagnosis of IMH relies on the visualization of intramural blood or evidence of regional wall thickening of the aortic wall, usually >7 mm, in a circular or crescent shape [32]. As already seen with aortic dissection, IMH usually occurs at points of greatest hydraulic stress and may be typically identified in the right lateral wall of the ascending aorta or in proximity of the isthmus. Pericardial effusion may be present in nearly half of patients with involvement of the ascending aorta, and pleural effusion is present in nearly half of all patients with IMH [20].

A characteristic CT finding of IMH is the crescent-shaped high-attenuating rim along the aortic wall on non-contrast scans, corresponding to the hematoma in the

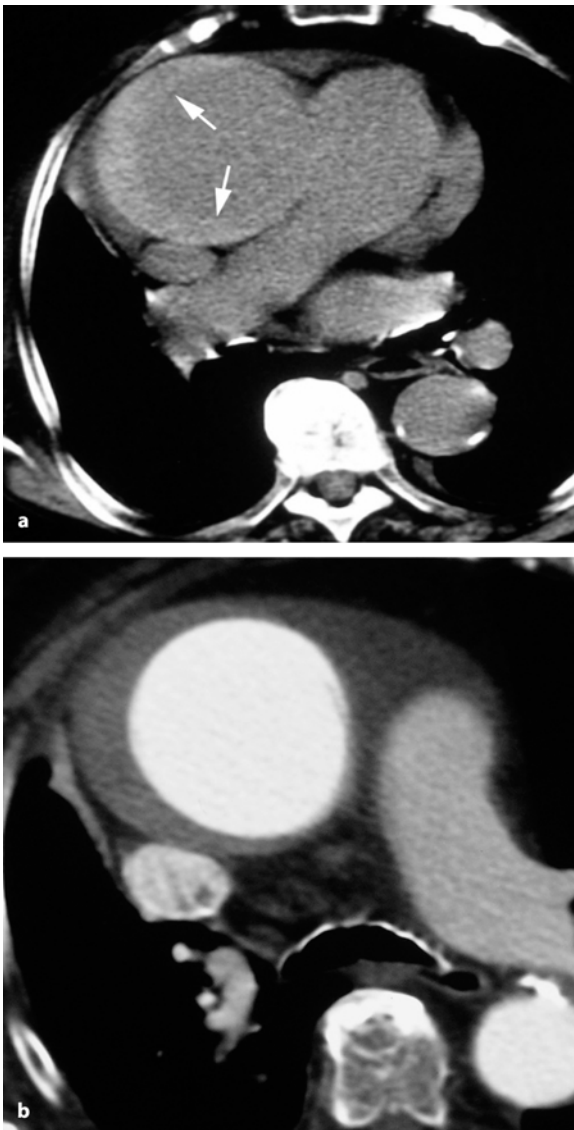


**Fig. 10.** Intramural hematoma of the ascending aorta in a 61-year-old man. Non-contrast CT scan (**a**) reveals a crescent area of high attenuation along the anterior, lateral and posterior walls of the ascending aorta (*arrows*), suggestive of intramural hematoma. On the CT scan performed at the same level after contrast medium administration (**b**), the hematoma does not enhance and appears as a hypoattenuating band relative to the aortic lumen; this latter shows an oval shape because of slight compression by the hematoma

medial layers (Figs. 2, 10), eventually associated with intraluminal displacement of calcifications [20, 41]. The hematoma may or may not compress the aortic lumen. Sometimes, the hyperdensity of the rim is better appreciated using narrow window settings (Fig. 11); recommended values are  $W=180-200$  HU;  $C=30$  HU [16]. After contrast administration, there is no enhancement of the hematoma, which appears relatively hypodense (Fig. 10). Distinction between an IMH and atherosclerotic wall thickening can

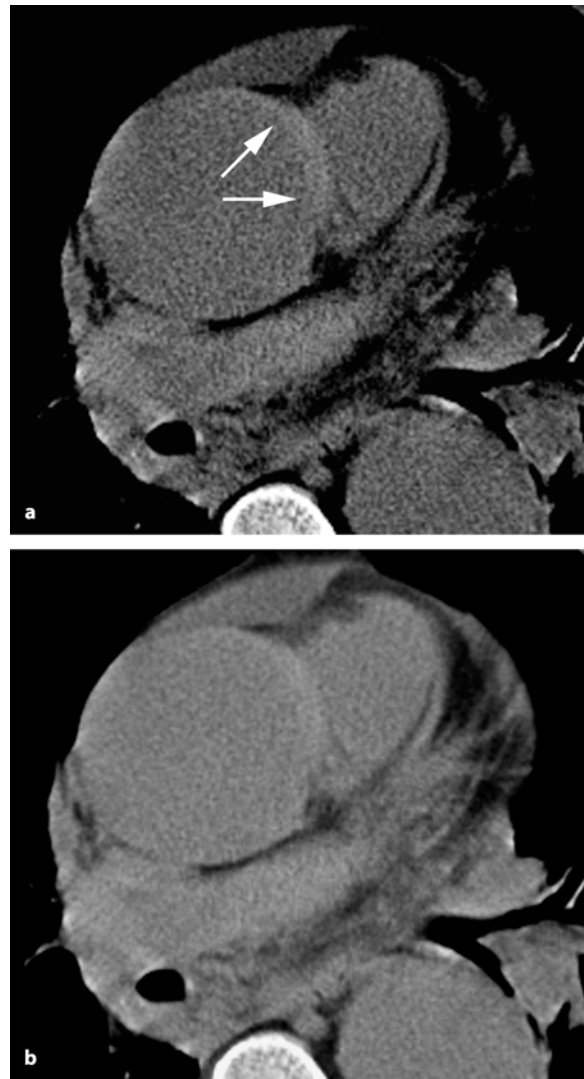


**Fig. 11.** Intramural hematoma of the ascending aorta; influence of window settings. Non-contrast CT scan photographed using narrow window settings ( $W=180$  HU,  $C=30$  HU; **a**) demonstrates a crescent-shaped high attenuation within the ascending aorta. This is less evident on the non-contrast CT scan (**b**) photographed with standard soft tissue window settings ( $W=400$  HU;  $L=40$  HU). A minimal pericardial effusion is also present. The patient underwent surgical repair of a type-A intramural hematoma

be problematic, although helpful findings include the absence of irregular inner margins, quite common in atherosclerosis [20], and the smooth extension of hematoma along the aorta which is in contrast with the patchy distribution of atherosclerosis. Moreover, atherosclerotic wall thickening is rarely present in the ascending aorta.

The MR appearance of IMH (Fig. 12) varies depending on its age. Fresh hematoma is isointense with the aortic wall on T1-weighted sequences and shows high signal in-



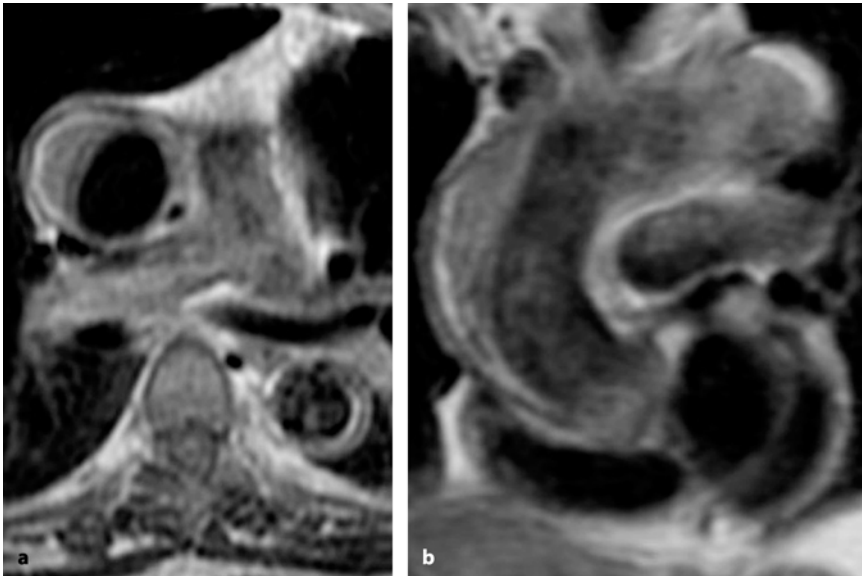


**Fig. 12.** Type-A intramural hematoma. Axial (a) and oblique (b) spin-echo MRI show a crescentic, hyperintense thickening along the right lateral wall of ascending aorta

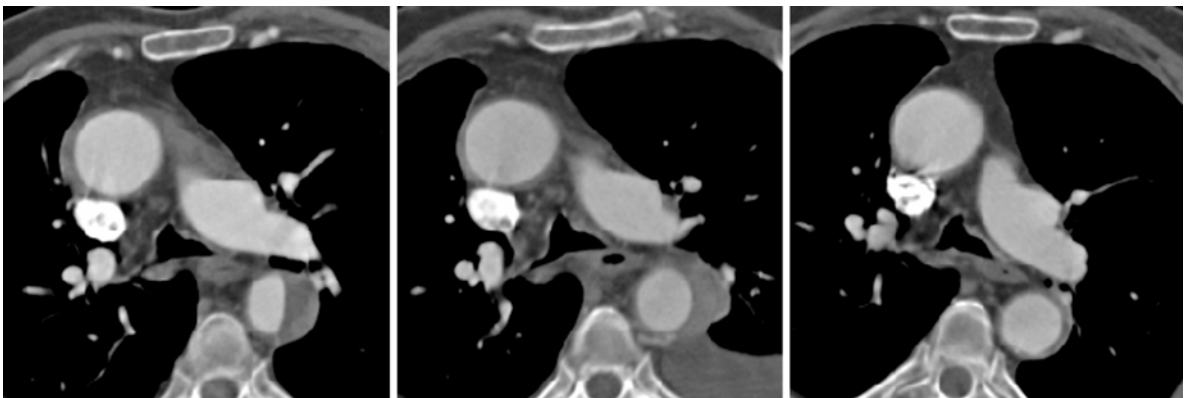


**Fig. 13.** Progressive resolution of intramural hematoma. Contrast-enhanced CT scan (left) shows an intramural hematoma along the right antero-lateral aspect of ascending aorta and the left lateral aspect of descending aorta. The true lumen in the descending aor-

ta is compressed. The follow-up CT scan performed 1 week later (center) shows an interval reduction of hematoma that completely resolved after 2 weeks (right)

tensity on T2-weighted images. In the few days after hemorrhage, IMH has low signal intensity, whereas subacute hematoma reveals a high signal intensity on both T1 and T2 images due to formation of methemoglobin [32, 35]. Signal intensity changes consistent with recurrent bleeding have been reported in patients with early subacute complications [17]. In some cases, failure to progression from intermediate to high signal intensity can be associated with symptoms of recurrent hemorrhage [22].

Echocardiographic criteria for IMH are a >7-mm crescentic or circular thickening of the aortic wall extending 1–20 cm longitudinally, with absence of intimal laceration or flap and no evidence of Doppler flow within the thickened wall [27, 49]. Complementary, but less diagnostic, features

include a thrombus-like consistency and layered appearance with echolucent areas of the widened aortic wall. Differentiation from severe atherosclerosis with local wall thickening may be difficult on the basis of TEE findings, and IMH may sometimes be diagnosed retrospectively with serial evaluation demonstrating resolution or progression of the hematoma. Moreover, false-positive findings of focal thickening on tangential scans and around the hemiazygos vein are possible [32].

Reported sensitivity for TEE, contrast-enhanced CT scanning, and MRI for identification of IMH exceed 96% [34].

The natural history of IMH is unpredictable. Several reports in the literature indicate that the hematoma may resolve completely (Fig. 13), or evolve after a variable inter-

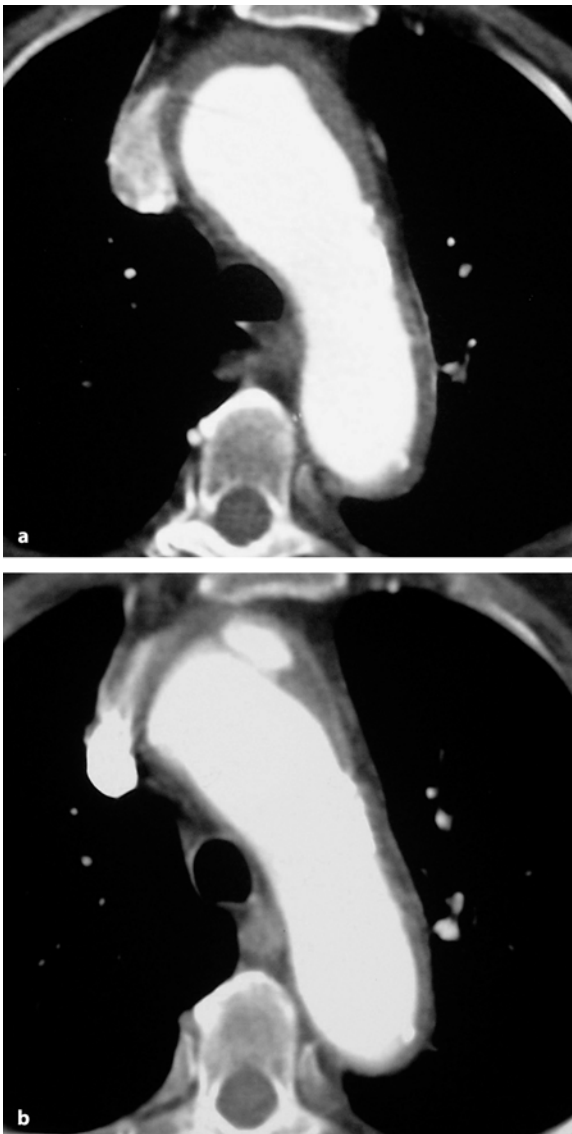


**Fig. 14.** Evolution of intramural hematoma to typical dissection. Contrast-enhanced CT scan (a) shows an intramural hematoma along the anterior and left lateral walls of aortic arch. A CT scan performed 3 days later because of persistent chest pain (b) shows focal enlargement of hematoma with development of dissection

val time into classical aortic dissection or aneurysm (Fig. 14) [17, 20, 42, 46]. The risk of complications is higher in patients with IMH involving the ascending aorta, particularly if the initial diameter of the ascending aorta exceeds 5 cm or when the hematoma fails to resolve on follow-up imaging [35]. In a recent study including 22 consecutive patients with type-A IMH, the maximum ascending aorta diameter resulted to be a significant predictor of hematoma progression on CT scans [17]. Use of a cut-off value of 5 cm for the initial aortic diameter resulted in a negative predictive value of 100% and positive predictive value of

83%. Other findings, including thick hematoma with compression of the true lumen and pericardial effusion, can be useful for predicting a progression to aortic dissection [3, 5]. A thicker hematoma may indicate more active bleeding and may be responsible for weakening of the intimal layer.

On follow-up studies, patients with IMH may show ulcer-like projections, indicative of a new intimal disruption [22]. This finding is more frequently observed in the ascending aorta rather than the descending aorta.

#### 4.1.3.3 Penetrating Atherosclerotic Ulcer

The term penetrating atherosclerotic ulcer describes the condition in which ulceration of an atherosclerotic lesion penetrates the internal elastic lamina, often resulting in hematoma within the media of the aortic wall [20, 38]. The absence of an ulcer crater distinguishes intramural hematoma from penetrating ulcers with intraparietal hemorrhage [46].

The clinical presentation of penetrating atherosclerotic ulcer may mimic classic dissection and IMH; however, patients with penetrating ulcers tend to be older, with an heavier burden of atherosclerotic disease, and are often active smokers [34]. In more than 40% of patients, penetrating ulcers are associated with abdominal aortic aneurysms [6]. Moreover, ulcers typically affect the mid to distal portion of the descending aorta and are not usually associated with extensive longitudinal propagation or branch vessel involvement. Accordingly, they are not accompanied by the pericardial, neurovascular, or visceral complications seen with classic dissection and IMH. Occasionally, aortic ulcers may represent an incidental finding in asymptomatic patients undergoing a CT scan of the chest for other reasons [38].

The diagnosis of penetrating atherosclerotic ulcer is made on CT, MRI, and TEE by demonstration of an out-pouching of the aortic wall with jagged edges, usually in the presence of extensive aortic atheroma and adjacent subintimal hematoma (Fig. 15) [41, 46, 49]. The intramural hematoma indicates an aggressive behavior of the atherosclerotic lesion and is a useful finding in the differential diagnosis between penetrating atherosclerotic ulcer and an irregular atherosclerotic plaque without disruption [22]. In the latter, the lesion does not extend beyond the level of intima and therefore is not accompanied by intramural hematoma.

On CT scans penetrating ulcers show well-defined margins, are filled with contrast material, and project outside the opacified aortic lumen [38]. Lesions are predominantly located in the descending aorta where atherosclerosis tends to be more severe. Concomitant aneurysms of the descending aorta are commonly found.

Little is known about the natural history of penetrating ulcers. The process may progress to aneurysm and pseudoaneurysm formation, typical dissection, aortic rupture, or

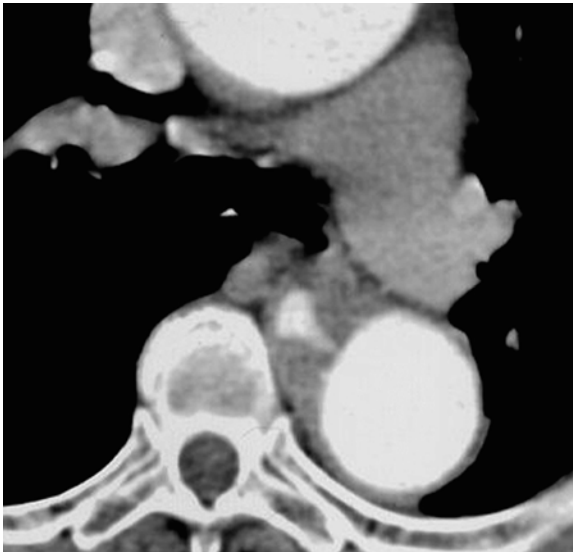


**Fig. 15.** Penetrating atherosclerotic ulcer. Contrast-enhanced CT scan in a 78-year-old woman demonstrates a focal contrast collection along the right lateral wall of descending aorta and projecting beyond the confines of aortic lumen. An adjacent subintimal hematoma is present. This is almost typical of penetrating atherosclerotic ulcer

may be spontaneously contained [20, 34, 46, 49]. Ganaha et al. reported that persistent or recurrent pain despite therapy and interval increase of pleural effusion were significant indicators of disease progression; moreover, penetrating atherosclerotic ulcer with an initial diameter  $\geq 20$  mm or a depth  $\geq 10$  mm were at higher risk of progression [10].

In a recent study, 56 ulcer-like lesions of the aorta were retrospectively evaluated in 38 patients [38]. Follow-up CT scans were available for 33 lesions and showed stability of the lesion and adjacent aorta in 21 cases, whereas mild to moderate increase in aortic diameter with or without lesion enlargement was observed in 8 cases. Two lesions were incorporated into the aortic wall contour with subsequent increase in aortic diameter. In the remaining 2 cases, the ulcer remained unchanged, although the associated intramural hematoma regressed. Similar results had been previously reported by Harris et al. [14]. Imaging follow-up in 10 patients with a total of 17 aortic ulcers showed no change over time in 9 cases and progression to saccular aneurysm for 4 ulcers. In 4 other cases, concentric aortic dilatation developed with loss of definition of the ulcer crater. The results of these studies point out that most aortic ulcers remain unchanged over time and do not require surgery or interventional procedures; however, a limitation of both studies is the lack of histopathological proof so that it is possible that some of the lesions assumed to be penetrating aortic ulcers may have represented different entities, such as atypical dissection with intimal tear, aneurysm with atherosclerotic debris, or a contained aortic rupture.

#### 4.1.4 Multidetector-Row CT and Acute Chest Pain

In recent years, fast imaging with electron beam tomography (EBT) has been proposed as a screening tool for patients in the emergency department presenting with acute chest pain and non-specific ECG findings [12, 19, 24]. A number of investigators have demonstrated that the presence of coronary artery calcium in a symptomatic cohort is a strong predictor of future cardiac events [19, 24]. On the contrary, the absence of coronary calcifications is associated with a very low likelihood of acute cardiac ischemia and should prompt early discharge of patients with non-diagnostic ECG and negative scans. These data have been recently confirmed in a study of 192 patients admitted to the emergency department for chest pain and undergoing EBT scanning in addition to the usual care for chest pain syndromes [12]. Patients were followed-up for a period of  $50 \pm 10$  months using chart review. Fifty-eight patients had cardiac events during the follow-up period. The mean calcium score of patients who did not suffer a cardiac event was significantly lower than the score of patients who suffered a hard event and the score of patients with any cardiovascular event.

The latest generation of multidetector-row CT scanners now provide adequate evaluation of coronary artery anatomy and significant disease and is gaining clinical acceptance for non-invasive cardiac imaging. In fact, considerable improvements of temporal and spatial resolution have been achieved with 16-detector-row or faster scanners which are fundamental for imaging of fast moving vessels as small as 1 mm. A CT coronary angiography is typically performed in a spiral mode with simultaneous registration of the patient's ECG; data are then retrospectively referenced to the ECG signal to reconstruct images during the diastolic phase of the cardiac cycle [37, 39]. This allows to obtain nearly motionless images in patients with regular and relatively low heart rates. Overlapping axial images are obtained with a minimum section thickness and eventually reformatted into 2D and 3D images for better visualization of coronary arteries along their course (Fig. 16) and of cardiac chambers along their major axis. If necessary (heart rate  $>60$ – $70$  bpm), beta-blockers may be used in order to reduce the heart rate and to increase the cardiac rest period.

In early reports, the number of assessable coronary artery segments with 4-detector-row scanners ranged between 68 and 74% [1, 29, 40]. The most frequent causes for non-assessability of coronary vessel segments were cardiac motion, extensive calcifications, small size, and adjacent contrast-filled structures such as veins or cardiac chambers [29]. Because of their oblique course and complex motion during the cardiac cycle, the right coronary artery and the left circumflex artery were the most difficult to assess at CT. Using state-of-the-art 16-detector row scanners, visibil-

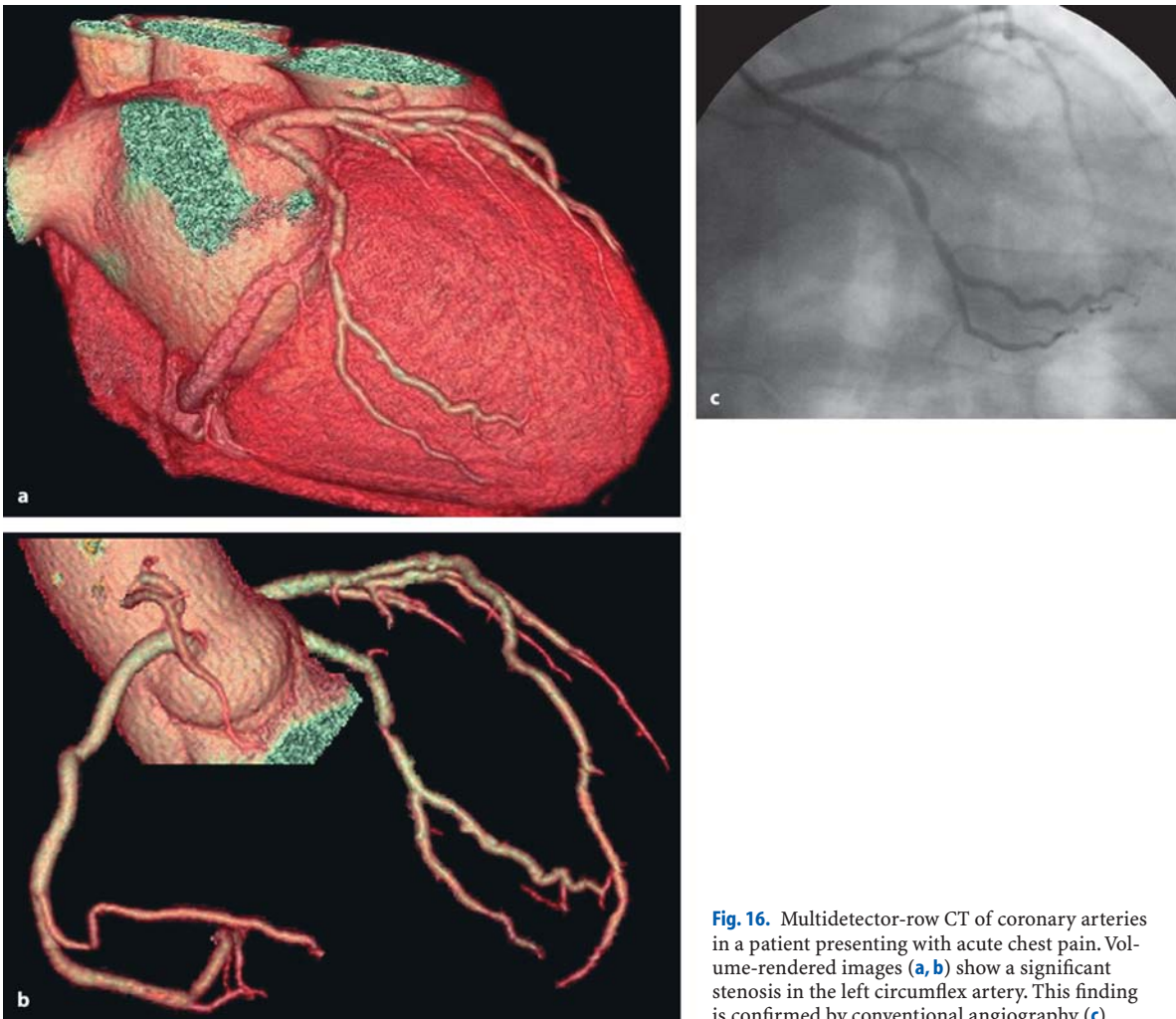


**Fig. 16.** Multidetector-row CT of coronary arteries in a patient presenting with acute chest pain. Volume-rendered images (**a, b**) show a significant stenosis in the left circumflex artery. This finding is confirmed by conventional angiography (**c**)

ity of coronary artery segments is significantly improved with about 10% of poorly assessable segments [28, 39].

When compared with conventional angiography, the sensitivity of multidetector-row CT to detect significant (>50%) stenoses of coronary arteries is in the range of 83–85% with 4-detector-row CT and 92–95% with 16-detector-row scanners [39]. Corresponding values of specificity are 76–90 and 86–93%, respectively. Although in most investigations accuracy of multidetector-row CT has been determined on the basis of analyzable segments rather than the total number of coronary segments, excellent results have been reported even when no vascular segments were excluded from the analysis. Nieman et al. reported sensitivity and specificity of 92 and 93%, respectively, for identifying  $\geq 50\%$  stenosis using 16-detector-row scanners and including non-evaluable segments in the statistical analysis [30]. Similarly, Mollet et al. compared 16-detector row CT and conventional angiography in a large series of 128 patients with stable angina pectoris and

found a sensitivity of 92% and a specificity of 95% for detection of significant stenoses with CT [28]. Image quality was considered poor in 7% of segments; however, these segments were included in the comparative analysis.

Coronary arterial calcifications may represent a limitation of CT angiography for assessment of coronary vessel stenoses. Calcifications are high density structures causing beam-hardening artifacts and partial-volume averaging that may impair assessment of adjacent plaque structures and result in false-positive detection or overestimation of stenoses [28, 39].

Multidetector-row CT also allows noninvasive assessment of patients with history of myocardial revascularization [23, 39]. Patency or occlusion of bypass grafts can be established by the presence or absence of contrast enhancement, respectively. In a recent investigation including 57 patients with a total of 122 grafts (95 arterial and 27 venous), the sensitivity and specificity of 4-detector-row CT for assessment of graft patency were 93 and 97.8%, re-



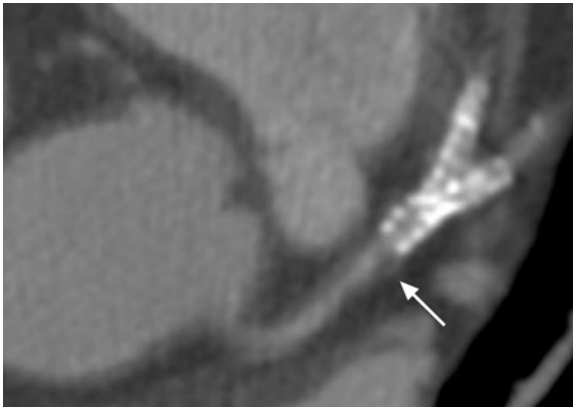


**Fig. 17.** Multidetector-row CT coronary angiography in a patient with sequential stents within the left descending coronary artery. Stent patency is revealed by flow to distal segments of the artery. A mural filling defect can be seen close to the proximal end of the stent (arrow)

spectively [23]. High-grade (>50%) stenoses of coronary grafts could be assessed with a sensitivity of 80% and a specificity of 96%; however, 33% of grafts were excluded from evaluation of stenosis because of artifacts from coarse surgical clips or motion artifacts, a common situation for conduits grafted to the lateral and inferior cardiac walls [23].

Similarly to surgical clips, the high attenuation metallic mesh of coronary stents precludes confident evaluation of in-stent restenosis with CT due to partial-volume effect. However, stent patency can be inferred on the basis of the presence or absence of coronary luminal enhancement distal to the stent (Fig. 17); moreover, evaluation of stenosis at the leading or trailing ends of a stent is possible [39].

The feasibility and usefulness of multidetector-row CT scans in patients with acute chest pain syndrome have been recently assessed with encouraging results. In one study, 66 patients hospitalized for acute chest pain syndrome underwent conventional coronary angiography and CT angiography using a 16-detector-row scanner without routine administration of beta-blockers [11]. The overall accuracy of multidetector-row CT for detection of significant stenoses in the left main, left anterior descending, left circumflex, and right coronary arteries were 93, 88, 86, and 86%, respectively. Seven patients were ultimately diagnosed as having non-specific chest pain. Moreover, multidetector-row CT has been shown to be effective in the diagnosis of different diseases presenting with the symptom chest pain, including aortic dissection and pulmonary embolism, and can then be used for a comprehensive evaluation of patients admitted to the emergency department with acute chest pain. In a pilot study of 69 clinically stable patients with acute chest pain, White et al. reported an overall sensitivity and specificity of 16-detector-row CT for diagnosis of cardiac and non-cardiac conditions of 87 and

96%, respectively [47]. Thirteen patients had significant CT findings concordant with the final diagnosis (10 cardiac and 3 non-cardiac); however, CT failed to suggest a clinically significant diagnosis in 2 patients and overdiagnosed a coronary stenosis in 2 other patients.

Although further studies are needed, multidetector-row CT seems to be a valuable method for excluding significant cardiogenic causes of chest pain and for suggesting non-cardiac diagnoses.

## References

- Achenbach S, Giesler T, Ropers D et al. (2001) Detection of coronary artery stenoses by contrast-enhanced, retrospectively electrocardiographically-gated, multislice spiral computed tomography. *Circulation* 103: 2535–2538
- Autore C, Agati L, Piccininno M et al. (2000) Role of echocardiography in acute chest pain syndrome. *Am J Cardiol* 86 (Suppl): 41G–42G
- Castaner E, Andreu M, Gallardo X et al. (2003) CT in nontraumatic acute thoracic aortic disease: typical and atypical features and complications. *Radiographics* 23: S93–S110
- Chambers J, Bass C, Mayou R (1999) Non-cardiac chest pain: assessment and management. *Heart* 82: 656–657
- Choi SH, Choi SJ, Kim JH et al. (2001) Useful CT findings for predicting the progression of aortic intramural hematoma to overt aortic dissection. *J Comput Assist Tomogr* 25: 295–299
- Coady MA, Rizzo JA, Elefteriades JA (1999) Pathologic variants of thoracic aorta dissections. Penetrating atherosclerotic ulcers and intramural hematomas. *Cardiol Clin* 17: 637–657
- Erbel R, Engberding R, Daniel W (1989) Echocardiography in diagnosis of aortic dissection. *Lancet* 4: 457–461
- Fallon EM, Roques J (1999) Acute chest pain. *AACN Clin Issues* 8: 383–397
- Filipek MS, Primak SL, Hronas TN et al. (2000) Transient aortic thrombus in a sickle-cell patient with chest pain. *AJR* 175: 1287–1288
- Ganaha F, Miller DC, Sugimoto K et al. (2002) Prognosis of aortic intramural hematoma with and without penetrating atherosclerotic ulcer. A clinical and radiological analysis. *Circulation* 106: 342–348
- Ghersin E, Litmanovich D, Dragu R et al. (2006) 16-MDCT coronary angiography versus invasive coronary angiography in acute chest pain syndrome: a blinded prospective study. *AJR* 186: 177–184
- Georgiou D, Budoff MJ, Kaufer E et al. (2001) Screening patients with chest pain in the emergency department using electron beam tomography: a follow-up study. *J Am Coll Cardiol* 38: 105–110
- Gomes AS, Bettmann MA, Boxt LM et al. (2000) Acute chest pain: suspected aortic dissection. *American College of Radiology. ACR Appropriateness Criteria. Radiology* 215 (Suppl): 1–5
- Harris J, Bis K, Glover J et al. (1994) Penetrating atherosclerotic ulcers of the aorta. *J Vasc Surg* 19: 90–99
- Hartnell GG (2001) Imaging of aortic aneurysms and dissection: CT and MRI. *J Thorac Imaging* 16: 35–46
- Holden A (2000) The value of narrow CT window settings in the recognition of subtle acute aortic intramural haematoma. *Australas Radiol* 44: 128–129
- Kaji S, Nishigami K, Akasaka T et al. (1999) Prediction of progression or regression of type-A aortic intramural hematoma by computed tomography. *Circulation* 100 (Suppl 2): 281–286
- Kapoor V, Ferris JV, Fuhrman CR (2004) Intimomedial rupture: a new CT finding to distinguish true from false lumen in aortic dissection. *AJR* 183: 109–112

19. Laudon DA, Vukov LF, Breen JF et al. (1999) Use of electron-beam computed tomography in the evaluation of chest pain patients in the emergency department. *Ann Emerg Med* 33: 15–21
20. Ledbetter S, Stuk JL, Kaufman JA (1999) Helical (spiral) CT in the evaluation of emergent thoracic aortic syndromes: traumatic aortic rupture, aortic aneurysm, aortic dissection, intramural hematoma, and penetrating atherosclerotic ulcer. *Radiol Clin North Am* 37: 575–589
21. LePage MA, Quint LE, Sonnad SS et al. (2001) Aortic dissection: CT features that distinguish true lumen from false lumen. *AJR* 177: 201–211
22. Macura KJ, Szarf G, Fishman EK et al. (2003) Role of computed tomography and magnetic resonance imaging in assessment of acute aortic syndromes. *Semin US CT MRI* 24: 232–254
23. Marano R, Storto ML, Maddestra N et al. (2004) Non-invasive assessment of coronary artery bypass graft with retrospectively ECG-gated four-row multidetector spiral computed tomography. *Eur Radiol* 14: 1353–1362
24. McLaughlin VV, Balogh T, Rich S (1999) Utility of electron beam computed tomography to stratify patients presenting to the emergency room with chest pain. *Am J Cardiol* 84: 327–328
25. Mesurolle B, Qanadli SD, Merad M et al. (2000) Dual-slice helical CT of the thoracic aorta. *J Comput Assist Tomogr* 24: 548–556
26. Mészáros I, Mórocz J, Szlávi J et al. (2000) Epidemiology and clinicopathology of aortic dissection: a population-based longitudinal study over 27 years. *Chest* 117: 1271–1278
27. Mohr-Kahaly S (2001) Aortic intramural hematoma: from observation to therapeutic strategies. *J Am Coll Cardiol* 37: 1611–1613
28. Mollet NR, Cademartiri F, Nieman K et al. (2004) Multislice spiral computed tomography coronary angiography in patients with stable angina pectoris. *J Am Coll Cardiol* 43: 2265–2270
29. Nieman K, Oudkerk M, Rensing BJ et al. (2001) Coronary angiography with multi-slice computed tomography. *Lancet* 357: 599–603
30. Nieman K, Cademartiri F, Lemos PA et al. (2002) Reliable non-invasive coronary angiography with fast submillimeter multislice spiral computed tomography. *Circulation* 106: 2051–2054
31. Nienaber CA, Kodolitsch Y von, Nicolas V (1993) The diagnosis of thoracic aortic dissection by noninvasive imaging procedures. *N Engl J Med* 328: 1–9
32. Nienaber CA, von Kodolitsch Y, Petersen B et al. (1995) Intramural hemorrhage of the thoracic aorta: diagnostic and therapeutic implications. *Circulation* 92: 1465–1472
33. Novelline RA, Rhea JT, Rao PM et al. (1999) Helical CT in emergency radiology. *Radiology* 213: 321–339
34. O’Gara PT, DeSanctis RW (1995) Acute aortic dissection and its variants. Toward a common diagnostic and therapeutic approach. *Circulation* 92: 1376–1378
35. Oliver TB, Murchison JT, Reid JH (1997) Serial MRI in the management of intramural haemorrhage of the thoracic aorta. *Br J Radiol* 70: 1288–1290
36. Oliver TB, Murchison JT, Reid JH (1999) Spiral CT in acute non-cardiac chest pain. *Clin Radiol* 54: 38–45
37. Ohnesorge B, Flohr T, Becker C et al. (2000) Cardiac imaging by means of electrocardiographically gated multisection spiral CT. *Radiology* 217: 564–571
38. Quint LE, Williams DM, Francis IR et al. (2001) Ulcerlike lesions of the aorta: imaging features and natural history. *Radiology* 218: 719–723
39. Schoenhagen P, Halliburton SS, Stillman A et al. (2004) Noninvasive imaging of coronary arteries: current and future role of multi-detector row CT. *Radiology* 232: 7–17
40. Schroeder S, Kopp AF, Kuettner A et al. (2002) Influence of heart rate on vessel visibility in noninvasive coronary angiography using new multislice computed tomography. *J Clin Imaging* 26: 106–111
41. Sebastia C, Pallisa E, Quiroga S et al. (1999) Aortic dissection: diagnosis and follow-up with helical CT. *Radiographics* 19: 45–60
42. Shimizu H, Yoshino H, Udagawa H et al. (2000) Prognosis of aortic intramural hemorrhage compared with classic aortic dissection. *Am J Cardiol* 85: 792–795
43. Sommers T, Fehske W, Holzknecht N et al. (1996) Aortic dissection: a comparative study of diagnosis with spiral CT, multiplanar transesophageal echocardiography, and MR imaging. *Radiology* 199: 347–352
44. Stanford W, Levin DC, Bettmann MA et al. (2000) Acute chest pain: non ECG evidence of myocardial ischemia/infarction. American College of Radiology. ACR Appropriateness Criteria. *Radiology* 215 (Suppl): 79–84
45. Therasse E, Soulez G, Giroux MF et al. (2005) Stent-graft placement for the treatment of thoracic aortic diseases. *Radiographics* 25: 157–173
46. Vilacosta I, San Román JA (2001) Acute aortic syndrome. *Heart* 85: 365–368
47. White CS, Kuo D, Kelemen M et al. (2005) Chest pain evaluation in the emergency department: Can MDCT provide a comprehensive evaluation? *AJR* 185: 533–540
48. Wilkinson K, Severance H (2001) Identification of chest pain patients appropriate for an emergency department observation unit. *Emerg Med Clin North Am* 19: 35–66
49. Willens HJ, Kessler KM (1999) Transesophageal echocardiography in the diagnosis of diseases of the thoracic aorta. Part 1. Aortic dissection, aortic intramural hematoma, and penetrating atherosclerotic ulcer of the aorta. *Chest* 116: 1772–1779
50. Yoshida S, Akiba H, Tamakawa M et al. (2003) Thoracic involvement of type-A aortic dissection and intramural hematoma. Diagnostic accuracy: comparison of emergency helical CT and surgical findings. *Radiology* 228: 430–435



# CT Diagnosis of Acute Pulmonary Embolism

B. Ghaye, R.F. Dondelinger

## 4.2

### Contents

4.2.1	Introduction	347
4.2.2	History	348
4.2.3	The CTPA Technique	348
4.2.3.1	Acquisition Protocols	348
4.2.3.2	Contrast Medium Administration	349
4.2.4	Image Interpretation	349
4.2.4.1	Direct Demonstration of PE	349
4.2.4.1	Ancillary Findings	351
4.2.5	Estimation of the Age of the Embolus	354
4.2.6	Results	354
4.2.6.1	Sensitivity and Specificity	354
4.2.6.2	Interobserver Variability	354
4.2.6.3	Comparison of CTPA and V/Q Scanning	355
4.2.6.4	Subsegmental PE	356
4.2.6.5	Negative Predictive Value of CTPA	357
4.2.7	Interpretation Pitfalls	358
4.2.8	Severity Assessment of Pulmonary Embolism	361
4.2.9	Alternative Diagnoses	362
4.2.10	Other Advantages	363
4.2.10.1	Wide Availability	363
4.2.10.2	Rapidity	363
4.2.10.3	Minimally Invasive Technique	363
4.2.10.4	Cost-Effectiveness	363
4.2.10.5	Follow-up	364
4.2.11	Limitations of CTPA	364
4.2.11.1	Contraindications to Iodinated Contrast Medium Injection	364
4.2.11.2	Moderate Amount of Irradiation	364
4.2.11.3	Inconclusive Examinations	364
4.2.11.4	Large Number of Images	364
4.2.11.5	Small Size or Obliquely Oriented Arteries	364
4.2.12	CT of PE in Emergency Conditions	364
4.2.13	Conclusion	365
	References	365

### 4.2.1 Introduction

The overall incidence of pulmonary embolism (PE) has been estimated to be approximately 1 per 1000 people in the U.S. [1]. The clinical diagnosis alone is inaccurate for patients with suspected pulmonary embolism. The prevalence of PE detected at autopsy among hospitalized patients is 15–26% [2–4]. One-third of PE caused or contributed to death of the patients, more than 70% of which was unsuspected clinically [3]. These results have not changed over 3 decades despite progress in medicine and prophylaxis [1, 2]. Approximately 10% of patients with PE do not survive the initial embolic event. When untreated, PE is fatal in up to 30% of patients, which can be reduced to 2–10%, if diagnosed and treated promptly with anticoagulation [1, 5–7]. Such therapy, however, is not without risk, with an estimated 10–30% complication rate [8–13]. Pulmonary embolism therefore requires sensitive and specific diagnostic examinations. Older imaging tests, such as chest X-ray, ventilation/perfusion (V/Q) lung scan, and pulmonary angiography (PA), suffer from a lack of specificity or are invasive. The V/Q lung scan together with chest X-ray have been the first-line tests for more than 30 years. Normal results on V/Q lung scan may be considered to rule out PE, whereas a high-probability lung scan is diagnostic of PE with a probability >90%; however, 60–70% of V/Q scans are nondiagnostic [14] and require additional tests, such as serial venous imaging of the lower limbs (US or impedance plethysmography). If the diagnosis is still unclear, the patient would undergo pulmonary angiography, a procedure which carries a small but definite risk [15].

This diagnostic algorithm, however, has generally been underused [4, 16–19]. In the beginning of the 1990s it was stressed that there is a clear need for a technique which is accurate, safe, noninvasive, easily and rapidly performed, widely accepted, and cost-effective, for direct detection and demonstration of intraluminal PE [20–22]. Now spiral CT pulmonary angiography (CTPA) of the pulmonary arteries has the potential to fulfill these requirements. Magnetic resonance imaging is also a promising diagnostic tool, but to date it has not a widespread use in emergency medicine and in critically ill patients, mainly because of long examination time, difficulties in patient monitoring, higher costs, and limited availability or access of MR in most centers [21, 23, 24].



## 4.2.2 History

In 1978 Sinner initially described the diagnosis of PE with CT [25]. In 1980 Godwin et al. reported for the first time the direct demonstration of endovascular clots in central PEs [26]. Technical parameters were a dynamic sequential contrast enhanced scanning, 5- or 10-mm collimation, and a rotation time of 2.4–4.8 s. In 1984 Breatnach and Stanley reported the first demonstration of a segmental embolus with CT [27]. During the 1980s incremental contrast-enhanced CT was occasionally performed, when the risk of complication of pulmonary angiography was high, for the follow-up of central thromboembolism and for preoperative delineation of organized central thrombus. In addition, the incidental detection of proximal clots on CT scans among patients with clinically unsuspected PE has been reported [28–30]. Nevertheless, the potential interest of CT for the diagnosis of PE remained doubtful until recent technical development of helical CT. New technology allowed the acquisition of a volume data set in a single breathhold at the peak of contrast enhancement using only a moderate amount of IV contrast material [31]. The first prospective study comparing CTPA with pulmonary angiography in 42 patients was published in 1992 and reported a 100% sensitivity and 96% specificity for the diagnosis of central PE [32]. The following year, Teigen et al. reported similar results with electron-beam computed tomography (EBCT) for the diagnosis of central PE in 86 patients [33]. Since those preliminary studies, CTPA dramatically improved the evaluation of pulmonary arteries in routine clinical practice. It has progressively gained widespread acceptance thanks to the ability to obtain a uniform opacification of pulmonary vessels down to 2–3 mm in diameter, and to analyze the peripheral pulmonary circulation with more anatomical details than those available with conventional studies. Since 2000 and the advent of multidetector-row CT, CTPA has become the one of the first-line tests in patients suspected of PE in many institutions or recommended diagnostic algorithms [34–36].

## 4.2.3 The CTPA Technique

### 4.2.3.1 Acquisition Protocols

Depending on the patient's clinical status and CT technology, a 3- to 40-s breathhold is required to scan the pulmonary vasculature. Hyperventilation before the start of the examination is recommended, to facilitate prolonged breath holds. Based on the breathhold capabilities of the patient, two acquisition protocols may be considered: (a) one enabling an optimal CT examination of the pulmonary arteries from the lung apex to the bases, but requiring 8- to 25-s breathhold according to whether single-slice or multidetector-row CT is used; and (b) a second protocol enabling scanning of dyspneic patients from the aortic arch to the level of the inferior pulmonary veins in a shorter period of time but at the expense of spatial resolution. The multidetector-row CT reduces examination time and reduces collimation, which increases the Z-axis resolution. It also reduces partial-volume averaging and increases total volume scanned, or influences favorably any combination of the factors listed above. Example of CT parameters for single-slice up to 16-multidetector-row CT scanners for eupneic and dyspneic patients are presented in Table 1. Using 64-multidetector-row CT, almost every patient is able to maintain a strict apnea of minimum 5 s, which is necessary to comply with the fastest examination protocol. When apnea cannot be maintained in a patient with severe lung impairment, acquisition should be performed while the patient is gently breathing. This will result nevertheless in a confident interpretation limited to the central vessels. Intubated patients referred from the intensive care units should have their ventilation manually suspended in deep inspiration for the duration of the acquisition. Thin collimation may result in increased signal-to-noise ratio, and 2- to 2.5-mm collimation may be indicated for large patients. Scanning the patient in a caudocranial or in a craniocaudal direction is not a major issue, as it does not affect the overall quality of the examination. Whenever possible, patients should be scanned at total lung capacity owing to the direct relationship between the quality of arterial opacification and the level of pulmonary arterial resistance [37].

**Table 1.** Suggested acquisition protocols for spiral CT imaging of pulmonary embolism

	Eupneic patient						Dyspneic patient					
	Single-slice CT		Multislice CT			Single-slice CT		Multislice CT				
			4,	8,	16 <sup>a</sup>			4,	8,	16 <sup>a</sup>		
Collimation (mm)	2		1	1.25	0.75	0.6	5		2.5	2.5	1.5	1.2
Table feed per revolution (mm)	4		7.2	17	18	16.3	10		18	34	36	32.6
Pitch	2		1.8	1.7	1.5	1.7	2		1.8	1.7	1.5	1.7
Z-axis coverage (cm)	10		30	30	30	30	10		30	30	30	30
Rotation time (s)	0.5	1	0.5	0.5	0.5	0.5	0.5	1	0.5	0.5	0.5	0.5
Breathhold duration (s)	12.5	25	20.8	8.8	8.3	9.2	5	10	8.3	4.4	4.2	4.6

<sup>a</sup> Data collected from different manufacturers

### 4.2.3.2 Contrast Medium Administration

A bolus of iodinated contrast medium is injected with an automatic injector. Different protocols of contrast medium administration have been reported, either low concentration/high volume or high concentration/low volume, resulting in a compromise between the quality of vascular enhancement and the total amount of iodine injected. The goal is to scan the region of interest in the limited time window at the peak enhancement phase of the pulmonary arteries. This is generally achieved by setting a fixed scan delay time varying from 15 to 25 s, depending on the hemodynamic status of the patient and the distance of the venous access to the pulmonary circulation. Clinical parameters are usually not helpful to predict the scan delay, which may show large variations [38]. The test-bolus technique, which consists of measuring the individual transit time from the puncture site to the pulmonary arteries following injection of 15 ml of contrast medium, adds to the total volume of contrast, and lengthens examination time and increases radiation dose [38]. Bolus-triggering software programs may become useful or necessary with the use of multidetector-row CT for precise timing of scanning and eventually reduction of the dose of contrast medium [39]. Increased flow concentration of iodine obtained when using high-concentration contrast material or high injection flow rate increases attenuation and visualization of peripheral pulmonary arteries, and potentially pulmonary emboli conspicuity [40, 41]. The advent of ultrafast CT may favor the use of gadolinium as contrast medium agent in patients with contraindications to iodine injection [42].

### 4.2.4 Image Interpretation

#### 4.2.4.1 Direct Demonstration of PE

The CTPA can demonstrate endoluminal clots, whereas pulmonary angiography and V/Q lung scan shows most commonly indirect signs of PE, such as a regional perfusion defect or abrupt cut-off of the pulmonary arteries [32]. Furthermore, central PEs are often more apparent on CTPA than on pulmonary angiography or V/Q lung scan [33, 43]. The vascular signs of acute PE on CTPA include (Figs. 1–4) [32, 44–46]:

- Central partial intravascular filling defect surrounded by contrast-medium (CM) presenting the “polo mint” sign when perpendicular to the long axis of the vessels or the “railway sign” when parallel to the long axis.
- Eccentric partial filling defect or mural defect surrounded by CM presenting an acute angle with the vessel wall.
- Complete filling defect not surrounded by CM and occupying the entire arterial vessel section. The corresponding artery is frequently dilated compared with the other side.

Occasionally, large and central PE are suspected at unenhanced CT, manifesting as hyper- or hypoattenuating filling defects (Fig. 5) [47]. Two studies reported detection of PE in main or lobar pulmonary arteries at unenhanced CT in 41–45% of patients with proved central PE at CTPA [47, 48].

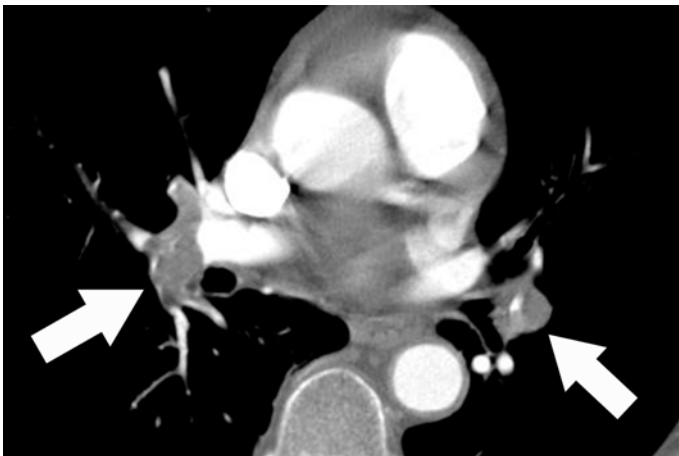


**Fig. 1.** Massive acute pulmonary embolism in an 85-year-old woman presenting with dyspnea. A 2-mm-thick-axial CT angiogram obtained with single slice CT demonstrates multiple clots in the central pulmonary arteries (*arrows*)

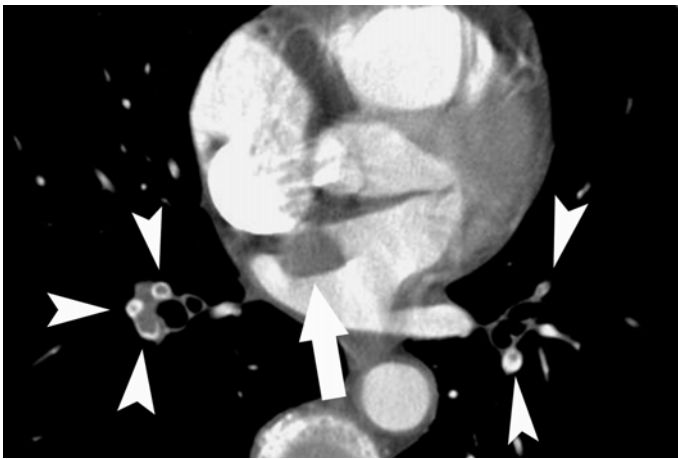


**Fig. 2.** Acute segmental pulmonary embolism and incidental demonstration of myxoma in a 70-year-old woman presenting with suspicion of pulmonary embolism 2-mm-thick axial CT angiogram obtained with single-slice CT demonstrates multiple acute clots in the segmental pulmonary arteries of both lower lobes (*arrowheads*). Note incidental demonstration of a mass in the left atrium appended to the inter-atrial septum corresponding to a myxoma (*arrow*)

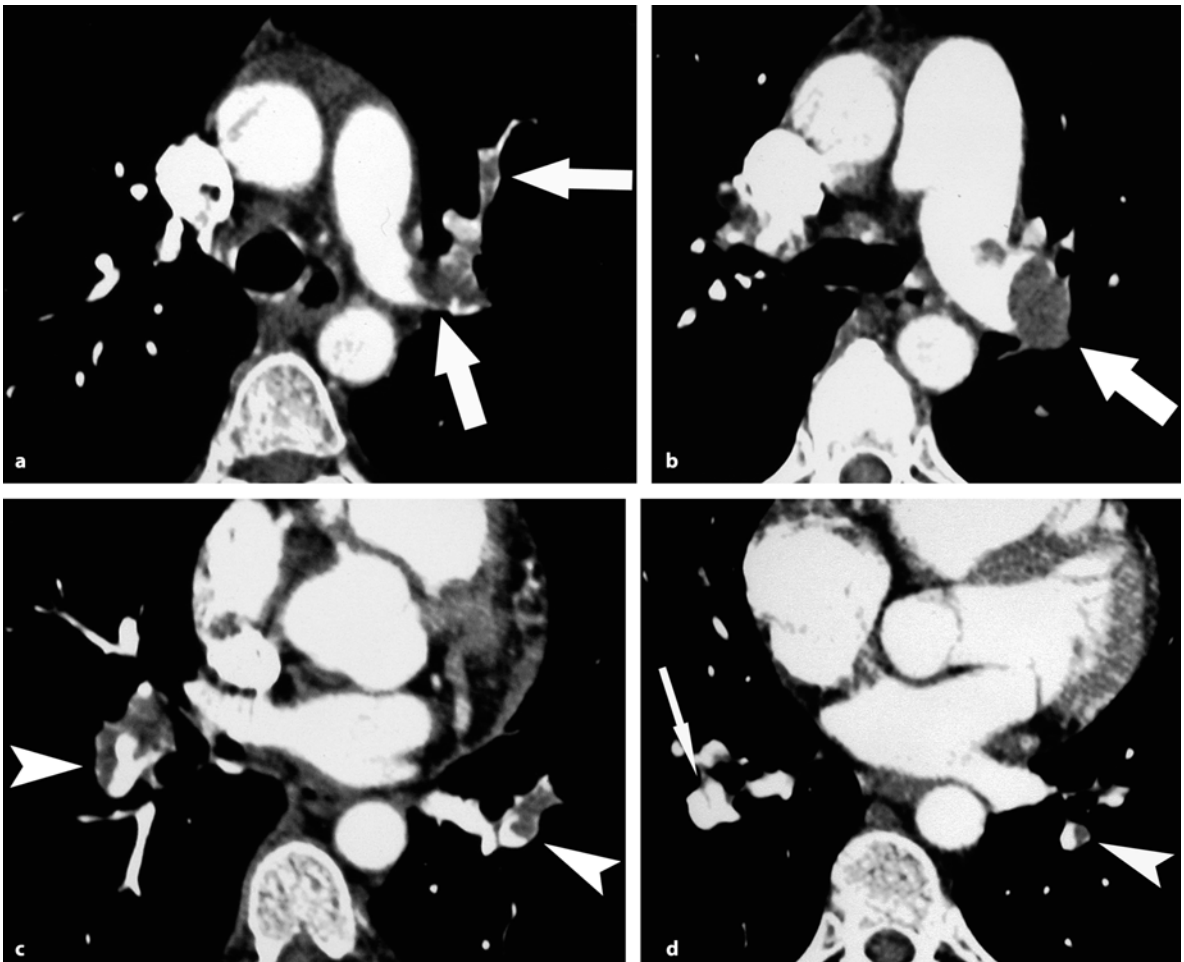


**Fig. 3.** Massive acute and subacute pulmonary embolism in a 56-year-old woman presenting with circulatory collapse syndrome and chest pain. **a–d** Four 1.25-mm-thick reconstructed axial CT angiograms obtained with multidetector row CT demonstrate multiple clots in the central and peripheral pulmonary arteries.

Acute clots (*arrows*) in the left pulmonary artery present as a filling defect in the column of contrast material, which forms an acute angle with the vessel wall. Older clots (*arrowheads*) adhere to the vessel wall or form an obtuse angle with the vessel wall. Intraluminal web is also depicted (*thin arrow*)

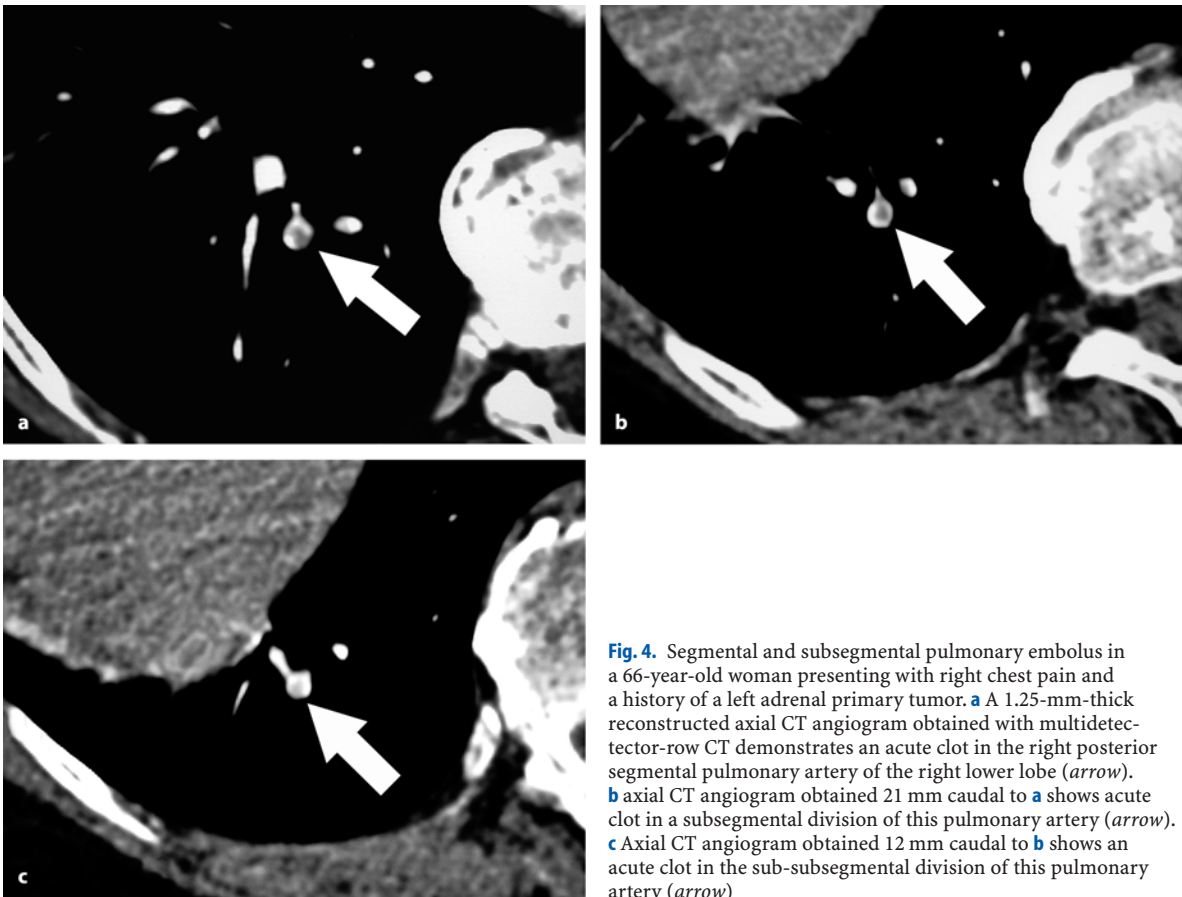


**Fig. 4.** Segmental and subsegmental pulmonary embolus in a 66-year-old woman presenting with right chest pain and a history of a left adrenal primary tumor. **a** A 1.25-mm-thick reconstructed axial CT angiogram obtained with multidetector-row CT demonstrates an acute clot in the right posterior segmental pulmonary artery of the right lower lobe (*arrow*). **b** axial CT angiogram obtained 21 mm caudal to **a** shows acute clot in a subsegmental division of this pulmonary artery (*arrow*). **c** Axial CT angiogram obtained 12 mm caudal to **b** shows an acute clot in the sub-subsegmental division of this pulmonary artery (*arrow*)

#### 4.2.4.2 Ancillary Findings

Computed tomography is also more sensitive than chest X-ray for demonstrating the ancillary findings related to PE [25, 49], as described below:

- The most commonly found ancillary finding is the wedge-shaped pleural-based consolidation corresponding to the Hampton's hump (Fig. 6). It is more frequently found in patients with PE than in patients without PE [50, 51]. Its frequency in patients with PE varied from 25 to 62% [50–53]. The CT-pathological correlation has demonstrated that the finding of a wedge-shaped opacity with a large pleural base and a truncated apex at CT is likely to represent pulmonary infarction with or without necrosis [54]. The contrast enhancement of the lesion after i.v. injection of contrast medium is related to pulmonary hemorrhage (76%), whereas a nonenhancing lesion corresponds to pulmonary infarct (24%) [50]. In more than 50% of pulmonary infarctions, low-attenuation areas may be seen within the lesion and represent preserved, uninfarcted secondary pulmonary lobules [54]. Nevertheless, the decreased enhancement in collapsed lung is not a specific sign of pulmonary infarct as it can be seen in some forms of pneumonia [55].

Wedge-shaped consolidation has typical lower lobe predominance [25, 50, 51, 54]. Infarction is uncommon in healthy patients and is more common in patients who have impaired bronchial collateral circulation or pulmonary venous hypertension, such as left ventricular dysfunction or shock [56, 57]. Wedge-shaped consolidation is also nonspecific as they may be seen in pneumonia, tumor, hemorrhage, edema, atelectasis, and fibrosis [58]. On the other hand, infarcts are not always wedge-shaped or subpleural on CT [25, 53, 54].

- The “vascular sign” is a thickened vessel leading to the apex of the consolidation, increasing the specificity for infarction, but is infrequent or difficult to recognize [54, 58].
- Other signs, such as non-wedge-shaped consolidation, areas of oligemia, atelectasis, linear bands, pleural effusion, and dilatation of central arteries have also been studied on CT. Atelectasis and pleural effusion are frequent but unspecific findings [50, 51, 53]. Only dilatation of the right main pulmonary artery and the left interlobar pulmonary artery and linear bands, representing opacities, <3 mm thick and perpendicular to the pleura, have been found most commonly in patients with PE in one study [50]. Especially, areas of oligemia are considered to be of limited utility for the diagnosis of acute PE [50, 53].



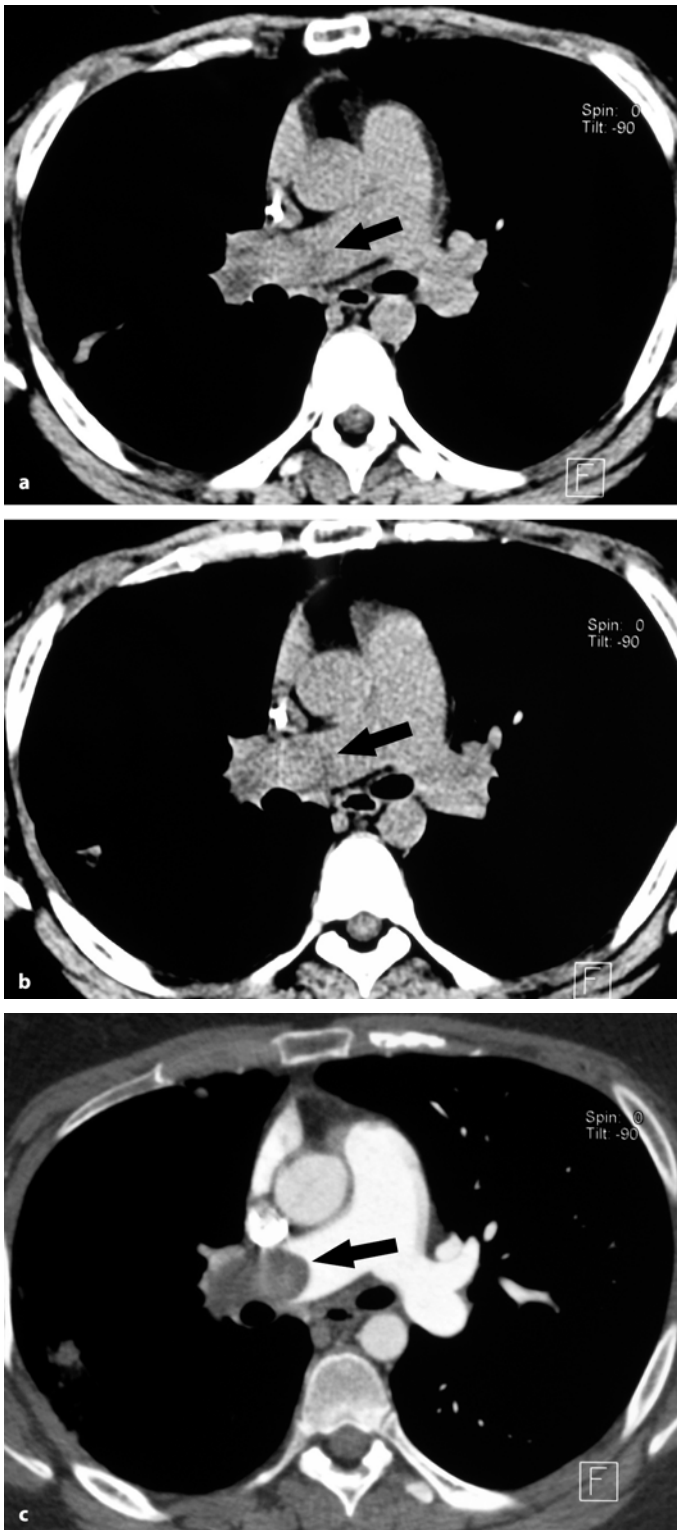


**Fig. 5.** Asymptomatic pulmonary embolism detected on unenhanced CT in a 26-year-old woman with a past history of metastatic sarcoma. **a, b** One-millimeter-thick reconstructed axial CT slices show large and central mixed hypo- and hyperattenuating filling defect in the right and interlobar pulmonary arteries (*arrows*). **c, d** Injection of contrast material confirmed the presence of emboli (*arrows*)



Fig. 5. (continued)

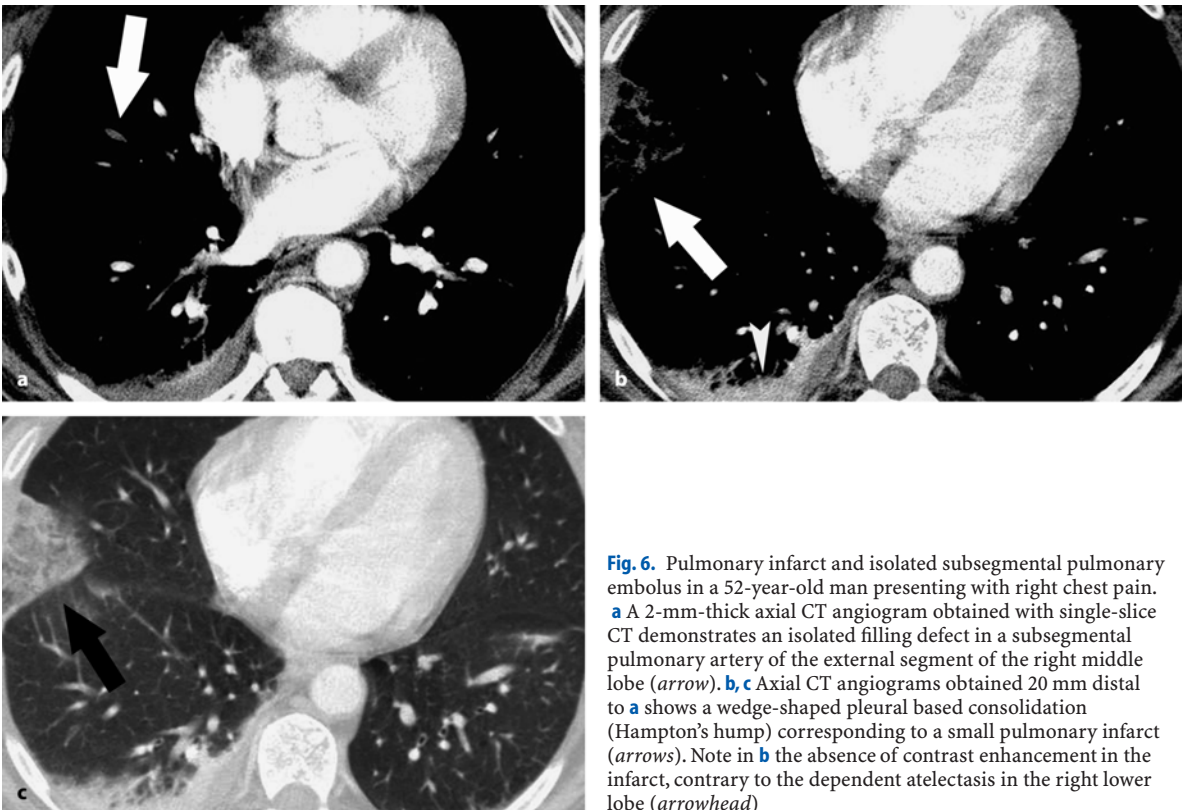


**Fig. 6.** Pulmonary infarct and isolated subsegmental pulmonary embolus in a 52-year-old man presenting with right chest pain. **a** A 2-mm-thick axial CT angiogram obtained with single-slice CT demonstrates an isolated filling defect in a subsegmental pulmonary artery of the external segment of the right middle lobe (*arrow*). **b, c** Axial CT angiograms obtained 20 mm distal to **a** shows a wedge-shaped pleural based consolidation (Hampton's hump) corresponding to a small pulmonary infarct (*arrows*). Note in **b** the absence of contrast enhancement in the infarct, contrary to the dependent atelectasis in the right lower lobe (*arrowhead*)

Whereas CT is more sensitive than chest X-ray for demonstrating ancillary findings, the absence of abnormalities on CT does not rule out PE, as 29% of the patients with PE had no pleuro-parenchymal abnormalities described on CT

[53]. All those studies are retrospective and the positive and negative predictive value of all ancillary findings have to be studied by large prospective studies.

**Table 2.** Criteria for the CT pulmonary angiography diagnosis of pulmonary embolism (PE). (Modified from [59])

Criteria	Acute PE	Subacute PE	Chronic PE
Filling defect	Central, eccentric, intraluminal; lack of opacification	Wall adherent (acute angle), convex; lack of opacification	Wall adherent (obtuse angle), concave; intraluminal webs; signs of thrombus recanalization; calcification; lack of opacification
Vascular wall			Irregular wall thickening
Intra-pulmonary vessels size	Dilated or normal	Dilated or normal	Variation in size of segmental vessels; abnormal proximal to distal tapering; complete retraction of segmental vessels (cut-off)
Parenchyma	Infiltration (hemorrhage) Round or wedge-shaped pleural-based consolidation	Pleural-based wedge-shaped consolidation	Translobular lines; plate-like atelectasis; mosaic perfusion; bronchial dilatation in abnormal areas
Pleura	Pleural effusion	Pleural effusion	Pleural effusion
Pulmonary hypertension	Right heart enlargement with normal wall thickness (<5 mm)	Right heart enlargement, interventricular septal shift; dilation of central pulmonary arteries	Right heart enlargement with thickening of the wall (> 5mm); negative axis of interventricular septum; dilation of central pulmonary arteries; dilation and tortuosity of bronchial or non-bronchial systemic arteries; pericardial effusion, ascite

### 4.2.5 Estimation of the Age of the Embolus

Differences in morphology of clots and arteries can be used to estimate the age of the thromboembolic event (Table 2) [59]. The CTPA is superior to V/Q scan in this setting (Fig. 3). In the Pioped study, 74% of patients with past history of PE and in whom a high-probability V/Q scan was obtained, actually had PE, whereas 91% of patients without a history of PE had PE [14].

## 4.2.6 Results

### 4.2.6.1 Sensitivity and Specificity

By comparing experimentally CTPA (1-mm collimation) and pulmonary angiography with a true gold standard (cast in a pig model), both techniques were comparable for detecting subsegmental-sized emboli [60]. Even until a few years ago, clinicians remained reluctant to acknowledge the effectiveness of single-slice CTPA [61, 62]. Reviewing the results of CTPA in the 1990s, the wide range of sensitivity and specificity may be related to differences in patients selection (nondiagnostic V/Q scan or discordance between V/Q scan and the level of clinical suspicion and/or normal US), extent of PE, extent of pulmonary vascular bed studied, methods of interpretation, and reader experience. Moreover, the most important factor affecting the results was the dramatic and continuous improvement of the spiral CT technology during this decade. Among others, early CT scan studies used a collimation of 5 mm, which resulted in partial-volume effect at the level of small-sized vessels and limited the detection of peripheral filling defects. For

5-mm collimation, results varied from 53 to 100% (sensitivity) and 67 to 100% (specificity). For 3-mm collimation, results varied from 67 to 92% and 91 to 100%, respectively, and for 2-mm collimation, results varied from 94 to 96% and 94 to 100%, respectively (Table 3) [23, 32, 63–86]. Using 1-mm collimation on multidetector CT, Coche et al. reported a sensitivity of 96% and a specificity and 98% [85].

### 4.2.6.2 Interobserver Variability

Good to excellent interobserver variability was demonstrated and compared favorably with pulmonary angiography and V/Q scan (Table 4). The interobserver agreement is significantly dependent of the technical quality of the examination for CTPA and PA, and independent for V/Q [87]. The interobserver variation was good to very good until the segmental level ( $K=0.72-0.90$ ) [46, 73, 82, 88] and until the subsegmental level ( $K=0.71-0.97$ ) [70, 79–81, 87, 86]. The interobserver agreement is nevertheless superior for proximal than distal level [84]. Although some authors found a considerable learning curve for interpreting CTPA, especially for the detection of small emboli [89, 90], excellent interobserver agreement was found for six observers with different levels of experience ( $K=0.85$ ) [46], between senior and junior CT radiologists without prior experience with CTPA ( $K=0.90$ ) [91] and between a senior and junior chest radiologist ( $K=0.97$ ) [81]. The intraobserver variation was also excellent ( $K=0.87-1.0$ ) [46, 92]. Multidetector-row CT using thin collimation significantly should improve the interobserver agreement as most causes of disagreement concern partial volume effects, small sized arteries, motion artifacts, and technically suboptimal examination [85, 92, 93].

**Table 3.** Published studies for the diagnosis of pulmonary embolism using CT pulmonary angiography

Reference	No. of patients	Collimation (mm)	Lowest anatomic level of interpretation	Sensitivity (%)	Specificity (%)
[32]	42	5	Segmental	100	96
[63]	10	5	Segmental	100	100
[64]	38	5	Segmental	100	100
[65]	25	5	Segmental	82	67
[66]	20	5	Segmental	86	92
			Subsegmental	63	89
[67]	33	5	Segmental	86	100
[68]	75	3–5	Segmental	91	78
[23]	28	5	Subsegmental	Five readers: 62–92 (75)	73–100 (89)
[69]	77	5	Subsegmental	95	97
[70]	149	5	Subsegmental	Observer 1: 94 Observer 2: 82	96 93
[71]	70	5	Segmental	90	96
			Subsegmental	86	92
[72]	164	5	Segmental	NA	NA
[73]	139	3	Segmental	87	95
[74]	49	5	Subsegmental	97	90
[75]	47	5	Segmental	Group A: 60 Group B: 53	81 97
[76]	26	3	Subsegmental	67	100
[77]	391	3 (2–5)	Subsegmental	Local reading: 95 Expert reading: 87	97 90
[78]	110	3	(Sub)segmental	92	96
[79]	179	2–3	Subsegmental	Observer 1: 94 Observer 2: 94	94 95
[80]	158	2.5 (MDCT)	Subsegmental	90	94
[81]	370	2–3	Subsegmental	96	100
[82]	299	3	Subsegmental	70	91
[83]	230	5	Segmental	86	NA
			Subsegmental	69	86
[84]	66	3	Subsegmental	Observer 1: 91 Observer 2: 88	81 86
[85]	94	1 (MDCT)	Subsegmental	96	98
[86]	93	2.5 (MDCT)	Subsegmental	100	89

**Table 4.** Interobserver variation for CT pulmonary angiography (CTPA), ventilation/perfusion (V/Q), and pulmonary angiography (PA)

Reference	CTPA	V/Q	PA
[73]	K=0.85	K=0.61	88%
[77]	K=0.72	K=0.39	K=0.46
[79]	K=0.72	K=0.22	K=0.83
[80]	K=0.86		K=0.78
[85]	K=0.94	K=0.94	K=0.66
[86]	K=0.71		K=0.83

#### 4.2.6.3 Comparison of CTPA and V/Q Scanning

In the Pioped study, 25–30% variation was reported for low- and intermediate-probability lung scan [14]. In studies including patients with nondiagnostic V/Q scan (some with further negative results for US of the lower limbs), CTPA demonstrated 14–44% of positive results for PE in this particular subgroup of patients [68, 69, 72, 76], which is similar to results (22%) obtained using pulmonary angiography

[14]. This confirmed that treatment decision in patients with nondiagnostic V/Q based on the clinical probability is not reliable. A correct diagnosis was provided with CTPA in 80% of the patients in which the V/Q scans were intermediate-probability [73]. Table 5 demonstrates comparison of results of CTPA and V/Q scan in patients with suspicion of acute PE. These correlative studies have demonstrated that the accuracy of CTPA is greater than V/Q. When the results of CTPA and V/Q scans were discordant, the interpretation of CTPA was correct in 92% [73]. Another study comparing CTPA and V/Q scans as the initial investigation for acute PE found a significant higher proportion of confident diagnosis when CTPA was used as the initial investigation (90 vs 54%) [95]. A review study compared a meta-analysis of seven single-slice CTPA studies with the V/Q scanning results in the Pioped study. Compared with high-probability lung scan, CTPA has a higher sensitivity (77–81 vs 41%) and a similar specificity. Compared with high- and intermediate-probability lung scan together, CTPA has similar sensitivity and higher specificity (91–98% vs 52%) [96]. Overall accuracy of CTPA is superior to V/Q lung scan and CTPA provides significantly higher rates of conclusive results [85, 96].



**Table 5.** Comparison of CTPA and V/Q scan. PPV positive predictive value, NPV negative predictive value

Reference	Diagnostic	Results				Conclusion
		Sensitivity (%)	Specificity (%)	PPV (%)	NPV (%)	
[73]	CTPA	87	95	NC	NC	CTPA is more accurate ( $p < 0.01$ )
	V/Q	65	94	NC	NC	
[94]	CTPA	75	90	93	90	CTPA is more accurate ( $p < 0.01$ )
	V/Q	49	74	96	85	
[78]	CTPA	92	96	NC	NC	NC
	V/Q	72	94	NC	NC	
[79]	CTPA	First observer: 94	94	95	96	CTPA performs better ( $p < 0.05$ )
	CTPA	Second observer: 94	95	95	97	
	V/Q	First observer: 81	74	82	76	
	V/Q	Second observer: 76	80	78	82	
[85]	CTPA	96	98	NC	NC	CTPA performs better ( $p < 0.05$ )
	V/Q	86	88	NC	NC	

#### 4.2.6.4 Subsegmental PE

The arteries beyond the segmental level are more difficult to interpret due to small vessel diameter, limited spatial resolution, insufficient enhancement, and spatial orientation of vessels and thrombi [59]. The CTPA has been criticized for its inability to detect subsegmental PE; however, this limitation also seems to be inherent to both pulmonary angiography and V/Q scanning [97–99]. It is well known from balloon-occlusion angiography studies that peripheral PE are missed during conventional angiography [100, 101]. In the Pioped study, all but one of the patients with subsegmental PE as the largest clot had low or intermediate results (non-diagnostic) [102]. Using a dual-slice CT, CTPA detected more subsegmental PE than pulmonary angiography (92 vs 56) and 75% of isolated PE seen at pulmonary angiography. In this setting, CTPA performed better than pulmonary angiography [80]. Nevertheless, using a four-row MDCT, another study reported that CT failed to demonstrate subsegmental PE in 53% of patients having subsegmental vessel involvement at pulmonary angiography [86].

#### Analyzability of Pulmonary Vessels

One of the main advantages of cross-sectional imaging is the absence of overlapping structure conversely to pulmonary angiography. Since its introduction, spiral CT technology has progressively improved and subsequently influenced the overall accuracy of CTPA in the evaluation of peripheral pulmonary arteries. Initially performed with a 5 mm collimation and 1-s rotation time, 78% of segmental arteries could be correctly analyzed with this protocol [72]. The reduction of the collimation to 3 mm with a pitch of 1.7 and 180° linear interpolator algorithm (actual slice thickness 3.86 mm) enables correct depiction of 85% of segmental arteries and 37–43% of subsegmental arteries. Reduction of the collimation to 2 mm with a pitch of 2 and

0.75 s rotation time (actual slice thickness 2.65 mm, which is more adapted to the evaluation of subsegmental arteries of 2–3 mm in diameter) further improves the analyzability of subsegmental arteries to 61–65% in both anatomical and clinical studies [103, 104]. The introduction of multi-detector-row CT offers further increase of performance, in particular the ability to scan larger anatomical volume with high spatial resolution. An anatomical study demonstrated that using 4×1 mm collimation, 0.5 s rotation time and a reconstruction slice thickness of 1.25 mm, 88.5% of the segmental arteries (namely 100% of these after excluding the anatomical variants) and 94% of subsegmental arteries (namely 96%) were correctly analyzable. Furthermore, 74% of subsegmental arteries and 35% of their division were also correctly depicted [105].

#### Frequency of Isolated Subsegmental PE

The correct diagnosis of acute PE with CTPA is improved by the presence of multiple emboli, whereas only one needs to be confidently recognized for the diagnosis. When a clot breaks off the deep veins of the leg and is washed to the lungs, it fragments in the right heart, showering the lung with emboli of variable size [20]; thus, PE splits into an average of 3–11 fragments with one or more large enough to be detected by CT [8, 32, 33, 51, 72, 79, 80, 106]. There is a wide range of reported isolated subsegmental embolus both on pulmonary angiography and on CTPA (6–30%). The true incidence of isolated PE is unknown even in studies using pulmonary angiography as the interobserver agreement at the subsegmental level varies from 13 to 66% [15, 98, 107]. It seems that in a broad selection of patients, <10% will have isolated subsegmental PE [14, 36, 68, 79–81, 84, 102, 108–110], whereas in highly selected population, limited clinical series or retrospective evaluation, higher frequency will be obtained [22, 66, 70, 106]. Nevertheless, large studies reported frequency of 2.3–5.9% of all patients and 12–24.4% of patients with proven acute PE [85, 92, 97, 111–113].

### Clinical Significance of Subsegmental PE

The clinical importance of subsegmental PE is controversial [120]. Small emboli are frequent and a healthy lung acts as a filter to protect the systemic circulation [20]. Its dual blood supply helps to preserve the integrity of the embolized segment. Small subsegmental PE has been untreated in angiographic studies with <1.6% of patients presenting with symptomatic PE in 6–12 months of follow-up [114]. In the Pioped population, among patients with only segmental arteries or smaller branches showing PE on pulmonary angiography, fatal and nonfatal events were non significantly different between untreated and treated patients [115]. In a recent study on 67 patients having isolated subsegmental PE at CTPA, no recurrent PE was observed at 3 months in the 42 patients that did not receive anticoagulation [112]. Nevertheless, small emboli can be of clinical importance in three settings. Firstly, they are relevant for patients with underlying impaired cardiopulmonary reserve [68, 116]. Secondly, they may be an important indicator for silent DVT, which potentially heralds more severe embolic events. Lower-limb investigation for DVT can be used as an alternative method in some patients with adequate cardiopulmonary reserve or a low or moderate clinical suspicion of VTE [117–119]. Thirdly, small emboli detection may be relevant for the diagnosis of chronic pulmonary hypertension in patients with thromboembolic disease, representing the “tip of the iceberg” [106].

Until this controversy is resolved (Will it ever be?), all PE must be considered important [66, 120]. One solution to determine the fate of those small missed or potentially missed clots is to evaluate the outcome of patients with negative CTPA, namely to determine the rate of subsequent PE (negative predictive value).

### Multidetector-Row CT

Four studies evaluated the benefit of multidetector-row CT on the detection of subsegmental PE. The first study compared single-slice CT (3-mm collimation) and multidetector-row CT (2.5-mm collimation) and found that the latter technique improved the conspicuity of peripheral arteries and identified significantly more peripheral filling defects. Improvements were attributed to the thinner collimation, faster scanning, and more homogeneous contrast enhancement using multidetector-row CT [121]. The second study assessed the influence of reconstructed slice thickness on the detection of subsegmental PE using multidetector-row CT. Following acquisition with 4×1-mm collimation, 1-mm-thick reconstructed sections allowed detection of 14 and 40% more of subsegmental PE compared with 2- and 3-mm-thick reconstructed sections, respectively. The benefit was more substantial for vessels with an oblique course to the scan plane (i.e., middle lobe and lingula). Diagnostic confidence, interobserver agreement, and reproducibility of findings were increased and the number of indeterminate results were decreased [93].

The third study evaluated the impact of multidetector-row CT on image quality and diagnostic value for PE compared with single-slice CT. The overall quality of CTPA was significantly higher using multidetector-row CT, particularly for subsegmental arteries. This was related to a higher spatial resolution along the longitudinal axis of the patient and to a decrease of respiratory and cardiac motion artifacts. Interestingly, accurate interpretation of subsegmental vessels was particularly improved in patients with underlying pulmonary disease, a patient population in which the diagnosis of PE is known to be difficult [122]. The fourth study compared single- (3 mm) and multidetector-row (1.25 and 2.5 mm) CT pulmonary angiograms (1.25 and 2.5 mm, respectively). The 1.25-mm collimation significantly improved visualization of subsegmental arteries and interobserver agreement in the detection of PE [123].

The traditional limitations of single-slice CT have been overcome with the advent of multidetector-row CT [124].

### 4.2.6.5 Negative Predictive Value of CTPA

Indeterminate results of CTPA generally means that PE can only be ruled out until the lobar level. Although most clinicians readily accept a CTPA-based positive diagnosis of PE, many are hesitant to accept a negative CTPA as a definite indication to exclude PE [125]. The majority of subsequent PE occur within the first weeks after treatment for PE or exclusion of PE: 50% of PE recurrence and 90% of PE-related death in treated patients occurred within 1–2 weeks [6, 126]; therefore, a mean follow-up of 3 months is acceptable to differentiate missed venous thromboembolism (VTE) and new episode of VTE in a high-risk patient. Nevertheless, the rate of subsequent VTE remains an indirect indicator of the false-negative rate of a test, as in patients with high risk factors a new episode of PE does not necessarily mean that the first test was a false negative [79]. The results of 23 series published in the literature are reported in Table 6. It appears that even single-slice CTPA is reliable for excluding clinically significant PE, even in patients with underlying respiratory disease [129, 139]. A meta-analysis performed in 2005 over 3500 patients showed a negative predictive value for VTE of 99.1% (95% CI 98.7–99.5%) and for VTE mortality of 99.4% (95% CI 98.7–99.9%) [140]. A negative CTPA excludes clinically significant VTE with the same level of confidence as negative pulmonary angiography (0–4.2%) [11, 36, 108, 114, 141–145] or even normal lung scintigraphy (0–0.7%) [89, 117, 125, 128, 146, 147].

**Table 6.** Follow-up of patients with negative CTPA

Reference	CT technology	Entry criteria	No. of patients	No. of patients with negative (or indeterminate) CTPA <sup>a</sup>	No. of nonanticoagulated patients with follow-up	Mean length of follow-up (months)	NVP (%)
[72]	SSCT	Nondiagnostic V/Q; normal US	164	125	109	3	94.6
[76]	SSCT	Clinical suspicion of PE	126	82	78	6	98.7
[127]	SSCT	Clinical suspicion of PE	143	113	100	6	100
[125]	SSCT	Clinical suspicion of PE; abnormal chest X-ray	393	285	198	3	99
[81]	SSCT	Clinical suspicion of PE	370	217 39 <sup>a</sup>	59 12	3	100 83.3 <sup>a</sup>
[99]	SSCT	Clinical suspicion of PE	305	244	215	3	98.6
[90]	SSCT	High clinical suspicion of PE; nondiagnostic V/Q	103	71	43	6	93–96
[128]	EBCT	Clinical suspicion of PE	1512	1010	993	3	99.5
[122]	SSCT MDCT	Clinical suspicion of PE	125 <sup>b</sup> 134 <sup>c</sup>	98 110	62 91	3	100 99
[129]	SSCT	Clinical suspicion of PE	334	253	185	12	98
[130]	SSCT	Clinical suspicion of PE	739	581	441	3	99.3
[109]	SSCT	Low or intermediate pretest clinical probability of PE, US	1041	525	507	3	98.2
[131]	SSCT	Clinical suspicion of PE, US	510	386	376	3	99.2
[132]	SSCT	Clinical suspicion of PE	62	51	41	3	95.1
[133]	SSCT	Clinical suspicion of PE	433	314	239	3	98.3
[134]	SSCT	Clinical suspicion of PE	209	132	99	3	99.1
[135]	SSCT	Clinical suspicion of PE; D-imer test, US	175	117	81	21±11	97.5
[136]	SSCT	Clinical suspicion of PE	485	325	220	>3	99.5
[137]	MDCT	Clinical suspicion of PE	102	85	79	9	98
[138]	SSCT MDCT	Clinical suspicion of PE; D-dimer test, US	965	458	406	3	98.3
[36]	MDCT	Clinical suspicion of PE; d-dimer test	756	562	523	3	98.5
[139]	SSCT MDCT	Clinical suspicion of PE	112 109	98 100	98 100	6	100 98
[110]	MDCT	Clinical suspicion of PE; d-dimer test	329	221	221	3	99.1

<sup>a</sup> Indeterminate results<sup>b</sup> Multidetector-row CT<sup>c</sup> Single-slice CT

#### 4.2.7 Interpretation Pitfalls

The correct interpretation of a CTPA examination requires a minimal experience and the knowledge of interpretative pitfalls. Interpretative pitfalls may be technique, anatomy or patient related [33, 37, 44, 45, 148]. They should be known by the radiologist but are easily recognized once the radiologist has gained experience. Technique-related pitfalls include inadequate selection of injection parameters, such as flow rate, concentration, and scan delay, or improper selection of the duration of the apnea, according to the patient's respiratory condition, both resulting in pseudo-

filling defects. The best compromise has to be chosen between high longitudinal spatial resolution and short duration of the apnea. Breathing artifacts can result in inhomogeneous opacification of pulmonary arteries in addition to hypodense doubling or blurring of vessel contour. Soft tissue reconstruction algorithms are mandatory, as high spatial frequency reconstruction algorithms, frequently used for imaging the thorax, show a high attenuation rim around vertically oriented vessels mimicking PE (Fig. 7). Image noise can degrade image quality, especially in heavy patients or in patients with large pleural effusion. Using a larger collimation or thicker reconstructed scans (i.e., 2.5 mm) may improve analysis of pulmonary arteries in

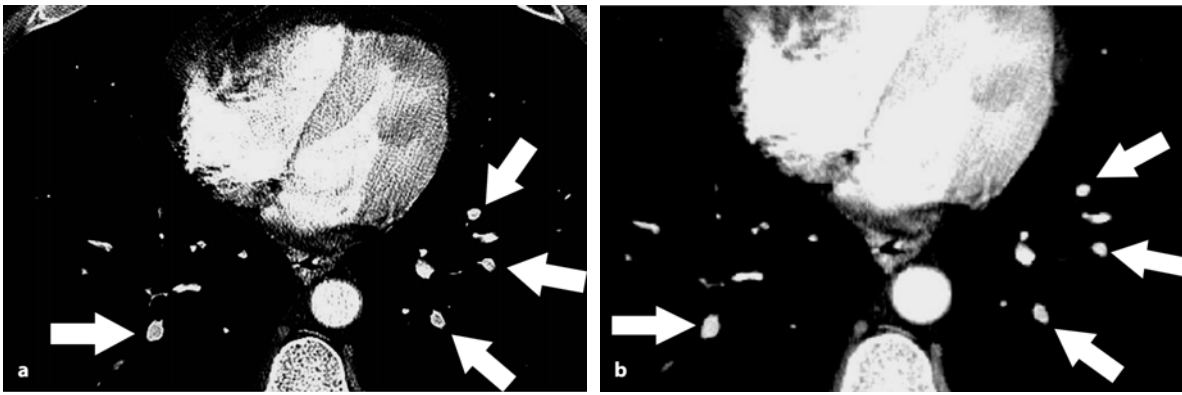


**Fig. 7.** Pseudo-filling defect with the use of high spatial frequency reconstruction algorithm mimicking pulmonary embolism. **a** A 2-mm-thick axial CT angiogram, reconstructed using a high spatial frequency algorithm, shows a high attenuation rim around verti-

cally oriented vessels, mimicking filling defects (*arrows*). **b** Same slice as **a**, reconstructed using a soft tissue algorithm. Pseudo-filling defects are no longer seen (*arrows*)

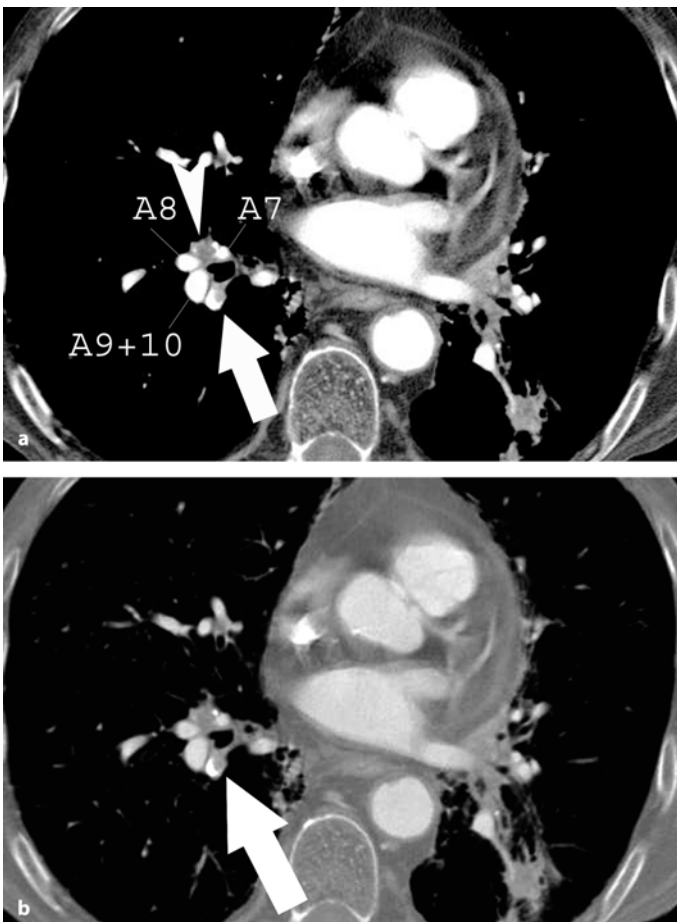


**Fig. 8.** Intersegmental lymph nodes mimicking pulmonary embolism in a 66-year-old man presenting with dyspnea. **a** A 2-mm-thick axial CT angiogram demonstrates a partially calcified lymph node mimicking a filling defect (*arrow*). Noncalcified lymph node is also demonstrated (*arrowhead*). A7 paracardiac segmental artery, A8 antero-basal segmental artery, A9+10 common trunk of latero-basal and postero-basal segmental arteries. **b** Same slice as **a** in bone window setting. The calcified lymph node (*arrow*) is well differentiated from contrast enhanced pulmonary arteries. CTPA showed no pulmonary embolism (not shown)

such cases. Beam-hardening artifacts from contrast in the superior vena cava may create pseudo-filling defects in the pulmonary arteries of the right upper lobe. Such artifacts may be reduced using a saline push immediately after con-

trast medium injection, which produces a washout of the contrast medium in the superior vena cava [149]. Central Swan-Ganz catheter that may also create pseudo-filling defects in the pulmonary arteries are easily recognized on





**Fig. 9.** Poor focal vascular enhancement due to peripheral systemic to pulmonary arteries shunt in a 63-year-old man. **a** A 5-mm-thick axial CT angiogram shows normal enhancement of the main and left pulmonary arteries (*thick arrows*) and left superior pulmonary vein (*thin arrow*), whereas right upper lobe pulmonary arteries and veins show poor contrast enhancement (*arrowheads*) which is similar to that of descending aorta. **b** A 5-mm-thick axial CT angiogram, located 3 cm cranial to **a** shows abnormal high contrast uptake of the subpleural tissue and pleura (*arrowheads*) on the right side, and dilated systemic vessels in the right axilla (*white arrow*). Note also dilated bronchial vessels in the mediastinum (*black arrow*). **c** A 5-mm-thick axial CT angiogram, shown in parenchymal window setting, demonstrates direct communications between parietal systemic vessels and pulmonary vessels (*arrowheads*) responsible for reversed flow within the pulmonary arteries of the right upper lobe (left-to-right shunt)

topogram, and should be placed in the heart or SVC before CTPA. Transient interruption of contrast enhancement may be observed over a substantial length of the acquisition, particularly when using multidetector-row CT. This artifact is likely related to inspiration and to unenhanced blood from the IVC entering the right heart and the pulmonary arteries [150].

Anatomical landmarks and variants should be known for accurate interpretation. Knowledge of the size and loca-

tion of intersegmental lymph nodes is important, as they frequently mimic mural filling defects for the inexperienced observer [151]. Sagittal or coronal reformatted images can help in difficult cases. Peripherally calcified lymph nodes exhibiting a hypodense center are seen on a few contiguous slices (Fig. 8). Knowledge of bronchovascular anatomy is also an important prerequisite, as veins may exhibit pseudo-filling defect due to slow flow and poor mixture of contrast material and unenhanced blood. Similarly,

dilated bronchial arteries in some patients may exhibit a peribronchovascular course simulating mural clots. In some conditions, the peribronchovascular soft tissues can enhance markedly, which may complicate differentiation between intra- and extravascular filling defect.

Finally, physiological or pathological factors related to the patient may influence the technique of CTPA or result in examinations difficult to interpret: superior vena cava obstruction, cardiomyopathy, focal or globally increased pulmonary resistance, and cardiac or pulmonary shunts may require longer scan delay, whereas circumferential perivascular edema or mucous plugging of small bronchi may simulate PE (Figs. 9, 13). Altering the window and the level can increase confidence in interpretation of a suspected filling defect, but it can also increase the conspicuity of artifacts caused by image noise, beam hardening, and motion.

#### 4.2.8 Severity Assessment of Pulmonary Embolism

Right heart failure is a major cause of mortality in patients with acute PE [152–164]. Obstruction of >30% of the pulmonary circulation causes sufficient elevation of the pulmonary vascular resistance to produce significant pulmonary hypertension resulting in RV afterload increase and dilatation [154, 155]. The cardiovascular effects of any acute PE must be regarded not only as the result of the degree of pulmonary vascular bed obstruction but also as the potential for RV to turn into a high-pressure pump. In other words, failure occurs if thin RV walls do not succeed in compensating for sudden elevation in parietal tension [162]. It is uncoupling of RV resources to pulmonary vascular load rather than obstruction index per se that leads to RV dilation and dysfunction, including successively decreased stroke volume, tricuspid regurgitation, reduced venous return, and finally, circulatory collapse.

Several recent studies have investigated multiple CT parameters to predict the prognosis of patients having PE [156–162]. Currently, CT parameters have to be classified in controversial or noncontroversial. In the noncontroversial parameters, quantitative cardiac CT measurements, such as the RV/LV short-axes ratio, have shown a significant correlation with the severity of PE [159] or with fatal outcome (Fig. 10) [160, 161]. When obtained on axial CT images, a RV/LV ratio >1.5 indicates a severe episode of PE [154, 159, 160–163]. When obtained on a reconstructed four-chamber view, a RV/LV ratio >0.9 was shown to be associated with a higher mortality rate [156].

On the other hand, the current literature shares some discrepancies regarding the potential of PA clot load scores, as described by Qanadli et al. or Mastora et al., to predict the prognosis of PE, probably due to differences in the populations studied in terms of severity of PE [157, 158,

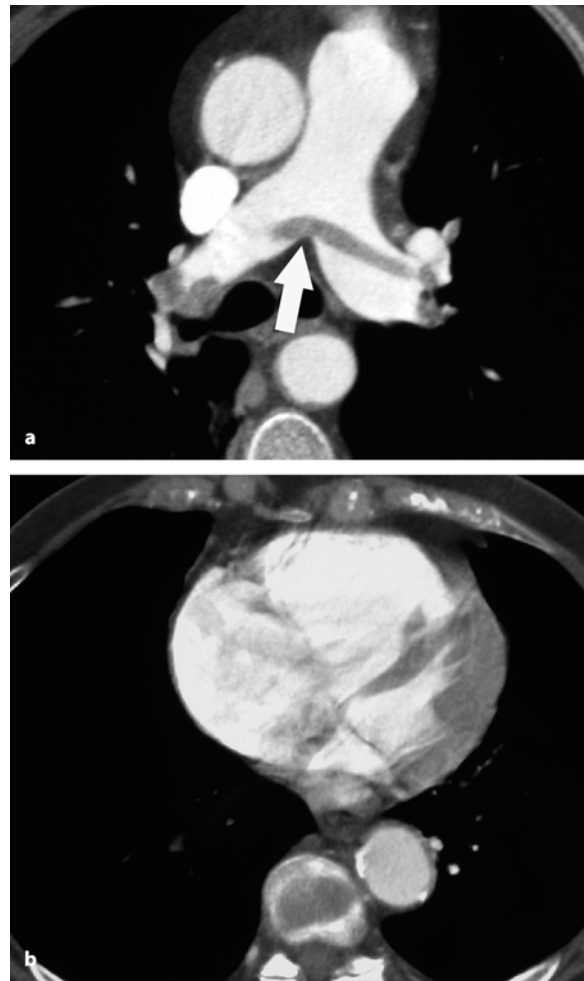


**Fig. 10.** Acute dilation of the right ventricle (RV) with leftward septal bowing in a 68-year-old woman presenting with severe dyspnea and severe hypotension. **a** A CT pulmonary angiography shows massive pulmonary embolism (*arrow*). The patient underwent a Trendelenburg intervention but eventually died during the first 24 h after admission. **b** Axial CT pulmonary angiogram at the level of the heart shows signs of cor pulmonale. Note the severe dilation of RV and the compression of left ventricle (LV), showing short axes of 59.4 and 24 mm, respectively. The RV/LV ratio was 2.5. Note also leftward bowing of the interventricular septum

160, 161, 164–166]. While PA clot load scores can be an indicator of the severity of the current episode of PE or treatment effectiveness, it seems that it cannot be used as a predictor of RV failure and death of the patient [157, 159, 160].

Pulmonary vascular resistance is not only related to mechanical obstruction by intravascular clot load, but can be further increased by the release of vasoactive agents from plasma, platelets or tissue, reflex pulmonary artery vasoconstriction, and systemic arterial hypoxemia occurring during pulmonary embolism [153, 155]. Furthermore, PA clot load scores do not consider clots located in small peripheral PA, possible unresolved previous episodes of PE,

emphysema, or other restrictive pleuro-parenchymal disease, which may contribute to an increase of pulmonary arterial pressure [155, 156, 160, 164–166].

The advent of multidetector CT and data acquisition coupled with ECG-gating recording is leading to the ability of providing dynamic and functional assessment of the RV. Two recent studies have assessed the feasibility of cardiac function measurement obtained on a retrospective ECG-gated multidetector CT angiography acquisition and have demonstrated that measurement of RV ejection fraction is reproducible and comparable to scintigraphic technique [167, 168]. Contiguous thin slices can be reconstructed every 5–10% of the R–R interval and RV and LV ejection fraction can be calculated by using dedicated 3D software. Work-in-progress is currently assessing if the measured ejection fraction of RV on CT pulmonary angiography can provide further refinements in the prediction of the outcome of patients with PE. New areas of research are dedicated to provide morphological and functional information of the effect of PE on lung perfusion using a single modality, similar to MR imaging [169–171]. The advent of the new generation of CT with increased number of detector rows and/or X-ray tubes should result in emergence of research on this topic.

#### 4.2.9 Alternative Diagnoses

One of the main advantages of CTPA is to provide alternative or additional diagnoses responsible for the symptoms of the patients that were not suggested by other diagnostic imaging, such as V/Q scan, pulmonary angiography, or US (Figs. 11–13). The CTPA demonstrated pleural or parenchymal abnormalities that could explain a defect seen at V/Q scanning with low or indeterminate-probability in 57% of patients [69]. The rate of alternative findings supporting alternative diagnoses varied from 11 to 85% [67, 72, 76, 78, 81, 85, 89, 94, 95, 129, 131, 132, 137, 172–174]. Alternative diagnoses are provided more frequently and with more precision than on pulmonary angiography [175]. The most common alternative diagnosis in patients without PE included pneumonia, atelectasis, pneumothorax, pneumomediastinum, pericardic or pleural effusion, aortic dissection, cardiovascular disease, interstitial lung disease, traumatic changes, post-operative changes, abscess, esophagitis, mucous plugging, bronchial infection, COPD, bronchopleural fistula, mediastinitis, arterial pulmonary hypertension, aspiration pneumonia, septic emboli, dia-

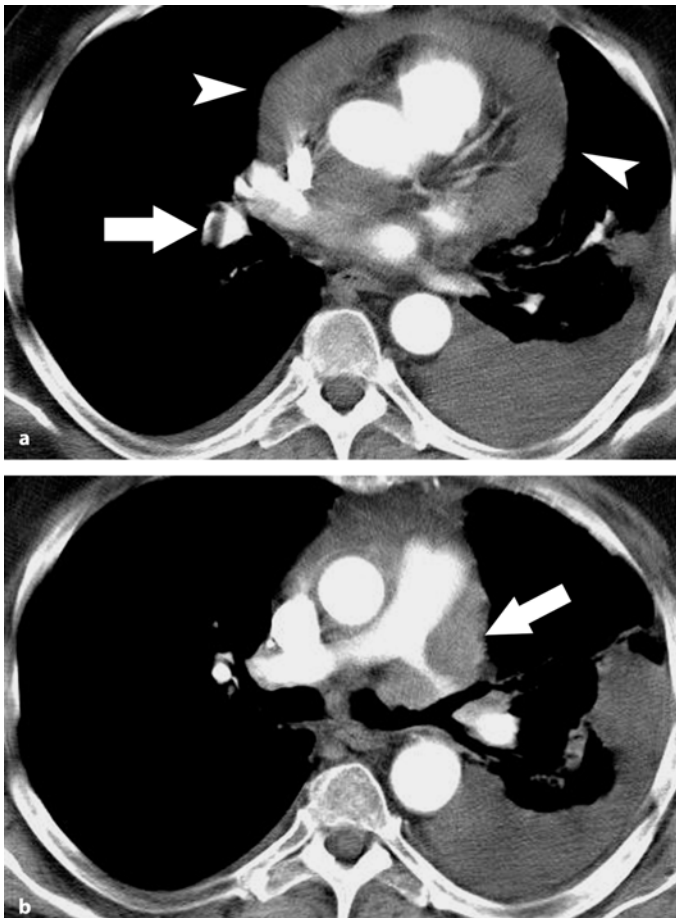


**Fig. 11.** Pulmonary emboli, cardiac tamponade, and central bronchogenic tumor demonstrated on CTPA in a 54-year-old man presenting with high clinical suspicion of pulmonary embolism and nondiagnostic V/Q lung scan. **a** A 5-mm-thick axial CT angiogram shows clot in the right lower lobe pulmonary artery (*arrow*) and large pericardial effusion (*arrowheads*). Note also left pleural effusion. **b** A 5-mm-thick axial CT angiogram 25 mm cranial to **a** reveals unsuspected bronchogenic tumor compressing the left pulmonary artery (*arrow*)

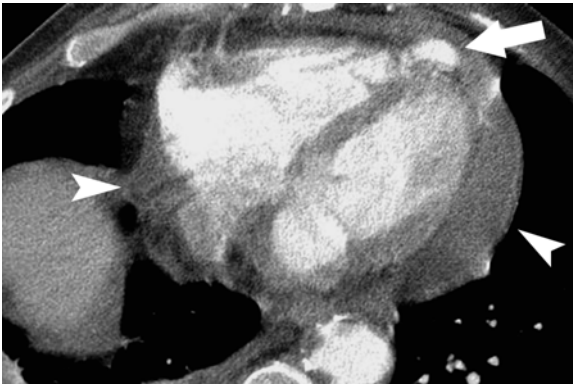


**Fig. 12.** Sudden dyspnea in a 60-year-old man with clinical suspicion of pulmonary embolism and a history of heart transplantation. A 2-mm-thick axial CT angiogram shows pericardial effusion (*arrowheads*) and cardiac pseudo-aneurysm (*arrow*). The patient had undergone endovascular myocardial biopsy a few days earlier



**Fig. 13.** Pulmonary edema in a 73-year-old woman suspected of having pulmonary embolism. A 2-mm-thick axial CT angiogram demonstrates peribroncho-vascular thickening (*arrowheads*) associated with bilateral pleural effusion and dilation of left atrium, findings highly suggestive of hemodynamic pulmonary edema, which was confirmed subsequently. No pulmonary embolism was seen

phragmatic hernia, esophageal rupture, malignancies, and even cardiac or coronary disease when ECG gating is used [176]. Nevertheless, alternative findings may be equally seen in patients with and without PE [51].

## 4.2.10 Other Advantages

### 4.2.10.1 Wide Availability

The CTPA is a routine 24 h/day technique. The CT scan is more readily accessible than a nuclear medicine study. This is one of the main reasons for considering CTPA as the first choice for the diagnosis of PE in many institutions [35].

### 4.2.10.2 Rapidity

The average time for CTPA is 10 min and for V/Q scan 45 min; therefore, the time spent outside the ward is far less for patients undergoing CTPA rather than V/Q scan, a difference that can be extremely important in critically ill patients requiring special care and monitoring [174, 177].

### 4.2.10.3 Minimally Invasive Technique

The CTPA obviates the complications encountered by heart catheterization in pulmonary angiography in high-risk patients.

### 4.2.10.4 Cost-Effectiveness

There is evidence that the use of CTPA in the diagnostic work-up of PE is cost-effective [177, 178]. The CTPA is less expensive than V/Q (1.4 fold) and pulmonary angiography (two to eight fold) although it can vary among institutions and countries [179, 180]. Using a study model, the cost-effectiveness of various algorithms for PE diagnosis was evaluated including V/Q scan, D-dimer assay, pulmonary angiography, lower-limb vein US, and single-slice CTPA. They analyzed the probability of PE and DVT, the accuracy and complications of the different modalities, the prognosis in treated and untreated patients, and the cost of diagnosis and treatment. The five strategies with the lowest mortality rate at 3 months and the lowest associated cost-per-life-saved included CTPA, usually in combination with examination of the lower limbs (US) [178]. Further refinements of this model concluded that the most cost-effective approach was US of the lower limbs followed by single-slice CTPA if the US findings were negative [181]. A slightly different study model found that the use of single-slice CTPA without or without US of lower limbs as a first line test was associated with the highest expected survival, but at a higher cost compared with other diagnostic strategies [182]. Difficulties in such study models are large variations in the cost of different tests (i.e., V/Q lung scan) and in the current performance of an evolving test (i.e., CTPA). Despite being one of the most important advantages compared with other diagnostic methods, the ability of CTPA to provide alternative diagnoses was not considered. As patient survival is primarily influenced by sensitivity of CTPA, even better results can be expected with multidetector-row CT. Perrier et al. demonstrated that, in opposition to single-slice CTPA, multidetector CTPA is the most cost-effective strategy when combined with D-dimer test and lower extremity US [183].



#### 4.2.10.5 Follow-up

The CTPA may be useful for evaluating the resolution and recanalization of emboli [26, 32, 64, 184, 185]. Although perfusion lung scans are commonly used for this purpose, changing patterns of perfusion may be misleading in some patients with central clots. The dissolution and fragmentation of central emboli with a peripheral migration can lead to an apparent worsening of perfusion defects with chest pain and a misleading diagnosis of recurrent PE [8, 186].

#### 4.2.11 Limitations of CTPA

##### 4.2.11.1 Contraindications to Iodinated Contrast Medium Injection

Renal failure, allergic reaction to contrast medium, and severe heart failure may account for a contraindication in 2.4–12% of the patients [72, 104]. The use of gadolinium as a contrast medium agent may be effectively used in the future with multidetector-row CT [42].

##### 4.2.11.2 Moderate Amount of Irradiation

The radiation exposure of CTPA may be up to four times lower than that of classical pulmonary angiography depending on CT technique or technology used [187–189]. The CTPA is responsible of a higher effective dose of irradiation than V/Q lung scan [190]; however, CTPA provides less radiation dose to the fetus compared with lung perfusion scanning [191]. Reducing the collimation may be associated with a substantial increase in the radiation dose delivered to the patient, particularly with the use of multidetector-row CT [93]. As CTPA is increasingly performed in patients suspected of PE, the collective radiation dose while ruling out PE is increasing [189]. Dose reduction in accordance with patient's body size is therefore needed. The use of adaptive modulation of dose system can result in substantial dose savings without compromising the image quality. Studies on "low-dose" CT angiograms by reducing mAs or other parameters are needed [192].

##### 4.2.11.3 Inconclusive Examinations

The most common reasons for inconclusive examinations are poor contrast enhancement of pulmonary arteries, motion artifacts, and excessive image noise in obese patient. The range of failed or indeterminate CTPA is reported between 2 and 13% [46, 68, 69, 70, 73, 78–82, 84, 85, 89, 90, 92, 94, 99, 109, 110, 112, 122, 127, 129, 131, 136, 138]. This contrasts with the rate of nondiagnostic V/Q scan, which

varies considerably (within the range of 30–80%) and is in the same range of nondiagnostic pulmonary angiography (0–17%) [14, 15, 108, 142–144, 193, 194]. Technical problems are encountered in <3% of the patients [81]. Inconclusive examinations are usually related to breathing artifacts (very dyspneic patients are allowed to breath quietly during acquisition), poor signal-to-noise ratio, and insufficient opacification of pulmonary arteries, which may occur in 1–10% of cases [44, 68–70, 78]. The use of thin sections (1 mm) significantly decreases the number of arteries classified as indeterminate and improves interobserver agreement in detection of PE [85, 92, 93, 105, 123].

##### 4.2.11.4 Large Number of Images

The total number of images resulting from CTPA are in the range of 100–200 using single-slice CT and 500–1500 using multidetector-row CT. The use of monitor reading has become essential for the analysis of pulmonary arteries, using cine-mode or scroll-through viewing, and has resulted in an increased detection rate of PE [30, 125]. Monitors are also helpful for multiplanar reconstruction (MPRs) for differentiation of intra- and extravascular structures and for improvement of diagnostic confidence [195]. Double screen monitors presenting simultaneously the acquisition in mediastinal and parenchymal windows can provide more accurate diagnosis, impeding false-positive results due to artifacts caused by respiratory or vascular artifacts. Window settings should also be adapted to the degree of vascular enhancement, in order not to miss small emboli [196]. Computer-aided detection of PE is currently under evaluation and may be helpful in the future to identify pulmonary emboli in large CTPA data sets [197].

##### 4.2.11.5 Small Size or Obliquely Oriented Arteries

Arteries from the lingula remain the most difficult to interpret due to their small caliber, oblique or horizontal course, or susceptibility to cardiac artifacts. Multidetector-row CT with the adjunct of cardiac gating should improve analysis of the vessels, although no additional relevant information for PE diagnosis was gained when using a ECG-gated eight-slice CT in one study [198].

#### 4.2.12 CT of PE in Emergency Conditions

In patients presenting with acute clinical signs of PE, chest X-ray and ECG are usually obtained to look for other conditions that may account for the patient's symptoms [34, 199]. D-dimers assay, a low-cost test with a high negative predictive value, may be used to safely rule out PE in patients with a low or intermediate clinical suspicion [82, 138, 109, 110].

Positive US of the lower limbs is usually sufficient to initiate anti-coagulant treatment, whereas a negative result does not exclude PE. In hemodynamically unstable patients with clinical suspicion of PE, bedside echocardiography appears to be an appropriate initial diagnostic test to evidence right ventricular overload, which is frequently associated with massive PE, and to demonstrate clots in cardiac cavities or in central pulmonary arteries, or other conditions, such as pericardial tamponade, acute valvular disease, myocardial infarction, or aortic dissection [74]. Nevertheless, CTPA is an appropriate initial diagnostic test to directly identify the presence and extent of PE in patients with intermediate or high clinical suspicion of PE in emergency conditions [199].

In the Pioped study, three major clinical presentations were encountered in patients with PE and with no history of cardiopulmonary disease. The pulmonary infarction syndrome (pleuritic pain or hemoptysis), the isolated dyspnea syndrome (dyspnea in the absence of pleuritic pain, hemoptysis, or circulatory collapse), and circulatory collapse syndrome (loss of consciousness or blood pressure <80 mm Hg) were seen in 65, 22, and 8% of the patients, respectively. Patients with circulatory collapse or isolated dyspnea had more severe angiographic scores than patients with pulmonary infarction syndrome. The severity of PE increased from mild, with the pulmonary infarction syndrome, to moderate, with the isolated dyspnea syndrome, and to severe with the circulatory collapse syndrome [200]. In patients presenting with circulatory collapse, severe dyspnea or in uncooperative patient, the presence of central emboli up to the segmental vessels must be evaluated in a few seconds. For this purpose, acquisition with 4×2.5 mm collimation allows scanning of the entire thorax in 8 s with optimal image quality [124]. In patient with pulmonary infarction syndrome or poor cardiopulmonary reserve, acquisition with 4×1 mm would increase the detection of small segmental or subsegmental clots within a 20 s breathhold. Scanning time will probably not be longer a limitation with the new generation of multi-detector-row CT with <0.4 s rotation time.

### 4.2.13 Conclusion

Positive results are widely accepted as accurate demonstration of PE, but negative results are still interpreted cautiously by some authors. The ability to provide alternative diagnoses in patients without PE is an undisputed advantage of CT. Examination of the leg veins may be indicated in negative CT. The widespread use of multidetector-row CT is expected to increase overall accuracy of the test. Follow-up studies of patients without anticoagulation are mandatory. The CTPA should be considered the initial imaging modality of choice, particularly in patients subgroups, which are known to be associated with a high rate of nondiagnostic V/Q scans, such as in-patients, patients with a history of cardiopulmonary disease, or abnormal chest X-ray.

## References

1. Goldhaber SZ, Elliott CG. Acute pulmonary embolism. Part I: epidemiology, pathophysiology, and diagnosis. *Circulation* 2003;108:2726–2729
2. Lindblad B, Sternby NH, Bergqvist D (1991) Incidence of venous thromboembolism verified by necropsy over 30 years. *Br Med J* 302:709–711
3. Stein PD, Henry JW (1995) Prevalence of acute pulmonary embolism among patients in a general hospital and at autopsy. *Chest* 108:978–981
4. Patriquin L, Khorasani R, Polak JF (1998) Correlation of diagnostic imaging and subsequent autopsy findings in patients with pulmonary embolism. *Am J Roentgenol* 171:347–349
5. Dalen JE, Alpert JS (1975) Natural history of pulmonary embolism. *Progr Cardiovasc Dis* 17:259–270
6. Carson JL, Kelley MA, Duff A et al. (1992) The clinical course of pulmonary embolism. *N Engl J Med* 326:1240–1245
7. Matsumoto AH, Tegtmeier CJ (1995) Contemporary diagnostic approaches to acute pulmonary emboli. *Radiol Clin North Am* 33:167–183
8. Urokinase Pulmonary Embolism Trial (1973) A National Cooperative Study. *Circulation* 47 (Suppl 2):1–108
9. Gervin AS (1975) Complications of heparin therapy. *Surg Gynecol Obstet* 140:789–796
10. Kashan J, Conti S, Blaisdell FW (1980) Heparin therapy for deep venous thrombosis. *Am J Surg* 140:836–840
11. Cheely R, McCartney WK, Perry JR et al. (1981) The role of noninvasive tests versus pulmonary angiography in the diagnosis of pulmonary embolism. *Am J Med* 70:17–22
12. Fihn SD, McDonnell M, Martin D et al. (1993) Risk factors for complications of chronic anticoagulation. A multicenter study. Warfarin optimized outpatient follow-up study group. *Ann Intern Med* 118:511–520
13. Landefeld CS, Beyth RJ (1993) Anticoagulant-related bleeding: clinical epidemiology, prediction and prevention. *Am J Med* 95:315–328
14. Pioped Investigators (1990) Value of the ventilation/perfusion scan in acute pulmonary embolism. Results of the Prospective Investigation of Pulmonary Embolism Diagnosis (PIOPED). *J Am Med Assoc* 263:2753–2759
15. Stein PD, Athanasoulis C, Alavi A et al. (1992) Complications and validity of pulmonary angiography in acute pulmonary embolism. *Circulation* 85:462–468
16. Henschke CI, Mateescu I, Yankelevitz DF (1995) Changing practice patterns in the workup of pulmonary embolism. *Chest* 107:940–945
17. Schluger N, Henschke C, King T et al. (1994) Diagnosis of pulmonary embolism at a large teaching hospital. *J Thorac Imaging* 9:180–184
18. Sostman HD, Ravin CE, Sullivan DC, Mills SR, Glickman MG, Dorfman GS (1982) Use of pulmonary angiography for suspected pulmonary embolism: influence of scintigraphic diagnosis. *Am J Roentgenol* 139:673–677
19. Khorasani R, Gudas TF, Nikpoor N, Polak JF (1997) Treatment of patients with suspected pulmonary embolism and intermediate-probability lung scans: Is diagnostic imaging underused? *Am J Roentgenol* 169:1355–1357
20. Gurney JW (1993) No fooling around: direct visualization of pulmonary embolism. *Radiology* 188:618–619
21. Gefter WB, Hatabu H, Holland GA, Gupta KB, Henschke CI, Palevsky HI (1995) Pulmonary thromboembolism: recent developments in diagnosis with CT and MR imaging. *Radiology* 197:561–574
22. Goodman LR, Lipchik RJ (1996) Diagnosis of acute pulmonary embolism: time for a new approach. *Radiology* 199:25–27
23. Sostman HD, Layish DT, Tapson FV et al. (1996) Prospective comparison of helical CT and MR imaging in clinically suspected acute pulmonary embolism. *J Magn Reson Imaging* 6:275–281

24. Oudkerk M, van Beek EJ, Wielopolski P et al. (2002) Comparison of contrast-enhanced magnetic resonance angiography and conventional pulmonary angiography for the diagnosis of pulmonary embolism: a prospective study. *Lancet* 359:1643–1647
25. Sinner WN (1978) Computed tomographic patterns of pulmonary thromboembolism and infarction. *J Comput Assist Tomogr* 2:395–399
26. Godwin JD, Webb WR, Gamsu G, Ovenfors CO (1980) Computed tomography of pulmonary embolism. *Am J Roentgenol* 135:691–695
27. Breatnach E, Stanley RJ (1984) CT diagnosis of segmental pulmonary artery embolus. *J Comput Assist Tomogr* 8:762–764
28. Verschakelen JA, Vanwijck E, Bogaert J, Baert AL (1993) Detection of unsuspected central pulmonary embolism with conventional contrast-enhanced CT. *Radiology* 188:847–850
29. Winston CB, Wechsler RJ, Salazar AM, Kurtz AB, Spirn PW (1996) Incidental pulmonary emboli detected at helical CT: effect on patient care. *Radiology* 201:23–27
30. Gosselin MV, Rubin GD, Leung AN, Huang J, Rizk NW (1998) Unsuspected pulmonary embolism: prospective detection on routine helical CT scans. *Radiology* 208:209–215
31. Vock P, Soucek M, Daepf M, Kalender WA (1990) Lung: spiral volumetric CT with single-breathhold technique. *Radiology* 176:864–867
32. Remy-Jardin M, Remy J, Wattinne L, Giraud F (1992) Central pulmonary thromboembolism: diagnosis with spiral volumetric CT with the single-breathhold technique: comparison with pulmonary angiography. *Radiology* 185:381–387
33. Teigen CL, Maus TP, Sheedy PF, Johnson CM, Stanson AW, Welch TJ (1993) Pulmonary embolism: diagnosis with electron-beam CT. *Radiology* 188:839–845
34. Schoepf UJ, Goldhaber SZ, Costello P (2004) Spiral computed tomography for acute pulmonary embolism. *Circulation* 109:2160–2167
35. Goldhaber SZ (2005) How chest CT for the diagnosis of pulmonary embolism (PE) has changed my professional life: reflections from a PE doctor. *Semin Roentgenol* 40:8–10
36. Perrier A, Roy PM, Sanchez O et al. (2005) Multidetector-row computed tomography in suspected pulmonary embolism. *N Engl J Med* 352:1760–1768
37. Remy-Jardin M, Remy J, Artaud D, Deschildre F, Fribourg M, Beregi JP (1997) Spiral CT of pulmonary embolism: technical considerations and interpretive pitfalls. *J Thorac Imaging* 12:103–117
38. Hartmann IJ, Lo RT, Bakker J, De Monye W, Van Waes PF, Pattynama PM (2002) Optimal scan delay in spiral CT for the diagnosis of acute pulmonary embolism. *J Comput Assist Tomogr* 26:21–25
39. Kirchner J, Kickuth R, Laufer U, Noack M, Liermann D (2000) Optimized enhancement in helical CT: experiences with a real-time bolus tracking system in 628 patients. *Clin Radiol* 55:368–373
40. Fleischmann D (2003) High-concentration contrast media in MDCT angiography: principles and rationale. *Eur Radiol* 13 (Suppl 3):N39–N43
41. Schoellnast H, Deutschmann HA, Fritz GA, Stessel U, Schaffler GJ, Tillich M (2005) MDCT angiography of the pulmonary arteries: influence of iodine flow concentration on vessel attenuation and visualization. *Am J Roentgenol* 184:1935–1939
42. Remy-Jardin M, Dequiedt P, Ertzbischoff O et al. (2005) Safety and effectiveness of gadolinium-enhanced multi-detector row spiral CT angiography of the chest: preliminary results in 37 patients with contraindications to iodinated contrast agents. *Radiology* 235:819–826
43. Enzweiler CN, Wiese TH, Lembcke AE et al. (2002) Electron beam tomography of interpulmonary saddle embolism: extent and vascular distribution. *J Comput Assist Tomogr* 26:26–32
44. Kuzo RS, Goodman LR (1997) CT evaluation of pulmonary embolism: technique and interpretation. *Am J Roentgenol* 169:959–965
45. Hansell DM (1997) Spiral computed tomography and pulmonary embolism: current state. *Clin Radiol* 52:575–581
46. Chartrand-Lefebvre C, Howarth N, Lucidarme O et al. (1999) Contrast-enhanced helical CT for pulmonary embolism detection: inter- and intraobserver agreement among radiologists with variable experience. *Am J Roentgenol* 172:107–112
47. Kanne JP, Gotway MB, Thoongsuwan N, Stern EJ (2003) Six cases of acute central pulmonary embolism revealed on unenhanced multidetector CT of the chest. *Am J Roentgenol* 180:1661–1664
48. Cobelli R, Zompatori M, De Luca G, Chiari G, Bresciani P, Marcato C (2005) Clinical usefulness of computed tomography study without contrast injection in the evaluation of acute pulmonary embolism. *J Comput Assist Tomogr* 29:6–12
49. Lourie GL, Pizzo SV, Ravin C, Putnam C, Thompson WM (1982) Experimental pulmonary infarction in dogs. A comparison of chest radiograph and computed tomography. *Invest Radiol* 17:224–232
50. Coche EE, Müller NL, Kim KI, Wiggs BR, Mayo JR (1998) Acute pulmonary embolism: ancillary findings at spiral CT. *Radiology* 207:753–758
51. Shah AA, Davis SD, Gamsu G, Intriere L (1999) Parenchymal and pleural findings in patients with and patients without acute pulmonary embolism detected at spiral CT. *Radiology* 211:147–153
52. Chintapalli K, Thorsen K, Olson DL, Goodman LR, Gurney J (1988) Computed tomography of pulmonary thromboembolism and infarction. *J Comput Assist Tomogr* 12:553–559
53. Johnson PT, Wechsler RJ, Salazar AM, Fisher AM, Nazarian LN, Steinter RM (1999) Spiral CT of acute pulmonary thromboembolism: evaluation of pleuroparenchymal abnormalities. *J Comput Assist Tomogr* 23:369–373
54. Balakrishnan J, Meziane MA, Siegelman SS, Fishman EK (1989) Pulmonary infarction: CT appearance with pathologic correlation. *J Comput Assist Tomogr* 13:941–945
55. Donnelly LF, Klosterman LA (1997) Pneumonia in children: decreased parenchymal contrast enhancement: CT sign of intense illness and impending cavitory necrosis. *Radiology* 205:817–820
56. Dalen JE, Haffajee CI, Alpert JS, Howe JP, Ockene IS, Paraskos JA (1977) Pulmonary embolism, pulmonary hemorrhage and pulmonary infarction. *N Engl J Med* 296:1431–1435
57. Greaves SM, Hart EM, Brown K, Young DA, Batra P, Aberle DR (1995) Pulmonary thromboembolism: spectrum of findings on CT. *Am J Roentgenol* 165:1359–1363
58. Ren H, Kuhlman JE, Hruban RH, Fishman EK, Wheeler PS, Hutchins GM (1990) CT of inflation-fixed lungs: wedge-shaped density and vascular sign in the diagnosis of infarction. *J Comput Assist Tomogr* 14:82–86
59. Kauczor HU, Heussel CP, Thelen M (1999) Update on diagnostic strategies of pulmonary embolism. *Eur Radiol* 9:262–275
60. Baile EM, King GG, Muller NL et al. (2000) Spiral computed tomography is comparable to angiography for the diagnosis of pulmonary embolism. *Am J Respir Crit Care Med* 161:1010–1015
61. Rathbun SW, Raskob GE, Whitsett TL (2000) Sensitivity and specificity of helical computed tomography in the diagnosis of pulmonary embolism: a systematic review. *Ann Intern Med* 132:227–232
62. Mullins MD, Becker DM, Hagspiel KD, Philbrick JT (2000) The role of spiral volumetric computed tomography in the diagnosis of pulmonary embolism. *Arch Intern Med* 160:293–298
63. Blum AG, Delfau F, Grignon B et al. (1994) Spiral-computed tomography versus pulmonary angiography in the diagnosis of acute massive pulmonary embolism. *Am J Cardiol* 74:96–98
64. Steiner P, Phillips F, Wesner D, Lund GK, Kreymann G, Nicolas V, Crone-Munzebrock W (1994) Primary diagnosis and follow-up in acute pulmonary embolism: comparison of digital subtraction angiography and spiral CT. *Rofo Fortschr Geb Rontgenstr Neuen Bildgeb Verfahr* 161:285–291

65. Dresel S, Stabler A, Scheidler J, Holzknrecht N, Tatsch K, Hahn K (1995) Diagnostic approach in acute pulmonary embolism: perfusion scintigraphy versus spiral computed tomography. *Nucl Med Commun* 16:1009–1015
66. Goodman LR, Curtin JJ, Mewissen MW et al. (1995) Detection of pulmonary embolism in patients with unresolved clinical and scintigraphic diagnosis: helical CT versus angiography. *Am J Roentgenol* 164:1369–1374
67. Senac JP, Vernhet H, Bousquet C et al. (1995) Pulmonary embolism: contribution of spiral X-ray computed tomography. *J Radiol* 76:339–345
68. Remy-Jardin M, Remy J, Deschildre F et al. (1996) Diagnosis of pulmonary embolism with spiral CT: comparison with pulmonary angiography and scintigraphy. *Radiology* 200:699–706
69. Van Rossum AB, Treurniet FE, Kieft GJ, Smith SJ, Schepers-Bok R (1996) Role of spiral volumetric computed tomographic scanning in the assessment of patients with clinical suspicion of pulmonary embolism and an abnormal ventilation/perfusion lung scan. *Thorax* 51:23–28
70. Van Rossum AB, Pattynama PM, Tjin A, Ton ER et al. (1996) Pulmonary embolism: validation of spiral CT angiography in 149 patients. *Radiology* 201:467–470
71. Christiansen F (1997) Diagnostic imaging of acute pulmonary embolism. *Acta Radiol* 38 (Suppl):1–33
72. Ferretti GR, Bosson JL, Buffaz PD et al. (1997) Acute pulmonary embolism: role of helical CT in 164 patients with intermediate-probability at ventilation–perfusion scintigraphy and normal results at duplex US of the legs. *Radiology* 205:453–458
73. Mayo JR, Remy-Jardin M, Müller NL et al. (1997) Pulmonary embolism: prospective comparison of spiral CT with ventilation–perfusion scintigraphy. *Radiology* 205:447–452
74. Pruszczyk P, Torbicki A, Pacho R et al. (1997) Noninvasive diagnosis of suspected severe pulmonary embolism. *Chest* 112:722–728
75. Drucker EA, Rivitz SM, Shepard JA et al. (1998) Acute pulmonary embolism: assessment of helical CT for diagnosis. *Radiology* 209:235–241
76. Garg K, Welsh CH, Feyereabend AJ et al. (1998) Pulmonary embolism: diagnosis with spiral CT and ventilation–perfusion scanning: correlation with pulmonary angiographic results or clinical outcome. *Radiology* 208:201–208
77. Herold CJ, Hahne J, Ghaye B et al. (1999) Prospective evaluation of pulmonary embolism: diagnostic performance of spiral CT angiography in the ESTIPEP trial. *Radiology* 213(P):126–127(Abstract)
78. Kim KI, Müller NL, Mayo JR (1999) Clinically suspected pulmonary embolism: utility of spiral CT. *Radiology* 210:693–697
79. Blachere H, Latrabe V, Montaudon M et al. (2000) Pulmonary embolism revealed on helical CT angiography: comparison with ventilation–perfusion radionuclide lung scanning. *Am J Roentgenol* 174:1041–1047
80. Qanadli SD, El Hajjam M, Mesurole B et al. (2000) Pulmonary embolism detection: prospective evaluation of dual-section helical CT versus selective pulmonary arteriography in 157 patients. *Radiology* 217:447–455
81. Remy-Jardin M, Remy J, Baghaie F, Fribourg M, Artaud D, Duhamel A (2000) Clinical value of thin collimation in the diagnostic workup of pulmonary embolism. *Am J Roentgenol* 175:407–411
82. Perrier A, Howarth N, Didier D et al. (2001) Performance of helical computed tomography in unselected outpatients with suspected pulmonary embolism. *Ann Intern Med* 135:88–97
83. Van Strijen MJ, De Monye W, Kieft GJ, Bloem JL (1999) Diagnosis of pulmonary embolism with spiral CT: a prospective cohort study in 617 consecutive patients. *Radiology* 213 (Suppl):128 (Abstract)
84. Ruiz Y, Caballero P, Caniego JL et al. (2003) Prospective comparison of helical CT with angiography in pulmonary embolism: global and selective vascular territory analysis. Interobserver agreement. *Eur Radiol* 13:823–829
85. Coche E, Verschuren F, Keyeux A et al. (2003) Diagnosis of acute pulmonary embolism in outpatients: comparison of thin-collimation multi-detector row spiral CT and planar ventilation–perfusion scintigraphy. *Radiology* 229:757–765
86. Winer-Muram HT, Rydberg J, Johnson MS et al. (2004) Suspected acute pulmonary embolism: evaluation with multi-detector row CT versus digital subtraction pulmonary arteriography. *Radiology* 233:806–815
87. Herold CJ, Remy-Jardin MJ, Grenier PA et al. (1998) Prospective evaluation of pulmonary embolism: initial results of the European multicenter trial (ESTIPEP). *Radiology* 209(P):299(Abstract)
88. Domingo ML, Marti-Bonmati L, Dosda R, Pallardo Y (2000) Interobserver agreement in the diagnosis of pulmonary embolism with helical CT. *Eur J Radiol* 34:136–140
89. Garg K, Sieler H, Welsh CH, Johnston RJ, Russ PD (1999) Clinical validity of helical CT being interpreted as negative for pulmonary embolism: implications for patient treatment. *Am J Roentgenol* 172:1627–1631
90. Ost D, Rozenshtein A, Saffran L, Snider A (2001) The negative predictive value of spiral computed tomography for the diagnosis of pulmonary embolism in patients with nondiagnostic ventilation–perfusion scans. *Am J Med* 110:16–21
91. Van Rossum AB, Van Erkel AR, Van Persijn Van Meerten EL, Tjin A, Ton ER, Rebergen SA, Pattynama PM (1998) Accuracy of helical CT for acute pulmonary embolism: ROC analysis of observer performance related to clinical experience. *Eur Radiol* 8:1160–1164
92. Brunot S, Corneloup O, Latrabe V, Montaudon M, Laurent F (2005) Reproducibility of multi-detector spiral computed tomography in detection of sub-segmental acute pulmonary embolism. *Eur Radiol* 15:2057–2063
93. Schoepf UJ, Holzknrecht N, Helmlinger TK et al. (2002) Subsegmental pulmonary emboli: improved detection with thin-collimation multi-detector row spiral CT. *Radiology* 222:483–490
94. Van Rossum AB, Pattynama PM, Mallens WM, Hermans J, Heijerman HG (1998) Can helical CT replace scintigraphy in the diagnostic process in suspected pulmonary embolism? A retrospective–propective cohort study focusing on total diagnostic yield. *Eur Radiol* 8:90–96
95. Cross JJ, Kemp PM, Walsh CG, Flower CD, Dixon AK (1998) A randomized trial of spiral CT and ventilation perfusion scintigraphy for the diagnosis of pulmonary embolism. *Clin Radiol* 53:177–182
96. Cueto SM, Cavanaugh SH, Benenson RS, Redcliff MS (2001) Computed tomography scan versus ventilation–perfusion lung scan in the detection of pulmonary embolism. *J Emerg Med* 21:155–164
97. Diffin DC, Leyendecker JR, Johnson SP, Zucker RJ, Grebe PJ (1998) Effect of anatomic distribution of pulmonary emboli on interobserver agreement in the interpretation of pulmonary angiography. *Am J Roentgenol* 171:1085–1089
98. Stein PD, Henry JW, Gottschalk A (1999) Reassessment of pulmonary angiography for the diagnosis of pulmonary embolism: relation of interpreter agreement to the order of the involved pulmonary arterial branch. *Radiology* 210:689–691
99. Gottsäter A, Berg A, Centergard J, Frennby B, Nirhov N, Nyman U (2001) Clinically suspected pulmonary embolism: Is it safe to withhold anticoagulation after a negative spiral CT? *Eur Radiol* 11:65–72
100. Bynum LJ, Wilson JE, Christensen EE, Sorensen C (1979) Radiographic techniques for balloon–occlusion pulmonary angiography. *Radiology* 133:518–520
101. Ferris EJ, Holder JC, Lim WN et al. (1984) Angiography of pulmonary emboli: digital studies and balloon-occlusion cine-angiography. *Am J Roentgenol* 142:369–373
102. Stein PD, Henry JW (1997) Prevalence of acute pulmonary embolism in central and subsegmental pulmonary arteries and relation to probability interpretation of ventilation/perfusion lung scans. *Chest* 111:1246–1248



103. Remy-Jardin M, Remy J, Artaud D, Deschildre F, Duhamel A (1997) Peripheral pulmonary arteries: optimization of the spiral CT acquisition protocol. *Radiology* 204:157–163
104. Remy-Jardin M, Baghaie F, Bonnel F, Masson P, Duhamel A, Remy J (2000) Thoracic helical CT: influence of subsecond scan time and thin collimation on evaluation of peripheral pulmonary arteries. *Eur Radiol* 10:1297–1303
105. Ghaye B, Szapiro D, Mastora I et al. (2001) Peripheral pulmonary arteries: How far in the lung does multi-detector row spiral CT allow analysis? *Radiology* 219: 629–636
106. Oser RF, Zuckerman DA, Gutierrez FR, Brink JA (1996) Anatomic distribution of pulmonary emboli at pulmonary angiography: implications for cross-sectional imaging. *Radiology* 199:31–35
107. Quinn MF, Lundell CJ, Klotz TA et al. (1987) Reliability of selective pulmonary arteriography in the diagnosis of pulmonary embolism. *Am J Roentgenol* 149:469–471
108. Nilsson T, Turen J, Billström A, Mare K, Carlsson A, Nyman U (1999) Validity of pulmonary cine arteriography for the diagnosis of pulmonary embolism. *Eur Radiol* 9:276–280
109. Musset D, Parent F, Meyer G et al. (2002) Diagnostic strategy for patients with suspected pulmonary embolism: a prospective multicentre outcome study. *Lancet* 360:1914–1920
110. Ghanima W, Almaas V, Aballi S et al. (2005) Management of suspected pulmonary embolism (PE) by D-dimer and multislice computed tomography in outpatients: an outcome study. *J Thromb Haemost* 3:1926–1932
111. De Monye W, Van Strijen MJ, Huisman MV et al. (2000) Suspected pulmonary embolism: prevalence and anatomic distribution in 487 consecutive patients. *Radiology* 215:184–188
112. Eyer BA, Goodman LR, Washington L (2005) Clinicians' response to radiologists' reports of isolated subsegmental pulmonary embolism or inconclusive interpretation of pulmonary embolism using MDCT. *Am J Roentgenol* 184: 623–628
113. Revel MP, Petrover D, Hernigou A, Lefort C, Meyer G, Frija G (2005) Diagnosing pulmonary embolism with four-detector row helical CT: prospective evaluation of 216 outpatients and inpatients. *Radiology* 234:265–273
114. Henry JW, Relyea B, Stein PD (1995) Continuing risk of thromboemboli among patients with normal pulmonary angiograms. *Chest* 107:1375–1378
115. Stein PD, Henry JW, Relyea B (1995) Untreated patients with pulmonary embolism. Outcome, clinical, and laboratory assessment. *Chest* 107:931–935
116. Hull RD, Raskob GE, Pineo GF, Brant RF (1995) The low-probability lung scan. A need for change in nomenclature. *Arch Intern Med* 155:1845–1851
117. Hull RD, Raskob GE, Ginsberg JS et al. (1994) A noninvasive strategy for the treatment of patients with suspected pulmonary embolism. *Arch Intern Med* 154:289–297
118. Wells PS, Ginsberg JS, Anderson DR et al. (1998) Use of a clinical model for safe management of patients with suspected pulmonary embolism. *Ann Intern Med* 129:997–1005
119. Perrier A, Desmarais S, Miron MJ et al. (1999) Non-invasive diagnosis of venous thromboembolism in outpatients. *Lancet* 353:190–195
120. Goodman LR (2005) Small pulmonary emboli: What do we know? *Radiology* 234:654–658
121. Raptopoulos V, Boiselle PM (2001) Multi-detector row spiral CT pulmonary angiography: comparison with single-detector row spiral CT. *Radiology* 221:606–613
122. Remy-Jardin M, Tillie-Leblond I, Szapiro D et al. (2002) CT angiography of pulmonary embolism in patients with underlying respiratory disease: impact of multislice CT on image quality and negative predictive value. *Eur Radiol* 12:1971–1978
123. Patel S, Kazerooni EA, Cascade PN (2003) Pulmonary embolism: optimization of small pulmonary artery visualization at multi-detector row CT. *Radiology* 227:455–460
124. Schoepf UJ, Kessler MA, Rieger CT et al. (2001) Multislice CT imaging of pulmonary embolism. *Eur Radiol* 11:2278–2286
125. Goodman LR, Lipchik RJ, Kuzo RS, Liu Y, Mcauliffe TL, O'Brien DJ (2000) Subsequent pulmonary embolism: risk after a negative helical CT pulmonary angiogram. Prospective comparison with scintigraphy. *Radiology* 215:535–542
126. Hirsh J (1998) Low-molecular-weight heparin: a review of the results of recent studies of the treatment of venous thromboembolism and unstable angina. *Circulation* 98:1575–1582
127. Lomis NN, Yoon HC, Moran AG, Miller FJ (1999) Clinical outcomes of patients after a negative spiral CT pulmonary arteriogram in the evaluation of acute pulmonary embolism. *JVIR* 10:707–712
128. Swensen SJ, Sheedy PF 2nd, Ryu JH et al. (2002) Outcomes after withholding anticoagulation from patients with suspected acute pulmonary embolism and negative computed tomographic findings: a cohort study. *Mayo Clin Proc* 77:130–138
129. Tillie-Leblond I, Mastora I, Radenne A et al. (2002) Risk of pulmonary embolism after a negative spiral CT angiogram in patients with pulmonary disease: 1-year clinical follow-up study. *Radiology* 223:461–467
130. Nilsson T, Olausson A, Johansson H, Nyman U, Aspelin P (2002) Negative spiral CT in acute pulmonary embolism. *Acta Radiol* 43:486–491
131. Van Strijen MJ, de Monye W, Schiereck J et al. (2003) Single-detector helical computed tomography as the primary diagnostic test in suspected pulmonary embolism: a multicenter clinical management study of 510 patients. *Ann Intern Med* 138:307–314
132. Lombard J, Bhatia R, Sala E (2003) Spiral computed tomographic pulmonary angiography for investigating suspected pulmonary embolism: clinical outcomes. *Can Assoc Radiol J* 54:147–151
133. Donato AA, Scheirer JJ, Atwell MS, Gramp J, Duszak R Jr (2003) Clinical outcomes in patients with suspected acute pulmonary embolism and negative helical computed tomographic results in whom anticoagulation was withheld. *Arch Intern Med* 163:2033–2038
134. Frieria A, Olivera MJ, Suarez C, Ruiz-Gimenez N, Caballero P (2004) Clinical validity of negative helical computed tomography for clinical suspicion of pulmonary embolism. *Respiration* 71:30–36
135. Bourriot K, Couffinal T, Bernard V, Montaudon M, Bonnet J, Laurent F (2003) Clinical outcome after a negative spiral CT pulmonary angiographic finding in an inpatient population from cardiology and pneumology wards. *Chest* 123:359–365
136. Krestan CR, Klein N, Fleischmann D et al. (2004) Value of negative spiral CT angiography in patients with suspected acute PE: analysis of PE occurrence and outcome. *Eur Radiol* 14:93–98
137. Kavanagh EC, O'Hare A, Hargaden G, Murray JG (2004) Risk of pulmonary embolism after negative MDCT pulmonary angiography findings. *Am J Roentgenol* 182:499–504
138. Perrier A, Roy PM, Aujesky D et al. (2004) Diagnosing pulmonary embolism in outpatients with clinical assessment, D-dimer measurement, venous ultrasound, and helical computed tomography: a multicenter management study. *Am J Med* 116:291–299
139. Prologo JD, Gilkeson RC, Diaz M, Cummings M (2005) The effect of single-detector CT versus MDCT on clinical outcomes in patients with suspected acute pulmonary embolism and negative results on CT pulmonary angiography. *Am J Roentgenol* 184:1231–1235
140. Quiroz R, Kucher N, Zou KH et al. (2005) Clinical validity of a negative computed tomography scan in patients with suspected pulmonary embolism: a systematic review. *J Am Med Assoc* 293:2012–2017
141. Novelline RA, Baltarowich OH, Athanasoulis CA, Waltman AC, Greenfield AJ, Mckusick KA (1978) The clinical course of patients with suspected pulmonary embolism and a negative pulmonary arteriogram. *Radiology* 126:561–567

142. Hull RD, Hirsh J, Carter CJ et al. (1983) Pulmonary angiography, ventilation lung scanning, and venography for clinically suspected pulmonary embolism with abnormal perfusion lung scan. *Ann Intern Med* 98:891–899
143. Van Rooij WJJ, Den Heeten GJ, Sluzewski M (1995) Pulmonary embolism: diagnosis in 211 patients with use of selective pulmonary digital subtraction angiography with a flow-directed catheter. *Radiology* 195:793–797
144. Van Beek EJR, Bakker AJ, Reekers JA (1996) Pulmonary embolism: interobserver agreement in the interpretation of conventional angiographic and DSA images in patients with nondiagnostic lung scan results. *Radiology* 198:721–724
145. Van Beek EJR, Reekers JA, Batchelor DA, Brandjes DPM, Buller HR (1996) Feasibility, safety and clinical utility of angiography in patients with suspected pulmonary embolism. *Eur Radiol* 6:415–419
146. Van Beek EJ, Kuyper PM, Schenk BE, Brandjes DP, Ten Cate JW, Buller HR (1995) A normal perfusion lung scan in patients with clinically suspected pulmonary embolism. Frequency and clinical validity. *Chest* 108:170–173
147. Van Beek EJR, Brouwers EM, Song B, Bongaerts AH, Oudkerk M (2001) Lung scintigraphy and helical computed tomography for the diagnosis of pulmonary embolism: a meta-analysis. *Clin Appl Thromb Hemost* 7:87–92
148. Gotway MB, Patel RA, Webb WR (2000) Helical CT for the evaluation of suspected acute pulmonary embolism: diagnostic pitfalls. *J Comput Assist Tomogr* 24:267–273
149. Vogel N, Kauczor HU, Heussel CP, Ries BG, Thelen M (2001) Artifact reduction in bolus-enhanced spiral CT of pulmonary arteries using a saline bolus. *Rofo Fortschr Geb Rontgenstr Neuen Bildgeb Verfahr* 173:460–465
150. Gosselin MV, Rassner UA, Thieszen SL, Phillips J, Oki A (2004) Contrast dynamics during CT pulmonary angiogram: analysis of an inspiration associated artifact. *J Thorac Imaging* 19:1–7
151. Remy-Jardin M, Duyck P, Remy J et al. (1995) Hilar lymph nodes: identification with spiral CT and histologic correlation. *Radiology* 196:387–394
152. Jardin F, Dubourg O, Gueret P et al. (1987) Quantitative two-dimensional echocardiography in massive pulmonary embolism: emphasis on ventricular interdependence and leftward septal displacement. *J Am Coll Cardiol* 10:1201–1206
153. Lualdi JC, Goldhaber SZ (1995) Right ventricular dysfunction after acute pulmonary embolism: pathophysiologic factors, detection, and therapeutic implications. *Am Heart J* 130:1276–1282
154. Reid JH, Murchison JT (1998) Acute right ventricular dilatation: a new helical CT sign of massive pulmonary embolism. *Clin Radiol* 53:694–698
155. Wood KE (2002) Major pulmonary embolism: review of a pathophysiologic approach to the golden hour of hemodynamically significant pulmonary embolism. *Chest* 121:877–905
156. Schoepf UJ, Kucher N, Kipfmüller F, Quiroz R, Costello P, Goldhaber SZ (2004) Right ventricular enlargement on chest computed tomography: a predictor of early death in acute pulmonary embolism. *Circulation* 110:3276–3280
157. Araoz PA, Gotway MB, Trowbridge RL et al. (2003) Helical CT pulmonary angiography predictors of in-hospital morbidity and mortality in patients with acute pulmonary embolism. *J Thorac Imaging* 18:207–216
158. Wu AS, Pezzullo JA, Cronan JJ, Hou DD, Mayo-Smith WW (2004) CT pulmonary angiography: quantification of pulmonary embolus as a predictor of patient outcome: initial experience. *Radiology* 230:831–835
159. Collomb D, Paramelle PJ, Calaque O et al. (2003) Severity assessment of acute pulmonary embolism: evaluation using helical CT. *Eur Radiol* 13:1508–1514
160. Ghaye B, Ghuysen A, Willems V et al. (2006) Severe pulmonary embolism: pulmonary artery clot load scores and cardiovascular parameters as predictors of mortality. *Radiology* 239:884–891
161. Van der Meer RW, Pattynama PM, van Strijen MJ et al. (2005) Right ventricular dysfunction and pulmonary obstruction index at helical CT: prediction of clinical outcome during 3-month follow-up in patients with acute pulmonary embolism. *Radiology* 235:798–803
162. Ghuysen A, Ghaye B, Willems V et al. (2005) Computed tomographic pulmonary angiography and prognostic significance in patients with acute pulmonary embolism. *Thorax* 60:956–961
163. Lim KE, Chan CY, Chu PH, Hsu YY, Hsu WC (2005) Right ventricular dysfunction secondary to acute massive pulmonary embolism detected by helical computed tomography pulmonary angiography. *Clin Imaging* 29:16–21
164. Ghaye B, Ghuysen A, Bruyere PJ, D’Orio V, Dondelinger RF (2006) Can CT pulmonary angiography assess severity and prognosis of patients presenting with pulmonary embolism: What the radiologist needs to know. *Radiographics* 26:23–39
165. Qanadli SD, El Hajjam M, Vieillard-Baron A et al. (2001) New CT index to quantify arterial obstruction in pulmonary embolism: comparison with angiographic index and echocardiography. *Am J Roentgenol* 176:1415–1420
166. Mastora I, Remy-Jardin M, Masson P et al. (2003) Severity of acute pulmonary embolism: evaluation of a new spiral CT angiographic score in correlation with echocardiographic data. *Eur Radiol* 13:29–35
167. Coche E, Vlassenbroek A, Roelants V et al. (2005) Evaluation of biventricular ejection fraction with ECG-gated 16-slice CT: comparison with radionuclide ventriculography. *Eur Radiol* 15:1432–1440
168. Kim TH, Ryu YH, Hur J et al. (2005) Evaluation of right ventricular volume and mass using retrospective ECG-gated cardiac multidetector computed tomography: comparison with first-pass radionuclide angiography. *Eur Radiol* 15:1987–1993
169. Schoepf UJ, Bruening R, Konschitzky H et al. (2000) Pulmonary embolism: comprehensive diagnosis by using electron-beam CT for detection of emboli and assessment of pulmonary blood flow. *Radiology* 217:693–700
170. Wildberger JE, Schoepf UJ, Mahnken AH et al. (2005) Approaches to CT perfusion imaging in pulmonary embolism. *Semin Roentgenol* 40:64–73
171. Wildberger JE, Klotz E, Ditt H, Spuntrup E, Mahnken AH, Gunther RW (2005) Multislice computed tomography perfusion imaging for visualization of acute pulmonary embolism: animal experience. *Eur Radiol* 15:1378–1386
172. Gotway MB, Nagai BK, Reddy GP, Patel RA, Higgins CB, Webb WR (2001) Incidentally detected cardiovascular abnormalities on helical CT pulmonary angiography: spectrum of findings. *Am J Roentgenol*;176:421–427
173. Lorut C, Ghossains M, Horellou MH, Achkar A, Fretault J, Laaban JP (2000) A noninvasive diagnostic strategy including spiral computed tomography in patients with suspected pulmonary embolism. *Am J Respir Crit Care Med* 162:1413–1418
174. Montgomery AB, Gilkeson RC, Glauser J, Applegate KE (2000) The role of spiral CT using the pulmonary embolus protocol: a comparison of emergency department and hospitalized populations. *Emerg Radiol* 7:25–30
175. Van Beek EJR, Reekers JA (1999) The value of pulmonary angiography for the differential diagnosis of pulmonary embolism. *Eur Radiol* 9:1310–1316
176. Coche E, Verschuren F, Kefer J (2005) Acute coronary artery occlusion revealed by ECG-gated 16-slice CT scan of the whole chest. *Eur Heart J* 26:2098
177. Russi TJ, Libby DM, Henschke CL (1997) Clinical utility of computed tomography in the diagnosis of pulmonary embolism. *Clin Imaging* 21:175–182

178. Van Erkel AR, Van Rossum AB, Bloem JL, Kievit J, Pattynama PM (1996) Spiral CT angiography for suspected pulmonary embolism: a cost-effectiveness analysis. *Radiology* 201:29–36
179. Goodman LR, Lipchik RJ, Kuzo RS (1997) Acute pulmonary embolism: the role of computed tomography imaging. *J Thorac Imaging* 12:83–86
180. Van Erkel AR, Van Den Hout WB, Pattynama PM (1999) International differences in health care costs in Europe and the United States: Do these affect the cost-effectiveness of diagnostic strategies for pulmonary embolism? *Eur Radiol* 9:1926–1931
181. Van Erkel AR, Pattynama PM (1998) Cost-effective diagnostic algorithms in pulmonary embolism: an updated analysis. *Acad Radiol* 5 (Suppl 2):321–327
182. Paterson DI, Schwartzman K (2001) Strategies incorporating spiral CT for the diagnosis of acute pulmonary embolism: a cost-effectiveness analysis. *Chest* 119:1791–1800
183. Perrier A, Nendaz MR, Sarasin FB, Howarth N, Bounameaux H (2003) Cost-effectiveness analysis of diagnostic strategies for suspected pulmonary embolism including helical computed tomography. *Am J Respir Crit Care Med* 167:39–44
184. Remy-Jardin M, Louveigny S, Remy J et al. (1997) Acute central thromboembolic disease: posttherapeutic follow-up with spiral CT angiography. *Radiology* 203:173–180
185. Van Rossum AB, Pattynama PM, Tjin A Ton E, Kieft GJ (1998) Spiral CT appearance of resolving clots at 6 week follow-up after acute pulmonary embolism. *J Comput Assist Tomogr* 22:413–417
186. Moser KM, Longo AM, Ashburn WL, Guisan M (1973) Spurious scintiphotographic recurrence of pulmonary emboli. *Am J Med* 55:434–443
187. Resten A, Mausoleo F, Valero M, Musset D (2003) Comparison of doses for pulmonary embolism detection with helical CT and pulmonary angiography. *Eur Radiol* 13:1515–1521
188. Kuiper JW, Geleijns J, Matheijssen NA, Teeuwisse W, Pattynama PM (2003) Radiation exposure of multi-row detector spiral computed tomography of the pulmonary arteries: comparison with digital subtraction pulmonary angiography. *Eur Radiol* 13:1496–1500
189. Diederich S (2003) Radiation dose in helical CT for detection of pulmonary embolism. *Eur Radiol* 13:1491–1493
190. Robinson PJ (1996) Ventilation–perfusion lung scanning and spiral computed tomography of the lungs: Competing or complementary modalities? *Eur J Nucl Med* 23:1547–1553
191. Winer-Muram HT, Boone JM, Brown HL, Jennings SG, Mabie WC, Lombardo GT (2002) Pulmonary embolism in pregnant patients: fetal radiation dose with helical CT. *Radiology* 224:487–492
192. Tack D, De Maertelaer V, Petit W et al. (2005) Multi-detector row CT pulmonary angiography: comparison of standard-dose and simulated low-dose techniques. *Radiology* 236:318–325
193. Dalen JE, Brooks HL, Johnson LW, Meister SG, Szucs MM, Dexter L (1971) Pulmonary angiography in acute pulmonary embolism: indications, techniques, and results in 367 patients. *Am Heart J* 81:175–185
194. Nilsson T, Carlsson A, Mare K (1998) Pulmonary angiography: a safe procedure with modern contrast media and technique. *Eur Radiol* 8:86–89
195. Remy-Jardin M, Remy J, Cauvain O, Petyt L, Wannebroucq J, Beregi JP (1995) Diagnosis of central pulmonary embolism with helical CT: role of two-dimensional multiplanar reformations. *Am J Roentgenol* 165:1131–1138
196. Brink JA, Woodard PK, Horesh L et al. (1997) Depiction of pulmonary emboli with spiral CT: optimization of display window settings in a porcine model. *Radiology* 204:703–708
197. Zhou C, Chan HP, Patel S et al. (2005) Preliminary investigation of computer-aided detection of pulmonary embolism in three-dimensional computed tomography pulmonary angiography images. *Acad Radiol* 12:782–792
198. Marten K, Engelke C, Funke M, Obenauer S, Baum F, Grabbe E (2003) ECG-gated multislice spiral CT for diagnosis of acute pulmonary embolism. *Clin Radiol* 58:862–868
199. Ryu JH, Swensen SJ, Olson EJ, Pellikka PA (2001) Diagnosis of pulmonary embolism with use of computed tomographic angiography. *Mayo Clin Proc* 76:59–65
200. Stein PD, Henry JW (1997) Clinical characteristics of patients with acute pulmonary embolism stratified according to their presenting syndromes. *Chest* 112:974–979

# CT Venography in an Integrated Diagnostic Strategy of Acute Pulmonary Embolism and Venous Thrombosis

B. Ghaye, R.F. Dondelinger

## 4.3

### Contents

4.3.1	Introduction	371
4.3.2	History	372
4.3.3	Diagnostic Imaging of DVT	372
4.3.4	Direct CT Venography	372
4.3.5	Indirect CT Venography	373
4.3.5.1	Examination Protocol	373
4.3.6	Venous Anatomy	375
4.3.6.1	Normal Anatomy	375
4.3.6.2	Anatomic Anatomy	377
4.3.7	Image Interpretation	378
4.3.7.1	CT Signs of Acute DVT	378
4.3.7.2	CT Signs of Chronic DVT	378
4.3.7.3	CT Signs of Recurrent DVT	379
4.3.8	Interpretive Pitfalls	379
4.3.8.1	Pitfalls Related to the Technique	379
4.3.8.2	Normal or Pathological Structures	383
4.3.8.3	Streak Artefacts	383
4.3.9	Potential Benefits of Combined CTPA and CTV	383
4.3.10	Clinical Results	388
4.3.10.1	CTV vs Other Imaging Tests	388
4.3.10.2	Incremental Value of CTV	388
4.3.11	Conclusion	388
	References	388

### 4.3.1 Introduction

Deep venous thrombosis (DVT) and pulmonary embolism (PE) are the two aspects of the same disease process, termed venous thrombo-embolism (VTE), and constitutes major health problems that result in significant morbidity and mortality [1–4]. It is estimated that VTE is associated with 300,000–900,000 hospitalizations per year in the US and will result in 50,000 to 150,000 deaths [1, 5, 6]. Early diagnosis and treatment significantly improve survival in

patients with VTE [7]. Clinical diagnosis and treatment of DVT and/or PE is difficult. The use of non-invasive and invasive testings will vary, as the clinical manifestations of VTE are diverse [6]. Although ventilation-perfusion (V/Q) lung scanning has been a common screening test in the evaluation of suspected PE, single-slice spiral CT pulmonary angiography (CTPA) was used increasingly in the 1990s, as it accurately defines emboli down to level of the segmental pulmonary arteries, while revealing other non-embolic causes of thoracic symptoms [8–10]. Criticism was raised against single-slice CTPA as a screening test for VTE. First, small clots located distally to the segmental level may be missed even on a high quality examination, exposing untreated patients to the risk of recurrent PE. Second, patients may be unable to hold their breath up to 40 s, and CTPA may be difficult to interpret in case of breathing artifacts (i.e. intensive care units patients). Third, CTPA has been considered indeterminate in 2–13% of the patients [10]. Some of the limitations have been overcome with the use of multidetector-row CT (MDCT) that allows accurate delineation of clots down to subsegmental pulmonary arteries in 5- to 20-s breathhold [11, 12]. Nevertheless a small pulmonary embolus may herald larger emboli, which imposes intensive evaluation of venous clots [13, 14]. While clots in the lungs clearly influence the cardio-pulmonary status of the patients, the major risk of death is from recurrent PE. In the PIOPED study, a recurrent embolic event was the cause of death in 90% of the patients dying of PE [15]. The DVT is often asymptomatic, and about 90% of PE arise from deep veins of the legs and pelvis [1]. Therefore it appears that optimization of resolution of CTPA may be of less clinical importance than accurate assessment of residual DVT. Furthermore, dual assessment of both aspects of the disease is important with respect to therapeutic implications [6]. A common strategy emerged that included CTPA, followed by ultrasound (US) to rule out DVT in the extremities [13, 16]. Although at our institution, US of the lower limbs is the primary imaging modality for the diagnosis of DVT, a single examination that accurately depicts both PE and the presence of DVT would be desirable to avoid delay in the diagnosis of VTE and limit cost.



### 4.3.2 History

Before the 1970s, the diagnosis of DVT was almost exclusively based on conventional venography (VG). Injection of contrast medium in the veins of the lower extremities was among the first descriptions of diagnostic angiography [17]. Because of the relative invasive nature of VG, many non-invasive techniques have been developed, including blood tests (i.e. d-dimers), radionuclide venography, impedance plethysmography (IPG), ultrasound (US), computed tomography (CT) and magnetic resonance (MR). Introduced in the mid-1980s, US of legs veins is currently the most commonly used and usually unique test in patients suspected of DVT [18]. In 1978, Steele et al. first reported incidental detection of inferior vena cava (IVC) thrombosis with CT in two patients [19]. In 1980, Zerhouni et al. reported 5 cases demonstrating CT findings of ilio-femoral venous thrombosis [20]. Thereafter, CT findings of DVT were refined in many papers published during the early 1980s [21–26]. In 1987, Pillari et al. reported a series of 14 patients suspected of DVT, who underwent CT of the legs after a negative venography. Computed tomography was performed from the patella to the inferior third of the calves during infusion of 30% contrast medium in a foot vein. No further DVT was demonstrated, but abnormalities such as muscular hemorrhage or occult knee joint effusion, responsible for the clinical symptoms were shown [27]. In 1988 Bauer and Flynn reported the clinical use of indirect CT venography in patients with inconclusive venography, or when venous access in the foot was impossible. CT scanning of the lower extremities and pelvis was obtained during a slow infusion of 150 ml of contrast medium in an arm vein for 10 min [28]. In 1991 Langer et al. reported a series of indirect CTV from the ankles to the pelvis in 15 patients. In the 6 patients suspected of PE, the thorax was also scanned and concomitant pleuro-parenchymal changes were demonstrated. This report was the first to promote a combined incremental CT examination of the thorax, lower limbs and pelvis in patients suspected of VTE [29]. In 1994 Stehling et al. reported the first case of direct spiral CT venography of the lower limbs following injection through a catheter inserted in a dorsal vein of the foot [30]; however, it was not until 1998, that Loud et al. reported the combination of spiral CT angiography of the pulmonary arteries and CT venography in 5 patients suspected of VTE. Veins were imaged from the lower calves to the diaphragm thanks to contrast medium recirculation that follows rapid infusion for CTPA [3].

### 4.3.3 Diagnostic Imaging of DVT

Ascending venography (VG) is still currently accepted as the most reliable test for the diagnosis of DVT and the gold standard against which all diagnostic tests should be evaluated [17, 28]. Venography is considered the only technique available that accurately depicts all calf and muscular venous thrombi. A variation of the basic technique may be necessary if initial results are doubtful. Using proper technique in a cooperative patient, it is almost always possible to define the deep venous system and to determine whether occlusion is acute or chronic. This invasive test is limited only by technical factors and complications which may be minimized by using a careful technique [17]. Inter- and intra-observer variability confirmed important operator-dependence and the need for experience to perform and interpret [31, 32].

Ultrasound (US) is an established and widely available technique for evaluation of the veins of both the lower and upper extremities. Advantages include non-invasive and inexpensive technique, and the ability to perform the examination at the patient's bedside. In a large meta-analysis, US showed sensitivities of 92–100% and specificities of 80–100%, when compared to VG for proximal veins in symptomatic patients. For distal or calves veins, sensitivity was 40–87%, depending on the technique used. In asymptomatic patients, sensitivity was 38–100% for the proximal level, and 38–58% for the calf level, confirming that none of the US examination techniques had a sufficiently high sensitivity for calves veins [18].

Similar to CT, magnetic resonance (MR) has the ability to allow for a combined evaluation of pulmonary embolism and venous thrombosis. Preliminary results of MR venography showed results similar to ascending VG [33–35]. Widespread availability, lower cost, shorter examination time and higher accuracy for peripheral pulmonary arteries are currently the main advantages of CT over the emerging MR imaging.

In nuclear medicine imaging, radiolabeled thrombus-detecting agents are investigated, with the potential of screening the whole body for thromboembolic disease in a single examination, and differentiating between acute or chronic thrombosis [36].

### 4.3.4 Direct CT Venography

Stehling reported the first case of direct spiral CT venography in 1994 [30]. Diluted contrast medium was injected through a catheter placed in a dorsal foot vein. Tourniquets around the ankle were used to direct the injected contrast medium into the deep venous system. Axial, multiplanar and maximum intensity projection images allowed differentiation of acute DVT from chronic thrombus in a patient with ambiguous sonographic and venographic findings.

Potential advantages over venography were the ability to perform 3D imaging, a tenfold reduction of contrast medium volume, increased patient comfort due to the low concentration of contrast medium, a supine position, and a decreased risk of post-injection phlebitis. Layering of contrast medium in the vein may remain nevertheless a factor of suboptimal opacification [30]. One study compared direct spiral CT venography with conventional venography in 52 patients [37]. Sensitivity of direct spiral CTV was 100%, specificity 96%, PPV 91% and NPV 100%. The extension of DVT, particularly in pelvic veins and IVC was better demonstrated with CTV. Interobserver agreement was 0.81–0.93 and 0.71–0.88, for direct CTV and conventional venography respectively. Intra-observer agreement was 0.91–0.94 and 0.75–0.92, respectively. Global venous opacification was significantly better with direct CTV, despite a 80% reduction of the volume of contrast medium (40 vs 200 ml). Major differences were found in the IVC, pelvic veins and deep femoral veins. Only 11% (compared with 25% with venography) of all deep veins were not opacified. The technique is less operator-dependent than US or venography, but remains susceptible to inflow phenomena that can mimic intraluminal filling defect. The deep venous system is not always opacified entirely, and puncture of both feet veins is required [37, 38]. The same group also applied the technique to evaluation of venous thrombosis in the upper extremities [38, 39]. Direct CTV better demonstrates the relation between thrombi and vessel wall, confirming that conventional venography overestimated the prevalence of free-floating clots [40]. With a four-detector rows CT, a 5 mm collimation, 1.5–2.0 pitch, 100 mAs spiral covering both legs from the ankles to the diaphragm may be sufficient. For preoperative imaging of venous insufficiency, the contrast medium may be injected directly inside the varicose veins and the spiral length limited to the region of interest. A combination with CTPA of the pulmonary arteries is impossible, and any further imaging will require additional contrast medium injection; thus, direct CTV must be used either for DVT, with the same rationale as VG, or in selected patients with venous insufficiency requiring preoperative three-dimensional diagnostic work-up.

### 4.3.5 Indirect CT Venography

Combined CTPA of the pulmonary arteries and indirect CTV of the lower limbs allow for a complete one-session evaluation of VTE [3, 41–45].

#### 4.3.5.1 Examination Protocol

##### How to Perform Data Acquisition

Patients are positioned supine on the CT table with the feet directed towards the gantry. Feet are placed in the head

holder or on a table extender and immobilized together with tape to limit leg motion. This patient orientation allows for scanning from the ankle to the cervico-thoracic junction without repositioning the patient. Legs are maintained slightly elevated on a folded blanket to avoid compression of the calf veins. In some centres tourniquets are used for preferential opacification of the deep venous system [46]. The use of compressive elastic stockings or isosmolar contrast material (in comparison of low-osmolar contrast media which are hyperosmolar to blood) have recently been shown to significantly increase delayed venous enhancement [47–49]. Further studies are needed to investigate if such refinements can be beneficial for the diagnostic rate of indirect CTV. The arms are placed over the patient's head as for CTPA. Firstly, a scout view of the thorax is obtained. Next, 120–150 ml of 240–300 mg iodine/ml contrast medium are injected at a flow rate of 3–5 ml/s through an antecubital vein for acquisition of CTPA. After completion of pulmonary arteries examination, the table is manually moved and the reference laser placed at the level of the ankles. The CTV starts about 210 s following the start of injection using either sequential or spiral scanning.

With sequential technique, 5- to 10-mm-thick slices are acquired every 20–50 mm. Only 2.1% of the patients had DVT visible on one single slice when using a 20 mm slice interval. A slice interval greater than 2 cm can potentially lead to either false negative findings on CTV or an underestimation of the extent of DVT [50]. Using spiral technique, 1.5- to 10-mm-thick slices are usually obtained [44, 46, 51–57]. With multi-slice CT, a length of 100 cm can be scanned in approximately 20 s, using 4×5 mm collimation, 0.5 s rotation time and a pitch of 1.8 [58, 59].

##### Which Level of Irradiation Dose

Advantages of spiral scanning include faster acquisition, 3D imaging capability and absence of interslice gap. Drawbacks of the spiral technique include minimal increase in sensitivity for DVT, while resulting in a substantial increase in radiation dose and in number of images [60]. Although their clinical significance is unknown, isolated short segmental DVT are not uncommon findings, especially in asymptomatic patients [43]; thus, as for the optimisation of multi-detector CTPA of the pulmonary arteries, the justification of spiral CTV will become in the near future an additional matter of debate. Technical parameters influencing the dose delivered to the patient have to be carefully selected. To the best of our knowledge, currently there is no published study comparing different irradiation parameters for CTV. Spiral technique requires careful selection of scanning parameters, in order to obtain acceptable radiation doses in comparison with sequential technique. For example, with sequential scanning (PQ 5000, Phillips, Eindhoven, The Netherlands), we used 100 mA, 1 s rotation speed and 130 kVp per slice [61]. Wildberger et al. used a 4×5 mm collimation, 30-mm/rotation table speed, 0.5 s ro-

tation speed, 120 kVp and 170 mAs and calculated the dose of CTV to be 9.3 mSv [59]. Begemann et al. reported an 8.26 mSv median cumulative effective dose and 3.87 mSv effective gonadal dose when using 4×2.5 mm [56]. Using 4×2.5 mm, 15 mm/s, 120 kV and 130 mAs, a CTDI of 12.22 mGy and DLP of 1200 mGy cm were reported. Using 16×1.5 mm, 24 mm/s, 120 kV and 130 mAs, results were 10.50 mGy for CTDI and 1090 mGy cm for DLP [62]. In other published clinical studies using spiral technology, CT parameters were variable (75–260 mA and 120–150 kVp and a pitch of 1–1.5) [44, 46, 52, 53]. One study estimated the dose of CTV to be slightly less than that of a standard pelvic CT [44]. In another study, the effective radiation dose of combined spiral CTPA-CTV was calculated to be approximately 57% of a dual-phase spiral CT of the liver (4.75 vs 8.3 mSv) [63]. Although such an evaluation depends on the specific technical parameters and type of scanner used, it was demonstrated that spiral CTV was responsible of 50% of the effective dose of the combined CTPA-CTV technique and of a significant increase in gonadal dose. Dose modulation systems, minimizing the dose required without compromise in image quality, are currently developed by all manufacturers and could reduce the dose by 35–60% [64]. Nevertheless although the risk-benefit ratio remains limited in a mainly aged population, indications of CTV should be considered carefully in younger patients [63].

### When to Perform Data Acquisition

Screening during the optimal time window for CTV is important for proper clot detection. Optimal vein analysis requires high level of luminal attenuation, homogeneous opacification and a sufficient vein to surrounding muscle gradient and vein to clot gradient. A gradient of 30 HU is generally considered to be sufficient. Morphology and density of clots measured *in vivo* appear to vary with thrombus composition and age. Venous thrombus, generated in slow flow conditions, are “red thrombus” composed predominantly of red blood cells. The relative concentration of protein, particularly globin, is responsible for high CT density values. Acute red thrombi have a higher hematocrit value than blood, due to increased concentration of globin [65]. Recent clots (<8 days) appear homogeneous with average densities of 31–76 HU [34, 41, 44, 65]. With time, globin is broken down and removed by phagocytes, resulting in decreased attenuation values, which are sometimes at a lower level than normal blood [65]. Subacute or chronic clots (>8 days) tend to become heterogeneous with areas of high attenuation and average densities of 28–55 HU [37, 65, 66].

Time–density curves of venous enhancement following CTPA have been studied using sequential, or spiral or multi-slice CT [45, 61]. The time–density curves for the veins of lower limbs are presented in Fig. 1. Curves at different levels of the lower limbs showed that all density values comprised in the time interval from mean peak venous en-

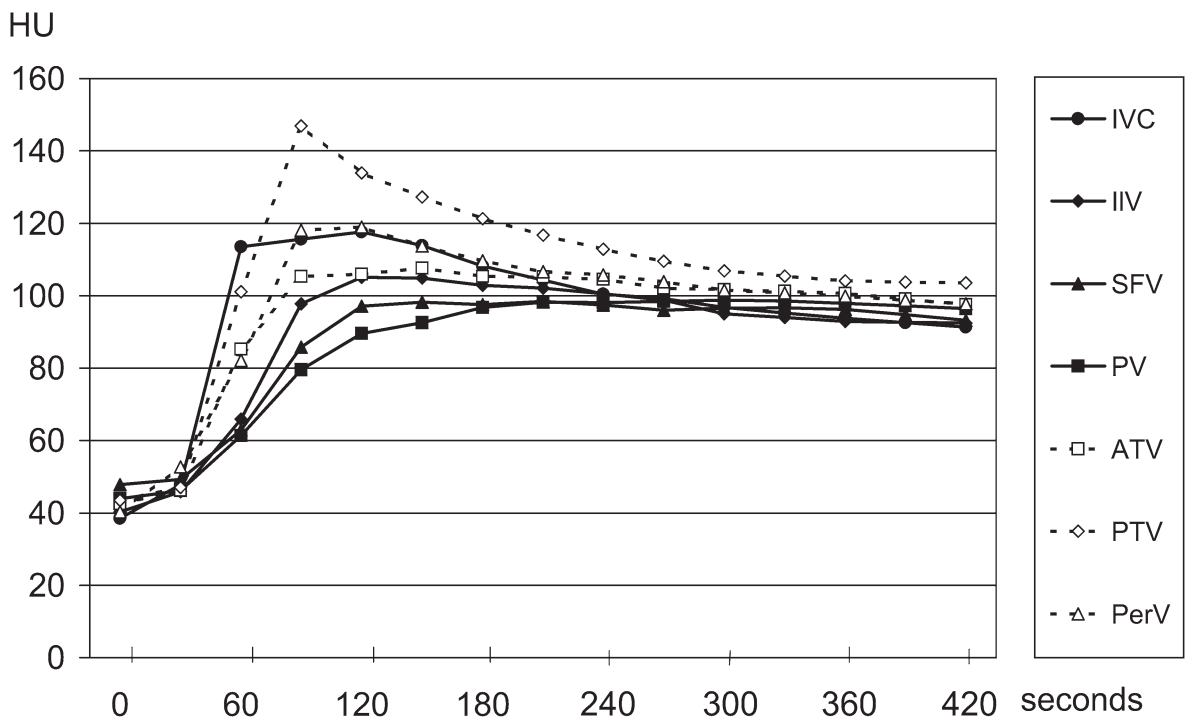
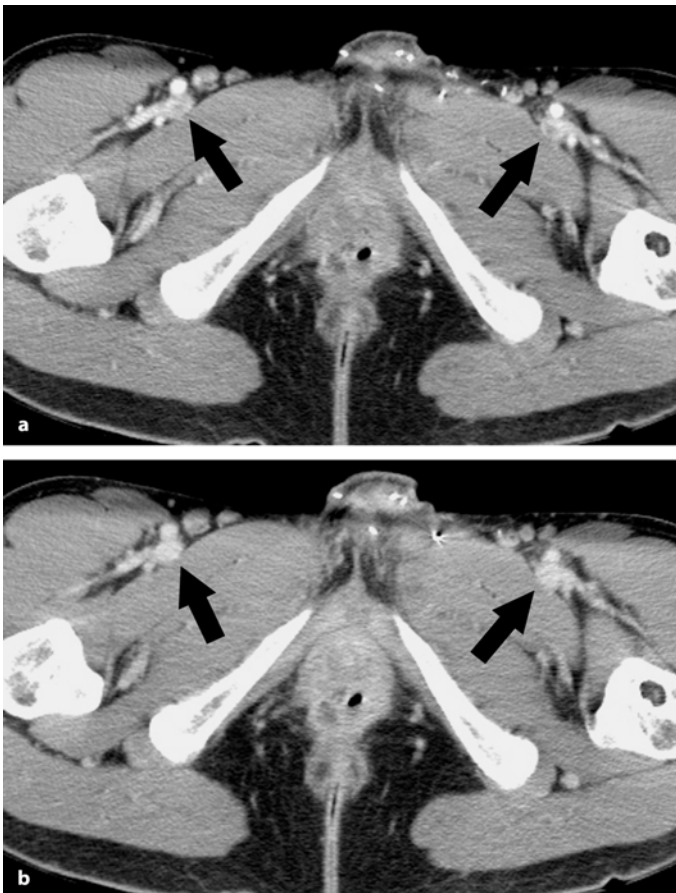


Fig. 1. Mean CT time–density curves of above- and below-knee veins



**Fig. 2.** Heterogeneous venous enhancement. **a** Axial CT venogram at the groin level shows a pseudo-filling defect in both common femoral veins (*arrows*). Scanning was performed <180 s after start of contrast medium injection. **b** Axial CT venogram shows normal enhancement after rescanning 30 s later (*arrows*)

hancement (ranging from 93 to 137 HU) to mean densities at 420 s (ranging from 88 to 103 HU) were above reported attenuation of recent clots. Time to reach maximum enhancement increased from IVC ( $93 \pm 9.5$  s) to popliteal veins ( $141 \pm 57$  s) and decreased for calf veins ( $124 \pm 32$  s) [61].

Homogeneity of venous enhancement is another parameter affecting clot detection during CTV. Homogeneous enhancement is obtained after 150 s for above-knee veins, except for femoral vein (180 s), and 210 s for veins below the knee (Fig. 2) [61]. When considering time–density curves, homogeneous venous opacification, vein to muscles and vein to clot gradients at different levels, an optimal time window for CTV was determined between 210 and 240 s for the calf level and 180–300 s for above-knee veins. When using a sequential acquisition for CTV, a caudo-cranial acquisition is recommended, which starts at 210 sec for the sural level (optimal time window). For faster CTV technique, such as multi-slice CT, the choice of direction of acquisition is irrelevant [61]. Similar levels of enhancement (91–101 HU) were reported in clinical practice for above-knee veins, when starting CTV 180–210 s after contrast medium injection [41, 44, 59, 67].

### 4.3.6 Venous Anatomy

The CTV enables recognition of DVT in veins that are difficult to assess with US or ascending venography, such as deep femoral vein, internal iliac vein, gonadal vein, renal vein and hepatic vein. Combination with CTPA may further demonstrate clots in the right heart, superior vena cava, right and left innominate veins and the distal part of subclavian and jugular veins.

#### 4.3.6.1 Normal Anatomy

Figure 3 shows the normal anatomy on an ascending venography with correlated CTV sections at different levels. Diameter of the veins reflects their capacious role. The venous caliber is similar to that of the corresponding artery for popliteal vein, superficial and common femoral veins, external and common iliac veins, and IVC. Veins below the popliteal level, deep femoral vein and internal iliac vein have a calibre superior to the corresponding artery. Greater and lesser saphenous veins, as other superficial veins, are not accompanied by a corresponding artery.



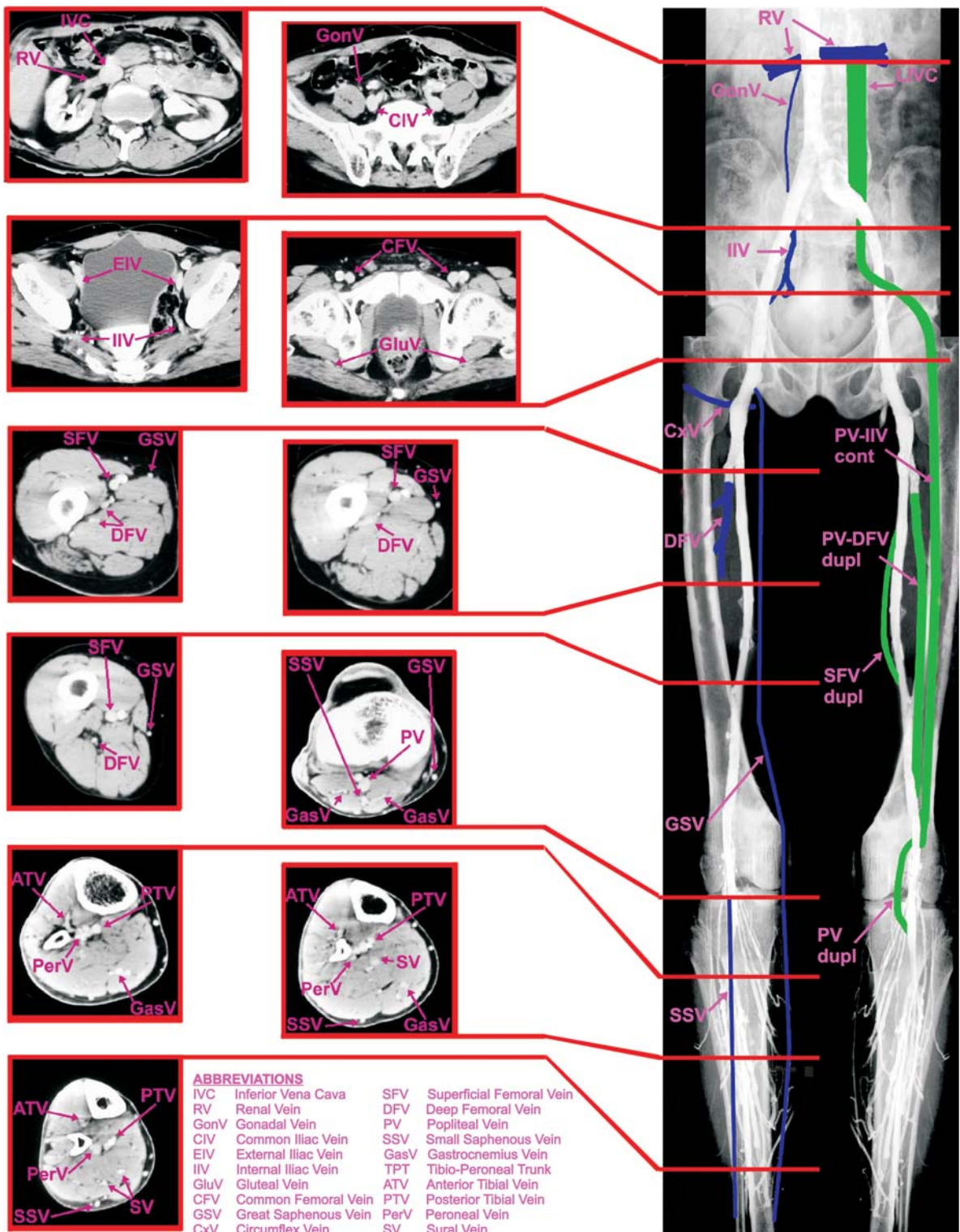


**Fig. 3.** Venous anatomy of the lower limbs. Normal venous anatomy is shown on venography and corresponding slices obtained by CTV. The veins that could be correctly analyzed on axial CT venograms are annotated on the slices. Veins represented in *blue* are visible on CTV and are usually poorly or non-opacified on state-of-the-art venography (RV, GonV, IIV, GSV, DFV, and SSV).

Most of these veins are also among the most difficult to study on US examinations. Veins represented in *green* are anatomic variants and include duplicated IVC or left-sided IVC (LIVC), direct continuation of the PV in the IIV (PV-IIV cont), direct continuation of the PV in the DFV (PV-DFV cont), and duplication of PV (PV dupl) or SFV (SFV dupl)



**Fig. 4.** Left-sided inferior vena cava resulting in “inverse” Cockett syndrome in a 60-year-old woman. **a** Axial CT venogram shows an endoluminal filling defect corresponding to an acute DVT in the right common iliac vein (*arrow*). **b** Axial CT venogram acquired 20 mm cranial to **a** shows a compression of the right common iliac vein (*arrow*) by the left common iliac artery (*arrowhead*). **c** Axial CT venogram acquired 20 mm cranial to **b** shows a left-sided inferior vena cava (*arrow*), resulting in an “inverse” Cockett syndrome

#### 4.3.6.2 Anatomic Variants

Anatomic variants should be recognized to avoid false negative results of CTV. Duplication is usual for posterior tibial, anterior tibial and peroneal veins. Partial duplication of popliteal and/or superficial femoral veins may be frequently encountered, particularly in patients with DVT.

The IVC may be occasionally duplicated or left-sided (Fig. 4) [68, 69]. Duplication represents a classic pitfall in US [70, 71]. Embryological remnants of the sciatic vein may rarely be seen with popliteal vein draining either in deep femoral vein (partial form), or in internal iliac vein (complete form; Fig. 3). Unusual venous pathways may be associated with absence of usual normal venous segment.

### 4.3.7 Image Interpretation

In clinical practice, the differentiation between acute and chronic DVT is important for determination of the need of anticoagulation and duration of treatment [17, 50, 72].

#### 4.3.7.1 CT Signs of Acute DVT

Basic CT signs of acute DVT have been described in case reports published in the 1980s [19–26, 73–75]. The primary CT sign used to diagnose DVT is the demonstration of intra-vascular clot, presenting as a complete, partial or mural filling defect, depending on the degree of venous occlusion (Figs. 5, 6). Recognition of clot with CT may be difficult in some cases, as fresh thrombus may exhibit similar attenuation values than contrast-enhanced blood [20, 42]. Additional findings may contribute to establish the diagnosis: venous dilation compared with the normal contralateral side, obliteration of perivenous fat suggestive of edema, high contrast ringlike rim of the venous wall due to contrast staining in the vasa vasorum or contrast accumulation around intraluminal clot, muscular swelling and

opacification of collateral veins [3, 42]. A non-opacified venous segment, that is sandwiched by an opacified distal and proximal segment has to be interpreted with caution. Prolonged arterial phase of enhancement may occasionally be seen in patients with extensive bilateral deep venous thrombosis [51].

#### 4.3.7.2 CT Signs of Chronic DVT

Chronic DVT classically manifests as clots with an irregular margin, and occasionally containing calcifications (Fig. 7a). Thrombus is often eccentric with a large portion anchored to the vein wall. Thickening of the vein wall corresponds either to a hyperplastic response of the endothelium, or to residual thrombus incorporated in the vein wall. Partial clot recanalisation may result in a heterogeneous lumen and strands. Multiple deep or superficial collaterals are commonly encountered. Other signs include small retracted veins and ultimately a fibrous cord replacing the vein [70]. Some chronic clots may show vein dilation, or perivascular and soft tissue edema, which makes differentiation between acute and chronic disease sometimes difficult [72, 71].



**Fig. 5.** Proximal acute DVT in a 69-year-old woman. Axial CT venogram at the level of the thigh shows typical findings of DVT in the right groin. An endoluminal filling defect is demonstrated in the right common femoral vein (*arrow*), which is enlarged compared with the normal left side. Note also extensive peri-focal edema infiltrating the fat. A clot is also demonstrated in the right greater saphenous vein (*arrowhead*)

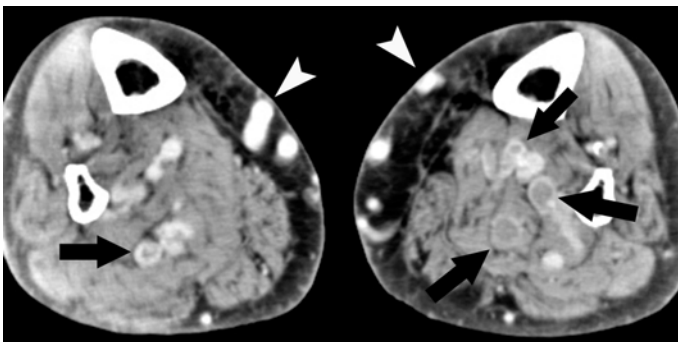


**Fig. 6.** Distal acute DVT in an 87-year-old woman. Axial CT venogram at the calf level shows bilateral DVT. Multiple endoluminal filling defects are demonstrated in left posterior tibial and peroneal veins as well as in sural veins bilaterally (*arrows*). Thrombosed veins are enlarged. Note discrete infiltration of subcutaneous fat and strongly enhanced dilated superficial collateral veins on both sides (*arrowheads*)



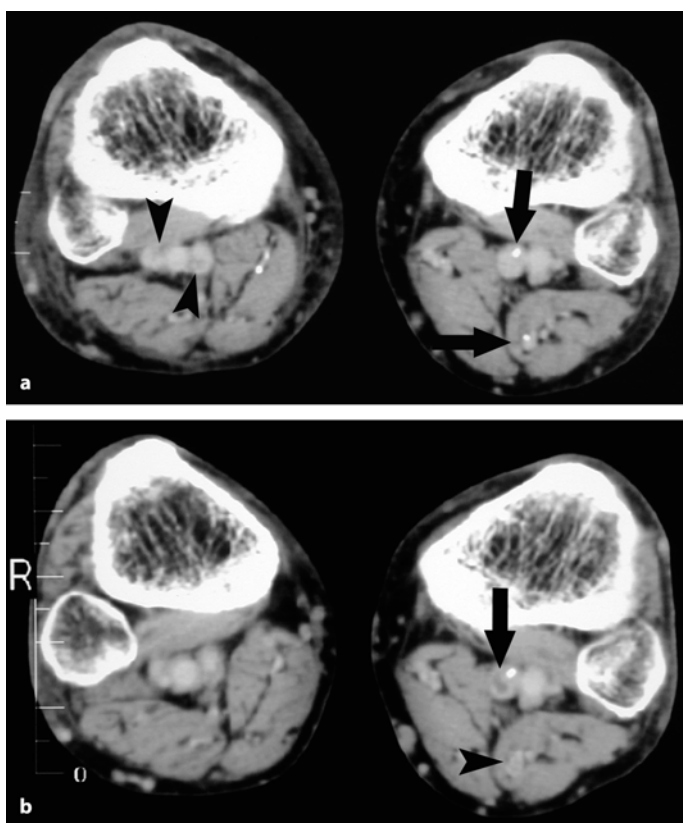


**Fig. 7.** Chronic and recurrent DVT in a 73-year-old man. **a** Axial CT venogram at the popliteal level shows calcified chronic thrombi in left popliteal and left external gastrocnemius veins (*arrows*). Non-calcified chronic thrombi are demonstrated on the right side (*arrowheads*). Note multiple venous collaterals in the sub-cutaneous fat on both sides. **b** Axial CT venogram at the same level, obtained 3 months later, demonstrates recurrent DVT, showing a fresh thrombus anchored to the popliteal calcified thrombus seen in **a** (*arrow*). Recurrent DVT is also visible in the left external gastrocnemius vein (*arrowhead*). No recurrent DVT was seen on control examination (not shown), performed after 6 months of anti-coagulation

### 4.3.7.3 CT Signs of Recurrent DVT

Association of findings of acute and chronic DVT on CTV suggests the diagnosis of recurrent DVT (Fig. 7b) [72]. Recurrent DVT is a major challenge on diagnostic imaging [76,77]. Comparison with previous examinations improves confidence in diagnosis. CTV and US have been suggested to have a complementary role in unsolved cases [72]. The accuracy of CTV in predicting the age of the thrombus and recurrent DVT needs to be assessed.

## 4.3.8 Interpretive Pitfalls

### 4.3.8.1 Pitfalls Related to the Technique

Theoretical advantages of the sequential technique is to reduce the number of slices and total irradiation. We found that a maximum 5-mm collimation is necessary to avoid partial-volume averaging on small veins, particularly veins presenting a transaxial or oblique course, and that a 15-mm interslice gap is acceptable. Small non-occlusive DVT involving a short venous segment, especially in asymptomatic patients, has been detected, although its clinical sig-

nificance is not clear (Fig. 8) [43]. We perform a “live” interpretation of CTV on the screen during and after acquisition. For doubtful images, a short spiral sequence is acquired over the problematic area (Fig. 9). Another option is to correlate findings with sonography [72]. With spiral scanning, the risk of missing a short clot is almost completely minimised. Furthermore, spiral technique offers orthogonal reformatting capability that may be useful in equivocal cases.

Inhomogeneous opacification of the veins may cause pseudo-filling defects, which may simulate DVT [70, 72]. Such artefacts may be flow-related or due to improper selection of scanning time (see Fig. 2) [43, 55, 70, 78–80]. The time to peak venous enhancement is highly variable among patients [45]. The influence of individual physiologic parameters on venous enhancement, such as age, body weight and height, cardiac output, hydration, and renal function, has to be evaluated. In patients with heart failure, severe distal arterial obstruction or impaired flow dynamics, such as abdominal vein compression, adding a further delay of 60 sec is recommended before CTV acquisition [43]. A contrast-blood interface can rarely be observed in dilated varicosities, due to local low flow [70, 81]. Rescanning the area 1–2 min later shows homogeneous filling in varicosities with normal lumen; however, insufficient venous opacification can occur in an unpredictable manner, which may limit



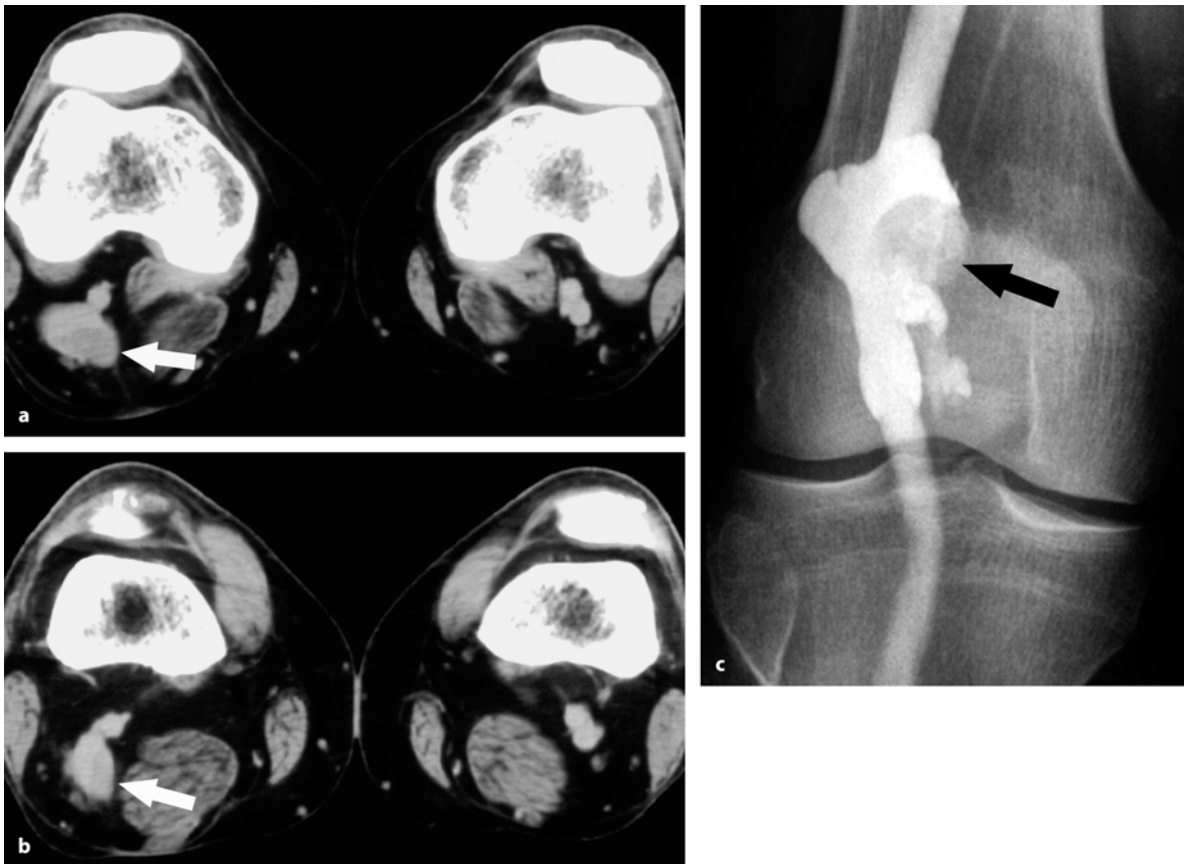


**Fig. 8.** Clots located between two sections in sequential CTV in a 45-year-old man presenting with acute pulmonary embolism. **a, b** Five-millimeter-thick axial CT venograms at the popliteal level, 20 mm apart, demonstrate an aneurysm of the right popliteal

vein. A slightly hypoattenuated area (*arrows*) was seen a posteriori, due to partial-volume averaging on each section. **c** Venography confirmed a limited clot in the popliteal vein (*arrow*)

CTV in some patients. Figure 10 shows quality of venous enhancement obtained in our experience. In clinical practice, sufficient and homogeneous enhancement is obtained in 84–99% of the patients depending on the anatomic level (Fig. 10). Poor opacification leading to indeterminate results for CTV has been reported in 1–5% of the patients

[41, 43, 44, 50, 51, 67]. In one study, patients with fair to poor quality CTPA (5%; 27 of 541) were more likely to have fair to poor quality CTV (52%; 14 of 27) [44].

Finally, CTV acquired with “low dose” or too thin slices can produce noisy images with lumen of the vessels difficult to interpret, particularly in obese patients.

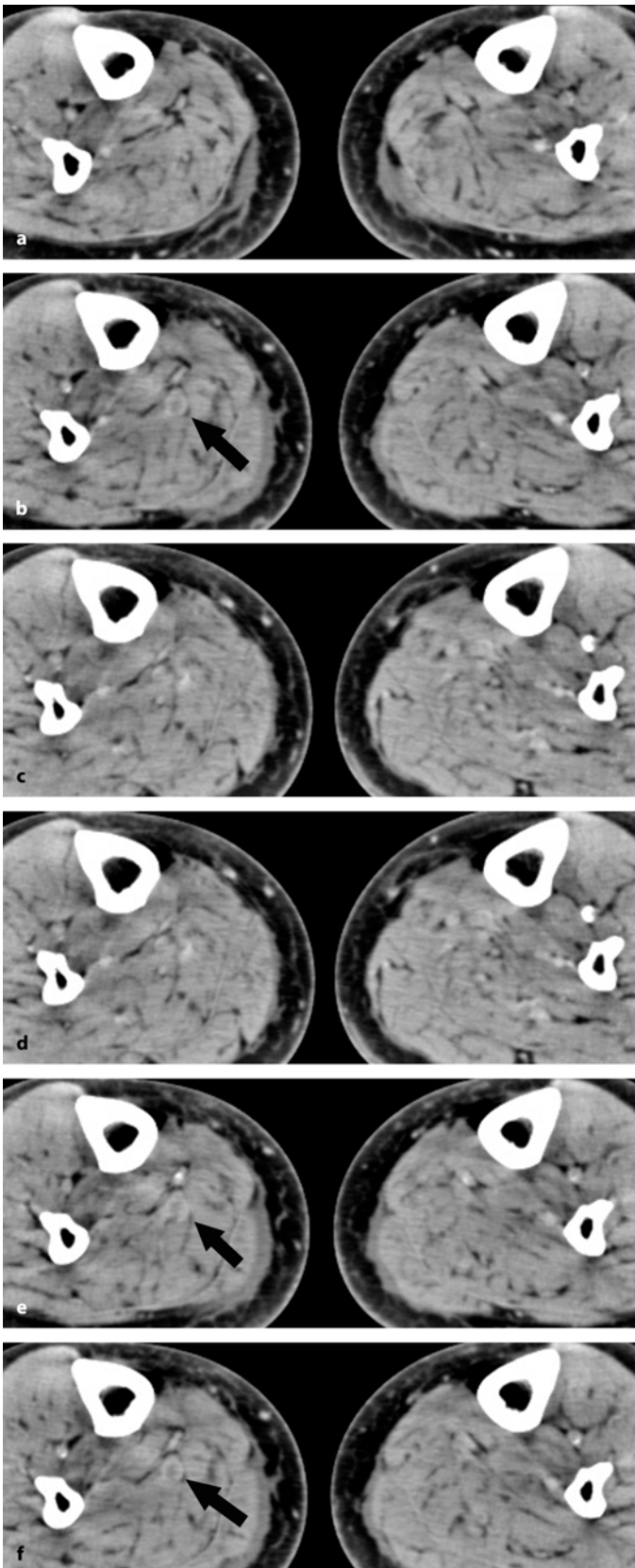


**Fig. 9.** Comparison of sequential scanning and spiral scanning at the calf level in a 61-year-old woman. **a–c** Five-millimeter-thick axial CT venograms were acquired sequentially 20 mm apart. Suspicion of DVT in a right sural vein (*arrows*). **d–h** Five-millimeter-thick axial CT venograms were acquired using spiral technique on the same area without reinjection of contrast medium. The DVT was confirmed in a right sural vein (*arrows*) as well as in other locations (*arrowheads*)

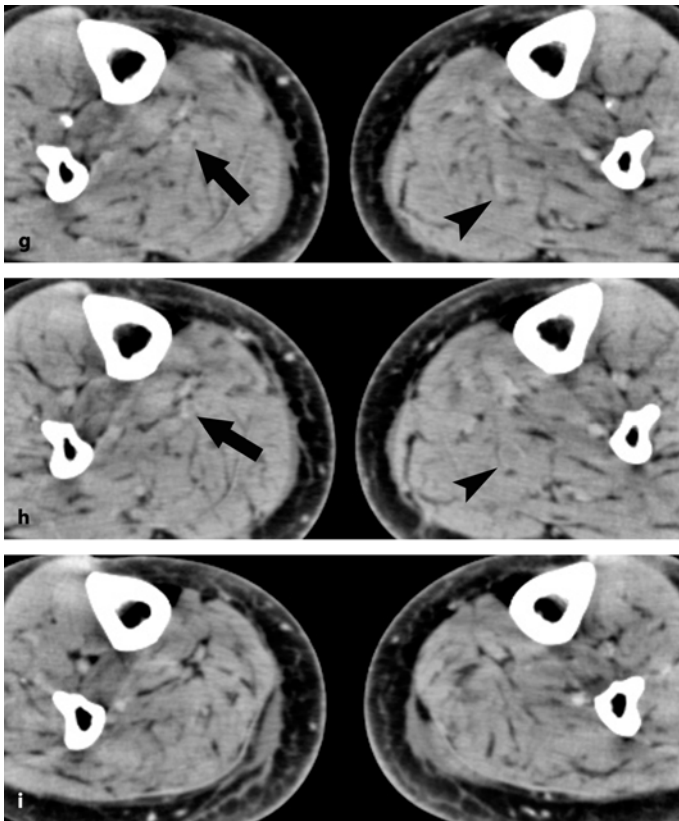


Fig. 9. (continued)

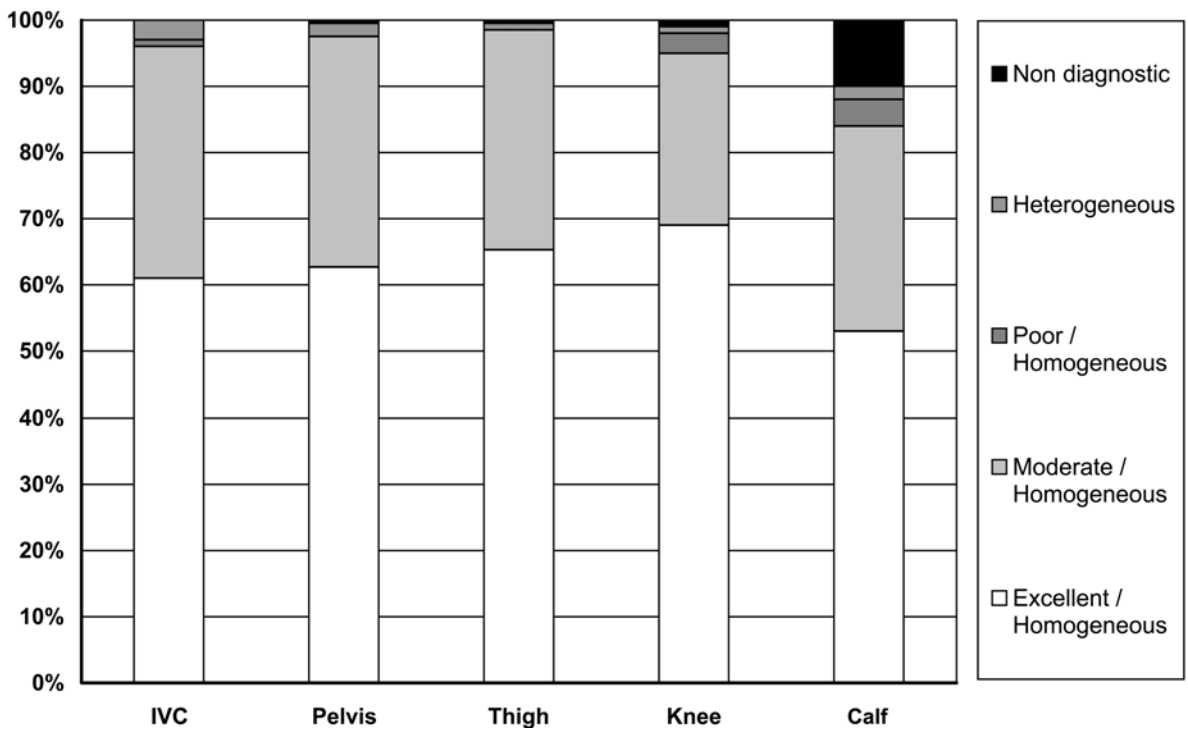


Fig. 10. Subjective assessment of quality of contrast enhancement in CTV. Evaluation was performed in 261 consecutive patients. Scanning was performed 210 s after start of contrast medium injection. Endoluminal enhancement was defined as homogeneous

or heterogeneous. Homogeneous filling was further divided into excellent (high degree of enhancement), moderate (lower degree of enhancement but sufficient for evaluation of patency), or poor (non-diagnostic) contrast. IVC inferior vena cava

#### 4.3.8.2 Normal or Pathological Structures

Some normal structures may present with a hypervascular rim and a central hypodensity mimicking DVT: volume averaging integrating a venous valve, lymph node, sciatic nerve, aponeurosis or tendon, obstructed and dilated ureter or bowel loop with non-opacified lumen (Fig. 11) [20, 25, 51, 70, 82]. Abnormal or pathologic structures may also wrongly suggest DVT, including thrombosed arteries or by-pass, hematoma, abscess, popliteal cyst and acute compartment syndrome [70]. Minor anatomic variants, such as venous ectasia, should also not be confused with venous dilation secondary to DVT [82].

#### 4.3.8.3 Streak Artefacts

Orthopedic material, bone, calcification and opacified bladder or ureter can produce streak or beam hardening artefacts, which may be responsible for endovascular hypodensities when crossing a normally opacified vessel

(Fig. 12). The sharp and straight appearance of these artefacts that extend in the surrounding tissues may help to the correct diagnosis [44, 70]. Such artefacts seem to be reduced by the use of multiple-detector CT compared to single slice CT.

#### 4.3.9 Potential Benefits of Combined CTPA and CTV

The potential benefits of combining CTPA and CTV are multiple. It is a rapid one-stop-shop examination of both aspects of VTE, which allows for immediate treatment of patients who have isolated DVT, without further delay of other types of diagnostic examinations. No separate venipuncture nor additional contrast medium injection are necessary as only the contrast medium already in circulation from CTPA is used. Little time (30–240 s) is added to the overall examination duration, depending on the technique used, with negligible additional cost, although this may vary from country to country [55]. Total room transit

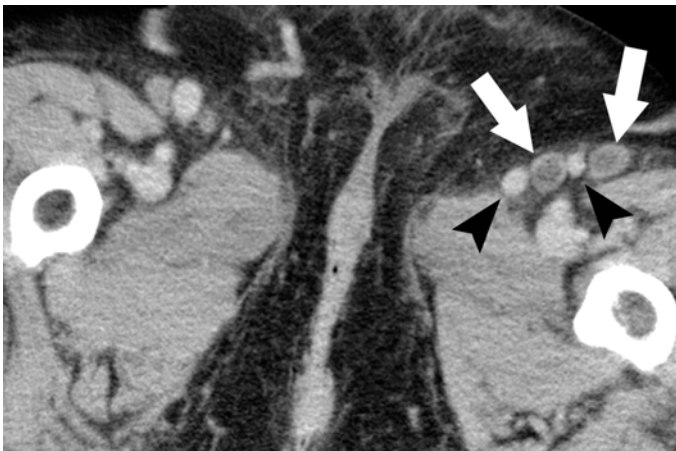


**Fig. 11.** Normal lymph nodes simulating DVT in a 47-year-old woman. Axial CT venogram at the level of the groin shows two left-sided structures with a hypodense center and an enhancing peripheral rim (arrows), mimicking endoluminal filling defects. This aspect corresponds to normal lymph nodes exhibiting lipodystrophy. Note normally enhancing branches of the greater saphenous vein (arrowheads)



**Fig. 12.** Beam-hardening artifact from opacified ureter in a 55-year-old man. Axial CT venogram at the level of the pelvis demonstrates a linear filling defect in the right internal iliac vein (arrow) that corresponds to streak or beam-hardening artifact from contrast in the right ureter located anteriorly



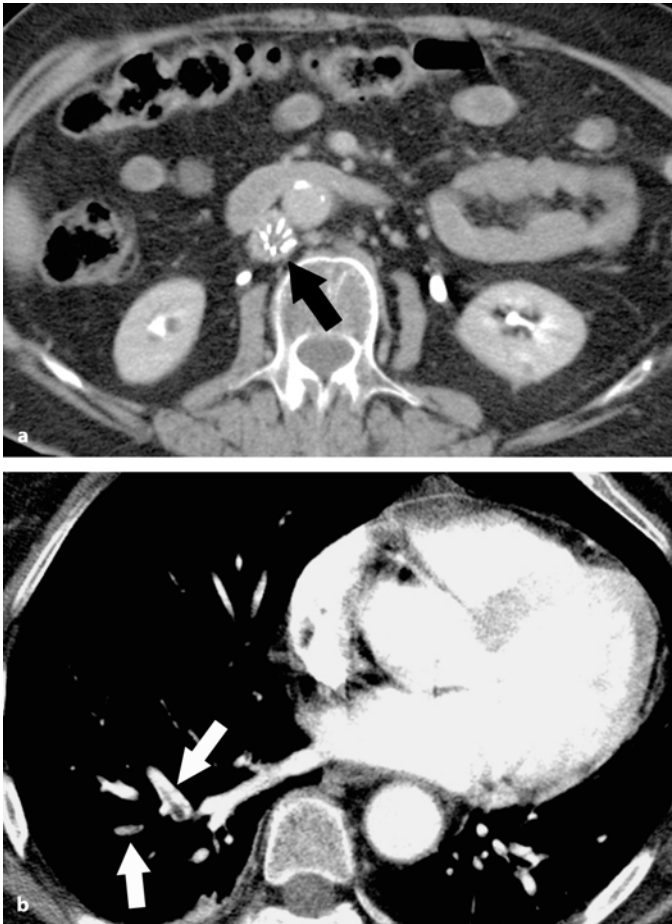


**Fig. 13.** Recurrent PE in an 83-year-old woman with a history of venous thrombo-embolism treated with percutaneous insertion of an inferior vena cava filter (IVCF). **a** Axial CT venogram at the level of the infrarenal IVC demonstrates tilting of the IVCF by showing the asymmetric aspect of the struts (*arrow*). Recurrent DVT was evidenced in the right lower limb (not shown). **b** Spiral CT angiography shows recurrent PE in the right lower lobe (*arrows*)

time of the patient is between 15 and 25 min. Preliminary results have suggested that combined CTPA-CTV is more cost-effective in selected patients than a combination of other tests [83]. The technical quality of CTV is not dependent of patient collaboration or mobility; therefore, it may be useful in ICU patients who are intubated, or who are unable to hold their breath, or in whom leg symptoms cannot be assessed [43]. The CTV is not limited by leg cast or painful compression, dressing, edema, open wounds, severe burns or trophic changes of lower limbs or obesity [43, 46, 84]. Patient comfort is increased, as no further mobilisation is required. CTV provides adequate visualisation of veins, that are difficult to image with other techniques, such as iliac veins and IVC, which is advantageous to guide further interventions, such as catheter placement for thrombolysis or IVC filter introduction [3]. The CTV also demonstrates unsuspected DVT in the opposite limb [28],

adjacent disease or other anomalies compressing the venous system [28, 42]. These findings may be responsible for the symptoms and may have an impact on patient management. Examples are given by GI tract perforation, abdominal tumor, hematoma or other fluid collection, ascitis, portal vein thrombosis, arterial embolism, etc. (Figs. 13–15) [42, 46, 52, 85]. The CTV may also decrease multiple referrals to CT units for suspected malignancy as an underlying cause for VTE [58]. Combined CTPA-CTV results in a complete evaluation of potential sources of clots by screening the lower limbs veins, IVC, SVC and the heart chambers (Figs. 16, 17). It is a valuable baseline for follow-up of VTE or against which any further development can be evaluated [3]. The technique is less operator dependent than US or venography. A potential role in the work-up of paradoxical embolism has been suggested [86].

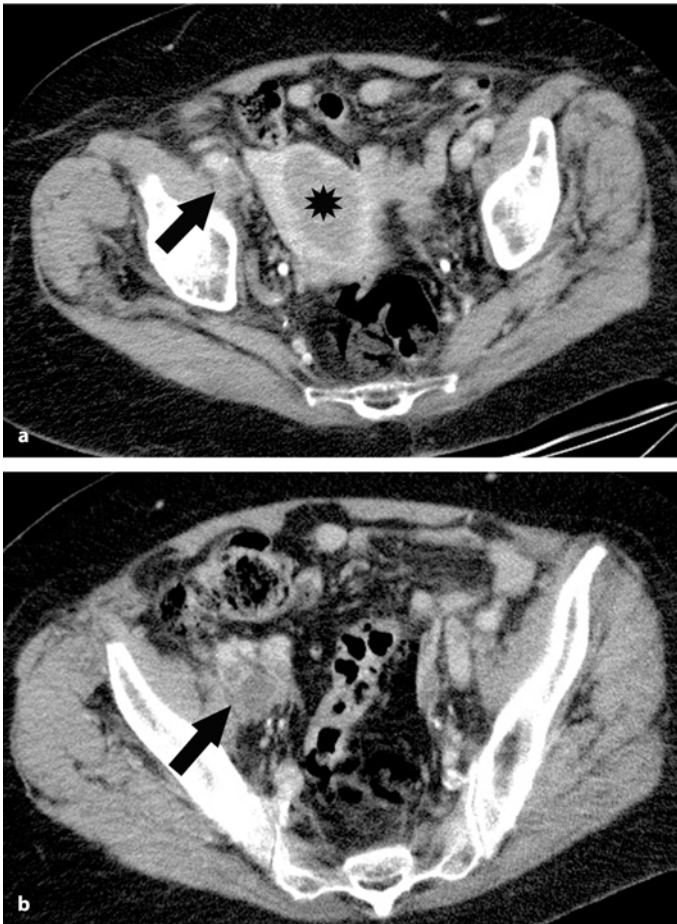


**Fig. 14.** Incidental demonstration of a pelvic tumor compressing the right iliac veins in an 81-year-old woman with acute deep venous thrombosis and non-symptomatic subacute PE. **a** Axial CT venogram at the level of the pelvis shows DVT in the right external iliac vein (*arrow*). A hematic collection is demonstrated in the uterine cavity (*star*). **b** Axial CT venogram acquired 20 mm cranial to **a** demonstrates large necrotic lymph nodes, metastasis of a neoplasia of the endometrium, compressing the right iliac vein (*arrow*)

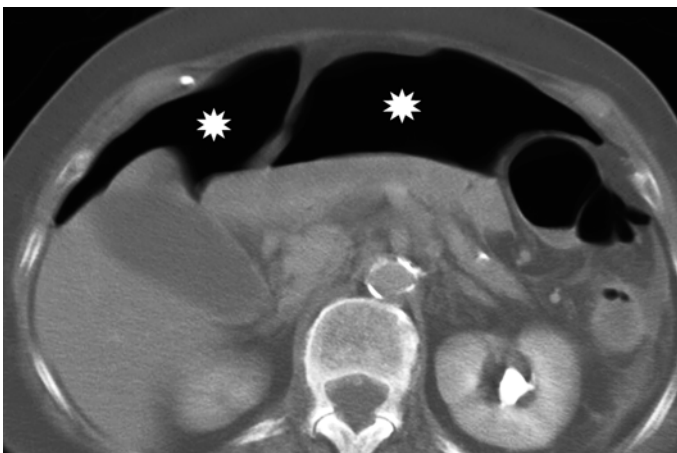


**Fig. 15.** Alternative diagnosis in a 78-year-old woman presenting with acute dyspnea and lower chest pain. Axial CT venogram at the level of upper abdomen shows a large pneumoperitoneum (*stars*) secondary to bowel perforation

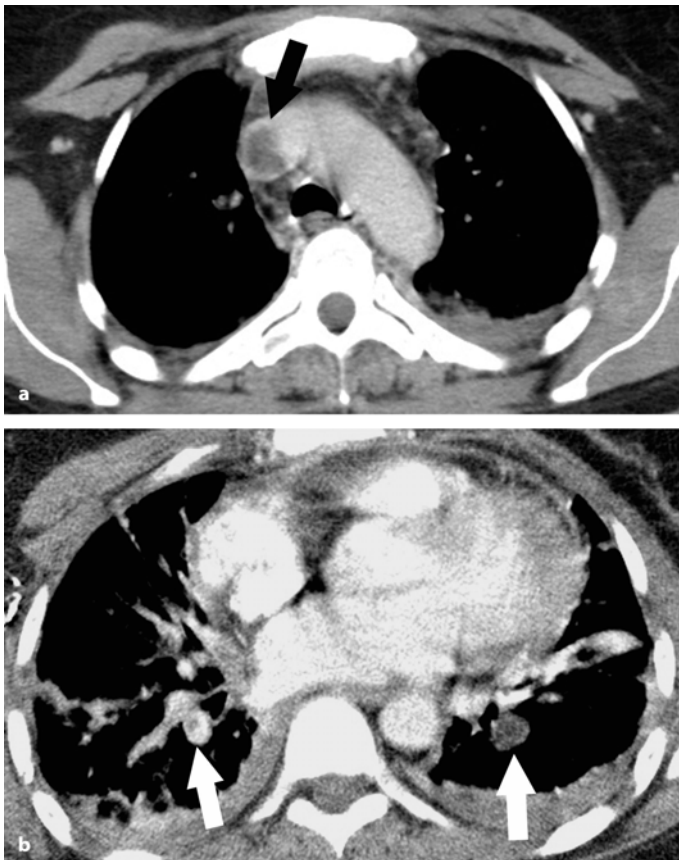


**Fig. 16.** Pulmonary embolism originating from thrombosis of the superior vena cava in a 48-year-old woman. **a** Late phase of CTPA shows clot in the SVC (*arrow*). The CTV of lower limb and abdomen was negative for DVT. **b** A CT angiogram shows segmental PEs in both lower lobes (*arrows*)

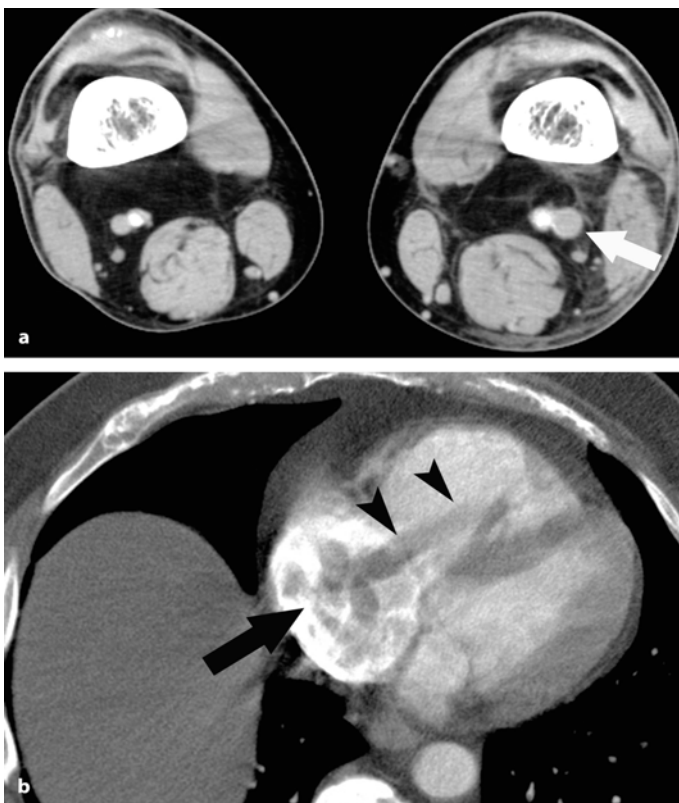


**Fig. 17.** Clot in the right heart chambers in a 66-year-old man. **a** Axial CT venogram at the popliteal level shows focal acute DVT in the left popliteal vein (*arrow*). **b** Late phase of CTPA at the level of the heart shows an elongated clot and packed in the right atrium (*arrow*) and protruding through the tricuspid valve in the dilated right ventricle (*arrowheads*). The clot was not evidenced on the early phase of CTPA, due to strong contrast enhancement and inflow artifacts from the IVC (not shown). The right heart chambers would probably be better studied when using ECG-gated MDCT

**Table 1.** Published clinical studies of combined spiral CT angiography of pulmonary arteries and CT venography of lower limbs and abdomen. US ultrasound, VG venography, IVC inferior vena cava, NA not available, PPV positive predictive value, NPV negative predictive value

Reference	No. of patients	Technique	Slice thickness (mm)	Increment (mm)	Region studied	Standard of reference (n)	Sensitivity (%)	Specificity (%)	PPV (%)	NPV (%)	Inter-technique agreement
[52]	100	Double-detector spiral	5.5	na	mid-calf to retro-hepatic IVC	US (100)	na	na	na	na	k = 1.00
[44]	541	Spiral	10	10	iliac crest to knee	US (116)	na	na	na	na	93 %
[51]	74	Spiral	10	na	iliac crest to knee	US (74)	89	94	67	98	na
[43]	70	Sequential	10	20	knee to renal vein	US (70)	100	97	71	100	na
[42]	209	Sequential	5	20	ankle to diaphragm	US (199) VG (51)	na	na	na	na	k = 0.84 k = 0.53
[85]	150	Sequential	10	50	diaphragm to ankle	US (150)	97	100	na	na	na
[41]	71	Sequential	5–10	50	upper-calf to diaphragm	US (71)	100	100	100	100	na
[46]	65	Double-detector spiral (lower limbs); sequential (abdomen)	6.5 10	5	Mid-calf to pelvis	US (65)					
[71]	650	Sequential	5–10	40	Pelvis to retro-hepatic IVC	VG (2)	93	97	93	97	na
				50	Diaphragm to upper calf or reverse direction	US (308)	97	100	100	99	na
[54]	152	Spiral (lower limbs); sequential (abdomen)	5	3	Pelvis to retro-hepatic IVC	US (18)	na	na	na	na	na
[53]	70	Multi-detector CT	3.75	na	Mid-calf to pelvis Calf to diaphragm	US (46) VG (10)	na	na	na	na	na
[59]	73	Multi-detector CT	5	na	Iliac crest to knee	US (47), VG (24), autopsy (2)	na	na	na	na	na
[55]	136	Spiral	7.5	3.75	Iliac crest to knee	US	71	93	53	97	na
[56]	41	Multi-detector CT	3–8	2–8	Iliac crest to knee	US	100	96.6	91.7	100	na



### 4.3.10 Clinical Results

#### 4.3.10.1 CTV vs Other Imaging Tests

The CTV has been performed using sequential [41–43, 50, 71, 82, 85], spiral [44, 51–53, 55, 56, 59, 87] or mixed technique [46, 54]. Results are most often compared to US which is known to be a weak standard of reference (Table 1). Compared to US, the results of CTV were 71–100% sensitivity, 94–100% specificity, 53–100% positive predictive value and 97–100% negative predictive value, and did not show any difference whether sequential or spiral technique was used. Global inter-technique agreement was 0.84–1.00 between CTV and US [42, 52, 88]. Agreement was lower for infra-popliteal veins ( $k=0.57$ ) than for popliteal and supra-popliteal veins ( $k=0.78-0.87$ ) [52]. The moderate agreement ( $k=0.53$ ) between CTV or US and venography in one study can be partially explained by the fact that venography was mainly applied to patients with discordant results of CTV and US [42].

#### 4.3.10.2 Incremental Value of CTV

Except in two series, CTV increased the percentage of positive results for VTE by 11–36% (mean 23%) [43, 44, 46, 54, 56, 57, 71, 85, 89, 90]. In one study, the addition of CTV to CTPA increased the accuracy of detection of VTE from 69 to 88% [83]. Other advantages were more accurate demonstration of extension of DVT, particularly in pelvic and abdominal veins [42, 43, 71, 54, 88]. When using multidetector technology, the interest of adding CTV to CTPA is currently debated. One recent prospective study shows that US of the common femoral and popliteal vein added <1% of new patients with VTE when multidetector CTPA was negative [10]. In opposition, a recent retrospective study showed that even when using multidetector CTPA, CTV added another 17–27% of patients when scanning from the ankle to the diaphragm [57, 91].

Inter-observer agreement was 0.59–0.95 [46, 50, 87, 88]. The overall detection rate of DVT in CTV in patients with PE was 32–89% (mean 59%). Additional findings and alternative diagnoses for the clinical symptoms were also provided by CTV [42, 46, 52, 85]. Other authors have suggested to perform limited CTV of the pelvis only or pelvis and abdomen, in combination with CTPA, when a previous US was negative. In this condition, additional DVT was demonstrated in 2–8% of the patients suspected of PE [90, 92, 93].

### 4.3.11 Conclusion

Regarding all advantages, combined CTPA–CTV appears as an outstanding imaging technique for patients suspected having VTE which will challenge the current standards

in diagnostic work up in the near future. The technique is time and cost-effective and allows an “all-in-one” accurate visualization of the pulmonary arteries, cardiac chambers, limb, pelvic, retroperitoneal and mediastinal veins. Correct choice of imaging parameters and reasonable use of the spiral mode while imaging the veins decrease the irradiation dose to an acceptable level. Clinical results suggest that CTV should be performed in combination with CTPA in patients suspected having PE, except in young patients, unless US has recently been performed.

### References

1. Moser KM (1990) Venous thromboembolism. *Am Rev Respir Dis* 141:235–249
2. Goldhaber SZ (1998) Pulmonary embolism. *N Engl J Med* 339:93–104
3. Loud PA, Grossman ZD, Klippenstein DL, Ray CE (1998) Combined CT venography and pulmonary angiography: a new diagnostic technique for suspected thromboembolic disease. *Am J Roentgenol* 170:951–954
4. Shah AA, Buckshee N, Yankelevitz DE, Henschke CI (1999) Assessment of deep venous thrombosis using routine pelvic CT. *Am J Roentgenol* 173:659–663
5. National Institutes of Health (1986) Prevention of venous thrombosis and pulmonary embolism. *J Am Med Assoc* 256: 744–749
6. Ferris EJ (1992) George W. Holmes Lecture. Deep venous thrombosis and pulmonary embolism: correlative evaluation and therapeutic implications. *Am J Roentgenol* 159:1149–1155
7. Dalen JE, Alpert JS (1975) Natural history of pulmonary embolism. *Progr Cardiovasc Dis* 17:259–270
8. Remy-Jardin M, Remy J, Deschildre F et al. (1996) Diagnosis of pulmonary embolism with spiral CT: comparison with pulmonary angiography and scintigraphy. *Radiology* 200:699–706
9. Ghaye B, Remy J, Remy-Jardin M (2002) CT diagnosis of acute pulmonary embolism: the first ten years. *Eur Radiol* 12:1886–1905
10. Perrier A, Roy PM, Sanchez O et al. (2005) Multidetector-row computed tomography in suspected pulmonary embolism. *N Engl J Med* 352:1760–1668
11. Ghaye B, Szapiro D, Mastora I et al. (2001) Peripheral pulmonary arteries: How far in the lung does multi-detector row spiral CT allow analysis? *Radiology* 219:629–636
12. Schoepf UJ, Holzkecht N, Helmberger TK et al. (2002) Subsegmental pulmonary emboli: improved detection with thin-collimation multi-detector row spiral CT. *Radiology* 222:483–490
13. Goodman LR, Lipchik RJ (1996) Diagnosis of acute pulmonary embolism: time for a new approach. *Radiology* 199:25–27
14. Goodman LR (2000) CT diagnosis of pulmonary embolism and deep venous thrombosis. *Radiographics* 20:1201–1205
15. Carson JL, Kelley Ma, Duff A, et al. (1992) The clinical course of pulmonary embolism. *N Engl J Med* 326:1240–1245
16. Fishman EK, Horton KM (2000) CT of suspected pulmonary embolism: study design optimization. *Am J Roentgenol* 175: 1002–1003
17. Bettmann MA (1997) Venography. In: Baum S (ed) *Abrams’ angiography*, vol 2. Little, Brown and Company, Boston, pp 1743–1754
18. Lensing AW, Kraaijenhagen R, Van Beek EJR, Buller HR (1999) Diagnosis of venous thrombosis. In: Oudkerk M, van Beek EJR, ten Cate JW (eds) *Pulmonary embolism*. Blackwell, London, pp 44–70

19. Steele JR, Sones PJ, Heffner LT (1978) The detection of inferior vena caval thrombosis with computed tomography. *Radiology* 128:385–386
20. Zerhouni EA, Barth KH, Siegelman SS (1980) Demonstration of venous thrombosis by computed tomography. *Am J Roentgenol* 134:753–758
21. Van Breda A, Rubin BE, Drury EM (1979) Detection of inferior vena cava abnormalities by computed tomography. *J Comput Assist Tomogr* 3:164–169
22. Pawar SV, Kay CJ (1984) Soft-tissue CT changes in pelvic venous thrombosis. *Am J Roentgenol* 143:605–607
23. Pagani JJ, Thomas JL, Bernardino ME (1982) Computed tomographic manifestations of abdominal and pelvic venous collaterals. *Radiology* 142:415–419
24. Vujic I, Stanley J, Tyminski LJ (1981) Computed tomography of suspected caval thrombosis secondary to proximal extension of phlebitis from the leg. *Radiology* 140:437–441
25. Allgayer B, Reiser M, Ries G, Feuerbach S (1981) Computed tomographic demonstration of venous thrombosis of different etiologies. *Eur J Radiol* 1:204–206
26. Hidalgo H, Korobkin M, Breiman RS, Heaston DK, Moore AV, Ram PC (1982) CT demonstration of subcutaneous venous collaterals. *J Comput Assist Tomogr* 6:514–518
27. Pillari G, Zito J, Chang JB et al. (1987) Lower extremity swelling: computerized tomography following negative venography. *Cardiovasc Intervent Radiol* 10:261–263
28. Bauer AR, Flynn RR (1988) Computed tomography diagnosis of venous thrombosis of the lower extremities and pelvis with contrast material. *Surg Gynecol Obstet* 167:12–15
29. Langer B, Kauffman P, Bechara M, Aguiar ET, Aun R (1991) Diagnosis of deep venous thrombosis of the lower limbs by computed tomography. *Rev Paul Med* 109:149–152
30. Stehling MK, Rosen MP, Weintraub J, Kim D, Raptopoulos V (1994) Spiral CT venography of the lower extremity. *Am J Roentgenol* 163:451–453
31. McLachlan MS, Thomson JG, Taylor DW, Kelly ME, Sackett DL (1979) Observer variation in the interpretation of lower limb venograms. *Am J Roentgenol* 132:227–229
32. Picolet H, Leizorovicz A, Revel D, Chirossel P, Amiel M, Boissel JP (1990) Reliability of phlebography in the assessment of venous thrombosis in a clinical trial. *Haemostasis* 20:362–367
33. Carpenter JB, Holland GA, Baum RA, Owen RS, Carpenter JT, Cope C (1993) Magnetic resonance venography for the detection of deep venous thrombosis: comparison with contrast venography and duplex Doppler ultrasonography. *J Vasc Surg* 18:734–741
34. Ruehm SG, Wiesner W, Debatin JF (2000) Pelvic and lower extremity veins: contrast-enhanced three-dimensional MR venography with a dedicated vascular coil: initial experience. *Radiology* 215:421–427
35. Fraser DG, Moody AR, Morgan PS, Martel AL, Davidson I (2002) Diagnosis of lower-limb deep venous thrombosis: a prospective blinded study of magnetic resonance direct thrombus imaging. *Ann Intern Med* 136:89–98
36. Blum JE, Handmaker H (2000) Role of small-peptide radiopharmaceuticals in the evaluation of deep venous thrombosis. *Radiographics* 20:1187–1193
37. Baldt MM, Zontsich T, Stumpflen A et al. (1996) Deep venous thrombosis of the lower extremity: efficacy of spiral CT venography compared with conventional venography in diagnosis. *Radiology* 200:423–428
38. Baldt MM, Zontsich T, Kainberger F, Fleischmann G, Mostbeck G (1997) Spiral CT evaluation of deep venous thrombosis. *Semin Ultrasound CT MR* 18:369–375
39. Zontsich T, Turetschek K, Baldt M (1998) CT-phlebography. A new method for the diagnosis of venous thrombosis of the upper and lower extremities. *Radiologie* 38:586–590
40. Gartenschlager M, Klose KJ, Schmidt JA (1996) Floating venous thrombi: diagnosis with spiral-CT-phlebography. *Rofo Fortschr Geb Rontgenstr Neuen Bildgeb Verfahren* 164:376–381
41. Loud PA, Katz DS, Klippenstein DL, Shah RD, Grossman ZD (2000) Combined CT venography and pulmonary angiography in suspected thromboembolic disease: diagnostic accuracy for deep venous evaluation. *Am J Roentgenol* 174:61–65
42. Ghaye B, Szapiro D, Willems V, Dondelinger RF (2000) Combined CT venography of the lower limbs and spiral CT angiography of pulmonary arteries in acute pulmonary embolism: preliminary results of a prospective study. *JBR-BTR* 83:271–278
43. Garg K, Kemp JL, Wojcik D et al. (2000) Thromboembolic disease: comparison of combined CT pulmonary angiography and venography with bilateral leg sonography in 70 patients. *Am J Roentgenol* 175:997–1001
44. Cham MD, Yankelevitz DF, Shaham D et al. (2000) Deep venous thrombosis: detection by using indirect CT venography. *Radiology* 216:744–751
45. Yankelevitz DF, Gamsu G, Shah A et al. (2000) Optimization of combined CT pulmonary angiography with lower extremity CT venography. *Am J Roentgenol* 174:67–69
46. Coche EE, Hamoir XL, Hammer FD, Hainaut P, Goffette PP (2001) Using dual-detector helical CT angiography to detect deep venous thrombosis in patients with suspicion of pulmonary embolism: diagnostic value and additional findings. *Am J Roentgenol* 176:1035–1039
47. Abdelmoumene Y, Chevallier P, Barghouth G et al. (2003) Optimization of multidetector CT venography performed with elastic stockings on patients' lower extremities: a preliminary study of nonthrombosed veins. *AJR* 180:1093–1094
48. Michel SJ, Fried AM, Sinha S et al. (2004) Comparison of iodixanol with iohexol for delayed pelvic venous opacification: a preliminary study of potential use for CT venography. *Am J Roentgenol* 183:123–126
49. Goodman LR, Gulsun M, Nagy P, Washington L (2005) CT of deep venous thrombosis and pulmonary embolus: Does isosmolar contrast agent improve vascular opacification? *Radiology* 234:923–928
50. Garg K, Kemp JL, Russ PD, Baron AE (2001) Thromboembolic disease: variability of interobserver agreement in the interpretation of CT venography with CT pulmonary angiography. *Am J Roentgenol* 176:1043–1047
51. Duwe KM, Shiau M, Budorick NE, Austin JH, Berkmen YM (2000) Evaluation of the lower extremity veins in patients with suspected pulmonary embolism: a retrospective comparison of helical CT venography and sonography. *Am J Roentgenol* 175:1525–1531
52. El Hajjam M, Qanadli SD, Mignon F, Sissakian J, Chagnon S, Lacombe P (1999) Combined double helical CT phlebography of the lower extremities and CT pulmonary angiography: new approach for thromboembolic disease diagnosis. *Radiology* 213 (Suppl):126 (Abstract)
53. Muller C, Kopka L, Funke M, Funke C, Grabbe E (2001) Diagnosis of lung embolism and underlying venous thrombosis in multi-slice spiral CT. *Rofo Fortschr Geb Rontgenstr Neuen Bildgeb Verfahren* 173:528–535
54. Nicolas M, Debelle L, Laurent V et al. (2001) Incremental lower extremity CT venography, a simplified approach for the diagnosis of deep venous thrombosis in patients with pulmonary embolism. *J Radiol* 82:251–256
55. Peterson DA, Kazerooni EA, Wakefield TW et al. (2001) Computed tomographic venography is specific but not sensitive for diagnosis of acute lower-extremity deep venous thrombosis in patients with suspected pulmonary embolus. *J Vasc Surg* 34:798–804
56. Begemann PG, Bonacker M, Kemper J et al. (2003) Evaluation of the deep venous system in patients with suspected pulmonary embolism with multi-detector CT: a prospective study in comparison to Doppler sonography. *J Comput Assist Tomogr* 27:399–409

57. Richman PB, Wood J, Kasper DM et al. (2003) Contribution of indirect computed tomography venography to computed tomography angiography of the chest for the diagnosis of thromboembolic disease in two United States emergency departments. *J Thromb Haemost* 1:652–657
58. Schoepf UJ, Kessler MA, Rieger CT et al. (2001) Multislice CT imaging of pulmonary embolism. *Eur Radiol* 11:2278–2286
59. Wildberger JE, Mahnken AH, Sinha AM, Haage P, Schaller S, Gunther RW (2002) A differentiated approach to the diagnosis of pulmonary embolism and deep venous thrombosis using multi-slice CT. *RoFo* 174:301–307
60. Katz DS, Loud PA, Bruce D et al. (2002) Combined CT venography and pulmonary angiography: a comprehensive review. *Radiographics* 22:S3–S19
61. Szapiro D, Ghaye B, Willems V, Zhang L, Albert A, Dondelinger RF (2001) Evaluation of CT time–density curves of lower-limb veins. *Invest Radiol* 36:164–169
62. Martin-Bouyer Y (2002) Phleboscanner. Presented at the 2nd Symposium on Volumetric Multislice CT, Nancy, France, 7–8 October
63. Rademaker J, Griesshaber V, Hidajat N, Oestmann JW, Felix R (2001) Combined CT pulmonary angiography and venography for diagnosis of pulmonary embolism and deep vein thrombosis: radiation dose. *J Thorac Imaging* 16:297–299
64. Greess H, Wolf H, Suess C, Kalender WA, Bautz W, Baum U (2004) Automatic exposure control to reduce the dose in subsecond multislice spiral CT: phantom measurements and clinical results. *RoFo* 176:862–869
65. Lomas DJ, Britton PD (1991) CT demonstration of acute and chronic iliofemoral thrombosis. *J Comput Assist Tomogr* 15:861–862
66. Gmelin E, Link J, Judaschke S, Marienhoff N (1992) Non-enhanced CT of thrombosed calf veins. *Rofo Fortschr Geb Rontgenstr Neuen Bildgeb Verfahr* 156:338–341
67. Bruce D, Loud PA, Klippenstein DL, Grossman ZD, Katz DS (2001) Combined CT venography and pulmonary angiography: How much venous enhancement is routinely obtained? *Am J Roentgenol* 176:1281–1285
68. Wagner M, Mark L (1969) Duplication of the inferior vena cava and its role in recurrent pulmonary emboli. *J Am Med Assoc* 209:108–109
69. Kouroukis C, Leclerc JR (1996) Pulmonary embolism with duplicated inferior vena cava. *Chest* 109:1111–1113
70. Ghaye B, Szapiro D, Willems V, Dondelinger RF (2002) Pitfalls in CT venography of the lower limbs and abdominal veins. *Am J Roentgenol* 178:1465–1471
71. Loud PA, Katz DS, Bruce DA, Klippenstein DL, Grossman ZD (2001) Deep venous thrombosis with suspected pulmonary embolism: detection with combined CT venography and pulmonary angiography. *Radiology* 219:498–502
72. Garg K, Mao J (2001) Deep venous thrombosis: spectrum of findings and pitfalls in interpretation on CT venography. *Am J Roentgenol* 177:319–323
73. Vogelzang RL, Gore RM, Anschuetz SL, Blei AT (1988) Thrombosis of the splanchnic veins: CT diagnosis. *Am J Roentgenol* 150:93–96
74. Lien HH, Lund G (1983) Collateral veins in inferior caval vein occlusion demonstrated via CT. *Eur J Radiol* 3:319–323
75. Seem E, Stranden E, Stiris MG (1985) Computed tomography in deep venous thrombosis with limb oedema. *Acta Radiol Diagn* 26:727–730
76. Hull RD, Carter CJ, Jay RM et al. (1983) The diagnosis of acute, recurrent, deep-vein thrombosis: a diagnostic challenge. *Circulation* 67:901–906
77. Cronan JJ, Leen V (1989) Recurrent deep venous thrombosis: limitations of US. *Radiology* 170:739–742
78. Glazer GM, Callen PW, Parker JJ (1981) CT diagnosis of tumor thrombus in the inferior vena cava: avoiding the false-positive diagnosis. *Am J Roentgenol* 137:1265–1267
79. Barnes PA, Bernardino ME, Thomas JL (1982) Flow phenomenon mimicking thrombus: a possible pitfall of the pedal infusion technique. *J Comput Assist Tomogr* 6:304–306
80. Vogelzang RL, Gore RM, Neiman HL, Smith SJ, Deschler TW, Vrla RF (1985) Inferior vena cava CT pseudothrombus produced by rapid arm–vein contrast infusion. *Am J Roentgenol* 144:843–846
81. Youssefzadeh S, Liskutin J, Dorffner R, Bankier A, Hubsch P (1998) Venous contrast fluid level in computed tomography. *Clin Radiol* 53:528–531
82. Ciccotosto C, Goodman LR, Washington L, Quiroz FA (2002) Indirect CT venography following CT pulmonary angiography: spectrum of findings. *J Thorac Imaging* 17:18–27
83. Censullo ML, Ernst RD, Kawashima A, Caskey CI, Sandler CM (1999) CT venography as an adjunct to CT pulmonary angiography for the detection of pulmonary thrombo-embolic disease. *Radiology* 213 (Suppl):558 (Abstract)
84. Balakrishnan C, Gheiler EL (1993) Computed tomography for diagnosis of deep venous thrombosis in burn patients. *Plast Reconstr Surg* 91:1174–1175
85. Katz DS, Loud PA, Klippenstein DL, Shah RA, Grossman ZD (2000) Extra-thoracic findings on the venous phase of combined computed tomographic venography and pulmonary angiography. *Clin Radiol* 55:177–181
86. Delalu P, Ferretti GR, Bricault I, Ayanian D, Coulomb M (2000) Paradoxical emboli: demonstration using helical computed tomography of the pulmonary artery associated with abdominal computed tomography. *Eur Radiol* 10:384–386
87. Ciccotosto C, Filippone A, Storto ML, Ricciardi M, Salcuni M, Bonomo L (2002) Accuracy of multislice CT for acute deep venous thrombosis: variability of observer performance related to clinical experience. *Eur Radiol* 12 (Suppl):150 (Abstract)
88. Landragin E, Delval O, Corneloup O, Tallon JB, Morin M, Vandermarcq P (2001) Can CT venography replace US in the diagnosis of deep venous thrombosis? *J Radiol* 82:1444 (Abstract)
89. Jonetz-Mentzel L, Basche S, Eger C (2001) CT phlebography and CT angiography of the pulmonary arteries in the diagnosis of acute lung embolism. *Eur Radiol* 11 (Suppl):137 (Abstract)
90. Walsh G, Redmond S (2002) Does addition of CT pelvic venography to CT pulmonary angiography protocols contribute to the diagnosis of thromboembolic disease? *Clin Radiol* 57: 462–465
91. Ghaye B, Nchimi A, Noukoua C, Dondelinger RF (in press) Does multi-detector row thin-collimation CT pulmonary angiography reduce the incremental value of indirect CT venography compared to single-detector row CT pulmonary angiography? *Radiology*
92. Ferretti GR, Ayanian D, Ranchoup Y, Thony F, Bosson JL, Coulomb M (1998) CT assessment of abdominal and pelvic veins in patients suspected of acute pulmonary embolism and presenting with normal sonography of the lower limbs. *J Radiol* 79:327–330
93. Au VW, Walsh G, Fon G (2001) Computed tomography pulmonary angiography with pelvic venography in the evaluation of thrombo-embolic disease. *Australas Radiol* 45:141–145

# Imaging and Treatment of Thoracic Fluid and Gas Collections

C. Noukoua Tchuisse, B. Ghaye, R.F. Dondelinger

## 4.4

### Contents

4.4.1	Introduction	391
4.4.2	Diagnostic Imaging	391
4.4.2.1	Pleural Fluid Collection	391
4.4.2.2	Pneumothorax	392
4.4.2.3	Pneumomediastinum	393
4.4.2.4	Pericardial Effusion	394
4.4.3	Imaging Guidance Modalities	394
4.4.3.1	Fluoroscopy	394
4.4.3.2	Computed Tomography	395
4.4.3.3	Ultrasound	395
4.4.3.4	Magnetic Resonance imaging	395
4.4.4	Percutaneous Drainage of Thoracic Fluid Collections	395
4.4.4.1	Pleural Collections	395
4.4.5	Pulmonary Collections	401
4.4.5.1	Pulmonary Abscess	401
4.4.5.2	Aspergilloma	401
4.4.5.3	Pneumatocele and Bulla	401
4.4.6	Mediastinal Collections	403
4.4.6.1	Mediastinal Abscess	403
4.4.7	Complications of Percutaneous Catheter Drainage	406
4.4.8	Conclusion	406
	References	406

### 4.4.1 Introduction

Percutaneous nonoperative procedures in the chest were applied before the advent of imaging. Leyden [1] performed the first transthoracic needle lung biopsy in 1882 to confirm pulmonary infection. Percutaneous insertion of drainage catheters in fluid collections of the pleura, lung, or mediastinum, guided by imaging, has been applied on a large scale since the late 1970s using basic catheter-guidewire techniques, which had been used already in the abdomen [2]. These procedures are recognized as standard and are part of the clinical radiological therapeutic armamentarium.

### 4.4.2 Diagnostic Imaging

#### 4.4.2.1 Pleural Fluid Collection

##### Chest Radiography

Minimal pleural effusion confined to the subpulmonary space is either responsible of slight elevation of the right hemidiaphragm or increased distance between the gastric air and left lung base on upright films. Fluid obliterating the posterior pleural sulcus occurs early and is more easily depicted with lateral chest radiographs. Blunting of the costo-phrenic angle is the characteristic plain-film presentation of pleural effusion in a lateral location. With the fluid volume increasing, lateral chest wall exhibits an ascending concave meniscus, the so-called meniscus sign or described as Damoiseau's curve, delineating the pleural fluid. Massive effusions in the absence of underlying lung atelectasis usually have an accompanying mediastinal shift to the contralateral side. Both transudative and exudative effusions present similar chest radiographic appearances. Radiographic abnormalities, such as pleural nodules, mediastinal, hilar, or pulmonary masses, indicate possible malignancy as a cause of pleural effusion [3].

##### Ultrasound

Typically, pleural fluid appears as a mobile and gravity-dependent echo-free layer between the visceral and parietal pleural membranes. Transudative effusions are anechoic, exudative appearances, and are complex and vary from anechoic to echoic with or without septations [4–6]. Mobile strands of echoic tissue and septations are frequently observed in complicated pleural effusion. Ultrasound can reveal cellular debris in empyema as hyperechoic spots that do not move with respiration [7]. Empyema, particularly at a chronic stage, can result in an echogenic collection that mimics a solid lesion. Pleural nodularity and complex effusion should draw attention to a possibly associated malignancy [8]; however, biopsy is necessary to distinguish benign from malignant lesion and warrant definitive diagnosis.



### Computed Tomography

Computed tomography has been established as the optimal technique to simultaneously demonstrate pleural space, pulmonary parenchyma, and mediastinum. Free pleural collections accumulate in a gravity-dependent position. They have a lentiform shape, an obtuse chest wall angle, with displacement of adjacent lung parenchyma. Characteristic increased enhancement and thickened parietal pleura is visible in patients with exudative effusions [9–11]. Pleural effusions containing proteins show higher density values than transudates (25–45 vs 0–25 HU). Recent hemothorax shows characteristic high densities (35–70 HU). The separation of thickened and enhancing parietal and visceral pleurae often seen at CT in empyemas is called the “split-pleural” sign [12]. Although CT has ability to determine the presence of pleural fluid loculations, its sensitivity for the detection of fibrinopurulent and organizing phases of effusions are reportedly fair. Computed tomography has high sensitivity and specificity in the detection of pleural disease in patients with suspected malignant effusions [13]. Multidetector-row CT with three-dimensional reconstruction improves both the accuracy of tumor detection and its local extent. Moreover, CT easily differentiates benign from malignant pleural thickening in most cases.

### Magnetic Resonance Imaging

Pleural fluid collections and pleural thickening remaining undetermined after CT may undergo magnetic resonance imaging (MRI). Gadolinium-enhanced fat-saturated T1-weighted images appear optimal in the detection of pleural thickening caused by malignancy, and T2-weighted sequences are useful in detecting pleural nodules in the presence of an effusion [14].

### Positron Emission Tomography

Fluorodeoxyglucose-18 positron emission tomography (18-FDG-PET) accurately detects both focal and diffuse glucose-avid pleural abnormalities. When analyzed with

the knowledge of the patient’s history, 18-FDG-PET appears to have a low false-positive rate and high accuracy in determining the malignant nature of a pleural effusion [15, 16]. On PET pleural abnormalities predict the nature of pleural effusion with an accuracy of 90% [15]. Moreover, PET is useful in the evaluation of mediastinal nodes metastases [17]. A 96% sensitivity and 88% specificity for FDG-PET was reported in detecting pleural malignancies in patients with exudative effusions and pleural thickening [18].

## 4.4.2.2 Pneumothorax

### Chest Radiography

Chest radiography (CR) has long been the most effective diagnostic examination for pneumothorax. In complete detachment of the visceral pleura, CR typically shows collapse of the lung, delineated by a linear shadow representing the visceral pleura beyond which peripheral markings of the normal lung are not visible (Fig. 1). The ipsilateral hemithorax is widened. In supine patients the detection of a pneumothorax may be difficult. Deep sulcus sign with radiolucency along the costophrenic sulcus may help to identify occult pneumothoraces. Mediastinal shift toward the contralateral lung and flattening of the diaphragm reflect tension pneumothorax. Pleural adhesions may prevent complete detachment of the visceral pleura, resulting in partial pneumothorax that may be difficult to detect on CR according to its volume, location, and the position of the patient.

### Ultrasound

Sonography is also useful for excluding pneumothorax [19]. The key sonographic signs used to diagnose pneumothorax include absent lung sliding, exaggerated horizontal artifacts, loss of comet-tail artifacts, and broadening of the pleural line to a band. Absent lung-sliding movement of the visceral pleura in patients with a pneumothorax is



**Fig. 1.** Posteroanterior chest radiograph in a 58-year-old man with dyspnea following insertion of a central venous access shows a right-sided pneumothorax (arrow) with loss of lung volume

the most sensitive criterion for the diagnosis but should not be used as the sole criterion because of its low specificity [20]. The combination of absent lung sliding and the loss of comet-tail artifact has a reported sensitivity of 100%, specificity of 96.5%, and negative predictive value of 100% [21]. Ultrasound was found to be more sensitive than CR in the detection of pneumothorax in a selected group of patients with percutaneous lung biopsy [22].

### Computed Tomography

Computed tomography is the most sensitive and specific modality in clinical setting, and has become the reference standard for the detection of pneumothorax because of high contrast differentiation between free air and lung parenchyma [23]. Differential diagnosis with large bullae and panlobular emphysema is usually easily estab-

lished. Moreover, CT warrants anatomical display of all thoracic structures, and percutaneous access to the pleural space.

### 4.4.2.3 Pneumomediastinum

#### Chest Radiography

Typically, pneumomediastinum appearance at CR is a radiolucent line between the left heart border and the mediastinal pleura. Other locations of mediastinal air are more difficult to detect; thus, posteroanterior CR may overlook 50% of cases. If CT is not available, lateral chest radiographs should be performed, which increase significantly the sensitivity of CR [24]. With lateral views, air is visualized in the retrosternal space or as lucent streaks outlining the aorta and other mediastinal structures [25].

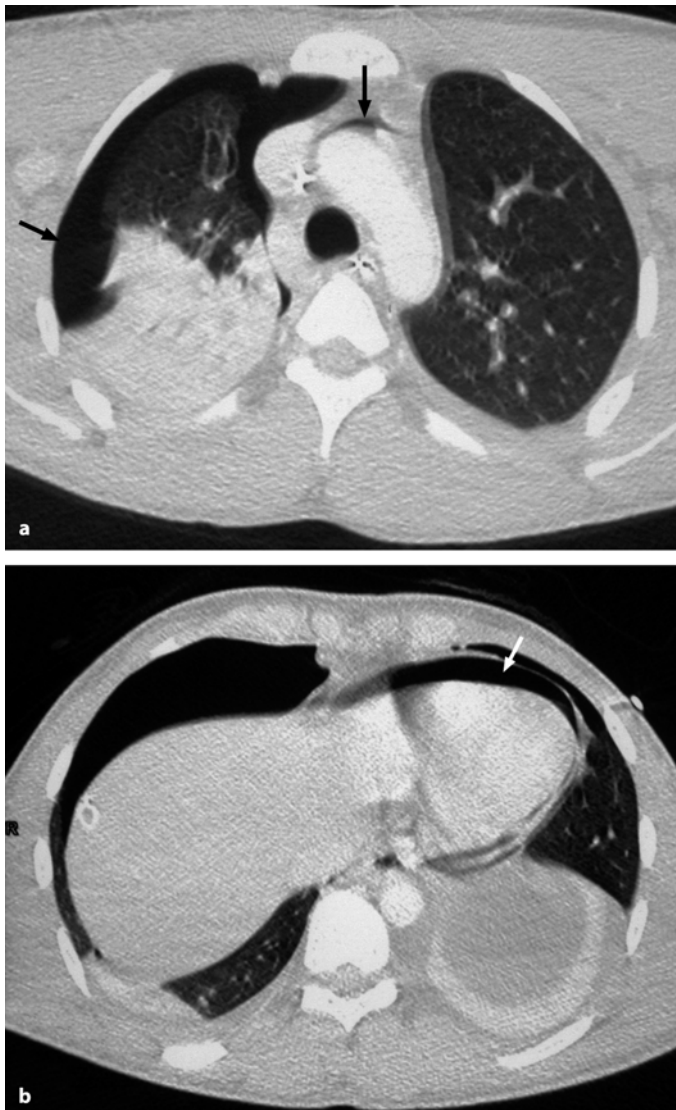


**Fig. 2.** Contrast-enhanced CT following trauma in a 44-year-old man shows **a** pneumothorax and pneumomediastinum (*arrows*), and **b** pneumopericardium (*arrow*)

### Computed Tomography

Similarly to pneumothorax, CT has become the standard of reference for the diagnosis of pneumomediastinum. The utility of chest CT in diagnosing small pneumomediastinum not visible on CR is well established (Fig. 2). The use of CR alone leads to a missed diagnosis in 30% of patients presenting with pneumomediastinum [26].

#### 4.4.2.4 Pericardial Effusion

##### Chest Radiography

Chest radiography may display a variable degree of heart shadow enlargement, depending on the amount of pericardial fluid and distribution. Massive effusions produce a large cardiac shadow, causing the characteristic water-bottle heart or triangular heart with smoothed-out cardiac borders.

##### Ultrasound

Echocardiography is the primary procedure for diagnosis and quantification of the effusion, and has a 96% diagnostic accuracy. Ultrasound appearance is an echo-free space between the epicardial and pericardial reflections (Fig. 3). Small volume effusion accumulates posterior to the left ventricle, whereas large effusion is observed around the heart.

##### Computed Tomography

Computed tomography also detect as little as 50 cc of fluid in the pericardial space, and determines composition of the fluid. The CT is able to evaluate thickness and density of the pericardium and characterize to some extent the content of the pericardial space. Highly attenuating pericardial effusion (>30 HU) had a sensitivity of 100%, a specificity of 70%, and a predictive value of 33% for hemorrhage [27]. The CT easily detects pericardial calcifications and helps identification of constrictive pericarditis by providing additional information on the status of the vena cava, atria, and ventricles [28].

##### Magnetic Resonance Imaging

Magnetic resonance imaging has great ability to characterize pericardial effusion and abnormalities with the use of T1, T2 spin-echo (SE), and gradient-recalled-echo (GRE) sequences. The MRI distinguishes hemorrhagic from non-hemorrhagic pericardial effusion. Nonhemorrhagic effusion has a low signal intensity on T1-weighted SE and high intensity on T2-weighted GRE images [28]. Hemorrhagic effusion often contains signal areas of mixed medium and high intensity signal on T1-weighted SE and low intensity on T2-weighted GRE images [29]. The MRI easily depicts thickening or nodular neoplastic pericardial disease, and

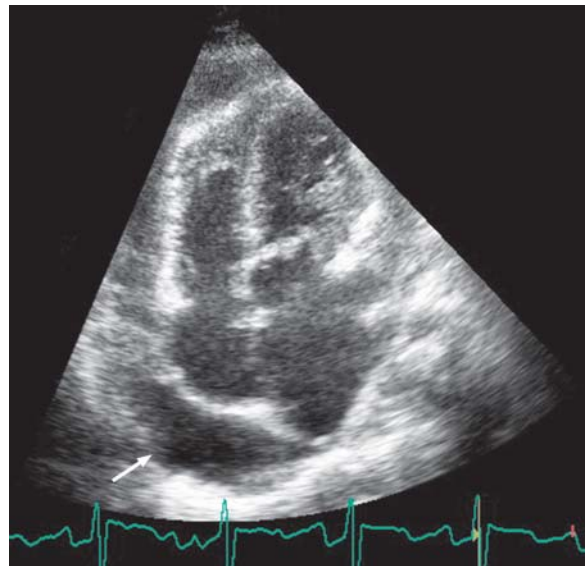


**Fig. 3.** Echocardiography in a 52-year-old man admitted for dyspnea shows an anechoic fluid collection in the posterior pericardial space (arrow)

also distinguishes constrictive thickening of the pericardium from effusion and restrictive cardiomyopathy with an accuracy of 93%. Pericardial thickness >4 mm associated with typical clinical symptoms is highly suggestive of constrictive pericarditis [28, 29].

### 4.4.3 Imaging Guidance Modalities

Imaging techniques used for diagnosis and the guidance of interventional procedures include fluoroscopy and cross-section imaging, or a combination of both [30]. A comparison of the different imaging modalities for percutaneous biopsy or drainage of thoracic lesions is given in Table 1 [31].

#### 4.4.3.1 Fluoroscopy

Uni- or bi-planar fluoroscopy was the first technique to be used as a guidance of percutaneous transthoracic needle biopsy and drainage of gas and fluid collections [32–42]. Advantages are familiarity to most elderly operators, real-time control of the procedure, rapidity, and its wide availability in radiology departments. Fluoroscopy allows adjustment of the tip of a catheter previously inserted into a fluid collection with US or CT control [43]. Opacification of fistulous tracts is best documented with fluoroscopy and plain films, sometimes in combination with CT. Fluoroscopy carries the drawbacks of projection imaging and lacks the anatomical precision of cross-sectional images.

**Table 1.** Comparison of imaging techniques for guidance of thoracic interventions. (Modified from [31])

Modality	Cost	Availability	Radiation (patient/physician)	Length of procedure	Access to central lesion	Real-time control	Mobilization of the patient
Fluoroscopy	+	+++	+/+	+	+	+++	+++
CT	++	++	++/0	+++	+++	0	+
Fluoro-CT	++	++	++/+	++	+++	++	+
Ultrasonography	+	+++	0/0	++	0	+++	+++
MR	+++	+	0/0	+++	+++	+	+

The plus symbols represent a qualitative assessment; the greater the number of pluses, the greater the parameter

#### 4.4.3.2 Computed Tomography

Computed tomography offers exquisite anatomical display of all the thoracic structures and allows percutaneous access to all spaces with almost equal ease [38, 41–47]. Intravenous contrast medium injection is mandatory for identification of fluid content, necrosis, inflammatory thickened pleura, normal vascular structures, and false aneurysm, located, for instance, in an abscess wall. The CT allows for determination of an optimal cutaneous entry point, in such a way as to avoid transgression of a pleural fissure or puncture of a large vessel, a bronchus, or the esophagus. Spiral scanning capability was not proved to be superior to sequential scanning for guiding percutaneous puncture [48]. Real-time CT (fluoro-CT or continuous CT) is now widely available and combines the advantages of cross-section imaging and almost real-time control of the procedure [49, 50]. A limited number and short acquisition sequences are mandatory to reduce radiation exposure of the operator's hands.

#### 4.4.3.3 Ultrasound

Apart from it being the primary imaging guidance for biopsies of the chest wall or pleural lesions as well as lesions located in the anterior mediastinum, US is particularly indicated to guide bedside percutaneous aspiration and catheter drainage of a pleural or pericardial fluid collection, even of only small amounts [34–37, 43, 51–54]. A subpleural pulmonary collection can also be punctured with US control [55]. The percutaneous approach is performed in the patient's position which optimally displays access to the collection.

#### 4.4.3.4 Magnetic Resonance imaging

Guidance of percutaneous interventions is a promising application of MRI. Little clinical experience has been gained thus far in thoracic interventions.

#### 4.4.4 Percutaneous Drainage of Thoracic Fluid Collections

Image-guided percutaneous aspiration or drainage of fluid (or air) collections is considered a valid alternative to surgery. Increased safety and effectiveness compared with blind techniques have been largely demonstrated. Access to any collection located in the pleural space, pericardium, lung, or mediastinum can be gained under imaging guidance.

##### 4.4.4.1 Pleural Collections

Pleural effusions, including empyema, hemothorax, chylothorax, and pneumothorax can be considered for percutaneous closed catheter drainage. Intrapleural fibrinolytic agents are used in the drainage of multiloculated pleural empyema.

##### Empyema

Indications for catheter drainage depend on the evolutionary stage of the pleural effusion, according to the classification of Light (Table 2) [56] and Light and Rodriguez [57]. The early stage (exudative phase) corresponds to the secretion of a protein rich fluid by the pleura. This is a mandatory transitional phase for empyemas and does not require drainage. The second stage (fibrinopurulent phase) is characterized by a viscous and opaque fluid with increased cellularity. Deposition of fibrin layers on the pleural surface promotes the formation of pleural pockets and progressive lung entrapment. Medical treatment without effective fluid drainage might fail. The third stage (organizing phase) is characterized by fibroblastic infiltration of the pleura, limiting the expansion of the underlying lung due to pleural peels. Early drainage of a complicated effusion is necessary to prevent progression to the organized phase, which requires surgical decortication. In surgical treatment, blind placement of a thoracostomy tube (30–34 F) is followed by open surgical drainage if unsuccessful, although some surgeons recommend early open drainage, and pleural decortication, as the initial therapeutic approach [56, 58].



**Table 2.** Classification and treatment of pleural effusions. (Adapted from [57])

Type of effusion	Class 1: nonsignificant	Class 2: typical parapneumonic	Class 3: borderline complicated	Class 4: simple complicated	Class 5: complex complicated	Class 6: simple empyema	Class 7: complex empyema
Imaging aspect	<10 mm on decubitus chest X-ray free flowing	>10 mm on decubitus chest X-ray free flowing	Usually not loculated	Not loculated	Multi-loculated	Single loculated or free flowing	Multiloculated
Fluid aspect	Clear	Clear	Clear	Not frank pus	Not frank pus	Frank pus	Frank pus
pH	>7.2	>7.2	>7.0 and <7.2	<7.0	<7.0		
Glucose (mg/dl)	>40	>40	>40	<40	<40		
LDH, (U/l)	<1000	<1000	>1000				
Gram stain or culture	Negative	Negative	Negative	Positive	Positive		
Treatment	Not indicated (antibiotics)	Antibiotics alone; thoracocentesis if ineffective	Antibiotics and serial thoracocentesis	Antibiotics and thoracostomy catheter	Thoracostomy catheter and thrombolytics (thoracoscopy if ineffective)	Thoracostomy tube; decortication	Thoracostomy tube and thrombolytics; decortication

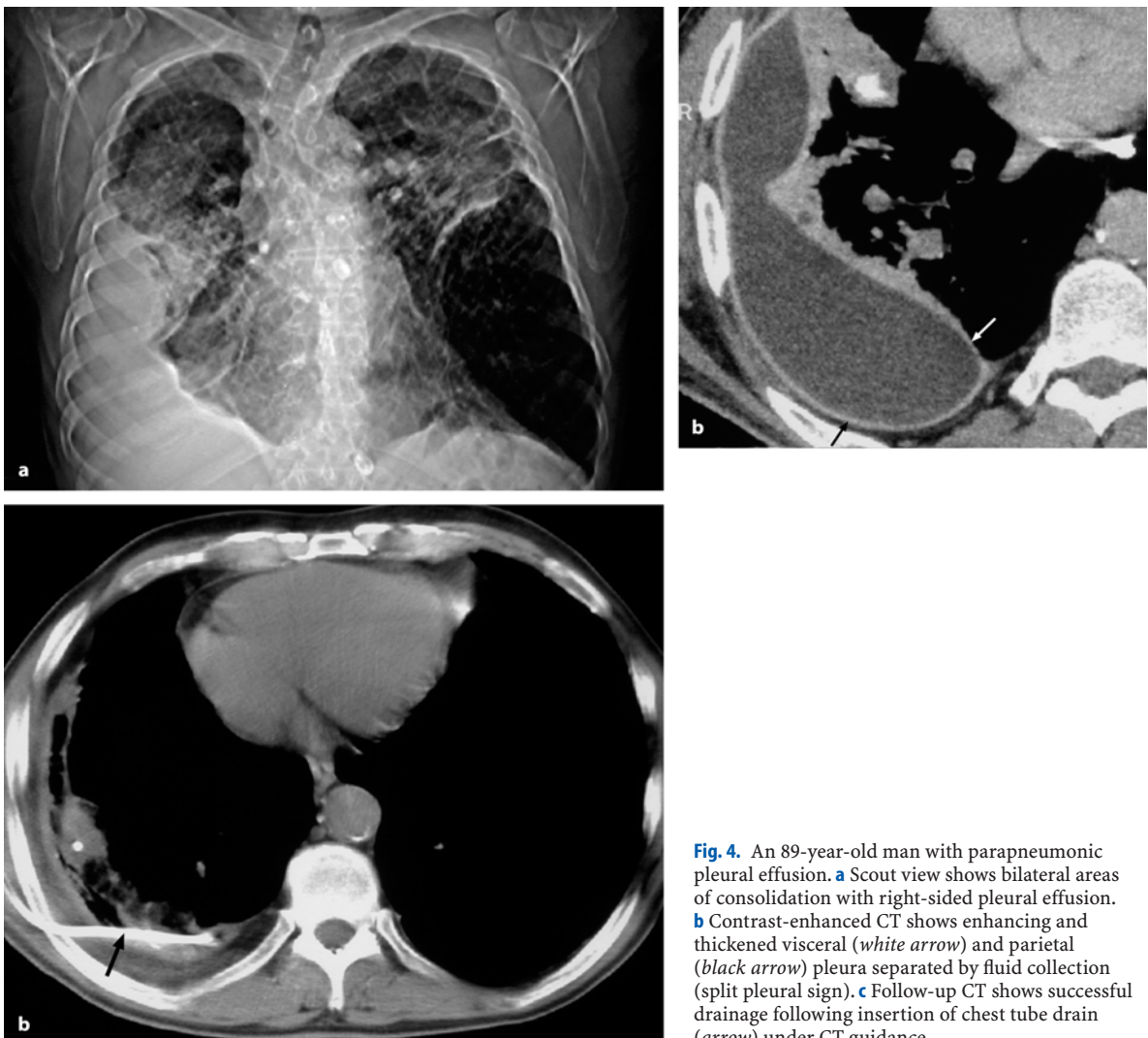


**Fig. 4.** An 89-year-old man with parapneumonic pleural effusion. **a** Scout view shows bilateral areas of consolidation with right-sided pleural effusion. **b** Contrast-enhanced CT shows enhancing and thickened visceral (*white arrow*) and parietal (*black arrow*) pleura separated by fluid collection (split pleural sign). **c** Follow-up CT shows successful drainage following insertion of chest tube drain (*arrow*) under CT guidance

**Table 3.** Percutaneous drainage of pleural empyema in a first attempt

Reference	No. of patients	Guidance modality (%)	Clinical success (%)
[43]	17	CT (59) US (41)	88
[33]	12	Fluoroscopy	83
[52]	17	US	88
[36]	16	CT	75
[35]	20	Fluoroscopy (5) CT (25), US (40) Combination (30)	80
[40]	42	US (72) CT (20) Fluoroscopy (8)	80
[38]	13	Fluoroscopy CT	100
[46]	12	US (80) CT (20)	83
[53]	13	US	85
[41]	10	Fluoroscopy	100
[42]	27	CT or US or Fluoroscopy	70
[45]	22	CT	82
[61]	63	CT or US	84

Imaging-guided percutaneous drainage avoids the potential failures associated with blind chest tube placement, which can occur in about 50% of patients due to inadequate positioning of the tube or to undrained satellite pleural pockets [59, 60]. The size of the percutaneous catheters that are in regular use varies from 7 to 30 F and is chosen according to the viscosity of the fluid to be drained (Fig. 4). Computed tomography discloses all satellite non-communicating pleural pockets, that are usually drained with multiple catheters. Pleural fluid, which is encapsulated in a fissure, can also be adequately drained with CT control, most often without transgression of normal lung by the catheter. Technical success is achieved in almost all cases. Clinical success is achieved in 70–89% of the patients treated in a first attempt, depending on the stage of empyema (Table 3) [30, 33, 35–37, 40, 42, 43, 45, 46, 52, 53, 61]. A similar success rate of 80% is obtained in patients treated in a second attempt following failed surgical chest tube drainage (Table 4) [30, 33, 36–38, 42, 43]. Failure of percutaneous drainage varies from 11 to 30%, and usually occurs in chronic empyema (stage III), when extensive pleural peels have formed, which may prevent catheter insertion, or prevent the cavity to collapse and obliterate. The CT may have its difficulties in accurately differentiating between the fibrinopurulent and organizing phase of empyema [62]. Medium-sized catheters are better tolerated by the patient than large thoracostomy tubes, but their lumen is more prone to obstruction by fibrin products.

Intrapleural injection of fibrinolytic agents was proven to be efficient in preventing fibrin deposit and formation of secondary loculation of the empyema, with a clinical suc-

**Table 4.** Percutaneous drainage of pleural empyema in a second attempt

Reference	No. of patients in whom thoracostomy tube failed	No. of patients with successful drainage by radiologically placed catheter
[43]	13	12 (92)
[33]	4	4 (100)
[37]	3	3 (100)
[36]	7	4 (57)
[38]	5	5 (100)
[42]	8	4 (50)
[61]	40	28 (70)

Numbers in parentheses are percentages

cess rate of 62–100% [30, 38, 41, 63–77]. The most commonly used fibrinolytic is streptokinase and urokinase. The mean dose of streptokinase was 250,000 IU in 100 ml normal saline solution, whereas the range of dose for urokinase varied from 50,000 IU to 250,000 IU in 100 ml normal saline solution. Local instillation of fibrinolytics also reduces the number of drainage catheters that are necessary to drain all loculations, duration of drainage, and prevents fibrosis of the pleural surface. Intrapleural fibrinolytics associated to chest tube drainage significantly improve the outcome of medically treated multiloculated empyema [78–80].

In a recent study fibrinolytics did not improve mortality, the need of surgical drainage, or the duration of hospital stay [81].

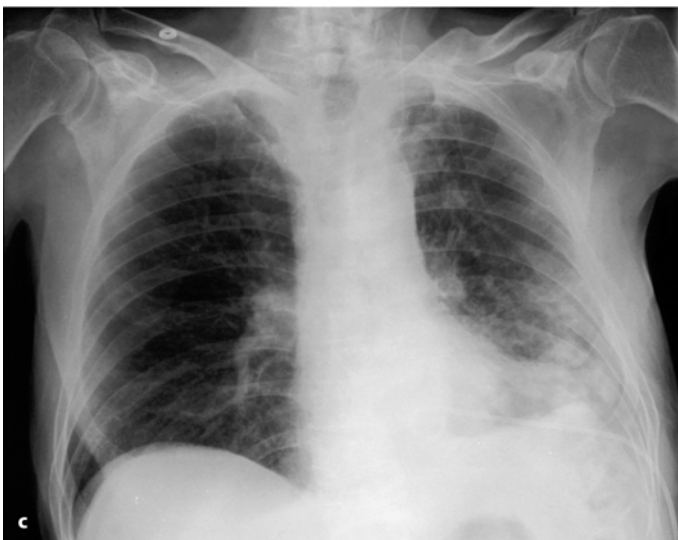
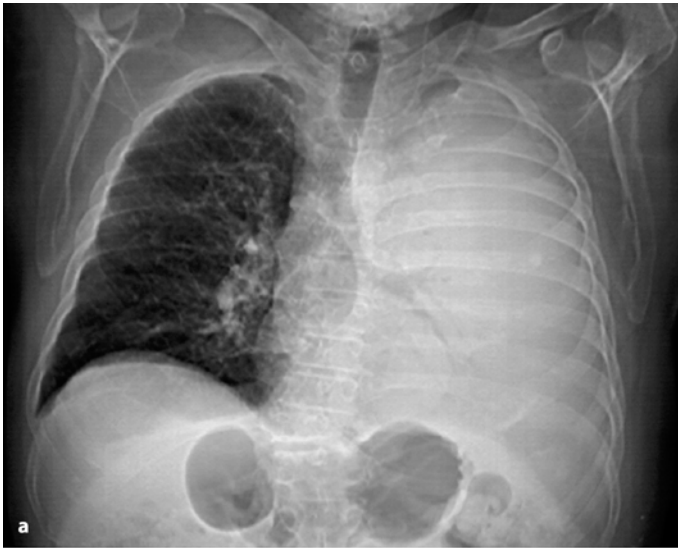


**Fig. 5.** A 78-year-old man presented with dyspnea, chest pain, and poor general condition. **a** Anteroposterior chest radiograph shows a massive left-sided pleural effusion without mediastinal shift. **b** Contrast-enhanced CT demonstrates pleural effusion with complete lung atelectasis. A 9-F pigtail catheter was inserted under CT guidance and drained a mixed (serous hemorrhagic) fluid. Vibromycin injection was performed for pleural talcage. **c** Follow-up chest radiograph a few months later shows re-expansion of the lung and residual pleural opacities

### Malignant Pleural Effusion

Recurrent malignant pleural effusion, which is not controlled by systemic treatment, is usually drained with a soft and small catheter (8 F) followed by pleural sclerosis by intrapleural injection of talcum, doxycyclin, bleomycin, or other drugs. Advantages of small catheters as compared with classic large-bore thoracostomy tubes are the possibility of treatment on an outpatient basis and increased patient comfort. Advantages of imaging guidance is the proper insertion of the catheter inside the pleural cavity, thus avoiding injury of a pleural mass, which may bleed during catheter insertion, nonrecognition of persistent undrained loculations, and incomplete lung re-expansion before pleural sclerosis (Fig. 5). Complete regression of a malignant pleural effusion is obtained in 53–81% and partial resolution in up to 95% of cases, which is a similar response rate than that obtained with large thoracostomy tubes [39, 54, 82–84].

### Hemothorax

Posttraumatic hemothorax is usually drained by large-bore surgical chest tubes. In selected cases with persistent intercostal or phrenic artery bleeding, angiography and transcatheter embolization is indicated before drainage. Long-lasting multiloculated hemothorax is an indication for image-guided catheter drainage. Fibrinolytic agents can be safely injected in a pleural hematoma at 1 week following trauma (Fig. 6) [70, 71]. Uncontrolled intrapleural bleeding is an absolute contraindication of intrapleural fibrinolysis.

### Pneumothorax

Pneumothorax is the most frequent potential complication following percutaneous pulmonary and mediastinal biopsy. The incidence of pneumothorax following percutaneous biopsy is 7–15% [85]. Less than 5% of patients have persistent clinical signs and need aspiration or drainage. Factors influencing pneumothorax are number of needle passes, type, diameter and flexibility of the needle, emphysema, difficult localization of the target, and cooperation of the patient. The best prevention of complications is to perform the procedure rapidly and to reduce the number of passes by inspecting the quality of smears after each puncture. Coaxial needle puncture reduces also pleural injury. A clinically significant pneumothorax is prevented by the roll-over technique, which consists in turning the patient following biopsy for 15–30 min on the side which has been punctured. When biopsy was performed with fluoroscopy

control on an outpatient basis, a chest X-ray is often obtained immediately following the procedure. When no pneumothorax is present, chest X-ray is repeated after 4 h of surveillance before the patient is discharged. When no pneumothorax is detected on CT slices following biopsy with CT guidance, chest X-ray is postponed for 4 h. When the X-ray is normal, the patient is sent home, with the usual instructions. The patient and his relatives are advised to return to the hospital when suggestive signs of complications (cough, chest pain, shortness of breath, etc.) are noticed. When an asymptomatic or partial pneumothorax is diagnosed following transthoracic needle biopsy, aspiration of air is performed with a 16-G teflon sheathed needle and a syringe. The patient is put again on the side that was biopsied and chest X-ray is repeated after 1 h. When control chest X-ray is normal, the patient is discharged after 4 h of surveillance and the above-mentioned recommendations are given. When a large or symptomatic pneumothorax persists, a Heimlich valve is inserted under fluoroscopy control by an anterolateral transthoracic approach. A 7-F catheter with a straight tip and multiple sideholes is inserted in the pleural cavity with the angiographic catheter-exchange technique. The pneumothorax is aspirated before the valve is connected and good function of the valve is checked before the patient is discharged. The catheter is sutured to the skin and the Heimlich valve is loosely attached to the waist. The patient is sent home and called back on the next day for a control chest X-ray. In our experience, pneumothorax disappeared in all cases. If the pneumothorax occurs during mediastinal biopsy, due to pulmonary transgression by the needle, biopsy is completed before the pneumothorax is treated.

Hemoptysis is encountered in less than 10% of percutaneous lung biopsy [85]. This complication is worrisome for the patient but rarely requires specific treatment. Bleeding inside a pulmonary nodule during puncture enhances its density on fluoroscopy but does not limit CT guidance. A perinodular alveolar hemorrhage is commonly observed and can obscure the nodule, rendering further punctures impossible. Alveolar blood usually does not appear on the exterior. Codeine can be given to reduce cough. Other complications, such as mediastinal emphysema, thoracic wall hematoma, hemothorax, empyema, air embolism, and sudden death, are extremely rarely reported following transthoracic fine-needle lung biopsy. The success rate of drainage of iatrogenic pneumothorax is 75–97%, the vast majority resolving within 24–72 h [34, 40, 59, 84, 86]. Recurrent pneumothorax can be treated with chemical pleurodesis if surgical therapy is not an option.



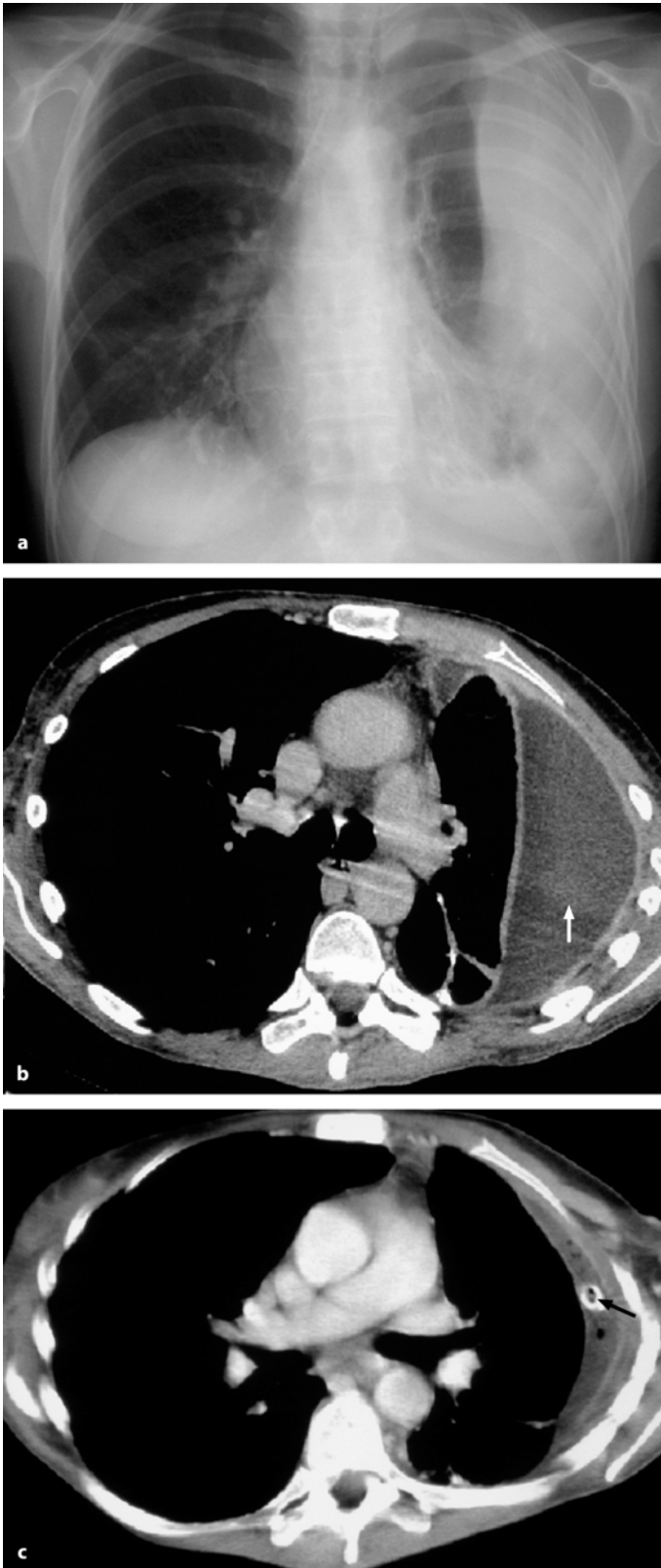


**Fig. 6.** A 35-year-old woman presented with increasing posttraumatic dyspnea. **a** Anteroposterior chest radiograph shows left-sided pleural effusion. **b** Contrast-enhanced CT confirmed a large pleural collection with areas of high density (*arrow*), suggesting the presence of fresh clot. **c** Aspiration with a Teflon-sheathed catheter confirms the presence of blood. A 24-F chest tube (*arrow*) was inserted into the collection. Follow-up CT demonstrates regression of the pleural collection

---

## 4.4.5 Pulmonary Collections

---

### 4.4.5.1 Pulmonary Abscess

Pulmonary abscesses occur mainly in adult patients, whose general condition is debilitated for instance by cancer, alcoholism, denutrition, diabetes, and immune deficiency. Pulmonary abscess may result from hematogenous origin (bacterial endocarditis), or from infection of a pre-existing pulmonary cavity (emphysematous bulla, post-traumatic pneumatocele or pseudocyst, tuberculosis, fungus), pulmonary infarction, or tumor. A pulmonary abscess can complicate pneumonia with or without bronchial obstruction (Fig. 7). Other facilitating conditions are chronic obstructive pulmonary disease, steroid therapy, general anesthesia, epilepsy, stroke, or esophageal motility disorders. Pulmonary abscesses which resist to medical treatment, postural, and bronchoscopic drainage need drainage [38]. In the past, surgical treatment of a lung abscess was required in about one-fifth of patients, and pulmonary lobectomy was standard treatment, then practice changed to limited wedge resection and open surgical abscess drainage without lung resection.

A percutaneous diagnostic aspiration with a 18- or 22-G needle can precede catheter insertion in doubtful cases, e.g. in a bulla with an air fluid level, which is not necessarily infected. An abscess with a diameter of 1–3 cm is adequately treated by a single percutaneous aspiration without insertion of a drainage catheter. Endoscopic transbronchial placement of a catheter inside a lung abscess can be planned with CT control and monitored with fluoroscopy control. Transbronchial drainage is less comfortable for the patient than the percutaneous approach. Contamination of the opposite lung is also a risk with the transbronchial technique. Mechanical ventilation is not a contraindication to percutaneous abscess drainage. Lung abscesses are often located in the periphery of the lung and usually they do not break through the lobar fissure. Pleural symphyses are rapidly established. The broad pleural contact allows planning of a percutaneous access in such a way that normal lung parenchyma is not crossed by the drainage catheter. There is no significant technical difference in draining empyema or a large pulmonary abscess. Pleural empyema by direct contamination is unlikely to occur. The trocar technique is the preferred drainage modality to avoid bacterial contamination during the over-wire catheter exchange.

Generally, 7- to 14-F catheters are adequate for drainage of most lung abscesses. Flexible pigtail catheters can be curled inside the cavity. The drainage catheter is sutured to the skin and must be connected to a negative waterseal aspiration. Pulmonary abscesses have a more or less thick wall and do not collapse rapidly after aspiration. Duration of drainage is variable, and the cavity closes after 4–5 weeks. Immediate decompression should be slow in order to avoid rupture of a vessel or pseudo-aneurysm incorporated in the abscess wall. Lavage of a pulmonary abscess is dangerous, due to risk of bronchogenic spread of pus. Injection of contrast medium through the drainage catheter does not add significant information, but patency of the catheter can be checked daily by injection of a minimal amount of fluid. Daily chest radiographs are imperative for monitoring regression of the abscess cavity and early detection of complications. Cure is obtained in 73–100% of cases following 10–15 days of drainage (Table 5) [2, 44, 45, 47, 51, 87–92]. Surgery remains indicated when extensive necrosis of lung parenchyma and life-threatening hemorrhage are present. Temporizing percutaneous drainage cures the abscess, but surgery can be required for removal of necrotized tissue or for decortication.

---

### 4.4.5.2 Aspergilloma

Life-threatening hemoptysis due to intracavitary aspergilloma may be recurrent, despite an initially successful bronchial embolization, and eventually may require surgical resection [93–96]. Open thoracotomy, however, can be contraindicated in some patients who present with a severe underlying pulmonary condition [94, 96]. Transthoracic instillation of amphotericin B has been described with a success rate of 50% for resolution of the aspergilloma and 75–100% for acute control of hemoptysis [95–98].

---

### 4.4.5.3 Pneumatocele and Bulla

Percutaneous drainage of infected or tension pulmonary pneumatocele has been described [30, 99]. A percutaneous diagnostic aspiration with an 18-G needle can precede catheter insertion in doubtful cases, as bullae may frequently contain an air–fluid level, without infection.

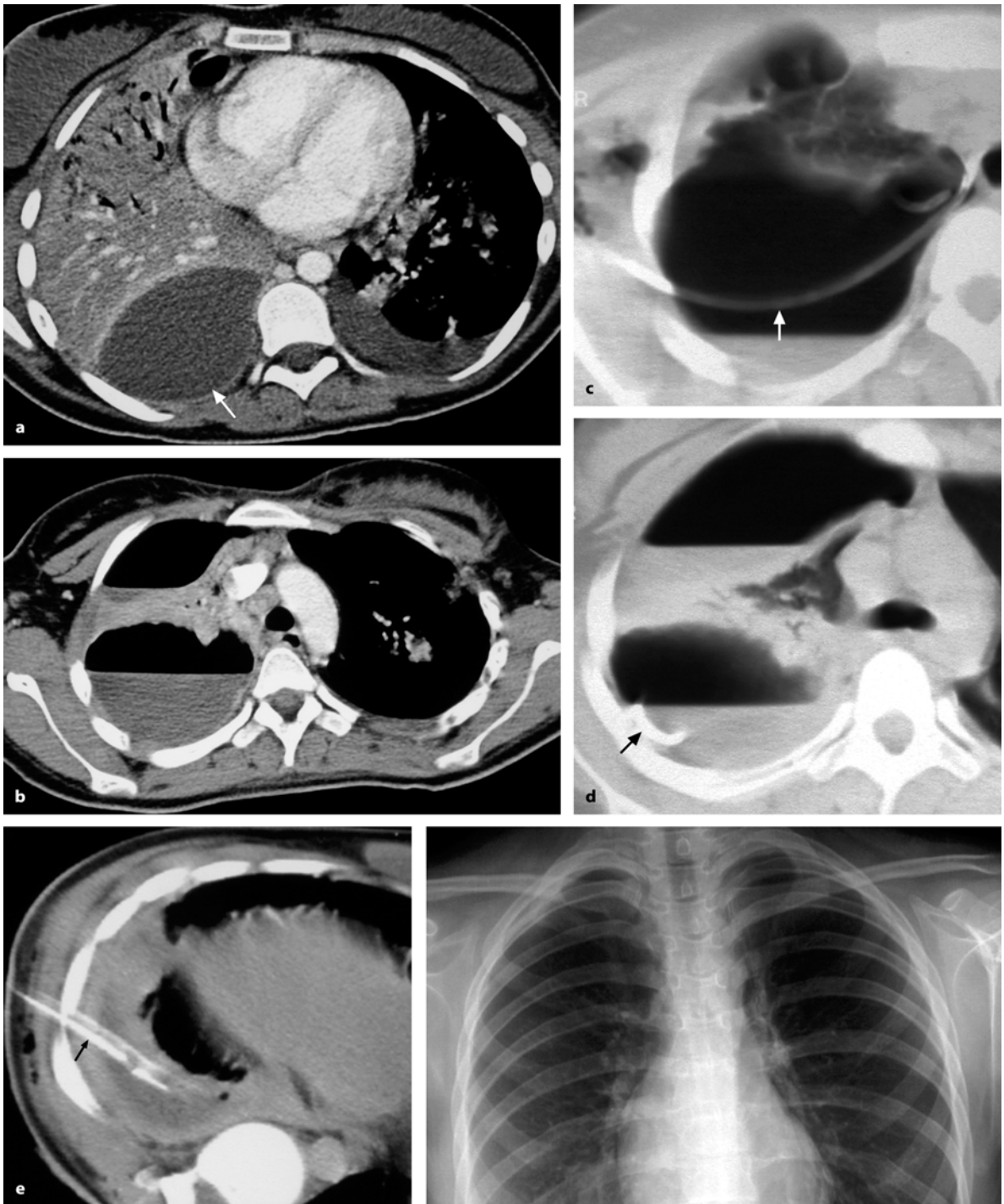


**Fig. 7.** A 21-year-old woman was admitted with fever, cough, and dyspnea. **a** Contrast-enhanced CT shows right-sided lung consolidation with empyema (arrow). **b** Air–fluid level within lung consolidation indicates the presence of a pulmonary abscess. **c, d** A 9-F pigtail catheter (arrow) was inserted into the abscess under CT guidance and pus was aspirated while **e** a 24-F catheter (arrow) was inserted into the empyema. **f** Follow-up chest radiograph 3 months later shows successful drainage

**Table 5.** Percutaneous drainage of pulmonary abscess

Reference	No. of patients	Guidance modality	Caliber of drainage catheter	Duration of drainage (days)	Clinical success (%)
[2]	3	Fluoroscopy	16–18 F		100
[87]	5	Fluoroscopy	18-G Teflon Sheathed needle	Aspiration	100
[88]	13	–	Repeat aspiration 5–30 F	15	100
[89]	7	Fluoroscopy	–	15	100
[51]	6	Fluoroscopy	10 F	–	100
[90]	11	Fluoroscopy	–	–	73
[45]	7	CT	8–14 F	12	43 <sup>a</sup>
[47]	19	CT	9–20 F	10	84
[91]	35	US	18–20F	Aspiration	94

<sup>a</sup> Four of seven patients died within 1 month from underlying disease after successful drainage

## 4.4.6 Mediastinal Collections

### 4.4.6.1 Mediastinal Abscess

Mediastinal abscesses result from circumscribed mediastinitis. Prognosis of diffuse mediastinitis is often poor. Computed tomography is able to distinguish between diffuse infiltration of mediastinal planes and a circumscribed abscess, but separation between acute mediastinitis and postsurgical changes can remain problematic in the early postoperative period. Most purulent mediastinal collections result from trauma, either penetrating transthoracic injury or perforation of the esophagus. Esophageal rupture is due to cancer, corrosion, ulceration, breakdown of surgical anastomoses, protracted vomiting, or following endoscopic laser therapy, resection, bouginage, or balloon dilatation. Thoracic and mediastinal surgery can be followed by mediastinal abscess formation, and a pleural, pulmonary, or cervical infection can spread to the mediastinum (descending mediastinitis). Computed tomography is by far the most useful modality for diagnosis and planning of percutaneous drainage of mediastinal collections (Fig. 8). Abscesses that are located in the anterior mediastinum are drained by a parasternal approach avoiding the internal mammary vessels which are regularly evidenced with CT. Abscesses that are located in the middle and posterior compartment are treated by a paravertebral and extrapleural approach [30, 42]. It is also possible to drain the mediastinal compartments by a percutaneous cervical descending approach. Multiple catheters are often necessary, to be placed either at both sides of the thoracic spine or the sternum, or in the upper and lower part of the mediastinum. Conservative treatment is commonly applied to esophageal perforation.

An endo-esophageal catheter can be inserted together with a percutaneous drainage catheter placed at the site of perforation [100]. When a fistulous tract is present between the mediastinal abscess and an empyema or a subphrenic abscess, percutaneous drainage of these collections may resolve the mediastinal abscess. Other mediastinal fluid collections, such as pancreatic pseudocysts, or pleuroperi-

cardial or bronchogenic cysts, can be aspirated or drained percutaneously during a short time period. Only a limited number of patients with percutaneous drainage have been reported (Table 6) [45, 100–105]. Cure can be obtained in 83–100% of cases, but 30 days mortality is high, owing to the underlying disease.

### Pericardial Fluid Collection

Pericardial effusion is suspected on the basis of clinical signs and electrocardiography. Diagnosis is confirmed with imaging techniques. Causes of pericardial effusion include cardiac insufficiency, malignant tumors, postoperative effusion, pericarditis, hypothyroidism, connective tissue disease, and trauma. Percutaneous aspiration of pericardial fluid is indicated for diagnosis. Percutaneous drainage prevents cardiac tamponade. Clinical signs of tamponade include dyspnea, tachycardia, compromised venous return, and paradoxical pulse. Pericardial fluid of large amount can be drained with CT control (Fig. 9) [106], but most effusions are evacuated with echocardiographic guidance by a subcostal or a subxiphoid approach. The angiographic technique is used to avoid cardiac injury, and the initial puncture is performed with a 18-G or a 5-F Teflon-sheath needle. A 5- to 7-F pigtail catheter is placed in the pericardial space over the guidewire after dilatation of the percutaneous track. Technical success of the procedure and decompression of the heart is achieved in almost all cases, when the effusion is sufficient. Duration of drainage is short, lasting several days. Chylopericardium can be difficult to drain and needs thoracic duct ligation of pericardectomy.

### Tension Pneumomediastinum

Mediastinal emphysema or pneumomediastinum is generated by distinct pathophysiological mechanisms: disruption of air-containing structures; gas producing infection; and so-called spontaneous mediastinal emphysema, which occurs in patients with or without a clinical abnormality and is caused by a large variety of conditions. In hospital patients, the main cause of mediastinal emphysema is mechanical



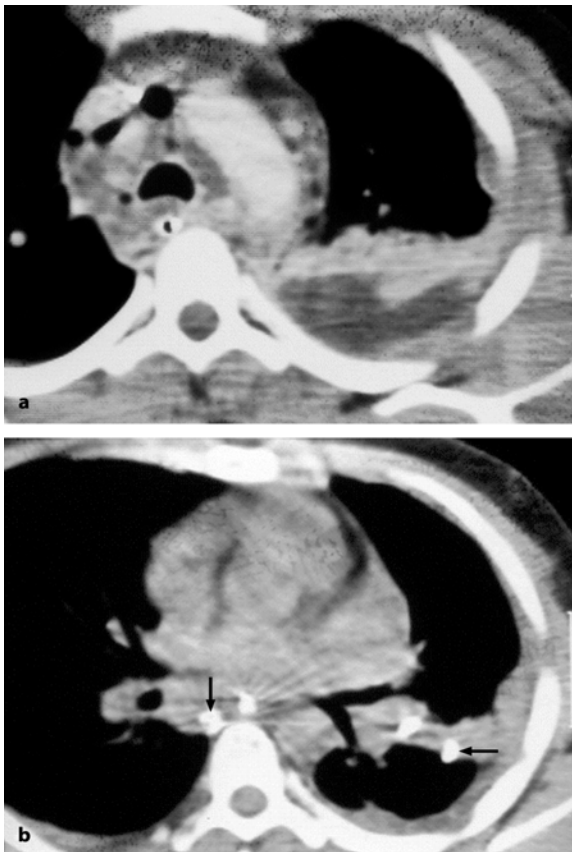


**Fig. 8.** A CT scan in a patient with recent history of cervical trauma shows **a** diffuse descending mediastinitis with air dissection of the mediastinal fat planes and left pleural empyema. **b** Percutaneous insertion of an 8-F pigtail catheter in the left pleural fissure (arrow). Two 14-F drainage catheters were inserted by a cervical approach in the left posterior mediastinum (arrow)

ventilation with high PAP and PEEP. The basic condition for mediastinal emphysema is interstitial pulmonary emphysema, due to alveolar rupture caused by increased alveolar pressure. Penetration of air in the mediastinum occurs along the interstitial tissue contained in the bronchovascular sheaths. When mediastinal pressure rises abruptly, the mediastinal pleura may rupture, resulting in pneumothorax.

Dyspnea and precordial chest pain are the most common clinical symptoms. Physical examination may reveal a thoracic or cervical subcutaneous emphysema and occa-



**Fig. 9.** A 38-year-old woman presented with sudden dyspnea and severe chest pain. **a** A CT scan demonstrates a large pericardial fluid collection (arrow). **b** Percutaneous insertion of a 5-F catheter (arrows) in the posterolateral part of the pericardial space under CT guidance allows aspiration of a sterile blood collection

sionally a crunch can be heard over the mediastinal area. Radiological recognition of pneumomediastinum can be problematic on chest radiographs when mediastinal air volume is limited. The mediastinal air collection is best recognized with CT (Fig. 10), particularly when extensive

**Table 6.** Percutaneous drainage of mediastinal abscess

Reference	No. of patients	Guidance modality	Caliber of drainage catheter (Fr)	Duration of drainage	Clinical success (%)
[100]	6	CT and fluoroscopy	8.3–12	5–91 days (mean 35 days)	83
[103]	8	Fluoroscopy	8.3–12	2–4 weeks	88
[102]	5	CT	–	–	100
[44]	5	Fluoroscopy, US, CT	8–12	Mean 28 days	100
[104]	2	Fluoroscopy and CT	23–17	46–25 days (mean 30 days)	100

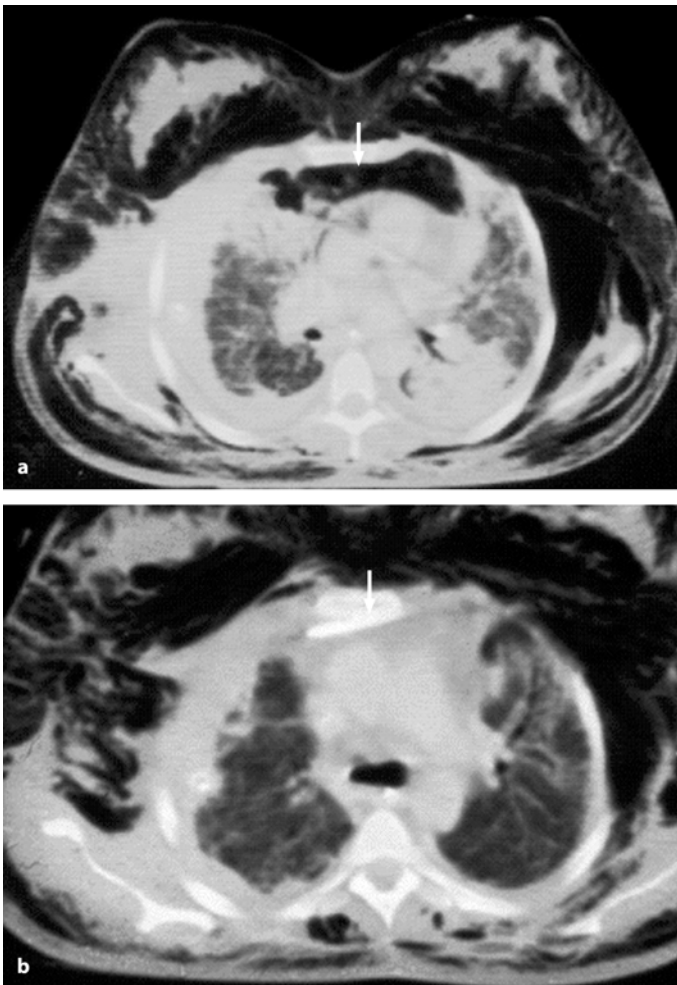


**Fig. 10.** Patient of ICU with sudden oligo-anuria. **a** A CT scan demonstrates tension pneumomediastinum (*arrow*), bilateral pleural effusion and pulmonary consolidation, and subcutaneous emphysema. **b** Percutaneous insertion of a 14-F catheter (*arrow*) in the anterior mediastinum behind the sternum relieved signs of tension pneumomediastinum

subcutaneous emphysema overlies endothoracic structures on bedside chest radiographs. Identification of the source of mediastinal air is crucial for management. In most cases, mediastinal emphysema is well tolerated. Conservative management is sufficient and spontaneous regression is the rule [107]. The most severe clinical presentation is tension mediastinal emphysema, which was reported in single patients [108–110] or in limited series, mainly children and newborn [111]. Tension mediastinal emphysema may develop in ventilated patients if cervical or subphrenic escape routes for mediastinal air were obliterated by previous surgery or scars. Tension within a large air collection confined to the mediastinum is responsible for compromised venous return, which may evolve into a life-threatening condition, if refractory to medical management. Clinical symptoms include dyspnea, cyanosis, hypotension, oligo-anuria, and cardiovascular collapse mimicking acute cardiac tamponade. Association with tension pneumothorax worsens the clinical symptoms.

Prompt therapy must be established before clinical evidence of cardiac tamponade or increase of intracranial

pressure. Limited mediastinostomy is usually performed by an incision above or below the sternum, below the clavicle, or lateral to the sternum, followed by blunt dissection to open the retrosternal space or by insertion of a chest tube in the mediastinum under direct vision. These maneuvers proved generally to be efficient, without serious complications [107, 108, 110]. A suprasternal incision may occasionally fail and need full sternotomy [107].

Percutaneous CT-guided insertion of a mediastinal drainage catheter is a useful therapeutic adjunct following confirmation of tension mediastinal emphysema and avoids the hazards of blind catheter insertion or limited mediastinostomy [112]. Usual percutaneous drainage catheters or chest tubes with variable diameters are used. Catheters with multiple sideholes are necessary to avoid obstruction of the sideholes by the connective mediastinal tissue. The optimal percutaneous approach is anterolateral, the extremity of the catheter being placed behind the sternum in the superior or inferior mediastinal compartment when large mediastinal vessels or the heart are pushed posteriorly by the pneumomediastinum. The internal mam-

mary vessels and large mediastinal vessels are avoided by the course of the catheter. When a pneumothorax is present, insertion of the mediastinal catheter is facilitated before the pneumothorax is treated. The trocar technique is usually adequate for catheter insertion in the mediastinum. A continuous waterseal aspiration with slight negative pressure is maintained during 1–3 weeks until signs of tension have vanished without recurrence. Mediastinal emphysema without symptoms of tension may persist in patients undergoing mechanical ventilation following percutaneous decompression.

### Others

Ectopic pancreatic pseudocysts, pleuropericardial, parathyroid or bronchogenic cysts, necrotic tumors, lymphocele, and hematomas can be drained or aspirated percutaneously using imaging guidance [30].

## 4.4.7 Complications of Percutaneous Catheter Drainage

Complications resulting from percutaneous drainage of thoracic fluid collections guided by imaging techniques occur in 5% of patients and are due mainly to inadequate technique during percutaneous insertion of the catheter. Life-threatening hemorrhage is rare but can be observed following rupture of the wall of a pulmonary abscess, erosion of a branch of the pulmonary artery, or transfixation of the internal mammary or mediastinal vessels by the catheter. Pericardial drainage is prone to most clinically significant complications such as hemopericardium with tamponade, dysrhythmia, pneumopericardium, or superinfection.

A thoracic catheter can be introduced erroneously into the subdiaphragmatic space, the liver, or spleen, when cross-sectional imaging is not used properly. When the catheter creates a communication between a pulmonary abscess and the pleural space, a secondary empyema or a bronchopleural fistula can be established. When the normal lung is crossed with a large-bore catheter using the trocar technique, pulmonary infarction can result. Pneumothorax is a potentially frequent complication, but can be avoided during percutaneous drainage of most pleural collections and pulmonary abscesses, provided that there is pleural contact. During pleural drainage under fluoroscopic guidance, a rate of pneumothorax of 6% has been noted; under US guidance a rate of 25% has occurred. When fluoroscopy is used predominantly as a guidance modality for thoracic drainage procedures, the overall complication rate is as high as 20%, most being minor problems. Other side effects include subcutaneous emphysema, local skin infection at the entry point of the catheter, and discomfort during breathing, rib erosion, catheter leakage, bending, breakage, and obstruction.

## 4.4.8 Conclusion

Thoracic fluid and gas collections may result from benign, malignant, traumatic, and nontraumatic diseases. The role of imaging is well established for diagnosing the cause. Image-guided percutaneous drainage of thoracic gas and fluid collection appear as a safe and effective alternative to surgery.

## References

- Leyden OO (1883) Über infectiöse Pneumonie. *Dtsch Med Wochenschr* 9:52–55
- Vainrub D, Husher DM, Guinn GA et al. (1978) Percutaneous drainage of lung abscess. *Am Rev Respir Dis* 117:153–157
- Maher GG, Berger HW (1972) Massive pleural effusion: malignant and nonmalignant causes in 46 patients. *Am Rev Respir Dis* 105:458–460
- Goerg C, Schwerk WB, Goerg K et al. (1991) Pleural effusion: an “acoustic window” for sonography of pleural metastases. *J Clin Ultrasound* 19:93–97
- Yang PC, Luh KT, Chang DB et al. (1992) Value of sonography in determining the nature of pleural effusion: analysis of 320 cases. *Am J Roentgenol* 159:29–33
- Lomas DJ, Padley SG, Flower CD (1993) The sonographic appearances of pleural fluid. *Br J Radiol* 66:619–624
- Tu CY, Hsu WH, Hsia TC et al. (2004) Pleural effusions in febrile medical ICU patients: chest ultrasound study. *Chest* 12:1274–1280
- Gorg C, Restrepo I, Schwerk WB (1997) Sonography of malignant pleural effusion. *Eur Radiol* 7:1195–1198
- Stark DD, Federle MP, Goodman PC et al. (1983) Differentiating lung abscess and empyema: radiography and computed tomography. *Am J Roentgenol* 141:163–167
- Waite RJ, Carbonneau RJ, Balikian JP et al. (1990) Parietal pleural changes in empyema: appearances at CT. *Radiology* 175:145–150
- Aquino SL, Webb WR, Gushiken BJ (1994) Pleural exudates and transudates: diagnosis with contrast-enhanced CT. *Radiology* 192:803–808
- Kearney SE, Davies CW, Davies RJ et al. (2000) Computed tomography and ultrasound in parapneumonic effusions and empyema. *Clin Radiol* 55:542–547
- Trall ZC, Davies RJ, Gleeson FV (2001) Thoracic computed tomography in patients with suspected malignant pleural effusions. *Clin Radiol* 56:193–196
- Falasci F, Battolla L, Mascalchi M et al. (1996) Usefulness of MR signal intensity in distinguishing benign from malignant pleural disease. *Am J Roentgenol* 166:963–968
- Bury T, Paulus P, Dowlati A et al. (1997) Evaluation of pleural diseases with FDG–PET imaging: preliminary report. *Thorax* 52:187–189
- Toaff JS, Metser U, Gottfried M et al. (2005) Differentiation between malignant and benign pleural effusion in patients with extra-pleural primary malignancies: assessment with positron emission tomography–computed tomography. *Invest Radiol* 40:204–209
- Wang ZJ, Reddy GP, Gotway MB et al. (2004) Malignant pleural mesothelioma: evaluation with CT, MR imaging, and PET. *Radiographics* 24:105–119
- Duysinx B, Nguyen D, Louis R et al. (2004) Evaluation of pleural disease with 18-fluorodeoxyglucose positron emission tomography imaging. *Chest* 125:489–493



19. Lichtenstein DA, Menu Y (1995) A bedside ultrasound sign ruling out pneumothorax in the critically ill. Lung sliding. *Chest* 108:1345–1348
20. Chung MJ, Goo JM, Im JG et al. (2005) Value of high-resolution ultrasound in detecting a pneumothorax. *Eur Radiol* 15:930–935
21. Wu RG, Yang PC, Kuo SH et al. (1995) “Fluid color” sign: a useful indicator for discrimination between pleural and non-pleural effusion. *J Ultrasound Med* 14:767–769
22. Goodman TR, Traill ZC, Phillips AJ et al. (1999) Ultrasound detection of pneumothorax. *Clin Radiol* 54:736–739
23. Wall SD, Federle MP, Jeffrey RB et al. (1983) CT diagnosis of unsuspected pneumothorax after blunt abdominal trauma. *Am J Roentgenol* 141:919–921
24. Miller WE, Spiekerman RE, Hepper NG (1972) Pneumomediastinum resulting from performing Valsalva maneuvers during marijuana smoking *Chest* 62:233–234
25. Bratton SL, O’Rourke PP (1993) Spontaneous pneumomediastinum. *J Emerg Med* 11:525–529
26. Kaneki T, Kubo K, Kawashima A et al. (2000) Spontaneous pneumomediastinum in 33 patients: yield of chest computed tomography for the diagnosis of the mild type. *Respiration* 67:408–411
27. Rifkin RD, Mernoff DB (2005) Noninvasive evaluation of pericardial effusion composition by computed tomography. *Am Heart J* 149:1120–1127
28. Wang ZJ, Reddy GP, Gotway MB et al. (2003) CT and MR imaging of pericardial disease. *Radiographics* 23 (Suppl):167–180
29. Aviram G, Fishman JE (2004) Magnetic resonance imaging of the heart and great vessels. *Can Assoc Radiol J* 55:96–101
30. Ghaye B, Dondelinger RF. (2001) Imaging guided thoracic interventions. *Eur Respir J* 17:507–528
31. Klein JS, Zarka MA (2000) Transthoracic needle biopsy. *Radiol Clin N Am* 38:235–266
32. Dahlgren S, Nordenstrom B (1966) Transthoracic needle biopsy. *Almqvist and Wiksell, Stockholm*
33. Westcott JL (1985) Percutaneous catheter drainage of pleural effusion and empyema. *Am J Roentgenol* 144:1189–1193
34. Casola G, van Sonnenberg E, Keightley A et al. (1988) Pneumothorax: Radiologic treatment with small catheters. *Radiology* 166:89–91
35. Hunnam GR, Flower CDR (1988) Radiologically guided percutaneous catheter drainage of empyemas. *Clin Radiol* 39:121–126
36. Merriam MA, Cronan JJ, Dorfman GS et al. (1988) Radiographically guided percutaneous catheter drainage of pleural fluid collections. *Am J Roentgenol* 151:1113–1116
37. Silverman SG, Mueller PR, Saini S et al. (1988) Thoracic empyema: management with image guided catheter drainage. *Radiology* 169:5–9
38. Moulton JS, Moore PT, Mencini RA (1989) Treatment of loculated pleural effusions with transcatheter intracavitary Urokinase. *Am J Roentgenol* 153:941–945
39. Parker LA, Charnock GC, Delany DJ (1989) Small bore catheter drainage and sclerotherapy for malignant pleural effusions. *Cancer* 64:1218–1221
40. Reinhold C, Illescas FF, Atri M et al. (1989) Treatment of pleural effusions and pneumothorax with catheters placed percutaneously under imaging guidance. *Am J Roentgenol* 152:1189–1191
41. Lee KS, Im JG, Kim YH et al. (1991) Treatment of thoracic multiloculated empyemas with intracavitary urokinase: a prospective study. *Radiology* 179:771–775
42. Lambiase RE, Deyoe L, Cronan JJ et al. (1992) Percutaneous drainage of 335 consecutive abscesses: result of primary drainage with 1-year follow-up. *Radiology* 184:167–179
43. Van Sonnenberg E, Nakamoto SK, Mueller PR et al. (1984) CT and ultrasound-guided catheter drainage of empyemas after chest tube failure. *Radiology* 151:349–353
44. Ball WS Jr, Bisset GS, Towbin RB (1989) Percutaneous drainage of chest abscesses in children. *Radiology* 171:431–434
45. Dondelinger RF, Kurdziel JC (1990) Percutaneous drainage of thoracic fluid collections. In: Dondelinger RF, Rossi P, Kurdziel JC, Wallace S (eds) *Interventional radiology*. Thieme, Stuttgart, pp 142–155
46. Neff CC, van Sonnenberg E, Lawson DW et al. (1990) CT follow-up of empyemas: pleural peels resolve after percutaneous catheter drainage. *Radiology* 176:195–197
47. Van Sonnenberg E, D’Agostino HB, Casola G et al. (1991) Lung abscess: CT-guided drainage. *Radiology* 178:347–351
48. Ghaye B, Dondelinger RF (1999) Percutaneous CT guided lung biopsy: sequential versus spiral scanning. A randomized prospective study. *Eur Radiol* 9:1317–1320
49. Katada K, Kato R, Anno H et al. (1996) Guidance with real-time CT fluoroscopy: early clinical experience. *Radiology* 200:851–856
50. White CS, Meyer CA, Templeton PA. (2000) CT fluoroscopy for thoracic interventional procedures. *Radiol Clin North Am* 38:303–322
51. Parker LA, Melton JW, Delany DJ et al. (1987) Percutaneous small bore catheter drainage in the management of lung abscesses. *Chest* 92:213–218
52. O’Moore PV, Mueller PR, Simeone JF et al. (1987) Sonographic guidance in diagnostic and therapeutic interventions in the pleural space. *Am J Roentgenol* 149:1–5
53. Cummin ARC, Wright NL, Joseph AE (1991) Suction drainage: a new approach to the treatment of empyema. *Thorax* 46: 259–260
54. Morrison MC, Mueller PR, Lee MJ et al. (1992) Sclerotherapy of malignant pleural effusion through sonographically placed small-bore catheters. *Am J Roentgenol* 158:41–43
55. PC, Luh KT, Lee YC, Chang DB (1991) Lung abscesses: US examination and US-guided transthoracic aspiration. *Radiology* 180:171–175
56. Light RW (1985) Parapneumonic effusions and empyema. *Clin Chest Med* 6:55–62
57. Light W, Rodriguez RM (1998) Management of parapneumonic effusions. *Clin Chest Med* 15:373–382
58. Vianna NJ (1971) Nontuberculous bacterial empyema in patients with and without underlying disease. *J Am Med Assoc* 215:69–75
59. Ghaye B, Dondelinger RF, Dorthu L (1994) Aspiration et drainage percutané des collections thoraciques. In: Gangi A, Dietemann JL (eds) *Tomodensitométrie interventionnelle*. Vigot, Paris, pp 113–131
60. Moulton JS (2000) Image-guided management of complicated pleural fluid collections. *Radiol Clin N Am* 38:345–374
61. Shankar S, Gulati M, Kang M et al. (2000) Image-guided percutaneous drainage of thoracic empyema: Can sonography predict the outcome? *Eur Radiol* 10:495–499
62. Cassina PC, Hauser M, Hillejan L et al. (1999) Video-assisted thoracoscopy in the treatment of pleural empyema: stage-based management and outcome. *J Thorac Cardiovasc Surg* 117:234–238
63. Bergh NP, Ekroth R, Larsson S et al. (1977) Intrapleural streptokinase in the treatment of haemothorax and empyema. *Scan J Thorac Cardiovasc Surg* 11:265–268
64. Berglin E, Ekroth R, Teger-Nilsson AC et al. (1981) Intrapleural instillation of streptokinase: effects on systemic fibrinolysis. *Thorac Cardiovasc Surg* 29:124–126
65. Fraedrich G, Hoffman D, Effenhauser P et al. (1982) Instillation of fibrinolytic enzymes in treatment of pleural empyema. *Thorac Cardiovasc Surg* 30:36–38
66. Aye RW, Froese DP, Hill LD (1991) Use of purified streptokinase in empyema and hemothorax. *Am J Surg* 161:560–562
67. Henke CA, Leatherman JW (1992) Intrapleurally administered streptokinase in the treatment of acute loculated nonpurulent parapneumonic effusions. *Am Rev Respir Dis* 145:680–684
68. Robinson LA, Moulton AL, Fleming WH et al. (1994) Intrapleural fibrinolytic treatment of multiloculated thoracic empyemas. *Ann Thorac Surg* 57:803–814



69. Taylor RFH, Rubens MB, Pearson MC et al. (1994) Intrapleural streptokinase in the management of empyema. *Thorax* 49: 856–859
70. Pollack JS, Passik CS (1994) Intrapleural urokinase in the treatment of loculated pleural effusions. *Chest* 105:868–873
71. Moulton SM, Benkert RE, Weisiger KH et al. (1995) Treatment of complicated pleural fluid collections with image-guided drainage and intracavitary urokinase. *Chest* 108:1252–1259
72. Park CS, Chung WM, Lim MK et al. (1996) Transcatheter instillation of urokinase into loculated pleural effusion: analysis of treatment effect. *Am J Roentgenol* 167:649–652
73. Jerjes-Sanchez C, Ramirez-Rivera A, Elizalde JJ et al. (1996) Intrapleural fibrinolysis with streptokinase as an adjunctive treatment in hemothorax and empyema. *Chest* 109:1514–1519
74. Temes RT, Follis F, Kessler RM et al. (1996) Intrapleural fibrinolytics in management of empyema thoracis. *Chest* 110: 102–106
75. Davies RJO, Traill ZC, Gleeson FV (1997) Randomised controlled trial of intrapleural streptokinase in community acquired pleural infection. *Thorax* 52:416–421
76. Bourros D, Schiza S, Patsourakis G et al. (1997) Intrapleural streptokinase versus urokinase in the treatment of complicated parapneumonic effusions. A prospective, double-blind study. *Am J Respir Crit Care Med* 155:291–295
77. Chin NK, Lim TK (1997) Controlled trial of intrapleural streptokinase in the treatment of pleural empyema and complicated parapneumonic effusions. *Chest* 111:275–279
78. Davies CW, Traill ZC, Gleeson FV (1999) Intrapleural streptokinase in the management of malignant multiloculated pleural effusions. *Chest* 115:729–733
79. Diacon AH, Theron J, Schuurmans MM et al. (2004) Intrapleural streptokinase for empyema and complicated parapneumonic effusions. *Am J Respir Crit Care Med* 170:49–53
80. Yao CT, Wu JM, Liu CC et al. (2004) Treatment of complicated parapneumonic pleural effusion with intrapleural streptokinase in children. *Chest* 125:566–571
81. Maskell NA, Davies CW, Nunn AJ et al (2005) U.K. Controlled trial of intrapleural streptokinase for pleural infection. *N Engl J Med* 352:865–874
82. Seaton KG, Patz EF Jr, Goodman PC (1995) Palliative treatment of malignant pleural effusions: value of small-bore catheter thoracostomy and doxycycline sclerotherapy. *Am J Roentgenol* 164:589–585
83. Patz EF Jr, McAdams P, Goodman PC et al. (1996) Ambulatory sclerotherapy for malignant pleural effusions. *Radiology* 199: 133–135
84. Erasmus JJ, Goodman PC, Patz EF Jr (2000) Management of malignant pleural effusions and pneumothorax. *Radiol Clin N Am* 38:375–383
85. Westcott JL (1990) Lung biopsy. In: Dondelinger RF, Rossi P, Kurdziel JC, Wallace S (eds) *Interventional radiology*. Thieme, Stuttgart, pp 9–17
86. Conces DJ Jr, Tarver RD, Gray WC et al. (1988) Treatment of pneumothoraces utilizing small caliber chest tubes. *Chest* 94:55–57
87. Lorenzo RL, Bradford BF, Black J (1985) Lung abscesses in children: diagnostic and therapeutic needle aspiration. *Radiology* 157:79–80
88. Rami-Porta R, Bravo-Bravo JL, Alix-Trueba A (1985) Percutaneous drainage of lung abscess. *J Thorac Cardiovasc Surg* 89:314–317
89. Yellin A, Yellin EO, Lierman Y (1985) Percutaneous tube drainage: the treatment of choice for refractory lung abscess. *Ann Thorac Surg* 39:266–270
90. Rice TW, Ginsberg RJ, Todd TRJ (1987) Tube drainage of lung abscesses. *Ann Thorac Surg* 44:356–359
91. Yang PC, Luh KT, Lee YC et al. (1991) Lung abscesses: US examination and US-guided transthoracic aspiration. *Radiology* 180:171–175
92. Ha HK, Kang MW, Park JM et al. (1993) Lung abscess. Percutaneous catheter therapy. *Acta Radiol* 34:362–365
93. Shirakusa T, Ueda H, Saito T, Matsuba K, Kouno J, Hirota N (1989) Surgical treatment of pulmonary aspergilloma and *Aspergillus* empyema. *Ann Thorac Surg* 48:779–782
94. Munk PL, Vellet AD, Rankin RN et al. (1993) Intracavitary aspergilloma: transthoracic percutaneous injection of amphotericin gelatin solution. *Radiology* 188:821–823
95. Giron JM, Poey CG, Fajadet PP et al. (1993) Inoperable pulmonary aspergilloma: percutaneous CT-guided injection with glycerin and amphotericin B paste in 15 cases. *Radiology* 188:825–827
96. Klein JS, Fang K, Chang MC (1993) Percutaneous transcatheter treatment of an intracavitary aspergilloma. *Cardiovasc Intervent Radiol* 16:321–324
97. Giron J, Poey C, Fajadet P et al. (1998) CT-guided percutaneous treatment of inoperable pulmonary aspergillomas: a study of 40 cases. *Eur J Radiol* 28:235–242
98. Jackson M, Flower CD, Shneerson JM (1993) Treatment of symptomatic pulmonary aspergillomas with intracavitary instillation of amphotericin B through an indwelling catheter. *Thorax* 48:928–930
99. Sewall LE, Franco AI, Wojtowycz MM (1993) Pneumatoceles causing respiratory compromise. Treatment by percutaneous decompression. *Chest* 103:1266–1267
100. Gobien RP, Stanley JH, Gobien BS et al. (1984) Percutaneous catheter aspiration and drainage of suspected mediastinal abscesses. *Radiology* 151:69–71
101. Callahan JA, Seward JB, Nishimura RA et al. (1985) Two-dimensional echocardiographically guided pericardiocentesis: experience in 117 consecutive patients. *Am J Cardiol* 55:476–479
102. Carrol CL, Jeffrez RB Jr, Federle MP et al. (1987) CT evaluation of mediastinal infections. *J Comput Assist Tomogr* 11:449–453
103. Meranze SG, Le Veen RF, Burke DR et al. (1987) Transesophageal drainage of mediastinal abscesses. *Radiology* 165:395–398
104. Tanaka T, Inaba Y, Arai Y et al. (1991) Lung abscesses: US examination and US-guided transthoracic aspiration. *Radiology* 180:171–175
105. Gevenois PA, Sergent G, De Myttenaere M et al. (1995) CT-guided percutaneous drainage of an anterior mediastinal abscess with a 16-F catheter. *Eur Respir J* 8:860–870
106. Szapiro D, Ghaye B, Dondelinger RF (1996) Pericardial tamponade: CT-guided percutaneous drainage. *J Interv Radiol* 11:129–131
107. Pfenninger J, Bossi E, Biesold J, Blumberg A (1982) Treatment of pneumothorax, pneumopericardium and pneumomediastinum. *Helv Paediatr Acta* 37:353–360
108. Tyler DC, Redding G, Hall D, Lynn A (1984) Increased intracranial pressure: an indication to decompress a tension pneumomediastinum. *Crit Care Med* 12:467–468
109. Shennib HF, Barkun AN, Matouk E, Blundell PE (1988) Surgical decompression of a tension pneumomediastinum. *Chest* 93:1301–1302
110. Beg MH, Reyazuddin Ansari MM (1988) Traumatic tension pneumomediastinum mimicking cardiac tamponade. *Thorax* 43:576–577
111. Rosenfeld DL, Cordell CE, Jadeja N (1990) Retrocardiac pneumomediastinum: radiographic finding and clinical implications. *Pediatrics* 85:92–97
112. Dondelinger RF, Coulon M, Kurdziel JC (1992) Tension mediastinal emphysema: emergency percutaneous drainage with CT guidance. *Eur J Radiol* 15:7–10



## **Section Five**

# **Non-Traumatic Abdominal Emergencies: Imaging and Intervention**

# Acute Abdominal Pain: Diagnostic Strategies

S. Leschka, H. Alkadhi, S. Wildermuth, B. Marincek

## 5.1

### Contents

5.1.1 Introduction	411
5.1.2 Clinical Findings	411
5.1.2.1 Patient's History	412
5.1.2.2 Physical Examination	412
5.1.3 Imaging	413
5.1.3.1 Imaging Modalities	413
5.1.3.2 Imaging Findings in Common Causes of Acute Abdominal Pain	415
5.1.4 Conclusion	429
References	431

### 5.1.1 Introduction

Acute abdominal pain unrelated to trauma is a common cause in patients who present to the emergency ward. The term “acute abdomen” defines a clinical syndrome characterized by the sudden onset of severe abdominal pain requiring emergency medical or surgical treatment [1]. Although a large number of potentially life-threatening processes can cause acute abdominal pain, eight conditions account for approximately 90% of patients who are referred to hospital and are seen on surgical wards: acute appendicitis; acute cholecystitis; small bowel obstruction; acute gynecological disease; acute pancreatitis; renal colic; perforated peptic ulcer; and acute diverticulitis [2]; however, in up to one-third of cases the etiology cannot be determined, and is often explained as being non-specific, non-surgical abdominal pain (“dyspepsia”) [2].

A rapid and accurate diagnosis is essential to reduce morbidity and mortality in patients with an acute abdomen. In general, the need for immediate surgical exploration can be identified by history and physical examination; however, establishing an accurate working diagnosis is often difficult because the clinical presentation of many entities overlap and physical and laboratory examinations are often non-specific. In many centers plain abdominal radiography, despite significant diagnostic limitations, traditionally serves as first step in the diagnostic work-up [3, 4].

Ultrasound (US) and computed tomography (CT) are used as secondary imaging modalities. Although US has gained widespread acceptance, CT is now considered as first-line imaging modality for triaging patients with acute abdominal pain [5–9]. It can facilitate appropriate therapeutic decisions in 95% of patients with an acute abdomen [5]. Undoubtedly, the introduction of multi-detector CT (MDCT) has further increased its role in these patients [8, 10–12]. Although cost-effectiveness is a dictum in health care, cost-effectiveness is not only determined by the direct cost of the imaging modality, but also by its ability to eliminate unnecessary surgical exploration and to reduce unnecessary hospital stay for observation. Inaccurate diagnosis may lengthen hospital stay, a major contributor to the costs of health care. For example, Rao and colleagues [13] reviewed the economic impact of CT in 100 patients with suspected appendicitis. In 13 of these patients unnecessary surgery and in 39 patients unnecessary hospital stay for observation could be avoided, resulting in a cost saving of US\$447 per patient; therefore, an expensive modality, such as CT, may even be cost-effective [13].

While many of acute abdominal disorders are discussed in greater detail elsewhere in this book, this chapter focuses on a systematic discussion of imaging strategies in common causes of acute abdominal pain depending on their topographic location.

### 5.1.2 Clinical Findings

When confronted with a patient complaining of acute abdominal pain, the physician must first rule out catastrophic causes of pain including ruptured aortic aneurysm or perforated viscus. If a life-threatening condition for the acute abdominal pain is probable, the patient must be treated without a formal diagnosis and sometimes even with minimal history and only a cursory initial physical examination. Once the need of immediate surgical intervention has been reasonably excluded, the physician becomes challenged with a long list of possible diagnoses of acute abdominal pain. At this point, as much history as possible must be obtained and a thorough physical examination is



mandatory to either suggest a specific diagnosis or guide further radiological investigation.

The patient's age and gender deserve special focus from the physician during the initial evaluation. The most challenging problem is to establish a diagnosis in very young and elderly patients. These patients often present atypically and special attention has to be paid to avoid missing the diagnosis. In the young, obviously a history is not obtainable and pain is often poorly localized. In the elderly, symptoms and early signs are often long-time masked and at time of presentation complex findings may be present. In women, the list of probable diagnoses is longer than in men due to additional pelvic organs (e.g., ovary, fallopian tubes, uterus) that may develop problems. Childbearing women may have atypical locations for abdominal conditions such as pain in the right upper quadrant for appendicitis. In later pregnancy, the possibility of abruptio placentae has to be considered as well. Pain may be also simple derive from pregnancy, but this is generally a diagnosis of exclusion. In the postoperative patient, the signs of previous surgery can mask complications.

---

#### 5.1.2.1 Patient's History

A thorough history is the initial step in evaluation. Specific features alone can suggest a diagnosis for a variety of causes of acute abdominal pain. The location and quality of pain is important in forming a differential diagnosis. Visceral pain arises from the walls of hollow viscera and solid organs due to stretching or distension, ischemia, or inflammation. It is usually described as crampy, dull, and gaseous, usually of insidious onset, poorly localized, and little or no change in pain with activity. On the other hand, somatic pain arises from the parietal peritoneum, mesenteric roots, and anterior abdominal wall due to inflammation. It is usually well localized, sharp in quality, often of acute onset, and usually increases with activity. In some conditions, abdominal diseases could present with pain referred to extra-abdominal locations due to central-nervous overlapping with pathways from cutaneous site (e.g., diaphragmatic irritation refers pain to the shoulder known as the Kehr's sign). Although atypical presentation can occur for any condition, many causes of abdominal pain have characteristic locations which can help guide the diagnostic approach; however, pain may also migrate over time. In acute appendicitis, the patient initially experiences periumbilical pain, while as the inflammation progresses and involves the parietal peritoneum, the pain is experienced in the right lower quadrant; therefore, the patient's description of the pain is vital in formulating a good working differential diagnosis list. The history should encompass the chronicity, onset, duration, quality, location, and radiation of the pain. In addition, associated symptoms as well as alleviating and aggravating factors should be determined. For example, pain which is gradual in onset sug-

gests an inflammatory or infectious process. The duration of pain can often aid in diagnosis as well, for instance, biliary colic typically lasts for several minutes or hours, whereas acute pancreatitis can cause pain lasting days. Radiation of pain can also help refine the differential diagnosis. For example, pancreatic pain typically radiates to the back. The intensity of pain does not always reflect the seriousness of the condition causing the pain. Severe abdominal pain can be from mild conditions such as gas of the cramping of viral gastroenteritis. On the other hand, relatively mild pain may be present with life-threatening conditions such as early appendicitis, especially in the elderly. Associated signs and symptoms can also be helpful in clarifying the diagnosis and have to be directly questioned, including nausea, vomiting, diaphoresis, gastrointestinal bleeding, weight loss, jaundice, diarrhea, constipation, dysphagia, bloating, and early satiety. A past history of previous symptoms is helpful in establishing the present problem particularly in ulcer disease, biliary colic, and diverticular disease. A drug history should include details concerning prescription and illicit drug use. Steroids and immunosuppressive drugs may increase the risk of gastrointestinal tract perforation with relatively little pain or leukocytosis.

---

#### 5.1.2.2 Physical Examination

Physical examination is the second step in the initial evaluation of a patient with abdominal pain and serves to confirm suspicions from history, to localize the area of disease, and to avoid missing extra-abdominal causes of pain. Shock, pallor, sweating, or fainting can accompany abdominal pain and implies the severity of disease. The physical examination should also include assessment of the sclera for jaundice, pulmonary examination for pneumonia which may cause abdominal irritation, and a pelvic examination for gynecological causes of abdominal pain. In addition, an electrocardiogram should be always performed in patients presenting with epigastric pain, because myocardial ischemia often radiates into the epigastrium and may be accompanied with nausea and diarrhea; however, the focus of examination is the abdomen with inspection, auscultation, and palpation being the key factors. Operative scars suggest possible adhesions and intestinal obstruction, and abnormal orifices can be the site of external hernia. Bleeding in the subcutaneous tissues in hemorrhagic pancreatitis may be indicated by a dissecting bluish discoloration of the costovertebral angles (Grey-Turner's sign) or around the umbilicus (Cullen's sign). By auscultation, bowel sounds have to be identified. Active peristalsis of normal pitch suggests a non-surgical disease (e.g., gastroenteritis), whereas severe pain with a silent abdomen is indicative of intestinal paralysis and the need of immediate exploration. With palpation, the physician can confirm if the process causing the abdominal pain is localized to one

area. Examination for tenderness, rebound tenderness, guarding, degree of distention, and palpable masses is of utmost importance to reduce the list of probable differential diagnoses. Ascites can be identified by percussion.

Laboratory tests are the third vital part in the work-up for abdominal pain. For patients presenting with acute abdominal pain, initial laboratory evaluation should include a complete blood cell count with differential, electrolytes (i.e., sodium, potassium, chloride, calcium, magnesium, phosphorus), serum chemistries (i.e., bicarbonate, blood urea nitrogen, creatinine, serum glucose, amylase, lipase), liver function tests, urinalysis, coagulation parameters, and a pregnancy test in women. These laboratory tests can aid in making a rapid diagnosis and prepare the patient for possible surgery.

### 5.1.3 Imaging

After an experienced observer carefully obtained history and physical examination, clinical findings and laboratory examinations often focus a differential diagnosis to a particular anatomic region or specific diagnosis. Various radiographic imaging modalities are used to either confirm the clinical diagnosis or to narrow the differential diagnosis further. In general, the referring physician directs the sequence of imaging modalities depending on the patient's initial presentation, the working clinical diagnosis, and the examiner's experience; however, because of training and experience, the radiologist's role is to guide the referring physician to the appropriate available examinations. To reduce the time penalty, the initial diagnostic imaging should gain enough information to confirm the working clinical diagnosis, or, if the diagnosis is incorrect, to provide sufficient information for an alternative diagnosis.

#### 5.1.3.1 Imaging modalities

The radiological approach in diagnosing patients with acute abdominal pain may include plain abdominal radiography, US examination, and/or CT imaging. In many emergency centers, plain radiography of the abdomen serves as the initial imaging modality. Because of the low diagnostic yield of abdominal radiography and the widespread availability of more precise modalities, such as US and CT, the need for plain abdominal radiography has declined.

The optimal diagnostic approach for evaluation of patients with acute abdominal pain considerably depends on the time-effective availability of imaging modalities close to the emergency ward. For instance, in urban medical centers with a CT imaging suite next to the emergency ward, CT imaging is preferred for most abdominal disorders, whereas in peripheral hospitals without around-the-clock CT evaluation availability, US examination should be more efficient. Table 1 summarizes the diagnostic imaging approach depending on the location of acute abdominal pain as established in the authors' hospital.

#### Plain Abdominal Radiography

Two views are usually taken, a supine and an erect. If the patient is unable to stand, a decubitus view is performed. The analysis of these abdominal radiographs is focused on the detection of gaseous distention of the bowel, gas outside the bowel lumen, mass or fluid collections, displacement of organs or bowel loops, abnormal calcifications, and skeletal pathology. The diagnostic yield of abdominal radiography is small due to its inherent low soft tissue contrast and the fact that many abdominal diseases do not have specific radiographic features [4]. Because of significant diagnostic limitations, the impact of plain abdominal

**Table 1.** Recommended diagnostic imaging approach for patients with acute abdominal pain. *RUQ* right upper quadrant, *LUQ* left upper quadrant, *LLQ* left lower quadrant, *PAR* plain abdominal radiography, *IVU* intravenous urography

Location of pain	PAR	US	CT	Comments
RUQ	-	+	(+)	US preferred initial modality in acute cholecystitis, CT for evaluation of complications of acute cholecystitis
LUQ	-	+	(+)	US for "screening," CT when US findings equivocal
RLQ	-	+	+	US preferred in children and in child-bearing women, CT initial modality in other patients with atypical clinical presentation
LLQ	-	(+)	+	CT preferred initial modality, US performed first when CT not available
Diffuse pain	(+)	(+)	+	Most conditions best visualized with CT; PAR may be initial modality in bowel obstruction
Flank/epigastric pain	(+)	(+)	+	US or CT initial modality in suspected ureteral stones; PAR combined with IVU if US or CT not available; CT modality of choice in acute pancreatitis

+ indicated for establishing diagnosis, (+) helpful adjunct but only in special situations, -generally not helpful for establishing diagnosis

radiography has declined even for traditional indications, including bowel obstruction, pneumoperitoneum, and detection of ureteral calculi. Several studies have demonstrated the superiority of CT for defining site, level, and underlying cause of small bowel obstruction [14, 15], for detecting a subtle pneumoperitoneum [16, 17], and for identifying ureteral calculi [18, 19]. Ahn and colleagues [4] compared the diagnostic yield of abdominal radiography and CT in 1000 consecutive patients with acute abdominal pain. The highest sensitivity of abdominal radiography was 90% for intra-abdominal foreign body and 49% for bowel obstruction, whereas sensitivity was 0% for appendicitis, pyelonephritis, pancreatitis, and diverticulitis. Sensitivities of CT were highest for bowel obstruction and urolithiasis at 75 and 68%, respectively.

### Abdominal Ultrasound

A US examination in patients with acute abdominal pain should include the entire abdomen and requires a specific technique of graded compression to displace or compress fat and bowel. This will often eliminate the disturbing of bowel gas and reduces the distance from the transducer to the structure of interest, allowing the use of a high-frequency probe with improved image quality. In addition, graded compression allows assessment of the rigidity of a structure by evaluating its reaction on compression. For assessment of the distal ureters, and of uterus and ovaries in women, a moderately filled bladder allows a better survey by serving as an acoustic window; however, a fully filled bladder prevents proper graded compression. Transvaginal US may be reserved for specific gynecological questions and assessment of Douglas' abscess.

Ultrasound is particularly valuable for patients with right upper quadrant pain [20] or in whom radiation exposure is a major concern (e.g., children, childbearing women, patients of reproductive age) [21]. In particular, the small body size of children usually allows for high-quality sonograms. In young women, many causes of abdominal pain are related to gynecological causes and have to be excluded initially. Specific advantages of US include the dynamic, real-time imaging of peristalsis or absence of peristalsis as in paralytic ileus, and the mobility and flexibility of US making it readily available in the emergency ward. In addition, US allows for close interaction with the patient. Information provided by the patient may lead to a specific search for a US finding, whereas certain US findings may lead to a specific question to the patient.

Disadvantages of US examination include operator dependency and the need for a proper acoustic window, and disturbance by gas, bone, and obesity. In addition, the time burden of US examination is often higher than for CT, particularly when the CT suite is located next to the emergency ward.

### Computed Tomography

Computed tomography is increasingly replacing US as first-line imaging modality for the evaluation of patients with acute abdominal pain. Compared with US, CT provides major advantages: it is extremely fast, is not disturbed by gas, bone or obesity, and is not operator dependent; therefore, it can be reviewed by others, even at a distance. The evolution from single-slice CT to current MDCT scanners results in several important advantages. Firstly, shortening in acquisition time increases scanner productivity, facilitates faster radiological interpretation, and reduces motion artifacts by scanning the entire abdomen in a single breath-hold, an essential prerequisite in acutely ill patients [22]. Secondly, thin-collimated submillimeter isotropic imaging enables high-quality reconstructions in any arbitrary plane with a spatial resolution similar to that of the axial plane. Thirdly, contrast bolus exploitation is improved allowing precise separation of multiple phases of enhancement, which is especially useful in the evaluation of vascular diseases. Major disadvantages of CT imaging includes radiation exposure, the risks inherent with iodinated contrast material if indicated, and the large amount of data and images produced [23], making efficient and accurate reporting on hard-copy images difficult [24]; therefore, dedicated post-processing has often to be performed for shortening evaluation time [25].

In general, the CT protocol has to be tailored to the specific questions; thus, the list of probable clinical diagnoses should be shortened prior to the CT examination by historical and physical examination and laboratory tests to gain the best results from CT imaging. Based on the clinical working diagnosis, optimizing the CT acquisition parameters and the contrast material application protocol are essential to maximize diagnostic accuracy [10]. At our institution, patients presenting with acute abdominal pain are scanned on a 16-slice CT scanner (Sensation 16, Siemens, Forchheim, Germany) located next to the emergency ward. The following scanning parameters are used: tube voltage 120 kV; tube current 225 mAs; and slice collimation 16×0.75 mm. Transverse slices are routinely reconstructed at a thickness of 2 mm with 1 mm increment for evaluation and at a thickness of 5 mm (5 mm increment) for reporting. Narrow collimation (1 mm slice thickness, 0.5 mm increment) is suggested for CT angiography. Different strategies for the application of contrast agent (oral/rectal/intravenous) are used depending on the clinical working diagnosis [7]. Non-contrast scanning is the fastest, but most limited, strategy; however, Malone [26] reported a high diagnostic accuracy of this strategy in patients with acute abdomen. If the clinical presentation is equivocal or the "short list" of probable diagnoses does not fit a single imaging protocol, the application of oral, rectal, and intravenous contrast is beneficial in most patients. We usually administer intravenous contrast material in all patients presenting with acute abdominal pain, with exception of suspected ureteral stone or in patients with renal insufficiency. Intravenous contrast enhancement of solid organs is

helpful to identify infarctions, abscesses, and in distinguishing bile ducts from normal intrahepatic vessels. Mural enhancement is also helpful in a variety of inflammatory bowel disorders, especially in patients with paucity of intra-abdominal fat. When intravenous contrast is indicated, depending on the patient's body weight a total volume of 120–150 ml of iodinated contrast material (270 mg iodine/ml) injected at a rate of 3 ml/s is adequate. The CT angiography is useful in patients with suspected hemorrhage and bowel ischemia with arterial or venous occlusion. Then scanning for the arterial phase of attenuation should be initiated 20–30 s after the start of injection; otherwise, scanning begins with a delay of 85 s after injection for portal venous phase imaging. Delayed images acquired 8 min after injection are helpful in cases of suspected pyelonephritis or when opacification of the bladder is desired. Use of oral contrast material is recommended in most cases, if severity of symptoms allow for delay in diagnosis, because most patients require at least 1 h transit time for adequate bowel opacification. Combination of oral and intravenous enhancement may help distinguishing common intestinal diseases by depicting variations in bowel wall attenuation [27]. When oral contrast is indicated, 800–1000 ml water-soluble contrast agent containing 2% iodine is used. Exceptions include cases in which high-grade bowel obstruction, ureteral stone, acute hemorrhage, or acute pancreatitis is suspected. Rectal contrast agent (100 ml water-soluble contrast containing 2% iodine) instilled via rectal enema can be indicated to optimally evaluate colonic abnormalities such as diverticulitis or appendicitis. On occasion, oral and rectal contrast material may obscure important information such as a coprolith in appendicitis.

### 5.1.3.2 Imaging Findings in Common Causes of Acute Abdominal Pain

For practical reasons it is helpful to discuss the imaging approach depending on the location of the acute pain, i.e., pain in an abdominal quadrant, diffuse abdominal pain, and flank or epigastric pain.

#### Acute Pain in an Abdominal Quadrant

Although there is overlapping in clinical presentation, the identification of patients with localized pain in an abdominal quadrant is pivotal for shortening the list of probable diagnoses (Table 2).

#### Right Upper Abdominal Quadrant Pain

Acute cholecystitis is the most common cause of acute pain in the right upper quadrant (RUQ); however, more than one-third of patients with acute RUQ pain do not have acute cholecystitis. Various diseases may mimic acute cholecystitis, including choledocholithiasis, hepatitis, liver abscess, spontaneous rupture or hemorrhage of a hepatic neoplasm (in particular hepatic adenoma and hepatocellular carcinoma), pancreatitis, peptic ulcer disease, right-sided (cecal) diverticulitis, and retrocecal appendicitis [20].

In most patients acute cholecystitis is caused by calculous obstruction of the gallbladder neck or cystic duct leading to increased intraluminal pressure and distension. Inflammation results from chemical injury of the mucosa

**Table 2.** Common causes of acute abdominal pain in an abdominal quadrant

Right upper abdominal quadrant	Left upper abdominal quadrant	Right lower abdominal quadrant	Left lower abdominal quadrant
Acute calculous/acalculous cholecystitis	Splenic infarction	Intestinal conditions	Sigmoid diverticulitis
Emphysematous cholecystitis	Splenic abscess	Acute appendicitis	Obstructive sigmoid carcinoma
Choledocholithiasis	Sickle cell disease	Crohn's disease	Epiploic appendagitis
Hepatitis	Gastritis	Mesenteric adenitis	Urinary tract obstruction
Liver abscess	Gastric ulcer	Mucocele of the appendix	Gynecological conditions
Spontaneous rupture of a hepatic neoplasm		Perforated cecal and appendiceal carcinoma	
Pancreatitis		Epiploic appendagitis	
Peptic ulcer disease		Right-sided omental infarction	
Right-sided (cecal) diverticulitis		Right-sided (cecal) diverticulitis	
Retrocecal appendicitis		Infectious ileocolitis	
		Urological conditions	
		Urinary tract obstruction	
		Gynecological conditions	
		Pelvic inflammatory disease	
		Ovarian vein thrombosis	
		Hemorrhagic ovarian cyst	
		Rupture of ovarian dermoid	
		Ovarian torsion	
		Rupture of ectopic pregnancy	
		Endometriosis	
		Necrotic uterine leiomyoma	





**Fig. 1.** An 83-year-old man with right upper abdominal quadrant pain. **a** Ultrasound demonstrates a gallstone (*arrow*) with acoustic shadowing in a distended gallbladder, asymmetric thickening of the gallbladder wall with echogenic foci (*arrowheads*), and small amounts of pericholecystic fluid. Although US is considered as the

basic imaging modality in patients with suspicion of acute cholecystitis, complications are usually better seen on CT. **b** Transverse CT image clearly shows small amounts of gas within the gallbladder wall (*arrowheads*) indicating gangrenous cholecystitis

by bile salts and/or superimposed infection. Gallbladder perforation and complicating pericholecystic abscess may occur if the obstruction persists. Acalculous cholecystitis accounts for approximately 5–10% of all patients with acute cholecystitis. It usually occurs in the setting of prolonged illness or in intensive care unit patients. Prolonged bile stasis results in increased viscosity of the bile that ultimately leads to functional cystic duct obstruction.

Ultrasound is the preferred initial imaging procedure. Findings include impacted calculi in the gallbladder neck or cystic duct, a positive sonographic Murphy's sign [28], which is considered positive if maximal tenderness is elicited over the gallbladder visualized at sonography, gallbladder distension, wall thickening, and pericholecystic fluid. Of these findings, the first two are considered the most specific with a positive predictive value of 92% for the diagnosis of acute cholecystitis [29]. In the setting of advanced inflammation or in elderly patients, the pain may not be clearly localized in the RUQ.

Computed tomography may be performed initially when the clinical presentation of the patient is unclear or when US findings are equivocal. If CT is used as initial imaging investigation, demonstration of typical findings may eliminate the need for any additional imaging modality, thus facilitating appropriate and expedient management. For most patients a standard CT protocol with intravenous contrast agent and portovenous phase imaging is adequate, but narrow collimation and increment can help to detect small calculi in the bile duct system. The

CT findings in acute cholecystitis are mural thickening >3 mm with increased attenuation in the setting of a distended gallbladder, pericholecystic fluid or haziness, increased attenuation of the gallbladder bile, and subserosal edema [30]. Transient focal increased attenuation of the liver can develop adjacent to the inflamed gallbladder indicating hepatic arterial hyperemia and early venous drainage [31, 32]. Of all these CT findings, pericholecystic inflammatory change is the most specific [33]. In acalculous cholecystitis, the diagnosis is difficult to establish by US [34]; CT is more specific and should be performed initially [35].

For the investigation of complications related to acute cholecystitis, CT has a higher accuracy than US [36]. Gangrenous cholecystitis results from cystic duct obstruction leading to marked gallbladder distension with ischemic wall necrosis [33]. This complication is more frequent in men, in patients of advanced age, or in those with coexisting cardiovascular disease [34]. On US, a typical finding is the presence of an irregular or striated gallbladder wall thickening [37]. A positive sonographic Murphy's sign is observed only in one-third of the patients with acute gangrenous cholecystitis because of denervation of the gallbladder wall [38]. The CT findings of gangrenous cholecystitis include intraluminal membranes, intraluminal hemorrhage, gas within the wall or lumen of the gallbladder, irregularity or absence of the gallbladder wall, pericholecystic abscess, and lack of gallbladder wall enhancement (Figs. 1, 2) [33].

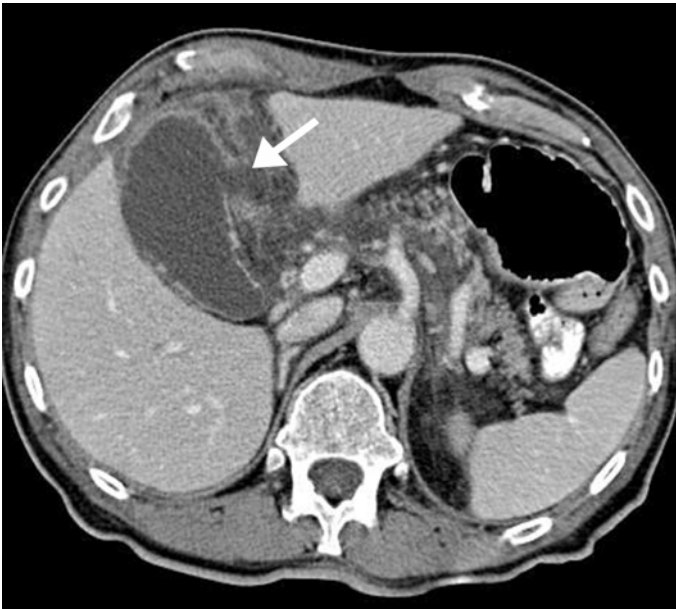


**Fig. 2.** A 78-year-old woman with acute pain in the right upper abdominal quadrant. Transverse CT image shows an irregular and disrupted gallbladder wall with an adjacent inhomogeneous unenhanced mass (arrow), representing a pericholecystic abscess due to transmural wall necrosis in gangrenous cholecystitis

Emphysematous cholecystitis is a variant of acute cholecystitis characterized by the presence of gas in the gallbladder lumen, wall, or pericholecystic tissues in the absence of an abnormal communication between the biliary system and the gastrointestinal tract (Fig. 3) [39]. It commonly occurs in elderly men and is associated with diabetes mellitus. It is postulated that gas-forming bacteria thrive in devitalized tissue resulting from vascular insufficiency of the gallbladder wall in arteriopathic patients. Cholecystolithiasis is often absent. In advanced cases the gaseous collections inherent with emphysematous cholecystitis can be diagnosed on plain abdominal radiographs; however, in milder cases plain abdominal radiography is relatively insensitive and only US or CT will be diagnostic [39]. In the past the diagnosis has relied on plain abdominal radiography, which failed to separate milder from severe cases. This provoked many previous reports of emphysematous cholecystitis being a rapidly progressing disease requiring early surgical intervention [39].

#### Left Upper Abdominal Quadrant Pain

Localized abdominal pain in the left upper quadrant (LUQ) is not frequent. The most important causes are splenic infarction, splenic abscess, sickle cell disease, gastritis, and gastric ulcer. In suspected pathologies of the spleen, US is usually used for “screening” and CT to confirm the diagnosis when US findings are equivocal. Splenic infarction may be caused by bacterial endocarditis, portal hypertension, underlying splenomegaly, and involvement in pancreatitis [40]. Focal splenic infarctions typically appear as peripheral wedge-shaped areas extending to the surface, which are hypoechoic on US and hypodense on CT. Findings in glob-

al infarction can mimic splenic abscess or tumor [41]. Splenic abscess is a rare pathology and most frequently caused by hematogenous dissemination of infection. On US, splenic abscesses are hypo- or anechoic. On CT, they are typically rounded lesions with decreased attenuation [41] and occasional rim enhancement. For evaluation of splenic pathologies, intravenous contrast in an arterial and portovenous phase are recommended for better depiction of surrounding splenic vasculature and associated pancreatic changes [25].

Gastric pathology is generally established by endoscopy and radiological imaging plays a minor role. Computed tomography is probably most important in detecting complications of gastric ulcers including inflammatory changes in adjacent tissue, and clinically unsuspected perforation (Fig. 4) [42]. Adequate gastric distension with either water or oral contrast agent is essential. Intravenous contrast administration is also necessary if water is used. Primary findings on CT may be non-specific and include focal thickening of the gastric or duodenal wall, pneumoperitoneum, and fat stranding adjacent to the peptic ulcer [42].

#### Right Lower Abdominal Quadrant Pain

Acute appendicitis is one of the most common causes of acute abdominal pain. It occurs when the lumen of the appendix is obstructed, e.g., by a fecolith or lymphoid hyperplasia. The obstruction leads to fluid accumulation, luminal distention, and inflammation. If appendicitis is allowed to progress, the wall becomes ischemic and the appendix perforates because of necrosis. Classic clinical symptoms and signs are periumbilical pain migrating to the right lower quadrant (RLQ), fever, and leukocytosis. Because of



**Fig. 3.** A 76-year-old man with known diabetes mellitus presents with acute abdominal pain in the right upper quadrant. **a** Supine plain abdominal radiography shows gas in the wall and in the lumen of the distended gallbladder (*arrow*). **b** Computed tomography depicts the distended gallbladder with intraluminal and intramural gas (*arrow*) indicative of emphysematous cholecystitis

the variable anatomical location of the appendix, however, in up to 30% of patients present with atypical symptoms [43] and the clinical presentations of alternative conditions of RLQ pain may be indistinguishable from appendicitis [44]. The misdiagnosis of acute RLQ pain has led to “nega-

tive” appendectomies, which are reported to be as high as 45% in women of childbearing age [45]; thus, many centers today request appendiceal imaging for clinically equivocal diagnosis. Both US and CT have become important imaging options for the evaluation of patients with suspected

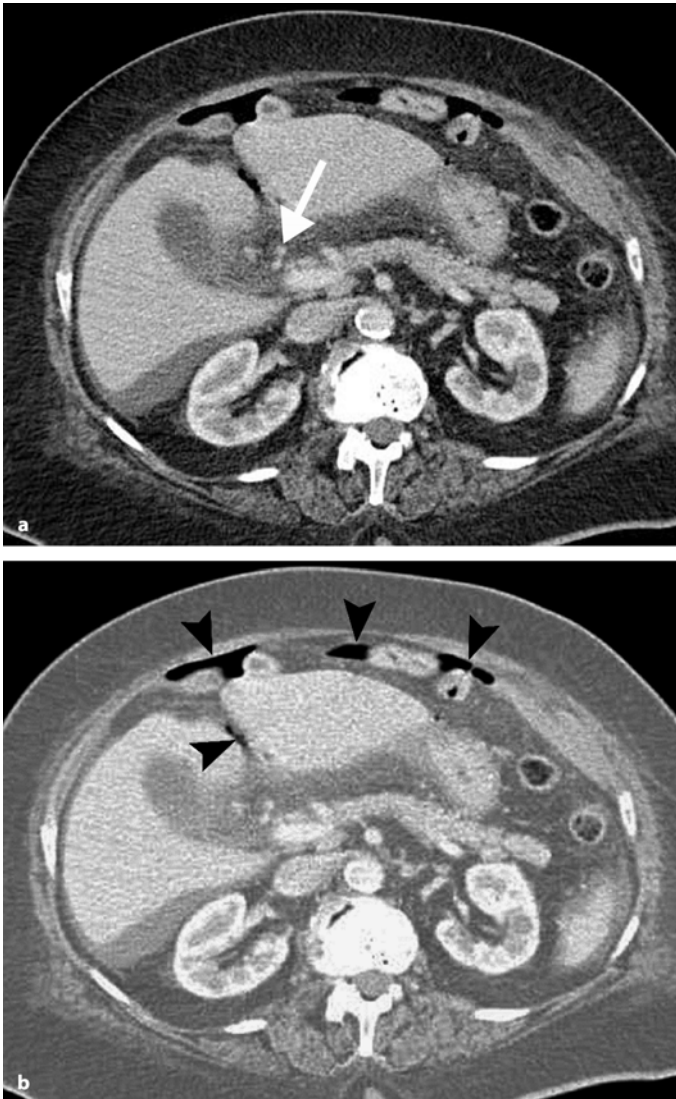


**Fig. 4.** An 81-year-old woman with a history of non-steroidal anti-inflammatory drug medication for over 10 years presents with sudden pain in the left upper quadrant. **a** Transverse CT image in a soft tissue window setting (width 350 HU, center 80 HU) delineates massive duodenal wall thickening with mural enhancement and ulcerations (*arrow*), and fluid collections in the right paracolic space. **b** The same image in a lung window setting (width 1500 HU, center -400 HU) better depicts the small pockets of free gas in the umbilical fissure and adjacent to the anterior abdominal wall (*arrowheads*). These findings are highly suggestive of perforated duodenal ulcer

appendicitis. Key findings include appendiceal thickening, periappendiceal inflammation, and appendicolith [46, 47].

Appendiceal thickening has been defined as transverse diameter >6 mm; however, recent literature suggests that because of considerable overlap between the normal and abnormal appendix the appendiceal diameter should be interpreted in the context of clinical findings: in symptomatic patients a diameter measuring >10 mm correlates with definite appendicitis, whereas a diameter measuring 6–10 mm has to be considered as indeterminate [48, 49].

Periappendiceal inflammation includes periappendiceal fat stranding, thickening of the lateroconal fascia and mesoappendix, extraluminal fluid, phlegmon, abscess, and ileocecal mild lymph node enlargement.

The identification of one or more appendicoliths increases the probability of appendiceal perforation, possibly because appendicoliths accelerate the occurrence of a per-

foration; therefore, the presence of appendicoliths in association with periappendiceal inflammation is virtually diagnostic of perforation [50].

Because US is widely available and cost-effective, it has been proposed as first-line imaging modality in patients with clinically suspected appendicitis (Fig. 5). When examined by experienced operators, the sensitivity and specificity of US are 76–90 and 86–100%, respectively [44, 51, 52]. Computed tomography, conversely, has corresponding values that are all >95% [45, 53]. In addition, when contrast material is used (contrast-enhanced CT), the results are more reproducible than with US (Fig. 6) [54, 55]. Furthermore, a recent comparative study has shown that more inconclusive images are obtained with US than with unenhanced MDCT [49]. This exceptional accuracy has emerged CT in many centers as the primary imaging modality for patients with suspected acute appendicitis.





**Fig. 5.** A 12-year-old boy with acute abdominal pain starting in the epigastrium and migrating to the right lower abdominal quadrant within hours. Physical examination and laboratory tests with elevated white blood cell counts raised the suspicion of acute appendicitis. Longitudinal and perpendicular (*inset*) graded compression US shows an increased diameter ( $>10$  mm) of the appendix, confirming the diagnosis of acute appendicitis

Different CT techniques and contrast agent application protocols have been proposed for evaluation of acute appendicitis, including non-contrast evaluation [56], imaging with oral and intravenous contrast [54], with oral and colonic contrast agent [47], and with colonic contrast only [46]. In our experience, for optimal diagnostic accuracy as well as for identification of alternative diagnoses oral, rectal, and intravenous contrast is recommended.

The list of differential diagnoses of RLQ pain is long. Common intestinal conditions that mimic appendicitis include Crohn's disease, mesenteric adenitis, mucocele of the appendix, perforated cecal and appendiceal carcinoma, epiploic appendagitis, right-sided omental infarction, right-sided (cecal) diverticulitis, and infectious ileocolitis. Other mimickers include urinary tract obstruction and gynecological conditions (pelvic inflammatory disease, ovarian vein thrombosis, hemorrhagic ovarian cyst, rupture of ovarian dermoid, ovarian torsion, rupture of ectopic pregnancy (Fig. 7), endometriosis, and necrotic uterine leiomyoma) [48, 57, 58]. Non-specific signs seen with appendicitis, such as fat stranding, adjacent bowel wall thickening, and free fluid collection, also occur in these conditions. Then the identification of a normal appendix is the key to exclude appendicitis [46].

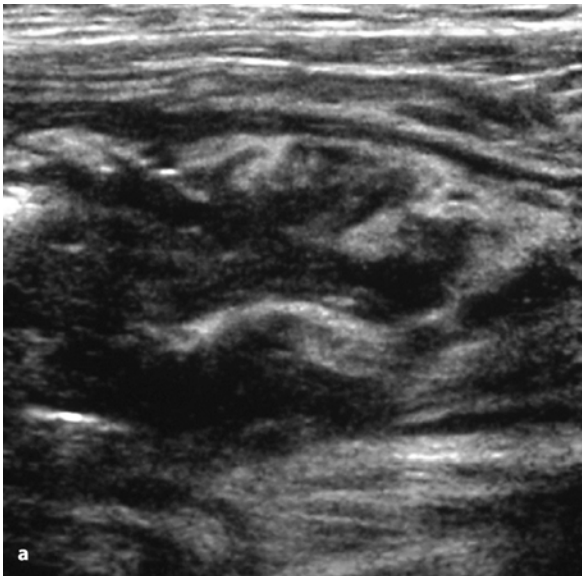


**Fig. 6.** A 27-year-old woman with fever, elevated white blood cells, and acute pain in the right lower abdominal quadrant. **a** Ultrasound examination of the right lower abdomen reveals an irregularly configured, hypoechoic mass with hyperechogenicity of the wall and of the adjacent fat tissue. **b** Coronal CT reconstruction and transverse image (*inset*) after intravenous contrast administration depict at the ileal-cecal junction a hypodense mass with rim enhancement and several gas collections. This mass was correctly diagnosed as a perityphlitic abscess in the setting of acute appendicitis. The *arrowhead* marks an appendicolith within the abscess

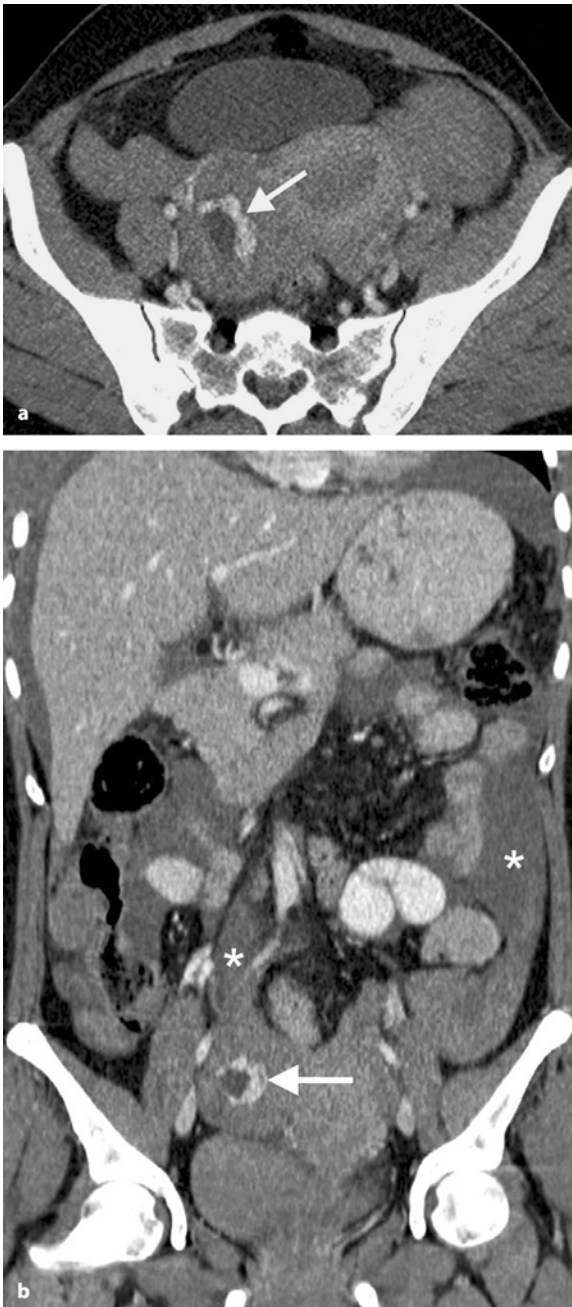


**Fig. 7.** A 40-year-old woman with acute pain in the right lower abdominal quadrant. **a** Transverse CT image demonstrates an enlarged uterus with an adjacent rounded mass. This mass exhibits central necrosis and extravasation of contrast material (arrow in **a** and **b**). **b** Coronal CT reconstruction shows a hemoperitoneum (asterisks) in mesenteric and paracolic location. The cause of pain was identified as rupture of an extra-uterine pregnancy

### Left Lower Abdominal Quadrant Pain

In western countries left lower abdominal quadrant (LLQ) pain most often derives from sigmoid diverticulitis. Diverticulitis occurs in 10–25% of patients with diverticula [59]. Prevalence of colonic diverticulosis rises with age, from <10% in people younger than age 40 years to 50–66% in patients older than age 80 years [59]. Asian patients have predominantly right-sided diverticula and usually present with RLQ pain [60]. The process by which diverticulitis arises is similar to that of appendicitis: the neck of a diverticulum becomes obstructed by a fecolith, causing inflammation and localized ischemia, ultimately leading to perforation. Small perforations are contained by pericolic fat and mesentery and cause pericolic phlegmonous changes. Large perforations result in an abscess, which can be extensive and extend to other organs. Free perforation into the peritoneum causes feculent peritonitis but is rare.

Most patients with diverticulitis present with signs and symptoms sufficient to justify clinical diagnosis [61]. Both US and CT are the preferred imaging modalities to confirm diagnosis and have replaced contrast enema, once the standard investigation. A set of four criteria is considered diagnostic: (a) presence of diverticula; (b) thickening of the bowel wall >4 mm; (c) inflammatory pericolic fat; and (d) pericolic abscess [62]. On US examination, the inflamed diverticulum presents as a hypoechoic mass surrounded by hyperechoic fat. Diverticular inflammation and pericolic abscesses located near the anterior abdominal wall are in most cases accessible with US, whereas changes in the posterior abdominal space can be very difficult to visualize due to disturbing bowel gas [63]. The overall sensitivity and specificity of US for the evaluation of patients suspected of having diverticulitis is reported to be 85 and 84%, respectively [62].

More recent studies have shown CT to be the preferable initial examination because of its high accuracy (sensitivity 97–98%, specificity 98%) [64, 65]. Computed tomography is also the imaging technique of choice in depicting complications such as abscess formation, fistulas (most commonly colovesicular and colovaginal), and obstruction caused by pericolic inflammation [61]. The administration of intravenous contrast material accentuates the characteristic rim enhancement of pericolic abscesses and helps differentiate neighboring bowel loops from surrounding inflammatory changes (Fig. 8) [10]. A very recent study suggests that in patients suspected of having acute colon diverticulitis, low-dose unenhanced multidetector-row CT has a diagnostic performance that is similar to that of contrast-enhanced standard-dose multidetector-row CT [66]. Additional benefits of CT include guiding therapeutic interventions in complicated forms of diverticular disease [68] and providing an alternative diagnosis in patients without diverticulitis [65, 67].

Alternative diagnoses include colon obstruction secondary to sigmoid carcinoma, gynecological diseases, urinary tract obstruction, or epiploic appendagitis. The most



**Fig. 8.** A 74-year-old man presents with acute pain in the left lower abdominal quadrant. Computed tomography reveals acute sigmoid diverticulitis with a complicating abscess (*white arrow*) and gas (*black arrow*) in the bladder lumen indicating a colovesical fistula. A colovesical fistula in sigmoid diverticulitis can be suspected when gas is seen in the bladder lumen and a focal bladder wall thickening adjacent to the diseased bowel segment

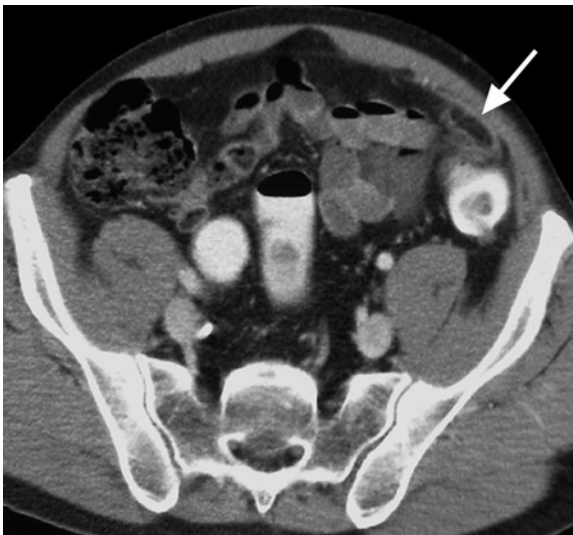


**Fig. 9.** A 52-year-old man presents with left lower abdominal quadrant pain. Transverse CT image shows an oval, fatty mass adjacent to the normal-appearing descending colon with surrounding mesenteric stranding (*arrow*). These findings are indicative of inflammation of one of the appendices epiploicae

common CT appearance of epiploic appendagitis is a 1.5- to 3.5-cm fat-density oval lesion with surrounding inflammatory changes abutting the anterior wall of the sigmoid colon (Fig. 9) [69]. The inflammation of epiploic ap-

pendages can be the result of torsion or venous occlusion [69]. When US is performed, the inflamed epiploic appendage appears as an echogenic finger-like projection arising from the colonic wall. Adjacent pericolonic fat also becomes echogenic and mass-like when inflamed [70].

### Acute Diffuse Abdominal Pain

Any disorder that irritates a large portion of the gastrointestinal tract and/or peritoneum usually results in poorly localizable diffuse abdominal pain. This is most frequently caused by bowel obstruction, acute bowel ischemia, infectious or inflammatory bowel disease, and gastrointestinal tract perforation (Table 3).

### Bowel Obstruction

Bowel obstruction is responsible for approximately 20% of surgical admissions for acute abdominal pain, with small bowel obstruction (SBO) accounting for approximately 75% and large bowel obstruction (LBO) for 25% [71, 72]. The leading cause of SBO in the western world has become adhesions. In a retrospective study encompassing 552 patients the etiology of SBO was adhesions (74%), followed by Crohn's disease (7%), neoplasia (5%), hernia (2%), radiation (1%), and miscellaneous (11%) [73]. In LBO, the three main causes are carcinoma (60%), volvulus (10–15%), and diverticulitis (10%) [74].

In order to ensure appropriate treatment, the goal of imaging in a patient with suspected SBO is to determine the site and cause of obstruction and the presence of strangulation [75]. Plain abdominal radiography is usually performed as the first radiological procedure. Several centers use US as a complementary imaging modality. On US, the cause of SBO is often well definable [76, 77]. In a study by Ko et al. [78], the diagnosis of obstruction was correct in 89% of cases with US and in 71% with plain abdominal radiography, whereas the level of obstruction was correctly predicted in 76% with US and in 51% with plain radiography. The cause of obstruction was identified in 20% of cases with US and in only 2% with plain radiography [78]. Although US can recognize dilated, fluid-filled bowel loops, the presence of a large amount of gas within the bowel often hinders its diagnostic use. The main advantage of US is the real-time visualization of peristalsis. In patients with mechanical obstruction, hyperperistalsis with a to-and-fro movement may be observed. Once the obstruction becomes complete or in the paralytic bowel, peristalsis is absent.

Because of the diagnostic limitations of plain abdominal radiography, CT is increasingly used to identify the site, severity, and underlying cause of SBO [79]. The CT is reported to have an accuracy of up to 96% in cases of high-grade obstruction [80], whereas it is less reliable for low-grade bowel obstruction [15, 81]. The MDCT brings additional information as compared with conventional CT by way of high-resolution multiplanar capabilities. This abili-



**Table 3.** Common causes of acute diffuse abdominal pain

Bowel obstruction	Acute bowel ischemia	Infectious bowel disease	Inflammatory bowel disease	Gastrointestinal tract perforation
Small bowel obstruction	Mesenteric arterial occlusion	Gastroenterocolitis	Ulcerative colitis	Diverticulitis
Adhesion	Thromboembolism	Pseudo-membranous colitis	Crohn's disease	Peptic ulcer disease
Crohn's disease	Atherosclerosis			Endoscopic procedures (biopsy, sphincterotomy)
Neoplasia	Dissection			
Hernia	Vasculitis			
Radiation	Mesenteric venous occlusion			
Miscellaneous (intussusception, gallstone ileus, volvulus)	Hypercoagulable states			
Large bowel obstruction	Neoplastic disease			
Carcinoma	Strangulation			
Volvulus	Volvulus			
Diverticulitis	Intussusception			
	Prestenotic bowel overdistension			
	Non-occlusive (low flow)			
	Cardiac failure			
	Hypovolemia			
	Septic shock			
	Drugs			



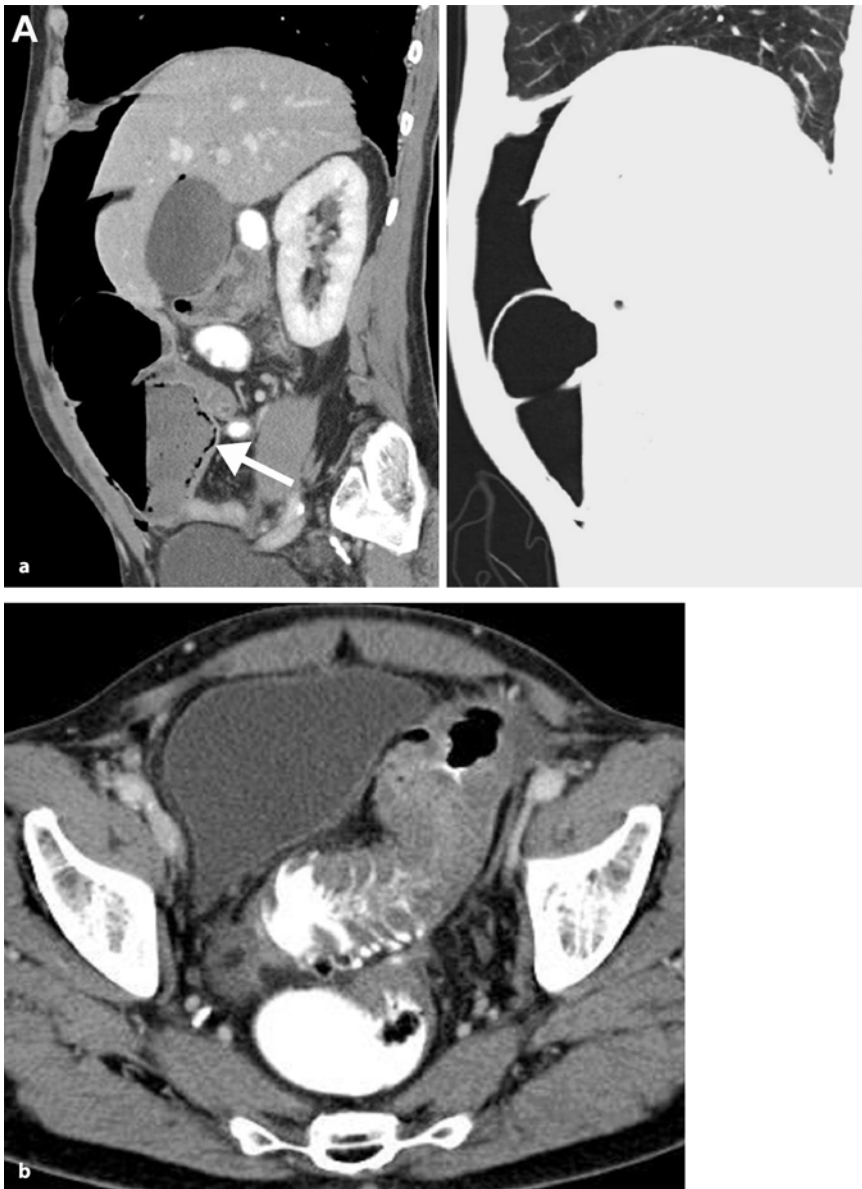


**Fig. 10.** A 61-year-old man with constipation and diffuse acute abdominal pain. **a** Sagittal CT reconstruction in a soft tissue window setting (left side: width 350 HU; center: 80 HU) shows intramural gas in the cecum (arrow) and free gas adjacent to the anterior abdominal wall. The same image in a lung window setting (right side: width 1500 HU; center: -400 HU) better shows the intraluminal and free extraluminal gas collections. **b** Transverse CT image identifies high-grade obstructing chronic sigmoid diverticulitis complicated by free perforation of the cecum due to ischemia

ty to acquire high-resolution multiplanar views provides greater diagnostic confidence as compared with standard axial images [12]. The CT diagnosis of SBO is based on the presence of a dilated bowel proximal to a definable transition zone and a collapsed distal bowel. The detection of a mass, lymphadenopathy, or abrupt transition with irregular bowel wall thickening are indicative of malignant obstruction [82]. In the absence of a mass or other abnormality in the area of obstruction, adhesions constitute the diagnosis of exclusion in the majority of patients [82]. Multiplanar images enable assessment of the site of obstruction from a different perspective and help to determine the transition zone with greater confidence [8, 12, 83, 84]. The CT is also very helpful in differentiating mechani-

cal obstruction from paralytic ileus [81] and in identifying strangulated SBO [85, 86], often secondary to adhesion or hernia. Complications from strangulation, such as ischemia, may be identified on coronal views.

The LBO will present as an emergency in patients with high-grade colonic obstruction. High-grade colonic obstruction can cause perforation with fecal peritonitis (Fig. 10). Patients with a competent ileocecal valve have a marked distention of the cecum due to the accumulated back pressure from the obstructive site. In contrast to SBO, which has been studied extensively, the reports on the value of CT in the diagnosis of LBO are scarce [87, 88]. In one study sensitivity and specificity were 96 and 93%, respectively [87].

### Acute Bowel Ischemia

Acute bowel ischemia is classified into three categories:

1. Acute mesenteric ischemia: acute ischemia of the small bowel with or without involvement of the colon
2. Focal mesenteric ischemia: acute ischemia of short small bowel segments
3. Acute ischemia of the colon

Thromboembolic occlusion of the superior mesenteric artery (SMA) with the thrombus originating from the heart as a consequence of atrial fibrillation, recent myocardial infarction, or valvular disease is the most common cause of acute mesenteric ischemia and is responsible for approxi-

mately 50% of cases. Thrombosis of an existing atherosclerotic plaque and dissection in the SMA account for 25% of the total, whereas thrombosis of the mesenteric and portal veins (observed in patients with hypercoagulable states, neoplastic disease, strangulated herniation or strangulated closed-loop obstruction, volvulus, intussusception) and non-occlusive ischemia, occurring in patients with low flow (cardiac failure, hypovolemia, septic shock, drugs), are less common, accounting together for approximately 25% of cases. Superior mesenteric vein (SMV) thrombosis has a better prognosis because extensive venous collaterals prevent infarction in most cases.

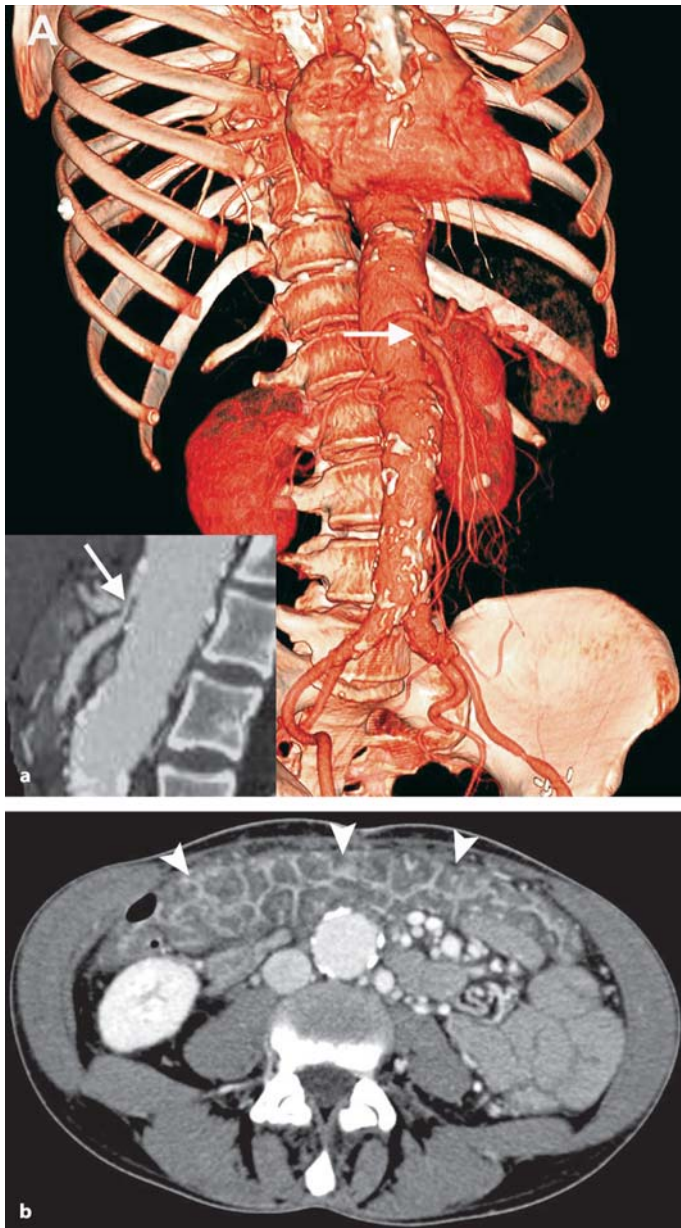


**Fig. 11.** A 45-year-old woman with known Takayasu arteritis with diffuse acute abdominal pain. **a** Volume-rendered reconstruction of CT angiography and maximum-intensity projection (*inset*) depict a high-grade stenosis of the celiac trunk and of the origin of the superior mesenteric artery (*arrow*) due to aortic wall changes. **b** Transverse CT image shows massive wall thickening of the small bowel (*arrowheads*), highly suggestive of bowel ischemia



**Fig. 12.** A 46-year-old man with diffuse acute abdominal pain and on immunosuppressive medication after kidney transplantation 1 week previously.

Contrast-enhanced CT in a coronal and transverse view (*inset*) demonstrates colonic wall thickening with a halo pattern caused by submucosal edema. In the setting of immunosuppressive therapy these CT findings are highly suggestive of pseudomembranous colitis

Focal mesenteric ischemia is an ischemic insult to a short bowel segment in which there is adequate collateral circulation to prevent transmural infarction. Common causes are strangulation from obstruction or volvulus, vasculitis (Fig. 11), radiation, and distal emboli to branch vessels. Limited tissue necrosis may result in complete healing or stricture formation.

The etiology of acute ischemia of the colon is unclear, probably related to low-flow states, small vessel disease, or both. Prestenotic intestinal overdistension causing bowel ischemia is usually observed in the colon (see Fig. 10) [89].

The US findings of acute mesenteric ischemia are non-specific and include bowel wall thickening, hyperechogenic pericolic fat, and free-fluid collections [90]. With duplex ultrasound, up to 90% of superior mesenteric artery stenosis and greater than 80% of celiac stenosis are identifiable [91].

Computed tomography is increasingly used as first-line imaging modality for the evaluation of patients with sus-

pected acute bowel ischemia. In the study by Klein et al. the sensitivity of spiral CT for the detection of acute mesenteric ischemia was 82% [90]. A common CT finding is bowel wall thickening, which is non-specific. The attenuation of the bowel wall may be low secondary to edema, or high secondary to intramural hemorrhagic infarction. Following intravenous contrast, the enhancement of the affected bowel segment may be absent, delayed, or persistent; hyperemia and hyperperfusion of mucosal/submucosal and serosal/subserosal layers in addition to the surrounding mural edema cause the "target sign" [89, 92]. Other CT findings include luminal dilatation, mesenteric edema, ascites, pneumatosis, and portomesenteric gas [89]. In addition to detecting ischemic bowel wall changes, CT allows identification of the cause by visualizing the mesenteric vasculature. In most cases of acute mesenteric ischemia thrombus or emboli occur at the origin or in the proximal part of the SMA. The MDCT, because of the thin collimation coupled with faster scanning and intravenous contrast bolus injec-

tion, is particularly well suited to display not only this segment of the SMA but also their branches [93]. It has a prospective sensitivity of 80% in diagnosing acute bowel ischemia in the daily routine and its overall sensitivity is therefore comparable to that of angiography [94].

### Infectious Bowel Disease

Gastroenterocolitis is responsible for approximately 70% of patients with abdominal pain admitted to the emergency department [95]. The vast majority of patients do not require imaging; however, in patients with atypical clinical findings colicky abdominal pain may be the predominant symptom. In these cases, CT may be necessary to differentiate gastroenterocolitis from alternative diagnoses. At CT, wall thickening with usually homogenous enhancement, inflammation of the pericolic fat, ascites, and multiple air–fluid levels may be present. Although these findings are non-specific, the portion of colon affected may suggest a specific organism [96].

In patients on antibiotic, chemotherapeutic, or immunosuppressive therapy, the normal bacterial flora of the colon is decreased, resulting in overgrowth of *Clostridium difficile* causing pseudomembranous colitis. Although non-specific, CT findings include mural thickening with a halo or target pattern caused by submucosal edema, pericolic inflammatory changes, and ascites (Fig. 12) [97, 98]. The extent of bowel wall thickening in pseudomembranous colitis is usually greater than in other infectious or inflammatory bowel disease except Crohn's disease [99]. Sometimes contrast material is caught between thickened haustra producing an accordion-like appearance [97], which is suggestive of pseudomembranous colitis but typically only occurs in severe cases [96].

### Inflammatory Bowel Disease

The vast majority of patients with chronic inflammatory bowel disease, such as ulcerative colitis or Crohn's disease, experience chronic symptoms; however, in some patients acute exacerbations or complications may lead to acute abdominal pain. The diagnostic value of CT is based on the excellent visualization and documentation of extent and severity of bowel wall inflammation and the estimation of inflammatory activity of the disease. Although there is considerable overlap in the CT findings of ulcerative colitis and Crohn's disease, the location of the involved segment and the extent and appearance of wall thickening may help to distinguish the two. Extensive involvement of the right colon and small intestine is more common in Crohn's disease, whereas ulcerative colitis is typically left sided (Fig. 13). Bowel wall thickening in ulcerative colitis is usually diffuse and symmetric, whereas wall thickening in Crohn's disease may be eccentric and segmental with skip regions and may result in pseudodiverticula. Proliferation of mesenteric fat and mesenteric lymphadenopathy sug-

gests Crohn's disease rather than ulcerative colitis. On the other hand, the target sign, which represents a low-attenuation ring in the bowel wall due to deposition of submucosal fat, is seen more commonly in ulcerative colitis than in Crohn's disease [96].

### Gastrointestinal Tract Perforation

Gastrointestinal tract perforation may be found complicating diverticulitis, peptic ulcer disease, or following endoscopic procedures particularly endoscopic biopsy or sphincterotomy [100]. Free intraperitoneal gas can be visualized on an erect chest radiograph or an erect abdominal or left lateral decubitus radiograph. The amount of free gas is indicative of the site of perforation: large amounts of free gas are seen with perforation of the large bowel, moderate quantities are seen with perforation of the stomach, and small amounts are seen with perforation of the small bowel, which usually does not contain gas. With the introduction of CT, the role of plain abdominal radiography for assessing pneumoperitoneum has diminished, because CT is far more sensitive in assessing gastrointestinal tract perforation as it allows detection of even small amounts of extraluminal gas in the abdomen (see Figs. 4, 10) [17]. Viewing on a “lung window” setting will enhance the sensitivity of detecting subtle extraluminal gas. Although evaluation of patients with suspected gastrointestinal tract perforation can be made on unenhanced CT images, administration of oral and intravenous contrast is recommended for identifying the site of perforation and for diagnosing the underlying cause. While the localization of extraluminal gas varies depending on the position of the patient and is usually not identical to the site of perforation, helpful CT signs for localization may be focal fluid, oral contrast extravasation, and local inflammatory changes.

### Acute Flank or Epigastric Pain

The most common cause of flank pain is due to ureteral stones. Localized epigastric pain is frequently caused by acute pancreatitis, in typical cases with pain radiating to the back (Table 4).

**Table 4.** Common causes of acute flank or epigastric pain

Urolithiasis
Non-calculous urinary tract abnormalities
Pyelonephritis
Renal cell carcinoma
Extraordinary disease
Appendicitis
Diverticulitis
Bowel obstruction
Abdominal aortic aneurysm
Retroperitoneal hemorrhage
Acute pancreatitis





**Fig. 13.** A 30-year-old man with a history of bloody diarrhea once per week for 6 months, now with acute pain in the left abdomen. Computed tomography in a sagittal and a transverse view (*inset*) delineates concentric thickening of colonic wall, absence of haustra, and transverse ulcerations indicative of ulcerative colitis. Colonoscopy revealed exudative inflammation of the mucosa and multiple ulcerations confirming the diagnosis

### Ureteral Stones

For a long time, plain abdominal radiography combined with intravenous urography (IVU) have been the standard imaging modality for the evaluation of acute flank pain. Direct visualization of ureteral calculi is achieved in 40–60% of cases, whereas using indirect signs, such as ureteral and renal pelvic dilatation diagnosis of renal colic, is possible in up to 80–90% of cases [101]; however, IVU might be hampered by poor quality due to lack of bowel preparation. The use of US has been growing and the sensitivity can be up to 96% when combining the findings of direct visualization of stones, pyeloureteral dilatation, and the absence of ureteral ejaculation [101]. Recently, unenhanced CT imaging has been introduced and rapidly evolved as the initial imaging modality because of its high sensitivity and specificity for the evaluation of acute flank pain (Fig. 14). On CT, almost all ureteral stones are radiopaque, regardless of their chemical composition. Uric-acid stones have attenuation values ranging from 300 to 500 HU, whereas calcified stones have attenuation values of more than 1000 HU [102]. Small ureteral stones may be detectable by the presence of focal periureteral stranding.

Secondary CT signs of urolithiasis include hydronephrer, hydronephrosis, perinephric stranding, and renal enlargement. The advantages of unenhanced CT are its high sensitivity and specificity for detection of ureteral stones from 98 to 100% regardless of size, location, and chemical composition, its high accuracy for identifying extraordinary causes of flank pain in about one-third of all patients presenting with acute flank pain, the avoidance of contrast media, and that it can be performed within 5 min, providing important time saving in the emergency work-up compared with IVU and US [101]. Because of the radiation penalty to be paid if CT is performed instead of IVU, the dose can be reduced by modulating the milliampere-second settings. Tack et al. have demonstrated reduction in radiation dose by using a low-dose CT protocol (120 kV, 30 mAs) without impairing diagnostic accuracy for the detection of ureteral calculi or obscuring alternative diagnoses [103]. The MDCT is favored over conventional CT because it provides coronal views, which often portray the urinary tract more effectively than transverse images for precise stone location [103].

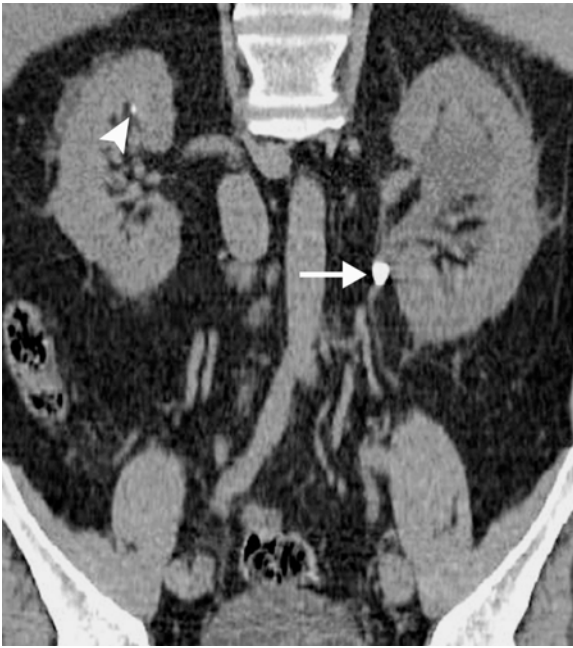


**Fig. 14.** A 56-year-old man with acute left-sided flank pain and a negative US examination in another hospital. Intravenous urography showed only delayed contrast excretion on the left side. The final diagnosis was made on unenhanced CT demonstrating a left-sided hydronephrosis with perinephric stranding caused by a stone in the proximal ureter (*arrow*). In addition, a small stone was identified in the right kidney (*arrowhead*). Coronal reconstructions often portray the urinary tract more effectively than transverse images

If non-enhanced CT is unable to detect a stone in the setting of acute flank pain, the CT imaging protocol can easily be tailored to alternative diagnoses by administration of intravenous contrast agent. Then acalculous urinary tract abnormalities (acute pyelonephritis, renal cell carcinoma) or extraurinary diseases (appendicitis, diverticulitis, bowel obstruction, acute pancreatitis, abdominal aortic aneurysm, retroperitoneal hemorrhage) may be observed as mimicking urinary colic.

### Acute Pancreatitis

Steady upper abdominal pain is the hallmark feature of acute pancreatitis. The pain often radiates to the back and may be associated with variable degrees of nausea and vomiting. The severe forms of acute pancreatitis are characterized by delayed or absent response to conservative therapy. Complications, such as superinfection of necrotic tissue, hemorrhage, abscess formation, and vascular erosion, present clinically as an acute abdomen.

On physical examination, tenderness is often located in the epigastrium in mild cases and may be generalized with guarding and rigidity in severe cases.

The diagnosis of acute pancreatitis depends on the history, physical examination, and confirmatory elevations in either amylase or lipase levels. Gallstones, dilatation of the common bile duct, and enlargement of the pancreas may be identified on US; however, overlying bowel gas often obscures accurate visualization of the pancreas. Computed tomography is the imaging modality of choice to classify pancreatitis and to detect complications such as pseudoaneurysms, porto-mesenteric vein occlusion, pseudocysts, or abscess (Fig. 15). The CT findings correlate well with the severity of disease [104, 105]: Mild forms present with peripancreatic inflammatory exudate or with a normal appearing or homogeneously enlarged gland. In severe forms, small intrapancreatic fluid collections are present as a result of intraglandular necrosis. Necrotizing pancreatitis exhibits necrotic regions as unenhanced areas sharply demarcated from normally enhancing parenchyma. Peripancreatic exudates may penetrate along fascial planes and extend to adjacent organs. Fluid collections typically accumulate in the anterior pararenal space, lesser sac, mesenteric root, and transverse mesocolon.

### 5.1.4 Conclusion

The optimal imaging strategy in patients presenting with acute abdominal pain highly depends on the topographical localization of pain, the ability of clinical examination to shorten the list of probable diagnoses in the individual patient, the radiological equipment readily available in the emergency situation, and the experience of the radiologist investigating the imaging studies. In the past few years, CT has gained widespread acceptance as the first-line imaging modality in the diagnostic work-up of most patients presenting with acute abdominal pain, because it is the most time-effective and accurate imaging technique, and, if the working clinical diagnosis is incorrect, CT provides sufficient information for an alternative diagnosis. However, in general, for optimal diagnostic accuracy the CT imaging technique has to be tailored to specific questions; therefore, the initial history and physical examination have to focus the abdominal pain to a particular anatomic region or specific diagnosis and close cooperation between referring physician and radiologist is a prerequisite for rapid and accurate diagnosis.

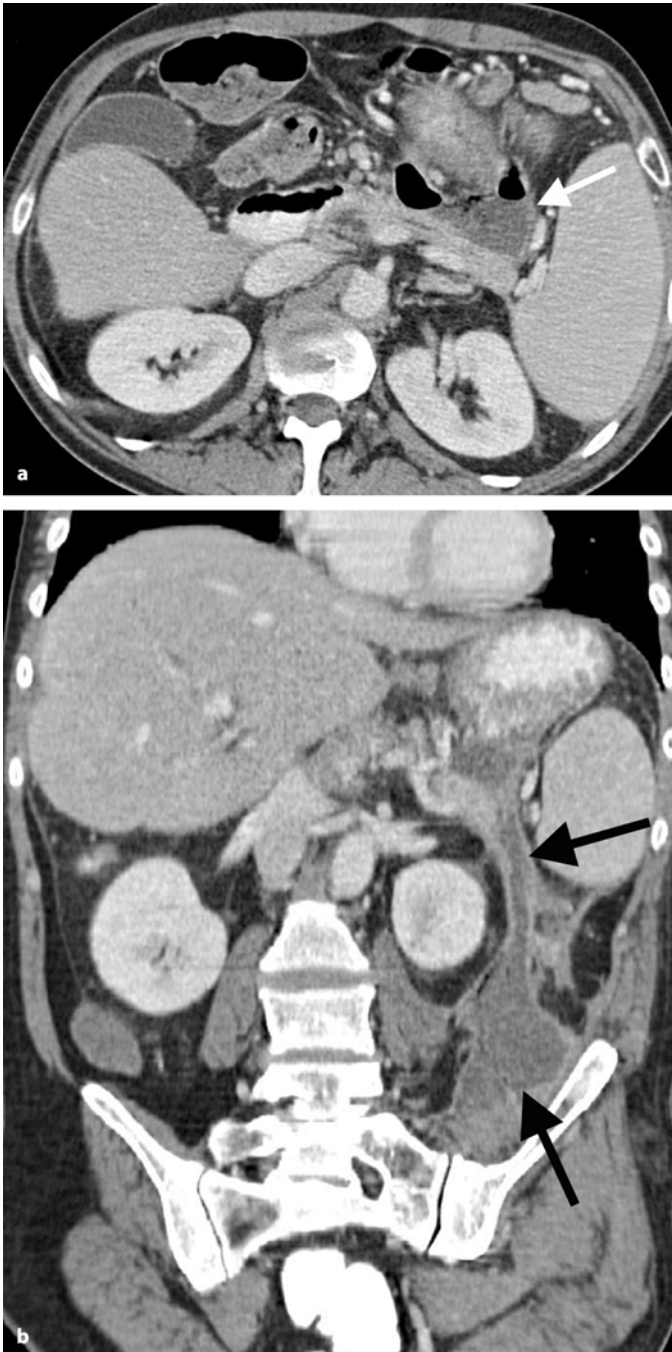


**Fig. 15.** A 44-year-old man with a history of alcohol abuse and acute pancreatitis 2 years previously now complains about acute epigastric pain. **a** Computed tomography revealed an extensive retroperitoneal encapsulated fluid collection with rim enhancement, corresponding to an abscess, originating from an infected pseudocyst (*arrow*). **b** Coronal reformation allows a better demonstration of the complete extent of the abscess (*arrows*)

## References

- Silen W (1996) Cope's early diagnosis of the acute abdomen, 19th edn. Oxford University Press, New York
- de Dombal FT (1991) Introduction. In: de Dombal FT (ed) Diagnosis of acute abdominal pain, 2nd edn. Churchill Livingstone, New York, pp 1–10
- Levine MS (1985) Plain film diagnosis of the acute abdomen. *Emerg Med Clin North Am* 3:541–562
- Ahn SH, Mayo-Smith WW, Murphy BL, Reinert SE, Cronan JJ (2002) Acute nontraumatic abdominal pain in adult patients: abdominal radiography compared with CT evaluation. *Radiology* 225:159–164
- Taourel P, Baron MP, Pradel J, Fabre JM, Senerterre E, Bruel JM (1992) Acute abdomen of unknown origin: impact of CT on diagnosis and management. *Gastrointest Radiol* 17:287–291
- Siewert B, Raptopoulos V, Mueller MF, Rosen MP, Steer M (1997) Impact of CT on diagnosis and management of acute abdomen in patients initially treated without surgery. *Am J Roentgenol* 168:173–178
- Mindelzun RE, Jeffrey RB (1999) The acute abdomen: current CT imaging techniques. *Semin Ultrasound CT MR* 20:63–67
- Marincek B (2002) Nontraumatic abdominal emergencies: acute abdominal pain: diagnostic strategies. *Eur Radiol* 12:2136–2150
- Rosen MP, Siewert B, Sands DZ, Bromberg R, Edlow J, Raptopoulos V (2003) Value of abdominal CT in the emergency department for patients with abdominal pain. *Eur Radiol* 13:418–424
- Urban BA, Fishman EK (2000) Tailored helical CT evaluation of acute abdomen. *Radiographics* 20:725–749
- Gore RM, Miller FH, Pereles FS, Yaghami V, Berlin JW (2000) Helical CT in the evaluation of the acute abdomen. *Am J Roentgenol* 174:901–913
- Caoili EM, Paulson EK (2000) CT of small-bowel obstruction: another perspective using multiplanar reformations. *Am J Roentgenol* 174:993–998
- Rao PM, Rhea JT, Novelline RA, Mostafavi AA, McCabe CJ (1998) Effect of computed tomography of the appendix on treatment of patients and use of hospital resources. *N Engl J Med* 338:141–146
- Maglinte DD, Gage SN, Harmon BH, Kelvin FM, Hage JP, Chua GT, Ng AC, Graffis RF, Chernish SM (1993) Obstruction of the small intestine: accuracy and role of CT in diagnosis. *Radiology* 188:61–64
- Frager D, Medwid SW, Baer JW, Mollinelli B, Friedman M (1994) CT of small-bowel obstruction: value in establishing the diagnosis and determining the degree and cause. *Am J Roentgenol* 162:37–41
- Jeffrey RB, Federle MP, Wall S (1983) Value of computed tomography in detecting occult gastrointestinal perforation. *J Comput Assist Tomogr* 7:825–827
- Maniatis V, Chryssikopoulos H, Roussakis A, Kalamara C, Kavadias S, Papadopoulos A, Andreou J, Stringaris K (2000) Perforation of the alimentary tract: evaluation with computed tomography. *Abdom Imaging* 25:373–379
- Smith RC, Rosenfield AT, Choe KA, Essenmacher KR, Verga M, Glickman MG, Lange RC (1995) Acute flank pain: comparison of non-contrast-enhanced CT and intravenous urography. *Radiology* 194:789–794
- Smith RC, Verga M, McCarthy S, Rosenfield AT (1996) Diagnosis of acute flank pain: value of unenhanced helical CT. *Am J Roentgenol* 166:97–101
- Hanbidge AE, Buckler PM, O'Malley ME, Wilson SR (2004) Imaging evaluation for acute pain in the right upper quadrant. *Radiographics* 24:1117–1135
- Puylaert JB, van der Zant FM, Rijke AM (1997) Sonography and the acute abdomen: practical considerations. *Am J Roentgenol* 168:179–186
- Cahir JG, Freeman AH, Courtney HM (2004) Multislice CT of the abdomen. *Br J Radiol* 77:S64–S73
- Rubin GD (2000) Data explosion: the challenge of multidetector-row CT. *Eur J Radiol* 36:74–80
- Reiner BI, Siegel EL, Hooper FJ (2002) Accuracy of interpretation of CT scans: comparing PACS monitor displays and hard-copy images. *Am J Roentgenol* 179:1407–1410
- Leschka S, Alkadhi H, Marincek B, Wildermuth S (2005) MDCT of acute abdomen. *Eur Radiol* 15:2435–2447
- Malone AJ (1999) Unenhanced CT in the evaluation of the acute abdomen: the community hospital experience. *Semin Ultrasound CT MR* 20:68–76
- Wittenberg J, Harisinghani MG, Jhaveri K, Varghese J, Mueller PR (2002) Algorithmic approach to CT diagnosis of the abnormal bowel wall. *Radiographics* 22:1093–1107
- Laing FC (1998) The gallbladder and bile ducts. In: Rumack CM, Wilson SR, Charboneau JW (eds) *Diagnostic ultrasound*, 2nd edn. Mosby, St. Louis, pp 187–193
- Ralls PW, Colletti PM, Lapin SA, Chandrasoma P, Boswell WD Jr, Ngo C, Radin DR, Halls JM (1985) Real-time sonography in suspected acute cholecystitis. Prospective evaluation of primary and secondary signs. *Radiology* 155:767–771
- Fidler J, Paulson EK, Layfield L (1996) CT evaluation of acute cholecystitis: findings and usefulness in diagnosis. *Am J Roentgenol* 166:1085–1088
- Yamashita K et al (1995) CT finding of transient focal increased attenuation of the liver adjacent to the gallbladder in acute cholecystitis. *Am J Roentgenol* 164:343–346
- Ito K, Awaya H, Mitchell DG, Honjo K, Fujita T, Uchisako H, Moritani K, Nomura S, Higuchi M, Kada T, Matsumoto T, Matsunaga N (1997) Gallbladder disease: appearance of associated transient increased attenuation in the liver at biphasic, contrast-enhanced dynamic CT. *Radiology* 204:723–728
- Paulson EK (2000) Acute cholecystitis: CT findings. *Semin Ultrasound CT MR* 21:56–63
- Bennett GL, Balthazar EJ (2003) Ultrasound and CT evaluation of emergent gallbladder pathology. *Radiol Clin North Am* 41:1203–1216
- Mirvis SE, Vainright JR, Nelson AW, Johnston GS, Shorr R, Rodriguez A, Whitley NO (1986) The diagnosis of acute acalculous cholecystitis: a comparison of sonography, scintigraphy, and CT. *Am J Roentgenol* 147:1171–1175
- Bennett GL, Rusinek H, Lisi V, Israel GM, Krinsky GA, Slywotzky CM, Megibow A (2002) CT findings in acute gangrenous cholecystitis. *Am J Roentgenol* 178:275–281
- Teefey SA, Baron RL, Radke HM, Bigler SA (1991) Gangrenous cholecystitis: new observations on sonography. *J Ultrasound Med* 10:603–606
- Simeone JF, Brink JA, Mueller PR, Compton C, Hahn PF, Saini S, Silverman SG, Tung G, Ferrucci JT (1989) The sonographic diagnosis of acute gangrenous cholecystitis: importance of the Murphy sign. *Am J Roentgenol* 152:289–290
- Gill KS, Chapman AH, Weston MJ (1997) The changing face of emphysematous cholecystitis. *Br J Radiol* 70:986–991
- Fishman EK, Soyer P, Bliss DF, Bluemke DA, Devine N (1995) Splenic involvement in pancreatitis: spectrum of CT findings. *Am J Roentgenol* 164:631–635
- Urban BA, Fishman EK (1998) Helical CT of the spleen. *Am J Roentgenol* 170:997–1003
- Jacobs JM, Hill MC, Steinberg WM (1991) Peptic ulcer disease: CT evaluation. *Radiology* 178:745–748
- Berry J, Malt RA (1984) Appendicitis near its centenary. *Ann Surg* 200:567–575
- Birnbaum BA, Jeffrey RB Jr (1998) CT and sonographic evaluation of acute right lower quadrant abdominal pain. *Am J Roentgenol* 170:361–371
- Balthazar EJ, Rofsky NM, Zucker R (1998) Appendicitis: the impact of computed tomography imaging on negative appendectomy and perforation rates. *Am J Gastroenterol* 93:768–771



46. Rao PM, Rhea JT, Novelline RA (1997) Sensitivity and specificity of the individual CT signs of appendicitis: experience with 200 helical appendiceal CT examinations. *J Comput Assist Tomogr* 21:686–692
47. Rao PM, Rhea JT, Novelline RA, McCabe CJ, Lawrason JN, Berger DL, Sacknoff R (1997) Helical CT technique for the diagnosis of appendicitis: prospective evaluation of a focused appendix CT examination. *Radiology* 202:139–144
48. Pinto Leite N, Pereira JM, Cunha R, Pinto P, Sirlin C (2005) CT evaluation of appendicitis and its complications: imaging techniques and key diagnostic findings. *Am J Roentgenol* 185:406–417
49. Keyzer C, Zalcman M, de Maertelaer V, Coppens E, Bali MA, Gevenois PA, van Gansbeke D (2005) Comparison of US and unenhanced multi-detector row CT in patients suspected of having acute appendicitis. *Radiology* 236:527–534
50. Sivit CJ (1993) Diagnosis of acute appendicitis in children: spectrum of sonographic findings. *Am J Roentgenol* 161:147–152
51. Jeffrey RB Jr, Laing FC, Townsend RR (1988) Acute appendicitis: sonographic criteria based on 250 cases. *Radiology* 167:327–329
52. Rioux M (1992) Sonographic detection of the normal and abnormal appendix. *Am J Roentgenol* 158:773–778
53. Ege G, Akman H, Sahin A, Bugra D, Kuzucu K (2002) Diagnostic value of unenhanced CT in adult patients with suspected acute appendicitis. *Br J Radiol* 75:721–725
54. Balthazar EJ, Birnbaum BA, Yee J, Megibow AJ, Roshkow J, Gray C (1994) Acute appendicitis: CT and US correlation in 100 patients. *Radiology* 190:31–35
55. Wise SW, Labuski MR, Kasales CJ, Blebea JS, Meilstrup JW, Holley GP, LaRusso SA, Holliman J, Ruggiero FM, Mauger D (2001) Comparative assessment of CT and sonographic techniques for appendiceal imaging. *Am J Roentgenol* 176:933–941
56. Malone AJ Jr, Wolf CR, Malmel AS, Melliere BF (1993) Diagnosis of acute appendicitis: value of unenhanced CT. *Am J Roentgenol* 160:763–766
57. Yu J, Fulcher AS, Turner MA, Halvorsen RA (2005) Helical CT evaluation of acute right lower quadrant pain. Part I: Common mimics of appendicitis. *Am J Roentgenol* 184:1136–1142
58. Yu J, Fulcher AS, Turner MA, Halvorsen RA (2005) Helical CT evaluation of acute right lower quadrant pain. Part II: Uncommon mimics of appendicitis. *Am J Roentgenol* 184:1143–1149
59. Parks TG (1975) Natural history of diverticular disease of the colon. *Clin Gastroenterol* 4:53–69
60. Markham NI, Li AK (1992) Diverticulitis of the right colon: experience from Hong Kong. *Gut* 33:547–549
61. Stollmann N, Raskin JB (2004) Diverticular disease of the colon. *Lancet* 363:631–639
62. Pradel JA, Adell JF, Taourel P, Djafari M, Monnin-Delhom E, Bruel JM (1997) Acute colonic diverticulitis: prospective comparative evaluation with US and CT. *Radiology* 205:503–512
63. Meuwly JY, Felley C, Vuilleumier H, Schnyder P, Hewig U (2002) Ultrasound examination of non-traumatic acute abdomen. *Ultraschall Med* 23:13–21 [in German]
64. Ambrosetti P, Jenny A, Becker C, Terrier F, Morel P (2000) Acute left colonic diverticulitis: compared performance of computed tomography and water-soluble contrast enema. Prospective evaluation of 420 patients. *Dis Colon Rectum* 43:1363–1367
65. Werner A, Diehl SJ, Farag-Soliman M, Düber C (2003) Multi-slice spiral CT in routine diagnosis of suspected acute left-sided colonic diverticulitis: a prospective study of 120 patients. *Eur Radiol* 13:2596–2603
66. Tack D, Bohy P, Perlot I, De Maertelaer V, Alkeilani O, Sourtzis S, Gevenois PA (2005) Suspected acute colon diverticulitis: imaging with low-dose unenhanced multi-detector row CT. *Radiology* 237:189–196
67. Lawrimore T, Rhea JT (2004) Computed tomography evaluation of diverticulitis. *J Intensive Care Med* 19:194–204
68. Mueller PR, Saini S, Wittenburg J, Simeone J, Hahn PF, Steiner E, Dawson SL, Butch RJ, Stark DD, Ottinger LW (1987) Sigmoid diverticular abscesses: percutaneous drainage as an adjunct to surgical resection in 24 cases. *Radiology* 164:321–325
69. Singh AK, Gervais DA, Hahn PF, Rhea J, Mueller PR (2004) CT appearance of acute appendagitis. *Am J Roentgenol* 183:1303–1307
70. Rioux M, Langis P (1994) Primary epiploic appendagitis: clinical, US, and CT findings in 14 cases. *Radiology* 191:523–526
71. Welch JP (1990) General consideration and mortality in bowel obstruction. In: Welch JP (ed) *Bowel obstruction: differential diagnosis and clinical management*. Saunders, Philadelphia, pp 59–95
72. Taourel P, Kessler N, Lesnik A, Blayac PM, Morcos L, Bruel JM (2002) Non-traumatic abdominal emergencies: imaging of acute intestinal obstruction. *Eur Radiol* 12:2151–2160
73. Miller G, Boman J, Shrier I, Gordon PH (2000) Etiology of small bowel obstruction. *Am J Surg* 180:33–36
74. Taourel P, Kessler N, Lesnik A, Pujol J, Morcos L, Bruel JM (2003) Helical CT of large bowel obstruction. *Abdom Imaging* 28:267–275
75. Herlinger H, Maglinte DDT (1989) Small-bowel obstruction. In: Herlinger H, Maglinte DDT (eds) *Clinical radiology of the small intestine*. Saunders, Philadelphia, pp 479–507
76. Grunshaw ND, Renwick IG, Scarisbrick G, Nasmyth DG (2000) Prospective evaluation of ultrasound in distal ileal and colonic obstruction. *Clin Radiol* 55:356–362
77. Seitz K, Merz M (1998) Ultrasound ileus diagnosis. *Ultraschall Med* 19:242–249
78. Ko YT, Lim JH, Lee DH, Lee HW, Lim JW (1993) Small bowel obstruction: sonographic evaluation. *Radiology* 188:649–653
79. Maglinte DD, Reyes BL, Harmon BH, Kelvin FM, Turner Jr WW, Hage JE, Ng AC, Chua GT, Gage SN (1996) Reliability and role of plain film radiography and CT in the diagnosis of small-bowel obstruction. *Am J Roentgenol* 167:1451–1455
80. Megibow AJ, Balthazar EJ, Cho KC, Medwid SW, Birnbaum BA, Noz ME (1991) Bowel obstruction: evaluation with CT. *Radiology* 180:313–318
81. Gazelle GS, Goldberg MA, Wittenberg J, Halpern EF, Pinkney L, Mueller PR (1994) Efficacy of CT in distinguishing small-bowel obstruction from other causes of small-bowel dilatation. *Am J Roentgenol* 162:43–47
82. Urban BA, Fishman EK (2000) Targeted helical CT of the acute abdomen: appendicitis, diverticulitis, and small bowel obstruction. *Semin Ultrasound CT MR* 21:20–39
83. Paulson EK, Jaffe TA, Thomas J, Harris JP, Nelson RC (2004) MDCT of patients with acute abdominal pain: a new perspective using coronal reformations from submillimeter isotropic voxels. *Am J Roentgenol* 183:899–906
84. Alkadhi H, Boehm T, Hahnloser D, Marincek B, Wildermuth S (2005) Adenocarcinoma of the ileum. *J Gastroenterol Hepatol* 20:648
85. Balthazar EJ, Birnbaum BA, Megibow AJ, Gordon RB, Whelan CA, Hulnick DH (1992) Closed-loop and strangulating intestinal obstruction: CT signs. *Radiology* 185:769–775
86. Ha HK, Kim JS, Lee MS, Lee HJ, Jeong YK, Kim PN, Lee MG, Kim KW, Kim MY, Auh YH (1997) Differentiation of simple and strangulated small-bowel obstructions: usefulness of known CT criteria. *Radiology* 204:507–512
87. Frager D, Rovno HDS, Baer JW, Bashist B, Friedman M (1998) Prospective evaluation of colonic obstruction with computed tomography. *Abdom Imaging* 23:141–146
88. Taourel P, Kessler N, Lesnik A, Pujol J, Morcos L, Bruel JM (2003) Helical CT of large bowel obstruction. *Abdom Imaging* 28:267–275
89. Wiesner W, Khurana B, Ji H, Ros PR (2003) CT of acute bowel ischemia. *Radiology* 226:635–650
90. Klein HM, Lensing R, Klosterhalfen B, Tons C, Gunther RW (1995) Diagnostic imaging of mesenteric infarction. *Radiology* 197:79–82

91. Zwolak RM (1999) Can duplex ultrasound replace arteriography in screening for mesenteric ischemia? *Semin Vasc Surg* 12:252–260
92. Mirvis SE, Shanmuganathan K, Erb R (1994) Diffuse small bowel ischemia in hypotensive adults after blunt trauma (shock bowel): CT findings and clinical significance. *Am J Roentgenol* 163:1375–1379
93. Horton KM, Fishman EK (2002) CT angiography of the GI tract. *Gastrointest Endosc* 55:S37–S41
94. Wiesner W, Hauser A, Steinbrich W (2004) Accuracy of multi-detector row computed tomography for the diagnosis of acute bowel ischemia in a non-selected study population. *Eur Radiol* 14:2347–2356
95. Trott AT, Lucas RH (1998) Acute abdominal pain. In: Rose P (ed) *Emergency medicine*, 4th edn. Mosby, St. Louis, pp 1888–1903
96. Horton KM, Corl FM, Fishman EK (2000) CT evaluation of the colon: inflammatory disease. *Radiographics* 20:399–418
97. Kawamoto S, Horton KM, Fishman EK (1999) Pseudomembranous colitis: spectrum of imaging findings with clinical and pathologic correlation. *Radiographics* 19:887–897
98. Gluecker TM, Williamson EE, Fletcher JG, Hough DM, Huppert BJ, Carlson SK, Casey MB, Farrell MA (2003) Diseases of the cecum: a CT pictorial review. *Eur Radiol* 13 (Suppl 4):L51–L61
99. Ros PR, Buetow PC, Pantograg-Brown L, Forsmark CE, Sobin LH (1996) Pseudomembranous colitis. *Radiology* 198:1–9
100. Kuhlman JE, Fishman EK, Milligan FD, Siegelman SS (1989) Complications of endoscopic retrograde sphincterotomy: computed tomographic evaluation. *Gastrointest Radiol* 14: 127–132
101. Heidenreich A, Desgrandschamps F, Terrier F (2002) Modern approach of diagnosis and management of acute flank pain: review of all imaging modalities. *Eur Urol* 41:351–362
102. Smith RC, Verga M, Dalrymple N, McCarthy S, Rosenfield AT (1996) Acute ureteral obstruction: value of secondary signs of helical unenhanced CT. *Am J Roentgenol* 167:1109–1113
103. Tack D, Sourtzis S, Delpierre I, de Maertelaer V, Gevenois PA (2003) Low-dose unenhanced multidetector CT of patients with suspected renal colic. *Am J Roentgenol* 180:305–311
104. Balthazar EJ, Robinson DL, Megibow AJ, Ranson JH (1990) Acute pancreatitis: value of CT in establishing prognosis. *Radiology* 174:331–336
105. Baron TH, Morgan DE (1999) Acute necrotizing pancreatitis. *N Engl J Med* 340:1412–1417



# Imaging of Acute Intestinal Obstruction

P. Taourel, C. Uriot, G. Laffargue,  
A. Lesnik, F. Guillon, J.M. Bruel

## 5.2

### Contents

5.2.1 Introduction	435
5.2.2 Diagnosis of Mechanical Obstruction	435
5.2.2.1 Clinical Considerations	435
5.2.3 Diagnosis of Site	437
5.2.3.1 Clinical Considerations	437
5.2.4 Diagnosis of Cause	437
5.2.4.1 Clinical Considerations	437
5.2.5 Diagnosis of Complications	446
5.2.5.1 Clinical Considerations	446
5.2.6 Impact and Diagnostic Strategy	449
5.2.6.1 Impact of Imaging on Management	449
5.2.6.2 Diagnostic Strategy	450
References	450

### 5.2.1 Introduction

Acute intestinal obstruction is defined by the hindrance to the progression of the intestinal content due to a mechanical obstacle. It is responsible for approximately 20% of surgical admissions for acute abdominal conditions, with small bowel obstruction (SBO) counting for approximately 75% of the obstruction and large bowel obstruction (LBO) for 25%. The goals of imaging in a patient with suspected intestinal obstruction were defined by Mondor et al. [1] in 1943 and were summarized by Herlinger and Maglinte [2], and are as follows:

1. To confirm that it is a true obstruction and to differentiate it from an ileus
2. To determine the level of obstruction
3. To determine the cause of the obstruction
4. To look for findings of strangulation
5. To allow a good management either medically or surgically by laparotomy or laparoscopy

### 5.2.2 Diagnosis of Mechanical Obstruction

#### 5.2.2.1 Clinical Considerations

The clinical diagnosis of bowel obstruction (BO) classically depends on four cardinal findings: abdominal pain; constipation or obstipation; and abdominal distension; however, diagnosis can be difficult because clinical findings vary with the degree and level of bowel obstruction and with the vascular status of the obstructed segment. In typical mechanical obstruction, abdominal pain is crampy and gradually increases in intensity, only to abate and recur. With time, increasing bowel distention inhibits motility and the pain tends to subside. Furthermore, in patients with most colonic obstructions due to cancer, patients are often elderly and have symptoms related to the tumor location, with less acute symptoms than with SBO. On the other hand, crampy abdominal pain can occur with other causes of acute abdomen such as renal colic. In the same way, vomiting or constipation is not specific to mechanical obstruction. Abdominal plain film is the classic imaging modality used to confirm the diagnosis of BO; however, about one-third of patients thought to have mechanical obstruction on clinical examination and abdominal plain film have no obstruction. Conversely, about 20% of patients suspected of having colonic pseudoobstruction have mechanical BO.

#### Imaging Findings

The distinction between bowel obstruction and ileus is classically based upon clinical exam and abdominal plain film. In complete obstruction, distended loops of small bowel containing gas and fluid are usually present within 3–5 h of the onset. The interface between gas and fluid forms a straight horizontal margin in the upright or lateral decubitus view. Although gas-fluid levels are occasionally present normally, more than two gas-fluid levels in the small bowel are generally considered to be abnormal; however, gas-fluid levels are also very common in ileus. The presence of gas-fluid levels at different heights in the same loop has traditionally been considered strong evidence of





**Fig. 1.** Feces finding in a patient with small bowel obstruction (SBO) due to adhesive band. Axial slice (a) shows small bowel fluid-filled loops. Fecal material in a distended bowel loop is present in front of the collapsed sigmoid colon. On coronal reformatting the small bowel and collapsed right and left colon are well seen (b), and the feces finding permits localization of the transition zone (arrow) between distended and collapsed small bowel (c)



mechanical obstruction; however, it has been shown [3] that this pattern is insensitive and can also be demonstrated in some patients with nondynamic ileus. Furthermore, in severe complete obstruction, the bowel proximal to an obstruction may contain no gas and be completely filled with fluid, producing sausage-shaped water-density shadows that can be difficult to diagnose. The collapsed loops beyond the obstruction may be difficult to identify, and the presence of air in the rectum, even in the lack of rectal exam, does not rule out a mechanical obstruction.

The CT diagnosis of bowel obstruction is based on the presence of dilated bowel proximal to a transition zone and a collapsed distal bowel [4, 5]. Small bowel is considered dilated when its diameter is wider than 2.5 cm [5] and large bowel when it is wider than 8 cm. The amount of intraluminal air vs fluid and the degree of dilatation of the small bowel are not reliable criteria to differentiate mechanical obstruction from ileus. Fluid-filled loops as large as 5 cm in

diameter can be present in a nonobstructive ileus [6]. In the same way, colon with diameter superior to 10 cm may be present in colonic reflex ileus. On the other hand, a large discrepancy of the caliber of the bowel loops at the transition zone and a high degree of collapse at the distal loops are reliable and convincing findings of mechanical obstruction. In the same way, fecal retention in a small bowel concomitant with collapsed colon is a finding indicative of SBO (Fig. 1). It is encountered in half of the patients with SBO and is more frequently present in patient with moderate and high degrees of SBO than in patients with mild degrees of SBO [7]. The small bowel feces finding is not perfectly specific and may be seen in the small bowel of patients with ileus.

Computed tomography is particularly helpful in the following cases:

1. Clinical findings of obstruction with abdominal plain film showing no gas, likely meaning that bowel loops are completely filled with fluid.
2. Dilatation of the small bowel and of the colon up to the splenic flexure which may be shown in obstruction with tumor of the splenic flexure, but also in some cases of ileus, in patients with a pattern of dilated small bowel and right and transverse colon, not being able to identify a lesion at the splenic flexure, is an argument for ileus.
3. Gas within one or two dilated bowel loops. Computed tomography has limitations in the diagnosis of a low-grade partial obstruction or in patients with numerous adhesions for whom a transition zone is not clearly identified, making it difficult to differentiate obstruction from ileus.

left indicates an obstruction in the proximal jejunum, whereas involvement of pelvic loops suggests a lower obstruction.

Computed tomography determines the site of SBO by detecting the site of the transition zone and by surveying all the abdominal axial images and comparing the relative lengths of the prestenotic vs collapsed intestine [6]. Attempting to determine the level of SBO solely on the basis of the site of transition can be misleading. Jejunal loops can be located in the pelvis, and ileal loops can be obstructed in the upper abdomen. When present, the small bowel feces finding is helpful to locate the transition zone in patients with small bowel obstruction (Fig. 1) [7].

It is much easier to follow the large bowel than the small bowel on CT slices, and CT is accurate in establishing the exact point of transition between dilated and collapsed colon; however, misinterpretations may be encountered between obstructing terminal ileal lesion and cecal lesion.

## 5.2.3 Diagnosis of Site

### 5.2.3.1 Clinical Considerations

The diagnosis of the site of a mechanical obstruction is not easily performed with just clinical data, even if vomiting is more pronounced in proximal SBO and abdominal distension in distal obstruction.

The accurate determination of the site of the obstruction is becoming a major point when considering the management of patients with SBO, by permitting a safe laparoscopic division of adhesions that may be a suitable form of treatment of adhesive bands. Additionally, it may represent a valuable predictive factor in the management of adhesive SBO, since it has been shown that most of the patients with proximal SBO healed with conservative management, whereas distal SBO more frequently required surgery [8].

The determination of the site of a large bowel obstruction due to cancer is important for the surgical procedure, particularly when a laparoscopic surgery is scheduled.

### Imaging Findings

The identification of loops of bowel that contain abnormally large amounts of gas is essential to differentiate small and large bowel obstruction. Small bowel loops generally occupy the more central portion of the abdomen, whereas colonic loops are positioned laterally around the periphery of the abdomen or inferiorly in the pelvis. Gas within the lumen of the bowel also permits to outline and to differentiate the valvulae conniventes in the small bowel from the colonic haustra. Valvulae conniventes are finer and closer together than colonic haustra, and they completely encircle the small bowel, whereas colonic haustra occupy only a portion of the diameter of the colon. The presence of a few dilated loops of small bowel located high and slightly to the

## 5.2.4 Diagnosis of Cause

### 5.2.4.1 Clinical Considerations

#### Small Bowel Obstruction

The pattern of major causes of SBO has changed during the past five decades. Originally, the most common cause was external hernia. Now, postoperative adhesions comprise 50–80% of the total number of SBO in the U.S. [9]. The second most common causes are neoplasm and hernias, each counting for 10–15%. A fourth miscellaneous group of causes includes inflammatory processes, intussusception, volvulus, endometriosis, ischemia, hematoma, congenital lesions, gallstones, foreign bodies, or bezoars; however, the prevalence of the different causes of SBO varies according to the clinical context. In patients without any past surgery, adhesions are less common even if congenital band may occur. In patients with previously treated cancer, obstruction is very common. It occurs in up to 28% of patients with a history of colorectal cancer and in as many as 42% of patients with ovarian cancer [10]. Determining the cause of obstruction becomes a vexing problem since it may be benign postoperative adhesions, a focal malignant deposit, peritoneal carcinomatosis, ischemic stenosis due to raditis enteritis or incisional entrapment. Malignant lesions represent the most common cause of obstruction; however, the percentage of benign causes of obstruction ranges from 18 to 38% on the basis of the distribution of the primary cancer [11–12]. Benign obstruction is more likely if pelvic irradiation was used in the management of the primary tumor [12], whereas the risk of malignant obstruction is increased if the patient had known metastatic cancer or if the primary cancer was in an advanced stage or of gynaecological origin. In patients with small bowel obstruction due to advanced intra abdominal malignancy,

**Table 1.** Causes of small bowel obstruction in adults

Extrinsic lesions	Intrinsic lesions	Intraluminal causes
Adhesions	Tumors infiltrating wall of small intestine	Obturation
Hernia	Adenocarcinoma	Gallstone
External	Carcinoid tumour	Bezoar
Inguinal	Lymphoma (rare)	Foreign body
Femoral	Leiomyosarcoma (rare)	Ascaris
Obturator	Inflammatory conditions	Meconium
Sciatic	Crohn's disease	Intussusception
Perineal	Tuberculosis	Adhesions
Supravesical	Potassium chloride stricture	Tumour
Spigelian	Eosinophilic gastroenteritis	Duplication
Lumbar	Vascular	Inverted Meckel's diverticulum
Incisional	Radiation enteropathy	
Umbilical	Ischaemia	
Internal	Haematoma	
Paraduodenal	Post-traumatic	
Epiploic foramen	Thrombocytopenia	
Diaphragmatic (traumatic)	Anticoagulants	
Transomental	Henoch-Schönlein purpura	
Transmesenteric		
Iliac fossa		
Masses		
Extrinsic tumours in mesentery		
Lymphoma		
Peritoneal metastasis		
Carcinoid		
Desmoid		
Abscesses		
Diverticulitis		
Pelvic inflammatory disease		
Crohn's disease		
Appendicitis		
Aneurysm		
Haematoma		
Endometriosis		

occult synchronous colic obstruction are present in nearly half of the patients [13]. This must be kept in mind before bypass surgery.

The diagnostic hypothesis for the cause of a SBO must take these probability data into account; however, systematic evaluation of imaging data must also be performed by looking for one of the three major categories of SBO, as stated by Herlinger and Rubesin [14]: intraluminal; intrinsic; and extrinsic (Table 1). Most extrinsic causes obstruct by flattening, twisting or kinking the small bowel. Intrinsic lesions constrict the lumen by thickening of the bowel wall, and intraluminal causes obturate the bowel lumen.

The practical value of knowing the cause of SBO before surgery has dramatically improved treatment in the last decade. The philosophy of never let the sun set or rise on SBO [9] has been succeeded by management according to the cause and the severity of the obstruction [15]. Most modern surgeons actually recommend and emergent operative management in hernias, a more delayed surgical management in malignant focal tumor, a medical management in most cases of jejunal hematoma, and a treatment of adhesions, balancing between medical treatment and sur-

gical exploration according to the patient's status, the location of the adhesions and overall the suspicion of strangulation [8].

### Imaging Findings

Intraluminal causes of obstruction include gallstones (mostly in elderly women) which may be visible at CT and not at plain radiography, fecal impaction in patients with cystic fibrosis, ingested foreign bodies occurring in mentally disturbed or retarded or elderly patients (Fig. 2), or bezoars which are most frequent in patients who have undergone gastric outlet resection or who have small bowel diverticula [16]. The detection of a small bowel foreign body or bezoars needs to look for an underlying obstructive lesion. Intussusception may be considered as an intraluminal cause of SBO, since it obturates the lumen by pushing a proximal small bowel loop and part of its mesentery into the lumen of a small bowel distal to it, even if various extrinsic or intrinsic processes may result in intussusception. The typical imaging features of enterointestinal intussusception are: a distended loop of bowel (the intussusciens) with a thickened wall; an eccentrically positioned in-

**Fig. 2.** Small bowel obstruction due to foreign body. Axial slice (a) and coronal reformatted (b) show a foreign body that was a peach stone ingested per os responsible for an SBO. Note that this foreign body is not visualized on the abdominal plain film (c). The patient was not treated surgically, and 2 days later the peach stone was in the colon (d)



traluminal intussusception (Fig. 3); and a crescentic area of fat-density mass representing invaginated fat from the mesentery of the intussusceptum. Computed tomography can also demonstrate the cause of the intussusception by showing the leading point and can suggest its nature by its

density: lipoma; cystic mass from a mucocele; or solid mass. In some cases CT may show multiple polypoid tumors, which suggest a diagnosis of metastases, especially from malignant melanoma, or Peutz-Jeghers syndrome; however, as demonstrated in a recent study [17]





**Fig. 3.** Small bowel obstruction due to intussusception. Axial slices show the intussusception (**a, b**) and its cause, which is a lipoma (**c**)

and contrary to the generally accepted idea, half of adult cases of enteroenteric intussusception are idiopathic. Additionally, CT has shown that most of the intussusceptions are transient, non-obstructive, and do not have a lead point.

Intrinsic causes include tumor, inflammatory disease, ischemia, and hematoma. Tumors that are responsible for SBO by infiltration of the bowel wall are mainly adenocar-

cinoma, primary carcinoid, and metastases. Adenocarcinomas present as an annular infiltrating lesion located in the duodenum or in the proximal jejunum. Conversely, bowel metastases (e.g., from melanoma) usually involve the distal small bowel making an annular infiltrative lesion in the distal ileum more likely to be a metastasis, especially in the setting of a known primary malignancy. Primary carcinoids obstruct bowel more by desmoplastic changes than



**Fig. 4.** Small bowel obstruction due to Crohn's disease. Axial slices (**a, b**) and coronal reformatting (**c**) show a thickening of the wall of the distal ileum due to Crohn's disease responsible for a SBO. Note also a sclerolipomatosis characteristic of the disease



**Fig. 5a, b.** Small bowel obstruction due to adhesive band. Oblique axial and coronal reformatting clearly show the transition zone (*arrow*) between the dilated and collapsed bowel

by the tumor itself, which may be difficult to visualize. The SBO consecutive to inflammatory disease is more often due to Crohn's disease and BO may be the first manifestation of the disease [19]. Ultrasound and CT (Fig. 4) show circumferential inflammatory thickening of the bowel wall, fibrofatty changes, and abscess in some cases. Other primary inflammatory causes of SBO include tuberculosis and Behcet's disease, both invading the terminal ileum and ul-

cerative jejunoileitis complicating celiac disease and occurring in the proximal jejunum. Chronic mesenteric ischemia is responsible for a thickening of the bowel wall, which may be responsible for an SBO. Radiation enteropathy is a form of ischemia since radiation-induced small-vessel occlusions may produce chronic ischemia anywhere in the alimentary tract. Computed tomography shows bowel wall thickening with occasional visualization of the target sign.

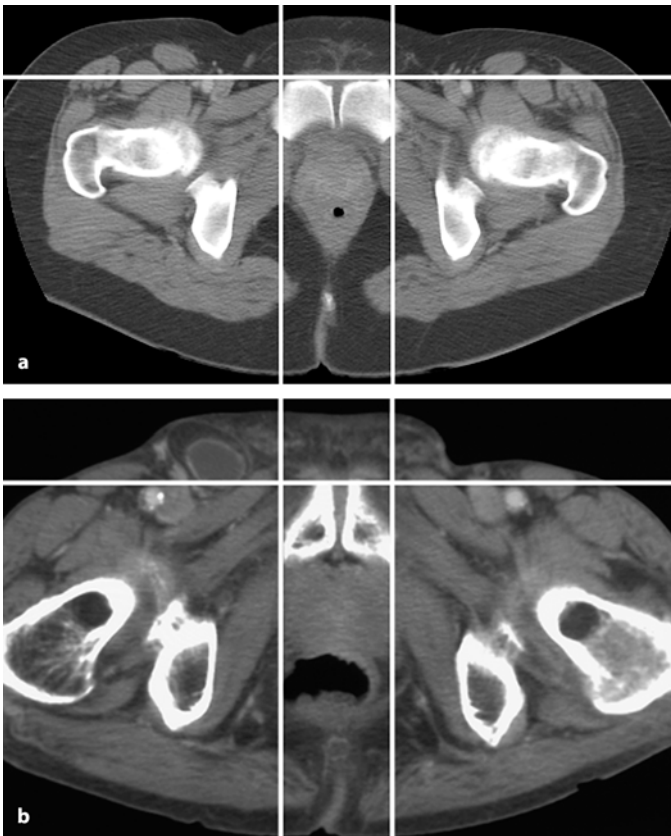


**Fig. 6.** Reference point in groin hernia. Construction of orthogonal lines (a) focused on the pubic tubercles allows to differentiate direct inguinal hernia located ventral to the axial axis and lateral to the sagittal axis, indirect inguinal hernia located ventral to the axial axis and crossing medially the sagittal axis, and the femoral hernia located dorsal to the axial axis and lateral to the sagittal axis. Computed tomography (b) shows direct inguinal hernia

An important clue for diagnosis is that bowel changes are confined to the radiation port. Spontaneous intramural hematoma is most commonly caused by excessive anticoagulation. Other etiologies include coagulopathy, collagen vascular disease, and Henoch-Schönlein purpura. Computed tomography shows thickening of the bowel wall occurring mainly in the duodenum and in the proximal jejunum with a characteristic ring pattern of high attenuation on unenhanced slices.

Extrinsic causes are the most common causes of SBO. Most extrinsic lesions are adhesions, which are the causes of SBO in approximately 60% of cases of hernias. The CT diagnosis of adhesion can be difficult because it is based on negative findings. The diagnosis is evoked from the presence of an abrupt change in bowel caliber without evidence of another cause of obstruction, the adhesive band itself being unidentifiable at CT [4, 5]. Thin slices and multiplanar reformations [20] allow the transition point to be viewed with more confidence and to individualize a beak-like narrowing without any mass at the transition zone (Fig. 5) increasing the confidence for adhesion diagnosis [21]. In patients without a history of surgery, the diagnosis of adhesive band is still possible, since 5% of the adhesive bands are encountered in such patients. Even if it is very rare, small bowel volvulus may occur in patients without adhesions or predisposing abnormalities such as mal-

rotation or hernia, and the differential diagnosis between primary small bowel volvulus and volvulus complicating congenital band is impossible before surgery.

Hernias are the second most common cause of SBO. Approximately 95% of obstruction caused by hernias are external. External hernias, which include inguinal, femoral, umbilical, spigelian, and incisional hernias, consist of a peritoneal sac that protrudes through a weakness or defect in the muscular layers of the abdomen. Diagnosis of external hernias is based on clinical examination, and generally external hernias are treated before occlusive complications; however, in obese patients the clinical diagnosis may be difficult and patient imaging is required. Indirect inguinal hernias are by far the most common cause of hernias. This type of hernia is localized laterally to the inferior epigastric vessels and anteromedially to the spermatic cords and may reach the scrotum. Femoral hernias are far less frequent than inguinal hernias, are encountered in women, and generally reach the superior part of the thigh, at the level of Scarpa's triangle, and when they are small, they may be difficult to distinguish from inguinal hernias. The CT is very helpful in differentiating direct inguinal hernia, indirect inguinal hernia, and femoral hernia by using the pubic tubercle as a reference point (Fig. 6) [22]. Umbilical and subumbilical hernias are the second most common cause of external hernias and are easily diag-



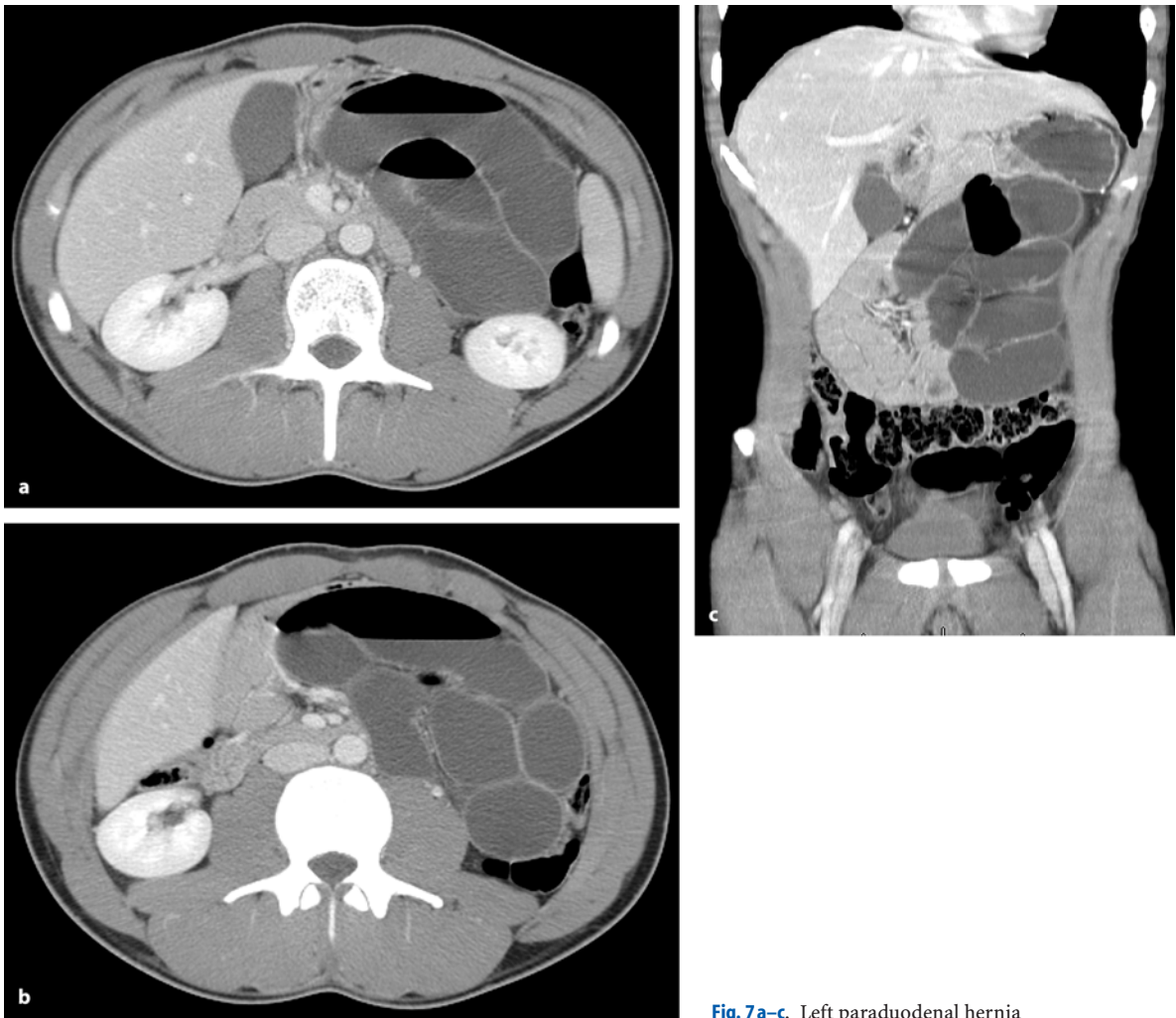


Fig. 7a-c. Left paraduodenal hernia

nosed by CT. Obturator hernias constitute a rarer form of external hernia for which CT has a great contribution to the diagnosis [23].

In comparison with external hernias, internal hernias are uncommon and remain a vexing problem for CT [24]. The most common internal hernias are paraduodenal hernias, which account for approximately 50% of all internal hernias. The small bowel is entrapped between the posterior peritoneum and the mesocolon in a hernia sac (Fig. 7). The CT shows that the anterior wall of the sac contains the inferior mesenteric vein and left colic artery in left paraduodenal hernia and the superior mesenteric vein and the right colic artery in right paraduodenal hernia, and these vessels constitute a landmark above the encapsulated bowel loops [25]. Other internal hernias include transmesenteric hernias which result from prior abdominal surgery with the creation of a Roux-en-Y anastomosis [26],

herniation through the foramen of Winslow, hernia through the transverse mesocolon which occurs after gastric surgery, and pericecal, intersigmoid, supravesical, and pelvic hernias including hernias through the broad ligament [25].

Extrinsic causes of SBO other than adhesions and hernias include a wide variety of neoplastic, inflammatory, and vascular processes. Extrinsic masses obstruct by two main mechanisms: compression of the lumen by the mass and distortion of the lumen by a desmoplastic process. The most common cause of extrinsic masses is carcinomatosis, most often from ovarian carcinoma; however, any peritoneal process, such as carcinoid desmoplastic reaction, tuberculous peritonitis, desmoid tumors, severe radiation changes, or peritoneal endometriosis from the small bowel serosa, may mimic peritoneal metastases.

In patients with occlusion and fever, the cause of occlusion is often an inflammatory process nearby, such as sigmoid diverticulitis or an appendicitis which may cause a paralytic ileus and/or a mechanical obstruction [27].

### Large Bowel Obstruction

The three main causes of large bowel obstruction are carcinoma, volvulus, and diverticulitis.

#### Colon Carcinoma

Colon carcinoma is the cause of the bowel obstruction in about 60% of cases, the sigmoid colon being the most common site of obstructive colon cancer because of its relatively narrow diameter and solid fecal contents. Nearly 20% of colon cancers are complicated by some degree of obstruction. Contrast enema is classically the recommended radiological examination for evaluating patients with suspected obstructing colon carcinoma; however, contrast enema may be non-diagnostic because the patient may not keep the contrast or tolerate insertion of the rectal tube [28]. Additionally, the search of other more proximal tumor is difficult with contrast enema and the evaluation of the viability of the cecum is impossible.

#### Volvulus

Volvulus represents about 10–15% of the causes of large bowel obstruction [29]. Colonic volvulus needs a segment of redundant mobile colon and relatively fixed points around which the volvulus may occur. Consequently, the sigmoid colon (70%), the cecum (25%), and the transverse colon (5%) are the most common sites of volvulus. Other contributing factors include distention of the colon by feces or gas, increased muscular activity, and changes in intra-peritoneal relationship as seen in pregnancy or parturition, previous abdominal surgery resulting in adhesions, congenital abnormalities, such as malrotation, and acquired obstructive lesions in the distal colon. The diagnosis of colon volvulus is often evoked on abdominal plain film. It shows a greatly distended paralyzed loop with fluid–fluid levels, mainly on the left side, extending toward diaphragm on erect film, with a “coffee bean sign” on supine film in sigmoid volvulus and a distended cecum, typically positioned in the left upper quadrant in cecum volvulus; however, in nearly half of the patients with cecal volvulus, the cecum twists in the axial plane, rotating around its long axis and appears in the right lower quadrant.

#### Diverticulitis

Diverticulitis accounts also for about 10% of the causes of large bowel obstruction. As noted by Welch [30], several mechanisms may lead to an obstruction in patients with

diverticulitis: adherence of small bowel loops to inflammatory focus; angulated pelvic colon by adhesions; pericolic fibrosis; and compression by intramural or extramural abscesses.

### Imaging Findings

Computed tomography may diagnose intraluminal, intrinsic, and extrinsic causes of LBO, as follows:

1. Intraluminal causes of colic obstruction are often located at the sigmoid colon, which is the narrowest portion of the colon. The most frequent one is fecal impaction which is a common cause of LBO in elderly and inactive patients. Other intraluminal objects that may cause LBO include gallstones (mostly in elderly women), foreign bodies which occur in mentally ill or disturbed patients, medications, such as antacid containing nonabsorbable aluminium hydroxide antacid gel given to prevent hyperphosphatemia, or bezoars that usually do not affect the colon unless there is a stricture. Intussusception may be considered as an intraluminal cause of LBO, since it occludes the lumen of the colon by pushing an ileal loop or proximal colon and part of its mesentery into the lumen of the colon distal to it, even if various extrinsic or intrinsic processes may result in intussusception [31]. The typical CT features of ileocolic or colocolic intussusception include a distended loop of bowel (the intussusciens) with a thickened wall, an eccentrically positioned intraluminal intussusceptum, and a crescentic area of fat-density mass representing invaginated fat from the mesentery of the intussusceptum. Computed tomography can also demonstrate the cause of intussusception by showing the leading mass suggesting its nature by its density: fat-containing lipoma; cystic mass from a mucocoele; or solid tumor. Conversely to ileo-ileal intussusception [17], colocolic intussusceptions are usually due to a primary bowel cancer.
2. Intrinsic causes include tumor, diverticulitis, inflammatory disease, and ischemic colitis. In colon cancer, CT shows an asymmetric and short thickening of the colon wall or an enhancing soft tissue mass. The dilatation of the colon proximal to the tumor makes easier the identification and the analysis of the tumor. Three-dimensional reconstruction images can demonstrate the transition point between dilated colon and collapsed colon (Fig. 8) [21, 32]. In diverticulitis, the thickening of the bowel wall is symmetric, more moderate, and extended on a longer segment; moreover, pericolic changes are more important with fat stranding, and in some cases phlegmon or intramural or extramural abscesses. In typhlitis, which occur more often in neutropenic patients undergoing chemotherapy for acute leukemia, CT demonstrates cecal distention and circumferential thickening of the cecal wall [33]. Crohn's disease and ulcerative colitis are rarely responsible for LBO. The location of the involved segment and the extent and



**Fig. 8 a, b.** Large bowel obstruction due to colon cancer. Axial slice and coronal reformatting show a tumor of the left corner responsible for a large bowel obstruction. The relationship between the distended transverse colon proximal to the tumor and the tumor is better seen on the axial reformatting

appearance of wall thickening may help distinguish them. In ischemic colitis, CT typically demonstrates circumferential, symmetric wall thickening, with often a double halo or a target sign. Pericolonic fat stranding is present in 60% of patients with ischemic colitis [34]. Ischemic colitis is rarely responsible for bowel obstruction, the ischemia being more often the consequences of an obstruction due to tumor or to fecal impaction [34]. The CT is helpful in distinguishing tumoral from ischemic segments in patients with ischemic colitis proximal to colonic carcinoma. The tumoral segment has an irregular thickening and heterogeneous enhancement by contrast with the ischemic segment more often smoothly thickened and homogeneously enhanced [35]. Radiation colitis is a form of ischemic colitis, with stricture responsible for obstruction more commonly. The sigmoid colon and the rectum are the most frequently affected because radiation therapy is often given for pelvic disease [36].

3. Extrinsic causes include volvulus, hernias adhesions, and compression by diseases from adjacent organs. In sigmoid volvulus, CT shows a whirl pattern of the collapsed colon, twisted mesentery, and enhancing engorged vessels, with a bird beak aspect of the afferent and efferent segments [37]. In cecal volvulus, the findings are the same with the whirl sign composed of spiraled vessels and loops of collapsed cecum distal ileum and with a progressive tapering of efferent and afferent loops ending at the site of torsion. The cecum may be in the right lower quadrant when it twists in the axial plane or in the left upper quadrant when it both twists

and inverts. Three-dimensional imaging could be interesting by allowing to select the optimal plane for viewing the volvulus and to locate the precise source of torsion [38]. The LBO attributable to hernias or to adhesions are much less common than SBO because of the relatively fixed nature of the colon and its larger caliber. Extrinsic compression may come from endometriosis which involves the rectum and the distal sigmoid colon with a colic thickening which may evoke a colon cancer on CT, from actinomycosis which must be considered in a woman with prolonged use of an intrauterine device [39], from pancreatitis, or more often from involvement due to extracolonic neoplasm either directly or by serosal metastasis. The rectum or the sigmoid are obstructed by direct invasion with gynecological and prostatic neoplasms, as well as by drop metastases to the pouch of Douglas. Pelvic lipomatosis, benign pelvic masses, retroperitoneal fibrosis, and pregnancy are causes of compression of the colon which rarely lead to LBO.

## 5.2.5 Diagnosis of Complications

### 5.2.5.1 Clinical Considerations

Strangulation occurs in about 10% of SBO. It represents the main factor of morbidity and mortality, with a mortality above 10%. It is characterized by an impaired vascular circulation to the obstructed intestine. Balthazar [6] has very

clearly summarized the mechanisms which lead to a strangulation:

1. The first event is a closed-loop or incarcerated intestinal obstruction due to adhesions or hernias, in which a loop of bowel is occluded at two adjacent points along its course. There is a mechanical obstruction proximal to the involved bowel segment. The length of the closed loop is variable from a single to several loops of bowel. If the length of the closed loop is sufficient, the loop may twist and produce a volvulus. If the length of the closed loop is short (e.g., in some external hernias), the bowel proximal to the obstacle may twist. Volvulus is a common but not invariable complication of incarcerated loop. It tends to occur in patients with high degrees of obstruction, but once developed, it further aggravates the mechanical obstructive process and contributes to the development of mesenteric ischemia.
2. The second event is strangulation, which is defined as a closed-loop obstruction associated with intestinal ischemia. The severity and duration of the intestinal and mesenteric obstructive process determines the severity of the ischemia. Initially, the venous return of blood from the involved bowel segment is compromised, with congestive changes affecting the bowel wall and the mesentery, while the influx of arterial blood continues. Ischemia may resolve with an emergent surgical treatment of the cause. Then arterial insufficiency follows, aggravating the anoxia and further contributing to the rapid development of gangrene and perforation.

The clinical diagnosis of strangulation is difficult. Intestinal strangulation is suspected when the intermittent crampy pain becomes continuous and increases in severity, and in patients with tachycardia, fever, peritoneal irritation, and leukocytosis; however, these findings cannot reliably differentiate simple from strangulated obstruction, which means that before the development of CT, strangulation was not diagnosed preoperatively in about 75% of patients with surgically proved strangulation.

In LBO ischemia may be due to volvulus of the cecum or of the sigmoid with the same mechanism as in small bowel strangulation or may occur proximal to the obstruction.

### Imaging Findings

In strangulating SBO, the CT findings can be divided into two categories: findings indicative of closed-loop obstruction; and findings indicative of strangulation.

### Closed-Loop Obstruction

In closed-loop obstruction CT shows [40, 42] findings of incarcerated small bowel with radial distribution and stretched mesenteric vessels converging toward torsion and a U- or C-shaped dilated bowel loop and at the site of torsion, the presence of two adjacent collapsed, round, oval, or triangular loops, the beak sign appearing as a fusiform tapering when the bowel is imaged in longitudinal section, and a whirl sign, meaning a twist of the mesentery.

### Strangulation

Computed tomography shows [40, 43] bowel wall abnormalities with circumferential thickening, increased attenuation, target or halo sign, or, on the contrary, lack of enhancement of the wall of the incarcerated bowel after intravenous administration of contrast (Fig. 9), which is the most specific finding of strangulation or bowel wall thinning that corresponds to late mucosal desquamation [43], and mesentery abnormalities (Fig. 9) with congestion, blurring, haziness, or obliteration of the mesenteric vessels and fluid or hemorrhage in the mesentery or in the mesosigmoid in sigmoid volvulus.

In LBO due to cancer, one must look for CT findings of ischemia in the colon proximal to the tumor. Pneumatosis affecting the colon wall is a classical finding of infarct in the setting of a LBO; however, we have shown that it does not always indicate transmural infarction, and that cecal pneumatosis, when in a bubble-like pattern in opposition to curvilinear pattern, and when not associated with other ischemia findings, may be related to viable bowel [44]. In the same way, colon wall thickening proximal to BO due to colon cancer is common and may represent a reversible, pre-ischemic CT finding [45]. On the other hand, dilatation of the cecum, proximal to an obstructing colic cancer superior to 12 cm, is a risk factor for a diastatic perforation. The perforation may come from the distended cecum above the tumor or may be located in the tumor itself. In this last case, free pneumoperitoneum is rare, and more commonly, small air bubbles with fluid and mesenteric stranding are detected in the pericolic fat.

In colic volvulus, CT findings of ischemia are sought on both the colic wall and the mesocolon. Bowel wall abnormalities include circumferential thickening, increased attenuation, target or halo sign or, on the contrary, lack of enhancement of the wall of the incarcerated bowel after intra-venous administration of contrast. Mesocolic abnormalities include congestion, blurring, haziness, or obliteration of the mesocolic vessels, and fluid or hemorrhage in the mesocolon. This may be crucial for the therapeutic choice between sigmoidoscopic decompression with insertion of a rectal tube in patients without findings of infarct



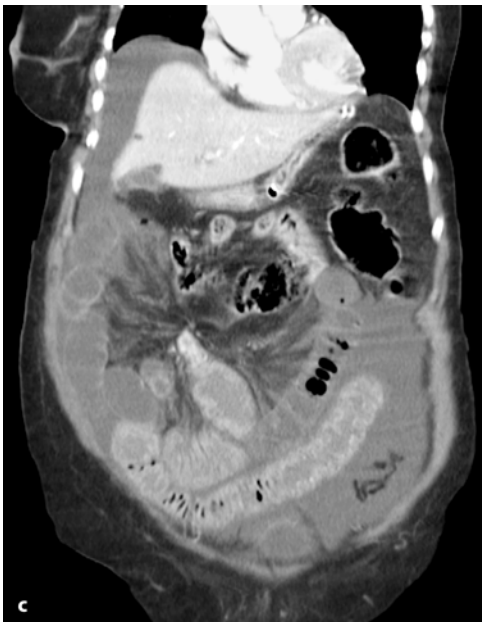
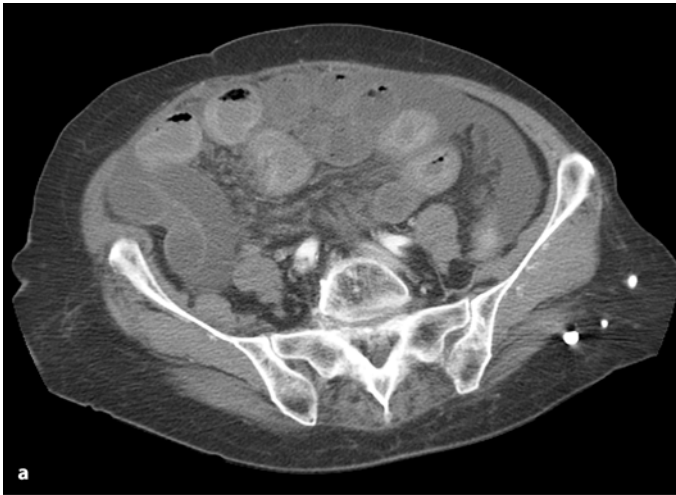


**Fig. 9 a–d.** Strangulating SBO. The wall of the strangulated small bowel loops have a decreased (a) and delayed (b) enhancement. Note also the congestion of the mesentery well shown on coronal reformatting (c, d)

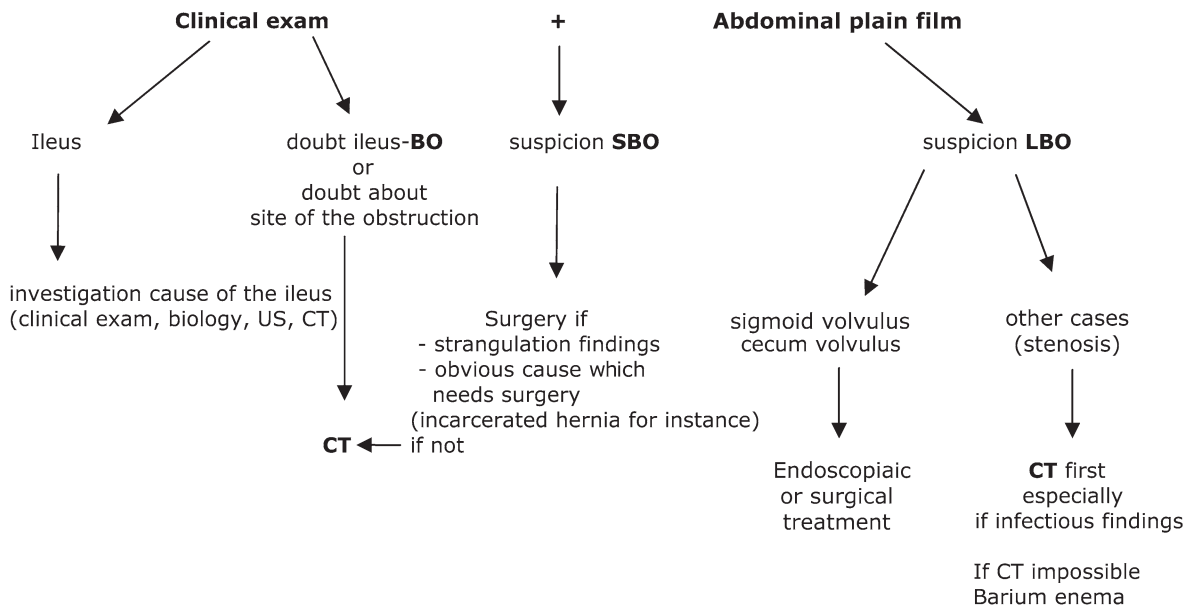


**Fig. 10.** Diagnosis strategy in patients with suspected bowel obstruction (BO). LBO large bowel obstruction, SBO small bowel obstruction

or perforation, and emergent sigmoid resection for other patients; however, the value and the impact of CT to differentiate sigmoid volvulus with or without infarct has not been evaluated to date.

## 5.2.6 Impact and Diagnostic Strategy

### 5.2.6.1 Impact of Imaging on Management

Traditionally, the diagnosis of bowel obstruction has been performed by clinical exam and abdominal plain film, the key point being to differentiate mechanical obstruction from ileus. Bowel obstruction was treated by surgery performed in emergency, whereas ileus was medically managed; however, in patients with bowel obstruction, the management should depend on the site and the cause of the obstacle, and of the viability of the bowel. The following rules are generally applied for management:

1. An SBO with strangulation needs emergency surgery.
2. A bowel obstruction due to a small bowel tumor needs a resection of the tumor with bowel anastomosis in the same operative time.
3. A bowel obstruction due to adhesion without strangulation may be initially medically managed, in an attempt to avoid a surgical procedure, itself at the origin of adhesions.
4. An SBO due to radiation enteritis, hematoma, or peritoneal carcinomatosis is managed medically.

5. A sigmoid volvulus is initially treated by endoscopic detorsion, unless it is complicated with peritonitis which requires surgery.
6. An obstruction due to colic cancer ideally is first medically managed in order to prepare the colon for a surgery with resection of the tumor and colic anastomosis.

These rules underline how important it is to diagnose the mechanism as well as the site and cause of an obstruction. Computed tomography is the most accurate modality for these different diagnostic steps; consequently, it has a significant impact on the management of patients with bowel obstruction [8, 15], especially when the clinical diagnosis is difficult and the abdominal plain film is not helpful. It is the case more particularly in post-operative patients, in obstruction with fever, and in obstruction in patients with a history of surgery for abdominal cancer.

### Post-operative Obstruction

Post-operative obstruction occurs after abdominal surgery, and three mechanisms must be individualized to explain the clinical findings in the patients: a paralytic ileus due to hydroelectric changes or to intra-abdominal abscess; a mechanical obstruction by an extrinsic compression by an abscess; or a mechanical obstruction due to adhesion or post-operative internal hernia.

### Obstruction with Fever

Obstruction with fever could be a clinical finding of strangulation; if not, it may evoke two main diagnoses: appendicitis in young patient and diverticulitis in older patient. Other diagnoses include pelvic inflammatory disease and Meckel's diverticulitis.

### Obstruction in Patients Past Surgery

Obstruction in patients with past surgery for abdominal cancer is a relatively common situation [46] for which CT has a strong impact to differentiate local recurrence, peritoneal carcinomatosis, radiation enteritis, parastomal hernia, or post-operative adhesions which constitute the most common cause of obstruction, even in this context.

#### 5.2.6.2 Diagnostic Strategy

In patients with suspected intestinal obstruction, the first diagnostic triage is based on clinical, laboratory, and abdominal plain-film findings, which allow schematic individualization of four situations (Table 1):

1. There is a strong suspicion of paralytic ileus. The cause of this ileus must be investigated by the clinical and laboratory exams, and in some cases by ultrasound and CT.
2. There is a strong suspicion of SBO: If there are findings of strangulation or if the cause of the SBO is obvious and needs emergency surgical management, surgery must be performed without other investigation. In other patients with acute symptoms, CT must look for the mechanism and the cause of the occlusion. If a small bowel obstruction due to adhesion is diagnosed, CT is not always precise enough to identify patients who need surgery and patients who need a medical management with certainty; however, the presence of some bowel signs at CT, especially the presence of reduced wall enhancement, would be helpful for surgical decision-making. Furthermore, the use of clinical criteria when CT findings are equivocal may overcome the inherent limitations of CT for diagnosing strangulated small bowel obstruction [47]. In patients with non-acute symptoms (suspicion of low-grade obstruction), enteroclysis is a good alternative to CT and should be performed first.
3. There is a strong suspicion of LBO. If the abdominal plain film shows signs of volvulus, more common on the sigmoid colon than on the cecum, a treatment of the volvulus must be performed (colonoscopic or surgical detorsion in sigmoid volvulus, surgery in cecal volvulus). Even if promising, the value of CT for therapeutic choice in sigmoid volvulus remains to be evaluated. If there is no finding of volvulus, a stenosis is presumed to be the cause of the LBO. Computed tomography must be

performed to look for the cause of the stenosis if there are inflammatory findings, but also in the absence of inflammatory findings since CT is preferred to contrast enema to search for a colic tumor responsible for the obstruction. Reformating is helpful in localizing the tumor on the colon and particularly in sigmoid tumor to localize the tumor on the sigmoid loop, which is very important for the surgical procedure.

4. There are some doubts between an obstruction and an ileus or some doubts about the localization of the obstruction. Computed tomography should be performed to investigate the nature, site, and cause of the obstruction, and to look for signs of strangulation.

These guidelines give an important role to CT in the management of patients with suspected bowel obstruction. This role, considered in studies published 15 years ago, has been justified by recent developments in technique and interpretation of CT including contiguous 1-mm slices which allows multiplanar reformating adequate injection permitting an accurate evaluation of bowel wall enhancement, and interpretation using picture archiving and communication system (PACS) with stack mode evaluation that permits a faster identification of the transition zone than tile mode evaluation [48].

## References

1. Mondor H, Porcher P, Olivier C (1943) Radiodiagnosics urgents. Abdomen. Masson, Paris, p 340
2. Herlinger H, Maglante DDT. Small-bowel obstruction. In: Herlinger H, Maglante DDT (eds) Clinical radiology of the small intestine. Saunders, Philadelphia, 1989, pp 479–507
3. Harlow CL, Stears RL, Zeligman BE, Archer PG. Diagnosis of bowel obstruction on plain abdominal radiographs: significance of air–fluid levels at different heights in the same loop of bowel. *Am J Roentgenol* 1993; 161:291–295
4. Megibow AJ, Balthazar EJ, Cho KC, Medwid SW, Birnbaum BA, Noz ME. Bowel obstruction: evaluation with CT. *Radiology* 1991; 180:313–318
5. Fukuya T, Hawes DR, Lu CC, Chang PJ, Barloon TJ. CT diagnosis of small bowel obstruction: efficacy in 60 patients. *Am J Roentgenol* 1992; 158:765–769
6. Balthazar EJ, George W. Holmes lecture. CT of small bowel obstruction. *Am J Roentgenol* 1994; 162:255–261
7. Lazarus DE, Slywotsky C, Bennett GL, Megibow AJ, Macari M. Frequency and relevance of the “small bowel feces” sign on CT in patients with small-bowel obstruction. *AJR* 2004; 183:1361–1366.
8. Donckier V, Closset J, Van Gansbeke D, Zalzman M, Sy M, Houben JJ, Lambilliotte JP. Contribution of computed tomography to decision making in the management of adhesive small bowel obstruction. *Br J Surg* 1998; 85:1071–1074
9. Mucha P. Small intestinal obstruction. *Surg Clin North Am* 1987; 67:597–620
10. Tang E, Davis J, Silberman H. Bowel obstruction in cancer patients. *Arch Surg* 1995; 130:832–837

11. Osteen RI, Guyton S, Steele G Jr, Wilson RE. Malignant intestinal obstruction. *Surgery* 1980; 1987:611–615
12. Walsh HPJ, Schofield PF. Is laparotomy for small bowel obstruction justified in patients with previously treated malignancy? *Br J Surg* 1984; 71:933–935
13. Hentel KD, Gollub MJ. Contrast enema before bypass surgery for small-bowel obstruction in the oncologic patient: Is it necessary? *AJR* 2003; 181:1361–1364
14. Herlinger H, Rubesin E. Obstruction. In: Gore RM, Levine MS, Laufer I (eds) *Textbook of gastrointestinal radiology*. Saunders, Philadelphia, 1994, pp 931–966
15. Taourel P, Fabre N, Pradel J, Seneterre EJ, Megibow AL, Bruel JM. Value of CT in the diagnosis and management of patients with suspected acute small bowel obstruction. *Am J Roentgenol* 1995; 165:1187–1192
16. Lo CY, Lau PWK. Small bowel phytobezoars: an uncommon cause of small bowel obstruction. *Aust N Z J Surg* 1994; 64: 187–189
17. Warshauer OM, Lee JK. Adult intussusception detected at CT or MR imaging: clinical-imaging correlation. *Radiology* 1999; 212:853–860
18. Sandrasegaran K, Kopecky KK, Rajesh A, Lappas J. Proximal small bowel intussusceptions in adults: CT appearance and clinical significance. *Abdom Imaging* 2004; 29:653–657
19. Zissin R, Hertz M, Paran H, Bernheim J, Shapiro-Feinberg M, Gayer G. Small bowel obstruction secondary to Crohn disease: CT findings. *Abdom Imaging* 2004; 29:320–325
20. Caoili EM, Paulson EK. CT of small bowel obstructions: another perspective using multiplanar reformations. *Am J Roentgenol* 2000; 174:993–998
21. Aouf S, Charra L, Lesnik A, Bruel JM, Taourel P. Multidetector CT of bowel obstruction: value of post-processing. *Eur Radiol* 2005; 15:2323–2329
22. Delabrousse E, Michalakis D, Sarliève P, Paratte B, Rodière E, Kastler B. Valeur de l'épine du pubis comme repère TDM des hernies. *J Radiol* 2005; 86:651–654
23. Yokoyama Y, Yamaguchi A, Isogai M, Hori A, Kaneoka Y. Thirty-six cases of obturator hernia: Does computed tomography contribute to postoperative outcome? *World J Surg* 1999; 23: 214–216
24. Zarvan NP, Lee FT, Yandow DR, Unger JS. Abdominal hernias: CT findings. *Am J Roentgenol* 1995; 164:1391–1395
25. Takeyama N, Gokan T, Ohgiya Y et al. CT of internal hernias. *Radiographics* 2005; 25:997–1015
26. Blachar A, Federle MP. Bowel obstruction following liver transplantation: clinical and CT findings in 48 cases with emphasis on internal hernia. *Radiology* 2001; 218:384–388
27. Kim AY, Bennett GL, Bashist B, Perlman B, Megibow AJ. Small bowel obstruction associated with sigmoid diverticulitis: CT evaluation in 16 patients. *Am J Roentgenol* 1998; 170:1311–1313
28. Frager D, Rovno HDS, Baer JW, Bashist B, Friedman M. Prospective evaluation of colonic obstruction with computed tomography. *Abdom Imaging* 1998; 23:141–146
29. Gore RM, Eisenberg RL. Large bowel obstruction. In: Gore RM, Levine MS, Laufer I, (eds) (2000) *Textbook of gastrointestinal radiology*. Saunders, Philadelphia, pp 1247–1260
30. Welch JP. Diverticular disease. In: Welch JP (ed) *Bowel obstruction*. Saunders, Philadelphia, 1990, pp 589–599
31. Orlando R III. Intussusception in adults. In: Welch JP (ed) *Bowel obstruction*. Saunders, Philadelphia, 1990, pp 229–240
32. Horton KM, Abrams RA, Fisherman EK. Spiral CT of colon cancer: imaging features and role in management. *Radiographics* 2000; 20:419–430
33. Horton KM, Corl FM, Fisherman EK. CT evaluation of the colon: inflammatory disease. *Radiographics* 2000; 20:399–418
34. Balthazar EJ, Yen BC, Gordon RB. Ischemic colitis: CT evaluation of 54 cases. *Radiology* 1999; 211:381–388
35. Ko GY, Ha HK, Lee HJ et al. Usefulness of CT in patients with ischemic colitis proximal to colonic cancer. *Am J Roentgenol* 1997; 168:951–956
36. Philpotts LE, Heiken JP, Westcott MA, Gore RM. Colitis: use of CT findings in differential diagnosis. *Radiology* 1994; 190: 445–449
37. Catalano O. Computed tomographic appearance of sigmoid volvulus. *Abdom Imaging* 1996; 21:314–317
38. Moore CJ, Corl FM, Fishman EK. CT of cecal volvulus: unraveling the image. *AJR* 2001; 177:95–98
39. Yeguez JF, Martinez SA, Sands LR, Hellinger MD. Pelvic actinomycosis presenting as malignant large bowel obstruction: a case report and a review of the literature. *Am Surg* 2000; 66:85–90
40. Balthazar EJ, Birnbaum BA, Megibow AJ, Gordon RB, Whelan CA, Hulnick DH (1992) Closed-loop and strangulating intestinal obstruction: CT signs. *Radiology* 185:769–775
41. Ha HK, Kim JS, Lee MS et al. Differentiation of simple strangulated small bowel obstructions: usefulness of known CT criteria. *Radiology* 1997; 204:507–512
42. Balthazar EJ, Liebeskind ME, Macari M. Intestinal ischemia in patients in whom small bowel obstructions is suspected: evaluation of accuracy, limitations, and clinical implications of CT in diagnosis. *Radiology* 1997; 205:519–522
43. Catel L, Lefèvre F, Lauren V et al. Occlusion du grêle sur bride: quels critères scanographiques de gravité rechercher? *J Radiol* 2003; 84:27–31
44. Taourel P, Garibaldi F, Arrigoni J, Le Guen V, Lesnik A, Bruel JM. Cecal pneumatosis in patients with obstructive colon cancer: correlation of CT findings with bowel viability. *Am J Roentgenol* 2004; 183:1667–1671
45. Xiong Lin, Chintapalli KN, Dodd GD et al. Frequency and CT patterns of bowel wall thickening proximal to cancer of the colon. *AJR* 2004; 182:905–909
46. Ha HK, Shin BS, Lee SI et al. Usefulness of CT in patients with intestinal obstruction who have undergone abdominal surgery for malignancy. *Am J Roentgenol* 1998; 171:1587–1593
47. Kim JH, Ha HK, Kim JK et al. Usefulness of known computed tomography and clinical criteria for diagnosing strangulation in small-bowel obstruction: analysis of true and false interpretation groups in computed tomography. *World J Surg* 2004; 28:63–68
48. YJ Kim, JK Han, SH Kim et al. Small-bowel obstruction in a phantom model of ex vivo porcine intestine: comparison of PACS stack and tile modes for CT interpretation. *Radiology* 2005; 236:867–871





# Imaging and Intervention in Gastrointestinal Hemorrhage and Ischemia

J.I. Bilbao Jaureguizar, I. Vivas Pérez,  
D. Cano Rafart, A. Martínez de la Cuesta

## 5.3

### Contents

5.3.1	Introduction	453
5.3.1.1	Vascular Anatomy	453
5.3.2	Gastrointestinal Hemorrhage	454
5.3.2.1	Etiology	454
5.3.2.2	Clinical Findings	454
5.3.2.3	Diagnosis	454
5.3.2.4	Endovascular Treatment	457
5.3.3	Intestinal Ischemia	461
5.3.3.1	Acute Ischemia	461
5.3.3.2	Chronic Ischemia	464
5.3.3.3	Endovascular Treatment of Intestinal Ischemia	465
	References	467

### 5.3.1 Introduction

Acute gastrointestinal (GI) bleeding is a frequent cause of hospitalization of patients that commonly present melena, hematemesis, or hematochezia. The source of most bleedings can usually be identified through an initial work-up including barium studies and endoscopy; however, 5% of all patients with intestinal bleeding have obscure bleeding in which no definitive source has been identified though routine diagnostic examinations [1]. Detection and localization of the source of acute intraabdominal hemorrhage is one of the major challenges in the early diagnostic work-up of acute intraperitoneal bleeding. It is very helpful in providing prompt hemostasis accomplished by means of transarterial embolization or surgery.

Helical computed tomography (CT) has been shown to be an effective method for detecting a wide variety of causes of obscure GI bleeding [2, 3]. Advantages over routine diagnostic exams include its ability to localize lesions, identify vascular abnormalities, and evaluate adjacent anatomical structures that may be related to the bleeding.

Bowel ischemia (BI) is not an uncommon disorder representing an increasing threatening abdominal condition as the overall population ages. Bowel and mesenteric ischemia occurs in a variety of conditions that carries out a

reduction or an absence of blood supply [4, 5]. This may be acute or chronic depending on the onset and clinical presentation and may involve the small or large bowel, may be partial mural or transmural, and may be segmental or diffuse. Bowel ischemia is a challenging abdominal disease because of its wide range of clinical and pathological manifestations and its high mortality rate, which has remained high over the past 30 years despite technical and medical advances (50–90%) [6]. If suspected, early diagnosis and treatment is crucial because partial mural ischemia may progress to fatal infarction. Clinical onset and plain radiographic findings are nonspecific mainly in early stages of the disease. With recent technical advances improving its sensitivity CT has become the procedure of choice when mesenteric ischemia is suspected because of its capacity to show vascular occlusions, bowel changes, or other related abdominal signs [7]. Multidetector row CT are faster and allow thinner collimation than traditional spiral CT in imaging the entire mesenteric vessels, which is crucial in patients with suspected mesenteric ischemia [8]. In the same way CT and magnetic resonance (MR) may also be helpful in determining other primary causes of BI.

Other imaging techniques, such as ultrasound (US) and barium studies (BS), are less sensitive. The MR is an emerging diagnostic tool and in some studies is as reliable as CT for demonstrating bowel wall changes and vascular anomalies.

#### 5.3.1.1 Vascular Anatomy

The arterial blood supply of the bowel loops is provided by three main arteries: the celiac trunk; the superior mesenteric artery; and the inferior mesenteric artery. Venous drainage is performed mainly by the superior and inferior mesenteric veins [9].

Gastrointestinal tract vascular flow from distal esophagus to the third portion of duodenum depends on the celiac trunk. The first branch of the common hepatic artery (gastroduodenal artery) represents an anastomosis between the superior mesenteric artery and the celiac trunk [6].

The superior mesenteric artery (SMA) arises from the abdominal aorta at the level of the L1 vertebral body, <1.5 cm below the celiac origin, and is just superior to the origin of the renal arteries. The SMA provides blood supply to the distal part of duodenum, the rest of small bowel loops, and the ascending and transverse large bowel to the splenic flexure. Main branches of the SMA are jejunal arteries, ileocolic artery, right colic artery (although absent in 80% of population it aids the ileocolic and middle colic in supplying blood to the ascending colon) and middle colic artery. Other branches include an artery for the right angle of colon and one for the transverse colon. The marginal arteries of Dwight and Drummond supply the vasa recta to the small intestine and colon and provide a channel of potential collateral blood supply to the entire gut. The vasa recta arise from the marginal artery and supply the bowel wall. The arc of Riolan is an inconstant artery parallel to a portion of the middle colic artery. Aberrant branches from the SMA are relatively common (common hepatic artery, right hepatic artery, splenic artery) [10-13].

The inferior mesenteric artery (IMA) arises from the aorta 7 cm below the origin of SMA at the level of L3. IMA supplies the splenic flexure, the descending colon, sigma and rectum. There are several anastomosis to lumbar, sacral and internal iliac arteries. Main branches are left colic artery (absent in 12% or may arise from the SMA), the colosigmoid artery, sigmoid branches and the superior rectal arteries. The branches of these arteries form several arcades to supply the muscularis propria, submucosa and mucosa.

The superior mesenteric vein (SMV) is a single trunk and receives several veins including the ileocolic, gastrocolic, right colic, and middle colic veins. The SMV lies at the right side of the SMA. In patients with complete malrotation of the gut this relationship is reversed [10, 12, 13].

The inferior mesenteric vein (IMV) receives blood flow from superior hemorrhoidal vein, sigmoid vein, and left colic vein. It may end at the splenic vein, at the splenoportal angle, or in the SMV [14].

## 5.3.2 Gastrointestinal Hemorrhage

### 5.3.2.1 Etiology

Intraabdominal hemorrhage may result from known conditions, such as bleeding diathesis or blunt abdominal trauma, or may be idiopathic. The latter condition may result from several incidentally discovered etiologies, including rupture of a vascular neoplasm, perforation of a duodenal ulcer, or other gastrointestinal pathologies; and inflammatory erosive processes, such as pancreatitis with subsequent pseudocyst or pseudoaneurysm formation.

Regarding lower GI bleeding, approximately 70% of cases are due to diverticular disease, neoplasms, and benign anorectal diseases that have a focal bleeding site.

### 5.3.2.2 Clinical Findings

The clinical presentation of spontaneous abdominal hemorrhage, although variable, frequently consists of sudden abdominal pain and distension associated with an acute drop in hematocrit. Uncommon signs include hypovolemic shock and discoloration around the umbilicus and flanks [15]. Signs and symptoms of abdominal hemorrhage may be equivocal, and hematocrit levels obtained during acute phase may not reflect its diagnosis [16]. In addition, clinical signs obtained during physical examination also may be independent from the severity and initiation of the intraabdominal hemorrhage, which is the reason why imaging plays a pivotal role in the diagnosis and assessment of this potentially lethal entity.

### 5.3.2.3 Diagnosis

Digestive endoscopy is highly effective and provides many solutions in the management of GI hemorrhage; however, it is necessary to point out that its efficacy depends on the experience of the operator and on good intestinal preparation. It should also be remembered that this technique is not useful in a large number of patients with hemorrhages whose origin is in the small bowel. For this reason, several angiodysplastic lesions and inflammatory or tumoral pathologies of this area of the intestine cannot be detected by endoscopy.

### Nuclear Medicine

Although these are not equally well accepted in all the clinical management protocols, gammagraphic techniques constitute the next step after endoscopy for diagnosing digestive hemorrhage. They make it possible to detect bleeding with debits as low as 0.2 ml/min, and they are useful in locating the abdominal region in which the bleeding originates; however, they are not able to determine either the cause of the hemorrhage or the exact anatomical location.

### Computed Tomography

Among the radiological techniques, CT and angiography are the most frequently used techniques for the study of patients with digestive hemorrhage. In 1989 Sivit et al. [17] were the first researchers to describe the CT appearance of active intraabdominal arterial extravasation in a patient with splenic rupture caused by blunt trauma. In 1991 Jeffrey et al. described 18 patients with active intraabdominal arterial hemorrhage diagnosed using dynamic contrast-enhanced CT [18].

Yamaguchi and Yoshikawa [19] believed that enhanced CT had the potential to show active GI bleeding getting

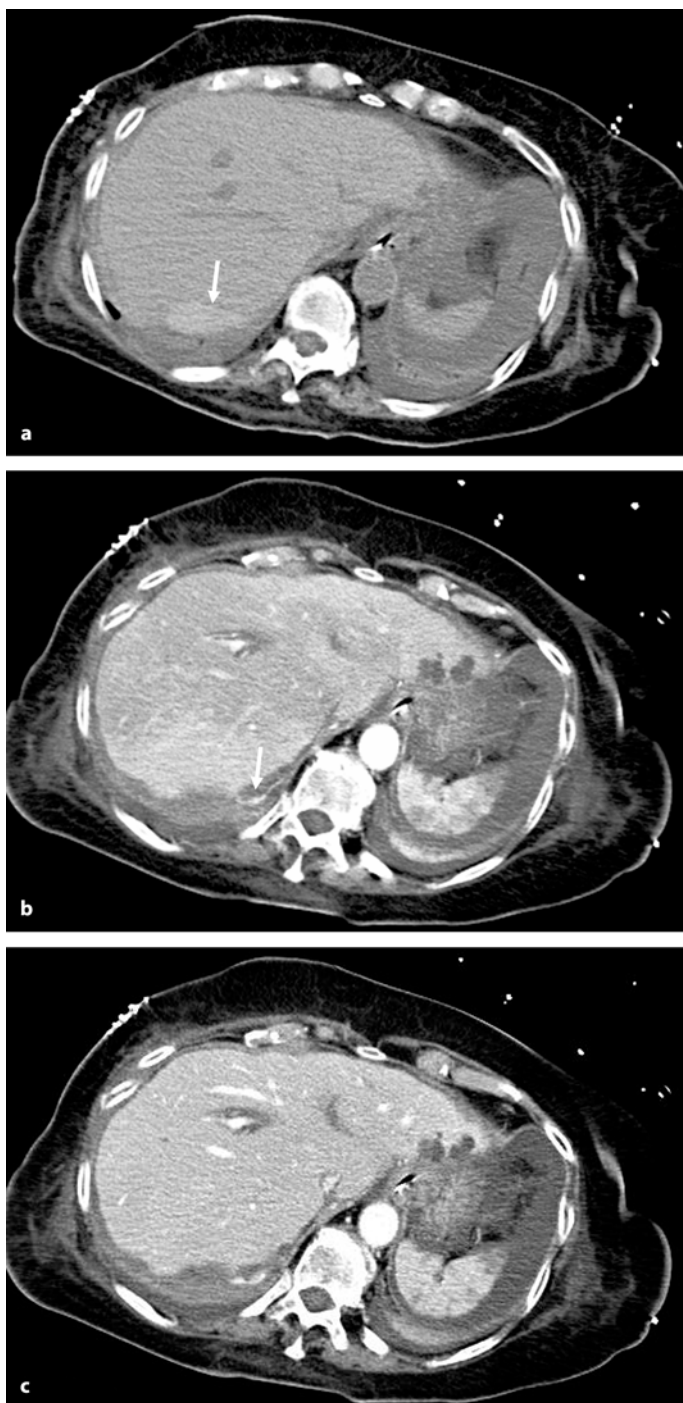


**Fig. 1.** A 74-year-old woman with hypotension after pancreatic, duodenal, renal, and adrenal resection due to malignant retroperitoneal fibrous histiocytoma. **a** Transversal section of unenhanced multidetector CT scan shows a perihepatic hematoma (arrow). **b** A clear jet of extravasated contrast material from a branch of the right phrenic artery, indicating active hemorrhage, is clearly depicted (arrow). **c, d** In addition, accumulation of extravasated contrast material is seen. **e** After the catheterization of the right phrenic artery two leaking points of contrast media were found. The bleeding point was successfully embolized with spherical particles (300–500  $\mu\text{m}$ ). (Although this interesting case is not a GI bleeding, it has been selected because the accurate information of the MDCT allowed a quick identification and embolization of the bleeding point in a hemodynamically unstable patient. The clinical results and the follow-up was good without any bleeding relapse.)

positive rates for GI bleeding on CT reached 80% [20]. Enhanced helical CT might provide information about the bleeding site [18, 21, 22] and indicates a specific diagnosis, but it is only a diagnostic tool and never therapeutic. When pooling of contrast material is found in the lower GI tract, the next strategy should be adopted immediately. For example, if the bleeding site is the rectum, proctoscopy or

colonoscopy is chosen, followed by angiography, if found necessary. Conversely, if the bleeding site is in the right colon or small intestine, angiography is the first choice because colonoscopy has difficulties in reaching the bleeding portion. Then, when enhanced CT promptly provides a map of the bleeding site, an appropriate treatment method can quickly be selected (Fig. 1) [23].



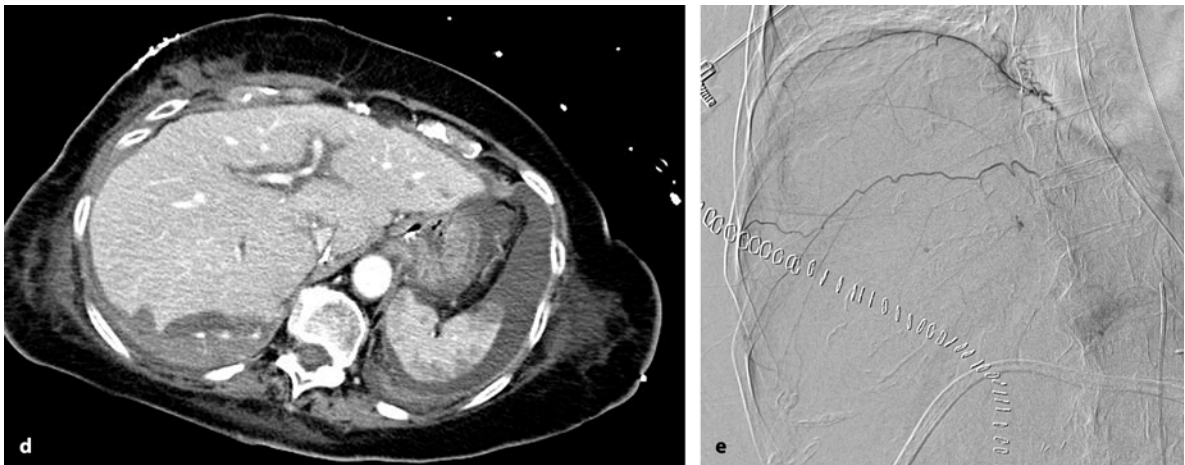


Fig. 1. (continued)

Computed tomography can provide indirect signs of bleeding, such as the hematoma, in the wall of the digestive tube, or the presence of localized or diffuse hematic collections. It can also pick up direct signs such as a jet of contrast (“active extravasation”) exiting from the bleeding vessel. Active extravasation has been defined as CT evidence of a contrast material collection with attenuation similar to that of the aorta or major adjacent arteries and greater than that of a surrounding parenchymal organ [24].

Recently, with the advent of multidetector-row CT (MDCT) scanners, CT is undergoing further improvement, especially for the evaluation of vascular disease, and subsequently in the evaluation of hemorrhagic complications leading to intraabdominal bleeding.

Direct detection of the bleeding point depends on the technique used for exploration. When using MDCT and high-flow intravenous contrast injection, it is possible to identify the bleeding point directly in 20% of cases.

The administration of an oral contrast agent [24] is not considered to be useful in patients presenting at the emergency department with suspicion of active hemorrhage. The extravasated contrast agent in a patient with active hemorrhage may not be detected when a high concentration of oral contrast material is present within the intestine. In addition, oral application of contrast material, even via a gastric tube, is another time-consuming procedure, usually impractical in the acute clinical setting of these patients, and may interfere with another radiological techniques such as angiography.

Combined with the use of IV-administered contrast material, the faster scanning speed of MDCT and its ability to use a narrow collimation increases opacification of contrast material in the mesenteric, retroperitoneal, and portal vasculatures [25, 26]. The superior spatial resolution provided by MDCT enables a more detailed assessment of the parenchymal organs and abdominal vasculature and improves the ability to identify and evaluate abdominal vessels on both

axial source images and multiplanar reformations [27, 28]. Computed tomography also makes it possible to identify the lesion responsible (i.e., tumor) and obtain information about its morphology, the degree of affection of the intestinal wall, and possible distant repercussions [29].

#### Ultrasound

Although US is insensitive in detecting injury in solid organs, in some patients it has demonstrated a relatively high sensitivity in detecting free fluid within the lower abdomen. The sonographic appearance of acute intraperitoneal hemorrhage usually is that of hypoechoic fluid. There may be mixed echoes in this hypoechoic fluid, isolated echogenic clots, or fluid–fluid interfaces [30]. As clot formations occurs, the US appearance may vary, although the clot is usually hypoechoic compared with solid organs.

#### Magnetic Resonance Imaging

Magnetic resonance imaging also can be used to demonstrate intraperitoneal hemorrhage. A hematoma less than 48 h old may have nonspecific signal intensity features [31]. Intraabdominal hematoma older than 3 weeks typically has a specific appearance referred to as the concentric ring sign, in which a thin peripheral rim, dark on all sequences, surrounds a bright inner ring, most distinctive on T1-weighted images. The MR imaging can readily distinguish blood from ascites. Acute blood, in the form of deoxyhemoglobin, is low in signal intensity on T2-weighted images. On the other hand, subacute blood, in the form of extracellular methemoglobin, has high signal intensity on T1- and T2-weighted images. The use of fat-suppression techniques accentuates this finding. In a chronic stage, a low signal intensity rim develops around the hematoma on both T1- and T2-weighted sequences. This rim corresponds to hemosiderin or fibrosis.

## Angiography

Conventional angiography performed through direct intravascular catheterization is still for many specialists the gold-standard technique in the radiological diagnosis of digestive hemorrhage; however, it is an aggressive technique, which requires training, and the results of which are influenced by some factors including those caused by the patient movements or intestinal peristalsis.

Angiographic detection of the bleeding lesion is based on obtaining direct signs (visualizing the leak of contrast) and indirect signs (tumor vessels, vascular malformations, and others). It is important to remember that in order to detect the bleeding point, the patient has to be bleeding at the moment of the exploration, at least minimally. Although it depends on the equipment and technique used to perform the angiography, several authors have specified that it is necessary for a bleeding of at least 0.3–0.5 ml/min to be detected [32]. Obviously, when the angiography is more selective and precise, it is easier to detect the lesion. When the bleeding point is not found, other techniques can be applied; the first is to use lower-viscosity contrast, such as CO<sub>2</sub> [33]. Management of this contrast medium must be carried out carefully, not because of risks or complications, which are negligible or nonexistent, but because imaging artifacts may occur. Moreover, CO<sub>2</sub> is useful since it can detect very small leaks of contrast medium. Another technical possibility is to “induce” hemorrhage in cases when there is a high clinical suspicion that a particular artery can be the source of the bleeding but the angiography is normal. In those cases, bleeding can be provoked by mechanical stimulation [34] or with drugs. For this purpose, “bleeding stimulation” has been described with urokinase (50–100,000), tolazoline (25–200 mg i.a.), heparin (3–10,000 units i.v.), and tPA (10–50 mg i.a.) [35–39]. The aim of these technique is to open the bleeding point, temporarily occluded by the clot, confirm the precise site of the hemorrhage, and, ultimately, to apply embolizing agents to achieve secure and lasting occlusion of the lesion.

There are indirect signs that suggest the presence of a hemorrhage even without seeing the exact bleeding point. These signs may be clear as the presence of aneurysm, or subtle like the presence of neovascularization or a vessel network. Other signs are hard to interpret, such as the presence of premature venous drainage or a vessel-caliber increase.

Active GI bleeding is a potentially dangerous situation because patients with this condition may go into shock. Colonoscopy, angiography, and scintigraphy have been used widely to localize the source of bleeding, but time is needed to perform these examinations. Enhanced CT may be an alternative to more invasive procedures for evaluation of hemodynamically stable patients with suspicion of hemorrhage [18]. Its simplicity and its ability to detect a wide variety of causes of intestinal bleeding not possible using other methods makes helical CT, and specially MD-

CT, an ideal method for detecting vascular lesions such as angiodysplasia and aortoenteric fistulas, small bowel masses, such as lipomas and stromal cell tumors, bowel wall thickening due to radiation enteritis and Crohn's disease, extraintestinal neoplasms, such as pancreatic cancer with metastases, and unusual lesions such as cholesterol emboli [40].

In the context of GI hemorrhage, CT has been proven to be an excellent imaging modality with a rapid diagnostic capability that contributes to a decrease in morbidity and mortality from patients presenting with suspicion of active hemorrhage.

---

### 5.3.2.4 Endovascular Treatment

The therapeutic approach to GI hemorrhage must be multidisciplinary and, at the same time, personalized to each patient's circumstance according to the clinical situation and the degree and source of the hemorrhage [41, 42]. Regardless of whether the method chosen is surgery, endoscopy, or endovascular treatment, the aims of therapy have to be the same: to obtain hemostasis and to treat the underlying lesion.

Below we shall analyze the techniques, results, and complications obtained with therapeutic embolization in gastrointestinal bleeding, depending on its origin and cause.

#### GI Hemorrhage of Hepatic Origin

A hepatic arterial lesion may present as a free intraperitoneal bleeding, as an intrahepatic or subcapsular hematoma, or as hemobilia that is clinically difficult to distinguish from other gastrointestinal hemorrhages [43–46]. If the lesion is in the common or proper hepatic artery, which is uncovered by liver parenchyma, the hemorrhage will generally be massive and difficult to control. The most common cause is the presence of a pseudoaneurysm related in most of the cases to earlier surgery (e.g., liver transplant) [34]. For its treatment, two therapeutic possibilities have been described: the first is to place a covered endoprostheses to seal the bleeding point and maintain the arterial flow at the same time; the second is to embolize the lesion as well as the hepatic artery. With the aim of preventing liver ischemia after the embolization, the gastro-duodenal artery should be left patent, to ensure hepatic arterial perfusion.

Intrahepatic vascular lesions causing hemobilia and GI hemorrhage can be divided mainly into four types:

1. Lesions of small terminal vessels. These lesions are generally caused by hepatic biopsy needles or biliary catheters, and can cause large hemorrhages. As these are distal vessels with a low possibility of connection and re-perfusion from other arteries, the treatment consists of superselective embolization using particles (100–500 μm) or microcoils.

2. Vascular lacerations. These lacerations are almost always caused by the insertion of drainage catheters, or by injuries or lacerating trauma. The artery must be embolized (coils or microcoils) first in the distal part to the lesion (“the back door”), the reason being to prevent “re-perfusion” distal to the bleeding point from occurring through intrahepatic collaterals [47]. Finally, the artery is embolized proximally to the lesion. In cases where there is a stable transhepatic access (e.g., from a biliary drainage), the lesion can be catheterized and treated using this approach. The therapeutic method is similar to the “endovascular,” and at times this is the quickest and most useful solution in solving the problem.
3. Vascular lesions with arterio-portal shunt. Sometimes (e.g., after a liver trauma), when performing an arteriography in a patient with a massive hemobilia and arterioportal shunting, opacification of a bile duct is also seen (this sign reflects the massive passage of arterial blood to the bile duct); however, the arterio-portal shunt of traumatic/iatrogenic origin is in most cases the only angiographic manifestation of nonmassive, intermittent hemobilia. Since the bile duct is close to the portal vein, the arterio-portal connection is assumed to be accompanied by an arterio-biliary communication as a result of vascular laceration [48]. By occluding the arterio-portal connection, the bleeding point is thereby also sealed.

It is also important to realize that an arterio-portal shunt produces “arterialization” of the porta, with an increase in pre-sinusoidal portal pressure and therefore an increase in the porto-systemic gradient. This hemodynamic situation, in patients with previous portal hypertension (e.g., cirrhotics), results in a raised risk of bleeding from gastroesophageal varices.

For all of these reasons, it is clinically useful to close the “high-flow” arterio-portal connections. The technique consists of inserting the catheter either well within the shunt or in the artery closest to the lesion. Embolization is performed with coils or microcoils, and the aim is to close the connection directly. If the catheter cannot be advanced to the desired point, it is perhaps better not to embolize, as an excessively proximal occlusion would favor the opening of collaterals distal to the coils, leading to rechannalization of the shunt. In these technically difficult cases, which are uncommon, percutaneous treatment can be performed transparietohepatically by injecting alcohol or thrombin to sclerose the fistula, or by gaining transportal access to reach and occlude the fistula.

4. Vascular laceration with formation of pseudoaneurysm. The most frequent example is that of a lesion in the right hepatic or the proper hepatic artery that appears after open liver surgery, or especially after laparoscopic cholecystectomy [49–51]. In such large pseudoaneurysms, as in the case of vascular injury, the most

suitable percutaneous treatment consists of distal and proximal occlusion of the arteries to exclude the arterial lesion while preserving distal flow. On occasions this procedure is not technically possible or is ineffective, so other possibilities must be considered such as direct puncture and sealing of the lesion using coils, gelatine sponge, or thrombin, which is perhaps the best option.

### Hemorrhages of Pancreatic Origin

Vascular lesions associated with pancreatic diseases can sometimes manifest in the form of hemosuccus (bleeding through the duct of Wirsung) and then GI hemorrhage. They may originate after surgery and in these cases the treatment consists to embolize the bleeding vessel. Inflammatory lesions of the pancreas frequently cause vascular lesions (pseudoaneurysms), the clinical manifestation of which could be as a massive GI hemorrhage. The most usual endovascular treatment consists of the embolization/occlusion of the bleeding artery. As in lesions of the common hepatic artery, a possible treatment is to seal and exclude the lesion using covered metal stents; however, there is some controversy about this modality of treatment, since the insertion of an endovascular prosthesis in an inflammatory area can, at least theoretically, be contraindicated as the device may become infected.

### Hemorrhages of the Upper GI Tract

Upper digestive hemorrhages are those which have their origin above the angle of Treitz. This section focuses on arterial hemorrhages that originate in the stomach and duodenum [52, 53].

#### Stomach

Gastric vascularization is characterized by the fact that it comes from many different arterial pedicles and, at least, the left gastric, the right gastric (from the hepatic arteries), the gastro-duodenal (with its right gastro-epiploic branch) and the splenic (with the short gastric and left gastro-epiploic arteries) are involved. In cases of digestive hemorrhage from a single bleeding point (e.g., stress ulcers), selective embolization, using segments of gelatine sponge, is highly effective, and necrosis due to post-embolization ischemia is very infrequent.

In cases of diffuse gastric hemorrhage, not controlled by endoscopy, owing to the above-mentioned network of collaterals, nonselective therapeutic embolization has been described as a possible treatment. The aim of this procedure is to reduce temporarily the blood supply to encourage hemostasis. It should not be carried out in patients who have undergone previous gastric surgery, as the stomach will have lost collaterals in some areas. The technique is performed using segments of gelatine sponge and embolizing two “main” pedicles, e.g., the left gastric and gas-

tro-epiploic arteries [54]. Finally, although there are series which contemplate the safe use of this type of nonselective embolization, other authors who have used similar techniques on similar patients have observed gastric necrosis [55].

### Duodenum

An important feature of the duodenal vascularization is its dual supply from the hepatic artery and the SMA. Then the pancreato-duodenal arcades function like a true high-flow connection between the celiac trunk and the SMA; therefore, a hemorrhage with its origin in a vascular lesion (caused, for example, by a duodenal ulcer) must be treated bearing this double supply in mind (Fig. 2) [53]. This means that if the lesion is reached by catheterization of the gastro-duodenal artery the end of the catheter or microcatheter should be initially placed distal to the lesion so that a distal seal (e.g., coils) will prevent the entry of blood from another vessel (“re-perfusion”). Once the distal artery is sealed, coils, segments of gelatine sponge, particles (300–500 or 500–700  $\mu\text{m}$ ), or glues can be used to treat the bleeding point. The success rate of embolization in duodenal bleeding is around 80% [53]. After obtaining hemostasis, the artery can be closed proximally with coils, although there is some controversy in this regard, since, by doing this, access to the lesion is impeded should further bleeding occur. Similarly, it is not recommended to insert the embolic material inside the lesion since the intracavitary pressure rises and so does the risk of active bleeding during the procedure. Although embolization of the duodenal area is safe and effective, cases of duodenal stenosis have been observed in long-term follow-up, which are caused by fibrosis after ischemia [56].

In addition to the above-mentioned dual supply, the duodenum also has some highly peculiar anatomical characteristics such as aberrant arteries which originate from accessory hepatic arteries, or tumoral areas with their own vascular supply (other than the arcade). For these reasons, every case must be studied in detail so that the therapeutic decision has to be taken individually. The choice of material is also important, not only to prevent long-term complications, but also to achieve the primary aim of embolization, which is hemostasis. For example, in cirrhotic patients or patients with clotting disorders, the application of microcoils alone may be insufficient, and other materials such as gelatine sponge have to be used in addition to them in order to achieve immediate stopping of the bleeding [57].

### Hemorrhages of the Lower GI Tract

As indicated previously, this section includes all the hemorrhages whose origin is distal to the angle of Treitz. The most common causes of bleeding in the large bowel are diverticula, tumors, and vascular malformations. The ma-

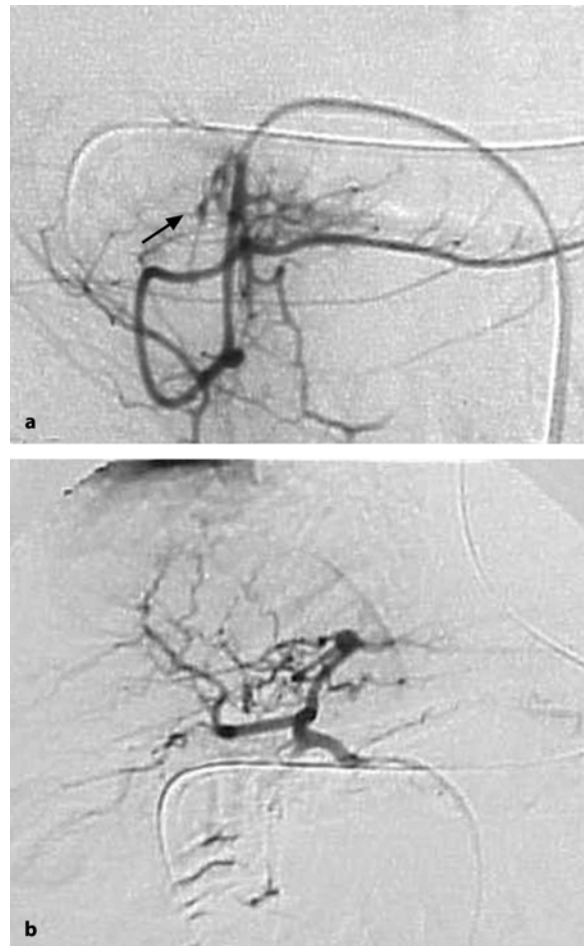


**Fig. 2.** Active hemorrhage in a patient with a duodenal ulcer. **a** Extravasation of contrast medium coming from the gastro-duodenal artery (arrow) is observed. **b** Hepatic arteriography after the embolization of the gastro-duodenal artery

majority of these lesions are detected and treated by endoscopic techniques and only in a few cases are surgery or embolization needed. On the other hand, the small bowel is, at this moment, inaccessible to endoscopy, so other diagnostic techniques (such as angiography) and methods of treatment (such as embolization or surgery) acquire greater importance. When a therapeutic decision has to be taken, angiography and surgery do not have to be exclusive or competitive. In some cases of angiodysplasia, aneurysms, tumors, or metaplastic gastric mucosa, the lesion can be detected and identified using angiographic techniques before being surgically resected. For example, patients with multiple vascular lesions and a localized bleeding in just one can benefit from a “pre-surgical angiographic marking” with microcoils or superselective injection of dye in the bleeding vessel, which facilitates a highly economical and extremely precise resection of a short segment of the intestine [35, 58].



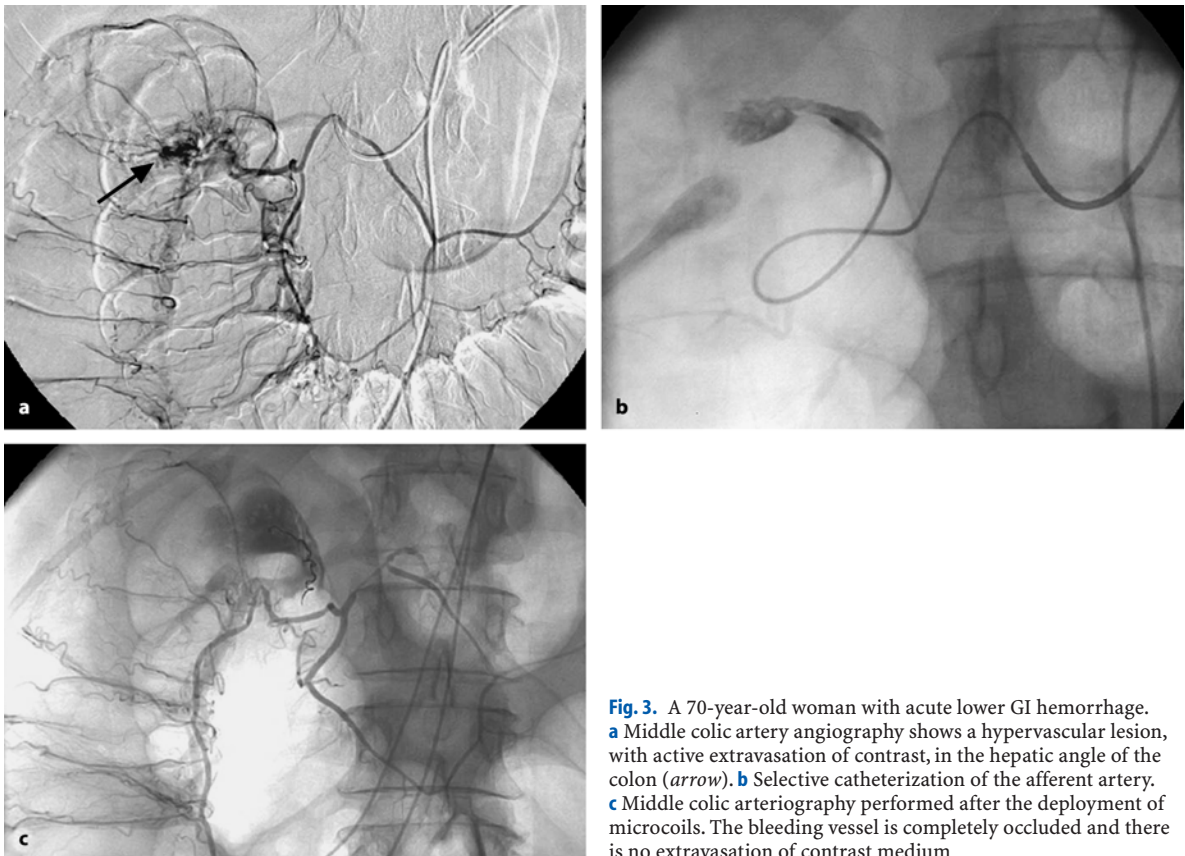


**Fig. 3.** A 70-year-old woman with acute lower GI hemorrhage. **a** Middle colic artery angiography shows a hypervascular lesion, with active extravasation of contrast, in the hepatic angle of the colon (*arrow*). **b** Selective catheterization of the afferent artery. **c** Middle colic arteriography performed after the deployment of microcoils. The bleeding vessel is completely occluded and there is no extravasation of contrast medium

In the early 1980s, different techniques and embolizing materials were developed to achieve safe hemostasis in a bleeding intestinal vessel; however, complications were observed, mainly ischemia and re-bleeding, probably due to poor technique and incorrect use of the embolizing agent. For this reason, at that time, other methods, such as the local infusion of vasoconstrictors (e.g., vasopressin), were developed. This treatment requires special hospital care, and is not free from cardiac (myocardial ischemia) and intestinal (caused by excessive vasoconstriction) complications. Although results vary according to the area of the bleeding, as it is more effective in colon hemorrhages than in the small intestine, recurrence of the bleeding has been described in up to 50% of cases [59, 60]. Owing to these obvious drawbacks, further attention has been paid to the development of new embolization techniques. New materials, such as microcatheters, spherical particles for embolization, and microcoils, have appeared on the market, making embolization safer and more accurate. As a result, embolization is presently an effective alternative to endoscopy and surgery, and can be recommended, from the technical point of view, for bleeding originating in any lesion of any localization. At present, the indications to perform an embolization for the treatment of a GI hemorrhage are: rebleeding after an unsuccessful endoscopic treatment, and when endoscopy is not

feasible, for example, in the small intestine or in patients who have recently undergone abdominal surgery [61]. Another clinical indication is patients who present with massive bleeding and with an unstable hemodynamic situation. An urgent occlusion of the bleeding vessel can be performed in order to improve the clinical situation of the patient, even if embolization may generate intestinal ischemia. In such cases, the “exclusive” purpose of the procedure is to allow the patient to be treated for his or her underlying intestinal lesion in a better hemodynamic condition.

Once the decision to embolize has been taken attention should be paid not only to obtain hemostasis (which in itself is important), but also to the specific treatment of the underlying lesion (technique and materials will be different if, for example, the bleeding comes from an angiodysplasia or from a bleeding aneurysm). In general, for the vast majority of cases, it is recommended that the vascular occlusion be performed at a point, usually the “vasa recta,” that is sufficiently distal to prevent rebleeding from collaterals, but proximal enough to prevent infarction of a segment of the intestinal wall. The “vasa recta” differ in morphology and characteristics according to whether it is in the jejunum, ileum, or colon [62]. In the jejunum, they are sparse, long (2–3 cm), and relatively thick, whereas in the ileum they are more abundant, well connected through col-

laterals, but also very thin, and in the colon they are less abundant, and with the origin from the marginal artery. Embolization of the “vasa recta” prevents, in most cases, ischemia of the intestinal wall and facilitates hemostasia by temporarily reducing the blood flow in the affected area. The materials that should be used are microcoils or particles such as “non-spherical” polyvinyl alcohol (500–700  $\mu\text{m}$ ) or, even better, the new “spherical” particles (700–900  $\mu\text{m}$ ; Fig. 3) [63–65]. The results obtained with embolization can be evaluated as “local success” (occlusion of the lesion) and “clinical success” (absence of bleeding and appearance of complications). Rebleeding ranges from 0 to 20% and complications from 0 to 42% [66]. This wide variation of figures is related with the time of the publication and, at this moment, using adequate materials and an accurate technique, both can be <5%.

The statement made in previous paragraphs that “any bleeding vessel can be embolized” is not completely correct since embolization can be ineffective in some situations and also the possibility of an ischemic complication is always present. This is particularly the case with two groups of patients. The first group are those with diffuse hemorrhage and clotting disorders. In such cases, infusion of vasoconstrictors could be a good option; however, another possibility to obtain “vasoconstriction” without drugs has been recently published. The technique consists in obtaining a temporary vasoconstriction by using catheters and guidewires manipulating them in such a way that they cause an arterial spasm. The spasm will produce a temporary decrease of the blood flow that facilitates hemostasia and the healing of the lesion [67]. The second group of patients are those who have a lesion (aneurysm, rupture, etc.) in a large artery, in whom surgery is contraindicated. In such cases, embolization should not be performed and covered stents could be used to seal the lesion and exclude the bleeding point; however these devices are still not flexible enough to be driven through tortuous curves of some splanchnic vessels.

### 5.3.3 Intestinal Ischemia

#### 5.3.3.1 Acute Ischemia

Acute mesenteric ischemia may be manifested by the clinical triad of sudden onset of abdominal pain, diarrhea, and vomiting in a patient with pre-existing cardiac disease. These symptoms are nonspecific and result in delayed diagnosis and treatment [68].

#### Etiology

Acute BI may be secondary to occlusions of the arteries or veins or due to nonocclusive reduction of intestinal perfusion (NOMI). Acute occlusions of arterial trunks, mainly SMA, accounts for most cases whereas venous thromboses

are involved in 5–10% of cases and NOMI conditions represent about 20–30% of the total [6].

Acute occlusion of SMA could be due to embolism (50%) or thrombus (25%). The most common source of embolism is the heart (atrial fibrillation, ventricular thrombi, or valvular lesions). About 95% of patients with SMA acute embolism occlusion have previous diagnosis of cardiac disease. Although embolism may be placed at the origin of the artery, the occlusion is usually placed in the middle or distal part of the SMA (Fig. 4). Thrombosis of SMA is most likely to occur proximal and is secondary to atherosclerosis. In these patients the degree of collateral vessels developed and the systemic blood pressure play an important role in the extent and severity of the bowel ischemia [6].

Acute occlusions may be related to other embolic conditions including embolisms from aorta, aortic dissection, cholesterol embolization, aortic surgery, or therapeutic embolization of mesenteric vessels [9, 10].

Antiphospholipid antibody syndrome affects females and among others causes major abdominal vascular thromboses, typically venous, and visceral infarctions [69]. Vasculitis comprises a diverse group of conditions that cause inflammation and necrosis of vessels walls. Pathogenic causes and mechanisms are multiple and not completely understood. The classification accepted presently is the Chapel Hill International Consensus Conference in 1994 in which vasculitis were classified in different categories depending on the size of the vessels affected. There are vasculitis affecting large vessels (aorta and the major trunks; Takayasu arteritis or giant cell arteritis), vasculitis of the medium sized vessels (visceral arteries and their branches; panarteritis nodosa or Kawasaki disease), and small vessel vasculitis (lupus erythematosus, Wegener's granulomatosis, Churg-Strauss syndrome, Schönlein-Henoch purpura), among others. Radiological findings in those patients often overlap. These diseases must be considered in young patients presenting ischemia at unusual sites, affecting small and large bowel and with systemic involvement (lung, genitourinary) [70].

Ischemia caused by the occlusion of mesenteric veins represents about 15–20% of cases and could be secondary to infiltrative tumours (colorectal or pancreas typically), inflammatory conditions (pancreatitis, diverticulitis, inflammatory bowel disease) various types of abdominal infections, blunt abdominal trauma, hypercoagulable states, portal hypertension, oral contraceptive use, or bowel obstruction (volvulus or intussusception). Primary venous thrombosis, when there is no predisposing condition, is unusual. When the thrombosis is proximal and isolated it probably will not cause a severe ischemia due to collateral drainage venous. Acute mesenteric venous thrombosis is defined when symptoms have been present for less than 4 weeks. Typical symptoms include abdominal pain, nausea and vomiting, and constipation with or without bloody diarrhea. Diffuse and intermittent abdominal pain



**Fig. 4.** Coronal maximum intensity projection (MIP) reconstruction shows an abrupt occlusion of the superior mesenteric artery due to embolism in a woman previously diagnosed with cardiac disease

may be present for days or even weeks. Abdominal distension is the most usual sign. All those symptoms and signs are not specific and may delay the diagnosis, and contribute to the high morbidity and mortality of this condition. The differential diagnosis must include all the causes of acute mesenteric ischemia (arterial and venous) and the radiological findings are similar [71].

Abdominal trauma may produce BI directly when mesenteric vessels and bowel wall are lacerated or indirectly when trauma leads to hemorrhagic shock and subsequent nonocclusive bowel ischemia. Radiological findings include focal bowel wall thickening, perienteric fluid collections, interloop mesenteric hematoma, and hemoperitoneum [72, 73].

### Pathology

There are three stages of acute BI. In the first stage there are mucosal necrosis, erosions, and ulcers with hemorrhage. This condition is reversible and usually heals without consequences. If the ischemia extends more deeply into the bowel wall and leads to necrosis of the deep submucosal and muscular layers, strictures and stenosis may develop (second stage). The third stage represents a transmural bowel wall necrosis and infarction. This stage is associated with a high mortality and requires surgery [6].

When mural or mucosal necrosis is present, there is associated wall edema with hemorrhage being more prominent in patients with venous thrombosis, which also presents mesenteric fat edema not present in arterial vascular occlusion.

### Imaging

Plain radiography findings are nonspecific with very low sensitivity. Most common findings include an unspecific ileus pattern with dilated loops of the bowel fluid-filled, but the image obtained, in some cases, can be “normal.” Focal mural thickening secondary to submucosal hemorrhage (thumbprinting), separated bowel loops by mesenteric fat thickened, intramural gas (pneumatosis), and mesenteric or portal ve-

nous gas is seen rarely and indicates late-stage disease. If BI is detected with a plain film, it is usually at late stage of the disease representing severe intestinal changes [7].

Barium studies are useful in patients with atypical presentation, when BI is not suspected and in the postoperative period of an ischemic bowel loop resection in cases when ischemic loops were left in place. Findings include bowel dilatation, thumbprinting, fold thickened, abnormal mucosal pattern, ulceration, and stasis of barium. Barium studies should not be performed if an angiography study will be performed later [7].

### Ultrasound

Findings on ultrasound studies are not specific. Vascular thrombus or blood flow changes in duplex and color Doppler studies, distended bowel, hypoechoic and thickened bowel walls, ileus, and fluid collections in peritoneal cavity are common findings in patients with bowel ischemia. Intramural gas can also be detected and, as occurs with the presence of fluid collections, represents a sign of transmural necrosis.

Detection of proximal vascular thrombus and complete occlusion may be diagnosed with color Doppler sonography, but the absence of occlusion in proximal vessels does not exclude the presence of small peripheral thrombus. Although ultrasound has several limitations, such as narrow window by distended bowel loops, its operator dependency or the poor correlation between Doppler flow index anomalies and the severity of ischemia can help identify patients who require angiography [7].

### Computed Tomography

To obtain a high sensitivity CT study in a patient with suspected bowel ischemia, performing and following an accurate protocol is essential. Oral and rectal preparation is required, if possible: oral administration of 600–750 ml of high-attenuation contrast material or water (low attenuation) 30–120 min before scanning and rectal administration of 400–800 ml of contrast material or water. Water as oral



**Fig. 5.** Axial CT. Typical radiological findings of acute large bowel ischemia: circumferential wall thickening; low submucosal attenuation; and mesenteric fat stranding

contrast material offers two advantages respect to traditional oral contrast: it allows better visualization of the enhancing bowel wall and does not interfere with three-dimensional reformatting techniques (maximum intensity projection, volume rendering and shaded-surface display) [8]. Rectal contrast is essential when ischemic colitis is suspected, to distinguish focal areas of ischemic colitis from colonic contractions [6]. Intravenous administration of contrast material is necessary to show vascular occlusions and to evaluate bowel enhancement. From 120 to 150 ml of nonionic contrast agent are necessary at an injection rate of 3–5 ml/s. A biphasic acquisition is performed with the multidetector row CT. The arterial phase begins 25–30 s after initiation of contrast injection and the portal venous phase at 60 s. Multiplanar reformatted images are created at workstations [74].

The two main roles of CT when BI is suspected are to detect ischemic changes in bowel loops affected, and to determine, if possible, the cause of the ischemia (Fig. 4; vascular occlusion secondary to embolus, thrombus or atherosclerosis, vascular compression due to bowel occlusion, or vascular tumor invasion).

The most common sign in BI is the circumferential thickening of bowel wall. Normal small bowel wall thickness is 5 mm or less. Large bowel can measure in contracted areas >5 mm. The most common sign in BI is the circumferential thickening of bowel wall (Fig. 5). Normal small bowel wall thickness is 5 mm or less. Large bowel wall can measure in contracted areas more than 5 mm of thickness. The thickened wall will show low attenuation due to submucosal edema. If thickened bowel loops show high attenuation, it might be due to submucosal hemorrhage that is usually associated to ischemia. The degree of bowel wall thickening does not reflect the severity of the ischemia. It has been demonstrated that reversal ischemia usually shows a much more significant bowel wall thickening than transmural infarction. Some authors have described the thickness of infarcted bowel wall as paper thin reflecting that wall thickening is not proportional to the

severity of the ischemia. Reversible shock small bowel wall may manifest with a mild and diffuse wall thickened and nontransmural ischemic colitis may manifest with pronounced wall thickening due to submucosal hemorrhage, inflammation, and/or superinfection being indistinguishable in some cases from transmural colonic infarction.

Enhancement of ischemic loops is less significant compared with normal loops and is highly specific for acute mesenteric ischemia. Bowel walls may show hyperattenuation due to hyperemia or hyperperfusion. Hyperemia of bowel walls is secondary to mesenteric venous occlusion, whereas hyperperfusion appears during reperfusion following occlusive or nonocclusive bowel ischemia or as a result of superinfection and subsequent inflammation. Hyperemia or hyperperfusion of an ischemic bowel segment may be diffuse or segmental and involve the mucosa and submucosa [6–8]. Dilatation of bowel loops and air fluid levels are quiet common in acute bowel infarction and both signs are less common in patients with reversible ischemia and in superficial ischemic colitis. Mesenteric fat stranding, mesenteric fluid, and ascites are nonspecific CT findings but are related bowel obstruction complicated by mesenteric venous occlusion. Partial or transmural ischemia may present these signs [75].

Pneumatosis and portomesenteric gas are signs of late stage of the disease representing severe intestinal changes (Fig. 6). Both signs are less common than the signs previously described but are more specific of acute BI [76,77].

### Magnetic Resonance Imaging

Magnetic resonance imaging might be comparable to CT to show changes of bowel wall and mesenteric vascular anomalies associated to intestinal ischemia. Vascular visualization is markedly improved by the introduction of three-dimensional MR angiography. The MR studies for bowel ischemia are usually performed in patients who cannot undergo CT [7].



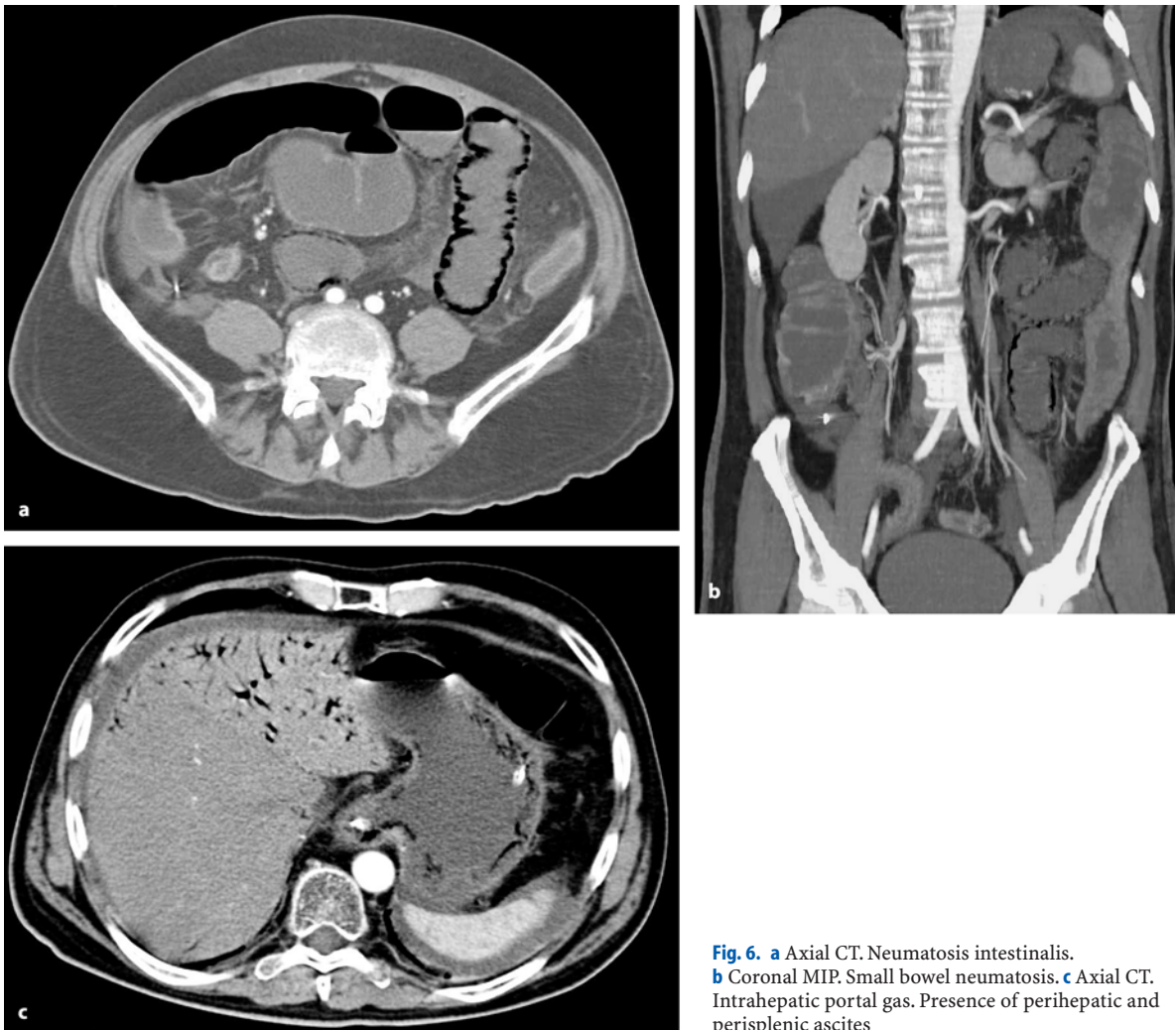


**Fig. 6.** **a** Axial CT. Neumatosis intestinalis. **b** Coronal MIP. Small bowel pneumatosis. **c** Axial CT. Intrahepatic portal gas. Presence of perihepatic and perisplenic ascites

### 5.3.3.2 Chronic Ischemia

Chronic mesenteric ischemia (CMI), or “abdominal angina,” is characterized by weight loss and abdominal epigastric pain that typically occurs 15–60 min after meals, due to the increased demand for splanchnic blood flow, and lasts for several hours. Other symptoms include constipation, flatulence, diarrhea, nausea, and vomiting. Chronic ischemia may produce mucosal damage leading to malabsorption. Symptoms develop insidiously contributing to diagnostic delay.

#### Etiology

Atherosclerotic disease is the main cause of CMI. In the majority of cases proximal segments of visceral arteries are usually involved. Infiltration of arterial walls by fatty plaques leads to stenosis or occlusion of one or more visceral arteries.

Other less frequent causes of vessel obstruction include fibromuscular dysplasia, Takayasu arteritis, thromboangiitis obliterans, radiation enteritis, drug-induced enteropathy, or extrinsic obstruction or vessel encasement by a tumor.

#### Pathology

The CMI is a slowly progressive disease. The degree of stenosis or obstruction capable of determining clinical symptoms depends on the anatomic configuration, the speed of progression, and the presence of collateral vessels. The number of arteries that must be involved before symptoms of abdominal angina appear is not clear but it has been suggested that while the three main supplying vessels are variably occluded or narrowed at least two vessels should be significantly compromised. Collateral vessels delay the clinical onset of the disease. These collateral can be divided into two major systems. The first system

connects celiac trunk to the SMA and is composed mainly of the pancreaticoduodenal arteries running between gastroduodenal artery and the proximal SMA. Blood can flow in both directions. The other system connects SMA and IMA and comprises the paracolic arcade (arch of Riolan) and the marginal artery of Drummond. When the three main trunks are occluded or stenotic, the phrenic, lumbar, and pelvic collateral vessels become prominent.

Patients with a single lesion can present pain, whereas patients that present lesions in all three trunks may be asymptomatic. This fact suggests that occurrence of ischemia also depends on the site of the lesion with respect to systems that connect the main trunks. Distal lesions to the collateral systems develop clinical symptoms of ischemia earlier than proximal lesions. Diffuse atherosclerosis of the distal visceral vessels is present in patients with diabetes or end-stage renal disease. These patients are unable to develop collateral vessels.

Another factor in the appearance of ischemia is the speed of progression of the lesions. Inflammatory lesions develop earlier and severe occlusion may be present before collateral vessels are present [78, 79].

### Imaging

#### Ultrasound

Ultrasound is the preferred noninvasive screening test for SMA and celiac trunk artery stenosis. A peak systolic velocity >275 cm/s or greater is highly specific for significant SMA stenosis [80, 81].

#### Computed Tomography

The CT findings suggesting CMI include the presence of atherosclerotic calcified plaque at or near the origins of proximal splanchnic arteries and focal vascular stenosis of proximal mesenteric vessels with prominent collateral development. These findings can be well demonstrated with MDCT. New computer reconstruction techniques allow accurate measurement of arterial stenosis [80, 81].

#### Magnetic Resonance Imaging

Magnetic resonance angiography shows a good agreement with conventional angiography for the evaluation of visceral arteries and evaluation of significant arterial stenosis. The advantage compared with CT is that it is a safe technique, even when patients have renal disease. The major disadvantage is that it is less sensitive for detecting calcified plaques and oversensitive for assessing vascular stenosis [7].

### 5.3.3.3 Endovascular Treatment of Intestinal Ischemia

As has been stated previously, intestinal ischemia can be classified into three major categories, as proposed by the American Gastroenterological Association (AGA) in 2000, according to the clinical features: AMI; CMI, also known as “abdominal angina”; and colonic ischemia (CI) or ischemic colitis. The AMI may be further classified into arterial thromboembolism, venous thrombosis, and NOMI [82].

This classification is important from a practical viewpoint because, for example, an arterial thromboembolism represents a true emergency, whereas CMI does not. Also, the mortality associated with each of them is different, and mesenteric venous thrombosis is not as lethal as an acute thromboembolism of the SMA or NOMI.

#### Acute Ischemia

Despite the progress made in the understanding of the pathophysiology, diagnosis, and treatment of this group of diseases, mortality still remains as high as decades ago, ranging between 59 and 93% in different published series [82, 83]. The mortality increases with age, the extension of bowel infarction and, most importantly, the time delay between onset of symptoms and intervention; the latter is the most important one, as it is entirely dependent on us. Thus, instituting an early diagnosis and treatment, before BI develops, results in marked improvement in survival rate [84].

The choice of treatment in many cases depends largely on the local availability for performing emergency angiography. Endovascular techniques do have a role to play, either alone or in conjunction with surgical treatment, but controlled trials are lacking because of the relative infrequency of these conditions.

Several therapeutic options are available from an endovascular viewpoint for the treatment of GI ischemia; these may be grouped into two broad categories depending on whether they are based on the use of mechanical devices (balloon catheters and stents) or pharmacological agents (fibrinolytics and vasodilators).

From a practical viewpoint there are four distinct entities that may result in acute mesenteric ischemia: SMA embolus; SMA thrombosis; and NOMI and mesenteric venous thrombosis.

In the presence of peritoneal signs and symptoms, there is uniform agreement that the treatment should consist of an exploratory laparotomy, together with resection of any necrotic portion of bowel. A primary anastomosis may be fashioned but, when blood perfusion of the anastomosis is not confirmed, it has been postulated that a second-look operation should be done within 12–24 h to confirm intestinal viability [85–92]. A recently published study, however, questioned the efficacy of the second-look operation in improving patient survival [93].



**Fig. 7a, b.** A CT reconstruction and digital subtraction angiography show a filling defect within the superior mesenteric artery. The ileocolic artery is patent as well as the middle colic artery. The jejunal branches are underfilled with contrast. Note the absence of collateral circulation. A diagnosis of superior mesenteric embolus

was made. **c** A microcatheter was placed with its tip just proximal to the thrombus and an infusion of urokinase (500,000 U in total) was started. **d** Six hours later, the embolus dissolved completely, and the arteries were patent. (Note, however, the severe vasospasm present, which mainly affects the jejunal and ileal branches.)

Establishing whether the occlusion is embolic or thrombotic may be difficult at times, as the angiographic findings may be similar. The presence of a meniscus sign or collateral circulation may help to point to one or the other. Differentiation between acute and chronic thrombosis can also be difficult at times, but visualization of collateral circulation with late filling of SMA branches favors the diagnosis of chronic disease.

In the presence of an embolus, an embolectomy with a Fogarty catheter may be performed through a SMA arteriotomy. A thrombosis, on the other hand, may be treated with an aortomesenteric bypass. Employing the saphenous vein as a graft has the advantage of reducing the risk of infection in comparison with a prosthetic one, but the risk of it kinking is higher [94].

When peritoneal signs are absent, in the presence of an embolus, an endovascular treatment consisting on the infusion of fibrinolytic agents (urokinase, streptokinase, or recombinant tissue plasminogen activator, t-PA) may be performed [95–102]. Different doses have been reported in case studies and series. Typically for streptokinase a 250,000-U intraarterial bolus followed by a low-dose continuous infusion of 5000–10,000 U/h. This is the least expensive of all but bears the drawbacks of potential allergic reactions (3%) and neutralization with antibodies to streptococcus. Urokinase, being an endogenous substance, does not have such shortcomings but is more expensive. The dosage used is 200,000–250,000 U as an intraarterial bolus followed by an infusion of 60,000–120,000 U/h. Finally, t-PA is the most expensive but has the advantage of being fibrin

selective, acting primarily on fibrin-bound plasminogen. A typical dose would be a 20-mg slow intraarterial bolus, followed by a subsequent 20-mg bolus 12 h later (Fig. 7) [103].

The outcome of this kind of treatment improves when the embolus is distal to the origin of the ileocolic artery or partially occluding the SMA trunk. Vasodilators have also been used on their own when the distal vascular bed is well founded; however, their main application is in conjunction with surgical embolectomy. In this context they have proved to be particularly helpful by relieving the vasoconstriction present in association with an embolus that may persist even after an embolectomy [104].

The use of angioplasty and stent placement for acute SMA thrombosis has also been reported [105, 106].

Patients suffering from NOMI may greatly benefit from the infusion of vasodilators on their own or in association with surgical resection of necrotic bowel. Early angiography before intestinal necrosis develops may prove useful in order to prevent an unnecessary laparotomy that would exacerbate vasoconstriction [94, 197]. An infusion of papaverine hydrochloride (60-mg bolus followed by an infusion at a dose of 30–60 mg/h) may be started at the time of angiography [108–111]. There are small series published in which the high mortality rate from this condition has been greatly reduced by this therapy [112]. This is in addition to any measures needed to revert the underlying condition, which predisposes to hypotension, such as hypovolemia, heart failure, or arrhythmia.

The treatment for mesenteric venous thrombosis depends on whether the diagnosis has been made incidentally in an asymptomatic patient or not. In asymptomatic individuals, in whom the diagnosis is an incidental finding, it has been proposed to rely either on no therapy or on a 3- to 6-month course of anticoagulation, although there are no studies published to support such a decision. Such regime consists of heparin for 7–10 days followed by oral anticoagulants for 3–6 months [113]. Symptomatic patients with peritoneal signs are candidates for urgent laparotomy with resection of necrotic bowel. Symptomatic patients with absence of peritoneal signs may be treated in the same way as asymptomatic patients, but the local infusion of fibrinolytic agents has also been proposed, either transarterially or directly into the vein through a transhepatic approach [114].

### Chronic Ischemia

The CMI (“abdominal angina”) does not require emergency treatment. It is usually the result of atheromatous involvement of the splanchnic circulation, but there is a specific entity (extrinsic compression of the celiac trunk by the median arcuate ligament of the diaphragm) which tends to affect younger individuals that requires separate consideration.

The first consideration should be to decide which stenosis requires treatment, as it is not uncommon to find asymptomatic patients with atheromatous lesions in one or

more vessels. It is generally accepted that patients with abdominal angina and unexplained weight loss, in whom other types of GI disease have been excluded, whose angiograms reveal stenosis in two of the three vessels, should be treated.

Traditionally, surgical revascularization has been the preferred therapy for these patients [115]. Presently, balloon dilatation and stent placement seem to be a reasonable alternative, although it is difficult to establish which treatment is better. From the published series the rates of clinical success seem to be similar; however, the recurrence rate of angioplasty (without stent placement) is higher [116]. It is likely that the use of stents diminishes the recurrence rate; therefore, making this the therapy of choice. The evidence to support this is still scanty but promising [117, 118].

Celiac artery compression syndrome is a controversial entity and is thought to be a syndrome of abdominal pain caused by compression of the celiac trunk by the median arcuate ligament and perhaps by dense encasement by periarterial neural tissue. Compression of the celiac artery is thought to cause intimal fibrosis that leads to luminal stenosis and impaired splanchnic blood flow. This would result in symptoms similar to those of atherosclerotic mesenteric ischemia compression, which nearly always is caused by at least two major visceral artery occlusive lesions. Patients are typically young adults, especially women, and the clinical features are asthenic body habitus, intermittent abdominal pain, epigastric bruits, and rapid weight loss, but the patients often do not have symptoms. Symptoms may be the result of compression of a single visceral artery in the absence of adequate collateral vessels. Mesenteric steal or neurogenic mechanisms have been proposed as other possible causes. This entity does not benefit from angioplasty and stenting alone. In this situation surgical decompression together with arterial reconstruction or dilatation appears to be the preferred therapy, particularly when there is a persistent vessel deformation [119].

## References

1. Thompson JN, Salem RR, Hemingway AP et al. (1987) Specialist investigation of obscure GI bleeding. *Gut* 28:47–51
2. Pretorius ES, Fishman EK, Zinreich SJ (1997) CT of hemorrhagic complications of anticoagulation therapy. *J Comput Assist Tomogr* 21:44–51
3. Federle MP, Jeffrey Jr RB (1983) Hemoperitoneum studied by computed tomography. *Radiology* 148:187–192
4. Routoulo RA, Evans SRT (1999) Mesenteric ischemia in the elderly. *Gastroenterology* 115:527–557
5. McKinsey JF, Gewertz BL (1997) Acute mesenteric ischemia. *Surg Clin North Am* 77:275–288
6. Weisner W, Khurana B, Hoon J, Ros P (2003) CT of acute bowel ischemia. *Radiology* 226:635–650
7. Kim AY, Ha HK (2003) Evaluation of suspected mesenteric ischemia. Efficacy of radiologic studies. *Radiol Clin North Am* 41:327–342



8. Horton KM, Fishman EK (2001) Multi-detector row CT of mesenteric ischemia. Can it be done. *Radiographics* 21:1463–1473
9. Geboes K, Geboes KP, Maleux G (2001) Vascular anatomy of the gastrointestinal tract. *Baillieres Best Pract Res Clin Gastroenterol* 15:1–15
10. Horton KM, Fishman EK (2002) Volume-rendered 3D CT of the mesenteric vasculature: normal anatomy, anatomic variants and pathologic conditions. *Radiographics* 22:161–172
11. Rosenblum JD, Boyle CM, Schwartz LB (1997) The mesenteric circulation: anatomy and physiology. *Surg Clin North Am* 77:289–306
12. Kornblith PL, Boley SJ, Whitehouse BS (1992) Anatomy of the splanchnic circulation. *Surg Clin North Am* 72:1–30
13. Lin PH, Chaidof EL (2000) Embryology, anatomy and surgical exposure of the great abdominal vessels. *Surg Clin North Am* 80:417–433
14. Graf O, Boland GW, Kaufman JA et al. (1997) Anatomic variants of mesenteric veins: depiction with helical CT venography. *Am J Roentgenol* 168:1209–1213
15. Mc Cott JJ (1976) Intraoperative and retroperitoneal hemorrhage. *Radiol Clin North Am* 14:391–405
16. Scott WW, Fishman EK, Siegelman SS (1984) Anticoagulants and abdominal pain: the role of computed tomography. *J Am Med Assoc* 252:2053–2056
17. Sivit CJ, Pecllet MH, Taylor GA (1989) Life-threatening intraoperative bleeding: demonstration with CT. *Radiology* 71:430
18. Jeffrey RB, Cardoza JD, Olcott EW (1991) Detection of active intraabdominal arterial hemorrhage: value of dynamic contrast-enhanced CT. *Am J Roentgenol* 156:725–729
19. Yamaguchi T, Yoshikawa K (2003) Enhanced CT for initial localization of active lower gastrointestinal bleeding. *Abdom Imaging* 28:634–636
20. Zuckerman GR, Prakash C (1998) Acute lower intestinal bleeding. *Gastrointest Endosc* 48:606–616
21. Yao DC, Jeffrey RB, Mirvis SE et al. (2002) Using contrast-enhanced helical CT to visualize arterial extravasation after blunt abdominal trauma: incidence and organ distribution. *Am J Roentgenol* 178:17–20
22. Morteale KJ, Cantisani V, Brown DL et al. (2003) Spontaneous intraoperative hemorrhage: imaging features. *Radiol Clin North Am* 41:1183–1201
23. Vernava AM, Longo WE, Virgo KS et al. (1996) A nationwide study of the incidence and etiology of lower gastrointestinal bleeding. *Surg Res Commun* 23:113–120
24. Willmann JK, Roos JE, Platz A et al. (2002) Multidetector CT: detection of active hemorrhage in patients with blunt abdominal trauma. *Am J Roentgenol* 179:437–444
25. Horton KM, Fishman EK (2000) 3D CT angiography of the celiac and superior mesenteric arteries with multidetector CT data sets: preliminary observations. *Abdom Imaging* 25:523–525
26. Laghi A, Iannaccone R, Catalano C et al. (2001) Multislice spiral computed tomography angiography of mesenteric arteries. *Lancet* 358:638–639
27. Weshaupt D, Pfammatter T, Hilfiker PR et al. (2002) *Am J Roentgenol* 178:399–401
28. Rubin GD, Shiau MC, Leung AN et al. (2000) Aortic and iliac arteries: single versus multiple detector-row helical CT angiography. *Radiology* 215:670–676
29. Elliot K. Fishman (2001) From the RSNA Refresher Courses. CT angiography: clinical applications in the abdomen. *Radiographics*:21:3
30. Mc Kenney MG, Martin L, Lentz K et al. (1996) 1000 Consecutive ultrasounds for blunt abdominal trauma. *J Trauma* 40:607–610
31. Unger EC, Glazer HS, Lee JKT et al. (1986) MRI of extracranial hematomas: preliminary observations. *Am J Roentgenol* 146:403–417
32. Kruger K, Heindel W, Dolken W et al. (1996) Angiographic detection of gastrointestinal bleeding. An experimental comparison of conventional screen-film angiography and digital subtraction angiography. *Invest Radiol* 31:451–457
33. Sandhu C, Buckenham TN, Belli A (1999) Using CO2 enhanced arteriography to investigate acute gastrointestinal hemorrhage. *Am J Roentgenol* 173:1299–1402
34. De Villa V, Calvo FA, Bilbao JI et al. (1992) Arteriodigestive fistula: a complication associated with intraoperative and external beam radiotherapy following surgery for gastric carcinoma. *J Surg Oncol* 49:52–57
35. Remzi FH, Dietz DW, Unal E et al. (2003) Combined use of preoperative provocative angiography and highly selective methylene blue injection to localize an occult small-bowel bleeding site in a patient with Crohn's disease: report of a case. *Dis Colon Rectum* 46:260–263
36. Gerber T, Bontikous S, Smolka G et al. (2002) Cystic lymphangioma with endosalpingiosis as a rare cause of gastrointestinal bleeding. *Z Gastroenterol* 40:183–188
37. Shetzline MA, Suhoki P, Dash R et al. (2000) Provocative angiography in obscure gastrointestinal bleeding. *South Med J* 93:1205–1208
38. Miller FH, Kline MJ, Vanaganas AD (1999) Detection of bleeding due to small bowel cholesterol emboli using helical CT examination in gastrointestinal bleeding of obscure origin. *Am J Gastroenterol* 94:3623–3625
39. St George JK, Pollak JS (1991) Acute gastrointestinal hemorrhage detected by selective scintigraphic angiography. *J Nucl Med* 32:1601–1604
40. Miller FH, Hwang CM (2004) An initial experience using helical CT imaging to detect obscure gastrointestinal bleeding. *J Clin Imaging* 28:245–251
41. Jackson JE, Stabile B (2000) Visceral embolization. In: Dyet JF, Ettles DF, Nicholson AA, Wilsson SE (eds) *Textbook of endovascular procedures*. Churchill Livingstone, Philadelphia, pp 328–340
42. Defreyne L, Vanlangenhove P, De Vos M et al. (2001) Embolization as a first approach with endoscopically unmanageable acute nonvariceal gastrointestinal hemorrhage. *Radiology* 218:739–748
43. Green MH, Duell RM, Johnson CD et al. (2001) Hemobilia. *Br J Surg* 88:773–786
44. Hidalgo F, Narvaez JA, Rene M et al. (1995) Treatment of hemobilia with selective hepatic artery embolization. *J Vasc Interv Radiol* 6:793–798
45. Moodley J, Singh B, Lalloo S et al. (2001) Non-operative management of haemobilia. *Br J Surg* 88:1073–1076
46. Doussot B, Sauvanet A, Bardou M et al. (1997) Selective surgical indications for iatrogenic hemobilia. *Surgery* 121:37–41
47. L'Hermine C, Ernst O, Delemazure O et al. (1996) Arterial complications of percutaneous transhepatic biliary drainage. *Cardiovasc Intervent Radiol* 19:160–164
48. Tarazov PG (1993) Intrahepatic arterioportal fistulae: role of transcatheter embolization. *Cardiovasc Intervent Radiol* 16:368–373
49. Nicholson T, Travis S, Ettles D et al. (1999) Hepatic artery angiography and embolization for hemobilia following laparoscopic cholecystectomy. *Cardiovasc Intervent Radiol* 22:20–24
50. Rivitz SM, Waltman AC, Kelsey PB (1996) Embolization of an hepatic artery pseudoaneurysm following laparoscopic cholecystectomy. *Cardiovasc Intervent Radiol* 19:43–46
51. Delgadillo X, Berney T, de Perrot M et al. (1999) Successful treatment of a pseudoaneurysm of the cystic artery with microcoil embolization. *J Vasc Intervent Radiol* 10:789–792
52. Dempsey DT, Burke DR, Reilly RS et al. (1990) Angiography in poor-risk patients with massive nonvariceal upper gastrointestinal bleeding. *Am J Surg* 159:282–286
53. Aina R, Oliva VL, Therasse E et al. (2001) Arterial embolotherapy for upper gastrointestinal hemorrhage: outcome assessment. *J Vasc Intervent Radiol* 12:195–200

54. Morris DC, Nichols DM, Connell DG et al. (1986) Embolization of the left gastric artery in the absence of angiographic extravasation. *Cardiovasc Intervent Radiol* 9:195–198
55. Lang EV, Picus D, Marx MV et al. (1992) Massive upper gastrointestinal hemorrhage with normal findings on arteriography: value of prophylactic embolization of the left gastric artery. *Am J Roentgenol* 158:547–549
56. Shapiro N, Brandt L, Sprayregen S et al. (1981) Duodenal infarction after therapeutic Gelfoam embolization of a bleeding duodenal ulcer. *Gastroenterology* 80:176–180
57. Encarnacion CE, Kadir S, Beam CA et al. (1992) Gastrointestinal bleeding: treatment with gastrointestinal arterial embolization. *Radiology* 183:505–508
58. Schmidt SP, Boskind JF, Smith DC et al. (1993) Angiographic localization of small bowel angiodysplasia with use of platinum coils. *J Vasc Intervent Radiol* 4:737–739
59. Darcy M (2003) Treatment of lower gastrointestinal bleeding: vasopressin infusion versus embolization. *J Vasc Intervent Radiol* 14:535–543
60. Gomes AS, Lois JF, McCoy RD (1986) Angiographic treatment of gastrointestinal hemorrhage: comparison of vasopressin infusion and embolization. *Am J Roentgenol* 146:1031–1037
61. Funaki B (2004) Superselective embolization of lower gastrointestinal hemorrhage: a new paradigm. *Abdom Imaging* 29:434–438
62. Lederhann HP, Schoch E, Jost R et al. (1998) Superselective coil embolization in acute gastrointestinal hemorrhage: personal experience in 10 patients and review of the literature. *J Vasc Intervent Radiol* 9:753–760
63. Funaki B, Kostelic K, Lorenz J et al. (2001) Superselective micro-coil embolization of colonic hemorrhage. *Am J Roentgenol* 177:829–836
64. Nicholson AA, Ettles DF, Hartley JE et al. (1998) Transcatheter coil embolotherapy: a safe and effective option for major colonic haemorrhage. *Gut* 43:79–84
65. Bandi R, Shetty PC, Sharma RP et al. (2001) Superselective arterial embolization for the treatment of lower gastrointestinal hemorrhage. *J Vasc Intervent Radiol* 12:1399–1405
66. Kuo WT, Lee DE, Saad WE et al. (2003) Superselective micro-coil embolization for the treatment of lower gastrointestinal hemorrhage. *J Vasc Intervent Radiol* 14:1503–1509
67. Cynamon J, Atar E, Steiner A et al. (2003) Catheter-induced vasospasm in the treatment of acute lower gastrointestinal bleeding. *J Vasc Intervent Radiol* 14:211–216
68. Wilson C, Gupta R, Gilmour DC (1987) Acute superior mesenteric ischemia. *Br J Surg* 74:279–281
69. Kaushik S, Federle MP, Schur PH et al. (2001) Abdominal thrombotic and ischemic manifestations of the antiphospholipid antibody syndrome: CT findings in 42 patients. *Radiology* 218:768–771
70. Ha HK, Lee SH, Rha SE et al. (2000) Radiologic features of vasculitis involving the gastrointestinal tract. *Radiographics* 20:779–794
71. Bradbury M, Kavanagh PV, Bechtold RE et al. (2002) Mesenteric venous thrombosis: diagnosis and noninvasive imaging. *Radiographics* 22:527–541
72. Martson A (1977) Focal ischemia of the small intestine: ischemic stricture. In: *Intestinal ischemia*. Edward Arnold, London, pp 132–142
73. Winton TL, Girotti MJ, Manby PN et al. (1985) Delayed intestinal perforation after nonpenetrating abdominal trauma. *Can J Surg* 28:347–391
74. Kirkpatrick I, Kroeker MA, Greenberg HM (2003) Biphasic CT with mesenteric CT angiography in the evaluation of acute mesenteric ischemia: initial experience. *Radiology* 229:91–98
75. Zalcman M, Sy M, Donckier V et al. (2001) Helical CT signs in the diagnosis of intestinal ischemia in small bowel obstruction. *Am J Roentgenol* 176:1167–1171
76. Alpern MB, Glazer G, Francis IR (1988) Ischemic or infarct bowel: CT findings. *Radiology* 166:149–152
77. Sebastià C, Quiroga S, Espin E et al. (2000) Portomesenteric vein gas: pathologic mechanisms, CT findings and prognosis. *Radiographics* 20:1213–1226
78. Cognet F, Ben Salem D, Dransart M et al. (2002) Chronic mesenteric ischemia: imaging and percutaneous treatment. *Radiographics* 22:863–880
79. Cademartini F, Raaijmakers R, Kuiper JW et al. (2004) Multi-detector row CT angiography in patients with abdominal angina. *Radiographics* 24:969–984
80. Moneta GL, Lee RW, Yeager RA et al. (1993) Mesenteric duplex scanning: a blinded prospective study. *J Vasc Surg* 17:79–84
81. Perko MJ (2001) Duplex ultrasound for assessment of superior mesenteric artery blood flow. *Eur J Vasc Endovasc Surg* 21:106–117
82. Brandt LJ, Boley SJ (2000) AGA technical review on intestinal ischemia. *Gastroenterology* 118:954–968
83. Gray BH, Sullivan TM (2001) Mesenteric vascular disease. *Curr Treat Options Cardiovasc Med* 3:195–206
84. Ritz JP, Runkel N, Berger G et al. (1997) Prognostic factors in mesenteric infarct. *Zentralbl Chir* 122:332–338
85. Shaw RS (1965) The second look after superior mesenteric embolotomy or reconstruction for mesenteric infarction. In: *Current surgical management*. Saunders, Philadelphia, p 509
86. Boley SJ, Feinstein FR, Sammartano R et al. (1981) New concepts in the management of emboli of the superior mesenteric artery. *Surg Gynecol Obstet* 153:561–569
87. Sachs SM, Morton JH, Schwartz SI (1982) Acute mesenteric ischemia. *Surgery* 92:646–653
88. Lindblad B, Hakansson H (1987) The rationale for “second-look operation” in mesenteric vessel occlusion with uncertain intestinal viability at primary surgery. *Acta Chir Scand* 153:531–533
89. Endean ED, Barnes SL, Kwolek CJ et al. (2001) Surgical management of thrombotic acute intestinal ischemia. *Ann Surg* 233:801–808
90. Clark RA, Gallant TE (1984) Acute mesenteric ischemia: angiographic spectrum. *Am J Roentgenol* 142:555–562
91. Levy P, Krausz MM, Manny J (1990) The role of second-look procedure in improving survival time for patients with mesenteric venous thrombosis. *Surg Gynecol Obstet* 170:287–291
92. Whitehill T, Rutherford RA (1990) Acute mesenteric ischemia caused by arterial occlusion. Optimal management to improve survival. *Semin Vasc Surg* 3:149–155
93. Kaminsky O, Yampolski I, Aranovich D et al. (2005) Does a second-look operation improve survival in patients with peritonitis due to acute mesenteric ischemia? A five-year retrospective experience. *World J Surg* 29:645–648
94. Yasuhara H (2005) Acute mesenteric ischemia: the challenge of gastroenterology. *Surg Today* 35:185–195
95. Simó G, Echenagusía AJ, Camúñez F et al. (1997) Superior mesenteric arterial embolism: local fibrinolytic treatment with urokinase. *Radiology* 204:775–779
96. Badiola CM, Scoppetta DJ (1997) Rapid revascularization of an embolic superior mesenteric artery occlusion using pulse-spray pharmacomechanical thrombolysis with urokinase. *Am J Roentgenol* 169:55–57
97. Boyer L, Delorme J M, Alexandre M et al. (1994) Local fibrinolysis for superior mesenteric artery thromboembolism. *Cardiovasc Intervent Radiol* 17:214–216
98. Flickinger EG, Johnsrude IS, Ogburn N L et al. (1983) Local streptokinase infusion for superior mesenteric artery thromboembolism. *Am J Roentgenol* 140:771–772
99. McBride KD, Gaines PA (1994) Thrombolysis of a partially occluding superior mesenteric artery thromboembolus by infusion of streptokinase. *Cardiovasc Intervent Radiol* 17:164–166
100. Pillari G, Doscher W, Fierstein J et al. (1983) Low-dose streptokinase in the treatment of celiac and superior mesenteric artery occlusion. *Arch Surg* 118:1340–1342

101. Regan F, Karistad RR, Magnusan TH (1996) Minimally invasive management of acute superior mesenteric artery occlusion: combined urokinase and laparoscopic therapy. *Am J Gastroenterol* 91:1019–1021
102. Gallego AM, Ramírez P, Rodríguez JM et al. (1996) Role of urokinase in the superior mesenteric artery embolism. *Surgery* 120:111–113
103. Kozuch PL, Brandt LJ (2005) Review article: diagnosis and management of mesenteric ischaemia with an emphasis on pharmacotherapy. *Aliment Pharmacol Ther* 21:201–215
104. Clavien PA (1990) Diagnosis and management of mesenteric infarction. *Br J Surg* 77:601–603
105. Rundback JH, Rozenblat GN, Poplasky M et al. (2000) Re-jejunal artery angioplasty and coronary stent placement for acute mesenteric ischemia. *Cardiovasc Intervent Radiol* 23:410–412
106. VanDeinse WH, Zawacki JK, Phillips D (1986) Treatment of acute mesenteric ischaemia by percutaneous transluminal angioplasty. *Gastroenterology* 91:475–478
107. Bender J, Ratner LE, Hagnuson TH et al. (1995) Acute abdomen in the hemodialysis patient population. *Surgery* 117:494–497
108. Boley SJ, Sprayregan S, Siegelman SS et al. (1977) Initial results from an aggressive approach to acute mesenteric ischemia. *Surgery* 82:848–855
109. John AS, Tuerff SD, Kerstein MD (2000) Nonocclusive mesenteric infarction in hemodialysis patients. *J Am Coll Surg* 190:84–88
110. Zeier M, Wiesel M, Rambusek M et al. (1995) Non-occlusive mesenteric infarction in dialysis patients: the importance of prevention and early intervention. *Nephrol Dial Transplant* 10:71–773
111. Ward D, Vernava AM, Kaminski DL et al. (1995) Improved outcome by identification of high-risk nonocclusive mesenteric ischemia, aggressive reexploration, and delayed anastomosis. *Am J Surg* 170:577–581
112. Morano JU, Harrison RB (1991) Mesenteric ischemia: angiographic diagnosis and intervention. *Clin Imaging* 15:91–98
113. Rhee RY, Gloviczki P, Mendonca CT et al. (1994) Mesenteric venous thrombosis: still a lethal disease in the 1990s. *J Vasc Surg* 20:688–697
114. Bilbao J I, Vivas I, Elduayen B et al. (1999) Limitations of percutaneous techniques in the treatment of portal vein thrombosis. *Cardiovasc Intervent Radiol* 22:417–422
115. Wolf Y G, Verstandig A, Sasson T et al. (1998) Mesenteric bypass for chronic mesenteric ischaemia. *Cardiovasc Surg* 6:34–41
116. Rose SC, Quigley TM, Raker EJ (1995) Revascularization for chronic mesenteric ischemia: comparison of operative arterial bypass grafting and percutaneous transluminal angioplasty. *J Vasc Interv Radiol* 6:339–349
117. Kasirajan K, O'Hara PJ, Gray B H et al. (2001) Chronic mesenteric ischemia: open surgery versus percutaneous angioplasty and stenting. *J Vasc Surg* 33:63–71
118. Matsumoto AH, Angle JF, Spinosa DJ et al. (2002) Percutaneous transluminal angioplasty and stenting in the treatment of chronic mesenteric ischemia: results and long-term follow-up. *J Am Coll Surg* 194:S22–S31
119. Kokotsakis JN, Lambidis CD, Lioulas AG et al. (2000) Celiac artery compression syndrome. *Cardiovasc Surg* 8:219–222

# Imaging and Intervention in Sepsis

T. Geoghegan, M.J. Lee

## 5.4

### Contents

5.4.1 Introduction	471
5.4.2 Ultrasound	471
5.4.3 Computed Tomography	472
5.4.4 Radionuclide Scintigraphy	472
5.4.5 Diagnostic Fluid Aspiration	473
5.4.6 Percutaneous Abscess Drainage	474
5.4.6.1 Guidance Modality and Access Route	474
5.4.6.2 Patient Preparation	474
5.4.6.3 Abscess Drainage Technique	475
5.4.6.4 Follow-up	475
5.4.7 Results of Percutaneous Abscess Drainage	476
5.4.7.1 Clinical Applications	476
5.4.7.2 Complications	478
5.4.8 Conclusion	479
References	479

### 5.4.1 Introduction

Modern imaging techniques facilitate the early diagnosis and characterisation of abdominal fluid collections and abscesses, enabling the interventional radiologist to safely perform procedures which significantly reduce the morbidity and mortality associated with intra-abdominal sepsis. Radiological guided techniques in the management of abdominal sepsis have become the standard of care, reducing the complications associated with surgical intervention.

Ultrasound and computed tomography (CT) provides the mainstay for the detection and depiction of intra-abdominal fluid and abscess collections. These modalities enable the radiologist to accurately evaluate often complex intra-abdominal collections and abscesses facilitating their drainage. This is particularly true in the post-operative patient, where further surgical intervention can be avoided. Ultrasound and CT have virtually replaced plain-film radiography and radionuclide scintigraphy in the detection of

intra-abdominal collections. Magnetic resonance imaging has an evolving role in the imaging and intervention of abdominal sepsis.

### 5.4.2 Ultrasound

Ultrasound has many advantages in the detection of intra-abdominal fluid collections [1–4]. It is quite a flexible examination in that it can be performed at the bedside for ICU patients who cannot travel to the radiology department. It can also be used to guide needles for aspiration and/or to guide catheters for drainage. Ultrasound is best at identifying sub-phrenic and right upper quadrant collections (Fig. 1), intra-hepatic abscesses and pelvic abscesses. Ultrasound has some limitations, particularly related to the presence of gas. Patients with free intraperitoneal air or large amounts of intestinal air are not suitable for ultrasound examination. Air causes reflection of the ultrasound beam, resulting in lack of visualisation of structures distal to any air present. This is particularly of concern in post-operative patients with an ileus or indeed any sick patient with an ileus; therefore, a negative ultrasound should not halt the search for an intra-abdominal abscess if

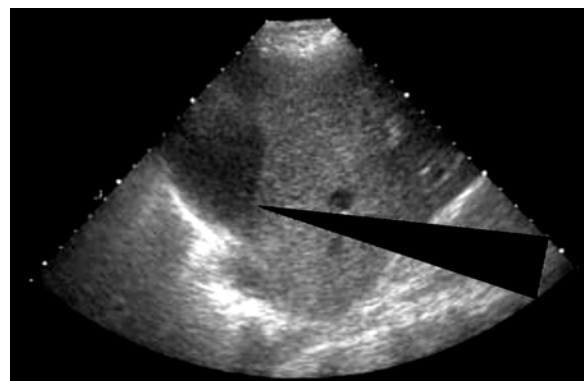


**Fig. 1.** Right subphrenic collection detected by ultrasound. Ultrasound shows a right subphrenic collection (arrows) interposed between the diaphragm and the liver



this is clinically suspected. Additionally, ultrasound is limited in obese patients, and overlying surgical dressings can severely limit access to the abdomen for scanning.

### 5.4.3 Computed Tomography

In recent years CT has emerged as the imaging modality of choice for the evaluation of patients with suspected intra-abdominal sepsis [5–7]. Availability of multi-slice CT scanners with the ability to perform sub-second scanning means that even in sick patients who are unable to breath-hold a diagnostic-quality CT examination can be performed. It is vitally important to obtain thorough opacification of the bowel with positive contrast agents. Labelling of the bowel with contrast material ensures that abscesses are not mistaken for fluid-filled loops of unopacified bowel, and vice versa. As with ultrasound, the CT appearances of fluid collections are non-specific in that sterile collections cannot be differentiated from infected collections. Helpful criteria to identify an abscess include intra-cavitary gas, thick or irregular walls, contrast enhancement and heterogeneous internal debris. Distribution of gas in an intra-abdominal or pelvic abscess is associated with suitability for drainage. Abscesses with superficial gas (superficial bubbles or air–fluid levels) have a greater chance of being drained successfully than do abscesses with deep trapped gas. The sensitivity of CT in identifying intra-abdominal fluid collections and abscesses approaches 90–100% in many studies [8–11]. This compares with an ultrasound sensitivity of 80–85% [8, 12] in experienced hands. A major advantage of CT over ultrasound is in the detection of abscesses in the retro-peritoneum and intra-loop abscesses (Fig. 2).

These are often impossible to see with ultrasound because of overlying bowel gas. CT is also invaluable in the evaluation of patients with acute, severe pancreatitis, where CT confers both diagnostic and prognostic information which is almost impossible to obtain with ultrasound [13]. For these reasons CT is our preferred modality for the detection of intra-abdominal abscesses particularly in sick patients with a high clinical suspicion of intra-abdominal sepsis.

### 5.4.4 Radionuclide Scintigraphy

Indium-111 [14, 15] and gallium-67 [16] are the predominant radio-pharmaceuticals used for the localisation of abdominal inflammation and abscess. Gallium localises inflammatory reactions by binding to leukocytes and/or tissue proteins. Indium-111 is labelled with leukocytes and therefore accumulates when there is leukocytic infiltration of an infected or inflamed area (Fig. 3). Both agents display areas of active inflammation or abscess formation as hot spots; however, they have been largely relegated to a secondary role in the imaging of patients with suspected intra-abdominal sepsis. If ultrasound or CT are negative, radionuclide scintigraphy can be performed. If a hot spot is seen, that area is carefully scrutinised on CT to determine whether there is a visible fluid collection. In addition, in patients with chronic pyrexia of unknown origin radionuclide scintigraphy can be useful particularly when ultrasound and CT have been negative. The long delay between injection and imaging makes these techniques of limited value in acutely ill patients who require urgent evaluation and drainage.

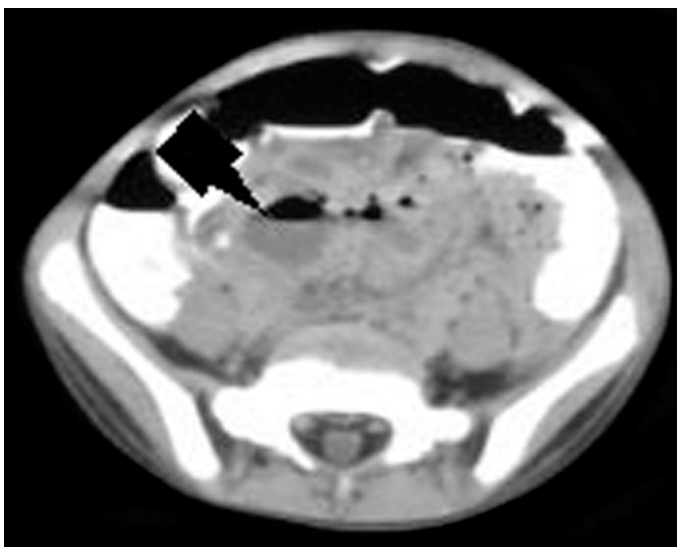


**Fig. 2.** Intra-loop abscess in a 9-year-old patient who presented with perforation of acute appendicitis. A CT scan of the abdomen with good bowel opacification shows an intra-loop abscess (*arrow*). A previous ultrasound did not show this collection. The associated ileus and overlying bowel gas would make this collection difficult to visualise by ultrasound.



**Fig. 3.** This patient with Crohn's disease had a persistent pyrexia, and an indium-111 scan was performed. This shows a localised abscess in the right lower quadrant (*arrow*). This was later confirmed by CT

### 5.4.5 Diagnostic Fluid Aspiration

Diagnostic fluid aspiration is frequently requested by clinicians because ultrasound and CT are unable to distinguish between sterile and infected fluid collections. Fluid aspiration plays an important role in abscess diagnosis (Fig. 4). The access route must be carefully selected to avoid contamination of a potentially sterile aspirate. Ultrasound is the imaging modality of choice with the exception of collections obscured by bowel gas shadowing or collections localised to the retroperitoneal spaces. Diagnostic fluid aspiration is performed with local anaesthesia and a 20-G needle. If the aspirate is dry, an 18-G needle may be placed in tandem with the 20-G needle into the fluid collection. One to 2 ml of sterile saline may be injected into the cavity and aspirated for the purposes of Gram stain and culture. Two to three millilitres of fluid are forwarded to the microbiology laboratory for Gram stain and culture. If pus is obtained at the time of diagnostic aspiration, a catheter is placed straight away. If clear fluid is obtained, a catheter

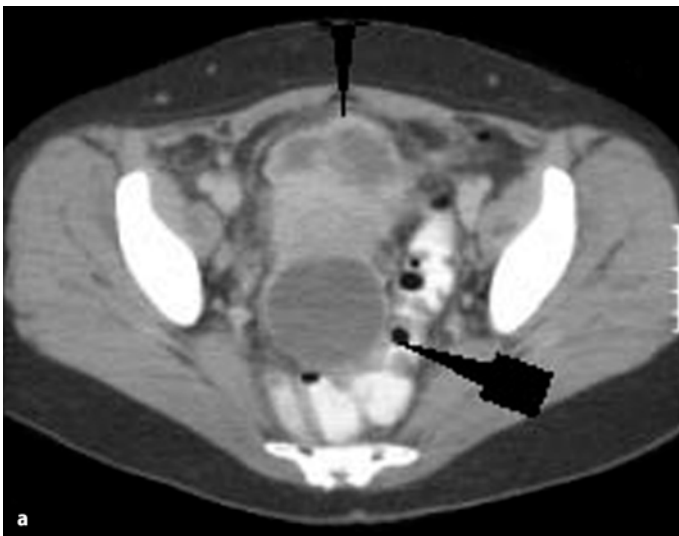


**Fig. 4a, b.** Pelvic abscess in a patient after appendectomy. **a** A CT scan shows a collection (*large arrow*) between the rectum and bladder. Apart from the thick wall, there are no features to suggest that this is an abscess, and thus sampling is necessary. Note also the smaller collection anterior to the bladder (*small arrow*). **b** Trans-vaginal ultrasound before drainage shows a collection with multiple echoes. The collection almost has a solid appearance. Pus was aspirated on placement of a needle, and a catheter was placed into the collection for drainage. Because of the lack of helpful criteria to definitively diagnose abscesses on ultrasound or CT, sampling is usually necessary

is usually not placed, but a sample is sent for Gram stain and culture (aerobic and anaerobic). If the fluid obtained is grossly cloudy in appearance, a catheter is placed depending on the index of clinical suspicion and the clinical state of the patient. If the patient is sick, with a high index of suspicion of intra-abdominal sepsis, a catheter is usually placed, and results of Gram stain and culture are awaited. If these are negative, the catheter can be removed. Alternatively, some interventional radiologists prefer to wait for the Gram stain result. If the Gram stain reveals abundant bacteria and white cells, the fluid collection is an abscess and should be drained. Alternatively, a sample that yields bacteria without white cells is more representative of bowel content and should prompt reassessment of the diagnosis of a fluid collection or indeed the access route used to sample the fluid collection. Occasionally the Gram stain reveals white cells without bacteria. This often represents a sterile abscess, particularly if the patient is taking antibiotics, and necessitates placement of a drainage catheter.

## 5.4.6 Percutaneous Abscess Drainage

Percutaneous abscess drainage was first proposed for simple uniloculated collections, whereas more difficult, multi-loculated collections and collections associated with fistula were the remit of the surgeon. Advances in imaging and advances in abscess drainage techniques have broadened the use of PAD to include the treatment of multiple abscesses, multi-loculated collections, collections in difficult anatomical locations, such as the spleen and pelvis, and abscesses associated with enteric fistula. The PAD has proved to be an enduring technique over the past 20 years, with a high success rate even in these difficult situations.

### 5.4.6.1 Guidance Modality and Access Route

Either CT or ultrasound can be used to guide abscess drainage. Fluoroscopy is now rarely used. The guidance route depends to a large extent on the size and location of the collection and the availability of ultrasound and CT imaging. Obviously if a collection is seen clearly with ultrasound, and there is a clear access route, ultrasound guidance is faster, cheaper and also portable if drainage needs to be performed in the intensive care unit (Fig. 5). Additionally, many operators prefer to use ultrasound if at all possible so that real-time imaging of the needle or catheter is available throughout the procedure; others prefer to use CT because of the more precise definition of the access route to the collection. The CT guidance is mandatory for collections that are not seen clearly by ultrasound, and where the access route is not clearly defined

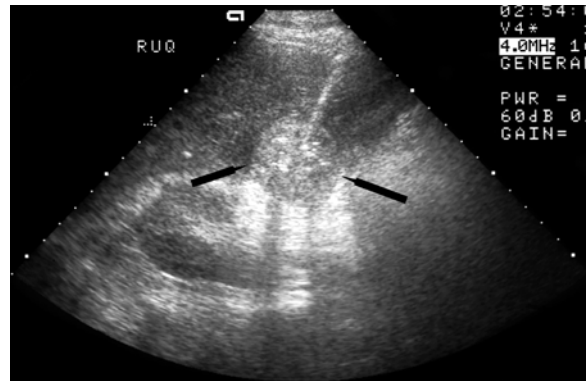


**Fig. 5.** Ultrasound guidance. Ultrasound was used to guide a catheter into this collection in the gallbladder fossa in a patient after cholecystectomy with a high fever. Real-time guidance is advantageous in that the catheter (*large arrow*) can be visualised at all times and can be guided precisely into the collection (*small arrows*)

by ultrasound; these include deep-seated collections such as retroperitoneal collections and intra-loop abscesses. The access route chosen should avoid all viscera between the collection and the skin surface; however, in some cases this may not be possible, and interposed organs can be traversed, such as when using a transgastric approach to drain pseudocysts or a transhepatic approach to the lesser sac.

### 5.4.6.2 Patient Preparation

When a decision has been made to drain an abscess, a number of preliminary steps need to be undertaken. Informed consent should be obtained from the patient or the patient's family. This should include an explanation of the drainage technique, potential benefits and risks, alternative methods of treatment and a description of the expected length of catheter drainage and follow-up catheter care. A coagulation screen should be obtained, and any coagulation deficiency corrected before proceeding to abscess drainage. It is also imperative to ensure that the patient is on antibiotic therapy before proceeding to abscess drainage. Drainage of the abscess induces a bacteraemia, which may produce a septicaemia if the patient is not appropriately treated with antibiotic therapy. If the patient is not on antibiotic therapy, a broad spectrum antibiotic regimen, such as gentamicin, ampicillin and metronidazole, should be commenced. A combination of local anaesthesia, intravenous sedation and analgesia are used for pain relief during the procedure. A combination of midazolam and fentanyl is the preferred combination for sedoanalgesia in our practice.

### 5.4.6.3 Abscess Drainage Technique

In our practice the abscess drainage technique preferred is that of the trocar technique (Fig. 6). An access route to the collection is chosen that avoids interposed viscera. A 20-G needle is inserted into the collection under ultrasound or CT guidance, and fluid is aspirated for Gram stain and culture. A catheter with a sharp stylet is then trocared alongside the needle into the abscess cavity. The 20-G needle is left in situ while the catheter is being inserted into the cavity. The needle acts as a guide with regard to the angle of entry for the catheter, and indeed the catheter follows the needle path once properly aligned with the needle. When using this technique, a good skin dissection is required with an artery forceps. This opens up the skin and superficial tissues for the abscess catheter. The advantage of this technique is that it is a one-step procedure and is ideally suited to either CT or ultrasound drainage when fluoroscopy is not available to monitor guidewire and dilator exchanges. When the catheter enters the cavity, a “pop” is usually felt. The position of the catheter tip in the abscess cavity can be confirmed by removing the stylet and aspirating with a syringe. If the catheter is in situ, the central metal trocar is removed, and the catheter is advanced into the cavity. In general, 10- to 16-F catheters are used for the majority of intra-abdominal abscesses. In rare instances larger catheter sizes (16–30 F) are required (e.g. pancreatic abscess or necrosis).

Some operators prefer the Seldinger technique. This is similar to techniques used for angiography. A needle is placed in the abscess cavity, through which a 0.035-in. guidewire is coiled in the abscess cavity.

track is then serially dilated, and the abscess catheter is inserted over the guidewire into the abscess cavity. This technique is slightly more cumbersome when using ultrasound or CT guidance and takes a little more time to perform.

When the catheter has been inserted into the cavity, the abscess cavity contents are evacuated using a three-way stopcock and a drainage bag. A 50-ml luer-lock syringe is attached to the stopcock and the syringe is filled from the abscess cavity and then the pus is flushed into the drainage bag. This avoids possible contamination of the operator and other personnel in the room at the time of the drainage procedure. When the abscess cavity is fully evacuated, the cavity is gently irrigated with sterile saline until the effluent becomes clear. The drainage catheter is then secured and is left to gravity drainage. When the drainage procedure is completed, a repeat CT or ultrasound scan of the abscess is obtained to document complete resolution. At this time any undrained locules should be treated by placing a second or further catheters. It is essential that this last step is performed because otherwise the patient's condition will not improve after drainage.

### 5.4.6.4 Follow-up

Close supervision of patients with abscess drainage is mandatory for best results [17]. In our practice this involves daily rounds on patients with abscess drainage catheters. The amount drained, tubing connections, and the overall status of the patient is checked during these rounds. Decisions are made with regard to repeat imaging or intervention as required. We generally have the catheters irrigated

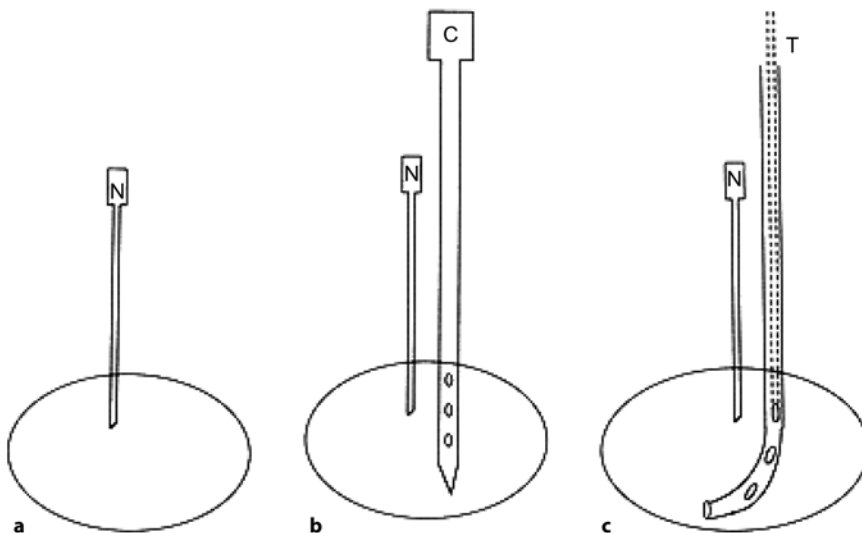


**Fig. 6a–c.** The trocar technique. **a** After planning an appropriate access route, a 20-G needle (N) is inserted into the cavity. Some 2- to 3-ml fluid is aspirated from the 20-G needle to confirm the presence of pus. **b** After adequate skin dissection, the catheter (C) is trocared alongside the needle into the cavity. A “pop” is usually

felt when the catheter enters the abscess cavity. This can be confirmed by removing the central stylet and aspirating pus from the catheter. **c** Holding the central metal trocar (T) firmly, the catheter is then moved forward into the abscess cavity. Lastly, the 20-G needle is removed



with 5–10 cc of sterile saline three to four times a day depending on the viscosity of the abscess cavity contents. If a catheter is not draining, the catheter can be flushed on the ward by a member of the interventional team to ensure that it is not blocked. If the patient remains febrile despite an adequately draining catheter, a search for an undrained locule or another collection should be performed with CT or ultrasound; however, it is important that the interventional radiologist be involved in this decision-making process. This improves relationships with referring physicians and optimises patient care. End points for successful catheter drainage include defervescence, improvement in clinical well-being, decrease in white cell count and daily catheter drainage of <10–15 ml per day. In patients who have a unilocular abscess cavity repeat imaging is not usually performed. If the patient clinically improves, defervesces and catheter drainage decreases to <10–15 ml per day, the catheter is simply removed; however, for more complicated collections repeat imaging is often obtained before catheter removal, and of course if the patient does not improve or indeed deteriorates, repeat imaging is mandatory.

#### 5.4.7 Results of Percutaneous Abscess Drainage

The Society of Cardiovascular and Interventional Radiology Standards of Practice Committee have published quality-improvement guidelines for PAD [18]. Curative drainage is defined as complete resolution of infection requiring no further operative intervention. In general, curative drainage has been achieved in >80% of patients treated by PAD. Partial success (defined as either adequate drainage of the abscess, with surgery subsequently performed to repair an underlying problem, or temporising drainage performed to stabilise the patient prior to surgery) occurs in 5–10% of patients. Lastly, failure occurs in 5–10% and recurrence in 5–10% of patients. These figures represent guidelines for operators performing PAD and were gleaned from the literature [19–30]. Currently collections which are unilocular or situated within parenchymal organs should be successfully drained in over 90% of patients (Fig. 7); however, more complicated collections, such as multi-locular collections, collections with fistulous communications, recent haematomas and pancreatic abscesses, have lower success rates varying from 70 to 80% [26, 31–33].

##### 5.4.7.1 Clinical Applications

###### Gastrointestinal Tract

Percutaneous drainage reduces the morbidity and mortality associated with abscess formation complicating acute intra-abdominal inflammatory processes, namely acute appendicitis, diverticulitis and inflammatory bowel dis-

ease. The surgical management of these complications is complex. Percutaneous abscess drainage in combination with antibiotic therapy promotes the resolution of sepsis prior to definitive surgery. The key to effective management of acute diverticulitis is the early and accurate assessment of the extent of the inflammatory process by CT, as this is the only parameter proven to have a definitive predictive value in the outcome of the disease. Pericolonic abscess formation complicates 35% of patients presenting with acute diverticulitis. The CT facilitates the drainage of pericolonic collections, enhancing the efficacy of antibiotics. Successful spontaneous resolution of the inflammatory process may be achieved in up to 75% of cases; thus, the requirement for emergency surgical intervention is avoided, although interval sigmoid colectomy with primary anastomosis becomes feasible.

High success rates can be anticipated in the management of abscess formation complicating acute appendicitis. Interval surgery is now performed up to 6 weeks following the initial presentation. Percutaneous abscess drainage may also be performed for the management of abscesses complicating inflammatory bowel disease, as a temporising measure prior to definitive surgery.

###### Hepatobiliary Tract and Pancreas

Liver or biliary surgery is the commonest cause of hepatic abscess formation having superseded acute inflammatory conditions such as appendicitis and diverticulitis. Targeted drainage of all intra-hepatic abscesses is recommended as a rapid clinical response can be anticipated. A subcostal or intercostal approach may be taken with fine needle aspiration of smaller intra-hepatic abscesses and catheter drainage of larger collections. The management of larger pyogenic abscesses is controversial. Tan et al. (2005) have recently compared surgical and percutaneous drainage for pyogenic abscesses >5 cm in diameter. In their experience of 80 consecutive patients, surgical drainage provided better clinical outcomes than percutaneous drainage in terms of treatment success, the number of secondary procedures, and hospital stay with comparable morbidity and mortality rates. Similarly, sub-phrenic collections are most commonly surgical in origin. Sub-phrenic collections were traditionally drained through a subpleural or extrapleural approach under ultrasound or fluoroscopic guidance. The author's unit advocates an intercostal approach for the majority of subphrenic collections. The lowest intercostal approach is recommended to reduce the risk of pneumothorax or empyema formation complicating the procedure.

Pancreatic pseudocyst may be complicated by infection or pain. The CT-guided drainage is preferable as the exact anatomical relationship to the surrounding viscera can be displayed. An 8- or 10-F catheter is usually sufficient for successful drainage. A transgastric approach may be used in selected cases, namely where a communication with the pancreatic duct is established or in patients who will not

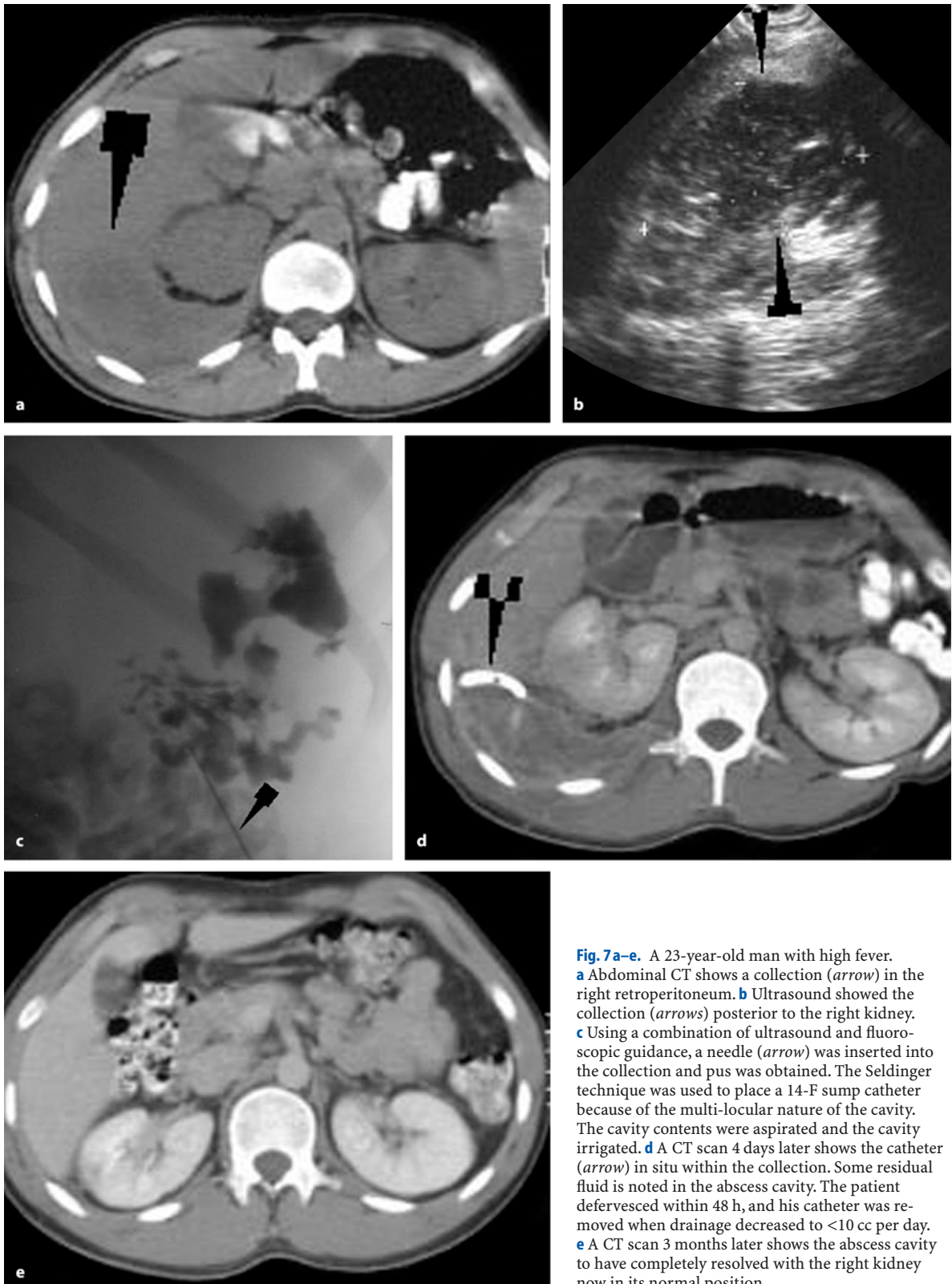


**Fig. 7a–e.** A 23-year-old man with high fever. **a** Abdominal CT shows a collection (*arrow*) in the right retroperitoneum. **b** Ultrasound showed the collection (*arrows*) posterior to the right kidney. **c** Using a combination of ultrasound and fluoroscopic guidance, a needle (*arrow*) was inserted into the collection and pus was obtained. The Seldinger technique was used to place a 14-F sump catheter because of the multi-locular nature of the cavity. The cavity contents were aspirated and the cavity irrigated. **d** A CT scan 4 days later shows the catheter (*arrow*) in situ within the collection. Some residual fluid is noted in the abscess cavity. The patient defervesced within 48 h, and his catheter was removed when drainage decreased to <10 cc per day. **e** A CT scan 3 months later shows the abscess cavity to have completely resolved with the right kidney now in its normal position

tolerate a tube for a protracted period of time. If a communication with the pancreatic duct occurs, drainage for a period of 8 weeks may be necessary. Successful percutaneous drainage of pancreatic cysts can be anticipated in up to 90% of cases.

Acute severe pancreatitis may be complicated by abscess formation necessitating the placement of large (16- to 30-F catheters) for drainage. Acute severe pancreatitis is commonly associated with an ileus making ultrasound-guided puncture difficult. The CT guidance is the imaging modality of choice, whereas fluoroscopy is required for the placement of catheters larger than 16 F. Due to the viscous nature of the abscess, multiple catheters may be required. Interventional radiologists may be required to distinguish between sterile and infected pancreatic necrosis, as the presence of the latter is an indication for emergent necrosectomy. This is achieved by percutaneous sampling of the area of necrosis utilising a 20-G needle under CT guidance. Avoiding the intervening viscera is of paramount importance to avoid the introduction of bacteria into a potentially sterile collection.

### Retroperitoneum and Kidneys

Retroperitoneal abscess formation most commonly occurs in the ilio-psoas compartment and may occur secondary to haematogenous spread, inflammatory bowel disease or seeding from spinal osteomyelitis. Due to the communication between the iliacus and psoas muscle, placement of a 12- or 14-F catheter in the iliacus muscle may be sufficient. Failure of resolution of the psoas abscess necessitates placement of a second catheter under fluoroscopic guidance. Success rates approaching 90% can be anticipated.

Perinephric or perirenal abscesses not responding to antibiotic treatment require drainage and can be placed under ultrasound or CT guidance. Urinomas complicated by infection require drainage. Placement of a nephrostomy is required if there is an obstructive uropathy or there is communication with the collecting system. Success rates of 90% can be anticipated for the drainage of renal or perirenal abscesses.

### Spleen

Previous reluctance to drain splenic abscesses due to the vascularity of the organ has been overcome using CT guidance and careful attention to technique. Transgressing the smallest volume of splenic tissue on the way to the abscess reduces the risk of haemorrhage. Because of splenic vascularity, small-calibre (8–10 F) catheters are used.

### Pelvic Abscesses

Access to pelvic collections requires special consideration due to the anatomy of the pelvis. Access may be accomplished by a transperitoneal, transgluteal, transvaginal or transrectal approach. Deep pelvic abscesses were most commonly drained by a transgluteal route under CT guidance. Localisation using a 20-G needle is performed followed by introduction of a 14- to 16-F catheter into the abscess cavity; however, more recently, transvaginal or transrectal catheter placement is preferred using a high-frequency endocavitary probe. The endocavitary probe is fitted with a 9-F peel-away sheath which is attached to the probe with rubber bands. Following localization of the abscess, local anaesthesia is introduced through the vaginal wall using a 20-G 20-cm (Chiba) needle. Locking 8-F pigtail catheters are introduced into the abscess cavity to avoid displacement. Presacral access may be used for collections in the presacral space using CT guidance with needle placement through the gluteal cleft below the coccyx and directed parallel to the sacrum with the patient positioned prone. The latter access is rarely used.

### 5.4.7.2 Complications

Percutaneous abscess drainage requires careful planning of the access route and close follow-up of the patient following catheter placement. Major complications include septic shock, haemorrhage (Fig. 8), superinfection of a sterile fluid collection and bowel wall transgression requiring intervention. The reported major complication rate varies from approximately 3 to 10% [18, 20–27]. Complications can be prevented by close attention to patient preparation and access route planning. Cover with a broad-spectrum antibiotic is mandatory to reduce the risk of bacteraemia following catheter placement. Once specific culture results have been obtained, specific antibiotic treatment is commenced. Similarly, choosing an access route that avoids bowel helps to decrease the incidence of bowel wall transgression. Additionally, the correction of any bleeding diathesis and avoiding major blood vessels should help decrease the risk of haemorrhage during the abscess drainage procedure. Due to the vascular nature of abscesses, selection of appropriate catheter size is required to reduce the risk of bleeding. Occasionally, placement of a large French catheter is required to achieve haemostasis by tamponade. Emergent embolisation may also be necessary. Delayed catheter complications, such as blockage, kinking or displacement should be identified by daily clinical rounds.

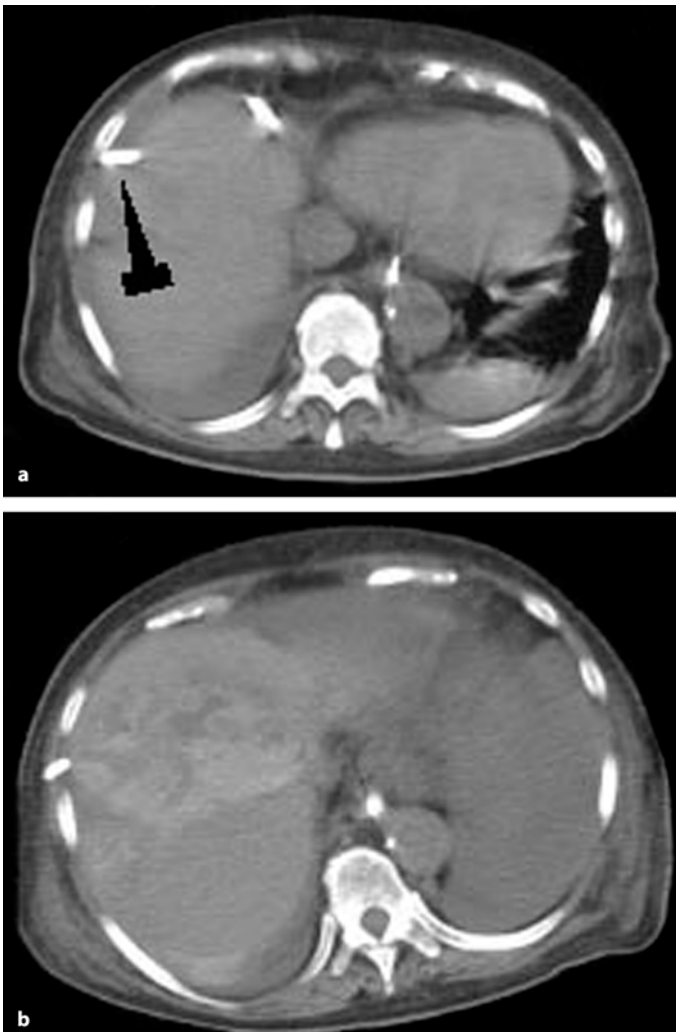


**Fig. 8a, b.** Life-threatening haemorrhage after insertion of a subphrenic abscess drainage catheter. **a** A CT obtained immediately post-drainage shows the catheter (*arrow*) in situ with the cavity completely aspirated. **b** Three days later, the patient developed what was thought to be a pulmonary embolus and was commenced on heparin. After 24 h, the patient suddenly became hypotensive and suffered a haemoglobin drop of approximately 5 g. Repeat CT showed considerable hepatic haemorrhage. It is likely that this haemorrhage resulted from the commencement of the heparin. The location of the haemorrhage was undoubtedly due to the recent catheter insertion

### 5.4.8 Conclusion

Percutaneous abscess drainage has become established as a central component in the management of patients with acute abdominal sepsis. Careful patient preparation, procedure planning and close follow-up enables the interventional radiologist to safely perform procedures which significantly reduce the morbidity and mortality associated with intra-abdominal sepsis. New techniques, such as CT fluoroscopy, are evolving as a useful method for guiding the accurate and safe drainage of abdominal and pelvic fluid collections.

### References

1. Doust BD, Quiroz F, Stewart JM (1977) Ultrasonic distinction of abscesses from other intra-abdominal fluid collections. *Radiology* 125:213–218
2. Doust BD, Thompson R (1978) Ultrasonography of abdominal fluid collections. *Radiology* 3:273–279
3. Korobkin M, Callen PW, Filly RA et al. (1980) Comparison of computed tomography, ultrasonography, and gallium-67 scanning in the evaluation of suspected abdominal abscess. *Radiology* 129:89–93
4. Taylor KM, Sullivan DC, Wasson JF et al. (1978) Ultrasound and gallium for the diagnosis of abdominal and pelvic abscess. *Gastrointest Radiol* 3:281–286
5. Filly RA (1979) Detection of abdominal abscesses: a combined approach employing ultrasonography, computed tomography, and gallium-67 scanning. *J Can Assoc Radiol* 30:202–210
6. Haaga JR, Alfydi RJ, Havrilla TR et al. (1977) CT detection and aspiration of abdominal abscesses. *Am J Roentgenol* 123:465–474



7. Wolverson MK, Jagannadharao B, Sundaram M et al. (1979) CT as a primary diagnostic method in evaluating intraabdominal abscess. *Am J Roentgenol* 133:1089–1095
8. Knochel JO, Koehler PR, Lee TG (1980) Diagnosis of abdominal abscesses with computed tomograph, ultrasound, and In-111 leukocyte scans. *Radiology* 137:427
9. Haaga JR, Alfidri RJ, Havrilla TR (1977) CT detection and aspiration of abdominal abscess. *Am J Roentgenol* 128:465
10. Dorbrin PB, Gully PH, Greenlee HB, Freeark RJ, Moncada R, Churchill R, Reynes C, Henkin R (1986) Radiologic diagnosis of an intraabdominal abscess. Do multiple tests help? *Arch Surg* 121:41
11. Roche J (1981) Effectiveness of computed tomography in the diagnosis of intraabdominal abscess. *Med J Aust* 25:85
12. Carroll B, Sliverman PM, Goodwin DA, McDougall IR (1981) Ultrasonography and Indium 111 white blood cell scanning for the detection of intraabdominal abscesses. *Radiology* 140:155
13. Silverstein W, Isikoff MB, Hill MCMC et al. (1980) Diagnostic imaging of acute pancreatitis: prospective study using CT and sonography. *Am J Roentgenol* 137:497–501
14. Baldwin JE, Wraight EP (1990) Indium labelled leucocyte scintigraphy in occult infection: a comparison with ultrasound and computed tomography. *Radiology* 42:199–202
15. Datz FL, Luers P, Baker WJ, Christian PE (1985) Improved detection of upper abdominal abscesses by combination of 99m Tc sulfur colloid and 111n leukocyte scanning. *Am J Roentgenol* 144:319
16. Muroff LR (1982) Detection of abdominal abscesses with gallium-67 citrate: correlative studies with computed tomography. *Semin Nucl Med* 21:173
17. Goldberg MA, Mueller PR, Saini S et al. (1991) Importance of daily rounds by the radiologist after interventional procedures of the abdomen and chest. *Radiology* 180:767–770
18. Society of Cardiovascular and Interventional Radiology Standards of Practice Committee (1995) Quality improvement guidelines for adult percutaneous abscess and fluid drainage. *SCVIR* 6:68–70
19. Gerzof SG, Robbins AH, Johnson WC et al. (1981) Percutaneous catheter drainage of abdominal abscesses: a five-year experience. *N Engl J Med* 305:653–657
20. Lambiase RE, Deyoe L, Cronan JJ, Dorfman GS (1992) Percutaneous drainage of 335 consecutive abscesses: results of primary drainage with 1-year follow-up. *Radiology* 184:167–179
21. Sones PJ (1984) Percutaneous drainage of abdominal collections. *Am J Roentgenol* 142:35–59
22. Van Sonnenberg E, Wing VW, Cassola G et al. (1984) Temporizing effect of percutaneous drainage of complicated abscesses in critically ill patients. *Am J Roentgenol* 142:821–826
23. Casola G, Van Sonnenberg E, Neff CC, Saba RM, Withers C, Emarine CW (1987) Abscesses in Crohn's disease: percutaneous drainage. *Radiology* 163:19–22
24. Jeffery RB Jr, Federie MP, Tolentino CS (1988) Periappendiceal inflammatory masses: CT-directed management and clinical outcome in 70 patients. *Radiology* 167:13–16
25. Mueller PR, Saini S, Wittenberg J et al. (1987) Sigmoid diverticular abscesses: percutaneous drainage as an adjunct to surgical resection in 24 cases. *Radiology* 164:321–325
26. Lee MJ, Rattner DW, Legemate DA et al. (1992) Acute complicated pancreatitis: redefining the role of interventional radiology. *Radiology* 183:171–174
27. Lambiase RE (1991) Percutaneous abscess and fluid drainage. A critical review. *Cardiovasc Intervent Radiol* 14:143–157
28. Haaga JR (1990) Imaging intraabdominal abscesses and non-operative drainage procedures. *World J Surg* 14:204–209
29. VanSonnenberg E, D'Agostino HB, Casola G et al. (1991) Percutaneous abscess drainage: current concepts. *Radiology* 181:617–626
30. Gazelle GS, Mueller PR (1994) Abdominal abscess: imaging and intervention. *Radiol Clin North Am* 32:913–931
31. Van Sonnenberg E, Mueller P, Ferrucci J (1982) Percutaneous catheter drainage of abscesses and fluid collections: technique, results, and applications. *Radiology* 142:110
32. Lambiase RE, Cronan JJ, Dorfman GS et al. (1989) Postoperative abscesses with enteric communication: percutaneous treatment. *Radiology* 171:497–500
33. Boland GW, Lee MJ, Dawson SL, Mueller PR (1994) Percutaneous abscess drainage: complications. *Semin Intervent Radiol* 11:267–275
34. Tan YM, Chung AY, Chow PK, Cheow PC, Wong WK, Ooi LL, Soo KC (2005) An appraisal of surgical and percutaneous drainage for pyogenic liver abscesses larger than 5 cm. *Ann Surg* 241:485–490

## Non-traumatic Abdominal Emergencies: Imaging and Intervention in Acute Biliary Conditions

Y. Menu, M.-P. Vuillerme

# 5.5

### Contents

5.5.1	Introduction	481
5.5.2	Acute Cholecystitis	481
5.5.2.1	Ultrasonography	482
5.5.2.2	CT and MRI	484
5.5.2.3	Cholescintigraphy	485
5.5.4	Emphysematous Cholecystitis	485
5.5.5	Gangrenous Cholecystitis	485
5.5.6	Perforation of the Gallbladder	485
5.5.7	Mirizzi Syndrome	485
5.5.8	Cholecystostomy	487
5.5.9	Acute Cholangitis	487
5.5.9.1	Ultrasonography	487
5.5.9.2	Computed Tomography	488
5.5.9.3	Magnetic Resonance	489
5.5.10	Emergency Intervention	490
5.5.11	Conclusion	491
	References	491

### 5.5.1 Introduction

Emergency conditions involving the bile ducts and the gallbladder are common radiological challenging problems. Radiology is the standard method for the diagnosis of most situations. In some instances, emergency treatment relies on radiological techniques.

In all situations, a combination of medical, radiological, surgical and endoscopic skills allows the patient to have the benefit of an optimal diagnosis and treatment.

Evaluation of such patients has dramatically changed in recent years. The onset of ultrasonography has been a revolution, but still, the development of CT, and more recently MR cholangiography and endoscopic ultrasonography, has provided additional tools for a better and less invasive diagnosis.

In the meantime, direct cholangiography, percutaneous or endoscopic, is now only dedicated to interventional procedures.

In this article we review the clinical impact of modern imaging in emergency conditions of the gallbladder (acute cholecystitis) and bile ducts (cholangitis).

### 5.5.2 Acute Cholecystitis

Acute inflammatory conditions of the gallbladder is a complication of gallbladder stones in most cases. It is very unusual that a patient with no history of biliary symptoms, such as colic pain, develop an acute cholecystitis. Conversely, <15% of the patients with cholelithiasis experience clinical symptoms and <5% an acute cholecystitis. It may be difficult, from a clinical point of view, to differentiate an acute but regressive attack of pain related to the stone, and acute inflammation. In the first situation, the symptoms disappear within 1 day when treated with anti-inflammatory and antispasmodic agents. In cases of acute cholecystitis, the symptoms are more likely to last longer, and to be resistant to this treatment.

Imaging provides valuable information for several reasons:

1. To ensure the final diagnosis, as up to 20% of patients clinically classified as having acute cholecystitis have another disease that does not require surgery. Conversely, it has been demonstrated that surgery was required in all patients with clearly symptomatic gallstones, even without evidence of cholecystitis, as it is more than likely that an emergency treatment will be necessary within months [1].
2. To prevent the patient from complications in case of delayed diagnosis
3. To detect complications such as perforation or gangrenous cholecystitis, which may urge the surgical treatment

In most instances, the surgeon will favour a conservative treatment at the acute phase, and perform delayed surgery. The optimal period seems to be 2 months after the initial inflammatory episode, as the patient may relapse in a less favourable way if surgery is performed beyond this delay

[2]. Recently, laparoscopic surgery has gained acceptance, and it is critical for the surgeon to rule out the indication for open surgery, on the basis of imaging methods. Endoscopic surgery is so safe that it has been proposed to perform cholecystectomy within the 48 h after the onset of acute cholecystitis, with a lower rate of conversion than in cases of delayed surgery [3].

Ultrasonography plays a major role in the diagnosis, but other methods may have a significant value in selected cases.

### 5.5.2.1 Ultrasonography

Typical appearance of acute cholecystitis is well known. Usually, in association with gallstones, a combination of wall thickening, intraluminal sludge and sonographic Murphy's sign is observed (Figs. 1, 2); the latter seems to be the most reliable symptom. The definition of Murphy's sign is very precise, and should not be misunderstood: pain is provoked by either the transducer or the sonographer's palpation under guidance, in the exact area of the gallbladder. The pain is the same as the spontaneous pain, blocking deep breathing.

Thickening of the gallbladder wall over 3 mm is a common appearance but is, by far, not characteristic of acute cholecystitis, as it is possible to observe such a finding in various conditions such as cirrhosis, acute hepatitis and cavernous transformation of the portal vein. Appearance of a striated thickening, and irregular thickening, has been claimed to be more characteristic for cholecystitis but may not prove valuable as a single sign; therefore, it is mandatory to rule out the other conditions associated with gallbladder thickening and not requiring surgery. Acute hepatitis may mimic acute cholecystitis very closely, and it is advisable to compare the imaging results with biological data, especially the level of transaminases.

Ancillary findings of uncomplicated acute cholecystitis are pericholecystic fluid and gallbladder distension.

Doppler imaging, either colour, power or pulsed Doppler, may show the presence of mural hypervascularization. Power Doppler may be more sensitive in demonstration of "hot spots" within the wall, but still is subjective (Fig. 3).

As most patients are examined on the basis of emergency, it has sometimes been questioned if the younger radiologists would perform as well as experienced radiologists, who are not always available at the time of examination. This has been studied in a series of 50 patients with different gallbladder diseases by Grantcharov et al. [4]. The authors failed to see any statistical difference between the junior radiologist and the senior radiologist for this kind of patient in the detection of gallbladder stones, but there was a statistical difference of appreciation of the wall thickening, and the calibre of the common bile duct. This means that the junior radiologist can reliably identify gallbladder stones, but the advice of a senior radiologist is required in order to assess more sophisticated findings such as the evaluation of the gallbladder wall thickening.



**Fig. 1.** Acute calculous cholecystitis. A large stone is seen in the gallbladder, as well as wall thickening and some amount of sludge. Patient was positive for Murphy's maneuver

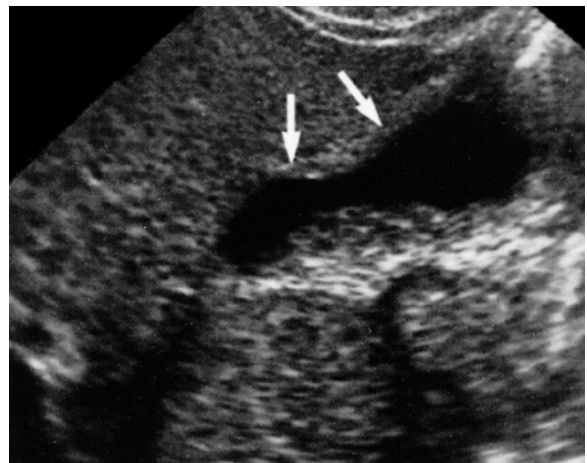


**Fig. 2.** Acute cholecystitis associated with microlithiasis. Wall thickening of the gallbladder is seen (arrows), irregular and less echogenic than in Fig. 1. Large amount of sludge

Acalculous cholecystitis is a common disease affecting trauma patients, and any patient in intensive care unit (Fig. 4). Similar disease, but much less severe, is seen in patients with AIDS. Inflammation of the gallbladder is not related to the cystic duct obstruction by a stone, but it is commonly thought that intravesicular haemorrhage, even moderate, may produce clotting and cystic duct obstruction, favouring infection and inflammatory process. Acalculous cholecystitis is a challenging problem, besides the fact that no stone is seen, because the patients are often in a poor condition, and localized palpation of the abdomen is not very informative. In such cases, percutaneous cholecystostomy may be recommended for diagnosis.

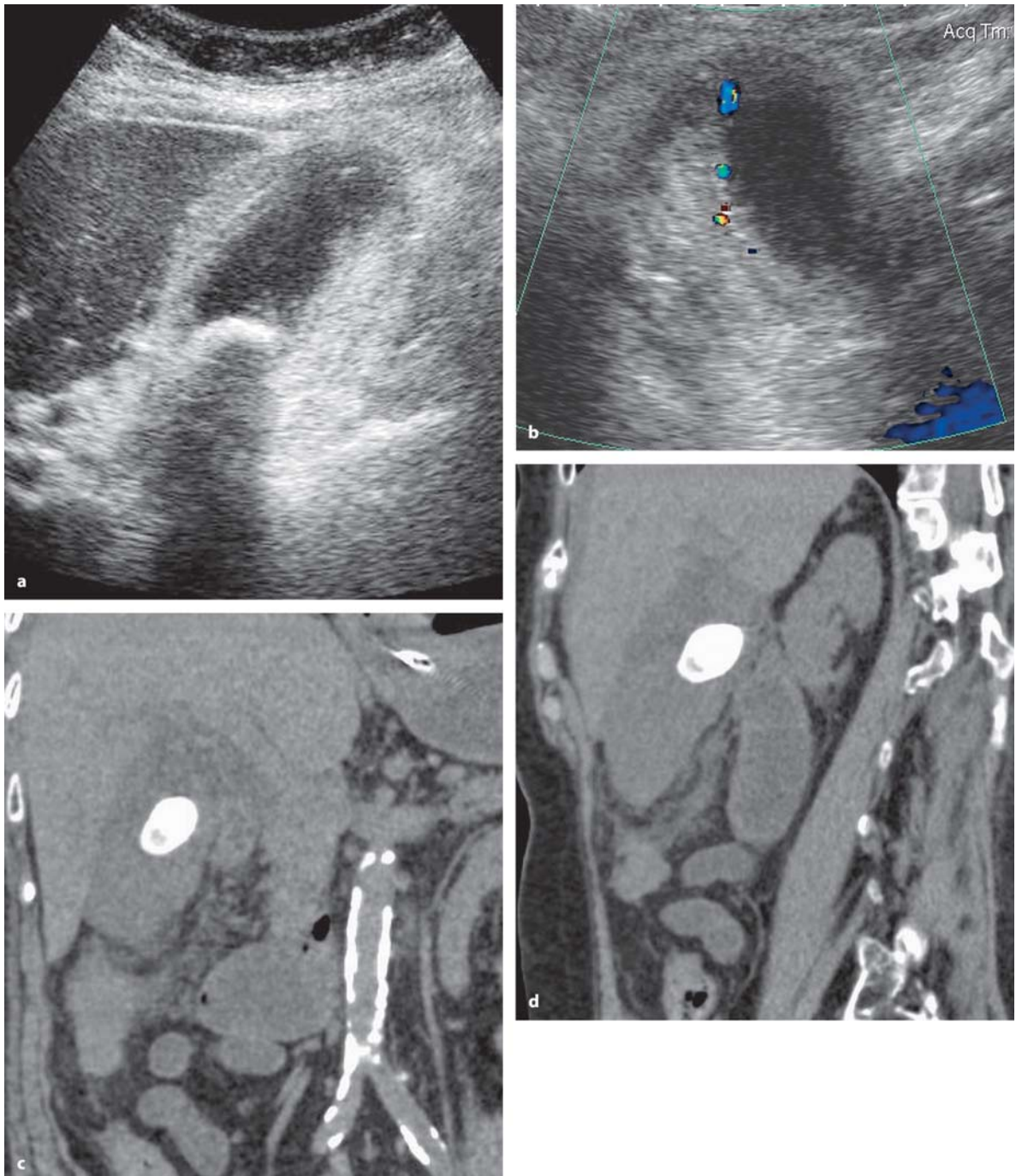


**Fig. 3.** Acute cholecystitis. Ultrasonography, colour Doppler and plain CT. **a** This patient had a common cholecystitis with a gallbladder stone, and marked wall thickening. **b** Colour Doppler shows some vessels in the gallbladder wall, consistent with inflammation

and hypervascularization. **c, d** Oblique reconstructions of thin slices acquired on multidetector-row CT without contrast injection show an enlarged gallbladder, with a large calcified stone, and stranding of the surrounding peritoneal fat, consistent with inflammation



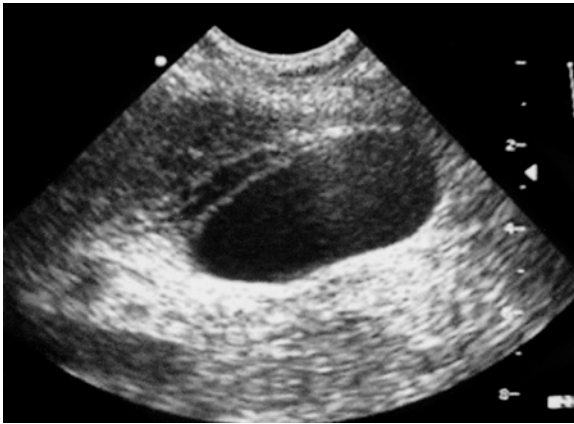


**Fig. 4.** Acalculous cholecystitis in a trauma patient. The gallbladder was distended, and wall was not clearly thickened, but there is some amount of pericholecystic fluid. Murphy's maneuver was negative in this comatose patient. Percutaneous cholecystostomy was performed in order to assess the diagnosis and treat the patient

### 5.5.2.2 CT and MRI

Both CT and MRI add little information to ultrasonography for the diagnosis of acute cholecystitis; both are helpful in cases with subacute presentation, when the palpation reveals a pseudomass in the right upper quadrant, corresponding to pericholecystic inflammation of peritoneum, even in the absence of perforation. In selected cases, the diagnosis between gallbladder cancer and cholecystitis may be difficult. Both CT and MR show an enhancing and smooth inflammatory mass, very different from heterogeneous cancer. A special problem is the so-called porcelain gallbladder (Fig. 5). Extensive calcification of the gallbladder wall may be misinterpreted on ultrasonography as gas in the wall. Mural calcification are known to be associated with a high probability of gallbladder cancer, and then cholecystectomy should be recommended.

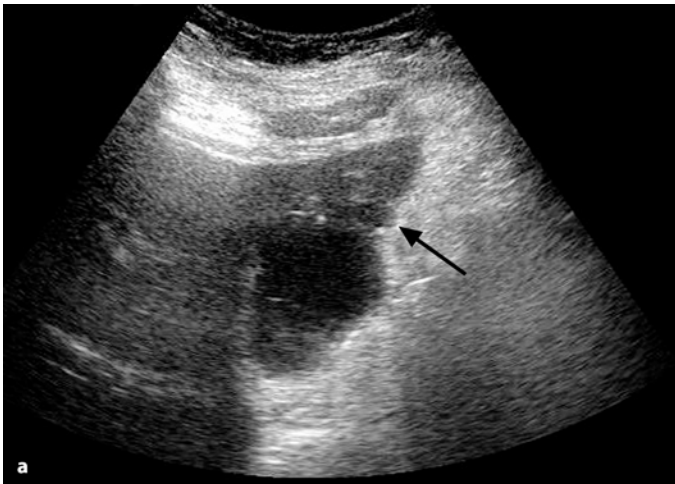


**Fig. 5.** Acute cholecystitis with gallbladder perforation. **a** On Ultrasonography, the gallbladder had a thin wall, and a small fluid-filled area was seen at the lower pole of the gallbladder (*arrow*), but it was difficult to find the relationship with the gallbladder. The patient had peritoneal fluid as well. **b** On contrast-enhanced CT, the gallbladder wall is not thickened but there is a clear disruption in the fundus. Biliary fluid spreads to the subcapsular area, as well as peritoneal space. At surgery, clear perforation of the gallbladder was observed

### 5.5.2.3 Cholescintigraphy

This method is widely used in some countries and completely ignored in others. The principle is to show that the radiopharmaceuticals (diisopropyl-iminodiacetic acid, or DISIDA) fills in the gallbladder within 30 min in normal subjects. In case of cystic duct obstruction, gallbladder will not enhance, even after hours. This very sensitive technique carries a lower specificity, as chronic cholecystitis, and other conditions, such as pancreatitis, hyperalimentation or absence of fasting before the examination, may lead to a similar finding. It is unlikely that cholescintigraphy would become popular in countries where it presently is not used.

### 5.5.4 Emphysematous Cholecystitis

Gas in the gallbladder wall is called an emphysematous cholecystitis. Gas formation is related to the presence of a micro-organism and is the landmark of a severe life-threatening disease. Emphysematous cholecystitis is more common in patients with diabetes mellitus and in older patients.

On sonograms, an echogenic line with ring-down artefacts is seen in some cases; in others, with a larger amount of gas, this line becomes broader and irregular. In very severe cases, the gallbladder may even be very difficult to differentiate from bowel gas, and this may be an advantage of CT [5].

### 5.5.5 Gangrenous Cholecystitis

Gangrenous cholecystitis is a severe form of the disease. It is related to wall necrosis. The perforation of the gallbladder wall is a major and early complication. Sonography is not very specific for the detection of this complication. Gallbladder wall may be thickened or even thinner than a normal wall. In some instances, intraluminal membranes are seen, but this may be difficult to assess. It has been reported that cholescintigraphy may help when it shows a pericholecystic activity. Computed tomography is probably the best method for identification of gangrenous cholecystitis, although sensitivity, specificity and accuracy of CT for acute gangrenous cholecystitis were 29.3, 96.0 and 64.1%, as compared with 91.7, 99.1 and 94.3%, respectively, for acute cholecystitis examined by the same authors [6]. The CT signs in these series were the following: gas in the wall or lumen; intraluminal membranes; irregular wall; pericholecystic abscess; and association with a lack of mural enhancement, pericholecystic fluid, and a greater degree of gallbladder distension and wall thickening.



**Fig. 6.** Porcelain gallbladder. Extensive calcifications are seen in the gallbladder wall. Difference between gas and calcification in the gallbladder wall could be assessed on sonography

### 5.5.6 Perforation of the Gallbladder

Perforation of the gallbladder is now a rare complication, as early treatment reduces its occurrence. Sonography may show intraperitoneal fluid, with sometimes an accumulation in the pericholecystic area, although the presence of pericholecystic fluid is not a synonym for perforation, as this may be observed in simple inflammatory cases without any perforation. Computed tomography is also helpful and may help in the depiction of the perforation. It is stressed that there should not be an additional delay related to imaging because surgical treatment is an emergency (Fig. 6). In rare cases, gallstones are seen outside of the gallbladder, in the peritoneal cavity. A report of two cases have showed that Doppler ultrasonography would be able to depict the perforation as flow signal passing through the perforated site [7].

### 5.5.7 Mirizzi Syndrome

Mirizzi syndrome is a manifestation of the impaction of a gallstone in the gallbladder neck that results in obstruction of the bile duct, causing jaundice and/or cholecystocholedochal fistula. The anatomic arrangement of the cystic duct at the gallbladder neck, such that it runs parallel to the common hepatic duct, leads to the possibility of common duct obstruction by a cystic expanding process such as impaction of a stone. Obstruction of the common hepatic duct is mechanical by the stone itself or by secondary inflammation, causing intermittent or constant jaundice and/or possible recurrent cholangitis. From a clinical point of view, Mirizzi syndrome may present as a tumor in most

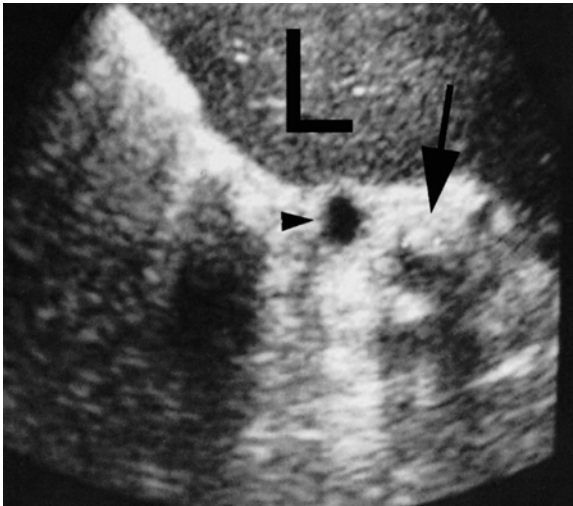


**Fig. 7.** Impacted stone in the gallbladder neck (*arrow*). This is very difficult to detect on sonography as there is no bile surrounding the stone. Posterior shadowing could be overlooked. *Arrowhead* indicates gallbladder infundibulum; *L* segment IV of the liver

cases as slowly progressive jaundice is the main symptom, rarely as an acute disease due to cholangitis. Mirizzi syndrome is very unusual as Johnson et al. were able to retrieve 11 cases among 4180 patients with biliary stones [8]. Diagnosis relies on the identification, either by sonography or CT, of a stone in the gallbladder neck area. Sometimes, inflammation is prominent and it may be difficult to localize the stone in the gallbladder neck or in the common bile duct (Figs. 7, 8). This is very important as the management of Mirizzi syndrome is mainly surgical and not endoscopic. Endoscopic retrograde cholangiopancreatography (ERCP), in these exceptional cases, may nevertheless represent the gold standard for imaging as it delineates the cholecystocholedochal fistula and the intracystic localization of the stone.



**Fig. 8a-d.** Mirizzi's syndrome. **a-c** Enhanced CT showing thickening of gallbladder wall, dilatation of intrahepatic bile duct, inflammatory mass in the porta hepatis, circumscribing the common bile duct. High-density stone is seen in the middle of the inflammatory

mass. **d** Percutaneous cholangiography in the same patient showing the dilated bile ducts, and the extrinsic compression of the common bile duct. Note the dense oval-shaped stone (*arrows*)



## 5.5.8 Cholecystostomy

Surgery, either laparoscopic or open, remains the treatment of choice for acute cholecystitis. In some patients, when surgery would carry a very high mortality, percutaneous cholecystostomy may help the patient to go through the acute phase of the disease. Sometimes, cholecystostomy is used as a diagnostic tool in intensive care patients with inflammation of unknown origin and confusing appearance on ultrasonography. In a series of 55 cases, one hepatic bleeding requiring surgery occurred in 1 patient and dislodgment of the catheter in 9 patients. Fifty-two patients recovered and 31 were able to undergo delayed cholecystectomy [9].

Cholecystostomy may well be the definitive treatment for the disease, especially when the patient condition remains poor. Conversely, in patients who recover, delayed surgery remains the recommendation.

Technique of percutaneous cholecystostomy is simple and may be a bedside procedure in intensive care units, using mobile ultrasonography. Computed tomography may be used as the guidance method as well. The gallbladder is punctured through the liver with a catheter needle (22–18 G). In fact, it has been reported that the bile leakage was not more frequent in patient with a direct transperitoneal approach, but still it should be recommended to go through the liver when possible. A sample of the bile is used for bacteriological studies. Cholecystostomy should remain in the gallbladder for 8–10 days. Cholecystography may be obtained to show the cystic duct patency and the bile ducts. A controversy still exists about the usefulness of early cholecystography through the catheter, but late cholecystography is always useful, especially to check if the cystic duct is patent or not.

## 5.5.9 Acute Cholangitis

Cholangitis is the result of a combination of bacterial colonization of the bile ducts and bile stasis. Most common organisms found in infected bile ducts are *Escherichia Coli*, *Enterococcus* and different other gram-negative coliforms. Although anaerobes are very seldom found in the gallbladder (only in cases of emphysematous cholecystitis), up to 30% of cases of common bile duct stones are associated with such bacteria, especially in older patients. *E. Coli* produces  $\beta$ -glucuronidase which favours deconjugation of the bilirubin in bile. The result is the formation of bile stones with high bile pigment content. Obstruction favours infection, and infection favours stone formation. This is the reason why any chronic bile duct obstruction may be associated with stones. In other words, when there are stones in the common bile ducts, imaging should rule out another cause of obstruction. The normal bile ducts are free of bacteria.

One-third of the patients with bile duct obstruction, and up to 80% of patients with common bile duct stones have bacteria in the bile ducts.

Sepsis associated with cholangitis is usually very severe, due to the general condition of the patients, who are commonly in their seventh or eighth decade, and may have significant associated diseases such as renal failure or cardiovascular disease. Although not yet well defined, it has been established that hyperbilirubinaemia increases the general risk by itself. The serum bilirubin level is also a predictor of the risk of sepsis. It is generally accepted that bile stasis inhibits the anti-toxin effect of the bile salts in the bile ducts and the alimentary tract. Endotoxins, produced by the gram-negative bacteria, may then go in the general circulation and activate an inflammatory response, with several secondary effects such as endothelial cell injury, reduction of blood flow leading to hypotensive shock, deficiency of different immune mechanisms, and changes in platelet function.

The role of imaging in acute cholangitis is essential: diagnosis of bile duct stasis; localization of the obstruction level; and characterization of the obstruction. In emergency patients, common duct stones are the main findings, because the other aetiologies, such as tumour conditions, are usually revealed by a chronic jaundice.

### 5.5.9.1 Ultrasonography

Ultrasonography is the technique of choice for the detection of bile duct obstruction in emergency patients. It may be the only method available for patients in intensive care unit, using bedside examinations. The main application for ultrasonography is the detection of bile duct dilatation. Technically, the examination may be difficult, because emergency patients commonly experience an ileus and abdominal gas distension, which does not favour the examination of the lower part of the common bile duct. Conversely, in most cases, at least the intrahepatic bile ducts are seen and usually the upper part of the common bile duct is also seen. The level of bile duct dilatation is not exactly correlated with the severity, but rather to the duration of the obstruction. It is possible that an acute obstruction may cause cholangitis, and not yet bile duct dilatation. Another possibility is that the obstruction varies, with a ball-valve mechanism. In such cases, the obstruction may not lead to severe dilatation. Nevertheless, these situations are unusual, and it should be remembered that in most cases of cholangitis, a bile duct dilatation is present.

Ultrasonography is able to predict the level of obstruction in 80% of the cases. The ability of ultrasonography to detect common bile duct stones is more controversial (Fig. 9). Sensitivity has been reported to be between 22 and 85% [10].

The reasons for these discrepancies are the biases in patient recruitment and bile duct stone prevalence in the studied population. It is commonly thought that ultra-





**Fig. 9.** Common bile duct stone seen on sonography. The common bile duct was seen until the papilla, allowing the identification of a small stone

sonography detects one-third of the stones. Conversely, specificity is very high, which means that once the diagnosis of common bile duct stones is made by ultrasonography, there is no need for further diagnostic evaluation, unless additional data are required for other abdominal organs.

Detection of stones in the common bile duct is difficult mainly due to the possibility of gastric or duodenal gas preventing the examination of the lower bile duct. Other reasons are the absence of bile duct dilatation, small size of the stones and mild shadowing behind crumbly stones. The only problems with false positives are gas in a parapapillary duodenal diverticulum, pancreatic calcification adjacent to the bile duct and associated with bile duct obstruction of pancreatic origin, and finally some cases of unusual appearance of the right branch of the hepatic artery.

Endoscopic sonography is a recognized method for the detection of common bile duct stones with a reported sensitivity of 94.9%, a specificity of 97.8%, and an accuracy of 95.9% [11].

### 5.5.9.2 Computed Tomography

Computed tomography is not routinely used to assess the dilatation of the bile ducts, due to the accuracy of ultrasonography, but may help in cases difficult to examine with ultrasound, especially in the extrahepatic course of the common duct, and to evaluate the surrounding organs such as the duodenum and the pancreas which are sometimes involved in biliary processes.

The detection of stones in the common duct is better achieved with CT than with ultrasonography, but still the sensitivity is lower than that of magnetic resonance cholangiopancreatography (MRCP). The CT sensitivity is

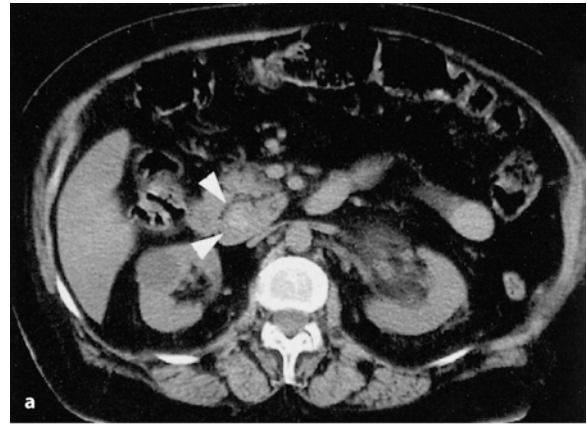


**Fig. 10 a, b.** Patient with a large stone in the lower common bile duct. **a** Unenhanced CT showing a faint hyperdensity in the common bile duct (*arrow*). **b** Enhanced CT: The image could be overlooked for a dilated bile duct without any stone if no reference had been made to the plain CT

usually reported as 70–80%. In a series of 40 patients with endosuspected common bile duct stones, Jimenez Cuenca et al. found 19 stones with ERCP, and 15 of these 19 stones were identified using unenhanced helical CT [12]. As most common bile duct stones are faintly hyperdense, there is no chance to detect them after contrast injection (Figs. 10, 11). Helical CT is helpful as it provides true contiguous and even overlapping slices. Thin slices are useful to avoid the partial-volume effect, but conversely, too thin slices are inadequate to evaluate true density of the stone. A better combination would be achieved with multidetector CT, which allows the reconstruction of a double set of images: Thick slices (6 mm) should be used for density measurements, and thin slices (2–3 mm) for the precise localization of density abnormalities. Reconstruction may help in some instances and are facilitated by multidetector CT and thin slices (Fig. 12). The appearance of stones varies according to the size and content: stone density varies from bile density, then indistinguishable, to calcium density. In most cases calcification is mild and should be carefully exam-

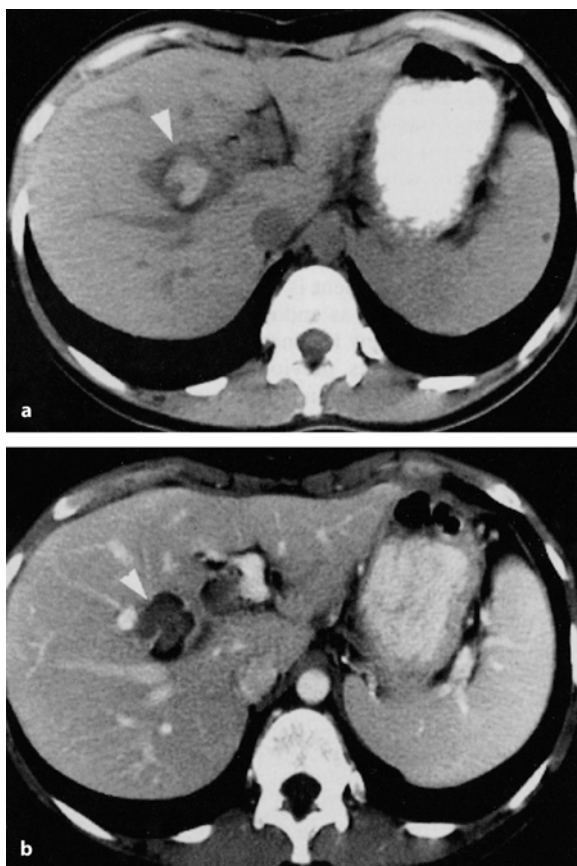


**Fig 11a, b.** Patient with intrahepatic stones. **a** Unenhanced CT showing a calcified intrahepatic stone in the right hepatic duct. **b** After injection, this dense stones is hypodense

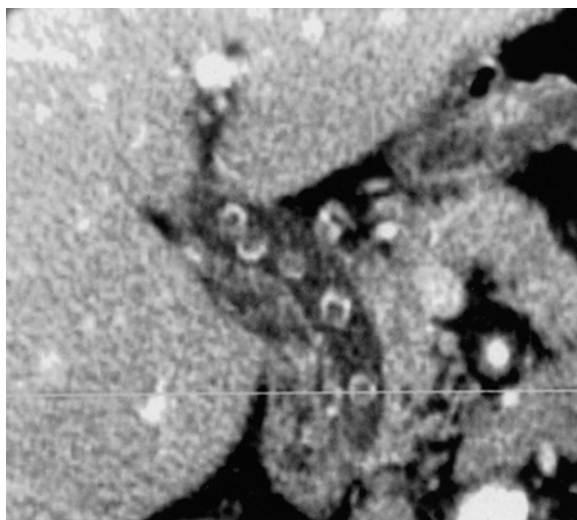


**Fig. 12.** A CT reconstruction through the common bile duct in a patient with multiple stones. This multiplanar reformation has been performed with 3-mm-thick slices and a 1.5-mm reconstruction interval

ined on plain slices. When increasing in size, the stones have a layered appearance, with one or several dense layers, and low-density intermediate layers.

Computed tomographic cholangiography has been claimed to increase CT sensitivity for the detection of stones. In a series of 101 patients with suspected common bile duct stones, CT cholangiography was positive in 21 of 22 proved stones, and no false positive was observed [13]. Despite these results, CT cholangiography has not gained acceptance, because MRCP sensitivity remains better, and biliary contrast injection is not allowed in case of severe obstruction.

### 5.5.9.3 Magnetic Resonance

Magnetic resonance cholangiopancreatography has had a tremendous impact on the management of bile duct diseases, as for the first time, images with anatomical details very similar to those of direct cholangiography were made available with a totally noninvasive procedure. There are varieties of sequences dedicated to MRCP, and still there is no standard protocol. The basis of the examination is that thin slices of the bile ducts should be acquired as well as “cholangiographic” views (usually thick slices in coronal, sagittal, or oblique planes). Most authors favor a combination of bile duct imaging and parenchymal imaging (liver and pancreas) in the same session (Fig. 13). Recently, advances in MRCP with contrast injection have been presented but are not yet accepted in a routine examination.

In a representative series of 51 patients, 26 patients (51%) had stones [14], sensitivity was 65% for unenhanced helical CT, 92% for CT cholangiography, and 96% for MRCP. Specificity was 84% for unenhanced helical CT, 92% for CT cholangiography and 100% for MR cholangiography, the difference being statistically significant. Differences in specificity were not significant.

In a series of 286 consecutive patients [15] MRCP was compared with ERCP, percutaneous transhepatic cholangiography, intraoperative cholangiography and surgical or imaging follow-up findings. Prevalence of stones was 27% in this series. The MRCP sensitivity was 92% and specificity was 97%. Interobserver agreement was excellent with a 0.84 kappa.

These two series are representative of very homogeneous reports from the literature. Pitfalls for MRCP are the following: it is difficult to examine patients with a poor general condition, and especially patients with a systemic shock; aerobilia may be overlooked as stones, if no reference is made to the axial slices (Fig. 14); even if the sequence time is very short, a minimal cooperation from the patient remains necessary. These are a few reasons why not all MRCP examinations are optimal. One last pitfall of MRI is a low availability in many centres, especially for emergency patients. Finally, the main limitation of MRCP is the size of the stones. When smaller than 2 or 3 mm, the prob-

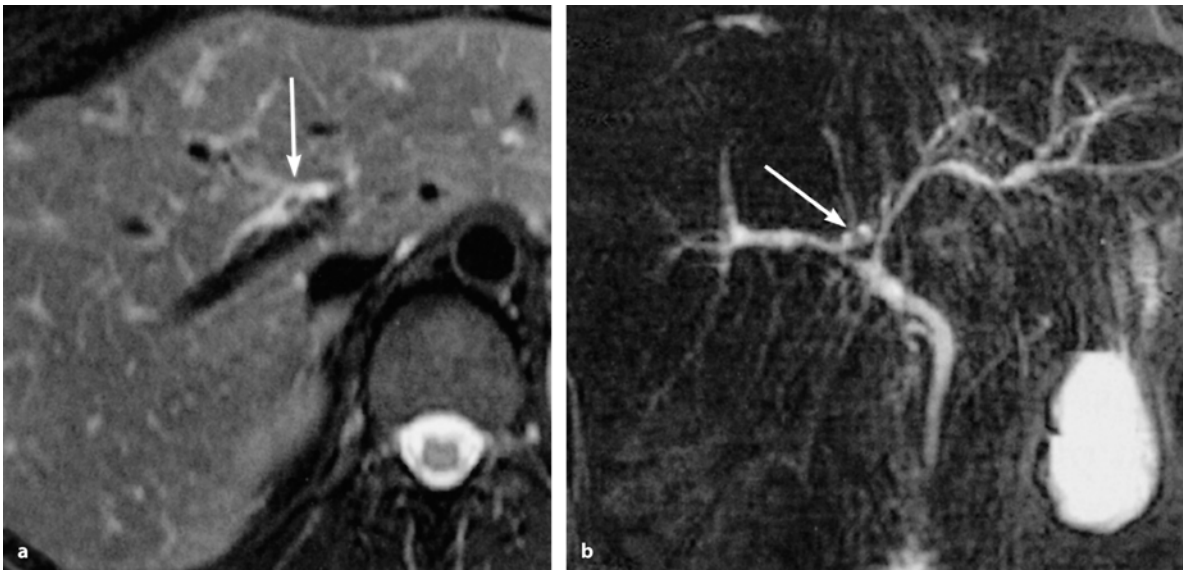


**Fig. 13.** Magnetic resonance cholangiopancreatography showing a very small stone in the right hepatic duct. Combination of axial and coronal slices allows more confidence for the diagnosis of small stones



**Fig. 14.** Patient with aerobilia. Air, like stones, is seen as a black area, with no signal. Axial slices show that the stones lay on the posterior aspect of the common bile duct, as they are heavier than the bile. In this case, there is an air-fluid level

ability to be overlooked is high. Even larger stones, up to 6 mm, may be difficult to detect [16]. Technical improvements may enhance the capability of MRCP to detect small stones, but it is likely that imaging of very small stones will remain a challenging issue.

#### 5.5.9.10 Emergency Intervention

It is very uncommon that cholangitis would require an emergency intervention, percutaneous, endoscopic, or surgical. Treatment includes fluid resuscitation and antimicrobial agents that cover enteric flora. Biliary decompression is required when patients do not rapidly respond to conservative therapy. Definitive therapy can be performed by a surgical, percutaneous, or endoscopic route. Historically, surgery has been the gold standard, but in the past 20 years or so, endoscopic removal of stones has gained wide acceptance. One question was the prevalence of complications of long-term endoscopic sphincterotomy, especially in young patients. In a series of 94 patients less than 60 years old with a mean follow-up of 15 years, late complication rate was 24% [17]. Most of these problems were stone recurrence, and almost all could be treated during a new endoscopic session. These results explain why endoscopy is now the treatment of choice for common bile duct stones, whether it be associated with laparoscopic cholecystectomy or not when gallstones are seen.

Percutaneous treatment is seldom necessary for common bile duct stones, as endoscopic removal is feasible in most cases. In a few instances, when endoscopy is not possible (local variants, previous surgery with biliary enteric anastomosis), percutaneous management is useful. Advantages of the percutaneous route are the following: possibility to perform an associated choledocoscopy, although endosonography and cholangioscopy have similar results [18]; possibility to perform intraluminal lithotripsy or lithotomy; and absence of permanent sphincterotomy. Dif-



ferent techniques should be used to treat the stones. Balloon dilatation of the sphincter will allow to push and flush the stones through the papilla: in a series of 31 patients, the success rate was 87% [19] with a mean treatment time of 16 days. Dormia baskets help to retrieve the stones, as long as they are large enough to be strongly tightened in it. Endocavitary lithotomy or lithotripsy can be performed to burst large stones in smaller fragments with a high success rate [20]. A combination of these different methods may be used according to each situation. In fact, it may be hazardous to compare the results of endoscopic and percutaneous treatment, because the patients referred to the latter have usually been unsuccessfully treated by the endoscopic approach.

### 5.5.11 Conclusion

Imaging methods are necessary for the management of acute biliary conditions. Ultrasonography remains the most simple method, and should always be performed first. At the end of this examination, the radiologist should be able to decide which patients require additional exploration, and to be able to choose between CT and MRCP, and in some instances endosonography. Intervention is seldom necessary during the first hours, but it may be critical in the integrated management of these patients in general with endoscopist and surgeon.

### References

1. Cheruvu CV, Eyre-Brook IA (2002) Consequences of prolonged wait before gallbladder surgery. *Ann R Coll Surg Engl* 84:20–22
2. Cameron IC, Chadwick C, Phillips J et al. (2002) Acute cholecystitis: room for improvement? *Ann R Coll Surg Engl* 84:10–13
3. Madan AK, Aliabadi-Wahle S, Tesi D et al. (2002) How early is early laparoscopic treatment of acute cholecystitis? *Am J Surg* 183:232–236
4. Grantcharov TP, Rasti Z, Rossen B et al. (2002) Interobserver agreement in ultrasound examination of the biliary tract. *Acta Radiol* 43:77–79
5. Konno K, Ishida H, Naganuma H et al. (2002) Emphysematous cholecystitis: sonographic findings. *Abdom Imaging* 27:191–195
6. Bennett GL, Rusinek H, Lisi V et al. (2002) CT findings in acute gangrenous cholecystitis. *Am J Roentgenol* 178:275–281
7. Konno K, Ishida H, Sato M et al. (2002) Gallbladder perforation: color Doppler findings. *Abdom Imaging* 27:47–50
8. Johnson LW, Sehon JK, Lee WC et al. (2001) Mirizzi's syndrome: experience from a multi-institutional review. *Am Surg* 67:11–14
9. Spira RM, Nissan A, Zamir O et al. (2002) Percutaneous transhepatic cholecystostomy and delayed laparoscopic cholecystectomy in critically ill patients with acute calculus cholecystitis. *Am J Surg* 183:62–66
10. Contini S, Dalla Valle R, Campanella G (1997) Reliability of ultrasound in detecting common bile duct stones before biliary surgery. A retrospective analysis. *Panminerva Med* 39:106–110
11. Palazzo L, Girollet PP, Salmeron M et al. (1995) Value of endoscopic ultrasonography in the diagnosis of common bile duct stones: comparison with surgical exploration and ERCP. *Gastrointest Endosc* 42:225–231
12. Jimenez Cuenca I, del Olmo Martinez L, Perez Homs M (2001) Helical CT without contrast in choledocholithiasis diagnosis. *Eur Radiol* 11:197–201
13. Cabada Giadas T, Sarria Octavio de Toledo L, Martinez-Berganza Asensio MT et al. (2002) Helical CT cholangiography in the evaluation of the biliary tract: application to the diagnosis of choledocholithiasis. *Abdom Imaging* 27:61–70
14. Soto JA, Alvarez O, Munera F et al. (2000) Diagnosing bile duct stones: comparison of unenhanced helical CT, oral contrast-enhanced CT cholangiography, and MR cholangiography. *Am J Roentgenol* 175:1127–1134
15. Boraschi P, Neri E, Braccini G et al. (1999) Choledocolithiasis: diagnostic accuracy of MR cholangiopancreatography. Three-year experience. *Magn Reson Imaging* 17:1245–1253
16. Zidi SH, Prat F, Le Guen O et al. (1999) Use of magnetic resonance cholangiography in the diagnosis of choledocholithiasis: prospective comparison with a reference imaging method. *Gut* 44:118–122
17. Bergman JJ, van der Mey S, Rauws EA et al. (1996) Long-term follow-up after endoscopic sphincterotomy for bile duct stones in patients younger than 60 years of age. *Gastrointest Endosc* 44:643–649
18. Tamada K, Ohashi A, Tomiyama T et al. (2001) Comparison of intraductal ultrasonography with percutaneous transhepatic cholangioscopy for the identification of residual bile duct stones during lithotripsy. *J Gastroenterol Hepatol* 16:100–103
19. Van der Velden JJ, Berger MY, Bonjer HJ et al. (2000) Percutaneous treatment of bile duct stones in patients treated unsuccessfully with endoscopic retrograde procedures. *Gastrointest Endosc* 51:418–422
20. Yoshimoto H, Ikeda S, Tanaka M et al. (1989) Choledochoscopic electrohydraulic lithotripsy and lithotomy for stones in the common bile duct, intrahepatic ducts, and gallbladder. *Ann Surg* 210:576–582





# Imaging and Intervention in Acute Pancreatic Conditions

G. Mansueto, D. Cenzi, A.A. Gumbs, M. D'Onofrio

## 5.6

### Contents

5.6.1 Introduction	493
5.6.2 Pancreatic Infections	493
5.6.2.1 Diagnosis of Pancreatic Infection	493
5.6.2.2 Percutaneous Management of Pancreatic Infection	499
5.6.2.3 Results of Percutaneous Management of Pancreatic Infection	502
5.6.3 Involvement of Adjacent Organs, Structures and Spaces	503
5.6.3.1 Gastrointestinal Obstruction	503
5.6.3.2 Splenic Involvement	504
5.6.3.3 Pancreatic Fistulas	504
5.6.4 Vascular Involvement	510
5.6.4.1 Diagnosis and Embolization Therapy of Arterial Lesions	510
5.6.4.2 Diagnosis and Management of Venous Complications	517
References	519

### 5.6.1 Introduction

Non-traumatic pancreatic emergencies can occur as a consequence of primary pancreatic pathologies (acute and chronic pancreatitis, tumors) or secondary to interventional or surgical therapy.

Acute pancreatic conditions are represented by pancreatic infections, involvement of adjacent organs, structures and spaces, and vascular complications. The role of radiology in the management of these complications is twofold: firstly, it must identify the lesion, diagnose and define the lesion's topographic characteristics; then it must proceed with treatment. Specifically, whenever an interventional procedure is preferable to surgery or when it would optimize surgical results.

In this chapter, all pancreatic complications with "emergency" characteristics are taken into account with the exception of hepatobiliary involvement, which is discussed in a previous chapter.

### 5.6.2 Pancreatic Infections

Infection is the most serious risk factor in patients suffering from pancreatic inflammatory diseases. The early detection of this complication is extremely important, because interventional or surgical rather than medical treatments are necessary (Farthmann 1993).

#### 5.6.2.1 Diagnosis of Pancreatic Infection

Infected pancreatic necrosis, pancreatic abscess, and infected pseudocyst are three different forms of pancreatic infection (Procacci et al. 2002). They differ in etiological clinical and pathological characteristics (Bradley 1993), and this distinction is important as it influences the therapeutic management (Morgan et al. 1997).

#### Infected Pancreatic Necrosis

Infected pancreatic necrosis is defined as infected pancreatic and/or peri-pancreatic tissue (Balthazar et al 1994). It can occur only in those patients suffering from severe acute pancreatitis. Its incidence varies between 30 and 70% (Beger et al. 1997), but 80% of patients affected by acute pancreatitis (AP) die secondary to septic complications following infection of the pancreatic necrotic tissue (Beger et al. 1997; Robinson and Sheridan 2000). Infection is due mainly to Gram-negative bacteria, especially *E. Coli* and *Enterococcus*. Infections from anaerobic bacteria or fungi are much less common (Beger et al. 1997). Contamination is usually due to diapedesis through the colonic wall, whereas hematogenous or biliary infection due to bile reflux in the pancreatic duct is rare (Reber 2001). Infection rates correlate proportionately with the seriousness of the acute pancreatitis, as measured by Ranson's criteria and CT findings. Infection in acute pancreatitis has been reported to be as high as 58% in cases with five or more Ranson's criteria signs (Laws and Kent 2000).

Because infected pancreatic necrosis reaches a peak 15–20 days after the onset of clinical acute pancreatitis (Laws and Kent 2000), it is, therefore, clinically important to

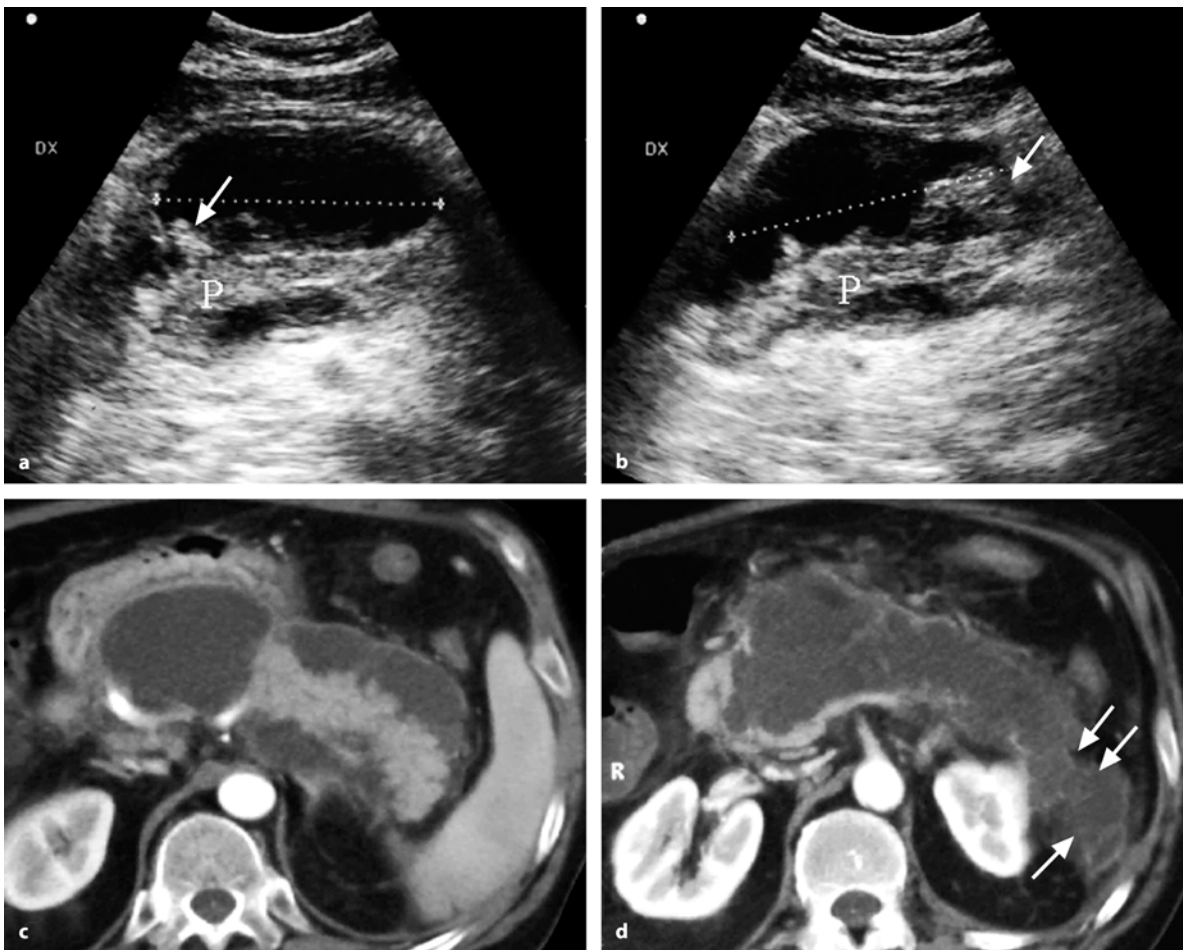


**Fig. 1 a–d.** Infected pancreatic fluid collection. **a, b** Axial ultrasound scans highlight a hypoechoic collection (*calipers*) with necrotic debris (*arrow*) in front of the pancreas (*P*) **c, d** Another case. Computed tomography, in the arterial contrastographic

phase, displays a large collection, surrounding the pancreas and occupying the lesser sac (**c**) and the left anterior pararenal space (*arrows* in **d**). (From Procacci et al. 2002)

suspect it. If the infection sets in earlier, the septic phase superimposes the toxic one so that the two are clinically indistinguishable; however, fever with acute necrotic pancreatitis must lead to the suspicion of infection. A prompt diagnosis is mandatory to prevent septic shock, which is the natural evolution of untreated infection. Septic patients die of multiple organ failure (MOF). The death rate of nontreated infected necrosis is 100% (Lumsden and Bradley 2000).

Ultrasonography can demonstrate the collection (Fig. 1a,b), but the exploration of the pancreatic area is often hindered by intestinal meteorism. A CT exam is the gold standard imaging technique in acute pancreatitis: the collections have an irregular morphology, conform to the anatomic space in which they reside, and frequently cross the lesser sac, the left anterior pararenal space, the transverse mesocolon or the mesenteric root (Fig. 1c,d). False-negative exams are extremely rare: a fluid collection is very seldom misinterpreted as a fluid-filled intestinal loop or as

a dilated gallbladder when located in the latter's area. The CT can indicate the presence and the extent of the necrotic collections, as well as their topographic location (Balthazar 1989; Laws and Kent 2000; Siegel and Sivit 1997). The site and extent of the necrosis correlates with the seriousness of the disease (Kemppainen et al. 1996). The CT shows one or more hypodense collections which do not change after contrast medium administration (Fig. 2a). Infection is suspected only in the presence of gas bubbles within the collections (Fig. 3a,b). Nevertheless, this sign is not pathognomic of this complication, and it occurs in no more than 20% of cases as a consequence of infection due to anaerobic bacteria (Balthazar 1989; Siegel and Sivit 1997; Laws and Kent 2000). Furthermore, the presence of gas related to sterile necrosis has also been reported, even though it is an extremely rare condition (Gandini et al. 1996). A definitive diagnosis of infected pancreatic necrosis can only be obtained by means of needle aspiration (Fig. 3c). When the

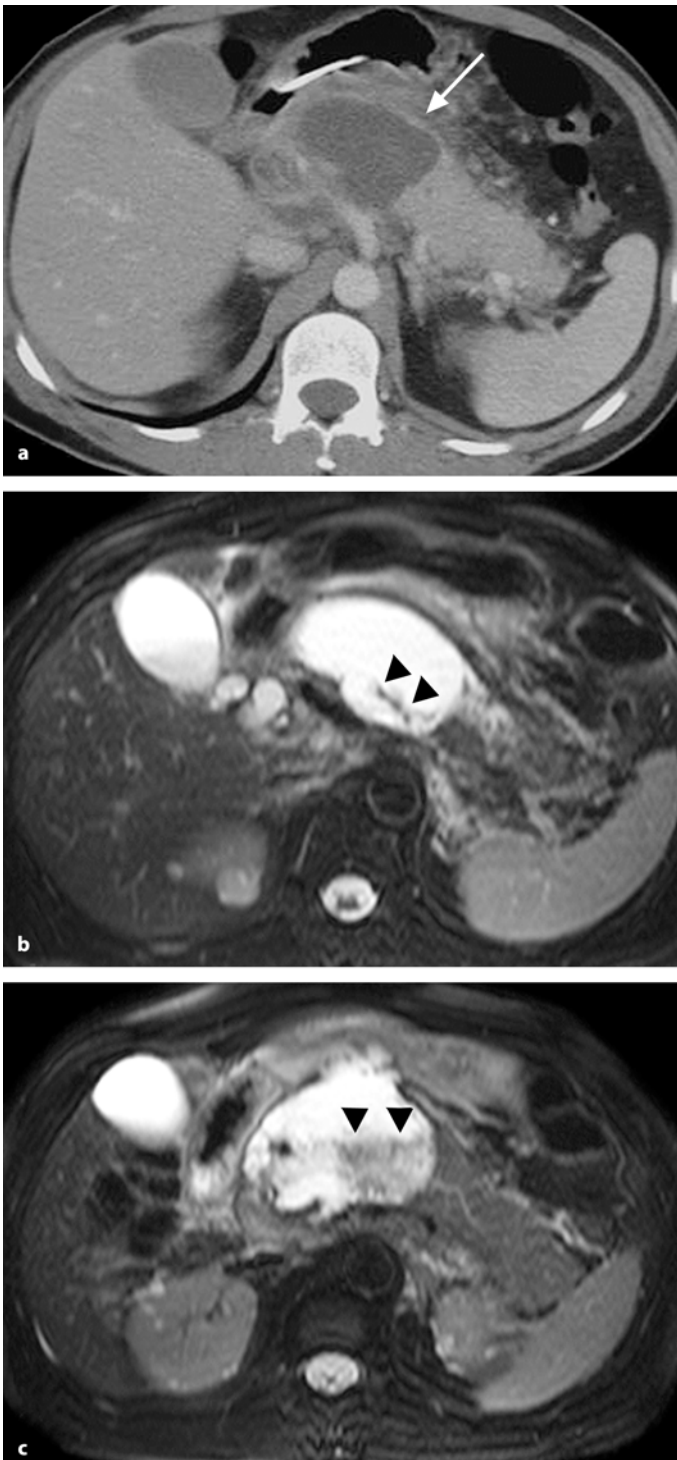


**Fig. 2 a–c.** Infected pancreatic necrosis. **a** A CT scan in the contrastographic phase demonstrates a hypodense area (*arrow*) in the cephalic site, hypovascularized, compatible with necrosis. **b, c** On a T2-weighted MR sequence, it is possible to distinguish the hyperintense fluid component from the hypointense necrotic tissue (*arrowheads*)

purulent nature of the aspirated fluid is not clear, a culture must be carried out (Balthazar 1989; Farthmann 1993; Siegel and Sivit 1997; Apte et al. 1999; Laws and Kent 2000). In order to make a therapeutic decision, it is also necessary

to establish the collection's degree of fluidity. In fact, the presence of necrotic debris or of actual infected parenchymal sequestrations makes surgery necessary, since it is impossible to remove them by means of percutaneous



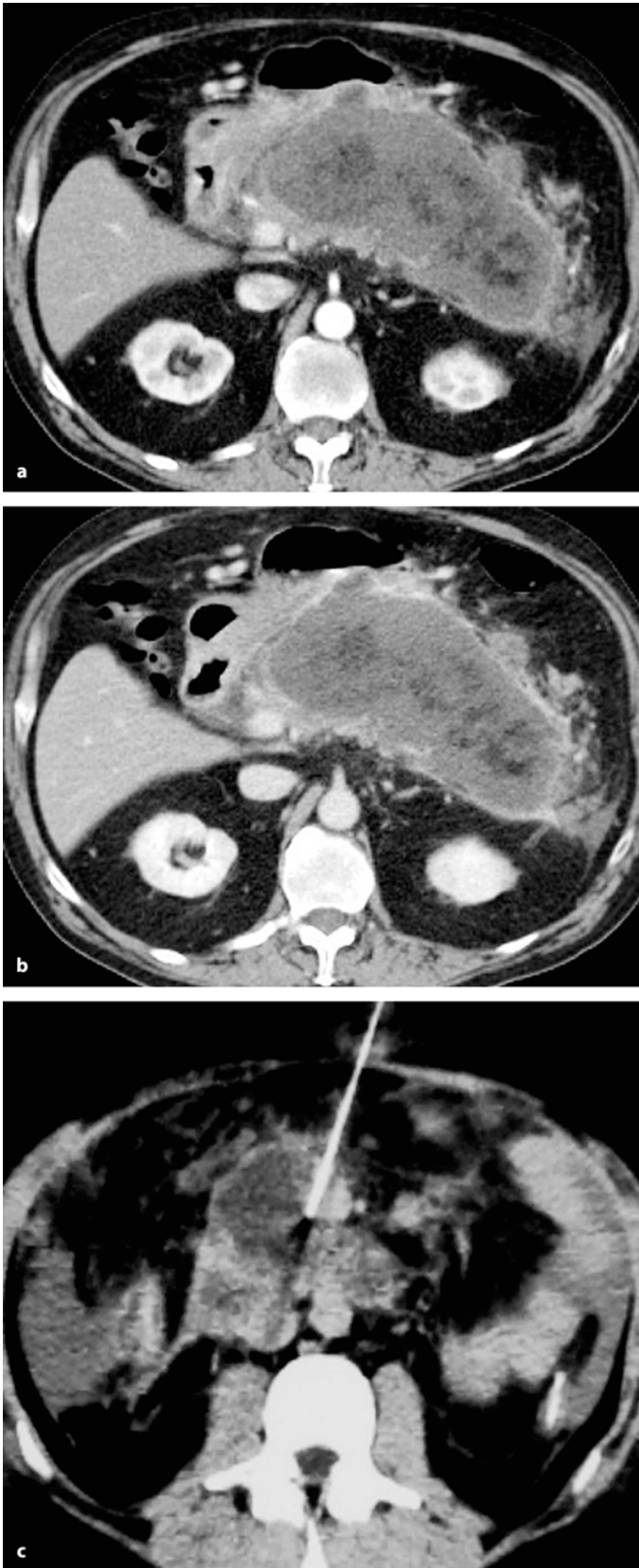


**Fig. 3 a–c.** Infected pancreatic necrosis. **a, b** The CT scans in the contrastographic phase show a large fluid collection occupying pancreatic body and tail. The presence of multiple gas bubbles demonstrate the infection of pancreatic necrosis. **c** Another case. A CT-guided needle aspiration of a small collection without gas, located under the pancreatic head (**c**). (From Procacci et al. 2002)



**Fig. 4.** Pancreatic abscess. A CT scan, in the contrastographic phase, highlights a voluminous mainly liquid hypodense collection bordered by a thin dense capsule; within it, multiple gas bubbles are seen

drainage (Bassi 1994; Rau et al. 1997). Defining the collection's content is difficult with CT (Fig. 2a), whereas it is more easily obtainable with MR (Fig. 2b,c). On T2-weighted sequences it is possible to distinguish the hyperintense infected fluid from the necrotic tissue, which appears clearly hypointense (Morgan et al. 1997).

### Pancreatic Abscess

A pancreatic abscess is defined as a well-circumscribed pus collection that occurs in areas of limited pancreatic necrosis, which has become infected (Farthmann 1993; Siegel and Sivit 1997; Ferrucci and Mueller 2003; Maher et al. 2004). Multiple abscesses occur in about 30–39% of cases. Abscesses can arise as a consequence of acute pancreatitis or pancreatic surgery. It occurs in about 3% of patients affected by severe acute pancreatitis, so that it is much less common than infected necrosis (Bradley 1993).

An abscess secondary to acute pancreatitis probably starts off as infected pancreatic necrosis. The pathogenic agents are mainly of intestinal origin, as in infected necrosis. The progressive necrotic tissue liquefaction leads to the formation of a mainly liquid collection of pus and pancreatic secretion.

An abscess appears later than infected necrosis, usually after the fourth week with fever and leukocytosis (Farthmann 1993; Begger et al. 1997; Siegel and Sivit 1997), and is usually preceded by a period of relative well-being, albeit short.

Computed tomography shows a mainly liquid hypodense collection on the pancreatic gland, outlined by a thin, dense wall (Fig. 4). The differential diagnosis between infected necrosis and the abscess is important, since the latter has a better prognosis and most often can be successfully treated with percutaneous catheter drainage (Morgan

et al. 1997; Siegel and Sivit 1997; Gervais et al 2001). To date, MR is the most reliable investigation in this respect, as it can better characterize the internal consistency of collections (Fig. 3b,c) (Morgan et al. 1997).

The post-operative abscess occurs as a complication of the dehiscence of intestinal or biliary pancreatic anastomoses and has the same imaging features (Berberat et al. 1999; Gervais et al 2001). A pancreatic abscess complicates the post-operative course in 10% of patients who undergo pancreatoduodenectomy. Post-operative abscesses can have a peripancreatic location or develop in the peritoneal spaces, and can be found in the sub-diaphragmatic, sub-hepatic, or pelvic space (Berberat et al. 1999; Gervais et al 2001).

### Infected Pseudocyst

Infected pseudocyst is a collection of infected fluid within a fibrous capsule located in the pancreatic area. The supra-infection of a pseudocyst is an uncommon condition and a high index of clinical suspicion is extremely important for the definitive diagnosis. Most of the patients suffering from infected pancreatic pseudocyst are septic. Pseudocyst can be recognized by ultrasound (Fig. 5a) or CT (Fig. 5b). Diagnosis of infection is possible at imaging if gas bubbles are present in the pseudocyst (Fig. 5c,d). When there are no gas bubbles inside the fluid collection, only fluid aspiration can provide the exact diagnosis.

Pseudocysts can communicate with the pancreatic ductal system. Demonstrating this communication, by means of CT or endoscopic retrograde cholangiopancreatographic (ERCP) examinations (Fig. 6), is important for therapeutic planning, negatively influencing the results of percutaneous treatment (Bradley and Warshaw 1993; Mithöfer et al. 1997).

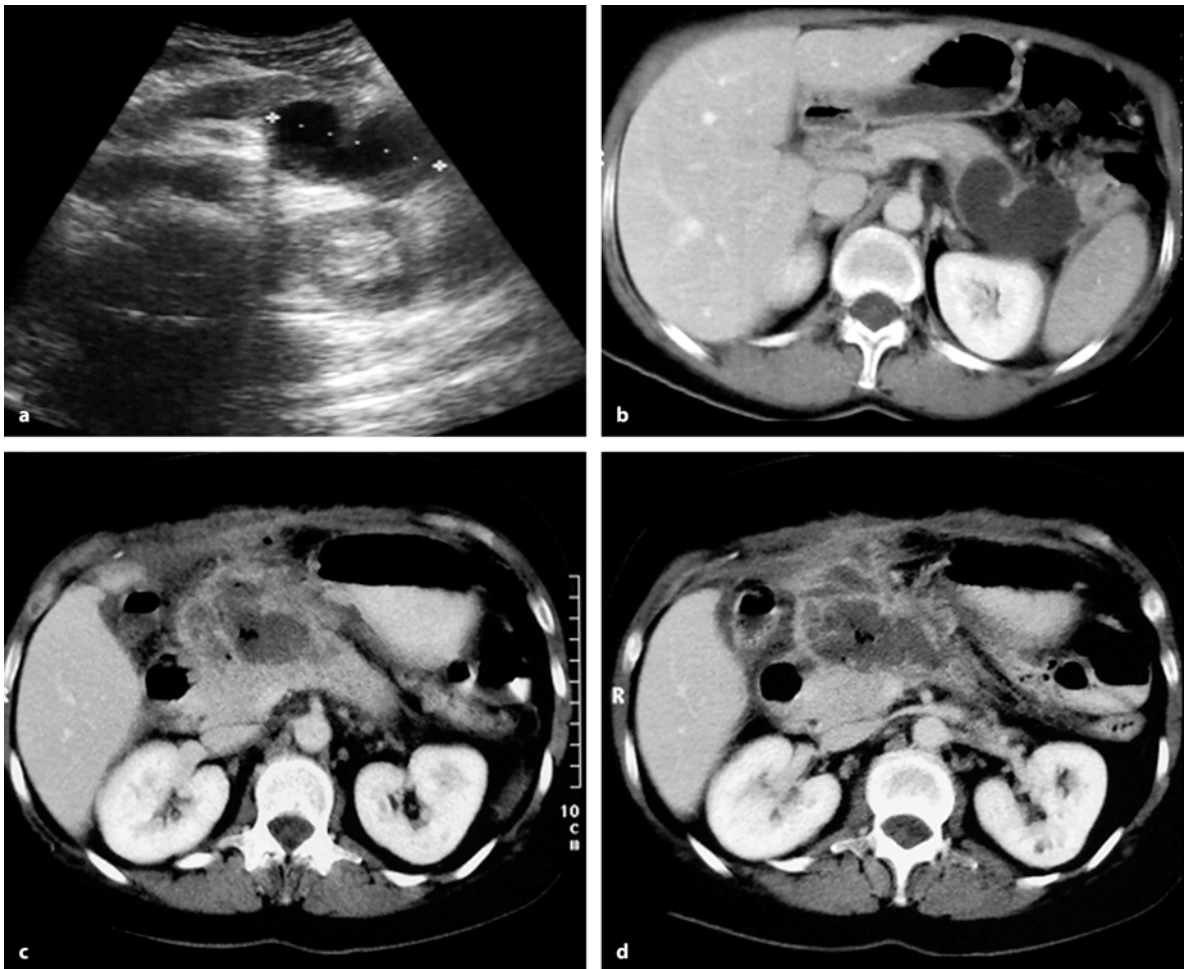


**Fig. 5 a–d.** Infected pseudocyst. **a–b** On axial US **(a)** and CT **(b)** scans, taken at the pancreatic tail level, a bilobed anechoic formation with well-defined margins is seen, delimited by a thin fibrous

wall. **c, d** Another case. On CT scans carried out in the venous contrastographic phase, a large pseudocyst with gas bubbles is present in front of the pancreas. (From Procacci et al. 2002)



**Fig. 6 a–c.** Infected pseudocyst communicating with the main duct. On contrast-enhanced CT scans **(a, b)** a slight dilation of the duct of Wirsung **(arrow)**, and a voluminous pseudocyst of the head

and uncinata process, with thick walls, are evident. An ERCP **(c)** displays the communication between the duct of Wirsung **(arrow)** and the infected pseudocyst **(asterisk)**. (From Procacci et al. 2002)

### 5.6.2.2 Percutaneous Management of Pancreatic Infection

Percutaneous catheter drainage is a well-established interventional option in the management of pancreatic infection. As a general rule, the more infected pancreatic collection contents are viscous and corpuscular, necessitating larger-sized catheters, preferably with a double-lumen sump and large-bore diameter (vanSonnenberg et al. 1991; vanSonnenberg et al. 1997; vanSonnenberg et al. 2001; Ferrucci and Mueller 2003; Maher et al. 2004; Shankar et al. 2004).

#### Infected Pancreatic Necrosis

In cases of infected pancreatic necrosis, surgical “debridement” should be the treatment of choice. Percutaneous approaches should be considered in patients at high surgical risk. It is difficult to completely remove the infected necrotic debris and the parenchymal sequestrations by means of percutaneous drainage (Farthmann 1993; Morgan et al. 1997; Beger et al. 1997; Robinson and Sheridan 2000; Laws and Kent 2000; Ferrucci and Mueller 2003). The treatment must be planned and carried out under CT guidance. At least two collection catheters have to be placed in the most appropriate positions to obtain a combined washout (Fig. 7). The Trocar technique is the best, initially using 8 to 10 F catheters. When the subcutaneous drainage channel has consolidated, it is easier to position larger catheters with the Seldinger technique under fluoroscopic control (Fig. 8). The size of the catheters used varies from 20 to 24 F (Lee et al. 1998), up to 30 F (Fig. 9a,b) (Balthazar et al. 1994). The “debridement” procedure typically needs a great deal of washout fluid. A long-term aftercare catheter drainage follows with frequent irrigation, periodic debridement and strict monitoring of the catheter output (Freeny et al. 1998; Echenique et al. 1998; Ferrucci and Mueller 2003; Shankar et al. 2004; Maher et al. 2004); however, even with several large-sized catheters, further debridement and scrupulous aftercare catheters, the necrotic component is always difficult to remove completely and the necrotic debris often perpetuates the infection and hence the septic condition. Early studies in selected patients have shown promise using percutaneous basketing (or other percutaneous devices such as snares and forceps) and mechanical removal of solid debris to treat necrosis. Clinical success rates have generally varied between 40 and 60%, but they require refinement and evaluation in larger patient populations before they can be widely used in clinical practice (Shonnard et al. 1997; Carter et al. 2000; Maher et al. 2004; Shankar et al. 2004). For this reason, both the surgical and radiological literature are in general agreement that surgical debridement is the best treatment modality

(Lee et al. 1998; Laws and Kent 2000). However, the percutaneous approach is awarded an important additional role, since, when used as a first step, it can make the subsequent surgical “debridement,” if required, definitive (Baril et al. 2000).

#### Pancreatic Abscess and Infected Pancreatic Pseudocyst

Percutaneous drainage under the guidance of imaging is highly efficient in the treatment of both pancreatic abscess and infected pseudocyst (Siegel and Sivil 1997; Morgan et al. 1997; Laws and Kent 2000; Robinson and Sheridan 2000). The mainly fluid content and the fact that this lesion is frequently solitary explains the great clinical success of this procedure. Percutaneous drainage can be carried out under US or CT guidance (Berberat et al. 1999), although CT is usually preferable, especially where deep lesions are concerned (Fig. 9c,d). On the whole, the shortest and most direct access route to the pancreas is preferable, avoiding involvement of the neighboring structures. When going through a viscus is inevitable, the trans-gastric approach is preferable. Positioning of the drain, usually single, can be carried out with the Trocar technique, or, less often, the Seldinger technique (Gervais et al. 2001). The latter is better for positioning larger-sized catheters. Usually, we start with a small catheter, substituting it with a larger one later. The size of the catheters used varies from 12 to 14 F, preferably of the double lumen type (Lee et al. 1998). The timing of catheter removal is decided on by evaluating the drainage parameters (reduction of the output) and the imaging aspects (considerable reduction or collapse of the cavity). Even in the remission period, before removing the drainages, fluoroscopic or CT contrastographic study through the drainages must be performed to detect any communication with the main pancreatic duct. The presence of a connection would considerably increase the risk of relapse (Gervais et al. 2001; Ferrucci and Mueller 2003).

A sample of the fluid is taken during the procedure to assess for the presence of amylase, which would indicate a communication with the duct of Wirsung. The presence and the extent of the communication with the main pancreatic duct have important consequences for the percutaneous treatment. A slight communication with the secondary ducts indicates that watchful waiting may lead to resolution of the lesion, whereas communication with the duct of Wirsung that is associated with a downstream obstruction can lead to the development of an external pancreatic fistula and/or a relapse in the pancreatic collection. In these cases the surgical approach is mandatory (Lee et al. 1998). In treating pancreatic abscess or infected pseudocyst communicating with the main pancreatic duct, the endoscopic approach by means of trans-papillary drainage has been reported (Venu et al. 2000).



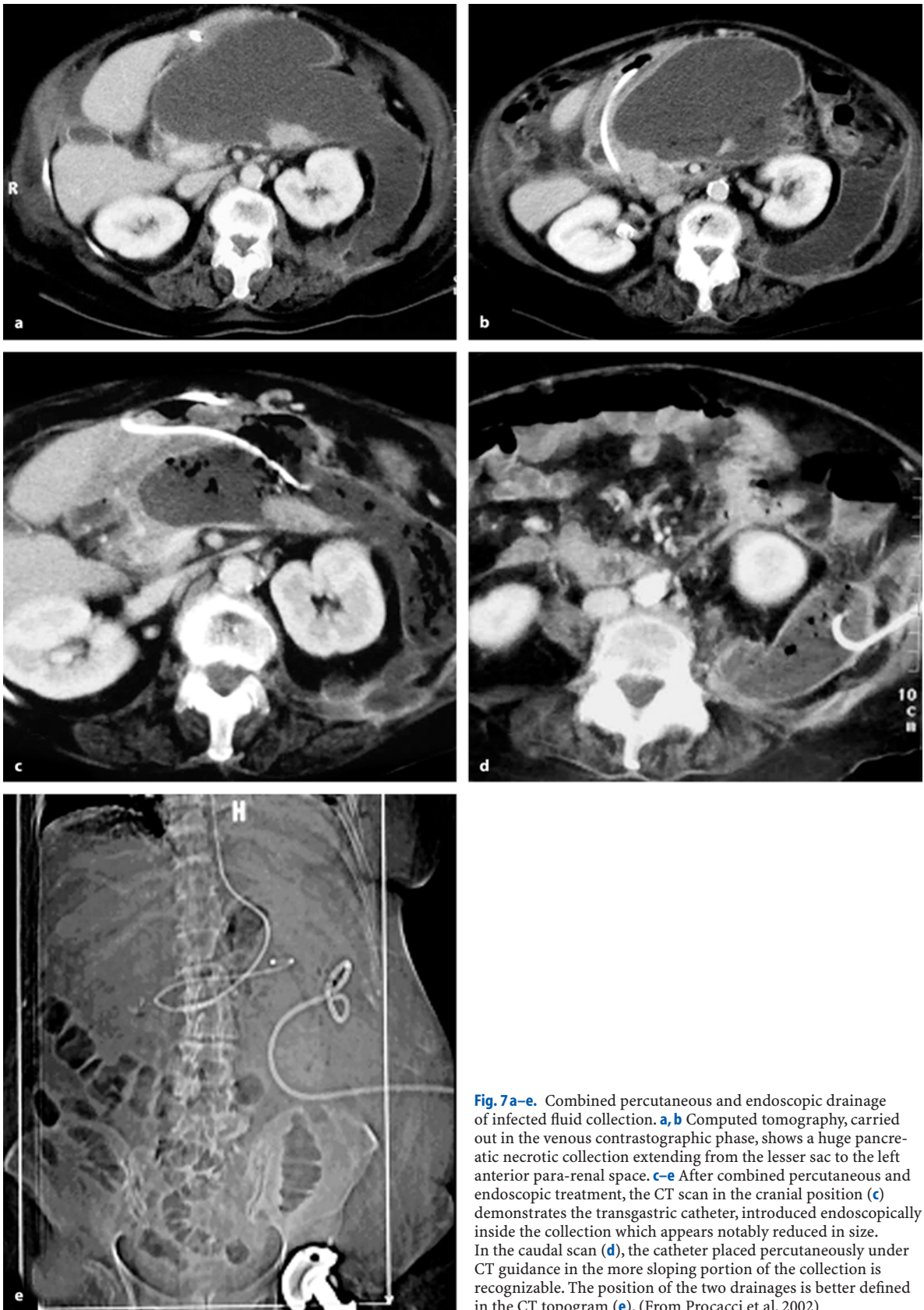


**Fig. 7 a-e.** Combined percutaneous and endoscopic drainage of infected fluid collection. **a, b** Computed tomography, carried out in the venous contrastographic phase, shows a huge pancreatic necrotic collection extending from the lesser sac to the left anterior para-renal space. **c-e** After combined percutaneous and endoscopic treatment, the CT scan in the cranial position (**c**) demonstrates the transgastric catheter, introduced endoscopically inside the collection which appears notably reduced in size. In the caudal scan (**d**), the catheter placed percutaneously under CT guidance in the more sloping portion of the collection is recognizable. The position of the two drainages is better defined in the CT topogram (**e**). (From Procacci et al. 2002)

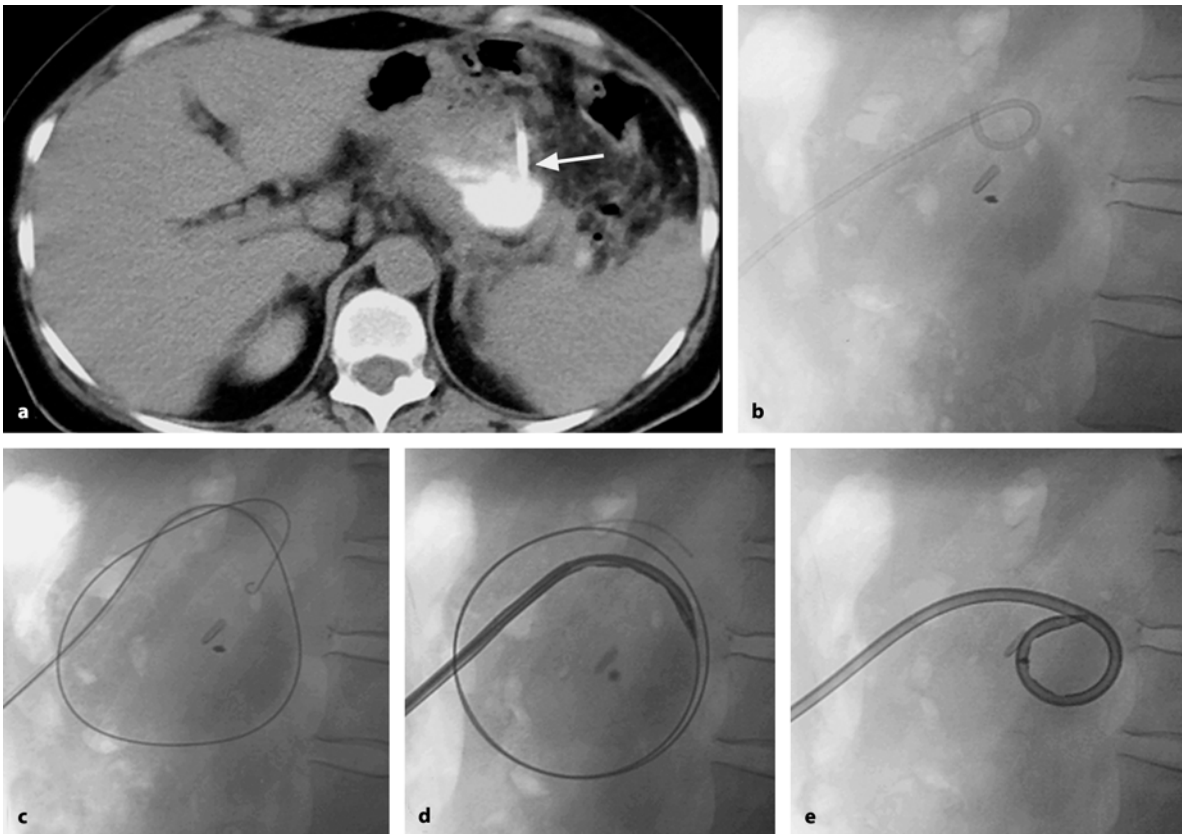


**Fig. 8 a–e.** Percutaneous drainage of pancreatic infection. **a** The CT scan shows percutaneous drainage (*arrow*), of small caliber (8 F), placed under CT guidance in the collection located at the tail of the pancreas. **b–e** Exchange of the drainage positioned under

CT guidance with a larger-sized one (14 F) using the Seldinger technique under fluoroscopic control in the latero-lateral projection. (From Procacci et al. 2002)

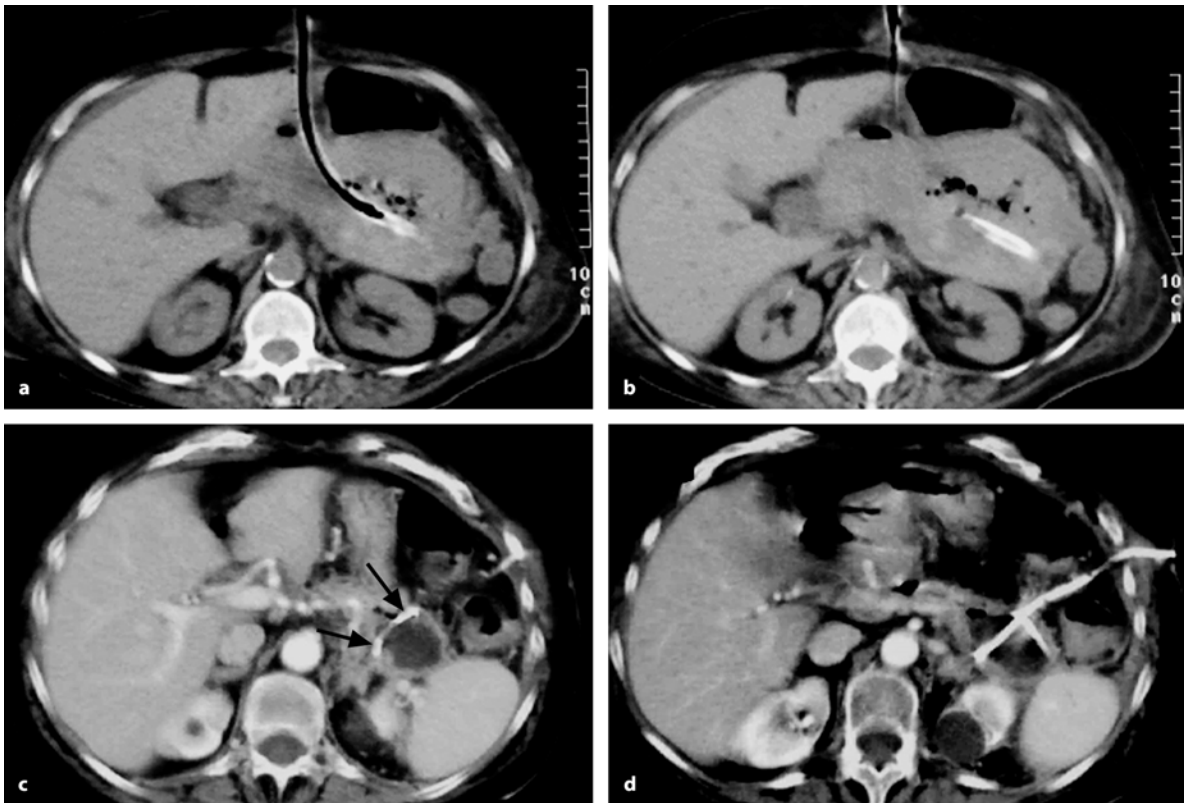


**Fig. 9 a–d.** Percutaneous drainage of pancreatic infection. **a, b** First case. The CT scans show large caliber percutaneous drainage positioned through anterior transgastric access, and with its extremity lodged inside the infected necrotic collection located at the left anterior para-renal space. **c, d** Another case. Computed tomography, in scans carried out in the contrastographic phase, shows infected

pseudocyst of the pancreatic tail in which the distal extremity of the percutaneous drainage is seen (*arrows*). In the more caudal scan (**d**) it is evident that the CT guidance has allowed for the positioning of the drainage through the only possible pathway above the left colic flexure. (From Procacci et al. 2002)

### 5.6.2.3 Results of Percutaneous Management of Pancreatic Infection

The results of radiological treatment reported in the literature vary greatly depending on the different types of lesions treated. The fluidity of the infected contents explains the different success rates reported in the literature. Percutaneous drainage of infected pseudocysts has a clinical success rate of more than 90%, whereas the results for

the percutaneous treatment of pancreatic abscess vary from 32 to 90%, and is <50% in infected necrosis (Table 1). The percutaneous approach under radiographic guidance has a low occurrence of complications (Ferrucci and Mueller 2003). The worst is acute bleeding caused by the loss of the compression that the distended collection had on the arterial and venous vessels involved. Location and treatment of this acute vascular complication is often possible during an angiographic examination, as described later.

**Table 1.** Clinical success rates of percutaneous drainage for pancreatic infection

	No. of patients	No. of necroses	No. of abscesses	No. of pseudocysts	Success (%)
Freeny et al. (1998)	34	34	–	–	47
Carter et al. (2000)	14	14	–	–	86
Steiner et al. (1988)	25	–	25	–	32
Lee et al. (1992)	30	–	41	–	47
Stanley et al. (1988)	14	–	16	–	64
Freeny et al. (1988)	23	–	23	–	65
Adams et al. (1990)	58	–	58	–	79
vanSonnenberg (1997)	59	–	80	–	86
vanSonnenberg et al. (1989)	48	–	–	48	94
Cantademir et al. (2003)	30	–	–	30	96

### 5.6.3 Involvement of Adjacent Organs, Structures and Spaces

Pancreatic inflammatory diseases often involve adjacent organs and structures. The strict relationship of the pancreatic head with the duodenum and the common bile duct, of the pancreatic body with the anteriorly lying transverse colon, the splenic flexure to the left, and of the pancreatic tail with the splenic vessels and hilum explains the frequent involvement of these structures in pancreatic diseases.

#### 5.6.3.1 Gastrointestinal Obstruction

An acute intestinal obstruction, high or low depending on the structure involved, is very rare in pancreatic diseases. Stenosis of the digestive tract with the consequent delayed emptying is more common (Safrit and Rice 1989).

Bowel involvement can occur via a compressive mechanism, usually due to a voluminous collection or pseudocyst (Fig. 10a,b). If the diameter is particularly large, the compression can be marked: in this case, radiology is necessary to not only demonstrate the cause of obstruction, but also to proceed with percutaneous drainage (Fig. 10c,d), as a temporary solution while awaiting surgery.

Visceral stenosis can be a sign of neoplastic infiltration of the viscus, more commonly due to ductal adenocarcinoma or the late complication of a severe AP. In this latter condition, stenosis can occur secondary to the fibrous reaction of the viscus on reabsorbing the fluid collection located in the transverse mesocolon or in the left anterior pararenal space. In the past, diagnosis of stenosis or obstruction was obtained by direct examination of the abdomen (signs of intestinal blockage) and/or with the contrastographic study of the digestive tract. It was possible to show not only the compression due to voluminous masses, but also the nature of the stenosis, whether fibrotic (un-

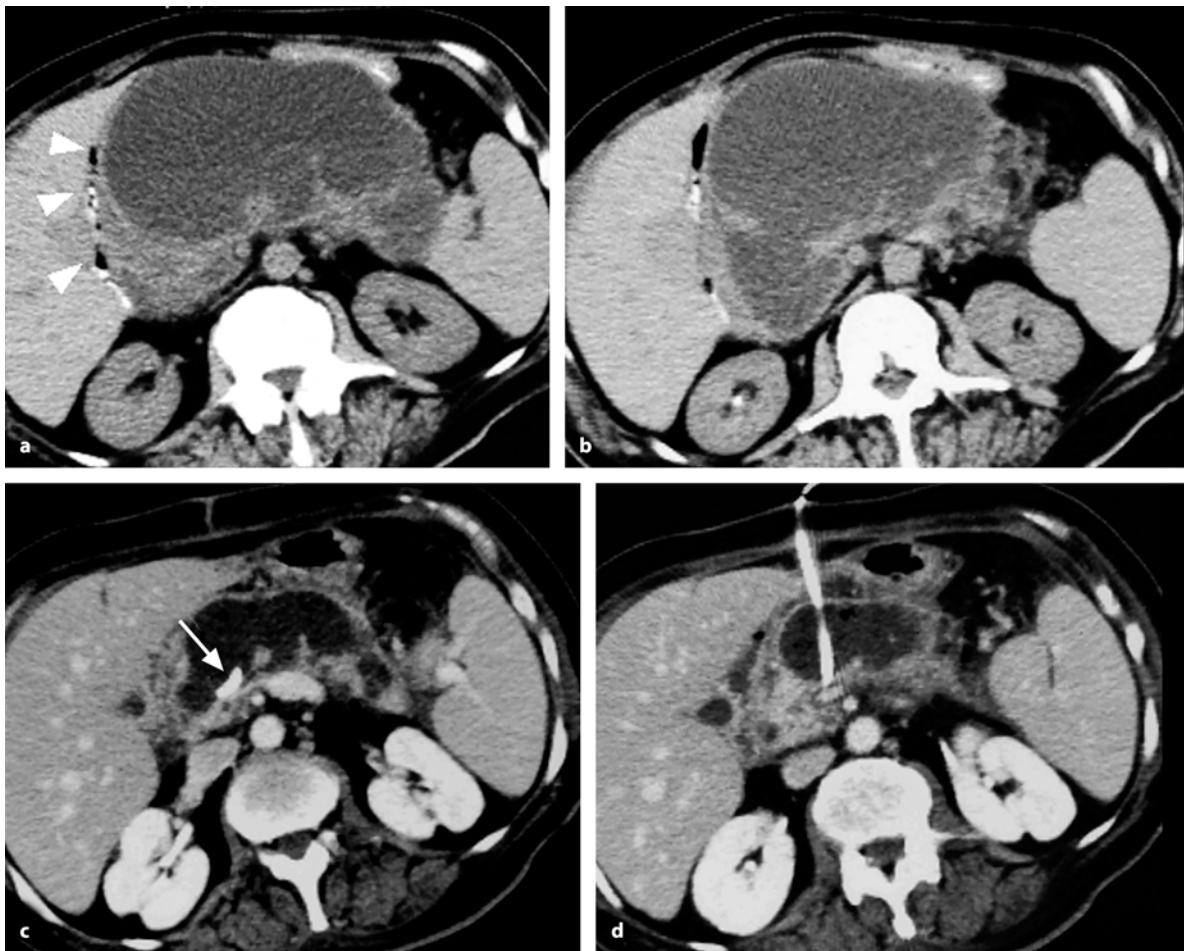


**Fig. 10a–d.** Percutaneous drainage of the pseudocyst responsible for duodenal stenosis. **a, b** The CT scans show a voluminous pancreatic pseudocyst, causing compression of the duodenal route (*arrowheads*). **c, d** The CT scans, carried out after positioning the

percutaneous drainage, show the considerable reduction in volume of the pseudocyst within which the end of the drainage is visible (*arrow*). The drainage runs between the liver and the stomach. (From Procacci et al. 2002)



damaged mucosa) or neoplastic (parietal infiltration). Presently, CT can demonstrate the cause of obstruction and its relationship to the viscus involved.

### 5.6.3.2 Splenic Involvement

During pancreatic inflammatory disease, splenic involvement is rare (from 1 to 5%) and includes intrasplenic pseudocyst, abscess, hemorrhage, infarction and splenic rupture (Fishman et al. 1995). Since these complications can be life threatening, the extent and course of the disease are closely followed up with CT, to determine if, and when, aggressive intervention is necessary to avoid catastrophic clinical outcomes (Fishman et al. 1995). Both mechanisms of splenic involvement in pancreatitis are possible: indirect and direct. Indirect involvement of the spleen may occur either by damage to splenic vessels (vascular involvement) or by lytic action of necrotic hemorrhagic collections on the peritoneal layer of the spleen (Fig. 11). Direct involvement of the spleen is less common (Pistolesi et al. 1987) and occurs through the lieno-pancreatic ligament, which is the only pathway through which both acute and, above all, chronic pancreatic processes directly penetrate into the spleen (Fig. 12a–c).

Intrasplenic pseudocyst is a homogeneous fluid collection at the central or sub-capsular location. Diagnosis is easy with CT, which demonstrates the fluid density (Fig. 12d–f).

Splenic hemorrhage and hematoma arise from erosion by activated pancreatic enzymes of small intrasplenic vessels, preserving capsule integrity. In this case, faced with an ultrasound diagnosis of an intra- or peri-splenic fluid collection, CT and MR immediately demonstrate the hemorrhagic content of the collection (Fig. 13). If the hemorrhage is massive, laceration and capsular disruption may occur.

Splenic rupture results from the erosion of the capsule by activated pancreatic enzymes, and appears with hemoperitoneum. Although small splenic parenchymal lesions, such as small intra-splenic pseudocysts or subcapsular hematomas, probably heal themselves spontaneously, the risk of splenic disruption requires surgery. The early detection of direct splenic involvement is extremely important to determine the need for immediate splenectomy, thus, avoiding hemorrhagic life-threatening complications.

### 5.6.3.3 Pancreatic Fistulas

Fistulas are increasing in incidence as a consequence of the considerable increase in the number of major pancreatic surgical procedures. Furthermore, the improvement in imaging techniques, especially CT, can give the diagnosis or at least the suspicion of pancreatic fistula. This is particularly true for internal fistulas, which often went unrecognized in the past. Pancreatic fistula is not usually consid-

ered an emergency because of the severity of the basic disease (severe AP, ductal adenocarcinoma) or the clinical condition (sepsis), even though it often represents a serious complication. There are also fistulas that can appear acute, such as the pancreo-mediastinal and pancreo-pleural fistulas, characterized by thoracic pain and dyspnea; or the intra-peritoneal fistula, which gives acute abdominal pain and ascites (Cole and Bradley 1992).

Pancreatic fistulas can be distinguished into two different groups: internal and external ones, characterized by different etiological mechanisms and clinical manifestations. The radiological approach to pancreatic fistulas differs significantly when dealing with internal or external ones. Internal fistulas are often an incidental finding at imaging, even though they are characterized by serious symptomatology, whereas external fistulas can be diagnosed by examination of the quantitative and qualitative characteristics of the fluid and require imaging to supply the extension of the lesion (Pistolesi et al. 1992). The therapeutic approach is also different for both cases (Sunderland and Imrie 1992).

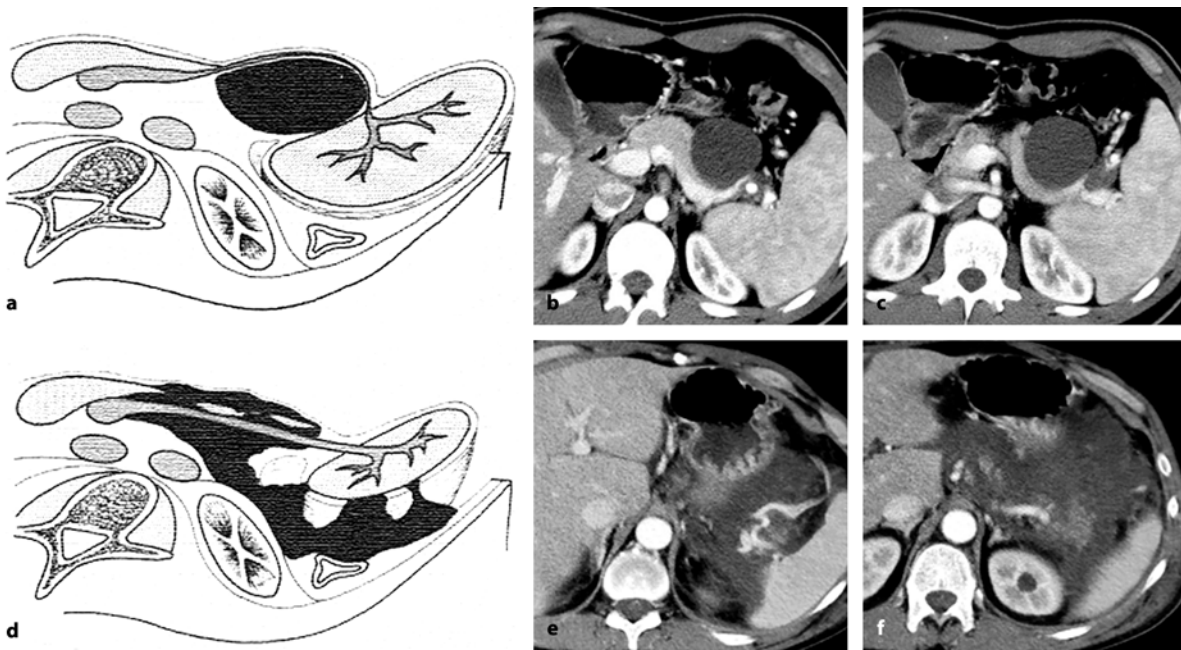
#### Internal Pancreatic Fistula

Internal pancreatic fistula is quite rare and due to the communication of the pancreatic duct with other structures and spaces (Cole and Bradley 1992).

The digestive fistula, pancreato-digestive fistula, is more common. In this case, the proteolytic action of the activated pancreatic enzymes, coming out of the duct or present in a peripancreatic collection, are the cause of intestinal wall erosion. This is sometimes due to necrosis, secondary to inflammatory thrombosis. The pancreato-colic fistula is clinically the worst due to frequent infection and bleeding complications, with a mortality rate of around 50%. On the contrary, the pancreato-gastric or pancreato-duodenal fistula can paradoxically appear with an improvement in the clinical picture (De Baker et al. 2001).

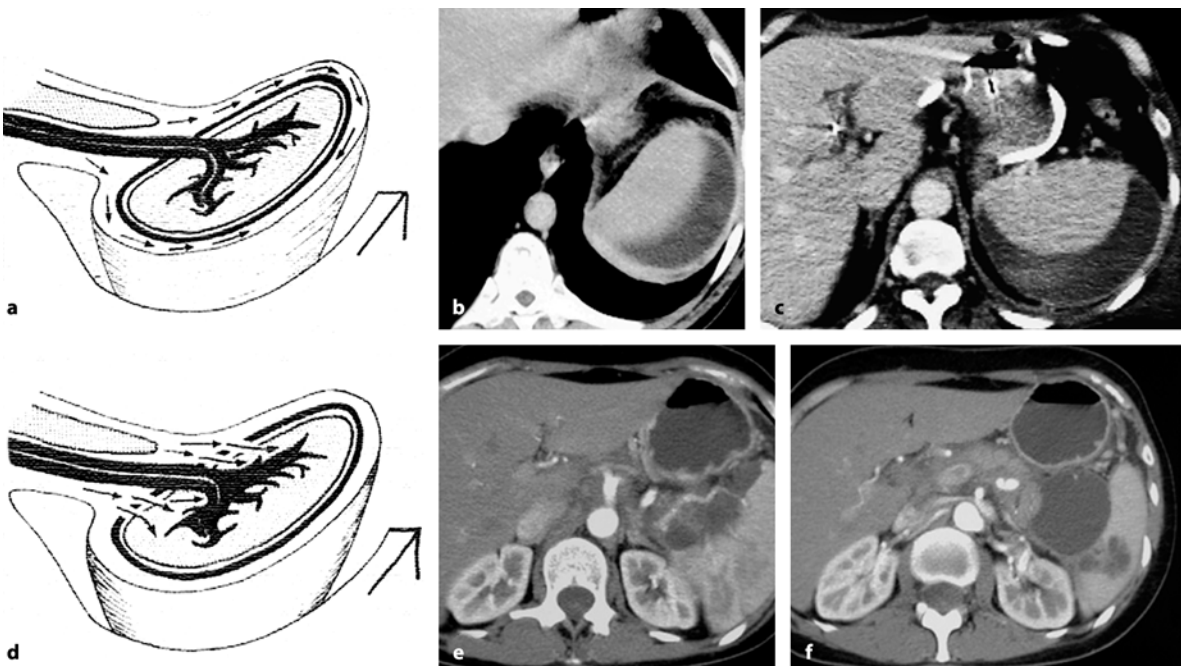
Demonstration of the pancreato-digestive fistula is achievable during a contrast study of the digestive tract. This investigation can be justified by the suspicion of such a complication on the basis of symptoms and, above all, CT recognition of gas in the pancreatic collection (Fig. 14a) in the absence of sepsis (Pistolesi et al. 1992). Currently, diagnostic confirmation with ERCP can be made with MRCP, especially using secretin stimulation, which demonstrates the site of the ductal rupture and eventually the fluid collection and/or the viscus involved (Fig. 14b,c) (Bohlman et al. 1976).

Intra-peritoneal fistula results from the pancreatic collection's erosion through the peritoneal parietal layer and can cause the intra-peritoneal spreading of pancreatic juice (Cole and Bradley 1992), with the appearance of pancreatic ascites. The hepatic origin of ascites can be excluded with paracentesis and amylase dosage (Cameron et al. 1976). At imaging the drastic and sudden volumetric reduction of an intra- or peripancreatic pseudocyst, in the



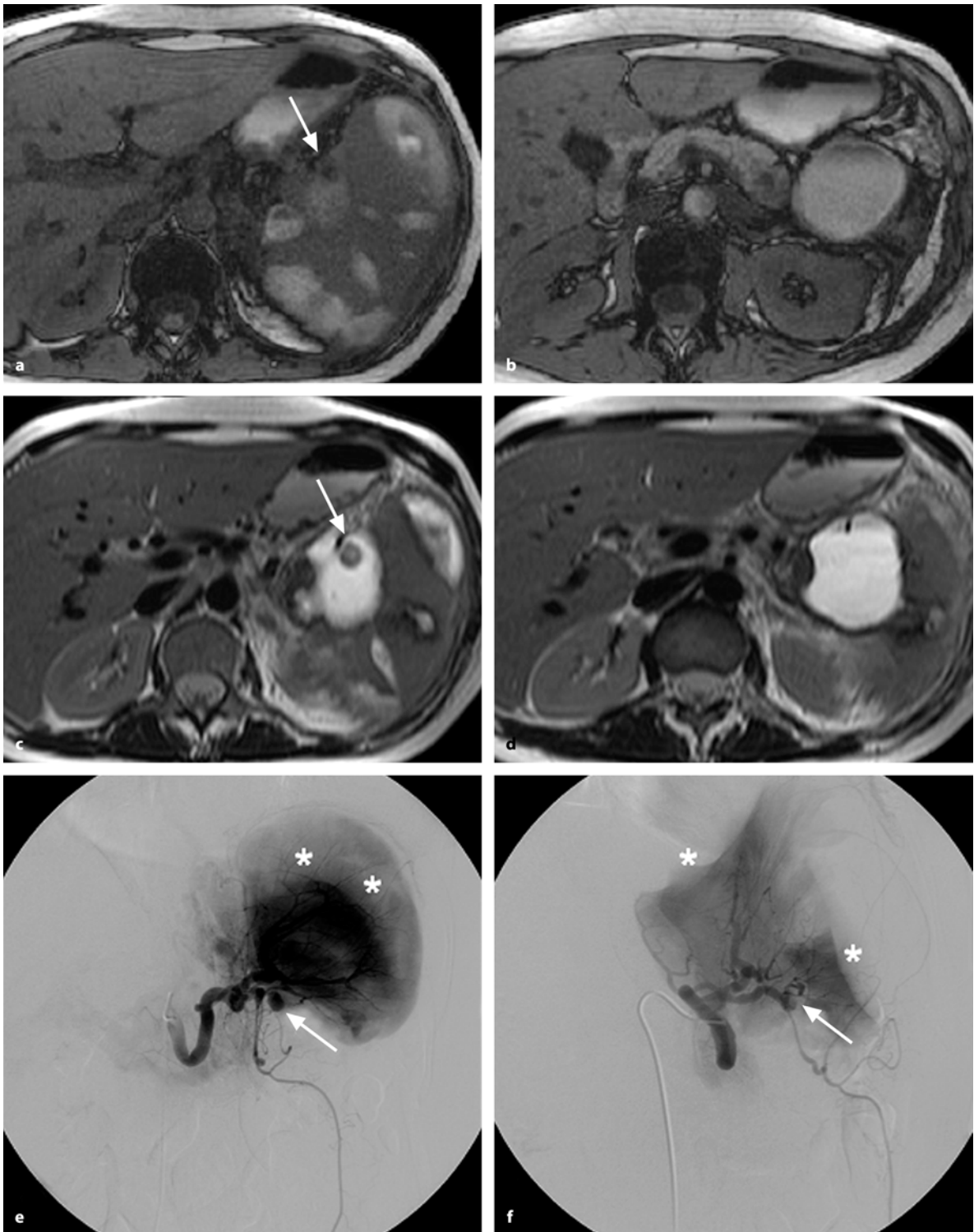
**Fig. 11 a–f.** Indirect involvement of the spleen. **a–c** In the scheme (a) the pseudocyst of the pancreatic tail compresses the splenic vascular peduncle. The CT scans in the arterial contrastographic phase (b, c) highlight a pseudocyst at the pancreatic tail, causing dislocation and compression of the vascular structures of the

hilum of the enlarged spleen. **d–f** In the scheme (d) fluid collection of the pancreatic tail surrounds the splenic vessels. The CT scans in the arterial contrastographic phase (e, f) display a necrotic collection without capsule, involving the splenic hilum and the lower pole of the spleen (a, d–f). (From Procacci et al. 2002)



**Fig. 12 a–f.** Direct involvement of the spleen. **a–c** In the scheme (a) the collection dissects, through the spleno-pancreatic ligament, the visceral peritoneal layer, settling itself in the subcapsular area. The CT scans in the venous contrastographic phase (b, c) show the subcapsular fluid collection. **d–f** In the scheme (d) the collection penetrates the splenic parenchyma through the spleno-pancreatic liga-

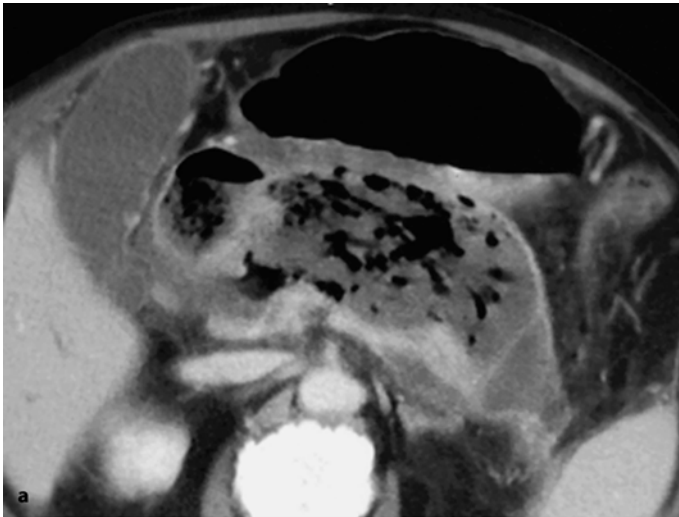
ment, with development of intra-splenic pseudocyst. The CT scans, in the arterial contrastographic phase, highlight a pseudocyst at the pancreatic tail, causing dislocation and compression of the vascular structures of the hilum of the spleen (e). A fluid hypodense collection is inside the spleen, inducing the suspicion of development of an intrasplenic pseudocyst (f) (From Procacci et al. 2002)



**Fig. 13a–f.** Intrasplenic pseudocyst and pancreatic tail bleeding pseudocyst in chronic pancreatitis (same case as in Fig. 12e,f). **a–d** In MR sequences, a pancreatic tail pseudocyst has eroded the splenic hilum creating a voluminous intra- and peri-splenic fluid collection, which appears hyperintense both on T1-weighted fat suppression (**a, b**) and on T2-weighted images (**c, d**). The hyperin-

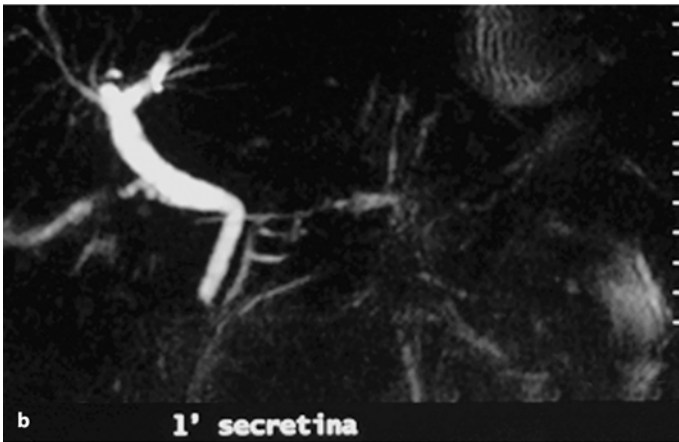
tensity is due to the hemorrhagic content. In fact, the pancreatic tail pseudocyst has eroded the left gastroepiploic artery and has been transformed into a bleeding pseudocyst. The arterial lesion (*arrow*) is clearly highlighted at angiography, which also demonstrates the subcapsular location of intrasplenic pseudocyst (*asterisks* in **e, f**)





**Fig. 14 a–c.** Pancreo-digestive internal fistula.

**a** A CT scan in the arterial contrastographic phase demonstrates voluminous pancreatic collection with gas bubbles in a nonseptic patient, a direct sign of pancreateo-digestive fistula. **b, c** Another case. The MRCP, carried out after secretin stimulation, highlights well the duct of Wirsung 1 min after stimulation (**b**), and the colon at the splenic flexure level 15 min after stimulation (**c**), confirming the communication between the main pancreatic duct and the viscus. (From Procacci et al. 2002)





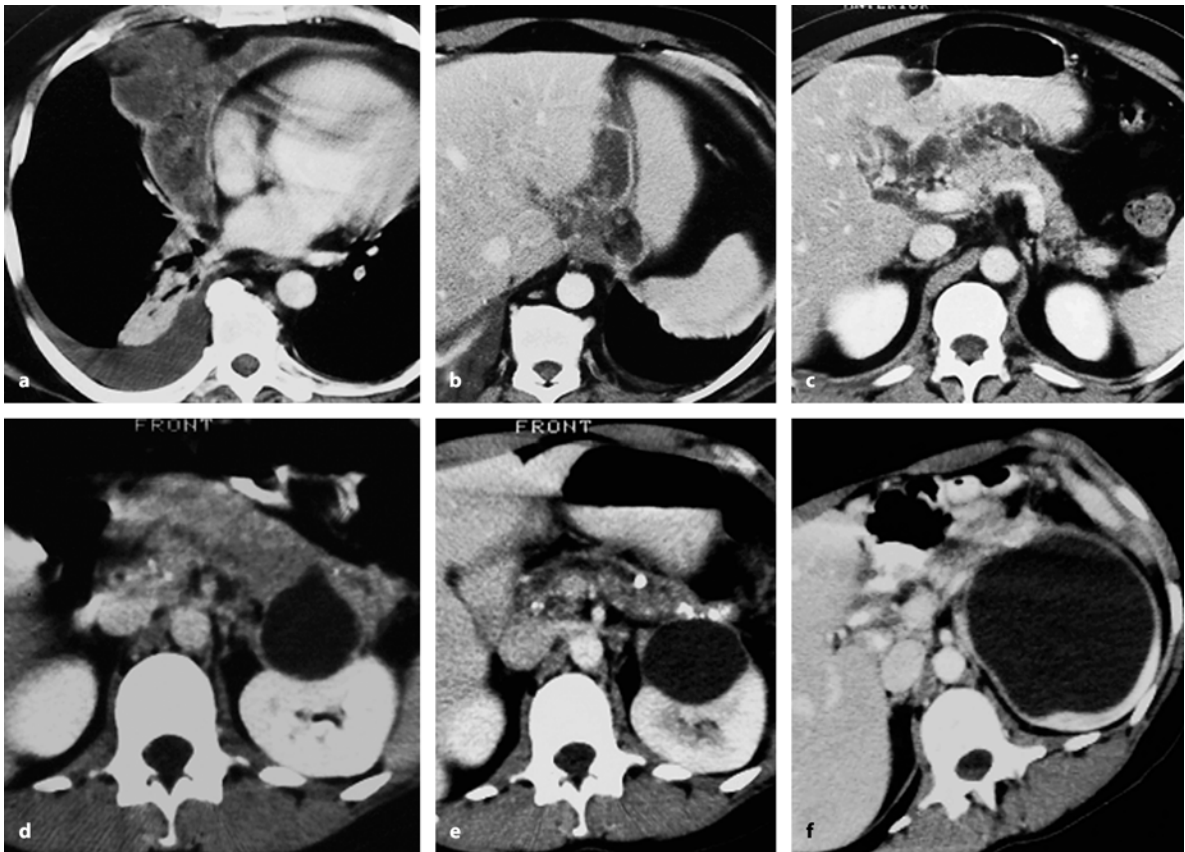


**Fig. 15a-f.** Complicated retroperitoneal internal fistulas. **a-c** Pancreo-pleural fistula. Computed tomography scans carried out in the cranio-caudal direction after contrast medium administration document the presence of pleuritis which assumes a sac-like appearance in the para-mediastinal area (**a**), and the fluid-containing fistulous link situated between the diaphragm (**b**) and the body of the pancreas (**c**). **d-f** Pancreo-renal fistula. A CT scan in the contrastographic phase (**d**) highlights a pseudocyst at the tail of the

pancreas which imprints the kidney; 2 years later, CT scan (**e**) shows the persisting pseudocyst impression on the kidney. There is concomitant dilation of the duct of Wirsung and a large calcification at the body-tail passage. After 4 years, CT (**f**) highlights the kidney's direct involvement with the pseudocyst situated inside the renal capsule and the consequent serious parenchymal compression. (From Procacci et al. 2002)

presence of ascites, should induce the suspicion of an intraperitoneal fistula. The ERCP, when able to directly demonstrate the rupture of the duct of Wirsung into the peritoneum, is definitive for the diagnosis.

Sometimes the fistula can develop in the retro-peritoneum. The retroperitoneal fistula can involve the kidney, the ureter or the psoas muscle. During its development, it can go back and up reaching through the esophageal or the aortic hiatus into the mediastinum (Fig. 15a-c). At this level pancreatico-mediastinal fistulas and mediastinitis can set in with catastrophic complications when the pancreatic enzymes are activated (Pistolesi et al. 1978; Alexander et al. 1982). Pseudocyst or erosion into the esophagus or the pericardium is also possible (Procacci et al. 1987). Erosion of the parietal pleura - pancreatico-pleural fistula - more commonly causes pancreatic pleuritis (Fig. 16a), which can be the cause of acute dyspnea in relation to the massive effusion. Much more rare is the erosion into the visceral

pleura with the onset of a pancreatico-pleuro-bronchial fistula (Iglehart et al. 1986).

Small retroperitoneal fistulas can be found by chance at CT examination required to define the cause of acute pain; US diagnosis is much more difficult. The lesion, constantly refilled, can become a pseudocyst. Its rupture can occur in an abdominal organ such as the spleen, the liver, or, more rarely, the kidney, causing a subcapsular collection (Fig. 15d-f) that is often hemorrhagic (Pistolesi et al. 1992). In this case US can highlight the fluid collection, but the lesion's characteristics and their relationship with the pancreatic gland are better documented by CT. In the past, diagnostic confirmation was only obtainable with ERCP, which showed the communication between the duct of Wirsung and the fistula (Pistolesi et al. 1992). Currently, a definitive role in the study of this disease is carried out by MRCP, especially using secretin stimulation, which appears to be alternative to ERCP.

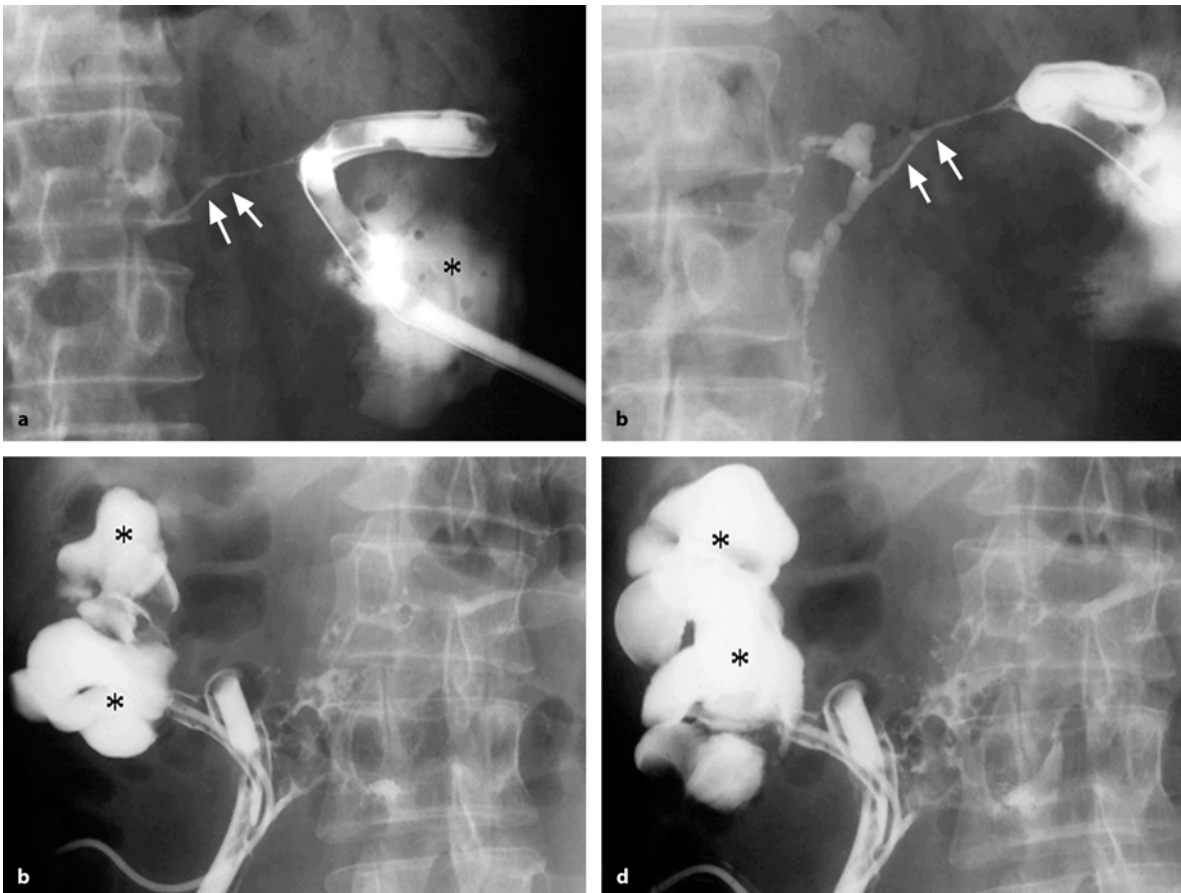


**Fig. 16a–d.** External pancreatic fistula. **a, b** The fistulography by means of surgical drainage highlights the pancreatic collection (*asterisk*), in communication with the pancreatic duct (*arrows*): simple pancreatic fistula. **c, d** Another case. The collection, opaci-

fied through the surgical drainages, is in communication with the right colon (*asterisks*) and the duct of Wirsung: complicated pancreatic fistula. (From Procacci et al. 2002)

There are few reports in the literature which are consistent with the rarity of this pathology (Kay et al. 1997; Fulcher et al. 1999; Materne et al. 2000). Massive pleural effusions can be seen on imaging without being able to define their origin. The diagnosis of pancreatico-pleural fistula can immediately be assessed by the amount of amylase in the pleural fluid (Cole and Bradley 1992). Both ERCP and MRCP can document retroperitoneal fistula and/or the mediastinal pseudocyst without, however, being able to confirm the direct relationship with the pleural cavity or the bronchial tree.

Treatment of the internal fistula is almost exclusively surgical. Only in selected cases, such as when infection complicates the fistula, might it be necessary to insert a percutaneous drain (Cole and Bradley 1992).

#### External Pancreatic Fistula

External pancreatic fistula is more common, as a consequence of surgery or, much less commonly, due to a pancreatic biopsy (Iglehart et al. 1986). It develops along the

pathway of the drain inserted during the operation. This complication may follow surgical resection (pancreaticoduodenectomy, distal pancreatectomy; Papachristou et al. 1981; Lerut et al. 1985; Sheiman et al. 2001) or drainage procedures (pancreatico-jejunostomy or cysto-jejunostomy). In most cases, it is caused by the dehiscence of the pancreatico-digestive anastomosis or, in the absence of this, a leakage at the pancreatic stump. The fistula can complicate the drainage of a simple pancreatic collection (Fotoohi et al. 1999) or other surgical abdominal procedures: such as after surgery for a gastric or duodenal ulcer, which penetrates into the pancreas or after an emergency splenectomy, or after a left nephrectomy secondary to excessive surgical handling of the pancreatic tail (Spirnak et al. 1984). The external fistula may be simple, with direct communication of the duct of Wirsung with the skin (Fig. 16a,b) or complicated by the involvement of other structures, particularly the digestive tract (Fig. 16c,d) (Pistolesi et al. 1992).

Diagnosis is mostly clinical, since evaluation of the output and analysis of the fluid leads to the diagnosis of fistu-

la and also to an indication of the viscus involved. To date, fistulography is the primary investigation and often the only one carried out, to define the viscus involved (Pistolesi et al. 1992). A study of the digestive tract should be considered in cases of complex fistulas, to better define the extent of its involvement. In selected cases, a CT examination with the opacification of the fistula may be useful to achieve more exact information as to the spatial extension.

Usually, when there are low-output fistulas, spontaneous closure is expected in 68–100% of cases after 6–26 days (Pederzoli et al. 1986) and medical therapy almost always resolves the problem (Sunderland and Imrie 1992). High-output external fistulas (>200 ml/24 h) require a different therapeutic modality, as they are less inclined to spontaneous closure. Standard management includes total parenteral nutrition, somatostatin analogues, and, more recently, endoscopic stent placement in the pancreatic duct (Saeed et al. 1993; Bassi et al. 1996; Falconi et al. 1999; Bassi et al. 2000; Boerma et al. 2000; Costamagna et al. 2001) or percutaneous radiological catheterization of the main pancreatic duct (Cabay et al. 1998), with the aim of aiding the physiological efflux of the pancreatic juice. Surgery is indicated when this therapy has failed. Although some authors have observed that high-output fistulas show a greater tendency to cause complications, Bassi et al. observed neither a greater nor a lesser infection tendency in fistulas in relation to output, but rather a greater bacterial concentration (and enhanced risk of the clinical onset of infection) in low-output fistulas, perhaps caused by a reduced intrinsic washout mechanism. This mechanism is rapidly interrupted by inhibitory therapy and may account for the occurrence of so-called false closure of the fistula (Bassi 1992).

## 5.6.4 Vascular Involvement

The erosive action of activated pancreatic proteolytic enzymes in acute pancreatitis, the decubitus of a pseudocyst and the drainage in the surgically treated pancreas can involve pancreatic or peri-pancreatic vessels. The result of these conditions are arterial lesions, such as pseudoaneurysm or disruption, and venous complications, in particular, venous thrombosis.

### 5.6.4.1 Diagnosis and Embolization Therapy of Arterial Lesions

Major severe hemorrhagic arterial complications in pancreatitis are infrequent but life-threatening conditions (Frey et al. 2002; Procacci et al. 2002). Massive bleeding may be due to pseudoaneurysm or arterial disruption. Usually it occurs late in the disease course and in post-operative patients (Beattie et al. 2003). According to our experience, spontaneous bleeding always occurs in the same sites, at

the pancreatic tail, next to the spleen hilum or at the head of the pancreas. The more commonly involved vessels are the splenic artery, the gastroduodenal artery, the pancreatico-duodenal arcades, and lastly, the left gastric artery.

Anatomy explains these clinical presentations. On the left side, arterial lesions usually involve the last tract of the splenic artery, immediately upstream the origin of the left gastroepiploic artery and the collateral omental branches. At this site, retroperitoneal splenic branches become intraperitoneal, so they are more mobile and may induce traction onto the stable retroperitoneal vessels until they break down (Fig. 17a,b). The same mechanism can be observed on right sided bleeds. We look for arterial lesions at the point in which the gastroduodenal artery divides into the right gastroepiploic artery and the pancreatico-duodenal branches, as this site corresponds to a “locus minoris resistentiae,” in which the artery enters from the retroperitoneum into the omental root and becomes intraperitoneal (Fig. 17d,e).

### Pseudoaneurysm

When pancreatitis is associated with a pseudocyst, both the progressive enlargement and the mechanic decubitus of the pseudocyst cause necrotizing arteritis, with maceration of the vessel walls and hemorrhage into it. The hemorrhage is initially contained by a fibrous tissue capsule that progressively enlarges due to the unrelenting arterial pressure.

The size of the pseudocyst depends on the type of the lesion developed: bleeding in a small pseudocyst is contained and more commonly ends up as a pseudoaneurysm. In the case of a larger pseudocyst, the arterial lesion is defined as a bleeding pseudocyst and, therefore, has a significant risk of rupture in the gastrointestinal tract or into the peritoneal and/or retroperitoneal cavities. Angiography demonstrates the presence of pseudoaneurysm, without bleeding, in 10–21% of patients with chronic pancreatitis (Burke et al. 1986). The occurrence is higher (10–31%) in patients with pseudocyst (Kiviluoto et al. 1989; Frey et al. 1992). Hemorrhagic complications are expected in 6–31% of patients with pancreatic pseudocyst (Sankaran and Walt 1975) and in 7–14% of those suffering from chronic pancreatitis (Bresler et al. 1991). The preventive vascular study of patients with pancreatic pseudocyst must be carried out since arterial pseudoaneurysm, although infrequent, is a potentially catastrophic complication. Currently, noninvasive vascular imaging (Doppler US, MSCT, MRA) is almost as sensitive as angiography and should be chosen as the first choice in asymptomatic patients (Ammori et al. 1998).

Asymptomatic pseudoaneurysm is occasionally reported in the course of an ultrasound examination. Duplex Doppler ultrasonography immediately recognizes the blood flow inside the pseudoaneurysm and, in some cases, may identify the vessel of origin. A bleeding pseudocyst may be suspected at ultrasound if a cystic pancreatic mass rapidly enlarges or suddenly changes echogenicity (Fig. 18a).



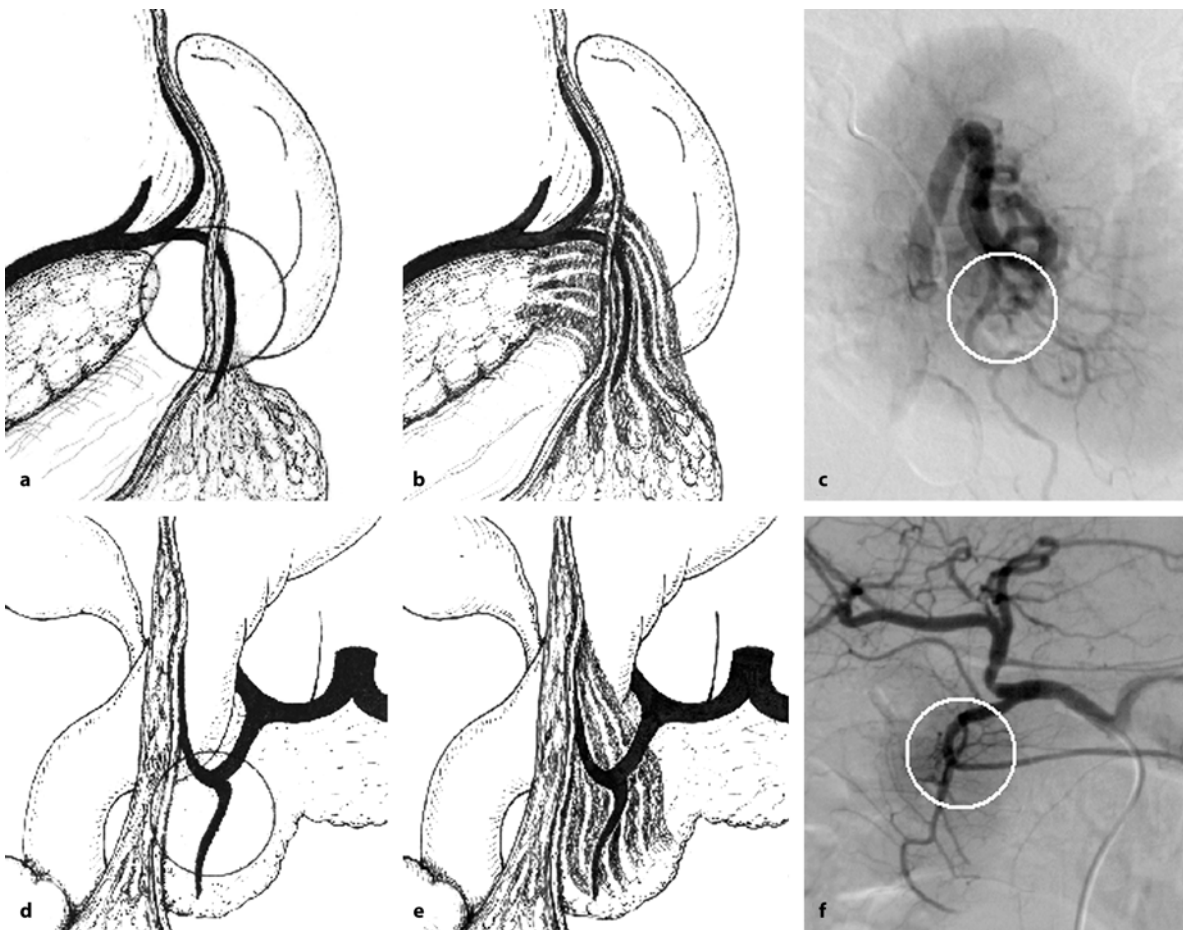


**Fig. 17 a–f.** Arterial involvement in pancreatitis. **a–c** The scheme highlights pancreatic left side arterial anatomy (**a**); arterial lesions usually occur in the last tract of splenic artery, immediately upstream the origin of the left gastroepiploic artery and the collateral omental branches (scheme) (**b**). Selective angiography of splenic artery in an oblique projection (**c**) displays how these retroperitoneal branches become intraperitoneal, so more mobile

and vulnerable to lesion (*circle*). **d–f** Right side vascular anatomy is shown in the scheme (**d**). At this site the “locus minoris resistentiae” is the point in which the gastroduodenal artery divides into the right gastroepiploic artery and the pancreatico-duodenal branches (scheme) (**e**). Selective angiography of coeliac trunk demonstrates arterial branches becoming intraperitoneal (*circle*; **f**)

Pseudoaneurysm identification more often occurs during CT examination (Fig. 18b,c), carried out following complaints of acute, usually gastrointestinal, pain associated with or without bleeding. Multiple recurrences of gastrointestinal hemorrhage, especially in association with transient pancreatic pain, must lead to the suspicion of a pseudoaneurysm or a bleeding pseudocyst, especially when endoscopic examinations are negative for concurrent peptic diseases.

The intermittence of the bleeding is characteristic of “wirsungorrhage” or “hemosuccus pancreaticus.” Described for the first time by Lower and Farrell in 1931 (Lower and Farrell 1931), it appears as intermittent hemorrhagic flow from the major papilla, a rare finding but pathognomonic for pancreatic arterial hemorrhage (Nabi Yattoo et al. 1999; Dasgupta et al. 2002; Feng and Mauro 2003). In the presence of chronic gastrointestinal bleeding

in a pancreatic inflammatory disease and of a pseudoaneurysm on CT examination (Fig. 19a), ERCP has the task of looking for an abnormal communication between the main pancreatic duct and the pseudoaneurysm, with direct endoscopic visualization of wirsungorrhage or indirect confirmation due to the opacification of the pseudoaneurysm (Fig. 19b).

Regarding symptomatic pseudoaneurysms and chronic gastrointestinal bleeding, the acute bleeding is a consequence of the pseudoaneurysm or ruptured bleeding pseudocyst. As already stated, the progressive expansion of the arterial lesion, owing to unrelenting arterial pressure, can result in a sudden and immediate rupture in the gastrointestinal tract, the peritoneal cavity, or the retroperitoneal space. Its clinical presentation is characterized by sudden hemorrhagic shock, with a mortality rate of 50% (Lendrum 1994). Computed tomography can highlight the



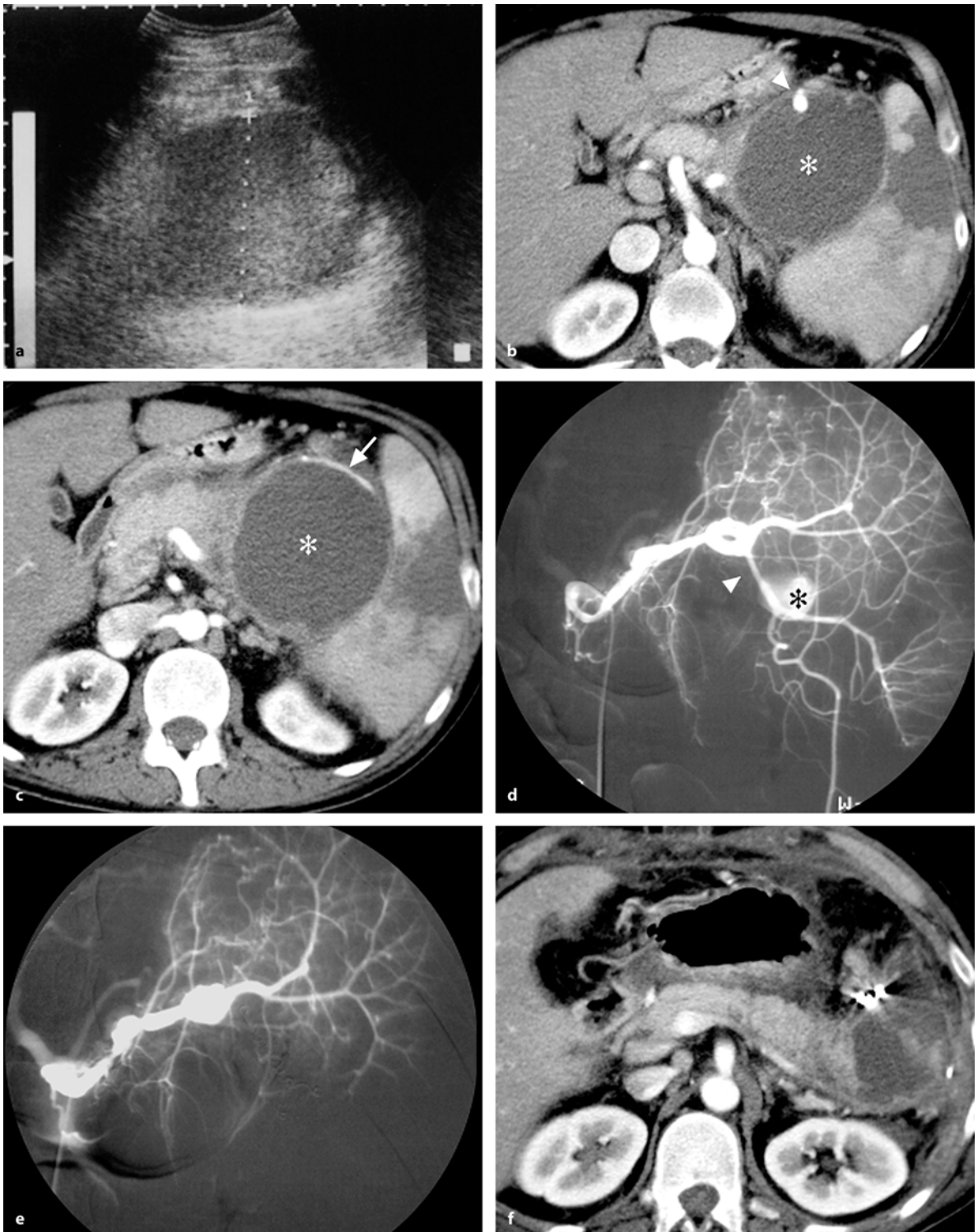


**Fig. 18a–f.** Bleeding pseudocyst of the left gastroepiploic artery, radiologically and surgically treated. The ultrasound examination (a) highlights a voluminous pseudocyst of the tail of the pancreas with a finely corpuscular hyper-echoic content. The CT scans in the arterial contrastographic phase (b, c) demonstrate the pancreatic tail pseudocyst (asterisk) compressing the splenic artery. In front of the pseudocyst, a small pseudoaneurysm is visible (arrowhead), adhering to the left gastroepiploic artery, which is stretched and displaced

frontward (arrow). There is a vast infarcted area in the spleen. Selective angiography of the splenic artery (d) shows the pseudoaneurysm (asterisk) slightly downstream of the left gastroepiploic artery origin (arrowhead). Selective angiography after placing coils at the pseudoaneurysm afferences (e) demonstrates its complete exclusion. Axial CT scans (f), carried out following splenectomy and cysto-jejunostomy demonstrate that the arterial embolizing material placed radiologically is still in position. (From Procacci et al. 2002)



**Fig. 19a–e.** Pseudoaneurysm in chronic pancreatitis, radiologically treated. The axial CT scan in the arterial phase (**a**) demonstrates the presence of a pseudoaneurysm (*asterisk*) embedded in the pancreatic head; ERCP (**b**) reveals the passing of contrast medium from the main pancreatic duct (*arrow*) to the lumen of the pseudoaneurysm (*arrowheads*). Angiography (**c**) shows that the

pseudoaneurysm (*asterisk*) is fed by the gastroduodenal artery and the pancreato-duodenal arcades. The coils (*arrows*) mimic the course of the embolized vessels (**d**) recreating their anatomy. The axial CT scan (**e**), carried out a year later, shows the collapse of the aneurysmatic sac with the coils positioned in the arcade. (From Procacci et al. 2002)

pseudoaneurysm and its contiguity with the gastrointestinal tract or the presence of hemoperitoneum.

To date, MSCT, with image reconstruction programs (MPR, MIP, SSD, VR), or MR, with 3D sequences in contrast phases, are extremely sensitive in defining a detailed arterial map of the pancreatic region as well as the site of the arterial lesion.

Angiography, therefore, plays no role in the diagnostic phase but is immediately used for treating lesions identified with noninvasive imaging. Embolization, in particular, has high success rates in the treatment of these lesions (Beattie et al. 2003; Deshmukh et al. 2004; Bergert et al. 2004, 2005). Initially, all the afferent and efferent arteries involved must be defined (Fig. 19c). Only the occlusion of all of them results in the complete and definite exclusion of the pseudoaneurysm or bleeding pseudocyst from the arterial flow, with its resultant progressive collapse (Fig. 19d,e). The best embolizing materials are Gianturco

coils; both the coaxial technique and the micro-coils lead to a particularly high success rates. The occlusion of all the efferents and, therefore, all of the afferents to the lesion with coils is technically similar to surgical tying, but it is clearly much less invasive. It is better not to place coils inside the pseudoaneurysm, unless this is required to occlude the efferent vessels, which would otherwise be inaccessible (Schoder et al. 2000). Notably, pseudoaneurysms have a pseudo-wall of variable thickness that can derive from the fibrotic wall of the pseudocyst. Moreover, without coils inside the pseudoaneurysm, CT can better demonstrate the reduction of the sac until it collapses during follow-up. This is because it is not hidden by the artifacts (Fig. 19e). When the pseudoaneurysm is ruptured, the emergency condition can justify the use of acrylic glue together with coils (Schoder et al. 2000; Yamakado et al. 2000) to obtain a quicker occlusion of the bleeding vessel, as described later. Recently, a direct US and/or CT guided percutaneous em-

bolization of pseudoaneurysms with thrombin has been proposed as an alternative to endovascular embolization with glue (Sparrow et al. 2003; Puri et al. 2003; Geoghegan et al. 2004; Krueger et al. 2005). In the presence of a copiously bleeding pseudocyst, radiological treatment is a priority, but not mandatory. By proceeding in this manner, the hemorrhage can be stopped and the patient can proceed to surgery in a controlled and hemodynamically stable condition (Fig. 18d–f). In acute hemorrhage, the surgical approach is in fact subject to a high mortality rate, varying from 12 to 64% (Stabile et al. 1983; El Hamel et al. 1991).

### Arterial Disruption

Arterial disruption is one of the most serious emergency conditions in pancreatic pathology. It is an uncommon complication of inflammatory pancreatic disease, but mortality is >50%. Survival depends greatly on quick and accurate diagnostic and therapeutic views.

Clinical presentation is characterized by hemorrhagic shock at the moment of diagnosis. Bleeding can occur in the gastrointestinal lumen, the peritoneal cavity, the retroperitoneum, or simultaneously in several anatomic cavities.

Arterial disruption in acute pancreatitis follows the powerful proteolytic action of activated enzymes present in the inflammatory pancreatic fluid combined with maceration of the arterial wall. The most commonly involved arterial vessel is the splenic artery, but all the peripancreatic vessels can be involved, depending on the location of the fluid collection. Bleeding from the right and middle colic arteries is common when the collection occupies the mesenteric root. Superior mesenteric artery and the celiac trunk can also be involved, but to a lesser degree. When hemorrhagic shock occurs, spiral CT is first imaging technique: it can highlight the collections that completely surround the arterial vessels and often when there is hemodynamic instability, it can identify the spreading hemorrhage inside the collection (Fig. 20a) and its vessel of origin. Nevertheless, diagnosis remains the great challenge, as it may fail in emergency conditions and immediate treatment is required. In such situations, the gold standard imaging technique is angiography, which has the advantage of being diagnostic and therapeutic at the same time (Fig. 20b–g).

Arterial bleeding in acute pancreatitis is a dramatic occurrence that is subject to a high mortality rate. Stopping it may be very difficult both surgically and radiologically. Emergency surgery is associated with a high degree of failure and mortality. A >80% recurrence rate of bleeding has been reported in the literature (Stanley et al. 1976; Stabile et al. 1983; El Hamel et al. 1991). Surgical resection has a more than 50% mortality (Bresler et al. 1991).

The radiological treatment of arterial disruption in “necrotic hemorrhagic” pancreatitis can fail due to the excessive extent of the maceration of the vessel or the involvement of multiple arterial branches. The goal of em-

bolization is control of the vessel proximally and distally to the site of bleeding (Fig. 20c–e).

Embolization of the vessel with spongostan has a high rate of rebleeding. This is because the fibrin sponge is sensitive to the lytic action of the activated pancreatic enzymes (Golzarian et al. 1997) and the vessel is practically without walls at the disruption site, as a result, its plugging is useless since the re-establishment of the pressure system would re-open the arterial breach. For the same reason, stopping the bleeding following an accidental proximal dissection of an arterial vessel is rarely definitive. Metal coils can completely embolize the arterial lesion only when they are placed up and downstream of the breach in the bleeding arterial vessel, where the wall is not affected by enzymatic erosion.

According to our experience, acrylic glue has proved to be the most efficient embolizing agent when hemodynamic instability requires rapid embolic action, or when catheterization of the vessel downstream of bleeding is impossible (Yamakado et al. 2000). Injected upstream of the arterial lesion and correctly diluted, the glue is able to reach the arterial tract downstream and, with its progressive polymerization, brings about the proximal and distal occlusion. Another useful advantage is that the glue's polymerization has an exothermic reaction, which creates a germicidal action in the usually infected collection. Whenever possible, it is better to precede the injection of the glue with partial embolization with coils. This is in order to slow down the arterial flow and avoid distal progression of the embolizing material, whose polymerization time cannot be calculated accurately.

The incidence of hemorrhagic complications due to arterial disruption after pancreatic surgery, especially pancreatoduodenectomy, has not changed in the past 20 years (2–18%) (Rumstadt et al. 1998). Bleeding is a serious complication, the second most frequent after sepsis due to dehiscence of the pancreatic anastomosis. In the first 2 weeks, early bleeding can be due to insufficient intra-operative hemostasis at the abdominal vessel level or in correspondence with the anastomosis and requires a second laparotomy. After the first to second week, late bleeding can occur. Its diagnosis as well as its treatment are often a challenge. The dehiscence of the pancreato-jejunal anastomosis can cause the liberation of lytic enzymes activated by the enteric contents, with consequent arterial disruption with massive hemorrhage. More than 2 weeks following surgery, even modest bleeding must be considered a potential sign of anastomotic dehiscence. This initial bleed is known as “sentinel bleeding” because it often precedes massive hemorrhage from erosion of a large arterial branch by 6 h to 10 days. Rumstadt et al. suggest that when “sentinel bleeding” appears at the drainage or the gastrointestinal tract, immediate surgical intervention with a revision of the pancreatic–digestive anastomosis should be undertaken (Rumstadt et al. 1998). When dehiscence of the anastomosis occurs, the massive hemorrhage results in





**Fig. 20a-h.** Emergency radiological treatment of arterial disruption in bleeding pancreatitis. **a** Contrast-enhanced CT scan highlights a fluid collection at the site of pancreatic head, almost completely destroyed by necrosis. A tiny hyperdensity inside the collection induces the suspicion of arterial disruption, even though bleeding source cannot be clearly identified. **b** Selective angiography demonstrates an active bleeding from gastroduodenal artery, immediately before the origin of right gastroepiploic artery. The angiographic image is pathognomonic of an arterial disruption in acute pancreatitis with contrast medium spreading directly into the peripancreatic fluid collection. **c-e** Emergency radiological treatment is carried out positioning microcoils downstream and

upstream to the arterial lesion (*arrows*), at the origin of gastroduodenal artery, superior pancreaticoduodenal artery and into gastroduodenal artery till the origin of common hepatic artery (**c**). Selective angiography of superior mesenteric artery is then performed and coils are positioned along the inferior pancreaticoduodenal arcades (*arrows*), to definitely exclude the arterial lesion and reduce the risk of rebleeding (**d, e**). **f-g** At the end of the procedure, digital subtraction angiography angiographies of superior mesenteric artery (**f**) and coeliac trunk (**g**) confirm the complete embolization of arterial lesion. **h** At 15 days CT control coils are clearly demonstrated and there is no evidence of arterial bleeding recurrence

mortality in 15–58% of cases (Rumstadt et al. 1998; Sato et al. 1998).

If the patient is hemodynamically stable, CT examination may fail to demonstrate the source of bleeding, but it is very useful for highlighting peri-anastomotic collections, which could be responsible for the arterial lesion. When a

greater amount of bleeding is noted from the drains, and/or the gastrointestinal tract, CT is usually effective in revealing the site of hemorrhage, but in this case the unstable hemodynamic condition of the patient makes it preferable to perform angiography immediately because it can diagnose and treat the site of bleeding. Bleeding associated



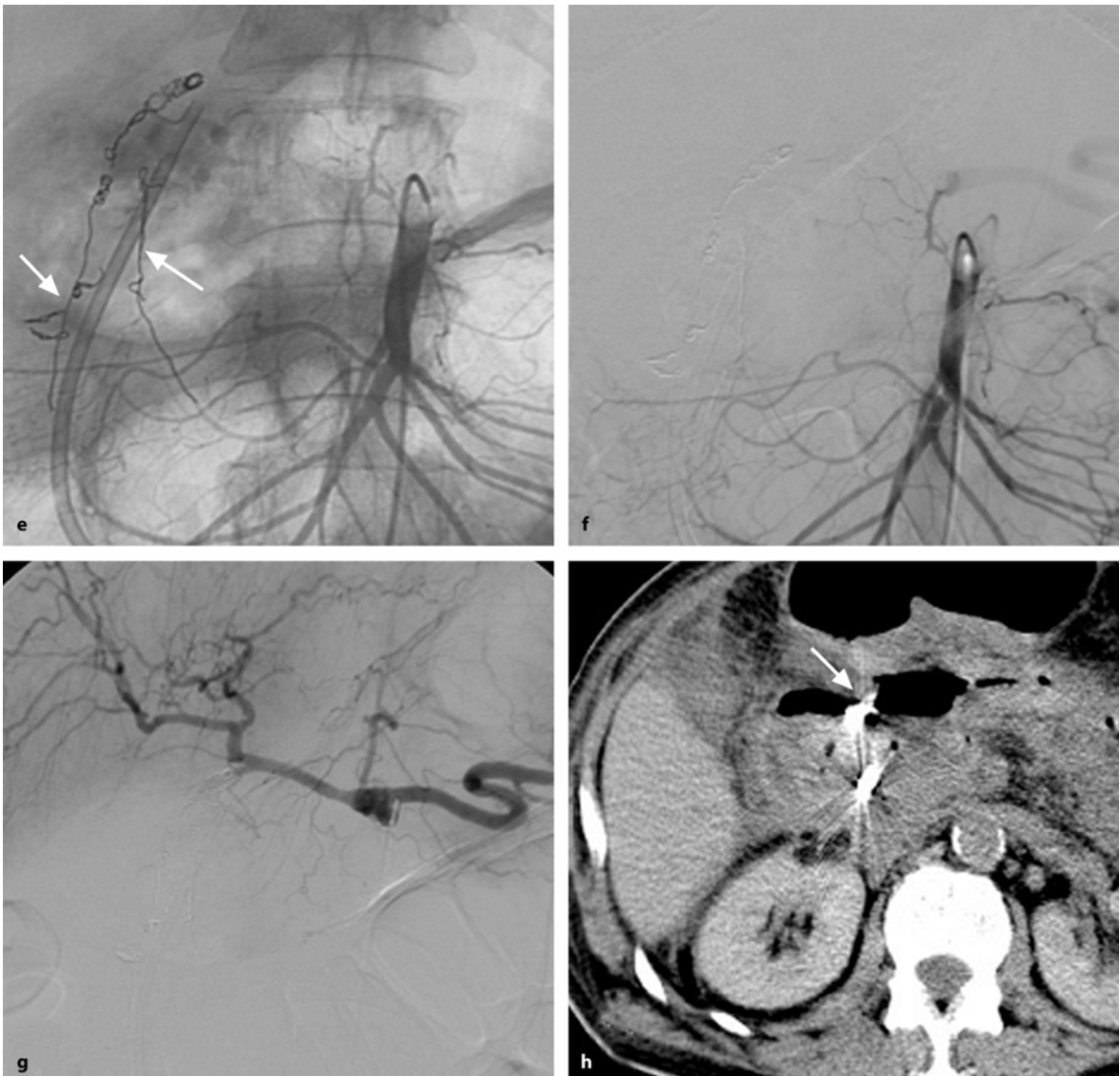


Fig. 20a–h. (continued)

with anastomotic dehiscence requires an embolization technique similar to that used in acute pancreatitis. The most commonly involved vessels are the gastroduodenal artery and the common hepatic artery (Aranha et al. 1984; Brodsky and Turnbull 1991; Balladur et al. 1996; Rumstadt et al. 1998; Sato et al. 1998). Embolization with coils leads to definite stoppage of the bleeding only when the gastroduodenal artery is occluded in a tract not involved by septic maceration or, alternatively, the common hepatic artery is directly occluded. Embolization is sometimes used as a temporary procedure to stop or slow down bleeding so that a patient can be operated on electively rather than emergently (Vujic 1989). There are few articles in the literature that report late hemorrhage following a pancreatoduodenectomy treated with embolization.

The arterial disruption in neoplastic pathology is the result of infiltration of the pancreatic and peri-pancreatic vessels. Arterial bleeding is, however, an uncommon complication of the very advanced stages, when even palliative treatment loses its effectiveness. Neuroendocrine tumors at the cephalo-pancreatic site are an exception: they grow slowly and require response to chemotherapy. Their bleeding is usually due to infiltration of the duodenal wall, so endoscopic examination can make the definite diagnosis. Palliative treatment consists of embolization of the arterial vessels involved. The best embolizing material is spongostan or microspheres of polyvinyl alcohol, whereas the afferent arteries to the neoplasm are occluded with coils.

### Embolization Therapy Complications

Complications due to embolization therapy in the pancreatic and visceral area are limited. Often patients complain of the so-called postembolization syndrome, in which there is a modest rise in temperature, leukocytosis, pain and nausea. Symptoms usually resolve in a few days with anti-inflammatory and anti-emetic therapy and intravenous resuscitation. The risk of ischemia is minimal in the upper gastrointestinal tract if the normal collateral pathways are patent and the appropriate embolic agents are used. In this region, the left gastric, gastroduodenal, gastroepiploic, and pancreaticoduodenal arteries can be safely embolized (Rosen and Sanchez 1994). Using a technique that leads to the most proximal occlusion possible with coils or fast polymerization acrylic glue, the recruitment of collateral circulation downstream allows for the re-vascularization of the occluded vessel. Splenic artery occlusion determines the onset of sectorial infarcts, which usually resolve with no further consequences. Occlusion of a short tract up- and downstream of the bleeding of arterial branches, such as the middle colic artery, is tolerated. Occlusion of the common hepatic artery, with normal patency of the portal vein, has no clinical consequences. Embolization is inadvisable in the presence of thrombosis or compression of the portal vein (Cardella et al. 1997). Treatment of bleeding from the common hepatic artery or from the short stump of the gastroduodenal artery following a pancreatoduodenectomy is often problematic for the surgeon. In fact, after surgery, there is a reduction in the number of arteries available for collateralization. Moreover, compression, even as far as thrombosis, of the portal vein is common due to the adjacent hematic collection. In these cases the alternative treatment to embolization is the placement of covered stents, which maintain the patency of the hepatic artery in emergencies. There are still only a few reports in the literature concerning the use of this technique in repairing the hepatic artery (Bürger et al. 2000; Paci et al. 2000). Occlusion of the stent over time due to intimal hyperplasia is predictable. Nevertheless, the treatment stops the bleeding immediately and maintains the blood flow to the liver. The slow occlusion of the stent can then be compensated by the recruitment of collateral intra-hepatic arterial circulation and the return to normal portal flow or the growth of a collateral portal network.

A rare complication of interventional treatment is infection. This is related to the introduction of foreign embolic material or the covered stents. Preventive treatment is therefore advisable by administering a second-generation cephalosporin on the day of the procedure. If fever or leukocytosis appear in the immediate post-procedure period, the differential diagnosis between post-embolization syndrome and infection can be difficult. Gas bubbles in the infarcted foci are not a definite sign of infection. If fever persists, the suspicion of infection is more certain. A blood culture usually confirms the diagnosis. Nevertheless, an-

tibiotic therapy is necessary if the fever persists over the sixth day. If imaging displays the presence of a collection in the embolized area, it is possible to perform percutaneous drainage.

#### 5.6.4.2 Diagnosis and Management of Venous Complications

##### Venous Thrombosis of the Peripancreatic Tributaries of the Portal Vein

Venous thrombosis is a frequent complication of pancreatitis. Thrombosis of the splenic vein is the most common vascular complication of pancreatitis. This is because of its location in a groove along the upper posterior border of the pancreas. It has been reported to be occluded in up to 45% of patients with pancreatitis (Vujic 1989). Chronic pancreatitis, especially when calcified, is the most common cause of splenic vein thrombosis with 5–37% of patients affected. All the signs of pre-hepatic segmental portal hypertension are also present. Compression and/or venous infiltration induces thrombosis that leads to the formation of esophageal or gastric varices, which can be responsible for acute bleeding. The development of esophageal varices occurs in >50% of patients with splenic artery thrombosis, whereas gastric varices can bleed in 45–69% of patients with splenic vein thrombosis (Moossa and Gadd 1985). Ultrasound and/or CT imaging can easily demonstrate the presence of varices but not actual bleeding. Diagnosis is the task of endoscopy, which is also often required to carry out sclerotherapy. Splenic vein thrombosis and sinistral hypertension may be treated by splenectomy (Vujic 1989).

##### Pancreatic Duct/Portal Vein Fistula

Pancreatic duct/portal vein fistula results from a spontaneous rupture of a pancreatic pseudocyst into the portal vein. The onset of this venous complication is very unusual: only a few cases have been reported in the literature (Procacci et al. 1995; Yamamoto et al. 1999; Ko et al. 2003; Riddel et al. 2005). The diagnosis of the fistula cannot be obtained by angiography because the portal tree is excluded from the systemic circulation and it develops a cystic transformation. The ERCP can highlight the fistula if the latter directly involves the pancreatic duct (Willis and Brewer 1989). Whenever the fistula is induced by a pseudocyst, ERCP may not be diagnostic. On contrast-enhanced CT, the portal lumen is easily recognizable with a liquid-type density (Fig. 21). Sometimes, communication between the venous lumen and the pseudocyst can be demonstrated. Confirmation of the fistula is obtainable by trans-hepatic portography carried out under US or CT guidance. Presently, magnetic resonance can also diagnose the development of pancreatic duct/portal vein fistula (Riddel et al. 2005).



**Fig. 21 a–d.** Pancreatic duct/portal vein fistula. The CT scans, carried out in the cranio-caudal direction in the contrastographic phase, show hypodense hepatic areas, due to the reduced contribution of the hematic portal flow caused by the total thrombosis of the portal

tree (*arrowheads*), involved by a voluminous pseudocyst of the pancreatic body (*asterisk*). The lumen of the portal vessels has the same liquid density of the pseudocyst, as a consequence of its spontaneous rupture into the portal vein. (From Procacci et al. 2002)

### Thrombophlebitis of the Peripancreatic Tributaries of the Portal Vein

Thrombophlebitis of the peripancreatic tributaries of the portal vein is defined as acute infection of the portal system associated with hepatic involvement. It can arise from the extension of pancreatic necrosis infection along the portal venous tree. The pyogenic diffusion through the portal system is followed by hepatic involvement, with the formation of one or more abscesses. At CT, the intra-hepatic abscesses

appear as badly defined hypodense collections, which may or may not contain small gas bubbles (Fig. 22a–c). The early detection of septic ascending thrombophlebitis and its adequate treatment (Fig. 22d–f) may decrease the mortality rate and the serious prognosis reported in the surgical literature (Balthazar and Gollapudi 2000).

**Acknowledgement.** The authors dedicate this chapter to the memory of Prof. Carlo Procacci.

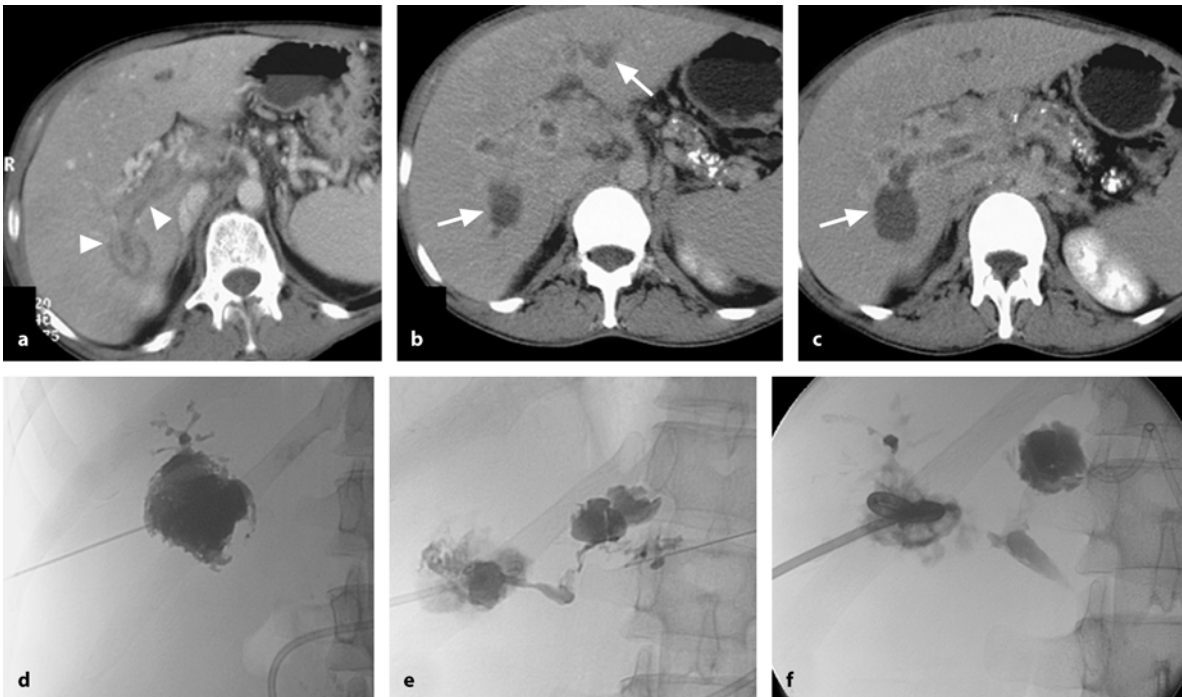


**Fig. 22a–f.** Pylephlebitis in chronic pancreatitis. **a–c** Contrast-enhanced CT scans show portal thrombosis (*arrowheads* in **a**) and adjacent hypodense hepatic areas with hyperdense walls (*arrows* in **b, c**), liver abscesses consequent to the pyogenic diffusion through the portal system. **d–f** Percutaneous transhepatic

drainage of liver abscesses can contribute to the definite diagnosis and treatment. It was carried out with a fine needle (**d**) then exchanged by a percutaneous catheter. The communication between fluid collections and thrombosed portal vein is demonstrated by the spreading of contrast medium directly into portal tree (**e, f**)

## References

- Adams DB, Harvey TS, Anderson MC (1990) Percutaneous catheter drainage of infected pancreatic and peripancreatic fluid collections. *Arch Surg* 125: 1554–1557
- Alexander ES, Weinberg S, Clark RA, Belkin RD (1982) Fistulas and sinus tract: radiographic evaluation, management and outcome. *Gastrointest Radiol* 7: 135–140
- Ammori B J, Alexander D J, Madan M (1998) Hemorrhagic complications of pancreatitis: presentation, diagnosis and management. *Ann R Coll Surg Engl* 80: 316–325
- Apte MV, Keogh GW, Wilson JS (1999) Chronic pancreatitis: complications and management. *J Clin Gastroenterol* 29: 225–240
- Aranha GV, Prinz RA, Greenlee HB, Freark RJ (1984) Gastric outlet and duodenal obstruction from inflammatory pancreatic disease. *Arch Surg* 119: 833–835
- Balladur P, Christophe M, Tiret E, Parc R (1996) Bleeding of the pancreatic stump following pancreatoduodenectomy for cancer. *Hepatogastroenterology* 43: 268–270
- Balthazar EJ (1989) CT diagnosis and staging of acute pancreatitis. *Radiol Clin North Am* 27: 19–37
- Balthazar EJ, Freeny PC, vanSonnenberg E (1994) Imaging and intervention in acute pancreatitis. *Radiology* 193: 297–306
- Balthazar EJ, Gollapudi P (2000) Septic thrombophlebitis of the mesenteric and portal veins: CT imaging. *J Comput Assist Tomogr* 24: 755–760
- Baril NB, Ralls PW, Wren SM, Selby RR, Radin R, Parekh D, Jabbar N, Stain SC (2000) Does an infected peripancreatic fluid collection or abscess mandate operation? *Ann Surg* 231: 361–367
- Bassi C (1992) Microbiological aspects of pancreatic fistulas. In: Pederzoli P, Bassi C, Vesentini S (eds) *Pancreatic fistulas*. Springer, Berlin Heidelberg New York, pp 121–128
- Bassi C (1994) Infected pancreatic necrosis. *Int J Pancreatol* 16: 1–10
- Bassi C, Falconi M, Caldiron E, Bonora A, Salvia R, Pederzoli P (1996) Somatostatin analogues and pancreatic fistulas. *Digestion* 57 (Suppl 1): 94–96
- Bassi C, Butturini G, Salvia R, Contro C, Valerio A, Falconi M, Pederzoli P (2000) A single-institution experience with fistulojejunostomy for external pancreatic fistulas. *Am J Surg* 179: 203–206
- Beattie GC, Hardman JG, Redhead D, Siriwardena AK (2003) Evidence for a central role for selective mesenteric angiography in the management of the major vascular complications of pancreatitis. *Am J Surg* 185: 96–102
- Beger HG, Rau B, Mayer J, Pralle U (1997) Natural course of acute pancreatitis. *World J Surg* 21: 130–135
- Berberat PO, Friess H, Kleeff J, Uhl W, Büchler MW (1999) Prevention and treatment of complications in pancreatic cancer surgery. *Dig Surg* 16: 327–336
- Bergert H, Dobrowolski F, Caffier S, Bloomenthal A, Hinterseher I, Saeger HD (2004) Prevalence and treatment of bleeding complications in chronic pancreatitis. *Langenbecks Arch Surg* 389: 504–510
- Bergert H, Hinterseher I, Kersting S, Leonhardt J, Bloomenthal A, Saeger HD (2005) Management and outcome of hemorrhage due to arterial pseudoaneurysms in pancreatitis. *Surgery* 137: 323–328



- Boerma D, Rauws EAJ, van Gulik TM, Huibregtse K, Obertop H, Gouma DJ (2000) Endoscopic stent placement for pancreaticocutaneous fistula after surgical drainage of the pancreas. *Br J Surg* 87: 1506–1509
- Bohlman TW, Katon RM, Lee TG, Eidemiller LR (1976) Use of endoscopic retrograde cholangiopancreatography in the diagnosis of pancreatic fistula. *Gastroenterology* 70: 582–584
- Bradley EL III (1993) A clinically based classification system for acute pancreatitis. Summary of the International Symposium on Acute Pancreatitis, Atlanta, 11–13 September 1992. *Arch Surg* 128: 586–590
- Bradley EL III, Warshaw AL (1993) Pancreatic abscess. In: Go VLW, DiMagno EP, Gardner JD, Leberthal E, Reber HA, Scheele GA (eds) *The pancreas. Biology, pathobiology, and disease*, 2nd edn. Raven Press, New York, pp 649–662
- Bresler L, Boissel P, Grosdidier J (1991) Major hemorrhage from pseudocysts and pseudoaneurysms caused by chronic pancreatitis: surgical therapy. *World J Surg* 15: 649–653
- Brodsky JT, Turnbull AD (1991) Arterial hemorrhage after pancreatoduodenectomy. The “sentinel bleed”. *Arch Surg* 126: 1037–1040
- Bürger T, Halloul Z, Meyer F, Grote R, Lippert H (2000) Emergency stent-graft repair of a ruptured hepatic artery secondary to local postoperative peritonitis. *J Endovasc Ther* 7: 324–327
- Burke JW, Erickson SJ, Kellum CD, Tegtmeyer CJ, Williamson BRJ, Hansen MF (1986) Pseudoaneurysms complicating pancreatitis: detection by CT. *Radiology* 161: 447–450
- Cabay JE, Boverie JH, Dondelinger RF (1998) Percutaneous catheter drainage of external fistulas of the pancreatic ducts. *Eur Radiol* 8: 445–448
- Cameron JL, Kieffer RS, Anderson WJ, Zuidema GD (1976) Internal pancreatic fistulas: pancreatic ascites and pleural effusion. *Ann Surg* 184: 587–593
- Cantademir M, Kara B, Kantarci F, Mihmanli I, Numan F, Erguney S (2003) Percutaneous drainage for treatment of infected pancreatic pseudocysts. *South Med J* 96: 136–140
- Cardella Cardella JE, Vujic I, Tadavarthy SM, Beltran M, Castañeda-Zúñiga WR (1997) Gastrointestinal bleeding Part I. Vasoactive drugs and embolotherapy in the management of gastrointestinal bleeding. In: Castañeda-Zúñiga WR (ed) *Interventional radiology*, 3rd edn, vol 1. Williams and Wilkins, Baltimore, pp 207–252
- Carter CR, McKay CJ, Imrie CW (2000) Percutaneous necrosectomy and sinus tract endoscopy in the management of infected pancreatic necrosis: an initial experience. *Ann Surg* 232: 175–180
- Cole DJ, Bradley EL III (1992) Internal pancreatic fistulas: classification, recognition, and management. In: Pederzoli P, Bassi C, Vesentini S (eds) *Pancreatic fistulas*. Springer, Berlin Heidelberg New York, pp 107–120
- Costamagna G, Mutignani M, Ingrosso M, Vamvakousis V, Alevras P, Manta R, Perri V (2001) Endoscopic treatment of postsurgical external pancreatic fistulas. *Endoscopy* 33: 317–322
- Dasgupta R, Davies NJ, Williamson RC, Jackson JE (2002) Haemorrhage in pancreatic necrosis: treatment by arterial embolization. *Clin Radiol* 57: 1021–1027
- De Baker AI, Mortelé KJ, Vaneerdeweg W, Ros PR (2001) Pancreatocolonic fistula due to severe acute pancreatitis: imaging findings. *JBR-BTR* 84: 45–47
- Deshmukh H, Rathod K, Garg A, Sheth R, Kulkarni S (2004) Transcatheter embolization as primary treatment for visceral pseudoaneurysms in pancreatitis: clinical outcome and imaging follow up. *Indian J Gastroenterol* 23: 56–58
- Echenique AM, Sleeman D, Yrizarry J, Scagnelli T, Guerra JJ, Casillas VJ, Huson H, Russell E (1998) Percutaneous catheter-directed debridement of infected pancreatic necrosis: results in 20 Patients. *J Vasc Interv Radiol* 9: 565–571
- El Hamel A, Parc R, Adda G, Bouteloup PY, Huguot C, Malafosse M (1991) Bleeding pseudocysts and pseudoaneurysms in chronic pancreatitis. *Br J Surg* 78: 1059–1063
- Falconi M, Sartori N, Caldiron E, Salvia R, Bassi C, Pederzoli P (1999) Management of digestive tract fistulas. A review. *Digestion* 60 (Suppl 3): 51–58
- Farthmann EH, Lausen M, Schöffel U (1993) Indications for surgical treatment of acute pancreatitis. *Hepatogastroenterol* 40: 556–562
- Feng DH, Mauro MA (2003) SIR 2003 film panel case 6: hemococcus pancreaticus secondary to chronic pancreatitis. *J Vasc Interv Radiol* 14: 803–805
- Ferrucci JT, Mueller PR (2003) Interventional approach to pancreatic fluid collections. *Radiol Clin North Am* 41: 1217–1226
- Fishman EK, Soyer P, Bliss DF, Bluemke DA, Devine N (1995) Splenic involvement in pancreatitis: spectrum of CT findings. *AJR* 164: 631–635
- Fotoohi M, D'Agostino HB, Wollman B, Chon K, Shahrokni S, van Sonnenberg E (1999) Persistent pancreaticocutaneous fistula after percutaneous drainage of pancreatic fluid collections: role of cause and severity of pancreatitis. *Radiology* 213: 573–578
- Freney PC, Lewis GP, Traverso LW, Ryan JA (1988) Infected pancreatic fluid collections: percutaneous catheter drainage. *Radiology* 167: 435–441
- Freney PC, Hauptmann E, Althaus SJ, Traverso LW, Sinanan M (1998) Percutaneous CT-guided catheter drainage of infected acute necrotizing pancreatitis: techniques and results. *AJR* 170: 969–975
- Frey CF, Stanley JC, Eckhauser F (1992) Hemorrhage. In: Bradley EL (ed) *Complications of pancreatitis*. Saunders, Philadelphia, pp 96–123
- Frey CF, Stanley JC, Eckhauser F (2002) Hemorrhage. In: Bradley EL (ed) *Complications of pancreatitis*. Saunders, Philadelphia, pp 96–123
- Fulcher AS, Capps GW, Turner MA (1999) Thoracopancreatic fistula: clinical and imaging findings. *J Comput Assist Tomogr* 23:181–187
- Gandini G, Grosso M, Bonardi L, Cassinis MC, Regge D, Righi D (1988) Results of percutaneous treatment of sixty-three pancreatic pseudocysts. *Ann Radiol* 31: 117–122
- Geoghegan T, Tuite D, McAuley G, O'Keeffe S, Torreggiani WC (2004) Percutaneous thrombin injection for the treatment of a post-pancreatitis pseudoaneurysm of the gastroduodenal artery. *Eur Radiol* 14: 2144–2145
- Gervais DA, Fernandez-del Castillo C, O'Neill MF, Hahn PF, Mueller PR (2001) Complications after pancreatoduodenectomy: imaging and imaging-guided interventional procedures. *Radiographics* 21: 673–690
- Golzarian J, Nicaise N, Devière J, Ghysels M, Wery D, Dussaussois L, Van Gansbeke D, Struyven J (1997) Transcatheter embolization of pseudoaneurysms complicating pancreatitis. *Cardiovasc Intervent Radiol* 20: 435–440
- Iglehart JD, Mansback C, Postlethwait R, Roberts L Jr, Ruth W (1986) Pancreatico-bronchial fistula: case report and review of the literature. *Gastroenterology* 90: 759–763
- Kay CL, Aabakken LE, Tarnasky P, Feldman D, Hawes RH, Cunningham J, Cotton PB (1997) Magnetic resonance cholangiopancreatography: a problem solving modality. *Gastrointest Endosc* 46: 363–366
- Kemppainen E, Sainio V, Haapiainen R, Kivisaari L, Kivilaakso E, Puolakkainen P (1996) Early localization of necrosis by contrast-enhanced computed tomography can predict outcome in severe acute pancreatitis. *Br J Surg* 83: 924–929
- Kiviluoto T, Kivisaari L, Kivilaakso E, Lempinen M (1989) Pseudocysts in chronic pancreatitis. Surgical results in 102 consecutive patients. *Arch Surg* 124: 240–243
- Ko HS, Anders M, Diehl S, Dominguez E, Lohr M, Duber C (2003) Portal vein erosion and acute abdominal hemorrhage as a complication of acute pancreatitis. *Abdom Imaging* 28: 700–702
- Krueger K, Zaehring M, Lackner K (2005) Percutaneous treatment of a splenic artery pseudoaneurysm by thrombin injection. *J Vasc Interv Radiol* 16: 1023–1025

- Laws HL, Kent RB III (2000) Acute pancreatitis: management of complicating infection. *Am Surg* 66: 145–152
- Lee MJ, Rattner DW, Legemate DA, Saini S, Dawson SL, Hahn PF, Warshaw AL, Mueller PR (1992) Acute complicated pancreatitis: redefining the role of interventional radiology. *Radiology* 183: 171–174
- Lee MJ, Wittich GR, Mueller PR (1998) Percutaneous intervention in acute pancreatitis. *Radiographics* 18: 711–724
- Lendrum R (1994) Chronic pancreatitis. In: Misiewicz JJ, Pounder RE, Venables CW (eds) *Diseases of the gut and pancreas*. Blackwell, London, pp 441–454
- Lerut J, Giannello P, Reynaert M, Otte JB, Kestens PJ (1985) Postoperative pancreatic fistulas: clinical study of a series of 114 consecutive cephalic duodeno-pancreatectomies. *Acta Chir Belg* 85: 205–210
- Lower WE, Farrell JT (1931) Aneurysm of the splenic artery: report of a case and review of the literature. *Arch Surg* 23: 182–190
- Lumsden A, Bradley EL III (1990) Secondary pancreatic infections. *Surg Gynecol Obstet* 170: 459–467
- Maher MM, Lucey BC, Gervais DA, Mueller PR (2004) Acute pancreatitis: the role of imaging and interventional radiology. *Cardiovasc Intervent Radiol* 27: 208–225
- Materne R, Vranckx P, Pauls C, Coche EE, Deprez P, Van Beers BE (2000) Pancreaticopleural fistula: diagnosis with magnetic resonance pancreatography. *Chest* 117: 912–914
- Mithöfer K, Mueller PR, Warshaw AL (1997) Interventional and surgical treatment of pancreatic abscess. *World J Surg* 21: 162–168
- Moossa AR, Gadd MA (1985) Isolated splenic vein thrombosis. *World J Surg* 9: 384–390
- Morgan DE, Baron TH, Smith JK, Robbin ML, Kenney PJ (1997) Pancreatic fluid collections prior to intervention: evaluation with MR imaging compared with CT and US. *Radiology* 203: 773–778
- Nabi Yattoo G, Sultan Khuroo M, Ahmad Wani N, Alam Wani K, Ahmad Bhat F (1999) Haemosuccus pancreaticus: a clinical challenge. *J Gastroenterol Hepatol* 14: 172–175
- Paci E, Antico E, Candelari R, Alborino S, Marmorale C, Landi E (2000) Pseudoaneurysm of the common hepatic artery: treatment with a stent-graft. *Cardiovasc Intervent Radiol* 23: 472–484
- Papachristou DN, Fortner JG (1981) Pancreatic fistula complicating pancreatectomy for malignant disease. *Br J Surg* 68: 238–240
- Pederzoli P, Bassi C, Falconi M, Albrigo R, Vantini I, Micciolo R (1986) Conservative treatment of external pancreatic fistulas with parenteral nutrition alone or in combination with continuous intravenous infusion of somatostatin, glucagon or calcitonin. *Surg Gynecol Obstet* 163: 428–432
- Pistolesi GF, Procacci C, Pederzoli P, Lombardi C (1978) Computer tomography in the diagnosis of mediastinitis due to pancreas ascites. *J Belge Radiol* 61: 439–442
- Pistolesi GF, Caudana R, Procacci C, Pederzoli P, Tinazzi Martini P, Graziani R, Mansueto GC, Spiller M (1987) Direct involvement of the spleen in pancreatitis; a pictorial essay. *J Magn Reson Imaging* 1: 145–154
- Pistolesi GF, Procacci C, Residori E, Bicego E, Bertocco M, Moore F, Bergamo Andreis IA (1992) Radiologic imaging of pancreatic fistulas. In: Pederzoli P, Bassi C, Vesentini S (eds) *Pancreatic fistulas*. Springer, Berlin Heidelberg New York, pp 10–38
- Procacci C, Pederzoli P, Caudana R, Bergamo Andreis IA, Iacono C, Tinazzi Martini P, Volino C, Zonta L, Moore F (1987) The role of computed tomography in pancreatic pseudocysts with mediastinal extension. *Med Imaging* 1: 39–46
- Procacci C, Mansueto GC, Graziani R, Bicego E, Pederzoli P, Mainardi P, Bergamo-Andreis IA, Valdo M, Azzolini D (1995) Spontaneous rupture of a pancreatic pseudocyst into the portal vein. *Cardiovasc Intervent Radiol* 18: 399–402
- Procacci C, Mansueto G, D'Onofrio M, Gasparini A, Ferrara RM, Falconi M (2002) Non-traumatic abdominal emergencies: imaging and intervention in acute pancreatic conditions. *Eur Radiol* 12: 2407–2434
- Puri S, Nicholson AA, Breen DJ (2003) Percutaneous thrombin injection for the treatment of a post-pancreatitis pseudoaneurysm. *Eur Radiol* 13 (Suppl 4): L79–L82
- Rau B, Uhl W, Buchler MW, Beger HG (1997) Surgical treatment of infected necrosis. *World J Surg* 21: 155–161
- Reber HA (2001) Pathogenesis of infection in pancreatic inflammatory disease. *Pancreatol* 1: 207–209
- Riddell A, Jhaveri K, Haider M (2005) Pseudocyst rupture into the portal vein diagnosed with MRI. *Br J Radiol* 78: 265–268
- Robinson PJA, Sheridan MB (2000) Pancreatitis: computed tomography and magnetic resonance imaging. *Eur Radiol* 10: 401–408
- Rosen RJ, Sanchez G (1994) Angiographic diagnosis and management of gastrointestinal hemorrhage. *Current concepts. Radiol Clin North Am* 32: 951–967
- Rumstadt B, Schwab M, Korth P, Samman M, Trede M (1998) Hemorrhage after pancreatoduodenectomy. *Ann Surg* 227: 236–241
- Saeed ZA, Ramirez FC, Hepps KS (1993) Endoscopic stent placement for internal and external pancreatic fistulas. *Gastroenterology* 105:1213–1217
- Safrit HD, Rice RP (1989) Gastrointestinal complications of pancreatitis. *Radiol Clin North Am* 27: 73–79
- Sankaran S, Walt AJ (1975) The natural and unnatural history of pancreatic pseudocyst. *Br J Surg* 62: 37–44
- Sato N, Yamaguchi K, Shimizu S, Morisaki T, Yokohata K, Chijiwa K, Tanaka M (1998) Coil embolization of bleeding visceral pseudoaneurysms following pancreatectomy: the importance of early angiography. *Arch Surg* 133: 1099–1102
- Schoder M, Cejna M, Langle F, Hittmaier K, Lammer J (2000) Glue embolization of a ruptured celiac trunk pseudoaneurysm via the gastroduodenal artery. *Eur Radiol* 10: 1335–1337
- Shankar S, vanSonnenberg E, Silverman SG, Tuncali K, Banks PA (2004) Imaging and percutaneous management of acute complicated pancreatitis. *Cardiovasc Intervent Radiol* 27: 567–580
- Sheiman RG, Chan R, Matthews JB (2001) Percutaneous treatment of a pancreatic fistula after pancreaticoduodenectomy. *J Vasc Interv Radiol* 12: 524–526
- Shonnard KM, McCarter DL, Lyon RD (1997) Percutaneous debridement of infected pancreatic necrosis with nitinol snares. *J Vasc Interv Radiol* 8: 279–282
- Siegel MJ, Sivit CJ (1997) Pancreatic emergencies. *Radiol Clin North Am* 35: 815–830
- Sparrow P, Asquith J, Chalmers N (2003) Ultrasonic-guided percutaneous injection of pancreatic pseudoaneurysm with thrombin. *Cardiovasc Intervent Radiol* 26: 312–315
- Spirnak JP, Resnick MI, Persky L (1984) Cutaneous pancreatic fistula as a complication of left nephrectomy. *J Urol* 132: 329–330
- Stabile BE, Wilson SE, Dibas HT (1983) Reduced mortality from bleeding pseudocysts and pseudoaneurysms caused by pancreatitis. *Arch Surg* 118: 45–51
- Stanley JC, Frey CF, Miller TA, Lindenaer SM, Child CG III (1976) Major arterial hemorrhage. *Arch Surg* 111: 435–438
- Stanley JH, Gobien RP, Schabel SI, Andriole JG, Anderson MC, Wesley Smith R (1988) Percutaneous drainage of pancreatic and peripancreatic fluid collections. *Cardiovasc Intervent Radiol* 1: 21–25
- Sunderland GT, Imrie CW (1992) Pancreatic fistulas in acute pancreatitis. In: Pederzoli P, Bassi C, Vesentini S (eds) *Pancreatic fistulas*. Springer, Berlin Heidelberg New York, pp 61–69
- vanSonnenberg E, Wittich GR, Casola G, Brannigan TC, Karnel F, Stabile BE, Varney RR, Christensen RR (1989) Percutaneous drainage of infected and noninfected pancreatic pseudocysts: experience in 101 Cases. *Radiology* 170: 757–761
- vanSonnenberg E, D'Agostino HB, Casola G, Halasz NA, Sanchez RB, Goodacre BW (1991) Percutaneous abscess drainage: current concepts. *Radiology* 181: 617–626

- vanSonnenberg E, Wittich GR, Chon KS, D'Agostino HB, Casola G, Easter D, Morgan RG, Walser EM, Nealon WH, Goodacre B, Stabile BE (1997) Percutaneous radiologic drainage of pancreatic abscesses. *AJR* 168: 979–984
- vanSonnenberg E, Wittich GR, Goodacre BW, Casola G, D'Agostino HB (2001) Percutaneous abscess drainage: update. *World J Surg* 25: 362–372
- Venu RP, Brown RD, Marrero JA, Pastika BJ, Frakes JT (2000) Endoscopic transpapillary drainage of pancreatic abscess: technique and results. *Gastrointest Endosc* 51: 391–395
- Vujic I (1989) Vascular complications of pancreatitis. *Radiol Clin North Am* 27: 81–91
- Willis SM, Brewer TG (1989) Pancreatic duct–portal vein fistula. *Gastroenterology* 97: 1025–1027
- Yamakado K, Nakatsuka A, Tanaka N, Takano K, Matsumura K, Takeda K (2000) Transcatheter arterial embolization of ruptured pseudoaneurysms with coils and n-butyl cyanoacrylate. *J Vasc Interv Radiol* 11: 66–72
- Yamamoto T, Hayakawa K, Kawakami S, Nishimura K, Katsuma Y, Hayashi N, Maeda M, Ishii Y (1999) Rupture of a pancreatic pseudocyst into the portal venous system. *Abdom Imaging* 24: 494–496

# Non-traumatic Uroradiological Emergencies

D. Rickards

## 5.7

### Contents

5.7.1	Introduction	523
5.7.2	Obstruction of the Upper Urinary Tract	523
5.7.2.1	Clinical Findings	524
5.7.2.2	Diagnostic Imaging	524
5.7.2.3	Plain Films and Excretory Urography	524
5.7.2.4	Ultrasound	526
5.7.2.5	Computed Tomography	527
5.7.2.6	Magnetic Resonance Urography	529
5.7.3	Treatment of Acute Urinary Obstruction	530
5.7.3.1	Patient Preparation and Consent	530
5.7.3.2	Localisation of the Pelvi-calyceal System	531
5.7.3.3	Puncture of the Pelvi-calyceal System, Track Dilatation and Tube Placement	531
5.7.3.4	Post-operative Care	532
5.7.4	Spontaneous Haemorrhage from the Urinary Tract	533
5.7.4.1	Clinical Findings	533
5.7.4.2	Radiological Findings	533
5.7.5	Spontaneous Bladder Rupture	534
5.7.6	Testicular Torsion	534
5.7.7	Priapism	535
	References	535

### 5.7.1 Introduction

Urinary obstruction is the leading cause of damage to the urinary tract and is frequently in need of urgent treatment, especially when complicated by sepsis. Obstruction, its diagnosis and treatment necessitate all the skills that form the bedrock of uroradiology and no hospital with an emergency department can adequately operate without such skills. Any part of the urinary tract can be obstructed from a single calyx to a stone lodged behind a urethral stricture that causes acute urinary retention. The role of imaging and intervention is to define the site and cause of obstruction and then to relieve it until the cause has been dealt with or if it cannot be, to provide long-term relief. Obstruction can occur in utero as well as at any age and is the most

common cause of paediatric end-stage renal failure needing transplantation and dialysis.

Non-traumatic catastrophic haemorrhage from the urinary tract is uncommon, but can occur secondary to tumours and congenital lesions, e.g. aneurysms of the renal artery. Bladder haemorrhage requiring emergency treatment is rare.

Spontaneous bladder rupture is uncommon, usually occurring in alcoholics or following cystoplasty.

Torsion of the testicle or the appendix of the testicle and priapism may require emergency imaging.

### 5.7.2 Obstruction of the Upper Urinary Tract

Obstruction of the upper urinary tract is only an emergency if it is acute, and even more so when obstruction occurs in a single kidney or transplant. The physiology of urine transportation is rapidly disrupted by obstruction. Under normal circumstances, urine is stored with the collecting system at low pressures, 10 cm of water and periodic rises in pressure (up to 15 cm water) and expels urine into the ureter, which propels urine at pressures between 20 and 60 cm of water into the bladder. In an obstructed state, the upper tract compensates by increasing renal blood flow and increasing both the frequency and pressure of ureteric peristalsis, but such compensation is transient. Peristalsis becomes inefficient, and the ureter dilates rendering peristalsis even more ineffectual. Dilatation of the collecting system initially compensates for increasing pressure within it, but eventually it loses the battle and glomerular filtration rate falls secondary to a decreasing blood flow. Vascular resistance increases and progressive nephron damage ensues.

Rupture of the pelvi-calyceal system with extravasation temporarily decreases the intra-pelvi-calyceal pressure [1], but within hours of the onset of obstruction, nephron damage occurs which, if left untreated, will be irreversible. To minimise the extent of potential renal impairment, obstruction must first be confirmed and then treated. The cause of obstruction is largely irrelevant. It does not matter whether it is due to a stone, sloughed papilla or blood clot.



They present with the same symptoms and signs, and are investigated and treated the same way.

### 5.7.2.1 Clinical Findings

Patients experience acute loin pain which can be severe, even intolerable. The pain is not alleviated by any position the patient might adopt. Vomiting and nausea are common. Initially urinary output will not fall, but will eventually fail because of dehydration, especially in children [2]. Renal function will deteriorate if left untreated, but the danger lies in hyperkalaemia, which can rapidly occur endangering cardiac function which can prove fatal. In a single functioning kidney, complete anuria is possible. Obstruction in a transplant kidney may be silent as the kidney is denervated. Renal output will be noticeably reduced if not non-existent, but transplant patients who know their transplant and renal status well will know there is something amiss.

Haematuria may be macroscopic but is usually not. The great danger other than hyperkalaemia is sepsis. Obstruction occurring in infected upper tract systems or due to infected stones can rapidly lead to septicaemia. In such circumstances, both the septicaemia and the obstruction demand treatment. Treating the septicaemia alone is unlikely to prove successful.

The causes of obstruction are numerous and largely irrelevant in the emergency situation. The commonest cause is calculus disease, where a stone has become lodged in part of the upper tract, usually the ureter, but it can obstruct a single calyx at its infundibulum or a calyceal diverticulum at its neck, where it communicates with the pelvicalyceal system [3]. Other luminal causes are a sloughed papilla, blood clot or a fungus ball, to name a few. Extraluminal or luminal abnormalities do not cause acute obstruction and are therefore not an emergency.

### 5.7.2.2 Diagnostic Imaging

Where the clinical signs and symptoms all too clearly point to acute obstruction, imaging is needed to (a) confirm obstruction, (b) guide interventional therapeutic measures and (c) to determine the level and cause of obstruction once it has been relieved, and the sepsis, if present, is treated.

Plain films and excretory urography are being surpassed by non-contrast computed tomography and ultrasound. The availability of CT is a problem in many centres and might not be available at all, so all techniques need to be considered. Prior to imaging, the patient needs resuscitation with analgesia and an IV access with or without a saline infusion depending on status. The majority, if not all, patients with acute obstruction will require hospitalisation.

### 5.7.2.3 Plain Films and Excretory Urography

Stones are radio-opaque in 90% of cases, and a careful search over the renal outlines and along the ureters is required (Figs. 1, 2). Lucent stones will not be seen, nor very small stones (less likely to cause obstruction), and stones will be missed or over-diagnosed because of phleboliths, etc. The size of the stone is important. Up to 90% of stones 5 mm or less can be expected to pass spontaneously within 4 days [4], and it is probable that the osmotic diuresis engendered by excretory urography pre-empt this. The affected kidney may show some modest enlargement.

Following IV contrast, the classic features are as follows:

1. Prolonged and dense nephrogram (Fig. 3)
2. Delayed pyelogram (Fig. 4)
3. Dilatation of the upper urinary tract above the point of obstruction (Fig. 5)
4. Extravasation of contrast (Fig. 6)
5. Nephromegaly

There is no point in prescribing exactly what sequence of films are needed, because each unit has its own protocol and the examination needs to be tailored to the patient's clinical condition as well as to available resources. The emergency protocol in the present author's unit is a plain film followed by a 10-min full-length film, which is likely to show a normal pyelogram on one side and a dense pyelogram on the affected side. At this point, no further films are necessary, as the

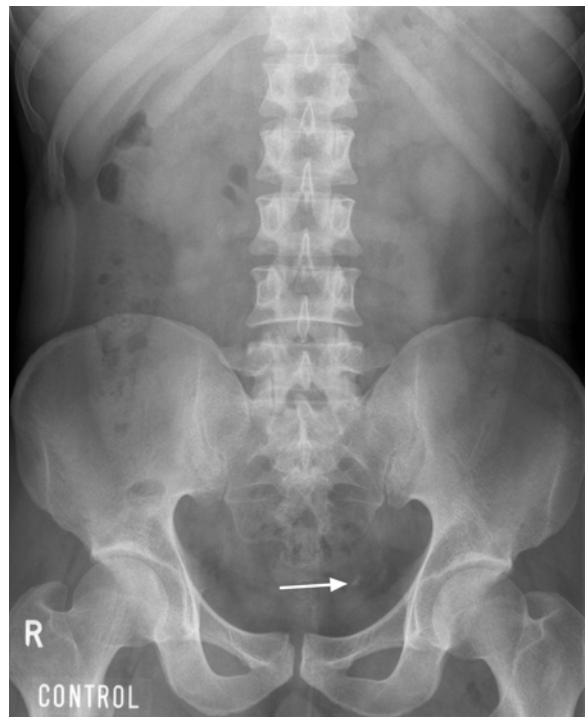


Fig. 1. A faint left distal ureteric stone (arrow)



**Fig. 2.** A small calculus overlying the transverse process of L4 on the left (*arrow*)



**Fig. 3.** At 5 min there is a normal right pyelogram and a dense left nephrogram with no pyelogram. Classic signs of acute obstruction

clinical diagnosis has been confirmed and all efforts are concentrated on treatment. Delayed films can be made, which will reveal the level and perhaps the cause of obstruction. The usual sequence involves doubling times until the anatomical information is clear, i.e. 20, 40, 80 and 160-min full-length films as are needed.

Where extravasation occurs, contrast is seen where contrast should not be, but the appearances can be very confusing. This can be expected in up to 33% of cases [5]. Pyelosinus extravasation is the most common situation, obscuring the normal sharp calyceal pattern, extending



**Fig. 4.** At 30 min there is a normal right pyelogram, but on the left, there is dilatation of the pelvi-calyceal system and the contrast within the left side is not as dense as that on the right. This is due to dilution of contrast within a urine-distended pelvi-calyceal system. There is a small stone (not seen) at the left vesico-ureteral junction (VUJ). This is partial obstruction



**Fig. 5.** Obstruction due to a distal left ureteric stone. Full-length KUB done 20 min after IV contrast. There is dilatation of the left pelvi-calyceal system and ureter down to the VUJ where an intraluminal filling defect is seen. This represents partial obstruction



**Fig. 6.** The left upper tract is normal. The appearances on the right are confusing, but there are dilated calyces and there is contrast where contrast should not be. This must represent obstruction and extravasation. In this case, the extravasation is into the perinephric space and contrast is mingling with peri-nephric fat

around the renal pelvis and outlining the proximal ureter. Less common is extravasation into the renal capsule. Once extravasation occurs, there is a decrease in renal pelvic pressures and glomerular filtration and urine formation continue despite obstruction. It is at this stage that a pyelogram rapidly appears. Although the appearances are alarming, extravasation is always benign and self-limiting. Where there is obstruction to a part of a kidney, similar, but segmental, abnormalities are seen.

Obstruction occurring in a poorly functioning kidney does not come under the heading of an emergency.

#### 5.7.2.4 Ultrasound

In acute obstruction, pyelocaliectasis is typically absent or there is only slight pelvi-calyceal dilatation. Stones within the collecting system are easily seen (Fig. 7); the latter can be seen in normal and unobstructed patients [6]. Dilatation of the collecting system is not synonymous with

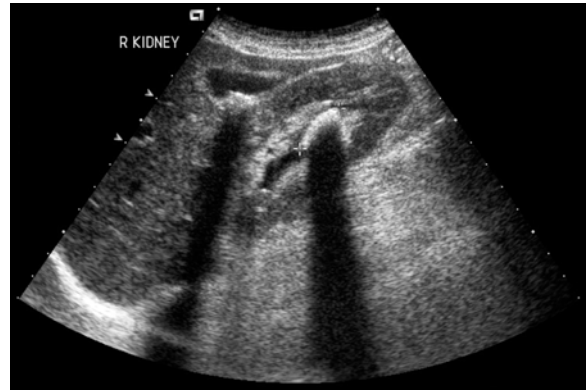


**Fig. 7.** There is a large calculus in the right renal pelvis. It is causing some obstruction as suggested by dilatation of upper pole calyces

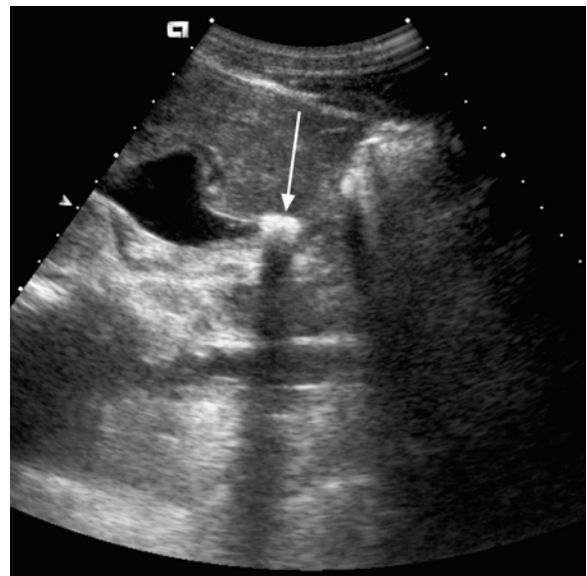


**Fig. 8.** There is an obstructing left ureteric calculus (*arrow*) causing a lot of proximal dilatation of the pelvi-calyceal system. This was a single kidney in a young man whose other kidney was removed due to a Wilm's tumour

obstruction, nor does the absence of dilatation exclude obstruction; therefore, grey-scale imaging has a limited role. Where there has been a delay in patient presentation, dilatation will be seen and may be complicated by infection, either an infected hydronephrosis or a pyonephrosis, which is associated with suppuration of renal parenchyma. If debris is seen with the collecting system, a pyonephrosis is more likely [7], but it is irrelevant as both conditions require urgent drainage. Unobstructing stones may be seen, which suggests a dislodged calculus is the cause. An attempt should be made to image the ureter, which is slightly easier if it is dilated, and to follow it down to an obstructing calculus (Fig. 8). If the bladder is distended, the distal

ureters can be seen as well as the vesico-ureteric junction. Stones must be sought there. Peri-nephric urinomas and subcapsular fluid collections are suggestive of obstruction with extravasation.

Colour Doppler may help. Up to 90% of patients with acute obstruction have asymmetrical ureteric jets [8], and in complete obstruction, no jet is seen from the affected side. Prominent vessels simulating pelvi-calyceal dilatation are easily distinguished. A raised resistive index (RI) implies a raised impedance of renal blood flow, which occurs in acute obstruction. It is not always easy to get a good trace as patients will be in pain and not able to cooperate fully. Obesity compounds difficulties as do ectopic kidneys. The RIs in excess of 0.7 are suggestive of acute obstruction, but with sensitivities between 40 and 100% reported [9], it is not worth measuring.

### 5.7.2.5 Computed Tomography

Smith et al. in 1995 proposed the use of CT in acute obstruction [10]. Non-contrast CT findings correlate well with those on excretory urography [11], and for detecting stones is nearly 100% specific and sensitive [12]. The technique continues to evolve with new technology. The 64-slice scanners with 1-mm slices are the present gold standard. Immediate reformatting in the coronal and sagittal plane with manipulation of the image allow for easy definition of the ureter, but there is a trade-off with dose [13]. No preparation, no contrast media and no delayed studies are needed. Patients can be scanned supine or prone. The prone position can identify possible interposition of the splenic or hepatic flexure of the colon between the posterior abdominal wall and the kidney. If seen, this would alter placement of nephrostomy tubes.

The primary advantage of non-contrast CT is the ability to identify calculi, especially those small obstructing calculi overlying bone. Finding a calculus is one thing, but determining whether it is the cause of obstruction is another. Dilatation of the pelvi-calyceal system and ureter down the side of the calculus is strong evidence of obstruction, as with the excretory urogram. Comparison with the ipsilateral normal side is helpful (Figs. 9, 10). The presence of perinephric stranding both around the kidney and ureter (Figs. 11–13), renal enlargement and a lower attenuation value of the affected kidney increase the diagnostic likelihood of obstruction [14]. A decrease of 4 Hounsfield units in the affected kidney suggests obstruction [15]. It is a non-specific finding that can occur in acute pyelonephritis, which can mimic colic. Not all obstructing stones have high attenuation on CT. Indivar (a drug used in immunodeficiency virus infection) induces symptomatic nephrolithiasis in 4% of cases, and very poorly calcified matrix stones are not seen on CT [16, 17]. The degree of perinephric stranding gives some indication as to the degree of obstruction. When extensive, high-grade obstruction could be predicted and the opposite when mild [18], and indeed, when extensive, the more likely the spontaneous passage of a stone [19]. Also predicting spontaneous passage, stone size is helpful. Those stones <3 mm are likely to pass, whereas those above 8 mm are not.

In 90% of patients presenting with acute flank pain, the absence or presence of an obstructing calculus can easily be made, but there are pitfalls. Phleboliths are not surrounded by soft tissue and can be associated with a tail of soft tissue which is the collapsed associated vein (Figs. 14, 15) [19]. Looking at a reconstructions helps enormously in defining the dilated ureter above a possible stone (Fig. 16). The radiolucent centre that phleboliths have on plain films cannot be seen on CT. Vascular calcification is usually lin-



**Fig. 9.** The right renal pelvis is dilated as compared with the left. The perinephric fat is normal





**Fig 10.** Non-contrast CT. There is a dilated right mid ureter (*arrow*) which has a slightly thickened wall. The left ureter is normal



**Fig 11.** Non-contrast CT. There is marked stranding within the perinephric fat of the left kidney without any obvious pelvi-calyceal dilatation. This is strong evidence of obstruction

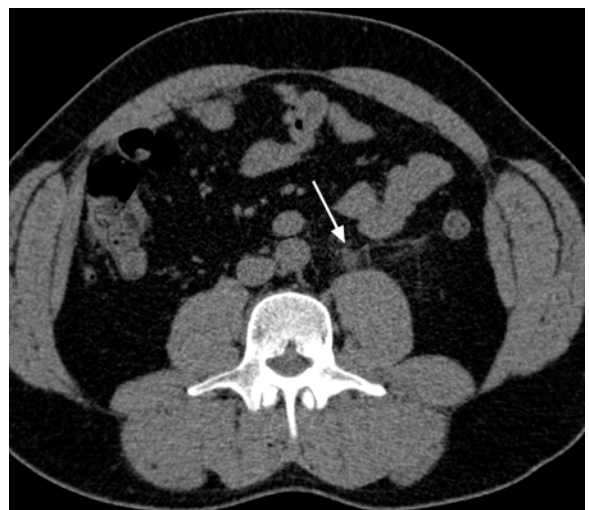


**Fig 12.** Non-contrast CT. There is marked stranding around the mid-left ureter (*arrow*), clear evidence of obstruction



**Fig 13.** Non-contrast CT. At a level just 1 cm below the scan in Fig. 12 is the obstructing calculus (*arrow*)

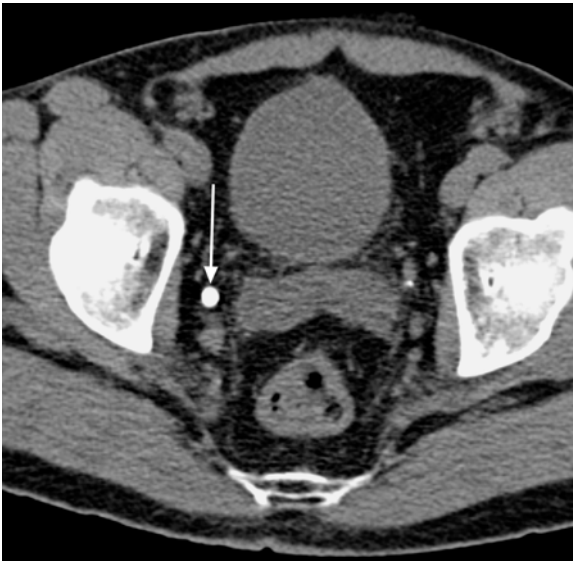


**Fig. 14.** Non-contrast CT. There is a large opacity in the right inferior hemipelvis (*arrow*). It is slightly posterior for the normally sited ureter and it is not surrounded by any soft tissue. This makes a phlebolith more likely



**Fig. 15.** Coronal reconstruction non-contrast CT. An opacity (*arrow*) in the right hemipelvis is a phlebolith. No surrounding soft tissue and no ureter is seen superiorly



**Fig. 16.** Reconstructed non-contrast CT. There is a calculus in the mid-left ureter and the dilated ureter can easily be seen above it. The amount of perinephric stranding can also be appreciated. There is very little in the way of pelvi-calyceal dilatation

ear and often quite symmetrical. Barium in diverticulae, brachytherapy seeds implanted for prostate cancer are but examples of other opacities that can mimic obstructing calculi. Conditions that mimic renal colic can be suspected on unenhanced CT and signs must be sought. Conditions include pancreatitis, appendicitis, hydrosalpinx and aortic aneurysm. Renovascular entities, e.g. renal vein thrombosis, are difficult to diagnose on unenhanced CT (Fig. 17).

#### 5.7.2.6 Magnetic Resonance Urography

Using T2-weighted sequences, MRU is a reliable and non-invasive method to demonstrate urinary tract dilatation and level of obstruction. The MRU cannot characterise small intraureteral filling defects and will miss most calyceal stones, but it is as good as CT is demonstrating perinephric stranding and other causes of acute flank pain [20].

The MRU is best reserved for selected patients, i.e. those pregnant, on indivar therapy and in whom the suspicion of extraordinary disease is high [21].



**Fig. 17.** Non-contrast CT. This patient presented with acute right renal colic and CT shows that the stone has passed into the bladder

### 5.7.3 Treatment of Acute Urinary Obstruction

The aim of any treatment is (a) to relieve obstruction to the upper urinary tract, thereby minimising or eradicating the possibility of permanent renal damage, (b) to relieve the pain associated with obstruction and (c) to treat infection caused by obstruction. This can be done antegradely by percutaneous nephrostomy or retrogradely by placing a JJ stent at cystoscopy. Cystoscopy involves a general anaesthetic, theatre time and it will often not be possible to bypass an obstructing calculus with any guidewire–catheter combination, so the ideal treatment of obstruction is nephrostomy. This involves the following:

1. Patient preparation and consent
2. Location of the pelvi-calyceal system
3. Puncture of the pc system, tract dilatation and drainage tube placement
4. Post-operative care

#### 5.7.3.1 Patient Preparation and Consent

Informed consent must be obtained and complications explained. Major complications, such as haemorrhage, must be stated, i.e. those that adversely affect the patient or need another procedure to correct. These can be expected in 3% [22]. Haematuria can be expected in all patients. Vascular damage needing surgical intervention is rare (<0.5%) [23]. Haemorrhage due to a pseudoaneurysm, arterio-venous malformation or vessel laceration are amenable to angiographic embolisation and can be expected in 2% of cases [24]. Any patient with a bleeding diathesis or on anticoagulants require special attention. In all patients, a coagulation profile and full blood and platelet count are mandatory. Ab-

normalities require correction to within acceptable limits, i.e. an INR (international normalized ratio) of <1.3, platelets of  $80,000 \times 10^9/l$  and a prothrombin time of <3 s. Clearly, a balance needs to be struck between the time taken to correct a bleeding diathesis and the danger to the patient with an obstructed kidney. This requires experience and an experienced operator to insert the nephrostomy for it to be shown that fewer complications can be expected [25].

Complications secondary to infection range from a low-grade fever to septic shock. Fevers and chills can be expected in 21% of cases [26]. Septic complications in patients with a pyonephrosis occur in at least 25% and can be very severe [27, 28]. Other factors that predispose to infection are diabetes, urinary diversions (ileal loop, ileocyclocystoplasty, etc.), bladder dysfunction and steroid therapy. These patients should have IV access via a saline drip and appropriate antibiotic cover [29]. Anaesthetic support should be sought and access to an ITU bed available should the patient develop septic shock requiring ventilatory support.

Sepsis can be minimised with less manipulation during nephrostomy placement and very little contrast instilled into the pc system, reducing any rise in pelvi-calyceal system, tract dilatation and tube placement pressure reducing bacteraemia [30, 31]. No diagnostic studies should be performed until the drained urine is clear of infection. It cannot be stressed enough that infection and sepsis can occur within minutes of nephrostomy placement, and it is the operator's responsibility to put in place all possible prophylactic procedures and to anticipate serious complications and have therapeutic measures in place. In our unit, even in the absence of a potential pyonephrosis, prophylactic antibiotics are given (e.g. 120 mg gentamicin IV, Hoechst Marion Roussel, West Malling, UK). Other complications are rare; these include puncture of adjacent organs, usually colon, hydrothorax and pneumothorax. Success rates in dilated kidneys of 98% can be stated [32, 33], but if undilat-



ed, success rates can fall to 85% [32], but these have improved with recent changes in technique.

All nephrostomies should be done under sedation and analgesia, and patients should be monitored with pulse oximetry and given oxygen. Where the patient, despite these measures, cannot cooperate, general anaesthesia must be considered, and is mandatory in children. The patient is then placed prone oblique on a fluoroscopy table, with the obstructed kidney uppermost.

### 5.7.3.2 Localisation of the Pelvi-calyceal System

#### Fluoroscopy

Those patients who have had a diagnostic excretory urogram may have a delayed pyelogram that allows for accurate puncture of the contrast filled collecting system under fluoroscopic control. Where the diagnosis has been made by CT or US, it is not worth giving contrast to opacify the pelvi-calyceal system because of the very considerable delay in the pyelogram that obstruction causes, which could be hours.

#### Ultrasound

If the pelvi-calyceal system is dilated, ultrasound can be used to define a point on the patient's back above a calyx and then the system is punctured. In systems that are only minimally dilated or non-dilated, continuous US is needed. For this, the probe is inserted in a sterile cover to allow the operator full use during needle placement.

#### Computed tomography

Computed tomography is useful where US cannot define the collecting system. In practice, this is rare in normal-sited kidneys, but in ectopic and displaced kidneys, it can be invaluable.

### 5.7.3.3 Puncture of the Pelvi-calyceal System, Track Dilatation and Tube Placement

Two methods in common practice depend on whether the pelvi-calyceal system is dilated or not. All punctures should ideally be directed towards the papillary tip of a posterior-facing lower pole calyx and approached through the relatively avascular line between the anterior and posterior branches of the renal artery (Brodel line 33). The patient's skin is cleansed, draped and local anaesthetic is infiltrated down to the capsule of the kidney and given sufficient time to take effect. If the pelvi-calyceal system is undilated, under guidance a 15-cm 22-g flexible Chiba needle (Becton Dickinson and Company, Franklin Lakes, N.J.) is passed into the most dilated part of the collecting system, whether that be the renal pelvis or infundibulum. Urine is aspirated

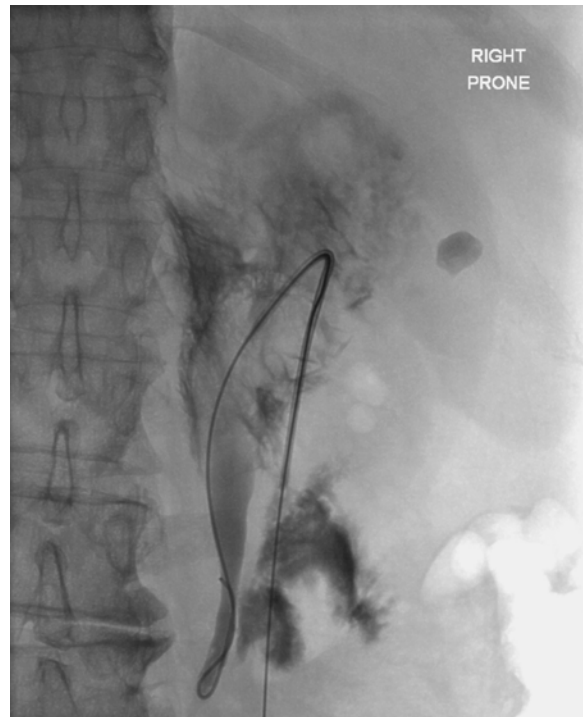


**Fig. 18.** Following opacification of the collecting system, a sheathed needle has been placed via a lower pole calyx, a guide wire passed through the sheath into the renal pelvis and down the ureter. There is extravasation of contrast confusing the picture. A dilator has been passed over the guide wire to dilate the tract

to confirm its intra-calyceal location, and that urine should be sent for bacteriology. Then, a little contrast and air is injected into the pelvi-calyceal system. Air will outline the posterior calyces and contrast the dependent ones [34–36]. Then a sheathed needle (18 G with a 5-F sheath Angiomed, Karlsruhe, Germany) is placed into a targeted calyx under fluoroscopic guidance. This method has the attendant danger of increasing intracalyceal pressure and thereby disseminating infection into the vascular space due to intrarenal reflux. In dilated systems, the initial step as outlined above can be omitted. Through the sheath, a 0.035-in. curved tip hydrophilic guidewire (Terumo, Leuven, Belgium) is advanced under fluoroscopy into the collecting system and sheath advanced over the guide wire to safely anchor its tip within the pelvi-calyceal system. By manipulating the curved tip of the wire, it is usually possible to get it down the ureter as long as it is not obstructed at the pelviureteric junction. If it is, then the guide wire needs to be passed into the upper pole calyces. The sheath then needs to be fully advanced over the wire and then the hydrophilic wire exchanged to a 0.035-in. metal wire (Superstiff Amplatz, Boston Scientific, Watertown, Mass.). Then, a track is dilated using facial dilators and a nephrostomy drain is inserted. Under all conditions, an 8-F catheter self-retaining (Soft drain, Angiomed) will suffice. To easily insert this, the track





**Fig. 19.** A drainage catheter has been passed over the guide wire and is located in the renal pelvis

should be dilated up to 10 F to accommodate the redundancy in the catheter by straightening with J shape that the catheter will ultimately assume. The drainage catheter is passed over the guide wire until all of its side holes are within the collecting system. In practice, this means that the end of the catheter will be down the ureter. The guide wire is removed, and under fluoroscopic guidance, the catheter is gently withdrawn while deploying its self-retaining properties. The catheter needs to be within the renal pelvis. It is wise to suture the catheter in place as well. Any temptation to extend the procedure, such as inserting a JJ stent, must be avoided. In acute obstruction, the aim is to relieve it. Stents can be placed at a later date, if appropriate.

This simplified description is not always borne out in practice. Initial puncture of the collecting system may well be associated with extravasation of any contrast instilled into the collecting system or contrast there following an IV injection of contrast (Figs. 18, 19).

#### 5.7.3.4 Post-operative Care

The patient should be carefully monitored for any signs of sepsis or significant blood loss [37, 38]. The drained urine volumes must be monitored and cultures performed to look for urosepsis. Diagnostic studies can be done within 24 h of nephrostomy insertion if there was no evidence of sepsis and infected urine; if there was, these must be delayed until the urine is crystal clear, and the patient apyrex-

ial and well. Any further interventions, e.g. JJ stent placement, ureteroscopy and percutaneous nephrolithomy must also be delayed until there is no sign of residual infection.

#### Complicated Cases

Not all kidneys are normally sited and body habitus can cause problems. A few examples are considered:

#### Transplant Kidneys

Obstructed transplants must be treated as an emergency [39]. They are superficially situated in an iliac fossa, denervated and extra-peritoneal in location and ideally suited to ultrasound-guided techniques. The basic technique is the same as for normally sited kidneys, but the puncture site must be kept as lateral as possible to avoid the peritoneum and colour Doppler is useful in avoiding major vessels. Blood loss can be expected to be more of a problem because Brodel's line cannot be accessed.

#### Ectopic Kidneys and Other Congenital Anomalies

Obstructed pelvic kidneys pose a major problem. They are extraperitoneal in location, usually have bowel between them and the anterior abdominal wall, and have pelvic bone posteriorly. No safe approach under any guidance is possible, and if a retrograde approach is for some reason impossible, a puncture through the anterior abdominal wall has to be done. Bowel perforation becomes a real problem and appropriate antibiotics must be given. Low-lying kidneys, malrotated kidneys and fused kidneys do not usually present a problem. Clearly, obstructed upper moieties of duplex kidneys require an upper pole approach often above the twelfth rib.

#### Horseshoe Kidneys

The lower poles of horseshoe kidneys are medially situated and both ureters and major vessels can be closely related to them. It is therefore wise to puncture through the laterally placed upper pole calyces which may involve a puncture above the twelfth rib.

#### Children

Essentially, this is the same approach as for adults, but smaller drainage catheters (5–6 F) are needed and tube stabilisation is difficult [40, 41]. General anaesthesia is mandatory.

#### Pyonephrosis

If pelvi-calyceal systems are full of thick and infected urine, aspiration of urine through either a Chiba or sheathed needle may be difficult or impossible. If the sys-



**Fig. 20.** An obstructed kidney due to a pelvic stone displaced anteriorly because of massive splenomegaly. Under CT, a needle has been advanced from the posterior abdominal wall into the collecting system, missing all other organs and with drainage safely achieved

tem is dilated, confirmation of needle tip placement is not too difficult, but if undilated, it is very difficult. There is no easy answer to this. An approach to the undilated pelvi-calyceal system will have to be made with a sheathed needle through which guide wires can be placed and manipulated under both US and fluoroscopic control. Once it is thought that the sheath is well into the collecting system, a little contrast can be injected, but this may show a bizarre appearance in a pyonephrosis, quite unlike the normal collecting system and often with no drainage down the ureter. These cases require great experience.

#### Displaced Kidneys

Kidneys can be very significantly displaced by other intra-abdominal pathologies. Because they are a posterior structure, they are usually displaced inferiorly or anteriorly. Computed tomography is then the best method of locating the collecting system and missing other intra-abdominal organs (Fig. 20).

### 5.7.4 Spontaneous Haemorrhage from the Urinary Tract

Spontaneous haemorrhage from the urinary tract is defined as bleeding with no history of preceding trauma, but due to a renal, systemic or coagulation abnormality. Common causes are malignant tumours, renal artery aneurysms, arterio-venous malformations [42], benign tumours (e.g. angiomyolipomas) [43] and vasculitis (e.g. polyarteritis nodosa and anticoagulant therapy), although 40% of anticoagulant-induced haemorrhage have significant underlying urinary tract disease [44]. Bleeding can occur in the collecting system, but it can also be intraparenchymal, sub-

capsular, perinephric or retroperitoneal. The extent of haematuria, if it occurs, does not indicate the severity of bleeding, as most bleeding occurs outside the luminal space.

Massive bladder haemorrhage can be caused by haemorrhagic cystitis [45], vascular tumours and arteriovenous malformations.

#### 5.7.4.1 Clinical Findings

Renal haemorrhage communicating with the collecting system presents with haematuria. Blood clots form within the renal pelvis and their passage down the ureter can result in typical renal colic and transient obstruction with hydronephrosis. Profuse bleeding can cause clot retention. Renal haemorrhage not communicating with the collecting system causes flank pain and a flank mass. Both types of haemorrhage can be associated with hypotension and a fall in the haematocrit requiring transfusion. Haematuria will occur in all patients with bladder haemorrhage and clot retention is common.

#### 5.7.4.2 Radiological Findings

Radiological findings depend on where the bleeding has occurred.

#### Intraluminal Bleeding

Clots within the collecting system cause filling defects on excretory urography and have a high attenuation on CT, typically 50–70 Hounsfield units [46]. Clot appears echogenic on US, but it is a non-specific finding. The underlying cause of bleeding may well be confirmed by all three modalities, but angiography may be needed.

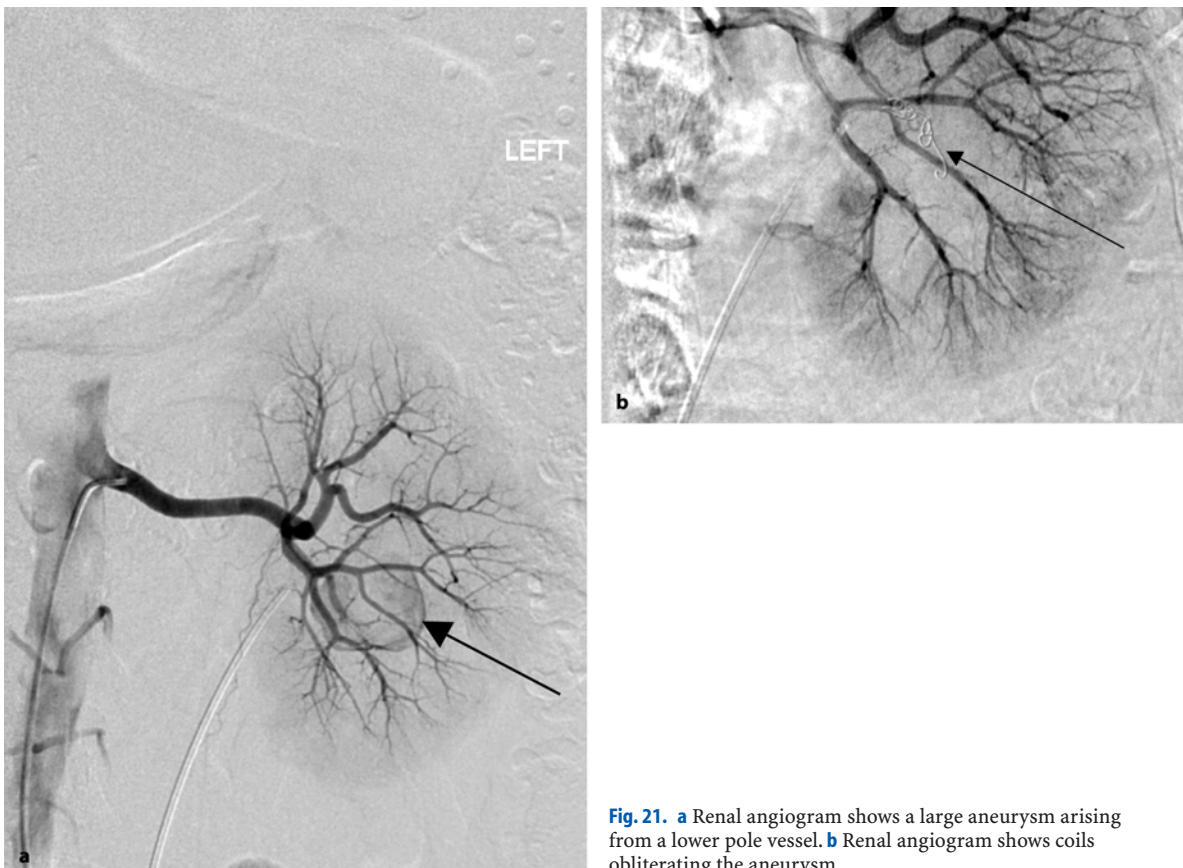


**Fig. 21.** **a** Renal angiogram shows a large aneurysm arising from a lower pole vessel. **b** Renal angiogram shows coils obliterating the aneurysm

### Subcapsular Haematomas

Subcapsular haematomas occur between the renal parenchyma and the renal capsule. The capsule is not elastic, so bleeding is usually limited and its cause will be tamponaded. The collecting system will be attenuated and displaced. Computed tomography will show a non-enhancing soft tissue mass around the kidney. Underlying pathology, e.g. tumour, must be carefully sought.

### Treatment of Haemorrhage

If surgery is not considered an option, embolisation is an option. Selective renal angiography will possibly pinpoint the bleeding vessel or vessels, and superselective cannulation can be followed by embolisation with coils (Figs. 21a,b). Bladder haemorrhage that does not respond to cystoscopic means may be controlled by embolising the anterior trunk of the internal iliac artery on both sides because of a rich anastomosis. Embolisation should be performed with gelfoam pledgets or the equivalent to minimize the risk of bladder wall necrosis [47].

## 5.7.5 Spontaneous Bladder Rupture

Spontaneous bladder ruptures are rarely reported. They have been reported in alcoholics who overdistend their bladders because of an excessive fluid intake [48]. Other causes are bladder tumours, radiation injury, during labour and chronic bladder inflammation [49]. Patients present with lower abdominal pain and anuria. The perforation is extraperitoneal and diagnosis is made by cystography or CT cystography. Treatment is either by surgery or catheterisation.

## 5.7.6 Testicular Torsion

In most units, the diagnosis of testicular torsion is made clinically. Where doubt exists, the scrotum is usually explored as an emergency, and if torsion is found, it is corrected. The degree and duration of torsion are crucial in determining the viability of the testicle. Complete torsion will result in necrosis of the testicle and its viability will only be salvaged if surgery is performed within 4 h. De-

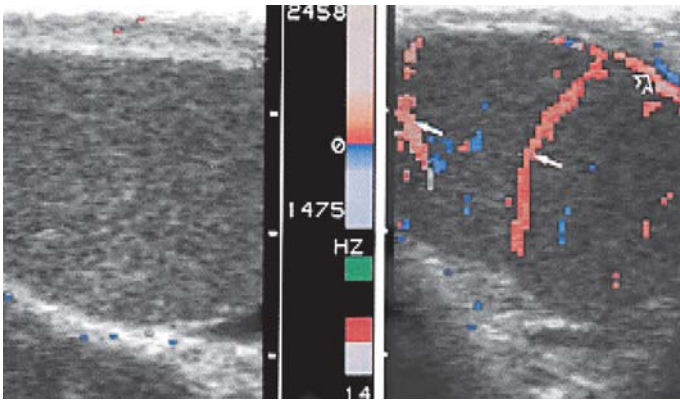


**Fig. 22.** Acute and complete testicular torsion. Flow is seen in the non-torted testicle

layed surgery will result in an infarcted testicle [50]. Ultrasound with colour Doppler will show either an avascular testicle (Fig. 22) or one with a decreased flow when compared with the non-torted testicle, but the delay in getting an ultrasound done and its relative limitations in defining the degree of torsion render the investigation a waste of precious time.

### 5.7.7 Priapism

Priapism is a prolonged and usually painful erection not initiated by sexual stimuli. Two types occur, high and low flow. Low-flow priapism results in stasis within the corpora that causes a decreased oxygen tension and acidosis which, if not corrected, will result in impotence. Emergency surgery to irrigate the corpora or perform shunts between the corpora and the spongiosum are needed. High-flow priapism is usually the result of perineal trauma; colour Doppler ultrasound will differentiate between the two. Low-flow cases will have a little flow within the corpora and is useful in directing treatment towards emergency surgery [51].

### References

1. Suziuki S, Saito Y. Effect of ureteral obstruction on proximal tubular functions of a rat kidney. *J Urol* 139:158–161, 1988
2. Klahr S. Pathophysiology of obstructive nephropathy. *Kidney Int* 23:414–426, 1983
3. Middleton AW. Stone-containing pyelocalyceal diverticulum. Embryogenic, anatomic, radiological and clinical characteristics. *J Urol* 41:2–6, 1974
4. Dawson C, Whitfield HN. ABC of urology: Urinary stone disease. *Br Med J* 312:1219–1221, 1996
5. Chen MY, ZagoriaRJ, Dyer RB. Radiologic findings in acute urinary tract obstruction. *J Emerg Med* 15:339–343, 1997
6. Dalla Palma L, Stacul F. Ultrasonography and plain film versus intravenous urography in ureteric colic. *Clin Radiol* 47:333–336, 1993
7. Vehmas T, Pasivansalo M et al. Ultrasound in renal pyogenic infection. *Acta Radiol* 29:675–678, 1988.
8. Deyoe LA, Cronan JJ et al. New techniques of ultrasound and color Doppler in the prospective evaluation of acute renal obstruction: Do they replace the intravenous urogram? *Abdom Imaging* 20:58–63, 1995
9. Older RA, Stoll HL et al. Clinical value to reno-vascular resistive index measurement in the diagnosis of acute obstructive uropathy. *J Urol* 157:2053–2055, 1997
10. Smith RC, Rosenfield AT, Choe KA et al. Acute flank pain: comparison on non-contrast CT and excretory urography. *Radiology* 194:789–794, 1995
11. Sourtzis S, Thibeau JF et al. Radiographic investigation of renal colic: unenhanced CT compared with excretory urography. *AJR* 172:1491–1494, 1999
12. Boulay I, Holtz P et al. Ureteral calculi: diagnostic efficiency of helical CT and implications for treatment of patients. *AJR* 172:1485–1490, 1999
13. Mamarsadeghi D, Heinz-Peerrl G et al. Unenhanced multidetector row CT in patients with suspected of having urinary stone disease: effects of sector width on diagnosis. *Radiology* 235:530–536, 2005
14. Georgiades CS, Moore CJ, Smith DP. Differences of renal parenchymal attenuation for acutely obstructed and unobstructed kidneys on unenhanced helical CT: A useful secondary sign? *Am J Roentgenol* 176:965–968, 2001
15. Baumgarten DA, Figueroa A. Decreased renal density: Another secondary sign of obstruction by noncontrast CT? 98th Annual Meeting of ARRS, San Francisco, 1998
16. Kohan AD, Armenakas NA, Fracchia JA. Indinavir urolithiasis: an emerging cause of colic in patients with human immunodeficiency virus. *J Urol* 161:1765–1768, 1999
17. Mathews LA, Spirnak JP. A matrix calculus causing bilateral ureteral obstruction and acute renal failure. *J Urol* 154:1125–1126, 1995
18. Boridy IC, Kawqashima A, Goldman SM et al. Acute ureterolithiasis: non-enhanced helical CT findings of perinephric edema for prediction of degree of ureteral obstruction. *Radiology* 213:663–667, 1999
19. Tahahashi N, Kawashima A, Ernst DR et al. Ureterolithiasis: Can clinical outcome be predicted with unenhanced helical CT? *Radiology* 208:97–102, 1998
20. Boridy IC, Nikolaidis P, Kawashima A et al. Ureterolithiasis: value of the tail sign in differentiating phleboliths from ureteral calculi at non-enhanced helical CT. *Radiology* 211:619–621, 1999
21. Sudah M, Vanninen RL, Partanen K et al. Patients with acute flank pain: comparison of MR urography with unenhanced helical CT. *Radiology* 223:98–105, 2002



22. Farral TA, Hicks ME. A review of radiologically guided percutaneous nephrostomies in 303 patients. *J Vasc Interv Radiol* 8:769-774, 1997
23. Kessaris DN, Bellman GC, Pardalidis NP et al. Management of haemorrhage after percutaneous surgery. *J Urol* 153:604-608, 1995
24. Dyer RB, Regan JD, Kavanagh PV et al. Percutaneous nephrostomy with extensions of the technique: step by step. *Radiographics* 22:503-525, 2002
25. Lee WJ, Mond DJ, Patel M et al. Emergency percutaneous nephrostomy. Technical success based on level of operator experience. *J Vasc Interv Radiol* 5:237, 1994
26. Lee WZJ, Patel U, Patel S et al. Emergency percutaneous nephrostomy: results and complications. *J Vasc Interv Radiol* 5:135, 1994
27. Ferral H, Stackhouse BJ, Bjarnason H et al. Complications of percutaneous nephrostomy tube placement. *Semin Intervent Radiol* 11:198-206, 1994
28. Cochran ST, Barnaric ZL, Lee JJ et al. Percutaneous nephrostomy tube placement: An outpatient procedure? *Radiology* 179:843-847, 1991
29. Spies JB, Rosen RJ, Lebowitz AS. Antibiotic prophylaxis in vascular and interventional radiology: a rational approach. *Radiology* 166:381, 1988
30. Ramchandani P, Cardella JF, Grassi CJ et al. Quality improvement guidelines for percutaneous nephrostomy. *J Vasc Interv Radiol* 12:1247-1251, 2001
31. Gerspach JM, Bellman GC, Stoller ML et al. Conservative treatment of colon injury following percutaneous renal surgery. *Urology* 47:831-836, 1997
32. Picus D, Weyman PL, Clayman RV et al. Intercostal space nephrostomy for percutaneous stone removal. *Am J Roentgenol* 147:393-396, 1986
33. Papanicolaou N. Renal anatomy relevant to percutaneous interventions. *Semin Intervent Radiol* 12:163-172, 1995
34. Patel U, Hussain FF. Percutaneous nephrostomy of nondilated renal collecting systems with fluoroscopic guidance: techniques and results. *Radiology* 233:226-233, 2004
35. Hunter DW, Salmonowitz E et al. Carbon dioxide as a lighter-than-contrast medium for percutaneous nephrostomy. *Radiology* 152:211-212, 1984
36. Dyer RB, Regan JD, Kavanagh PV et al. Percutaneous nephrostomy with extensions of the technique: step by step. *Radiographics* 22:503-525, 2002
37. Millward SF. Percutaneous nephrostomy: a practical approach. *J Vasc Intervent Radiol* 11:955-964, 2000
38. Maher MM, Fotheringham T, Lee ML. Percutaneous nephrostomy. *Semin Intervent Radiol* 17:329-339, 2000
39. Bennett LN, Voegli DR, Crummy AB et al. Urological complications following renal transplantation: role of interventional procedures. *Radiology* 160:531-535, 1986
40. O'Brien WM, Matsumoto AH, Grant EG et al. Percutaneous nephrostomy in infants. *Urology* 36:269-272, 1990
41. Stanley P, Bear JW, Reid BS. Percutaneous nephrostomy in infants and children. *AJR* 141:473-475, 1983
42. Takaha M, Matsumoto AQ, Ochi K et al. Intrarenal arteriovenous malformation. *J Urol* 124:315-318, 1980
43. Belville JS, Morgantaler A, Laughlin KR et al. Spontaneous perinephric and subcapsular renal haemorrhage: evaluation with CT, US and angiography. *Radiology* 172:733-740, 1989
44. Cuttino JT, Clark RL, Fester SH et al. The evaluation of gross haematuria in anticoagulated patients: efficacy of IV urography and cystoscopy. *AJR* 149:527-531, 1987
45. De Vries CR, Freiha FS. Hemorrhagic cystitis: a review. *J Urol* 143:1-9, 1990
46. Pqarienty RA, Ducellier R, Pradel J et al. Diagnostic value of CT numbers in pelvicalyceal filling defects. *Radiology* 145:743-760, 1982
47. Seiber PR. Bladder necrosis secondary to pelvic artery embolisation. Case report and review of the literature. *J Urol* 151:422-424, 1994
48. Kumar S, Rao MS. Concealed rupture of a normal bladder following an alcoholic bout. *J Trauma* 22:165-166, 1982
49. Huffman JL, Schraut W, Baley DH. Atraumatic perforation of the bladder. *Urology* 22:30-35, 1983
50. Williamson RC. Torsion of the testis and allied conditions. *Br J Surg* 20:465-468, 1976
51. Harmon WJ, Nehra A. Subspecialty clinics: urology, priapism. Diagnosis and management. *Mayo Clinic Proc* 72:350-355, 1997

## **Section Six**

# **Non-Traumatic Vascular Emergencies: Imaging and Intervention**



# Imaging and Intervention in Acute Non-traumatic Arterial Condition

W. Cwikiel

## 6.1

### Contents

6.1.1 Introduction . . . . .	539
6.1.2 Pulmonary and Bronchial Arteries . . . . .	539
6.1.2.1 Pulmonary Thromboembolism . . . . .	539
6.1.2.2 Bronchial Arteries . . . . .	542
6.1.2.3 Abdominal and Renal Arteries . . . . .	543
6.1.3 Acute Arterial Gastrointestinal Bleeding . . . . .	544
6.1.3.1 Peripheral Arteries . . . . .	544
6.1.4 Conclusion . . . . .	546
References . . . . .	546

### 6.1.1 Introduction

Radiological diagnosis is required on a regular basis in acute non-traumatic arterial conditions caused by thrombosis, emboli, or dissection. Methods of imaging and intervention in acute non-traumatic vascular arterial conditions have changed substantially during recent years. Computer tomography (CT), magnetic resonance angiography (MRA), and intravascular ultrasonography (IVUS) have replaced to large extent conventional diagnostic angiography. This is demonstrated by the rising number patients with suspicion of pulmonary embolism referred to CT scans, or evaluation of patients with aortic dissection by MRA or CT. In other acute non-traumatic arterial conditions, such as acute gastrointestinal bleeding, angiography is thus far a method of choice, but also encouraging MRI results have been reported [36]. The interventional treatment is being performed in an increasing number of patients with non-traumatic arterial conditions. Technical development of new equipment and instruments, increasing skill of interventional radiologists, and better understanding of events following interventions improve continuously results of the treatment. Development of MRI-guided interventions is in an early stage, but the preliminary results indicate future potential of these methods.

Acute non-traumatic acute arterial conditions can be categorized according to anatomic location as follows:

1. Coronary arteries
2. Supra-aortal and cranial arteries
3. Pulmonary and bronchial arteries
4. Aorta
5. Abdominal and renal arteries
6. Peripheral arteries.

According to the type of the disease, non-traumatic acute arterial conditions can be described as occlusive thromboembolic disease, occlusive or non-occlusive arterial dissection, and acute bleeding.

Patients with acute non-traumatic arterial condition require mainly immediate diagnosis and subsequent treatment. Some diagnostic delay is, however, generally accepted for patients without serious clinical symptoms such as peripheral occlusive disease or suspicion of pulmonary embolism. These patients can receive anticoagulant therapy during a short period of time, until the diagnosis is completed.

Diagnosis and treatment of acute non-traumatic arterial conditions is discussed herein (except those in coronary, supra-aortic, and cranial arteries, which are diagnosed and treated by cardiologists and neuroradiologists, respectively).

### 6.1.2 Pulmonary and Bronchial Arteries

#### 6.1.2.1 Pulmonary Thromboembolism

Pulmonary thromboembolism (PE) is a third most common cardiovascular disease and one of the leading causes of sudden death in western countries. Symptoms are similar to infectious disease, which can delay diagnosis of PE. The clinical suspicion of PE is conventionally verified on scintigraphy and/or pulmonary angiography. Pulmonary angiography, which remains the gold standard, has been, during recent years, increasingly replaced by spiral CT examination. The disadvantage of CT examination is inability to obtain diagnosis of small peripheral emboli and to



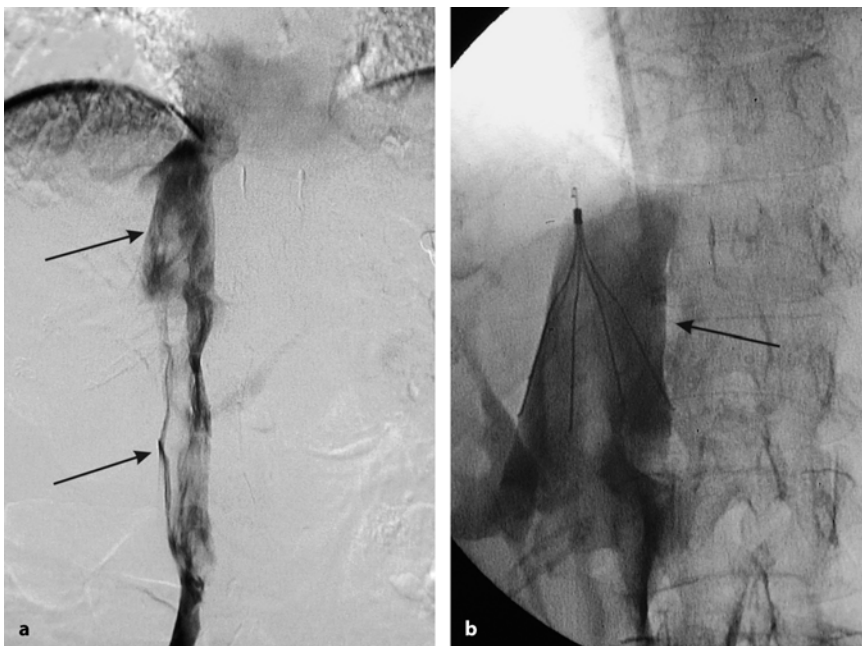


**Fig. 1.** Supraceliac inferior vena cava (IVC) filter. **a** Thrombus extending to infrahepatic IVC (arrows). **b** Filter encasing thrombus, placed by transjugular approach (arrow)

measure a pressure in the central circulation. Compared with pulmonary angiography, spiral CT is a non-invasive examination, usually done with less contrast medium, with short examination time, and is commonly available. Pulmonary angiography is now being used when spiral CT is inconclusive or endovascular treatment is intended. Both angiography and CT examination require use of iodinated contrast medium, whereas these methods may be unsuitable for patients with deteriorating renal function or with allergy. Magnetic resonance angiography has been proposed for diagnosis of PA [26, 27], but the results of MRA are inferior to those of spiral CT [2]. Improvement of MRA in diagnosis of PE may, however, be expected.

Conventional treatment of PE includes anticoagulant therapy, systemic administration of thrombolytic drugs, and, in severe cases, surgical embolectomy [20]. Anticoagulant therapy prevents further thrombus formation and permits endogenous fibrinolysis. Systemic administration of thrombolytic drugs (i.e., urokinase, r-TPA) increases perfusion to the lungs and reduces mortality rate [35]. If thrombolytic therapy is contraindicated, insertion of the inferior vena cava (IVC) filter can prevent further embolization and improve prognosis for the patient. Choice of the vena cava filter should be made according to diameter of the IVC, and possible necessity of the future filter retrieval. Placement of the filter can be done by transjugular, transfemoral, or peripheral approach, depending on extension of the thrombus, anatomic situation and type of the filter. The filter should be positioned in IVC caudal to the origin of the renal veins. For patients with IVC thrombosis stretching cranial to the origin of the renal veins, supraceliac position of the filter can be considered in life-threatening situations (Fig. 1).

Interventional treatment includes embolus aspiration, local administration of thrombolytic agent, mechanical thrombus fragmentation or combination of these methods [33]. Local infusion thrombolytic drugs through the catheter, with the tip wedged in the pulmonary embolus, can have good therapeutic effect (Fig. 2) [2]. Local cloth fragmentation can be obtained using the following techniques:

1. High pressure fluid injection Hydrolyser (Cordis, Warren, N.J.), shredding embolectomy catheter (Boston Scientific, Medi-Tech, Natick, Mass.), and Angio-jet (Possis, Minneapolis, Mich.)
2. Devices with rotating basket (impeller basket device, Cook Europe, Bjaeverskov, Denmark)
3. Thrombolizer (Angiocor, Lille Hellemmes, France)
4. Arrow-Trerotola device (Arrow, Reading, Pa.)
5. Impeller Kensey dynamic device (Dow Corning, Miami Fla.), Amplatz thrombectomy device (Microvena, White Bear Lake, Minn.), and Straub-Rotarex catheter (Straub Medical, Wangs, Switzerland)

For placement of these devices in pulmonary artery a long introducer sheath has to be used. During local fragmentation of a central embolus, cloth fragments are distributed to the more peripheral arterial branches (Fig. 3); however, several peripheral branches remain open, with subsequent decreased pressure in the pulmonary circulation and improved perfusion of the lungs. Aspiration, of the usually large central cloth, is often difficult but can be combined with mechanical fragmentation and the local thrombolysis. Balloon dilation and stenting of the pulmonary arteries is seldom necessary at emergency but can also be used for treatment of pulmonary embolism [10, 35].

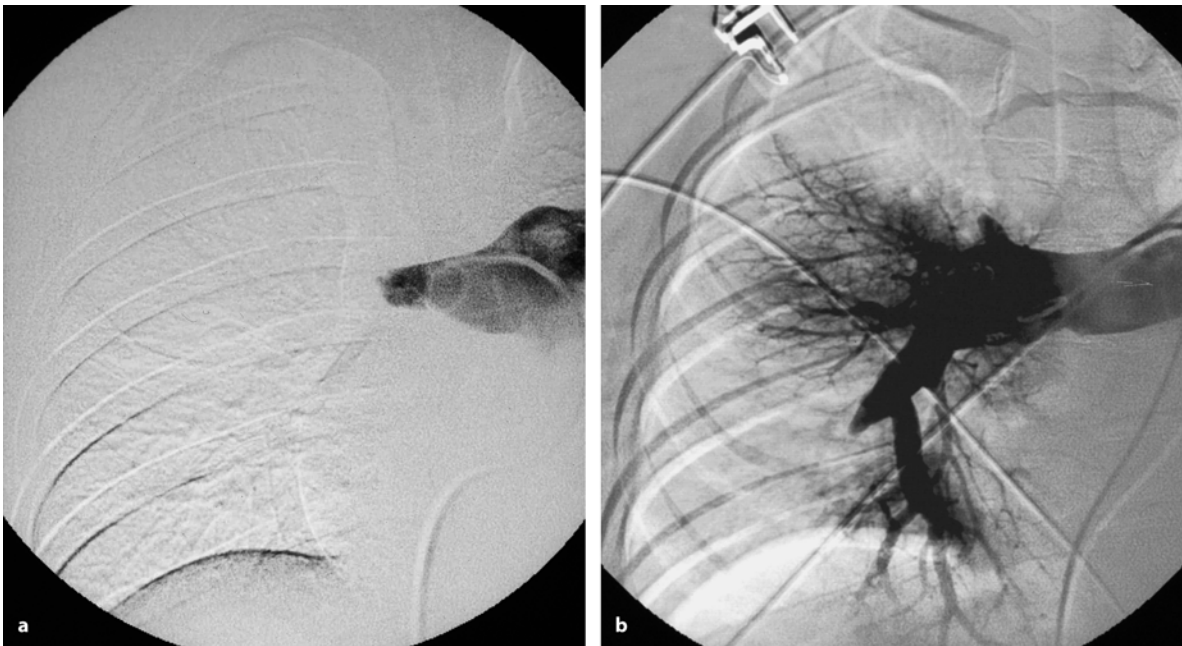


**Fig. 2.** Pulmonary embolism. Pharmacological thrombolysis. Totally blocked right main pulmonary artery. **a** Improved perfusion

after local thrombolysis for 24 h through the catheter wedged in the embolus

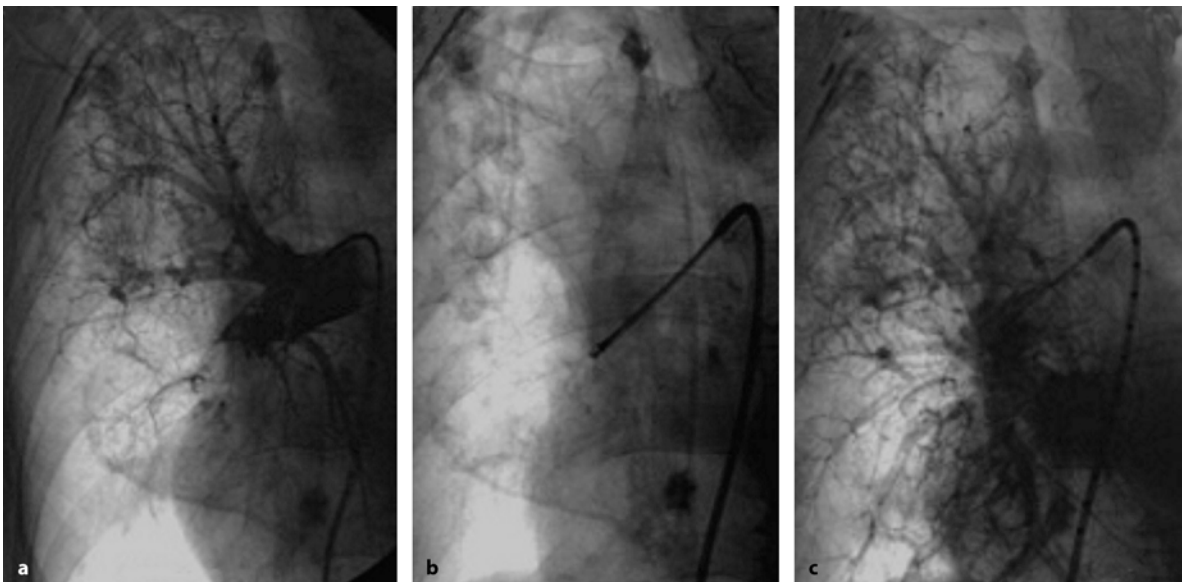


**Fig. 3.** Pulmonary embolism. Mechanical fragmentation. **a** Large clot in lower lobe bronchus. **b** Amplatz thrombectomy device in-

serted in the bronchus. **c** Increased perfusion to the lung after treatment

### 6.1.2.2 Bronchial Arteries

Massive hemoptysis is often a life-threatening condition and requires frequently emergent diagnosis and treatment. Acute hemoptysis can arise from pulmonary, intercostal, or other thoracic artery, but most frequently originates from the bronchial artery. Bronchial arteries arise usually from aorta at level of the left main bronchus, but the number of arteries, as well as their origin, can vary, and detailed angiographic work-up is often required. Bleeding can be caused by benign (common in tuberculosis) or malignant disease. Bronchoscopy, chest radiography, or CT can be helpful in approximating localization of the bleeding. Selective angiography of the thoracic (primary bronchial) arteries visualize site of the bleeding in up to 90% of patients (Fig. 4) [6]. Enlargement of arteries, aneurysms and shunts may also suggest site of bleeding. Intravascular embolization is a method of choice, and due to the small diameter of bronchial arteries, a coaxial catheter system is used for embolization. Embolization with Gelfoam, PVA particles, microspheres, or coils often has a prompt effect on the hemoptysis. Bronchial arteries can be embolized without serious consequences for the patient, but correlation to spinal arteries, which can have same origin, should always be revealed before embolization [6, 14, 21, 32, 41].

## Aorta

### Acute Aortic Dissection

Acute aortic dissection is a life-threatening condition. Etiological factors, including the Marfan syndrome and other conditions affecting connective tissue, uncontrolled hyper-

tension, and pregnancy, increase the risk of aortic dissection. Using the Stanford classification, dissection may be divided into type A, involving the ascending aorta, and type B, not involving the ascending aorta [15, 31]. Type-A dissection, which may affect the aortic valve, coronary arteries, or brachiocephalic arteries, requires emergent surgical treatment. Type-B dissection is usually treated medically, but in cases of rapidly increasing aorta diameter, malperfusion involving critical arterial branches, intractable hypertension, or severe pain more aggressive treatment is required. The diagnosis is usually established by CT, transesophageal echocardiography, or MRA. Due to availability, CT is probably the most commonly used diagnostic modality [11]. Multiplanar reconstruction of CT slices can provide information on the brachiocephalic arteries as well as non-vascular thoracic structures. Transesophageal echocardiography has the advantages of portability (allowing the diagnosis in the emergency department) and the ability to assess myocardial and valvular function prior to operation. Also MRA can provide sufficient information, particularly in patients with deteriorated renal function [22]. The role of angiography has evolved from the diagnosis of aortic dissection to treatment of the malperfusion syndrome, which frequently accompanies dissection [39]. In addition, angiography has a role in the emerging treatment of aortic dissection by means of endografts [11, 15, 31].

In the setting of aortic dissection, branch artery obstruction may be divided into static (or fixed) and dynamic obstruction [40]. In static obstruction, the dissection flap extends into a branch artery origin and narrows the true lumen. If the narrowing is hemodynamically significant, treatment consists of stent deployment across the nar-

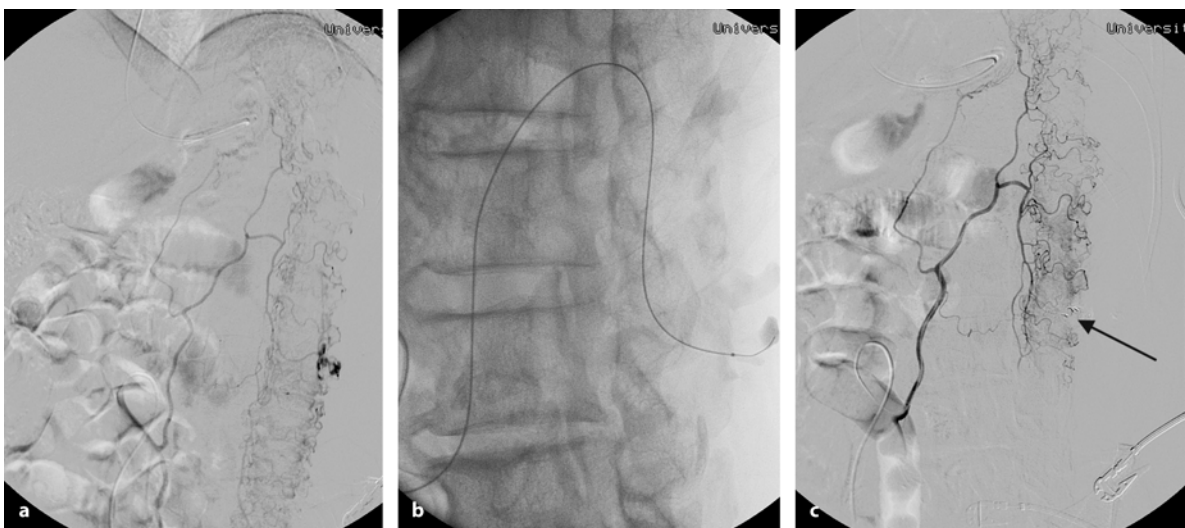


**Fig. 4.** Gastrointestinal bleeding. **a** Extravasation of the contrast medium from peripheral inferior mesenteric artery. **b** Superselective catheterization of the bleeding branch. **c** Following coil (arrow) embolization bleeding stopped

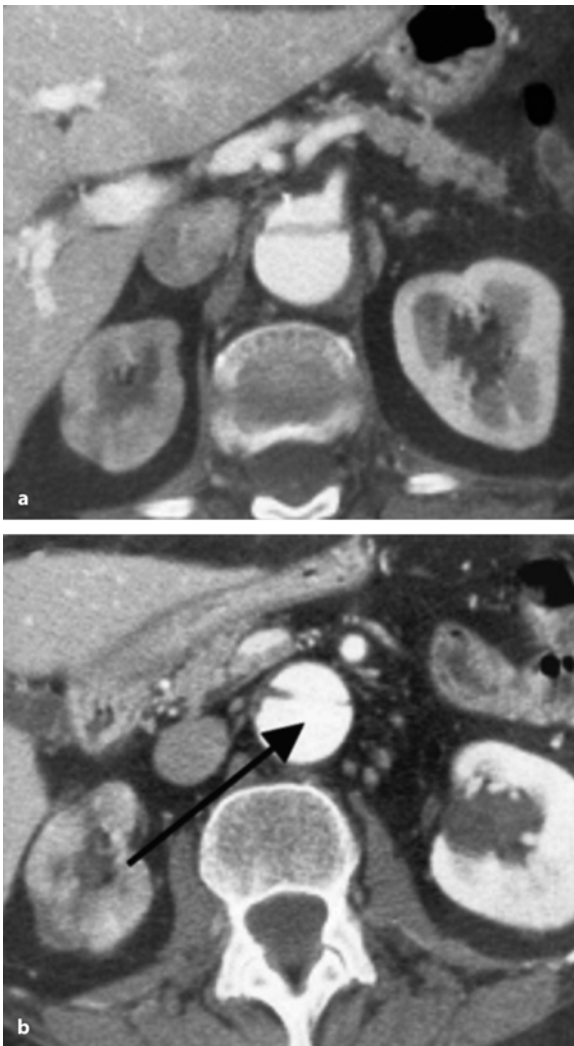


**Fig. 5.** Computed tomography of aortic dissection. **a** Compressed true aortic lumen with diminished blood flow to the small mesenteric artery. **b** Open fenestration (arrow) after 1 month

rowed segment. In dynamic obstruction, the flap does not extend into the origin but instead prolapses across the origin. Treatment consists of fenestration of the dissection flap, to allow flow and pressure equilibration between the true and false lumens (Fig. 5). For fenestration Rösch-Ushida TIPS instrument should be inserted in the smaller (usually true) lumen. Puncture of the intimal flap is guided by intravascular ultrasonography from the larger lumen, but also balloon or basket can be positioned in this lumen as a target for a puncture. The puncture hole in the intima is subsequently dilated over the guidewire with a 12- to 16-mm-diameter balloon. In some cases it is necessary to supplement fenestration by placing a large diameter stent in the aortic true lumen [40].

Recently, the use of endografts to cover the entry tear and restore transluminal pressure on the dissection flap

has been shown to be effective in treating the malperfusion syndrome. The use of endografts to induce thrombosis of the false lumen in uncomplicated type-B dissections appears promising [7, 25, 18].

### Rupture of Aortic Aneurysm

A moderate asymptomatic aortic aneurysm, with stable diameter, may be treated conservatively for several years. A rupture of aortic aneurysm, a highly fatal condition diagnosed frequently after acute onset of symptoms, may be found also in patients with no history of aortic disease.

Computed tomography is a modality of choice for diagnosis of ruptured aneurysm, but also transesophageal echocardiography and ultrasonography can be useful. Mortality rate is high and immediate treatment essential, traditionally as a surgical repair, but operative mortality rates up to 41% have been reported [13]. During recent years endovascular stent-graft placement has evolved as an alternative to surgery, diminishing substantially invasiveness of the treatment in the often hemodynamically unstable patient.

Assessment of anatomic suitability for possible endovascular repair may be done at primary CT examination. The endograft placement can be done under local anesthesia, and procedure is suitable for treatment of ruptured abdominal and thoracic aneurysms [13, 29]. A stent-graft treatment of ruptured aneurysm may convert the acute life-threatening situation to a stable situation, increasing survival of patients.

The possibility of late complications, requiring additional interventions, has been demonstrated, however, at midterm follow-up [8, 13].

### 6.1.2.3 Abdominal and Renal Arteries

#### Acute Thromboembolism of Renal Artery

Acute embolism of renal artery is most common in patients with heart disease (e.g., atrial fibrillation). Renal artery thrombosis can develop in grafts, but also after angioplasty or stent placement. Renal isotope scan, contrast-enhanced CT or angiography can confirm diagnosis [12]. Urgent treatment in the form of aspiration or thromboembolus, mechanical fragmentation, catheter-directed thrombolysis, or surgical intervention can save function of the kidney. The value of thrombolytic therapy has been documented in several case reports. Aspiration carries the risk of the spillover of thrombotic material both to the peripheral renal artery branches and through the aorta to the other, caudal arteries.

#### Visceral Thromboembolism

Visceral non-traumatic thromboembolism is most often secondary to heart disease, infection, atherosclerosis, malignant disease, or coagulopathy. Visceral thromboembolism can be suspected in case of rapid onset of bowel



symptoms, without signs of mechanical obstruction or other explanation. A CT examination can confirm deficient perfusion of the mesenteric branches in some cases, and show signs of bowel ischemia. Magnetic resonance imaging has the potential to improve on the diagnostic accuracy [1, 5, 36]. Diagnosis can be done by angiographic examination, but acute bowel resection is often performed due to the rapid progress of symptoms. Catheter embolectomy may be possible in case of more central embolus but practically is seldom attempted. Local or systemic thrombolysis carries risk of bleeding from the ischemic part of the bowel and can substantially delay surgery.

### 6.1.3 Acute Arterial Gastrointestinal Bleeding

Acute arterial gastrointestinal bleeding (GIB) can be divided in the upper GIB (proximal to the ligamentum of Treitz) and the lower GIB (distal to the ligamentum of Treitz).

Upper GIB is secondary to gastric or duodenal ulceration, hemorrhagic gastritis, tumor, pseudoaneurysm, angiodysplasia, inflammatory disease, or has iatrogenic origin. Endoscopy is commonly used for diagnosis and therapy. Angiographic work-up should include selective examination of the celiac trunk and superior mesenteric artery, followed by catheterization of left gastric artery, gastroduodenal artery, as well as hepatic and splenic artery. Aortography can be valuable if the aorto-enteric fistula is suspected. If the bleeding has gastric or duodenal origin, embolization can be performed safely; thus, a network of collaterals prevents ischemia. However, risk of ischemia is not negligible for patients with history of surgery in these organs. In case of bleeding from the gastroduodenal artery or its branch, embolization distally as well as proximally to the point of bleeding is required due to the double inflow of the blood (from common hepatic artery and superior mesenteric artery). Acute, non-traumatic hepatic arterial bleeding can be secondary to rupture of pseudoaneurysm, tumor erosion of the artery, or can have iatrogenic origin. Due to the double blood supply to the liver, embolization of branches of the hepatic artery is relatively safe; however, due to the rich collateral circulation in the liver, the artery should be embolized on both sides of the bleeding.

Acute arterial lower GIB originates usually from diverticula, angiodysplasia, or tumor, but may be secondary to inflammatory bowel disease, leukemic infiltration, or have iatrogenic origin.

Severe blood loss are frequent and the patients require often massive blood transfusion. Bleeding can be intermittent and stop due to lowered blood pressure and constriction of arteries. Consequently, the bleeding often cannot be visualized at acute angiography. If the patient is bleeding,

but is circulatory stable, red blood cells scan is valuable for localization of the bleeding. Provocation of the bleeding by intra-arterial administration of heparin or thrombolytic drugs during angiography has been proposed [30]. In acute active GIB angiography should be performed as soon as possible to identify bleeding site, followed by intra-arterial treatment. The GIB can be seen at angiography if extravasation of the blood is minimum of 0.5 ml/min. Selective intra-arterial injection of Vasopressin can be used (0.2–0.4 IU for 20 min, then 50% of the initial dose for 12 h), but this method has several disadvantages and contraindications. Embolization should be performed as close as possible to the source of bleeding. Use of coaxial catheter systems for superselective embolization is often necessary. Embolization of the peripheral arterial branch can be preferably done with micro-coils (Fig. 4) but can be combined with additional placement of pieces of gelfoam or other embolizing material; however, more central embolization of visceral arteries and embolization with liquids or particles should be avoided, due to risk for bowel necrosis. Endovascular treatment of GIB is effective first-line treatment, preventing bowel resection in many cases [24, 28, 30, 37].

#### 6.1.3.1 Peripheral Arteries

Acute peripheral arterial thromboembolic occlusion, which occurs predominantly in lower extremities, is a common problem for the interventional radiologists and vascular surgeons. Most patients have underlying vascular pathology, usually of atherosclerotic origin, but embolism secondary to cardiac disease may occur in patients with normal peripheral arteries. Embolus migration from the heart is most common cause, but emboli can originate from mural thrombus in the aortic aneurysm or central arteries. If acute peripheral occlusion is suspected, clinical diagnosis is usually confirmed by Doppler ultrasonography, but angiography is still a most important diagnostic tool, facilitating following endovascular intervention. Traditional treatment consisted of open embolectomy or bypass surgery. Over recent decades the treatment of peripheral thromboembolic disease become more efficient and cost-effective, due to introduction of the new thrombolytic agents, new catheters, mechanical thrombus fragmentation devices, and other tools.

In arteries and native grafts aspiration of embolic material is often the primary treatment. For the aspiration catheters of 5- to 8-F diameter, inserted preferably through the sheath with removable valve, are used [23]. In many cases aspiration is followed by catheter-directed thrombolytic therapy. In cases, of arterial thrombosis or combined thromboembolic disease, aspiration can be attempted, but thrombolytic therapy or mechanical thrombus fragmentation is usually necessary (Fig. 6). A mechanical thrombus fragmentation is effective in the synthetic grafts,



**Fig. 6.** Acute arterial graft thrombosis. **a** Thrombotic occlusion of a distal portion of femoro-popliteal graft. **b** Distal emboli following mechanical thrombus fragmentation and aspiration. **c** Restored distal flow after pharmacological thrombolysis and stenting of distal popliteal-proximal tibial artery (due to dissection)

**Table 1.** Properties of different thrombolytic agents

	Urokinase	Alteplase	Retaplaste	Tenecteplase
Plasma half-life	15 min	<5 min	13–16 min	18 min
Affinity for fibrin	Low	High	Low	Low
Fibrin specificity	Low	High	High	High
Clot penetration	Unknown	No	Yes	Yes
Vendor	Abbott Laboratories, Chicago	Boehringer Ingelheim, Basel	Centocor, Malvern PA,	Genetech, San Francisco CA, ancisco

but in the native artery it carries the risk of endothelial damage and more distal embolization. The use of the protection devices is recommended to prevent distal embolization [38]. After removal of the thrombus/embolus, balloon dilation or stent insertion is often necessary for a treatment of underlying stenosis.

Thrombolytic therapy can be risky for patients with arterial aneurysm and should be not performed right after surgery in patients with risk for intracranial bleeding, or in late pregnancy. Pharmacological thrombolysis also requires hospitalization and careful monitoring. Thrombolytic drugs, which have different properties, can be used (Table 1) [9, 16, 19, 34]. A relatively new group of thrombolytic agents are tissue plasminogen activators (rt-PA), converting plasminogen to plasmin. These drugs, for example, Tenecteplase, are produced by recombinant DNA technology, using an established mammalian cell line.

Treatment with Tenecteplase has been reported to be associated with decreased risk of non-cerebral bleeding and reduced need for blood transfusions in all patients [3]. Also, longer survival of patients treated with Tenecteplase with late presentation of acute myocardial infarction has been observed [34].

Good results for peripheral arterial applications has also been reported for combined therapy with Reteplase [9], which catalyzes the cleavage of endogenous plasminogen to generate plasmin, and IV Abciximab, a potent inhibitor of platelets aggregation [23]. Infusion of thrombolytic agents can be done through the multiple side-hole catheters or infusion wire into the thrombus as a graded, continuous, or pulse-spray infusion. A bolus injection may be done at the start of the treatment. Infusion should be stopped if fibrinogen is reduced to 40% of the initial levels (monitored at 4-h intervals), or if complications are suspected.

Complete or significant lysis is achieved in 75% of iliac, 58% of femoropopliteal, and 41% of crural vessels. Duration and type of presenting symptoms do not necessarily predict the outcome. Costs of the treatment are lower than for surgical treatment [17].

Patients presenting with acute upper limb ischemia tend to have significant co-existing more central disease; therefore, the angiographic examination should include proximal and distal arteries, as well as the aortic arch. Upper limb ischemia due to the arterial spasm can be managed with intra-arterial injection of vasodilators. In thromboembolic disease thrombolysis is a treatment of choice, with results comparable to those achieved in the lower extremities [4].

## 6.1.4 Conclusion

The importance of radiological imaging and intervention in diagnosis and treatment of the acute, non-traumatic arterial conditions increases continuously. Development of new diagnostic and interventional techniques and therapeutic modalities opens new possibilities for a less traumatic, safer, and efficient treatment of the patients with a acute, non-traumatic arterial diseases.

## References

- Baden JG, Racy DJ, Grist TM (1999) Contrast-enhanced three-dimensional magnetic resonance angiography of the mesenteric vasculature. *J Magn Reson Imaging* 10:369–75
- Blum A, Bellou A, Guillemin F et al. (2005) Performance of magnetic resonance angiography in suspected acute pulmonary embolism. *Thromb Haemost* 93:503–11
- Burkart DJ, Borsa JJ, Anthony JP et al. (2003) Thrombolysis of acute peripheral arterial and venous occlusions with tenecteplase and eptifibatid: a pilot study. *J Vasc Interv Radiol* 14:729–733
- Cejna M, Salomonowitz E, Wohlschlager H (2001) rt-PA thrombolysis in acute thromboembolic upper-extremity arterial occlusion. *Cardiovasc Intervent Radiol* 24:218–223
- Chow LC, Chan FP, Li KC (2002) A comprehensive approach to MR imaging of mesenteric ischemia. *Abdom Imaging* 27:507–516
- Corr PD (2005) Bronchial artery embolization for life-threatening hemoptysis using tris-acryl microspheres: short-term result. *Cardiovasc Intervent Radiol* 28:439–441
- Dake MD, Kato N, Mitchell RS et al. (1999) Endovascular stent-graft placement for the treatment of acute aortic dissection. *N Engl J Med* 340:1546–1552
- Doss M, Wood JB, Balzer J et al. (2005) Emergency endovascular interventions for acute thoracic aortic rupture: four-year follow-up. *J Thorac Cardiovasc Surg* 129:645–651
- Dresscher P, Crain, M R, Rilling WS (2002) Initial experience with the combination of Reteplase and Abciximab for thrombolytic therapy in peripheral arterial occlusive disease: a pilot study. *J Vasc Interv Radiol* 13:37–43
- Fontaine AB, Borsa JJ, Hoffer EK et al. (2001) Stent placement in the treatment of pulmonary artery stenosis secondary to fibrosing mediastinitis. *J Vasc Interv Radiol* 12:1107–1111
- Hagan PG, Nienaber CA, Isselbacher EM (2000) The International Registry of Acute Aortic Dissection (IRAD): new insights into an old disease. *J Am Med Assoc* 283:897–903
- Hazanov N, Somin M, Attali M et al. (2004) Acute renal embolism. Forty-four cases of renal infarction in patients with atrial fibrillation. *Medicine (Baltimore)* 83:292–299
- Hechelhammer L, Lachat ML, Wildermuth S et al. (2005) Midterm outcome of endovascular repair of ruptured abdominal aortic aneurysms. *J Vasc Surg* 41:752–757
- Kato A, Kudo S, Matsumoto K et al. (2000) Bronchial artery embolization for hemoptysis due to benign diseases: immediate and long-term results. *Cardiovasc Intervent Radiol* 23:351–357
- Kato N, Shimono T, Hirano T et al. (2001) Transluminal placement of endovascular stent-grafts for the treatment of type-A aortic dissection with an entry tear in the descending thoracic aorta. *J Vasc Surg* 34:1023–1028
- Kessel DO, Patel JV (2005) Current trends in thrombolysis: implications for diagnostic and interventional radiology. *Clin Radiol* 60:413–424
- Korn P, Khilnani NM, Fellers JC et al. (2001) Thrombolysis for native arterial occlusions of the lower extremities: clinical outcome and cost. *J Vasc Surg* 33:1148–1157
- Kusagawa H, Shimono T, Ishida M et al. (2005) Changes in false lumen after transluminal stent-graft placement in aortic dissections: six years' experience. *Circulation* 111:2951–2957
- Laird JR, Dangas G, Jaff M et al. (1999) Intra-arterial Reteplase for the treatment of acute limb ischemia. *J Invas Cardiol* 11:757–762
- Leacche M, Unic D, Goldhaber SZ et al. (2005) Modern surgical treatment of massive pulmonary embolism: results in 47 consecutive patients after rapid diagnosis and aggressive surgical approach. *J Thorac Cardiovasc Surg* 129:1018–1023
- Marshall TJ, Jackson JE (1997) Vascular intervention in the thorax: bronchial artery embolization for hemoptysis. *Eur Radiol* 7:1221–1227
- Matsunaga N, Hayashi K, Okada M et al. (2003) Magnetic resonance imaging features of aortic diseases. *Top Magn Reson Imaging* 14:253–266
- Morgan R, Bell A-M (2002) Percutaneous thrombectomy: a review. *Eur Radiol* 12:205–217
- Neuman HB, Zarzaur BL, Meyer AA et al. (2005) Superselective catheterization and embolization as first-line therapy for lower gastrointestinal bleeding. *Am Surg* 71:539–544
- Nienaber CA, Fattori R, Lund G et al. (1999) Nonsurgical reconstruction of thoracic aortic dissection by stent-graft placement. *N Engl J Med* 340:1539–1545
- Obernosterer A, Aschauer M, Portugaller H et al. (2005) Three-dimensional gadolinium-enhanced magnetic resonance angiography used as a “one-stop shop” imaging procedure for venous thromboembolism: a pilot study. *Angiology* 56:423–430
- Ohno Y, Higashino T, Takenaka D et al. (2004) MR angiography with sensitivity encoding (SENSE) for suspected pulmonary embolism: comparison with MDCT and ventilation-perfusion scintigraphy. *Am J Roentgenol* 183:91–98
- Patel TH, Cordts PR, Abcarian P, Sawyer MA (2001) Will transcatheter embolotherapy replace surgery in the treatment of gastrointestinal bleeding? *Curr Surg* 58:323–327
- Rousseau H, Dambrin C, Marcheix B et al. (2005) Acute traumatic aortic rupture: a comparison of surgical and stent-graft repair. *J Thorac Cardiovasc Surg* 129:1050–1055
- Ryan JM, Key SM, Dumbleton SA et al. (2001) Nonlocalized lower gastrointestinal bleeding: provocative bleeding studies with intraarterial tPA, heparin, and tolazoline. *J Vasc Interv Radiol* 12:1273–1277

31. Sailer J, Peloschek P, Rand T et al. (2001) Endovascular treatment of aortic type B dissection and penetrating ulcer using commercially available stent-grafts. *Am J Roentgenol* 177: 1365–1369
32. Stebbings AE, Lim TK (1999) Cause, treatment and outcome of patients with life-threatening haemoptysis. *Singapore Med J* 40:67–69
33. Tajima H, Murata S, Kumazaki T et al. (2005) Recent advances in interventional radiology for acute massive pulmonary thromboembolism. *J Nippon Med Sch* 72:74–84
34. Tsikouris JP, Tsikouris AP (2001) A review of available fibrin-specific thrombolytic agents used in acute myocardial infarction. *Pharmacotherapy* 21:207–217
35. Uflacker R (2001) Interventional therapy for pulmonary embolism. *J Vasc Interv Radiol* 12:147–164
36. Vossenrich R, Fisher U (2002) Contrast-enhanced MR-angiography of abdominal vessels: Is there still a role for angiography? *Eur Radiol* 12:218–230
37. Walsh RM, Anain P, Geisinger M et al. (1999) Role of angiography and embolization for massive gastroduodenal hemorrhage. *J Gastrointest Surg* 3:61–66
38. Wholey MH, Toursarkissian B, Postoak D et al. (2005) Early experience in the application of distal protection devices in treatment of peripheral vascular disease of the lower extremities. *Catheter Cardiovasc Interv* 64:227–235
39. Williams DM, Lee DY, Hamilton BH et al. (1997) The dissected aorta: III. Anatomy and radiologic diagnosis of branch-vessel compromise. *Radiology* 203:37–44
40. Williams DM, Lee DY, Hamilton BH et al. (1997) The dissected aorta: percutaneous treatment of ischemic complications: principles and results. *J Vasc Interv Radiol* 8:605–625
41. Witt C, Schmidt B, Geisler A et al. (2000) Value of bronchial artery embolisation with platinum coils in tumorous pulmonary bleeding. *Eur J Cancer* 36:1949–1954





# Imaging and Intervention in Acute Venous Occlusion

P. Haage, T. Krings

## 6.2

### Contents

6.2.1	Introduction	549
6.2.2	Acute Venous Occlusion of the Lower Extremity	549
6.2.2.1	Imaging	550
6.2.2.2	Intervention	551
6.2.2.3	Conclusions: Venous Occlusion of the Lower Extremity	552
6.2.3	Acute Pelvic Vein and Inferior Vena Cava Occlusion	552
6.2.3.1	Imaging	552
6.2.3.2	Intervention	553
6.2.3.3	Conclusions: Pelvic Vein and Inferior Vena Cava Occlusion	554
6.2.4	Acute Mesenteric Vein Occlusion	554
6.2.4.1	Imaging	555
6.2.4.2	Intervention	555
6.2.4.3	Conclusions: Mesenteric Vein Occlusion	556
6.2.5	Acute Venous Occlusion of the Upper Extremity	556
6.2.5.1	Imaging	556
6.2.5.2	Intervention	556
6.2.5.3	Conclusions Venous Occlusion of the Upper Extremity	557
6.2.6	Acute Venous Occlusion of Arteriovenous Hemodialysis Access	557
6.2.6.1	Imaging	557
6.2.6.2	Intervention	559
6.2.6.3	Conclusions: Venous Occlusion of Arteriovenous Hemodialysis Access	560
6.2.7	Acute Cerebral Vein Thrombosis	560
6.2.7.1	Imaging	561
6.2.7.2	Intervention	567
6.2.7.3	Conclusions: Cerebral Vein Thrombosis	568
	References	568

### 6.2.1 Introduction

Acute venous occlusion is a clinical entity, the importance of which cannot be emphasized enough. As a rule of thumb, 5% of the general population develops symptomatic acute venous occlusion in his or her lifetime. Diagnosis is established in 200,000 patients annually in Ger-

many alone [90]. The implications regarding morbidity, mortality, and cost are thus tremendous.

Due to its associated risks of pulmonary embolism (PE), renal failure, and phlegmasia cerulea dolens, acute venous occlusion is a potentially life-threatening disorder. Occlusion can emerge in any vein but is most frequently observed in the deep veins of the lower extremities. Chronic venous hypertension resulting in the “postphlebotic syndrome” as a consequence of deep venous thrombosis has been estimated to affect 500,000 individuals in the United States alone [79]. Timely diagnosis and treatment are therefore indispensable measures to provide adequate care for the patient. This claim is reinforced by the fact that the organization of a venous thrombus proceeds much faster than that of an arterial thrombus [102], thereby impeding successful treatment strategies. In addition, early clot clearance lowers the risk for PE and post-thrombotic sequelae [88].

This chapter focuses on the diagnostic tools and treatment options from the radiologist’s point of view in an emergency setting which includes acute venous occlusion of the lower extremities, pelvic vein, inferior vena cava, mesenteric vein, and the upper extremities. Furthermore, imaging and interventional treatment of acute venous occlusion of arteriovenous (AV) access and acute cerebral vein thrombosis are discussed.

### 6.2.2 Acute Venous Occlusion of the Lower Extremity

As many as 60% of patients with acute lower extremity venous occlusion are reported to develop PE, if left untreated [60]. Clinical signs are unreliable in establishing the correct diagnosis [31]. Many deep venous occlusions are clinically inconspicuous, because the thrombus does not completely occlude the vein or due to an ample collateral circulation. At present, the available diagnostic modalities are US, contrast venography, CT, and MR imaging. Once the diagnosis of acute venous occlusion has been verified, the next step is its adequate treatment. The objectives of an acute therapeutic regimen are restoration of unimpeded venous return, prevention of recurrent occlusion, preservation of venous valve function, and prevention of PE.

### 6.2.2.1 Imaging

Venography remains the reference gold standard of acute venous occlusion [8]. Even at present, with a variety of noninvasive tests, venography is essential especially for diagnosing symptomatic calf occlusions that do not extend proximally, recurrent venous occlusion in patients who are again symptomatic, and occlusions in patients who have a high clinical suspicion and a negative or equivocal, noninvasive study. The findings typical of acute venous thrombosis are a filling defect with surrounding contrast medium "tram-tracking," or abrupt vessel cut-off distant from a valve in the case of total occlusion. The sensitivity of venography is almost 100%, and the test accurately detects acute venous occlusions of the entire leg including the calf as well as the pelvic veins and the inferior vena cava, which may be overlooked by other diagnostic modalities such as US [24]; however, venography is invasive and has associated complications, such as allergic reactions, nephrotoxicity, and phlebitis, and thus its use is limited to carefully selected patients. Furthermore, venography may be nondiagnostic in up to 18% of cases through misinterpretations, artifacts, and interobserver disagreement [110]. Underfilling of vessels and vessel superposition are problems encountered especially in calf-vein phlebography.

In the hands of an experienced operator, duplex US with manual compression is the most sensitive and specific of the routinely available noninvasive tests. In many cases, US has replaced contrast venography. The advantages of US are that it also detects other pathologies such as Baker cysts, lymphadenopathy, hematomas, femoral artery aneurysms, superficial thrombophlebitis, and abscesses [13]. Also, it is widely available and inexpensive.

Criteria for the diagnosis of acute venous occlusion by Doppler ultrasound include failure of vein to collapse on direct compression, visualization of thrombus within the normally echo-free lumen, and absent or abnormal venous pulsation on Doppler scanning [48]. Inability to compress the common femoral or popliteal vein is usually diagnostic of a first episode of venous occlusion in symptomatic patients (positive predictive value of approximately 97%). Full compressibility of both of these sites indicates proximal patency in symptomatic patients (negative predictive value of approximately 98%) [48].

In general, duplex US is more accurate when the patient has symptoms of acute venous occlusion, and when the occlusion is in the thigh rather than above the groin or below the knee [49]. Venous US has a sensitivity of only 50–75% for isolated distal calf vein occlusion, and the clinical utility of venous US of the distal veins is vague. In one study, power Doppler demonstrated a sensitivity of 100%, a specificity of 79%, a positive predictive value of 71%, and a negative predictive value of 100% in detecting an isolated calf vein thrombosis [22]. The hazard of calf vein occlusions are that they can extend to the larger more proximal veins, thus posing an increased risk of PE. A repeat US

within 1 week is therefore indicated in those patients with a normal US exam at presentation [41].

Ultrasound can be technically difficult in obese patients or those with a large amount of lower extremity edema. In asymptomatic patients, the usefulness of US is even more limited. The Venous Thrombosis Group of Denmark compared US with venography in asymptomatic patients after elective hip surgery and found that in patients with contrast-venography-proven venous thrombosis, US had a sensitivity of 54%, specificity of 91%, a positive predictive value of 83%, and a negative predictive value of only 69% [11]. These limitations of sonography and its well-known low sensitivity in recurrent venous occlusion should be recognized in the diagnostic work-up of suspected lower limb venous occlusion.

Again, if the pretest probability is high and the results of sonography are nondiagnostic or are discordant with the clinical assessment, venography should be considered.

Spiral CT venography has been proposed as an accurate tool for the evaluation of acute venous occlusion. The CT can detect occluded veins and is considered superior to conventional venography by identifying intraluminal thrombi, possibly distinguishing new thrombi from older ones, and delineating soft tissue alterations such as extrinsic compression of the vein. The prevalence of unsuspected venous thrombosis detected by CT in a study was found to be 1.1% [108]. In one study spiral CT venography of the lower extremity showed a sensitivity of 100% and a specificity of 96% [114]. The quality of venous opacification with CT venography compared with ascending phlebography was rated superior in all segments; however, the application of CT venography alone is limited due to high costs and concomitant radiation dosage and is presently only applied as an adjunct to pulmonary CT angiography in case of suspected PE. If PE is proven, an indirect CT phlebography can be performed without the need of additional contrast medium application [109]. When compared with the results of US, phlebography, or autopsy, indirect CTP with multi-slice CT had a sensitivity of 94.3% and a specificity of 92.1% [109]. The CTP was also reported to be superior to venous sonography in one Japanese study [51].

One advantage of MR imaging over other techniques is that it can differentiate an acute occlusion from chronic thrombosis more accurately than US can [21]. Furthermore, MR imaging delineates the surrounding tissues and thus may indicate the cause of the occlusion. It is also less operator dependent than US. It is accurate for the diagnosis of acute venous occlusion of the calf which can easily be missed by US, and it can be performed in postoperative patients with full-length leg plaster casts. The sensitivity and specificity are reported to be as high as 100% for acute venous occlusion of the thigh and 87–100% and 97% for occlusion of the calf, respectively [13, 23, 61]. Because of its high cost and limited access, MR venography is not yet used for the routine diagnosis of lower extremity venous occlusion only; however, it can be useful after other inconclusive tests have been performed (Fig. 1).

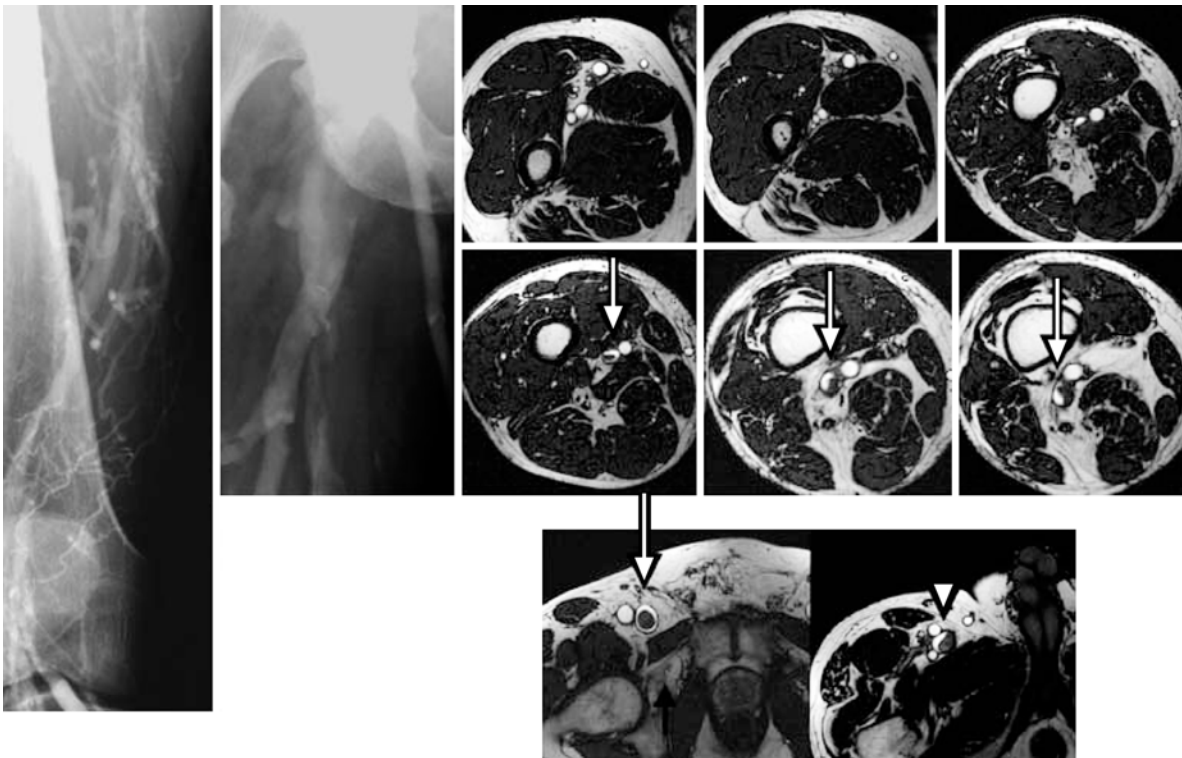


**Fig. 1.** High-resolution steady-state-free-precession (SSFP) MR venography of a superficial femoral vein thrombosis compared with venography. Transverse 2D balanced fast-field-echo [FFE; SSFP, true fast imaging with steady precession (FISP), FIESTA] with the following parameters: TR 5.0 ms; TE 2.5 ms; field of view

(FOV) 440 cm; and 512×512 matrix. Thrombus is displayed with low signal intensity (*arrows*), whereas venous blood pool is displayed as being signal enhanced due to the “T2-like” contrast in balanced FFE

### 6.2.2.2 Intervention

The current standard of care includes systemic anticoagulation with heparin followed by therapy with warfarin sodium [45] for acute venous femoro-popliteal occlusion. Such a regimen, however, does not promote lysis to reduce the thrombus load, nor does it contribute to restoration of venous valve function. Anticoagulation alone, therefore, does not protect the limb from postthrombotic syndrome, which can occur months to years after the acute thrombotic event [91]. Up to two-thirds of patients with acute iliofemoral venous occlusion develop edema and pain, and 5% develop ulcers albeit adequate anticoagulation [71, 91].

Thrombolysis is a potentially attractive form of therapy because it provides the prospect for rapid restitution of venous patency and preservation of venous valve function. This therapy can potentially help prevent the feared long-term sequelae of deep venous occlusion. It has been reported that thrombolytic agents, even when administered systemically, are superior to standard anticoagulation therapy for achieving early lysis of thrombus. In a meta-analysis of the results from 13 randomized studies, Comerota and Aldridge [18] demonstrated that only 4% of patients treat-

ed with heparin had substantial or complete lysis as compared with 45% of patients arbitrarily assigned to receive systemic streptokinase therapy.

Notwithstanding these outcomes, broad routine introduction was delayed. One of the reasons may be that via systemic administration the drug does not reliably reach and penetrate the occluded venous segment in sufficient concentration to provide most favorable results.

Delivery of the thrombolytic agent directly into the thrombus may offer substantial advantages over systemic administration. First indications on the potential of catheter-directed thrombolysis can be spotted from the study by Semba and Dake [86]. They observed complete lysis in 72% of patients, with associated resolution of symptoms.

Because thrombolytic agents activate plasminogen in the thrombus, delivery of the drug to that location improves its efficiency. By delivering higher concentrations of the drug, lysis rates can be improved, the length of treatment can be decreased, and problems associated with the exposure of the patient to systemic thrombolytic therapy may be reduced. The results were supported by the data from a multicenter venous registry, where marked lysis was achieved in 83% of patients with femoral-popliteal occlusion with a 1-year primary patency rate of 47% following catheter-direct-



ed thrombolysis [59]; however, the manifold contraindications to the use of thrombolytic agents may limit the usefulness of such therapy; it was reported to be feasible in only 7% of patients in one study [56]. Major bleeding complications were reported in 54 (11%) of 473 patients included in the registry [59]; of those, 21 (39%) occurred at the venous puncture site, and 7 (13%) resulted from a retroperitoneal hematoma. In an additional 15 (28%) patients, other bleeding complications were recorded. No immediate deaths occurred as a consequence of a major bleeding complication.

From an interventional radiologist's viewpoint, catheter-directed thrombolysis can be applied to dissolve thrombus securely and effectively from the deep veins in carefully selected patients with symptomatic venous lower limb occlusion and no contraindications to therapy. The best results can be anticipated in patients with acute symptoms and no history of previous thrombosis and who are treated with local thrombolysis. The longstanding benefits of this type of therapy are thus far not known and cannot decisively be derived. Thrombolytic therapy has the capability of shielding the patient against chronic venous insufficiency by attaining patency and preserving valve function. In cases of isolated calf vein occlusion, anticoagulation therapy should be sufficient to prevent chronic venous insufficiency [57]. Percutaneous mechanical thrombectomy devices currently are not indicated in cases of acute venous occlusion, which are merely situated in the lower extremity.

---

### 6.2.2.3 Conclusions: Venous Occlusion of the Lower Extremity

In acute venous occlusion of the lower extremity phlebography is still the reference gold standard. Presently, duplex ultrasound with manual compression is the most sensitive and specific noninvasive test. Limitations of ultrasonography include isolated distal calf vein occlusion, obesity, and patients with lower extremity edema. If sonography is non-diagnostic, venography should be considered. Magnetic resonance venography can differentiate an acute occlusion from chronic thrombus, but because of its high cost and limited availability, it is not yet used for the routine diagnosis of lower extremity venous occlusion only. Regarding interventional treatment, catheter-directed thrombolysis can be applied to dissolve thrombus in carefully selected patients with symptomatic occlusion and no contraindications to therapy.

---

## 6.2.3 Acute Pelvic Vein and Inferior Vena Cava Occlusion

Acute occlusion of the pelvic veins and the inferior vena cava (IVC) are frequently due to extension from the femoropopliteal system, representing a significant risk of clinically significant PE [37]. Isolated pelvic vein occlusion

is uncommon in an emergency situation and has been reported mainly as a complication in the postpartum period [2]. Furthermore, thrombosis of the pelvic veins, including the internal iliac veins, can be seen in women with pelvic inflammatory disease and in men with involvement of the prostatic plexus. Pelvic vein occlusion should be suspected in patients with abdominal pain, a unilateral pelvic mass, uterine infection, and fever that fails to respond to appropriate treatment, especially in trauma patients and post-operatively.

---

### 6.2.3.1 Imaging

Lately, the utilization of US has taken on greater importance for the diagnosis of venous occlusion. In the presence of thrombus, the vein is distended and incompressible. Sharp definition of the venous wall is lost and the presence of echogenic material inside the lumen may be observed. Very fresh thrombus may be nearly anechoic and consequently not openly perceptible [115]. Color flow is helpful in these cases, as the thrombus will appear as a color flow void. The most useful criterion for acute venous occlusion is failure of the vascular lumen to collapse entirely on gentle pressure. Under normal circumstances flow is identified as a spontaneous phasic pattern at rest with augmentation on calf compression. In the presence of occlusive thrombus, no flow is detected. Venous flow is generally phasic, decreasing in inspiration and increasing in expiration. A proximal obstruction will prevent such respiratory variation resulting in a continuous flow pattern and will also prevent venous distension normally seen when performing the Valsalva maneuver.

Color flow Doppler imaging is necessary for the evaluation of pelvic vessels [115] but is often limited due to the intrinsic difficulty in plainly outlining the pelvic structures. Ultrasonography is the primary diagnostic method in the pregnant patient and can also serve as a screening test in other patients, proceeding to more invasive testing if the results are uncertain.

Venography has long been considered the gold standard for identifying proximal venous occlusion, because it allows a complete work-up of the lower limb up to the IVC. In contrast to sonography, diagnosis is less restricted by obesity and bowel gas. It is generally a safe procedure and is often indispensable in cases of failure of sonography and in the absence of CT or MR facilities.

Both CT scanning and MR imaging can accurately provide the diagnosis of pelvic vein thrombosis. These diagnostic modalities are less dependent on the technical expertise of the investigator than US, and venography provides better information in some situations. The CT venography requires the application of IV contrast agent and is thus contraindicated in patients with renal failure. Pregnancy is another exclusion criterion for CT imaging. The MR venography, which does not have these limita-

tions, provides superior sensitivity and good specificity for the diagnosis of pelvic vein thrombosis compared with contrast venography, and ultimately could emerge as the study of choice for the diagnosis of pelvic vein thrombosis [54]. For pelvic deep venous thrombosis, the sensitivity and specificity are reported to be 100 and 95 %, respectively, [13]. Furthermore, MR venography can demonstrate other causes of symptoms, such as enlarged iliac lymph nodes and pelvic masses [54]. Obviously, MR imaging is restricted in patients with claustrophobia and contraindicated in patients with pacemakers or ferromagnetic clips.

In conclusion, all current imaging methods for the diagnosis of proximal venous occlusion have their specific disadvantages. Magnetic resonance imaging has the greatest potential for the future because it is noninvasive, does not require contrast agent, carries no exposure to ionizing radiation, and is highly accurate and reproducible. Its accuracy is maintained through comprehensive imaging of the full extent of the occlusion including the calf and pelvis, and sensitivity and specificity below the knee are high. Both legs can be evaluated simultaneously in one session and testing can be easily repeated to monitor thrombus evolution; thus, MR imaging has promising roles in the diagnosis of acute venous occlusion not only in pregnancy but also in high-risk patients. It is also well suited for diagnosis of recurrent thrombosis and asymptomatic disease. Lack of widespread availability of MRI and cost limit its use at present; however, as imagers become more abundant and scanning speed increases, expenses will decrease and may become comparable to those of other noninvasive tests.

### 6.2.3.2 Intervention

As mentioned previously, anticoagulation alone does not diminish thrombus burden or re-establish valve function. Surgical thrombectomy, although capable of adequately removing thrombus, has traditionally been associated with a high rate of recurrence of thrombosis and fair clinical results [55]; thus, surgical venous thrombectomy has not been broadly established or regularly employed. Catheter-directed thrombolysis is a potentially attractive alternative for restoration of venous patency and preservation of valve function. In a multicenter registry, marked lysis was observed in 88% of patients with acute iliofemoral occlusion. The 1-year primary patency rate following catheter-directed thrombolysis was 64% [59]. Additional treatment with stent placement was required to treat uncovered stenoses and/or short residual occlusions that were resistant to lysis in 33%; 94% were performed in the iliac segments. The average urokinase dose was 7.8 million IU and the mean duration of intervention was 53.4 h; however, pharmacological treatment of intravascular thrombus is limited by

the lengthy time to effect and medication-related side effects. In addition, thrombolytic therapy is costly, labor intensive, and may require several days of intensive care unit hospitalization. Also, this form of therapy entails a significant risk for hemorrhagic and embolic complications, and is contraindicated in the postoperative patient. Response may be hindered in a large clot burden resulting in incomplete lysis.

Considering these limitations and contraindications of anticoagulation, thrombolysis, and surgical removal, percutaneous interventional techniques have more recently been added to the therapeutic repertoire for the management of vascular pathologies. In order to perform a safe approach allowing rapid flow restoration several different types of percutaneous mechanical thrombectomy devices [89] have been developed and tested *in vitro* [34] and *in vivo* [97] which use combinations of mechanical dissolution, fragmentation, and aspiration [87]. Since then, mechanical thrombectomy devices have proved to be a valuable, rapid, and safe treatment modality in acute venous occlusion by enabling the recanalization of thrombotic occlusions in conjunction with minimal invasiveness and a low bleeding risk, thereby offering the potential of low (post)procedural morbidity and mortality (Fig. 2) [28, 63, 75, 82, 105, 111]. In cases where thrombolysis is not contraindicated, an adjunctive pharmacological thrombolytic therapy, balloon angioplasty, and/or endovascular stent deployment may be of assistance if hemodynamically significant thrombus remains that has not been cleared by the mechanical thrombectomy procedure. Even though only a limited number of patients in a study by Kasirajan received thrombolytic agents, the duration of therapy was significantly shorter than with lysis alone with  $20.2 \pm 19.4$  h [47]. After initial thrombus debulking, the consecutive reduction of the thrombus load led to an increase of the surface area of the thrombus exposed to lytic agent. In doing so, the risk of hemorrhagic complications can be decreased in light of the decreased quantity of lytic agents required and shortened overall agent exposure. Placement of an inferior vena cava filter should be considered when there is documented recurrent PE despite adequate anticoagulation or if anticoagulation is contraindicated. It should be kept in mind that the filter does not stop the progress of thrombosis, and thus additional treatment is necessary.

There are manifold treatment possibilities in ilio-caval thrombosis for the radiologist. For the sake of immediate clot removal with flow restoration and improved circulatory hemodynamics within minutes, fewer hemorrhagic complications, as well as less expense and room time, the primarily mechanical approach seems to be most promising. It is noted that any mechanical thrombectomy device should only be used in conjunction with a temporary cava filter to prevent procedure-related PE.

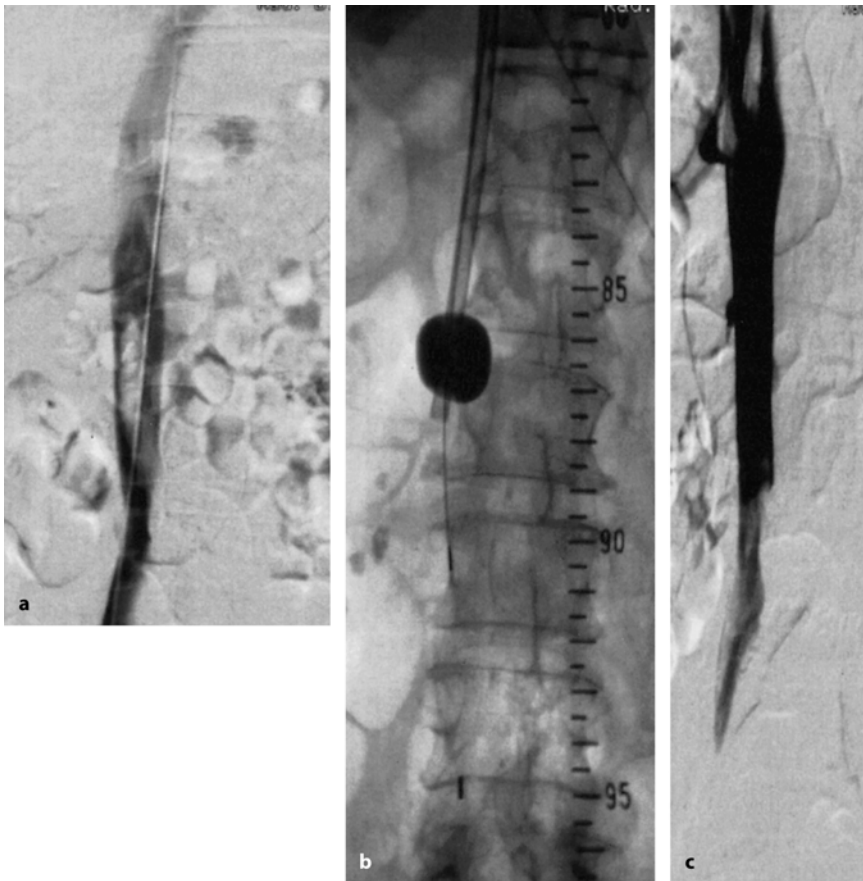


**Fig. 2a–c.** Balloon sheath thrombectomy of a caval thrombus. **a** Before thrombectomy. **b** Balloon sheath and co-axial basket catheter in place. **c** Post-thrombectomy complete extraction

### 6.2.3.3 Conclusions: Pelvic Vein and Inferior Vena Cava Occlusion

Acute occlusion of the pelvic veins and the inferior vena cava, often due to extension from the femoropopliteal system, represents a major risk for pulmonary embolism. Color flow Doppler imaging is often limited owing to obesity and bowel gas. Venography has long been considered the gold standard for identifying proximal venous occlusion. Both CT scanning and MR imaging, however, can even more accurately diagnose acute pelvic vein or inferior vena cava occlusion. The MRI is preferred because it is noninvasive, does not require contrast agent, carries no exposure to ionizing radiation, and is highly accurate and reproducible. Apart from catheter-directed thrombolysis, mechanical thrombectomy has been proven to be a quick and safe treatment modality by enabling the recanalization of thrombotic occlusions in conjunction with minimal invasiveness and a low bleeding risk. Mechanical thrombectomy devices should only be used in conjunction with a temporary cava filter.

### 6.2.4 Acute Mesenteric Vein Occlusion

Acute mesenteric vein occlusion is an exceptional and distinctive type of intestinal ischemia which was initially illustrated by Warren and Eberhard in 1935. Often idiopathic, precipitating factors range from liver cirrhosis, portal hypertension, neoplasm, intra-abdominal inflammatory diseases, trauma, and hypercoagulable states [17]. The acute appearance can be varied and includes poorly localized abdominal pain, nausea, vomiting, melena, bloody diarrhea, and ultimately circulatory collapse [30]. Preceding the onset of severe symptoms recurrent abdominal discomfort and a change in bowel habits are often reported.

A common etiology of this entity is discussed, because in up to 60% of patients a history of previous peripheral venous occlusion can be elicited. Total occlusion of the mesenteric vein brings about transmural infarction only when resulting thrombosis advances to the bowel wall and comprises the venous arcade and the vasa recta. Subsequently, hyperemia, edema, hemorrhage, and cyanosis emerge. Finally, even the arterial splanchnic circulation can occlude. As mortality rates for acute mesenteric vein occlusion can be as high as 80%, timely diagnosis is crucial [40].

### 6.2.4.1 Imaging

Plain radiographs of the abdomen are often inconspicuous. When dilated, small bowel loops with air–fluid levels, “thumbprinting,” or air in the bowel wall become visible, infarction has usually already taken place [1]. Ultrasonography, digital subtraction angiography (DSA), CT, and MR imaging are all possible imaging tools in the detection of acute venous occlusion. Contrast-enhanced CT has a sensitivity of 90% and is currently considered the examination of choice [84]. With CT, the extent of the occlusion and the collateral venous flow can be appraised. The remaining diagnostic modalities are afflicted by technical difficulties often due to bowel gas (US), invasiveness (angiography), and availability plus long examination duration (MRI); thus, with high clinical suspicion and a negative screening US, cross-sectional techniques are mandatory [107]. Selective mesenteric angiography is indicated once abdominal CT scan is nondiagnostic and the clinical suspicion still remains high. It can be expected that with the ongoing rapid technical development, MRI will be a welcome alternative to – or even replacement of – CT and conventional angiography in the near future (Fig. 3).

### 6.2.4.2 Intervention

Treatment of life-threatening acute mesenteric venous thrombosis is generally performed by surgical embolectomy. The decision to proceed surgically should be based on imaging findings, laboratory parameters, and clinical judgment.

Surgery permits the direct assessment of the bowel during embolectomy and resection of necrotic bowel. Additional thrombolytic therapy is nevertheless often necessary because complete thrombus removal from the small branches of the mesenteric veins may not be feasible. This in turn is associated with a substantial bleeding risk in the postoperative patient.

Exclusive infusion of thrombolytic agents is another treatment modality for mesenteric venous occlusion without bowel ischemia. Options comprise intra-arterial lysis, catheter-directed thrombolysis in the superior mesenteric artery, percutaneous transhepatic infusion of thrombolytic agents, and transhepatic placement of portal venous catheters for lytic agent infusion [77]. Direct superior mesenteric artery thrombolytic infusion permits lysis of even tiny splanchnic veins. The lack of direct agent infusion into the clot leads to long infusion times, however. Conversely, transhepatic catheter placement, although allowing direct infusion of the thrombolytic agent into the thrombus, neglects the smaller venous branches. It is also associated with a risk of subcapsular or intra-abdominal bleeding.

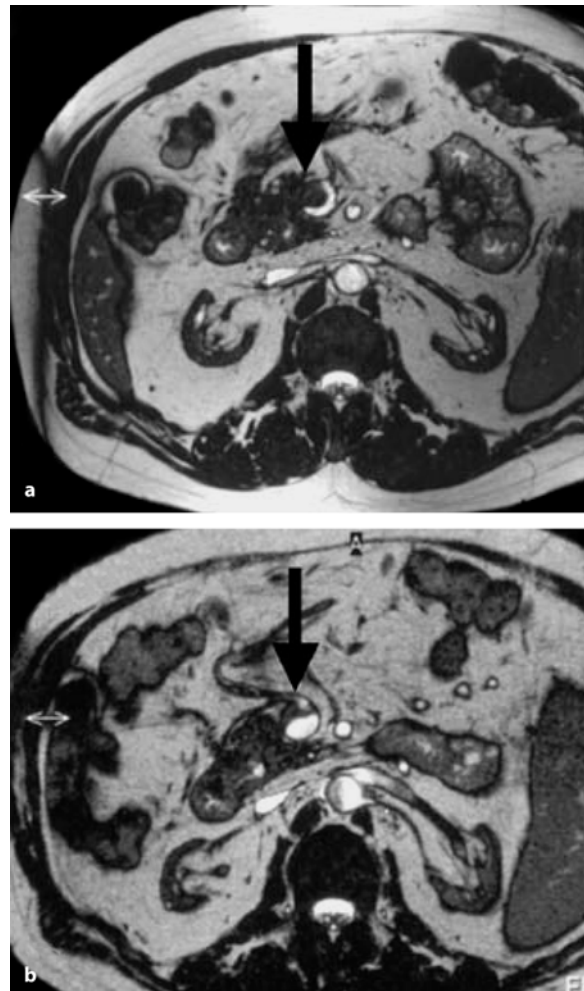


**Fig. 3.** A 47-year-old man with esophageal varices and incidental finding of venous mesenteric thrombosis **a** before and **b** after IV hyalination. Transverse true-FISP venography (TR 5.3 ms, TE 2.7 ms, flip angle 80°, FOV 450 cm, matrix 512×512) accurately depicts regression of thrombus size (arrows)

As fibrinolytic therapy can only be performed in select patients who are not actively bleeding and who do not present with bowel ischemia, a purely mechanical percutaneous approach for rapid thrombus fragmentation is a reasonable and rational alternative and mesenteric venous flow restoration. Balloon dilatation with mechanical thrombectomy and sometimes stent placement via a transjugular intrahepatic or a transhepatic route has been proposed and reported [10, 77]. The latter approach, while allowing direct access to the portal, splenic, and mesenteric veins, is possible with sheath sizes as small as 5 F. The percutaneous maneuvers have demonstrated effectiveness in cases with acute mesenteric venous occlusion [94].

Patients with proven acute mesenteric venous occlusion and contraindications to surgical therapy and no known bleeding disposition without imminent bowel ischemia or



infarction are thus potential candidates to the less invasive percutaneous approach either by (in)direct thrombolysis or mechanical means. Indeed, further research and larger trials in this area are needed to corroborate the clinical efficacy of this interventional treatment modality.

#### 6.2.4.3 Conclusions: Mesenteric Vein Occlusion

Contrast-enhanced CT is at present considered the examination of choice for acute mesenteric vein occlusion which has mortality rates as high as 80%. Patients with proven acute mesenteric venous occlusion and contraindications to surgical therapy and no identified bleeding disposition without looming bowel ischemia or infarction are possible candidates to the less invasive percutaneous approach either by (in)direct thrombolysis or mechanical means.

### 6.2.5 Acute Venous Occlusion of the Upper Extremity

Paget and von Schroetter independently described several cases of spontaneous upper extremity deep vein thrombosis in 1875 and 1884, respectively. They suggested that there was a relationship to repeated severe effort of the involved extremity, and thus the condition has been named spontaneous or effort vein thrombosis. Most cases can be related to strenuous arm activity or holding the arm for a prolonged period in a set position [78]. In many cases, an anatomic abnormality, such as a cervical rib or costoclavicular compression syndrome, is observed. The use of the term primary upper extremity deep venous thrombosis is intended to distinguish spontaneous or effort thrombosis from the more common secondary form caused by central venous lines, pacemaker wires, trauma, or intravenous drug use. Secondary acute venous upper extremity occlusion is also seen in inherited thrombophilia, malignancy, heart failure, acquired hypercoagulable states, and infection. Occurrence is also more frequent in patients with a medical history of thrombotic lower limb vein occlusion [72].

Primary upper extremity occlusions account for only 2% of all acute venous occlusions. The incidence of secondary occlusion seems to be rising, which could be related to the pervasive use of long-term indwelling central venous catheters, more liberal use of US to make the diagnosis, and an increased knowledge and awareness of this condition [81]; however, even in occlusive upper extremity thrombosis, the condition can be asymptomatic.

Whereas PE is seen in up to 50% of patients with proximal lower extremity occlusion, in contrast, upper extremity occlusion has been reported to have a 5–10% rate of PE. Clinical manifestations are nonspecific and can replicate lymph edema, local infection, or mediastinal malignancy.

Suspicion should arise with the occurrence of tenderness, swelling, functional deterioration of the upper extremity, skin discoloration, venous distension, or occasionally paresthesias.

#### 6.2.5.1 Imaging

By tradition, contrast venography has been the reference standard for the diagnosis of acute venous occlusion of the upper extremity. This technique has its disadvantages. Venous puncture can be problematic in a swollen extremity, the procedure may cause thrombophlebitis, and there is a minute risk of an allergic contrast medium reaction. Recent studies have revealed that compression US and color flow Doppler imaging of the axillary vein and lateral course of the subclavian vein to be both sensitive and specific for the diagnosis of upper extremity occlusion, with a sensitivity of 96 and 100%, and a specificity of 93 and 93%, respectively [72].

Ultrasonography is less reliable for the detection of thrombus in the central portions of the subclavian vein, the brachiocephalic veins, and the superior vena cava, however, owing to difficult access to these vessels. Enlarged collateral veins and nonocclusive thrombi may cause false-negative results and overlying bony structures and lung parenchyma may mask vessel segments. Sensitivity can be improved with the demonstration of normal cardiac pulsatility and respiratory phasicity within these vessels.

Computed tomography and MRI may also be valuable in diagnosing acute upper extremity occlusion. In several studies MRI had a sensitivity and specificity of almost 100% in evaluating the patency of the central chest veins [15, 52].

In summary, conventional venography, subtraction angiography, CT, and MRI can all be used to consistently detect upper extremity occlusion, but the excellent test characteristics of US favors its use as the primary imaging tool for the diagnosis of upper extremity thrombosis. Alternative imaging modalities should only be applied in case of equivocal sonographic findings due to the above-mentioned limitations.

#### 6.2.5.2 Intervention

Since complications of acute occlusion of upper extremity veins range from restriction or loss of central venous access, venous gangrene, postthrombotic syndrome, and superior vena cava (SVC) syndrome to PE, timely treatment is mandatory after the diagnosis has been established. In the acute phase, traditional treatment consisted of elevation of the affected extremity and full-dose anticoagulation with unfractionated heparin or low molecular weight heparin [72] followed by 6 weeks to 6 months of therapy with oral warfarin sodium. In secondary venous

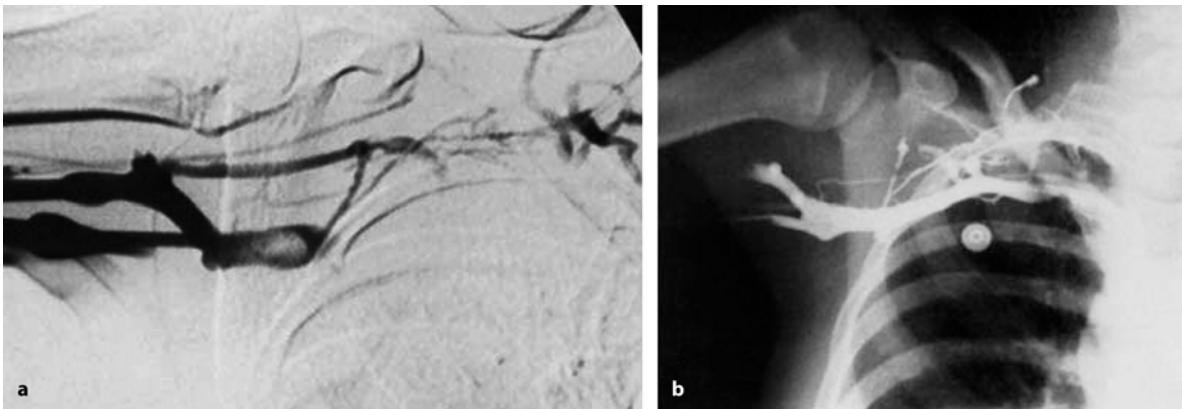


**Fig. 4a,b.** Paget-von Schroetter syndrome. **a** Fresh thrombosis of axillary and subclavian vein. **b** Complete recanalization after catheter-directed thrombolysis

occlusion, the removal of the triggering cause, such as the central venous catheter, is usually necessary.

The radiologist is infrequently involved in the treatment of this entity. Catheter-directed thrombolysis is known to improve lysis rates by delivering the thrombolytic agent in high concentrations directly to the site of the thrombus. In combination with balloon angioplasty, good results have been obtained (Fig. 4) [44]. If hemodynamically significant residual stenosis or thrombus remains after thrombolysis and angioplasty, stent placement should be considered [74].

Systemic thrombolysis is also effective for nonocclusive thrombi with reported excellent results in 32 of 36 primary upper extremity occlusion patients in a recent study [101]; however, in this patient collectively better results were demonstrated by aggressive thrombolysis and prompt first rib resection to relieve both the acute and chronic manifestations.

In patients where anticoagulation and thrombolysis are contraindicated, refractory, or difficult, and who are susceptible for PE the placement of a SVC filter may be necessary. Even though there is widespread familiarity with placement of inferior vena cava filters, only few data regarding placement of SVC filters exist. Available results nevertheless show that filters placed in the SVC appear to be a safe and effective means of preventing pulmonary thromboembolism [5]. Indications for SVC filter are recurrent PE despite full-dose anticoagulation, or a major complication as a result of anticoagulation treatment.

Due to the variety of underlying causes, a multidisciplinary treatment strategy for acute venous occlusion of the upper extremity is often needed. The interventional radiologist should participate in the primary treatment and in the prevention of thrombosis sequelae.

### 6.2.5.3 Conclusions Venous Occlusion of the Upper Extremity

Ultrasonography is the primary imaging modality for the diagnosis of upper extremity thrombosis. Computed tomography and MRI are additionally helpful in diagnosing central chest vein occlusions. The interventionalist is rarely involved in the treatment of this entity. Catheter-directed thrombolysis is known to improve lysis rates. Together with balloon angioplasty good results have been obtained. If stenosis or thrombus remains after thrombolysis and angioplasty, stent placement should follow.

## 6.2.6 Acute Venous Occlusion of Arteriovenous Hemodialysis Access

Timely recognition and treatment of access-related complications are essential to achieve long-term access function for the hemodialysis patient. Acute occlusions of dialysis grafts and fistulae represent a common complication [113]. Key predisposing factors include an underlying stenosis or aneurysmatic vein leading to flow turbulence [85, 103] as well as arterial hypotension, low cardiac output, compromised arterial inflow, and clotting disorders [106]. In the majority of cases, a venous stenosis is detected.

### 6.2.6.1 Imaging

Clinical examination of the dialysis access is the primary diagnostic method [99]. Digital palpation of the occluded access shows loss of thrill and very soft draining shunt veins. Development of arm swelling is highly suggestive of central venous occlusion. Among the numerous methods described for acute occlusion screening, US and MRI have

been proven to be accurate and noninvasive [66, 80, 92]. Magnetic resonance angiography (MRA) has been reported to be a useful, safe, and a practical diagnostic imaging modality in multifaceted fistulas with less complications and side effects in comparison with fistulography [68], and allows noninvasive evaluation of the arterial and venous system in one examination [38]. If MRA is performed, a contrast-enhanced (gadolinium) technique (CE-MRA) should be preferred, since the latter demonstrates a fine visualization of arm veins with diameter measurements closely correlating overall to conventional venography [58]. In one study, MRA depicted all 13 stenoses and two false-positive findings, resulting in a sensitivity of 100% and a specificity of 94% for the arterial and venous tree [38]. Froger et al. reported sensitivity, specificity, and positive and negative predictive values of MR in detection of

vessel segments with significant stenoses of 97, 99, 96, and 99%, respectively [27]. When central vein obstruction is suspected, angiography of the complete venous outflow system up to the right atrium is mandatory. An MRA of the central veins is accurate and even superior to contrast venography, which may fail to show all patent thoracic vessels [6, 39]; however, it is an elaborate procedure and therefore not possible in every hospital [33].

Nevertheless, if decreasing access flow, decrease in measurement of dialysis dose, deviant urea measurements, and elevation of venous dialysis pressure is observed during dialysis, immediate treatment is mandatory and imaging should then be performed directly by DSA before the percutaneous intervention. Access pathology is usually visualized by puncturing the brachial artery with a 22-G sheath needle for arteriovenography.

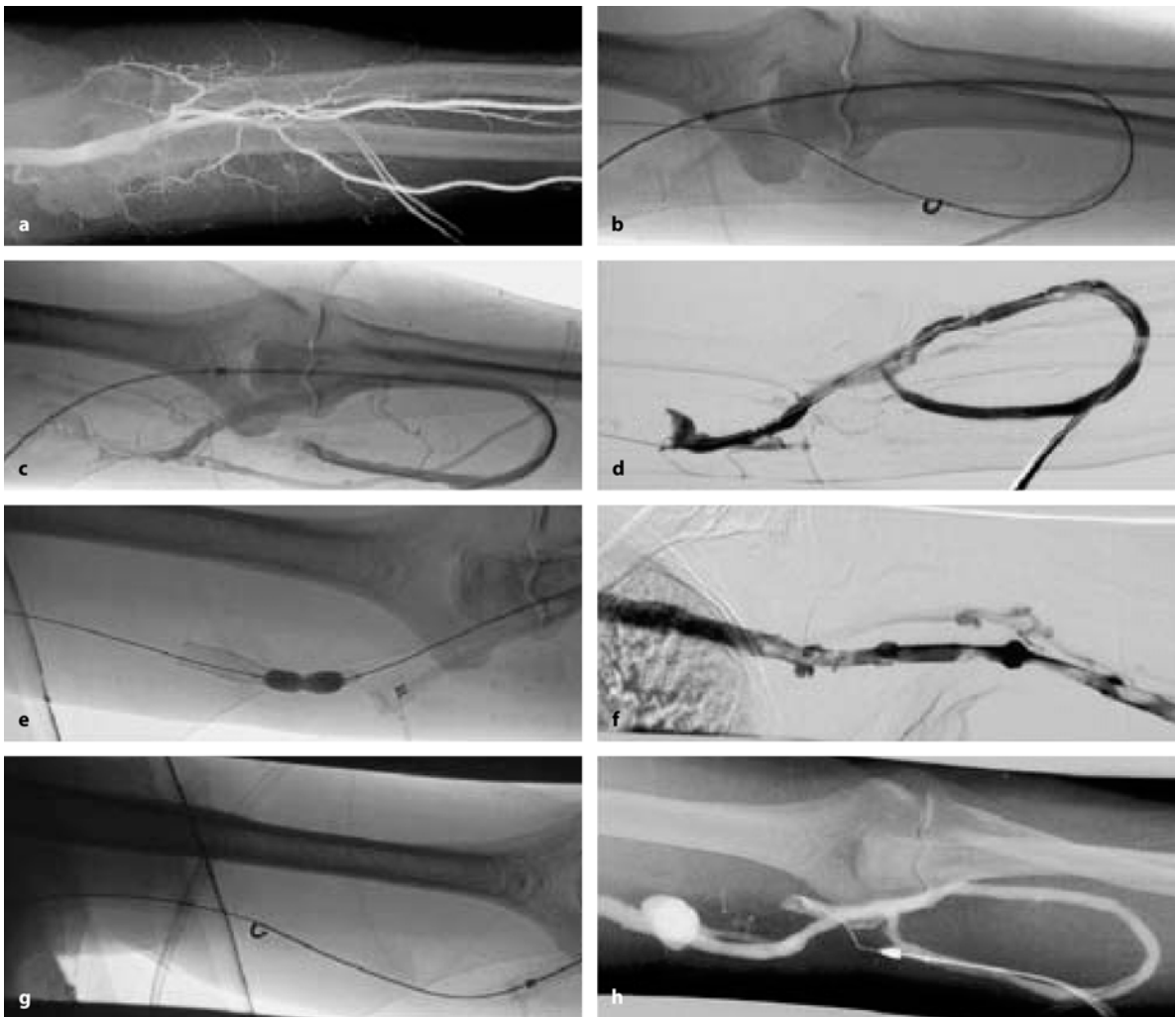


**Fig. 5 a–h.** Recanalization of a thrombosed hemodialysis graft. **a** Arterial angiography shows completely occluded graft. **b** Introduction of a pigtail rotation catheter. **c** Partial recanalization. **d** Occlusion by a valve-like thrombus in a puncture aneurysm. **e** Stent

placement bridging the aneurysm. **f** Thrombus in the basilic vein. **g** Treatment by pigtail rotation catheter. **h** Final result: complete recanalization

### 6.2.6.2 Intervention

The surgical approach has been limited by the lack of imaging guidance in the operating room concerning the detection of additional stenoses and obtaining information on the often complex vessel anatomy. A solely percutaneous approach therefore is a cost-reducing, attractive alternative. In the past decade, percutaneous interventional techniques have been evaluated and proven as a valuable alternative means in managing of dialysis access dysfunction. Poulain et al. combined a local low-dose infusion of urokinase with PTA and thromboaspiration to achieve a 12-month overall patency in 14 native fistulas of approximately 90% [70]. Zaleski et al. reported on 17 patients with complete thrombosis of their Brescia-Cimino fistulas, which were treated by angioplasty and urokinase infusion [112]. Procedural success was 82% with primary, primary assisted, and secondary patency rates at 12 months of 71, 93, and 100%, respectively. Twenty of 24 patients (83%) with occluded Brescia-Cimino fistulas were successfully recanalized by Overbosch et al. using the Hydrolyser catheter [67]. Median assisted patency was 34 weeks and was significantly shorter in fistulas than in PTFE grafts ( $p=0.002$ ). Turmel-Rodrigues et al. described an 81% initial success rate using thromboaspiration and PTA in 16 patients [100]. An 81% secondary patency at 1 year was reported. These results advocate that percutaneous interventions in occluded native arteriovenous fistulas are at least as effective as surgical treatment regarding technical success and patencies. Treatment results of thrombosis and associated stenosis in synthetic grafts have been summarized by Aruny et al. [4]. Clinical success rates for thrombolysis or mechanical thrombectomy range from 75 to 94% with primary patencies of 18–39% at 6 months. Reported 6- and 12-month secondary patencies for thrombolysis range from 62 to 80 and 57 to 69%, respectively. Trerotola et al. demonstrated a 95% technical success with a 3-month primary patency of 39% using the Arrow-Trerotola percutaneous thrombolytic device [96]. Schmitz-Rode reported a 100% success rate in 26 procedures (15 native fistulas, 11 PTFE grafts) in recanalizing occluded dialysis access with use of an easy-to-handle, cost-saving rotating mini-pigtail catheter (Fig. 5) [83].

Further results of our department demonstrated technical success rates of almost 90% in 81 native fistula procedures and a primary and overall fistula patency of 27 and 51% at 1 year, respectively, pinpointing the efficacy of percutaneous thrombosis treatment strategies (Fig. 6) [36]. It is our opinion that as long as less-invasive equivalent therapeutic alternatives to safeguard the access are on hand and viable, abandonment of the vascular access should be avoided and a percutaneous approach should be considered.

As a rule, the intervention should be performed as an outpatient procedure. It is advisable to perform the intervention as soon as possible once thrombosis is diagnosed, because occlusion period in our patients with primary

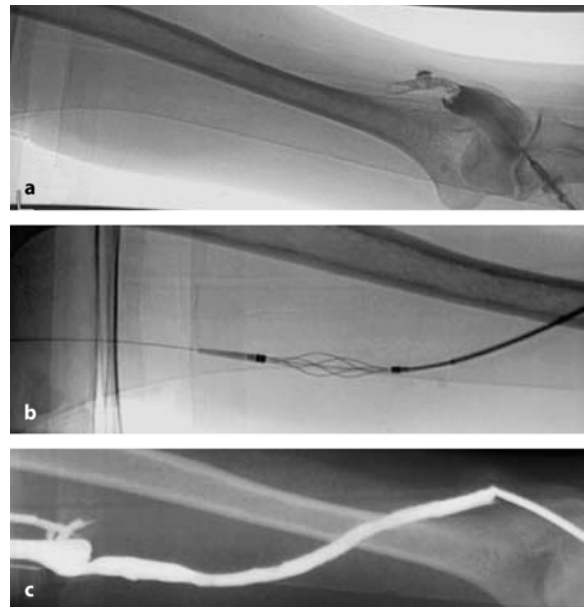


**Fig. 6 a–c.** Recanalization of a thrombosed forearm graft by rotating basket catheter (arrow). A 54-year-old female dialysis patient. **a** Digital subtraction angiography shows a complete occlusion of the thrombosed fistula draining PTFE segment distal to the arteriovenous anastomosis. **b** Arrow-Trerotola percutaneous thrombolytic device (PTD) in place. **c** Angiogram after mechanical thrombectomy demonstrates the recanalized PTFE graft segment with unimpeded postprocedural flow

technical failure was by far longer compared with the whole group ( $44\pm 22$  vs  $25\pm 12$  h). Involvement of large veins, such as the brachial vein, substantially complicates treatment and is another important factor determining technical success. Long-term access functionality depends on diverse factors such as cannulation trauma, tendency for restenosis, hypercoagulability, and frequency of reobstruction episodes [12].

In case of central venous occlusion related to dialysis access, initial stent deployment is very effective with improved long-term patency rates compared with other therapeutic modalities such as percutaneous balloon angioplasty alone, which has long been recommended as the primary treatment tool [35]. An appropriate endoprosthesis for central veins should be flexible enough to be used in curved and tortuous vessels. To evade stent dislocation and proximal embolization, a self-adjusting stent should be preferred, because venous occlusions may undergo progressive luminal enlargement after stent placement. Mechanical thrombectomy should not be regularly used as a primary therapy for dialysis-related central venous occlusions, mostly because of the sharp angles and slim vessel walls observed in this region. On the other hand, thrombectomy devices are effective tools in debulking neointimal tissue in case of stent reocclusion. Central and peripheral reocclusion is a commonly observed complica-



tion and is more likely to take place after thrombosis has occurred for the first time [29]. The radiologist should be ready for repeat interventions, occasionally multiple, over the months and years after the primary recanalization procedure.

### 6.2.6.3 Conclusions: Venous Occlusion of Arteriovenous Hemodialysis Access

In conclusion, initial percutaneous thrombectomy is very effective in the treatment of newly occluded dialysis access with good success rates and satisfactory primary and long-term patency rates comparable to other therapy regimens such as surgical thrombectomy. When percutaneous thrombolysis is available, surgical revision should be reserved for failures of percutaneous techniques. The choice of the appropriate percutaneous approach depends on size and location of the thrombus detected by angiography. A short-segment thrombosis can be easily treated with balloon angioplasty alone, whereas an extensive thrombosis requires a combination of mechanical devices and/or thrombolytic agents with adjunctive balloon angioplasty. The declotting method in dialysis grafts, whether pharmacomechanical or purely mechanical, has no major effect on short- or long-term patency [32]. Further studies have to be carried out to offer the hemodialysis access patient the most favorable and long-lasting percutaneous treatment strategy. To date, either type of method for access recanalization is suitable and should be based on the familiarity of the interventional radiologist with the particular therapeutic modality. Percutaneous thrombectomy is equally successful in native fistulae and grafts. Repetitive interventional failures should be referred to surgery, and vice versa. Prolonged successful preservation of the vascular access must be based on a multidisciplinary foundation with the interventional radiologist, vascular surgeon, and nephrologist cooperating with each other.

### 6.2.7 Acute Cerebral Vein Thrombosis

Veno-occlusive disorders of the brain may affect the dural sinuses, the superficial cortical veins, and the deep venous system. They may lead to a venous congestion of the brain and are an often underdiagnosed cause for acute or slowly progressive neurological deterioration. Since clinical symptoms can be unspecific and might demonstrate a high degree of variability, the (neuro-) radiologist plays an important part in diagnosing this potentially fatal disease.

Several etiological factors are known that can cause SVT, although in about 25% of all cases, no specific cause for SVT can be found [19]. One has to differentiate between aseptic SVT as the most common form, septic SVT, tumor-induced and trauma-induced SVT. Disease processes that

may cause aseptic SVT include hypercoagulopathic states such as present in polycythemia vera, sickle cell disease, deficiencies of fibrinolytic factors (antithrombin III, protein C, protein S), or disseminated intravascular coagulopathy [19]. Oral contraceptives, pregnancy, and puerperium are also known risk factors for developing an aseptic SVT [14]. In addition, systemic malignancies with paraneoplastic syndromes, lupus erythematoses, drug abuse or low-flow situations as present during dehydration or shock may cause SVT. Septic causes are most often encountered in childhood with a chronic or acute mastoiditis trespassing upon the neighboring transverse or sigmoid sinus [95]. Meningitis, brain abscesses or septicemia are, however, more seldom causes for septic SVT. Concerning tumor-induced SVT, meningiomas are prone to obliterate the lumen of the dural sinuses. However, this process evolves slowly over time; therefore, venous collaterals are often present and an acute venous congestion is an exemption rather than a rule. Apart from meningiomas, other tumor entities only rarely infiltrate the dural sinus walls. The SVT caused by trauma is also rare; however, fractures that lead to a laceration of the dural wall might cause a venous occlusion [93].

Sinus or venous thrombosis (SVT) is a disease that typically starts with thrombus formation within a large dural sinus, which in the further course might lead to a total occlusion of the sinus and then begins to involve cortical veins draining into the sinus. Most commonly, the superior sagittal sinus is affected followed by the transverse, sigmoid, and cavernous sinuses whereas the cortical veins draining into the sinuses are secondarily involved when thrombosis progresses from the sinus [26]. Cortical vein thrombosis and venous infarction without additional sinus thrombosis is a rare finding. Involvement of the internal cerebral venous system, including the vein of Galen and the internal cerebral veins, is also a rare event with specific bilateral basal ganglia and thalamic involvement of edema and/or hemorrhage [65].

The SVT generally shows a subacute onset and course of symptoms; however, clinical symptomatology is dependant on the cause, localization, extension and time of development of the venous occlusion. It might vary between a clinical asymptomatic course and a rapidly progressive deterioration with coma and death [73]. In asymptomatic cases, the occlusion of an isolated sinus is typically compensated by collaterals or in case of the transverse sinus by a contralateral sinus of adequate size. Neurological deficits and seizures occur in the group of patients in whom focal congestive and hemorrhagic lesions occur. The stroke-like symptoms depend on the localization of the brain damage and may be accompanied by seizures [3]. In these cases extension of the thrombus in cortical veins has occurred or the collateral drainage for a distinct area of the brain parenchyma is not sufficient. A typical example for this is the occlusion of a transverse sinus together with the vein of Labbé. Focal sensorimotor deficits and/or seizures are also

the clinical feature of the solitary thrombosis of a superficial cerebral vein which in our experience is rare. This entity may be accompanied by a cortical subarachnoid hemorrhage. Impaired consciousness and coma may develop with increasing intracranial pressure. A decrease in mental status, drowsiness, progressive confusion, and impaired consciousness may also be the major symptoms of deep cerebral venous thrombosis. Drainage impairment affects mainly the thalamus uni- or bilaterally with venous congestion and/or bleeding.

The most common initial symptoms are headaches, often associated with nausea and vomiting, that may persist for over a week. A decrease in mental status and drowsiness are often present. Abrupt and sudden clinical onsets with seizures and an impaired consciousness are, however, also not rare. If focal parenchymal lesions are present, neurological symptoms can occur in dependence of the localization; these can even present as stroke-like syndromes [3]. As a sign for an increased intracranial pressure, a bilateral papilla edema may be present [76]. The prognosis of SVT is unpredictable and variable: clinical uncomplicated courses can suddenly evolve into dramatic diseases, and a mortality of up to 33% was reported [14].

In conclusion, it is our policy to carefully check for the signs of SVT or even perform additional imaging procedures if the patient complains about headaches (as the most common symptom for SVT) in combination with one or more of the following criteria: (a) the patient is on oral contraceptives, pregnant, or in puerperium; (b) nausea and vomiting without a history of head trauma are present; or (c) neurological deficits, seizures, or bilateral papilla edema are found [95].

### 6.2.7.1 Imaging

To interpret imaging, it is necessary to know the normal anatomy of the cerebral venous system and to transfer this knowledge to the transversal cuts of the axial CCT and MRI. Moreover, the most important anatomical variants of the dural sinuses must be readily perceived. The normal venous angiogram as detected by MRI can be found in Fig. 7. Often encountered anatomical variants include (a) the unilateral hypoplastic transverse and sigmoid sinus with compensation via the contralateral transverse sinus, (b) the aplasia of the frontal sinus sagittalis superior anterior to the coronary suture with compensation via large bridging veins, and (c) the high division of the superior sagittal sinus (cranial to the protuberantia occipitalis interna where normally the confluens sinuum is encountered) [95].

#### Cranial Computed tomography

One has to differentiate direct and indirect signs of SVT, the direct signs proving the diagnosis by demonstrating thrombus within the dural sinus or pial veins, and the indirect signs just raising the suspicion of SVT by demonstrating venous congestions [16]. Direct signs include the hyperdense sinus in the non-contrast-enhanced scan (Fig. 8), the “cord sign” (hyperdense bridging vein), and the empty triangle sign in the contrast-enhanced CCT [104] (Fig. 9). Within the first 2 weeks, thrombosed blood is typically hyperdense on CCT compared with brain parenchyma (Fig. 10), whereas after the course of 2 weeks the thrombus will get isodense to the brain parenchyma and will therefore only be visible after contrast media injection as a hypodense area surrounded by contrast-enhancing meningeal venous tributaries, still patent lumen, or collateral

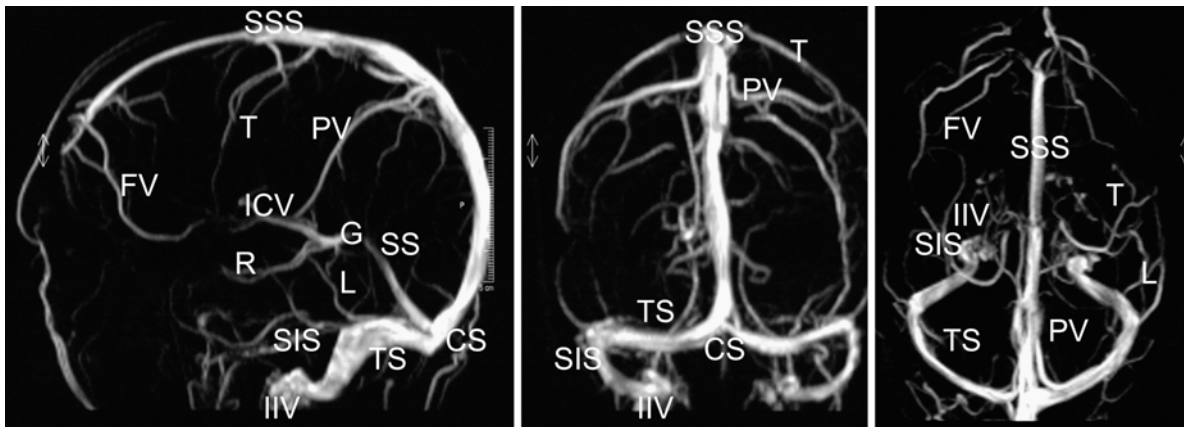


**Fig. 7.** Normal venous anomaly in a 3D phase-contrast venous angiogram performed at 1.5 T. *FV* frontal veins, *T* vein of Trolard, *PV* parietal veins, *SSS* superior sagittal sinus, *TS* transverse sinus, *SIS*

sigmoid sinus, *IIV* internal jugular vein, *SS* straight sinus, *CS* confluens sinuum, or torcular herophili, *L* Vein of Labbé, *G* vein of Galen, *ICV* internal cerebral vein, *R* vein of Rosenthal

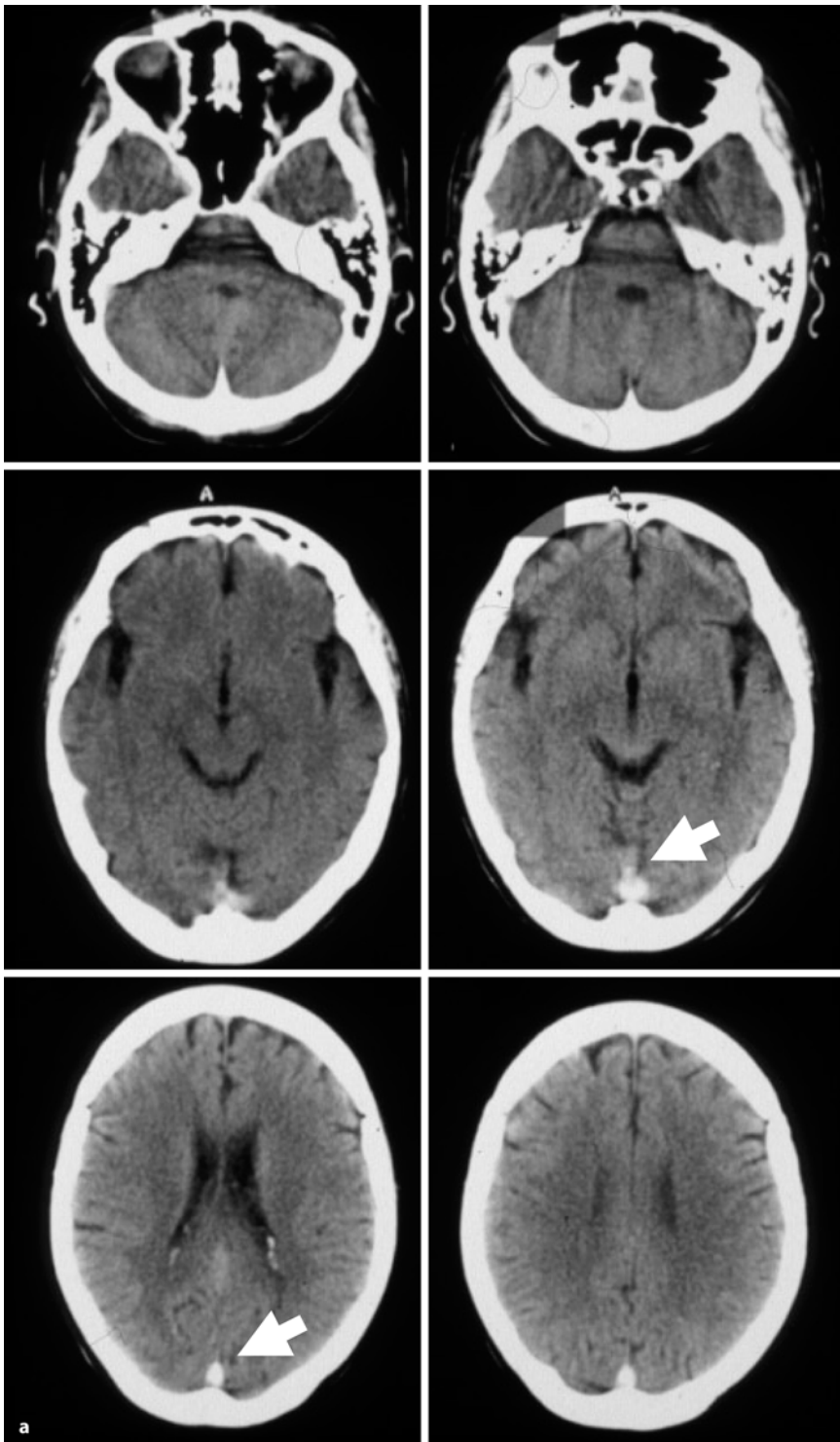


**Fig. 8.** A 21-year-old woman on oral contraceptives with progradient headaches for the previous 3 days. *Empty triangle* sign on contrast-enhanced CT (arrow in **a**), on axial gradient-echo sequences (T1 FFE, TR 20 ms, TE 7 ms, flip angle 40°), and thrombus material with surrounding flow can be seen (**b**), and on sagittal 2D phase-contrast angiography there is a normal depiction of the superior sagittal sinus (**c**), on contrast-enhanced T1-weighted spin-echo sequences thrombus material surrounded by blood can be visualized (arrowheads in **d**). The normal visualization of the superior sagittal sinus is presumably secondary to the still-present flow around the thrombus material

venous channels. This constitutes the empty-triangle or empty-delta sign on contrast-enhanced CCT. It is of utmost importance to obtain a native CCT scan in patients with suspected SVT, since the density of the thrombus might mimic contrast within the sinuses (Fig. 7).

Indirect signs include global and focal brain edema (Figs. 11, 12), intraparenchymal hemorrhages that might be single or multiple involving both gray and (preferentially) white matter, and intense tentorial enhancement. Concerning the edema that is demonstrated as a hypodense

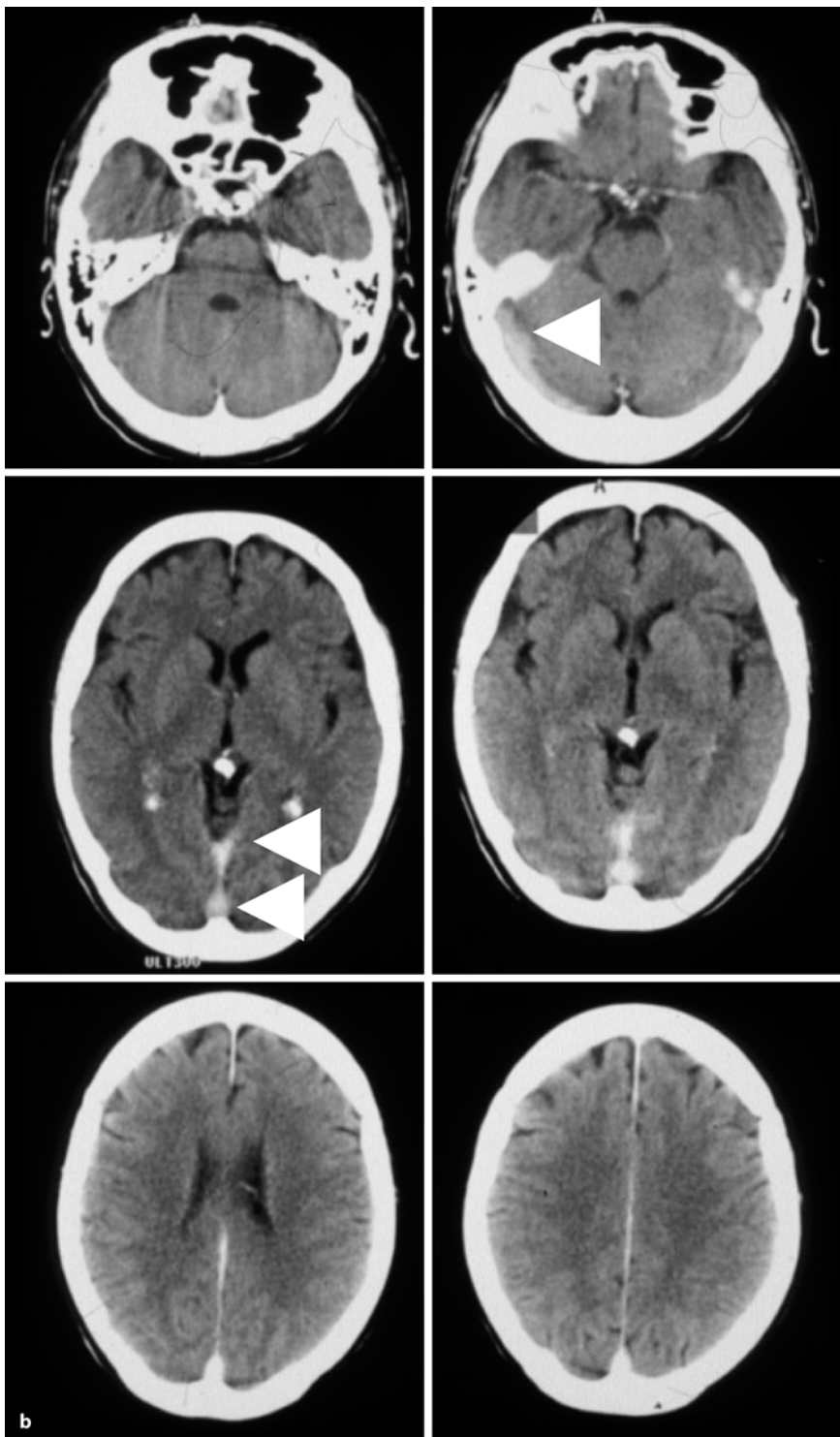


Fig. 8. (continued)

area the form and localization will typically not correspond to the classical arterial territories (Fig. 11). Hemorrhages will also not suit the typical localization of parenchymal hypertensive bleeds, but instead will typically also expand to the cortical surface. The tentorium and

the falx will appear thickened, engorged, and will demonstrate a pronounced enhancement that is presumably due to dural venous collaterals [65].

The CT angiography techniques will only help in establishing the diagnosis of SVT if the thrombus has a marked-



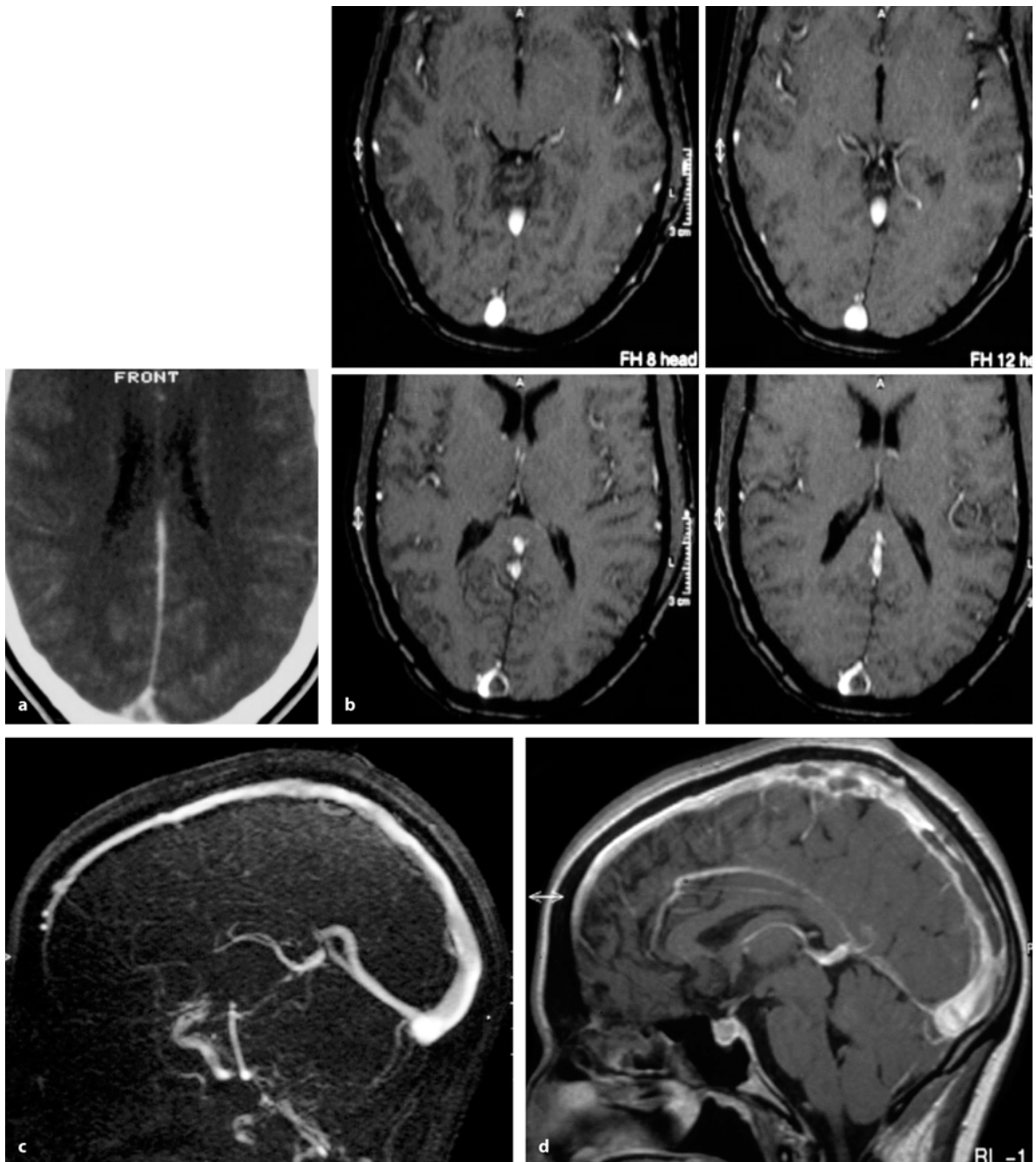


**Fig. 9.** This patient presented with confusion and headaches. On native CCT both internal cerebral veins and the straight sinus are markedly hyperdense (*arrows*) representing acute thrombus of the internal cerebral venous system. There is a discrete hypodensity of the right thalamus representing beginning edema (*arrowhead*)

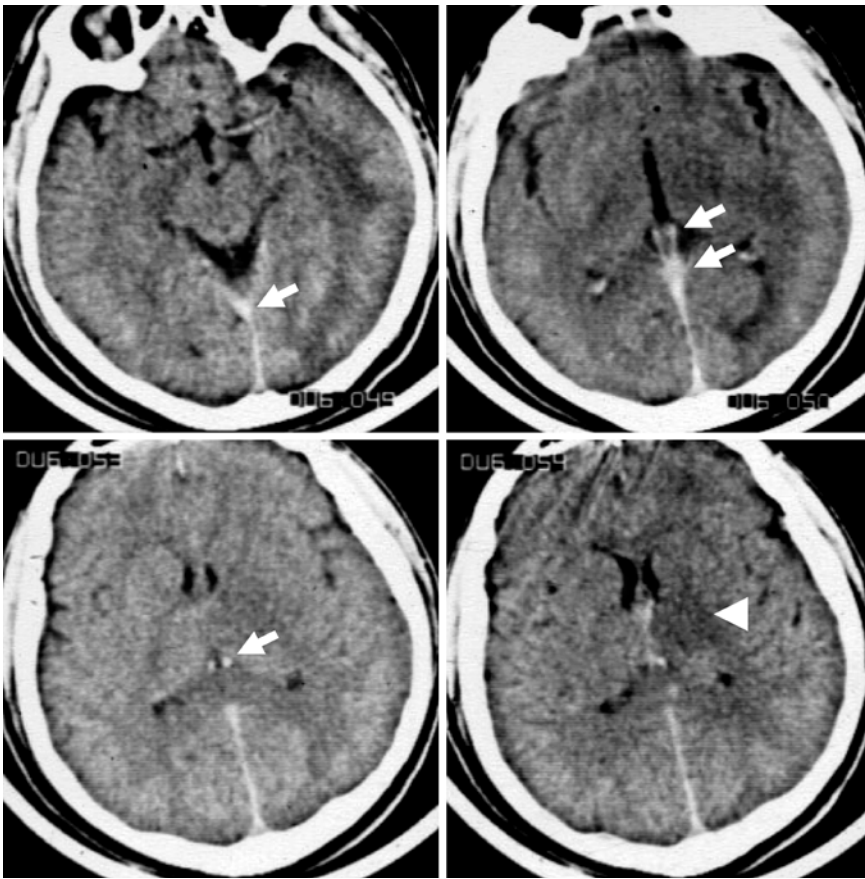


**Fig. 10.** This figure shows the importance of native CCT scans in obtaining the diagnosis of sinus thrombosis: the superior sagittal sinus is markedly hyperdense on the native scan (arrows in **a**). After contrast enhancement, all sinuses have the same density (arrowheads in **b**), with primary contrast-enhanced CCT scans; therefore, the sinus venous thrombosis would not have been detected

ly lower density compared with the contrast media. This again underlines the importance of native CT scans before contrast media is administered.

As a differential diagnosis of a hyperdense sinus a high hematocrit level has to be discussed, especially in newborns, the combination of unmyelinated brain and physiological polycythemia makes the dural sinuses appear very dense. Differential diagnoses of the indirect signs of SVT include certain forms of vasculitis, a posterior leucoencephalopathy, amyloidangiopathic bleedings, and infectious diseases.

### Magnetic Resonance Imaging

The MR signal on standard sequences varies with clot age; therefore, MR signal characteristics of blood and blood products during different stages of evaluation have to be taken into account. Acute thrombus is iso- to slightly hypointense to cortex (0–3 days) on T1-weighted sequences with a hypointense signal on T2-weighted images (12 h to 3 days). Late acute clots (3–7 days) are hyperintense on T1-weighted sequences and hypointense on T2-weighted images. Subacute thrombi (1.4 weeks after initial thrombosis) are hyperintense on both T1 and T2 scans, whereas

chronically thrombosed sinuses undergo fibrosis and may develop extensive collaterals [46]. Bearing this consideration in mind, the sinuses are best visualized using coronal sequences in which the superior and inferior sagittal sinus and the transverse sinus are well imaged. Using these standard sequences, it is possible to detect anatomic variations such as a hypoplasia of the transverse sinus. In addition to the routine sequences, coronal flow-sensitive gradient-refocused sequences should be obtained; these can demonstrate flow within the sinuses (Fig. 9). A phase-contrast (PC) MR angiogram, preferably a 3D PC venous angiogram, should be another standard sequence when evaluating SVT (Fig. 11) [98]. An axial fluid-attenuated inversion recovery sequence (FLAIR) is usually acquired additionally to demonstrate parenchymal involvement of the SVT. Contrast media might be helpful but is not mandatory and can demonstrate, similar to the contrast-enhanced CT, an empty-triangle sign (Fig. 9).

When evaluating a MR study for SVT one has to be aware of different artifacts that might mimic SVT. Hypoplasia or even aplasia of the sinus must be differentiated from thrombus by careful analysis of the standard anatomic sequences. When present, the CCT scan should also be taken into account, since a hypoplastic transverse and sig-

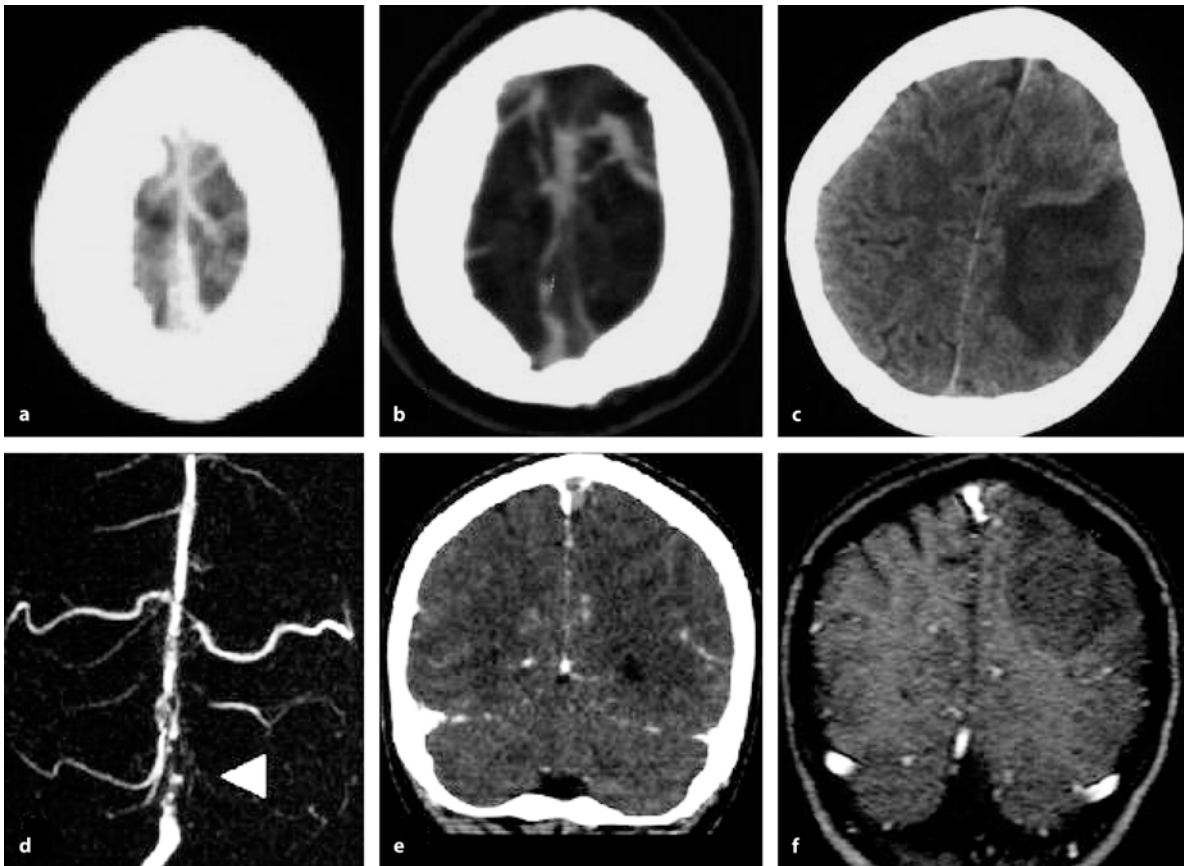


**Fig. 11.** Bridging vein thrombosis of a 29-year-old woman with a history of headaches for 5 days. Upon admission, the patient had experienced her first seizure ever. The native CCT scan in the most cranial cuts demonstrate a partly hyperdense superior sagittal sinus as a direct CT sign for sinus thrombosis (**a**), and CT angiography demonstrated thrombus material in the superior sagittal sinus slightly more on the left that is surrounded by flowing blood (**b, e**). The native CT scan demonstrated indirect signs of cerebral venous

thrombosis with edema within a non-arterial territory (**c**). A 3D phase-contrast MRA demonstrates thrombus within the superior sagittal sinus (**d**). Moreover, a large left bridging vein (presumably the parietal vein) is missing when compared with the right side (*arrowhead*), suiting the area of venous congestion visible on CT. Gradient-echo MR demonstrates flow within the right lateral part of the sinus and thrombus in the left superior sagittal sinus

moid sinus typically demonstrates a smaller iugular foramen when compared with the normal side. Slow or turbulent flow might lead to signal dephasing and false interpretation of impaired or even missing flow within the dural sinuses [53]. Non-thrombotic intraluminal notches as present in hypertrophic Pacchioni-granulation might also mimic hyperthrombus. On the other hand, thrombus characteristics as discussed above might also mask the presence of an acute SVT, since the hypointense visualization of acute thrombus (<3 days) on T2-weighted sequences might be mistaken as a flow void.

Our typical MR protocol for suspected SVT includes an axial FLAIR, axial diffusion-weighted MRI, coronal T1 SE and T2 TSE sequences, a coronal gradient-echo and a 3D PC venous angiogram with a total imaging time of approximately 20 min.

### Conventional Digital Subtraction Angiography

Conventional angiography is typically not needed unless endovascular treatment is necessary, since MRI, MRA, and CT usually is sufficient in making the correct diagnosis. When employing DSA to diagnose SVT, the head should be filmed in a slightly oblique position to better visualize both the anterior and the posterior portion of the sagittal sinus. A thrombosed sinus appears as an empty channel surrounded by dilated venous collaterals in the dural wall. Medullary veins might be enlarged and collaterals via the deep venous system including the cavernous sinus might be present. Within thrombosed cortical veins contrast material persists into the late venous phases, these vessels seem to “hang in space” [65].



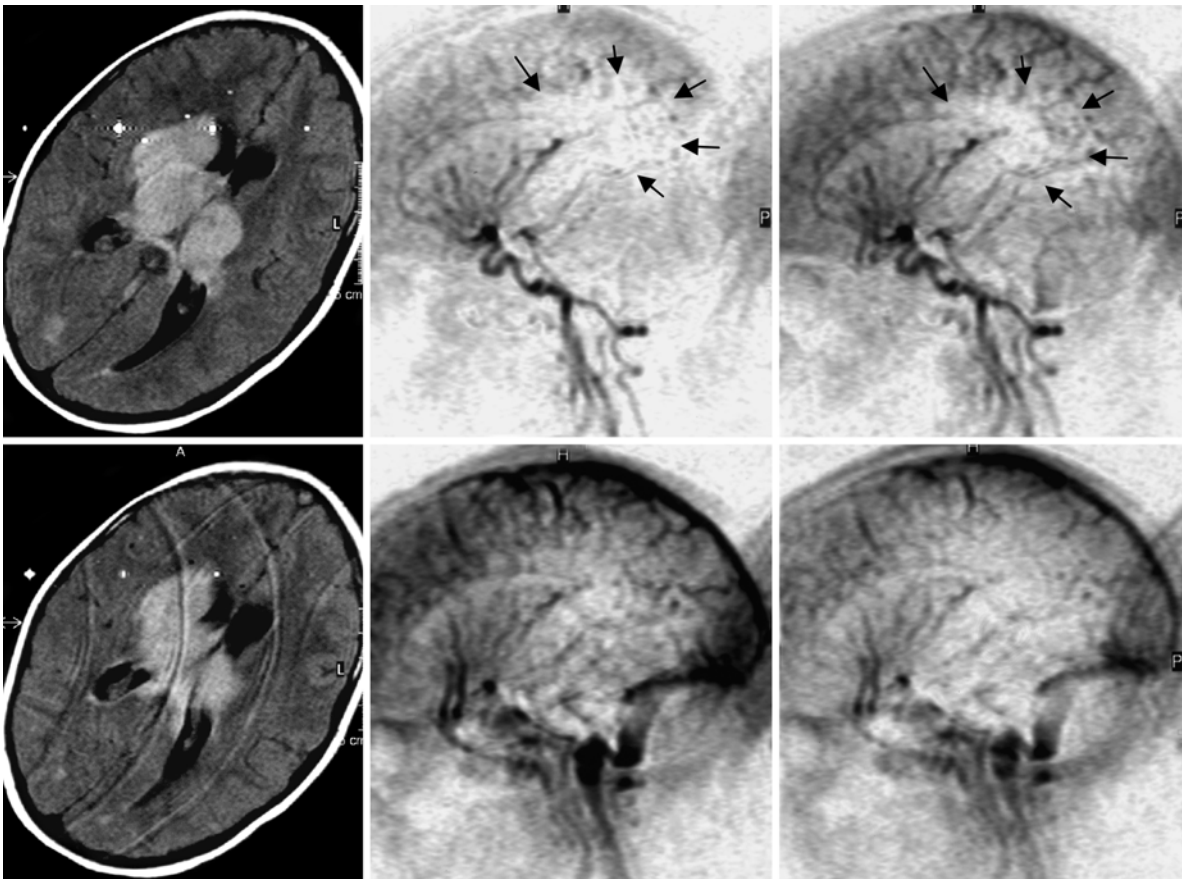


**Fig. 12.** Internal cerebral vein thrombosis in a 7-year-old girl who came to the emergency department with a progressive loss of consciousness over the previous few hours: a newly developed anisocoria. The patient had complained about headaches over the course of the previous 4 days and was severely dehydrated due to repeated vomiting. Fluid-attenuated inversion recovery images (TR/TE/TI: 6000/120/2000 ms) demonstrate swelling within both thalami, the right caudate nucleus and the corpus callosum typical

for internal cerebral vein thrombosis. A 2D dynamic contrast-enhanced MR subtraction angiography demonstrates not only the delayed filling within the edematous tissue consisting of venous congestion (arrows), but also the totally missing internal cerebral veins. Whereas the superior sagittal sinus and the transverse sinus are well filled with contrast media in the early and late venous phases, neither the internal cerebral vein, nor the basal vein of Rosenthal, the vein of Galen, or the sinus rectus is seen

### 6.2.7.2 Intervention

Typically, patients with confirmed SVT are treated with intravenous heparin. Placebo-controlled studies comparing systemic hyalinization with placebo therapy have reported an 80% favorable outcome with a very low mortality rate compared with only 10% of patients with a favorable outcome and 30% mortality rate in the placebo group [20]. The question of endovascular treatment of SVT therefore only arises when patients have an exacerbation of clinical symptoms or imaging signs of worsening disease despite sufficient anticoagulation therapy. Indications for intravenous treatment are therefore: development of cerebral venous hypertension; edema; and neurological decline with propagation of clot on heparin medication [62]. Endovascular techniques offer the potential for either direct pharmacological or physical dissolution of venous clot in the dural si-

nuses. The following techniques have been described in the literature: instillation of urokinase or recombinant tissue plasminogen activator (rTPA) via a microcatheter placed in the dural sinuses over a transvenous transfemoral approach [9, 25, 43, 50, 69]. Other approaches include direct puncture of the internal jugular artery, in infants even the direct puncture of the anterior cranial fontanelle has been described [42]. Doses are similar to that used in intra-arterial thrombolysis although the volume of clot is several orders of magnitude greater that encountered during arterial thrombosis. Therefore, the possibility of mechanical fragmentation or extraction of clot from the dural sinuses using a snare [7], balloons [62], or a rheolytic catheter [64] based on the Venturi effect (attraction and fragmentation of clot by a jet of high-pressure saline) has been proposed; however, to date their safety and efficacy are yet to be demonstrated. Still, the published results of treatment are encouraging and warrant further controlled prospective studies.



### 6.2.7.3 Conclusions: Cerebral Vein Thrombosis

Cerebral venous or sinus thrombosis is still an underdiagnosed disease since the clinical symptomatology varies considerably. We think that those patients deserve further investigation who complain about headaches (as the most common symptom for SVT) in combination with one or more of the following criteria: (a) the patient is on oral contraceptives, pregnant, or in puerperium; (b) nausea and vomiting without a history of head trauma are present; or (c) neurological deficits, seizures, or bilateral papilla edema can be found. Diagnosis can be either performed by venous CTA or multimodality MRA, including axial FLAIR, axial diffusion-weighted MRI, coronal T1 SE and T2 TSE sequences, or a coronal gradient-echo and a 3D PC venous angiogram.

### References

- Abdu RA, Zakhour BJ, Dallis DJ (1987) Mesenteric venous thrombosis 1911 to 1984. *Surgery* 101:383–388
- Acharya G, Singh K, Hansen JB, Kumar S, Maltau JM (2005) Catheter-directed thrombolysis for the management of postpartum deep venous thrombosis. *Acta Obstet Gynecol Scand* 84:155–158
- Ameri A, Bousser MG (1994) Cerebral venous thromboses. Clinical diagnosis. *Ann Radiol (Paris)* 37:101–107
- Aruny JE, Lewis CA, Cardella JF, Cole PE, Davis A, Drooz AT, Grassi CJ, Gray RJ, Husted JW, Jones MT, McCowan TC, Meranze SG, Van Moore A, Neithamer CD, Oglevie SB, Omary RA, Patel NH, Rholl KS, Roberts AC, Sacks D, Sanchez O, Silverstein MI, Singh H, Swan TL, Towbin RB, Trerotola SO, Bakal CW (1999) Quality improvement guidelines for percutaneous management of the thrombosed or dysfunctional dialysis access. *J Vasc Interv Radiol* 10:491–498
- Ascer E, Gennaro M, Lorenzen E, Pollina RM (1996) Superior vena caval Greenfield filters: indications, techniques, and results. *J Vasc Surg* 23:498–503
- Bacchini G, Cappello A, La Milia V, Andrulli S, Locatelli F (2000) Color doppler ultrasonography imaging to guide transluminal angioplasty of venous stenosis. *Kidney Int* 58:1810–1813
- Bagley LJ, Hurst RW, Galetta S et al. (1998) Use of a microsnare to aid direct thrombolytic therapy of dural sinus thrombosis. *Am J Roentgenol* 170:784–786
- Baker WF Jr (1998) Diagnosis of deep venous thrombosis and pulmonary embolism. *Med Clin North Am* 82:459–476
- Barnwell SL, Clark WM, Nguyen TT et al. (1994) Safety and efficacy of delayed intraarterial urokinase therapy with mechanical clot disruption for thromboembolic stroke. *Am J Neuro-radiol* 15:1817–1822
- Bilbao JJ, Vivas I, Elduayen B, Alonso C, Gonzalez-Crespo I, Benito A, Martinez-Cuesta A (1999) Limitations of percutaneous techniques in the treatment of portal vein thrombosis. *Cardiovasc Intervent Radiol* 22:417–422
- Borris LC, Christiansen HM, Lassen MR, Olsen AD, Schott P (1989) Comparison of real-time B-mode ultrasonography and bilateral ascending phlebography for detection of postoperative deep vein thrombosis following elective hip surgery. The Venous Thrombosis Group. *Thromb Haemost* 30:363–365
- Brotman DN, Fandos L, Faust GR, Doscher W, Cohen JR (1994) Hemodialysis graft salvage. *J Am Coll Surg* 178:431–434
- Burke B, Sostman HD, Carroll BA, Witty LA (1995) The diagnostic approach to deep venous thrombosis. Which technique? *Clin Chest Med* 16:253–268
- Cantu C, Barinagarrementeria F (1993) Cerebral venous thrombosis associated with pregnancy and puerperium. Review of 67 cases. *Stroke* 24:1880–1884
- Chang YC, Su CT, Yang PC (1998) Magnetic resonance angiography in the diagnosis of thoracic venous obstruction. *J Formos Med Assoc* 97:38–43
- Chiras J, Bousser MG, Meder JF et al. (1985) CT in cerebral thrombophlebitis. *Neuroradiology* 27:145–154
- Cohen J, Edelman RR, Chopra S (1992) Portal vein thrombosis: a review. *Am J Med* 92:173–182
- Comerota AJ, Aldridge SC (1993) Thrombolytic therapy for deep venous thrombosis: a clinical review. *Can J Surg* 36:359–364
- Deschiens MA, Conard J, Horellou MH et al. (1996) Coagulation studies, factor V Leiden, and anticardiolipin antibodies in 40 cases of cerebral venous thrombosis. *Stroke* 27:1724–1730
- Einhaupl KM, Villringer A, Meister W et al. (1991) Heparin treatment in sinus venous thrombosis. *Lancet* 338:597–600
- Evans AJ, Sostman HD, Knelson MH, Spritzer CE, Newman GE, Paine SS, Beam CA (1993) 1992 ARRS Executive Council Award. Detection of deep venous thrombosis: prospective comparison of MR imaging with contrast venography. *Am J Roentgenol* 161:131–139
- Forbes K, Stevenson AJ (1998) The use of power Doppler ultrasound in the diagnosis of isolated deep venous thrombosis of the calf. *Clin Radiol* 53:752–754
- Fraser DG, Moody AR, Morgan PS, Martel AL, Davidson I (2002) Diagnosis of lower-limb deep venous thrombosis: a prospective blinded study of magnetic resonance direct thrombus imaging. *Ann Intern Med* 136:89–98
- Fraser JD, Anderson DR (1999) Deep venous thrombosis: recent advances and optimal investigation with US. *Radiology* 211:9–24
- Frey JL, Muro GJ, McDougall CG et al. (1999) Cerebral venous thrombosis: combined intrathrombus rtPA and intravenous heparin. *Stroke* 30:489–494
- Fries G, Wallenfang T, Hennen J et al. (1992) Occlusion of the pig superior sagittal sinus, bridging and cortical veins: multistep evolution of sinus-vein thrombosis. *J Neurosurg* 77:127–133
- Froger CL, Duijm LE, Liem YS, Tielbeek AV, Donkers-van Rossum AB, Douwes-Draaijer P, Cuyppers PW, Butj J, van den Bosch HC (2005) Stenosis detection with MR angiography and digital subtraction angiography in dysfunctional hemodialysis access fistulas and grafts. *Radiology* 234:284–291
- Gandini R, Maspes F, Sodani G, Masala S, Assegnati G, Simonetti G (1999) Percutaneous ilio-caval thrombectomy with the Amplatz device: preliminary results. *Eur Radiol* 9:951–958
- Gaylord GM, Taber TE (1993) Long-term hemodialysis access salvage: problems and challenges for nephrologists and interventional radiologists. *J Vasc Interv Radiol* 4:103–107
- Gertsch P, Matthews J, Lerut J, Luder P, Blumgart LH (1993) Acute thrombosis of the splanchnic veins. *Arch Surg* 128:341–345
- Gorman WP, Davis KR, Donnelly R (2000) ABC of arterial and venous disease. Swollen lower limb. I. General assessment and deep vein thrombosis. *Br Med J* 27:1453–1456
- Gray RJ (1997) Percutaneous intervention for permanent hemodialysis access: a review. *J Vasc Interv Radiol* 8:313–327
- Haage P, Krings T, Schmitz-Rode T (2002) Nontraumatic vascular emergencies: imaging and intervention in acute venous occlusion. *Eur Radiol* 12: 2627–2643
- Haage P, Tacke J, Bovelander J, Wildberger JE, Klosterhalfen B, Vorwerk D, Günther RW (2001) Prototype percutaneous thrombolytic device: preclinical testing in subacute inferior vena caval thrombosis in a pig model. *Radiology* 220:135–141
- Haage P, Vorwerk D, Piroth W, Schürmann K, Günther RW (1999) Treatment of hemodialysis-related central venous stenosis or occlusion: results of primary Wallstent placement and follow-up in 50 patients. *Radiology* 212:175–180

36. Haage P, Vorwerk D, Wildberger JE, Piroth W, Schürmann K, Günther RW (2000) Percutaneous treatment of thrombosed primary arteriovenous hemodialysis access fistulae. *Kidney Int* 57:1169–1175
37. Haage P, Günther RW (2005) Iliofemoral and ilio caval interventions in deep venous thrombosis *Röfo* 177:670–680
38. Han KM, Duijm LE, Thelissen GR, Cuypers PW, Douwes-Draaijer P, Tielbeek AV, Wondergem JH, van den Bosch HC (2003) Failing hemodialysis access grafts: evaluation of complete vascular tree with 3D contrast-enhanced MR angiography with high spatial resolution: initial results in 10 patients. *Radiology* 227:601–605
39. Hartnell GG, Hughes LA, Finn JP, Longmaid HE (1995) Magnetic resonance angiography of the central chest veins. A new gold standard? *Chest* 107:1053–1057
40. Harward TR, Green D, Bergan JJ, Rizzo RJ, Yao JS (1989) Mesenteric venous thrombosis. *J Vasc Surg* 9:328–333
41. Heijboer H, Buller HR, Lensing AW, Turpie AG, Colly LP, ten Cate JW (1993) A comparison of real-time compression ultrasonography with impedance plethysmography for the diagnosis of deep-vein thrombosis in symptomatic outpatients. *N Engl J Med* 329:1365–1369
42. Higashida RT, Helmer E, Halbach VV et al. (1989) Direct thrombolytic therapy for superior sagittal sinus thrombosis. *Am J Neuroradiol* 10:S4–S6
43. Horowitz M, Purdy P, Unwin H et al. (1995) Treatment of dural sinus thrombosis using selective catheterization and urokinase. *Ann Neurol* 38:58–67
44. Huey H, Morris DC, Nichols DM, Connell DG, Fry PD (1987) Low-dose streptokinase thrombolysis of axillary subclavian vein thrombosis. *Cardiovasc Intervent Radiol* 10:92–95
45. Hull RD, Raskob GE, Rosenbloom D, Panju AA, Brill-Edwards P, Ginsberg JS, Hirsh J, Martin GJ, Green D (1990) Heparin for 5 days as compared with 10 days in the initial treatment of proximal venous thrombosis. *N Engl J Med* 322:1260–1264
46. Isensee C, Reul J, Thron A (1994) Magnetic resonance imaging of thrombosed dural sinuses. *Stroke* 25:29–34
47. Kasirajan K, Gray B, Ouriel K (2001) Percutaneous AngioJet thrombectomy in the management of extensive deep venous thrombosis. *J Vasc Interv Radiol* 12:179–185
48. Kearon C, Ginsberg JS, Hirsh J (1998) The role of venous ultrasonography in the diagnosis of suspected deep venous thrombosis and pulmonary embolism. *Ann Intern Med* 129:1044–1049
49. Kearon C, Julian JA, Newman TE, Ginsberg JS (1998) Noninvasive diagnosis of deep venous thrombosis. McMaster Diagnostic Imaging Practice Guidelines Initiative. *Ann Intern Med* 128:663–677
50. Kim SY, Suh JH (1997) Direct endovascular thrombolytic therapy for dural sinus thrombosis: infusion of alteplase. *Am J Neuroradiol* 18:639–645
51. Kim T, Murakami T, Hori M, Kumano S, Sakon M, Nakamura H (2004) Efficacy of multi-slice helical CT venography for the diagnosis of deep venous thrombosis: comparison with venous sonography. *Radiat Med* 22:77–81
52. Kroencke TJ, Taupitz M, Arnold R, Fritsche L, Hamm B (2001) Three-dimensional gadolinium-enhanced magnetic resonance venography in suspected thrombo-occlusive disease of the central chest veins. *Chest* 120:1570–1576
53. Lafitte F, Boukobza M, Guichard JP et al. (1999) Deep cerebral venous thrombosis: imaging in eight cases. *Neuroradiology* 41:410–418
54. Laissy JP, Cinqualbre A, Loshkajian A, Henry-Feugeas MC, Crestani B, Riquelme C, Schouman-Claeys E (1996) Assessment of deep venous thrombosis in the lower limbs and pelvis: MR venography versus duplex Doppler sonography. *Am J Roentgenol* 167:971–975
55. Lansing AM, Davis W (1968) Five-year follow-up study of iliofemoral venous thrombectomy. *Ann Surg* 168:620–628
56. Markel A, Manzo RA, Strandness DE Jr (1992) The potential role of thrombolytic therapy in venous thrombosis. *Arch Intern Med* 152:1265–1267
57. Meissner MH, Caps MT, Bergelin RO, Manzo RA, Strandness DE Jr (1997) Early outcome after isolated calf vein thrombosis. *J Vasc Surg* 26:749–756
58. Menegazzo D, Laissy JP, Durrbach A, Debray MP, Messin B, Delmas V, Mignon F, Schouman-Claeys E (1998) Hemodialysis access fistula creation: preoperative assessment with MR venography and comparison with conventional venography. *Radiology* 209:723–728
59. Mewissen MW, Seabrook GR, Meissner MH, Cynamon J, Labropoulos N, Haughton SH (1999) Catheter-directed thrombolysis for lower extremity deep venous thrombosis: report of a national multicenter registry. *Radiology* 211:39–49
60. Monreal M, Ruiz J, Olazabal A, Arias A, Roca J (1992) Deep venous thrombosis and the risk of pulmonary embolism. A systematic study. *Chest* 102:677–681
61. Moody AR (1997) Direct imaging of deep-vein thrombosis with magnetic resonance imaging. *Lancet* 350:1073
62. Morris P (2002) Interventional and endovascular therapy of the nervous system. A practical guide. Springer, Berlin Heidelberg New York
63. Moughabghab A, Socolovsky C, Lemaitre RM et al. (1995) Treatment of an ilio-caval thrombosis by mechanical thrombolysis. *Intensive Care Med* 21:440–442
64. Opatowsky MJ, Morris PP, Regan JD et al. (1999) Rapid thrombectomy of superior sagittal sinus and transverse sinus thrombosis with a rheolytic catheter device. *Am J Neuroradiol* 20:414–417
65. Osborn AG (1994) Diagnostic neuroradiology. Mosby, St. Louis
66. Oudenhoven L, Pattynama P, de Roos A, Seevers H, Rebergen S, Chang P (1994) Magnetic resonance, a new method for measuring blood flow in hemodialysis fistulae. *Kidney Int* 45:884–889
67. Overbosch EH, Pattynama PM, Aarts HJ, Schultze Kool LJ, Hermans J, Reekers JA (1996) Occluded hemodialysis shunts: Dutch multicenter experience with the Hydrolyser catheter. *Radiology* 201:485–488
68. Paksoy Y, Gormus N, Tercan MA (2004) Three-dimensional contrast-enhanced magnetic resonance angiography (3-D CE-MRA) in the evaluation of hemodialysis access complications, and the condition of central veins in patients who are candidates for hemodialysis access. *J Nephrol* 17:57–65
69. Philips MF, Bagley LJ, Sinson GP et al. (1999) Endovascular thrombolysis for symptomatic cerebral venous thrombosis. *J Neurosurg* 90:65–71
70. Poulain F, Raynaud A, Bourquelot P, Knight C, Rovani X, Gaux JC (1991) Local thrombolysis and thromboaspiration in the treatment of acutely thrombosed arteriovenous hemodialysis fistulas. *Cardiovasc Intervent Radiol* 14:98–101
71. Prandoni P, Lensing AW, Cogo A, Cuppini S, Villalta S, Carta M, Cattelani AM, Polistena P, Bernardi E, Prins MH (1996) The long-term clinical course of acute deep venous thrombosis. *Ann Intern Med* 125:1–7
72. Prandoni P, Polistena P, Bernardi E, Cogo A, Casara D, Verlato F, Angelini F, Simioni P, Signorini GP, Benedetti L, Girolami A (1997) Upper-extremity deep vein thrombosis. Risk factors, diagnosis, and complications. *Arch Intern Med* 157:57–62
73. Preter M, Tzourio C, Ameri A et al. (1996) Long-term prognosis in cerebral venous thrombosis. Follow-up of 77 patients. *Stroke* 27:243–246
74. Putnam JS, Uchida BT, Antonovic R, Rosch J (1988) Superior vena cava syndrome associated with massive thrombosis: treatment with expandable wire stents. *Radiology* 167:727–728
75. Reekers JA, Blank LE (2000) Iliocaval thrombosis: percutaneous treatment with hydrodynamic thrombectomy. *Eur Radiol* 10:326–328
76. Reul J, Weber U, Kotlarek F et al. (1997) Cerebral vein and sinus thrombosis: an important cause of benign intracranial pressure increase in childhood. *Klin Padiatr* 209:116–120
77. Rosen MP, Sheiman R (2000) Transhepatic mechanical thrombectomy followed by infusion of TPA into the superior mesenteric artery to treat acute mesenteric vein thrombosis. *J Vasc Interv Radiol* 11:195–198

78. Rutherford RB, Hurlbert SN (1996) Primary subclavian-axillary vein thrombosis: consensus and commentary. *Cardiovasc Surg* 4:420–423
79. Salzman EW, Hirsh J (1994) The epidemiology, pathogenesis and natural history of venous thrombosis. In: Colman RW, Hirsh J, Marder VJ, Salzman EW (eds) *Hemostasis and thrombosis. Basic principles and clinical practice*. Lippincott, Philadelphia, pp 1275
80. Sands J, Young S, Miranda C (1992) The effect of Doppler flow screening studies and elective revisions in dialysis access failures. *ASAIO J* 38:M524–M527
81. Schmittling ZC, McLafferty RB, Bohannon WT, Ramsey DE, Hodgson KJ (2004) Characterization and probability of upper extremity deep venous thrombosis. *Ann Vasc Surg* 18:552–557
82. Schmitz-Rode T, Vorwerk D, Schürmann K, Günther RW (1996) Experimental impeller fragmentation of ilio caval thrombosis under tulip filter protection: preliminary results. *Cardiovasc Intervent Radiol* 19:260–264
83. Schmitz-Rode T, Wildberger JE, Hübner D, Wein B, Schürmann K, Günther RW (2000) Recanalization of thrombosed dialysis access with use of a rotating mini-pigtail catheter: follow-up study. *J Vasc Interv Radiol* 11:721–727
84. Schmutz GR, Benko A, Billiard JS, Fournier L, Peron JM, Fisch-Ponsot C (1998) Computed tomography of superior mesenteric vein thrombosis following appendectomy. *Abdom Imag* 23:563–567
85. Schwab S, Raymond J, Saeed M, Newman G, Dennis P, Bollinger R (1989) Prevention of hemodialysis fistula thrombosis. Early detection of venous stenoses. *Kidney Int* 36:707–711
86. Semba CP, Dake MD (1994) Iliofemoral deep venous thrombosis: aggressive therapy with catheter-directed thrombolysis. *Radiology* 191:487–494
87. Sharafuddin MJ, Hicks ME (1997) Current status of percutaneous mechanical thrombectomy. I. General principles. *J Vasc Interv Radiol* 8:911–921
88. Sharafuddin MJ, Hicks ME (1998) Current status of percutaneous mechanical thrombectomy. III. Present and future applications. *J Vasc Interv Radiol* 9:209–224
89. Sharafuddin MJ, Hicks ME (1998) Current status of percutaneous mechanical thrombectomy. II. Devices and mechanisms of action. *J Vasc Interv Radiol* 9:15–31
90. Spengel FA, Liebe S von (1998) Venous thrombosis: a diagnostic and therapeutic challenge. *Radiologe* 38:549–553
91. Strandness DE Jr, Langlois Y, Cramer M, Randlett A, Thiele B (1983) Long-term sequelae of acute venous thrombosis. *J Am Med Assoc* 250:1289–1292
92. Strauch B, O'Connell R, Geoly K, Grundlehner M, Yakub Y, Tietjen D (1992) Forecasting thrombosis of vascular access with Doppler color flow imaging. *Am J Kidney Dis* 19:554–557
93. Taha JM, Crone KR, Berger TS et al. (1993) Sigmoid sinus thrombosis after closed head injury in children. *Neurosurgery* 32:541–546
94. Takahashi N, Kuroki K, Yanaga K (2005) Percutaneous transhepatic mechanical thrombectomy for acute mesenteric venous thrombosis. *J Endovasc Ther* 12:508–511
95. Thron A (2001) Diagnostik duraler Sinus- und zerebraler Venenthrombosen *Klin Neurorad* 11:185–196
96. Trerotola SO, Vesely TM, Lund GB, Soulen MC, Ehrman KO, Cardella JF (1998) Treatment of thrombosed hemodialysis access grafts: Arrow-Trerotola percutaneous thrombolytic device versus pulse-spray thrombolysis. *Radiology* 206:403–414
97. Truong TH, Spüntrup E, Staatz G, Wildberger JE, Schmitz-Rode T, Nolte-Ernsting CC, Günther RW, Haage P (2004) Mechanical thrombectomy of ilio caval thrombosis using a protective expandable sheath. *Cardiovasc Intervent Radiol* 27:254–258
98. Tsuruda JS, Shimakawa A, Pelc NJ et al. (1991) Dural sinus occlusion: evaluation with phase-sensitive gradient-echo MR imaging. *Am J Neuroradiol* 12:481–488
99. Turmel-Rodrigues L, Pengloan J, Bourquelot P (2002) Inter-ventricular radiology in hemodialysis fistulae and grafts: a multidisciplinary approach. *Cardiovasc Intervent Radiol* 25:3–16
100. Turmel-Rodrigues L, Sapoval M, Pengloan J, Billaux L, Testou D, Hauss S, Mouton A, Blanchard D (1997) Manual thromboaspiration and dilation of thrombosed dialysis access: midterm results of a simple concept. *J Vasc Interv Radiol* 8:813–824
101. Urschel HC Jr, Razzuk MA (2000) Paget-Schroetter syndrome: What is the best management? *Ann Thorac Surg* 69:1663–1668
102. Usui Y, Sauvage LR, Wu HD, Goff SG, Walker M (1987) A comparative experimental study of the organization of arterial and venous thrombi. *Ann Surg* 205:312–317
103. Valji K, Bookstein J, Roberts A, Davis G (1991) Pharmacomechanical thrombolysis and angioplasty in the management of clotted hemodialysis grafts: early and late clinical results. *Radiology* 178:243–248
104. Virapongse C, Cazenave C, Quisling R et al. (1987) The empty delta sign: frequency and significance in 76 cases of dural sinus thrombosis. *Radiology* 162:779–785
105. Vorwerk D, Günther RW, Wendt G, Neuerburg J, Schürmann K (1996) Iliac stenosis and iliac venous thrombosis in retroperitoneal fibrosis: percutaneous treatment by use of hydrodynamic thrombectomy and stenting. *Cardiovasc Intervent Radiol* 19:40–42
106. Vorwerk D, Schürmann K, Müller-Leisse C, Adam G, Bucker A, Sohn M, Kierdorf H, Günther RW (1996) Hydrodynamic thrombectomy of hemodialysis grafts and fistulae: results of 51 procedures. *Nephrol Dial Transplant* 11:1058–1064
107. Warshauer DM, Lee JK, Mauro MA, White GC (2001) Superior mesenteric vein thrombosis with radiologically occult cause: a retrospective study of 43 cases. *Am J Roentgenol* 177:837–841
108. Virman EE, Salzman EW (1994) Deep-vein thrombosis. *N Engl J Med* 15:1630–1641
109. Wildberger JE, Mahnken AH, Sinha AM, Stargardt A, Haage P, Schaller S, Günther RW (2002) A differentiated approach to the diagnosis of pulmonary embolism and deep venous thrombosis using multi-slice CT. *Rofo Fortschr Geb Röntgenstr Neuen Bildgeb Verfahr* 174:301–307
110. Wille-Jorgensen P, Borris L, Jorgensen LN, Hauch O, Lassen MR, Nehen AM, Kjaer L, Jensen R (1992) Phlebography as the gold standard in thromboprophylactic studies? A multicenter interobserver variation study. *Acta Radiol* 33:24–28
111. Yamauchi T, Furui S, Katoh R et al. (1993) Acute thrombosis of the inferior vena cava: treatment with saline-jet aspiration thrombectomy catheter. *Am J Roentgenol* 161:405–407
112. Zaleski GX, Funaki B, Kenney S, Lorenz JM, Garofalo R (1999) Angioplasty and bolus urokinase infusion for the restoration of function in thrombosed Brescia-Cimino dialysis fistulas. *J Vasc Interv Radiol* 10:129–136
113. Zibari GB, Rohr MS, Landreneau MD, Bridges RM, DeVault GA, Petty FH, Costley KJ, Brown ST, McDonald JC (1988) Complications from permanent hemodialysis vascular access. *Surgery* 104:681–686
114. Zontsich T, Turetschek K, Baldt M (1998) CT-phlebography. A new method for the diagnosis of venous thrombosis of the upper and lower extremities. *Radiologe* 38:586–590
115. Zwiebel WJ, Priest D (1990) Color duplex sonography of extremity veins. *Semin Ultrasound CT MR* 11:136–167

# Management of Occluded Hemodialysis Shunts, Grafts, and Venous Access

D. Vorwerk

## 6.3

### Contents

6.3.1 Introduction	571
6.3.2 Clinical Situation	571
6.3.2.1 Percutaneous Treatment	572
6.3.2.2 Endoluminal Clot Dissolution	575
6.3.2.3 Stenting	577
6.3.3 Conclusion	577
6.3.4 Venous Access Occlusion	578
6.3.4.1 Technique of Fibrinolysis	578
6.3.4.2 Technique of Catheter Stripping	578
References	578

### 6.3.1 Introduction

Shunt thrombosis is a relatively frequent complication of implant grafts but is less common in native fistulas; both may undergo percutaneous revascularization by thrombolysis or mechanical recanalization without thrombolysis.

While in native fistulas simple balloon angioplasty is a very useful tool for short segment thrombosis, extensive thrombosis in native veins or grafts requires use of different mechanical devices or aspiration catheters.

In venous access thrombosis, thrombolysis or fibrinous sheath stripping are percutaneous options. Shunt thrombosis is a frequent complication in hemodialysis shunts, particularly in grafts, but may also be found in autologous fistulas [1]. Besides an underlying stenosis, which is present in almost all cases, co-factors are manifold: clotting abnormalities, thrombocytosis, disturbed fluid balance, as well as hypotension may lead to shunt thrombosis. There are, however, different types of shunt thrombosis that require different strategies of percutaneous intervention.

### 6.3.2 Clinical Situation

Clinical examination of the shunt, and especially palpation of the venous outflow tract, gives an impression of the type of occlusion and its location and is an inevitable part of the clinical check-up prior to an intervention. Where there is doubt, sonography and duplex sonography may facilitate determination of the extent of a thrombosis and its location.

Shunt occlusions in Brescia-Cimino fistulas, especially in the very early phase, may be due to only a very short plug-like thrombus selectively obstructing the arteriovenous anastomosis or a segment of the venous outflow. In those cases, the draining shunt veins are soft and compressible at palpation. If digital manipulation to remove the thrombus fails, this type of obstruction is an ideal candidate for PTA, since the small thrombus can be macerated by balloon inflation alone and flow can be restored immediately. Treatment, however, should be started soon to avoid propagation of thrombosis. Palpation also depicts those cases in which shunt thrombosis is due to an underlying severe stenosis and a subsequent small thrombus formation. If this happens close to the arteriovenous anastomosis, the amount of thrombus is mostly small and balloon dilatation alone may be sufficient for recanalization and treatment of the underlying stenosis.

Long-segment thrombosis of Brescia-Cimino fistulas present with enlarged and incompressible veins that appear rather hard during palpation. The PTA alone is mostly insufficient in these cases.

In implant grafts there is almost always complete occlusion of the total graft from the arterial to the venous anastomosis and sometimes extending into the draining vein with thrombus at both ends. The thrombosis within the graft itself varies considerably in amount and grade of organization. There is always a whitish resistant arterial plug on the arterial anastomosis present that needs to be removed and almost always an outflow tract stenosis either directly at the venous anastomosis or within the draining vein.



Very rarely, arterial thrombosis or embolism may be a cause for shunt dysfunction. Percutaneous treatment depends on the location and amount of thrombus that has to be removed. It can vary from simple PTA to thrombolysis.

### 6.3.2.1 Percutaneous Treatment

There are several different approaches described in the literature with regard to percutaneous treatment with dialysis grafts and shunts:

1. Thrombolysis and spray lysis
2. Mechanical thrombectomy
3. Balloon angioplasty
4. Aspiration thrombectomy
5. Hydrodynamic thrombectomy
6. Mechanical clot dissolution
7. Stent placement

Frequently, a combination of a variety of methods becomes necessary to finalize a case. Different methods have been used with success, and interventional radiologists should be familiar with several of them to achieve the best possible results.

#### Thrombolysis and Spray Lysis

Thrombolysis has been described for treatment of thrombosis especially in grafts, and has been performed with different application techniques of the lytic agent [2–5]. Different technical success rates varying from 56 to 90 % have been reported in the literature [6–9]. It is not yet clear whether spray lysis [6] has a predominantly mechanical or lytic effect on thrombus material, since Beathard achieved comparable results using spray technique with and without lytic agents [10].

#### Mechanical Thrombectomy

##### Balloon Angioplasty

Simple balloon angioplasty is the easiest tool for treating small-segment thrombosis or small thrombus mass complicating a venous stenosis. It is very quick, inexpensive, and effective [11]. Its use is limited to native fistulas since grafts do not show circumscribed thrombosis unless they are treated in a very early stage of thrombus formation.

To avoid propagation of thrombosis, treatment should be performed on an emergency basis after the patient has shown up with circumscribed thrombosis. This should also be executed during evening hours and on weekends.

Access to the shunt depends on the location of the thrombus. In most instances it is located close to the anastomosis; thus, retrograde cannulation of the draining vein is most suitable. The arteriovenous anastomosis is then carefully passed by a 5-F multipurpose catheter and a hydrophilic guidewire which is advanced into the feeding

artery. There is only a minimal risk of arterial thrombus dislodgement during this maneuver; thereafter, the 5-F catheter is exchanged for a balloon catheter of 4–6 mm which is inflated at the area of thrombosis. This can be repeated until shunt flow is restored. Treatment should not be terminated unless an optimal opening of the underlying stenotic area has been achieved.

#### Combined Surgery and Balloon Angioplasty

Implant grafts are most frequently declotted using Fogarty balloons after surgical cut-down [3]. Combination with balloon dilatation and thrombus cracking for older thrombus formation has been recommended and combined surgical–radiological intervention is a suitable approach to that problem in order to image the shunt morphology after thrombectomy and to treat underlying stenosis by PTA [3, 4].

After removing all thrombus material, PTA catheters are advanced through the surgical cut-down to the underlying stenosis.

This approach is advantageous to be performed in the angiosuite since excellent X-ray facilities improve diagnosis and treatment of stenotic areas and residual thrombosis.

While this approach was our routine approach to graft occlusion during past years, it has become rare recently since we introduced purely percutaneous methods of mechanical thrombectomy.

#### Aspiration Thrombectomy

Clot removal may also be performed by use of simple end-hole aspiration catheter of 7–9 F. The technique used is similar to arterial thrombosuction. In case a residual flow is present, arterial inflow should be interrupted by digital compression to facilitate aspiration of a clot. It is a simple and cost-effective technique that is able to remove clot effectively.

Turmel-Rodrigues et al. [13] reported on their vast experience with aspiration thrombectomy in native fistulas and grafts with 257 declotting procedures. They achieved a technical success in 78–98 % depending on the nature of the shunt connection. Primary patency at 1 year was 50 % for native fistula and 25 % for implant grafts. Secondary patency at 1 year was between 80 and 86 %.

Technically, besides aspiration, stent placement became necessary in a considerable number of cases [13]. They placed stents in 41–45 % of declotting cases including those stents indicated to displace residual clot material.

The procedure itself was relatively time-consuming with a mean procedure time of 119 (grafts) to 134 min (forearm fistulas) [13].

Some authors used aspiration in combination with thrombolysis by urokinase. Raynaud et al. aspirate residual thrombus after thrombolysis that has been softened by

previous application of urokinase. They reported on 85 procedures with a complete success in 74%, partial success in 20%, and failure in 6%. A primary patency of 41% after 6 months was found [5].

Aspiration is also an excellent tool to remove embolized occlusion material from the radial or brachial artery that occurred during declotting procedures allowing treatment of complications caused by mechanical thrombectomy or lysis.

### Hydrodynamic Thrombectomy

Hydrodynamic thrombectomy has been recently introduced to the treatment of acute thrombosis of arteries, bypass grafts, and hemodialysis fistulas and grafts [12–15]. There have been three different devices tested for their usability in dialysis connections:

1. Hydrolyser (Cordis, Roden, The Netherlands), 7 F
2. Oasis catheter (Boston Scientific, Boston, Mass.), 7–8 F
3. Angiojet catheter (Possis, USA), 6 F

All of them work with the same principle: they are double-lumen catheters with retrograde saline injection from a very small supply lumen that is injected in a larger efferent lumen. Due to the resulting pressure gradient, known as the Venturi effect, between the jet flow and the larger exhaust lumen, the injected fluid instantaneously leaves the vessel via the exhaust lumen thus creating a turbulent flow zone close to the catheter tip and suction. The surrounding thrombus is fragmented by the flow vortex, sucked into the exhaust lumen, and removed as a mixture of saline and thrombus through it. Blood loss is low and the system is more or less isovolumetric.

Saline injection can be performed by conventional angiographic injectors for the Hydrolyser and the Oasis catheter but requires a specially designed power pump for the Angiojet catheter.

### Technique of Mechanical Thrombectomy

Different access techniques have to be used for native forearm fistulas (Fig. 1) and PTFE grafts (Fig. 2).

### PTFE Grafts

Three different approaches can be used for PTFE grafts. With the “double-sheath technique” the PTFE graft is cannulated twice [12]: in the arterial limb in an antegrade fashion (with flow direction) for venous thrombectomy; and in the venous limb in a retrograde fashion (against flow direction) for thrombectomy of the arterial limb. A sheath is inserted at each puncture site with no crossing. The venous limb is thrombectomized first by firstly guiding the nonactivated catheter centrally into a nonclotted venous segment. After activation, it is pulled back through the occluded segment; thereafter, the arterial limb is thrombectomized by advancing the activated catheter into the arterial limb up to 2–3 cm distally to the arterial anastomosis. Thrombus within the anastomosis is first dilated by a 5–6 mm balloon catheter and pulled into the graft where it is hydrolyzed.

Since two 7- to 8-F sheaths within the graft are flow-restricting a modified approach, the so-called single-sheath approach is applicable [15]. For that reason, only the arterial limb is cannulated in an antegrade fashion by a 7-F in-

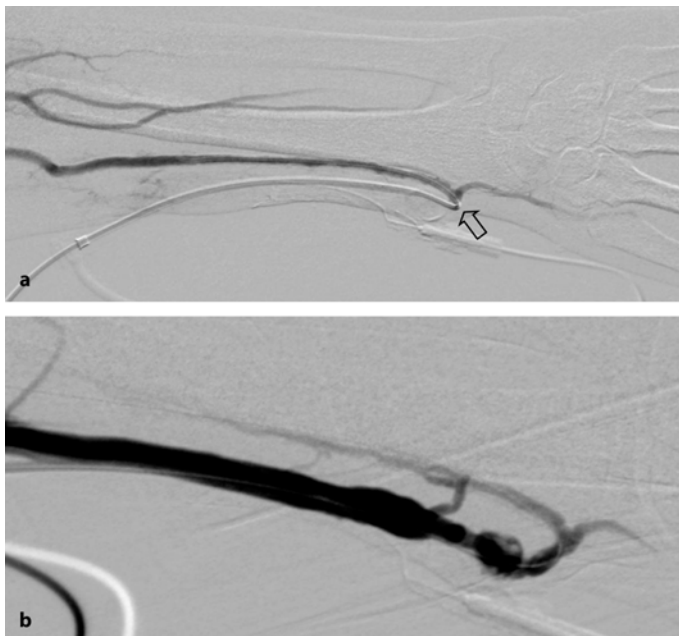


**Fig. 1.** Native fistula. **a** After retrograde passage of the cephalic vein across the arteriovenous anastomosis, complete occlusion by a tight stenosis combined with a small thrombus is visualized injecting contrast media into the radial artery. **b** After PTA with no additional thrombectomy maneuver, patency has been restored

troducer sheath. Hydrodynamic thrombectomy of the venous limb is subsequently performed as described above; thereafter, a retrograde puncture of the venous limb is performed just introducing a 5-F balloon catheter of 5–6 mm diameter without sheath that is guided over a 0.035-in. hydrophilic wire (Terumo Inc, Tokyo, Japan) into the brachial artery. The balloon is inflated in the most proximal part of the graft to dilate thrombus material that is regularly found in that location; thereafter, the inflated balloon is gently pulled back into the graft distally to the 7-F sheath entry point. The balloon is then deflated and pulled back to its puncture site. The dislodged thrombus material will then be hydrodynamically thrombectomized via the first 7-F sheath.

The third technique is the “apex-approach” [16], where the loop is punctured at the apex. A sheath is then inserted preferably in the venous limb first and after finishing one side, the sheath together with a dilator is pulled back and is tilted at the puncture side until, by the help of a guidewire, the other limb can be cannulated. This technique allows to use only one puncture, but sometimes a dead zone at the apex occurs where clot removal is difficult.

### Brescia-Cimino Fistulas

In native forearm BC fistulas, the draining vein is punctured in a retrograde fashion against flow direction. We prefer to advance the hydrodynamic catheter as close to the anastomotic region as possible or to cross it and then to retrieve the system while activated. Several passes of the system have to be performed until no residual thrombus can be detected or no more material removed. Individually, additional balloon dilatation has to be applied in order to press residual material aside or to treat an underlying stenosis. During activation, retrograde arterial embolization is prevented by digital compression of the arteriovenous anastomosis. In some cases, the most distal thrombus close to the anastomosis is dilated with a 5–6 mm balloon to allow some inflow into the proximal fistula prior to use of the hydrodynamic system. No special technique is used to prevent central venous embolization, since the introducer sheath is considered to sufficiently block the venous outflow for larger emboli.

In cases of upper-arm cephalic BC fistula, a modified protocol has to be used: In brachiocephalic upper-arm fistulas with its anastomosis in the elbow region, antegrade puncture close to the anastomosis may be performed. The anastomosis has to be compressed during thrombectomy to avoid retrograde dislodgement of thrombus material into the brachial artery.

### Results

Results are available for all three hydrodynamic systems. No comparison studies exist, however, neither comparing other hydrodynamic nor other mechanical devices.

### Hydrolyser

Evaluated from 51 procedures [15], hydrodynamic thrombectomy using the Hydrolyser was completed with 1–7 runs (mean  $3.2 \pm 1.1$  runs). Considerable fluid imbalance with over-infusion of 50–100 ml to the patient occurred in two cases.

The major amount of thrombus was removed by hydrodynamic thrombectomy in most cases. The estimated amount of residual thrombus was 8% (range 5–30%) on average in grafts and 21% (range 10–50%) in native fistulas. Despite residual thrombus in many cases, arterialized flow was completely established by combining hydrodynamic thrombectomy and PTA in 44 of 51 cases (86%). By additional use of aspiration thrombectomy, stent implantation or Fogarty embolectomy overall assisted technical success was therefore 46 of 51 procedures (90%).

Technical failure of combining hydrodynamic thrombectomy and balloon angioplasty occurred in 7 cases. Occlusion time in these cases ranged from 12 to 120 h (mean 65.2 h, median 60 h). In all cases, hydrodynamic thrombectomy was combined with balloon angioplasty and, in two cases, with directional atherectomy for treatment of an additional stenosis or remaining thrombus.

There was one retrograde arterial embolization to the radial artery that was treated by embolectomy using a minibasket and one case of temporary short breath that might be subsequent to pulmonary embolization of occluding material.

Clinical success was achieved in 39 of 46 technically successful cases (85%) in whom the access was used for hemodialysis again or remained patent for at least 1 week after thrombectomy without hemodialysis (3 patients).

Forty-six grafts and fistulas were followed from 1 week to 18 months. Cumulative patency was calculated 63% after 1 week, 57% after 1 month, 48% after 3 months, 37% after 6 months, and 32% after 12 months.

### Oasis Catheter

Barth and coworkers [17] evaluated the safety and efficacy of a hydrodynamic thrombectomy system in a prospective, multicenter randomized comparison with pulse-spray thrombolysis in hemodialysis grafts. Nine centers enrolled 120 adult patients with recently ( $\leq 14$  days) thrombosed hemodialysis grafts. Graft venography was used to confirm occlusion in 62 patients randomly assigned to thrombectomy and 58 to thrombolysis.

Technical success rates were 95% (59 of 62) for thrombectomy and 90% (52 of 58) for thrombolysis. Clinical success rates were 89% (55 of 62) and 81% (47 of 58). At 90 days, the rates were 40% (25 of 62) and 41% (24 of 58), respectively ( $P=0.91$ ). None of these differences or those for procedure-related blood loss and early and late complications were statistically significant. Thrombus treatment times of 16.8 min for thrombectomy and 23.4 min for thrombolysis were significantly different. They concluded that hydrodynamic thrombectomy system is at least as efficacious and safe as pulse-spray thrombolysis but shortened thrombus treatment time.

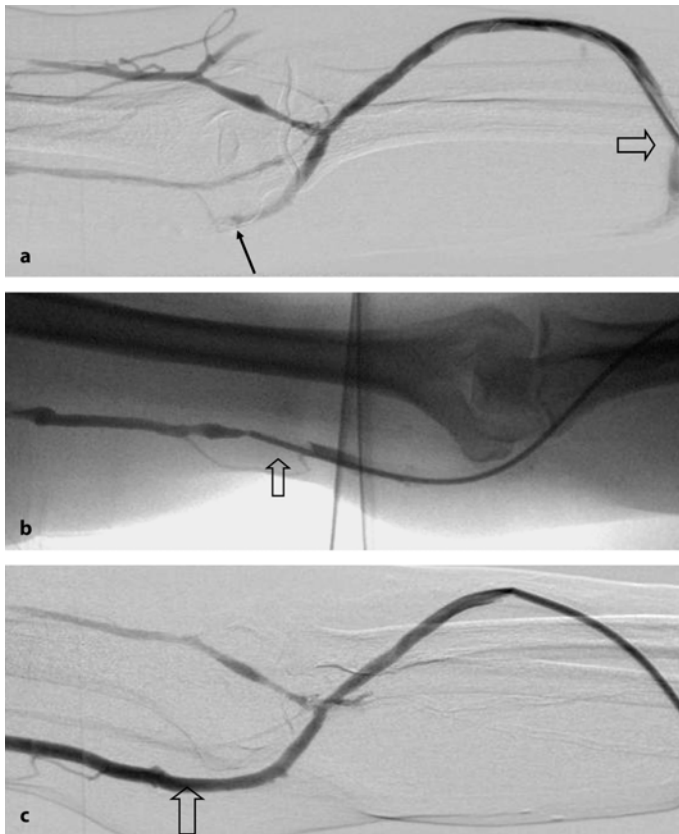


**Fig. 2.** Implant loop shunt. **a** After apex puncture (*large arrow*) of the implant loop, thrombotic occlusion (*small arrow*) of the venous outflow is visualized following successful thrombectomy from the loop. **b** After placing an 8-F aspiration catheter (*arrow*), suction thrombectomy has been performed. **c** Following aspiration, patency has been restored

### Angiojet Catheter

Vesely and coworkers compared the clinical effectiveness of the AngioJet F105 rheolytic catheter to that of surgical thrombectomy for the treatment of thrombosed hemodialysis grafts. A total of 153 patients were enrolled with 82 patients in the AngioJet group and 71 patients in the surgical thrombectomy group [18].

Technical success was 73.2% for the AngioJet group and 78.8% for the surgical thrombectomy group. The primary patency rates of the AngioJet group were 32, 21, and 15% at 1, 2, and 3 months, respectively. The primary patency rates for the surgical group were 41, 32, and 26 at 1, 2, and 3 months, respectively. The groups had similar complication rates: 14.6% in the AngioJet group and 14.1% in the surgical thrombectomy group. The AngioJet F105 catheter provides similar clinical results when compared with surgical thrombectomy for the treatment of thrombosed hemodialysis grafts, but the patency rate in surgically treated cases was significantly better.

In the meantime, larger 6-F catheters have been introduced on the market, and results are pending.

### 6.3.2.2 Endoluminal Clot Dissolution

Other than hydrodynamic thrombectomy that removes the thrombus from the body, endoluminal thrombus dissolution tries to break up thrombus formation into ultrasmall pieces allowing capillary passage of the fragments. Several different devices are clinically available, but the Amplatz clot buster device (Microvena, Minneapolis, Minn.) and the PTD Trerotola rotating basket (Arrow Inc., Reading Pa.) are the only available devices where clinical data are available for dialysis connections.

#### Clot Buster

The Clot buster is a 7- or 8-F flexible catheter with no guiding lumen that wears a housed impeller at its distal end. The impeller is driven by air pressure up to high rotational speed causing a large vortex around the catheter tip. Thrombus is sucked towards the impeller and breaks up, and its fragments recirculate into the vortex over and over again.

Technical application is similar to hydrodynamic thrombectomy and depends on the type of shunt that is going to be treated. Applicability is easy and quick, since pressured air is available in most angiosuites.



Sometimes guiding problems may occur since the 8-F device cannot be advanced over a wire (a 6-F over-the-wire version will be available soon) and hemolysis is possible. In large-diameter veins, such as the brachial, subclavian, and jugular veins, the Amplatz catheter, in our experience, seems to be more effective than hydrodynamic devices such as the Hydrolyser.

Uflacker et al. [19] reported the final results of the trial comparing the Amplatz thrombectomy device (ATD) with surgical thromboembolotomy to declot thrombosed dialysis access grafts. The study population consisted of 174 grafts, 109 of which were randomized to mechanical thrombectomy using the ATD and 65 of which were randomized to conventional surgical thromboembolotomy. Forty grafts were re-enrolled in the trial when they failed beyond the 90 days follow-up after the initial treatment; thirty-one were re-enrolled for mechanical thrombectomy and nine were re-enrolled for surgical thrombectomy, resulting in a total of 140 ATD procedures and 74 surgical thromboembolotomy.

Patency of the graft, with successful dialysis, at 30 days with the ATD procedure was 79.2% and with surgery was 73.4%. Patency of the graft, with successful dialysis, at 90 days with the ATD procedure was 75.2% and with ST was 67.8%. The results of the performance of both methods were comparable. No statistically significant differences were seen.

#### PTD Trerotola Device

The PTD device is a 7-F system that carries a nitinol basket which slowly rotates driven by a small motor. It can be closed and opened by moving an outer protecting catheter. It is an over-the-wire system that accepts an 0.025-in. guidewire.

In dialysis shunts and grafts, some clinical experience has been published. Lazzaro et al. [20] reported on the use of the Arrow-Trerotola percutaneous thrombolytic device (PTD) as the sole means of mechanical thrombolysis in hemodialysis access grafts. Fifty consecutive patients in whom mechanical thrombolysis of a thrombosed hemodialysis access graft using the PTD was planned were included in the study. In all patients, the PTD was used to treat the arterial plug in situ at the arterial anastomosis, instead of using a Fogarty catheter to reposition the plug, as indicated in the PTD product labeling. Prospective data collection included demographic information, technical details of the procedure, immediate outcomes, and complications. Patients were followed for 3 months. Immediate technical patency was 100%. Complications included arterial embolization (6%), venous rupture (6%), and sepsis in 1 patient. Three-month patency using life-table analysis was 42%.

Rocek et al. [21] evaluated the feasibility of use of the Arrow-Trerotola percutaneous thrombolytic device (PTD) in the treatment of thrombosed native fistulas. Ten patients

were treated: the technical success rate was 100% and the clinical success rate was 90%. In all 10 cases, the procedure was associated with angioplasty. The mean time of successful procedures was 126 min. The 3- and 6-month primary patency rates were 70 and 60%, respectively. The assisted primary patency rate at 6 months was 80%; thus, the device could be safely used also in native veins.

#### Intentional Pulmonary Embolization of Occlusion Material

Trerotola and coworkers described a technique of mechanical declotting that uses over-the-wire Fogarty balloons to clear grafts from clot material [22]. They intentionally embolized the occluding thrombus to the central circulation by pushing it through the graft or by pulling it into the graft when clearing the arterial limb. This relatively inexpensive technique had a technical success of 94% (32 of 34 procedures). Two arterial emboli were found; no clinical significance of pulmonary embolization was reported.

This technique has become a matter of discussion because intentional embolization to the pulmonary circulation appears to be of an unknown risk. This is especially significant if the procedure has to be repeated several times due to recurrent graft thrombosis. Swan and coworkers found that scintigraphic evidence of pulmonary embolism occurred in 59% of cases after combining mechanical maceration, lysis, and intentional embolization, although the vast majority remained without clinical significance [23]. Two patients, however, developed clinical signs of PE and died. From these findings, they concluded that patients with underlying cardiopulmonary disease and repeated procedures are of higher risk to develop symptoms from this procedure.

It is, however, true that pulmonary emboli may occur unintentionally with all other mechanical thrombectomy devices and also thrombolysis. Moreover, the amount of thrombus usually found in hemodialysis grafts is very small and mostly close to both anastomoses. Harp and co-workers [24] compared the prevalence of pulmonary hypertension between patients who underwent one or more hemodialysis access thrombectomy procedures with controls without prior thrombectomy. A retrospective case-control study was performed. Cases ( $n=88$ ) had undergone one or more hemodialysis graft thrombectomy procedures, with subsequent echocardiography during routine investigation of comorbid cardiovascular disease. Cases were compared with controls without end-stage renal disease ( $n=100$ ) and controls with ESRD but no prior thrombectomy procedures ( $n=117$ ).

The prevalence of pulmonary hypertension among cases was 52% (46 of 88). Prevalence of pulmonary hypertension among normal controls was 26% (26 of 100). Cases had 2.7 times greater odds of having pulmonary hypertension than group-1 controls ( $p=0.002$ ). The prevalence of pulmonary hypertension among dialysis patients without declotting procedures was 42%. Cases were slightly more

but insignificantly likely to have pulmonary hypertension than the latter group of patients.

To the best of our knowledge, however, whether or not the procedure can be repeated several times without danger for the patient, intentional embolization should be used with care and limited to very small clots and exceptional instances.

### 6.3.2.3 Stenting

Another possibility of mechanical “thrombectomy” is use of endoluminal stents to fix the thrombus to the venous wall by compression and flattening [25]. This technique can be especially very helpful in large veins where other techniques failed to remove thrombus material successfully. Due to the permanent stent placement and its costs, it is of course not an approach that should be used on a regular basis but offers additional possibilities in case an otherwise desperate situation has to be resolved.

## 6.3.3 Conclusion

Thrombosis of hemodialysis fistulae and grafts represents the most frequent complication of hemodialysis access [1]. As a late complication, they are more often found in grafts than in native fistulae. An underlying stenosis or aneurysmatic vein causing flow irregularities are predisposing factors for thrombosis and especially venous stenosis is found in the vast majority of cases [26]. Early reintervention to dilate an underlying stenosis has been shown to reduce the rate of thrombosis [26]. Venous stenosis in grafts is typically located at the venous graft anastomosis, whereas in native fistulas stenoses are more frequently located distally close to the arteriovenous anastomosis or within the cannulation area. Thrombosis may be, however, also caused by clotting abnormalities, low cardiac output, hypotension, or compromised proximal arterial inflow.

Standard therapy of access thrombosis includes surgical thrombectomy after cut-down in grafts and more proximal arteriovenous reanastomosis in native fistulas [27]; underlying stenosis frequently requires additional patch plasty.

Percutaneous techniques have been shown to be a promising alternative in fistula stenoses.

Technical success of hydrodynamic thrombectomy (90%) is comparable to those received by catheter-directed (97%) or pulse-spray lysis (96%) and mechanical declotting (94%) [6, 8, 22]. Comparing mechanical with pharmacomechanical spray-technique, Beathard [10] found an equal technical success of 93 vs 94%. We believe that an improvement of technical success was achieved in our series by introducing the single-sheath technique for grafts, since adequate thrombectomy was now more easy to determine with only one sheath inserted. Important factors influenc-

ing primary technical success were time of occlusion and involvement of larger veins such as the brachial vein: occlusion time in cases with primary technical failure was considerably longer compared with that of the total group. Furthermore, organization of thrombus material seemed to be more pronounced in native veins than in grafts. These findings support start of the intervention as early as possible once thrombosis has been detected. Involvement of larger veins, such as the brachial vein, complicated treatment since hydrodynamic thrombectomy failed to remove thrombus from this location.

Early thrombosis, despite technical success, is frequent after percutaneous treatment. It occurred in 7% of cases after catheter-directed thrombolysis [6], in 15% after mechanical declotting [22], and in 11% after hydrodynamic thrombectomy. The reasons are manifold including inadequate heparinization [6, 12, 22], hypotension, or residual stenosis [22], and there is no proven relation to the method of thrombectomy used.

Follow-up primary patency has been found to be low with no regard to which type of treatment has been used. Valji and co-workers [6] reported a cumulative patency rate (excluding technical failures) of 68% (1 month), 45% (3 months), 34% (6 months), and 26% (1 year). The results of Terrotola and co-workers [22] were 56% (1 month), 40% (3 months), and 20% (6 months). Beathard found a cumulative patency (mechanical vs pharmacomechanical) of 65 vs 74% (1 month) and 37 vs 46% (3 months) in a randomized trial [10]. These data correspond well to the patency rate found for hydrodynamic thrombectomy, which were almost equal or slightly better. Furthermore, patency after surgical thrombectomy is not better [29, 30]. Brotman and co-workers [30] described patency rates of 45% (1 month), 27% (3 months), and 3.5% (12 months). It has to be emphasized, however, that long-term success of repaired hemodialysis fistulas and grafts depends on several factors such as tendency for restenosis, cannulation trauma, reduced arterial inflow, hypotension, or hypercoagulability [30].

Complications of mechanical thrombectomy were only minor. Rate of arterial embolization is usually rare with no regard what technique was used.

Particularly in grafts, embolization across the arterial anastomosis is rare if manipulations are performed carefully. It is more likely to occur in case brisk injection into the clotted graft is applied causing arterial embolization by backflow into the brachial artery; thus, only downstream angiography should be used to image the declotting procedure.

In conclusion, mechanical thrombectomy with all its variations proved to be an effective percutaneous method for thrombectomy in haemodialysis grafts and native fistulas achieving results well comparable to alternative methods such as lysis therapy. What particular type of treatment should be used depends on the experience of each operator, the clinical situation, the extent of thrombosis, and the type and age of occlusion.

In our daily practice, we try to keep a procedure as simple as possible. In native fistulas, PTA is our first choice that may be combined with aspiration, hydrodynamic thrombectomy, or the PTD device if larger amounts of thrombus are present. In grafts, aspiration, hydrodynamic thrombectomy, or mechanical thrombectomy are well applicable.

Applying these strategies, percutaneous techniques have become the approach of first choice in our institution and surgical thrombectomy has been limited to cases where thrombosis is older than a week or failure of percutaneous approach had occurred. Thrombolysis has been nearly abandoned from treatment of shunt thrombosis.

### 6.3.4 Venous Access Occlusion

Occlusion of venous access may occur by three different mechanisms:

1. Catheter thrombosis. In this case neither injection of fluids nor aspiration of blood might be possible in tunneled catheters.
2. Formation of a fibrin sheath. In this case, injection of fluid is usually possible, but aspiration of blood is not possible which compromises the functionality especially in tunneled catheters for dialysis.
3. Pericatheter thrombosis of the hosting vein. In catheter thrombosis and venous thrombosis, thrombolysis is the only technique to save the access. Alternatively, a complete system exchange is an alternative option.

In fibrin sheath formation, fibrinolysis should be the first step followed by mechanical fibrin sheath stripping and eventually catheter exchange.

#### 6.3.4.1 Technique of Fibrinolysis

A bolus of 50,000 IU urokinase is administered into the catheter lumen. If, after 24 h, the catheter is not recanalized again, a urokinase infusion of 20,000 IU urokinase per hour and lumen over a period of 6 h up to a maximum dose of 240,000 IU may be administered. If this approach fails again, fibrin-sheath stripping or catheter exchange would be the next steps.

#### 6.3.4.2 Technique of Catheter Stripping

After accessing the femoral vein, a goose neck catheter of an appropriate size (15–20 mm) is advanced into the superior vena cava and the catheter is snared. After having moved the open snare to the distal portion of the catheter, the snare is closed and pulled centrally. This maneuver is repeated several times until aspiration becomes again possible.

If possible, a guidewire should be inserted through the catheter into the inferior vena cava which facilitates capture of the wire and safe upward placement of the snare around the catheter tip. This is especially helpful if the catheter's tip already protrudes into the right atrium to limit the danger of pericardial trauma.

## References

1. Zibari G, Rohr M, Landreneau M, Bridges R, DeVault G, Petty F, Costley K, Brown S, McDonald J: Complications from permanent hemodialysis vascular access Surgery 1988; 104: 681–686
2. Vorwerk D, Günther RW, Schürmann K, Sohn M: Perkutane Behandlungsmöglichkeiten beim thrombotischen Verschluss von Brescia-Cimino-Dialysehunt. Fortschr Röntgenstr 1995, 162: 236–240
3. Kistler D, Bohndorf K, Günther RW. Kombiniert chirurgisch-radiologisches Vorgehen beim Verschluss eines Hämodialysehunts. Chirurg 1990; 61: 84–86
4. Smith T, Hunter D, Darcy M, Castaneda-Zuniga W, Amplatz K: Thrombosed synthetic hemodialysis access fistulas: the success of combined thrombectomy and angioplasty (Technical note). Am J Roentgenol 1986; 147: 161–163
5. Raynaud A, Auguste M, Pagny J, Beyssen B, Bourquelot P: Acute angioaccess thrombosis. treatment by fibrinolysis associated to thromboaspiration. Abstract 138, p 79 Angioaccess for Hemodialysis, Tours 1996
6. Valji K, Bookstein J, Roberts A, Davis G: Pharmacomechanical thrombolysis and angioplasty in the management of clotted haemodialysis grafts: early and late clinical results. Radiology 1991; 178: 243–248
7. Davis G, Dowd C, Bookstein J, Maroney T, Lang E, Halasz N: Thrombosed dialysis grafts. Efficacy of intrathrombic deposition of concentrated urokinase, clot maceration and angioplasty Am J Roentgenol 1987; 149: 177–181
8. Poulain F, Raynaud A, Bourquelot P, Knight C, Rovani X, Gaux J: Local thrombolysis and thromboaspiration in the treatment of acutely thrombosed arteriovenous hemodialysis fistulas. Cardiovasc Intervent Radiol 1991; 14: 98–101
9. Young A, Hunter D, Castaneda-Zuniga W, So S, Mercado S, Cardella J, Amplatz K: Thrombosed synthetic hemodialysis access fistulas: failure of fibrinolytic therapy. Radiology 1985; 154: 639–642
10. Beathard G: Mechanical versus pharmacomechanical thrombolysis for the treatment of thrombosed dialysis access grafts. Kidney Int 1994; 45: 1401–1406
11. Haage P, Vorwerk D, Wildberger JE, Piroth W, Schürmann K, Günther RW: Percutaneous treatment of thrombosed primary arteriovenous hemodialysis access fistulae. Kidney Int 2000; 57: 1169–1175
12. Vorwerk D, Sohn M, Schürmann K, Hoogeveen Y, Gladziwa U, Günther RW: Hydrodynamic thrombectomy of hemodialysis fistulas: first clinical results. J Vasc Intervent Radiol 1994; 5: 813–821
13. Turmel-Rodrigues L, Pengloan J, Baudin S, Testou D, Abaza M, Dahdah G, Mouton A, Blanchard D: Treatment of stenosis and thrombosis in haemodialysis fistulas and grafts by interventional radiology. Nephrol Dial Transplant 2000; 15: 2029–2036
14. Turmel-Rodrigues L, Pengloan J, Rodrigue H, Brillet G, Lataste A, Pierre D, Jourdan JL, Blanchard D: Treatment of failed native arteriovenous fistulae for hemodialysis by interventional radiology. Kidney Int 2000; 57: 1124–1140
15. Vorwerk D, Schürmann K, Müller-Leisse C, Adam G, Bücker A, Sohn M, Kierdorf H, Günther RW: Hydrodynamic thrombectomy of haemodialysis grafts and fistulas: results of 51 procedures. Nephrol Dialys Transplant 1996; 11: 1058–1064

16. Hathaway PB, Vesely TM: The apex-puncture technique for mechanical thrombolysis of loop hemodialysis grafts. *J Vasc Interv Radiol* 1999; 10:775-779
17. Barth KH, Gosnell MR, Palestrant AM, Martin LG, Siegel JB, Matalon TA, Goodwin SC, Neese PA, Swan TL, Uflacker R: Hydrodynamic thrombectomy system versus pulse-spray thrombolysis for thrombosed hemodialysis grafts: a multicenter prospective randomized comparison. *Radiology* 2000; 217: 678-684
18. Vesely TM, Williams D, Weiss M, Hicks M, Stainken B, Matalon T, Dolmatch B: Comparison of the angiojet rheolytic catheter to surgical thrombectomy for the treatment of thrombosed hemodialysis grafts. *Peripheral Angiojet Clinical Trial. J Vasc Interv Radiol* 1999; 10: 1195-1205
19. Uflacker R, Rajagopalan PR, Selby JB, Hannegan C: Investigators of the Clinical Trial Sponsored by Microvena Corporation. Thrombosed dialysis access grafts: randomized comparison of the Amplatz thrombectomy device and surgical thromboembolctomy. *Eur Radiol* 2004; 14:2009-2014. Epub
20. Lazzaro CR, Trerotola SO, Shah H, Namyslowski J, Moresco K, Patel N: Modified use of the arrow-trerotola percutaneous thrombolytic device for the treatment of thrombosed hemodialysis access grafts. *J Vasc Interv Radiol* 1999; 10:1025-1031
21. Rocek M, Peregrin JH, Lasovickova J, Krajickova D, Slaviokova M: Mechanical thrombolysis of thrombosed hemodialysis native fistulas with use of the Arrow-Trerotola percutaneous thrombolytic device: our preliminary experience. *J Vasc Interv Radiol* 2000; 11: 1153-1158
22. Trerotola S, Lund G, Scheel P, Savader S, Venbrux A, Osterman F: Thrombosed dialysis access grafts: percutaneous mechanical declotting without urokinase. *Radiology* 1994; 191: 721-726
23. Swan TL, Smyth SH, Ruffenach SJ, Berman SS, Pond GD: Pulmonary embolism following hemodialysis access thrombolysis/thrombectomy. *J Vasc Interv Radiol* 1995; 6: 683-686
24. Harp RJ, Stavropoulos SW, Wasserstein AG, Clark TW: Pulmonary hypertension among end-stage renal failure patients following hemodialysis access thrombectomy. *Cardiovasc Intervent Radiol* 2005; 28: 17-22
25. Vorwerk D, Guenther RW, Schurmann K: Stent placement on fresh venous thrombosis. *Cardiovasc Intervent Radiol* 1997; 20: 359-363
26. Schwab S, Raymond J, Saeed M, Newman G, Dennis P, Bollinger R: Prevention of hemodialysis fistula thrombosis. Early detection of venous stenoses. *Kidney Int* 1989; 36: 707-711
27. Palder S, Kirkman R, Whittemore A, Hakim R, Lazarus M, Tilney N: Vascular access for hemodialysis. Patency rates and results of revision. *Ann Surg* 1985; 202: 235-239
28. Smith T, Hunter D, Darcy M, Castaneda-Zuniga W, Amplatz K: Thrombosed synthetic hemodialysis access fistulas: the success of combined thrombectomy and angioplasty (Technical note). *Am J Roentgenol* 1986; 147: 161-163
29. Etheredge E, Haid S, Maeser M, Sicard G, Anderson C: Salvage operations for malfunctioning PTFE hemodialysis access grafts. *Surgery* 1983; 94: 464-470
30. Brotman D, Fandos L, Faust G, Doscher W, Cohen J: Hemodialysis graft salvage. *J Am Coll Surg* 1994; 178: 431-434





## **Section Seven**

# **Imaging Pediatric Emergencies**



# Pediatric Neurological Emergencies

J.W.J. McCann, E. Phelan

## 7.1

### Contents

7.1.1	Introduction	583
7.1.2	Clinical Findings	584
7.1.3	Hypoxic–Ischaemic Encephalopathy	584
7.1.4	The Preterm Infant	585
7.1.5	The Term Infant	587
7.1.6	Congenital Infection	588
7.1.7	Acquired Infection	589
7.1.8	Non-accidental Injury	590
7.1.9	Acute Disseminated Encephalomyelitis	592
7.1.10	Hypertensive Encephalopathy	593
7.1.11	Cerebral Sinovenous Thrombosis and Venous Infarction	594
7.1.12	Arterial Infarction	595
7.1.13	Metabolic Disorders	595
7.1.14	Drugs: Asparaginase, Methotrexate and Cyclosporin	596
7.1.15	Epilepsy: Structural Abnormalities	596
7.1.16	Endocrine-Related Encephalopathy	597
7.1.17	Conclusion	597
	References	597

**Table 1.** Causes of acute encephalopathy in children

Trauma
Accidental
Non-accidental
Hypoxic–ischaemic injury
Cardio-respiratory arrest
SIDS, near SIDS
Near drowning
Smoke inhalation
Intracranial infection
Meningitis
Encephalitis
Para-infectious (acute disseminated encephalomyelitis)
Vascular
Hypertensive encephalopathy
Venous sinus thrombosis
Embolism
Arteritis
Hyperhomocysteinaemia
Migraine
Fluid and electrolyte imbalance
Seizure disorders
Complications of malignancy
Poisoning
Endocrine dysfunction
Hypoglycaemia
Diabetes mellitus
Diabetes insipidus
Hepatic failure
Reye's syndrome
Inherited metabolic disorders
Lactic acidosis
Urea cycle disorders
Iatrogenic
Overhydration–water intoxication
Drug related

### 7.1.1 Introduction

Children presenting with acute encephalopathy constitute the majority of emergencies requiring neurological imaging. The term encephalopathy implies a disorder of consciousness and may be applied to a continuum of worsening states of arousal from being fully alert and responsive to deep coma [1]. The causes of acute encephalopathy are numerous (Table 1), and may arise either within or outside

the central nervous system (CNS). For practical purposes, the causes of acute encephalopathy are quite different in the neonate compared with those in infants and older children. In the pre-term neonate, germinal matrix haemorrhage and periventricular leukomalacia (PVL) due to hypoxic–ischaemic injury (HII) are causative in the majority of cases. In the term neonate, causes are more widespread, and in addition to hypoxic–ischaemic encephalopathy (HIE), also include stroke, infection, structural abnormalities and inborn errors of metabolism. In infants and older



children HIE can also occur. Other potential causes of acute encephalopathy in this age group include infection, non-accidental injury (NAI), acute disseminated encephalomyelitis (ADEM), vascular causes such as stroke and hypertensive encephalopathy, as well as metabolic abnormalities, fluid and electrolyte imbalance and encephalopathy secondary to toxins. Epidemiologically, accidental and non-accidental head injuries are probably the major causes of acute encephalopathy in the paediatric group [1], but non-traumatic coma resulting from hypoxic–ischaemic injury and infection remain important causes, and contribute significantly to mortality and chronic morbidity. In a large population-based study, infection was the commonest cause of non-traumatic coma in 38% of cases with intoxication, epilepsy and complications of congenital abnormalities comprising 8–10% of cases each [2].

Conditions in which imaging has a major role in diagnosis and outcome are discussed. Cerebral neoplasm, acute hydrocephalus and accidental trauma are not discussed in any detail, as these represent acute neurosurgical emergencies.

---

## 7.1.2 Clinical Findings

Encephalopathy implies disturbed neurological function. Symptoms are varied, often non-specific and present diagnostic difficulties, particularly in the early stages in the neonate. Symptoms include poor feeding, vomiting, irritability, difficulty initiating and maintaining respiration, seizures and coma. Signs can also be non-specific and include abnormal tone, depressed reflexes, pyrexia and those related to raised intracranial pressure, such as a bulging fontanelle, scalp vein distension, false localising signs and hypertension. In the older child, CNS specific presentations are much more common, especially in those over 5 years of age [2], although non-specific findings with anorexia, nausea, vomiting, lethargy and seizures often occur. Use of the Glasgow coma scale or the modified James scale can give an assessment of the depth of coma, and can be serially measured to monitor the child's clinical status [3].

A careful history often provides clues to the underlying pathology. Acute deterioration is associated with trauma, cerebrovascular accidents, metabolic disturbance and ingestion of toxins. Sub-acute deterioration over days or weeks is suggestive of infection, chronic intoxication, or slowly developing raised intracranial pressure. Focal neurological abnormalities prior to the onset of coma suggests a cerebrovascular accident or encephalitis. The past medical history and family history may provide useful information, such as a history of seizures or sickle cell disease. A history of previous stillbirths or sibling infant death might suggest an inherited metabolic abnormality.

A general physical examination may provide signs of systemic disease, infection or trauma. The size and weight of the child might indicate failure to thrive, suggesting a long-

standing metabolic disease. Pyrexia may be present due to central causes but is much more likely due to infection. Hypertension may be as a result of raised intracranial pressure, or neurological signs may be secondary to hypertensive encephalopathy. Skin examination may reveal petechial haemorrhages associated with meningococcaemia, or may reveal lesions of a specific neurocutaneous syndrome. Examination of the head is important, especially in infants and young children, where bulging fontanelles and increased head circumference suggest hydrocephalus and raised intracranial pressure. Fundoscopy can demonstrate papilloedema but may also reveal retinal haemorrhages, which are associated with NAI. Signs of meningeal irritation must be sought, but these are often absent in the very young infant or in the critically ill child, even in the presence of subarachnoid haemorrhage or meningitis.

Intracranial hypertension almost invariably presents in acute encephalopathy, and early recognition and treatment is important. It is thought to cause brain damage by at least two mechanisms. Firstly, reduced cerebral perfusion causes cerebral ischaemia, which preferentially affects the arterial watershed zones. Secondly, differences in pressure between intracranial compartments can result in different herniation syndromes. Brain herniation causes direct mechanical damage and also ischaemia and haemorrhage secondary to vascular distortion [3]. As already described, the early signs and symptoms can be quite subtle, but signs become more obvious as intracranial pressure rises, but signs can be mimicked or masked by drugs, toxins and metabolic abnormalities, as well as in the post-ictal state. The role of emergent neuroimaging is to detect potentially reversible causes of encephalopathy, and also to detect complications. With these aims in mind, trans-cranial ultrasound is the initial imaging method of choice in neonates in part due to its portability and availability. Computerised tomography (CT) is more useful in older children. Magnetic resonance imaging (MRI) has well-defined roles in specific conditions [4, 5]. The conditions in which neuroimaging plays a pivotal role will be discussed further.

---

## 7.1.3 Hypoxic–Ischaemic Encephalopathy

The HIE can occur at any age secondary to any number of aetiologies including cardiac arrest, intracranial infection and NAI (Table 1). In the neonatal period the patterns of injury to the brain caused by HIE depend on the severity and duration of hypoxia and the gestational age of the patient at the time of injury. While intra-uterine first- or second-trimester HIE will result in hydranencephaly or neuronal migration disorders and can usually be readily distinguished from perinatal HIE [6, 7], the greatest difficulty is the differentiation between brain injuries which occur late during gestation and those which occur in the immediate perinatal period. This is made difficult because

there are no reliable factors which detect intra-uterine asphyxia. Similarly, in both preterm and term infants, clinical signs of cerebral insult in the postnatal period are very subtle [8]. While acute and profound hypoxia can cause acute encephalopathy with its associated significant morbidity and mortality, chronic or intermittent hypoxia can also have an adverse impact on development, behaviour and cognitive function in children with congenital heart disease and sleep disorders, with adverse effects seen at even mild levels of oxygen desaturation [9].

The focus of research in this field has concentrated on understanding the cellular mechanisms of brain injury and the definition of a therapeutic window, between the acute insult and cell death, in which specific neuroprotective therapeutic measures might prevent delayed injury [10]. The imaging signs of HIE in the term and preterm infant vary significantly and are discussed separately.

### 7.1.4 The Preterm Infant

The most common HI lesion in the immature nervous system is subependymal haemorrhage, the majority of these being clinically insignificant. Haemorrhage occurs through damaged walls in delicate cerebral vessels secondary to hypoxia, hypercapnia and increased venous pressure.

Ultrasound remains the mainstay of primary imaging and is sensitive to the detection of subependymal and intraventricular haemorrhage (IVH), which is seen in 30–35% of infants born at <32 weeks gestation or with a birth weight of <1500 g. The optimal time for ultrasound detection of IVH is between days 4 and 7 after birth, with 95% of haemorrhages detectable by day 5 [11]. The IVH is classified into four grades [12]:

1. Grade-1 haemorrhage (Fig. 1) can be unilateral or bilateral and is confined to the subependymal germinal matrix in the caudo-thalamic groove in the floor of the lateral ventricle.
2. Grade-2 haemorrhage indicates extension within the ventricles but without ventricular dilatation.
3. Grade-3 haemorrhage shows ventricular dilatation in addition to subependymal and intraventricular haemorrhage.
4. Grade-4 haemorrhage (Fig. 2) indicates extension into the cerebral parenchyma. The association of IVH with long-term neurological deficit is well known. The severity of IVH correlates with neurological outcome with major handicap seen in approximately 10% of grade-1 and grade-2 IVH, whereas those with grade-3 and grade-4 IVH have higher morbidity and mortality at 36 and 76%, respectively [13]. The presence of blood within the fourth ventricle has been shown to be a good predictor of subsequent hydrocephalus [14], as has the presence of blood in the subarachnoid space anterior to the temporal lobe on sagittal imaging [15].

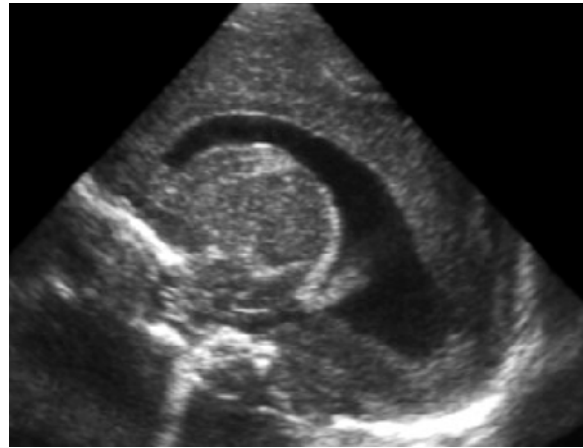


**Fig. 1.** Grade-I haemorrhage of the germinal matrix, seen as echogenic material expanding the caudothalamic groove on a sagittal ultrasound image

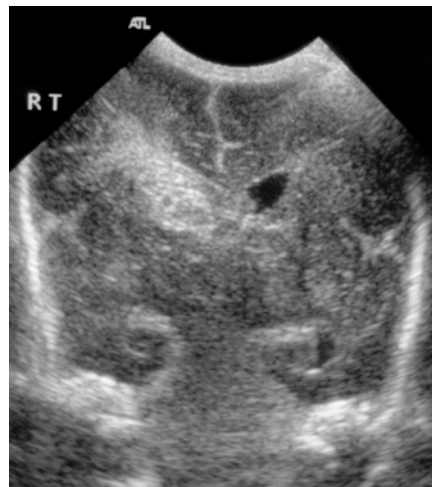


**Fig. 2.** Coronal ultrasound image demonstrates grade-IV haemorrhage within the left lateral ventricle extending into the adjacent brain parenchyma

Periventricular leukomalacia (PVL) is another manifestation of HII in the preterm neonate, and often occurs simultaneously with IVH. As a solitary manifestation of HII, this occurs almost exclusively in the preterm neonate. It is, at least in part, contributed to by the immaturity of the vascular supply to the deep white matter. Each of the three major cerebral arteries has both cortical and basal branches. Cortical branches are divided into two main types: long penetrators which terminate in the deep periventricular white matter, and short penetrators which extend only as far as the subcortical white matter [7]. At 24–28 weeks of gestation, there is a relative paucity of short penetrators and the long penetrators are spiral in configuration, and have very few side branches and intraparenchymal anastomoses.

From 32 weeks of gestation, the number of short penetrators increases substantially and the long penetrators increase in calibre, lose their spiral character and develop a greater number of side branches. Together, these changes provide a greater blood supply for the increasing metabolic requirements of the subcortical and deep white matter. Eventually, rich anastomotic channels develop between the long and short penetrators. Vulnerability of the highly metabolically active, developing oligodendrocytes in this region, to excitatory amino acids produced in response to ischaemia, is also thought to predispose the deep white matter to PVL [16]. The combination of inherent oligodendrocyte vulnerability, immature vascularisation of the white matter and the inability of the stressed preterm infant to autoregulate cerebral blood flow makes ischaemic change in the white matter in the form of PVL the commonest manifestation of HII in this group of patients. The detection of PVL is important because it is the major neuropathological form of brain injury and underlies most of the neurological morbidity in survivors of prematurity with spastic motor deficits classified as cerebral palsy (CP), seen in approximately 10% of survivors [8], and later cognitive and behavioural deficits seen in up to 50% [17].

Ultrasound can detect PVL, though the sensitivity is as low as 50% [18]; however, ultrasound enables identification of the vast majority of lesions associated with a poor outcome [19], with only 3% of children with normal ultrasound scans developing CP [20]. Findings include a featureless appearance of the parenchyma which may be associated with a generalised, patchy or focal increase in echogenicity. Multiple periventricular cysts (Fig. 3) may then evolve in association with cerebral atrophy, usually after the second week. The presence of periventricular flares (increased echogenicity; Fig. 4) persisting for 3 weeks or more is also strongly associated with clinical PVL in 86% of children [21]. The location affected is of critical importance in determining the outcome, with 91% of children with lesions in both the parietal and occipital lobes going on to develop CP, but less than 7% of those with lesions confined to the frontal lobes being similarly affected [20]. The same authors found no correlation between location and cognitive dysfunction, although this was directly proportional to the size and extent of white matter lesions as detected on ultrasound.

With the increasing use of MRI during the neonatal period, it has become clear that ultrasound underestimates the extent of white matter disease associated with PVL. Good correlation is seen between ultrasound and MRI for cystic periventricular white lesions but for other white matter lesions, MRI is more sensitive (Fig. 5) [22]. Conventional MRI alone is superior to ultrasound in identifying and quantifying cerebral white matter damage in very low birth weight infants [23], and may demonstrate areas of T2 shortening in the deep white matter within 2–3 days of injury, not visible on ultrasound. With the addition of MR spectroscopy (MRS) and diffusion-weighted imaging

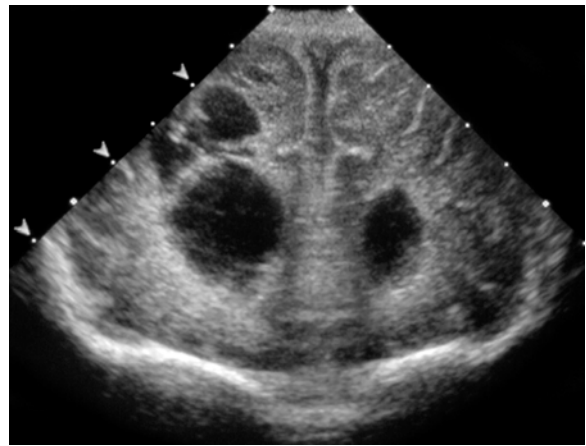


**Fig. 3.** Coronal ultrasound image demonstrates right-sided frontal periventricular cysts

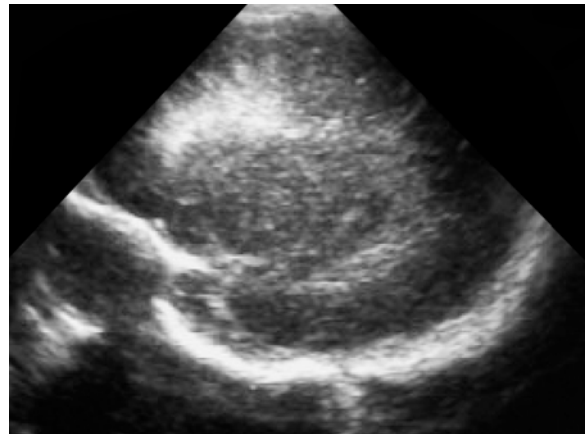


**Fig. 4.** Sagittal ultrasound demonstrates anterior periventricular flare

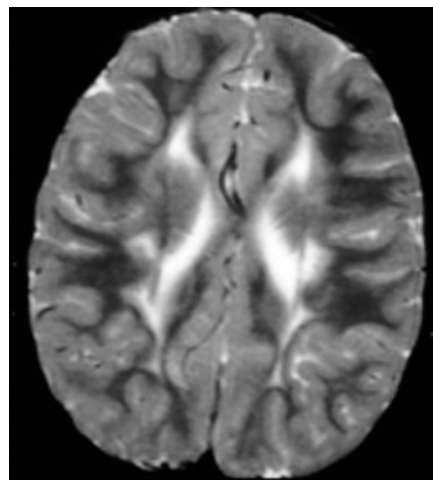


**Fig. 5.** Axial T2-weighted MR image demonstrates focal areas of high periventricular signal in the periventricular white matter consistent with periventricular leukomalacia (PVL)

(DWI), the sensitivity is increased further and earlier detection is possible [22, 23]; however, the need for MRI must be balanced against the difficulty of imaging an unstable infant outside the neonatal intensive care unit, and as a result, MRI cannot replace trans-cranial ultrasound as a routine diagnostic tool in most neonatal units.

### 7.1.5 The Term Infant

Acute perinatal asphyxia is the most common clinical insult causing HII and, in the term infant, has an incidence of between 0.2 and 1% of live births, accounting for 8–15% of patients with cerebral palsy [24]. Acute perinatal asphyxia refers to a condition of hypoxaemia, hypercapnia and insufficient cerebral perfusion of the neonate during labour and birth. Depressed fetal heart rate, meconium stained amniotic fluid, low Apgar scores, low scalp pH or clinical signs of neurological depression soon after birth signify the acute clinical condition in the neonate; however, the predictive value of such clinical indicators is quite poor with regard to the development of HII and neurodevelopmental outcome [25]. Soon after birth, neonates with significant HII may develop subtle or profound neurological signs, ranging from poor feeding, lethargy and decreased muscular tone to episodes of apnoea, seizures or coma. The pattern of neurological injury is very different to that seen in the preterm infant, as described previously.

Two major patterns of injury are present in the term infant [26, 27]. The watershed predominant pattern affects the white matter in the vascular watershed zones between major vascular territories. This is associated with mild to moderate injury. Ischaemic changes are most obvious in the frontal and parietal areas. Moderate to severe injury is associated with the basal ganglia/thalamus predominant pattern of injury. Changes are seen in the lateral thalami, posterior putamina, hippocampi and corticospinal tracts. The cortex, other than the perirolandic gyri, is relatively spared in all but the most severe injury, where it is also usually associated with the basal ganglia/thalamus pattern of injury. These regions of the brain are the most metabolically active and most actively myelinating at the time of birth. It is unclear whether these patterns are associated with specific antenatal risk factors. Not surprisingly, the basal ganglia/thalamus predominant pattern is more strongly associated with caesarean delivery, aggressive resuscitation, more severe encephalopathy and seizures, and more severe motor and cognitive impairment at 30 months [26]. Although many risk factors are prenatal [28], more recent data suggest that the vast majority of injuries occur in the immediate perinatal period, with only a very small proportion of infants having a definite established antenatal injury [29].

Ultrasound may detect deep grey nucleus and cortical injury in term infants as areas of increased echogenicity, followed by the development of cystic areas of encephalo-

malacia depending on the severity of the injury. On CT, areas of decreased attenuation may be seen in the watershed zones and/or within the deep grey nuclei; however, due to the high water content within the neonatal brain, early CT findings in HIE are often quite subtle or absent even in the presence of significant disease [30]. Because of its higher sensitivity and specificity to maturational changes, including accurate assessment of the degree of myelination and structural abnormalities, MRI has enormous advantages over both CT and ultrasound. Conventional MRI of the neonatal brain performed within the first few days after HII demonstrates affected areas as foci of increased signal intensity on T2-weighted sequences. When special attention is given to the internal capsule, thalamus, parietal cortex, hippocampus and medulla, the reproducibility and accuracy of MRI is substantially improved [31]. The normal term infant will have evidence of myelination within the posterior limb of the internal capsule from 37 weeks of gestation onwards. This is seen as high signal intensity on T1-weighted imaging. An absence or a decrease in this signal, in infants with HII, manifested sensitivities and specificities between 90 and 100% for the prediction of poor neurodevelopmental outcome at 1 year of age [31, 32]. This finding takes 1–2 days to evolve and becomes maximal at 1 week. Findings on conventional MRI in patients with inherited inborn errors of metabolism can be identical to those of HIE. If there is any clinical suspicion of such abnormalities, serial imaging can be beneficial and show progressive white matter disease in metabolic conditions, but will show typical evolution and cystic change with areas of encephalomalacia in patients with HIE.

More recently, researchers have concentrated on detecting changes earlier, with a view to providing a more accurate prediction of outcome and possibly instigating neuroprotective therapies. In the first 24 h after injury, DWI may show abnormalities before conventional MR sequences [33]. The DWI images will demonstrate restricted water diffusion in areas of ischaemic change associated with HII (Fig. 6). These regions are of high signal intensity on DWI. Interpretation of DWI may be complicated by pre-existing injuries where the T2 of abnormal tissue is elevated, known as T2 shine-through. The use of apparent diffusion coefficient (ADC) values in evaluating affected regions improves conspicuity of such injuries, which appear as regions of low signal, in the acute and sub-acute setting [34]; however, early DWI may underestimate the extent of injury, and may not detect changes in the deep grey matter and perirolandic cortex [33, 35, 36]. The MRS is based on the phenomenon of chemical shift, and can determine the concentration of many metabolites in the neonatal brain and play an important role in the evaluation of HIE and many metabolic disorders. In the first 24 h of life, MRS may show lactate elevation in ischaemic regions and can more accurately predict the severity of injury [36]. MRS can also distinguish between HIE and inborn errors of metabolism.



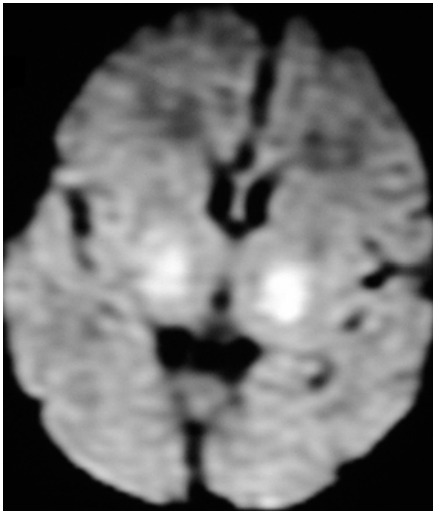


**Fig. 6.** Axial diffusion-weighted-imaging MR image demonstrates symmetrical areas of restricted diffusion in the posterior limbs of both external capsules, consistent with hypoxic-ischaemic encephalopathy



**Fig. 7.** Axial MR image demonstrates extensive neuronal migration abnormalities with typical findings of both lissencephaly and polymicrogyria

Neonatal alloimmune thrombocytopenia is a maternal/fetal platelet antigen incompatibility disorder which can have imaging findings somewhat similar to those of established HIE. Porencephalic cysts, primarily located in the temporal lobes, along with ventriculomegaly, commonly occur. Antenatal haemorrhage, be it extra-axial intraventricular or intraparenchymal, may also occur. Diagnosis can be confirmed with serological tests, but there is no current active screening program. The radiologist should be suspicious of this disorder when these abnormalities are present, and plays an important role in disease recognition in the absence of a screening program. Establishing the diagnosis has important management considerations in the affected neonate as well as in subsequent pregnancies which might be similarly affected [37].

### 7.1.6 Congenital Infection

The clinical manifestations of CNS infections in children vary depending on the infective agent, stage of development and maturation of the host CNS and the stage and development of the host immune defences [38]. The time point in gestation at which intrauterine infection occurs is vital because the stage of development of the fetus will determine whether a developmental structural abnormality occurs, as in the first two trimesters, or a destructive process, which is seen, if infection occurs in the last trimester or perinatal period.

The TORCH acronym (Toxoplasma, Other, e.g. Syphilis, Rubella, Cytomegalovirus, Herpes simplex type 2/HIV), defines infections acquired in the fetal or neonatal period.

These infections are acquired as a result of transplacental transmission with the exception of Herpes simplex type 2, which is usually acquired during parturition. The clinical manifestations of congenital infection include microcephaly, intrauterine growth retardation, seizures, ocular and other congenital anomalies, skin rash and hepatosplenomegaly. Neonatal infection may present with sepsis and meningoencephalitis [38].

The imaging manifestations of TORCH infection vary depending on the age of gestation or stage of embryological development at the time of insult. Infection in the first two trimesters of pregnancy may result in neuronal migration abnormalities such as lissencephaly and polymicrogyria (Fig. 7). Infections acquired in the third trimester and in the perinatal and neonatal period may result in destruction of developed brain secondary to meningoencephalitis causing aqueduct stenosis, hydrocephalus, hydranencephaly, porencephaly, multicystic encephalomalacia, calcification, haemorrhage, delayed myelination and atrophy [38]. The presence of parenchymal calcification is characteristic. Lenticulostriate vasculopathy may also be present and is manifested as linear increased echogenicity in the distribution of the thalamostriate vessels on ultrasound. Its branching pattern has the appearance of a candelabra (Fig. 8). This, however, is not specific to TORCH infection and may be seen in neonatal ischaemia, trisomy 13 and 21, twin-twin transfusion, intrauterine cocaine exposure, neonatal lupus, neonatal hypoglycaemia, fetal alcohol syndrome and head injury [39]. Herpes simplex type-2 infection is most commonly acquired during parturition or in the postnatal period but may rarely be acquired in utero. It presents in the neonatal period with sepsis and meningoencephalitis. The imaging manifestations include diffuse

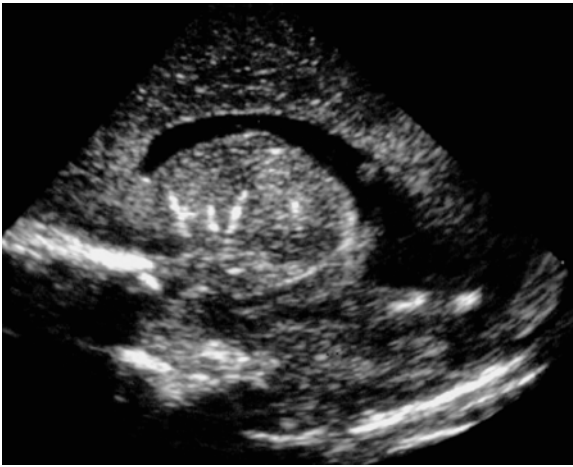


**Fig. 8.** Sagittal ultrasound image demonstrates the typical appearance of lenticulostriate vasculopathy, with a branched linear pattern of echogenicity in the region of the basal ganglia and thalamus

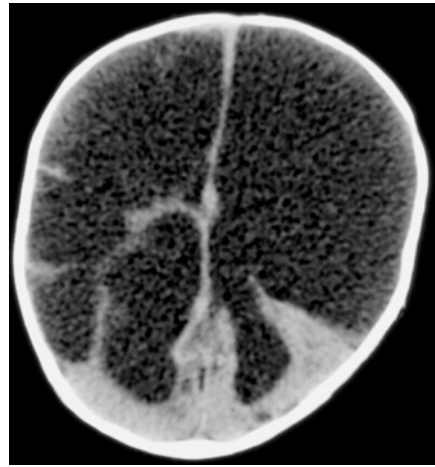


**Fig. 9.** Axial CT brain image demonstrates extensive septation and compartmentalisation following *Citrobacter* meningitis

brain swelling with multifocal areas of oedema seen on ultrasound, CT and MRI. The CT findings may not be apparent for the first 24–48 h. Vascular thrombosis and haemorrhage may occur [38].

### 7.1.7 Acquired Infection

Meningitis in the neonatal period is often bacterial in origin. The three most common organisms are group-B *Streptococcus*, Gram-negative *Enterobacter bacilli* and *Listeria monocytogenes* [40]. Factors contributing to infection in the immediate postnatal period include maternal urinary tract or genital infection, premature rupture of membranes, immature fetal immune responses or intensive care environmental conditions [38]. Infection is usually haematogenously transmitted via the choroid plexus with accompanying ventriculitis [38, 41]. This may be seen on ultrasound as increased echogenicity and thickening of the ventricular walls. Periventricular increased echogenicity may also be seen and is similar in appearance to that caused by premature flare in the premature infant. Subdural effusions can occur but are unusual with infections in the first week of life compared with those seen in the second or third weeks. Basal arachnoiditis and haemorrhagic infarction secondary to arteritis and phlebitis may occur. Hydrocephalus may be complicated by septation, adhesions and entrapment of the ventricular system [38].

In children aged between 3 months and 2 years, the most common cause of meningitis is *Haemophilus influenzae* type b. In older children, *Streptococcus pneumoniae* and *Neisseria meningitidis* predominate. Infection is usually haematogenous; however, direct extension from infected paranasal sinuses and mastoid air cells may occur as well

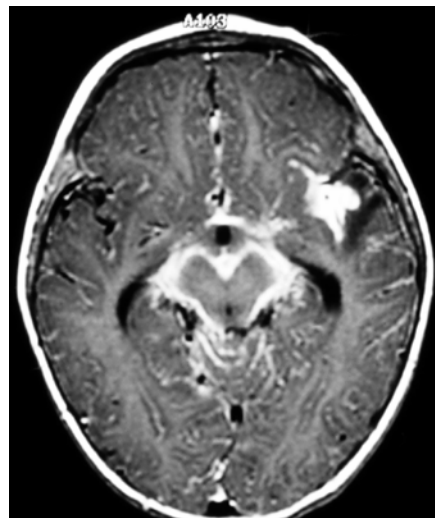


**Fig. 10.** Axial post-contrast T1-weighted MR image demonstrates extensive basilar meningeal enhancement in a patient with bacterial meningitis. Note also the meningeal enhancement in the Sylvian fissure

as a complication of penetrating injury or skull fracture. Associated subdural effusions are more common and are often bilateral. Early in the disease, mild hydrocephalus, leptomeningeal enhancement (Fig. 10) and cerebral oedema may be present. Infarction, either arterial or venous, may develop [38].

Chemical meningitis may be caused by dissemination of material from a ruptured craniopharyngioma or intracranial dermoid throughout the ventricular system and basal cisterns. Ventriculo-peritoneal shunt infection can also occur, and is usually caused by *Staphylococcus*.

Encephalitis, particularly that caused by Herpes simplex type 1 is most commonly seen in young children. When severe, the infection can be overwhelming and often rapidly fatal. In the first few days, CT or MRI shows diffuse oedema which progresses to necrosis resulting in multicystic encephalomalacia. Herpes simplex type-2 infection occurs more commonly in adults and predominantly affects the anterior temporal lobes. Focal oedema may be the only manifestation, but central areas of haemorrhagic transformation are sometimes seen.

Intracranial abscess may develop in Gram-negative infection such as *Citrobacter*, which is the causative organism in haematogenous infection in the majority of patients aged less than 1 month. Various streptococcus species are the most common isolates from abscess cultures in patients older than 1 month. The overall incidence of intracranial abscess is increasing in all paediatric age groups. This is, at least in part, as a result of longer survival in patients with congenital heart disease, which is the most common predisposing factor. Other factors strongly associated, include immunosuppression in patients post-bone-marrow and solid-organ transplantation, where abscess often occurs in association with systemic fungal infection [42]. Sinus disease with intracranial extension of infection can present with an acute neurological deterioration without any prior symptoms of sinus infection, although the incidence of intracranial abscess as a complication of sinus or otitic infection has decreased in recent years. In teenagers, particularly boys, this can present acutely with fever, headache and seizures mimicking meningitis or encephalitis. Examination of the sinuses on CT may give a clue to the diagnosis. One or all of the sinuses may be affected. Local osteomyelitis of the frontal bone may also occur [43].

Sinus infection secondary to fungal infection, most commonly *Aspergillus*, may also disseminate intracranially to involve the parenchyma and meninges. Mucormycosis is a virulent fungal organism of the *Zygomycetes* class of the *Mucoraceae* family. These fungi are found in soil, air, decaying vegetation, foods with a high sugar content and bread mould. Infection is typically airborne with primary infection of the upper and lower airways with associated development of sinusitis, rhinocerebral mucormycosis or pulmonary infection. The majority of presentations, approximately 80%, are in patients with poorly controlled diabetes mellitus; however, it is also seen in the immunocompromised host with only 4% of cases seen without underlying disease. The rhinocerebral form of this disease is the most common and may present with invasive sinusitis. The hallmark of the disease is invasion of blood vessels causing infarction and thrombosis which can involve both the intracranial circulation and the cavernous sinus. The mortality from this condition varies from 30 to 80% [44].

Neurological dysfunction is a common manifestation of HIV infection in both adults and children and because of its increasing incidence deserves special consideration. Pa-

tients can acquire infection vertically, from mother to infant, which accounts for the vast majority. Infection can also be secondary to transfusion of infected blood or infected blood products. Adolescents can acquire infection similar to adults, i.e., as a result of intravenous drug use and through sexual transmission. Young children can present with developmental delay, loss of developmental milestones or a decline in motor and neurocognitive function. Opportunistic infections can occur in immunosuppressed, HIV infected children. Direct HIV infection has been implicated as a possible cause of encephalopathy in the absence of other opportunistic or microbial pathogens. The CNS malignancies can also rarely occur, although these are much more common in adults. Cerebrovascular complications are also commonly seen in children with HIV infection, usually in those with severe immune suppression [45]. Cerebral aneurysms and infarctions are seen in a substantial number of patients, often without significant neurological signs or symptoms. The exact mechanism by which HIV induces arterial damage is not clear, but some authors suggest a synergistic effect from direct HIV infection and infection with other viral agents, particularly *Varicella-Zoster* [46]. There is also a well-recognised association between HIV infection and acquired protein-S and protein-C deficiency [47], which are independent risk factors for thrombotic complications. In addition, thrombocytopenia also occurs with HIV infection, again increasing the risk of thrombotic complications and stroke.

---

### 7.1.8 Non-accidental Injury

The intentional infliction of both emotional and physical pain and suffering on children is a common occurrence, with an estimated incidence of between 5.7 and 15.7 per 1000 children abused or neglected [48]. The majority of harm inflicted is in the form of neglect, which accounts for 63% of cases of NAI, with physical, sexual and psychological abuse accounting for 19, 10 and 8%, respectively [48]. In the U.S., the incidence of fatality associated with NAI is 1.7 per 100,000 children. Young children are particularly at risk, with those aged less than 1 year accounting for 44% of all abuse-related fatalities. The radiologist should always be alert to the possibility of NAI, as they may be the first to suggest such a diagnosis on the basis of imaging findings. In the presence of significant intracranial injury, a history of relatively minor trauma is incompatible, and the reliability of the history should be questioned and the possibility of NAI should be queried. Where NAI is suspected, further evaluation with radiographic skeletal survey is mandatory, in order to identify and document other injuries in "at risk" patients.

Non-accidental head injury occurs in approximately 12% of cases of NAI. Most children are under 2 years of age at the time of diagnosis, with an average age of 1.6 years

compared with an average age of 5.4 years for accidental injury [49]. Intracranial injury is the leading cause of death in these patients, with NAI-related head injury accounting for 80% of deaths from head injury in this age group. Evidence of significant recent injury associated with intracranial haemorrhage, is seen in 71% of fatalities [50]. Skull fractures are identified in approximately 50% of patients with intracranial injury [51]. The infant skull is relatively plastic and tends to be more resistant to fracture. Fractures occur in only 1–3% of children as a result of short (<6 feet) accidental falls [52]. There is no specific pattern of skull fracture specific to NAI [53], however, multiple fractures, complex fractures involving both side of the skull, diastatic fractures, fractures that cross sutures, depressed fractures especially of the occiput and fractures of differing ages occur more frequently with NAI [54].

The initial brain injury is termed the primary injury. The mechanisms of intracranial primary injury include direct injury, shaking, strangulation, either separately or in combination [55]. Subdural haemorrhage (SDH; Fig. 11) may occur from an acceleration/deceleration type injury as occurs with a direct impact, or may occur from whiplash-shaking injury alone [56]. The SDH is particularly prevalent in very young babies who can present to hospital with a wide range of symptoms. Subarachnoid haemorrhage (SAH) is also a common manifestation of NAI [57]. Neither SAH nor SDH are specific for NAI; however, since SDH may be present from birth. Typically, the relatively small volume of SDH or SAH associated with NAI is not, in itself, responsible for the neurological deterioration, but serves as a marker for the mechanism of injury. This primary injury in may be complicated by various pathophysiological responses, including cerebral oedema, cerebral congestion and vasospasm with a resultant decrease in cerebral perfusion. Seizures, apnoeic episodes and compression of brain parenchyma by a large SDH, although not often seen, can also occur. All these factors may contribute to secondary injury in the form of hypoxic-ischaemic damage [58]. Coma at presentation, apnoea, and diffuse brain swelling with HII are all associated with a poor prognosis.

The most common location for both SDH and SAH is in an interhemispheric parafalcine distribution, and in this location is highly suspicious for NAI. It is often difficult to differentiate the two forms of haemorrhage, particularly when interhemispheric, and both may coexist. Acute SDH appears, on CT, as a crescentic or interhemispheric area of high attenuation. As blood ages over days to weeks, it then becomes isoattenuating and finally hypoattenuating relative to brain. The exact timing for these changes in characteristics is not well established and may vary considerably in different patients. Certain features of SDH are seen infrequently in accidental injury and therefore are suspicious for NAI, such as SDH without associated skull fracture, bilateral SDH, more than one SDH of different ages, SDH in association with retinal haemorrhage and, as already mentioned parafalcine haemorrhage [54]. The MRI can be use-

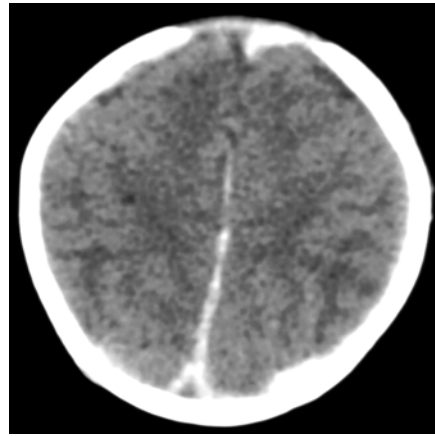


**Fig. 11.** A 9-week-old infant presenting in status epilepticus after a shaking episode. Axial CT demonstrates acute subdural haemorrhage



**Fig. 12.** Bilateral acute on chronic subdural haematomata in a 7-week-old infant following non-accidental injury (NAI)

ful and has shown that interhemispheric SDH is often associated with shallow surface collections of blood which may not be readily identified on CT [59]. It can also be very helpful in differentiating chronic or subacute SDH from cerebrospinal fluid and extraaxial fluid collections, and will more clearly demonstrate SDHs of differing ages (Fig. 12). Acute SDH is of low signal or isointense on T1 and of low signal on T2-weighted sequences. In the subacute phase, blood appears of high signal on T1 and varies from low to high signal on T2-weighted sequences, finally reverting to low signal or isointense on T1 and low signal on T2. As with CT, these are not fixed findings and signal characteristics may vary considerably in different patients. Ultrasound can occasionally be useful in differentiating SDH (Fig. 13) from diffuse enlargement of the subarachnoid space in in-





**Fig. 13.** Coronal ultrasound image demonstrates expansion of the subdural space with echogenic blood, secondary to NAI

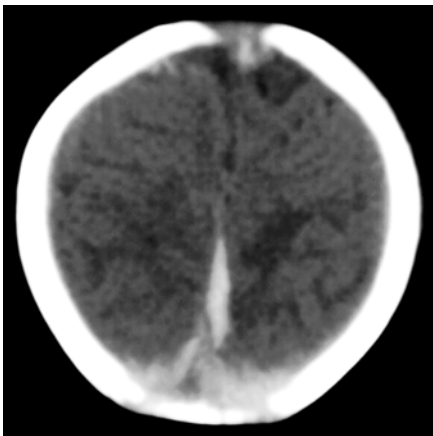


**Fig. 14.** Axial CT image shows an area of edema in the left posterior or frontal lobe subsequently demonstrated as contusion. Parafalline haemorrhage is also present

fants, and also in following up a known visible abnormality, previously fully evaluated with CT or MRI. Limitations include poor visualisation of the far convexities and posterior fossa.

The three most common types of parenchymal brain injury are shear injury, contusion and oedema (Fig. 14). Shear injury refers to an acceleration–deceleration type injury, which causes shear stress and axonal injury at the grey–white matter junction of the cerebral hemispheres. This can also be seen at the craniocervical junction and within the cervical spinal cord, where it is strongly associated with apnoea and is thought to be as a result of hyper-extension/flexion injury during shaking [60]. Axonal injury is not commonly haemorrhagic in infants and therefore is usually occult on CT examinations. High-attenuation petechiae are occasionally seen. There is usually exten-

sive background oedema, focal or diffuse, seen as diffuse or focal low attenuation. Magnetic resonance tends to be more revealing, and may demonstrate axonal injury as hyperintense foci at the grey–white interface on T2-weighted sequences, when non-haemorrhagic. When haemorrhagic, axonal injury is typically hyperintense on T1-weighted sequences.

Cerebral contusion is a focal haemorrhage within the brain substance from a direct compressive force. Such injuries are rare in infants, as are extradural haemorrhage and penetrating parenchymal injury.

Cerebral oedema is a common consequence of head injury associated with NAI. It may occur as a result of both the primary and the secondary injury (hypoxia due to HII). It can also be seen as a result of other forms of abuse such as strangulation, suffocation and post-traumatic apnoea due to axonal injury at the craniocervical junction and cervical spinal cord in victims of shaking [61]. Oedema is seen as diffuse or focal low attenuation on CT, associated with loss of grey–white differentiation. Mass effect may occur, with sulcal effacement and possible herniation. Profound diffuse oedema has a tendency to maintain normal attenuation in the basal ganglia, thalami, cerebellum and brain stem and may give rise to the “reversal sign” which has a poor prognosis [62]. This can occur in association with HII as a result of other brain insults, such as near drowning, prolonged seizure, status asthmaticus, cardiac arrest and accidental trauma, but when associated with acute inter-hemispheric SDH is highly suggestive of NAI. The reason for the retained normal attenuation within these deep structures, in the face of marked ischaemia and cerebral oedema elsewhere, is not well understood. MRI shows oedema as focal or global hyperintensity on T2-weighted sequences, but can be difficult to detect on standard MR in the very immature unmyelinated brain. The DWI will demonstrate areas of restricted water diffusion, which appears bright.

Complications of HII associated with NAI include herniation syndromes, hydrocephalus, cerebral atrophy, cerebral infarction and encephalomalacia. Clinical manifestations range from mild developmental delay and attention disorders to hemiplegia, motor and intellectual impairment and cerebral palsy.

### 7.1.9 Acute Disseminated Encephalomyelitis

Post-infectious encephalitis or acute disseminated encephalomyelitis (ADEM) is a monophasic inflammatory condition characterised by reactive demyelination of the white matter. In over 70% of patients, there is a prodromal illness and antibodies to specific infectious agents such as *Streptococcus*, *Mycoplasma* and Epstein-Barr virus may be isolated in a minority of patients. ADEM may also follow rubella, mumps or hepatitis vaccination [63]. Neurological

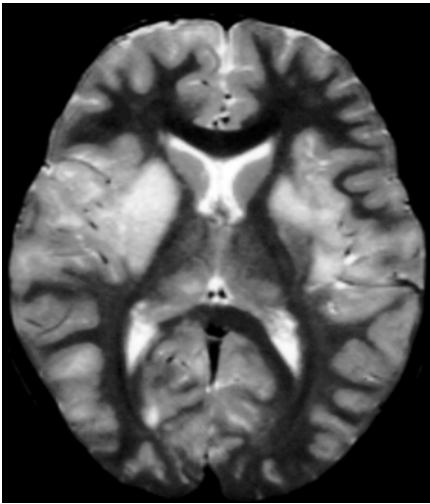


**Fig. 15.** Axial MR image demonstrates bilateral focal areas of high signal in the basal ganglia in a patient with acute disseminated encephalomyelitis

presentation varies from an acute explosive presentation to a more indolent progression over days or weeks. A polysymptomatic presentation is the general rule and systemic signs are often present. Diagnostic difficulties may therefore arise, as patients often present with headache, fever, meningism and seizures, and infection will need to be considered and excluded as an alternative diagnosis [63]. Acute encephalopathy with motor signs, cranial neuropathy, ophthalmoplegia, dysarthria and dysphagia can also occur, and occasionally patients will require ventilatory support. Cerebellar signs, myelitis and visual impairment may also occur and there is an association with bilateral optic neuritis [63]. Despite its monophasic nature, neurological signs and symptoms in patients with ADEM can evolve over time, and can relapse as part of the same acute monophasic immune process, particularly if treatment is withdrawn too soon. The term multiphasic disseminated encephalomyelitis (MDEM) has been suggested for such presentations. If, however, relapses occur that are disseminated in time and site, then multiple sclerosis (MS) is diagnosed.

Multiple sclerosis, the main differential diagnosis on combined clinical and imaging findings, is less commonly associated with a prodromal illness, which occurs in just over 30%. Systemic symptoms of headache, fever and meningism are much less frequent, and seizures are extremely rare. Most presentations are monosymptomatic. Myelitis, visual and cerebellar signs often occur. The CSF oligoclonal bands may occur in both groups but are relatively more common in patients with MS. Both conditions have a seasonal distribution and are more prevalent in the winter months. Patients with MS are older, and childhood presentation is uncommon, whereas ADEM shows early childhood predominance.

On neuroimaging, CT can show focal areas of low attenuation but has a sensitivity of only 60% for detection of such lesions. The MRI is the preferred imaging method and shows lesions of high signal on both T2-weighted and fluid-attenuated inversion recovery (FLAIR). Lesions are predominantly located in the subcortical white matter, with relative sparing of the periventricular white matter compared with MS. Cortical grey matter lesions, although not often seen, are thought to be specific for ADEM. Similarly, lesions in the thalamus and basal ganglia (Fig. 15) occur much more commonly in ADEM than MS, with thalamic lesions seen in 40% [63, 64]. The ADEM, like MS, can present as a tumour-like mass in the cerebrum or posterior fossa. Current opinion regarding treatment supports the use of high-dose intravenous methylprednisolone followed by oral prednisolone therapy. This can be instigated once infective encephalitis has been excluded. Rapid recovery is common with over 80% of patients making a complete recovery [65].

### 7.1.10 Hypertensive Encephalopathy

Hypertensive encephalopathy is induced by a significant acute elevation in blood pressure above the patient's baseline. In children, the mean systolic arterial pressure is lower than in adults, with an average systolic pressure of 105 mmHg at 1 year compared with 135 mmHg at 18 years. Consequently, hypertensive encephalopathy will occur at lower levels of systemic blood pressure in children [66]. The condition is characterised by rapidly progressive signs and symptoms including headache, seizures, altered mental status, visual disturbance and other focal or diffuse neurological signs. Early diagnosis is important as reversal of hypertension is associated with complete neurological recovery. If not recognised and treated, it can progress to progressive central nervous system failure with intracranial haemorrhage, cerebral infarction, coma and death [67]. This condition is under-reported in children but can occur in relation to renal diseases such as acute glomerulonephritis, renal vascular hypertension or chronic renal failure. It is not uncommonly diagnosed in adults in certain clinical conditions, such as pre-eclampsia/eclampsia syndrome and lupus nephritis. It is a subset of the more generalised reversible posterior leukoencephalopathy syndrome/posterior reversible encephalopathy syndrome (PRES), which is seen in patients receiving chemotherapy particularly cyclosporin, post-transplantation or transfusion, and can also be seen with HIV infection [68]. There may be no discernable change in blood pressure in patients in the above clinical situations.

Computed tomography and standard MRI, in uncomplicated cases, show oedema in the subcortical white matter of the posterior temporal, posterior parietal and occipital lobes as well as within the structures within the posterior fossa. The DWI demonstrates vasogenic oedema as

areas of normal slightly lower signal, corresponding to areas of high signal on standard T2-weighted and FLAIR sequences. Initial investigators had postulated that hypertensive encephalopathy was as a result of uncontrolled autoregulatory vasoconstriction leading to hypoperfusion, focal ischaemia and infarction; however, the presence of vasogenic oedema and lack of cytotoxic oedema on DWI does not support this theory. It is now widely accepted that the physiological mechanism involved is cerebrovascular vasodilatation caused by autoregulatory failure, as a result of hypertension, which causes increased vascular permeability and extravasation of protein and fluid [67, 69]. The relative paucity of sympathetic innervation in the posterior fossa accounts for the propensity for this region to be affected [67]. The cortex tends to be spared due to the vasogenic nature of the oedema seen; however, cortical involvement can be seen when infarction complicates, and can be recognised on DWI as areas of high signal restricted diffusion representing cytotoxic oedema.

### 7.1.11 Cerebral Sinovenous Thrombosis and Venous Infarction

Cerebral sinovenous thrombosis is a rare disorder but should be suspected where infarction occurs in a non-arterial distribution. Risk factors include young age, with over 50% of cases seen in children less than 1 year old. The relative high incidence in neonates and young infants is associated with dehydration and perinatal complications, such as HII, premature rupture of membranes, maternal infection, placental abruption and gestational diabetes [70]. Disorders of the head and neck, especially infections including meningitis, chronic systemic illness and prothrombotic disorders such as the presence of anticardiolipin antibody and factor-V Leiden, as well as protein-S and protein-C deficiency, and acquired thrombotic states as seen with DIC, liver disease or nephritic syndrome, are commonly seen in older children. Dehydration and hypernatraemia can also predispose in older patients, as can procoagulant drugs, such as Asparaginase used in an oncological setting [71], and the oral contraceptive used in adolescents. Presentation is non-specific, with seizures and diffuse neurological signs in neonates and with decreased consciousness, headache and focal neurological signs such as hemiparesis and cranial nerve palsies in older children.

In younger children, particularly in the neonate, patients may make a complete recovery without treatment. Thrombolytic therapy has been used successfully in older children in the acute setting [72], and anticoagulant therapy is often safely administered over a more protracted period. Recognised neurological deficits include motor impairment, cognitive impairment, developmental delay, speech and visual impairment. Overall mortality approaches 10%, with poor predictors of outcome being

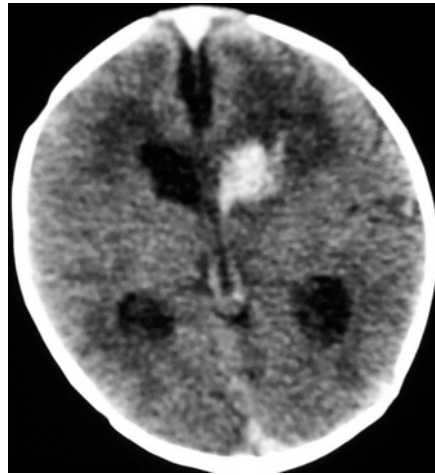


**Fig. 16.** Axial non-contrast CT image demonstrates a haemorrhagic venous infarct in a patient with sinovenous thrombosis, producing high attenuation in the sagittal sinus

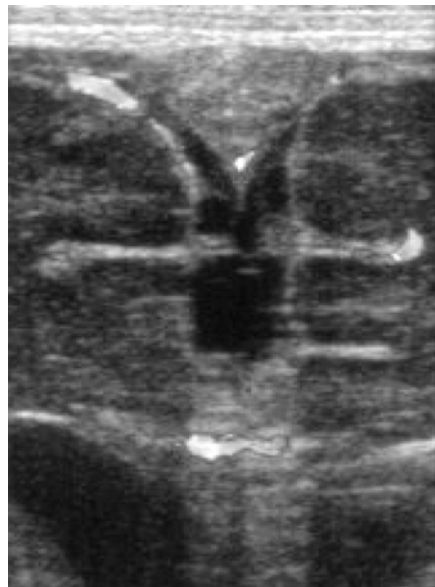


**Fig. 17.** Expansion of the superior sagittal sinus with echogenic thrombus with no evidence of flow on colour flow assessment

seizures at presentation in non-neonates, and the presence of venous infarcts, haemorrhagic and non-haemorrhagic, in both neonates and non-neonates [70].

Imaging findings include high attenuation in one or more of the venous sinuses on non-contrast CT (Fig. 16), with a filling defect, termed the delta sign, on post-contrast images. Venous infarction may occur and is haemorrhagic in up to 25% of patients. If the thrombosis affects the deep veins, such as the internal cerebral veins, thalamic infarction may occur. Similarly, thrombosis in the superior sagittal sinus may cause parasagittal infarction and thrombosis of the

vein of Labbe, transverse and sigmoid sinuses may cause temporal lobe infarction. Computed tomography, however, has a sensitivity of 84% [70], and may also have false-positive results in neonates because of an increased haematocrit, and a decreased attenuation because of high water content in the unmyelinated white matter. On MRI, subacute thrombus is seen as high signal on T1-weighted sequences. Acute thrombus is more difficult to detect as it is isodense with grey matter. The absence of the normal flow void within the sinuses on T2-weighted sequences is often helpful. Magnetic resonance venography should be interpreted in association with other imaging sequences, as the presence of transverse flow gaps may be seen in up to 30% of normal patients [73]. Ultrasound, with Doppler assessment, is a powerful tool in the detection of sinovenous thrombosis and venous infarction in the neonate (Fig. 17). It can also be very useful in temporal follow-up and obviate the need for multiple repeated invasive procedures such as CT and MRI.

### 7.1.12 Arterial Infarction

Stroke is rare in childhood, and the causes are different to those in the adult population. Traditionally, up to 50% of stroke in childhood was said to be idiopathic; however, risk factors for stroke are now recognised in up to 75% of children [74]. Common risk factors include congenital heart disease and sickle cell disease. Prothrombotic disorders are present in up to 50% of children [75]. Other less common risk factors include head and neck trauma, meningitis, tuberculosis, fungal infection, vasculopathies such as Moya-Moya disease, neurofibromatosis, fibromuscular dysplasia, Kawasaki disease, vascular malformations, arterial dissection often associated with trauma, maternal cocaine abuse, migraine and metabolic disorders such as MELAS and hyperhomocysteinaemia [24]. As previously mentioned in this section, HIV-related stroke is common, especially when associated with profound immunosuppression. Similarly, in sickle cell disease, the prevalence of stroke, which is often silent, is substantially higher than previously thought [76]. In approximately 25% of children, no cause is identified.

The initial presentation in children is most often with motor symptoms, which occur in up to 60% [77]. Altered mental state occurs in 21% and headache, unlike with adults, occurs in 32%. Aphasia, seizures, sensory symptoms, cranial nerve and cerebellar symptoms occur less frequently. The imaging features of stroke in childhood are similar to adults, appearing as focal areas of low attenuation on CT and of high signal on T2-weighted and FLAIR images on MRI (Fig. 18). The DWI will show restricted diffusion soon after onset, indicating cytotoxic oedema, when other modalities can appear normal. A haemorrhagic component can be seen in up to 20% of cases. Posterior circulation stroke is relatively uncommon in childhood and should raise the suspicion of dissection and trauma to the

vertebrobasilar circulation, or vasospasm secondary to migraine [24]. Thalamic infarcts typically occur in meningitis, congenital heart disease, migraine and trauma [24]. Unfortunately, due to its relative rarity compared with that in adults, the diagnosis of stroke is often delayed in children, and most delay is actually in seeking medical attention [77]. Very few children, even those with known risk factors, are imaged within the time frame of 3–6 h, which is regarded as the therapeutic window for treatment with thrombolytic agents or other forms of neuroprotection.

### 7.1.13 Metabolic Disorders

Few of these disorders present as an acute encephalopathy; however, mitochondrial disorders, such as mitochondrial encephalopathy, lactic acidosis and stroke (MELAS), may present with acute encephalopathy and stroke (Fig. 18). In MELAS, the lesions are seen in the periphery of the cerebral hemispheres and may have a wedge-shaped appearance (see Fig. 9). The lesions may be single or multiple. Signal abnormalities are also seen in the deep grey nuclei; however, these may not be present at first presentation. The diagnosis is made by the presence of high levels of lactic acid in the CSF. Other metabolic disorders which may cause stroke include Leigh's disease, the organic acidurias including hyperhomocysteinaemia and lysosomal storage disorders including cystinosis [24].

Urea cycle disorders may precipitate acute episodic clinical deterioration which may be reflected in an acute worsening of existing changes on MRI. The appearance may mimic dysmyelinating or demyelinating disorders including ADEM.

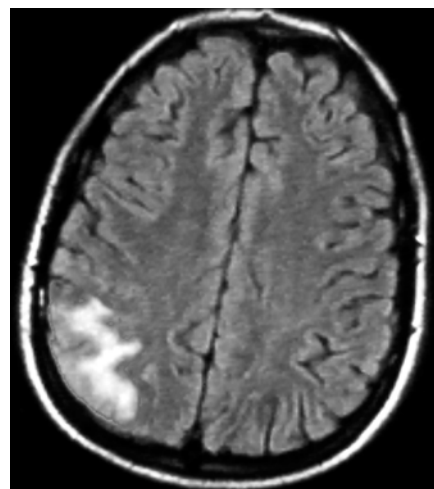


**Fig. 18.** Peripheral wedge-shaped area of increased signal on T2-weighted MR involving both grey and white matter, consistent with an infarct in a 14-year-old with mitochondrial encephalopathy, lactic acidosis and stroke



### 7.1.14 Drugs: Asparaginase, Methotrexate and Cyclosporin

These drugs are the most commonly implicated as causes of acute encephalopathy. The most common complication of Asparaginase therapy is sinovenous thrombosis as previously described. Cyclosporin therapy can be complicated by a form of reversible posterior leukoencephalopathy, which is discussed under the section describing hypertensive encephalopathy.

Methotrexate, given either intrathecally or intravenously in the treatment and prophylaxis of acute lymphoblastic leukaemia (ALL), may cause acute or delayed CNS sequelae. Acute neurotoxicity occurs within days to weeks of initialisation of therapy and includes encephalopathy, seizures, transient paresis, dysarthria and aphasia and severe headache. Long term effects may include gait abnormalities, memory deficits, learning disorders, declines in IQ scores as well as various behavioural difficulties. In the past, it was thought that a combination of methotrexate and craniospinal irradiation caused these abnormalities; however, it is now apparent that Methotrexate alone, either given intrathecally or even intravenously can be causative, although changes and neurological outcome are worse in combination [78–80]. The classical appearance of methotrexate related change is high signal intensity in the deep white matter on T2-weighted MR sequences (Fig. 19), which appears as low attenuation on CT. This is associated with hyperdense or calcified foci at the grey–white matter interface (Fig. 20), representing dystrophic calcification of the subcortical U-fibres adjacent to areas of intracerebral mineralising microangiopathy. When profound, this can even be visible on skull radiographs and can mimic Sturge-Weber syndrome. Minimal enhancement may occur after administration of intravenous contrast. The exact mechanism by which methotrexate causes these changes is not fully understood, but these lesions show evidence of vascular endothelial injury, infarction, focal demyelination and an atypical cellular response. Mineralising microangiopathy may also affect the basal ganglia and cerebellar grey matter and lead to calcifications in these regions also.

### 7.1.15 Epilepsy: Structural Abnormalities

Seizures in childhood are a common indication for imaging. In the neonate the first investigation is usually ultrasound. Specific causes of seizures, which may be evident on ultrasound, include calcification secondary to congenital infection or tuberous sclerosis. Disorders of neuronal migration and organisation are difficult to see with ultrasound except where the abnormalities are extensive as seen with lissencephaly. The presence of midline structural abnormalities, such as agenesis of the corpus callosum, or

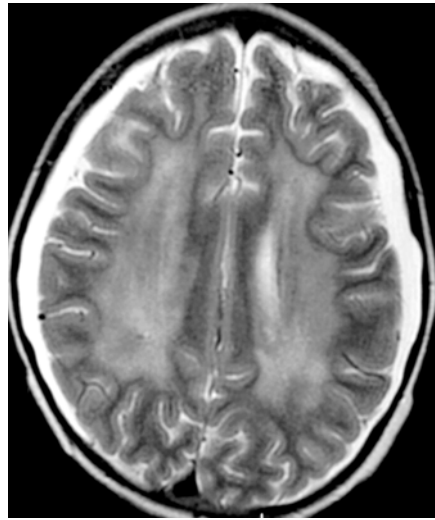


**Fig. 19.** Axial T2-weighted MR image shows bilateral symmetrical increased signal in the deep white matter typical of methotrexate-associated changes in a patient with a history of encephalopathy



**Fig. 20.** Axial CT image demonstrates the typical findings of subcortical calcification and low attenuation in deep white matter in a patient following treatment with intrathecal methotrexate

posterior fossa malformation, may alert the radiologist to the possibility of undetected neuronal migration or proliferation abnormalities which are best assessed with MRI.

In infants and older children CT is usually the first investigation. Unlike in adults, where the demonstration of a significant finding on neuroimaging in patients with new-onset seizures occurs in up to 45% of patients, in children, significant findings are seen in only 8%, with <1% caused by either a tumour or stroke [81]. Emergent neuroimaging in children with new onset afebrile seizures should therefore be restricted to those in high-risk populations, such as

children aged <33 months presenting with focal seizures, and those with a known predisposing condition, such as sickle cell disease, bleeding and coagulation disorders, cerebrovascular disease, malignancy, HIV infection and hydrocephalus [81]. Specific causes of status epilepticus, such as encephalitis or meningitis, may be evident in those patients imaged. Other conditions, such as haemorrhage associated with NAI, infarction or sinovenous thrombosis, may also be identified in “at-risk” groups. There may be evidence of ADEM or of a phakomatosis, particularly cortical tubers as seen in tuberous sclerosis. Remember, a new presentation of seizures in any group of patients should not be attributed to a known underlying abnormality without undertaking some form of neuroimaging. Patients with underlying brain abnormalities, such as cerebral palsy, are as much at risk of infection, NAI or other causes of seizures as the rest of the population.

Children not deemed suitable for emergent imaging can be imaged at a later date, if there is ongoing clinical concern. The MRI is the best investigation for detection of abnormalities of cerebral migration and organisation. Regression or evidence of neurodegeneration in a child with “cerebral palsy” should raise the possibility of metabolic disease.

Rasmussen’s encephalitis, or chronic localised encephalitis, is characterised by onset of seizures, progressive hemiplegia and psychomotor deterioration [82]. It presents in previously normal healthy children or young adults. Both viral and autoimmune aetiologies have been suggested as the cause. Imaging is typically normal at presentation; however, focal high signal on T2-weighted MR images may be seen in the cerebral cortex [83, 84]. Progressive atrophy of the involved hemisphere occurs over time, and with intractable seizures and hemiplegia, occasionally surgical removal of the affected cerebral hemisphere is the only treatment possible.

### 7.1.16 Endocrine-Related Encephalopathy

Diabetes mellitus, other than hypo- or hyperglycaemia, rarely presents as encephalopathy in childhood. Neonatal hypoglycaemia is, however, a common cause of encephalopathy which may mimic HIE.

### 7.1.17 Conclusion

Acute encephalopathy in childhood may vary in its presentation, aetiology and imaging compared with the adult population. Emergent neuroimaging, while often performed in order to exclude infection or neoplasia as a cause of acute neurological deterioration, may reveal imaging findings peculiar to a number of specific conditions. The

radiologist may be the first to recognise and suggest conditions such as NAI or neonatal alloimmune thrombocytopenia as causes of encephalopathy. Specific imaging features in conditions such as ADEM, MELAS, hypertensive encephalopathy and venous sinus thrombosis may also contribute to diagnosis and management. The role of the radiologist in the early diagnosis of neonatal HIE is increasing with newer imaging methods such as MR spectroscopy and DWI, giving potential future benefits with neuroprotective measures.

## References

1. Tasker RC, Cole GF. Acute encephalopathy of childhood and intensive care. In: Brett EM (ed) *Paediatric neurology*, 3rd edn. Churchill Livingstone, Edinburgh, 1996, pp 691–729
2. Wong CP, Forsyth RJ, Kelly TP, Eyre JA. Incidence, aetiology, and outcome of non-traumatic coma: a population based study. *Arch Dis Child* 2001;84:193–199
3. Kirkham FJ. Non-traumatic coma in children. *Arch Dis Child* 2001;85:303–312
4. Khong PL, Lam BCC, Tung HKS, Wong V, Chan FL, Ooi GC. MRI of neonatal encephalopathy. *Clin Radiol* 2003;58:833–844
5. Rutherford M, Ward P, Allsop J, Malamateniou C, Counsell S. Magnetic resonance imaging in neonatal encephalopathy. *Early Hum Dev* 2005;81:13–25
6. Barkovich AJ, Rowley H, Bollen A. Correlation of prenatal events with the development of polymicrogyria. *Am J Neuroradiol* 1995;16:822–827
7. Rorke LB. Anatomical features of the developing brain implicated in pathogenesis of hypoxic-ischaemic injury. *Brain Pathol* 1992;2:211–221
8. Volpe JJ. Neurobiology of periventricular leukomalacia in the premature infant. *Pediatr Res* 2001;50:553–562
9. Bass JL, Corwin M, Gozal D, Moore C, Nishida H, Parker S, Schonwald A, Wilker RE, Stehle S, Kinane TB. The effect of chronic or intermittent hypoxia on cognition in childhood: a review of the evidence. *Pediatrics* 2004;114:805–816
10. du Plessis AJ, Volpe J. Perinatal injury in the preterm and term newborn. *Curr Opin Neurol* 2000;15:151–157
11. Partridge JC, Babcock DS, Streichen JJ, Han BK. Optimal timing of cranial ultrasound in low birth weight infants: detection of intracranial hemorrhage and ventricular dilatation. *J Pediatr* 1983;102:281–287
12. Papile L, Burstein J, Koffler H. Incidence and evolution of subependymal and intraventricular hemorrhage: a study of infants with birth weights less than 1500 g. *J Pediatr* 1978;92:529–534
13. Babcock DS. Cranial sonography of the infant. In Ball WS Jr (ed) *Pediatric neuroradiology*. Lippincott-Raven, Philadelphia, 1997
14. Cramer BC, Walsh BA. Cisterna magna clot and subsequent post-hemorrhagic hydrocephalus. *Pediatr Radiol* 2001;31:153–159
15. Ryan SP. Subarachnoid blood in infants with intraventricular haemorrhage: an easier site to find this and still a good predictor of hydrocephalus (Abstract). *Pediatr Radiol* 2001;31:41–42
16. Martin E, Barkovich AJ. Magnetic resonance imaging in perinatal asphyxia. *Arch Dis Child* 1995;72:F62–F70
17. Wood NS, Marlow N, Costeloe K, Gibson AT, Wilkinson AR. Neurologic and developmental disability after extremely preterm birth. *N Engl J Med* 2000;343:378–384

18. Pinto-Martin JA, Riolo S, Cnaan A, Holzman C, Susser MW, Paneth N. Cranial ultrasound prediction of disabling and non-disabling cerebral palsy at age two in a low birth weight population. *Pediatrics* 1995;95:249–254
19. Rutherford MA, Pennock JM, Dubowitz LM. Cranial ultrasound and magnetic resonance imaging in hypoxic-ischaemic encephalopathy: a comparison with outcome. *Dev Med Child Neurol* 1994;36:813–825
20. Holling EE, Leviton A. Characteristics of cranial ultrasound white-matter echolucencies that predict disability: a review. *Dev Med Child Neurol* 1999;41:136–139
21. Hashimoto K, Hasegawa H, Kida Y, Takeuchi Y. Correlation between neuroimaging and neurological outcome in periventricular leukomalacia: diagnostic criteria. *Pediatr Int* 2001;43:240–245
22. Childs AM, Cornette L, Ramenghi LA, Tanner SF, Arthur RJ, Martinez D, Levene MI. Magnetic resonance and cranial ultrasound characteristics of periventricular white matter abnormalities in newborn infants. *Clin Radiol* 2001;56:647–655
23. Sie LT, van der Knaap MS, van Wezel-Meijler G, Taets van Amerongen AHM, Lafebre HN, Valk J. Early MR features of hypoxic-ischaemic brain injury in neonates with periventricular densities on sonography. *AJNR* 2000;21:852–861
24. Barkovich AJ. Brain and spine injuries. In: Barkovich AJ (ed) *Pediatric neuroimaging*. Lippincott, Williams and Wilkins, Philadelphia, 2000
25. Mercuri E, Rutherford M, Barnett A, Foglia C, Haataja L, Counsell S, Cowan F, Dubowitz L. MRI lesions and infants with neonatal encephalopathy. Is the Apgar score predictive? *Neuropediatrics* 2002;33:150–156
26. Miller SP, Ramaswamy V, Michelson D, Barkovich AJ, Holshouser B, Wycliffe N, Glidden DV, Deming D, Partridge C, Wu YW, Ashwal S, Ferriero D. Patterns of brain injury in term neonatal encephalopathy. *J Pediatr* 2005;April:453–460
27. Sie LT, van der Knaap MS, Oosting J, de Vries LS, Lafebre HN, Valk J. MR patterns of hypoxic-ischaemic brain damage after prenatal, perinatal or postnatal asphyxia. *Neuropediatrics* 2000;31:128–136
28. Badawi N, Kurinczuk JJ, Keogh JM, Alessandri LM, O'Sullivan F, Burton PR et al. Antepartum risk factors for newborn encephalopathy: the Western Australian case-control study. *Br Med J* 1998;317:1554–1558
29. Cowan F, Rutherford M, Groenendaal F, Elken P, Mercuri E, Bydder GM, Meiners LC, Dubowitz LMS, deVries L. Origin and timing of brain lesions in term infants with neonatal encephalopathy. *Lancet* 2003;361:736–742
30. Barkovich AJ. MR and CT evaluation of profound neonatal and infantile asphyxia. *Am J Neuroradiol* 1992;13:959–972
31. Juvet P, Cowan FM, Cox P, Lazda E, Rutherford MA, Wigglesworth J, Mehmet H, Edwards AD. Reproducibility and accuracy of MR imaging of the brain after severe birth asphyxia. *Am J Neuroradiol* 1999;20:1343–1348
32. Rutherford MA, Pennock JM, Counsell SJ et al. Abnormal magnetic resonance imaging in the internal capsule predicts poor neurodevelopmental outcome in infants with hypoxic-ischaemic encephalopathy. *Pediatrics* 1998;102:323–328
33. Robertson RL, Ben-Sira L, Barnes PD, Mulkern RV, Robson CD, Maier SE, Rivkin MJ, du Plessis AJ. MR line diffusion-weighted imaging of term neonates with perinatal brain ischemia. *Am J Neuroradiol* 1999;20:1658–1670
34. Wolf RL, Zimmerman RA, Clancy R, Haselgrove JH. Quantitative apparent diffusion coefficient measurements in term neonates for early detection of hypoxic-ischaemic brain injury: initial experience. *Radiology* 2001;218:825–833
35. Forbes KPN, Pipe JG, Bird R. Neonatal hypoxic-ischaemic encephalopathy: detection with diffusion-weighted MR imaging. *Am J Neuroradiol* 2000;21:1490–1496
36. Barkovich AJ, Westmark KD, Bedi HS, Partridge JC, Ferriero DM, Vigneron DB. Proton spectroscopy and diffusion imaging on the first day of life after perinatal asphyxia: preliminary report. *Am J Neuroradiol* 2001;22:1786–1794
37. Dale ST, Coleman LT. Neonatal alloimmune thrombocytopenia: antenatal and postnatal imaging findings in the pediatric brain. *Am J Neuroradiol* 2002;23:1457–1465
38. Barnes PD, Poussaint TY, Burrows PE. Imaging of pediatric central nervous system infections. *Neuroimaging Clin N Am* 1994;4:367–391
39. Siegal MJ. Brain in pediatric sonography. In: Siegal MJ (ed) Lippincott, Williams and Wilkins, Philadelphia, 2002
40. Klein JO. Bacteriology of neonatal sepsis. *Pediatr Infect Dis J* 1990;9:778
41. Fitz CR. Inflammatory diseases of the brain in childhood. *Am J Neuroradiol* 1992;13:551–567
42. Goodkin H, Harper MB, Pomeroy SL. Intracerebral abscess in children: historical trends at Children's Hospital Boston. *Pediatrics* 2004;113:1765–1770
43. Saxton VJ, Boldt DW, Shield LK. Sinusitis and intracranial sepsis: the CT imaging and clinical presentation. *Pediatr Radiol* 1995;25:S212–S217
44. Garces P, Mueller D, Trevenen C. Rhinocerebral mucormycosis in a child with leukemia: CT and MRI findings. *Pediatr Radiol* 1994;24:50–51
45. Patsalides AD, Wood LV, Atac GK, Sandifer E, Butman JA, Patronas NJ. Cerebrovascular disease in HIV-infected pediatric patients: neuroimaging findings. *AJR* 2002;179:999–1003
46. Dubrovsky T, Curless R, Scott G et al. Cerebral aneurysmal arteriopathy in childhood AIDS. *Neurology* 1998;51:560–565
47. Koh S, Chen L. Protein C and S deficiency in children with ischaemic cerebrovascular accident. *Pediatr Neurol* 1997;17:319–321
48. Lonergan GJ, Baker AM, Morey MK, Boos SC. From the archives of the AFIP. Child abuse: radiologic-pathologic correlation. *Radiographics* 2003;23:822–845
49. Golstein B, Kelly MM, Bruton D, Cox C. Inflicted versus accidental head injury in critically injured children. *Crit Care Med* 1993;21:1328–1332
50. Pollanen MS, Smith CR, Chiasson DA, Cairns JT, Young J. Fatal child abuse—maltreatment syndrome. A retrospective study in Ontario, Canada. 1990–1995. *Forensic Sci Int* 2002;126:101–104
51. Merton DF, Osborne DRS. Craniocerebral trauma in child abuse syndrome: radiological observations. *Pediatr Radiol* 1984;14:272–277
52. Tarantino CA, Dowd MD, Murdock TC. Short vertical falls in infants. *Pediatr Emerg Care* 1999;15:5–8
53. Carty H. The non-skeletal injuries of child abuse: the brain. *Yearbook of paediatric radiology*, vol 3. Miskolc, pp 17–24, 1991
54. Rao P, Carty H. Non-accidental injury: review of the radiology. *Clin Radiol* 1999;54:11–24
55. Duhaime AC, Christian CW, Rorke LB, Zimmermann RA. Nonaccidental head injury in infants: the “shaken-baby syndrome”. *N Engl J Med* 1998;338:1822–1829
56. Hadley MN, Sonntag VKH, Rekate HL, Murphy A. The infant whiplash-shake injury syndrome: a clinical and pathological study. *Neurosurgery* 1989;24:536–540
57. Reece RM, Sege R. Childhood head injuries: Accidental or inflicted? *Arch Pediatr Adolesc Med* 2000;154:11–15
58. Kleinman PK, Barnes PD. Head trauma. In: Kleinman PK (ed) *Diagnostic imaging of child abuse*. Mosby, St. Louis, p 314, 1998
59. Zimmermann RD, Bilianuk LT, Bruce D, Uzzell B, Goldberg HI. Computer tomography of craniocerebral injury in the abused child. *Radiology* 1979;130:687–690
60. Kemp AM, Stoodley N, Copley C, Coles L, Kemp KW. Apnoea and brain swelling in non-accidental head injury. *Arch Dis Child* 2003;88:472–476

61. Geddes JF, Whitwell HL, Graham DI. Traumatic axonal injury: practical issues for diagnosis in medicolegal cases. *Neuropathol Appl Neurobiol* 2000;26:105–116
62. Han KB, Towbin RB, De Courten-Myers G et al. Reversal sign on CT: effect of anoxic/ischaemic cerebral injury in children. *Am J Neuroradiol* 1989;10:1191–1198
63. Dale RC, Sousa C de, Chong WK, Cox TCS, Harding B, Neville BGR. Acute disseminated encephalomyelitis, multiphasic disseminated encephalomyelitis and multiple sclerosis in children. *Brain* 2000;123:2407–2422
64. Murthy SNK, Faden HS, Cohen ME, Bakshi R. Acute disseminated encephalomyelitis in children. *Pediatrics* 2002;110:21
65. Hynson JL, Kornberg AJ, Coleman LT, Shield L, Harvey AS, Kean MJ. Clinical and neuroradiologic features of acute disseminated encephalomyelitis in children. *Neurology* 2001;56:1308–1312
66. Jones BV, Egelhoff JC, Patterson RJ. Hypertensive encephalopathy in children. *Am J Neuroradiol* 1995;18:101–106
67. Cooney MJ, Bradley WG, Symko SC, Patel ST, Groncy PK. Hypertensive encephalopathy: complication in children treated for myeloproliferative disorders: report of three cases. *Radiology* 2000;214:711–716
68. Nag S, Robertson DM, Dinsdale HB. Cerebral cortical changes in acute hypertension: an ultrastructural study. *Lab Invest* 1977;39:150–161
69. Schwartz RB, Mulkern RV, Gudbjartsson H, Jolesz F. Diffusion-weighted MR imaging in hypertensive encephalopathy: clues to pathogenesis. *Am J Neuroradiol* 1998;19:859–862
70. deVeber G, Andrew M, Adams C, Bjornson B, Booth F, Buckley DJ, Camfield CS, David M, Humphreys P, Langevin P, Macdonald A, Gillet J. Cerebral sinovenous thrombosis in children. *N Engl J Med* 2001;345:417–423
71. Schick RM, Jolesz F, Barnes PD, Macklis JD. MR diagnosis of dural venous sinus thrombosis complicating L-asparaginase therapy. *Comput Med Imaging Graph* 1989;13:319–327
72. Griesemer DA, Theodorou AA, Berg RA, Spera TD. Local fibrinolysis in cerebral venous thrombosis. *Pediatr Neurol* 1995;10:78–80
73. Ayanzen RH, Bird CR, Keller PJ, Thoebald MR, Heiserman JE. Cerebral MR venography: Normal anatomy and potential diagnostic pitfalls. *Am J Neuroradiol* 2000;21:74–78
74. deVeber G, Roach ES, Riela AR, Wiznitzer M. Stroke in children: recognition, treatment and future directions. *Semin Pediatr Neurol* 2000;7:309–317
75. Chan AK, deVeber G. Prothrombotic disorders and ischaemic stroke in children. *Semin Pediatr Neurol* 2000;7:301–308
76. Steen RG, Emudianughe T, Hankins GM, Wynn LW, Wang WC, Xiong X, Helton KJ. Brain imaging findings in pediatric patients with sickle cell disease. *Radiology* 2003;228:2216–2225
77. Gabis, LV, Yangala R, Lenn NJ. Time lag to diagnosis in children. *Pediatrics* 2002;110:924–928
78. Lovblad KO, Kelkar P, Ozdoba C, Ramelli G, Remonda L, Schroth G. Pure methotrexate encephalopathy presenting with seizures: CT and MRI features. *Pediatr Radiol* 1998;28:86–91
79. Mahoney DH, Shuster JJ, Nitschke R, Lauer SJ, Steuber P, Winick N, Camitta B. Acute neurotoxicity in children with B-precursor acute lymphoid leukaemia: an association with intermediate-dose intravenous methotrexate and intrathecal triple therapy: a Pediatric Oncology Group Study. *J Clin Oncol* 1998;16:1712–1722
80. Hertzberg H, Huk WJ, Ueberall MA, Langer T, Meier W, Dopfer R, Skalej M, Lackner H, Bode U, Janssen G, Zintl F, Beck JD. CNS late effects after ALL therapy in childhood. Part I: Neuro-radiological findings in long-term survivors of childhood ALL: an evaluation of the interfaces between morphology and neuropsychological performance. *Med Pediatr Oncol* 1997;28:387–400
81. Sharma S, Riviello JJ, Harper MB, Baskin MN. The role of neuroimaging in children with new-onset afebrile seizures. *Pediatrics* 2003;111:1–5
82. Barkovich AJ. Infection of the nervous system. In: Barkovich AJ (ed) *Pediatric neuroimaging*. Lippincott, Williams and Wilkins, Philadelphia, 2000
83. Bien CG, Widman G, Urbach H, Sassen R, Kuczaty S, Wiestler OD, Schramm J, Elger CE. The natural history of Rasmussen's encephalitis. *Brain* 2002;125:1751–1759
84. Bien CG, Urbach H, Deckert M, Schramm J, Wiestler OD, Lassman H, Elger CE. Diagnosis and staging of Rasmussen's encephalitis by serial MRI and histopathology. *Neurology* 2002;58:250–257





# Thoracic Emergencies

L. Breyssem, M.-H. Smet

## 7.2

### Contents

7.2.1	Introduction	601
7.2.2	The Chest and Respiratory Tract in Children: Physiological Aspects and Differences with Adults	601
7.2.3	Clinical Symptoms	602
7.2.4	Imaging of Non-traumatic Pediatric Thoracic Emergencies	603
7.2.4.1	Extrathoracic Airway Obstruction	603
7.2.4.2	Parenchymal Disease	612
7.2.4.3	Pleural Collections	612
7.2.4.4	Large Diaphragmatic Defects	615
7.2.4.5	Chest Wall Pathology	615
7.2.5	Imaging of Traumatic Pediatric Thoracic Emergencies	617
7.2.6	Conclusion	618
	References	618

### 7.2.1 Introduction

Respiratory distress accounts for almost 10% of pediatric emergencies. Under 15 years of age, deaths from respiratory disorders accounts for 30% of childhood morbidity and almost 50% in those less than 1 year of age.

By definition, respiratory failure indicates an inability of the respiratory system to provide sufficient oxygen for metabolic needs or to excrete the CO<sub>2</sub> produced by the body. When a child presents with signs of respiratory distress, diagnosis and therapeutic decisions have to be made, and in some cases within a very short time scale. Many different diseases may lead to acute respiratory failure, including disorders outside the respiratory tract.

That children are not small adults is even truer regarding the airways and respiratory system. Consequently, children respond different to an insult (traumatic or non-traumatic) than adults. These differences between a child and an adult respiratory tract are also reflected in the multidisciplinary approach. The approach of the child has to be done with special care in a child friendly way; specific experience in pediatric or emergency medicine makes the diagnosis and immediate stabilization of the patient more

accurate, and in many situations imaging plays an essential role in completing or confirming the clinical suspicion. The older the patient, the more comparable with adults is the therapeutic management.

In this chapter, we focus on some important physiological and anatomical aspects of the pediatric airway and discuss the most encountered non-traumatic and traumatic thoracic emergencies in the pediatric age group.

Reviewing the causes of non-traumatic acute respiratory pathology in the different pediatric age groups, we choose to subdivide the pathologies inhibiting normal respiratory function in six main groups. We acknowledge, however, that some conditions can occur concomitantly:

- The airways can be obstructed and the pathology can anatomically be situated from the upper airways to the peripheral small airways.
- The most common cause of severe respiratory distress related to parenchymal disease is premature birth and hyaline membrane disease, acquired pneumonitides coming second.
- Changes in normal pleural negative pressure can compromise pulmonary function and pleural fluid collections can be susceptible for infection.
- Large diaphragmatic defects either congenital either acquired need surgical intervention on very short notice.
- Chest wall involvement with mechanical impairment can play a role in compromising normal respiratory function, especially with underlying cardiopulmonary disease.
- Since the airways and the esophagus have a common embryological origin, both arising from the foregut, pathology and especially in neonates and infants, symptomatology, can be associated.

### 7.2.2 The Chest and Respiratory Tract in Children: Physiological Aspects and Differences with Adults

Children have a large tongue and the narrowest point of the extrathoracic airway is the subglottic region. The airways in children are smaller, more collapsible, and the air flow is larger in the central airways than in the peripheral airways. Since the acini are smaller and the mucus production is in-

creased, more atelectasis and/or air trapping is present in cases of airway inflammation or foreign-body aspiration. The alveoli grow until 8 years. Collateral ventilation is underdeveloped until 8 years due to the decreased number of pores of Kohn, the increased thickness of the connective tissue septa, and the smaller alveolar size. This also results in more atelectasis compared with adults (Hedlund and Kirks 1990; Rotta and Wiryawan 2003). In emergency situations, intubation of a child needs special experience. The possibility of craniofacial malformations, such as the Pierre-Robin sequence or Apert syndrome with retrognathia and micrognathia, has to be taken into account (Dinwiddie 2004; Levy and Helfaer 2000; Nicolai 2004).

Also traumatic injuries of the chest do not have the same result in children as in the adult. Bony and cartilaginous structures are more deformable, the elasticity of mediastinal vessels is greater (Sivit 2002). Bony injuries are uncommon in children. If rib fractures are present, the likelihood of marked chest distortion and injury to the intrathoracic viscera is great (Fig. 1). Aortic and great vessel injury is uncommon in children, even following severe injury. Evaluation of the superior mediastinum, however, is more difficult in children because of the thymus. The age of the child, the absence of deviation of the midline structures, and, if present, the "sail sign" or "wave sign," must assure you that the large upper mediastinum is thymus. If the plain chest X-ray is doubtful, ultrasound can be very helpful. Using a superficial high-resolution linear or convex probe, the thymus between the ribs can be identified (Mendelson 2001).

All these features of the pediatric chest wall and respiratory system make the response to a thoracic trauma, infection, a thoracic mass, or respiratory obstruction in a young child different than in an adult.

### 7.2.3 Clinical Symptoms

Thoracic emergencies in children often result in life-threatening changes in cardiorespiratory function, anxious moments for the child as well as for the parents. The causes of these emergencies are often distinct in the pediatric patient; however, it is a problem of any age, it can occur as a "new" situation or in an already existing pathology, and it can be a medical or a surgical emergency. Non-traumatic acute chest pathology is more frequent than thoracic trauma. Inspection of the child's well-being is in many cases more informative than blood gases or respiratory rate. The patient presents with acute or more insidious onset of sometimes specific, and sometimes non-specific, signs or symptoms. Most frequently, symptoms are present since a few hours or days and are not always easy to appreciate, especially in the baby or infant (Eber 2004; Hammer 2003; Rotta and Wiryawan 2003).

Voice changes can help in refining the differential diagnosis, but tachypnea, cyanosis, and difficult breathing, defined as stridor or wheezing, are most frequently present. Associated inflammatory symptoms or a septic appearance are alerting. More severe signs are pulsus paradoxus and symptoms of pulmonary edema. Other worrying but less specific symptoms are apnea, cough, chest pain, and sore throat (Eber 2004). Feeding problems, swallowing problems, or dysphagia can sometimes be the initial symptoms of a tracheobronchial anomaly.

Stridor and wheezing are defined as an abnormal sound during breathing produced by turbulence of air flow through a partial obstruction. The characteristics and timing of stridor can indicate the site of airway obstruction and the effect

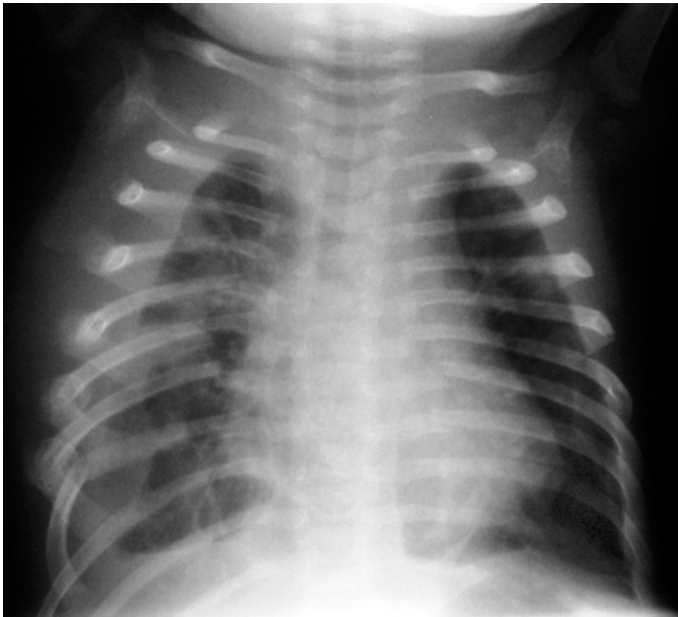


**Fig. 1.** Battered child with multiple rib fractures and a hemothorax on the right side. Posterior and lateral rib fractures are highly specific fractures for battered child (in a non-accidental clinical setting)

of the obstruction will be the greatest when the airway is the narrowest. Obstruction in the extrathoracic airway will be of more significance in inspiration and the child presents with inspiratory stridor. Obstruction in the intrathoracic airway will be of more significance in expiration and the child presents with expiratory stridor or wheezing. The lumen of the subglottic airway is defined by rigid cricoids cartilage and obstruction at that site produces stridor in the in- and expiratory phase, a biphasic stridor (Swischuk 2000a,b).

In first instance, it is obvious that the clinician has to be sure that all immediate necessary respiratory care to stabilize the child is given and secondly imaging can lead to the definitive diagnosis. In an urgent situation, rapid diagnosis and therapeutic action are mandatory.

## 7.2.4 Imaging of Non-traumatic Pediatric Thoracic Emergencies

Airway obstruction is potentially life-threatening and the pathology can be situated from the upper airways to the peripheral small airways. Airway obstruction in a child is potentially life threatening and, depending on the cause of the obstruction and the general well-being of the child, requires rapid and effective approach.

The worst scenario is an acute total airway obstruction with respiratory arrest, but is, fortunately, very uncommon. The most frequent causes are laryngeal edema or inhalation of aspirated foreign body with complete airway obstruction. Partial obstruction of the airways is more often the case and leads to stridor or wheezing (Bar-Ziv et al. 2001). We subdivide the causes of airway obstruction in extrathoracic and intrathoracic.

### 7.2.4.1 Airway Obstruction

#### Extrathoracic Airway Obstruction

Imaging of a child with upper airway or extrathoracic respiratory obstruction is not without danger. In some cases, imaging speed and minimal disturbance are of utmost importance and you start with non-invasive methods. Try to reassure the child and make easy movements with the head during the procedure. After evaluating the status of the child and possible etiology of the obstruction with the clinician, you start with a lateral view of the neck, with the neck in extension. When possible and necessary, an anteroposterior (AP) view or dynamic information under fluoroscopy of the airway is required. Chest X-ray has to be performed with chin up to exclude soft tissue superposition, with in- and expiration or lateral decubitus when necessary. Direct laryngoscopy is usually the next step (Duncan 1999).

If the most critical period is over tided, additional imaging is performed when diagnosis needs further evaluation: ultrasound (US); upper gastrointestinal (GI) series; spiral computed tomography (CT); or magnetic resonance imag-

**Table 1** Most frequent causes of inflammatory and non-inflammatory extrathoracic airway obstruction

<b>Inflammatory</b>
Viral laryngotracheobronchitis
Epiglottitis
Retropharyngeal abscess
Bacterial tracheitis (or laryngotracheobronchitis)
Allergy/laryngeal edema
Viral laryngotracheobronchitis
Epiglottitis
Retropharyngeal abscess
Bacterial tracheitis (or laryngotracheobronchitis)
Allergy/laryngeal edema
<b>Non-inflammatory</b>
Acquired or congenital anomalies
Foreign body
Angioneurotic edema
Tumors: subglottic hemangioma; vallecular cyst (uncommon: aryepiglottic cysts or dermoid cysts, cysts of the thyroglossal duct and laryngeal cyst)
Neck trauma
Vocal cord paralysis
Chronic stridor can become acute

ing (MRI) for specific indications (Table 1; Damm et al. 1999; Rencken et al. 1998).

Potential life-threatening causes of extrathoracic airway obstruction are usually febrile.

The acute onset of stridor in a young child, invariably accompanied with fever, usually presents viral laryngotracheobronchitis or croup. The circumferential localized airway inflammation is seen as a tapered narrowing of the subglottic region and should be visible on both AP and lateral views (Fig. 2a). When standard treatment fails, an artificial airway should be considered and other diagnoses must be excluded with radiology and endoscopy, particularly bacterial croup but also acute epiglottitis, foreign-body aspiration and retropharyngeal abscess.

Infectious symptoms in bacterial or membranous croup are more pronounced. Rare additional findings on conventional X-ray are thin, irregular opacities representing detached membranes, not to be confused with foreign bodies.

Epiglottitis, although less frequent since vaccination against *H. Influenzae*, remains an important emergency. The child is very sick with high fever and presents with inspiratory stridor or dyspnea, drooling, marked respiratory distress, dysphonia, and restlessness/anxiety. Only a true lateral view of the neck with the child upright and the head in extension visualizes the swollen epiglottis and aryepiglottic folds, also known as the “thumb sign,” ballooning of the hypopharynx, and associated subglottic edema (Fig. 2b). Although epiglottitis is mostly a clinical diagnosis, imaging is needed in selected cases to differentiate with croup, retropharyngeal abscess (Fig. 2), laryngeal foreign body, bacterial tracheitis or inhalation or ingestion injury, angioneurotic edema, and anaphylaxis. It has to be performed with great precaution and stand-by for respiratory resuscitation, especially when the neck has to be extended for optimal imaging technique. Chest X-ray with



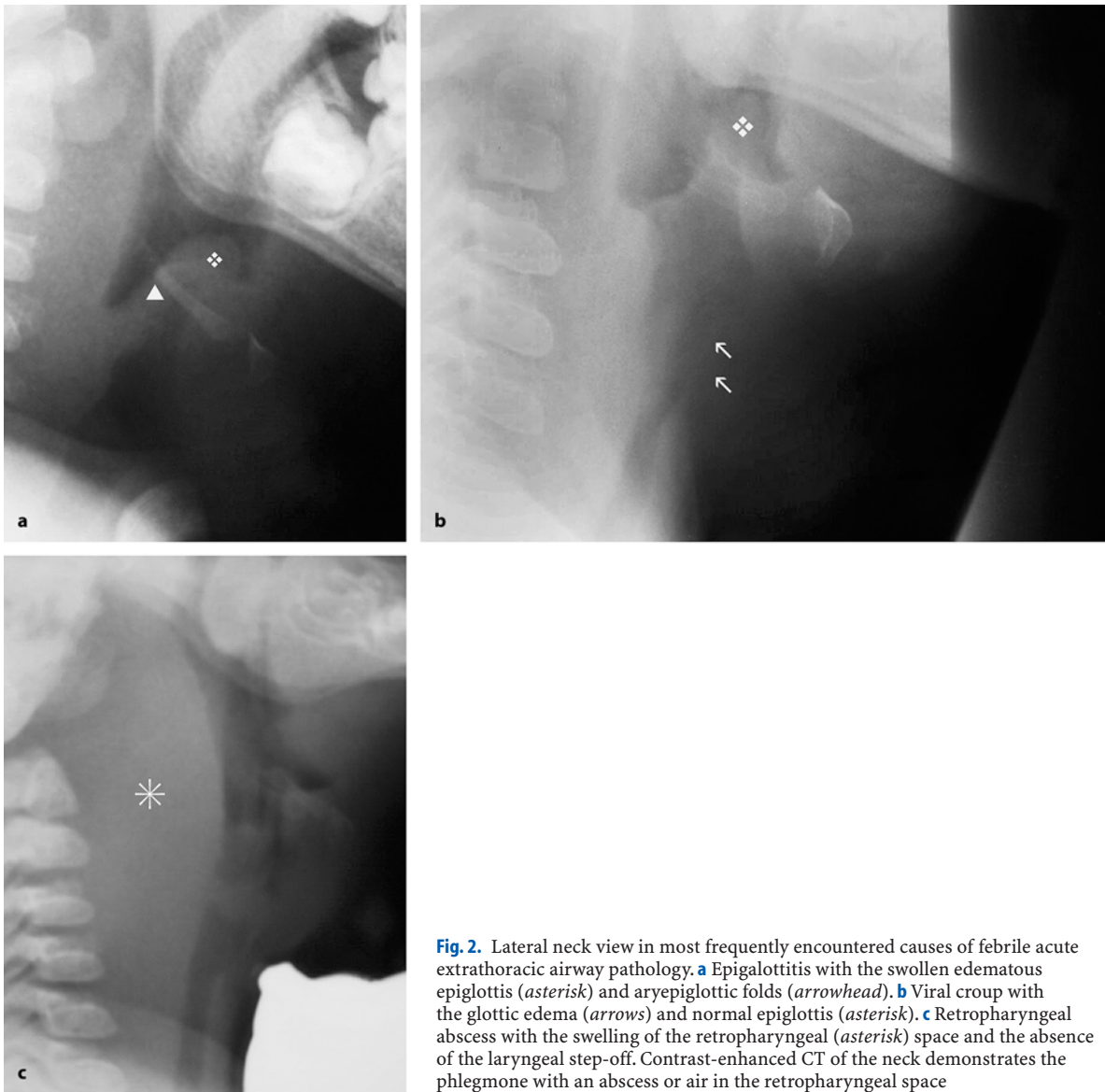


**Fig. 2.** Lateral neck view in most frequently encountered causes of febrile acute extrathoracic airway pathology. **a** Epiglottitis with the swollen edematous epiglottis (*asterisk*) and aryepiglottic folds (*arrowhead*). **b** Viral croup with the glottic edema (*arrows*) and normal epiglottis (*asterisk*). **c** Retropharyngeal abscess with the swelling of the retropharyngeal (*asterisk*) space and the absence of the laryngeal step-off. Contrast-enhanced CT of the neck demonstrates the phlegmone with an abscess or air in the retropharyngeal space

chin up permits evaluation of the glottic soft tissue and air space or other causes of acute respiratory symptoms.

In a retropharyngeal abscess, the enlarged retropharyngeal space can be seen clearly by the lateral neck view with the neck in extension. Sometimes additional dynamic fluoroscopy is necessary, but ultimately the abscess and the extension of the inflammation are confirmed by contrast-enhanced CT scan. According to the latest literature, retropharyngeal abscess as a cause of acute airway obstruction or respiratory distress are rare. An emergency complication, such as descending suppurative mediastinitis, is rarely described in one case (Craig and Schunk 2003; Dinwiddie 2004; Duncan 1999; Ghyepes and Nussbaum 1985; Lee et al. 2001; Markowitz 1984; Rotta and Wiryanan 2003; Stroud and Friedman 2001; Sztajn bok et al. 1999).

Afebrile life-threatening causes of the extrathoracic airway obstruction are congenital or secondary laryngeal or tracheal abnormalities (subglottic stenosis, neck trauma), tumors, foreign-body aspiration, angioneurotic edema (acquired/hereditary), and vocal cord paralysis. Congenital airway abnormalities (nasal masses, Pierre-Robin sequence, craniofacial anomalies, laryngomalacia, trachea or bronchomalacia, clefts, webs, atresia, or stenosis) are usually present in >85% in evaluation for persistent stridor and respiratory difficulties. Associated risk factors, including prematurity, cardiovascular malformations, as well as neurological and congenital or chromosomal abnormalities, increase the need for tracheotomy and endotracheal intubation (Altman et al. 1999). Especially in the neonate and infant, congenital airway anomalies can result in signifi-

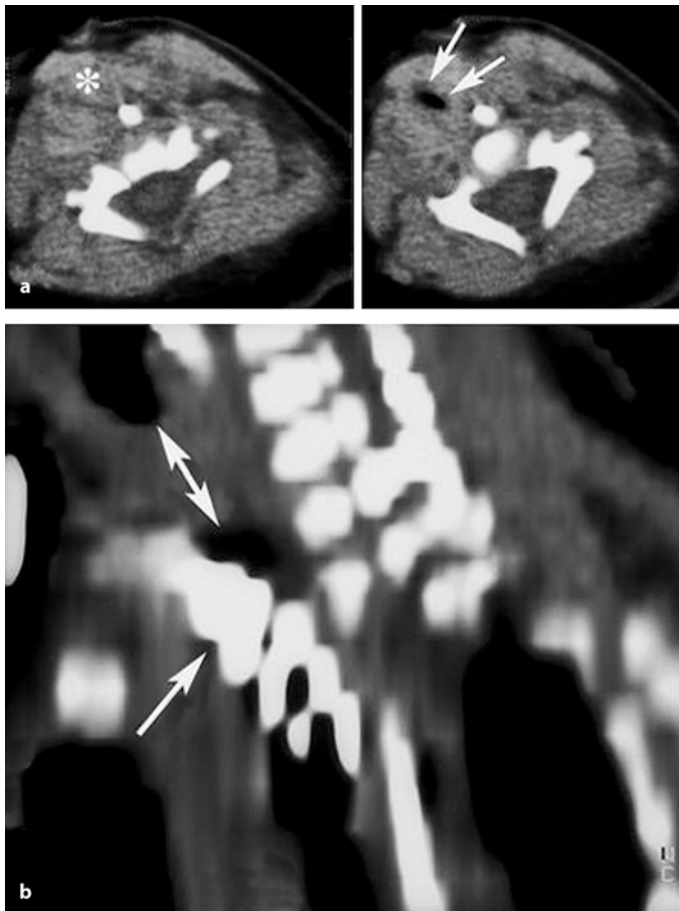


**Fig. 3.** Congenital stenosis of the trachea in a neonate with CHARGE syndrome. **a** Axial unenhanced CT scan (slice thickness 2 mm): narrow (*arrows*) and obliterated (*asterisk*) airway at consecutive levels compatible with stenosis of the infraglottic trachea. **b** Sagittal reconstruction: extent of stenosis (*double-headed arrow*), tracheostomy (*arrow*)

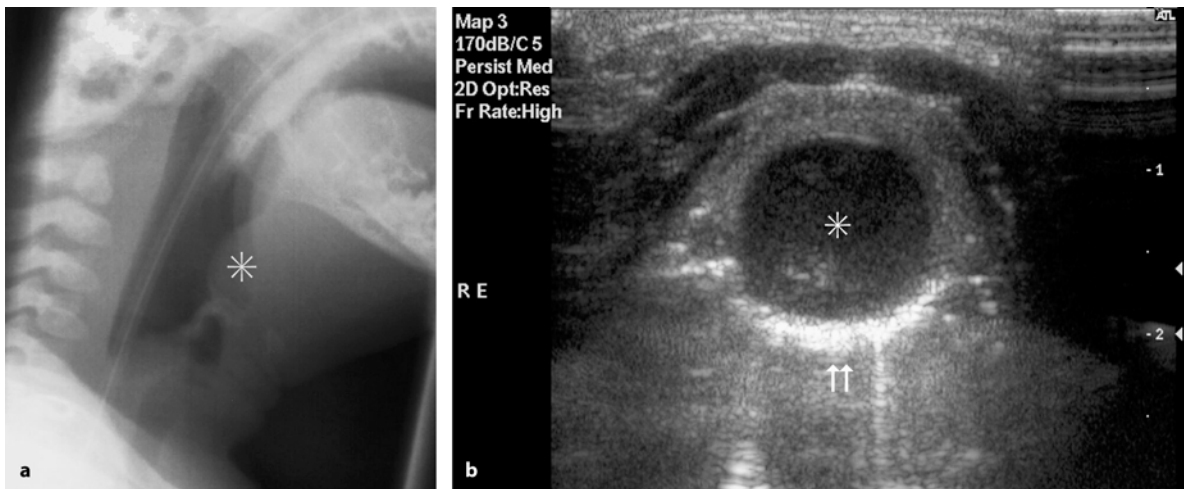


**Fig. 4.** A baby with severe stridorous breathing. **a** On the lateral neck view, there is a subtle swelling visible in the vallecular region (*asterisk*). Febrile signs are absent. **b** Ultrasound can make the diagnosis of a thick-walled cyst (*asterisk*) with the air in the pharynx at the dorsal side of the cyst (*arrows*). Regarding the location just

above the glottic region, a vallecular cyst is proposed. A CT scan will not add more information and can be omitted (radioprotection). Surgery cannot be delayed and, in this case, after marsupialization of the cyst, histology confirmed a vallecular origin

**Table 2.** Most common mediastinal masses in children

Anterior mediastinum	Middle mediastinum	Posterior mediastinum
Normal thymus (neonate and infant)	Foregut duplication cyst	Neurogenic tumor
Germ cell tumor	Enlarged lymph nodes (neoplastic, inflammatory)	Esophageal duplication cyst
Lymphoma, leukemia, histiocytosis	Lymphangioma	Lymphoma (non-Hodgkin), metastatic neuroblastoma
Thymic masses (thymolipoma, thymic cyst)	Pericardial cyst	Bochdalek hernia
Lymphangioma		
Morgagni hernia		

cant upper airway obstruction and are frequently associated with feeding disorders. They may require immediate tracheostomy after birth, followed by imaging. The CT with multiplanar imaging or 3D reconstruction is best suited to evaluate the extent of the anomaly, followed by an upper-GI series to evaluate the esophagus (Fig. 3). The history of the patient can aid in differentiating between congenital or acquired pathology, e.g., longstanding endotracheal intubation or granuloma in Wegener's vasculitis. Subglottic stenosis after intubation is a frequently encountered acquired cause of respiratory distress in children (Shinkwin and Gibbin 1996). Associations with other congenital abnormalities are common, e.g., VA(C)TER(L) in 25% of the cases or CHARGE syndrome (Dinwiddie 2004; Katz et al. 1995; Lander et al. 2004; Rencken et al. 1998).

The effect of the extrinsic airway compression depends on the size of the lesion; however, even with small lesions, intrinsic air-flow obstruction can occur when there is important additional mucosal edema during intercurrent viral infection. An optimal lateral and AP view are necessary to delineate the air column and evaluate the lumen and symmetry of the airway walls. Ultrasound can differentiate a simple cyst from a complicated cyst or a soft tissue mass. Computed tomography and/or MRI with contrast enhancement are performed for further characterization of the suspected mass and its extension.

Small soft tissue tumors can also become large and infiltrative and are an indication for surgery. In the neonate, subglottic hemangioma is most frequent and can be suspected if an asymmetrical impression of the subglottic airway is seen on the conventional AP neck films. The hemangioma can be demonstrated with US and CT scan (Chetty et al. 1997). Other types of upper airway masses are uncommon and consist of aryepiglottic cysts or dermoid cysts, cysts of the thyroglossal duct, and laryngeal cyst (Markowitz 1985, Rencken et al. 1998). A cyst in the vallecula can cause progressive stridor and can be confirmed with US when there is a – sometimes very subtle – vallecular distention of the soft tissue visible on the lateral neck X-ray, easily mistaken for tonsillar tissue (Fig. 4).

### Intrathoracic Airway Obstruction

Pathologies causing obstruction of the intrathoracic airways can be acquired or congenital and can be infectious, neoplastic, vascular, or congenital.

The mediastinum is a common site for tumors because of its midline location and the different embryological composition. In general, any patient with a tumor in the anterior or middle mediastinum should be admitted immediately and undergo urgent evaluation (Meyer et al. 2004). The causes of pathological mediastinal widening differ with age. In the infant, thymic teratoma, lymphangioma, and cardiovascular malformations are most common, additional causes in the older child are leukemia/lymphoma – especially non-Hodgkin's lymphoma – malignant germ cell tumor, and Langerhans cell histiocytosis (Table 2). Non-Hodgkin's lymphoma is one of the most common mediastinal tumors in childhood and respiratory symptoms are common: 25% may rapidly progress to life-threatening respiratory compromise with dyspnea, orthopnea, and stridor. A rapid progression may require immediate chemotherapy or radiotherapy to shrink a tumor mass.

Specific urgent complications related to large mediastinal tumoral masses are (Fig. 5):

- Superior vena cava syndrome causes headache, dyspnea, orthopnea and syncope, and vascular collapse.
- Inferior vena cava syndrome: cardiac inflow decreases dangerously and necessitates urgent surgery.
- Pericardial effusion is most often seen with a teratoma or cardiogenic tumor (Meyer et al. 2004).

Evaluation of mediastinal (neoplastic) masses requires a chest X-ray (AP and lateral view), completed with CT and/or MRI (Siegel 1999). Compression of more than one-third of the airways is putting the child in a dangerous position regarding respiratory symptoms, difficulty in intubation, and decrease in pulmonary function (Kirks et al. 1983).

Small mediastinal tumors can be tricky also (Table 3). If they are located nearby the airways (the trachea or the bronchi), they cause a partial compression that can become significant with superimposed airway infection or enlargement of the mass. When the mass is not directly seen on

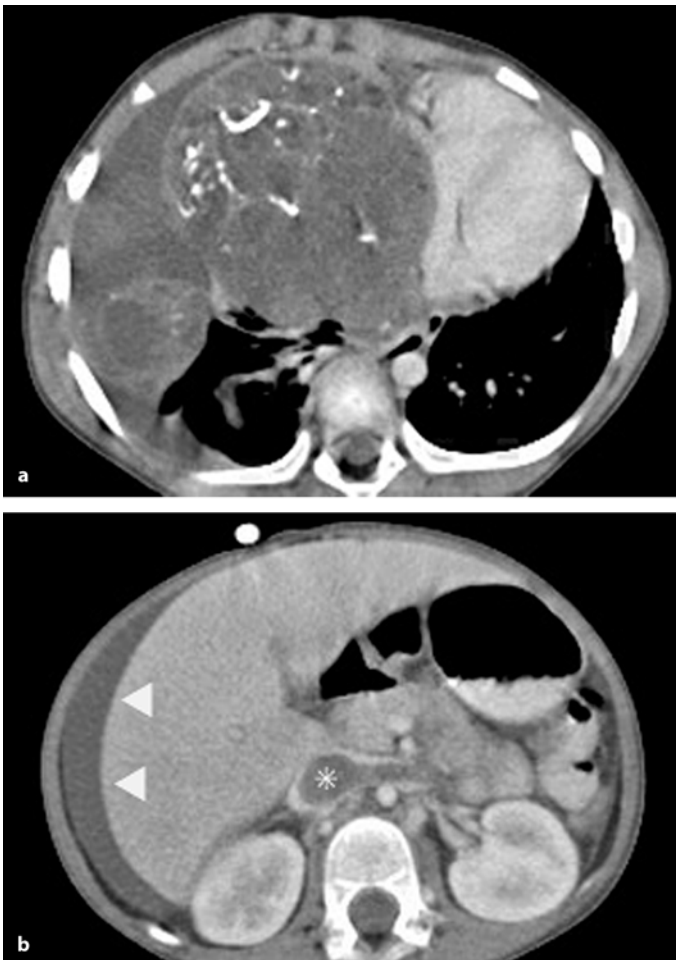


**Fig. 5.** A 5-year-old boy presented with semi-urgent respiratory symptoms and demonstrated a large right-sided thoracic consolidation, deviating the mediastinum and heart to the left. Histology revealed a malignant teratoma. **a** Even during chemotherapy, the mass increased significantly and resulted in increased compression of the heart, upper mediastinum, and airways, creating a dangerous situation. Important decrease of the cardiac inflow due to vessel and heart compression and the features of superior and inferior vena cava syndrome were present: headache; dyspnea; orthopnea with the risk of syncope; and vascular collapse. A CT scan was performed in urgency. **b** Additionally, ascites (*arrowheads*) and a large inferior vena cava (IVC) thrombus (*asterisk*) were seen compatible with inferior vena cava syndrome. Urgent surgical resection of the tumoral mass was performed

**Table 3.** Common non-neoplastic causes of intrathoracic airway obstruction

Bronchogenic cyst
Vascular compression
Intrinsic obstruction
Foreign-body aspiration
Mucus plug

chest X-ray, there are some indirect signs putting you on the right way such as mediastinal densities and bulging, comparing the lucency of both lungs is important. Is there air trapping or retro-obstructive atelectasis? In- and expiration film are mandatory. Further evaluation requires contrast-enhanced CT or MRI with multiplanar reconstructions (Alford et al. 1993).

A bronchogenic cyst is often asymptomatic in older children and adults, but can be more dangerous in neonates and infants. Stridor in newborns and young infants is an alarming symptom. As a foregut cyst, a bronchogenic cyst is a ventral budding abnormality and they

can have different anatomic locations anywhere along the tracheobronchial tree, including the neck, mediastinum and lung. They are usually unilocular, spherical or oval and generally close to the tracheobronchial tree, usually without patent communication to the airway, preferentially solitary located in the lower lobes. The central or peripheral location of a cyst will determine its mode of presentation. A mediastinal lesion, especially a carinal location, is likely to produce earlier compression of the trachea or proximal mainstem bronchi. Secondly, they can undergo rapid enlargement and surgery cannot be postponed. Contrast-enhanced CT is a highly reliable diagnostic tool to visualize bronchogenic cysts as a thin-walled round lesion that can contain fluid. Sometimes they are air filled. Magnetic resonance imaging remains an alternative imaging modality; however, one drawback in infancy is that general anesthesia is required. Surgical resection is usually necessary (Alford et al. 1993; Lazar et al. 1991).

Vascular rings and slings or anatomically normal vessels that are enlarged due to congenital cardiopathy can lead to respiratory problems, especially in the first months



of life when there is significant impression on the airways. Feeding difficulties and aspiration sequelae are frequently associated. These potential respiratory emergencies are the result of the proximity of the great vessels, heart, esophagus, and large intrathoracic airways. Symptomatic vascular rings and slings include right-sided aortic arch, aberrant left subclavian artery and ductal remnant completing the ring, double aortic arch, and pulmonary sling. The abnormal vessels form a ring and symptoms depend upon the tightness of the ring. It remains the most important vascular cause of tracheal obstruction (Table 4; Alford et al. 1993;

**Table 4.** Symptomatic vascular rings and slings

Right-sided aortic arch and aberrant left subclavian artery and ductal remnant  
Double aortic arch  
Pulmonary sling

Berdon 2000; Berrocal et al. 1999; Chun et al. 1992; Rencken et al. 1998; Subramanyan et al. 2003). In most cases, tracheal impression is not visible on conventional chest X-ray, and additional indirect signs can lead you towards the correct diagnosis. When evaluating a chest X-ray in a child with stridor or respiratory problems and/or feeding difficulties, always look at the aortic arch. A right-sided aortic arch is sometimes the first clue to a vascular ring, causing the sometimes severe respiratory symptoms. On barium swallow, the presence of a posterior esophageal impression reveals the abnormal course of a vessel. Cardiac Doppler ultrasound will confirm the vascular anomaly; however, when diagnosis is still doubtful, the evaluation can be completed with a CT with 3D reconstruction/MRI or – now less frequently – angiography (Beekman et al. 1998; Berdon 2000; Berrocal et al. 1999; Katz et al. 1995). Surgery may involve division and reanastomosis of obstructing vessels, which produces immediate relief of airway obstruction.

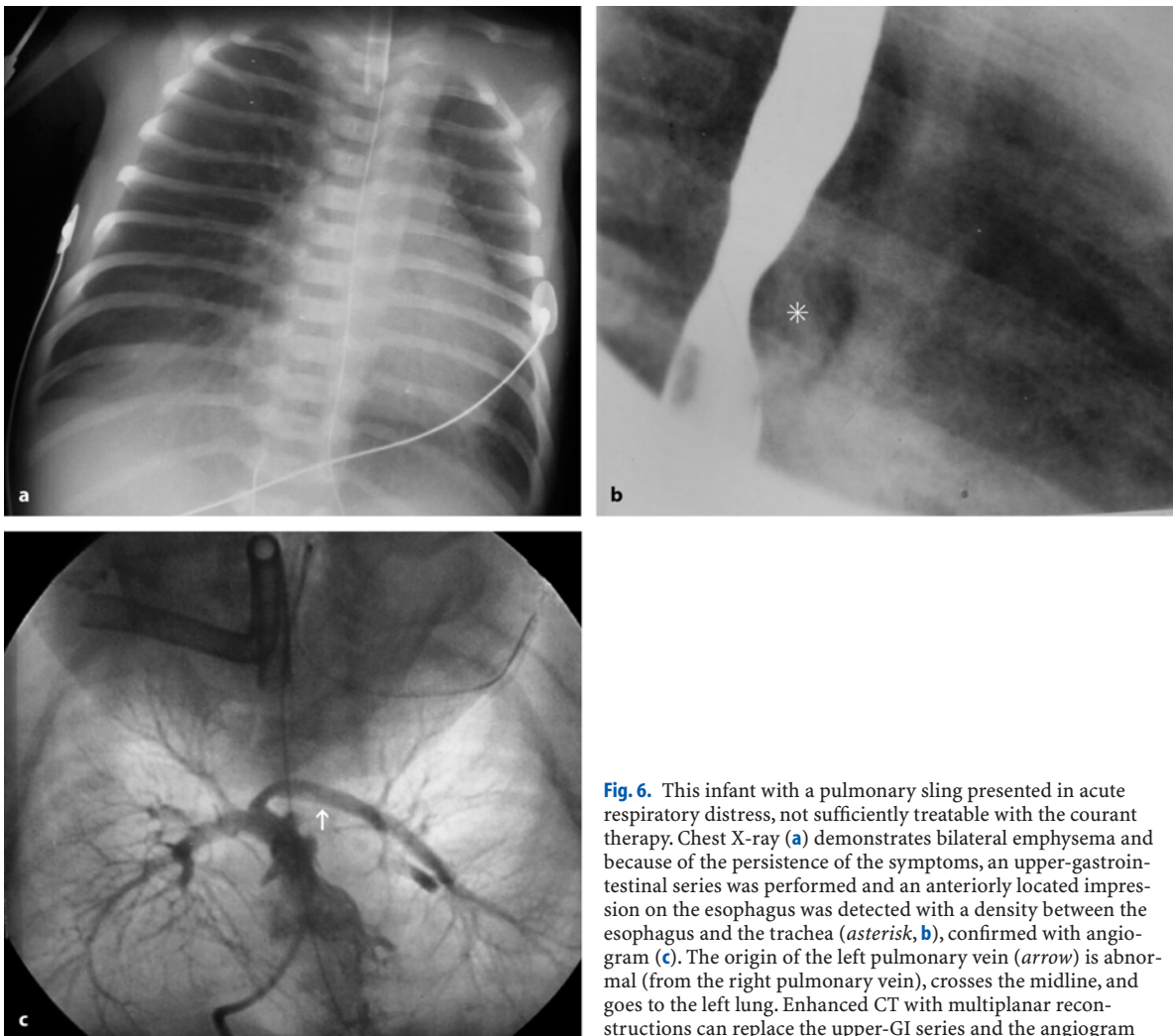


**Fig. 6.** This infant with a pulmonary sling presented in acute respiratory distress, not sufficiently treatable with the current therapy. Chest X-ray (a) demonstrates bilateral emphysema and because of the persistence of the symptoms, an upper-gastrointestinal series was performed and an anteriorly located impression on the esophagus was detected with a density between the esophagus and the trachea (asterisk, b), confirmed with angiogram (c). The origin of the left pulmonary vein (arrow) is abnormal (from the right pulmonary vein), crosses the midline, and goes to the left lung. Enhanced CT with multiplanar reconstructions can replace the upper-GI series and the angiogram

Anterior esophageal impression is due to an anomalous left pulmonary artery that comes off the right pulmonary artery at the level of the right main bronchus and carina and runs between the trachea and the esophagus to the left lung. Respiratory symptoms are common, which can be severe at early age. Cases with obstructive emphysema of the entire lung or of the middle and lower lobes are reported (Fig. 6). Accompanying tracheomalacia or intrinsic cartilaginous malformation is seen as sequelae and may result in persistent symptoms, even after surgical correction (Alford et al. 1993; Markowitz 1984; Rencken et al. 1998).

Partial airway obstruction in a child with a congenital cardiopathy presenting with respiratory deterioration is usually due to mechanical compression of the central airways (Alford et al. 1993; Rencken et al. 1998). Compression of the left lower lobe bronchus is most common (Markowitz 1984). Enlargement of the left atrium, left pulmonary artery, and pulmonary veins on the left are potential causes of airway compression with obstructive emphysema or atelectasis, requiring surgical repair or bronchial stenting in the near future. Computed tomography and/or MRI or angiography can be used to demonstrate the relation between the vessels and the airways.

Foreign-body aspiration is a common pediatric pathology and can have serious or sometimes fatal sequelae. Diagnosis can be easily overlooked when the aspiration event is missed and many children present with complications. Even more, there is also a moderate high rate of negative radiology findings (sensitivity 70.2%, specificity 62.5%). Management is variable and varies according to the type and location of the foreign body (Metrangolo et al. 1999; Silva et al. 1998; Zerella et al. 1998). Potential respiratory threat is a foreign body that is located in the upper airways (laryngeal or subglottic). Laryngeal spasm with cyanosis can occur. Laryngeal web, acute severe viral or bacterial croup, epiglottitis, hemangioma (or papilloma), angioneurotic edema, or hypocalcemic tetany are differential diagnoses. Differential diagnoses of a tracheal foreign body is vascular compression, bronchogenic cyst, enlarged lymph nodes, or other mediastinal mass. Bilateral retroobstructive emphysema can be seen on chest X-ray. A bronchial foreign body is most frequent. Abnormalities on chest X-ray can be the first abnormal sign or clue to the diagnosis, especially features secondary to the partial airway obstruction, e.g., retroobstructive emphysema. The hyperinflated lung with air trapping shows decreased pulmonary vascularity and this radiological sign can be used to determine the abnormal side: the large hyperlucent lung vs the smaller opaque lung (Rencken et al. 1998). If it is not clearly visible on the AP in- and expiratory film or in young children, additional dynamic fluoroscopic or conventional evaluation can be performed: either in a stand-up decubitus during normal respiration or in the right or left lateral decubitus with horizontal X-ray beam in infants. Cases are reported in which partial airway obstruction can change in a complete airway obstruction due to the mobility of the for-

ign body. But if clinical suspicion is strong, bronchoscopy is the modality of choice and confirms the presence. At the same time, the aspirated foreign body can be evacuated.

Serious complications are fatal asphyxia, atelectasis, pneumonia, associated pleural effusion, air leak in the interstitial space leading to pneumomediastinum, pneumothorax, or pneumopericardium. Aspiration of a foreign body is one of the common causes of massive atelectasis in the emergency room. An abrupt onset of an air leak in a child less than 2 years should raise the suspicion of an aspirated foreign body (Fig. 7; Bar-Ziv et al. 2001; Gay 1978), Metrangolo et al. 1999; Swischuk and John 1999; Zerella et al. 1998).

Congenital lesions based on intrinsic bronchial obstruction are congenital cystic adenomatoid malformation (CCAM) and congenital lobar emphysema (CLE). Especially in the neonate they can complicate with severe air trapping. Large lesions push away the normal mediastinal and pulmonary structures and lung growth can be compromised. Mediastinal compression can result in airway and vascular compromise, the lesion behaves as an “oncological” emergency. If they precipitate alarming symptoms in the first few days of life, surgery cannot be delayed. If the child is born in respiratory distress usually resulting from associated pulmonary hypoplasia and persistent fetal circulation, the mass can be removed after respiratory stabilization of the child. In the older child, acute presentation is usually associated with surinfection or abscedation of the lesion.

The CCAM is by definition disorganized lung tissue, rich in bronchial structures, with cystic lesions and poor in alveoli. A multilocular air-filled cyst is the most common presentation of a CCAM, but presentation can be variable. Symptomatic neonates are treated as surgical emergencies. Presentation later in life is also possible, often with unresolved pulmonary infections. The CCAM can become infected and a multicystic complex lesion can be seen and is difficult to differentiate from a sequestration or a necrotizing pneumonia.

Congenital lobar emphysema is overinflation of one lobe, rarely bilobar, usually due to a bronchial (partial) obstruction. Symptoms may be mild, but when lung fluid clears, overinflation of the lobe can occur and the lobe becomes overinflated due to ball valve phenomenon and air trapping. Severe respiratory distress can occur requiring urgent lobectomy. Before surgery, an extrabronchial compression or endobronchial plug has to be ruled out with bronchoscopy and CT of the chest with contrast enhancement and multiplanar views. Delayed congenital lobar emphysema also exists. Sometimes an underlying viral infection triggers the problem with mucosal edema and bronchospasm. Differentiation with a tension pneumothorax is possible with chest CT (Fig. 8). In an older infant, the differential diagnosis of an overinflated lobe is an extrinsic compression of a vessel or mass or an acquired cause of bronchial obstruction, e.g., foreign body, mucus plugs, endobronchial granulomas in primary tuberculosis (Gibson

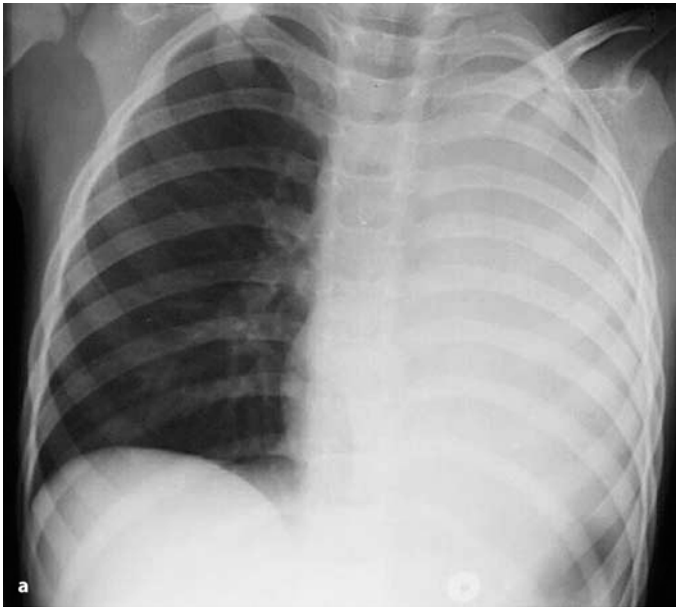


**Fig. 7.** In a child with symptoms of acute (upper or lower) airway obstruction, always consider aspiration of a foreign body. Complications can occur (a) unilateral atelectasis and (b) pneumomediastinum and subcutaneous emphysema in the neck

and Steiner 1997; Mercado-Deane and John 2001; Rencken et al. 1998; Seo et al. 1999).

Small airway obstruction caused by intrinsic or extrinsic edema/bronchospasm or plugs is seen in bronchiolitis, asthma, and cystic fibrosis.

Asthma is a classic example of hyperreactive airway disease, aggravated by allergies as well as viral and mycoplasma pneumoniae infections. The basic pathophysiology is

airway narrowing with increased resistance to air flow in the small airways (smooth muscle contraction, bronchospasm, bronchial wall inflammation, and excessive mucus production; Duiverman et al. 1999).

The goal of imaging in an acute asthmatic attack is the detection of complications: hyperinflation; atelectasis; emphysema of a lung or a lobe are common (mucus plug with obstruction); air leaks such as pneumomediastinum and

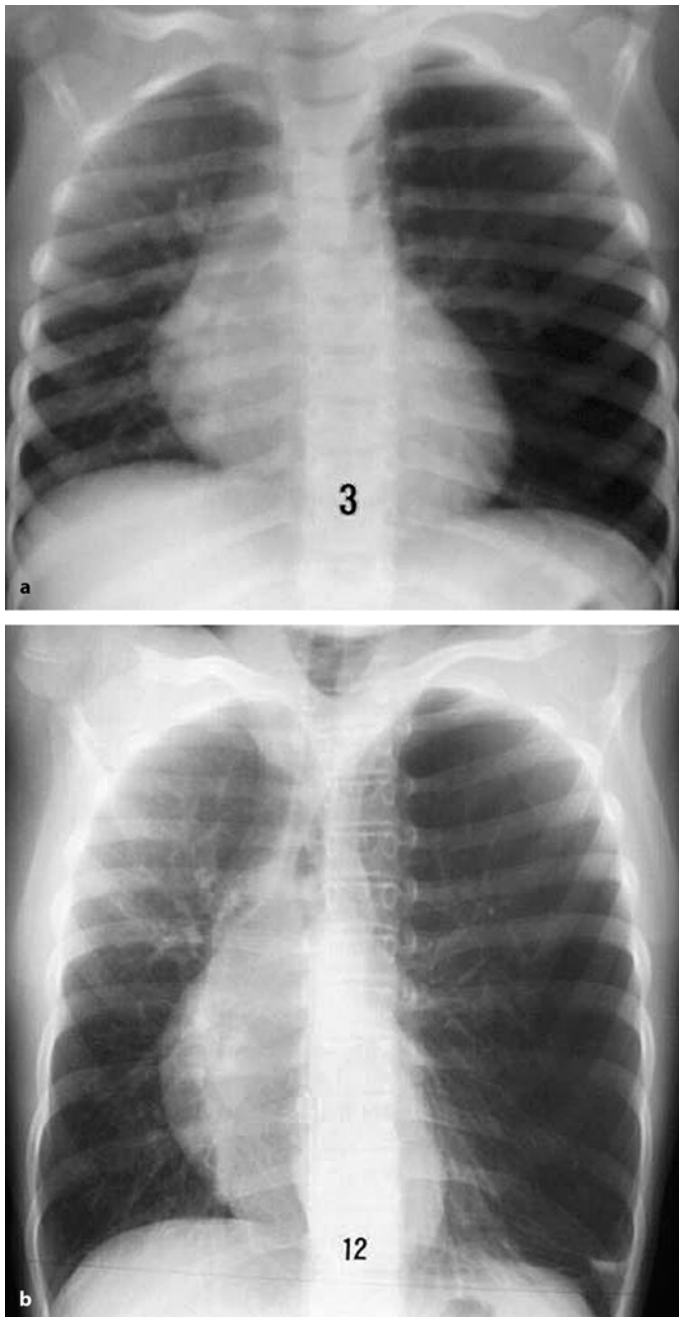


**Fig. 8.** Left-sided congenital lobar emphysema (CLE) in a boy at **a** 3 years of age presents as an acute episode of respiratory distress at **b** the age of 12 years. Due to the air trapping, there is enlargement of the CLE, deviation of the mediastinum and the heart to the right, spreading of the vascular markings in the lung, and compression of the lung parenchyma in the left lower lobe: the space-occupying effects or infection can result in acute distress. Additional CT helps in defining the topography of the CLE in a preoperative setting, and more urgently, in differentiating from pneumothorax, demonstrating the presence or absence of vascular marking in the CLE

pneumonia; or to exclude other causes of wheezing such as foreign-body aspiration, endobronchial or extrinsic mass lesions, and vascular rings.

A viral infection is an “airway” infection. Bronchiolitis is a seasonal viral infection in babies and can cause severe respiratory distress resulting in mechanical ventilation. It consists of bronchial wall thickening, parahilar-peribronchial streaking, central predominance due to parahilar edema or adenopathy: bronchospasm, mucus plugs

with narrowing of the already small airways. This leads to air trapping or emphysema or lobar or segmental atelectasis (Fig. 9). Emphysema can be the only finding in an acute ill infant with respiratory distress (Swischuk and John 1999). Pleural effusions or empyemas are not common with viral infections, except in very young infants and immunocompromised individuals. Acute interstitial viral pneumonitis presents as a diffuse hazy interstitial pattern on chest X-ray (Swischuk and John 1999).





**Fig. 9.** Bronchiolitis in an 11-month-old baby: important air trapping or lung emphysema bilaterally, perihilar streaks, and (sub)segmental atelectasis, requiring ventilation

**Table 5.** Causes of potential acute hypoxemic respiratory failure

Fungal infections
Allergic lung disease
Aspiration
Cystic fibrosis
Bone marrow transplantation

#### 7.2.4.2 Parenchymal Disease

The most common cause of severe respiratory distress related to parenchymal disease is premature birth with hyaline membrane disease, with acquired lung infections coming second. Severe respiratory distress in the premature baby is caused by RDS or hyaline membrane disease and most of these babies are admitted in the neonatal intensive care unit (Agrons et al. 2005; Gibson and Steiner 1997). A child in the emergency room with fever and an acute onset of pneumonia almost always has an infection, most frequently viral. Bacterial pneumonia is most often a *Streptococcus pneumoniae* or at later age mycoplasma pneumoniae. Occasionally, the infection is tuberculosis. As a viral infection is more an airway involvement, a bacterial pneumonia or inflammation of the lung tissue that may follow either a non-infectious or an infectious insult, is more an air-space involvement. Most patients can be treated as outpatients; however, in some cases the infection can worsen that intravenous medication is required. Consolidations begin at the periphery of the lung and frequently make contact with the pleural surface: pleural effusions and empyemas are common (Swischuk and John 1999). *Staphylococcus aureus* is a severe but infrequent pneumonia in young children and has a peculiar follow-up. It is the most common cause of bronchopneumonia. The child can be very ill with severe respiratory distress. It is characterized on chest X-ray as

rapidly evolving patchy parenchymal process with accompanying pleural fluid. On follow-up, the resolved parenchymal densities change in residual thin-walled peripheral air cysts. Any bacterial pneumonia can result in abscessation and empyema. When the infection or pleural effusion is extended, both can compromise the pulmonary function and the child can become septic. Major lung involvement with diffusely spread infiltrates is not infrequently seen in fungal infections, allergic lung disease, aspiration, cystic fibrosis, and after bone marrow transplantation (Table 5). Acute lung injury triggered by these systemic and/or pulmonary insults can result in acute hypoxemic respiratory failure (AHRF), a common reason for admission on the pediatric intensive care unit. On chest X-ray, patchy infiltrates are diffusely spread over both lungs, an ARDS image in the adults. The outcome, however, is preferentially determined by the causing pathology, but pulmonary status has to be followed carefully (Fig. 10; Boiko et al. 1995; Duncan 1999; Golder et al. 1998; Peters et al. 1998; Priestley and Helfaer 2004; Weiss et al. 1996). The acute chest syndrome in sickle cell disease results in more dense consolidations in the lung bases (Meyer et al. 2004; Swischuk and John 1999).

#### 7.2.4.3 Pleural Collections

Large pleural collections can compromise pulmonary function and pleural fluid can be susceptible for infection. Decrease in negative pressure is caused by presence of air, fluid, or a solid structure in the pleural space. The result is a varying degree of pulmonary collapse producing intrapulmonary shunting and a drop in the PaO<sub>2</sub>. The development of a positive pressure in the pleura is a more urgent situation than the loss of negative intrathoracic pressure. Positive intrapleural pressure is the result of pleural fluid



**Fig. 10.** Wegener's granulomatosis in a 6-year-old child with acute hypoxic respiratory failure.  
**a** Anteroposterior chest X-ray: patchy consolidations in both lungs, less pronounced in the upper lobe.  
**b** Axial-unenhanced CT scan: spontaneous hyperdense areas with a density of 60 HU (*asterisk*), suggestive for hemorrhagic consolidations. Respiratory distress became worse and ventilatory support on the intensive care unit was necessary for this child

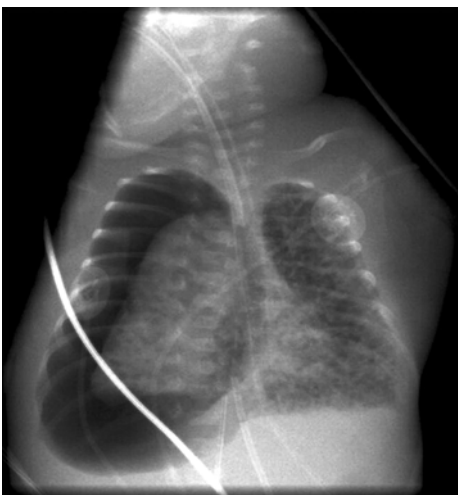


**Fig. 11.** Barotrauma and air leaks in a low birth weight premature infant, with severe RDS and mechanical ventilation. Anteroposterior chest X-ray: tension pneumothorax on the right with atelectasis of the ipsilateral lung, marked deviation of the mediastinum to the left. The pneumothorax is most likely the result of the combination of RDS, mechanical ventilation, and pulmonary interstitial emphysema, still present in the left lung

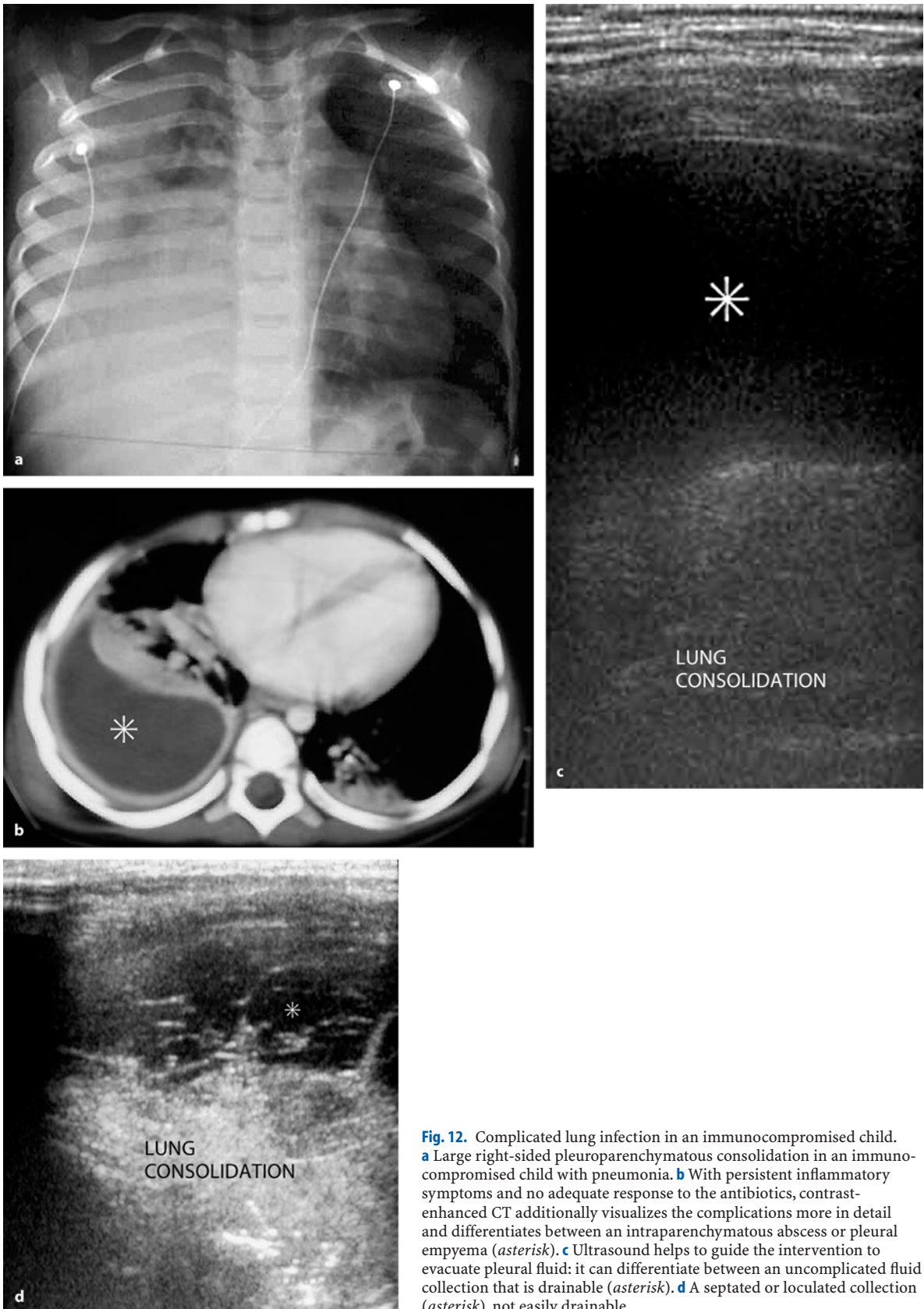


**Fig. 12.** Complicated lung infection in an immunocompromised child. **a** Large right-sided pleuroparenchymatous consolidation in an immunocompromised child with pneumonia. **b** With persistent inflammatory symptoms and no adequate response to the antibiotics, contrast-enhanced CT additionally visualizes the complications more in detail and differentiates between an intraparenchymatous abscess or pleural empyema (*asterisk*). **c** Ultrasound helps to guide the intervention to evacuate pleural fluid: it can differentiate between an uncomplicated fluid collection that is drainable (*asterisk*). **d** A septated or loculated collection (*asterisk*), not easily drainable

or air under tension or a tension pneumothorax. A tension pneumothorax acts as an air mass and produces lung and mediastinal compression. This results in impaired ventilation. Tension across the mediastinum with obstruction of the inferior vena cava (IVC) results in compromised pulmonary venous return and decreased cardiac output with circulatory collapse and collapse of the contralateral lung.

Severe respiratory distress in newborn babies and infants occurs secondary to prematurity and its adequate therapy, congenital cardiovascular or thoracic malformations (with or without prematurity), or to severe lung infection.

The most common acute complications in newborn (premature) babies with respiratory distress requiring artificial ventilation are air leaks. They result in intrathoracic extra-alveolar gas. The “free” air can be located at different sites: pneumothorax; pneumomediastinum; pulmonary interstitial emphysema (PIE); gas below the visceral pleura usually at the lung base; pneumopericardium; and pneumoperitoneum. A tension pneumothorax with deviation of the mediastinal structures can be fatal if not decompressed immediately (Fig. 11; Briassoulis et al. 2000; Gibson and Steiner 1997; Krul et al. 1997; Markowitz 1984). The ventrally located pneumothorax in the premature baby has characteristic features. On chest X-ray, a hypolucent paramediastinal region with sharp delineation of the mediastinal, cardiac, and diaphragmatic border, and a deep lucent cardiaphragmatic sinus are pathognomonic signs. A lateral film with horizontal beam with the child in a supine position can confirm the diagnosis (Agrons et al. 2005). The PIE is air that escapes in the pulmonary interstitium or lymphatic vessels from the terminal alveoli or airways. Thin-walled cystic or tubular lucent structures, raying from the hili, are seen on chest X-ray. Occasionally it can appear unilateral and acts as an air mass with mediastinal shift, compromising the venous return, and subsequently decreases cardiac output (Fig. 11).

In response to inflammation or infection, the pleura can produce large amounts of fluid, an exudation that is an environment for bacterial growth. Usually bacteria enter the pleural space from an adjacent pneumonia. This can result in toxemia when there is a pyothorax. With US, visualization of the pleural space with a high-resolution linear probe permits the radiologist to evaluate free fluid or loculated fluid and to guide possible intervention. The extension of the disease and the presence of an abscess or empyema is best evaluated with contrast-enhanced CT (Fig. 12; Kim et al. 2000).

#### 7.2.4.4 Large Diaphragmatic Defects

Large diaphragmatic defects, either congenital or acquired, need immediate surgical intervention. Diaphragmatic eventration is usually the result of a congenital paralysis, aplasia, or atrophy of the diaphragmatic muscle, and is seen on chest X-ray as an abnormally elevated diaphragm,

partially or totally. Left-sided eventrations are more likely to be complete. The severity of presentation depends on the location and whether it involves a complete leaflet. Occasionally, diaphragmatic eventration is bilateral and can lead to respiratory distress in infants, especially when associated with infection.

Congenital diaphragmatic defect (CHD) is usually severe and has an incidence of 1/2500–5000 live births. Around 8–10 weeks gestational age, the abdominal content can herniate to the thorax through a diaphragmatic defect, usually through the foramen of Bochdalek. Anterior CHD through the foramen of Morgagni (90% right sided) is less common (1–5%) and is usually asymptomatic. Approximately 5–30% of patients with CHD present after the neonatal period with severe neonatal asphyxia and pulmonary hypertension, occasionally with gastrointestinal symptoms (Alford et al. 1993; Ozturk et al. 2001; Singh et al. 2001). Prenatal US and/or prenatal MRI already detect the hernia in utero in most cases (Gibson and Steiner 1997). The intrathoracic space restriction results in ipsilateral lung hypoplasia. The associated pulmonary hypertension makes it very difficult to provide adequate oxygenation and there can be an indication for intensive therapy such as ECMO.

Chest X-ray in CHD is frequently abnormal but not always diagnostic. A “bubbly” hemithorax with obliteration of the costodiaphragmatic sinus, deviation of the mediastinum to the contralateral side, abnormal position of the nasogastric tube, and an airless abdomen are the most common findings on chest- and abdominal X-ray. Sometimes differential diagnosis with an aerated congenital cystic adenomatoid malformation (CCAM) is equivocal. In these cases, US can help in further diagnosis. The presence of mobile gastrointestinal structures and spleen, and in severe cases parts of the liver, confirm the hernia (Alford et al. 1993; Gibson and Steiner 1997; Rencken et al. 1998).

The CHD can also be found in older children (5–30% of CHD) presenting with acute distress or gastrointestinal symptoms, in most cases due to an episode of infection with involvement of the residual lung and airways (*Streptococcus-B pneumoniae*; Schafermeyer 1993). Other causes of delayed CHD are posttraumatic or, for instance, a complication of surgery (Fig. 13; Ozturk et al. 2001; Singh et al. 2001).

#### 7.2.4.5 Chest Wall Pathology

Chest wall pathology with mechanical impairment can play a role in compromising normal respiratory function, especially with underlying cardiopulmonary disease. Chest wall pathology with respiratory compromise is mostly the result of chest wall configuration anomalies or large tumoral masses, frequently associated with compression of the ipsilateral lung or a large pleural effusion (Donnelly and Frush 1999; Wong et al. 2004). Chest configuration anomalies with





**Fig. 13.** **a** A 2-month-old child with recurrent pericardial effusion (*asterisk*), demonstrated by cardiac ultrasound, was treated surgically creating a connection between the pericardium, the pleural, and the peritoneal space on the left. **b** A few days later, the child presented acutely in shock and respiratory distress. On chest X-ray, a large diaphragmatic hernia on the left with a smaller component on the right was seen, requiring urgent surgery

narrowing of the superior anterior mediastinal space can compress the mediastinal vessels and airways, in some cases leading to airway obstruction. The trachea at the thoracic inlet and the left main bronchus are most frequently involved (Donnelly and Bisset 1998). Lymphangiomatosis of the bone can also involve the chest wall. Frequently associated with a chylothorax, a large pleural effusion can cause respiratory distress and require immediate evacuation of the fluid. Malignant chest wall tumors are potentially life threatening (Wong et al. 2004). Conventional chest X-ray can give an initial diagnostic image concerning the severity of the lesion and bony involvement. Ultrasound differentiates between fluid or soft tissue and can guide the interventional procedure; however, contrast-enhanced CT will be performed to evaluate the extent and the tissue characteristics of the lesion (Fefferman and Pinkney 2005).

Since the airways and the esophagus have a common embryological origin, both arising from the foregut, pathology and symptoms can be associated, especially in neonates and infants.

Thoracic emergencies affecting the esophagus are found in congenital (tracheobroncho) esophageal malformations and tracheoesophageal fistula with severe aspiration pneumonia (Berrocal et al. 1999). Acquired stenosis of the esophagus causes foreign-body impaction in infants and older children. In this setting, the foreign-body impaction is usually associated with a secondary esophageal stenosis after surgical repair of atresia and needs immediate therapy (Lao et al. 2003). Esophageal perforation with pneumomediastinum in children is rare.

## 7.2.5 Imaging of Traumatic Pediatric Thoracic Emergencies

Traumatic emergencies related to the chest are less common, but the injuries tend to be serious, especially an arterial injury has a high mortality rate (Table 6). Concerning imaging, conventional imaging of the chest (completed with cervical spine and pelvis in polytrauma patients) and CT are the most sensitive methods of assessing thoracic trauma.

Due to blunt trauma, pulmonary contusion is leakage of blood into the interstitial spaces. As it occupies air space, it is seen as patchy infiltrates or large areas of consolidation with atelectasis. The extent is underestimated on radiography, CT is much more sensitive. Lung lacerations result in atelectasis, consolidations, interstitial air, or hydropneumothorax (due to air leak; Beaver and Laschinger 1992; Schafermeyer 1993; Sivit 2002). Rib fractures are rare in accidental injury. A single rib fracture involves a low risk of serious injury, but multiple rib fractures are associated with high mortality and morbidity, since they are often associated with head injury. If rib fractures are present in a child with no defined thoracic trauma, a non-accidental injury or battered child has to be considered, especially in the neonate and young infant (Fig. 1). Some signs strongly suggest non-accidental injury such as the location and type of fractures. Fractures of different ages and evaluation of the most vulnerable places can help in the diagnosis of non-accidental trauma. Even resuscitation uncommonly leads to rib fractures. Tracheobronchial injury results in cervical and mediastinal emphysema if it is a high lesion. A distal lesion is associated with a pneumothorax. A pneumothorax can occur secondary to injury of the lung, airways, or esophagus, or due to direct penetration of the chest. The lack of response to drainage may indicate a tracheal or bronchial tear. As in non-traumatic pathology, a tension pneumothorax can produce dramatic shifts in the mediastinum, leading to impaired venous return, and significantly decrease cardiac output. Pneumomediastinum and pneumopericard are occasionally seen in pediatric chest trauma. A large opaque hemithorax suggests a diaphragmatic tear or a hemothorax. A hemopericardium is present as the cardiac silhouette is enlarged. It can cause tamponade and needs urgent puncture.

Traumatic aortic rupture is frequently rapidly fatal and results in widening of the superior mediastinum; however, traumatic venous tears are more frequent and also result in widening of the mediastinum. The presence of normal thymus often obscures the widening of the mediastinum, but some signs can help you to identify traumatic rupture (Fig. 14): displacement of the trachea and esophagus, displacement of catheters or tracheal–esophageal tubes, the

**Table 6.** Pediatric thoracic trauma: common and less common posttraumatic lesions

Common	Less common
Pulmonary contusion	Aortic injury
Rib fractures	Great vessel injury
Pneumothorax	Diaphragmatic injury

presence of apical pleural fluid, blurring of the aortic outline, opacification of the angle between the aorta and the left pulmonary artery, depression of main-stem bronchus, the presence of left apical pleura, obscuration of the aortic knuckle if left-sided, loss of paraspinal shadow, a large associated hemothorax, a fracture of sternum, and first ribs are associated injuries. These are no 100% reliable signs; however, an aortic rupture is unlikely if those signs are absent. An esophageal ultrasound or angiogram is recommended when aortic rupture is suspected.

Traumatic lung cysts are the result of lung compression or alveolar rupture. The distal lung tissue burst in balloon like manner (usually due to blunt trauma), as result of a fracture of the small bronchi due to sudden compression restricting the air flow. A thin-walled air-filled cyst appears (similar radiographic appearance as pneumatoceles). They appear on a chest X-ray or CT within 1–3 days of injury and resolve spontaneously. If multiple, differential diagnosis with a diaphragmatic rupture and abdominal visceral herniation is difficult on chest X-ray. A pneumothorax can be a complication of a ruptured pneumatocele.

Esophageal rupture is rare and usually occurs in the lower third. The esophageal content enters the mediastinum and can cause mediastinitis. Associated signs are pneumomediastinum, pneumothorax, and pleural effusion. An esophagogram with low-osmolar non-ionic contrast swallow or CT will confirm the diagnosis.

A traumatic diaphragmatic rupture is also rare and is seen in association with other significant injuries. Recognition is imperative because catastrophic complications can occur. It is most frequently caused by compressive blunt trauma. On chest X-ray, the gas-filled loops of bowel in chest cavity but often the hemithorax is largely opaque. Look for the position of the nasogastric tube. Left-sided hernias are more common because of the protective effect of liver on the right side. If no bowel is seen, an elevated or abnormal contour to the left hemidiaphragm, particularly when associated with basal opacities and pneumothorax, should raise the possibility. The CT is the examination of choice. If CT is negative and diagnosis is doubtful, non-ionic low-osmolar contrast studies can bring definitive diagnosis (Beaver and Laschinger 1992; Dubinsky and Low 1997; Friedlaender and Tsarouhas 2003; Hodgkinson et al. 1993; Kevill et al. 2002; Mitchell et al. 2000; Schafermeyer 1993; Sivit 2002).

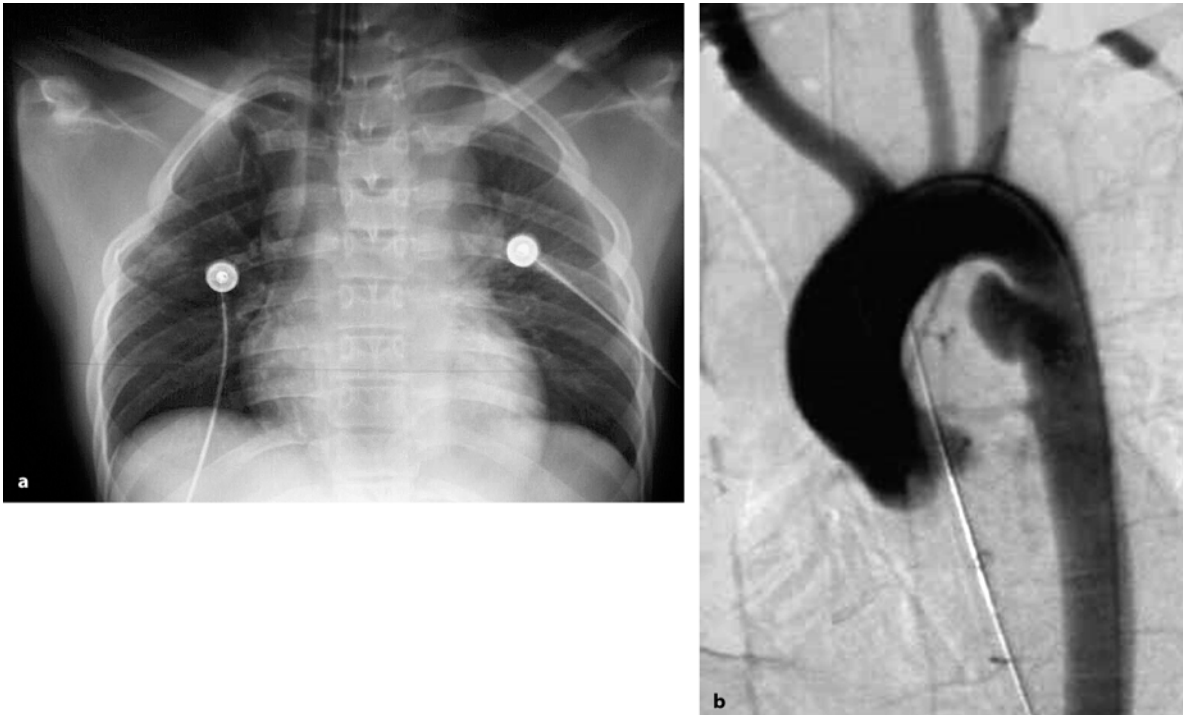


**Fig. 14.** **a** Indirect signs of a traumatic aortic rupture seen on chest X-ray in a polytrauma patient: Enlarged mediastinum displacement of the trachea and esophagus, displacement of catheters or tracheal–esophageal tubes, the presence of apical pleural fluid, blurring of the aortic outline, opacification of the angle between the aorta and the left pulmonary artery, depression of main-stem

bronchus, the presence of left apical pleura, obscuration of the aortic knuckle if left sided, loss of paraspinal shadow, a large associated hemothorax, a fracture of sternum, and first ribs are associated injuries. **b** The aortic rupture is demonstrated with an angiogram in this patient. More recently, esophageal ultrasound can be performed initially, followed by an angiogram if necessary

## 7.2.6 Conclusion

Pediatric thoracic emergencies can be situated at several levels. In first instance, the respiratory status of the child must be under control and then secondly, additional investigations can be performed. Airway obstruction is a common and dangerous emergency and can originate from the upper airway to the small airways. Clinical information can help to localize the pathology and avoid unnecessary imaging. When there is a superimposed infection of the airways or due to a carinal location, smaller mass lesions can evoke respiratory distress. A pulmonary infection that is not adequately responding to medical treatment can complicate with abscedation and empyema. A septic pleural effusion can result in a seriously ill child. Acute hypoxic respiratory failure needs intensive respiratory support and can be triggered by variable pulmonary insults. The premature baby in respiratory distress requiring artificial ventilation, barotrauma, and infection are emergencies. Surgical intervention for large intrathoracic masses, mostly congenital, cannot be delayed in a symptomatic baby. Perhaps more unexpectedly, respiratory emergencies can be the result of thoracic deformities or esophageal abnormalities. Traumatic thoracic emergencies can be fatal, but fortunately, the life-threatening traumatic lesions are rare.

## References

- Agrons GA, Courtney SE, Stocker JT et al. (2005) Lung disease in premature neonates: radiologic–pathologic correlation. *Radiographics* 25:1047–1073
- Alford BA, McIlhenny J, Jones JE et al. (1993) Asymmetric radiographic findings in the pediatric chest: approach to early diagnosis. *Radiographics* 13:77–93
- Altman KW, Wetmore RF, Marsh RR (1999) Congenital airway abnormalities in patients requiring hospitalization. *Arch Otolaryngol Head Neck Surg* 125:525–528
- Bar-Ziv J, Koplewitz BZ, Agid R (2001) Syllabus Postgraduate Course International Pediatric Radiology (Brunelle F, Strife JL eds), Paris, 28–29 May 2001. Springer, Berlin Heidelberg New York, pp 129–131
- Beaver BL, Laschinger JC (1992) Pediatric thoracic trauma. *Semin Thoracic Cardiovasc Surg* 4:255–262
- Beekman RP, Hazekamp MG, Sobotka MA et al. (1998) A new diagnostic approach to vascular rings and pulmonary slings: the role of MRI. *Magn Reson Imaging* 16:137–145
- Berdon WE (2000) Rings, slings, and other things: vascular compression of the infant trachea updated from the mid-century to the millennium. *Radiology* 216:624–632
- Berrocal T, Torres I, Gutierrez J et al. (1999) Congenital anomalies of the upper gastrointestinal tract. *Radiographics* 19:855–872
- Boiko T, Notterman D, Greenwald BM (1995) Acute hypoxic respiratory failure in children following bone marrow transplantation: an outcome and pathologic study. *Crit Care Med* 23:755–759

- Brissoulis GC, Venkataraman ST, Vasilopoulos AG et al. (2000) Air leaks from the respiratory tract in mechanically ventilated children with severe respiratory disease. *Pediatr Pulmonol* 29:127–134
- Chetty A, Mischler E, Gregg D (1997) Diagnosis of subglottic hemangioma by chest CT. *Pediatr Pulmonol* 23:464–467
- Chun K, Colombani PM, Dudgeon DL et al. (1992) Diagnosis and management of congenital vascular rings: a 22-year experience. *Ann Thorac Surg* 53:597–603
- Craig FW, Schunk JE (2003) Retropharyngeal abscess in children: clinical presentation, utility of imaging, and current management. *Pediatrics* 111:1394–1398
- Damm M, Eckel HE, Jungehülsing M et al. (1999) Management of acute inflammatory childhood stridor. *Otolaryngol Head Neck Surg* 121:633–638
- Dinwiddie R (2004) Congenital upper airway obstruction. *Paediatr Respir Rev* 5:17–24
- Donnelly LF, Bisset GS (1998) Airway compression in children with abnormal thoracic configuration. *Radiology* 206:323–326
- Donnelly LF, Frush DP (1999) Abnormalities of the chest wall in pediatric patients. *AJR* 173:1595–1601
- Dubinsky I, Low A (1997) Non-life-threatening blunt chest trauma: appropriate investigation and treatment. *Am J Emerg Med* 15:240–243
- Duiverman EJ, Sprij AJ, Nuysink M et al. (1999) Acute respiratoire benauwdheid bij kinderen. *Ned Tijdschr Geneesk* 143:197–201
- Duncan AW (1999) Emergency chest radiology in children. In: Carty H (ed) *Emergency pediatric radiology*. Springer, Berlin Heidelberg New York, pp 33–115
- Eber E (2004) Evaluation of the upper airway. *Paediatr Respir Rev* 5:9–16
- Fefferman NR, Pinkney LP (2005) Imaging evaluation of chest wall disorders in children. *Radiol Clin North Am* 43:355–370
- Friedlaender E, Tsarouhas N (2003) Traumatic diaphragmatic rupture in a pediatric patient: a case report. *Pediatr Emerg Care* 19:340–342
- Gay BB (1978) Radiologic evaluation of the nontraumatized child with respiratory distress. *Radiol Clin North Am* 16:91–112
- Ghyepes MT, Nussbaum E (1985) Radiographic–endoscopic correlations in the examination of airway disease in children. *Pediatr Radiol* 15:291–296
- Gibson AT, Steiner GM (1997) Imaging the neonatal chest. *Clin Radiol* 52:172–186
- Golder NDB, Lane R, Tasker RC (1998) Timing of recovery of lung function after severe hypoxemic respiratory failure in children. *Intensive Care Med* 24:530–533
- Hammer J (2004) Acquired upper airway obstruction. *Paediatr Respir Rev* 5:25–33
- Hedlund GL, Kirks DR (1990) Emergency radiology of the pediatric chest. *Curr Probl Diagn Radiol* 19:135–164
- Hodgkinson DW, O'Driscoll BR, Driscoll PA et al. (1993) Chest radiographs, vol II. *Br Med J* 307:1273–1277
- Katz M, Konen E, Rozenman J et al. (1995) Spiral CT and 3D image reconstruction of vascular rings and associated tracheo-bronchial anomalies. *J Comput Assist Tomogr* 19:564–568
- Kevill K, Wong AM, Goldman HS et al. (2002) Is a complete trauma series indicated for all pediatric trauma victims? *Pediatr Emerg Care* 18:75–77
- Kim et al (2000) US in the diagnosis of pediatric chest diseases. *Radiographics* 20:653–671
- Kirks DR, Fram EK, Vock P et al. (1983) Tracheal compression by mediastinal masses in children: CT evaluation. *AJR* 141:647–651
- Krul S, Heinonen KM, Kiekara O (1997) The first chest radiograph in neonates exhibiting respiratory distress at birth. *Clin Pediatr* 285–289
- Lander TA, Schauer G, Bendel-Stenzel E et al. (2004) Tracheal agenesis in newborns. *Laryngoscope* 114:1633–1636
- Lao J, Bostwick HE, Berezin S et al. (2003) Esophageal food impaction in children. *Pediatr Emerg Care* 19:402–407
- Lazar RH, Younis RT, Bassila MN (1991) Bronchogenic cysts: a cause of stridor in the neonate. *Am J Otolaryngol* 12:117–121
- Lee SS, Schwartz RH, Bahadori RS (2001) Retropharyngeal abscess: epiglottitis of the new millennium. *J Pediatr* 138:435–437
- Levy RJ, Helfaer MA (2000) Pediatric airway issues. *Crit Care Clin* 16:489–504
- Markowitz RI (1984) Radiologic assessment in the pediatric intensive care unit. *Yale J Biol Med* 57:49–82
- Mendelson DS (2001) Imaging of the thymus. *Chest Surg Clin N Am* 11:269–293
- Mercado-Deane M.-G., John SD (2001) Acute presentation of cystic and mass-like lesions of the chest in children. *Emerg Radiol* 8:75–84
- Metrangolo S, Monetti L, Meneghini L et al. (1999) Eight years' experience with foreign-body aspiration in children: What is really important for a timely diagnosis? *J Pediatr Surg* 34:1229–1231
- Meyer S, Reinhard H, Gottschling S et al. (2004) Pulmonary dysfunction in pediatric oncology patients. *Pediatr Hematol Oncol* 21:175–195
- Mitchell MW, Eichelberger MR, Newman KD et al. (2000) Thoracic injury in children: contemporary patterns of injury and management. *Pediatr Emerg Care* 16:69
- Nicolai T (2004) Therapeutic concepts in upper airway obstruction. *Paediatr Respir Rev* 5:34–39
- Ozturk H, Karnak I, Sakarya MT et al. (2001) Late presentation of Bochdalek hernia: clinical and radiological aspects. *Pediatr Pulmonol* 31:306–310
- Peters MJ, Tasker RC, Kiff KM et al. (1998) Acute hypoxemic respiratory failure in children: case mix and the utility of respiratory severity indices. *Intensive Care Med* 24:699–705
- Priestley MA, Helfaer MA (2004) Approaches in the management of acute respiratory failure in children. *Curr Opin Pediatr* 16:293–298
- Rencken I, Patton WL, Brasch RC (1998) Airway obstruction in pediatric patients. *Radiol Clin North Am* 36:175–187
- Rotta AT, Wiryawan B (2003) Respiratory emergencies in children. *Respir Care* 48:248–258
- Schafermeyer R (1993) Pediatric trauma. *Emerg Med Clin North Am* 11:187–205
- Seo T, Ando H, Watanabe Y et al. (1999) Acute respiratory failure associated with intrathoracic masses in neonates. *J Pediatr Surg* 34:1633–1637
- Shinkwin CA, Gibbin KP (1996) Tracheostomy in children. *J R Soc Med* 89:188–192
- Singh S, Bhende MS, Kinnane JM (2001) Delayed presentations of congenital diaphragmatic hernia. *Pediatr Emerg Care* 17:269–271
- Siegel MJ (1999) *Pediatric body CT*. Lippincott, Williams and Wilkins, Philadelphia, pp 65–100
- Silva AB, Muntz HR, Clary R (1998) Utility of conventional radiography in the diagnosis and management of pediatric airway foreign bodies. *Ann Otol Rhinol Laryngol* 107:834–838
- Sivit CJ (2002) Pediatric thoracic trauma: imaging considerations. *Emerg Radiol* 9:21–25
- Stroud RH, Friedman NR (2001) An update on inflammatory disorders of the pediatric airway: epiglottitis, croup, and tracheitis. *Am J Otolaryngol* 22:268–275
- Subramanyan R, Venugopalan P, Narayan R (2003) Vascular rings: an important cause of persistent respiratory symptoms in infants and children. *Indian Pediatr* 40:951–957
- Swischuk LE (2000a) The chest. In: Swischuk LE (ed) *Emergency imaging of acutely ill or injured child*, 4th edn. Lippincott, Williams and Wilkins, Baltimore, pp 1–150
- Swischuk LE (2000b) Upper airway, nasal passages, sinuses, and mastoids. In: Swischuk LE (ed) *Emergency imaging of acutely ill or injured child*, 4th edn. Lippincott, Williams and Wilkins, Baltimore, pp 151–184
- Swischuk LE, John SD (1999) *Emergency pediatric chest radiology*. Emerg Radiol 6:160–169



- Sztajn bok J, Grassi MS, Katayama DM et al. (1999) Descending suppurative mediastinitis: nonsurgical approach to this unusual complication of retropharyngeal abscesses in childhood. *Pediatr Emerg Care* 15:341–343
- Weiss I, Ushay HM, DeBruin W et al. (1996) Respiratory and cardiac function in children after acute hypoexemix respiratory failure. *Crit Care Med* 24:148–154
- Wong KS, Hung IJ, Wang CR et al. (2004) Thoracic wall lesions in children. *Pediatr Pulmonol* 37:257–263
- Zerella JT, Dimler M, McGill LC et al. (1998) Foreign body aspiration in children: value of radiography and complications of bronchoscopy. *J Pediatr Surg* 33:1651–1654

# Pediatric Emergencies: Non-traumatic Abdominal Emergencies

M.I. Tawil

## 7.3

### Contents

7.3.1 Introduction	621
7.3.2 Imaging	622
7.3.2.1 Abdominal Radiograph	622
7.3.2.2 Ultrasound	622
7.3.2.3 Contrast Radiographic Examination	622
7.3.2.4 Computed Tomography	622
7.3.2.5 Magnetic Resonance Imaging	623
7.3.3 The Diseases	623
7.3.3.1 Neonates	623
7.3.3.2 Infants and Young Children	628
7.3.3.3 Older Children	632
7.3.4 Conclusion	642
References	642

### 7.3.1 Introduction

Non-traumatic abdominal emergencies in children are different from those in adults and need to be treated with a greater degree of urgency than equivalent conditions in an adult. There are numerous disorders that can present as abdominal emergencies, ranging from a self-limiting condition, such as gastroenteritis, to life-threatening conditions

such as perforated appendicitis and midgut volvulus. These causes are age related and can broadly be divided into those that occur in the neonatal period, the infant and toddler, and the child aged 3 years to teenager (Table 1). It must be always kept in mind that, inevitably, there is some overlap and common entities can present atypically.

The presenting symptoms of an abdominal emergency in childhood are mainly vomiting, abdominal distension, abdominal pain and sometimes fever. A careful clinical history followed by thorough physical examination is extremely important in reaching a provisional diagnosis, although this may be difficult to achieve, particularly in a distressed child. Vomiting may be bilious or non-bilious. Distinction needs to be made between green bile-stained vomitus, which must always be taken seriously, and the sometimes yellowish colour of gastric content which is not necessarily indicative of pathology. Pain localisation in young children is poor, particularly in an irritable and uncooperative child, or in a child too young to communicate. The site of pain is therefore less helpful in making the diagnosis in children than adults. Findings on abdominal physical examination which can be challenging in young children depend on the cause and range from a normal abdomen on palpation to the rigidity of peritonitis, a palpable mass, or a distended abdomen. A provisional working diagnosis is made, based on history, examination and basic blood and urine analysis. A request for imaging will follow if immediate surgery is not indicated.

**Table 1.** Causes of abdominal emergencies

Neonates	Infants and toddlers	Toddler–teenage years
Atresia or stenosis of GIT	Gastroenteritis	Appendicitis
Malrotation with volvulus	Intussusception	Mesenteric adenitis
Meconium ileus	Mesenteric adenitis	Inflammatory bowel disease
Meconium plug syndrome	Bowel obstruction	Bowel obstruction
Hirschsprung's disease	Renal pathology	Renal pathology
Necrotising enterocolitis	Malrotation	Gynaecological disorders
Pyloric stenosis	Appendicitis	Abdominal malignancy
	Abdominal malignancy	Pancreatitis
	Metabolic disease	Metabolic disease
	Meckel's diverticulum	Meckel's diverticulum
	Abscess	Hepato-biliary pathology
		Abscess
		Haematological disorders

## 7.3.2 Imaging

The timing and the choice of the imaging technique are based on the clinical problem and best made after a discussion between the clinician and the radiologist. This is important for making the diagnosis and planning for specific therapy.

### 7.3.2.1 Abdominal Radiograph

Imaging usually starts with a supine abdominal radiograph. The entire abdomen from the dome of the diaphragm to the obturator foramina must be imaged; otherwise significant abnormalities, such as free air under the diaphragm and air in the hernial orifices, may be missed. A review of an abdominal radiograph should provide answers to the following questions:

1. Is gas present throughout large and small bowel?
2. If there is gaseous distension, is it both large and small bowel or is it confined to one?
3. Is the caecum visible in the right iliac fossa or right abdomen?
4. Are the stomach, large and small bowel correctly sited in the abdomen?
5. Is there air in the hernial orifices?
6. Is there organomegaly: liver, spleen, kidneys?
7. Is there a mass lesion? If so, what is the suspected organ of origin?
8. Is there any calcification within the organs, mass or peritoneum?
9. Are the psoas outlines visible? Loss of psoas outline is a soft sign of intra-abdominal pathology.
10. Are the properitoneal fat stripes displaced?
11. Are the lung bases clear?
12. Are the bones and disc spaces normal?

Although this is a long list of questions, each should be mentally answered and in practice this only takes a few seconds. If there is doubt about free air or a need to identify fluid levels, an erect or a decubitus film is useful in providing specific diagnostic information such as presence of intra-abdominal free air and bowel obstruction. The radiographic findings in abdominal emergencies may be minimal or non-specific, and further imaging is often required for making the diagnosis.

### 7.3.2.2 Ultrasound

Ultrasound is widely available and extremely helpful in both establishing and excluding abdominal pathology. Abdominal ultrasound should include both examination of the organs and bowel, the latter requiring the use of high-frequency linear-array transducer and graded compression. It must be

remembered that ultrasound is operator dependent and the findings should always be correlated with the clinical findings. The questions to be addressed with ultrasound are:

1. Are the liver, spleen, gallbladder, kidneys and pelvic organs present, correctly sited, and have they normal echo texture?
2. Is there free fluid?
3. Are there mesenteric nodes?
4. Is there free fluid, either in the pelvis, subdiaphragmatic areas, paracolic gutter or between bowel loops?
5. Is there a mass? If so, what is the likely organ of origin? Is it solid or cystic, or does it have a mixed echo texture? Are the margins well or poorly defined? Is there calcification?
6. Is the bowel wall of normal thickness?
7. Is the intestinal peristalsis normal, excessive or absent?

### 7.3.2.3 Contrast Radiographic Examination

Contrast studies are usually performed in newborn infants to investigate bowel obstruction or to answer questions raised by abdominal plain film. Non-ionic water soluble contrast media must be used because of the risk of lung aspiration and bowel perforation. The type of examination will depend on the clinical indication and should provide answers to the following questions:

1. Does the stomach lie on the left?
2. Is the gastric emptying normal?
3. Is the duodenojejunal junction normally positioned?
4. Are the large and small bowel correctly sited in the abdomen?
5. Is the bowel obstructed? If so, where is the level and what is the cause?
6. Is the calibre of the small and large bowel normal?
7. Is there inspissated meconium in the ileum or large bowel?
8. Is there a transitional zone in the large bowel?

### 7.3.2.4 Computed Tomography

The majority of abdominal emergencies in children can be adequately assessed using ultrasound. Computed tomography is required in selected circumstances but should be agreed on an individual basis. It is used more frequently in the United States than in Europe but is invaluable in appropriate circumstances. Because of the higher stochastic radiation risks in children as compared with adults the examination should be individually tailored with the area of coverage, slice thickness and pitch, and milliampere level adjusted to answer the clinical questions. Most paediatric radiologists presently carry out an IV contrast-enhanced CT exam without oral contrast and do not perform a non-contrast scan. The CT is required in abdominal tumours and is particularly helpful for the complete demonstration of intra-abdominal abscesses.

### 7.3.2.5 Magnetic Resonance Imaging

Magnetic resonance imaging is seldom required as a primary imaging technique but supplements CT and ultrasound in selected cases, e.g. magnetic resonance cholangiopancreatography (MRCP) in jaundice, or for staging of abdominal malignancy where, if it is freely available, the use of MR for GI studies is increasing.

## 7.3.3 The Diseases

### 7.3.3.1 Neonates

#### Necrotising Enterocolitis

Necrotising enterocolitis (NEC) is a severe illness primarily affecting preterm infants in the first few weeks of life. It is associated with multiple factors such as hypoxia, early and rapid enteral feeding, umbilical vessel catheterisation and polycythaemia. Ten to 15% of cases occur in full term infants, especially those with congenital heart disease (Ostlie et al. 2003). The condition is thought to be due to combination of ischaemia and infection from organisms colonising the bowel. It presents clinically with feeding intolerance, increased aspirate from the stomach, vomiting which may be bile stained and abdominal distension. The neonate may rapidly deteriorate and become shocked.

Diagnostic imaging has an important role in the early diagnosis of NEC. An antero-posterior supine abdominal film, supplemented by a cross-table lateral or left lateral decubitus film, should be performed if NEC is clinically suspected (Fotter and Sorantin 1994). The decubitus film is required to demonstrate small amounts of free air. The early radiographic findings are localised or generalised dilated bowel loops, with one or more loops becoming fixed on sequential films, bowel wall thickening and intraperitoneal fluid (Carty and Brereton 1983). These findings are non-specific, but in the appropriate clinical setting are suggestive of NEC. Intramural air is more specific feature for NEC and can be seen either as multiple bubble-like or curvilinear lucencies (Fig. 1). The former gas pattern can be seen in gas admixed with stool, which is rarely seen in premature infants (Patriquin et al. 1984). The intramural air can extend into the portal venous circulation and appear as branching linear lucencies extending to the periphery of the liver. The radiographic features of free intraperitoneal air on the supine film are air collection over the upper abdomen “football sign”, visualisation of both sides of the bowel wall “rigler’s sign” or air outlining the falciform ligament. A cross-table lateral film may show a small air collection just beneath the anterior abdominal wall. Radiographic detection of intraperitoneal free air is only possible in approximately 50% of perforated cases. This is probably because the site of perforation is quickly walled off by adjacent loops of bowel.



**Fig. 1.** Necrotising enterocolitis. Plain radiograph shows gas-filled dilated loops of bowel with linear and curvilinear intramural gas collections

Ultrasound is a useful examination particularly when the radiographic findings are non-specific. It is very sensitive for detection of portal venous air (Merritt et al. 1984), which appears as highly echogenic particles flowing within the portal vein and highly echogenic areas within the liver. Ultrasound can also demonstrate bowel wall thickening, intramural air and intraperitoneal fluid. The sonographic detection of NEC findings may precede the radiographic features (Bomelburg and von Lengerke 1992; Lindley et al. 1986). Contrast studies are not performed in the acute stage, but they are useful tools in the assessment of bowel strictures which are late complications of NEC.

#### Intestinal Obstruction

Intestinal obstruction can be divided into high and low intestinal obstruction. The distinction is important as neonates with high obstruction usually need little or no further imaging after radiography. Low intestinal obstruction requires a contrast enema examination which often provides a diagnosis and may be therapeutic for some conditions, such as meconium ileus and meconium plug syndrome. The common causes of intestinal obstruction in neonates are shown in Table 2. Anorectal malformations are usually evident on physical examination and are not discussed further.



**Table 2.** Common causes of intestinal obstruction in neonates

High intestinal obstruction	Low intestinal obstruction
Malrotation and midgut volvulus	Ileal atresia
Duodenal obstruction	Meconium ileus
Duodenal atresia/stenosis	Meconium plug syndrome
Duodenal web	Hirschsprung's disease
Annular pancreas	Anorectal malformation
Jejunal atresia	

### Duodenal Obstruction

Duodenal obstruction is a congenital malformation due to a variety of conditions which can be classified as either intrinsic or extrinsic lesions. Intrinsic lesions, including duodenal atresia, stenosis and a web, are believed to be due to failure of recanalisation of the bowel lumen (Bailey et al. 1993). Failure of the embryonic pancreatic tissue to rotate around the duodenum leads to the development of annular pancreas. Other causes of extrinsic compression of the duodenum are peritoneal bands, a duplication cyst and a preduodenal portal vein. Combinations of various anatomical abnormalities producing duodenal obstruction may occur. The presenting symptoms and signs include vomiting, which is usually bilious, abdominal distension and in severe cases dehydration. Neonates with duodenal atresia present acutely within the first few hours of life, whereas infants with internal or external duodenal stenosis present at a variable time depending on the severity of the obstruction.

In cases of complete duodenal obstruction, abdominal radiographs typically demonstrate a distended stomach and duodenal cap with air–fluid levels – the “double-bubble sign” (Fig. 2) – and gasless distal bowel unless a bifid hepatopancreatic duct is present (Kassner et al. 1972) which allows air to bypass the site of atresia; this latter is extremely rare. In cases of partially obstructing lesions, the double-bubble sign may or may not present and air is usually visible in the distal bowel. Ultrasound can demonstrate the double-bubble sign and allows visualisation of the rare causes of duodenal obstruction such as a duplication cyst and preduodenal portal vein. Complete obstruction of the duodenum may be identified on antenatal ultrasound as fluid-filled bubbles complicated by polyhydramnios (Lawrence et al. 2000). In the correct clinical setting, a contrast study is unnecessary in the presence of the classical double-bubble sign and gasless distal bowel; however, if the radiographic features are not typical, a contrast study is required to exclude malrotation.

Approximately 25% of patients with duodenal atresia have Down's syndrome (Dalla Vecchia et al. 1998). Other associations include malrotation, other intestinal atresia, congenital heart disease, biliary anomalies and Vater syndrome (vertebral, anorectal, cardiac, tracheo-oesophageal fistula and radial and renal dysplasia) spectrum (Bailey et al. 1993).



**Fig. 2.** Duodenal atresia. Abdominal radiograph shows distended stomach and duodenal bulb giving the appearance of “double bubble” sign. No air is present distal to the duodenum

### Small Bowel Atresia

Intestinal atresia is more common than stenosis and occurs more frequently in the ileum than in the duodenum and large bowel. Unlike duodenal atresia, it is generally considered to be due to an antenatal vascular accident leading to sterile ischaemia and obliteration of the small bowel lumen. The diagnosis may be suspected antenatally on ultrasound examination (Tam and Nicholls 1999), which demonstrates bowel dilatation and polyhydramnios. Neonates usually become symptomatic in the first day of life with bilious vomiting, abdominal distension and failure to pass meconium. The lower the atresia, the later the presentation as it takes time for obstruction to develop.

Abdominal radiographs will reveal a few dilated loops of bowel in cases of jejunal atresia and multiple dilated loops in cases of ileal atresia. A localised bowel dilatation immediately proximal to the atresia (Johnson and Robinson 1984) and calcification indicating meconium peritonitis may also be present. The radiographic features of ileal atresia may appear similar to those seen in meconium ileus and distinguishing these two conditions on plain films can be difficult. In the setting of low intestinal obstruction, neonates should be evaluated with contrast enema studies, rather than upper gastrointestinal contrast studies. On contrast enemas, neonates with distal ileal atresia typically show a narrow-calibre empty colon “microcolon”, and a collapsed terminal ileum with atresia. Contrast does not enter the dilated proximal bowel. The colon usually has a normal calibre and may contain a few meconium plugs in cases of jejunal and proximal ileal atresia. In a rare variant “apple peel atresia”, the distal ileum spirals around a rudi-

mentary mesentery and appears as an apple peel on reflux of contrast (Seashore et al. 1987).

Small bowel stenosis is shown on contrast follow-through examinations as calibre change. Approximately 30% of cases of jejunal and ileal atresia are associated with other gastrointestinal anomalies such as malrotation, meconium ileus or gastroschisis (Dalla Vecchia et al. 1998).

### Malrotation and Midgut Volvulus

Intestinal malrotation is a consequence of failure of complete rotation and fixation of the intestine during its return to the abdominal cavity in intrauterine life (Long et al. 1996). During normal embryonic development the proximal duodenojejunal and distal ileocolic segments of the bowel rotate 270° anticlockwise around the mesenteric vessels. This results in a broad-based small bowel mesentery with its attachment extending from the duodeno-jejunal junction in the left upper abdomen to the ileocaecal valve in the right iliac fossa. This prevents the mesentery from twisting around the superior mesenteric artery. Malrotation results in an abnormal position and shortening of the mesenteric root which predispose the small bowel to twisting and development of volvulus. Less frequently, the bowel obstruction in malrotation is secondary to peritoneal (Ladd's) bands or internal hernia. Of patients with malrotation, 75% present in the neonatal period and 80–90% of patients present during the first year of life (Torres and Ziegler 1993; Ford et al. 1992).

The most common presenting symptom is bilious vomiting which may be associated with abdominal pain. Older children may present with a long history of recurrent episodes of colicky abdominal pain and vomiting which may be non-bilious. Abdominal distension is often present when there is compromise of bowel vascularity due to the volvulus around the superior mesenteric artery. This is a surgical emergency requiring early diagnosis to prevent the catastrophic complications of the midgut volvulus and the ischaemic necrosis of the bowel. Presentation of malrotation later in life may also occur acutely with the same life-threatening implication if the diagnosis is missed.

The abdominal radiograph in acute presentation of malrotation may be normal if the obstruction is partial. In more total obstruction, there is air in the stomach but none distally. Presence of right-sided jejunal markings and colonic gas on the left are suggestive of the diagnosis (Fig. 3a; Berdon 1995). Dilatation of the proximal duodenum is rare and, when present, suggests duodenal atresia or duodenal stenosis. The diagnosis is made by upper gastrointestinal studies which should be performed in all suspected cases. In normal rotation, the duodenojejunal junction lies to the left of the midline at the same level or more superior to the duodenal bulb and should lie under the gastric antrum (Long et al. 1996). In malrotation, the duodenojejunal junction is abnormally positioned and usually lies inferior and to the right of this; however, in approximately



**Fig. 3.** Malrotation. **a** Abdominal radiograph shows the distribution of the small bowel gas on the right and colonic gas on the left. **b** Barium meal shows typical spiral configuration of the duodenum

2% cases the duodenojejunal junction may have a normal position and the malrotation is related to an abnormal caecal position. In such cases and when the position of the duodenojejunal junction is equivocal on upper gastrointestinal studies, following the contrast through the small bowel to determine the position of the caecum is helpful. In volvulus, the duodenum and the proximal small bowel have a spiral configuration “corkscrew appearance” because they twist around the superior mesenteric artery (Fig. 3b).

Ultrasound scan may allow the detection of malrotation by demonstrating abnormal relative positions of the superi-

or mesenteric artery (SMA) and superior mesenteric vein (SMV). A normal relationship between the SMA and SMV does not exclude malrotation, but an abnormal relationship is likely to predict malrotation (DuFour et al. 1992). All patients with abnormal vascular relationship on ultrasound should have contrast studies for further assessment (Weinberger et al. 1992). The sonographic diagnosis of volvulus is specific and appears as clockwise whirlpool sign due to clockwise rotation of the SMV and the mesentery around the SMA (Shimanuki et al. 1996; Pracros et al. 1992).

### Meconium Ileus

Meconium ileus (MI) accounts for approximately 20% of neonatal intestinal obstruction and results primarily from accumulation of a sticky and inspissated intraluminal meconium in the terminal ileum. Although it can rarely occur in otherwise normal neonates (Fakhoury et al. 1992), the majority of patients with this condition have cystic fibrosis. Meconium ileus is the initial presentation in 10–15% of all patients with cystic fibrosis due to intestinal and pancreatic dysfunction (Mushtaq et al. 1998; Ziegler 1994). Most patients are usually normal at birth but soon present clinically with bilious vomiting, abdominal distension and delayed passage of meconium. Some patients present at birth with an abdominal mass due to intrauterine volvulus caused by inspissated meconium.

The diagnosis of MI may be suspected on the abdominal radiograph which may demonstrate multiple dilated loops of bowel with few or no air–fluid levels, soap bubble appearance in the right lower quadrant due to mixed gas and inspissated meconium. These findings are non-specific and can be seen in other conditions such as ileal atresia and Hirschsprung's disease (Carty and Brereton 1983). The most frequent finding is of non-specific small bowel dilatation. At contrast enema a microcolon and multiple intraluminal filling defects representing inspissated meconium (Fig. 4) at the point of obstruction in the terminal ileum are seen. Half of neonates with MI present with uncomplicated intestinal obstruction (Agrons et al. 1996). In such cases, the obstruction can usually be relieved non-surgically by refluxing water-soluble contrast medium into the proximally dilated ileum. The fluid and electrolyte status of the patient must be closely monitored if hypertonic water-soluble contrast media are used. Though the reported success of enema relieving MI is up to 60% (Kao and Franken 1995; Docherty et al. 1992). This figure often includes those in whom meconium plug is the underlying diagnosis, in which an enema is virtually 100% successful. Repeated enemas may be required in some cases to relieve the obstruction completely provided the infant remains well.

Intra-peritoneal calcification is a result of meconium peritonitis secondary to perforation. The calcification is seen most typically in the paracolic gutters, subdiaphragmatically, and may extend through the hernial orifices into the scrotum.



**Fig. 4.** Meconium ileus. Contrast enema radiograph shows microcolon and contrast outlining inspissated pellets within the terminal ileum. The small bowel is grossly dilated

Operative intervention is reserved for those who fail non-operative treatment as well as those with complications. The complications of MI are intrauterine volvulus, atresia, perforation, meconium peritonitis and pseudocyst formation. Antenatal ultrasound may show dilated bowel, hyperechoic bowel, ascites and calcification (Irish et al. 1997); however, the sonographic findings have low specificity, being found in cases with jejunoileal atresia, volvulus and meconium peritonitis (Casaccia et al. 2003).

### Meconium Plug Syndrome

Meconium plug syndrome, also known as functional immaturity of the large bowel or small left colon syndrome, is the most common cause of functional large bowel obstruction in neonates. Risk factors associated with this condition include prematurity, neonatal hypoglycaemia, maternal diabetes and mothers who received magnesium sulphate for eclampsia (Krasna et al. 1996; Davis and Campbell 1975). Clinical presentation is with delayed passage of meconium, vomiting and abdominal distension, although these patients are generally not critically ill. Physiological passage of the first meconium stool may be delayed in tiny premature infants and this is usually not a cause of concern unless vomiting or abdominal distension develops.



**Fig. 5.** Meconium plug syndrome. Contrast enema radiograph shows small calibre sigmoid that gradually tapers proximally to the normal calibre colon that contains many meconium plugs. The dilated rectum differentiates this from Hirschsprung's disease



**Fig. 6.** Hirschsprung's disease. Lateral contrast enema radiograph shows a transitional zone from dilated ganglionic sigmoid colon to aganglionic rectum

Diffusing dilated loops of bowel and paucity of gas in the rectum are usually demonstrated on abdominal radiographs. Contrast enema studies show multiple filling defects due to retention of meconium within a relatively normal calibre large bowel "meconium plug syndrome". A transitional zone from slightly dilated ascending and transverse colon to a narrowed descending colon at the splenic flexure "small left colon syndrome" may be seen (Fig. 5). In contrast to Hirschsprung's disease, the calibre of the rectum is normal and the obstruction is usually relieved by contrast enema. Rectal biopsy, however, is indicated if the obstruction remains unresolved following the enema or the diagnosis of Hirschsprung's disease is suspected radiologically (Berdon et al. 1977).

### Hirschsprung's Disease

Hirschsprung's disease is the most common cause of true low intestinal obstruction in neonates, affecting approximately 1 in 5000 live births (Russell et al. 1994; Spouge and Baird 1985). The disease is characterised by congenital aganglionosis of the rectum and the distal large bowel. The involved bowel segment becomes hypertrophic and acts as a functional stenosis. The affected colon usually involves the rectum or the rectum and a short distal segment of the sigmoid colon, in 80% of cases. In a few cases, the aganglionosis is limited to the internal anal sphincter "ultrashort segment Hirschsprung's disease" or involves the entire colon "total colonic aganglionosis" (Cass and Myers 1987). In the majority of cases, the diagnosis is made during the neonatal period. The infants present with abdominal distension, vom-

iting and delayed passage of meconium. Approximately 10% of cases present outside the neonatal period with severe constipation, abdominal distension and failure to thrive. Enterocolitis associated with Hirschsprung's disease is a serious complication presenting with severe diarrhoea which can be difficult to differentiate from gastroenteritis. Delay in the diagnosis of Hirschsprung's disease increases the risk of developing enterocolitis associated with the disease (Vieten and Spicer 2005; Singh et al. 2003).

The abdominal radiographs typically show features of low intestinal obstruction with multiple dilated loops of bowel. Neonates with suspected Hirschsprung's disease require further evaluation with contrast enema studies. It is essential to obtain an early filling view in a lateral position using a soft catheter inserted just inside the anus in order to assess the anorectal junction and the rectum. Findings on contrast enema include an abrupt or gradual transitional zone from a dilated normally innervated proximal colon to an aganglionic narrow rectum and distal colon, mostly seen at the rectosigmoid junction (Fig. 6; Taxman et al. 1986; Rosenfield et al. 1984). Absence of the transitional zone does not exclude the diagnosis of Hirschsprung's disease. Irregular contraction "saw-tooth appearance" in the aganglionic segment and delayed clearance of the contrast from the colon are additional supportive features for the diagnosis of Hirschsprung's disease. When the disease is confined to the rectum, the sigmoid colon appears larger than the rectum "abnormal rectosigmoid ratio". In total colonic aganglionosis, the colon may appear normal or short and small in calibre mimicking microcolon (DeCampo et al. 1984). The diagnostic sensitivity of the contrast en-



ema decreases in cases of short lesions, total colonic aganglionosis and in newborns affected with the disease. Rectal biopsy provides a definitive diagnosis of Hirschsprung's disease, and is indicated in all suspected cases.

### 7.3.3.2 Infants and Young Children

#### Hypertrophic Pyloric Stenosis

Hypertrophic pyloric stenosis (HPS) is a relatively common condition in which the pyloric muscle is abnormally thickened resulting in gastric outlet obstruction. Although there is a family history in up to 16% of cases (Poon et al. 1996), the exact aetiology remains unknown. Male infants are more commonly affected than females and there is a predilection for the first born child (Van de Schouw et al. 1994). Infants with HSP typically present at age of 4–6 weeks with non-bilious projectile vomiting. The majority of cases are relatively well at presentation, but prolonged vomiting can lead to dehydration and eventually hypochloreaemic hypokalaemic metabolic alkalosis (Chen et al. 1996). The diagnosis is usually suspected from the typical clinical presentation and palpation of an olive-shaped mass in the epigastric region during a test feed.

Ultrasound is the imaging modality of choice for diagnosis of HSP with an accuracy approaching 100% (Neilson and Hollman 1994; Hernanz-Schulman et al. 1994). Ultrasonography allows objective measurement of the pyloric muscle thickness and length and is best performed using a linear-

array high-frequency probe with gentle abdominal pressure. The transverse scan demonstrates a thick hypoechoic ring representing hypertrophied pyloric muscle measuring 3 mm or more on one side of the lumen with echogenic central mucosa (Fig. 7). On the longitudinal scan the pyloric canal length measures more than 16 mm. Other findings include non-relaxed pyloric canal, protrusion of the central mucosa into the antrum “the nipple sign” and active gastric peristalsis. Pyloric muscle thickness <2 mm is normal (O’Keeffe et al. 1991). Pylorospasm may mimic hypertrophic pyloric stenosis for at least a portion of a sonographic study (Cohen et al. 1998). In infants with borderline measurements, particularly those who present early, a follow-up scan is often diagnostic. Over-distended stomach with air may displace the pylorus posteriorly rendering it difficult to visualise. In such cases, placement of a nasogastric tube and administration of small amounts of fluid to fill the gastric antrum may be required for adequate evaluation of the pylorus. The stomach should be emptied at the end of the scan. This, however, is invasive unless one is in place and a repeat attempt when the baby is burped may prove effective.

The diagnosis of HSP can also be established by upper gastrointestinal contrast studies (Olson et al. 1998). This is particularly helpful when the ultrasound is equivocal or there is still a clinical concern despite a normal scan. The typical contrast studies findings are active gastric peristalsis, failure of relaxation of the pylorus, elongated narrowed pyloric canal “string sign”, and linear tracks of contrast separated by folded compressed mucosa “double-track sign”.

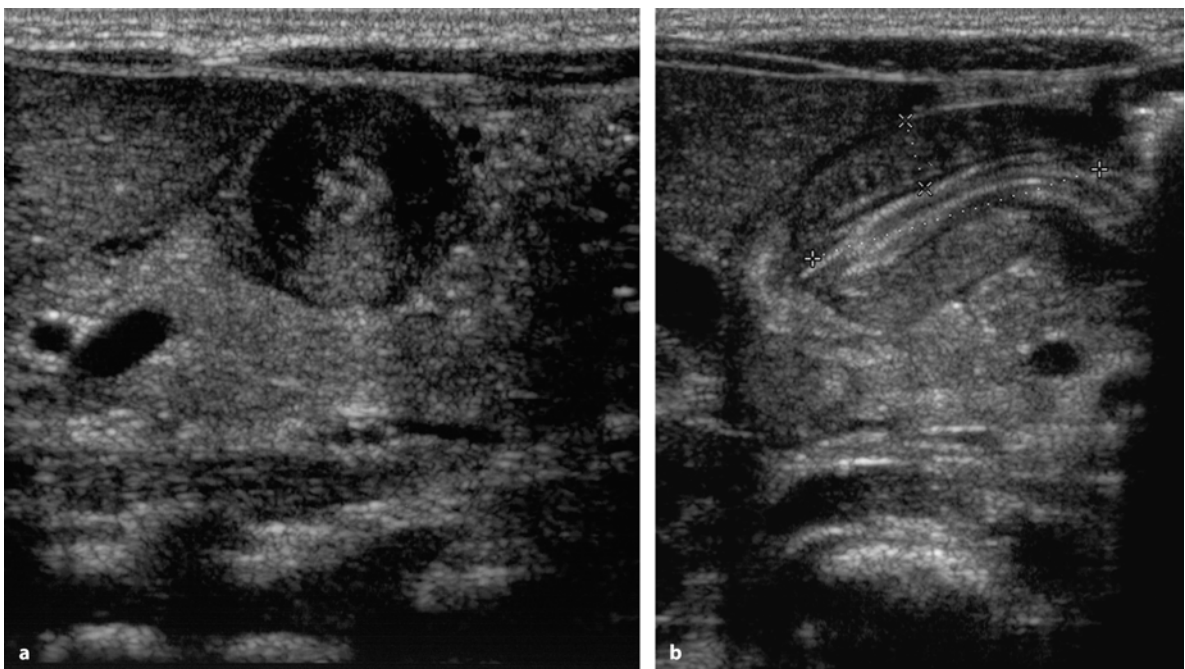


**Fig. 7.** Hypertrophic pyloric stenosis. **a** Transverse ultrasound section through the pylorus shows central compressed echogenic mu-

cosa surrounded by hypoechoic hypertrophied muscle. **b** Longitudinal section shows elongated pyloric canal and muscle thickening

### Intussusception

Intussusception is a common abdominal surgical emergency occurring when a segment of bowel, the intussusceptum, prolapses and invaginates into another segment, the intussusciptum. It predominantly occurs in the 6- to 24-month age group (Miller et al. 1995) but may occur in older children and even in adults (Azar and Berger 1997). It is often seasonal, being common in the UK in the later spring and autumn (Rosenfeld and McHugh 1999). The clinical presentation varies widely from shock with peripheral shut down to vomiting or lethargy alone. The classical symptoms and signs of abdominal pain, red currant jelly stool and palpable abdominal mass are only present in 50% of cases (Daneman and Alton 1996; Lim et al. 1994). Four types of intussusception are described: ileo-colic; ileo-ileocolic; colo-colic; and ileo-ileal. Ileo-colic is the most frequent and occurs in 90% of cases. In the vast majority of children, the cause is unknown “idiopathic” but is probably related to hyperplasia of lymphoid tissue in the distal ileum during a generalised viral infection (Stringer et al. 1992). Up to 5% of the cases are caused by abnormalities of the gastrointestinal tract that act as leading point (Table 3). The incidence of an identifiable pathological leading point increases with the patient’s age (Blakelock and Beasley 1998).

Although an abdominal radiograph is often requested, this examination is often unhelpful in the diagnosis of intussusception. The most frequent plain-film findings are a soft tissue mass, paucity of the right lower quadrant gas and small bowel obstruction (Ratcliffe et al. 1992b). The intussusceptum may be seen invaginating the distal bowel and is known as the “crescent sign”. The “target sign”, which consists of two concentric circles of fat density to the right of the spine, has been described (Ratcliffe et al. 1992a). The presence of normal gas and feces in the caecum located in the right iliac fossa excludes intussusception; however, in children the sigmoid colon may lie in the right lower quadrant of the abdomen and can be misinterpreted for the caecum (Fiorella and Donnelly 2001). The plain films are therefore unreliable diagnostically (Hernandez et al. 2004; Sargent et al. 1994) and generally taken to exclude complications such as a perforation, or other pathology.

Ultrasound is a reliable imaging technique for diagnosis of intussusception and has 100% diagnostic accuracy in expert hands (Verschelden et al. 1992; Wood et al. 1992). Ultrasound should be performed with a high-frequency linear-array probe. The intussusception in transverse section has a hypoechoic outer ring and a hyperechoic centre and is known as the target or doughnut sign (Fig. 8). In longitudinal section there are alternating hypoechoic and echogenic layers giving a pseudokidney or sandwich appearance. The hypoechoic layer is due to oedematous bowel wall and the echoic centre, the mucosa and trapped intraluminal content. Multiple layers indicate an ileo-ileocolic lesion. Enlarged lymphoid tissue may be seen in the intussuscepting mass. Small amount of free fluid are frequent between the bowel loops

**Table 3.** Common pathological lead points (PLP) in intussusception

Focal PLP	Diffuse PLP
Meckel’s diverticulum	Henoch-Schonlein purpura
Intestinal polyps	Cystic fibrosis
Duplication cyst	Coeliac disease
Lymphoma	

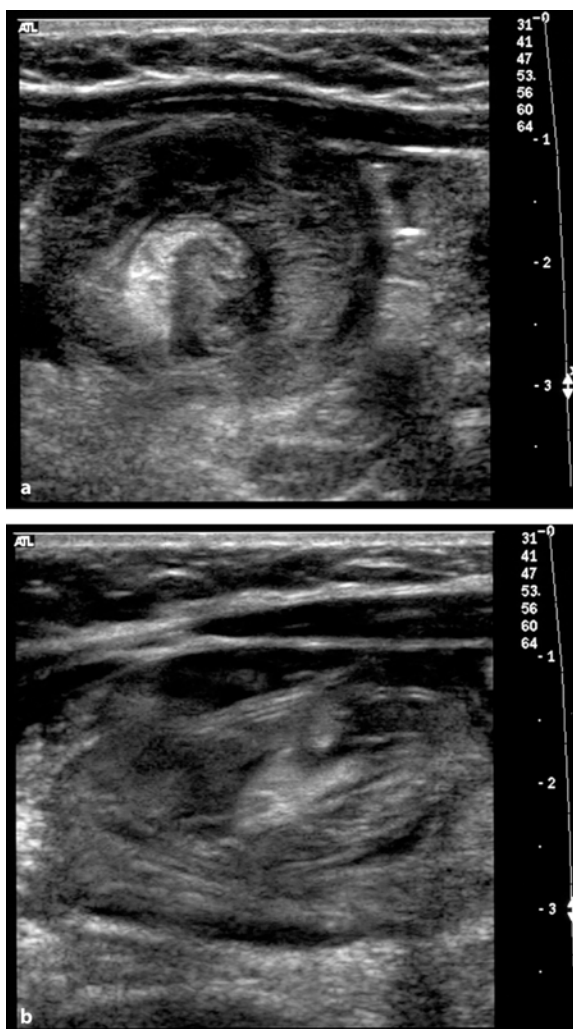


**Fig. 8.** Intussusception. **a** Transverse US image shows concentric layers of bowel and eccentric echogenic crescent of mesenteric fat. **b** Longitudinal section shows the appearance of “pseudokidney” sign

surrounding an intussusception, or in the pelvis or subhepatic region. Absence of colour flow and fluid trapped between the entering and returning limbs of the intussusceptum are said to be predictors of poor prognosis for reduction (Del-Pozo et al. 1996; Lim et al. 1994). Ultrasound can also be useful for documenting the presence of pathological lead point (Navarro et al. 2000).

Non-operative reduction is the treatment of preference. Reduction is only attempted once the patient is clinically stable and has been evaluated by the surgeon. Dehydration and shock must be corrected before reduction is attempted. Peritonitis and radiographic evidence of perforation are contraindications for enema reduction. Hydrostatic (barium, water soluble contrast, saline) or pneumatic reduction may be used either under fluoroscopic or sonographic guidance (Rosenfeld and McHugh 1999; Hadidi and El Shal 1999). Most paediatric radiologists presently use pneumatic reduction under fluoroscopic guidance, but hydrostatic reduction under ultrasound guidance is sometimes used. The choice of technique used will depend on the experience and personal preference, but the success rate of either technique should be at least 70% in experienced hands. Confirmation that the reduction has occurred is the demonstration of contrast or air in the small bowel. This may not occur if the ileo-caecal valve is oedematous and gives the impression that the reduction has been unsuccessful. The approach to this situation should be continued clinical observation of the patient. Successful reduction is confirmed by recovery and absence of pain. If symptoms present, a repeat attempt at reduction is an effective approach with a high success rate (Navarro et al. 2004). The perforation rate from attempted reduction enema should be <1% in experienced hands (Daneman and Navarro 2003). The recurrence rate of intussusception after successful reduction is approximately 10%. Intussusception reduction is painful and should be performed with adequate analgesia.

### Gastroenteritis

Gastroenteritis is a short, self-limiting, but common illness in infants and young children worldwide. Viruses are the leading cause and rotavirus accounts for up to 60% of cases, particularly during the winter months. Other viruses, particularly enteric adenovirus, astrovirus and norovirus, are also important causative agents (Boga et al. 2004; Oh et al. 2003). Children with viral gastroenteritis generally present with watery diarrhoea, vomiting and often with low-grade fever (Shinozaki et al. 1991; Uhnnoo et al. 1986). Severe abdominal pain, bloody stool, prolonged diarrhoea and raised white blood count and erythrocyte sedimentation rate are suggestive of a bacterial aetiology. The most common bacteria are *Salmonella*, *Campylobacter*, *Yersinia* and *Escherichia coli*. The abdominal pain may be severe and associated with tenderness or rectal bleeding, and may clinically simulate acute appendicitis (Puylaert et al. 1988) or intussusception.

The role of imaging is therefore to exclude other causes of an acute abdomen in those with atypical clinical presentation or severe cases. Radiographs in gastroenteritis are often normal but may have variable appearances. The most typical finding is the presence of multiple distended loops of bowel with air–fluid levels on decubitus or erect films.



**Fig. 9.** Abdominal radiograph in a child with cryptosporidium gastroenteritis shows severe gaseous distension

Gaseous distension can be very severe and is specially seen with cryptosporidial infection (Fig. 9). The ultrasound appearances vary with the stage of the disease and range from demonstration of excessive peristalsis to ileus with little movement. The bowel wall thickness is usually normal in viral infection, but changes in the ileal wall may be visualised during the acute stage (Bass et al. 2004). The hallmark of bacterial infection is mucosal and submucosal thickening of the bowel wall, most often the terminal ileum and caecum (Puylaert et al. 1989). Enlarged mesenteric lymph nodes are usually present and colour Doppler may demonstrate increased mucosal blood flow (Quillin and Siegel 1994). The differential diagnosis of bacterial ileo-cecitis is Crohn's disease. In Crohn's disease the bowel wall thickening and increased colour flow tend to involve all layers.

### Meckel's Diverticulum

Meckel's diverticulum is a common form of congenital abnormality of the small bowel, resulting from an incomplete obliteration of the omphalomesenteric duct. The condition becomes symptomatic due to development of complica-



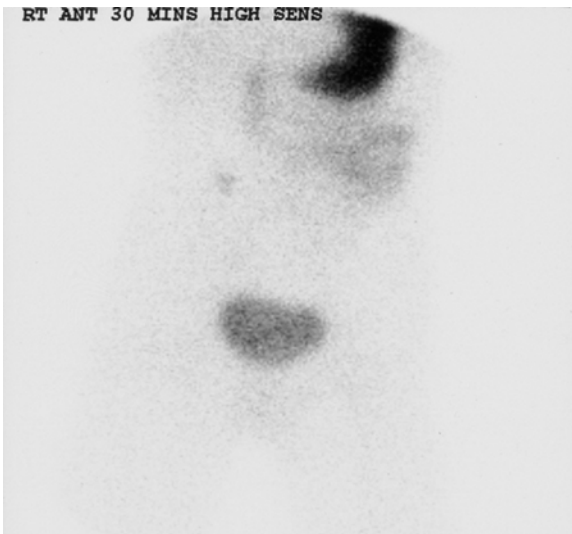


**Fig. 10.** Meckel's diverticulum. Image acquired 30 min after injection of technetium-99m pertechnetate demonstrates a focal area of tracer accumulation in the right lower abdomen

tions, which include gastrointestinal bleeding, secondary to the presence of ectopic gastric mucosa, inflammation, perforation and intestinal obstruction (St-Vil et al. 1991; Vane et al. 1987). The intestinal obstruction can occur as a result of an omphalomesenteric band, internal hernia through the omphalomesenteric duct remnant, volvulus, prolapse of the intestine through the patent duct at the umbilicus in neonate, or intussusception.

Plain radiographs of the abdomen may show a low obstructive pattern or perforation. The exact cause of the obstruction is usually established at laparotomy. Patients with acute Meckel's diverticulitis present with acute focal or diffuse abdominal pain, which is often mistaken for acute appendicitis (St-Vil et al. 1991). Nuclear scintigraphy, using technetium-99m pertechnetate isotope, is the imaging modality of choice for those patients who present with gastrointestinal bleeding. Increased tracer uptake in Meckel's diverticulum, usually located in the right lower abdominal quadrant, is the positive finding (Fig. 10).

### Inguinal Hernia

Inguinal hernia occurs when an intra-abdominal structure, such as a bowel or omentum protrudes, through the persistent processus vaginalis. There is an increased incidence of inguinal hernia in preterm babies. It is more common in boys than girls. Patients are usually asymptomatic, until bowel incarceration occurs, often in children less than 1 year of age, presenting with symptoms and signs of intestinal obstruction (Stylianou et al. 1993).

Abdominal radiographs show a low bowel obstructive pattern. Bowel gas may be visible within the scrotum or inguinal canal (Fig. 11). Absence of this sign does not exclude



**Fig. 11.** Obstructed inguinal hernia. Abdominal radiograph shows multiple dilated loops of air-filled bowel and bowel gas in the right inguinal region and scrotum

the diagnosis as the incarcerated bowel is usually collapsed or only contains fluid. This can sometimes be seen as widening of the scrotal shadow on the affected side. Other imaging studies are usually not required. Ultrasound can be helpful when there is a doubt about the diagnosis (Chen et al. 1998).

### Henoch-Schonlein Purpura

Henoch-Schonlein purpura (HSP) is a vasculitic condition which commonly affects the small blood vessels of the skin, gastrointestinal tract, kidneys and joints, and predominantly occurs in children between the ages of 2 and 10 years (Chang et al. 2004). Although this condition is frequently preceded by an upper respiratory tract infection, the exact aetiology is not known. The clinical diagnosis of HSP is usually made from the typical presentation with non-thrombocytopenic rash often associated with arthralgia or arthritis, abdominal pain and nephritis. The abdominal pain may precede the typical purpuric rash causing diagnostic problems and may lead to unnecessary laparotomy (Katz et al. 1991). The HSP is usually a benign and self-limited condition; however, serious gastrointestinal and renal complications may occur. Intussusception is the most common gastrointestinal complication (Cull et al.



1990). Bowel ischaemia, perforation, massive gastrointestinal haemorrhage, hydrops of the gallbladder, acute appendicitis and pancreatitis are less frequent complications. Some cases may present with acute scrotal pain which may mimic testicular torsion resulting in unnecessary exploration.

Abdominal radiographs are usually not indicated unless there is a clinical concern regarding an obstruction or perforation. Ultrasound is the imaging modality of choice in evaluating the bowel involvement and detecting the surgical complications (Ozdemir et al. 1995; Connolly and O'Halpin 1994; Hu et al. 1991). Ultrasound typically demonstrates small bowel wall thickening, which may be eccentric due to haemorrhage, usually associated with ileus, dilated bowel loops and free intraperitoneal fluid. Colour Doppler may show increased blood flow (Siegel et al. 1997). Intramural haemorrhage may act as a pathological lead point for an intussusception, which is often confined to the small bowel and therefore not detected on contrast enema. The intussusception is usually intermittent and reduces spontaneously (Hu et al. 1991), but intestinal obstruction warranting laparotomy may occur (Katz et al. 1991). Contrast studies are not routinely performed, but, if done, may show thickened valvulae conniventes which give the appearances of stack on coins.

### 7.3.3.3 Older Children

#### Acute Appendicitis

Acute appendicitis is the most frequent condition requiring emergency abdominal surgery in children (Reynolds and Jaffe 1992). The condition occurs usually in older children and adolescents. It is rare in children under 2 years and leads to considerable diagnostic difficulty (Alloo et al. 2004). The cause of appendicitis is obstruction of the appendiceal lumen by hard concretions which leads to distension, ischaemia and bacterial overgrowth with ultimate appendiceal infarction resulting in perforation, peritonitis and abscess formation. The presenting clinical features are usually right lower quadrant pain, vomiting, tenderness and guarding. One-third of the patients with the disease have an atypical presentation, particularly so in young children (Sivit et al. 1992). This can cause diagnostic confusion and delayed treatment which leads to appendiceal perforation and subsequently increased morbidity (Alloo et al. 2004).

The diagnosis is mainly clinical in older children (Kosloske et al. 2004). Imaging is most helpful in children with an unclear clinical diagnosis. In non-perforated appendicitis, the radiographic findings are non-specific (Rao et al. 1999a), except in the case of calcified appendicoliths. Appendicoliths are seen in 10–17% of cases (Siegel 1992; Olutola 1988) and in children with abdominal pain are highly suggestive of the diagnosis. Abdominal radiographs are more likely to show abnormalities in perforated appen-

ditis and these abnormalities include a mass in the right iliac fossa with displacement of bowel gas "flank strip sign", localised right lower quadrant ileus "sentinel loop", and when there is delayed diagnosis and rupture, signs of bowel obstruction. Free intra-peritoneal air is an uncommon finding of perforated appendicitis.

Ultrasound is an ideal modality for evaluation of children with an equivocal diagnosis, because it not only permits direct examination of the appendix but also the entire abdomen to exclude other conditions that can mimic appendicitis (Hernandez et al. 2005). The overall sensitivity and specificity of ultrasound in diagnosis of appendicitis is 85 and 92%, respectively (Orr et al. 1995). The appendix is optimally imaged with a linear-array high-frequency (7.5–12 MHz) transducer using a graded-compression technique and supplemented by colour Doppler. Scanning is performed in both longitudinal and transverse planes and must be done very gently to minimise pain and discomfort. Sonographically, the inflamed non-perforated appendix appears as distended and relatively sonolucent, non-compressible blind ended tubular structure measuring >6.0 mm in maximal transverse diameter. There may be an appendicolith, which casts an acoustic shadow, localised ileus and peri-appendiceal fluid (Fig 12a,b). Inflammation may be confined to the appendiceal tip and therefore the entire length of the appendix must be imaged to avoid false-negative scans (Lim et al. 1996; Nghiem and Jeffrey 1992). The rate of perforation in various paediatric reports has ranged from 15 to 50% (Smink et al. 2004; Pena et al. 2002; Rao et al. 1999b; Gamal and Moore 1990). The ultrasound findings of perforation include loss of the echogenic submucosal layer, focal peri-appendiceal or pelvic fluid collection or abscess. Mesenteric oedema, free peritoneal fluid or subphrenic abscess may be found. Colour Doppler sonography typically demonstrates increased blood flow in the appendiceal wall or right lower quadrant mass (Lim et al. 1996). Ultrasound is technically difficult in obese patients and rarely visualises retrocaecal appendix. If a normal appendix is not visualised, a negative ultrasound therefore, does not exclude appendicitis (Simonovsky 1999; Jeffrey et al. 1994).

Computed tomography has the same value in children in the diagnosis of doubtful appendicitis as it has in adults. The reported sensitivity and specificity of CT for the diagnosis of acute appendicitis have ranged from 90 to 100% and from 89 to 100%, respectively (Lowe et al. 2001; Lane et al. 1997; Rao et al. 1997a; Balthazar et al. 1994). The choice CT technique has varied widely, ranging from abdominopelvic study with or without IV and oral contrast material to a focused appendiceal study with or without enteric contrast material. At the author's institution, a full abdominal scan after intravenous contrast medium administration is the preferred technique. Rectal and oral contrast are not required. Signs of non-perforated appendicitis include demonstration of distended and thickened appendix, oedema of the surrounding mesenteric fat, calcified appen-

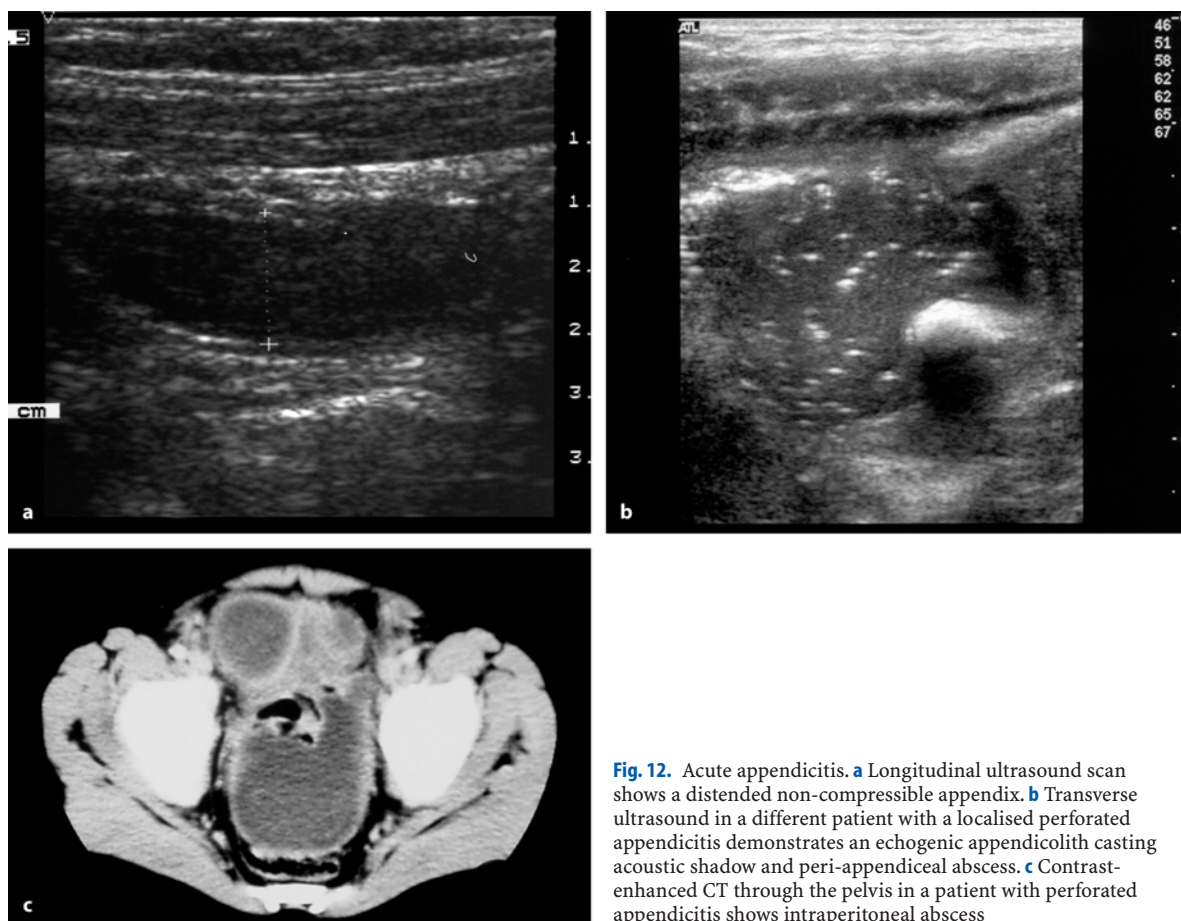


**Fig. 12.** Acute appendicitis. **a** Longitudinal ultrasound scan shows a distended non-compressible appendix. **b** Transverse ultrasound in a different patient with a localised perforated appendicitis demonstrates an echogenic appendicolith casting acoustic shadow and peri-appendiceal abscess. **c** Contrast-enhanced CT through the pelvis in a patient with perforated appendicitis shows intraperitoneal abscess

dicolith which is present in up to 65% of cases on CT (Lowe et al. 2000), apical caecal thickening (also known as the arrowhead sign; Rao et al. 1997c) and focal or free peritoneal fluid. Complications of appendicitis are best demonstrated by CT; these include peri-caecal phlegmon or abscess formation. Pus collection can develop in the pelvis or anywhere in the abdomen (Fig. 12c). In cases of perforation with abscesses and ileus, it can be difficult to distinguish the abscess from bowel. The abscess wall enhances intensely with IV contrast material. Appendicitis remains a fatal condition in children and must not be misdiagnosed. Full imaging is justified to resolve difficult cases.

### Mesenteric Adenitis

Mesenteric adenitis is a self-limited clinical entity that presents with abdominal pain, nausea, vomiting, and fever and sometimes raised white blood cell count (Rao et al. 1997b). The symptoms are due to non-specific inflammation of the mesenteric lymph nodes, usually in the right lower quadrant as a consequence of viral or bacterial infection (Van Noven et al. 1991). Mesenteric adenitis most frequently affects school age children, and may be recurrent. It is one

of the most frequent causes of acute abdominal pain in children with normal appendix at laparotomy (Quillin and Siegel 1993).

Ultrasound usually demonstrates clustered, enlarged mesenteric lymph nodes with a normal appendix (Fig. 13). Normal mesenteric nodes are <10 mm in longitudinal diameter. Clinically there is a considerable overlap with appendicitis and in up to 40% of appendicitis cases, right lower quadrant lymphadenopathy is identifiable; hence, the role of imaging. Mesenteric lymphadenopathy is associated with other conditions such as gastroenteritis and Crohn's disease, and is occasionally seen in asymptomatic children (Watanabe et al. 1997; Sivit et al. 1993).

### Omental Infarction

Omental infarction is a rare entity in children and typically presents with acute right lower abdominal pain and tenderness and sometimes vomiting. The condition is typically seen in obese children and is usually mistaken for acute appendicitis or cholecystitis (Theriot et al. 2003; Helmraht et al. 2001). Omental infarction is usually classified into idiopathic infarction and infarction associated with omental

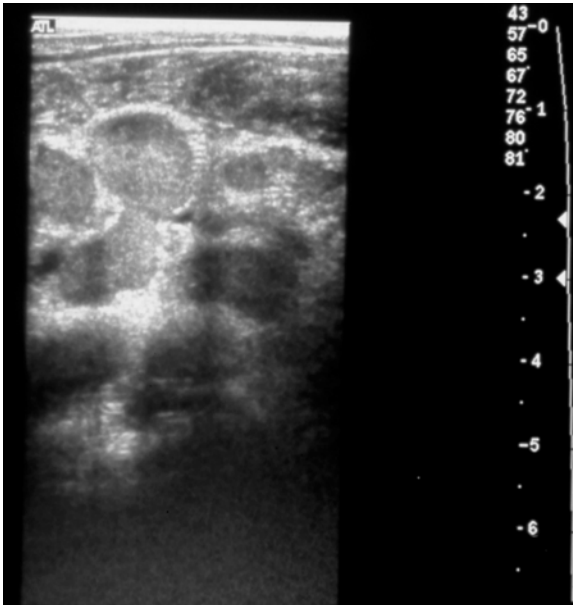


**Fig. 13.** Mesenteric adenitis. Ultrasound of the abdomen shows multiple enlarged mesenteric nodes

torsion; the latter is separated into primary and secondary torsion. The secondary torsion is caused by the attachment of the omentum to an acquired lesion such as a hernia or cyst.

The sonographic findings are similar to those seen in adults and include demonstration of hyperechoic, non-compressible, intra-abdominal masses between the anterior abdominal wall and the transverse or ascending colon with a localised tenderness (Bachar et al. 2005; Grattan-Smith et al. 2002). The mass has mixed attenuation on CT and is separate from a normal appendix.

### Pancreatitis

Pancreatitis is less common in children than in adults. It should be considered in the evaluation of children with acute abdominal pain because of its morbidity. The main difference between children and adults lies in the aetiologies. In

contrast to adults, the most frequent causes of pancreatitis in children are trauma, structural anomalies, multi-system disease and drugs (Table 4; Benifla and Weizman 2003; Yeung et al. 1996). Clinical presentation depends on the severity of the disease, but abdominal pain is invariable (Weizman and Durie 1988). Other symptoms include vomiting, fever, jaundice and an abdominal mass, if a pseudocyst is present. Severe fulminating pancreatic necrosis is rare in children, the symptoms of this being similar to those in adults.

Pancreatitis is classified into acute and chronic. Acute pancreatitis is a reversible inflammatory process, whereas chronic pancreatitis produces irreversible changes, and leads ultimately to pancreatic insufficiency. Clinical suspicion is required to make the diagnosis. An elevated plasma amylase level is usual. Imaging of the pancreas is an important adjunct to the clinical and biochemical diagnosis of pancreatitis and its complication. The imaging findings of pancreatitis on both ultrasound and CT in children are similar to those in adults; these include diffuse or focal, often hypoechoic pancreatic enlargement, dilatation of the pancreatic duct (Fig. 14a; Chao et al. 2000; Coleman et al. 1983), and on CT, in addition to the enlargement, peripancreatic fluid and mesenteric oedema, with a variable enhancement pattern with IV contrast material (Vaughn et al. 1998; King et al. 1995). Increased echogenicity, atrophy, focal or diffuse enlargement, ductal dilatation and calcification are the findings of chronic pancreatitis (Alpern et al. 1985).

Complications of acute pancreatitis include acute peripancreatic fluid collections, pseudocyst, pancreatic abscess, infected necrosis and haemorrhage (Fig. 14b). Pseudocyst formation occurs in 16–23% of cases (Yeung et al. 1996; Weizman and Durie 1988). This usually takes approximately 4–6 weeks to develop and clinically presents with recurrent pain. Pseudocysts may be single or multiple and when large, they may obstruct the upper gastrointestinal tract or the biliary tree. The ultrasound appearances are of a well-circumscribed, anechoic structure with acoustic enhancement unless complicated by infection or haemorrhage. In 50% of cases, pseudocysts resolve spontaneously. In children, congenital anomalies of the biliary or pancreatic tree are relatively frequent; hence, the role of MRCP which may obviate the need for invasive anatomic studies such as ERCP (Shimizu et al. 2001; Arcement et al. 2001).

**Table 4.** Causes of pancreatitis in children

Trauma	Structural abnormalities	Multi-systemic disease	Drugs and toxins	Metabolic	Familial
Blunt injury (accidental and NAI)	Pancreas divisum	Sepsis and shock	Steroid	Cystic fibrosis	Hereditary pancreatitis
Endoscopic manipulation	Choledochal cyst	Viral infection	L-asparaginase	Diabetic ketoacidosis	
	Duplication cyst	Haemolytic uraemic syndrome Reye's syndrome		Inborn error of metabolism	

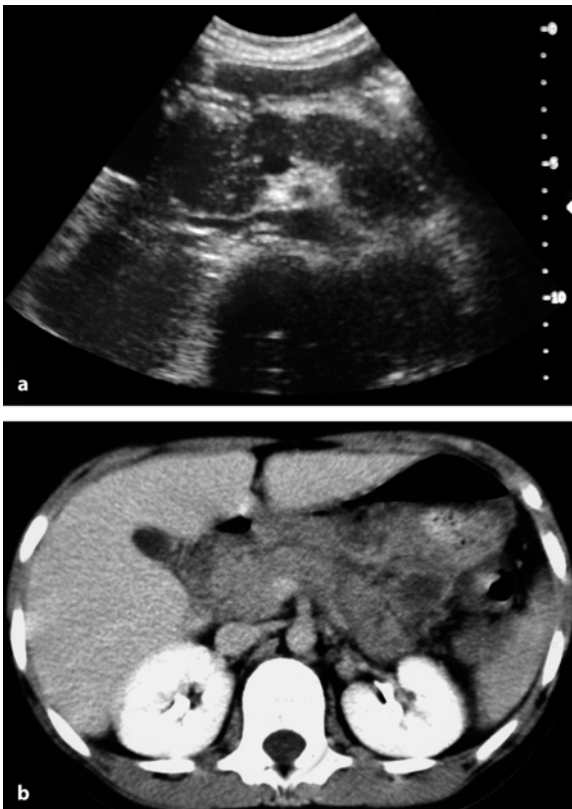


**Fig. 14.** Acute pancreatitis. **a** Transverse ultrasound of the pancreas shows an enlarged hypoechoic pancreas. **b** Contrast-enhanced CT of the abdomen shows inhomogeneous enhancement of the pancreatic tail and a pseudocyst formation within the lesser sac

### Constipation

Constipation is a common clinical problem in infants and children, estimated to occur in 5–10% in paediatric patients (Loening-Baucke 2005). The history is usually longstanding and in over 90% of cases the cause is functional. Acute presentation of fecal impaction is rare and usually has an organic cause, but it may occur with functional constipation; hence, it is discussed here under abdominal emergencies. Causes of constipation are listed in Table 5. Missed Hirschsprung's disease in older children may present with a fulminating enterocolitis (Vieten and Spicer 2005), but most commonly presents insidiously with a history of chronic constipation.

Imaging of children presenting with an abdominal emergency due to constipation usually includes an abdominal radiograph with a limited contrast enema examination. The contrast enema in these children should be done with a water-soluble contrast material to avoid barium impaction. Plain radiographs and contrast enema studies will show the degree of faecal loading and dilatation of the large bowel (Fig. 15). In functional constipation, the megarectum extends to the anal margin and may be very large, fills the pelvis and can cause sec-

**Table 5.** Causes of constipation in childhood

Functional	Organic
Hirschsprung's disease	Hirschsprung's disease
Neuronal intestinal dysplasia	Neuronal intestinal dysplasia
Hypoganglionosis	Hypoganglionosis
Chronic intestinal pseudo-obstruction	Chronic intestinal pseudo-obstruction
Spinal cord disorders	Spinal cord disorders
Cerebral palsy	Cerebral palsy
Metabolic and endocrine disorders	Metabolic and endocrine disorders



**Fig. 15.** Constipation. Plain film of the abdomen shows hugely distended rectum and sigmoid colon which are filled with feces

ondary urinary obstruction and hydronephrosis. Ultrashort segment of Hirschsprung's disease may appear similar to a functional constipation with no evidence of transitional zone (Taxman et al. 1986). A barium enema therefore, does not exclude Hirschsprung's disease. Ultrasound can be helpful to differentiate a faecal mass from a true intra-abdominal soft tissue mass. If spinal cord or sacral anomalies are suspected, spinal MRI is indicated.



**Table 6.** Common causes of intestinal obstruction in children

Adhesions
Intussusception
Perforated appendicitis
Incarcerated inguinal hernia
Distal intestinal obstruction syndrome in cystic fibrosis
Malrotation with volvulus
Meckel's diverticulum

### Intestinal Obstruction

Intestinal obstruction in children, though uncommon, should be suspected in any child with persistent vomiting and abdominal pain, as delayed diagnosis can cause vascular compromise and bowel ischaemia. Beyond the neonatal period, the commonest causes of intestinal obstruction are listed in Table 6.

Supine and erect, or cross-table lateral or left decubitus abdominal radiographs, are required for full assessment of suspected cases of intestinal obstruction. In mechanical obstruction, the abdominal gas pattern is similar to that in adults, i.e. distended loops of bowel proximal to the obstruction with air–fluid levels which are shorter than those seen in ileus. Evidence of underlying causes, such as masses, appendicolith or air trapped in the hernial orifices, as well as perforation, should be sought. Once a clinical diagnosis of obstruction is made and confirmed by plain radiographs, further investigation is not indicated. If the symptoms are intermittent and there is a doubt about the cause of the obstruction, oral water-soluble contrast studies with follow through examination may demonstrate the cause. This should be preceded by ultrasound, which can reveal many intestinal abnormalities, such as a mesenteric cyst and intussusception (Ikeda et al. 1993).

Computed tomography is being used increasingly in adults presenting with bowel obstruction (Burkill et al. 2001). In children, the diagnosis of bowel obstruction is usually based on the clinical, radiographic and contrast studies findings, and CT is generally not indicated; however, CT has proved helpful in selected cases (Jabra and Fishman 1997), such as in patients who have intermittent or subacute obstruction or those who present postoperatively.

### Intestinal Pseudo-obstruction

Intestinal pseudo-obstruction is an intestinal dysmotility condition characterised by the presence of mechanical bowel obstruction without organic occlusion (Rudolph et al. 1997). The cause is unknown. In some patients, histological or histochemical abnormalities have been identified in the intestinal muscles or nerves (Knowles et al. 2004; Goulet et al. 1999); in children, the condition is often a primary. Pseudo-obstruction secondary to systemic illnesses, such as infection, hypothyroidism and Kawasaki disease, is more common in older patients.

The clinical presentation is variable and includes vomiting, diarrhoea and constipation, but when the initial presentation is with acute abdominal pain and distension, the initial diagnosis is often acute intestinal obstruction and laparotomy is performed at which an organic cause for the obstruction is not identified. Plain radiographic findings are very variable and range from non-specific bowel dilatation, isolated loop dilation or a mechanical obstructive pattern. Contrast studies, if performed, may show non-propulsive peristalsis with to-and-fro movement, which may be segmental.

### Inflammatory Bowel Disease

The two major inflammatory bowel lesions, ulcerative colitis and Crohn's disease, affect primarily young adults, but 25% of cases present in children. Usually neither presents primarily as an acute abdominal emergency but may present acutely due to complications in a child with known disease. Intestinal obstruction due to inflammation, stricture formation or adhesions associated with previous surgery is relatively common. Abscess formation due to localised perforation may also occur (Ali and Carty 2000). Toxic megacolon is a rare complication of ulcerative colitis (von Allmen et al. 1995).

Ultrasound allows non-invasive diagnosis of these complications and assessment of other intra-abdominal organs; however, in some cases it is difficult, particularly in the post-operative period or in those with abdominal wall tenderness. In such patients, contrast-enhanced CT is an invaluable alternative in identifying intra-abdominal or pelvic abscesses (Gore 1987). These lesions are not discussed further as the radiological appearances are identical to those in adults.

### Haemolytic Uraemic Syndrome

Haemolytic uraemic syndrome is a distinct condition characterised by microangiopathic haemorrhagic anaemia, thrombocytopenia and acute renal failure. The syndrome predominantly occurs in young children and frequently follows gastroenteritis due to *Escherichia coli* O157:H7 (Pickering et al. 1994). Most of the patients present with gastrointestinal prodromes characterised by fever, vomiting, abdominal pain and watery diarrhoea that progresses to grossly bloody diarrhoea (Su and Brandt 1995). The renal disease manifests by oliguria. When the gastrointestinal manifestations precede the classical triad of haemolytic uraemic syndrome, the diagnosis is often delayed and other causes of bloody diarrhoea, such as inflammatory bowel disease and intussusception are often clinically suspected (Miller et al. 2001; Kawanami et al. 1984).

Imaging studies are particularly helpful when the clinical findings are non-specific. The radiographic features include thumbprinting and narrowing of the colon (Fig. 16). This can be confirmed by contrast enema study, but it is not

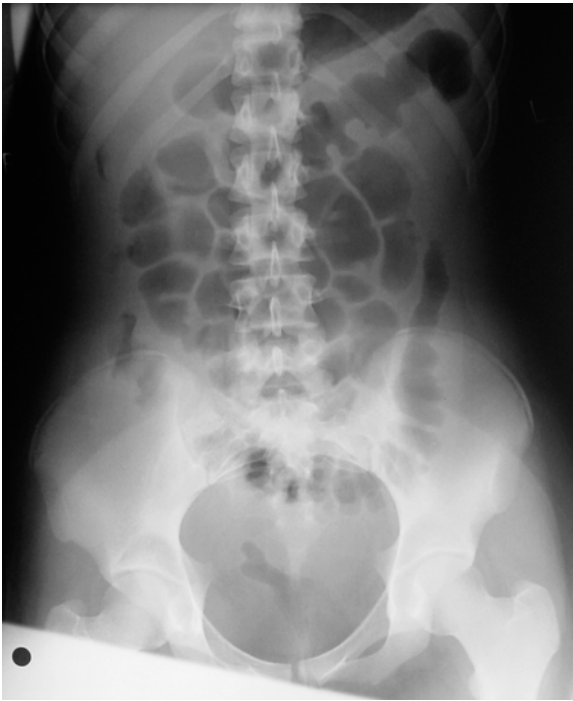


**Fig. 16.** Haemolytic uraemic syndrome. A plain abdominal film shows thumbprinting of the transverse colon

routinely indicated. Ultrasound and CT show colonic wall thickening which is often hypovascular, peri-colonic stranding and there may be some free fluid in the abdomen (Miller et al. 2001; Friedland et al. 1995). The caecum and ascending colon are most commonly involved, but any segment of the large bowel may be affected. Colonic stricture (Kirks et al. 1982), perforation (Whittington et al. 1979) and toxic megacolon are reported complications of HUS. Depending on the severity of the renal involvement, the kidneys may be normal or hyperechoic with loss of corticomedullary differentiation.

### Gynaecological Pathology

Acute abdominal pain in older girls and adolescents is a common problem and frequent cause for hospital admission. The gynaecological causes must be taken into account when considering the differential diagnosis (Table 7). Rare causes of abdominal pain include pelvic inflammatory disease, or the complication of pregnancy. The clinical and imaging features of these are similar to those in adults, and are not discussed further. Transabdominal ultrasound usually shows the lesion. Transvaginal ultrasound should not be routinely done as a primary investigation in adolescent girls but may supplement the abdominal examination in selected cases.

**Table 7.** Gynaecological causes of acute abdominal pain

Rupture of a functional ovarian cyst
Haemorrhagic ovarian cyst
Ovarian torsion
Congenital vaginal anomalies
Complications of pregnancy
Pelvic inflammatory disease
Tumours
Endometriosis
Pregnancy

### Functional Ovarian Cysts

Follicular and luteal cysts result from failure of involution during the normal menstrual cycle. Bleeding into, enlargement of, or rupture of a functional ovarian cyst is a frequent cause of acute lower abdominal pain in pubertal girls. This may occur during midcycle or may herald the onset of menstruation and may be recurrent. The pain may be severe and mimic acute appendicitis. Ultrasound is invaluable in assessing such situations. Non-haemorrhagic ovarian cysts are classically anechoic, thin-walled masses exhibiting posterior acoustic enhancement, and are avascular on Doppler sonography. The cysts may be quite large, but it is well recognised that even cysts of up to 6 cm may resolve spontaneously within a few months. Haemorrhagic ovarian cysts appear as an echogenic adnexal mass with increased through transmission, reflecting its cystic nature (Fig. 17) and may be associated with free fluid (Baltarowich et al. 1987).

### Ovarian Torsion

Ovarian torsion is an uncommon cause of abdominal pain in children and is usually seen in patients with predisposing ovarian lesions, such as ovarian cysts and ovarian masses (Kokoska et al. 2001; Surratt and Siegel 1991). Two-thirds of ovarian masses are benign mature teratomas. Torsion of a normal ovary is also encountered due to excessive mobility of the adnexa caused by abnormally long fallopian tubes, mesosalpinx, or meso-ovarium (Mordehai et al. 1991). The clinical presentation depends on the degree of torsion and can vary from intermittent lower abdominal pain to an acute abdominal crisis. Other symptoms may include nausea and vomiting, fever and urinary symptoms. A lower abdominal mass may be palpable. Torsion of the ovary occludes initially the venous circulation and, if untreated, progresses to occlude the arterial circulation resulting in haemorrhagic infarction, and may lead to peritonitis; therefore, early diagnosis of torsion is essential if the ovary is to be salvaged.

A mass may be seen on an abdominal radiograph and, if large enough, the gas shadows are displaced around it. The presence of fat calcification or teeth will occasionally be present and indicates the diagnosis of a dermoid cyst or a tumour. Ultrasound may reveal diffusely enlarged ovary with multiple peripheral follicles (Fig. 18), a complex

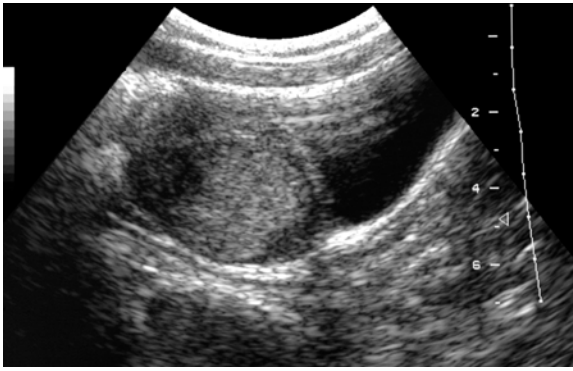


**Fig. 17.** Haemorrhagic ovarian cyst. Ultrasound scan of the pelvis shows an echogenic ovarian cyst due to bleeding within the follicular cyst

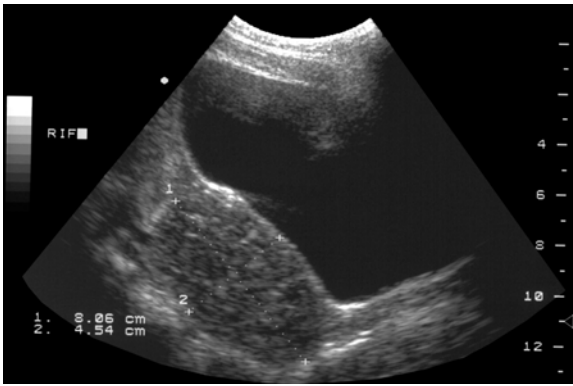


**Fig. 18.** Ovarian torsion. Longitudinal ultrasound scan of the pelvis shows diffusely enlarged echogenic ovarian mass in the pouch of Douglas

pelvic mass and occasionally free fluid in the pouch of Douglas (Graif and Itzhak 1988). Absence of colour flow on Doppler sonography suggests arterial occlusion; however, demonstration of normal colour flow on Doppler sonography does not exclude an ovarian torsion (Lee et al. 1998; Stark and Siegel 1994). Atypical cysts or ovarian masses demonstrated on ultrasound will require further imaging with CT or MRI.

### Congenital Uterovaginal Anomalies

Failure of the müllerian or para-mesonephric ducts to reach the urogenital sinus causes accumulation of the uterine secretion proximal to the vaginal occlusion. This is typically caused by an imperforate hymen, but there may also be transverse vaginal septum or vaginal or cervical atresia (Blask et al. 1991b). Vaginal obstruction can present in the neonatal period or at the time of menarche. Neonates present clinically with a palpable abdominal mass or with noticeable bulging mass between the labia which is the result of excessive uterine or vaginal secretion secondary to ma-

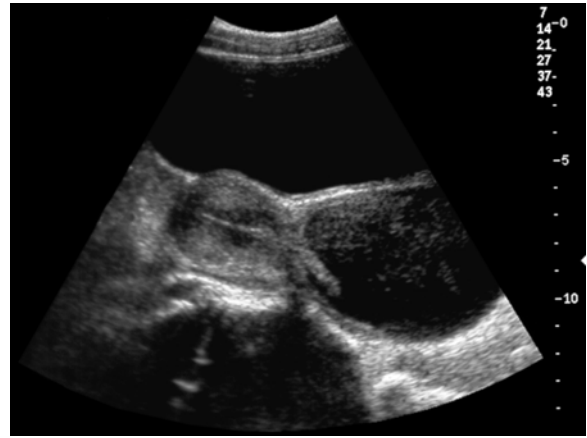


**Fig. 19.** Haematocolpos. Longitudinal ultrasound scan of the pelvis shows hugely distended fluid-filled vagina with multiple internal echoes indicating menstrual products

ternal hormone stimulation (Haha-Pedersen et al. 1984). Young teenagers typically present with amenorrhoea, lower abdominal pain or a mass which is the result of accumulation of the menstrual products predominantly in the vagina with dilatation of the uterus. In vaginal or cervical atresia the products may collect in the fallopian tubes and broad ligament.

The diagnosis is easily made with ultrasound by demonstrating a midline tubular, fluid-filled structure, representing the dilated vagina “hydrocolpos” (Blask et al. 1991a,b). The uterus may also be dilated and filled with fluid “Hydrometrocolpos”. Menstrual products appear as internal echoes within the dilated vagina “Haematocolpos” (Fig. 19) or the vagina and uterus “haematometrocolpos”. Dilatation of the fallopian tubes and hydronephrosis are rare findings (Davis et al. 1984). A more difficult diagnostic problem is the girl with a uterus Didelphys with one patent horn but an obstructed second horn. The patient presents with cyclic pain related to menstruation but has normal menses.

### Renal Disease

The most acute emergency presentation of renal disease is anuria due to renal failure. Ultrasound is required to identify surgically remedial causes such as obstruction, but this is rare. The other renal causes of an apparent acute abdomen are upper urinary tract infection, especially acute pyelonephritis, acute presentation of a pelvi-ureteric junction obstruction, or more rarely renal colic due to a stone in the urinary tract.

### Infection

Urinary tract infections (UTIs) are common in children. It has been estimated that 8% of girls and 2% of boys will develop a UTI during childhood (Hellstrom et al. 1991).

The clinical presentation varies with age and severity. Dysuria, lower abdominal pain and frequency in the absence of fever are indicative of lower UTI, whereas loin pain, vomiting, anorexia and fever are features of upper UTI; however, the distinction between the two on the basis of the clinical presentation is difficult particularly in young children. The symptoms in neonates and infants are usually non-specific and include diarrhoea, vomiting, fever and irritability. Acute pyelonephritis in children may lead to permanent renal damage (scarring) and subsequently to hypertension and end-stage renal disease (Hellerstine 2000).

Imaging of acutely ill patients during the acute infection can be helpful to confirm the presence or absence of acute pyelonephritis. Patients are then imaged later as part of the work-up for UTI. Plain abdominal radiographs are generally not indicated unless renal calculi or other intra-abdominal pathologies are also suspected (Kenney et al. 1991). The details of the kidneys are often obscured by gas and feces, and the renal outlines are difficult to see because of the paucity of the perinephric fat. On ultrasound the infected kidney appears enlarged with focal or diffuse areas of abnormal echogenicity and loss of corticomedullary differentiation (Fig. 20a; Ilyas et al. 2002; Lavocat et al. 1997). The acutely infected kidney may, however, appear normal. The sensitivity of ultrasound for detecting acute pyelonephritis increases by adding power Doppler, which shows decreased perfusion in the affected area of the kidney (Dacher et al. 1996; Halevy et al. 2004). Ultrasound also allows visualisation of complications of acute pyelonephritis, such as abscess formation which appears as a mass lesion with central necrosis. Structural abnormalities of the urinary tract, which may be found on ultrasound in children presenting with UTI include duplex systems with hydronephrosis of one moiety due to an obstructing ureterocele, or renal ectopia – horseshoe kidney, malrotation or a pelvic kidney. A simple duplex kidney is identified because of splitting of the renal sinus echo.

Technetium-99m-DMSA scintigraphy is more sensitive than ultrasound in detecting acute pyelonephritis and renal scarring, which both appear as focal or diffuse areas of reduced isotope uptake (Fig. 20b; Stokland et al. 1999; Ilyas et al. 2002). Computed tomography is less sensitive than DMSA (Lavocat et al. 1997) but may be helpful in selected cases (Dacher et al. 1993). Vesico-ureteric reflux has been identified as a predisposing factor for the development of UTIs, and is found in 25–40% of children with pyelonephritis (Hellerstine 1995). Vesico-ureteric reflux can be demonstrated by micturating cysto-urethrogram or indirect isotope cystography. This is not done in the acute phase but after infection is under control, and is not discussed further in this text.

Xanthogranulomatous pyelonephritis (XGP) is an uncommon form of pyelonephritis that is rarely seen in children. It is usually unilateral, presenting with abdominal pain, fever, anorexia, weight loss, anaemia and abdominal

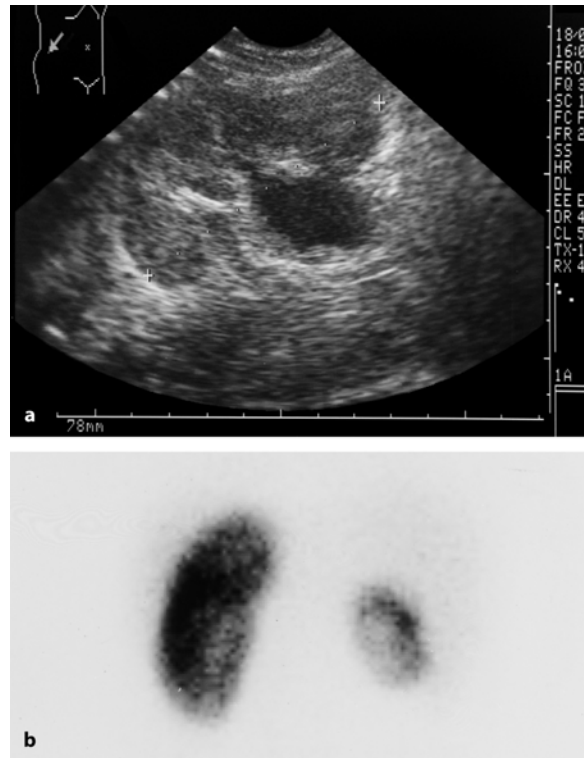


**Fig. 20.** Acute pyelonephritis. **a** Ultrasound of the right kidney shows diffuse alteration of the normal renal echogenicity and loss of the cortico-medullary differentiation. **b** Posterior view of the renal DMSA scan shows reduced isotope uptake by the right kidney

mass (Samuel et al. 2001; Bingol-Kologlu et al. 2002). The condition is characterised by destruction of the renal parenchyma and may involve the perinephric tissue; therefore, the lesion is often mistaken for a tumour. Ultrasound demonstrates a focal or diffuse ill-defined mass with mixed echoes due to fat, areas of calcification and dilated calyces filled with debris. Contrast-enhanced CT shows similar appearances with patchy areas of enhancement.

### Pelviureteric Junction Obstruction

Pelviureteric junction (PUJ) is the most common site of obstruction in the upper urinary tract, usually due to an intrinsic cause or less commonly due to an extrinsic compression secondary to bands, kinks or aberrant vessels. With the development of antenatal ultrasound, PUJ obstruction is now diagnosed more during the perinatal period in asymptomatic infants (Grignon et al. 1986); however, PUJ obstruction may go unnoticed antenatally and present with a palpable mass or abdominal distension in neonates. Older children may present clinically with severe abdominal pain, urinary tract infection or haematuria, but intermittent pain associated with vomiting is also recognised.

Ultrasound is the initial imaging of choice used in children with suspected urinary tract obstruction. It shows a



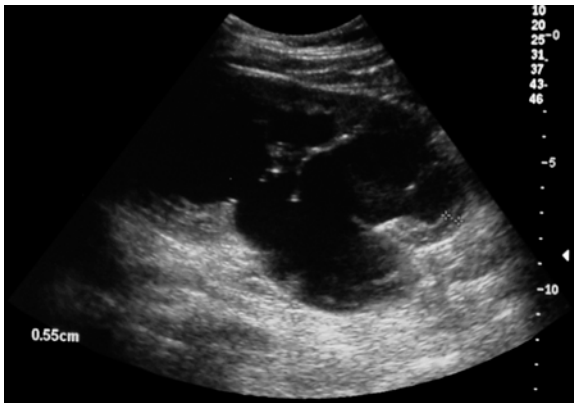


**Fig. 21.** Pelviureteric junction obstruction. Ultrasound of the left kidney shows dilated pelvis and calyces with no ureteric dilatation

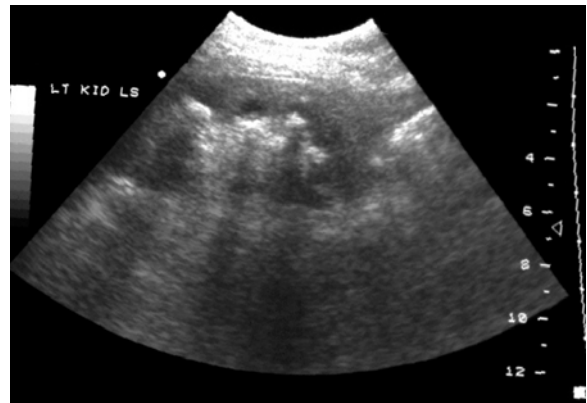


**Fig. 22.** Renal calculi. Left kidney ultrasound shows multiple echogenic foci associated with acoustic shadowing

dilated renal pelvis communicating with dilated calyces in the absence of visualisation of the distal ureter (Fig. 21). The renal cortex may appear thin, and a crossing blood vessel at the PUJ may be visualised on colour Doppler ultrasound (Veyrac et al. 2003). Occasionally, the distal ureter appears dilated due to associated vesico-ureteric reflux. The PUJ obstruction must be distinguished from a multicystic kidney; the latter appears as non-communicating areas of cystic dilation of variable size.

A functional study using Tc-99m-MAG3 is performed to assess the renal drainage and compare the function of the kidneys. The PUJ obstruction is confirmed by showing dilatation of the upper urinary tract, failure of tracer washout after diuretic administration and gradually rising activity on the time-activity graph. Intravenous urography (IVU) shows similar appearances. If facilities are available, MR urography will achieve the same result. If the ureter is dilated or the bladder wall is thick, an MCUG is indicated to exclude vesico-ureteric reflux and urethral valves. Acute management of a PUJ is usually placement of a percutaneous nephrostomy, and functional imaging is performed when acute symptoms have settled.

### Urolithiasis

Paediatric urolithiasis is not common. Most commonly, the cause is infection, particularly with proteus and *Klebsiella*, but metabolic diseases (Coward et al. 2003) must be considered if infection is eliminated. Hypercalcaemia is the most common metabolic cause of urinary tract calculi. The aetiology is undetermined in 25% of cases. Urolithiasis usually present with abdominal pain, haematuria or infection. Presentation with the classical combination of renal colic and haematuria is uncommon and, in some cases, the calculi may be discovered incidentally in asymptomatic children. Most of the calculi affect the upper urinary tract and they can be single or multiple.

The calculi are usually visible on plain radiographs, but sometimes they cannot be identified, either because they are radiolucent or obscured by overlying bowel gas or faeces. Ultrasound is the imaging modality of choice in children with suspected renal tract calculi (Smith et al. 2000). Calculi appear on ultrasound as echogenic areas with intense acoustic shadowing (Fig. 22; Middleton et al. 1988). Calculi, particularly when situated in the ureter, may cause obstruction and subsequently dilatation of the proximal upper tract. Ureteric calculi, especially in the mid-part of the ureter are difficult to identify on ultrasound (Smith et al. 2000); therefore, in children presenting with symptoms suggestive of urolithiasis and negative ultrasound and plain-film radiographs, an intravenous urography is a useful examination for conformation or exclusion.

An unenhanced CT is increasingly used in the United States for the primary diagnosis (Lowe et al. 2001). It may be especially useful for the diagnosis of very small calculi and calculi with poor radiographic density.

### Hepato-biliary Pathology

Compared with adults, acute presentation of hepato-biliary disease in children is rare. The symptoms are either acute abdominal pain due to cholecystitis – calculus or acalculous – or jaundice. Acalculous cholecystitis is often associated with systemic infections (Imamoglu et al. 2002). In addition, it has been also associated with parenteral nutrition, extensive burns and post-surgery. Primary cholelithiasis is rare in children (Rescorla 1997). Haemoglobinopathies account for many stones in children (O'Haller 1991). Stones are also complication of parenteral nutrition, cystic fibrosis, ileal resection and congenital anomalies of the biliary tree, the most frequent of which present as an emergency is a choledochal cyst. The clinical presentation and imaging investigations are similar to those in adults. For example, an abdominal radiograph is used to identify calcified gallstones and ultrasound of the pancreas, gallbladder and bil-

**Table 8.** Classification of choledochal cyst

Type 1:	fusiform dilatation of the common bile duct
Type 2:	localised cystic diverticula of the common bile duct
Type 3:	dilatation of the intra-duodenal segment of the bile duct
Type 4:	multiple cystic dilatation of the extrahepatic and possible the intrahepatic biliary duct
Type 5:	intrahepatic bile duct cysts (Caroli's disease)

iliary tree. The imaging appearances of cholecystitis, e.g. thickening of the gallbladder wall and the presence of stones causing an acoustic shadowing, are similar to those in adults. Dilatation of the common bile duct and intrahepatic radicles occur in obstructive jaundice.

Choledochal cysts are rare congenital cystic malformation of the biliary tree. Five types of cysts are described based on cyst morphology and location (Table 8). The commonest type is type 1, representing 80% of cases. The male-to-female ratio is 1:4. Clinical symptoms include episodic abdominal pain, jaundice and a right upper quadrant mass. Approximately one-third present under 1 year (Stringer et al. 1995). The typical ultrasonic appearance of a choledochal cyst is cystic dilatation of the common bile duct (CBD), which may be massive, with dilatation of the right and left hepatic duct but no dilatation of the intrahepatic radicles. The gallbladder is identified as a separate structure. Although the diagnosis is made by ultrasound, hepatobiliary scintigraphy can be used to confirm the diagnosis by showing accumulation of the radioisotope within the cyst. Some children have an endoscopic retrograde pancreatography, or more recently MRCP, to identify the distal CBD and pancreatic anatomy. Complications of the choledochal cyst include stones, cholangitis, recurrent pancreatitis and malignant transformation, the latter occurring in adulthood.

Hepatitis is usually a clinical diagnosis and children rarely present as an acute abdominal emergency. Clinical symptoms are nausea, vomiting, lethargy, abdominal pain and mild jaundice. The pain may be very severe and this with the jaundice leads to the clinical diagnosis of cholecystitis. Ultrasound is indicated to exclude other pathology. Imaging may be normal, but in severe cases the liver may be hypoechoic and there may be oedema of the gallbladder wall.

A liver abscess is a rare primary lesion in children most being secondary to intra-abdominal sepsis. It is may be a presenting feature of any of the immune-deficiency syndromes. The clinical and imaging features are similar to those in adults.

### Emergencies in Cystic Fibrosis

Although the respiratory involvement is the main clinical concern in children with cystic fibrosis, gastrointestinal complications are not uncommon and may lead to intestinal obstruction. Other complications are distal intestinal obstruction syndrome and fibrosing colonopathy.



**Fig. 23.** Meconium ileus equivalent. Plain abdominal film shows granular appearances in the right side of the abdomen associated with dilated loops of small bowel

The distal intestinal obstruction syndrome, also known as meconium ileus equivalent, affects older children with cystic fibrosis and is characterised by retention of inspissated, tenacious intestinal contents most commonly in the terminal ileum and right colon resulting in varying degrees of intestinal obstruction. The condition may be precipitated by an intercurrent chest infection, dehydration or stopping the oral pancreatic enzyme supplements (Gross et al. 1985). The clinical manifestations range from mild abdominal pain, usually in the right lower quadrant associated with a palpable mass to severe pain associated with vomiting, constipation and abdominal distension. The abdominal radiographs show a bubbly, granular appearance, predominantly in the right side of the abdomen in addition to the findings of intestinal obstruction (Fig. 23; Pilling and Steiner 1981). Distal intestinal obstruction syndrome is usually treated medically, but a gastrografin contrast enema is sometime requested for both diagnostic and therapeutic purposes. The contrast enema helps not only in confirming the diagnosis by showing multiple filling defects, but also in excluding other possible causes of abdominal pain and obstruction, such as intussusception. Gastrografin also acts as a mucolytic agent and relieves the obstruction.

Fibrosing colonopathy is a newly described entity in patients with cystic fibrosis, characterised by colonic thickening with varying degrees of stenosis and stricture. The condition is probably related to the intake of high-strength pancreatic enzyme supplements (Smyth et al. 1994). The symptoms are non-specific, including abdominal pain, distension and constipation, which fail to respond to the medical treatment of distal intestinal obstruction syndrome. The colonic wall thickening may be visible on the abdominal radiographs and ultrasound (King et al. 1994). Contrast enema studies show colonic wall thickening, mucosal irregularity, loss of the normal colonic haustration and stricture, usually involving the caecum and ascending colon with variable extension to the distal large bowel without skip lesions (Crisci et al. 1997; Zerin et al. 1995). It must be remembered that other conditions, such as acute appendicitis, Crohn's disease and gallbladder disease, should also be considered in the differential diagnosis of acute abdominal pain in children with cystic fibrosis.

### 7.3.4 Conclusion

There is a wide range of differential diagnoses of acute abdomen in paediatrics. Although many of these conditions are self-limiting, some of them are life-threatening and require prompt diagnosis and treatment to minimize morbidity. The initial diagnosis usually depends on a careful clinical evaluation, laboratory investigations and the knowledge of the likely causes within the specific age group. In many cases however, the diagnosis is uncertain and imaging studies are indicated. Although abdominal radiographs are traditionally requested initially, ultrasound is generally more useful in providing the diagnosis in many children with acute abdomen. Diagnosis of obstruction in neonates is usually made by plain abdominal radiographs and contrast studies. Computed tomography in children is required in selected patients whom the clinical and sonographic findings are indeterminate. Abdominal malignancy has not been specifically discussed as the clinical presentation is usually that of an obvious mass and subsequent pathways are well established.

**Acknowledgement.** Thanks to Prof. H. Carty, upon whose original work this chapter is based, for her help and advice.

### References

- Agrons GA, Corse WR, Markowitz RI et al. (1996) Gastrointestinal complications of cystic fibrosis: a radiologic-pathologic correlation. *Radiographics* 16:871-893
- Ali SI, Carty HML (2000) Paediatric Crohn's disease: a radiological review. *Eur Radiol* 10:1085-1094
- Allmen D von, Goretsky MJ, Ziegler MM (1995) Inflammatory bowel disease in children. *Curr Opin Pediatr* 7:547-552
- Alloo J, Gerstle T, Shilyansky J et al. (2004) Appendicitis in children less than 3 years of age: a 28-year review. *Pediatr Surg Int* 19:777-779
- Alpern MP, Sandler MA, Kellman GM et al. (1985) Chronic pancreatitis: ultrasound features. *Radiology* 155:215-219
- Arcement CM, Meza MP, Arumanla S et al. (2001) MRCP in the evaluation of pancreaticobiliary disease in children. *Pediatr Radiol* 31:92-97
- Azar T, Berger DL (1997) Adult intussusception. *Ann Surg* 226:134-138
- Bachar GN, Shafir G, Postnikov V et al. (2005) Sonographic diagnosis of right segmental omental infarction. *J Clin Ultrasound* 33:76-79
- Bailey PV, Tracy TF, Connors RH et al. (1993) Congenital duodenal obstruction: a 33-year review. *J Pediatr Surg* 28:92-95
- Baltarowich OH, Kurtaz AB, Pasto ME et al. (1987) The spectrum of sonographic findings in hemorrhagic ovarian cysts. *Am J Roentgenol* 148:901-905
- Balthazar EJ, Birnbaum BA, Yee J et al. (1994) Acute appendicitis: CT and US correlation in 100 patients. *Radiology* 190:31-35
- Bass D, Cordoba E, Dekker C et al. (2004) Intestinal imaging of children with acute rotavirus gastroenteritis. *J Pediatr Gastroenterol Nutr* 39:270-274
- Benifla M, Weizman Z (2003) Acute pancreatitis in childhood: analysis of literature data. *J Clin Gastroenterol* 37:169-172
- Berdon WE (1995) The diagnosis of malrotation and volvulus in the older child and adult: a trap for radiologists. *Pediatr Radiol* 25:101-103
- Berdon WE, Slovis TL, Campbell JD et al. (1977) Neonatal small left colon syndrome: its relationship to aganglionosis and meconium plug syndrome. *Radiology* 125:457-462
- Bingol-Kologlu M, Ciftci AO, Senocak ME et al. (2002) Xanthogranulomatous pyelonephritis in children: diagnostic and therapeutic aspects. *Eur J Pediatr Surg* 12:42-48
- Blakelock RT, Beasley SW (1998) The clinical implications of non-idiopathic intussusception. *Pediatr Surg Int* 14:163-167
- Blask AR, Sanders RC, Gearhart JP (1991a) Obstructed uterovaginal anomalies: demonstration with sonography. Part I. Neonates and infants. *Radiology* 179:79-83
- Blask AR, Sanders RC, Rock JA (1991b) Obstructed uterovaginal anomalies: demonstration with sonography. Part II. Teenagers. *Radiology* 179:84-88
- Boga JA, Melon S, Nicieza I et al. (2004) Etiology of sporadic cases of pediatric acute gastroenteritis in Asturias, Spain, and genotyping and characterization of norovirus strains involved. *J Clin Microbiol* 42:2668-2674
- Bomelburg T, Lengerke HJ von (1992) Sonographic findings in infants with suspected necrotizing enterocolitis. *Eur J Radiol* 15:149-153
- Burkill G, Bell J, Healy J (2001) Small bowel obstruction: the role of computed tomography in its diagnosis and management with reference to other imaging modalities. *Eur Radiol* 11:1405-1422
- Carty H, Brereton RJ (1983) The distended neonate. *Clin Radiol* 34:367-368
- Casaccia G, Trucchi A, Nahom A et al. (2003) The impact of cystic fibrosis on neonatal intestinal obstruction: the need for prenatal/neonatal screening. *Pediatr Surg Int* 19:75-78
- Cass DT, Myers N (1987) Total colonic aganglionosis: 30 years experience. *Pediatr Surg Int* 2:68-75
- Chang WL, Yang YH, Lin YT et al. (2004) Gastrointestinal manifestations in Henoch-Schonlein purpura: a review of 261 patients. *Acta Paediatr* 93:1427-1431
- Chao HC, Lin SJ, Kong MS et al. (2000) Sonographic evaluation of the pancreatic duct in normal children and children with pancreatitis. *J Ultrasound Med* 19:757-763
- Chen EA, Luks FI, Gilchrist BF et al. (1996) Pyloric stenosis in the age of ultrasonography: Fading skills, better patients? *J Pediatr Surg* 31:829-830
- Chen KC, Chu CC, Chou TY et al. (1998) Ultrasonograph for inguinal hernia in boys. *J Pediatr Surg* 33:1784-1787

- Cohen HL, Zinn HL, Haller JO et al. (1998) Ultrasonography of pylorospasm: findings may simulate hypertrophic pyloric stenosis. *J Ultrasound Med* 17:705–711
- Coleman BG, Arger PH, Rosenberg HK et al. (1983) Gray-scale sonographic assessment of pancreatitis in children. *Radiology* 146:145–50
- Connolly B, O'Halpin D (1994) Sonographic evaluation of the abdomen in Henoch-Schonlein purpura. *Clin Radiol* 49:320–323
- Coward RJM, Peters CJ, Duffy PG et al. (2003) Epidemiology of paediatric renal stone disease in the UK. *Arch Dis Child* 88:962–965
- Crisci KL, Greenberg SB, Wolfson BJ et al. (1997) Contrast enema findings of fibrosing colonopathy. *Pediatr Radiol* 27:315–316
- Cull DL, Rosario V, Lally KP et al. (1990) Surgical implications of Henoch-Schonlein purpura. *J Pediatr Surg* 25:741–743
- Dacher JN, Boillot B, Eurin D et al. (1993) Rational use of CT in acute pyelonephritis: findings and relationships with reflux. *Pediatr Radiol* 23:281–285
- Dacher JN, Pfister C, Monroc M et al. (1996) Power Doppler sonographic pattern of acute pyelonephritis in children: comparison with CT. *Am J Roentgenol* 166:1451–1455
- Dalla Vecchia LK, Grosfeld JL, West KW et al. (1998) Intestinal atresia and stenosis: a 25-year experience with 277 cases. *Arch Surg* 133:490–496
- Daneman A, Alton DJ (1996) Intussusception: issues and controversies related to diagnosis and reduction. *Radiol Clin North Am* 34:743–756
- Daneman A, Navarro O (2003) Intussusception. Part 2: An update on the evolution of management. *Pediatr Radiol* 34:97–108
- Davis WS, Campbell JB (1975) Neonatal small left colon syndrome. *Am J Dis Child* 129:1024–1027
- Davis GH, Wapner RJ, Kurtz AB et al. (1984) Antenatal diagnosis of hydrometrocolpos by ultrasound examination. *J Ultrasound Med* 3:371–374
- DeCampo JF, Mayne V, Boldt DW et al. (1984) Radiological findings in total aganglionosis coli. *Pediatr Radiol* 14:105–209
- Del-Pozo G, Gonzalez-Spinola J, Gomez-Anson B et al. (1996) Intussusception: trapped peritoneal fluid detected with US relationship to reducibility and ischemia. *Radiology* 201:379–383
- Docherty JG, Zaki A, Coutts JA et al. (1992) Meconium ileus: a review 1972–1990. *Br J Surg* 79:571–753
- Dufour D, Delaet MH, Dassonville M et al. (1992) Midgut malrotation, the reliability of sonographic diagnosis. *Pediatr Radiol* 22:21–23
- Fakhoury K, Durie PR, Levinson H et al. (1992) Meconium ileus in the absence of cystic fibrosis. *Arch Dis Child* 67:1204–1206
- Fiorella DJ, Donnelly LF (2001) Frequency of right lower quadrant position of the sigmoid colon in infants and young children. *Radiology* 219:91–94
- Ford EG, Senac MO Jr, Srikanth MS et al. (1992) Malrotation of the intestine in children. *Ann Surg* 215:172–178
- Fotter R, Sorantin E (1994) Diagnostic imaging in necrotising enterocolitis. *Acta Paediatr Suppl* 396:41–44
- Friedland AJ, Herman TE, Siegel MJ (1995) Escherichia coli O157:H7-associated hemolytic-uremic syndrome: value of colonic color Doppler sonography. *Pediatr Radiol* 25:S65–S67
- Gamal R, Moore TC (1990) Appendicitis in children aged 13 years and younger. *Am J Surg* 159:589–592
- Gore RM (1987) Cross-sectional imaging of inflammatory bowel disease. *Radiol Clin North Am* 25:115–131
- Goulet O, Jobert-Giraud A, Michel JL et al. (1999) Chronic intestinal pseudo-obstruction syndrome in pediatric patients. *Eur J Pediatr Surg* 9:83–90
- Graif M, Itzhak Y (1988) Sonographic evaluation of ovarian torsion in childhood and adolescence. *Am J Roentgenol* 150:647–649
- Grattan-Smith JD, Blews DE, Brand T (2002) Omental infarction in pediatric patients: sonographic and CT findings. *Am J Roentgenol* 178:1537–1539
- Grignon A, Filion R, Filiatrault D et al. (1986) Urinary tract dilatation in utero: classification and clinical applications. *Radiology* 160:645–647
- Gross K, Desanto A, Grosfeld JL et al. (1985) Intra-abdominal complications of cystic fibrosis. *J Pediatr Surg* 20:431–435
- Hadidi AT, El Shal N (1999) Childhood intussusception: a comparative study of nonsurgical management. *J Pediatr Surg* 34:304–307
- Haha-Pedersen J, Kvist N, Nielsen OH (1984) Hydrometrocolpos: current views on pathogenesis and management. *J Urol* 132:537–540
- Halevy R, Smolkin V, Bykov S et al. (2004) Power Doppler ultrasonography in the diagnosis of acute childhood pyelonephritis. *Pediatr Nephrol* 19:987–991
- Hellerstine S (1995) Urinary tract infections: old and new concepts. *Pediatr Clin North Am* 42:1433–1457
- Hellerstine S (2000) Long-term consequences of urinary tract infections. *Curr Opin Pediatr* 12:125–128
- Hellstrom A, Hanson E, Hansson S et al. (1991) Association between urinary symptoms at 7 years old and previous urinary tract infection. *Arch Dis Child* 66:232–234
- Helmrath MA, Dorfman SR, Minifee PK et al. (2001) Right lower quadrant pain in children caused by omental infarction. *Am J Surg* 182:729–732
- Hernandez JA, Swischuk LE, Angel CA (2004) Validity of plain films in intussusception. *Emerg Radiol* 10:323–326
- Hernandez JA, Swischuk LE, Angel CA et al. (2005) Imaging of acute appendicitis: US as the primary imaging modality. *Pediatr Radiol* 35:392–395
- Hernanz-Schulman M, Sells LL, Ambrosino MM et al. (1994) Hypertrophic pyloric stenosis in the infant without a palpable olive: accuracy of sonographic diagnosis. *Radiology* 193:771–776
- Hu SC, Feeney MS, McNicholas M et al. (1991) Ultrasonography to diagnose and exclude intussusception in Henoch-Schonlein purpura. *Arch Dis Child* 66:1065–1067
- Ikeda H, Matsuyama S, Suzuki N et al. (1993) Small bowel obstruction in children: review of 10 years experience. *Acta Paediatr Jpn* 35:504–507
- Ilyas M, Mastin ST, Richard GA (2002) Age-related radiological imaging in children with acute pyelonephritis. *Pediatr Nephrol* 17:30–34
- Imamoglu M, Sarihan H, Sari A, Ahmetoglu A (2002) Acute acalculous cholecystitis in children: diagnosis and treatment. *J Pediatr Surg* 37:36–39
- Irish MS, Ragi JM, Karamanoukian H, Borowitz DS et al. (1997) Prenatal diagnosis of the fetus with cystic fibrosis and meconium ileus. *Pediatr Surg Int* 12:434–436
- Jabra AA, Fishman EK (1997) Small bowel obstruction in the pediatric patient: CT evaluation. *Abdom Imaging* 22:466–470
- Jeffrey RB, Jain KA, Nghiem HV (1994) Sonographic diagnosis of acute appendicitis: interpretive pitfalls. *Am J Roentgenol* 162:55–59
- Johnson JF, Robinson LH (1984) Localised bowel distension in the newborn: a review of the plain film analysis and differential diagnosis. *Pediatrics* 73:206–215
- Kao SC, Franken EA Jr (1995) Nonoperative treatment of simple meconium ileus: a survey of the Society for Pediatric Radiology. *Pediatr Radiol* 25:97–100
- Kassner EG, Sulton A, DeGroot T (1972) Bile duct anomalies associated with duodenal atresia: paradoxical presence of small bowel gas. *Am J Roentgenol* 116:577–583
- Katz S, Borst M, Seekri I et al. (1991) Surgical evaluation of Henoch-Schonlein purpura. Experience with 110 children. *Arch Surg* 126:849–853
- Kawanami T, Bowen A, Girdany BR (1984) Enterocolitis: prodrome of the haemolytic-uremic syndrome. *Radiology* 151:91–92
- Kenney IJ, Arthur RJ, Sweeney LE et al. (1991) Initial investigation of childhood urinary tract infection: Does the plain abdominal X-ray still have a role? *Br Radiol* 64:1007–1009



- King SJ, Velzen D, Smyth RL et al. (1994) Strictures of the colon in cystic fibrosis. *Clin Radiol* 49:476-477
- King LR, Siegel MJ, Balfe DM (1995) Acute pancreatitis in children: CT findings of intra- and extrapancreatic fluid collections. *Radiology* 195:196-200
- Kirks DR (1982) The radiology of enteritis due to hemolytic-uremic syndrome *Pediatr Radiol* 12:179-183
- Knowles CH, Silk DB, Darzi A et al. (2004) Deranged smooth muscle alpha-actin as a biomarker of intestinal pseudo-obstruction: a controlled multinational case series. *Gut* 53:1583-1589
- Kokoska ER, Keller MS, Weber TR (2000) Acute ovarian torsion in children. *Am J Surg* 180:462-465
- Kosloske AM, Love CL, Rohrer JE et al. (2004) The diagnosis of appendicitis in children: outcomes of a strategy based on pediatric surgical evaluation. *Pediatrics* 113:29-34
- Krasna IH, Rosenfeld D, Salerno P (1996) Is it necrotizing enterocolitis, microcolon of prematurity, or delayed meconium plug? A dilemma in the tiny prematurity infant. *J Pediatr Surg* 31:855-858
- Lane MJ, Katz DS, Ross BA et al. (1997) Unenhanced helical CT for suspected acute appendicitis. *Am J Roentgenol* 168:405-409
- Lawrence MJ, Ford WD, Furness ME et al. (2000) Congenital duodenal obstruction: early antenatal ultrasound diagnosis. *Pediatr Surg Int* 16:342-345
- Lavocat MP, Granjon D, Allard D et al. (1997) Imaging of pyelonephritis. *Pediatr Radiol* 27:159-165
- Lee EJ, Kwon HC, Joo HJ et al. (1998) Diagnosis of ovarian torsion with color Doppler sonography: depiction of twisted vascular pedicle. *J Ultrasound Med* 17:83-89
- Lim HK, Bae SH, Lee KH et al. (1994) Assessment of reducibility of ileocolic intussusception in children: usefulness of color Doppler sonography. *Radiology* 191:781-785
- Lim HK, Lee WJ, Lee SJ et al. (1996) Focal appendicitis confined to the tip: diagnosis at US. *Radiology* 200:799-801
- Lindley S, Mollitt DL, Seibert JJ et al. (1986) Portal vein ultrasonography in the early diagnosis of necrotizing enterocolitis. *J Pediatr Surg* 21:530-532
- Loening-Baucke V (2005) Prevalence, symptoms and outcome of constipation in infants and toddlers. *J Pediatr* 146:359-363
- Long FR, Kramer SS, Markowitz RI et al. (1996) Radiographic patterns of intestinal malrotation in children. *Radiographics* 16:547-556
- Lowe LH, Penney MW, Schecker LE et al. (2000) Appendicolith revealed on CT in children with suspected appendicitis: How specific is it in the diagnosis of appendicitis? *Am J Roentgenol* 175:981-984
- Lowe LH, Penney MW, Stein SM et al. (2001) Unenhanced limited CT of the abdomen in the diagnosis of appendicitis in children: comparison with sonography. *Am J Roentgenol* 176:31-35
- Merritt CR, Goldsmith JB, Sharp MJ (1984) Sonographic detection of portal venous gas in infants with necrotizing enterocolitis. *Am J Roentgenol* 143:1059-1062
- Middleton WD, Dodds WJ, Lawson TL et al. (1988) Renal calculi: sensitivity for detection with US. *Radiology* 167:239-244
- Miller SF, Landes AB, Dautenhahn LW et al. (1995) Intussusception: ability of fluoroscopic images obtained during air enemas to depict lead points and other abnormalities. *Radiology* 197:493-496
- Miller FH, Ma JJ, Scholz FJ (2001) Imaging features of enterohemorrhagic *Escherichia coli* colitis. *AJR* 177:619-623
- Mordehai J, Mares AJ, Barki Y et al. (1991) Torsion of uterine adnexa in neonates and children: a report of 20 cases. *J Pediatr Surg* 26:1195-1199
- Mushtaq I, Wright VM, Drake DP et al. (1998) Meconium ileus secondary to cystic fibrosis. The east London experience. *Pediatr Surg Int* 13:365-369
- Navarro O, Dugougeat F, Kornecki A et al. (2000) The impact of imaging in the management of intussusception owing to pathologic lead points in children. A review of 43 cases. *Pediatr Radiol* 30:594-603
- Navarro OM, Daneman A, Chae A (2004) Intussusception: the use of delayed, repeated reduction attempts and the management of intussusceptions due to pathologic lead points in pediatric patients. *Am J Roentgenol* 182:1169-1176
- Neilson D, Hollman AS (1994) The ultrasonic diagnosis of infantile hypertrophic pyloric stenosis: technique and accuracy. *Clin Radiol* 49:246-247
- Nghiem HV, Jeffrey RB Jr (1992) Acute appendicitis confined to the appendiceal tip: evaluation with graded compression sonography. *J Ultrasound Med* 11:205-207
- Oh DY, Gaedicke G, Schreier F (2003) Viral agents of acute gastroenteritis in German children: prevalence and molecular diversity. *J Med Virol* 71:82-93
- O'Haller J (1991) Sonography of the biliary tract in infants and children. *AJR* 157:1051-1058
- Olson AD, Hernandez R, Hirschl RB (1998) The role of ultrasonography in the diagnosis of pyloric stenosis: a decision analysis. *J Pediatr Surg* 33:676-681
- Olutola PS (1988) Plain film radiographic diagnosis of acute appendicitis: an evaluation of the signs. *Can Assoc Radiol J* 39:254-256
- Orr RK, Porter D, Hartman D (1995) Ultrasonography to evaluate adults for appendicitis: decision making based on meta-analysis and probabilistic reasoning. *Acad Emerg Med* 2:644-650
- Ostlie DJ, Spilde TL, St Peter SD et al. (2003) Necrotizing enterocolitis in full-term infants. *J Pediatr Surg* 38:1039-1042
- Ozdemir H, Isik S, Buyan N et al. (1995) Sonographic demonstration of intestinal involvement in Henoch-Schonlein syndrome. *Eur J Radiol* 20:32-34
- Patriquin HB, Fisch CH, Bureau M et al. (1984) Radiologically visible faecal gas patterns in "normal" newborns and young infants. *Pediatr Radiol* 14:87-90
- Pena BM, Taylor GA, Fishman SJ et al. (2002) Effect of an imaging protocol on clinical outcomes among pediatric patients with appendicitis. *Pediatrics* 110:1088-1093
- Pickering LK, Obrig TG, Stapleton FB (1994) Hemolytic-uremic syndrome and enterohemorrhagic *Escherichia coli*. *Pediatr Infect Dis J* 13:459-475
- Pilling DW, Steiner CM (1981) The radiology of meconium ileus equivalent. *Br J Radiol* 54:562-565
- Poon TS, Zhang AL, Cartmill T et al. (1996) Changing patterns of diagnosis and treatment of infantile hypertrophic pyloric stenosis: a clinical audit of 303 patients. *J Pediatr Surg* 31:1611-1615
- Pracos JB, Sann L, Genin G et al. (1992) Ultrasound diagnosis of midgut volvulus: the "whirlpool" sign. *Pediatr Radiol* 22:18-20
- Puylaert JB, Lalisang RI, van der Werf SD et al. (1988) *Campylobacter* ileocolitis mimicking acute appendicitis: differentiation with graded-compression US. *Radiology* 166:737-740
- Puylaert JB, Vermeijden RJ, van der Werf SD et al. (1989) Incidence and sonographic diagnosis of bacterial ileocaecitis masquerading as appendicitis. *Lancet* 8:84-86
- O'Keeffe FN, Stansberry SD, Swischuk LE et al. (1991) Antropyloric muscle thickness at US in infants: What is normal? *Radiology* 178:827-830
- Quillin SP, Siegel MJ (1993) Color Doppler US of children with acute lower abdominal pain. *Radiographics* 13:1281-1293
- Quillin SP, Siegel MJ (1994) Gastrointestinal inflammation in children: color Doppler ultrasonography. *J Ultrasound Med* 13:751-756
- Rao PM, Rhea JT, Novelline RA et al. (1997a) Helical CT technique for the diagnosis of appendicitis: prospective evaluation of a focused appendix CT examination. *Radiology* 202:139-144
- Rao PM, Rhea JT, Novelline RA (1997b) CT diagnosis of mesenteric adenitis. *Radiology* 202:145-149
- Rao PM, Wittenberg J, McDowell RK et al. (1997c) Appendicitis: use of arrowhead sign for diagnosis at CT. *Radiology* 202:363-366
- Rao PM, Rhea JT, Rao JA et al. (1999a) Plain abdominal radiography in clinically suspected appendicitis: diagnostic yield, resource use, and comparison with CT. *Am J Emerg Med* 17:325-328

- Rao PM, Rhea JT, Rattner DW et al. (1999b) Introduction of appendiceal CT: impact on negative appendectomy and appendiceal perforation rates. *Ann Surg* 229:344–349
- Ratcliffe JE, Fong S, Cheong I et al. (1992a) The plain abdominal film in intussusception: the accuracy and incidence of radiographic signs. *Pediatr Radiol* 22:110–111
- Ratcliffe JE, Fong S, Cheong I et al. (1992b) Plain film diagnosis of intussusception: prevalence of the target sign. *Am J Roentgenol* 158:619–621
- Rescorla FJ (1997) Cholelithiasis, cholecystitis and common bile duct stones. *Curr Opin Pediatr* 9:276–282
- Reynolds SL, Jaffe DM (1992) Diagnosing abdominal pain in a pediatric emergency department. *Pediatr Emerg Care* 8:126–128
- Rosenfeld K, McHugh K (1999) Survey of intussusception reduction in England, Scotland and Wales: how and why we could do better. *Clin Radiol* 54:452–458
- Rosenfield NS, Ablow RC, Markowitz RI et al. (1984) Hirschsprung's disease: accuracy of the barium enema examination. *Radiology* 150:393–400
- Rudolph CD, Hyman PE, Altschuler SM et al. (1997) Diagnosis and treatment of chronic intestinal pseudo-obstruction in children: report of consensus workshop. *J Pediatr Gastroenterol Nutr* 10:157–163
- Russell MB, Russell CA, Niebuhr E (1994) An epidemiological study of Hirschsprung's disease and additional anomalies. *Acta Paediatr* 83:68–71
- Samuel M, Duffy P, Capps S et al. (2001) Xanthogranulomatous pyelonephritis in childhood. *J Pediatr Surg* 36:598–601
- Sargent MA, Babyn P, Alton DJ (1994) Plain abdominal radiography in suspected intussusception: a reassessment. *Pediatr Radiol* 24:17–20
- Seashore JH, Collins FS, Markowitz RI et al. (1987) Familial apple peel jejunal atresia: surgical, genetic, and radiological aspects. *Pediatrics* 80:540–544
- Siegel MJ (1992) Acute appendicitis in childhood: the role of US. *Radiology* 185:341–342
- Siegel MJ, Friedland JA, Hildebolt CF (1997) Bowel wall thickening in children: differentiation with US. *Radiology* 203:631–635
- Shimizu T, Suzuki R, Yamashiro Y et al. (2001) Magnetic resonance cholangiopancreatography in assessing the cause of acute pancreatitis in children. *Pancreas* 22:196–199
- Shimanuki Y, Aihara T, Takano H et al. (1996) Clockwise whirlpool sign at color Doppler US: an objective and definite sign of midgut volvulus. *Radiology* 199:261–264
- Shinozaki T, Fujita Y, Araki K et al. (1991) Clinical features of enteric adenovirus infection in infants. *Acta Paediatr Jpn* 33:623–627
- Simonovsky V (1999) Sonographic detection of normal and abnormal appendix. *Clin Radiol* 54:533–539
- Singh SJ, Croaker GDH, Manglick P et al. (2003) Hirschsprung's disease: the Australian paediatric surveillance unit's experience. *Pediatr Surg Int* 19:247–250
- Sivit CJ, Newman KD, Boenning DA et al. (1992) Appendicitis: usefulness of US in diagnosis in a pediatric population. *Radiology* 185:549–552
- Sivit CJ, Newman KD, Chandra RS (1993) Visualization of enlarged mesenteric lymph nodes at US examination. Clinical significance. *Pediatr Radiol* 23:471–475
- Smink DS, Finkelstein JA, Garcia Pena BM et al. (2004) Diagnosis of acute appendicitis in children using a clinical practice guideline. *J Pediatr Surg* 39:458–463
- Smith SL, Somers JM, Broderick N et al. (2000) The role of the plain radiograph and renal tract ultrasound in the management of children with renal tract calculi. *Clin Radiol* 55:708–710
- Smyth RL, Velzen DV, Smyth AR et al. (1994) Strictures of ascending colon in cystic fibrosis and high-strength pancreatic enzymes. *Lancet* 343:85–86
- Spouge D, Baird PA (1985) Hirschsprung disease in a large birth cohort. *Teratology* 32:171–177
- Stark JE, Siegel MJ (1994) Ovarian torsion in prepubertal and pubertal girls: sonographic findings. *Am J Roentgenol* 163:1479–1482
- Stokland E, Hellstrom M, Jakobsson B et al. (1999) Imaging of renal scarring. *Acta Paediatr (Suppl 431)*:13–21
- Stringer MD, Pablot SM, Brereton RJ (1992) Paediatric intussusception. *Br J Surg* 79:867–876
- Stringer MD, Dhawan A, Davenport M et al. (1995) Choledochal cysts: lessons from a 20 year experience. *Arch Dis Child* 73:528–531
- St-Vil D, Brandt ML, Panic S et al. (1991) Meckel's diverticulum in children: a 20-year review. *J Pediatr Surg* 26:1289–1292
- Stylianou S, Jacir NN, Harris BH (1993) Incarceration of inguinal hernia in infants prior to elective repair. *J Pediatr Surg* 28:582–583
- Su C, Brandt LJ (1995) *Escherichia coli* O157:H7 infection in humans. *Ann Intern Med* 123:698–714
- Surratt JT, Siegel MJ (1991) Imaging of pediatric ovarian masses. *Radiographics* 11:533–584
- Tam PK, Nicholls G (1999) Implications of antenatal diagnosis of small-intestinal atresia in the 1990s. *Pediatr Surg Int* 15:486–487
- Taxman TL, Yulish BS, Rothstein FC (1986) How useful is the barium enema in the diagnosis of infantile Hirschsprung's disease? *Am J Dis Child* 140:881–884
- Theriot JA, Sayat J, Franco S et al. (2003) Childhood obesity: a risk factor for omental torsion. *Pediatrics* 112:e460
- Torres AM, Ziegler MM (1993) Malrotation of the intestine. *World J Surg* 17:326–331
- Uhnou I, Olding-Stenkvist E, Kreuger A (1986) Clinical features of acute gastroenteritis associated with rotavirus, enteric adenoviruses, and bacteria. *Arch Dis Child* 61:732–738
- Vane DW, West KW, Grosfeld JL (1987) Vitelline duct anomalies. Experience with 217 childhood cases. *Arch Surg* 122:542–547
- Van de Schouw YT, Van der Velden MT, Hitge-Boetes C et al. (1994) Diagnosis of hypertrophic pyloric stenosis: value of sonography when used in conjunction with clinical findings and laboratory data. *Am J Roentgenol* 163:905–909
- Van Noven R, Selderslaghs R, Bekaert J et al. (1991) Causative role of *Yersinia* and other enteric pathogens in the appendicular syndrome. *Eur J Clin Microbiol Infect Dis* 10:735–741
- Vaughn DD, Jabra AA, Fishman FK (1998) Pancreatic disease in children and young adults: evaluation with CT. *Radiographics* 18:1171–1187
- Verschelden P, Filiatrault D, Garel L (1992) Intussusception in children: reliability of US in diagnosis: a prospective study. *Radiology* 184:741–744
- Veyrac C, Baud C, Lopez C et al. (2003) The value of colour Doppler ultrasonography for identification of crossing vessels in children with pelvi-ureteric junction obstruction. *Pediatr Radiol* 33:745–751
- Vieten D, Spicer R (2004) Enterocolitis complicating Hirschsprung's disease. *Semin Pediatr Surg* 13:263–272
- Watanabe M, Ishii E, Hirowatari Y et al. (1997) Evaluation of abdominal lymphadenopathy in children by ultrasonography. *Pediatr Radiol* 27:860–864
- Weinberger E, Winters WD, Liddell RM et al. (1992) Sonographic diagnosis of intestinal malrotation in infants: importance of the relative positions of the superior mesenteric vein and artery. *Am J Roentgenol* 159:825–828
- Weizman Z, Durie PR (1988) Acute pancreatitis in childhood. *J Pediatr* 113:24–29
- Whittington PF, Friedman AL, Chesney RW (1979) Gastrointestinal disease in the hemolytic-uremic syndrome. *Gastroenterology* 76:728–733
- Wood SK, Kim JS, Suh SJ et al. (1992) Childhood intussusception: US-guided hydrostatic reduction. *Radiology* 182:77–80
- Yeung CY, Lee HC, Huang FY et al. (1996) Pancreatitis in children: experience with 43 cases. *Eur J Pediatr* 155:458–463
- Zerin JM, Kuhn-Fulton J, White SJ et al. (1995) Colonic strictures in children with cystic fibrosis. *Radiology* 194:223–226
- Ziegler MM (1994) Meconium ileus. *Curr Prob Surg* 31:731–777



## Subject Index

- 3D
  - bony surface reconstruction 128, 134
  - surface reconstructions 126
- A**
- abciximab 317
- abciximab abdominal injury 91
- abdominal ultrasound 414
- abscess
  - acute pyelonephritis 639
  - liver 641
  - pancreatic 634
  - peri-appendiceal 632
  - retropharyngeal 604
  - splenic injury 82
  - subphrenic 632
- abscess drainage technique 475
  - post procedure care 475
  - technique 475
- acalculous cholecystitis 416
- acetabulum columns
  - anterior 227
  - posterior 227
- acute
  - appendicitis 417, 632
  - cholecystitis 415
  - disseminated encephalomyelitis (ADEM) 592
  - hypoxic respiratory failure 612
  - mesenteric ischemia 425
  - pyelonephritis 638, 639
- air leaks 615
- air-fluid levels 630, 636
- airway obstruction 603
- alloimmune thrombocytopaenia 588
  - neonatal 588
- aneurysm 316, 322
  - AVM 322
  - coil therapy 317
  - feeding arteries 322
  - intracranial 316
- anterior cruciate ligament injury 280
  - ACL tears 280
- aortic
  - injury 12
  - rupture 617
- arterial hypertension 87
  - renal injury 87
- arterio-venous fistula
  - embolization 89
  - liver injury 67
  - renal injury 86
  - SMA 89
  - spleen 80, 82
- arteriography 68
  - arteriovenous fistula 69
  - delayed hemorrhage 69
  - embolization 69
  - liver injury 67
  - pseudo-aneurysm 69
  - renal injury 86
  - spleen injury 76, 77
  - vascular complications 69
- asphyxia 587
  - perinatal 587
- asthma 610
- avulsion of the tibial eminence 278
- B**
- Bankart lesion 256
- Barton fractures 265
- Bennet's fracture 271
- bile duct injury
  - bile fistula 72
  - bile leakage 69, 72
  - bile peritonitis 72
  - bilhemia 69, 72
  - biloma 72
  - complications 62, 69, 72
  - stricture 74
- bladder rupture 10
- blow-out fracture 131, 132
- blunt abdominal trauma 6, 190
- bowel injuries 15
- Boxer's fracture 271
- Brescia-Cimino fistulas
  - occlusions 571
- bronchiolitis 611
- bronchogenic 607
- bullae
  - percutaneous drainage 401
- C**
- calcific myonecrosis 253
- cardiopathy 609
- carotid artery 314
  - balloon occlusion 315
  - pseudoaneurysms 314
- carotid
  - blow-out syndrome 314
  - cavernous fistulas 322
- carotido-cavernous fistula 135, 136
- catheter stripping 578
- cavernous sinus 322
- cerebral palsy 586
- cerebral venous thrombosis 319
  - dural sinus thrombosis 320
- cervical fracture 5
- Chauffeur (or Hutchinson) fracture 266
- chest wall 615
- children
  - non-operative management 64
  - surgery 64
- cholangitis 485, 487
- cholecystitis
  - calculous cholecystitis 415, 481, 640
  - acalculous cholecystitis 416, 482, 640
  - gangrenous cholecystitis 416, 485
  - emphysematous cholecystitis 417, 485
- cholecystostomy 482, 487
- choledochal cysts 641
- Chopart's dislocation 287
- collar sign 193
- Colles fracture 265
- common bile duct 488
  - complex
    - facial fractures 133
    - midfacial fractures 128
    - tripod fracture 128
  - computed tomography (CT)
    - cystogram 10
    - scanning protocols 8
- congenital cystic adenomatoid malformation 609
- congenital lobar emphysema 609
- constipation 635
- contrast-enhanced sonography 19
- coronoid fractures 263
- cost-effectiveness analyses 251
- cranio-facial dysjunction 129
- Crohn's disease 427
- croup 603
- Cullen's sign 412
- cystic fibrosis
  - distal intestinal obstruction syndrome 641
  - fibrosing colonopathy 642
- D**
- dependent viscera sign 193
- deQuervain fracture 269
- diagnostic
  - arteriography 19
  - fluid aspiration 473
    - gram stain and culture 473
    - sterile abscess 474
    - technique 473
  - peritoneal lavage 189
- diaphragm
  - pleural fistula 92
- diaphragmatic rupture 18, 617
- diffuse axonal injuries (DAI) 10
- diffusion-weighted imaging (DWI) 586, 587
- dislocations of the distal radioulnar joint 267
- duodenal injury
  - fistula 88
  - obstruction 88, 624
    - congenital 624
- dural arteriovenous fistulas 319
  - embolization 320



**E**

- embolization
  - arterial 577
  - arterio-venous fistula 67, 82
  - delayed hemorrhage 67, 77
  - liver injury 67
  - pancreatic pseudo-aneurysm 83
  - pseudo-aneurysm of the spleen 77
  - renal injury 86
  - spleen injury 80, 82
  - technique 67
- encephalitis
  - Rasmussen's 597
- encephalopathy
  - acute 583
  - PRES (Posterior Reversible Encephalopathy Syndrome) 593
- epicondylar fractures 261
- epiglottitis 603
- epiploic appendagitis 422
- epistaxis 313
- ERCP
  - bile fistula 72
  - pancreas injury 83
  - stricture 74
- ethmoid cells 131

**F**

- facial pillars 129
- fibrinolysis 578
- fistula
  - thoraco-biliary 72
- flares
  - periventricular 586
- floating palate 129
- focal mesenteric ischemia 425
- focused assessment sonography for trauma (FAST) 7, 191
- foreign body 133, 253
  - aspiration 609
  - impaction 616
- fractures of the
  - acetabulum 230, 243, 246
  - acromion 259
  - anterior tibial tubercle 280
  - capitellum 262
  - condyle 137
  - coracoid process 259
  - ethmoid cells 131
  - frontal sinuses 131
  - pelvic ring 231
  - scapular body 259
- frontal sinus 131
- functional immaturity of the large bowel
  - see meconium plug syndrom 626

**G**

- Galeazzi's fracture 264
- Gamekeeper's thumb 271
- gastroenteritis 630
- gastroenterocolitis 427
- gastrointestinal tract injury
  - perforation 15, 89
  - stenosis 88, 89
- general fracture signs 251
- germinal matrix haemorrhage 583
- Glenoid fractures 259
- Grey-Turner's sign 412
- groin disruption 276
- gunshot fracture of orbit 134

**H**

- haemobilia 67
- haemolytic uraemic syndrome 636

**haemorrhage**

- intraventricular 585
- subependymal 585
- hamate fractures 268
- head injury
  - non-accidental 590
- hemangioma, subglottic 606
- hemodialysis shunts 571
- hemorrhage
  - gastrointestinal, diagnosis 454
    - angiography 457
    - computed tomography 454
    - magnetic resonance 456
  - gastrointestinal treatment 457
    - arterio-portal connections 458
    - covered stents 461
    - diffuse gastric hemorrhage 458
    - duodenal ulcer 459
    - duodenal vascularization 459
    - gastrointestinal rebleeding 460
    - hemobilia 457
    - hemosuccus 458
    - ineffective embolization 461
    - microcoils 460
    - vasa recta 460
    - vasopressin 460
- hemothorax
  - percutaneous drainage 399
- Henoch-Schonlein purpura 631
- hepatitis 641
- Hill-Sachs lesion 256
- Hirschsprung's disease 627
- humeral avulsion of glenohumeral ligaments (HAGL) lesion 256
- hydranencephaly 584
- hydronephrosis 635, 639
- hypertrophic pyloric stenosis (HPS) 628
- hypoxic-ischaemic encephalopathy (HIE) 583
- hypoxic-ischaemic injury (HII) 583

**I**

- iliac artery injury
  - embolization 91
- implant grafts 571
- inferior vena cava injury
  - thrombosis 91
- inflammatory bowel disease 636
- inguinal hernia 631
- intercondylar fractures 277
- intestinal malrotation 625
- intestinal obstruction
  - neonates 623
  - in children 636
- intestinal pseudo-obstruction 636
- intraoperative
  - calcification 624, 626
  - perforation 631
  - peritoneal 633
    - air 623
    - fluid 623, 632
- intussusception 629, 630, 631, 632
- ischaemic stroke 323
- ischemia
  - gastrointestinal, acute 425, 461
  - gastrointestinal, chronic 464
  - gastrointestinal, treatment 465
    - angioplasty 467
    - bowel infarction 465
    - fibrinolytic agents 466
    - median arcuate ligament 467
    - vasodilators 467
- isolated facial fractures 131

**J**

- Jersey finger 272

**K**

- kidney injury
  - hypertension 87
  - parenchyma injury 18
  - pseudo-aneurysm 86
  - urinary leaks 88
  - urinary stenosis 88
  - vascular complications 86

**L**

- large bowel obstruction 422
- laryngotracheobronchitis 603
- Le Fort-type fractures 129
- lisfranc injuries 287
- liver injury 14
  - abscess 75
  - complications 62, 63, 67
  - cyst 75
  - embolization 62, 67
  - haemobilia 62, 67
  - sepsis 75
  - surgery 63
  - vascular complications 62, 67
- low-energy trauma 4
- lumbar artery injury
  - embolization 91
- lunate
  - dislocation 269
  - fractures 268

**M**

- magic-angle phenomenon 252
- magnetic resonance imaging 126, 132, 136
- magnetic resonance imaging (MRI) 584
- Maisonneuve injury 283
- malignant pleural effusion
  - percutaneous drainage 399
- Mallet finger 272
- mandibular fracture 136
- MDCT protocols 8
- mechanical bowel obstruction 424
- Meckel's diverticulum 630
- meconium ileus 626
  - equivalent see distal intestinal obstruction syndrome 641
- meconium plug syndrome 626, 627
- mediastinal abscess
  - percutaneous drainage 403
- MELAS 595
- meningitis
  - children 589
  - neonatal 589
- mesenteric
  - adenitis 633
  - injuries 16
- microcolon 624, 626
- midcarpal dislocation 269
- midtarsal dislocation 287
- Mirizzi syndrome 485, 486
- Monteggia's fracture 264
- Moore's fracture 267
- MR spectroscopy (MRS) 586
- MRCP 489, 490
- MRI 19, 127, 133
- multiple sclerosis 593
- Murphy's sign 482
- muscle
  - contusion 253
  - tears 253
- myositis ossificans 253

- N**  
nasal fractures 127  
naso-lacrimal duct 135  
native fistulas 571  
– thrombolysis 571  
necrotising  
– enterocolitis 623  
– pancreatitis 429  
Neer's classification 258  
neuronal migration disorders 584  
non-accidental injury (NAI) 590  
– shear injury 592  
– subdural haemorrhage 591  
non-operative management abdominal trauma  
– complications 61, 63
- O**  
olecranon fractures 263  
omental infarction 633  
optic canal fractures 133  
orbital emphysema 131  
ovarian  
– cysts 637  
– torsion 637, 638
- P**  
pancreas injury  
– complications 83, 85, 195  
– duct stricture 85  
– pseudo-cyst 83  
– transection 16, 196  
pancreatitis  
– acute pancreatitis 429, 634  
– chronic pancreatitis 634  
paralytic ileus 424  
patellar  
– dislocation 279  
– tendon ruptures 280  
pelvic trauma 226, 230  
pelviureteric junction (PUJ) obstruction 639  
penetrating  
– abdominal trauma 190  
– injuries 133  
penumbra 323  
percutaneous abscess drainage  
– complications 478  
– endocavitary access 478  
– fluoroscopy 474  
– gastrointestinal tract 476  
– hepato-biliary tract 476  
– pancreas 476  
– patient preparation 474  
– pelvic abscesses 478  
– post procedure care 475  
– pseudocyst 83  
– pulmonary abscess 401  
– retroperitoneum 478  
– spleen 83, 478  
– sub-phrenic collections were tra 476  
– technique 475  
– transgluteal access 478  
percutaneous biliary drainage 69, 72  
percutaneous needle lung biopsy  
– hemoptysis 399  
– pneumothorax 399  
percutaneous thoracic drainage  
– complications 406  
– fluid collections 395  
percutaneous treatment  
– shunt dysfunction 572  
pericardial effusion 394  
pericardial fluid  
– percutaneous drainage 403  
perilunate dislocation 269  
periventricular leukomalacia (PVL) 583  
pilon tibial fractures 283  
pisiform fractures 269  
plain abdominal radiography 413  
plain films pelvis 228  
pleural empyema  
– percutaneous drainage 395  
– results of percutaneous drainage 397  
pleural fluid collection 391  
– percutaneous drainage 395  
pneumatocele 401  
– percutaneous drainage 401  
pneumocephalus 131  
pneumomediastinum 393  
– percutaneous drainage 405  
pneumonia 612  
pneumothorax 392, 399  
– Heimlich valve 399  
posterior cruciate ligament injuries 280  
premature baby 615  
pseudo-aneurysm  
– liver injury 67  
– renal injury 86  
– spleen 13, 82  
pseudo-cysts  
– pancreatic injury 83  
pulmonary abscess  
– percutaneous drainage 401  
pulmonary aspergiloma  
– percutaneous treatment 401  
pulmonary contusion 617  
pyothorax 615  
pyramidal fracture 129
- Q**  
quadriceps tendon rupture 280
- R**  
radiocarpal dislocations 267  
renal injury – organ injury scale 199  
Rendu–Osler–Weber disease 313  
respiratory  
– failure 601  
Rolando's fracture 271  
rotator-cuff tears 260
- S**  
scapholunate dissociation 269  
scapular neck fractures 259  
scapulothoracic  
– dislocation 260  
– dissociation 260  
sentinel clot sign 199  
shattered  
– kidney 197  
– spleen 195  
shock bowel 196  
shunt 571  
– thrombosis 571  
sigmoid diverticulitis 421  
sinus infection 590  
– fungal 590  
– HIV 590  
skier's thumb 271  
skull-base fractures 136  
SMA injury 89  
small airway obstruction 610  
small bowel  
– atresia 624  
– obstruction 422, 437  
small left colon syndrome 627  
small left colon syndrome  
see meconium plug syndrom 626  
smash injuries 129  
Smith fracture 265  
soft tissue injury 125  
somatic pain 412  
sonographic Murphy's sign 416  
spinal catheter 323  
spleen injury  
– complications 75  
– CT-based scoring system 195  
– delayed rupture 77  
– embolization 80, 82  
splenic  
– abscess 417  
– infarction 417  
– injuries 13, 75, 195  
Stener lesion 271  
stomach injury 88  
stridor 602  
stroke  
– childhood 595  
subarachnoid haemorrhages 316  
subtalar dislocation 287  
subtrochanteric fractures 275  
superior labrum anterior posterior (SLAP) 260  
superior mesenteric artery (SMA) injury 89  
supracondylar fractures 261, 276
- T**  
target sign 426  
thrombolysis 317  
– intra-arterial 323  
– intravenous 323  
thymus 602  
Tillaux fractures 283  
TORCH 588  
total body scan 9  
transcondylar fractures 261  
transscaphoid perilunate dislocation 269  
trapezoid fractures 269  
trapezoid fractures 269  
trauma  
– high-energy 225  
– low-energy 225  
triage 7  
triplane fracture 283  
tripod fracture 127, 128  
triquetrum fractures 268  
tumors  
– mediastinal 606
- U**  
ulcerative colitis 427  
urethral injury 201  
urinary bladder injury 200  
urinary tract infection 638  
urokinase 319, 323  
– pseudoocclusion 324  
urolithiasis 428, 640
- V**  
vascular  
– rings and slings 607  
vasculopathy  
– lenticulostriate 588  
vasospasm  
– angioplasty 318  
venous access occlusion 578  
vesico-ureteric reflux 639

visceral pain 412  
volar plate avulsion 272  
Volkmann's fracture 283  
volvulus 422, 437, 625

**W**  
wheezing 602  
Winterstein's fracture 271

**X**  
xanthogranulomatous pyelonephritis  
(XGP) 639

**Z**  
zygomatico-maxillary complex  
fracture 127